Figure 47 shows a metal loss feature on the 11 3/4 in. casing ID from the UCI log. This feature is ~21 in. long (894.58–896.33 ft) and has an average width of 1.8 in and a maximum penetration of 48% (0.16/0.333 in.), denoted by an arrow. The length of the 7 in. axial rupture was measured as 19 in. long and .75 in wide [2]. The depth of this 11 3/4 in. longitudinal feature was very close to the depth in which we found the 7 in. axial rupture. The upper half of the feature was more defined than the lower half. The longitudinal feature was observed in the caliper and HRVRT logs but was best visualized by the UCI log.

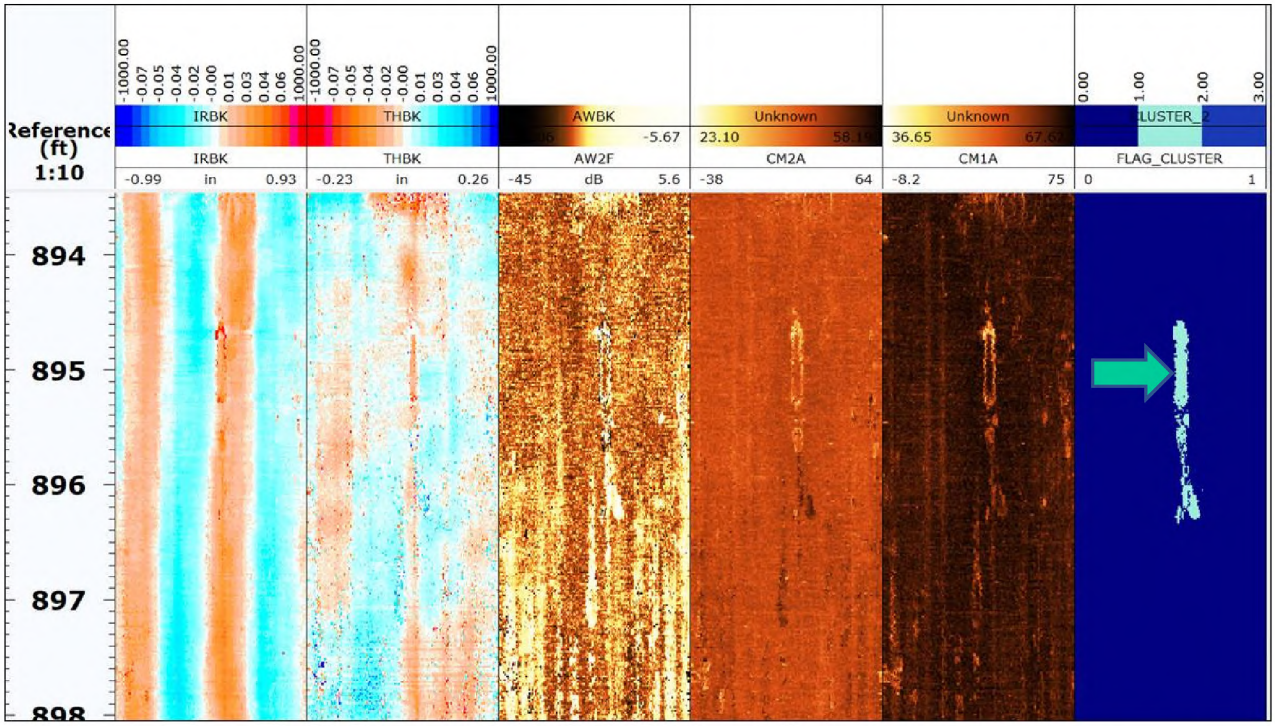

Figure 47: UCI Log [7] of 11 3/4 in. Longitudinal Feature in 11 3/4 in. Casing Resembling 7 in. Rupture

Figure 48 shows the caliper log of the 11 3/4 in. casing joint 23; Figure 49 is the same joint but zoomed into a 10 ft section from 888–898 ft. This joint was adjacent to the failed 7 in. casing joint 22. We estimated that, prior to its failure on October 23, 2015, the wall thickness of the 7 in. casing joint 22 was reduced by 85% at the rupture initiation site [2]; however, we did not observe any internal metal loss features in the 11 3/4 in. casing of the same magnitude (85%) in the external corrosion found on the 7 in. casing.

In addition to the longitudinal feature resembling the 7 in. axial rupture, there was a 1.2 ft tall metal loss feature at 892.4–893.6 ft and circumferential in nature; there was radial wall thinning where the average ID increased to 11.23 in. in this depth range (compared to this joint's average ID of 11.16 in.) as denoted by the green highlighted line. The 3D inset in Figure 49 shows a top down view of the same circumferential feature. Our interpretation is that these longitudinal and circumferential features were likely erosion related and the consequence of the flow of gas, liquids, and solids through the axial rupture and circumferential parting of the 7 in. casing joint 22. This interpretation is supported by the video imaging of 891-892 ft (Appendix C). The 11 3/4 in. casing ID was, at this depth, much more reflective than in other areas.

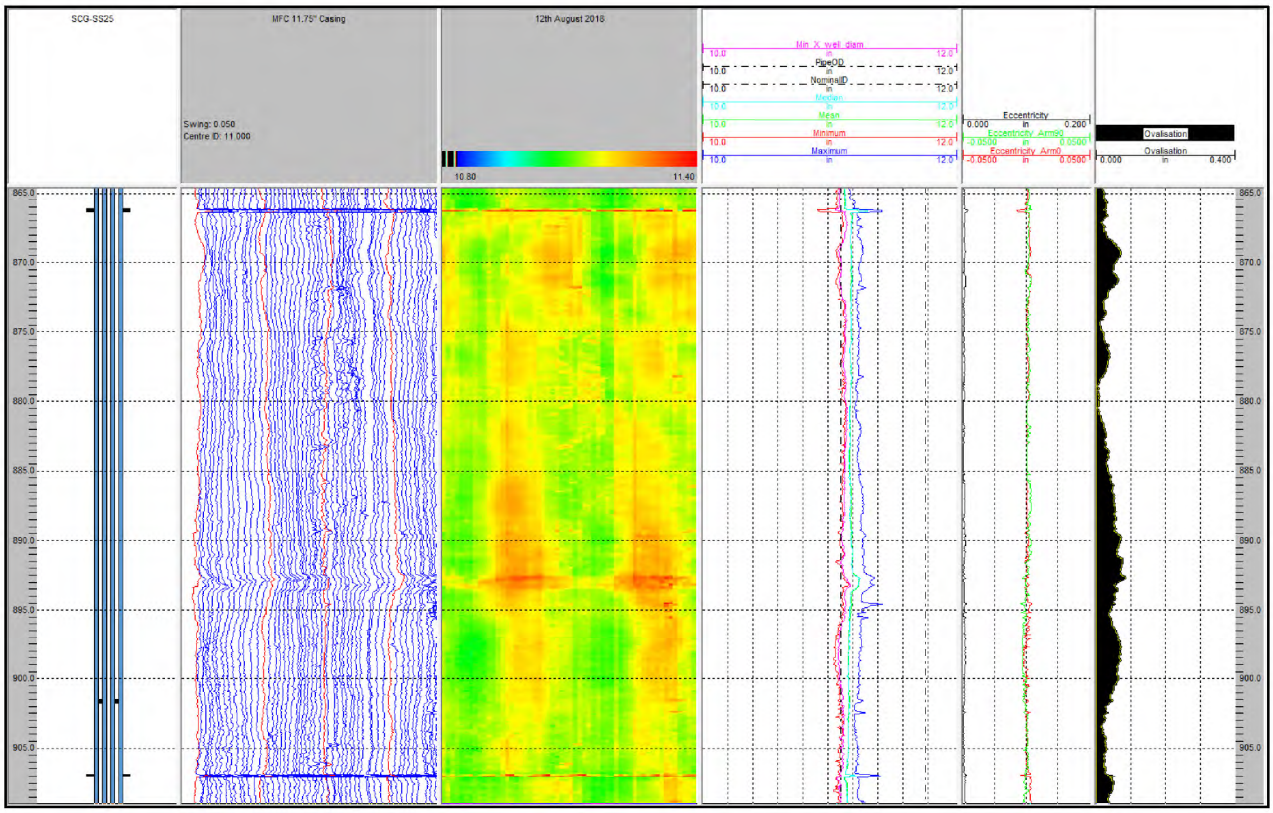

Figure 48: Caliper Log [7] of 11 3/4 in. Casing Joint 23

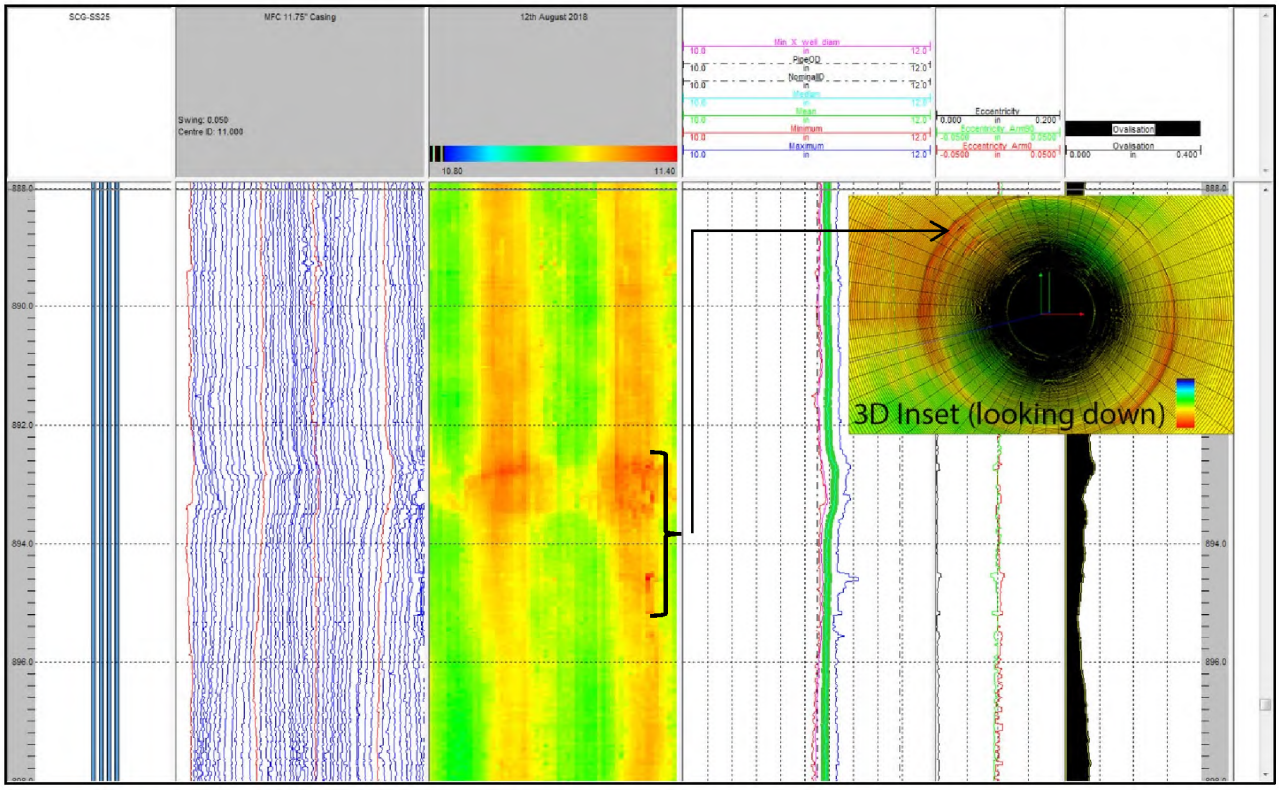

Figure 49: Caliper [7] Log of 11 3/4 in. Casing Joint 23, 888–898 ft, Mean ID Highlighted Green, 3D Inset

2.4.5 Ovality

Ovality was observed in the caliper and ultrasonic logs at various locations. Figure 50 shows the 11 3/4 in. caliper log from the surface to 990 ft. The right track shows ovalization (black) displayed in inches and is the half of the maximum ID minus minimum ID. EV-Epidote calculated ovalization using the caliper data [7] for the 11 3/4 in. casing and found a range of ovality of 1-2%[ii]. Our interpretation is that ovality of this magnitude is minor. Higher values of ovality were observed at the locations of the holes (e.g., at 180 ft) but were not valid because the measurements at the holes were not actually from the casing ID. Less than 1% ovality was observed in the location of the 7 in. casing failure.

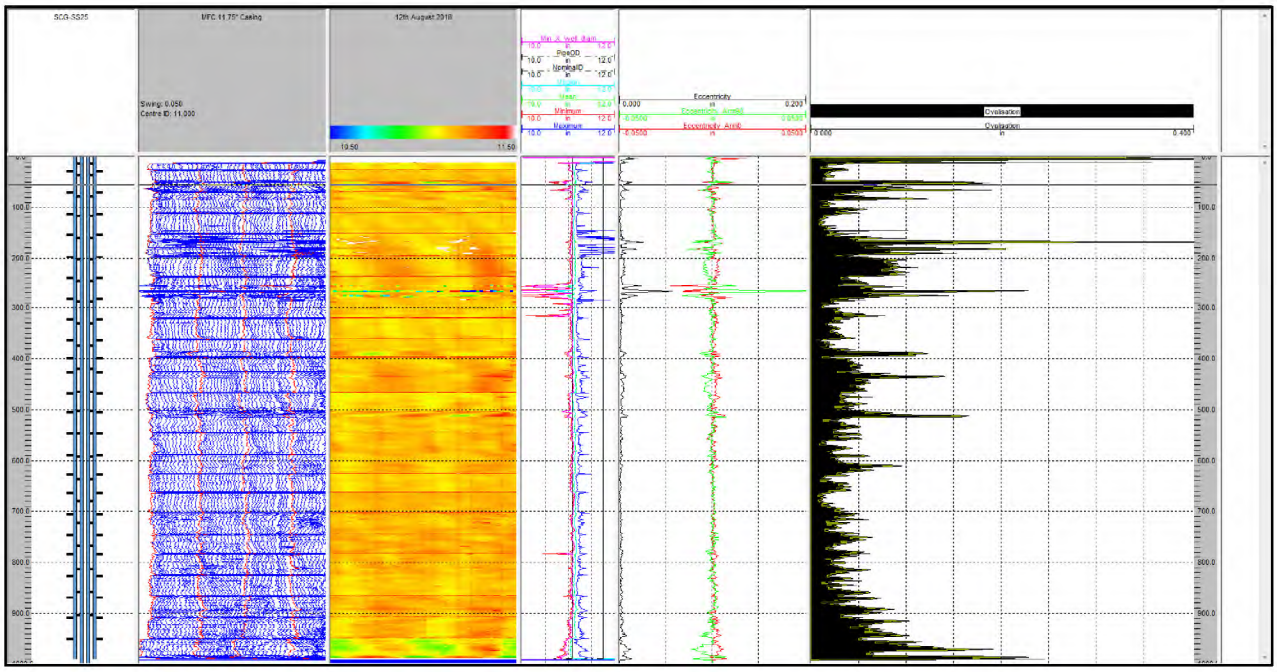

Figure 50: Caliper Log [7] of 11 3/4 in. Casing, Ovality (Right Track) Displayed Range 0–0.4 in. (0–3.6%)

2.4.6 Casing Wear

Casing wear was observed in caliper and ultrasonic logs at various locations and listed in Table 10. Figure 51 shows the UCI log of joints 13–14 with casing wear denoted by a red box. Note the internal metal loss features shown previously (Figure 39, Figure 40 and Figure 41) are highlighted by a blue box. These features seem to be within the casing wear groove. The other occurrences of casing wear are similar to that shown.

[ii] To express ovalization as a percentage, take the ovalization in inches, divide it by the nominal ID, and multiply it by 100 e.g. ovalization of 0.2 in. is 1.8% (0.2 in. / 11.084 in. *100).

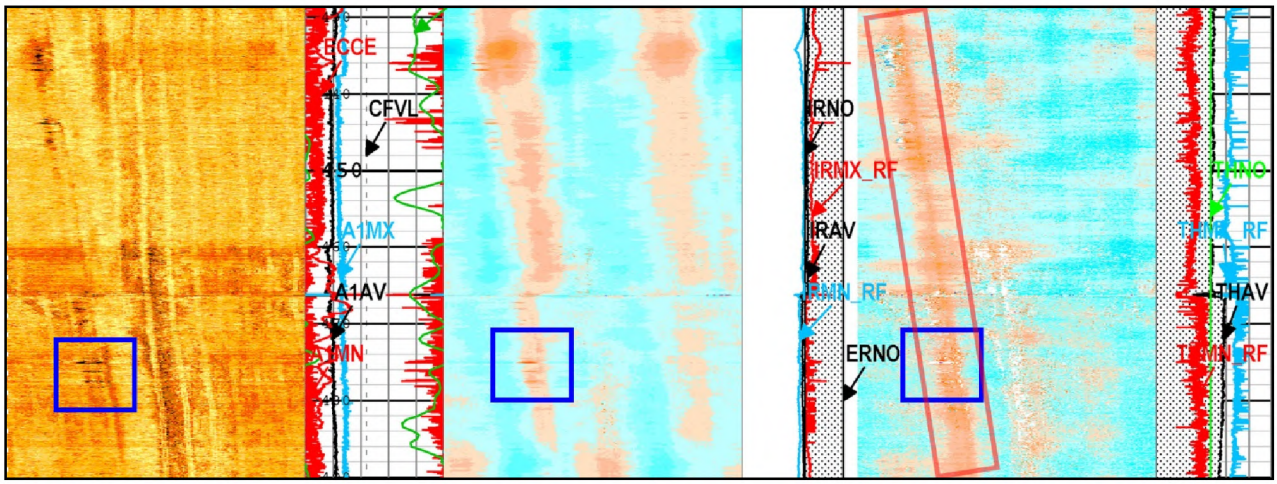

Figure 51: UCI Log [17] of 11 3/4 in., Joints 13–14, Casing Wear (Red Box) and Internal Metal Loss Feature (Blue Boxes)

2.4.7 Annulus Condition

Appendix E shows the HRVRT, IBC, and Integrity Explorer (INTeX) logs. There is excellent agreement between the IBC and INTeX logs—both show a poorly cemented casing annulus. The HRVRT log was placed beside these annulus logs to show where the metal loss was found relative to the annulus condition.

Schlumberger's interpretation was the following (reformatted for clarity):

- Above 400 ft, the cement coverage behind the casing is poor, apparent on both IBC and CBL/VDL. A correlation exists between the lack of cement and high corrosion in this area.
- From approximately 606 to 660 ft and approximately 950 to 985 ft, there is in general a good indication of presence of solids behind the casing. This is evident based on the azimuthal coverage of the acoustic impedance and flexural attenuation maps.
- From approximately 395 to 411 ft and approximately 660 to 668 ft, gas[iii] appears to be trapped.
- From approximately 625 to 655 ft, the cement coverage is good, but it also shows a channel lacking cement. This area without cement shows corrosion on the thickness map.
- From approximately 670 to 950 ft and at other isolated areas, a gas filled micro-annulus is observed. This is supported by the high attenuation readings.

Our interpretation is consistent with Schlumberger's.

Noise Logs Related to Annulus Condition

Fluid losses were evident during the extraction of the 7 in. casing [11]. Blade directed noise logs on May 20 and August 11, 2018 to determine the location of the losses. On the May 20, 2018, the noise tool was positioned at 990 ft, 400 ft, and 300 ft in the 7 in. production tieback and 7 in. casing while adding 9 ppg viscosified potassium chloride (aka Flowzan) into the 7 in. by 11 3/4 in. annulus. Two 5 bbl volumes of Flowzan were added from the surface via trip tank. With the first 5 bbl volume, no noise was detected

[iii] Our interpretation of the word gas is intended to communicate that gas, the phase, was observed (with no specific composition; e.g., natural gas or air).

with the noise tool positioned at 990 ft. With the second 5 bbl volume, noise was detected with the noise tool positioned at 300 ft, but no noise was detected at 400 ft. In the August 11, 2018 work, Flowzan was pumped at 3 bbl/min for 5 minutes down open-ended drill pipe that was positioned at 932 ft within the 11 3/4 in. casing. A noise tool was positioned at 990 ft—the 11 3/4 in. casing shoe depth. No noise was detected. Our interpretation is that the holes observed in the 11 3/4 in. casing from 134 to 300 ft were the location of the losses, not the 11 3/4 in. casing shoe.

3 Conclusions

The following is a summary of Blade's observations and interpretations of the inspection logs:

2 7/8 in. tubing:

- No metal loss features above 20% penetration was present.
- Deformation in the form of bulging and bent joints was present.

7 in. casing:

- Internal metal loss—penetration ranged from 15 to 41% and was prevalent from 1,780 to 2,230 ft.
- External metal loss—penetration ranged from 15 to 51% and was prevalent from surface down to 1,015 ft.
- Deformation in the form of ovality, which ranged from 1 to 2% for all but one location. At the whipstock depth, the maximum ovality was 6%.
- Cementing—the 7 in. annulus was cemented from the shoe at 8,585 ft to a depth of 6,980 ft. The area above the cement was filled with varying percentages of liquids, gases, and solids.

11 3/4 in. casing:

- Internal metal loss—pitting, uniform internal metal loss features, casing wear, erosion, and holes were present in various intervals. The penetration ranged from 15 to 100%.
- External metal loss was observed. The penetration ranged from 15 to 95% and was prevalent from 90 to 385 ft. There were other areas of isolated external metal loss.
- Deformation was observed in the form of ovality. The ovality ranged from 1 to 2%.
- Good cement was observed in short isolated portions of the 11 3/4 in. annulus, specifically at 606–660 ft and 950-985 ft. Cement was not observed above 400 ft. Areas without cement were filled with liquids, gases, and solids of varying percentages.

4 References

[1] Blade Energy Partners, "SS-25 Tubulars NDE Analysis," Houston, 2019.

[2] Blade Energy Partners, "SS-25 Casing Failure Analysis," Houston, 2019.

[3] Blade Energy Partners, "00_Summary of Vendors for Phase 3 Wireline Logging of SS25 v3 composite.pdf," Houston, 2016.

[4] Blade Energy Partners, "AC-RCA SS25 Phase 3 Tubing Casing Wellhead Extraction Protocol Ver 6 2017-07-14.pdf," Houston, 2017.

[5] Blade Energy Partners, "AC-RCA SS25 Phase 3A Contingency Part 2 Work Plan Rev 1 2018-15-04.pdf," Houston, 2018.

[6] Baker Hughes GE, "2_875_Baker_Hughes_GE_Logs.pdf," Houston, 2019.

[7] EV Epidote, "7_11_75_EV_Epidote_Logs.pdf," Houston, 2019.

[8] Scientific Drilling, "SS-25 INRUN Survey Report_01-16-2016 .pdf," 2016.

[9] Baker Hughes GE, "7_Baker_Hughes_GE_Logs.pdf," Houston, 2019.

[10] Schlumberger, "7_Schlumberger_Logs.pdf," Houston, 2019.

[11] Blade Energy Partners, "Phase 3 Report," Houston, 2019.

[12] SoCalGas, , "SS-25 Well Documentation (from SoCalGas)_N, AC_CPUC_0000056," Chatsworth, 2016.

[13] Blade Energy Partners, "SS-25 Summary of Trips in 7 in. Casing.pdf," Houston, 2019.

[14] Blade Energy Partners, "Aliso Canyon Field: Hydrology," Houston, 2019.

[15] Schlumberger, "OH_Schlumberger_Logs.pdf," Houston, 2019.

[16] Baker Hughes GE, "11_75_Baker_Hughes_GE_Logs.pdf," Houston, 2019.

[17] Schlumberger, "11_75_Schlumberger_Logs.pdf".

[18] Scientific Drilling, "Survey Report Default Wellbore - Default Wellbore View - SS-25," Bakersfield, 2018.

Appendix A Log Headers

Main Log
5"/100'

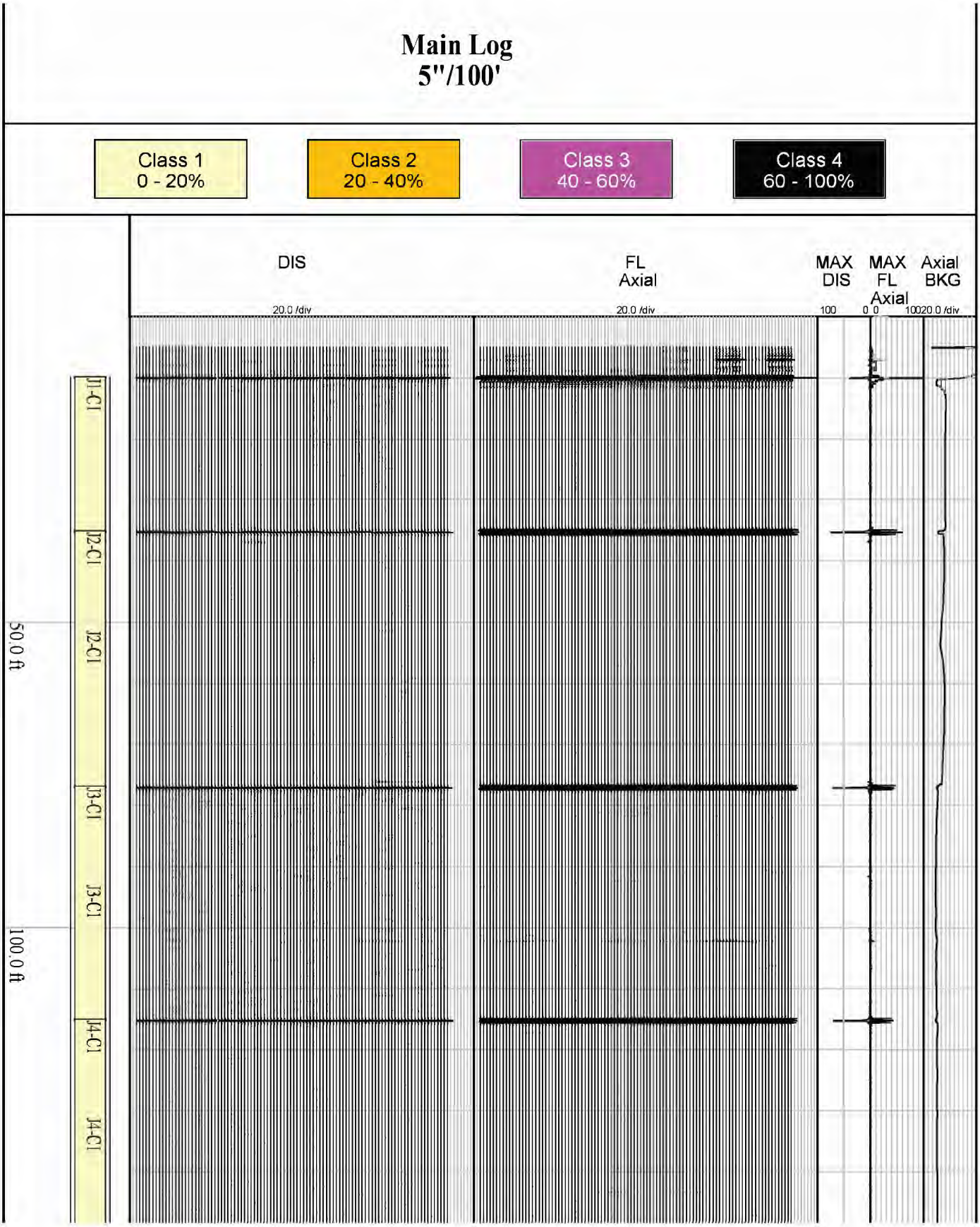

SS-IBC

Main Pass

Software Version

Acquisition System	Version
Maxwell 2017 SP3	7.3.92069.3100

Pass Summary

Run Name	Pass Objective	Direction	Top	Bottom	Start	Stop	DSC Mode	Depth Shift	Include Parallel Data
SS-IBC	Log[6]:Up	Up	26.73 ft	7551.80 ft	04-Dec-2017 6:13:20 PM	05-Dec-2017 10:19:25 AM	ON	3.31 ft	No

All depths are referenced to toolstring zero

Log

Company:Southern California Gas Company Well:Standard Session 25

SS-IBC: Log[6]:Up:S004

Description: USI IBC SLG Format: Log (IBC SLG VDLCBL) Index Scale: 5 in per 100 ft Index Unit: ft Index Type: Measured Depth Creation Date: 06-Dec-2017 18:09:22

TIME_1900 - Time Marked every 60.00 (s)

USIT Processing Flags (UFLG[0]) USIT-E

1 - UFLG 1 Value within [0.0 - 1.5] - :
2 - UFLG 2 Value within [1.5 - 2.5] -
3 - UFLG 3 Value within [2.5 - 3.5] -
4 - UFLG 4 UFLG 5 UFLG 6 Value within [3.5 - 6.5] - :
5 - UFLG 7 UFLG 8 UFLG 9 Value within [6.5 - 10] - :

UTIM Error
Pulse Origin Not Detected
WINLEN Error
Casing Thickness Error
Loop Processing Error

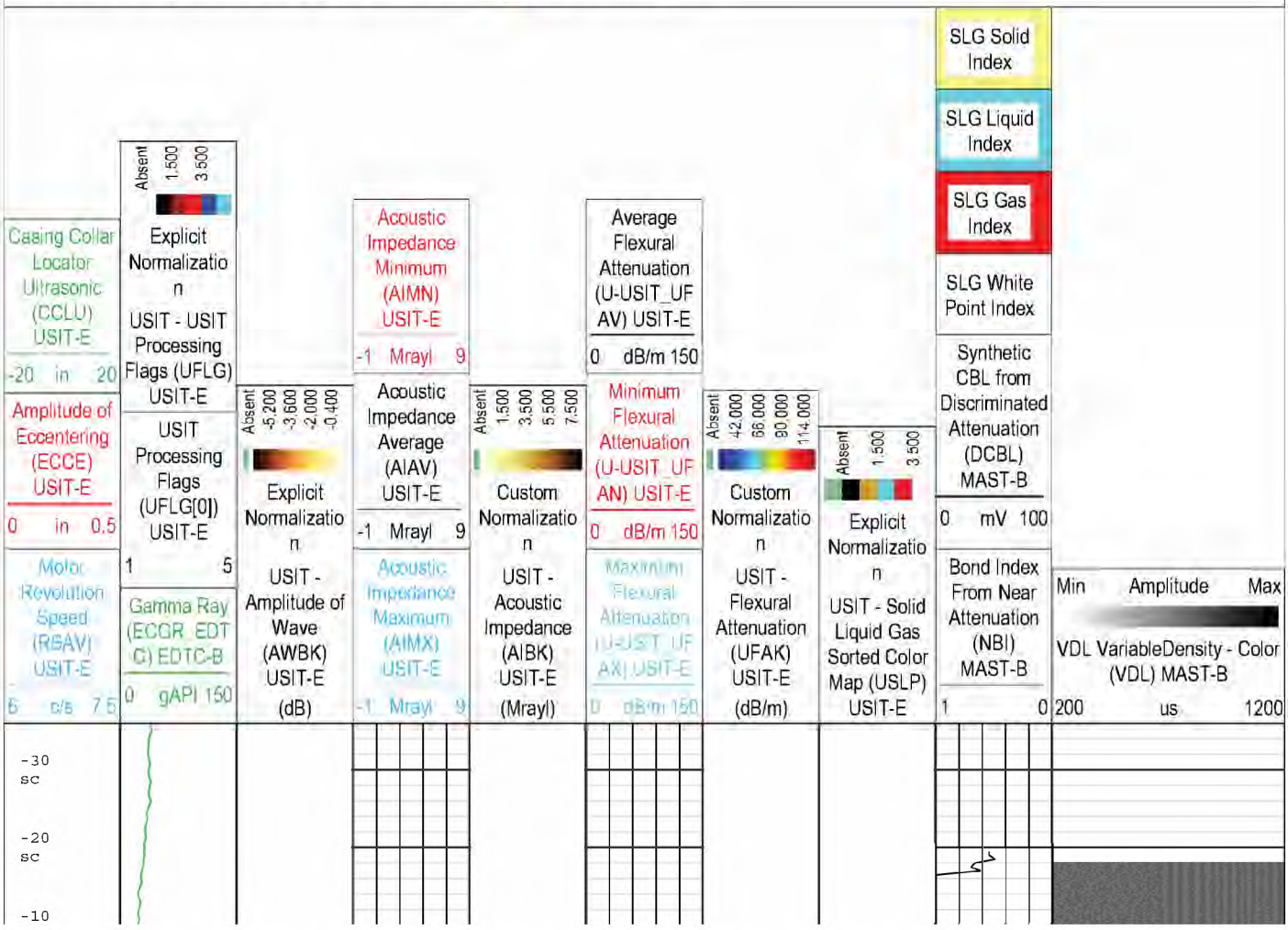

SS-IBC

CORROSION Main Pass

Software Version

Acquisition System	Version
Maxwell 2017 SP3	7.3.92069.3100

Pass Summary

Run Name	Pass Objective	Direction	Top	Bottom	Start	Stop	DSC Mode	Depth Shift	Include Parallel Data
SS-IBC	Log[6]:Up	Up	26.73 ft	7551.80 ft	04-Dec-2017 6:13:20 PM	05-Dec-2017 10:19:25 AM	ON	3.31 ft	No

All depths are referenced to toolstring zero

Log

Company:Southern California Gas Company Well:Standard Sesnon 25

SS-IBC: Log[6]:Up:S004

Description: USI Corrosion Format: Log (USI Corrosion 7inch) Index Scale: 5 in per 100 ft Index Unit: ft Index Type: Measured Depth Creation Date: 06-Dec-2017 18:09:07

TIME_1900 - Time Marked every 60.00 (s)

USIT Processing Flags (UFLG[0]) USIT-E

1 - UFLG 1 Value within [0.0 - 1.5] - :
2 - UFLG 2 Value within [1.5 - 2.44] - :
3 - UFLG 2 Value within [2.44 - 2.5] - :
4 - UFLG 3 Value within [2.5 - 3.5] - :
5 - UFLG 4 UFLG 5 UFLG 6 Value within [3.5 - 6.5] - :
6 - UFLG 7 UFLG 8 UFLG 9 Value within [6.5 - 10] - :

- UTIM Error
- Pulse Origin Not Detected
- Spiky Waveform
- WINLEN Error
- Casing Thickness Error
- Loop Processing Error

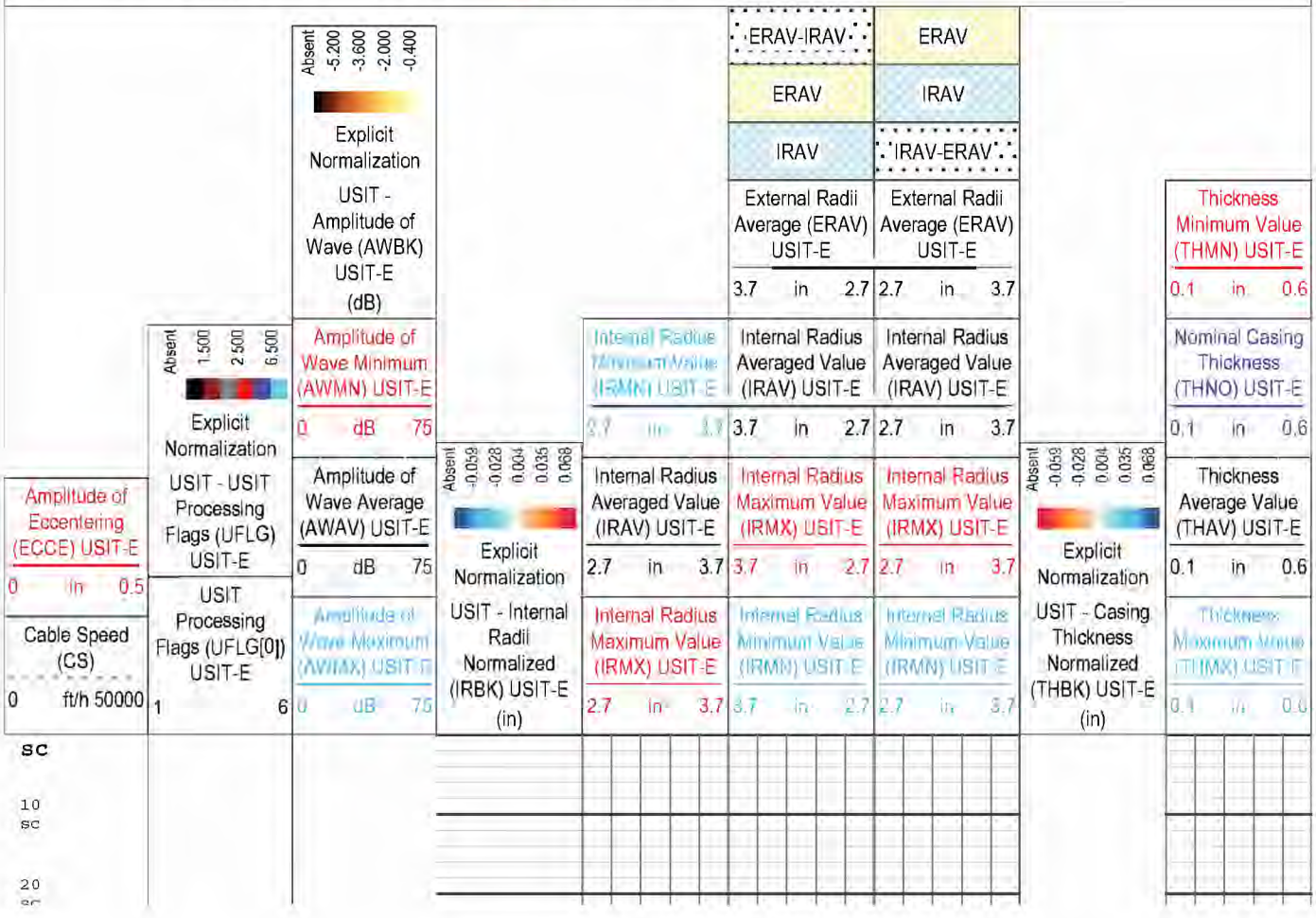

NEXT-HNGS-UCI

Main Pass 12 in = 100 ft

Log

Company:Southern California Gas Company Well:Standard Sesnon 25

NEXT-HNGS-UCI: Log[5]:Up:S006

Description: UCI MAIN Format: UCI MAIN Index Scale: 10 in per 100 ft Index Unit: ft Index Type: Measured Depth Creation Date: 07-Dec-2017 12:27:53

TIME_1900 - Time Marked every 60.00 (s)

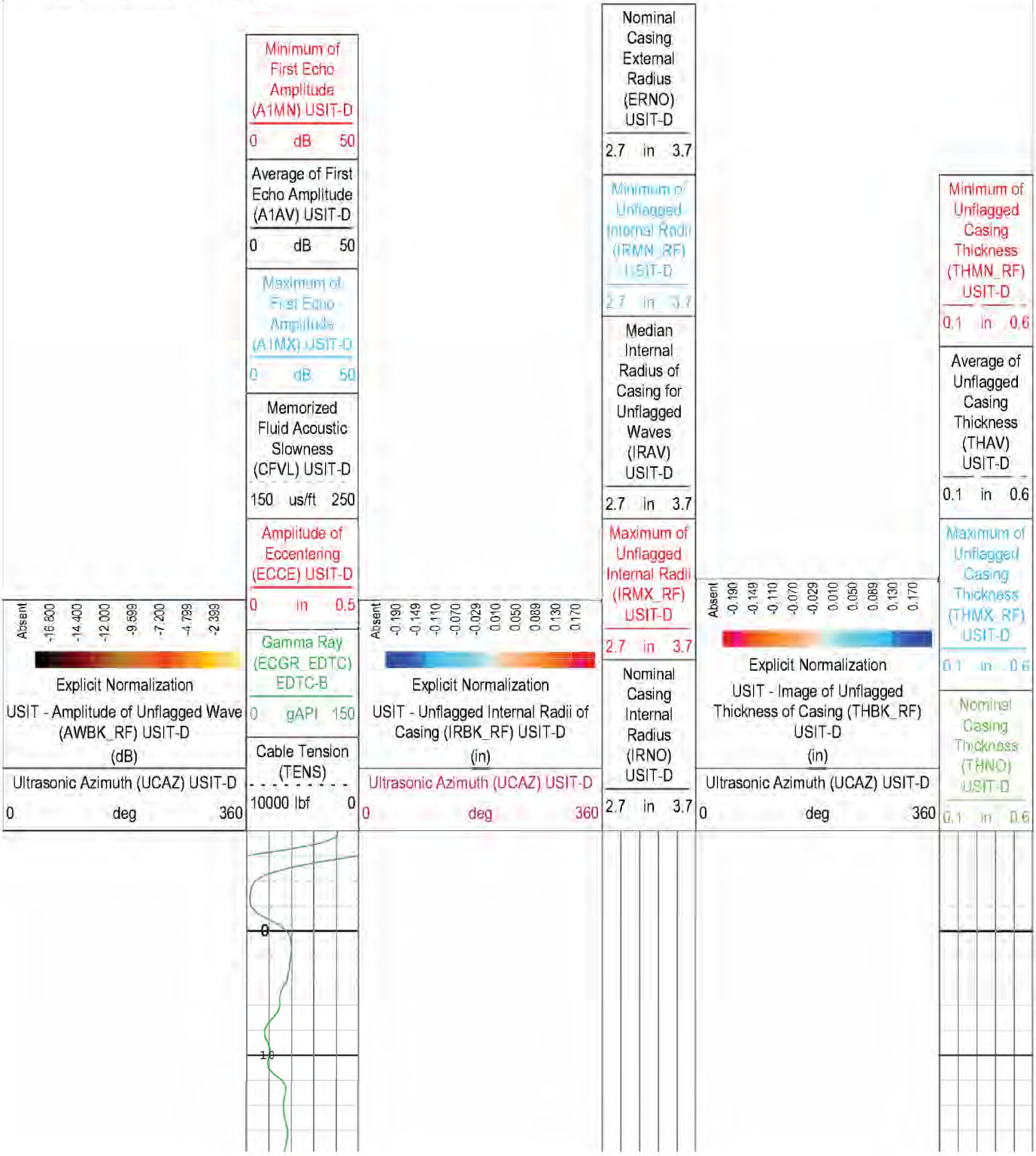

Appendix B 7 in. EV Camera Pictures

8/31/2017 9:42:01 AM
Res: MediumHigh
Temperature: 98.60 F
2.61°
Video Rate: 240 kbps
891.09 ft
-4.29 ft/min
Temperature: 98.60°
Video Rate: 240 kbps
Res: MediumHigh

8/31/2017 9:43:26 AM
Res: Medium
Temperature: 98.60 F
2.60°
Video Rate: 240 kbps
891.10 ft
0.00 ft/min
Temperature: 98.60°
Video Rate: 240 kbps
Res: Medium

8/31/2017 9:43:26 AM
Res: Medium
Temperature: 98.60 F
2.64°
Video Rate: 240 kbps
891.10 ft
0.11 ft/min
Temperature: 98.60°
Video Rate: 240 kbps
Res: Medium

8/31/2017 9:40:30 AM
Res: MediumHigh
Video Rate: 240 kbps
892.92 ft
-0.82 ft/min
Video Rate: 240 kbps

8/31/2017 9:44:20 AM
Res: Medium
Temperature: 99.05 F
2.64°
Video Rate: 240 kbps
890.08 ft
0.45 ft/min
Temperature: 99.05°
Video Rate: 240 kbps
Res: Medium

8/31/2017 9:44:21 AM
Res: Medium
Temperature: 99.05 F
2.46°
Video Rate: 240 kbps
890.02 ft
-1.39 ft/min
Temperature: 99.05°
Video Rate: 240 kbps
Res: Medium

8/31/2017 9:50:37 AM
Res: Medium
Temperature: 99.50 F
2.45°
Video Rate: 240 kbps
888.54 ft
-0.61 ft/min
Temperature: 99.50°
Video Rate: 240 kbps
Res: Medium

8/31/2017 9:50:48 AM
Res: Medium
Temperature: 99.50 F
Video Rate: 240 kbps
888.51 ft
-0.49 ft/min
Video Rate: 240 kbps

8/31/2017 9:50:45 AM
Res: Medium
Temperature: 99.50 F
2.61°
Video Rate: 240 kbps
888.13 ft
-6.33 ft/min
Temperature: 99.50°
Video Rate: 240 kbps
Res: Medium

8/31/2017 9:51:53 AM
Res: Medium
Temperature: 99.50 F
2.65°
Video Rate: 240 kbps
887.98 ft
0.00 ft/min
Temperature: 99.95°
Video Rate: 240 kbps
Res: Medium

8/31/2017 10:04:08 AM
Res: MediumHigh
Temperature: 102.20 F
3.32°
Video Rate: 240 kbps
887.67 ft
0.00 ft/min
Temperature: 102.65°
Video Rate: 240 kbps
Res: MediumHigh

8/31/2017 10:06:29 AM
Video Rate: 240 kbps
887.67 ft
0.00 ft/min

8/31/2017 10:07:33 AM
3.26°
pumping at .7 BBLs per minute
Video Rate: 240 kbps
887.67 ft
0.00 ft/min
Temperature: 102.65°
Res: MediumHigh

8/31/2017 10:09:18 AM
3.50°
pumping at .7 BBLs per minute
Video Rate: 240 kbps
887.60 ft
0.00 ft/min
Temperature: 102.65°
Res: MediumHigh

8/31/2017 10:12:15 AM
Res: MediumHigh
Temperature: 102.20 F
3.79°
Video Rate: 240 kbps
887.60 ft
0.00 ft/min
Temperature: 102.20°
Res: MediumHigh

8/31/2017 10:28:10 AM
Video Rate: 240 kbps
887.28 ft
0.00 ft/min

8/31/2017 10:28:47 AM
5.80°
Video Rate: 240 kbps
887.28 ft
0.00 ft/min
Temperature: 88.70°
Res: MediumHigh

8/31/2017 10:28:51 AM
5.60°
Video Rate: 240 kbps
887.28 ft
0.00 ft/min
Temperature: 88.70°
Res: MediumHigh

8/31/2017 10:28:56 AM
4.06°
Video Rate: 240 kbps
887.28 ft
0.00 ft/min
Temperature: 88.70°
Res: MediumHigh

8/31/2017 10:29:03 AM
Video Rate: 240 kbps
887.28 ft
0.00 ft/min

8/31/2017 10:29:09 AM
3.60°
Video Rate: 240 kbps
887.28 ft
0.00 ft/min
Res: MediumHigh

8/31/2017 10:29:16 AM
2.79°
Video Rate: 240 kbps
887.28 ft
0.00 ft/min
Temperature: 89.15°
Res: MediumHigh

8/31/2017 10:29:22 AM
4.68°
Video Rate: 240 kbps
887.28 ft
0.00 ft/min
Temperature: 89.15°
Res: MediumHigh

8/31/2017 10:29:34 AM
Video Rate: 240 kbps
887.28 ft
0.00 ft/min

8/31/2017 10:30:25 AM
Video Rate: 240 kbps
887.28 ft
0.00 ft/min
Temperature: 89.15°
Res: MediumHigh

8/31/2017 10:30:34 AM
Video Rate: 240 kbps
887.28 ft
0.00 ft/min
Temperature: 89.15°
Res: MediumHigh

8/31/2017 10:30:45 AM
Video Rate: 240 kbps
887.28 ft
0.00 ft/min
Temperature: 89.15°
Res: MediumHigh

8/31/2017 10:30:50 AM
Video Rate: 240 kbps
887.28 ft
0.00 ft/min

8/31/2017 10:31:02 AM
Video Rate: 240 kbps
887.28 ft
0.00 ft/min
Temperature: 88.70°
Res: MediumHigh

8/31/2017 10:31:12 AM
Video Rate: 240 kbps
887.28 ft
0.00 ft/min
Temperature: 89.15°
Res: MediumHigh

8/31/2017 10:31:23 AM
Video Rate: 240 kbps
887.28 ft
0.00 ft/min
Temperature: 88.70°
Res: MediumHigh

8/31/2017 10:31:29 AM
Video Rate: 240 kbps
887.28 ft
0.00 ft/min

8/31/2017 10:31:39 AM
Video Rate: 240 kbps
887.28 ft
0.00 ft/min
Temperature: 89.15°
Res: MediumHigh

8/31/2017 10:31:47 AM
Video Rate: 240 kbps
887.28 ft
0.00 ft/min
Temperature: 89.15°
Res: MediumHigh

8/31/2017 10:36:46 AM
Res: MediumHigh
Lighting Down: 100% Side: 59% Aux: 0%
Temperature: 89.15 F
Video Rate: 240 kbps
887.40 ft
1.96 ft/min
Temperature: 89.15°

8/31/2017 10:36:50 AM
Lighting Down: 100% Side: 59% Aux: 0%
Video Rate: 240 kbps
887.54 ft
2.30 ft/min

Res: MediumHigh
Lighting Down: 100% Side: 59% Aux: 0%
Temperature: 89.15°F
Video Rate: 240 kbps
887.57 ft
2.04 ft/min
Temperature: 89.15°

8/31/2017 10:36:52 AM
Lighting Down: 100% Side: 59% Aux: 0%
Video Rate: 240 kbps
887.59 ft
2.04 ft/min
Temperature: 89.15°

8/31/2017 10:36:54 AM
Lighting Down: 100% Side: 59% Aux: 0%
Video Rate: 240 kbps
887.66 ft
1.97 ft/min
Temperature: 89.15°

8/31/2017 10:36:56 AM
Res: MediumHigh
Lighting Down: 100% Side: 59% Aux: 0%
Temperature: 89.15°F
Video Rate: 240 kbps
887.75 ft
1.98 ft/min

8/31/2017 10:36:58 AM
Lighting Down: 100% Side: 59% Aux: 0%
Video Rate: 240 kbps
887.80 ft
1.38 ft/min
Temperature: 89.15°

8/31/2017 10:37:05 AM
Res: MediumHigh
Lighting Down: 100% Side: 59% Aux: 0%
Temperature: 89.15 F
Video Rate: 240 kbps
887.80 ft
0.00 ft/min
Temperature: 89.15°

8/31/2017 10:37:05 AM
Lighting Down: 100% Side: 59% Aux: 0%
Video Rate: 240 kbps
887.80 ft
0.00 ft/min
Temperature: 89.15°

8/31/2017 10:37:10 AM
Lighting Down: 100% Side: 59% Aux: 0%
Video Rate: 240 kbps
887.80 ft
0.00 ft/min

8/31/2017 10:37:10 AM
Lighting Down: 100% Side: 59% Aux: 0%
Video Rate: 240 kbps
887.80 ft
0.00 ft/min
Temperature: 89.15°

8/31/2017 10:37:13 AM
Lighting Down: 100% Side: 59% Aux: 0%
Video Rate: 240 kbps
887.80 ft
0.00 ft/min
Temperature: 89.15°

8/31/2017 10:37:35 AM
Lighting Down: 100% Side: 59% Aux: 0%
Video Rate: 240 kbps
887.80 ft
0.00 ft/min
Temperature: 89.15°

8/31/2017 10:37:37 AM
Lighting Down: 100% Side: 59% Aux: 0%
Video Rate: 240 kbps
887.80 ft
0.00 ft/min

8/31/2017 10:43:58 AM
3.06°
Video Rate: 240 kbps
887.64 ft
-0.07 ft/min
Temperature: 89.15°

8/31/2017 10:44:13 AM
3.99°
Res: MediumHigh
Temperature: 89.15 F
Video Rate: 240 kbps
887.56 ft
-0.88 ft/min
Temperature: 89.15°

8/31/2017 10:44:18 AM
4.65°
Res: MediumHigh
Temperature: 89.15 F
Video Rate: 240 kbps
887.54 ft
0.00 ft/min
Temperature: 89.15°

8/31/2017 10:44:23 AM
Res: MediumHigh
Temperature: 89.60 F
Video Rate: 240 kbps
887.54 ft
0.00 ft/min

8/31/2017 10:44:28 AM
3.40°
Res: MediumHigh
Temperature: 89.60 F
Video Rate: 240 kbps
887.54 ft
0.00 ft/min
Temperature: 89.60°

8/31/2017 10:44:32 AM
4.90°
Res: MediumHigh
Temperature: 89.15 F
Video Rate: 240 kbps
887.54 ft
0.00 ft/min
Temperature: 89.15°

8/31/2017 10:44:44 AM
4.62°
Res: MediumHigh
Temperature: 89.15 F
Video Rate: 240 kbps
887.56 ft
0.00 ft/min
Temperature: 89.15°

8/31/2017 10:44:48 AM
Res: MediumHigh
Temperature: 89.15°F
Video Rate: 240 kbps
887.56 ft
0.00 ft/min

8/31/2017 10:44:53 AM
3.68°
Res: MediumHigh
Temperature: 89.15 F
Video Rate: 240 kbps
887.56 ft
0.00 ft/min
Temperature: 89.60°

8/31/2017 10:44:59 AM
3.80°
Res: MediumHigh
Temperature: 89.15 F
Video Rate: 240 kbps
887.56 ft
0.00 ft/min
Temperature: 89.15°

8/31/2017 10:45:09 AM
3.98°
Res: MediumHigh
Temperature: 89.60 F
Video Rate: 240 kbps
887.56 ft
0.00 ft/min
Temperature: 89.15°

8/31/2017 10:45:16 AM
Res: MediumHigh
Temperature: 89.60 F
Video Rate: 240 kbps
887.56 ft
0.00 ft/min

8/31/2017 10:45:21 AM
3.88°
Res: MediumHigh
Temperature: 89.60 F
Video Rate: 240 kbps
887.56 ft
0.00 ft/min

8/31/2017 10:45:25 AM
2.43°
Res: MediumHigh
Temperature: 89.60 F
Video Rate: 240 kbps
0.00 ft/min

8/31/2017 10:46:03 AM
2.39°
Res: MediumHigh
Temperature: 89.15 F
Video Rate: 240 kbps
0.00 ft/min

8/31/2017 10:46:19 AM
Res: MediumHigh
Temperature: 89.15 F
Video Rate: 240 kbps
0.00 ft/min

8/31/2017 11:20:30 AM
2.65°
Res: Medium
Temperature: 102.20°F
Video Rate: 240 kbps
886.51 ft
2.07 ft/min
Temperature: 102.20°
Res: Medium

8/31/2017 11:20:33 AM
2.65°
Res: Medium
Temperature: 102.20°F
Video Rate: 240 kbps
886.65 ft
3.44 ft/min
Temperature: 102.20°
Res: Medium

8/31/2017 11:20:34 AM
2.95°
Res: Medium
Temperature: 102.20°F
Video Rate: 240 kbps
886.70 ft
3.81 ft/min
Temperature: 102.20°
Res: Medium

8/31/2017 11:20:35 AM
Res: Medium
Temperature: 102.20°F
Video Rate: 240 kbps
886.75 ft
2.66 ft/min

8/31/2017 11:20:35 AM
2.93°
Res: Medium
Temperature: 102.20°F
Video Rate: 240 kbps
886.75 ft
2.66 ft/min
Temperature: 102.20°
Res: Medium

8/31/2017 11:20:36 AM
2.63°
Res: Medium
Temperature: 102.20°F
end of 7 inch top section>>>
Video Rate: 240 kbps
886.83 ft
2.70 ft/min
Temperature: 102.20°
Res: Medium

8/31/2017 11:20:37 AM
2.97°
Res: Medium
Temperature: 102.20°F
end of 7 inch top section>>>
Video Rate: 240 kbps
886.87 ft
2.71 ft/min
Temperature: 102.20°
Res: Medium

8/31/2017 11:20:39 AM
Res: Medium
Temperature: 102.20°F
end of 7 inch top section>>>
Video Rate: 240 kbps
886.96 ft
2.66 ft/min

8/31/2017 11:20:44 AM
Res: Medium
Temperature: 102.20°F
Video Rate: 240 kbps
887.19 ft
2.52 ft/min

8/31/2017 11:20:45 AM
Res: Medium
Temperature: 102.20°F
Video Rate: 240 kbps
887.21 ft
2.88 ft/min

8/31/2017 11:20:46 AM
Res: Medium
Temperature: 102.20°F
Video Rate: 240 kbps
887.27 ft
2.72 ft/min

8/31/2017 11:20:47 AM
Res: Medium
Temperature: 102.20°F
Video Rate: 240 kbps
887.31 ft
2.76 ft/min

8/31/2017 11:20:50 AM
Res: Medium
Temperature: 102.20°F
Video Rate: 240 kbps
887.44 ft
2.90 ft/min

8/31/2017 11:20:52 AM
Res: Medium
Temperature: 102.20°F
Video Rate: 240 kbps
887.49 ft
2.37 ft/min

8/31/2017 11:21:00 AM
Res: Medium
Temperature: 102.20°F
Video Rate: 240 kbps
887.50 ft
0.09 ft/min

8/31/2017 11:21:02 AM
Res: Medium
Temperature: 102.20°F
Video Rate: 240 kbps
887.50 ft
0.20 ft/min

8/31/2017 11:21:26 AM
Res: Medium
Temperature: 102.20°F
Video Rate: 240 kbps
887.50 ft
0.00 ft/min

8/31/2017 11:22:00 AM
Res: Medium
Temperature: 101.75°F
<<<<Top of bottom section
Video Rate: 240 kbps
887.51 ft
0.00 ft/min

8/31/2017 11:22:15 AM
Res: Medium
Temperature: 101.75°F
Video Rate: 240 kbps
887.52 ft
0.20 ft/min

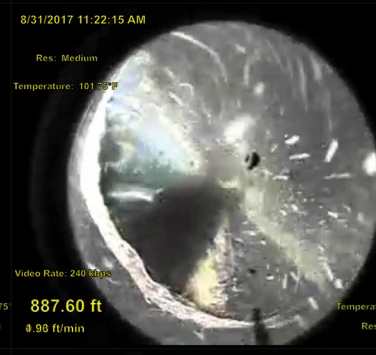
8/31/2017 11:22:15 AM
Res: Medium
Temperature: 101.75°F
Video Rate: 240 kbps
887.60 ft
0.99 ft/min

8/31/2017 11:22:16 AM
Res: Medium
Temperature: 101.75°F
Video Rate: 240 kbps
887.63 ft
1.38 ft/min

8/31/2017 11:22:18 AM
Res: Medium
Temperature: 101.75°F
Video Rate: 240 kbps
887.67 ft
3.42 ft/min

8/31/2017 11:22:20 AM
Res: Medium
Temperature: 101.75°F
Video Rate: 240 kbps
887.74 ft
2.06 ft/min

8/31/2017 11:22:20 AM
Res: Medium
Temperature: 101.75°F
Video Rate: 240 kbps
887.79 ft
2.24 ft/min

8/31/2017 11:22:22 AM
Res: Medium
Temperature: 101.75°F
Video Rate: 240 kbps
887.83 ft
2.21 ft/min

8/31/2017 11:22:23 AM
Res: Medium
Temperature: 101.75°F
Video Rate: 240 kbps
887.85 ft
1.33 ft/min

8/31/2017 11:22:24 AM
Res: Medium
Temperature: 101.75°F
Video Rate: 240 kbps
887.92 ft
2.24 ft/min

8/31/2017 11:22:30 AM
Res: Medium
Temperature: 101.75°F
Video Rate: 240 kbps
888.07 ft
2.35 ft/min

8/31/2017 11:22:31 AM
Res: Medium
Temperature: 101.75°F
Video Rate: 240 kbps
888.18 ft
2.42 ft/min

8/31/2017 11:22:33 AM
Res: Medium
Temperature: 101.75°F
Video Rate: 240 kbps
888.28 ft
2.52 ft/min

8/31/2017 11:22:35 AM
Res: Medium
Temperature: 101.75°F
Video Rate: 240 kbps
888.34 ft
2.35 ft/min

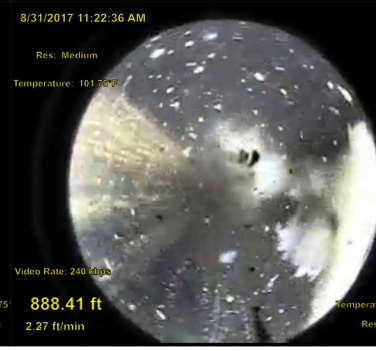
8/31/2017 11:22:36 AM
Res: Medium
Temperature: 101.75°F
Video Rate: 240 kbps
888.41 ft
2.27 ft/min

10/10/2017 10:04:57 AM
3.19°
sideview up
Res: Medium
Temperature: 79.70°F
313.47 ft

10/10/2017 10:11:08 AM
2.94°
sideview up
Res: Medium
Temperature: 80.15°F
285.61 ft

10/10/2017 10:28:57 AM
6.84°
Possible area to set RBP
Res: Medium
Temperature: 80.15°F
198.57 ft

10/10/2017 10:36:40 AM
3.43°
pulling out of hole
Res: Medium
Temperature: 117.05
198.48 ft

10/10/2017 8:29:06 AM
3.69°
Res: MediumHigh
Temperature: 96.35°F
19.34 ft

10/10/2017 8:37:09 AM
3.33°
Res: MediumHigh
Temperature: 99.05°F
37.11 ft

10/10/2017 8:53:56 AM
4.14°
Res: MediumHigh
Temperature: 101.75°F
59.57 ft

10/10/2017 8:57:22 AM
4.10°
Res: MediumHigh
Temperature: 101.75
61.30 ft

10/10/2017 8:38:39 AM
4.60°
Sideview up
Res: MediumHigh
Temperature: 74.30°F
63.38 ft

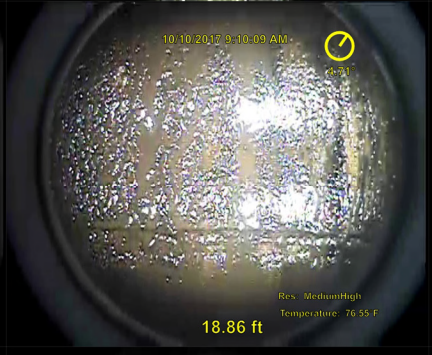
10/10/2017 9:10:09 AM
4.21°
Res: MediumHigh
Temperature: 76.55°F
18.86 ft

10/10/2017 9:21:00 AM
3.92°
Res: MediumHigh
Temperature: 110.30°F
58.96 ft

10/10/2017 9:21:20 AM
3.47°
Res: MediumHigh
Temperature: 110.30
61.30 ft

10/10/2017 9:28:36 AM
3.85°
Res: MediumHigh
Temperature: 110.30°F
66.80 ft

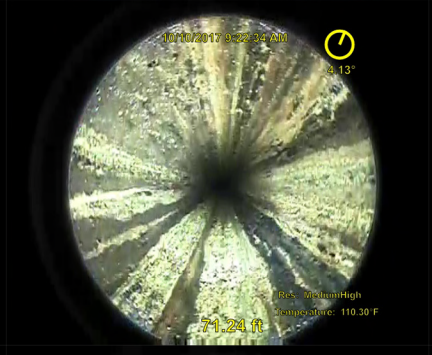
10/10/2017 9:22:24 AM
4.13°
Res: MediumHigh
Temperature: 110.30°F
71.24 ft

10/10/2017 9:23:16 AM
4.00°
Res: MediumHigh
Temperature: 110.30°F
76.78 ft

10/10/2017 9:23:32 AM
4.47°
Res: MediumHigh
Temperature: 110.75
78.98 ft

10/10/2017 9:23:59 AM
3.96°
Res: MediumHigh
Temperature: 110.30°F
81.18 ft

10/10/2017 9:25:35 AM
4.40°
Res: MediumHigh
Temperature: 110.30°F
95.57 ft

10/10/2017 9:31:25 AM
4.35°
Res: MediumHigh
Temperature: 109.40°F
142.95 ft

10/10/2017 9:34:35 AM
4.86°
Res: MediumHigh
Temperature: 109.40
174.20 ft

10/10/2017 9:35:22 AM
4.34°
Res: MediumHigh
Temperature: 109.40°F
181.60 ft

10/10/2017 9:49:24 AM
3.81°
Res: Medium
Temperature: 110.30°F
222.93 ft

10/10/2017 9:59:24 AM
3.23°
Res: Medium
Temperature: 114.35°F
304.07 ft

0.00 ft/min
12/10/2017 2:27:39 PM
5.13°
Pin connection 95
4007.70 ft
Temperature: 126.95°F
Video Rate: 170 kbps
Res: MediumHigh

0.00 ft/min
12/11/2017 10:29:22 AM
3.92°
4175.70 ft
Video Rate: 80 kbps
Temperature: 117.95°
Res: Medium

0.00 ft/min
12/11/2017 10:29:37 AM
3.75°
4175.70 ft
Video Rate: 80 kbps
Temperature: 117.95°
Res: Medium

0.00 ft/min
12/11/2017 10:29:10 AM
3.77°
4175.70 ft
Video Rate: 80 kbps
Res: Medium

0 ft/min
12/11/2017 10:30:24 AM
3.77°
175.70 ft
Rate: 80 kbps
Temperature: 118.40°
Res: Medium

0.00 ft/min
12/11/2017 10:30:49 AM
4.03°
Joint 99 pin
4175.70 ft
Video Rate: 80 kbps
Temperature: 118.40°
Res: Medium

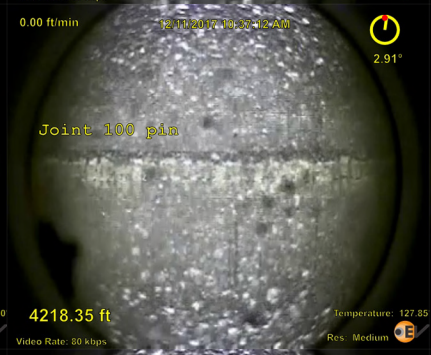
0.00 ft/min
12/11/2017 10:37:12 AM
2.91°
Joint 100 pin
4218.35 ft
Video Rate: 80 kbps
Temperature: 127.85°
Res: Medium

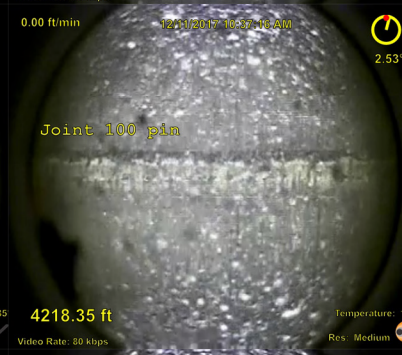
0.00 ft/min
12/11/2017 10:37:19 AM
2.53°
Joint 100 pin
4218.35 ft
Video Rate: 80 kbps
Res: Medium

0 ft/min
12/11/2017 10:54:56 AM
8.37°
Joint 101 pin
260.65 ft
Rate: 80 kbps
Temperature: 130.10°
Res: Medium

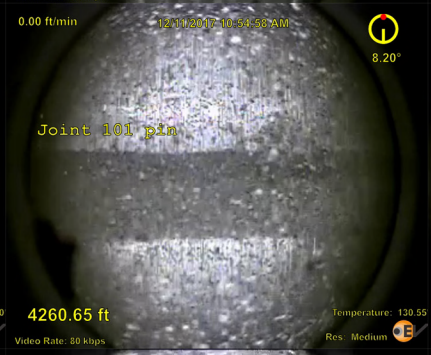
0.00 ft/min
12/11/2017 10:54:58 AM
8.20°
Joint 101 pin
4260.65 ft
Video Rate: 80 kbps
Temperature: 130.55°
Res: Medium

0.00 ft/min
12/11/2017 11:01:46 AM
8.47°
Joint 102 pin
4303.93 ft
Video Rate: 80 kbps
Temperature: 130.10°
Res: Medium

0.00 ft/min
12/11/2017 11:05:56 AM
8.67°
Joint 102 pin
4303.93 ft
Video Rate: 80 kbps
Res: Medium

2/11/2017 2:10:34 PM
8.17°
3967.00 ft
0.00 ft/min
Video Rate: 190 kbps
Res: High
Temperature: 125.15°F

12/11/2017 2:38:04 PM
Joint 102 pin
5.06°
4303.93 ft
0.00 ft/min
Video Rate: 190 kbps
Res: MediumHigh
Temperature: 117.05°F

12/11/2017 2:49:47 PM
Joint 103 pin
3.09°
4347.04 ft
0.83 ft/min
Video Rate: 190 kbps
Res: MediumHigh
Temperature: 117.95°F

12/11/2017 2:49:50 PM
Joint 103 pin
13.01°
4347.04 ft
0.00 ft/min
Video Rate: 19
Res: MediumHigh
Temperature: 117.95°F

2/11/2017 2:50:09 PM
oint 103 pin
9.48°
4347.04 ft
0.00 ft/min
Video Rate: 190 kbps
Res: MediumHigh
Temperature: 117.95°F

12/11/2017 2:58:51 PM
Joint 104 pin
9.30°
4389.35 ft
0.00 ft/min
Video Rate: 190 kbps
Res: MediumHigh
Temperature: 118.40°F

12/11/2017 2:58:54 PM
Joint 104 pin
1.74°
4389.35 ft
0.00 ft/min
Video Rate: 190 kbps
Res: MediumHigh
Temperature: 118.40°F

12/11/2017 3:13:27 PM
Joint 105 pin
8.01°
4431.78 ft
0.00 ft/min
Video Rate: 19
Res: MediumHigh
Temperature: 118.85°F

2/11/2017 3:37:48 PM
oint 106 pin
7.76°
4474.54 ft
0.00 ft/min
Video Rate: 190 kbps
Res: MediumHigh
Temperature: 119.30°F

12/11/2017 3:38:03 PM
Joint 106 pin
7.99°
4474.54 ft
0.00 ft/min
Video Rate: 190 kbps
Res: MediumHigh
Temperature: 119.30°F

12/11/2017 3:46:00 PM
Joint 107 pin
7.69°
4517.15 ft
0.00 ft/min
Video Rate: 190 kbps
Res: MediumHigh
Temperature: 119.75°F

12/11/2017 3:46:03 PM
Joint 107 pin
7.72°
4517.15 ft
0.00 ft/min
Video Rate: 19
Res: MediumHigh
Temperature: 119.75°F

oint 107 pin
7.69°
4517.15 ft
0.00 ft/min
Video Rate: 190 kbps
Res: MediumHigh
Temperature: 120.20°F

12/11/2017 3:47:41 PM
Joint 107 pin
10.57°
4517.15 ft
0.00 ft/min
Video Rate: 190 kbps
Res: MediumHigh
Temperature: 120.20°F

12/11/2017 3:52:27 PM
Joint 108 pin
6.82°
4560.80 ft
0.00 ft/min
Video Rate: 190 kbps
Res: MediumHigh
Temperature: 120.65°F

12/11/2017 3:52:47 PM
Joint 108 pin
4.87°
4560.80 ft
0.00 ft/min
Video Rate: 19
Res: MediumHigh
Temperature: 120.65°F

oint 109 pin
3.88°
4602.67 ft
0.00 ft/min
Video Rate: 190 kbps
Res: MediumHigh
Temperature: 121.10°F

12/11/2017 4:00:40 PM
4.68°
4602.67 ft
0.00 ft/min
Video Rate: 190 kbps
Res: MediumHigh
Temperature: 121.10°F

12/11/2017 4:01:10 PM
Joint 109 pin
2.89°
4602.67 ft
0.00 ft/min
Video Rate: 190 kbps
Res: MediumHigh
Temperature: 121.10°F

12/11/2017 4:01:40 PM
Joint 109 pin
5.87°
4602.67 ft
0.00 ft/min
Video Rate: 19
Res: MediumHigh
Temperature: 121.10°F

oint 110 pin
7.15°
4645.44 ft
0.00 ft/min
Video Rate: 190 kbps
Res: MediumHigh
Temperature: 122.00°F

12/11/2017 4:23:04 PM
Joint 111 pin
5.94°
4688.27 ft
0.00 ft/min
Video Rate: 190 kbps
Res: MediumHigh
Temperature: 122.45°F

12/11/2017 4:23:45 PM
Joint 111 pin
5.68°
4688.27 ft
0.00 ft/min
Video Rate: 190 kbps
Res: MediumHigh
Temperature: 122.45°F

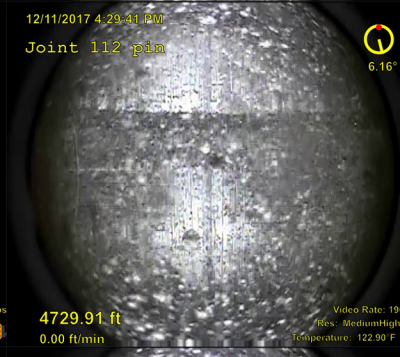
12/11/2017 4:29:41 PM
Joint 112 pin
6.16°
4729.91 ft
0.00 ft/min
Video Rate: 19
Res: MediumHigh
Temperature: 122.90°F

oint 113 pin
3.70°
4773.81 ft
0.00 ft/min
Video Rate: 190 kbps
Res: MediumHigh
Temperature: 123.35°F

12/11/2017 4:43:08 PM
Joint 113 pin
9.49°
4773.81 ft
0.00 ft/min
Video Rate: 190 kbps
Res: MediumHigh
Temperature: 123.80°F

12/11/2017 4:43:36 PM
Joint 113 pin
7.95°
4773.81 ft
0.00 ft/min
Video Rate: 190 kbps
Res: MediumHigh
Temperature: 123.35°F

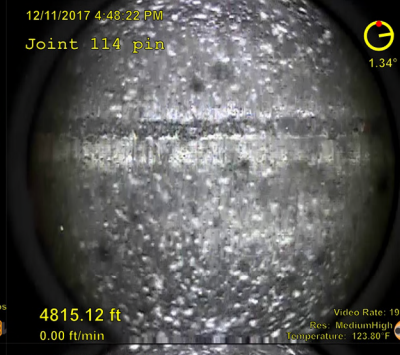
12/11/2017 4:48:22 PM
Joint 114 pin
1.34°
4815.12 ft
0.00 ft/min
Video Rate: 19
Res: MediumHigh
Temperature: 123.80°F

oint 115 pin
6.39°
4857.78 ft
0.00 ft/min
Video Rate: 190 kbps
Res: MediumHigh
Temperature: 124.25°F

12/11/2017 4:56:35 PM
Joint 115 pin
5.80°
4857.78 ft
0.00 ft/min
Video Rate: 190 kbps
Res: MediumHigh
Temperature: 124.25°F

12/11/2017 5:03:04 PM
Joint 116 pin
4.98°
4900.57 ft
0.00 ft/min
Video Rate: 160 kbps
Res: MediumHigh
Temperature: 125.15°F

12/11/2017 5:04:03 PM
Joint 116 pin
5.50°
4900.57 ft
0.00 ft/min
Video Rate: 16
Res: MediumHigh
Temperature: 125.15°F

oint 117 pin
5.17°
4942.49 ft
0.00 ft/min
Video Rate: 160 kbps
Res: MediumHigh
Temperature: 125.60°F

12/11/2017 5:11:35 PM
Joint 117 pin
4.79°
4942.49 ft
0.00 ft/min
Video Rate: 160 kbps
Res: MediumHigh
Temperature: 125.60°F

12/11/2017 5:17:03 PM
Joint 118 pin
4.70°
4984.66 ft
0.00 ft/min
Video Rate: 190 kbps
Res: MediumHigh
Temperature: 126.05°F

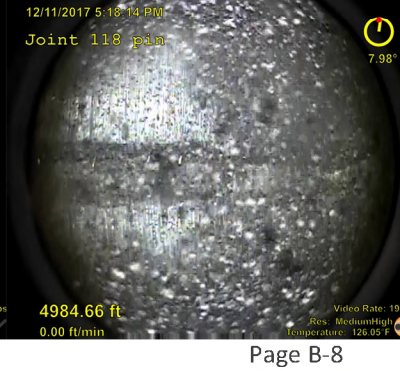
12/11/2017 5:18:14 PM
Joint 118 pin
7.98°
4984.66 ft
0.00 ft/min
Video Rate: 19
Res: MediumHigh
Temperature: 126.05°F

2/11/2017 5:25:43 PM
oint 119 pin
1.56°
5027.60 ft
0.00 ft/min
Video Rate: 190 kbps
Res: MediumHigh
Temperature: 126.50°F

12/11/2017 5:26:24 PM
Joint 119 pin
5.14°
5027.60 ft
0.00 ft/min
Video Rate: 190 kbps
Res: MediumHigh
Temperature: 126.50°F

12/11/2017 6:17:26 PM
Joint 177 pin
4.31°
7488.10 ft
0.00 ft/min
Video Rate: 190 kbps
Res: MediumHigh
Temperature: 158.45°F

12/11/2017 6:18:13 PM
6.46°
7488.10 ft
0.00 ft/min
Video Rate: 19
Res: MediumHigh
Temperature: 158.45°F

2/11/2017 6:18:16 PM
6.15°
7488.10 ft
0.00 ft/min
Video Rate: 190 kbps
Res: MediumHigh
Temperature: 158.00°F

12/11/2017 6:19:25 PM
2.16°
7488.10 ft
0.00 ft/min
Video Rate: 190 kbps
Res: MediumHigh
Temperature: 158.45°F

12/11/2017 6:20:35 PM
8.15°
7488.10 ft
0.00 ft/min
Video Rate: 190 kbps
Res: MediumHigh
Temperature: 158.45°F

12/11/2017 6:31:31 PM
Joint 178 pin
2.16°
7530.50 ft
0.00 ft/min
Video Rate: 19
Res: MediumHigh
Temperature: 158.45°F

2/11/2017 6:32:13 PM
7.07°
7530.50 ft
0.00 ft/min
Video Rate: 190 kbps
Res: MediumHigh
Temperature: 158.90°F

12/11/2017 6:33:23 PM
4.14°
7530.50 ft
0.00 ft/min
Video Rate: 190 kbps
Res: MediumHigh
Temperature: 158.90°F

12/11/2017 6:39:38 PM
2.62°
7543.80 ft
-4.06 ft/min
Video Rate: 190 kbps
Res: MediumHigh
Temperature: 172.40°F

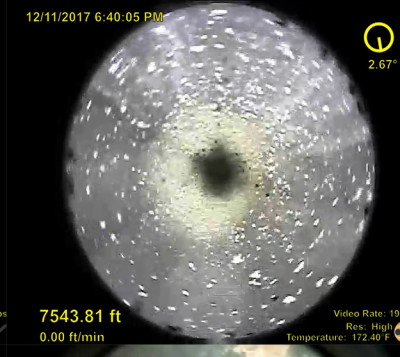
12/11/2017 6:40:05 PM
2.67°
7543.81 ft
0.00 ft/min
Video Rate: 19
Res: High
Temperature: 172.40°F

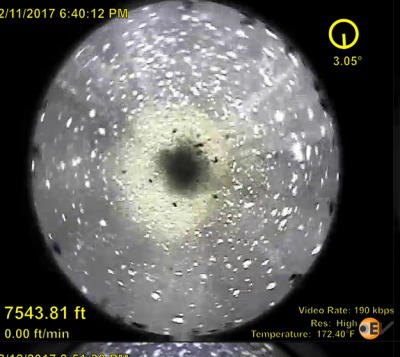
2/11/2017 6:40:12 PM
3.05°
7543.81 ft
0.00 ft/min
Video Rate: 190 kbps
Res: High
Temperature: 172.40°F

12/11/2017 6:41:59 PM
5.53°
7543.81 ft
0.00 ft/min
Video Rate: 190 kbps
Res: MediumHigh
Temperature: 158.90°F

12/11/2017 6:42:20 PM
5.53°
7543.81 ft
0.00 ft/min
Video Rate: 190 kbps
Res: MediumHigh
Temperature: 158.90°F

12/11/2017 8:02:44 PM
0.89°
3953.06 ft
0.00 ft/min
Video Rate: 12
Res: Medium
Temperature: 113.00°F

2/12/2017 2:51:30 PM
oint 42 pin
2.47°
1772.48 ft
161.02 ft/min
Video Rate: 160 kbps
Res: MediumHigh
Temperature: 90.05°F

12/12/2017 3:04:32 PM
Joint 41 pin
3.13°
1730.68 ft
0.00 ft/min
Video Rate: 160 kbps
Res: Medium
Temperature: 89.60°F

12/12/2017 3:04:53 PM
Joint 41 pin
3.38°
1730.68 ft
0.00 ft/min
Video Rate: 160 kbps
Res: MediumHigh
Temperature: 90.05°F

12/12/2017 3:05:17 PM
Joint 41 pin
3.22°
1730.68 ft
0.00 ft/min
Video Rate: 16
Res: MediumHigh
Temperature: 89.60°F

2/12/2017 3:11:39 PM
10.23°
1782.94 ft
0.00 ft/min
Video Rate: 190 kbps
Res: Medium
Temperature: 90.05°F

12/12/2017 3:18:56 PM
Joint 43 pin
3.07°
1813.72 ft
0.00 ft/min
Video Rate: 190 kbps
Res: MediumHigh
Temperature: 90.05°F

12/12/2017 3:27:12 PM
Joint 44 pin
25.90°
1856.44 ft
0.00 ft/min
Video Rate: 190 kbps
Res: MediumHigh
Temperature: 90.50°F

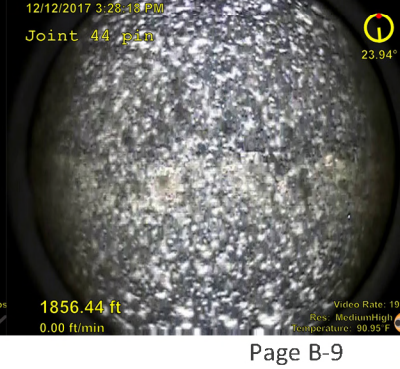
12/12/2017 3:28:18 PM
Joint 44 pin
23.94°
1856.44 ft
0.00 ft/min
Video Rate: 19
Res: MediumHigh
Temperature: 90.95°F

OI
2.86°
1886.48 ft
0.00 ft/min

12/12/2017 3:39:13 PM
AOI
23.77°
1897.13 ft
0.00 ft/min

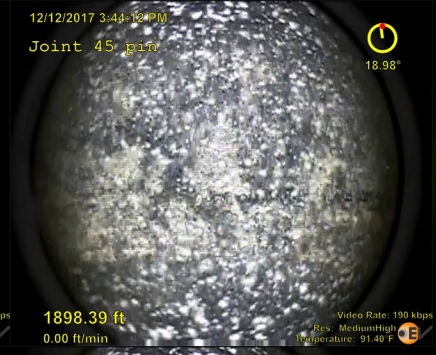
12/12/2017 3:44:12 PM
Joint 45 pin
18.98°
1898.39 ft
0.00 ft/min

12/12/2017 3:52:30 PM
AOI
14.43°
1932.05 ft
0.00 ft/min

oint 46 pin
12.69°
1940.71 ft
0.00 ft/min

12/12/2017 4:23:38 PM
Joint 47 pin
2.59°
1981.54 ft
0.00 ft/min

12/12/2017 4:24:07 PM
Joint 47 pin
4.59°
1981.54 ft
0.00 ft/min

12/12/2017 4:29:23 PM
Joint 48 pin
21.15°
2021.21 ft
0.00 ft/min

oint 48 pin
11.48°
2021.21 ft
0.00 ft/min

12/12/2017 4:30:48 PM
7.43°
2021.21 ft
0.00 ft/min

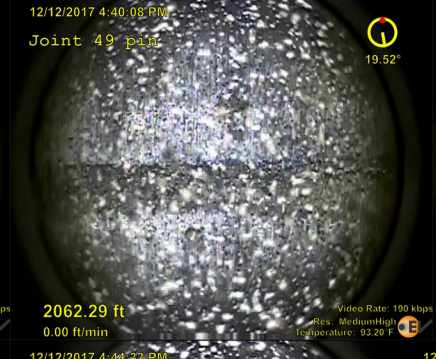
12/12/2017 4:40:08 PM
Joint 49 pin
19.52°
2062.29 ft
0.00 ft/min

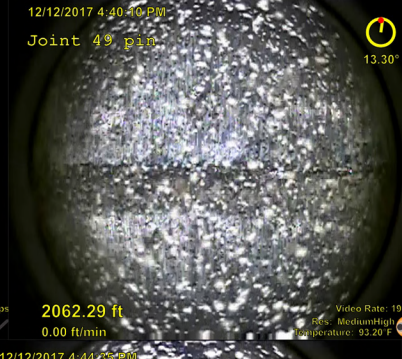
12/12/2017 4:40:10 PM
Joint 49 pin
13.30°
2062.29 ft
0.00 ft/min

oint 50 pin
4.92°
2104.53 ft
0.00 ft/min

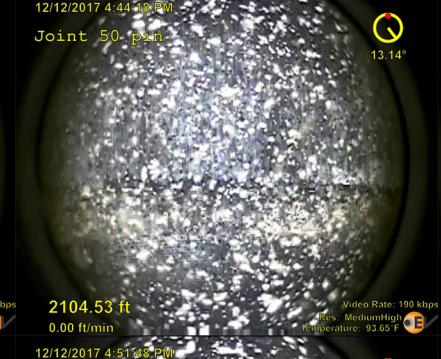
12/12/2017 4:44:18 PM
Joint 50 pin
13.14°
2104.53 ft
0.00 ft/min

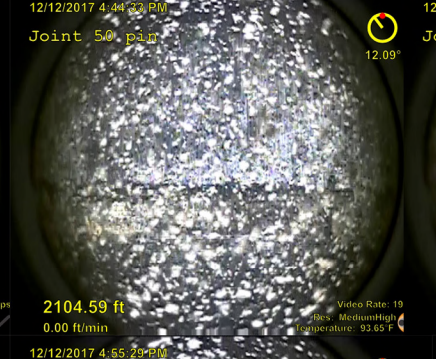
12/12/2017 4:44:33 PM
Joint 50 pin
12.09°
2104.59 ft
0.00 ft/min

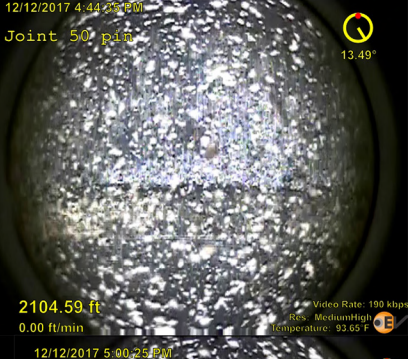
12/12/2017 4:44:45 PM
Joint 50 pin
13.49°
2104.59 ft
0.00 ft/min

oint 51 pin
17.76°
2143.85 ft
0.00 ft/min

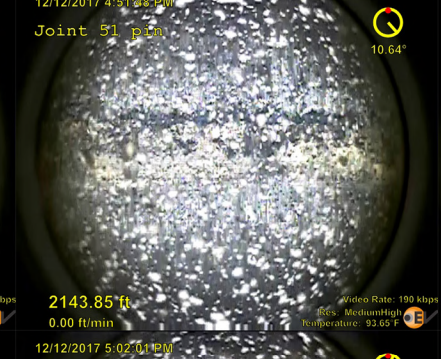
12/12/2017 4:51:48 PM
Joint 51 pin
10.64°
2143.85 ft
0.00 ft/min

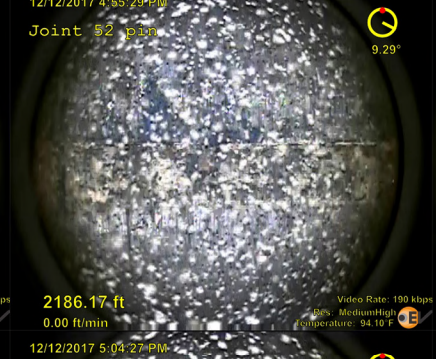
12/12/2017 4:55:29 PM
Joint 52 pin
9.29°
2186.17 ft
0.00 ft/min

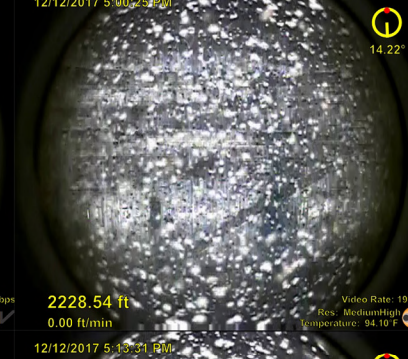
12/12/2017 5:00:25 PM
14.22°
2228.54 ft
0.00 ft/min

OI
4.85°
2228.54 ft
0.00 ft/min

12/12/2017 5:02:01 PM
4.31°
2228.54 ft
0.00 ft/min

12/12/2017 5:04:27 PM
Joint 53 pin
6.41°
2229.33 ft
0.00 ft/min

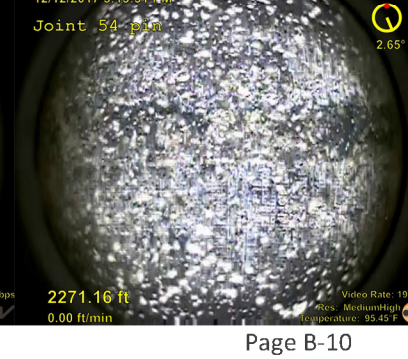
12/12/2017 5:13:31 PM
Joint 54 pin
2.65°
2271.16 ft
0.00 ft/min

oint 54 pin
2.66°
2271.16 ft
0.00 ft/min
Video Rate: 190 kbps
Res: MediumHigh
Temperature: 95.45°F

12/12/2017 5:19:58 PM
2.95°
2272.51 ft
13.20 ft/min
Video Rate: 190 kbps
Res: MediumHigh
Temperature: 95.45°F

12/12/2017 5:17:21 PM
Joint 55 pin
2.41°
2313.34 ft
0.00 ft/min
Video Rate: 190 kbps
Res: MediumHigh
Temperature: 95.45°F

12/12/2017 5:17:24 PM
Joint 55 pin
2.32°
2313.34 ft
0.00 ft/min
Video Rate: 19
Res: MediumHigh
Temperature: 95.45°F

oint 56 pin
2.22°
2355.47 ft
0.00 ft/min
Video Rate: 190 kbps
Res: MediumHigh
Temperature: 95.90°F

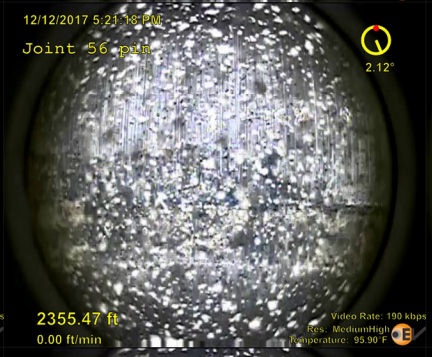
12/12/2017 5:21:18 PM
Joint 56 pin
2.12°
2355.47 ft
0.00 ft/min
Video Rate: 190 kbps
Res: MediumHigh
Temperature: 95.90°F

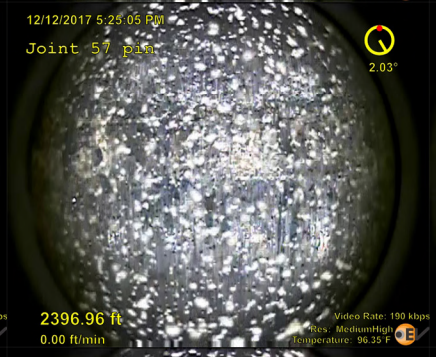
12/12/2017 5:25:05 PM
Joint 57 pin
2.03°
2396.96 ft
0.00 ft/min
Video Rate: 190 kbps
Res: MediumHigh
Temperature: 96.35°F

12/12/2017 5:28:30 PM
Joint 57 pin
16.74°
2396.96 ft
0.00 ft/min
Video Rate: 19
Res: Medium
Temperature: 96.35°F

oint 61 pin
12.05°
2567.26 ft
0.00 ft/min
Video Rate: 190 kbps
Res: MediumHigh
Temperature: 97.70°F

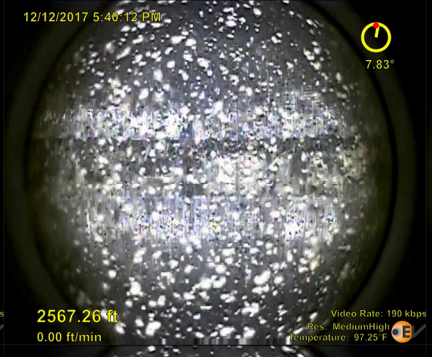
12/12/2017 5:40:12 PM
7.83°
2567.26 ft
0.00 ft/min
Video Rate: 190 kbps
Res: MediumHigh
Temperature: 97.25°F

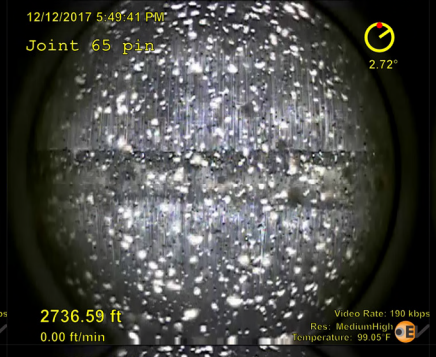
12/12/2017 5:49:41 PM
Joint 65 pin
2.72°
2736.59 ft
0.00 ft/min
Video Rate: 190 kbps
Res: MediumHigh
Temperature: 99.05°F

12/12/2017 5:51:20 PM
8.56°
2736.59 ft
0.00 ft/min
Video Rate: 19
Res: MediumHigh
Temperature: 99.50°F

oint 68 pin
6.78°
2864.75 ft
0.00 ft/min
Video Rate: 190 kbps
Res: MediumHigh
Temperature: 100.40°F

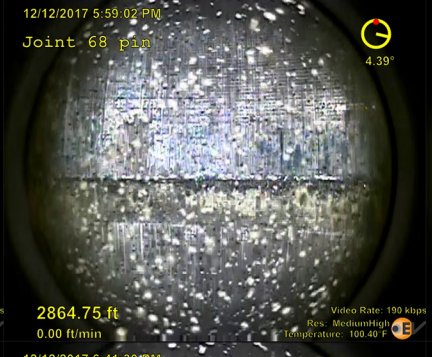
12/12/2017 5:59:02 PM
Joint 68 pin
4.39°
2864.75 ft
0.00 ft/min
Video Rate: 190 kbps
Res: MediumHigh
Temperature: 100.40°F

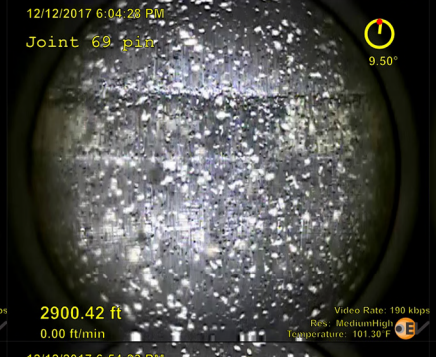
12/12/2017 6:04:28 PM
Joint 69 pin
9.50°
2900.42 ft
0.00 ft/min
Video Rate: 190 kbps
Res: MediumHigh
Temperature: 101.30°F

12/12/2017 6:15:46 PM
Joint 72 pin
18.90°
3028.87 ft
0.00 ft/min
Video Rate: 19
Res: MediumHigh
Temperature: 101.75°F

12/12/2017 6:16:35 PM
20.77°
3028.87 ft
0.00 ft/min
Video Rate: 190 kbps
Res: MediumHigh
Temperature: 101.75°F

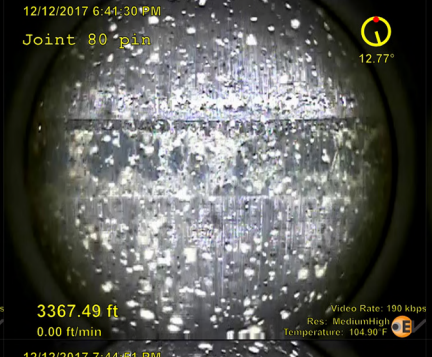
12/12/2017 6:41:30 PM
Joint 80 pin
12.77°
3367.49 ft
0.00 ft/min
Video Rate: 190 kbps
Res: MediumHigh
Temperature: 104.90°F

12/12/2017 6:54:22 PM
Joint 87 pin
9.27°
3668.22 ft
0.00 ft/min
Video Rate: 190 kbps
Res: MediumHigh
Temperature: 107.60°F

12/12/2017 6:55:04 PM
2.52°
3668.22 ft
0.00 ft/min
Video Rate: 19
Res: MediumHigh
Temperature: 107.60°F

12/12/2017 7:19:47 PM
oint 91 pin
10.60°
3837.79 ft
0.00 ft/min
Video Rate: 190 kbps
Res: MediumHigh
Temperature: 109.85°F

12/12/2017 7:44:01 PM
Joint 94 pin
2.88°
3965.11 ft
0.00 ft/min
Video Rate: 190 kbps
Res: MediumHigh
Temperature: 110.75°F

12/12/2017 7:51:34 PM
Joint 95 pin
9.18°
4007.67 ft
0.00 ft/min
Video Rate: 190 kbps
Res: MediumHigh
Temperature: 112.10°F

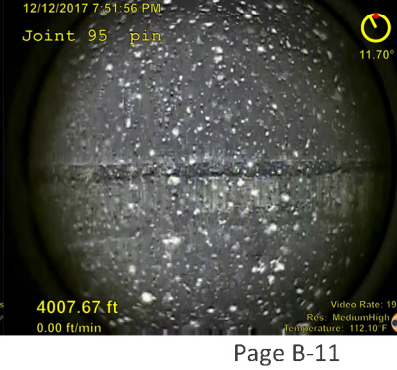
12/12/2017 7:51:56 PM
Joint 95 pin
11.70°
4007.67 ft
0.00 ft/min
Video Rate: 19
Res: MediumHigh
Temperature: 112.10°F

2/12/2017 7:52:14 PM
oint 95 pin
13.13°
4007.67 ft
0.00 ft/min
Video Rate: 190 kbps
Res: MediumHigh
Temperature: 112.10°F

12/12/2017 8:26:18 PM
1.38°
1722.98 ft
0.00 ft/min
Video Rate: 190 kbps
Res: MediumHigh
Temperature: 91.40°F

12/12/2017 8:26:18 PM
End of tubing
2.36°
1722.98 ft
0.00 ft/min
Video Rate: 190 kbps
Res: MediumHigh
Temperature: 91.40°F

12/13/2017 12:25:31 PM
5.72°
933.40 ft
0.00 ft/min
Video Rate: 19
Res: MediumHigh
Temperature: 81.50°F

2/13/2017 12:25:37 PM
4.40°
933.40 ft
0.00 ft/min
Video Rate: 190 kbps
Res: MediumHigh
Temperature: 81.50°F

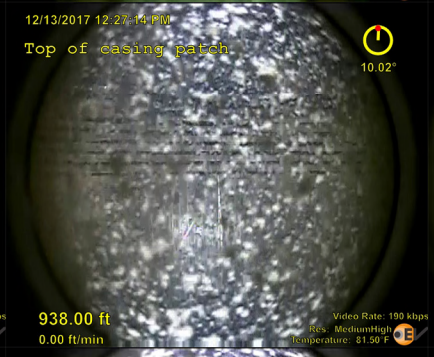
12/13/2017 12:27:14 PM
Top of casing patch
10.02°
938.00 ft
0.00 ft/min
Video Rate: 190 kbps
Res: MediumHigh
Temperature: 81.50°F

12/13/2017 12:29:02 PM
4.29°
939.14 ft
0.00 ft/min
Video Rate: 190 kbps
Res: MediumHigh
Temperature: 81.50°F

12/13/2017 12:29:18 PM
Top of 7 in. cut joint
3.42°
939.14 ft
0.00 ft/min
Video Rate: 19
Res: MediumHigh
Temperature: 81.95°F

2/13/2017 12:29:21 PM
op of 7 in. cut joint
15.21°
939.14 ft
0.00 ft/min
Video Rate: 190 kbps
Res: MediumHigh
Temperature: 81.95°F

12/13/2017 12:33:21 PM
AOI
10.39°
946.01 ft
0.00 ft/min
Video Rate: 190 kbps
Res: MediumHigh
Temperature: 81.95°F

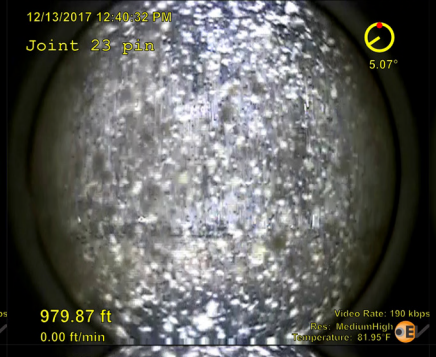
12/13/2017 12:40:32 PM
Joint 23 pin
5.07°
979.87 ft
0.00 ft/min
Video Rate: 190 kbps
Res: MediumHigh
Temperature: 81.95°F

12/13/2017 12:43:25 PM
AOI
2.12°
981.93 ft
0.00 ft/min
Video Rate: 19
Res: MediumHigh
Temperature: 82.40°F

2/13/2017 12:48:46 PM
OI
5.24°
1010.93 ft
0.00 ft/min
Video Rate: 190 kbps
Res: MediumHigh
Temperature: 82.85°F

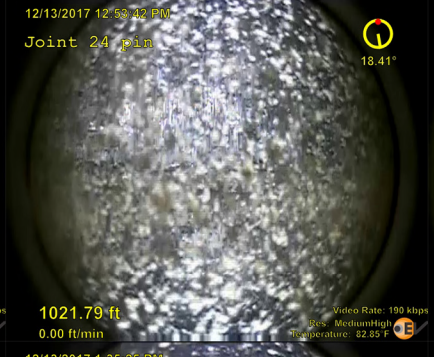
12/13/2017 12:52:42 PM
Joint 24 pin
18.41°
1021.79 ft
0.00 ft/min
Video Rate: 190 kbps
Res: MediumHigh
Temperature: 82.85°F

12/13/2017 1:06:15 PM
Joint 25 pin
8.17°
1064.30 ft
0.00 ft/min
Video Rate: 190 kbps
Res: MediumHigh
Temperature: 83.30°F

12/13/2017 1:13:28 PM
Joint 26 pin
16.64°
1106.46 ft
0.00 ft/min
Video Rate: 19
Res: MediumHigh
Temperature: 83.30°F

2/13/2017 1:19:53 PM
oint 27 pin
12.35°
1147.83 ft
0.00 ft/min
Video Rate: 190 kbps
Res: MediumHigh
Temperature: 83.75°F

12/13/2017 1:35:25 PM
AOI
16.93°
1254.89 ft
0.00 ft/min
Video Rate: 190 kbps
Res: MediumHigh
Temperature: 84.65°F

12/13/2017 1:39:56 PM
Joint 30 pin
21.11°
1275.75 ft
0.00 ft/min
Video Rate: 190 kbps
Res: MediumHigh
Temperature: 85.10°F

12/13/2017 1:41:48 PM
Joint 30 pin
15.46°
1275.75 ft
0.00 ft/min
Video Rate: 19
Res: MediumHigh
Temperature: 84.65°F

2/13/2017 1:49:27 PM
oint 33 pin
5.57°
1400.53 ft
0.00 ft/min
Video Rate: 190 kbps
Res: MediumHigh
Temperature: 85.55°F

12/13/2017 1:49:30 PM
Joint 33 pin
3.82°
1400.53 ft
0.00 ft/min
Video Rate: 190 kbps
Res: MediumHigh
Temperature: 85.55°F

12/13/2017 1:59:50 PM
Joint 36 pin
2.05°
1525.20 ft
0.00 ft/min
Video Rate: 190 kbps
Res: MediumHigh
Temperature: 86.45°F

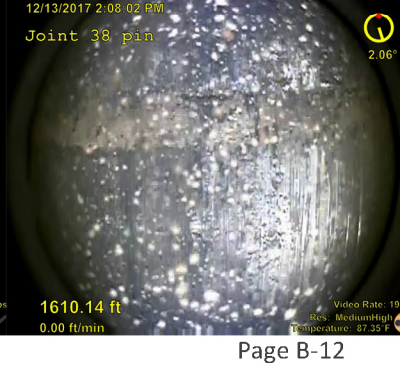
12/13/2017 2:08:02 PM
Joint 38 pin
2.06°
1610.14 ft
0.00 ft/min
Video Rate: 19
Res: MediumHigh
Temperature: 87.35°F

2/13/2017 2:08:05 PM
oint 38 pin
2.13°
1610.13 ft
0.00 ft/min
Video Rate: 190 kbps
Res: MediumHigh
Temperature: 87.35°F

12/13/2017 2:08:42 PM
Joint 38 pin
8.36°
1610.19 ft
0.00 ft/min
Video Rate: 190 kbps
Res: MediumHigh
Temperature: 87.35°F

12/13/2017 2:09:03 PM
Joint 38 pin
18.38°
1610.19 ft
0.00 ft/min
Video Rate: 190 kbps
Res: MediumHigh
Temperature: 87.35°F

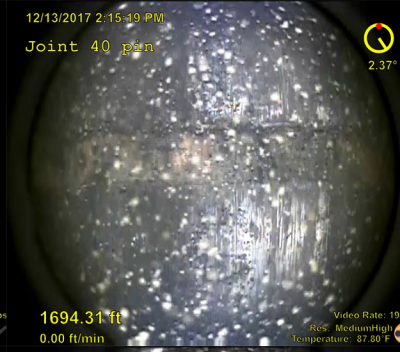
12/13/2017 2:15:19 PM
Joint 40 pin
2.37°
1694.31 ft
0.00 ft/min
Video Rate: 19
Res: MediumHigh
Temperature: 87.80°F

2/13/2017 2:15:21 PM
oint 40 pin
2.21°
1694.31 ft
0.00 ft/min
Video Rate: 190 kbps
Res: MediumHigh
Temperature: 87.80°F

12/13/2017 2:23:18 PM
Joint 41 pin
2.32°
1730.68 ft
0.00 ft/min
Video Rate: 190 kbps
Res: MediumHigh
Temperature: 88.70°F

12/13/2017 2:23:21 PM
Joint 41 pin
2.49°
1730.68 ft
0.00 ft/min
Video Rate: 190 kbps
Res: MediumHigh
Temperature: 88.25°F

12/13/2017 2:30:39 PM
Joint 44 pin
2.55°
1856.44 ft
0.00 ft/min
Video Rate: 19
Res: MediumHigh
Temperature: 90.95°F

2/13/2017 2:43:33 PM
OI
7.46°
1892.50 ft
0.00 ft/min
Video Rate: 190 kbps
Res: MediumHigh
Temperature: 92.30°F

12/13/2017 2:49:39 PM
9.33°
1898.39 ft
0.00 ft/min
Video Rate: 190 kbps
Res: MediumHigh
Temperature: 92.75°F

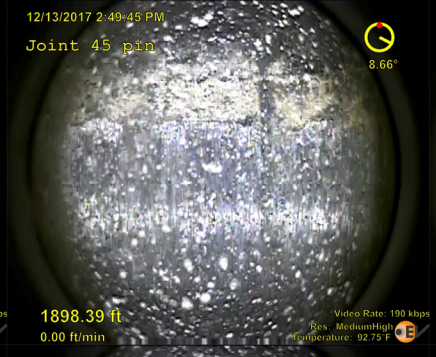
12/13/2017 2:49:45 PM
Joint 45 pin
8.66°
1898.39 ft
0.00 ft/min
Video Rate: 190 kbps
Res: MediumHigh
Temperature: 92.75°F

12/13/2017 2:49:48 PM
Joint 45 pin
5.49°
1898.39 ft
0.00 ft/min
Video Rate: 19
Res: MediumHigh
Temperature: 92.75°F

2/13/2017 2:54:23 PM
OI
9.16°
1931.98 ft
0.00 ft/min
Video Rate: 190 kbps
Res: MediumHigh
Temperature: 92.75°F

12/13/2017 2:55:19 PM
6.38°
1931.98 ft
0.00 ft/min
Video Rate: 190 kbps
Res: MediumHigh
Temperature: 92.30°F

12/13/2017 2:55:26 PM
8.36°
1931.98 ft
0.00 ft/min
Video Rate: 190 kbps
Res: MediumHigh
Temperature: 92.75°F

12/13/2017 2:57:40 PM
11.36°
1931.98 ft
0.00 ft/min
Video Rate: 19
Res: MediumHigh
Temperature: 92.75°F

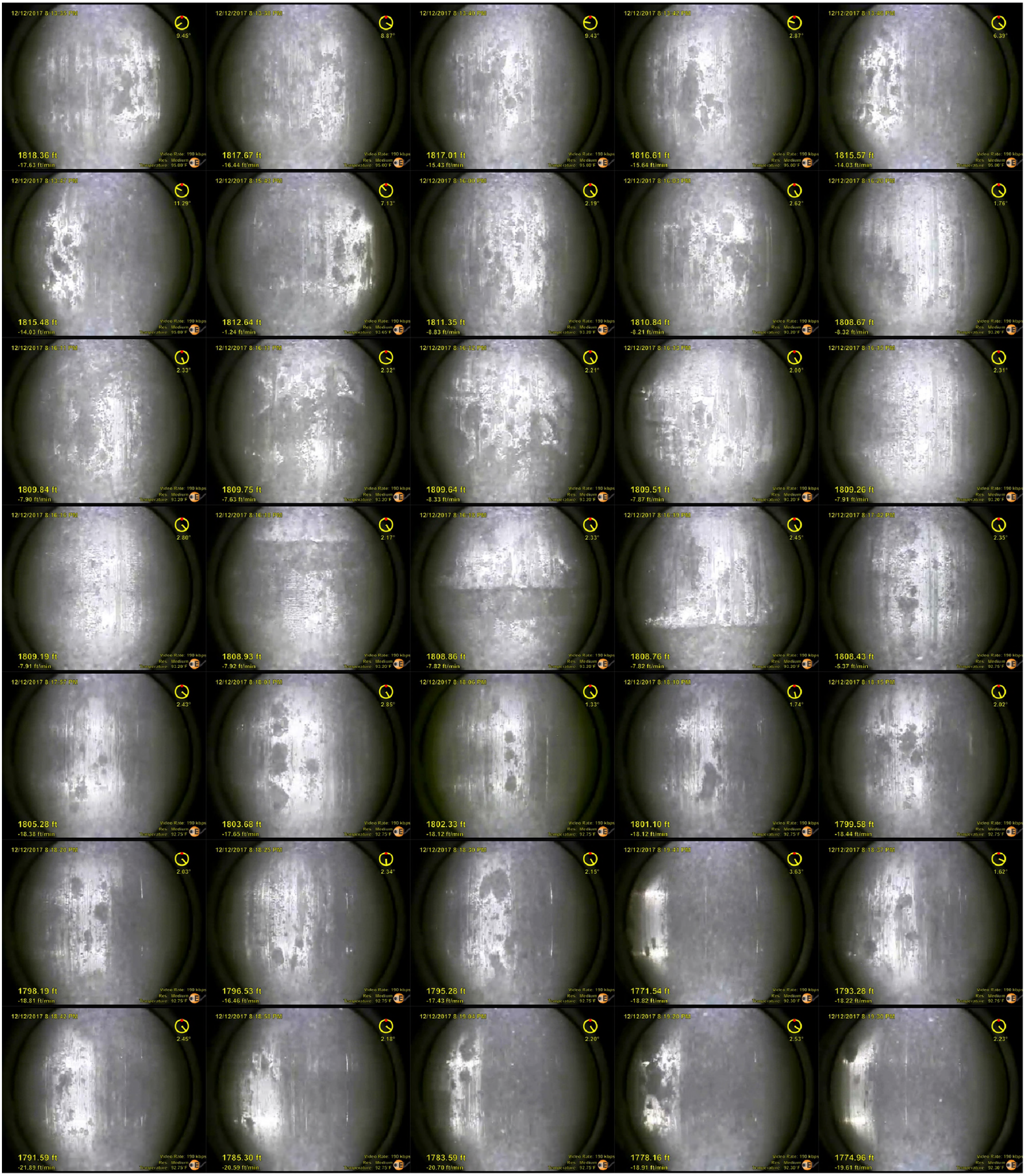

Appendix C 11 3/4 in. EV Camera Pictures November 7, 2017

Date	Report No.	Depth (ft)	Operations Summary
November 7, 2017	100	7,555	Pull, inspect, cut and LD 1 jt of 7" - upper parted section (C022). Transfer 1 jt to PS-20. Total of 22 joints extracted. RU Baker WL and EV Camera. Ran Camera to FL top at 275 ft. Ran Baker caliper from 875 ft. Ran 10.48" GR to 875 ft.

C.1 November 8–9, 2017 and November 13, 2017

Date	Report No.	Depth (ft)	Operations Summary
November 8, 2017	101	7,555	RU NOV pawl Extraction Tool and RIH on 22 jts of 7" casing/work string. RU, RIH with EV Camera to view TOF while pumping 1 bpm KCL. Ran camera to 890 ft. Fluid too cloudy to see TOF. 170 bbl pumped in total
November 9, 2017	102	7,555	PU, install 10 ft pup. Pump 3.2 bpm to clear area. SO to 892.82 ft. Could see TOF 2 ft inside NOV extraction tool. 120 bbl pumped in total. LD side entry sub, PU 6 ft pup. SO 4 ft over TOF, pull 5K tension. RIH with Baker MPC to 915 ft. Att to cut 7" - failed. Re-position MPC at 916 ft. Att cut - failed. POOH.
November 10, 2017	103	7,555	Pulled 7.5K OP - fish still engaged. Set slips with 5K. RIH with Baker MPC to 920 ft. Att cut - failed after several attempts.
November 11, 2017	104	7,555	RU WWL and RIH with Chemical Cutter to 939 ft. Good cut - hookload fell off and PU 1 ft. POOH with 7" workstring to surface - No fish. LD BHA, inspect pawls.
November 12, 2017	105	7,555	Att to MU new NOV Extraction Tool - damaged threads. SD and wait on Weatherford to re-dress threads. MU NOV Tool successfully, RIH with 22 jt of 7" workstring.
November 13, 2017	106	7,555	RU Baker WL. RIH with EV Camera. Pump at 2-3.5 bpm. Catch fish with NOV Tool. Pull 12K OP but unable to pull free. Ran EV Camera to cut location - observe partial cut. 260 bbl pumped in total.

C.2 August 18, 2018

Date	Report No.	Depth (ft)	Operations Summary
August 18, 2018	236	1,066	RU SLB. RIH with CPET tools. Log up from 400' to surface taking readings every 6'. Ran repeat section. RD SLB. RU Baker and EV Camera on the 11" 3M flange and shooting nipple. RIH with the camera. Observe and record casing holes from 190 to 133'. Tagged fluid at 213'. Logged out in side view mode. RD camera and Baker for the night.

C.3 August 19, 2018

Date	Report No.	Depth (ft)	Operations Summary
August 19, 2018	237	1,066	RU bell nipple. RIH to 990'. Pump 120 bbl 3% KCl to displace the Flowzan mud. RU Baker, EV Camera and Tiger side entry sub on the 3-1/2" DP. RIH camera to 990'. Pump clear fluid and observe surface casing from the shoe at 990' to 972'. POH camera. RD side entry sub. POH to 886'. RU Baker pump in sub. Observe casing around 892'. POH. RD pump in sub. POH DP to 740'. RU side entry sub. RIH with camera. Observe casing from 743' to 701'. RD Baker and EV camera. Shut well in for the night.

11/7/2017 12:25:20 PM
90.78°
Lighting Down: 100% Side: 59% Aux: 0%
Sideview Gain: Automatic Shutter: Automatic
Video Rate: 340 kbps
Quality Mode: Error Tolerant
Res: Medium
Surface test
-0.01 ft
Temperature: 95.45°F

11/7/2017 1:08:36 PM
2.22°
2.99 ft
Temperature: 113.45°F
Res: MediumHigh
Video Rate: 240 kbps

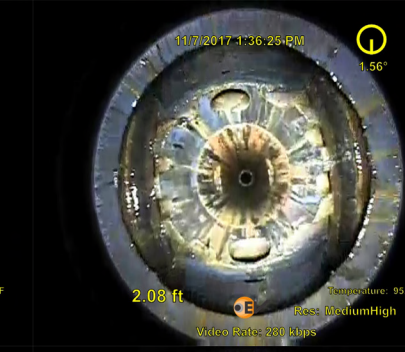
11/7/2017 1:36:25 PM
1.56°
2.08 ft
Temperature: 95.90°F
Res: MediumHigh
Video Rate: 280 kbps

11/7/2017 1:36:30 PM
2.54°
2.85 ft
Temperature: 95.90°F
Res: MediumHigh
Video Rate: 280 kbps

11/7/2017 1:36:32 PM
1.93°
3.27 ft
Temperature: 96.35°F
Res: MediumHigh
Video Rate: 280 kbps

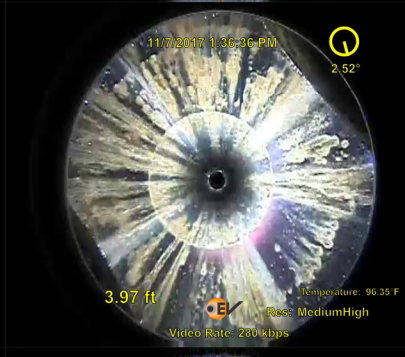
11/7/2017 1:36:36 PM
2.52°
3.97 ft
Temperature: 96.35°F
Res: MediumHigh
Video Rate: 280 kbps

11/7/2017 1:36:45 PM
0.63°
5.39 ft
Temperature: 96.35°F
Res: MediumHigh
Video Rate: 280 kbps

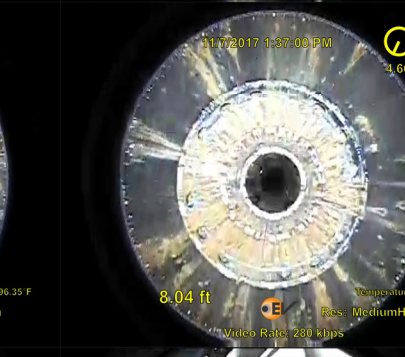
11/7/2017 1:37:06 PM
4.66°
8.04 ft
Temperature: 96.80°F
Res: MediumHigh
Video Rate: 280 kbps

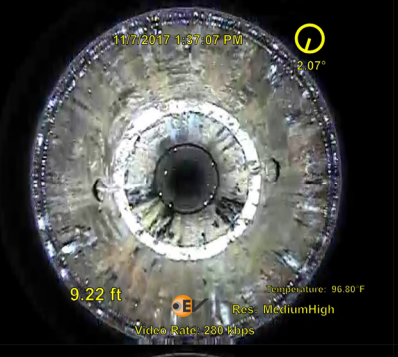
11/7/2017 1:37:07 PM
2.07°
9.22 ft
Temperature: 96.80°F
Res: MediumHigh
Video Rate: 280 kbps

11/7/2017 1:38:58 PM
2.97°
28.14 ft
Temperature: 98.15°F
Res: MediumHigh
Video Rate: 280 kbps

11/7/2017 1:48:13 PM
Side view
2.90°
39.83 ft
Temperature: 97.70°F
Res: MediumHigh
Video Rate: 280 kbps

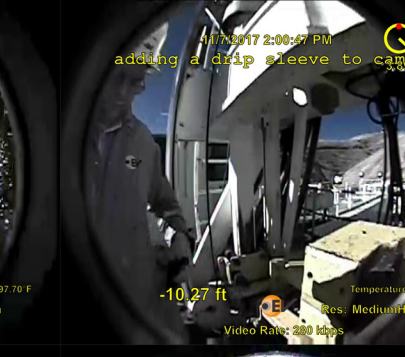
11/7/2017 2:00:47 PM
adding a drip sleeve to camera
-10.27 ft
Temperature: 102.20°F
Res: MediumHigh
Video Rate: 280 kbps

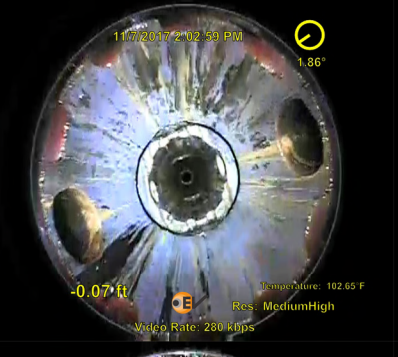
11/7/2017 2:02:59 PM
1.86°
-0.07 ft
Temperature: 102.65°F
Res: MediumHigh
Video Rate: 280 kbps

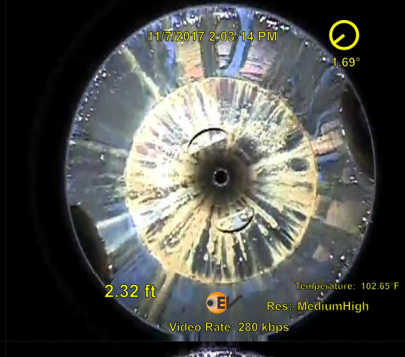
11/7/2017 2:03:14 PM
1.69°
2.32 ft
Temperature: 102.65°F
Res: MediumHigh
Video Rate: 280 kbps

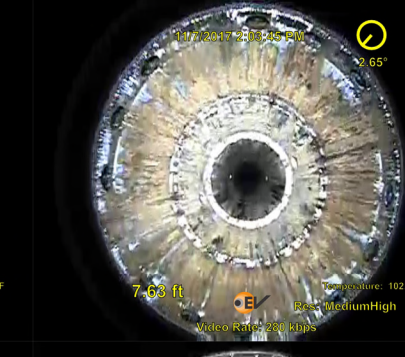
11/7/2017 2:03:45 PM
2.65°
7.63 ft
Temperature: 102.65°F
Res: MediumHigh
Video Rate: 280 kbps

11/7/2017 2:04:07 PM
2.08°
11.61 ft
Temperature: 102.65°F
Res: MediumHigh
Video Rate: 280 kbps

11/7/2017 2:05:32 PM
2.63°
26.37 ft
Temperature: 103.10°F
Res: MediumHigh
Video Rate: 280 kbps

11/7/2017 2:09:38 PM
1.22°
69.81 ft
Temperature: 103.55°F
Res: MediumHigh
Video Rate: 240 kbps

11/7/2017 2:13:36 PM
2.21°
110.57 ft
Temperature: 102.20°F
Res: MediumHigh
Video Rate: 175 kbps

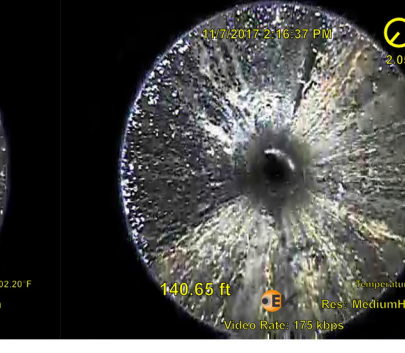
11/7/2017 2:16:37 PM
2.05°
140.65 ft
Temperature: 99.50°F
Res: MediumHigh
Video Rate: 175 kbps

11/7/2017 2:16:48 PM
2.33°
142.55 ft
Temperature: 99.50 F
Res: MediumHigh
Video Rate: 175 kbps

11/7/2017 2:17:54 PM
Sideview
5.86°
143.39 ft
Temperature: 98.60 F
Res: MediumHigh
Video Rate: 175 kbps

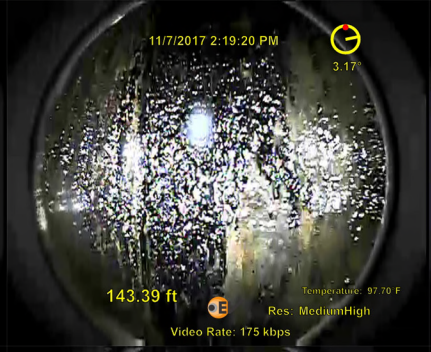
11/7/2017 2:19:20 PM
3.17°
143.39 ft
Temperature: 97.70 F
Res: MediumHigh
Video Rate: 175 kbps

11/7/2017 2:22:33 PM
2.80°
143.90 ft
Temperature: 95.90 F
Res: High
Video Rate: 175 kbps

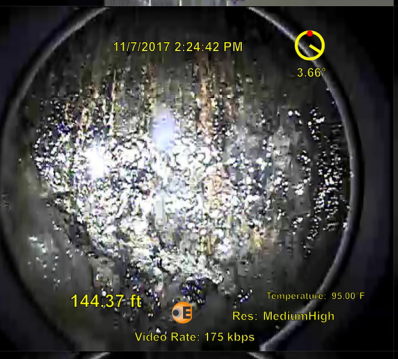
11/7/2017 2:24:42 PM
3.66°
144.37 ft
Temperature: 95.00 F
Res: MediumHigh
Video Rate: 175 kbps

11/7/2017 2:26:22 PM
8.49°
144.37 ft
Temperature: 94.55 F
Res: MediumHigh
Video Rate: 175 kbps

11/7/2017 2:26:35 PM
3.75°
144.37 ft
Temperature: 94.10 F
Res: MediumHigh
Video Rate: 175 kbps

11/7/2017 2:26:39 PM
0.87°
144.37 ft
Temperature: 94.10 F
Res: MediumHigh
Video Rate: 175 kbps

11/7/2017 2:26:43 PM
3.12°
144.37 ft
Temperature: 94.10 F
Res: MediumHigh
Video Rate: 175 kbps

11/7/2017 2:26:49 PM
3.07°
144.37 ft
Temperature: 94.10 F
Res: MediumHigh
Video Rate: 175 kbps

11/7/2017 2:26:56 PM
3.00°
144.37 ft
Temperature: 94.10 F
Res: MediumHigh
Video Rate: 175 kbps

11/7/2017 2:27:39 PM
2.06°
144.65 ft
Temperature: 93.65 F
Res: MediumHigh
Video Rate: 175 kbps

11/7/2017 2:27:48 PM
3.35°
144.65 ft
Temperature: 93.65 F
Res: MediumHigh
Video Rate: 175 kbps

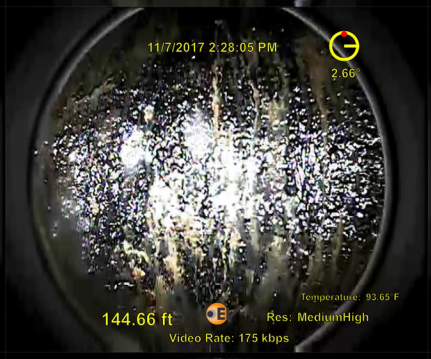
11/7/2017 2:28:05 PM
2.66°
144.66 ft
Temperature: 93.65 F
Res: MediumHigh
Video Rate: 175 kbps

11/7/2017 2:28:40 PM
1.23°
144.66 ft
Temperature: 93.20 F
Res: MediumHigh
Video Rate: 175 kbps

11/7/2017 2:28:49 PM
1.14°
144.66 ft
Temperature: 93.20 F
Res: MediumHigh
Video Rate: 175 kbps

11/7/2017 2:29:19 PM
2.33°
144.66 ft
Temperature: 93.20 F
Res: High
Video Rate: 280 kbps

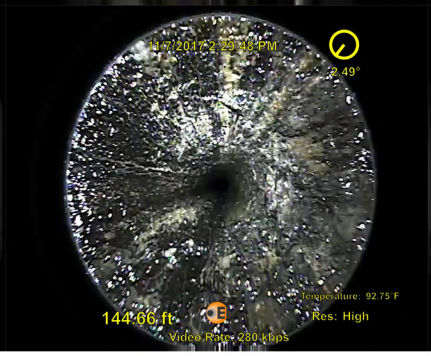
11/7/2017 2:29:48 PM
2.49°
144.66 ft
Temperature: 92.75 F
Res: High
Video Rate: 280 kbps

11/7/2017 2:31:31 PM
4.21°
145.17 ft
Temperature: 92.30 F
Res: MediumHigh
Video Rate: 240 kbps

11/7/2017 2:32:28 PM
3.86°
145.17 ft
Temperature: 91.85 F
Res: MediumHigh
Video Rate: 240 kbps

11/7/2017 2:34:22 PM
1.57°
Temperature: 91.85 F
145.67 ft
Res: MediumHigh
Video Rate: 240 kbps

11/7/2017 2:34:31 PM
1.86°
Temperature: 91.85 F
145.67 ft
Res: MediumHigh
Video Rate: 240 kbps

11/7/2017 2:35:39 PM
1.94°
Temperature: 91.85 F
145.67 ft
Res: High
Video Rate: 240 kbps

11/7/2017 2:42:16 PM
1.75°
Temperature: 91.40 F
144.82 ft
Res: MediumHigh
Video Rate: 80 kbps

11/7/2017 2:47:24 PM
1.57°
Temperature: 90.95 F
144.82 ft
Res: Medium
Video Rate: 80 kbps

11/7/2017 2:47:28 PM
1.75°
Temperature: 90.95 F
144.82 ft
Res: Medium
Video Rate: 80 kbps

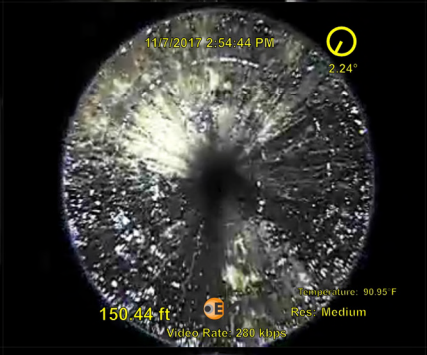
11/7/2017 2:54:44 PM
2.24°
Temperature: 90.95 F
150.44 ft
Res: Medium
Video Rate: 280 kbps

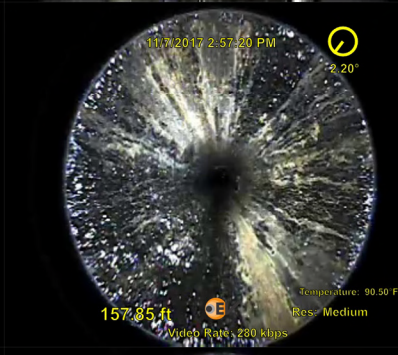
11/7/2017 2:57:20 PM
2.20°
Temperature: 90.50 F
157.85 ft
Res: Medium
Video Rate: 280 kbps

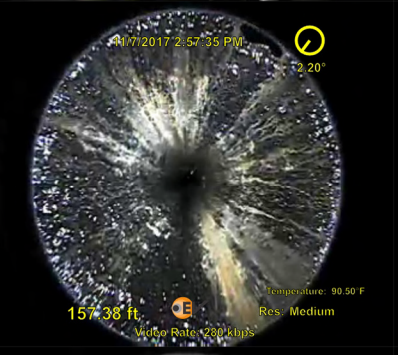
11/7/2017 2:57:35 PM
2.20°
Temperature: 90.50 F
157.38 ft
Res: Medium
Video Rate: 280 kbps

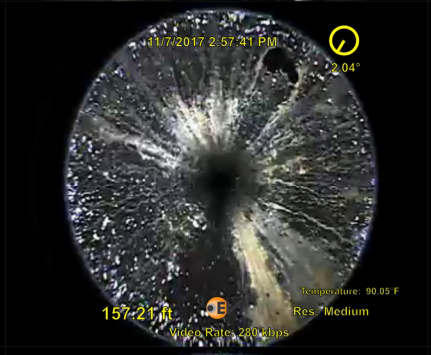
11/7/2017 2:57:41 PM
2.04°
Temperature: 90.05 F
157.21 ft
Res: Medium
Video Rate: 280 kbps

11/7/2017 2:57:48 PM
2.05°
Temperature: 90.50 F
157.02 ft
Res: Medium
Video Rate: 280 kbps

11/7/2017 2:59:07 PM
2.18°
Temperature: 90.05 F
154.64 ft
Res: Medium
Video Rate: 280 kbps

11/7/2017 3:00:45 PM
2.11°
Temperature: 89.60 F
156.00 ft
Res: Medium
Video Rate: 280 kbps

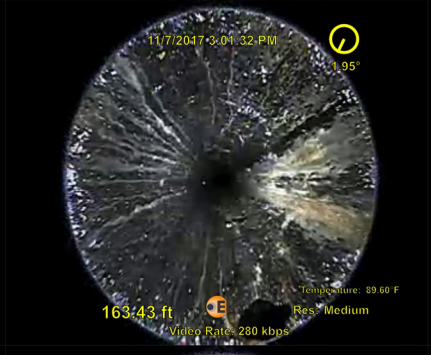
11/7/2017 3:01:32 PM
1.95°
Temperature: 89.60 F
163.43 ft
Res: Medium
Video Rate: 280 kbps

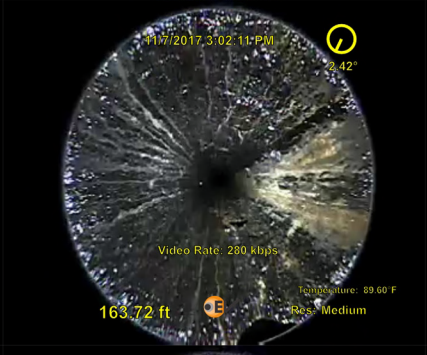
11/7/2017 3:02:11 PM
2.42°
Video Rate: 280 kbps
Temperature: 89.60 F
163.72 ft
Res: Medium

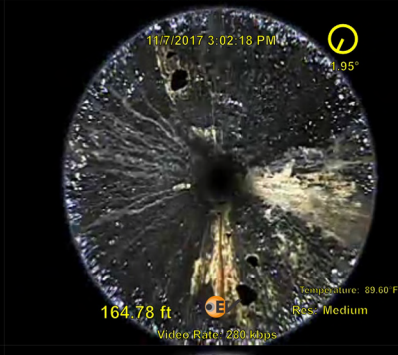
11/7/2017 3:02:18 PM
1.95°
Temperature: 89.60 F
164.78 ft
Res: Medium
Video Rate: 280 kbps

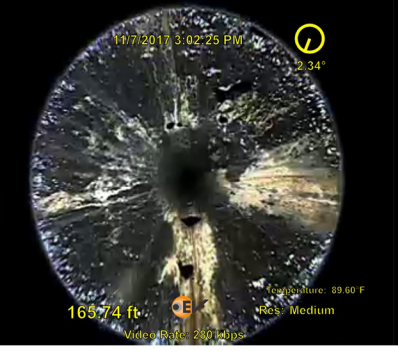
11/7/2017 3:02:25 PM
2.34°
Temperature: 89.60 F
165.74 ft
Res: Medium
Video Rate: 280 kbps

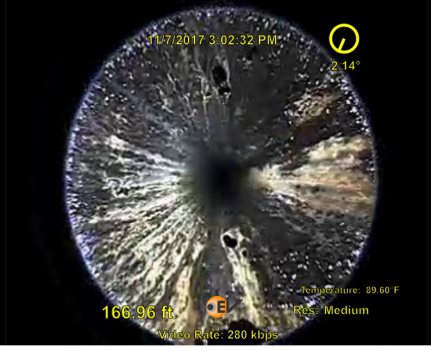
11/7/2017 3:02:32 PM
2.14°
Temperature: 89.60 F
166.96 ft
Res: Medium
Video Rate: 280 kbps

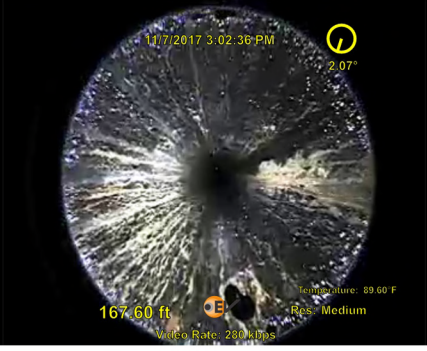
11/7/2017 3:02:36 PM
2.07°
Temperature: 89.60 F
167.60 ft
Res: Medium
Video Rate: 280 kbps

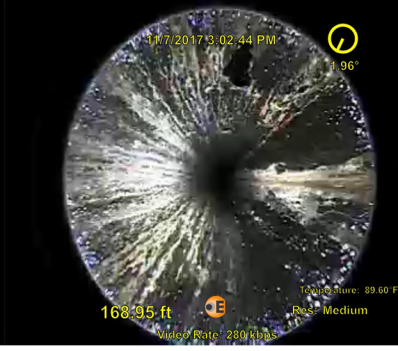
11/7/2017 3:02:44 PM
1.96°
Temperature: 89.60 F
168.95 ft
Res: Medium
Video Rate: 280 kbps

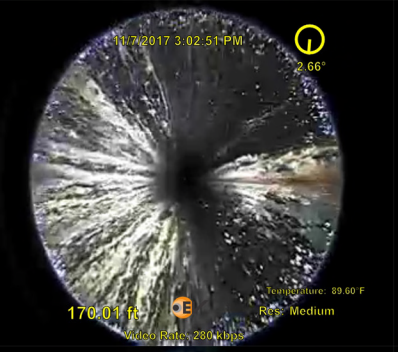
11/7/2017 3:02:51 PM
2.66°
Temperature: 89.60°F
170.01 ft
Res: Medium
Video Rate: 280 kbps

11/7/2017 3:03:05 PM
3.03°
Temperature: 89.60°F
172.32 ft
Res: Medium
Video Rate: 280 kbps

11/7/2017 3:03:30 PM
1.58°
Temperature: 89.60°F
176.51 ft
Res: Medium
Video Rate: 280 kbps

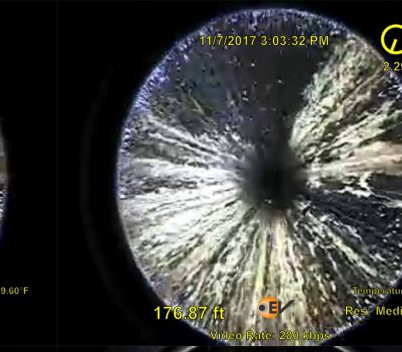
11/7/2017 3:03:32 PM
3.29°
Temperature: 89.15°F
176.87 ft
Res: Medium
Video Rate: 280 kbps

11/7/2017 3:03:38 PM
2.31°
Temperature: 89.60°F
177.84 ft
Res: Medium
Video Rate: 280 kbps

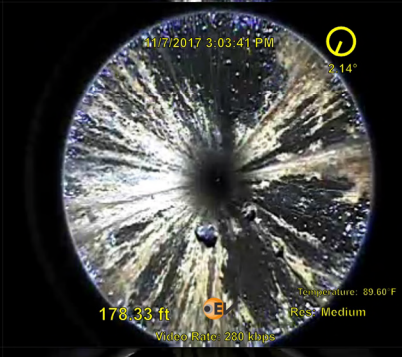
11/7/2017 3:03:41 PM
2.14°
Temperature: 89.60°F
178.33 ft
Res: Medium
Video Rate: 280 kbps

11/7/2017 3:04:28 PM
1.95°
Temperature: 89.15°F
179.47 ft
Res: Medium
Video Rate: 280 kbps

11/7/2017 3:08:49 PM
1.69°
Temperature: 88.25°F
179.94 ft
Res: Medium
Video Rate: 280 kbps

11/7/2017 3:09:33 PM
1.69°
Temperature: 88.25°F
180.25 ft
Res: Medium
Video Rate: 280 kbps

11/7/2017 3:10:01 PM
1.87°
Temperature: 88.25°F
180.25 ft
Res: High
Video Rate: 280 kbps

11/7/2017 3:12:28 PM
7.58°
Temperature: 88.25°F
180.25 ft
Res: High
Video Rate: 280 kbps

11/7/2017 3:12:32 PM
4.28°
Temperature: 88.25°F
180.25 ft
Res: High
Video Rate: 280 kbps

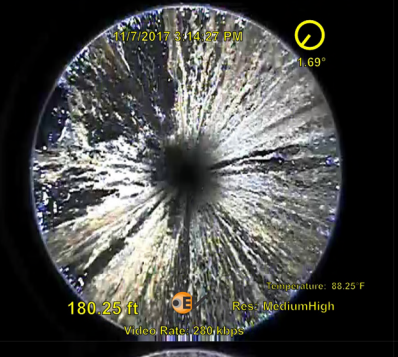
11/7/2017 3:13:27 PM
1.69°
Temperature: 88.25°F
180.25 ft
Res: MediumHigh
Video Rate: 280 kbps

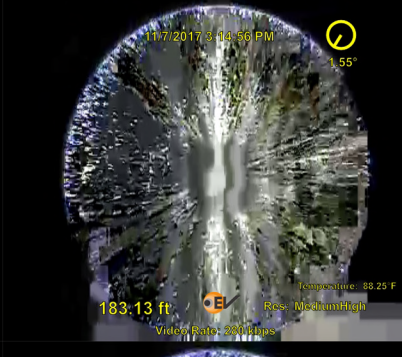
11/7/2017 3:14:56 PM
1.55°
Temperature: 88.25°F
183.13 ft
Res: MediumHigh
Video Rate: 280 kbps

11/7/2017 3:15:52 PM
1.69°
Temperature: 88.25°F
192.16 ft
Res: MediumHigh
Video Rate: 240 kbps

11/7/2017 3:17:58 PM
2.03°
Temperature: 88.25°F
212.99 ft
Res: Medium
Video Rate: 240 kbps

11/7/2017 3:18:03 PM
2.27°
Temperature: 88.25°F
213.90 ft
Res: Medium
Video Rate: 240 kbps

11/7/2017 3:18:23 PM
2.47°
Temperature: 88.25°F
218.87 ft
Res: Medium
Video Rate: 240 kbps

11/7/2017 3:18:57 PM
2.67°
Temperature: 88.25°F
222.75 ft
Res: Medium
Video Rate: 240 kbps

11/7/2017 3:19:48 PM
3.17°
Temperature: 88.25°F
231.41 ft
Res: Medium
Video Rate: 240 kbps

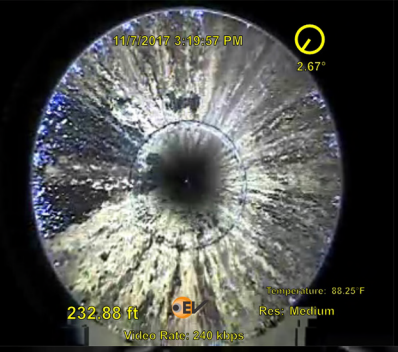

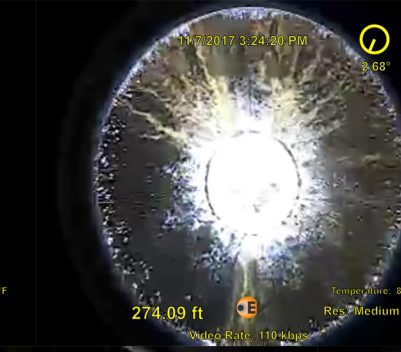

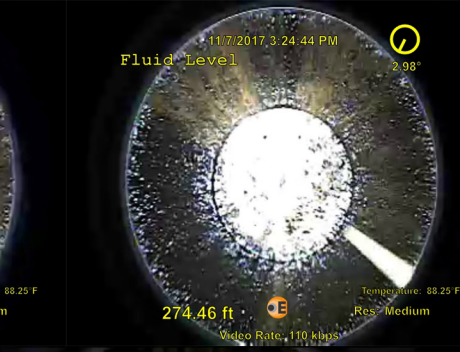

Configuration
Camera: E-Line Mk2 Colour Sideview Camera (EVCAMCSV-A) Lens: 26-00007
Image Size: 704x576 Pipe ID: 11in Environment: Gas Software Version: 0.5.3.0

Measurements assume that physical camera was centralised and pipe ID configured correctly.
Correct camera & lens must be selected in order to calibrate the calculations correctly.
Any accuracy figures quoted assume the above is correct. Any variations will significantly reduce the accuracy.

Same Plane Accuracy: ± 10% (central area) Accuracy: ± 20-30% (outer area)
Area Accuracy: ± 20%

Configuration
Camera: E-Line Mk2 Colour Sideview Camera (EVCAMCSV-A) Lens: 26-00007
Image Size: 704x576 Pipe ID: 11in Environment: Gas Software Version: 0.5.3.0

Measurements assume that physical camera was centralised and pipe ID configured correctly.
Correct camera & lens must be selected in order to calibrate the calculations correctly.
Any accuracy figures quoted assume the above is correct. Any variations will significantly reduce the accuracy.

Key: Same Plane Accuracy: ± 10% (central area) Accuracy: ± 20-30% (outer area)
Area Accuracy: ± 20%

Configuration
Camera: E-Line Mk2 Colour Sideview Camera (EVCAMCSV-A) Lens: 26-00007
Image Size: 704x576 Pipe ID: 11in Environment: Gas Software Version: 0.5.3.0

Measurements assume that physical camera was centralised and pipe ID configured correctly.
Correct camera & lens must be selected in order to calibrate the calculations correctly.
Any accuracy figures quoted assume the above is correct. Any variations will significantly reduce the accuracy.

Key: Same Plane Accuracy: ± 10% (central area) Accuracy: ± 20-30% (outer area)
Area Accuracy: ± 20%

Configuration
Camera: E-Line Mk2 Colour Sideview Camera (EVCAMCSV-A) Lens: 26-00007
Image Size: 704x576 Pipe ID: 11in Environment: Gas Software Version: 0.5.3.0

Measurements assume that physical camera was centralised and pipe ID configured correctly.
Correct camera & lens must be selected in order to calibrate the calculations correctly.
Any accuracy figures quoted assume the above is correct. Any variations will significantly reduce the accuracy.

Key: Same Plane Accuracy: ± 10% (central area) Accuracy: ± 20-30% (outer area)
Area Accuracy: ± 20%

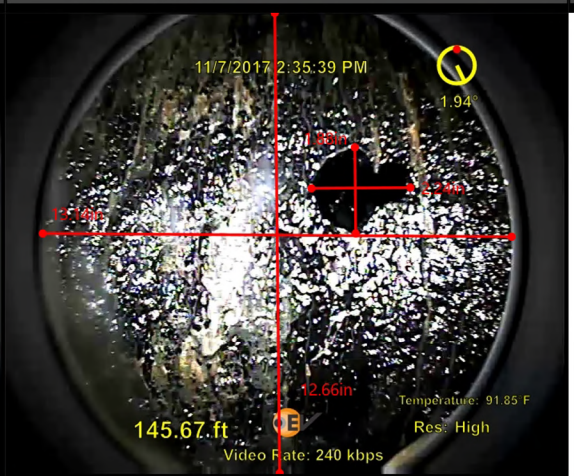

Configuration
Camera: E-Line Mk2 Colour Sideview Camera (EVCAMCSV-A) Lens: 26-00007
Image Size: 704x576 Pipe ID: 11in Environment: Gas Software Version: 0.5.3.0

Measurements assume that physical camera was centralised and pipe ID configured correctly.
Correct camera & lens must be selected in order to calibrate the calculations correctly.
Any accuracy figures quoted assume the above is correct. Any variations will significantly reduce the accuracy.

Key: Same Plane Accuracy: ± 10% (central area) Accuracy: ± 20-30% (outer area)
Area Accuracy: ± 20%

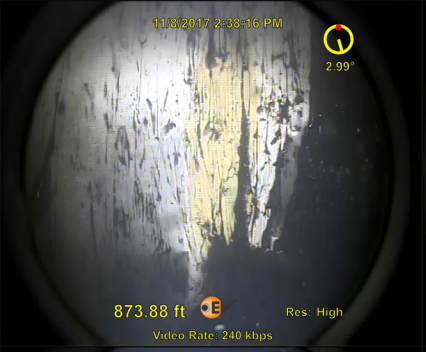
11/8/2017 2:38:16 PM
2.99°
873.88 ft
Res: High
Video Rate: 240 kbps

11/8/2017 2:48:59 PM
7.69°
871.83 ft
Res: MediumHigh
Video Rate: 240 kbps

11/8/2017 2:49:11 PM
9.03°
871.83 ft
Res: MediumHigh
Video Rate: 240 kbps

11/8/2017 2:49:28 PM
4.74°
871.83 ft
Res: MediumHigh
Video Rate: 240 kbps

11/8/2017 3:05:27 PM
3.38°
874.77 ft
Res: MediumHigh
Video Rate: 240 kbps

11/9/2017 12:59:27 PM
2.33°
883.72 ft
Res: Medium
Video Rate: 176 kbps

11/9/2017 1:28:58 PM
891.63 ft
2.52°
Video Rate: 240 kbps
Res: MediumHigh

11/9/2017 1:33:41 PM
892.11 ft
16.77°
Video Rate: 240 kbps
Res: MediumHigh

11/9/2017 1:35:42 PM
889.04 ft
1.56°
Video Rate: 240 kbps
Res: High

11/9/2017 1:36:28 PM
889.04 ft
2.03°
Video Rate: 240 kbps
Res: MediumHigh

11/9/2017 1:36:59 PM
889.18 ft
1.85°
Video Rate: 240 kbps
Res: MediumHigh

11/9/2017 1:37:05 PM
889.26 ft
2.32°
Video Rate: 240 kbps
Res: MediumHigh

11/9/2017 1:37:24 PM
889.52 ft
2.03°
Video Rate: 240 kbps
Res: MediumHigh

11/9/2017 1:37:40 PM
889.77 ft
2.33°
Video Rate: 240 kbps
Res: MediumHigh

11/9/2017 1:37:52 PM
889.96 ft
2.44°
Video Rate: 240 kbps
Res: MediumHigh

11/9/2017 1:38:02 PM
890.91 ft
2.46°
Video Rate: 240 kbps
Res: MediumHigh
inside 7 inch

11/9/2017 1:40:48 PM
2.47°
888.45 ft
Res: MediumHigh
Video Rate: 240 kbps

11/9/2017 1:40:52 PM
2.16°
888.21 ft
Res: MediumHigh
Video Rate: 240 kbps

11/9/2017 1:41:32 PM
2.54°
885.43 ft
Res: MediumHigh
Video Rate: 240 kbps

11/13/2017 12:50:33 PM
7.31°
889.91 ft
Res: Medium
Video Rate: 240 kbps

11/13/2017 9:32:18 AM
0.21°
885.67 ft
Res: MediumHigh
Video Rate: 280 kbps

11/13/2017 9:32:22 AM
9.89°
885.67 ft
Res: MediumHigh
Video Rate: 280 kbps

11/13/2017 9:32:32 AM
9.89°
885.67 ft
Res: MediumHigh
Video Rate: 280 kbps

11/13/2017 9:35:53 AM
2.90°
<<<Cut lip
885.67 ft
Res: MediumHigh
Video Rate: 280 kbps

11/13/2017 9:35:53 AM
2.90°
<<<Cut lip
885.67 ft
Res: MediumHigh
Video Rate: 280 kbps

1.07°
11/13/2017 11:06:37 AM
892.87 ft
Res: Medium
Video Rate: 110 kbps

1.07°
11/13/2017 11:06:37 AM
892.87 ft
Res: Medium
Video Rate: 110 kbps

1.35°
11/13/2017 11:06:59 AM
892.87 ft
Res: Medium
Video Rate: 110 kbps

1.35°
11/13/2017 11:06:59 AM
892.87 ft
Res: Medium
Video Rate: 110 kbps

4.75°
11/13/2017 12:23:28 PM
892.90 ft
Res: Medium
Video Rate: 280 kbps

4.75°
11/13/2017 12:23:28 PM
892.90 ft
Res: Medium
Video Rate: 280 kbps

5.43°
11/13/2017 12:24:52 PM
892.90 ft
Res: Medium
Video Rate: 280 kbps

8.45°
11/13/2017 12:26:43 PM
889.85 ft
Res: Medium
Video Rate: 280 kbps

1.68°
11/13/2017 12:27:12 PM
889.85 ft
Res: Medium
Video Rate: 280 kbps

6.26°
cut lip
11/13/2017 12:27:28 PM
889.85 ft
Res: Medium
Video Rate: 280 kbps

7.53°
11/13/2017 12:27:35 PM
889.85 ft
Res: Medium
Video Rate: 280 kbps

11/13/2017 12:28:12 PM
2.70°
889.85 ft
Res: Medium
Video Rate: 280 kbps

11/13/2017 12:28:28 PM
2.15°
889.85 ft
Res: Medium
Video Rate: 280 kbps

11/13/2017 12:44:41 PM
3.07°
889.91 ft
Res: Medium
Video Rate: 110 kbps

11/13/2017 1:46:24 PM
930.92 ft
Res: Medium

11/13/2017 12:58:06 PM
3.10°
896.28 ft
Res: Medium
Video Rate: 240 kbps

11/13/2017 12:58:09 PM
3.09°
896.28 ft
Res: Medium
Video Rate: 240 kbps

11/13/2017 12:59:49 PM
Video Rate: 240 kbps
3.34°
896.36 ft
Res: Medium

11/13/2017 1:01:46 PM
Video Rate: 240 kbps
1.90°
896.37 ft
Res: Medium

11/13/2017 1:08:29 PM
Video Rate: 240 kbps
2.42°
896.37 ft
Res: Medium

11/13/2017 1:08:36 PM
Video Rate: 240 kbps
2.65°
896.37 ft
Res: Medium

11/13/2017 1:13:39 PM
Video Rate: 240 kbps
2.48°
892.35 ft
Res: MediumHigh

11/13/2017 1:13:48 PM
Video Rate: 240 kbps
2.35°
892.24 ft
Res: MediumHigh

11/13/2017 1:14:09 PM
Video Rate: 240 kbps
2.33°
891.97 ft
Res: MediumHigh

11/13/2017 1:15:37 PM
Video Rate: 240 kbps
2.04°
890.78 ft
Res: MediumHigh

11/13/2017 1:15:41 PM
Video Rate: 240 kbps
2.33°
890.76 ft
Res: MediumHigh

11/13/2017 1:17:22 PM
Video Rate: 240 kbps
2.42°
890.76 ft
Res: MediumHigh

11/13/2017 1:19:22 PM
892.13 ft
Res: MediumHigh

11/13/2017 1:19:53 PM
892.58 ft
Res: MediumHigh

11/13/2017 1:20:12 PM
892.90 ft
Res: MediumHigh

11/13/2017 1:22:53 PM
896.26 ft
Res: MediumHigh

11/13/2017 1:26:10 PM
898.49 ft
Res: Medium

11/13/2017 1:26:17 PM
898.49 ft
Res: Medium

11/13/2017 1:43:44 PM
931.95 ft
Res: Medium

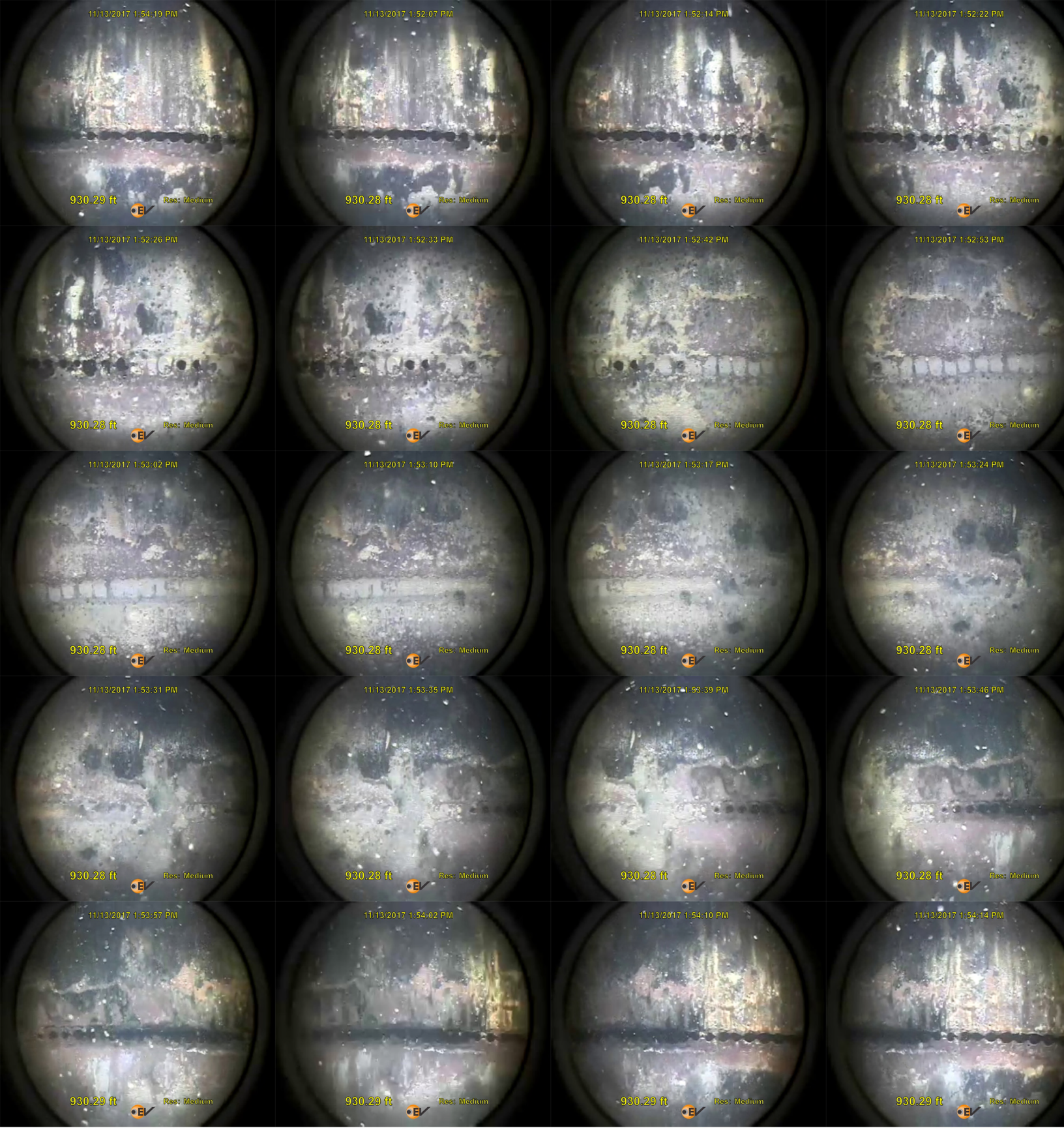
11/13/2017 1:54:19 PM
930.29 ft
Res: Medium
11/13/2017 1:52:07 PM
930.28 ft
Res: Medium
11/13/2017 1:52:14 PM
930.28 ft
Res: Medium
11/13/2017 1:52:22 PM
930.28 ft
Res: Medium
11/13/2017 1:52:26 PM
930.28 ft
Res: Medium
11/13/2017 1:52:33 PM
930.28 ft
Res: Medium
11/13/2017 1:52:42 PM
930.28 ft
Res: Medium
11/13/2017 1:52:53 PM
930.28 ft
Res: Medium
11/13/2017 1:53:02 PM
930.28 ft
Res: Medium
11/13/2017 1:53:10 PM
930.28 ft
Res: Medium
11/13/2017 1:53:17 PM
930.28 ft
Res: Medium
11/13/2017 1:53:24 PM
930.28 ft
Res: Medium
11/13/2017 1:53:31 PM
930.28 ft
Res: Medium
11/13/2017 1:53:35 PM
930.28 ft
Res: Medium
11/13/2017 1:53:39 PM
930.28 ft
Res: Medium
11/13/2017 1:53:46 PM
930.28 ft
Res: Medium
11/13/2017 1:53:57 PM
930.29 ft
Res: Medium
11/13/2017 1:54:02 PM
930.29 ft
Res: Medium
11/13/2017 1:54:10 PM
930.29 ft
Res: Medium
11/13/2017 1:54:14 PM
930.29 ft
Res: Medium

Configuration
Camera: E-Line Mk2 Colour Sideview Camera (EVCAMCSV-A) Lens: 26-00007
Image Size: 704x576 Pipe ID: 11.084in Environment: Gas Software Version: 0.6.3

Measurements assume that physical camera was centralised and pipe ID configured correctly.
Correct camera & lens must be selected in order to calibrate the calculations correctly.
Any accuracy figures quoted assume the above is correct. Any variations will significantly reduce the accuracy.

Key: Same Plane Area
Accuracy: ± 10% (central area) Accuracy: ± 20%
Accuracy: ± 20-30% (outer area)

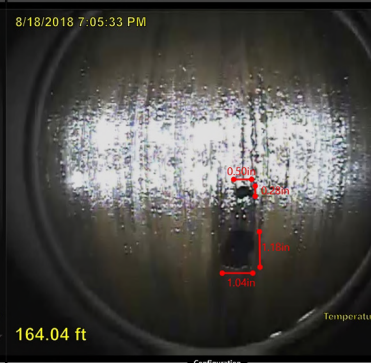

Configuration
Camera: E-Line Mk2 Colour Sideview Camera (EVCAMCSV-A) Lens: 26-00007
Image Size: 704x576 Pipe ID: 11.084in Environment: Gas Software Version: 0.6.3

Measurements assume that physical camera was centralised and pipe ID configured correctly.
Correct camera & lens must be selected in order to calibrate the calculations correctly.
Any accuracy figures quoted assume the above is correct. Any variations will significantly reduce the accuracy.

Key: Same Plane Area
Accuracy: ± 10% (central area) Accuracy: ± 20%
Accuracy: ± 20-30% (outer area)

Configuration
Camera: E-Line Mk2 Colour Sideview Camera (EVCAMCSV-A) Lens: 26-00007
Image Size: 704x576 Pipe ID: 11.084in Environment: Gas Software Version: 0.6.3

Measurements assume that physical camera was centralised and pipe ID configured correctly.
Correct camera & lens must be selected in order to calibrate the calculations correctly.
Any accuracy figures quoted assume the above is correct. Any variations will significantly reduce the accuracy.

Key: Same Plane Area
Accuracy: ± 10% (central area) Accuracy: ± 20%
Accuracy: ± 20-30% (outer area)

Configuration
Camera: E-Line Mk2 Colour Sideview Camera (EVCAMCSV-A) Lens: 26-00007
Image Size: 704x576 Pipe ID: 11.084in Environment: Gas Software Version: 0.6.3

Measurements assume that physical camera was centralised and pipe ID configured correctly.
Correct camera & lens must be selected in order to calibrate the calculations correctly.
Any accuracy figures quoted assume the above is correct. Any variations will significantly reduce the accuracy.

Key: Same Plane Area
Accuracy: ± 10% (central area) Accuracy: ± 20%
Accuracy: ± 20-30% (outer area)

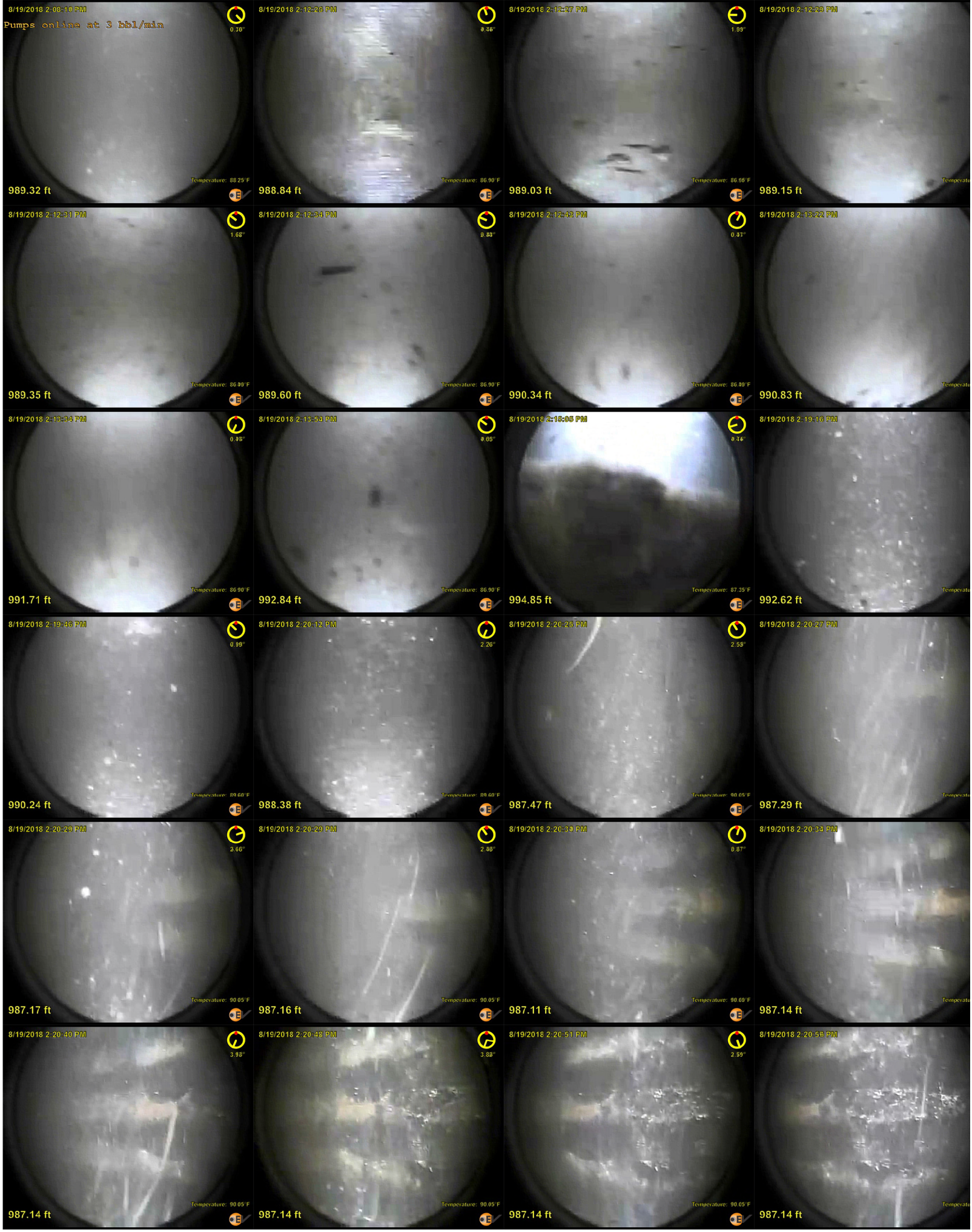
8/19/2018 2:08:10 PM
Pumps online at 3 bbl/min
989.32 ft
8/19/2018 2:12:25 PM
988.84 ft
8/19/2018 2:12:27 PM
989.03 ft
8/19/2018 2:12:29 PM
989.15 ft
8/19/2018 2:12:31 PM
989.35 ft
8/19/2018 2:12:34 PM
989.60 ft
8/19/2018 2:12:43 PM
990.34 ft
8/19/2018 2:13:22 PM
990.83 ft
8/19/2018 2:13:34 PM
991.71 ft
8/19/2018 2:13:54 PM
992.84 ft
8/19/2018 2:16:05 PM
994.85 ft
8/19/2018 2:19:16 PM
992.62 ft
8/19/2018 2:19:46 PM
990.24 ft
8/19/2018 2:20:12 PM
988.38 ft
8/19/2018 2:20:26 PM
987.47 ft
8/19/2018 2:20:27 PM
987.29 ft
8/19/2018 2:20:29 PM
987.17 ft
8/19/2018 2:20:29 PM
987.16 ft
8/19/2018 2:20:30 PM
987.11 ft
8/19/2018 2:20:34 PM
987.14 ft
8/19/2018 2:20:40 PM
987.14 ft
8/19/2018 2:20:48 PM
987.14 ft
8/19/2018 2:20:51 PM
987.14 ft
8/19/2018 2:20:56 PM
987.14 ft

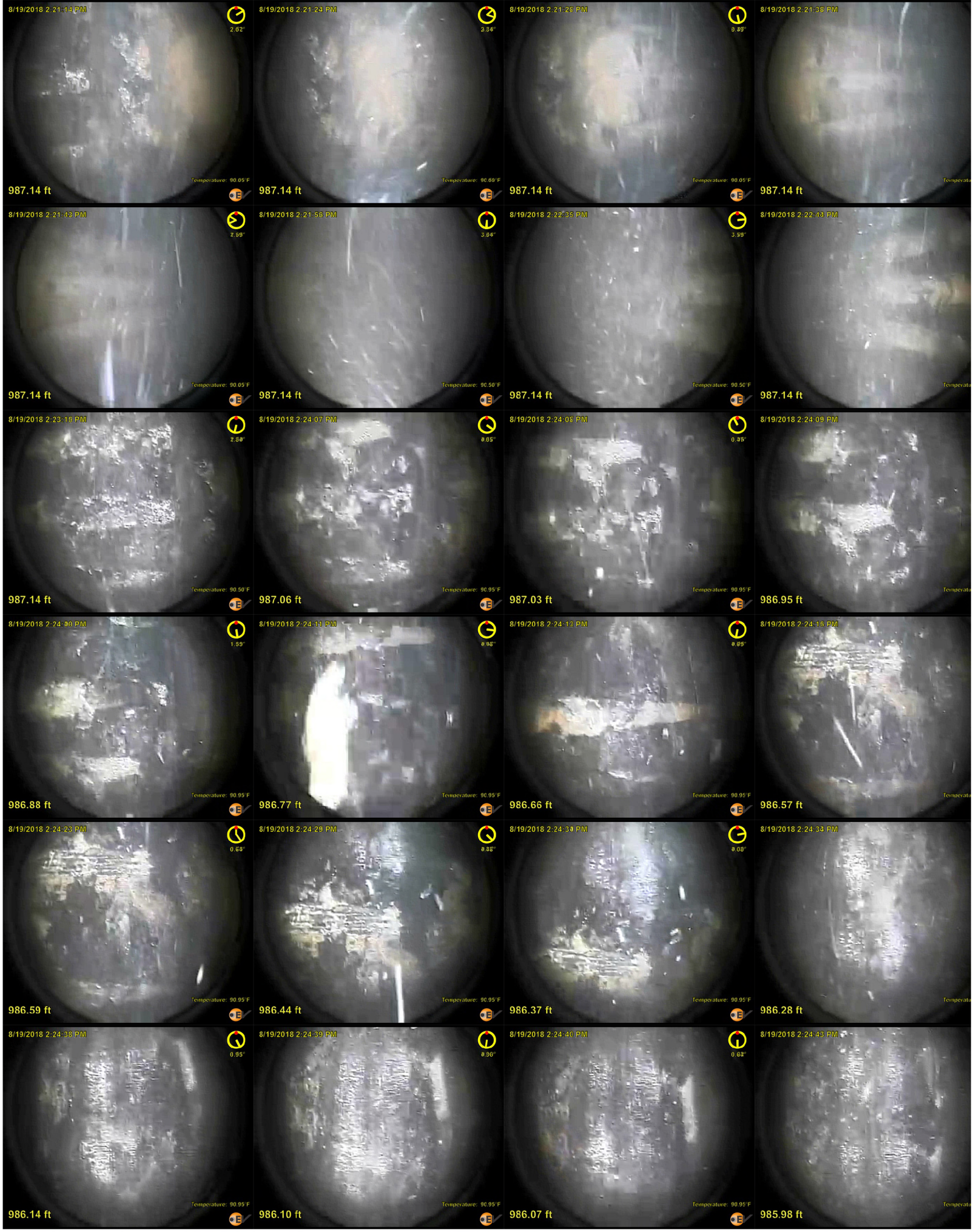
8/19/2018 2:21:14 PM
987.14 ft
8/19/2018 2:21:23 PM
987.14 ft
8/19/2018 2:21:26 PM
987.14 ft
8/19/2018 2:21:38 PM
987.14 ft
8/19/2018 2:21:43 PM
987.14 ft
8/19/2018 2:21:56 PM
987.14 ft
8/19/2018 2:22:36 PM
987.14 ft
8/19/2018 2:22:43 PM
987.14 ft
8/19/2018 2:23:16 PM
987.14 ft
8/19/2018 2:24:07 PM
987.06 ft
8/19/2018 2:24:08 PM
987.03 ft
8/19/2018 2:24:09 PM
986.95 ft
8/19/2018 2:24:10 PM
986.88 ft
8/19/2018 2:24:11 PM
986.77 ft
8/19/2018 2:24:13 PM
986.66 ft
8/19/2018 2:24:16 PM
986.57 ft
8/19/2018 2:24:23 PM
986.59 ft
8/19/2018 2:24:29 PM
986.44 ft
8/19/2018 2:24:30 PM
986.37 ft
8/19/2018 2:24:34 PM
986.28 ft
8/19/2018 2:24:38 PM
986.14 ft
8/19/2018 2:24:39 PM
986.10 ft
8/19/2018 2:24:40 PM
986.07 ft
8/19/2018 2:24:43 PM
985.98 ft

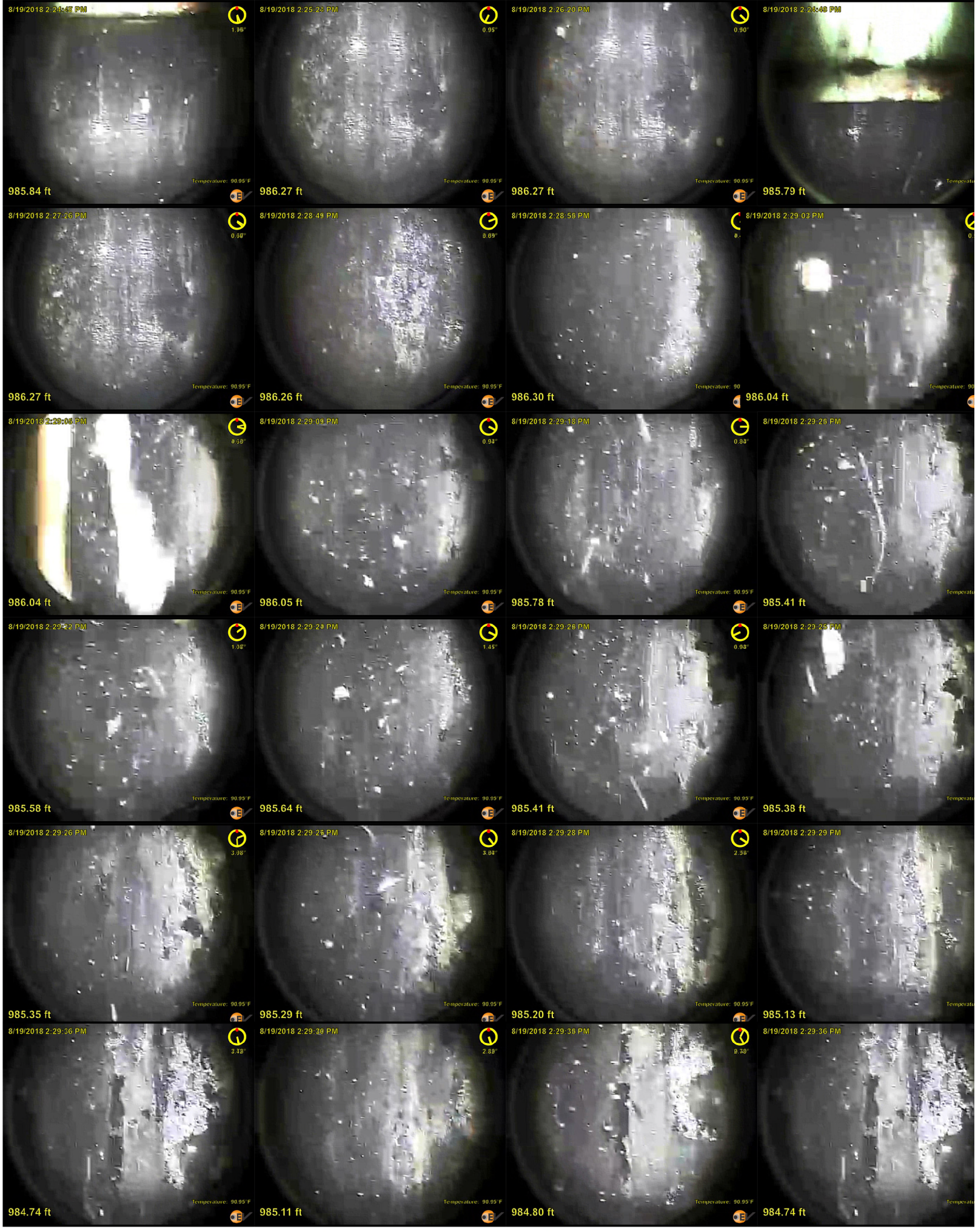
8/19/2018 2:24:45 PM
985.84 ft
8/19/2018 2:25:23 PM
986.27 ft
8/19/2018 2:26:20 PM
986.27 ft
8/19/2018 2:28:48 PM
985.79 ft
8/19/2018 2:27:26 PM
986.27 ft
8/19/2018 2:28:49 PM
986.26 ft
8/19/2018 2:28:56 PM
986.30 ft
8/19/2018 2:29:03 PM
986.04 ft
8/19/2018 2:29:05 PM
986.04 ft
8/19/2018 2:29:09 PM
986.05 ft
8/19/2018 2:29:18 PM
985.78 ft
8/19/2018 2:29:25 PM
985.41 ft
8/19/2018 2:29:22 PM
985.58 ft
8/19/2018 2:29:24 PM
985.64 ft
8/19/2018 2:29:26 PM
985.41 ft
8/19/2018 2:29:25 PM
985.38 ft
8/19/2018 2:29:26 PM
985.35 ft
8/19/2018 2:29:25 PM
985.29 ft
8/19/2018 2:29:28 PM
985.20 ft
8/19/2018 2:29:29 PM
985.13 ft
8/19/2018 2:29:36 PM
984.74 ft
8/19/2018 2:29:30 PM
985.11 ft
8/19/2018 2:29:36 PM
984.80 ft
8/19/2018 2:29:36 PM
984.74 ft

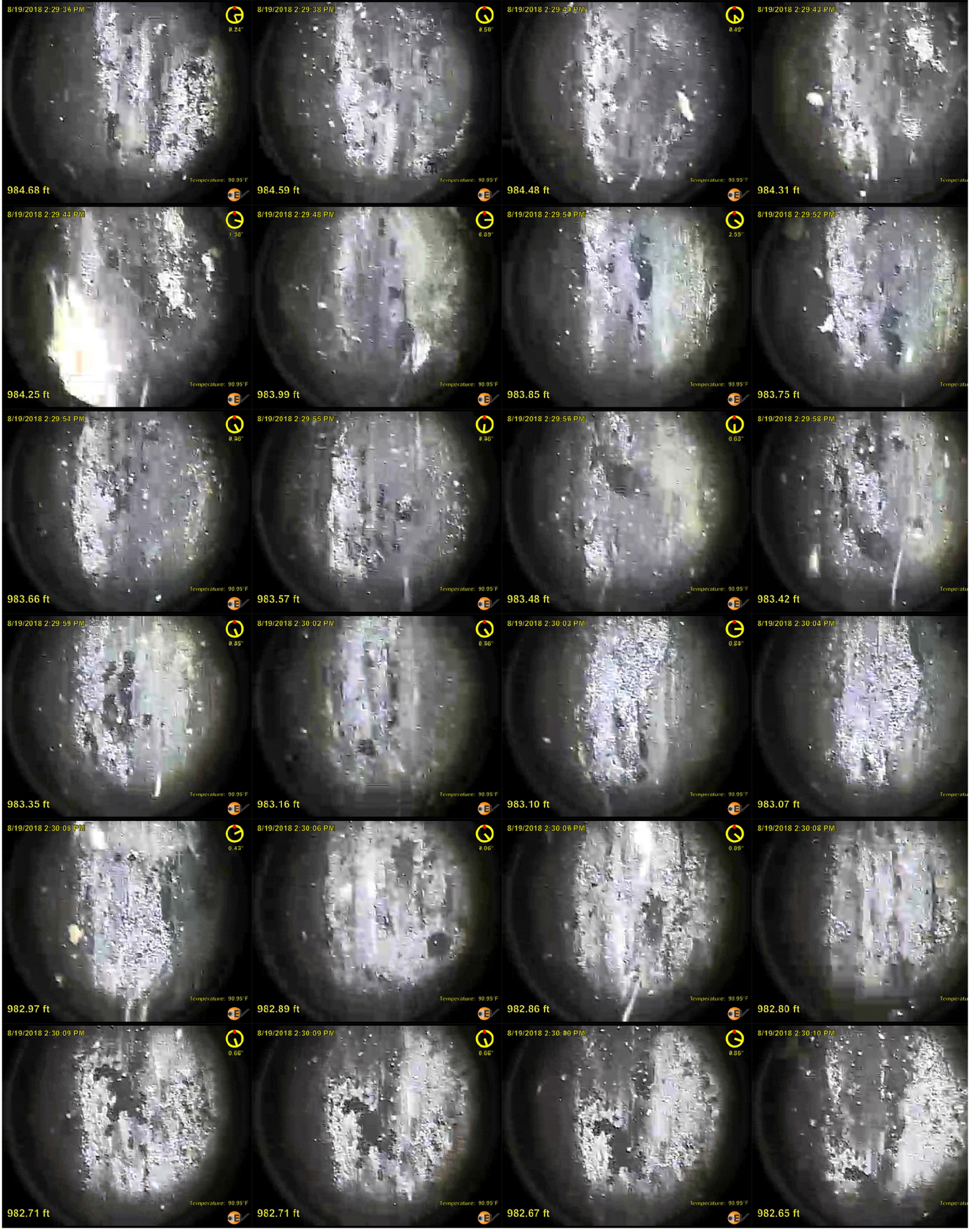
8/19/2018 2:29:36 PM
984.68 ft
8/19/2018 2:29:38 PM
984.59 ft
8/19/2018 2:29:40 PM
984.48 ft
8/19/2018 2:29:43 PM
984.31 ft
8/19/2018 2:29:44 PM
984.25 ft
8/19/2018 2:29:48 PM
983.99 ft
8/19/2018 2:29:50 PM
983.85 ft
8/19/2018 2:29:52 PM
983.75 ft
8/19/2018 2:29:53 PM
983.66 ft
8/19/2018 2:29:55 PM
983.57 ft
8/19/2018 2:29:58 PM
983.48 ft
8/19/2018 2:29:58 PM
983.42 ft
8/19/2018 2:29:59 PM
983.35 ft
8/19/2018 2:30:02 PM
983.16 ft
8/19/2018 2:30:03 PM
983.10 ft
8/19/2018 2:30:04 PM
983.07 ft
8/19/2018 2:30:06 PM
982.97 ft
8/19/2018 2:30:06 PM
982.89 ft
8/19/2018 2:30:08 PM
982.86 ft
8/19/2018 2:30:08 PM
982.80 ft
8/19/2018 2:30:09 PM
982.71 ft
8/19/2018 2:30:09 PM
982.71 ft
8/19/2018 2:30:10 PM
982.67 ft
8/19/2018 2:30:10 PM
982.65 ft

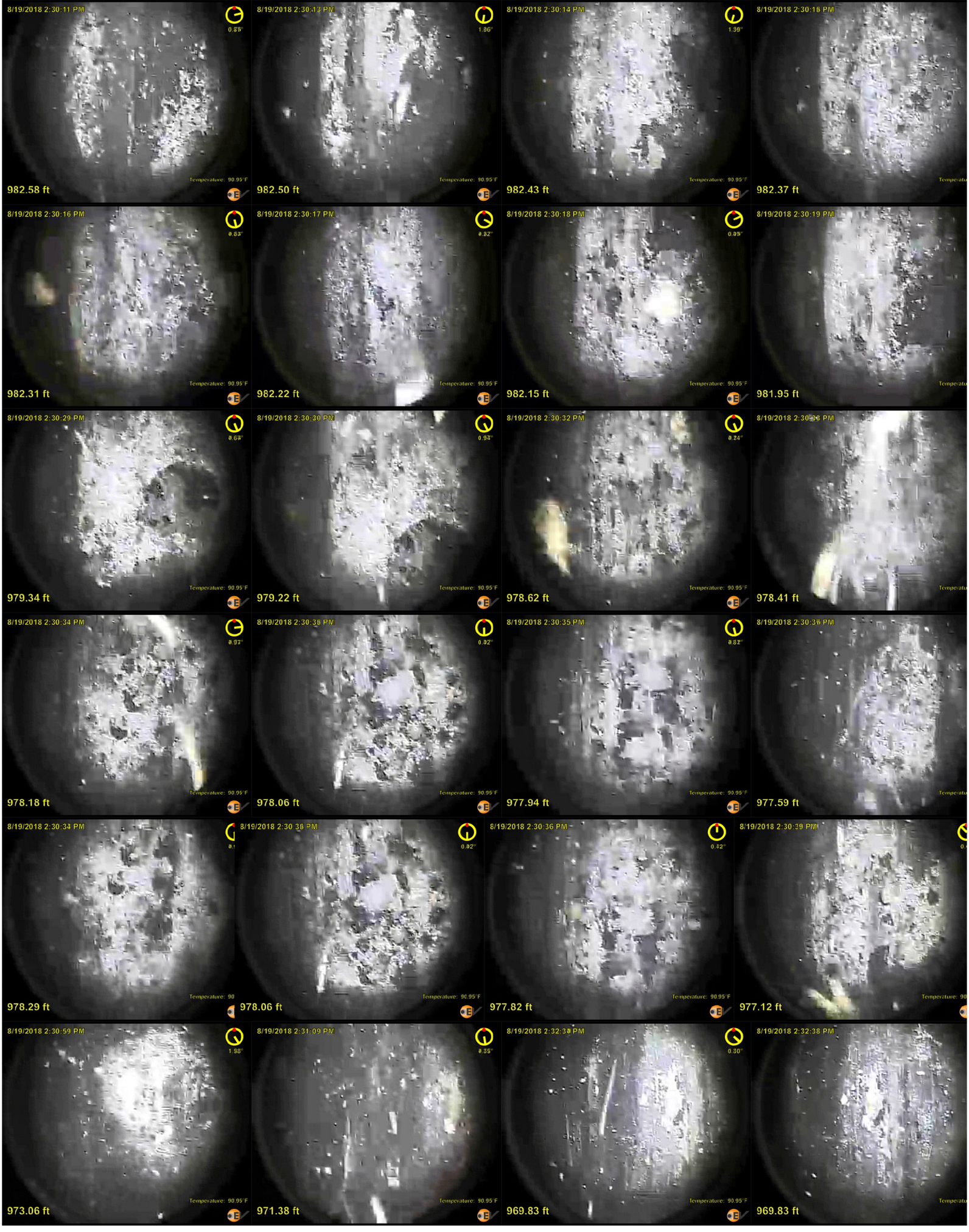
8/19/2018 2:30:11 PM
982.58 ft
8/19/2018 2:30:13 PM
982.50 ft
8/19/2018 2:30:14 PM
982.43 ft
8/19/2018 2:30:15 PM
982.37 ft
8/19/2018 2:30:16 PM
982.31 ft
8/19/2018 2:30:17 PM
982.22 ft
8/19/2018 2:30:18 PM
982.15 ft
8/19/2018 2:30:19 PM
981.95 ft
8/19/2018 2:30:29 PM
979.34 ft
8/19/2018 2:30:30 PM
979.22 ft
8/19/2018 2:30:32 PM
978.62 ft
978.41 ft
8/19/2018 2:30:34 PM
978.18 ft
8/19/2018 2:30:35 PM
978.06 ft
8/19/2018 2:30:35 PM
977.94 ft
977.59 ft
978.29 ft
978.06 ft
977.82 ft
977.12 ft
8/19/2018 2:30:59 PM
973.06 ft
971.38 ft
969.83 ft
969.83 ft

969.83 ft

8/19/2018 2:33:16 PM
970.48 ft

8/19/2018 2:33:15 PM
970.38 ft

8/19/2018 2:33:16 PM
970.43 ft

970.54 ft

8/19/2018 2:33:19 PM
970.74 ft

8/19/2018 2:33:23 PM
971.19 ft

8/19/2018 2:33:26 PM
971.46 ft

8/19/2018 2:33:38 PM
973.24 ft

8/19/2018 2:33:50 PM
973.92 ft

8/19/2018 2:33:57 PM
974.27 ft

8/19/2018 2:37:02 PM
974.97 ft

8/19/2018 2:37:03 PM
974.86 ft

8/19/2018 2:37:26 PM
973.38 ft

8/19/2018 2:37:27 PM
973.22 ft

8/19/2018 2:38:10 PM
971.86 ft

971.86 ft

971.86 ft

8/19/2018 2:38:33 PM
971.86 ft

8/19/2018 2:38:38 PM
971.86 ft

Resetdepth to EOT
886.00 ft

8/19/2018 4:07:15 PM
891.05 ft

8/19/2018 4:07:28 PM
891.05 ft

891.25 ft

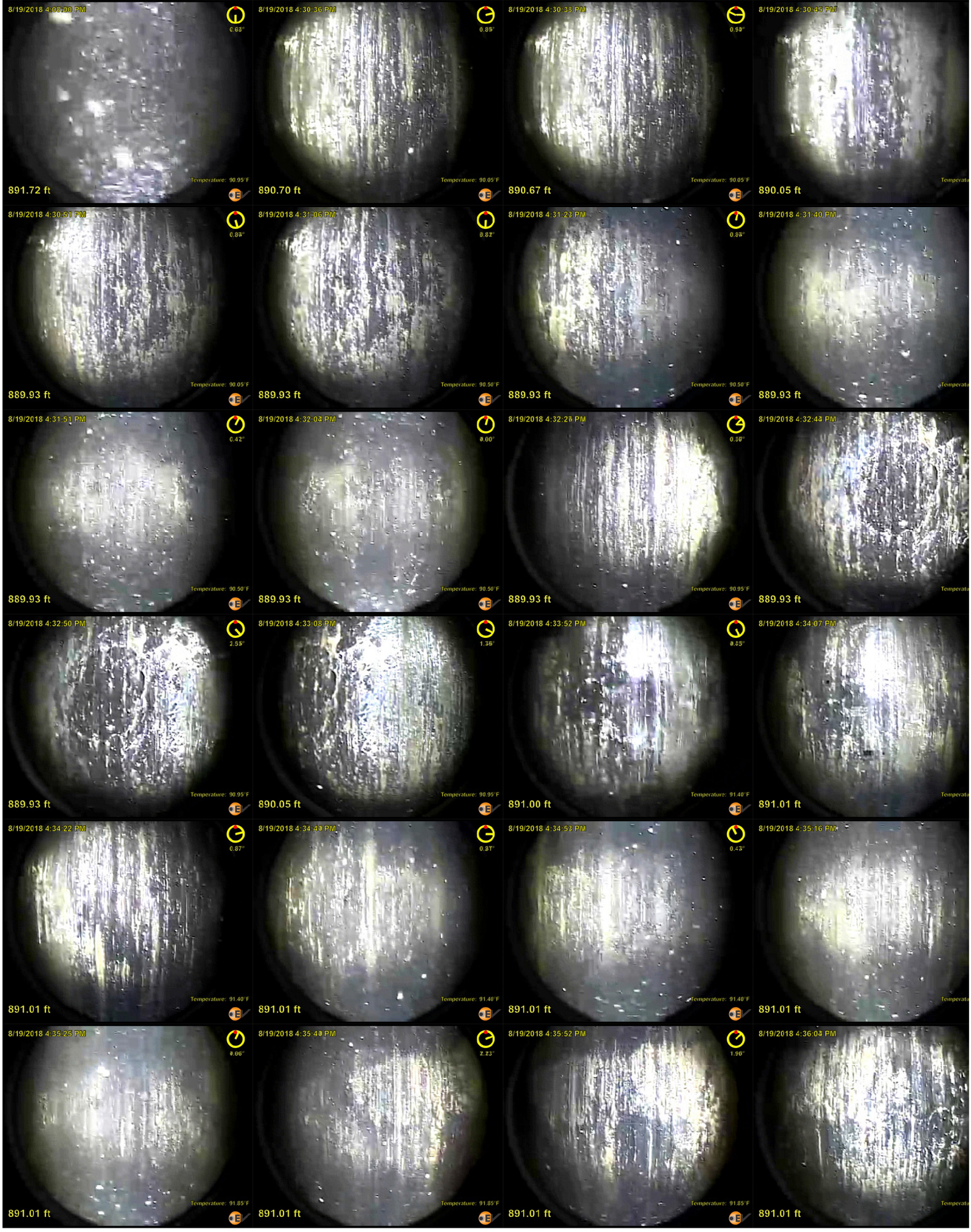
8/19/2018 4:29:30 PM
891.72 ft
Temperature: 90.95°F
8/19/2018 4:30:36 PM
890.70 ft
Temperature: 90.05°F
8/19/2018 4:30:38 PM
890.67 ft
Temperature: 90.05°F
8/19/2018 4:30:45 PM
890.05 ft
8/19/2018 4:30:51 PM
889.93 ft
Temperature: 90.05°F
8/19/2018 4:31:06 PM
889.93 ft
Temperature: 90.50°F
8/19/2018 4:31:23 PM
889.93 ft
Temperature: 90.50°F
8/19/2018 4:31:40 PM
889.93 ft
8/19/2018 4:31:51 PM
889.93 ft
Temperature: 90.50°F
8/19/2018 4:32:04 PM
889.93 ft
Temperature: 90.50°F
8/19/2018 4:32:23 PM
889.93 ft
Temperature: 90.95°F
8/19/2018 4:32:43 PM
889.93 ft
8/19/2018 4:32:50 PM
889.93 ft
Temperature: 90.95°F
8/19/2018 4:33:08 PM
890.05 ft
Temperature: 90.95°F
8/19/2018 4:33:52 PM
891.00 ft
Temperature: 91.40°F
8/19/2018 4:34:07 PM
891.01 ft
8/19/2018 4:34:22 PM
891.01 ft
Temperature: 91.40°F
8/19/2018 4:34:40 PM
891.01 ft
Temperature: 91.40°F
8/19/2018 4:34:53 PM
891.01 ft
Temperature: 91.40°F
8/19/2018 4:35:16 PM
891.01 ft
8/19/2018 4:35:25 PM
891.01 ft
Temperature: 91.85°F
8/19/2018 4:35:40 PM
891.01 ft
Temperature: 91.85°F
8/19/2018 4:35:52 PM
891.01 ft
Temperature: 91.85°F
8/19/2018 4:36:03 PM
891.01 ft

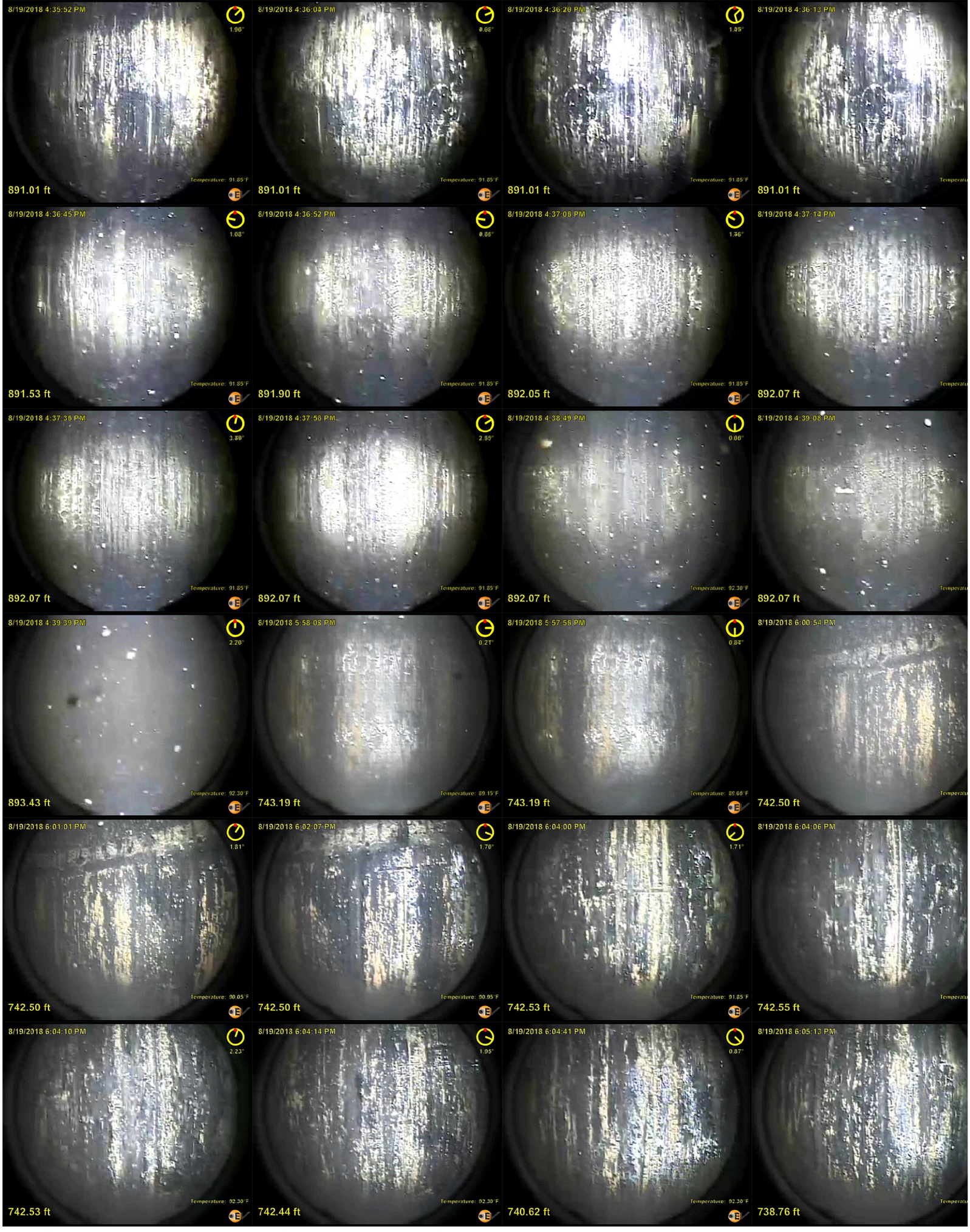
8/19/2018 4:35:52 PM
891.01 ft
8/19/2018 4:36:03 PM
891.01 ft
8/19/2018 4:36:29 PM
891.01 ft
8/19/2018 4:36:13 PM
891.01 ft
8/19/2018 4:36:45 PM
891.53 ft
8/19/2018 4:36:52 PM
891.90 ft
8/19/2018 4:37:06 PM
892.05 ft
8/19/2018 4:37:19 PM
892.07 ft
8/19/2018 4:37:36 PM
892.07 ft
8/19/2018 4:37:56 PM
892.07 ft
8/19/2018 4:38:49 PM
892.07 ft
8/19/2018 4:39:08 PM
892.07 ft
8/19/2018 4:39:39 PM
893.43 ft
8/19/2018 5:58:08 PM
743.19 ft
8/19/2018 5:57:56 PM
743.19 ft
8/19/2018 6:00:54 PM
742.50 ft
8/19/2018 6:01:01 PM
742.50 ft
8/19/2018 6:02:07 PM
742.50 ft
8/19/2018 6:04:00 PM
742.53 ft
8/19/2018 6:04:06 PM
742.55 ft
8/19/2018 6:04:10 PM
742.53 ft
8/19/2018 6:04:14 PM
742.44 ft
8/19/2018 6:04:41 PM
740.62 ft
8/19/2018 6:05:13 PM
738.76 ft

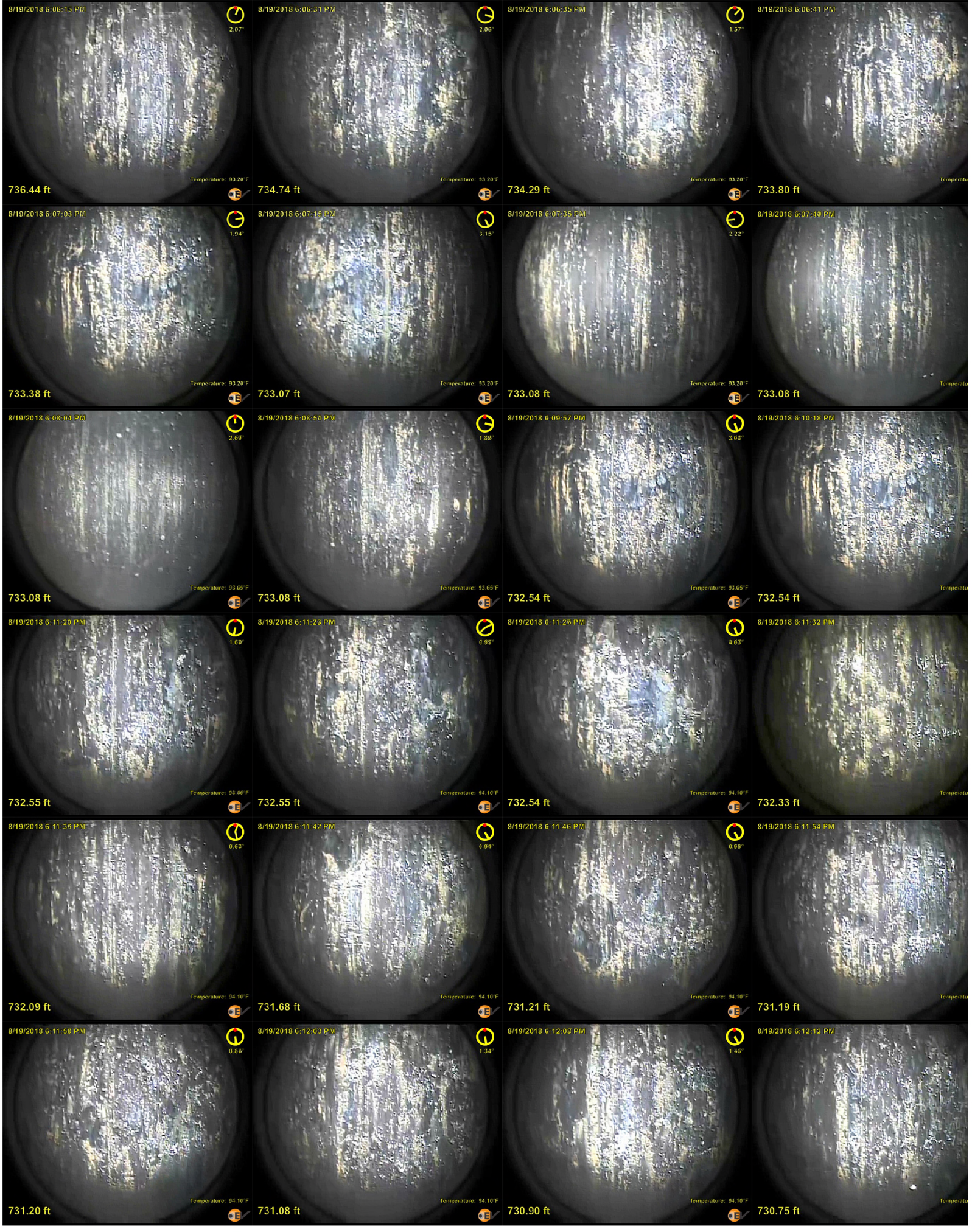
8/19/2018 6:06:15 PM
2.07°
Temperature: 93.20°F
736.44 ft
8/19/2018 6:06:31 PM
2.06°
Temperature: 93.20°F
734.74 ft
8/19/2018 6:06:35 PM
1.57°
Temperature: 93.20°F
734.29 ft
8/19/2018 6:06:41 PM
733.80 ft
8/19/2018 6:07:03 PM
1.94°
Temperature: 93.20°F
733.38 ft
8/19/2018 6:07:15 PM
3.15°
Temperature: 93.20°F
733.07 ft
8/19/2018 6:07:35 PM
2.22°
Temperature: 93.20°F
733.08 ft
8/19/2018 6:07:40 PM
733.08 ft
8/19/2018 6:08:04 PM
2.69°
Temperature: 93.65°F
733.08 ft
8/19/2018 6:08:50 PM
1.88°
Temperature: 93.65°F
733.08 ft
8/19/2018 6:09:57 PM
3.08°
Temperature: 93.65°F
732.54 ft
8/19/2018 6:10:18 PM
732.54 ft
8/19/2018 6:11:20 PM
1.69°
Temperature: 94.10°F
732.55 ft
8/19/2018 6:11:23 PM
0.95°
Temperature: 94.10°F
732.55 ft
8/19/2018 6:11:26 PM
3.02°
Temperature: 94.10°F
732.54 ft
8/19/2018 6:11:32 PM
732.33 ft
8/19/2018 6:11:38 PM
0.63°
Temperature: 94.10°F
732.09 ft
8/19/2018 6:11:42 PM
0.94°
Temperature: 94.10°F
731.68 ft
8/19/2018 6:11:46 PM
0.99°
Temperature: 94.10°F
731.21 ft
8/19/2018 6:11:54 PM
731.19 ft
8/19/2018 6:11:58 PM
0.86°
Temperature: 94.10°F
731.20 ft
8/19/2018 6:12:03 PM
1.34°
Temperature: 94.10°F
731.08 ft
8/19/2018 6:12:08 PM
1.36°
Temperature: 94.10°F
730.90 ft
8/19/2018 6:12:12 PM
730.75 ft

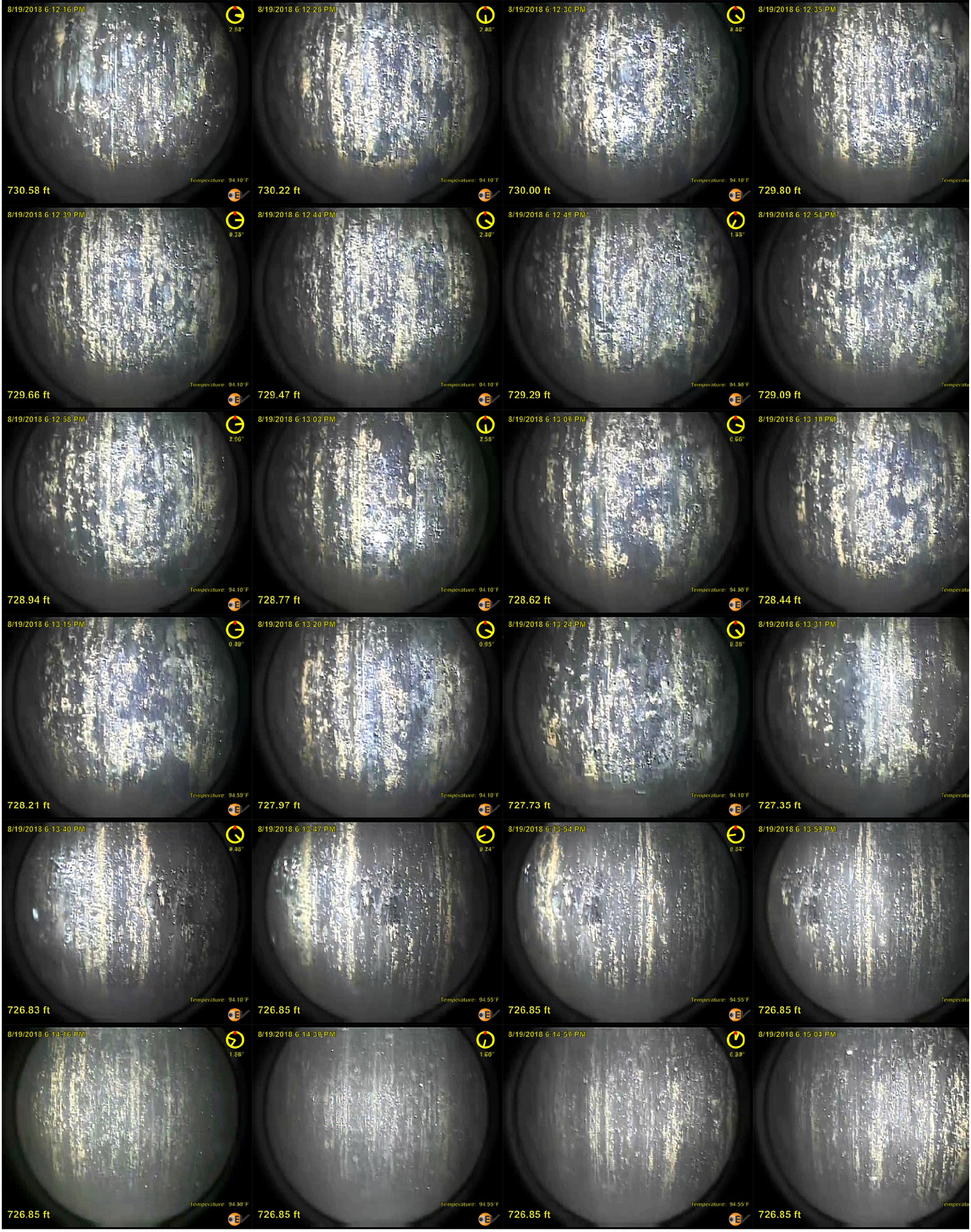
8/19/2018 6:12:16 PM
730.58 ft
8/19/2018 6:12:26 PM
730.22 ft
8/19/2018 6:12:30 PM
730.00 ft
8/19/2018 6:12:35 PM
729.80 ft
8/19/2018 6:12:39 PM
729.66 ft
8/19/2018 6:12:44 PM
729.47 ft
8/19/2018 6:12:49 PM
729.29 ft
8/19/2018 6:12:54 PM
729.09 ft
8/19/2018 6:12:58 PM
728.94 ft
8/19/2018 6:13:03 PM
728.77 ft
8/19/2018 6:13:08 PM
728.62 ft
8/19/2018 6:13:10 PM
728.44 ft
8/19/2018 6:13:15 PM
728.21 ft
8/19/2018 6:13:20 PM
727.97 ft
8/19/2018 6:13:24 PM
727.73 ft
8/19/2018 6:13:31 PM
727.35 ft
8/19/2018 6:13:40 PM
726.83 ft
8/19/2018 6:13:47 PM
726.85 ft
8/19/2018 6:13:54 PM
726.85 ft
8/19/2018 6:13:59 PM
726.85 ft
8/19/2018 6:14:16 PM
726.85 ft
8/19/2018 6:14:38 PM
726.85 ft
8/19/2018 6:14:59 PM
726.85 ft
8/19/2018 6:15:03 PM
726.85 ft

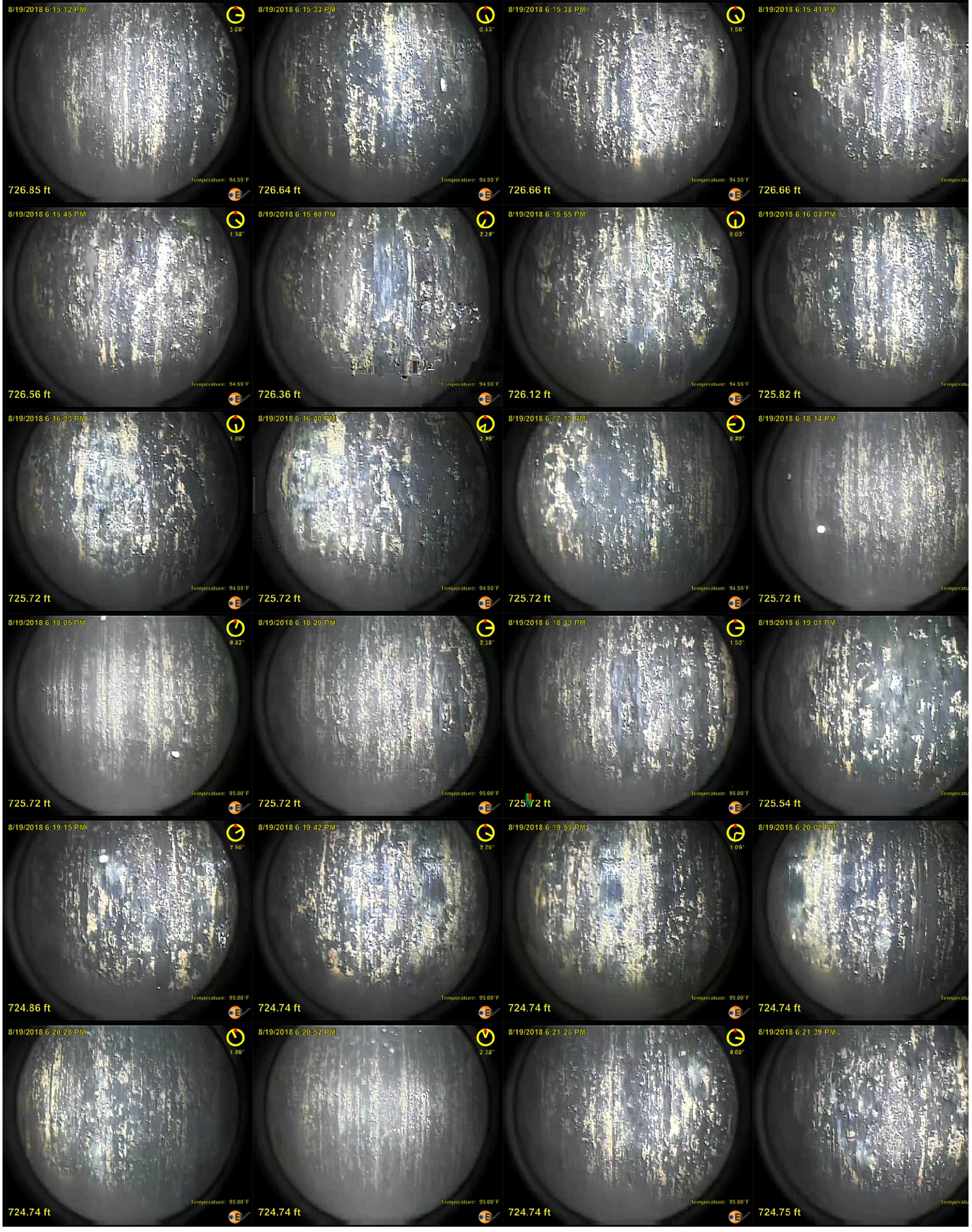
8/19/2018 6:15:12 PM
726.85 ft
8/19/2018 6:15:33 PM
726.64 ft
8/19/2018 6:15:38 PM
726.66 ft
8/19/2018 6:15:41 PM
726.66 ft
8/19/2018 6:15:45 PM
726.56 ft
8/19/2018 6:15:50 PM
726.36 ft
8/19/2018 6:15:55 PM
726.12 ft
8/19/2018 6:16:03 PM
725.82 ft
8/19/2018 6:16:33 PM
725.72 ft
8/19/2018 6:16:40 PM
725.72 ft
8/19/2018 6:17:10 PM
725.72 ft
8/19/2018 6:18:13 PM
725.72 ft
8/19/2018 6:18:05 PM
725.72 ft
8/19/2018 6:18:20 PM
725.72 ft
8/19/2018 6:18:30 PM
725.72 ft
8/19/2018 6:19:01 PM
725.54 ft
8/19/2018 6:19:15 PM
724.86 ft
8/19/2018 6:19:42 PM
724.74 ft
8/19/2018 6:19:53 PM
724.74 ft
8/19/2018 6:20:02 PM
724.74 ft
8/19/2018 6:20:28 PM
724.74 ft
8/19/2018 6:20:52 PM
724.74 ft
8/19/2018 6:21:26 PM
724.74 ft
8/19/2018 6:21:39 PM
724.75 ft

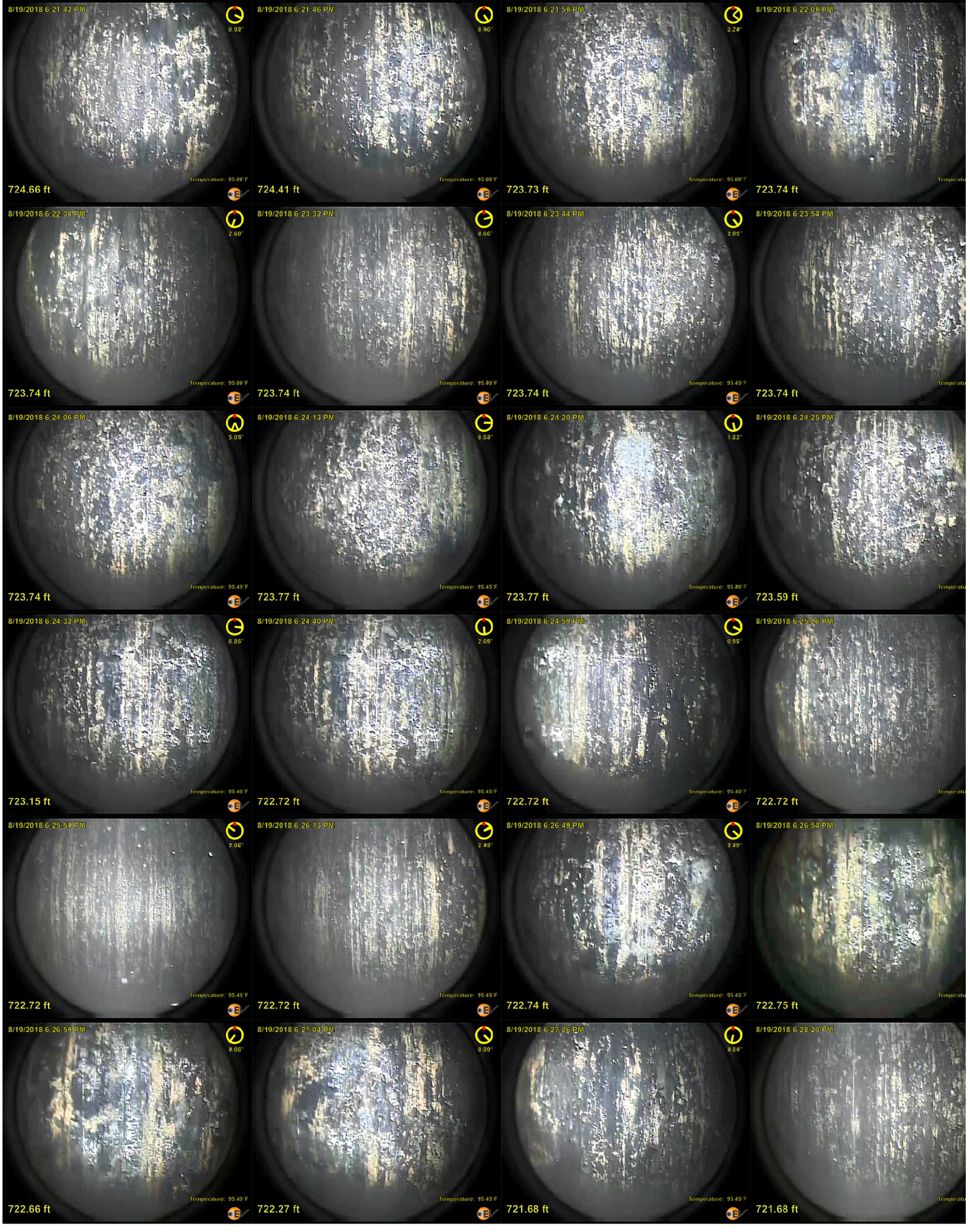
8/19/2018 6:21:42 PM
724.66 ft
8/19/2018 6:21:46 PM
724.41 ft
8/19/2018 6:21:56 PM
723.73 ft
8/19/2018 6:22:06 PM
723.74 ft
8/19/2018 6:22:34 PM
723.74 ft
8/19/2018 6:23:32 PM
723.74 ft
8/19/2018 6:23:44 PM
723.74 ft
8/19/2018 6:23:54 PM
723.74 ft
8/19/2018 6:24:06 PM
723.74 ft
8/19/2018 6:24:13 PM
723.77 ft
8/19/2018 6:24:20 PM
723.77 ft
8/19/2018 6:24:25 PM
723.59 ft
8/19/2018 6:24:32 PM
723.15 ft
8/19/2018 6:24:40 PM
722.72 ft
8/19/2018 6:24:59 PM
722.72 ft
8/19/2018 6:25:26 PM
722.72 ft
8/19/2018 6:25:50 PM
722.72 ft
8/19/2018 6:26:13 PM
722.72 ft
8/19/2018 6:26:49 PM
722.74 ft
8/19/2018 6:26:54 PM
722.75 ft
8/19/2018 6:26:59 PM
722.66 ft
8/19/2018 6:27:04 PM
722.27 ft
8/19/2018 6:27:26 PM
721.68 ft
8/19/2018 6:28:20 PM
721.68 ft

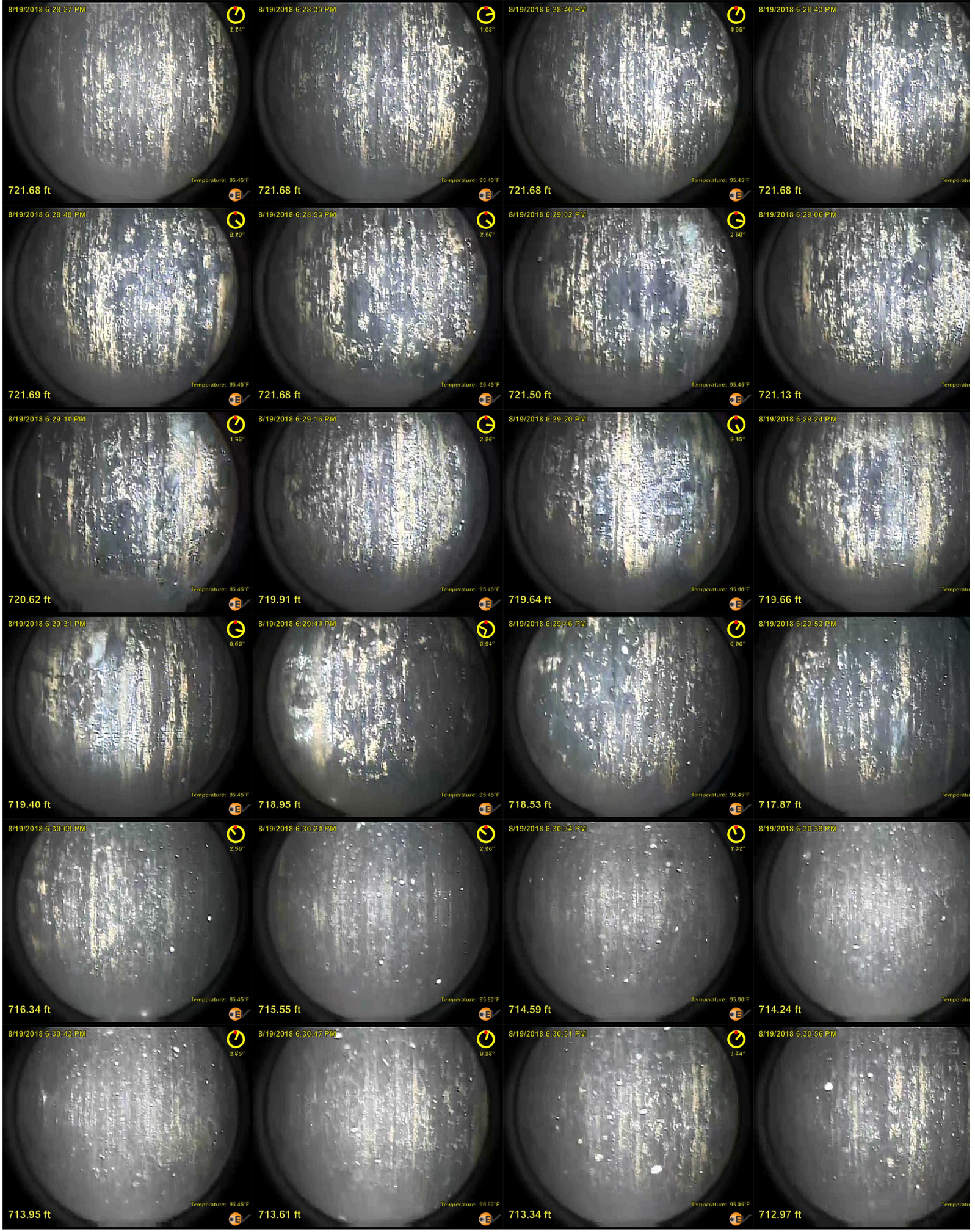
8/19/2018 6:28:27 PM
721.68 ft
8/19/2018 6:28:38 PM
721.68 ft
8/19/2018 6:28:38 PM
721.68 ft
8/19/2018 6:28:43 PM
721.68 ft
8/19/2018 6:28:48 PM
721.69 ft
8/19/2018 6:28:53 PM
721.68 ft
8/19/2018 6:29:02 PM
721.50 ft
8/19/2018 6:29:06 PM
721.13 ft
8/19/2018 6:29:10 PM
720.62 ft
8/19/2018 6:29:16 PM
719.91 ft
8/19/2018 6:29:20 PM
719.64 ft
8/19/2018 6:29:24 PM
719.66 ft
8/19/2018 6:29:31 PM
719.40 ft
8/19/2018 6:29:40 PM
718.95 ft
8/19/2018 6:29:46 PM
718.53 ft
8/19/2018 6:29:53 PM
717.87 ft
8/19/2018 6:30:09 PM
716.34 ft
8/19/2018 6:30:29 PM
715.55 ft
8/19/2018 6:30:33 PM
714.59 ft
8/19/2018 6:30:39 PM
714.24 ft
8/19/2018 6:30:43 PM
713.95 ft
8/19/2018 6:30:47 PM
713.61 ft
8/19/2018 6:30:51 PM
713.34 ft
8/19/2018 6:30:56 PM
712.97 ft

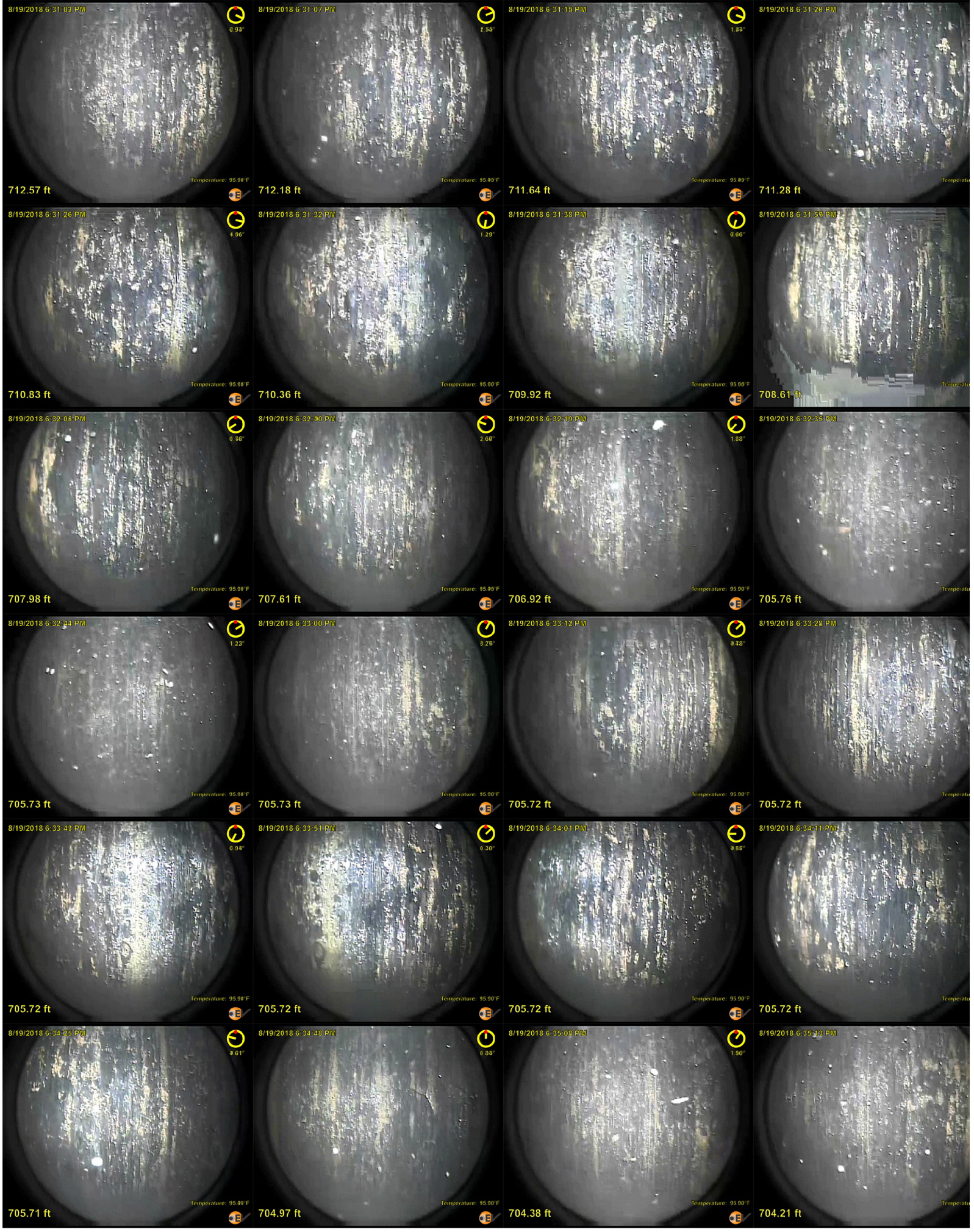
8/19/2018 6:31:02 PM
712.57 ft
8/19/2018 6:31:07 PM
712.18 ft
8/19/2018 6:31:15 PM
711.64 ft
8/19/2018 6:31:20 PM
711.28 ft
8/19/2018 6:31:26 PM
710.83 ft
8/19/2018 6:31:32 PM
710.36 ft
8/19/2018 6:31:38 PM
709.92 ft
8/19/2018 6:31:56 PM
708.61 ft
8/19/2018 6:32:05 PM
707.98 ft
8/19/2018 6:32:30 PM
707.61 ft
8/19/2018 6:32:19 PM
706.92 ft
8/19/2018 6:32:35 PM
705.76 ft
8/19/2018 6:32:44 PM
705.73 ft
8/19/2018 6:33:00 PM
705.73 ft
8/19/2018 6:33:12 PM
705.72 ft
8/19/2018 6:33:28 PM
705.72 ft
8/19/2018 6:33:43 PM
705.72 ft
8/19/2018 6:33:51 PM
705.72 ft
8/19/2018 6:34:01 PM
705.72 ft
8/19/2018 6:34:11 PM
705.72 ft
8/19/2018 6:34:25 PM
705.71 ft
8/19/2018 6:34:48 PM
704.97 ft
8/19/2018 6:35:08 PM
704.38 ft
8/19/2018 6:35:13 PM
704.21 ft

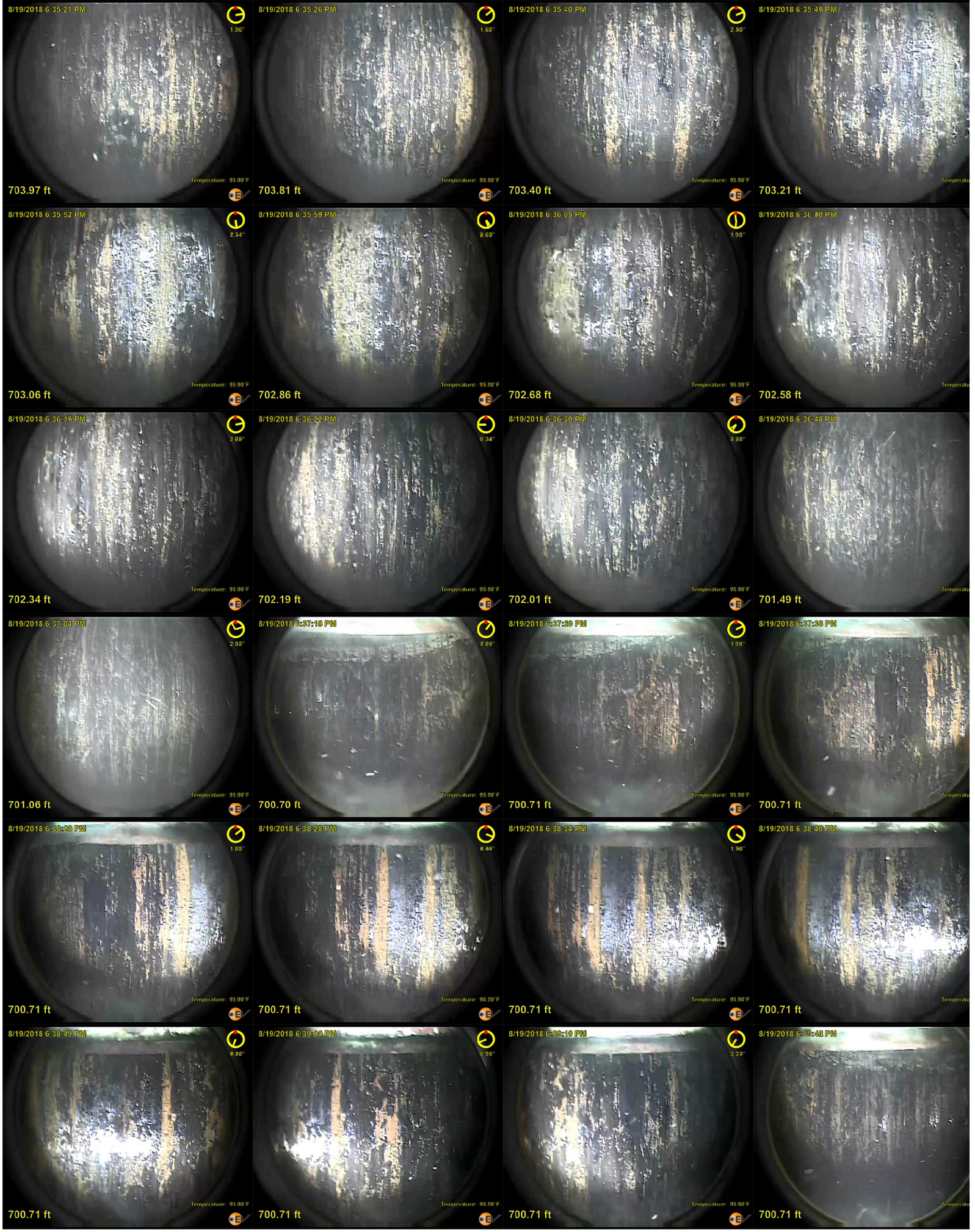
8/19/2018 6:35:21 PM
703.97 ft
8/19/2018 6:35:26 PM
703.81 ft
8/19/2018 6:35:40 PM
703.40 ft
8/19/2018 6:35:52 PM
703.06 ft
8/19/2018 6:35:59 PM
702.86 ft
8/19/2018 6:36:05 PM
702.68 ft
8/19/2018 6:36:16 PM
702.34 ft
8/19/2018 6:36:22 PM
702.19 ft
8/19/2018 6:36:30 PM
702.01 ft
8/19/2018 6:37:04 PM
701.06 ft
8/19/2018 6:37:10 PM
700.70 ft
8/19/2018 6:37:20 PM
700.71 ft
8/19/2018 6:38:20 PM
700.71 ft
8/19/2018 6:38:28 PM
700.71 ft
8/19/2018 6:38:34 PM
700.71 ft
8/19/2018 6:38:49 PM
700.71 ft
8/19/2018 6:39:00 PM
700.71 ft
8/19/2018 6:39:10 PM
700.71 ft

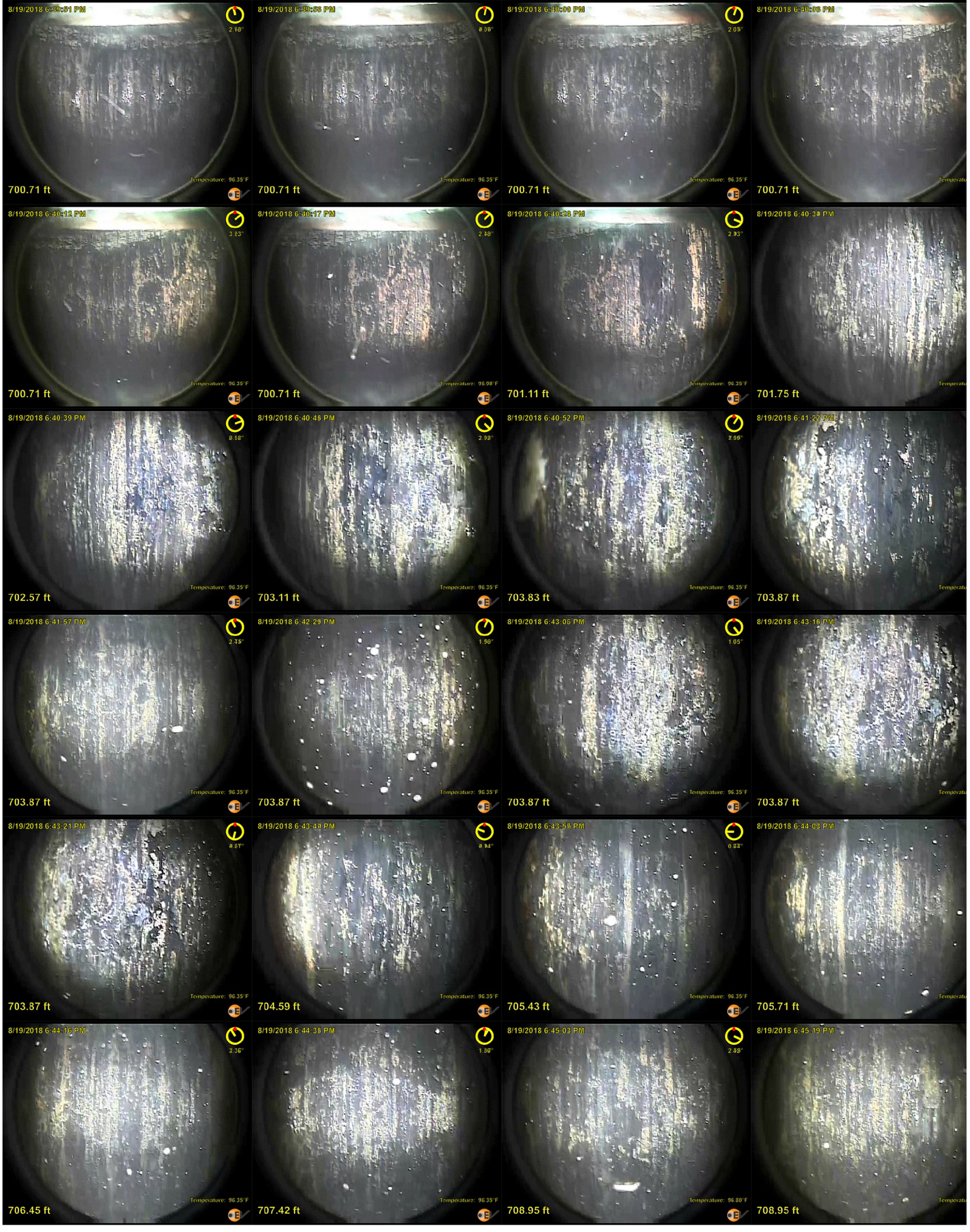
8/19/2018 6:39:51 PM
700.71 ft
8/19/2018 6:39:56 PM
700.71 ft
8/19/2018 6:40:00 PM
700.71 ft
8/19/2018 6:40:05 PM
700.71 ft
8/19/2018 6:40:12 PM
700.71 ft
8/19/2018 6:40:17 PM
700.71 ft
8/19/2018 6:40:23 PM
701.11 ft
8/19/2018 6:40:30 PM
701.75 ft
8/19/2018 6:40:39 PM
702.57 ft
8/19/2018 6:40:45 PM
703.11 ft
8/19/2018 6:40:52 PM
703.83 ft
8/19/2018 6:41:22 PM
703.87 ft
8/19/2018 6:41:57 PM
703.87 ft
8/19/2018 6:42:29 PM
703.87 ft
8/19/2018 6:43:06 PM
703.87 ft
8/19/2018 6:43:16 PM
703.87 ft
8/19/2018 6:43:21 PM
703.87 ft
8/19/2018 6:43:40 PM
704.59 ft
8/19/2018 6:43:56 PM
705.43 ft
8/19/2018 6:44:03 PM
705.71 ft
8/19/2018 6:44:16 PM
706.45 ft
8/19/2018 6:44:36 PM
707.42 ft
8/19/2018 6:45:03 PM
708.95 ft
8/19/2018 6:45:19 PM
708.95 ft

8/19/2018 6:45:45 PM
708.95 ft
Temperature: 96.80°F

8/19/2018 6:46:02 PM
708.95 ft
Temperature: 96.80°F

8/19/2018 6:46:15 PM
708.96 ft
Temperature: 96.80°F

8/19/2018 6:46:20 PM
709.98 ft

8/19/2018 6:46:25 PM
711.87 ft
Temperature: 96.80°F

8/19/2018 6:46:30 PM
714.44 ft
Temperature: 96.80°F

8/19/2018 6:46:35 PM
716.82 ft
Temperature: 96.80°F

8/19/2018 6:46:40 PM
719.53 ft

8/19/2018 6:46:46 PM
722.70 ft
Temperature: 96.80°F

8/19/2018 6:46:54 PM
726.30 ft
Temperature: 96.80°F

8/19/2018 6:46:59 PM
728.82 ft
Temperature: 96.80°F

8/19/2018 6:47:04 PM
731.52 ft

8/19/2018 6:47:10 PM
734.28 ft
Temperature: 96.80°F

8/19/2018 6:47:16 PM
736.91 ft
Temperature: 96.80°F

8/19/2018 6:47:20 PM
739.64 ft
Temperature: 96.80°F

8/19/2018 6:47:29 PM
743.89 ft

8/19/2018 6:48:28 PM
741.42 ft
Temperature: 96.35°F

8/19/2018 6:48:59 PM
729.83 ft
Temperature: 95.90°F

8/19/2018 6:50:03 PM
705.61 ft
Temperature: 95.45°F

Appendix D Comparison of 7 in. Laser Scan Data and 11 3/4 in. High-Resolution Vertilog

7 in. Laser Scan

11 3/4 in. HRVRT

11 3/4 in. Caliper

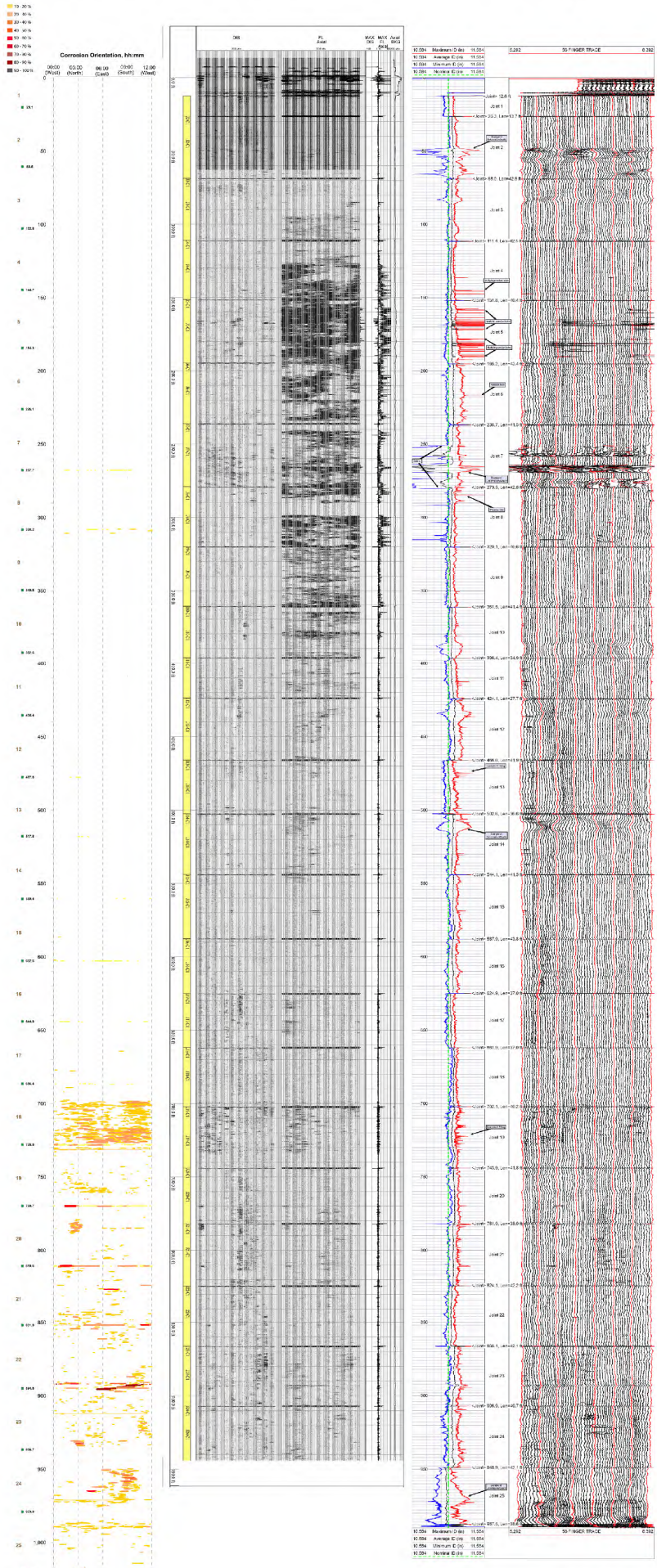

Appendix E 11 3/4 in. Composite Log

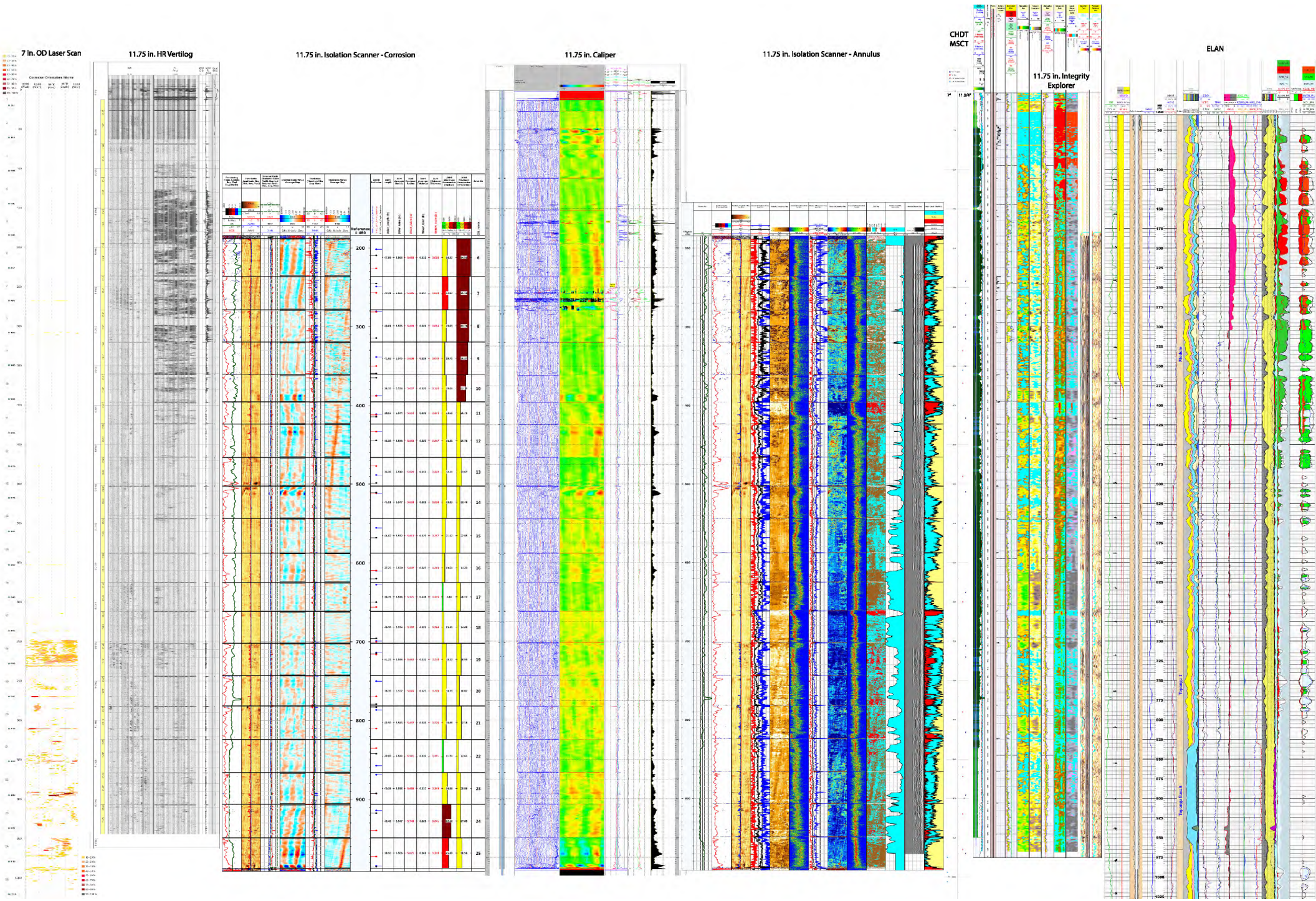
7 in. OD Laser Scan
11.75 in. HR Vertilog
11.75 in. Isolation Scanner - Corrosion
11.75 in. Caliper
11.75 in. Isolation Scanner - Annulus
CHDT
MSCT
11.75 in. Integrity
Explorer
ELAN

SS-25 RCA Supplementary Report

SS-25 Temperature, Pressure, and Noise Logs Analysis

Purpose:
Report on the SS-25 well temperature, pressure, and noise logs from before, during, and after the blowout.

Date:
May 31, 2019

BLADE ENERGY PARTNERS

2600 Network Boulevard, Suite 550
Frisco, Texas 75034

+1 972-712-8407 (phone)
+1 972-712-8408 (fax)

16285 Park Ten Place, Suite 600
Houston, Texas 77084

1-800-319-2940 (toll free)
+1 281-206-2000 (phone)
+1 281-206-2005 (fax)

www.blade-energy.com

Blade Energy Partners Limited, and its affiliates ('Blade') provide our services subject to our General Terms and Conditions ('GTC') in effect at time of service, unless a GTC provision is expressly superseded in a separate agreement made with Blade. Blade's work product is based on information sources which we believe to be reliable, including information that was publicly available and that was provided by our client; but Blade does not guarantee the accuracy or completeness of the information provided. All statements are the opinions of Blade based on generally-accepted and reasonable practices in the industry. Our clients remain fully responsible for all clients' decisions, actions and omissions, whether based upon Blade's work product or not; and Blade's liability solely extends to the cost of its work product.

Abstract

The gas storage well Standard Sesnon 25 (SS-25) in the Aliso Canyon Gas Storage Field located in Los Angeles County, California started leaking gas in October 2015. A relief well was drilled, and SS-25 was brought under control. The leak stopped in February 2016.

In January 2016, as part of their investigation of the leak, the California Public Utilities Commission (CPUC) and the Division of Oil, Gas, and Geothermal Resources (DOGGR) selected and gave provisional authority to Blade Energy Partners (Blade) to perform an independent Root Cause Analysis (RCA). The Blade Team and parties under Blade's direction were responsible for directing the work of subcontractors who performed the extraction of the SS-25's wellhead, tubing, and casings and the preservation and protection of associated evidence. Blade's RCA Reports, including this report, document and describe the key activities undertaken in support of the RCA effort.

This report provides details of Blade's examination and interpretation of all the temperature, pressure, and noise surveys before, during, and after the SS-25's blowout. Indications of a preexisting log anomaly before October 23, 2015 were not present. After the 7 in. casing failure had occurred, the temperature profile was significantly different than all historical temperature profiles for SS-25. Freezing temperatures in the top few hundred feet of the well were observed during the blowout. Almost three years after the 7 in. casing failure, temperatures remain cold.

Table of Contents

1 Introduction **5**
1.1 Abbreviations and Acronyms 5
2 Before the Incident **6**
2.1 Temperature, Pressure, and Noise Surveys 6
3 During the Blowout **16**
3.1 Temperature 16
3.2 Temperature Profile Comparison 16
4 After the Well Kill **24**
4.1 Wireline Temperature Surveys 24
4.2 Distributed Temperature Sensing 29
5 Conclusions **34**
6 References **35**
Appendix A **Pre-Incident Dates of Surveys** **A-1**
Appendix B **Weekly Pressure Measurements [5]** **B-1**
Appendix C **Comparison of Digitized Temperature Surveys to Raw Data** **C-1**

List of Figures

Figure 1: Dates of Pre-Incident Temperature, Pressure, and Noise Logs 6
Figure 2: Temperature Survey on October 21, 2014 7
Figure 3: SS-25 Temperature Surveys: 1984, 2000–2004 9
Figure 4: SS-25 Temperature Surveys: 1984, 2000–2014 9
Figure 5: SS-25 Temperature Surveys: 2005–2009 9
Figure 6: SS-25 Temperature Surveys: 1984, 2000–2014, 400–800 ft 9
Figure 7: SS-25 Temperature Surveys: 2010–2014 9
Figure 8: SS-25 Temperature Surveys: 1984, 2000–2014, 800–1,100 ft 9
Figure 9: Interpretation of Deflections: Pre-Incident and Post-Incident Temperature Surveys During the Blowout, Depths 100–1,200 ft 10
Figure 10: Noise Survey on June 01, 2012, (Surface–1,200 ft) 11
Figure 11: Noise Survey on November 07, 1991, (Surface–1,300 ft) 12
Figure 12: Pressure Survey from October 21, 2014 13
Figure 13: West Field Injection Line Pressures from October 22–24, 2015 15
Figure 14: Temperature Surveys: November 08, 2015, (Down Pass in Blue) Superimposed on October 21, 2014 (Red) 17
Figure 15: Frew-3 Operations Summary, Temperature Observations June 11–13, 1984 19
Figure 16: Temperature Survey from November 08, 2015, During Blowout [10] 20
Figure 17: Temperature Survey from November 08, 2015, (During Blowout) with Zoomed-in Areas at approximately 300 ft and 900 ft 22
Figure 18: Temperature Surveys During the Blowout [12] 23

Figure 19: SS-25 Temperature Surveys Post-Blowout 25
Figure 20: Temperature Surveys of SS-25, SS-25A, and SS-25B in April–May 2016 26
Figure 21: Wells Surveyed Using the High Precision Temperature Tool (Blue Stars) 27
Figure 22: Pressure and Temperature Survey of P-71 on July 18, 2016 28
Figure 23: Pressure and Temperature Survey of SS-9 on July 21, 2016 28
Figure 24: Pressure and Temperature Survey of SS-5 on July 19, 2016 28
Figure 25: Pressure and Temperature Survey of SS-1 on July 27, 2016 28
Figure 26: DTS Installation and Onsite Calibration Pictures 29
Figure 27: DTS Temperature Surveys Dates 31
Figure 28: SS-25 DTS Temperature Surveys Post-Blowout 0–1,200 ft 31
Figure 29: SS-25A DTS Temperature Surveys Post-Blowout 0–1,200 ft 31
Figure 30: SS-25B DTS Temperature Surveys Post-Blowout 0–1,200 ft 31
Figure 31: SS-25 DTS Temperature Surveys Post-Blowout 0–350 ft 32
Figure 32: SS-25A DTS Temperature Surveys Post-Blowout 0–350 ft 32
Figure 33: SS-25B DTS Temperature Surveys Post-Blowout 0–350 ft 32
Figure 34: SS-25 DTS Temperature Trends 33
Figure 35: SS-25A DTS Temperature Trends 33
Figure 36: SS-25B DTS Temperature Trends 33

List of Tables

Table 1: Dates of Temperature Logs During Blowout 16
Table 2: Pre-Incident Dates of Pressure, Temperature, and Noise Surveys (Chronological) A-1

1 Introduction

Changes in temperature, pressure, and sound occur when a leak is present in wells; temperature, pressure, and noise surveys can detect these changes. This report summarizes surveys before, during, and after the SS-25's blowout. SoCalGas directed the surveys that predated the SS-25 blowout. These data were provided by SoCalGas but was also publicly available on the DOGGR Well Finder website. Blade directed the surveys that were performed after SS-25 was killed as part of the RCA. The following questions are answered in this report:

- Was a preexisting casing integrity issue observed prior to October 23, 2015?
- What was observed during the blowout?
- What was observed after the blowout?

1.1 Abbreviations and Acronyms

Term	Definition
AC	Aliso Canyon
ASCII	American Standard Code for Information Interchange
Blade	Blade Energy Partners
CCL	Casing Collar Locator
CPUC	California Public Utilities Commission
DOGGR	Division of Oil, Gas, and Geothermal Resources
DTS	Distributed Temperature Sensing
EOT	End of Tubing
GR	Gamma Ray
GTC	General Terms and Conditions
HPT	High Precision Temperature
LAS	Log ASCII Standard
MIT	Mechanical Integrity Test
OD	Outside Diameter
P&A	Plug and Abandon
RBMW	Regional Board Monitoring Well
RCA	Root Cause Analysis
SS	Standard Sesnon
SSV	Surface Safety Valve

2 Before the Incident

2.1 Temperature, Pressure, and Noise Surveys

Figure 1 and Table 2 show the dates of the temperature, pressure, and noise surveys performed in the SS-25 from 1974 to 2015 (41 years). The totals are:

- 65 temperature surveys
- 8 noise surveys
- 41 pressure surveys

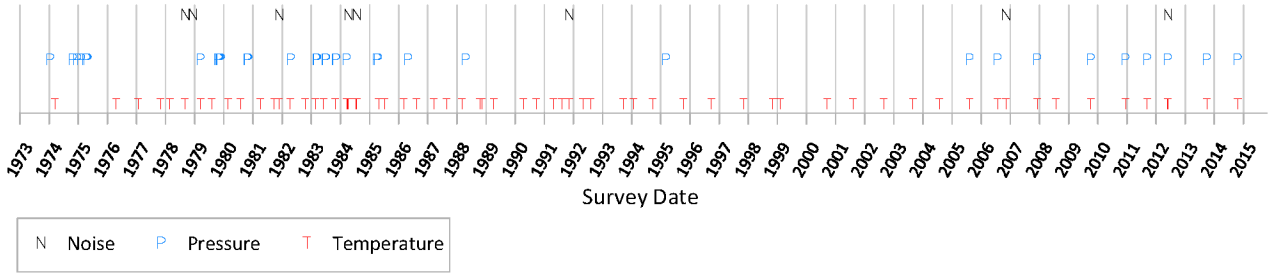

Figure 1: Dates of Pre-Incident Temperature, Pressure, and Noise Logs

2.1.1 Temperature Surveys

In a 1989 DOGGR Aliso Canyon letter [1], project approval was contingent on an annual Mechanical Integrity Test (MIT). The temperature logs were used as the MIT. At least one temperature log was run in SS-25 annually from 1974 to 2014. All the logs were run through tubing with the well shut in at the surface and open to the storage zone. Typically, the surveys were run beyond the end of tubing (EOT), below the 7 in. casing shoe and into the 5.5 in. liner.

Figure 2 shows the temperature survey from October 21, 2014, which is the *last* survey before the October 23, 2015, incident and shows no anomalies related to casing integrity. There is a cooling feature below approximately 8,200 ft related to gas injection and withdrawal; this is not related to a casing integrity issue.

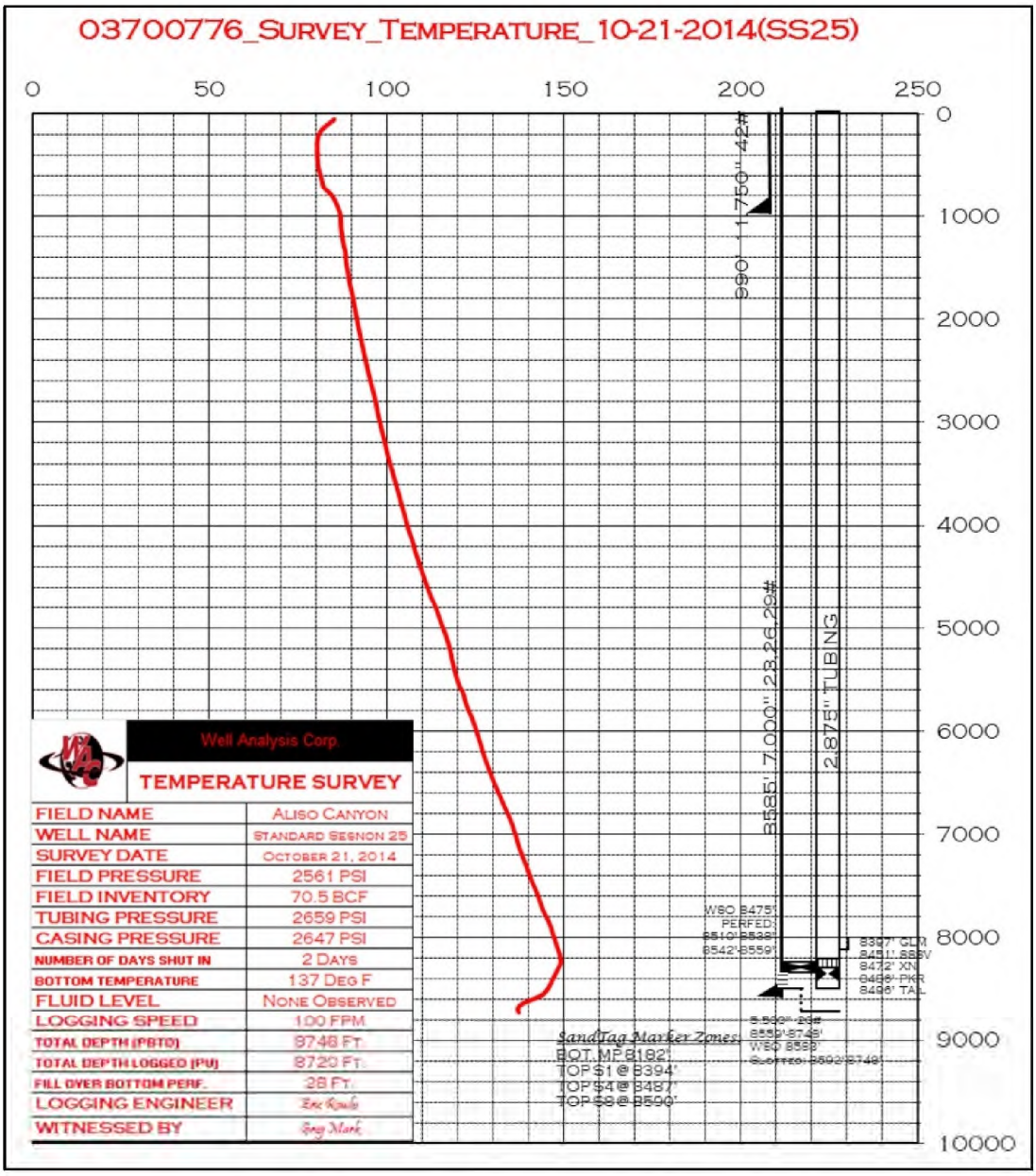

Figure 2: Temperature Survey on October 21, 2014

We analyzed some changes in the slope of the temperature at the top of the wellbore. Eighteen temperature surveys from 1984 and 2000–2014 were digitized from pdf for the top 1,200 ft of the well. Pdf files were provided initially, which is what this work was based on. On February 28, 2019, raw digital data in spreadsheet format (.xls) was provided for 10 years. We compared the digitized data to the raw digital data and showed no significant difference; we have used the digitized data. Appendix C shows this comparison. We evaluated temperature surveys before 2000 but did not include them because the spacing between points was not suitable for detailed analysis. We did include the 1984 survey because it had better resolution. Figure 3, Figure 4, Figure 5, and Figure 7 show the digitized temperature surveys to a depth of 1,200 ft. We did not show the top 100 ft because that region was heavily influenced by the surface ambient temperatures and was not useful.

We observed three small but noticeable deflections at approximately 400–500 ft, 700 ft, and 930–990 ft; the deflections are denoted by arrows on Figure 4, Figure 6, and Figure 8, respectively. The feature at 400–500 ft seemed to be present for almost all the years graphed. We hypothesized this feature to be shallow-geology driven and strongly related to the thermal diffusion of surface temperatures. Considering the major onset of internal corrosion on the 11 3/4 in. casing and external corrosion on the 7 in. casing at 700 ft [2], we surmised the temperature feature at 700 ft was related to the fluid level in the 7 in. by 11 3/4 in. annulus. The cooling feature at 930–990 ft was present on the 1984 and 2000–2009 surveys but was absent on the 2010–2014 temperature surveys. We surmised that this cooling feature was related to the presence of ground water below the Topanga Basalt, which was confirmed to exist in the nearby RBMW-1 water monitoring well [3]. We interpreted that these minor temperature deflections were not related to casing integrity issues. These features are shown again in Figure 9.

Figure 9 shows the 1984 and 2000–2014 pre-incident temperature surveys, plus the post-blowout temperature survey from November 8, 2015. There were no temperature anomalies at 892 ft, the 7 in. casing failure depth, until the temperature survey from November 8, 2015. The three small temperature deflections previously discussed are also highlighted. Although we observed some minor warming and cooling features in the 100–1,100 ft area, we found no temperature indications of the 892 ft casing failure that would have preceded the October 23, 2015 incident.

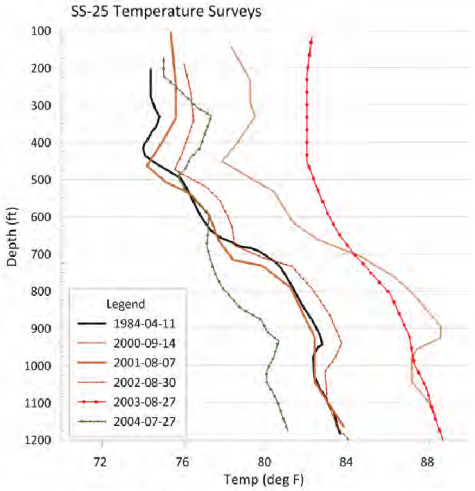

Figure 3: SS-25 Temperature Surveys: 1984, 2000–2004

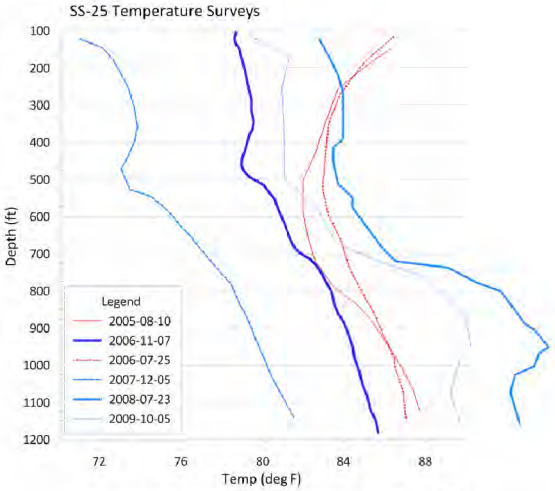

Figure 5: SS-25 Temperature Surveys: 2005–2009

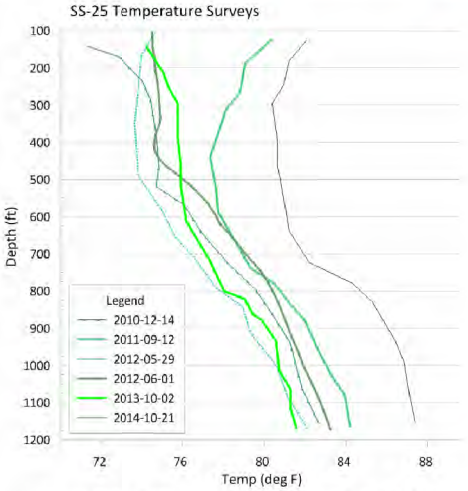

Figure 7: SS-25 Temperature Surveys: 2010–2014

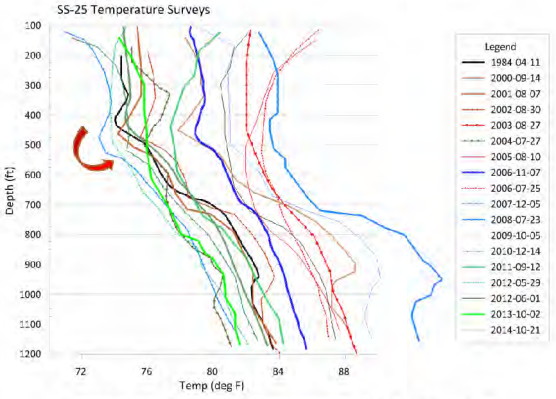

Figure 4: SS-25 Temperature Surveys: 1984, 2000–2014

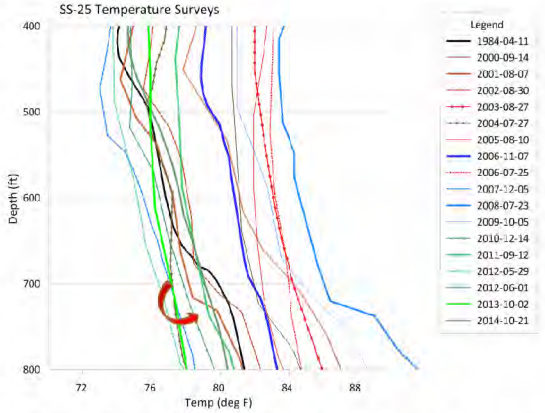

Figure 6: SS-25 Temperature Surveys: 1984, 2000–2014, 400–800 ft

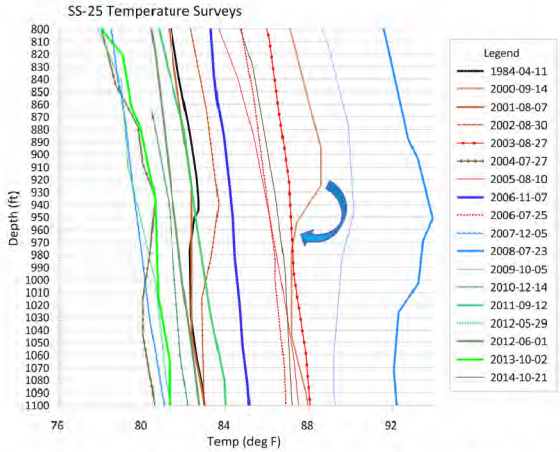

Figure 8: SS-25 Temperature Surveys: 1984, 2000–2014, 800–1,100 ft

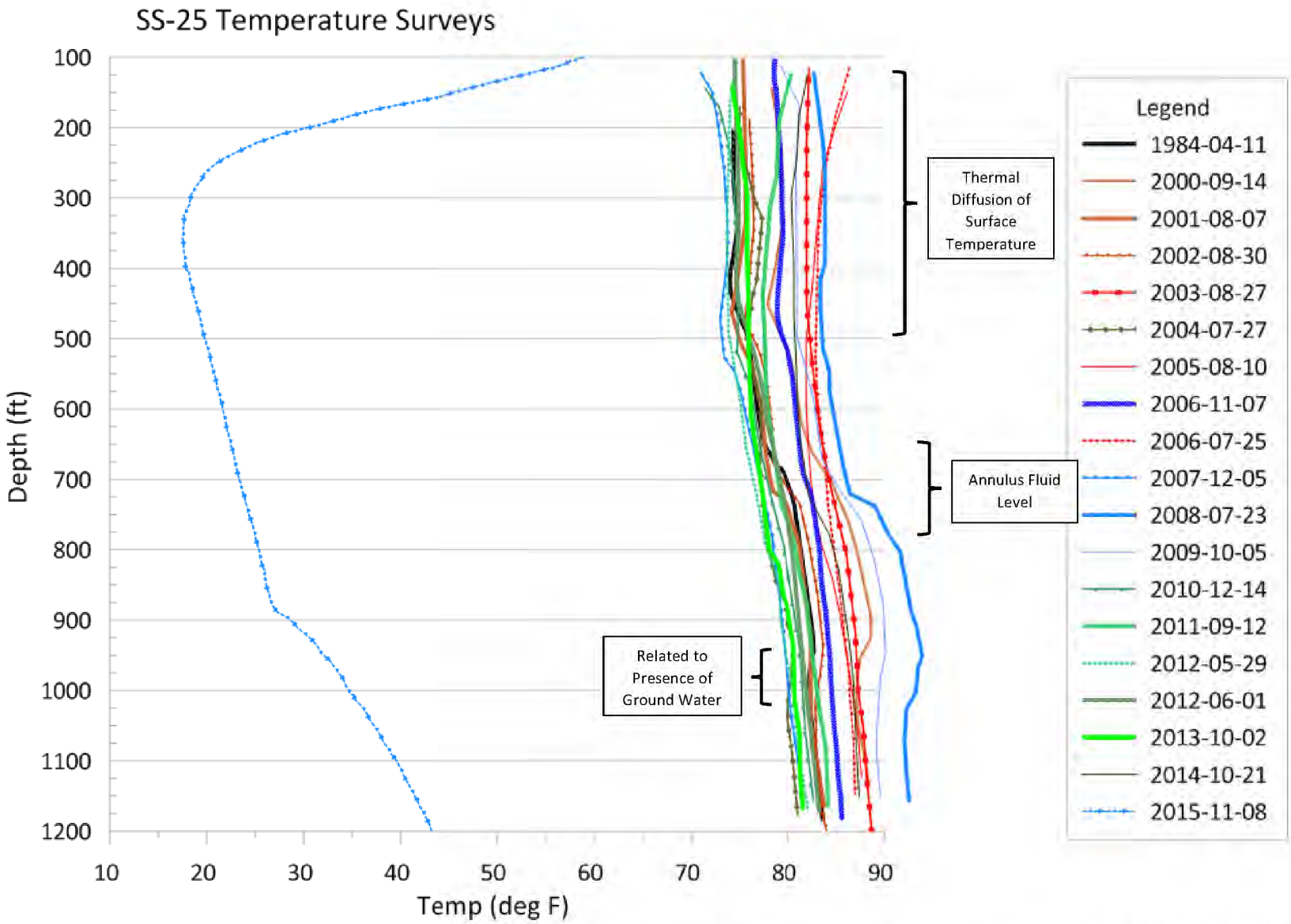

Figure 9: Interpretation of Deflections: Pre-Incident and Post-Incident Temperature Surveys During the Blowout, Depths 100–1,200 ft

2.1.2 Noise Logs

Figure 10 shows the most recent noise survey SoCalGas ran from 8,600 ft to surface on June 1, 2012. This figure only shows the portion from surface to 1,200 ft. We observed no casing integrity-related noise anomalies in this 2012 noise log and in all previous noise logs, with the exception of November 07, 1991.

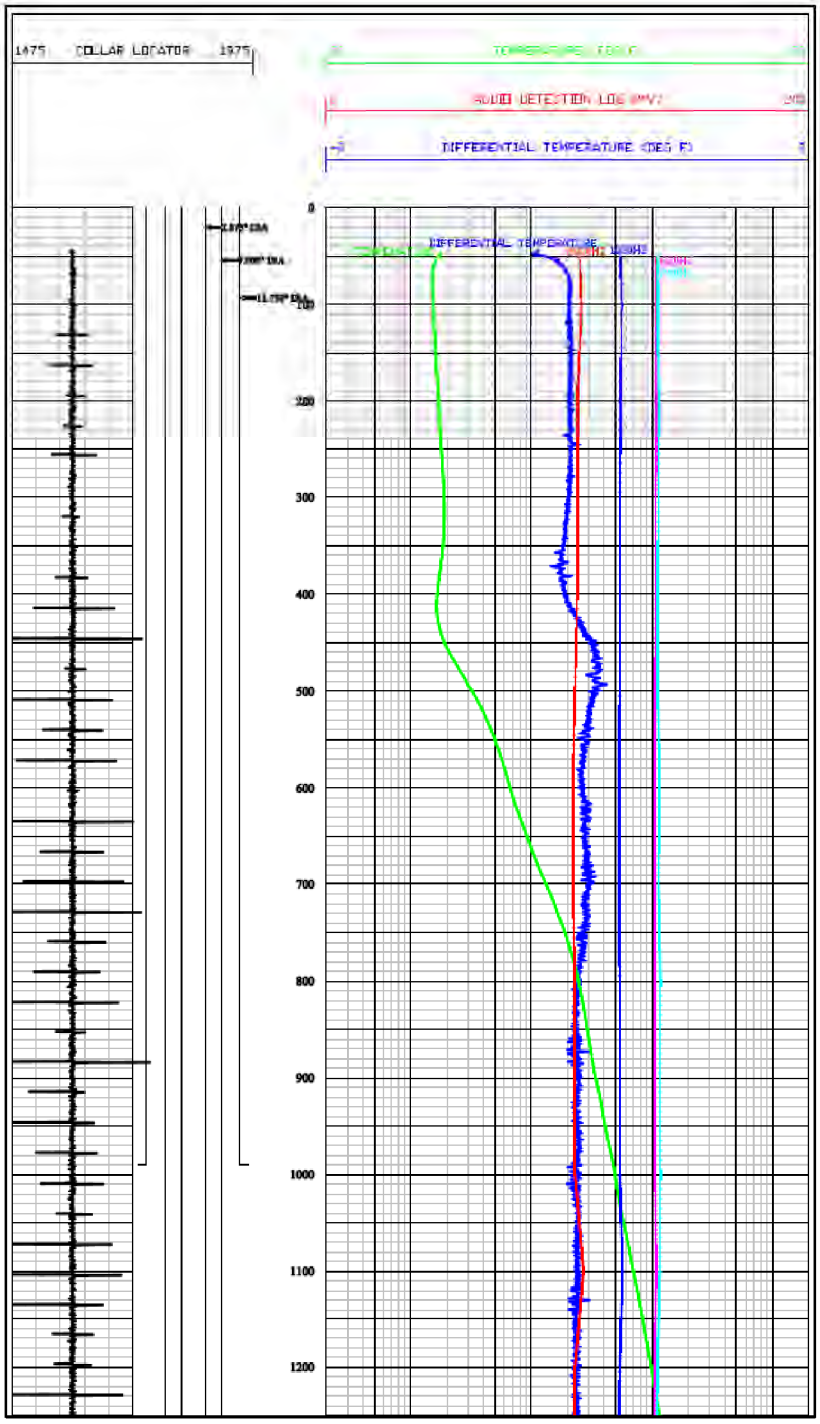

Figure 10: Noise Survey on June 01, 2012, (Surface–1,200 ft)

Figure 11 shows the noise log on November 7, 1991. Highlighted in purple is the temperature survey and it seems consistent with the minor deflections noted in Figure 9. Comments in the log header and noise readings on the graph that are related to shallow noise above 1,200 ft and at 500 ft are highlighted in yellow. We interpreted that the activities in "Bled Casing Kill Line on Well 25 A" were affecting the noise log of SS-25 at 500–1,200 ft. The next noise log was 15 years later on November 7, 2006. It was conducted at a higher shut-in tubing pressure of 2,808 psi than the 1991 noise log, which was conducted at 2,600 psi shut-in tubing pressure. No noise anomalies were detected. As discussed in the previous section, no shallow temperature anomalies related to casing integrity were detected.

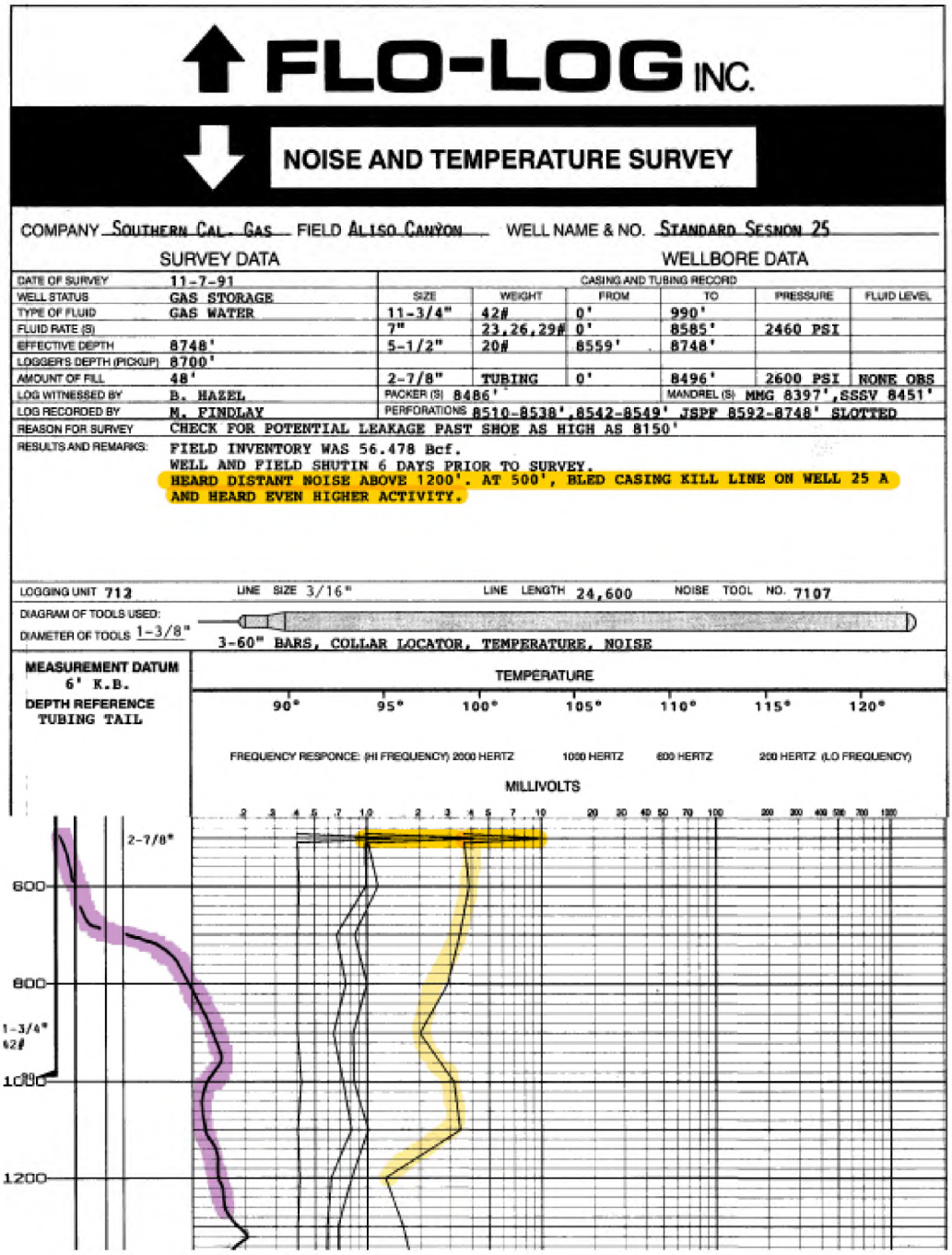

Figure 11: Noise Survey on November 07, 1991, (Surface–1,300 ft)

2.1.3 Pressure Surveys

Although SoCalGas ran 41 pressure surveys in 41 years, neither the DOGGR project approval letter [1] nor the SoCalGas Gas Inventory-Monitoring, Verification, and Reporting Company Operations Standard Gas Operations policy [4] required pressure surveys. Figure 12 shows the most recent pressure survey from October 21, 2014, run to 8,720 ft. There appears to be an error; the title block entry for "Tubing Pressure" (2659 psi) does not match the graphed data, which appears to be between 2550–2600 psi. Despite this error, no pressure anomalies are observed in the graphed data.

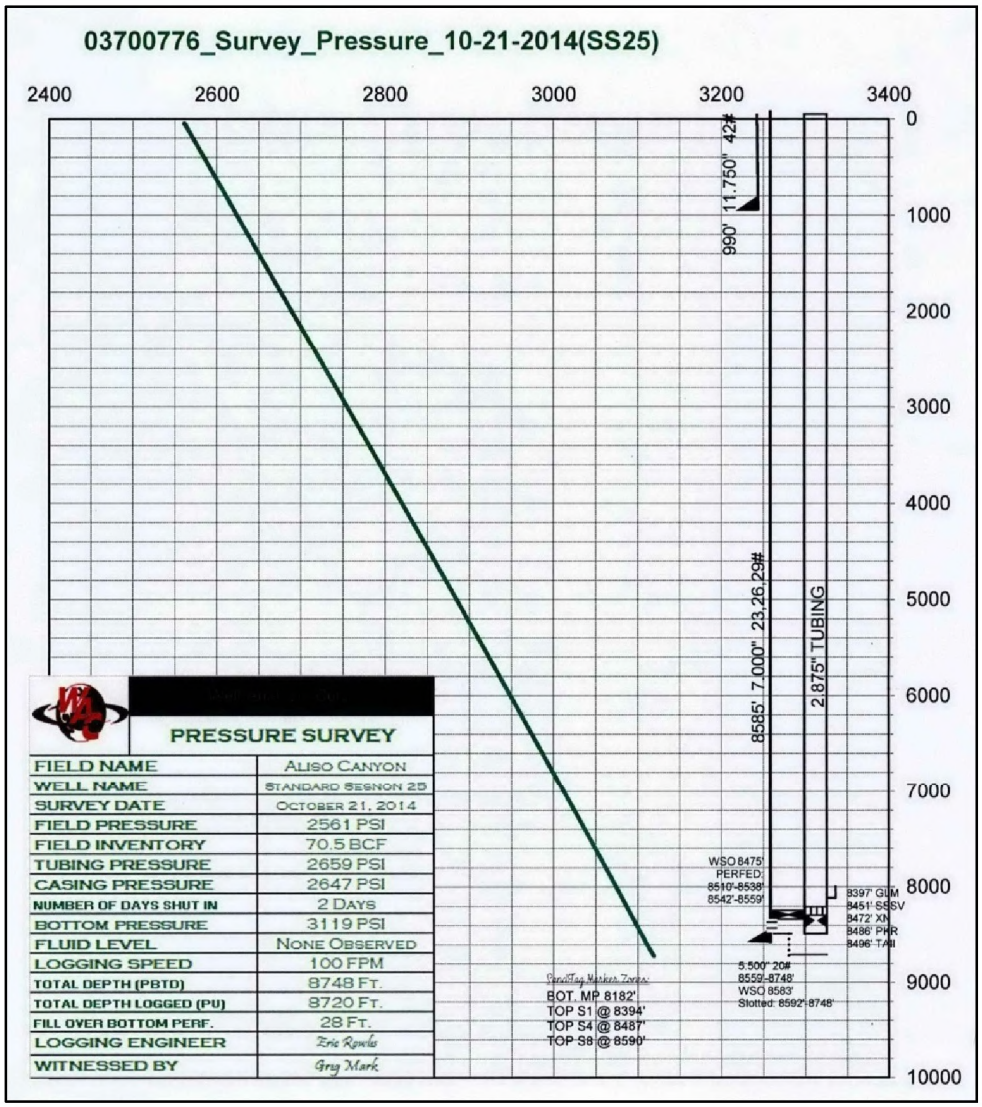

Figure 12: Pressure Survey from October 21, 2014

Because the pressures surveys are not of great use in determining the presence or location of a casing leak, they were not investigated in great detail. These pressure surveys provide a direct measurement of the pressures in the tubing only (and not the casing). If a leak in the casing were to occur, the pressure change would not transmit into the tubing at that same depth.

Another reason why pressure surveys are not of great use is because they differ from pressure tests. For pressure surveys, the well is open to the storage zone, and any gas that escapes into a casing leak is replenished by the storage zone; this is much different than in a pressure test. Additionally, the pressures observed during these pressure surveys are the shut-in pressures. It is important to highlight that pressure profiles during shut-in are *lower* than during standard gas injection operations. In other words, pressure surveys are taken at times when the casing is under less pressure than during gas injection.

2.1.4 Surface Pressure Measurements

SoCalGas took the weekly pressure measurements from the tubing and the production and surface casings' annuli. Appendix B shows these manually-collected pressure readings for the SS-25, SS-25A, and SS-25B wells for the year 2015 [5]. The surface locations of these three wells are within 40 ft of each other on the same well site. No sustained surface casing pressure was observed in SS-25 for the weeks leading up to the incident on October 23, 2015.

The SS-25 well site was last inspected on October 22, 2015, as part of a daily well inspection and no issues were detected then.

2.1.5 Injection Line Pressure

The first detection of an issue at SS-25 was the smell of gas reported at 15:15 on October 23, 2015, while SS-25 was on injection. The injection pressure was being recorded continuously at various locations in the field. The West Field Injection Line Y-Trench pressure is the closest upstream pressure transducer to SS-25 [6]. Figure 13 shows the pressure data from October 22–24, 2015. In the 24 hours that preceded the gas odor detection, gas injection occurred until approximately 16:00 October 22, 2015; a 12-hour period of no injection was then followed by the resumption of gas injection from about 04:00 on October 23, 2015. The pressure drop was approximately 30 psig when the gas injection stopped.

At 15:20, a team arrived at the SS-25's well site. At 15:30, they closed the injection header valve and observed the 3 in. WKM Surface Safety Valve (SSV) activated into the closed position almost immediately. Tubing, production casing, and surface casing pressure were monitored from that point onwards. These pressures are studied in the SS-25 Well Nodal Analysis with Uncontrolled Leak Estimation report [7] where a very large amount of gas was predicted to flow through the casing failure.

The West Field Injection Line Y-Trench pressure provided an important clue as to when the casing failure may have occurred. Had the casing failure occurred before or during the no gas injection period that began on October 22, 2015, then the West Field Injection Line Y-Trench pressure would have dropped substantially as the gas in the injection pipeline leaked through the failed SS-25 casing, which had a high flow rate capability. Since no substantial pressure drop in the West Field Injection Line pressure was observed during the 12 hours of no gas injection, it is likely that the casing failure occurred sometime after the start of injection on the morning of October 23.

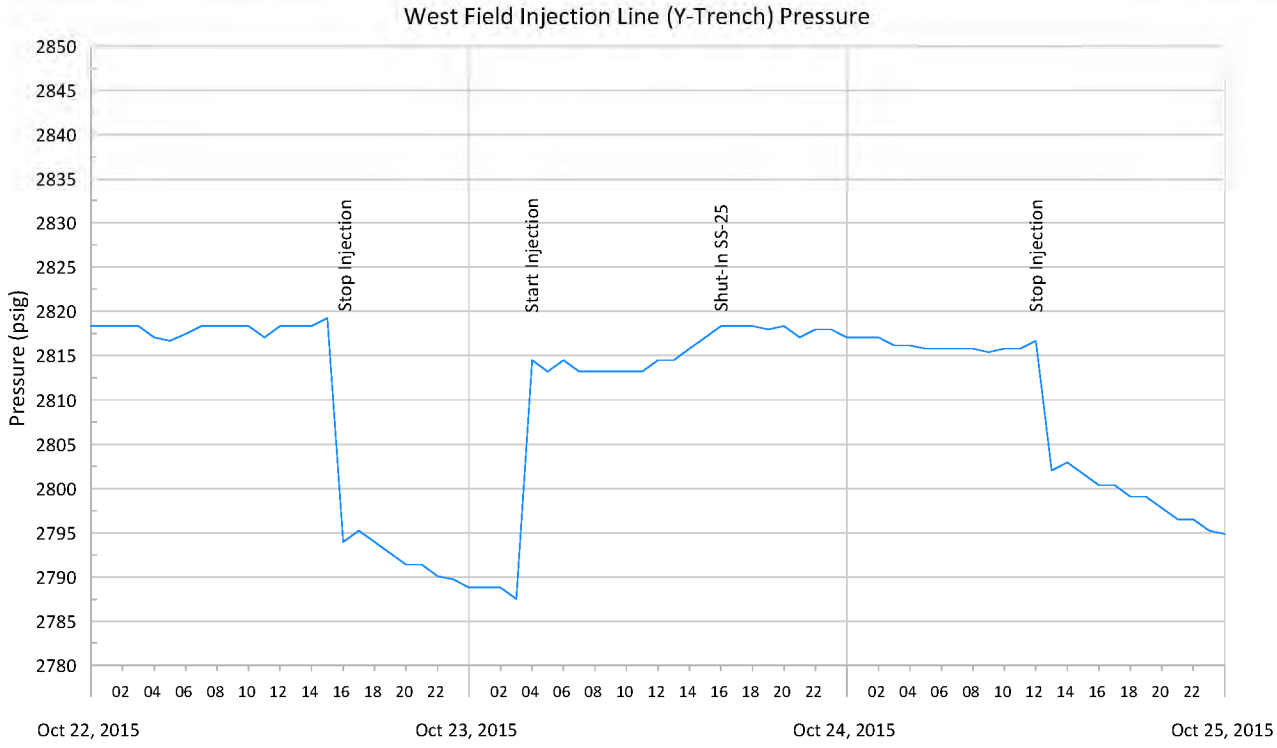

Figure 13: West Field Injection Line Pressures from October 22–24, 2015

3 During the Blowout

3.1 Temperature

Table 1 shows the dates of the temperature and other logs run during the blowout. All the logs were run through the tubing to a depth greater than 8,000 ft.

Table 1: Dates of Temperature Logs During Blowout

Date	Type
November 8, 2015	Temperature, Pressure, Spinner, GR, and CCL
November 9, 2015	Temperature, Noise
November 30, 2015	Temperature, Noise
January 15, 2016	Temperature, Pressure (in memory, no depths)
January 23, 2016	Temperature, Pressure

3.2 Temperature Profile Comparison

The 7 in. casing failure on October 23, 2015, caused a substantial change in the SS-25 wellbore temperature profile. Figure 14 shows the November 8, 2015, temperature profile (in blue) overlaid on an image of the October 21, 2014, temperature profile (in red). The November 08, 2015, data is from the down pass Log ASCII Standard (LAS) file [8]. For comparison, the two profiles' x and y axes are on the same scale. The two temperature curves pre- and post-failure are *substantially* different. The difference between the temperature profiles at 3,600 ft is approximately 14°F. The temperatures at 350 ft were approximately 18°F and 80°F for a difference of 62°F. The highest temperature logged on November 08, 2015, was approximately 129°F at 8,430 ft.

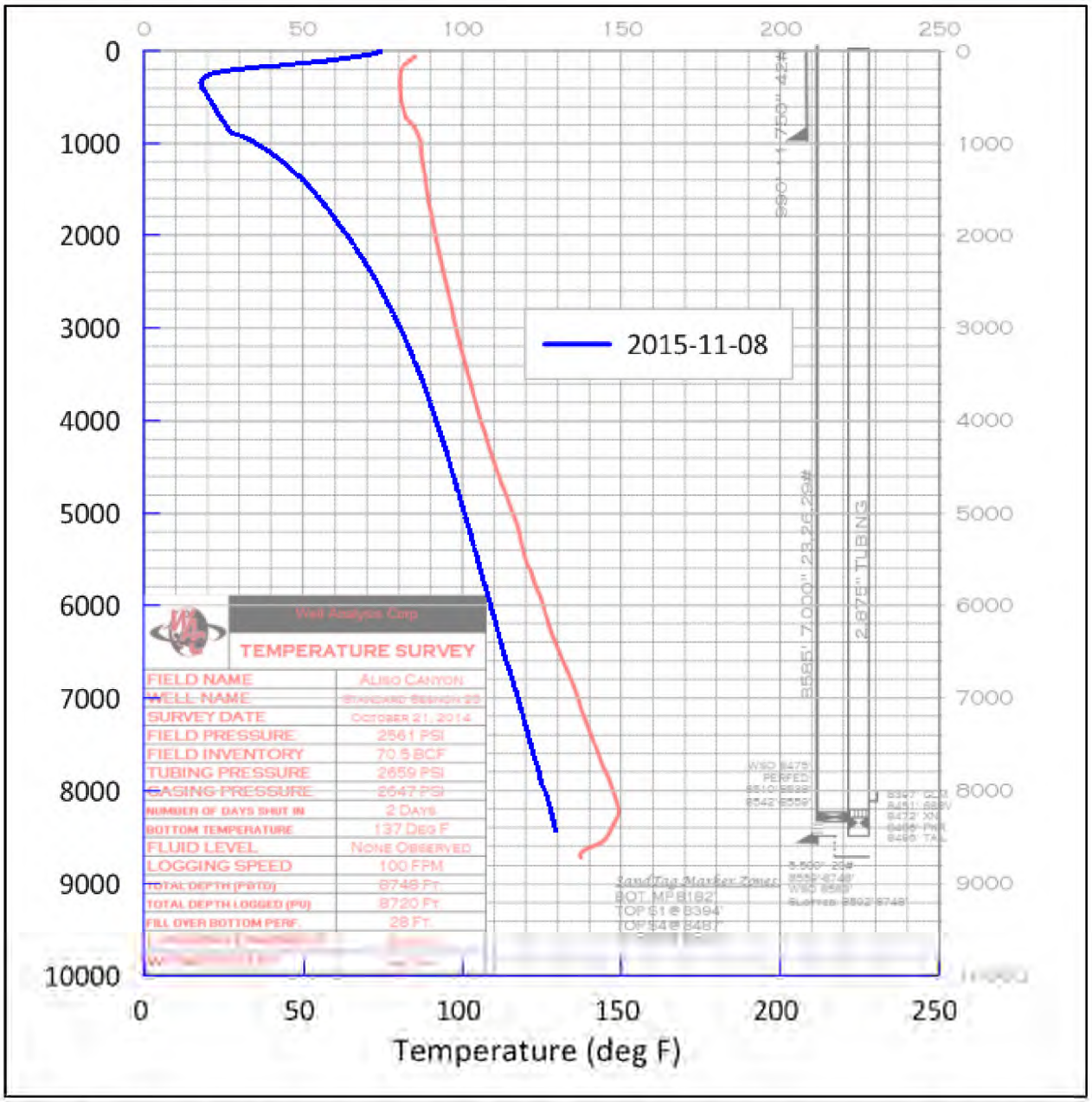

Figure 14: Temperature Surveys: November 08, 2015, (Down Pass in Blue) Superimposed on October 21, 2014 (Red)

Figure 15 shows the well activity reports during temperature logging of the Frew 3 (F-3) blowout in 1984. The report entries for June 11, 1984, highlighted in yellow, indicate that the highest temperature observed was only 80°F. Subsequently, the June 13, 1984, temperature survey yielded a range of 38–82°F. Freezing temperatures like the ones on SS-25 were *not observed* in F-3, although lower bottom hole temperatures were observed in F-3.

Highlighted in orange is an entry that both surveys on June 11 and 13, 1984, "could not be run through the tubing" and a remark regarding possible hydrates deep within the well [9]. It is possible that this restriction was not caused by hydrates, but instead, by the force from the upward gas flow at the EOT, which may have prevented the tools from exiting the end of the tubing.

Similar to 1984, the SS-25 November 8, 2015, temperature, pressure, spinner, gamma ray (GR), and casing collar locator (CCL) log was unable to reach the end of the tubing. The log analyst reports that the spinner's impeller was "exposed to an extreme flow rate or velocity above the design limits of the spinner" [10]. As a result of the spinner's failure, the flow rate of the escaping gas was not calculated.

11

WELL ACTIVITY REPORTS FOR FREW 3

DATE	ACTIVITY/REMARKS
8/18/81	Pruett pulled SSSV, cost $515.00
8/19/81	Pruett pulled choke, cost $265.34
8/20/81	Ran temperature survey
8/31/81	Triangle ran sound log, cost $3,172.04
9/15/81	Otis ran SSSV, test OK, cost $1,235.00
10/27/81	Otis rigged up to pull SSSV, no complete
12/3/81	Otis set SSSV & BHC, will test on 12/4
12/4/81	Otis set SSSV & BHC, test OK
1/11/82	Pruett pulled SSSV
1/16/82	Pruett pulled BHC, blew-out and re-ran BHC
1/17/82	Pruett pulled BHC, blew-out second time
1/18/82	Sand testing
3/30/82	Ran temperature survey
10/20/82	Ran temperature survey, anomaly @ 7650'. Run A/A
12/16/82	Noise log run, no noise
6/8/83	Ran temperature survey, no anomaly
12/12/83	Ran temperature survey, no anomaly
4/2/84	Ran temperature survey, cooling anomaly at shoe
4/10/84	Ran detail temperature survey, confirms cooling from 6750'-7791' at shoe. A noise log will be run at high inventory due to low structural position of well.
6/10/84	Operations noted sudden jump in surface annulus pressure to 550#; repeated attempts to blowdown annulus were unsuccessful
6/11/84	Ran temperature survey which looked very abnormal; hottest temperature noted was around 80 F so assumed temperature bomb had malfunctioned.
6/13/84	MacCarlisle checked seals on wellhead, neither seal was leaking. Ran temperature survey which showed extreme cooling. Surface temperature was 38 and temperature @ 7750' was only 82. It should be noted both surveys (11th & 13th) could not be run through the tubing, but the survey run on 4/2/84 could go through; possible hydrates (?) all the way to SSSV ports. Continued trying to blowdown annulus, but it will rise back to 460# from 250# in minutes.
6/14/84	Baker set 500 Bbl tank on site for well kill. Test center came out and took sample of gas coming from annulus. Helium content on annulus was 560 ppm thus showing it was definitely Aliso gas and it was coming from a leak somewhere. Checked DA-2 (Del Aliso 2) which is in close proximity but only showed 24 ppm. No movement in that direction. Annulus pressure on F-4 increased abruptly from 30# to 180#. Looks like definite migration to F-4.

84 Frew 3 Well Documentation from SoCal.pdf

AC_BLD_0031722

Figure 15: Frew-3 Operations Summary, Temperature Observations June 11–13, 1984

Figure 16 shows a section of the November 8, 2015, temperature data. The down pass (red) and up pass (blue) show significant shallow anomalies; note that 892 ft is the depth of the 7 in. casing failure. The analyst's comments annotated on the figure regarding the flow of gas through a surface casing leak were incorrect. We know now, from subsequent logging and camera images, that significant holes were found in the surface casing from approximately 134–300 ft and that the 7 in. casing had parted at 892 ft. The gas flow on November 08, 2015, was out of the ruptured and parted 7 in. casing, up to the surface casing holes, and then away from the wellbore.

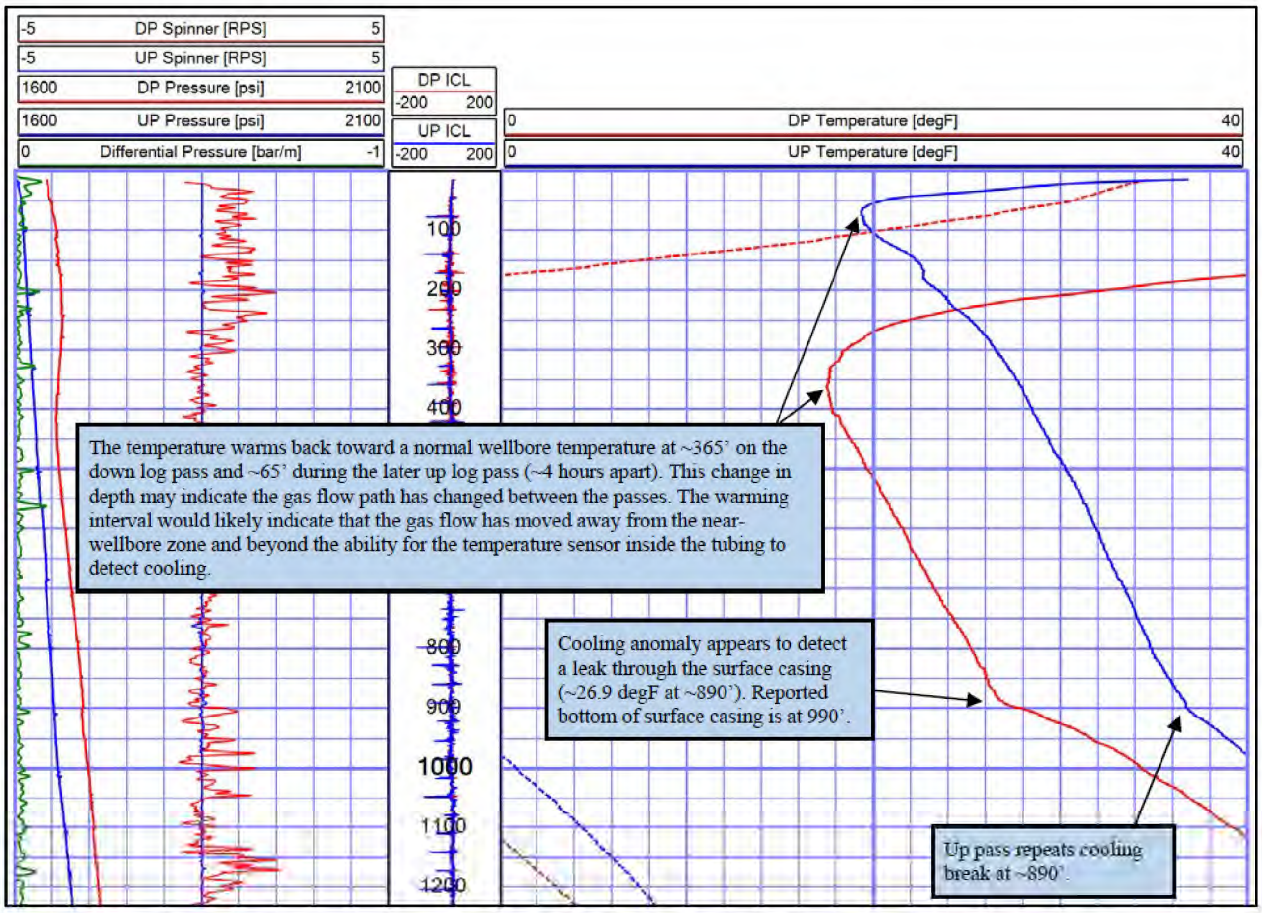

Figure 16: Temperature Survey from November 08, 2015, During Blowout [10]

Figure 17 shows the digital data from the November 8, 2015, down pass temperature survey, which is considered the best temperature data set because there are no telemetry or data quality issues and it is the earliest post-blowout temperature survey. The large change in temperature at 892 ft is best observed in the furthest right panel; we interpret this to be the temperature change occurring at the 7 in. casing rupture or part. We presume that the gas was traveling upward because the temperature decreased in the wellbore. Since no temperature anomaly was present at the surface casing shoe of 990 ft, the interpretation is that no gas was going through the shoe on November 8, 2015. The cooling was most prominent at 300–400 ft, which is interpreted as the area where the gas was exiting the casing.

Figure 18's left graph shows the temperature surveys from November 9 and November 30, 2015. The right graph adds the November 08, 2015, and January 23, 2016, temperature surveys. Warmer temperatures were observed as the blowout continued; this was related to a lower gas rate as a result of field-wide withdrawal, the lack of back pressure as the crater grew, and the 2 in. annulus valve unscrewing from the casing head and dropping into the crater during one of the kill attempts. A separate supplementary report [11] elaborates further on the rates, pressures, and temperatures during the blowout.

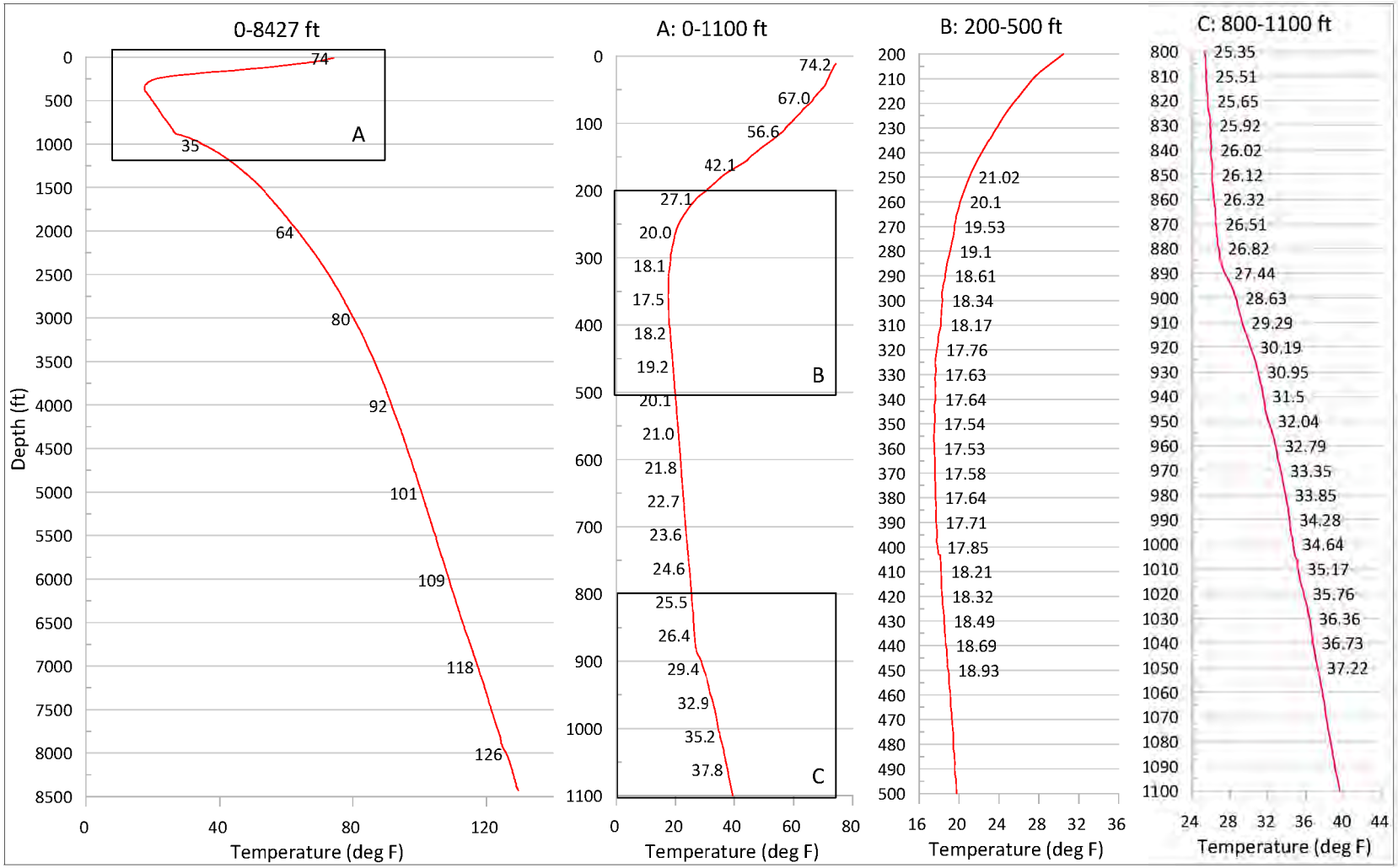

Figure 17: Temperature Survey from November 08, 2015, (During Blowout) with Zoomed-in Areas at approximately 300 ft and 900 ft

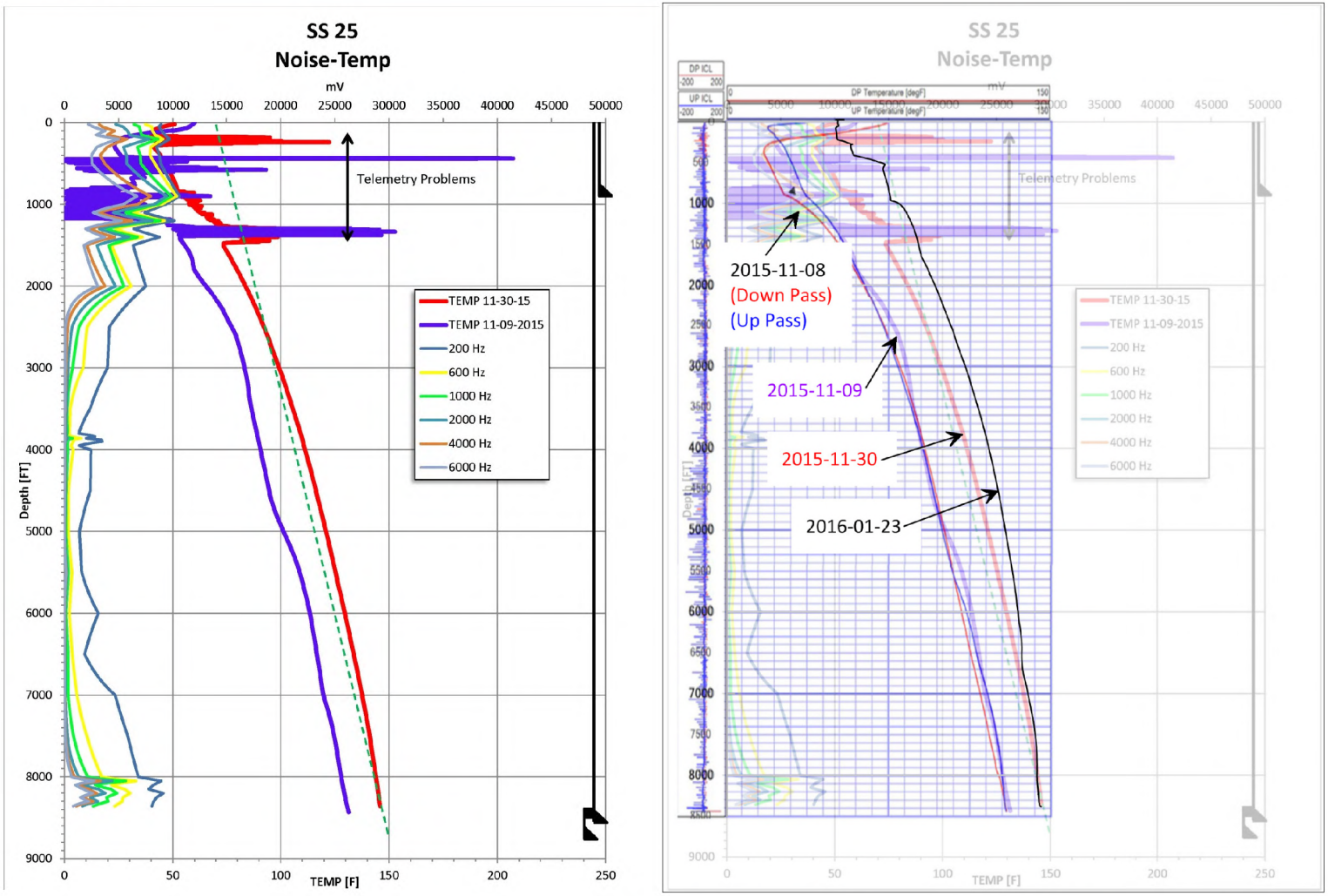

Figure 18: Temperature Surveys During the Blowout [12]

4 After the Well Kill

After the SS-25 well was killed in February 2016, at Blade's request, SoCalGas performed additional temperature surveys for the three wells on the SS-25 well site and four wells adjacent to the SS-25 well site. At Blade's request, SoCalGas also arranged for the installation of fiber optic lines in the three SS-25 well site wells at various times in 2016–2018. The fiber optic lines were used for distributed temperature sensing (DTS). This section provides the details of all the post-kill temperature measurements.

4.1 Wireline Temperature Surveys

Figure 19 shows the four wireline temperature surveys performed on the SS-25 after the well kill and the November 08, 2016 temperature survey—the first captured after the incident started. The February 16, 2016 temperature survey (blue) shows the cooling that occurred in the top 500 ft of the well; the lowest temperature it recorded was in the 60s°F. This survey was likely strongly impacted by the warm kill fluids originating from the P-39A relief well.

A subsequent temperature survey on April 12, 2016 (black) shows two shallow cool locations in the high 40s°F (approximately 20°F cooler than the February 16, 2016 survey). The temperature data was acquired using the High Precision Temperature (HPT) logging tool with a running speed of 15 ft/min, which is much slower than the field-typical 100 ft/min. The two distinct cool areas are demarked as upper and lower lobes. These lobes were observed during the earliest blowout temperature survey from November 08, 2015 (Figure 14) but not in the later blowout temperature surveys.

4.1.1 SS-25A and SS-25B

Figure 20 shows the HPT temperature surveys of SS-25, SS-25A, and SS-25B from April to May 2016. There are some general observations:

- The cold temperatures and lobes observed in SS-25 were also evident on the adjacent wells SS-25A and SS-25B.
- The temperature of the upper lobe was colder than the lower lobe.
- The SS-25's temperature was about 10°F colder than SS-25A and SS-25B in the lower lobe.
- The SS-25A and SS-25B's temperatures were about 4–5°F colder than SS-25 in the upper lobe.

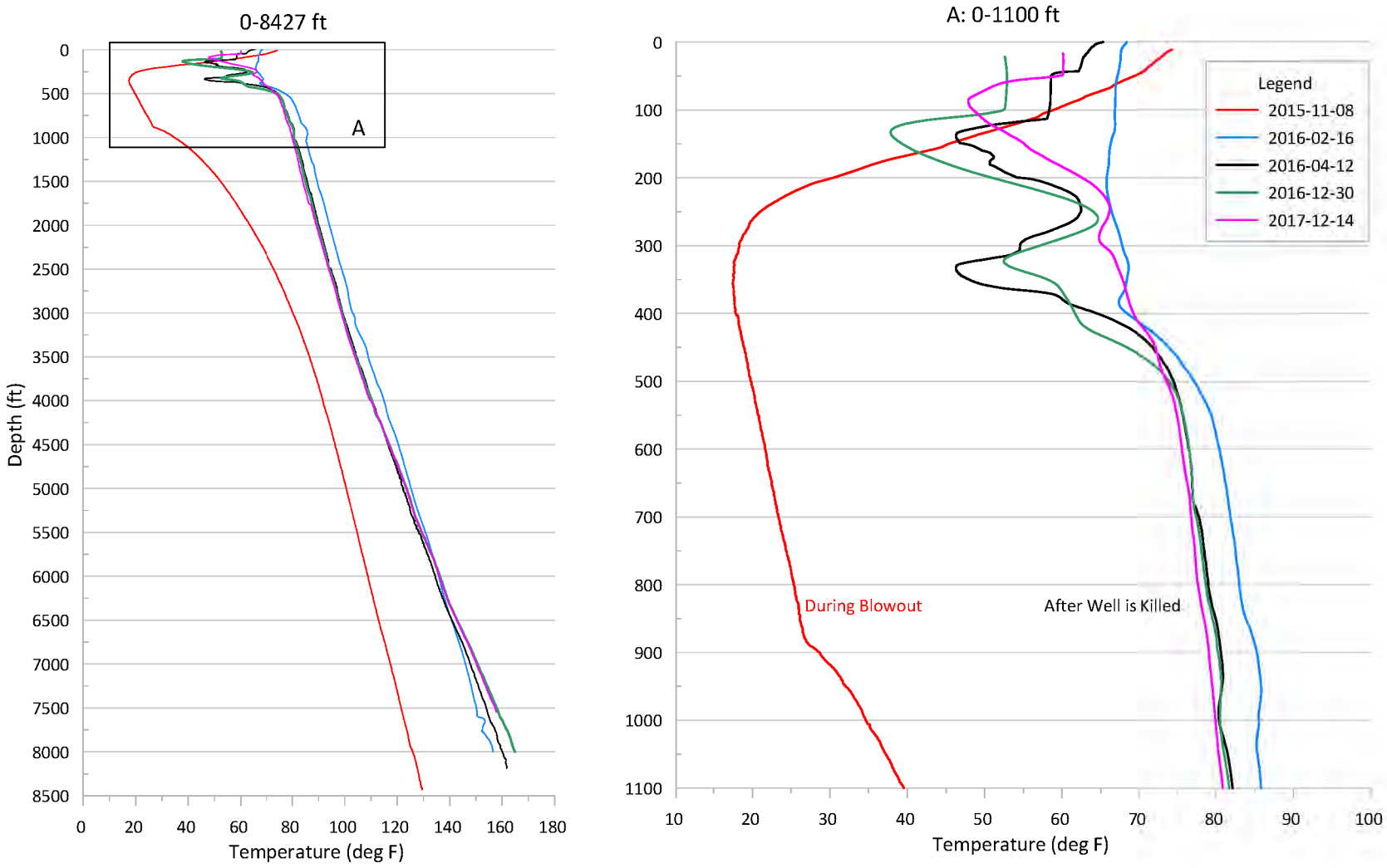

Figure 19: SS-25 Temperature Surveys Post-Blowout

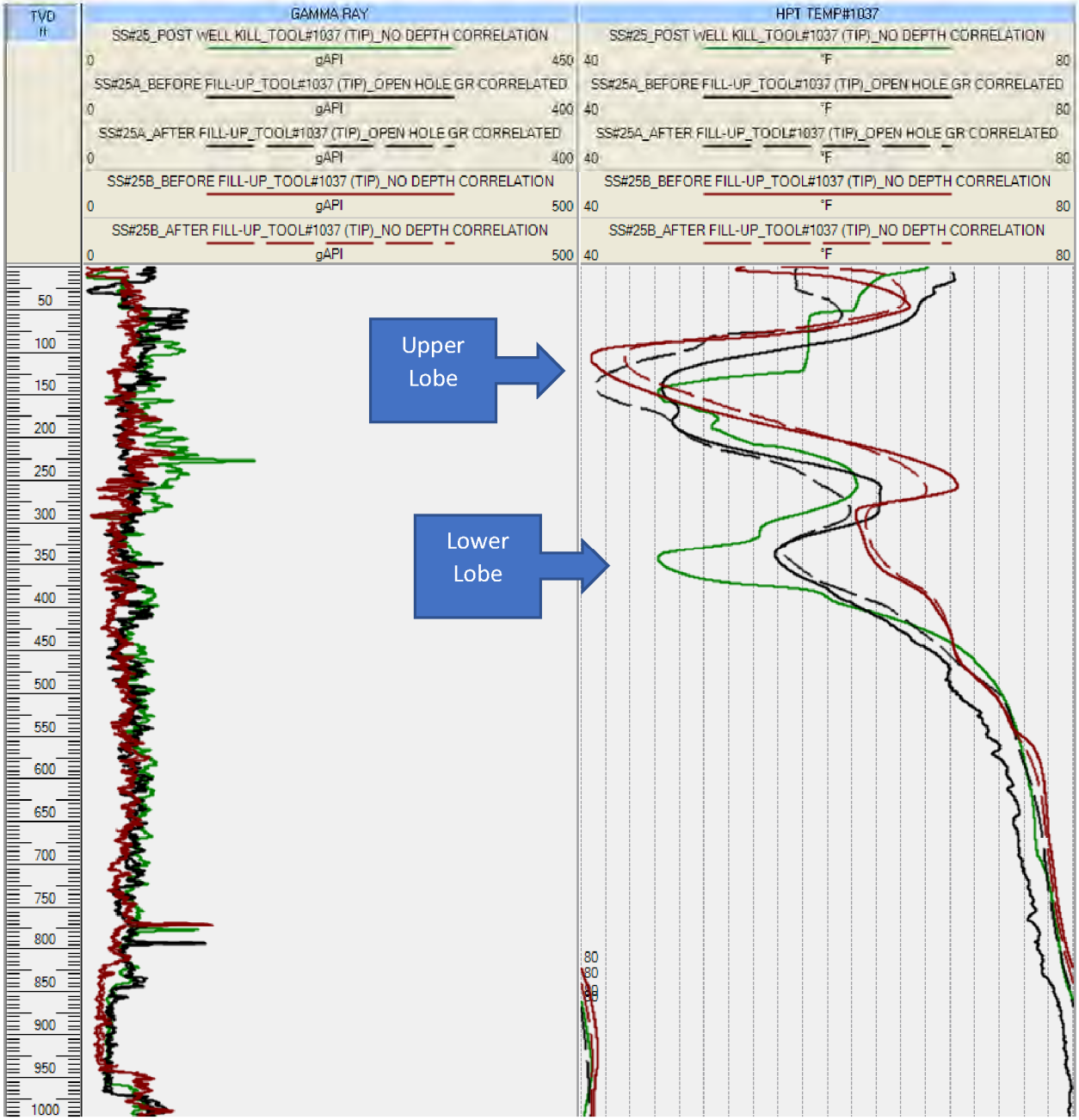

Figure 20: Temperature Surveys of SS-25, SS-25A, and SS-25B in April–May 2016

4.1.2 Offset Wells Beyond the SS-25 Well Site

Because SS-25 and adjacent wells on the same well site (SS-25A and SS-25B) had exhibited low temperatures in April 2016, additional wells were selected for investigation. At Blade's request, SoCalGas surveyed four offset wells around SS-25 in July 2016, namely P-71, SS-1, SS-5, and SS-9. Figure 21 shows the location of the wells surveyed using the HPT tool. We selected these wells because they were in close proximity to, and radially spread out from, the SS-25 well site. We were keenly interested in P-71 because we suspected shallow gas migration due to pressure observations of 140 psi from shallow production casing perforations on November 23, 2016 [13]. We were also interested in SS-5 because SoCalGas had historically used it as an observation well.

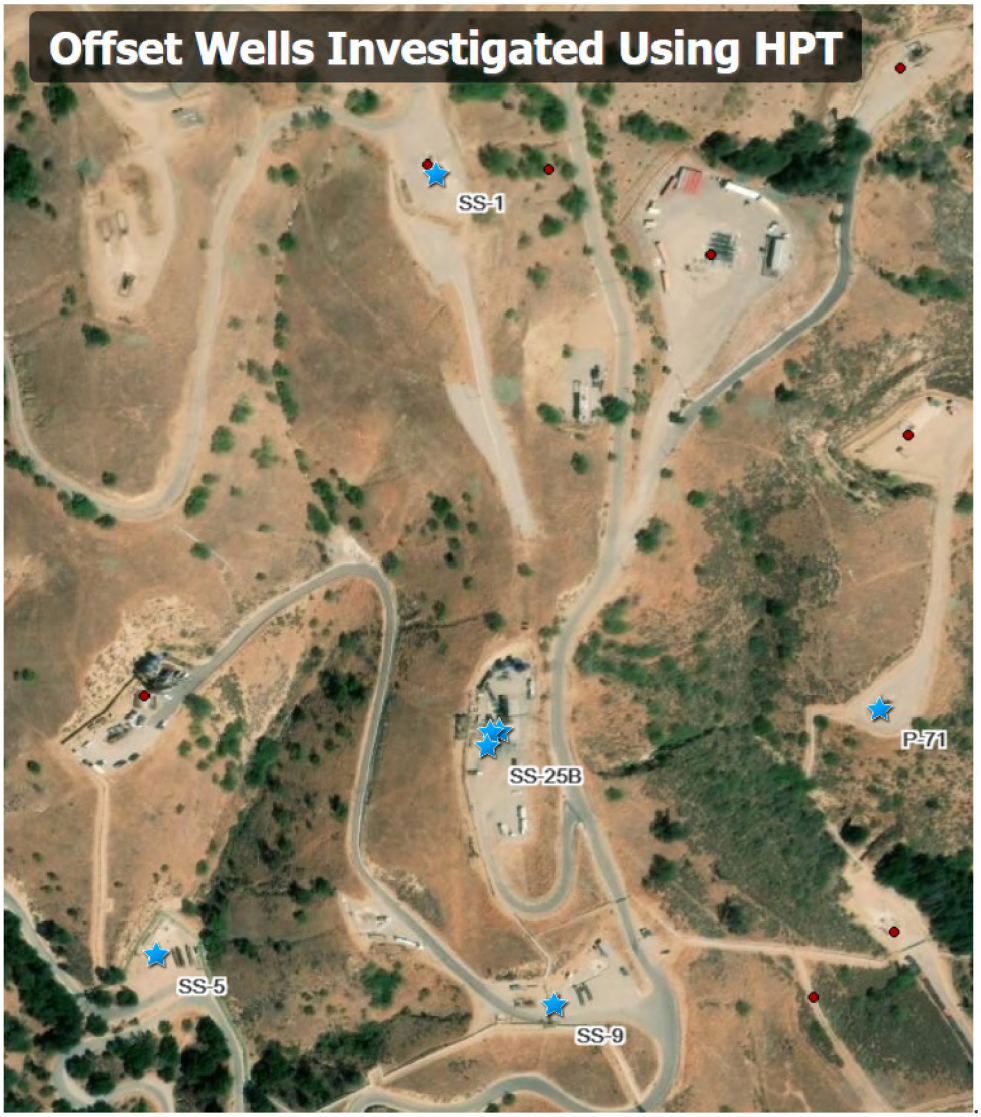

Figure 21: Wells Surveyed Using the High Precision Temperature Tool (Blue Stars)

Figure 22, Figure 23, Figure 24, and Figure 25 show the HPT temperature surveys from P-71, SS-9, SS-5, and SS-1 respectively. These wells *did not show* the same cold temperature lobes observed in the SS-25 wells.

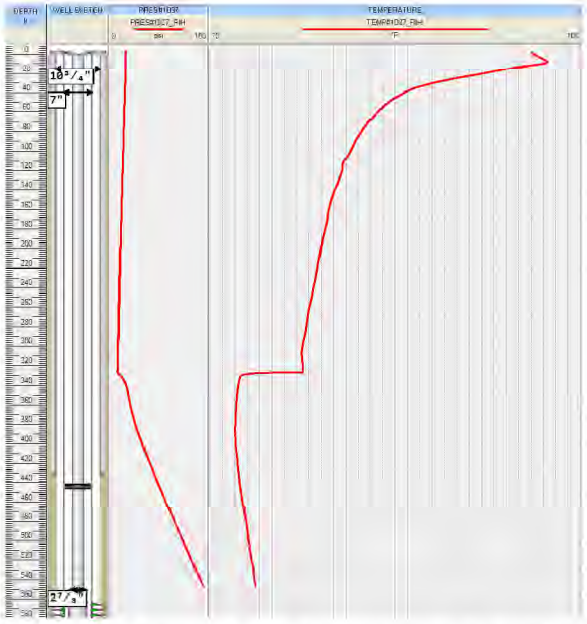

Figure 22: Pressure and Temperature Survey of P-71 on July 18, 2016

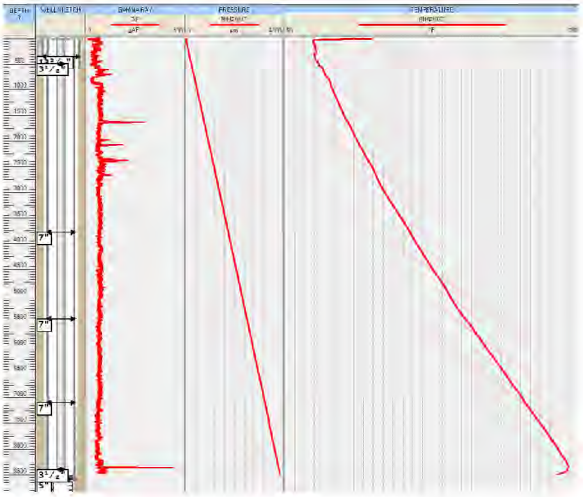

Figure 23: Pressure and Temperature Survey of SS-9 on July 21, 2016

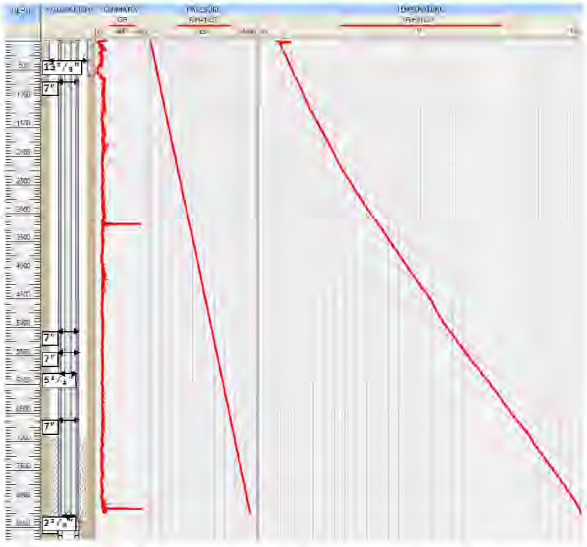

Figure 24: Pressure and Temperature Survey of SS-5 on July 19, 2016

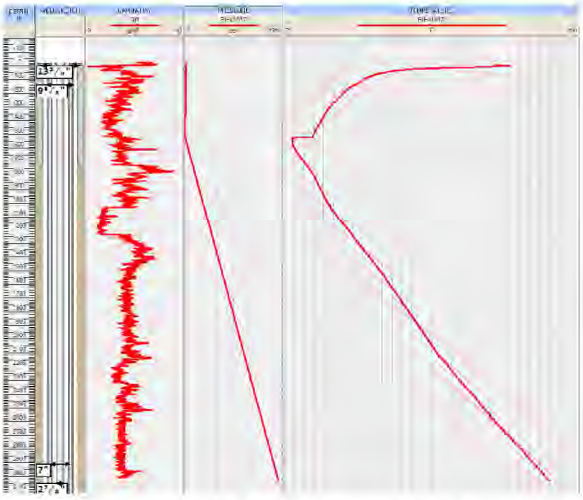

Figure 25: Pressure and Temperature Survey of SS-1 on July 27, 2016

4.2 Distributed Temperature Sensing

The wireline-deployed HPT surveys in April–May 2016 in SS-25, SS-25A, and SS-25B confirmed shallow cold areas. The reason why we see a limitation in the wireline surveys is that they were a snapshot in time, and multiple deployments to the well were required to get a trend of the temperatures. To understand what was happening to the well temperatures over a period of time, the Schlumberger WellWatcher BriteBlue Distributed Temperature Survey system was deployed to the SS-25, SS-25A, and SS-25B wells. The fiber optic line was encapsulated within a hollow 1/4 in. outside diameter (OD) stainless steel line (Inconel 825) and spool-mounted. The fiber optic line was installed within the production tubing to a depth greater than 1,200 ft and was suspended from an anchor above a pack-off mounted on the production tree swab valve. The DTS system provided a temperature profile every approximately 3.3 ft. The data for each point was averaged for 30 seconds and then averaged over a 30-minute period.

4.2.1 Distributed Temperature Sensing Calibration

Schlumberger performed a shop calibration of the DTS system prior to deployments and provided Blade with the calibration reports. Since cold temperatures are not common in wells, Blade performed an independent calibration of the DTS system onsite to confirm the accuracy of the temperatures and the depth. The AC-RCA SS-25A DTS Validation Report [14] contains the test protocol and results. Based on the onsite tests, the reported depths and temperatures by the DTS system were a good representation of the wells. Figure 26 shows pictures of a typical installation of the DTS system (upper left) and pictures of the onsite calibration setup.

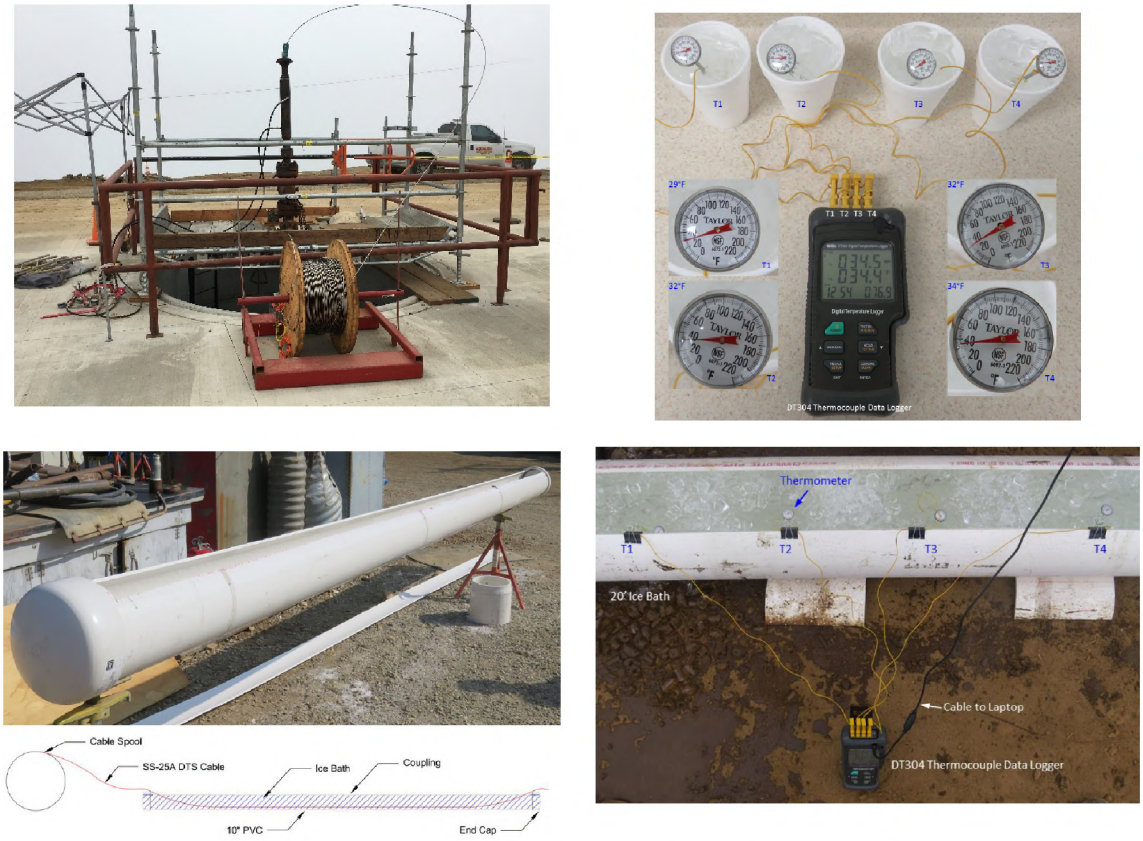

Figure 26: DTS Installation and Onsite Calibration Pictures

4.2.2 Distributed Temperature Sensing Observations

Figure 27 shows the date ranges for when the DTS was installed in SS-25, SS-25A, and SS-25B. Schlumberger collected the first DTS survey in SS-25B on August 02, 2016. The final DTS survey in SS-25A was on August 13, 2018. Each dot represents a survey. The frequency of the DTS surveys was originally twice each week but was later reduced to weekly and then biweekly. Blade directed this change in frequency because the temperatures in the well were not changing significantly. The removal of the DTS system from some wells was required due to well operations, but, overall, there was a DTS system installed in at least one well for the two-year period.

Figure 28 shows the DTS data for SS-25. Only depths to 1,200 ft are shown because there were no changes in temperature deeper than 1,000 ft, and most of the temperature features of interest occur in depths shallower than 350 ft. Figure 31 shows the same SS-25 DTS data zoomed in to the top 350 ft. The x-axis is time in terms of number of days from October 23, 2015, which was the start of the incident. The y-axis is the measured depth in feet. The plots are color-shaded by temperature with 13 bins from a gradient from blue to red. Each temperature bin is 6°F. Blue represents colder temperatures, and red represents warmer temperatures. Figure 9 shows the historical temperature range of approximately 75–90°F for the depths 0–1,200 ft; this is a significant difference to the DTS data. The two blue bands in the SS-25 DTS data are termed upper lobe and lower lobe.

Figure 29 and Figure 30 show SS-25A and SS-25B, respectively. The axes and temperature bins were set up the same way for SS-25 for easy comparison. The upper lobe was persistent in these wells and has remained cold for quite a long time. Figure 31, Figure 32, and Figure 33 show the same temperature data with the same temperature bins and axes but with the depths 0–350 ft zoomed in. The SS-25A data shows some anomalous temperature changes from about 320 days to 420 days. This is attributed to liquid movement related to convection within the tubing.

The color contour plots show the big picture of what regions are cold through time at the SS-25 well site. Figure 34, Figure 35, and Figure 36 show the trends at the specific locations: the upper and lower lobes and at 990 ft. The black line is the temperature at 990 ft, which is the depth of the SS-25 surface casing shoe. At 990 ft, the temperature is static, approximately 80°F, and consistent with the historical temperatures. The dark blue lines are the minimum temperatures of the upper lobe. The SS-25's minimum temperature in the upper lobe has remained static at approximately 32°F. The SS-25A's minimum temperatures in the upper lobe changed from the first installation and the second installation. The DTS system was removed for approximately six months while the well was partially plugged and abandoned. These operations increased the temperature of the upper lobe approximately 12°F but remained fairly stable for the year that followed. The lower lobe, in light blue, is approximately 15–25°F warmer than the upper lobe. The SS-25's lower lobe appears to be warming with time but remains static in SS-25A and SS-25B.

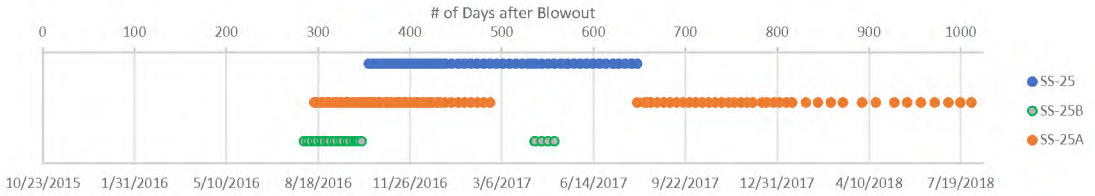

Figure 27: DTS Temperature Surveys Dates

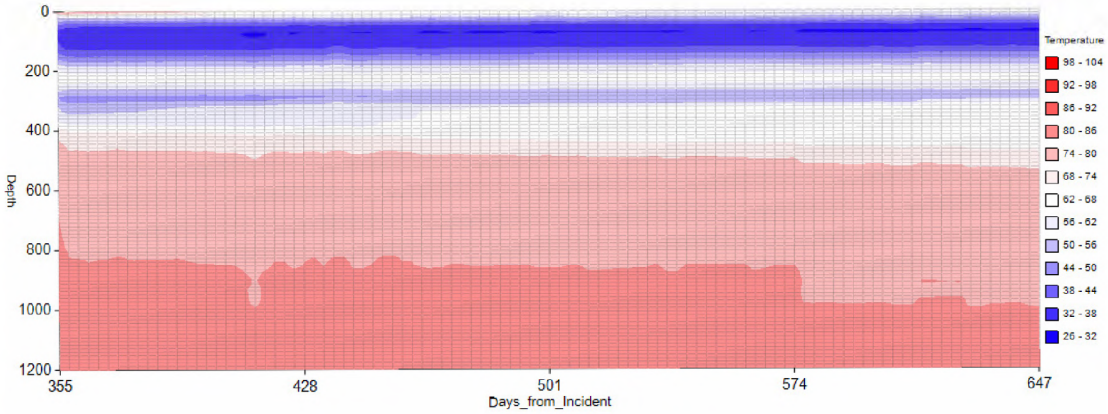

Figure 28: SS-25 DTS Temperature Surveys Post-Blowout 0–1,200 ft

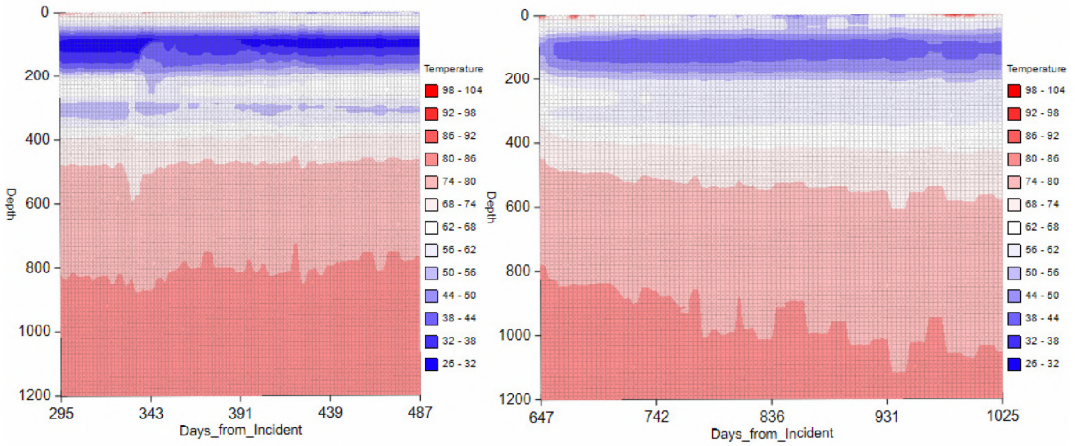

Figure 29: SS-25A DTS Temperature Surveys Post-Blowout 0–1,200 ft

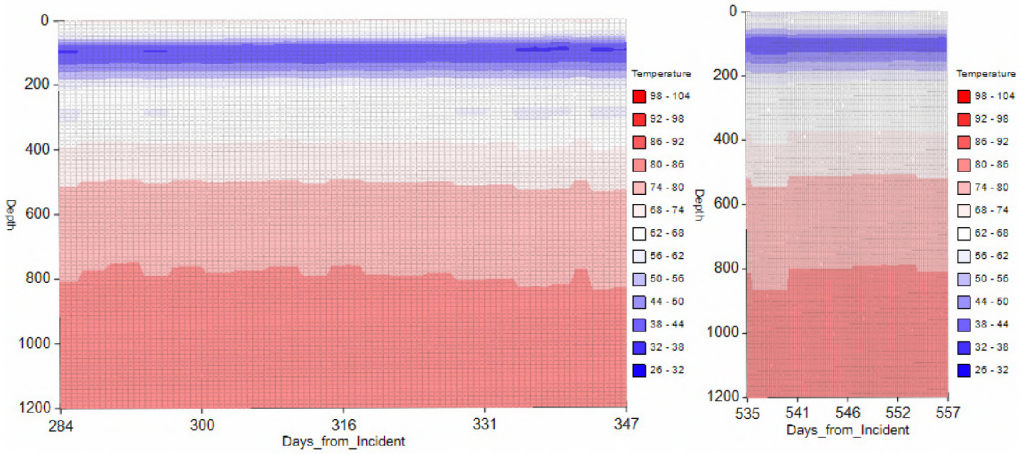

Figure 30: SS-25B DTS Temperature Surveys Post-Blowout 0–1,200 ft

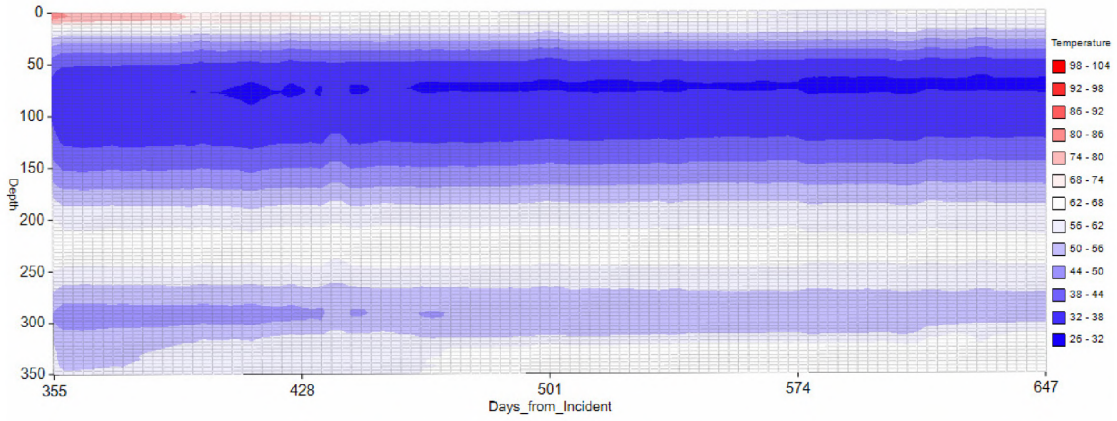

Figure 31: SS-25 DTS Temperature Surveys Post-Blowout 0–350 ft

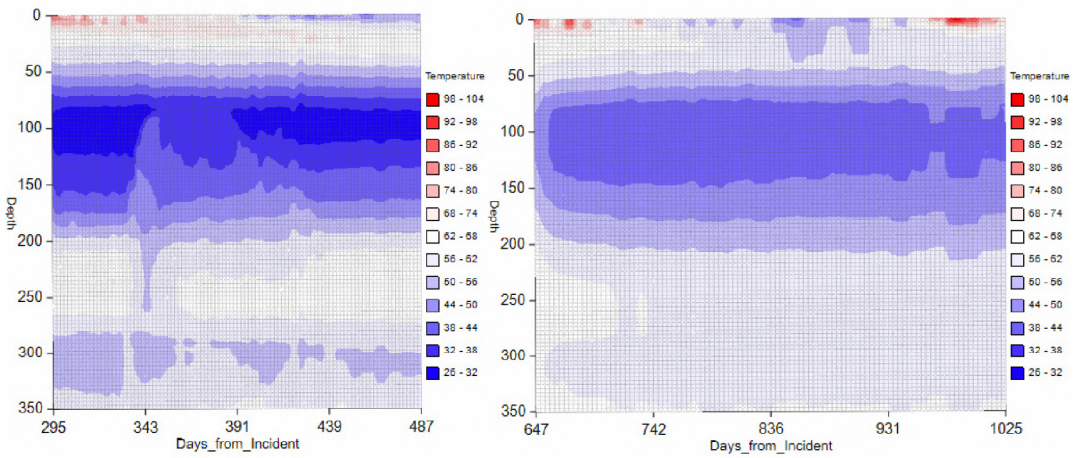

Figure 32: SS-25A DTS Temperature Surveys Post-Blowout 0–350 ft

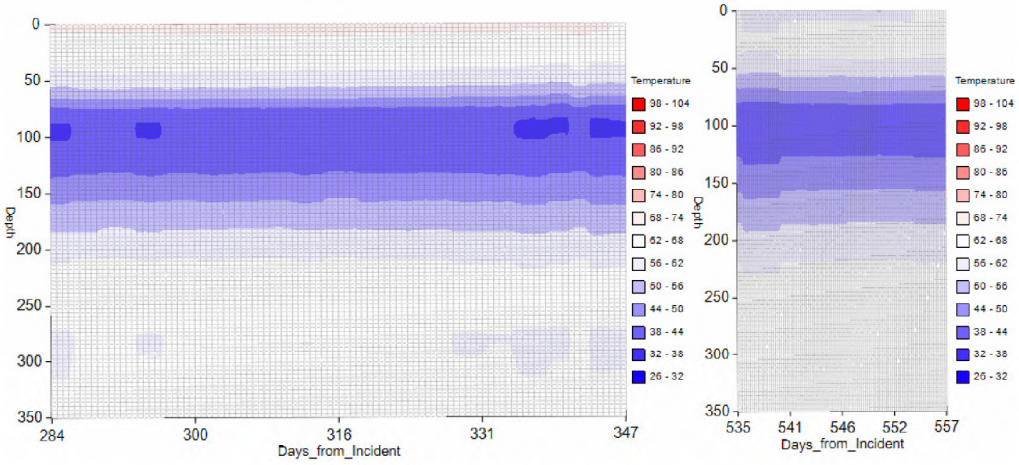

Figure 33: SS-25B DTS Temperature Surveys Post-Blowout 0–350 ft

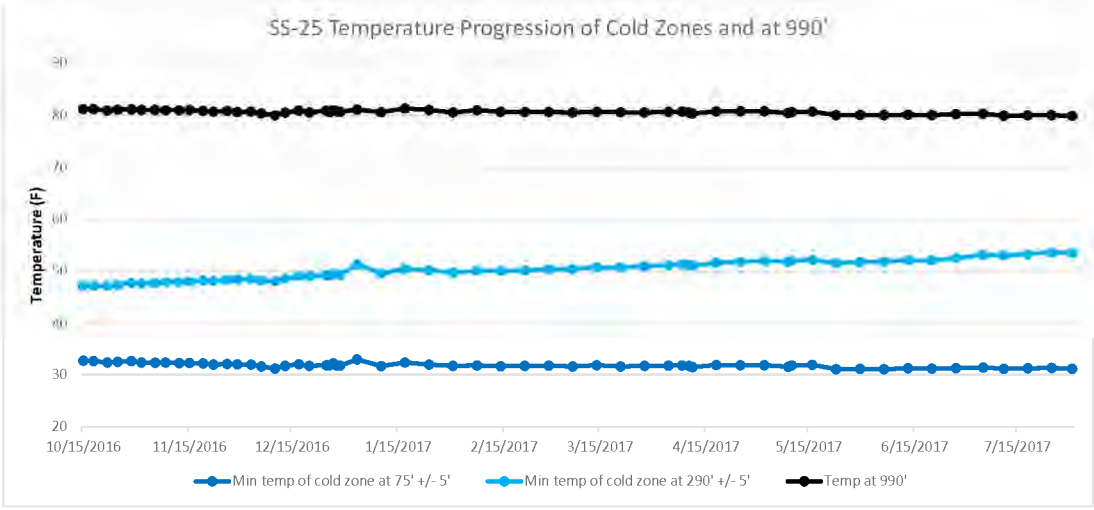

Figure 34: SS-25 DTS Temperature Trends

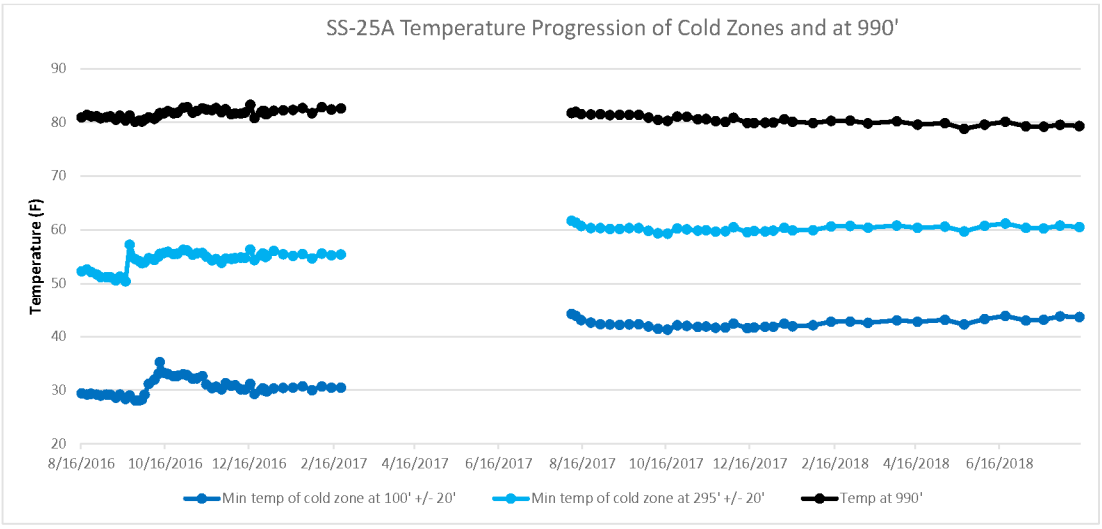

Figure 35: SS-25A DTS Temperature Trends

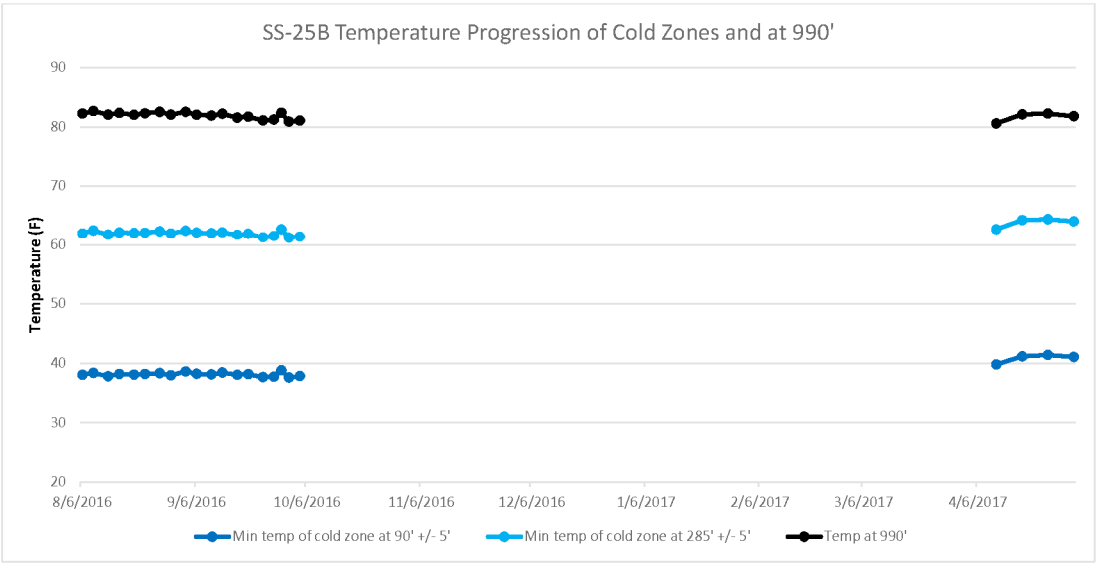

Figure 36: SS-25B DTS Temperature Trends

5 Conclusions

Before the SS-25 7 in. casing failure on October 23, 2015, there were no temperature, pressure, or noise anomalies in the surveys that indicated a preexisting problem. Additionally, there were no physical observations from well inspections and weekly pressure measurements that indicated a preexisting problem.

The temperature profiles during the blowout were significantly different than the historical temperature profiles. The November 08, 2015, temperature, pressure, spinner, GR, and CCL log was unable to identify the flow rate of the escaping gas because the gas flow exceeded its designed limits and was damaged. The log did identify significant temperature changes at approximately 892 ft, 365 ft, and 75 ft associated with the 7 in. casing failure, lower lobe, and upper lobe respectively. The lowest temperature observed was approximately 18°F, which was approximately 20°F lower than in the 1984 F-3 blowout.

After SS-25 was killed, SoCalGas performed numerous wireline surveys at Blade's request. The HPT logs revealed two shallow cold lobes in the SS-25, SS-25A, and SS-25B wells. The four nearby wells investigated did not show any cold temperatures. Schlumberger installed fiber optic lines encapsulated in stainless steel in SS-25, SS-25A, and SS-25B at various times over a two-year period (August 2016–August 2018). The installation depths were greater than 1,200 ft. The upper (75–100 ft) and lower lobes (285–290 ft) had remained cold through two years of observation.

6 References

[1] Division of Oil, Gas, and Geothermal Resources, *Letter, Gas Storage Project Approval,* Ventura, 1989.

[2] Blade Energy Partners, "SS-25 Inspection Logs Analysis," Houston, 2019.

[3] Blade Energy Partners, "Aliso Canyon Field Hydrology," Houston, 2019.

[4] SoCalGas, *Company Operations Standard Gas Operations, Gas Inventory - Monitoring, Verification and Reporting, SCG 224.070, AC_BLD_0012022,* 2014.

[5] SoCalGas, *Weekly Pressure Data for 2015, SS-25, SS-25A, SS-25B, AC_BLD_0075828.*

[6] SoCalGas, *Blade-Follow Up Request_82918_1, Response 4,* 2018.

[7] Blade Energy Partners, *SS-25 Well Nodal Analysis with Uncontrolled Leak Estimation,* 2019.

[8] CoreLab, *Socalgas_SS25_11-8-15_PLT_Protechniques.las,* 2015.

[9] SoCalGas, "Daily Well Activities Frew 3 AC_BLD_0031720 (Frew 3 Well Documentation from SoCal.pdf)".

[10] CoreLab, "03700776 CompletnProf_11-08-15.pdf," 2015.

[11] Blade Energy Partners, *Analysis of the Post-Failure Gas Pathways and Temperature Anomalies at the SS-25 Site,* 2019.

[12] Western Wireline, "03700776 Noise-Temp_11-2015.pdf," 2015.

[13] SoCalGas, "SS-25 Daily Summary from 11-15-15 to 12-2-2015, AC_BLD_0018309," 2015.

[14] Blade Energy Partners, "SS-25A DTS Validation Report," 2016.

[15] SoCalGas, "AC_CPUC_0000486_SS25_PressureSurvey1.15.1974.pdf," Chatsworth, 1974.

[16] SoCalGas, "AC_CPUC_0000527_SS25_TempSurvey3.14.1974.pdf," Chatsworth, 1974.

[17] SoCalGas, "AC_CPUC_0000485_SS25_PressureSurvey10.24.1974.pdf," Chatsworth, 1974.

[18] SoCalGas, "AC_CPUC_0000484_SS25_PressureSurveyDataSheet12.20.1974Pt2.pdf," Chatsworth, 1974.

[19] SoCalGas, "AC_CPUC_0000481_SS25_PressureSurvey2.6.1975.pdf," Chatsworth, 1975.

[20] SoCalGas, "AC_CPUC_0000480_SS25_PressureSurvey4.11.1975.pdf," Chatsworth, 1975.

[21] SoCalGas, "AC_CPUC_0000259_SS25_PressureSurvey4.23.1975.pdf," Chatsworth, 1975.

[22] SoCalGas, "AC_CPUC_0000257_SS25_PressureSurvey4.30.1975.pdf," Chatsworth, 1975.

[23] SoCalGas, "AC_CPUC_0000526_SS25_TempSurvey4.20.1976.pdf," Chatsworth, 1976.

[24] SoCalGas, "AC_CPUC_0000448_SS25_TempSurvey1.19.1977.pdf," Chatsworth, 1977.

[25] SoCalGas, "AC_CPUC_0000445_SS25_TempSurvey10.27.1977.pdf," Chatsworth, 1977.

[26] SoCalGas, "AC_CPUC_0000442_SS25_TempSurvey2.23.1978.pdf," Chatsworth, 1978.

[27] SoCalGas, "AC_CPUC_0000439_SS25_TempSurvey8.29.1978.pdf," Chatsworth, 1978.

[28] SoCalGas, "AC_CPUC_0000177_SS25_Noise9.8.1978.pdf," Chatsworth, 1978.

[29] SoCalGas, "AC_CPUC_0000176_SS25_Noise12.8.1978.pdf," Chatsworth, 1978.

[30] SoCalGas, "AC_CPUC_0000522_SS25_TempSurvey3.14.1979.pdf," Chatsworth, 1979.

[31] SoCalGas, "AC_CPUC_0000473_SS25_PressureSurvey3.14.1979.pdf," Chatsworth, 1979.

[32] SoCalgas, "AC_CPUC_0000518_SS25_TempSurvey8.3.1979.pdf," Chatsworth, 1979.
[33] SoCalGas, "AC_CPUC_0000472_SS25_PressureSurvey10.23.1979.pdf," Chatsworth, 1979.
[34] SoCalGas, "AC_CPUC_0000252_SS25_PressureSurvey11.5.1979.pdf," Chatsworth, 1979.
[35] SoCalGas, "AC_CPUC_0000468_SS25_PressureSurvey11.13.1979," Chatsworth, 1979.
[36] SoCalGas, "AC_CPUC_0000246_SS25_PressureSurvey11.26.1979.pdf," Chatsworth, 1979.
[37] SoCalGas, "AC_CPUC_0000519_SS25_TempSurvey2.22.1980.pdf," Chatsworth, 1980.
[38] SoCalGas, "AC_CPUC_0000517_SS25_TempSurvey7.19.1980.pdf," Chatsworth, 1980.
[39] SoCalGas, "AC_CPUC_0000465_SS25_PressureSurvey10.20.1980.pdf," Chatsworth, 1980.
[40] SoCalGas, "AC_CPUC_0000464_SS25_PressureSurvey10.27.1980.pdf," Chatsworth, 1980.
[41] SoCalGas, "AC_CPUC_0000463_SS25_PressureSurvey11.3.1980.pdf," Chatsworth, 1980.
[42] SoCalGas, "AC_CPUC_0000515_SS25_TempSurvey4.2.1981.pdf," Chatsworth, 1981.
[43] SoCalGas, "AC_CPUC_0000414_SS25_TempSurvey9.21.1981.pdf," Chatsworth, 1981.
[44] SoCalGas, "AC_CPUC_0000410_SS25_TempSurvey4.14.1982.pdf," Chatsworth, 1982.
[45] SoCalGas, "AC_CPUC_0000239_SS25_PressureSurvey4.20.1982.pdf," Chatsworth, 1982.
[46] SoCalGas, "AC_CPUC_0000407_SS25_TempSurvey10.18.1982.pdf," Chatsworth, 1982.
[47] SoCalGas, "AC_CPUC_0000405_SS25_TempSurvey2.23.1984.pdf," Chatsworth, 1984.

[48] SoCalGas, "AC_CPUC_0000238_SS25_PressureSurvey3.3.1983.pdf," Chatsworth, 1983.
[49] SoCalGas, "AC_CPUC_0000237_SS25_PressureSurvey3.9.1983.pdf," Chatsworth, 1983.
[50] SoCalGas, "AC_CPUC_0000236_SS25_PressureSurvey3.16.1983.pdf," Chatsworth, 1983.
[51] SoCalGas, "AC_CPUC_0000401_SS25_TempSurvey6.2.1983.pdf," Chatsworth, 1983.
[52] SoCalGas, "AC_CPUC_0000234_SS25_PressureSurvey7.1.1983.pdf," Chatsworth, 1983.
[53] SoCalGas, "AC_CPUC_0000232_SS25_PressureSurvey7.6.1983.pdf," Chatsworth, 1983.
[54] SoCalGas, "AC_CPUC_0000397_SS25_TempSurvey10.28.1983.pdf," Chatsworth, 1983.
[55] SoCalGas, "AC_CPUC_0000228_SS25_PressureSurvey11.7.1983.pdf," Chatsworth, 1983.
[56] SoCalGas, "AC_CPUC_0000230_SS25_PressureSurvey11.10.1983.pdf," Chatsworth, 1983.
[57] SoCalGas, "AC_CPUC_0000225_SS25_PressureSurvey3.21.1984.pdf," Chatsworth, 1984.
[58] SoCalGas, "AC_CPUC_0000393_SS25_TempSurvey3.23.1984.pdf," Chatsworth, 1984.
[59] SoCalGas, "AC_CPUC_0000390_SS25_TempSurvey4.2.1984.pdf," Chatsworth, 1984.
[60] SoCalGas, "AC_CPUC_0000171_SS25_Noise&Temp1984.pdf," Chatsworth, 1984.
[61] SoCalGas, "AC_CPUC_0000387_SS25_TempSurvey7.18.1984.pdf," Chatsworth, 1984.
[62] SoCalGas, "AC_CPUC_0000178_SS25_Noise&Temp1984.pdf," Chatsworth, 1984.
[63] SoCalGas, "AC_CPUC_0000224_SS25_PressureSurvey4.2.1985.pdf," Chatsworth, 1985.
[64] SoCalGas, "AC_CPUC_0000222_SS25_PressureSurvey4.17.1985.pdf," Chatsworth, 1985.
[65] SoCalGas, "AC_CPUC_0000506_SS25_TempSurvey4.24.1985.pdf," Chatsworth, 1985.
[66] SoCalGas, "AC_CPUC_0000372_SS25_TempSurvey7.10.1985.pdf," Chatsworth, 1985.
[67] SoCalGas, "AC_CPUC_0000368_SS25_TempSurvey3.5.1986.pdf," Chatsworth, 1986.
[68] SoCalGas, "AC_CPUC_0000220_SS25_PressureSurvey1986.pdf," Chatsworth, 1986.

[69] SoCalGas, "AC_CPUC_0000364_SS25_TempSurvey8.13.1986.pdf," Chatsworth, 1986.

[70] SoCalGas, "AC_CPUC_0000357_SS25_TempSurvey3.19.1987.pdf," Chatsworth, 1987.

[71] SoCalGas, "AC_CPUC_0000353_SS25_TempSurvey8.24.1987.pdf," Chatsworth, 1987.

[72] SoCalGas, "AC_CPUC_0000349_SS25_TempSurvey3.3.1988.pdf," Chatsworth, 1988.

[73] SoCalGas, "AC_CPUC_0000218_SS25_PressureSurvey1988.pdf," Chatsworth, 1988.

[74] SoCalGas, "AC_CPUC_0000345_SS25_TempSurvey10.18.1988.pdf," Chatsworth, 1988.

[75] SoCalGas, "AC_CPUC_0000342_SS25_TempSurvey11.9.1988.pdf," Chatsworth, 1988.

[76] SoCalGas, "AC_CPUC_0000338_SS25_TempSurvey4.6.1989.pdf," Chatsworth, 1989.

[77] SoCalGas, "AC_CPUC_0000334_SS25_TempSurvey4.12.1990.pdf," Chatsworth, 1990.

[78] SoCalGas, "AC_CPUC_0000330_SS25_TempSurvey9.20.1990.pdf," Chatsworth, 1990.

[79] SoCalGas, "AC_CPUC_0000327_SS25_TempSurvey4.23.1991.pdf," Chatsworth, 1991.

[80] SoCalGas, "AC_CPUC_0000322_SS25_TempSurvey8.12.1991.pdf," Chatsworth, 1991.

[81] Division of Oil, Gas, and Geothermal Resources, ""03700776 Noise-Temp_11-7-91.tif"," [Online]. Available: https://secure.conservation.ca.gov/WellRecord/037/03700776/03700776%20Noise-Temp_11-7-91.tif. [Accessed 9 01 2019].

[82] SoCalGas, "AC_CPUC_0000318_SS25_TempSurvey4.30.1992.pdf," Chatsworth, 1992.

[83] SoCalGas, "AC_CPUC_0000314_SS25_TempSurvey8.4.1992.pdf," Chatsworth, 1992.

[84] SoCalGas, "AC_CPUC_0000310_SS25_TempSurvey1993.pdf," Chatsworth, 1993.

[85] SoCalGas, "AC_CPUC_0000305_SS25_TempSurvey1.24.1994.pdf," Chatsworth, 1994.

[86] Division of Oil, Gas, and Geothermal Resources, SS-25 September 21, 1994 Temperature, [Online]. Available: https://secure.conservation.ca.gov/WellRecord/037/03700776/03700776%20Temp_9-21-94.pdf. [Accessed 7 January 2019].

[87] SoCalGas, "AC_CPUC_0000457_SS25_PressureSurvey3.8.1995.pdf," Chatsworth, 1995.

[88] SoCalGas, "AC_CPUC_0000294_SS25_TempSurvey1995.pdf," Chatsworth, 1995.

[89] SoCalGas, "AC_CPUC_0000289_SS25_TempSurvey1996.pdf," Chatsworth, 1996.

[90] Division of Oil, Gas, and Geothermal Resources, SS-25 November 5, 1997 Temperature, [Online]. Available: https://secure.conservation.ca.gov/WellRecord/037/03700776/03700776%20Temp_11-5-97.pdf. [Accessed 7 January 2019].

[91] Division of Oil, Gas, and Geothermal Resources, SS-25 November 6, 1998 Temperature, [Online]. Available: https://secure.conservation.ca.gov/WellRecord/037/03700776/03700776%20Temp_11-6-98.pdf. [Accessed 7 January 2019].

[92] SoCalGas, "AC_CPUC_0000282_SS25_TempSurvey1999.pdf," Chatsworth, 1999.

[93] SoCalGas, "AC_CPUC_0000281_SS25_TempSurvey2000.pdf," Chatsworth, 2000.

[94] SoCalGas, "AC_BLD_0068967.xls," Chatsworth, 2000.

[95] Division of Oil, Gas, and Geothermal Resources, SS-25 August 8, 2001 Temperature, [Online]. Available: https://secure.conservation.ca.gov/WellRecord/037/03700776/03700776%20Temp_8-7-01.pdf. [Accessed 7 January 2019].

[96] SoCalGas, "AC_BLD_0068958.xls," Chatsworth, 2001.

[97] SoCalGas, "AC_CPUC_0000279_SS25_TempSurvey2002.pdf," Chatsworth, 2002.

[98] SoCalGas, "AC_BLD_0068959.xls," Chatsworth, 2002.

[99] SoCalGas, "AC_CPUC_0000278_SS25_TempSurvey2003.pdf," Chatsworth, 2003.

[100] SoCalGas, "AC_BLD_0068961.xls," Chatsworth, 2003.

[101] Division of Oil, Gas, and Geothermal Resources, SS-25 July 27, 2004 Temperature , [Online]. Available: https://secure.conservation.ca.gov/WellRecord/037/03700776/03700776%20Temp_7-27-04.pdf. [Accessed 7 January 2019].

[102] SoCalGas, "AC_BLD_0068962.xls," Chatsworth, 2004.

[103] Division of Oil, Gas, and Geothermal Resources, SS-25 August 10, 2005 Temperature, [Online]. Available: https://secure.conservation.ca.gov/WellRecord/037/03700776/03700776%20Temp_8-10-05.pdf. [Accessed 7 January 2019].

[104] SoCalGas, "AC_BLD_0068964.xls," Chatsworth, 2005.

[105] Division of Oil, Gas, and Geothermal Resources, SS-25 August 10, 2005 Pressure, [Online]. Available: https://secure.conservation.ca.gov/WellRecord/037/03700776/03700776%20Pressure_8-10-05.pdf. [Accessed 7 January 2019].

[106] Division of Oil, Gas, and Geothermal Resources, SS-25 July 25, 2006 Temperature, [Online]. Available: https://secure.conservation.ca.gov/WellRecord/037/03700776/03700776%20Temp_7-25-06.pdf. [Accessed 7 January 2019].

[107] SoCalGas, "AC_BLD_0068966.xls," Chatsworth, 2006.

[108] Division of Oil, Gas, and Geothermal Resources, SS-25 July 25, 2006 Pressure, [Online]. Available: https://secure.conservation.ca.gov/WellRecord/037/03700776/03700776%20Pressure_7-25-06.pdf. [Accessed 7 January 2019].

[109] SoCalGas, "AC_CPUC_0000454_SS25_Noise11-7-2006.pdf," Chatsworth, 2006.

[110] SoCalGas, "AC_CPUC_0000274_SS25_TempSurvey2007.pdf," Chatsworth, 2007.

[111] SoCalGas, "AC_CPUC_0000212_SS25_PressureSurvey2007.pdf," Chatsworth, 2007.

[112] Division of Oil, Gas, and Geothermal Resources, "03700776 Temperature Surveys," [Online]. Available: ftp://ftp.consrv.ca.gov/pub/oil/Standard_Sesnon_25_API_037-00776_Well_File/03700776%20Temperature%20Surveys/03700776%20Temperature%20Surveys%201989-2014.pdf. [Accessed 9 January 2019].

[113] Division of Oil, Gas, and Geothermal Resources, SS-25 October 5, 2009 Temperature, [Online]. Available: https://secure.conservation.ca.gov/WellRecord/037/03700776/03700776%20Temp_10-05-09.pdf. [Accessed 7 January 2019].

[114] SoCalGas, "AC_BLD_0068969.xls," Chatsworth, 2009.

[115] SoCalGas, "AC_CPUC_0000211_SS25_PressureSurvey2009.pdf," Chatsworth, 2009.

[116] Division of Oil, Gas, and Geothermal Resources, SS-25 December 14, 2010 Temperature, [Online]. Available: https://secure.conservation.ca.gov/WellRecord/037/03700776/03700776%20Temp_12-14-10.pdf. [Accessed 7 January 2019].

[117] SoCalGas, "AC_CPUC_0000210_SS25_PressureSuvey2010.pdf," Chatsworth, 2010.

[118] Division of Oil, Gas, and Geothermal Resources, SS-25 September 12, 2011 Temperature, [Online]. Available:

https://secure.conservation.ca.gov/WellRecord/037/03700776/03700776%20Temp_09-12-11.pdf.

[119] SoCalGas, "AC_BLD_0068970.xls," Chatsworth, 2011.

[120] SoCalGas, "AC_CPUC_0000209_SS25_PressureSuvey2011.pdf," Chatsworth, 2011.

[121] Division of Oil, Gas, and Geothermal Resources, SS-25 May 29, 2012 Temperature, [Online]. Available: https://secure.conservation.ca.gov/WellRecord/037/03700776/03700776%20Temp_05-29-12.pdf. [Accessed 7 January 2019].

[122] SoCalGas, "AC_CPUC_0000208_SS25_PressureSurvey2012.pdf," Chatsworth, 2012.

[123] Division of Oil, Gas, and Geothermal Resources, SS-25 June 1, 2012 Noise, [Online]. Available: https://secure.conservation.ca.gov/WellRecord/037/03700776/03700776%20Noise_06-01-12.pdf. [Accessed 7 January 2019].

[124] Division of Oil, Gas, and Geothermal Resources, SS-25 October 2, 2013, [Online]. Available: https://secure.conservation.ca.gov/WellRecord/037/03700776/03700776%20Tempe_10-02-13.pdf. [Accessed 7 January 2019].

[125] SoCalGas, "AC_CPUC_0000207_SS25_PressureSurvey2013.pdf," Chatsworth, 2013.

[126] Division of Oil, Gas, and Geothermal Resources, SS-25 October 21, 2014 Temperature, [Online]. Available: https://secure.conservation.ca.gov/WellRecord/037/03700776/03700776%20Temp_10-21-14.pdf. [Accessed 7 January 2019].

[127] SoCalGas, "AC_BLD_0068974.xls," Chatsworth, 2014.

[128] SoCalGas, "AC_CPUC_0000205_SS25_PressureSurvey2014.pdf," Chatsworth, 2014.

Appendix A Pre-Incident Dates of Surveys

Table 2: Pre-Incident Dates of Pressure, Temperature, and Noise Surveys (Chronological)

Survey Date	Survey Type	Ref.
January 15, 1974	Pressure	[15]
March 14, 1974	Temperature	[16]
October 24, 1974	Pressure	[17]
December 20, 1974	Pressure	[18]
February 06, 1975	Pressure	[19]
April 11, 1975	Pressure	[20]
April 23, 1975	Pressure	[21]
April 30, 1975	Pressure	[22]
April 20, 1976	Temperature	[23]
January 19, 1977	Temperature	[24]
October 27, 1977	Temperature	[25]
February 23, 1978	Temperature	[26]
August 29, 1978	Temperature	[27]
September 08, 1978	Noise, Temperature	[28]
December 11, 1978	Noise, Temperature	[29]
March 14, 1979	Temperature	[30]
March 14, 1979	Pressure	[31]
August 03, 1979	Temperature	[32]
October 23, 1979	Pressure	[33]
November 05, 1979	Pressure	[34]
November 13, 1979	Pressure	[35]
November 26, 1979	Pressure	[36]
February 22, 1980	Temperature	[37]
July 29, 1980	Temperature	[38]
October 20, 1980	Pressure	[39]
October 27, 1980	Pressure	[40]
November 03, 1980	Pressure	[41]
April 02, 1981	Temperature	[42]
September 21, 1981	Temperature	[43]
April 14, 1982	Temperature	[44]
April 20, 1982	Pressure	[45]
October 18, 1982	Temperature	[46]
February 23, 1983	Temperature	[47]
March 03, 1983	Pressure	[48]
March 09, 1983	Pressure	[49]
March 16, 1983	Pressure	[50]
June 02, 1983	Temperature	[51]
July 01, 1983	Pressure	[52]
July 06, 1983	Pressure	[53]
October 28, 1983	Temperature	[54]
November 07, 1983	Pressure	[55]
November 10, 1983	Pressure	[56]
March 21, 1984	Pressure	[57]
March 23, 1984	Temperature	[58]
April 02, 1984	Temperature	[59]
April 11, 1984	Noise, Temperature	[60]
July 18, 1984	Temperature	[61]
July 27, 1984	Noise, Temperature	[62]
April 02, 1985	Pressure	[63]
April 17, 1985	Pressure	[64]
April 24, 1985	Temperature	[65]
July 10, 1985	Temperature	[66]
March 05, 1986	Temperature	[67]
April 29, 1986	Pressure	[68]
August 13, 1986	Temperature	[69]
March 19, 1987	Temperature	[70]
August 24, 1987	Temperature	[71]
February 26, 1988	Temperature	[72]
April 22, 1988	Pressure	[73]
October 18, 1988	Temperature	[74]
November 09, 1988	Temperature	[75]
April 06, 1989	Temperature	[76]
April 12, 1990	Temperature	[77]
September 20, 1990	Temperature	[78]
April 23, 1991	Temperature	[79]
August 12, 1991	Temperature	[80]

Survey Date	Survey Type	Ref.
November 07, 1991	Noise, Temperature	[81]
April 30, 1992	Temperature	[82]
August 04, 1992	Temperature	[83]
September 21, 1993	Temperature	[84]
January 25, 1994	Temperature	[85]
September 16, 1994	Temperature	[86]
March 08, 1995	Pressure	[87]
October 12, 1995	Temperature	[88]
September 24, 1996	Temperature	[89]
November 05, 1997	Temperature	[90]
November 06, 1998	Temperature	[91]
February 05, 1999	Temperature	[92]
September 14, 2000	Temperature	[93] [94]
August 07, 2001	Temperature	[95] [96]
August 30, 2002	Temperature	[97] [98]
August 27, 2003	Temperature	[99] [100]
July 27, 2004	Temperature	[101] [102]
August 10, 2005	Temperature	[103] [104]
August 10, 2005	Pressure	[105]
July 25, 2006	Temperature	[106] [107]
July 25, 2006	Pressure	[108]
November 07, 2006	Noise, Temperature	[109]
December 05, 2007	Temperature	[110]
December 05, 2007	Pressure	[111]
July 23, 2008	Temperature	[112]
October 05, 2009	Temperature	[113] [114]
October 05, 2009	Pressure	[115]
December 14, 2010	Temperature	[116]
December 14, 2010	Pressure	[117]
September 12, 2011	Temperature	[118] [119]
September 12, 2011	Pressure	[120]
May 29, 2012	Temperature	[121]
May 29, 2012	Pressure	[122]
June 01, 2012	Noise, Temperature (Figure 10)	[123]
October 02, 2013	Temperature	[124]
October 02, 2013	Pressure	[125]
October 21, 2014	Temperature (Figure 2)	[126] [127]
October 21, 2014	Pressure (Figure 12)	[128]

Appendix B Weekly Pressure Measurements [5]

SS25				SS25A				SS25B			
	A1 - Surface Casing Annulus (PSIG)	C - Production Casing Annulus (PSIG)	Tubing (PSIG)		A1	C	T		A1	C	T
01/03/15	1	2047	2045	01/03/15	1	500	2235	01/03/15	37	850	1997
01/09/15	0	1930	1930	01/09/15	0	480	2175	01/09/15	0	1930	1930
01/17/15	1	1882	1886	01/17/15	1	500	2122	01/17/15	36	1900	1900
01/22/15	0	1890	1890	01/22/15	0	475	2125	01/22/15	37	1920	1920
01/31/15	1	0	0	01/31/15	1	500	0	01/31/15	35	0	0
02/07/15	0	1940	1940	02/07/15	0	470	2120	02/07/15	36	1975	1975
02/13/15	0	1960	1960	02/13/15	0	470	2140	02/13/15	36	1995	1995
02/21/15	0	1975	1980	02/21/15	0	470	2130	02/21/15	36	2010	2010
03/06/15	0	1790	1790	03/06/15	0	470	1895	03/06/15	36	1785	1785
03/14/15	1	0	0	03/14/15	1	0	0	03/14/15	35	0	0
03/19/15	0	1850	1850	03/19/15	0	470	1900	03/19/15	35	1850	1850
03/27/15	0	2035	2005	03/27/15	0	470	2130	03/27/15	36	1980	1980
04/10/15	0	2145	2110	04/10/15	0	470	2260	04/10/15	36	2100	2100
04/18/15	1	2213	2280	04/18/15	1	480	2320	04/18/15	36	2165	2146
04/24/15	0	2255	2215	04/24/15	0	470	2370	04/24/15	36	2205	2205
05/01/15	0	2305	2265	05/01/15	0	470	2400	05/01/15	36	2250	2250
05/07/15	0	2335	2300	05/07/15	0	470	2460	05/07/15	36	2310	2310
05/22/15	0	2415	2340	05/22/15	0	470	2510	05/22/15	36	2405	2405
05/29/15	0	0	0	05/29/15	0	0	0	05/29/15	36	0	0
06/05/15	0	2425	2405	06/05/15	0	470	2455	06/05/15	36	2415	2415
06/15/15	0	2468	2461	06/15/15	0	500	2541	06/15/15	37	2530	0
06/19/15	0	2470	2470	06/19/15	0	470	2550	06/19/15	37	2550	2550
06/26/15	0	0	0	06/26/15	0	0	0	06/26/15	36	0	0
07/02/15	0	2335	2345	07/02/15	0	475	2480	07/02/15	38	2365	2365
07/11/15	20	2468	2460	07/11/15	1	500	2505	07/11/15	40	2500	2459
07/18/15	1	2516	2500	07/18/15	1	500	2584	07/18/15	40	2577	2485
07/24/15	0	2505	2495	07/24/15	0	470	2540	07/24/15	42	2540	2485
07/30/15	0	2505	2495	07/30/15	0	470	2540	07/30/15	42	2540	0.2485
08/07/15	0	2460	2460	08/07/15	0	475	2550	08/07/15	41	2480	2480
08/12/15	0	2490	2490	08/12/15	0	470	2580	08/12/15	41	2510	2510
08/20/15	0	2380	2380	08/20/15	0	470	2505	08/20/15	40	2415	2415
08/27/15	0	2445	2445	08/27/15	0	470	2575	08/27/15	41	2470	2470
09/05/15	1	2558	2537	09/05/15	1	500	2644	09/05/15	43	2633	2530
09/11/15	0	0	0	09/11/15	0	0	0	09/11/15	41	0	0
09/18/15	0	2540	2540	09/18/15	0	470	2640	09/18/15	44	2640	2635
09/25/15	0	2680	2680	09/25/15	0	470	2700	09/25/15	44	2680	2680
10/01/15	0	2610	2600	10/01/15	0	470	2635	10/01/15	46	2635	2595
10/15/15	0	2595	2595	10/15/15	0	470	2305	10/15/15	44	2620	2620

Appendix C Comparison of Digitized Temperature Surveys to Raw Data

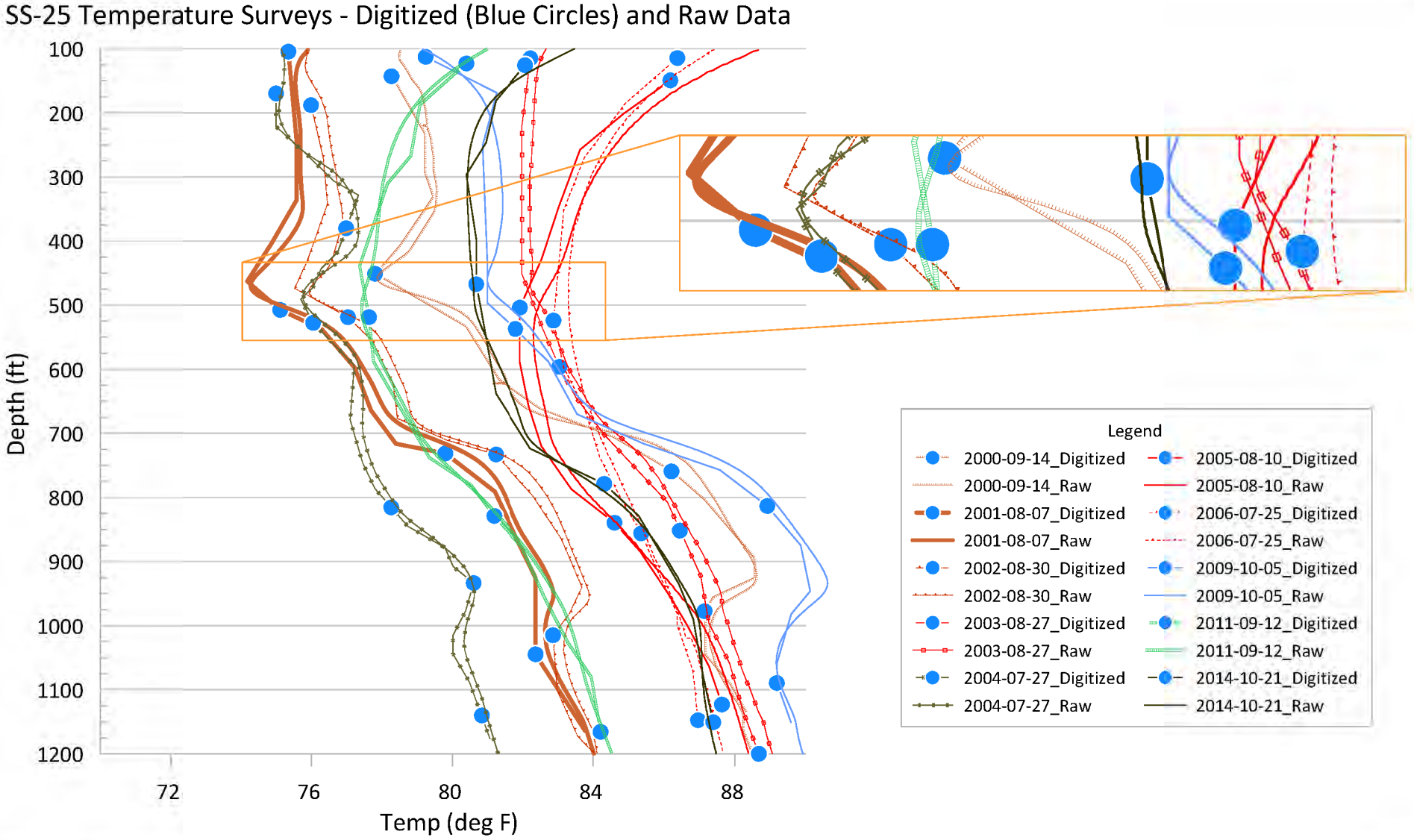

SS-25 RCA Supplementary Report

Aliso Canyon Field: Hydrology

Purpose:
Report on the hydrology of Aliso Canyon field in support of the Aliso Canyon Root Cause Analysis.

Date:
May 31, 2019

BLADE ENERGY PARTNERS

2600 Network Boulevard, Suite 550
Frisco, Texas 75034

+1 972-712-8407 (phone)
+1 972-712-8408 (fax)

16285 Park Ten Place, Suite 600
Houston, Texas 77084

1-800-319-2940 (toll free)
+1 281-206-2000 (phone)
+1 281-206-2005 (fax)

www.blade-energy.com

Blade Energy Partners Limited, and its affiliates ('Blade') provide our services subject to our General Terms and Conditions ('GTC') in effect at time of service, unless a GTC provision is expressly superseded in a separate agreement made with Blade. Blade's work product is based on information sources which we believe to be reliable, including information that was publicly available and that was provided by our client; but Blade does not guarantee the accuracy or completeness of the information provided. All statements are the opinions of Blade based on generally-accepted and reasonable practices in the industry. Our clients remain fully responsible for all clients' decisions, actions and omissions, whether based upon Blade's work product or not; and Blade's liability solely extends to the cost of its work product.

Abstract

The gas storage well Standard Sesnon 25 (SS-25) in the Aliso Canyon Gas Storage Field located in Los Angeles County, California started leaking gas in October 2015. A relief well was drilled, and SS-25 was brought under control. The leak stopped in February 2016.

In January 2016, as part of their investigation of the leak, the California Public Utilities Commission (CPUC) and the Division of Oil, Gas, and Geothermal Resources (DOGGR) selected and gave provisional authority to Blade Energy Partners (Blade) to perform an independent root cause analysis (RCA). The Blade Team and parties under Blade's direction were responsible for directing the work of subcontractors who performed the extraction of the SS-25's wellhead, tubing, and casings and the preservation and protection of associated evidence. Blade's RCA Reports, including this report, document and describe the key activities undertaken in support of the RCA effort.

Blade has studied the hydrology of the Aliso Canyon field to determine the presence, source, and properties of the groundwater in the field. This study was conducted through:

- Drilling two test wells.
- Collecting, and analyzing water samples from the test wells and surface seeps.
- Geophysical well logs.
- Analyzing local precipitation records.
- Reviewing documents related to hydrology of the region and nearby areas.

Groundwater is present at and below 2,512 ft Above Mean Sea Level (AMSL) elevation and occurs in two regimes (shallow and deep) with distinct pressures and chemistries. The source of groundwater is precipitation falling in the field. The groundwater elevation depends on the precipitation, with month-to-month and year-to-year variations depending on the rainfall amounts. This study has estimated that the groundwater level at the time of the SS-25 incident in October 2015 was at or near its lowest level since at least 1997. Finally, this study has developed a conceptual model to explain the movement of groundwater in the Aliso Canyon area.

Table of Contents

1 **Introduction** 5

1.1 Abbreviations and Acronyms 5

1.2 Well Nomenclature 5

2 **Principal Findings** 6

3 **Data Sources** 7

4 **Groundwater Presence and Pressure** 8

5 **Groundwater Chemistry** 12

5.1 Groundwater Type 12

5.2 Groundwater Source 18

6 **Well Log Analysis** 20

6.1 RBMW-1 Well Logs 20

6.2 SS-25 Logs 22

7 **Precipitation Analysis** 25

8 **Conceptual Groundwater Model** 30

9 **SS-25 Implications** 31

10 **References** 34

Appendix A **Water Chemistry Data** A-1

Appendix B **Water Seeps on Geologic Map** B-1

Appendix C **RBMW-1 NMR Log** C-1

Appendix D **RBMW-1 ELAN Log** D-1

Appendix E **SS-25 ELAN Log** E-1

List of Figures

Figure 1: Groundwater Investigation During Drilling of RBMW-1 Well 9
Figure 2: Hydrostatic Head/Water Level Measurements in RBMW-1 and RBMW-2 10
Figure 3: Piper Plot Construction and Uses 13
Figure 4: Piper Plot for EPA Water Samples 15
Figure 5: Piper Plot Comparing Grab Samples with EPA Samples 16
Figure 6: Piper Plot Comparing Seep Samples with EPA Samples 17
Figure 7: Regional Elevation Contour Map 18
Figure 8: Composite Geophysical Logs for RBMW-1 21
Figure 9: Composite Geophysical Logs for SS-25 23
Figure 10: Correlation of Aliso Canyon's Precipitation with San Fernando Valley's Precipitation 26
Figure 11: Aliso Canyon Annual Precipitation (1996–2017) 27
Figure 12: Annual Distribution of Rainfall in Aliso Canyon for Typical Dry, Normal, and Wet Years 28
Figure 13: Conceptual Groundwater Level in Aliso Canyon (1996–2018) 29
Figure 14: Conceptual Hydrologic Model 30
Figure 15: Possible Leak Paths for Escaping Gas 32

List of Tables

Table 1: Geophysical Well Logs Run in RBMW-1 to Investigate Subsurface Geology and Groundwater 20
Table A-1: List of EPA and Grab Samples A-1
Table A-2: Water Chemistry Data for Grab Samples and EPA Samples A-2
Table A-3: List of Seep Samples A-3
Table A-4: Water Chemistry Data for Seep Samples A-4

1 Introduction

The Aliso Canyon RCA project identified corrosion on the outside of the 11 3/4 in. surface casing and the 7 in. production casing. Corrosion of the production casing may have been the most proximate technical cause of the casing failure. All corrosion mechanisms require the presence of water, and groundwater is a possible source of water. Therefore, the RCA project undertook a study of the Aliso Canyon hydrology to determine the source and behavior of groundwater. This document summarizes the information and data generated by this study.

1.1 Abbreviations and Acronyms

Term	Definition
AIT	Array Induction Imager Tool
ALERT	Automatic Local Evaluation in Real Time
AMSL	Above Mean Sea Level
bgs	Below Ground Surface
Blade	Blade Energy Partners
CPUC	California Public Utilities Commission
DOGGR	Division of Oil, Gas and Geothermal Resources (State of California)
EC	Electrical Conductivity
ELAN	Electric Log Analysis (Schlumberger)
EPA	Environmental Protection Agency
FMI	Formation Micro Imager
NMR	Nuclear Magnetic Resonance
OH	Open Hole
PEX	Platform Express
RBMW	Regional Board (Groundwater) Monitoring Well
RCA	Root Cause Analysis
RCAR	Reverse Circulation Air Rotary
SCV	Santa Clarita Valley
SFV	San Fernando Valley
SS	Standard Sesnon
TD	Total Depth
TH	Test Hole

1.2 Well Nomenclature

Two wells were drilled near the SS-25 well site to investigate hydrology. The first well is referred to interchangeably as TH-1, or RBMW-1. The second well is referred to interchangeably as TH-2, or RBMW-2.

For the remainder of the report, these wells will be designated as RBMW-1 and RBMW-2; however, some supporting documents (e.g., well logs) may use the other (i.e., TH-1 and TH-2) designations.

2 Principal Findings

The following are the principal findings:

- The presence of shallow groundwater was confirmed.
- The groundwater occurred in two distinct regimes, designated 'shallow' and 'deep,' each with a different chemistry and pressure.
- The shallow groundwater regime contained Ca-HCO_3 water type, which is characteristic of shallow, fresh groundwaters [1]. The potentiometric[i] surface elevation of the shallow groundwater regime was 2,496 ft AMSL, which was equivalent to 431 ft bgs in the SS-25 well.
- The deep groundwater regime contained Na-HCO_3 water type, which is typical of deeper groundwaters influenced by ion exchange [1]. The potentiometric surface elevation of the deep groundwater regime was 2,354 ft AMSL, which was equivalent to 573 ft bgs in the SS-25 well.
- The transition from shallow to deep groundwater regime occurred around 500–600 ft, which coincided with the Modelo-Topanga transition.
- The source of the groundwater was precipitation.
- The occurrence of mobile groundwater was in distinct, high permeability, likely fractured layers.
- The groundwater level was expected to be affected by annual and year-to-year variation in precipitation. In a given rain year, almost all rainfall occurs between December and March (the rainy season). Therefore, groundwater level rises during these months, reaching a maximum at the end of the rainy season, and falls during the remaining months, reaching a minimum at the start of the next rainy season. Year-to-year variation of rainfall also affects the groundwater level: the groundwater level was expected to fall after drier-than-normal years, remain steady after normal years, and rising after wetter-than-normal years.
- The SS-25 incident in October 2015 occurred following four drier-than-normal rain years (2011–2012 through 2014–2015). It is estimated that the groundwater level at the time of the SS-25 was lower than it had been at any point since at least 1997. The groundwater level at the time of RBMW-1 and RBMW-2 investigation is estimated to be similar to the groundwater level at the time of the SS-25 incident.
- When SS-25 was drilled in 1953, the 11 3/4 in. surface casing was placed, likely inadvertently, in a permeable or fractured water zone. This zone was likely the source of water infiltrating into the 11 3/4 in. × 7 in. casing annulus.

[i] A potentiometric surface, also called a piezometric surface, is a "A surface representing the hydraulic head of ground water; represented by the water-table altitude in an unconfined aquifer or by the altitude to which water will rise in a properly constructed well in a confined aquifer" [14, p. 120]. At the elevation of potentiometric surface, groundwater will have zero (gauge) pressure.

3 Data Sources

This study used the following sources to generate the information about Aliso Canyon field hydrology:

- Groundwater monitoring wells: Two test wells were drilled in 2018 to relatively shallow depths to investigate the presence of groundwater. Because the area around the incident SS-25 well was disturbed during the incident, the test wells were drilled about 600 ft south of the SS-25 wellhead location. These wells were later converted to groundwater monitoring wells and designated RBMW-1 and RBMW-2, respectively.

  The primary data obtained from these wells were:

  - Groundwater elevations (potentiometric surface elevations).
  - Groundwater samples for chemical analysis. Two types of samples were obtained:
    - EPA samples, which were obtained using a 'low flow' method consistent with EPA guidance [2]. These are the best representatives of the groundwater chemistry.
    - Grab samples, which were obtained from water in the wellbore during RBMW-1 drilling.
- Seep samples: Several surface seeps in the vicinity of the SS-25 well pad were sampled for chemical analysis. The primary data obtained from these seeps were water chemistry.
- Geophysical well logs: Well logs of various types were run, principally in SS-25 and RBMW-1. The SS-25 well was restricted to cased hole logs only because of the presence of surface casing; therefore, the RBMW-1 well was used to run open hole (OH) logs. Primary data obtained from these geophysical logs are lithology and location of layers containing moveable (free) water.
- Meteorological data: Historical precipitation records were acquired for the Aliso Canyon area for 1997–2018. The principal use of the meteorological data is to estimate the groundwater level over time.
- Background research: Papers, reports, and theses related to geology, hydrology, and climate of the region were reviewed.

  The following reports were found to be especially useful:

  - *Report of Referee* [3] [4], which describes the hydrology of the Upper Los Angeles River area, including geology, soils, precipitation, water quality, water use, and groundwater recharge. Surface runoff from Aliso Canyon field is to the upper Los Angeles River.
  - Studies, reports, and models [5] generated during the site remediation and restoration of the Santa Susana Field Laboratory (SSFL), a former rocket engine test and nuclear research facility located approximately 10 miles southwest of Aliso Canyon field.
  - Annual hydrologic reports [6] prepared by the County of Los Angeles Department of Public Works.

  These reports were used to guide the development of the conceptual groundwater model, which is described in Section 8.

4 Groundwater Presence and Pressure

Before this RCA project, little information was available about the presence of groundwater in the Aliso Canyon field. When the field was originally put into production, surface casings were usually installed to approximately 500 ft bgs "essentially as anchorage for blow-out protection" [7, p. 16]. There were "no subsurface waters suitable for domestic or irrigation purposes to protect" [7, p. 16]. Surface casing depths were increased in later wells to approximately 1,000 ft bgs, although the reason for the increase is unclear.

Under Blade's guidance, two shallow wells (RBMW-1 and RBMW-2) were drilled to investigate groundwater. These wells were drilled from the SS-9 well site, which is located 630 ft south-southeast of the SS-25 location, to investigate an area unaffected by the SS-25 incident, and because of the limited access to the SS-25 well pad. The surface elevation for both wells is 2,837 ft AMSL.

RBMW-1 was first drilled dry (i.e., without a drilling fluid) in order to identify the depth of first groundwater influx.

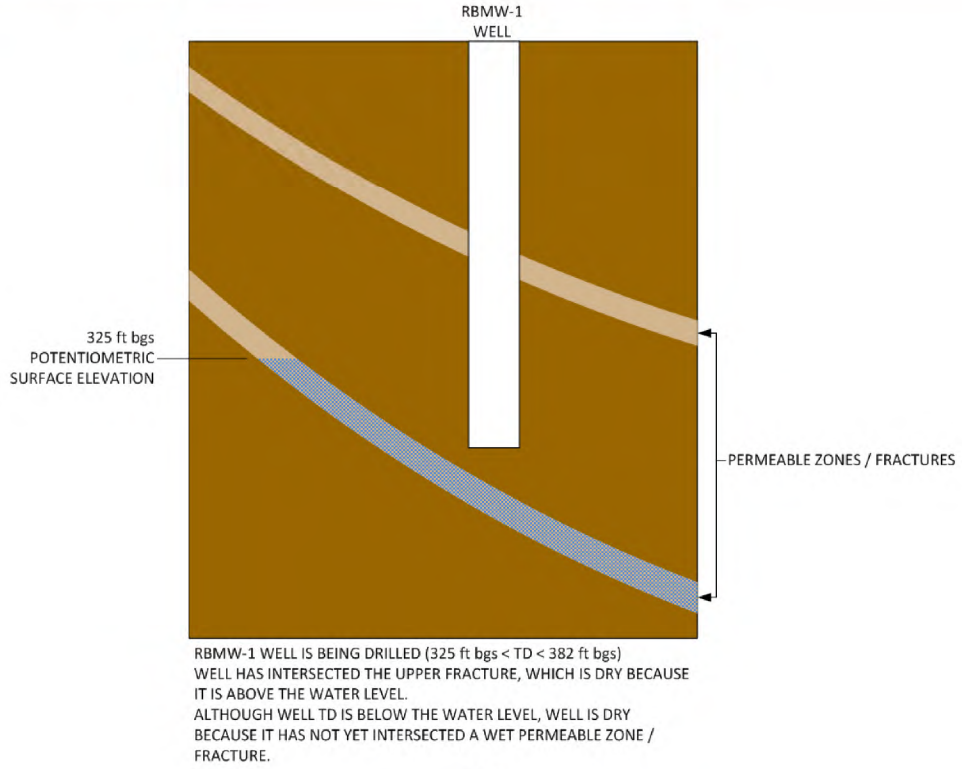

Figure 1: Groundwater Investigation During Drilling of RBMW-1 Well

The RBMW-1 well was first drilled dry using a Reverse Circulation Air Rotary (RCAR) technique (Figure 1) in order to identify the depth at which groundwater was present. The well first encountered groundwater at 382 ft bgs (2,455 ft AMSL). Drilling continued and the Modelo-Topanga interface was identified at 510 ft bgs (2,327 ft AMSL). Hole stability problems were encountered at 555 ft bgs (2,282 ft AMSL). After hole stability problems were addressed, the standing water level rose to 325 ft bgs (2,512 ft AMSL).

Drilling then continued to 1,110 ft bgs (1,727 ft AMSL) with complete loss of returns, so it was not possible to identify additional water zones during drilling. After reaching total depth (TD), RBMW-1 was completed as a monitoring well in the Topanga formation by installing a 100-ft screen between 900–1,000 ft bgs (1,837–1,937 ft AMSL).

RBMW-2 was drilled approximately 25 ft away from RBMW-1 to TD of 450 ft bgs (2,387 ft AMSL). RBMW-2 was completed as a monitoring well in the Modelo formation by installing a 100-ft screen between 340-440 ft bgs (2,397–2,497 ft AMSL).

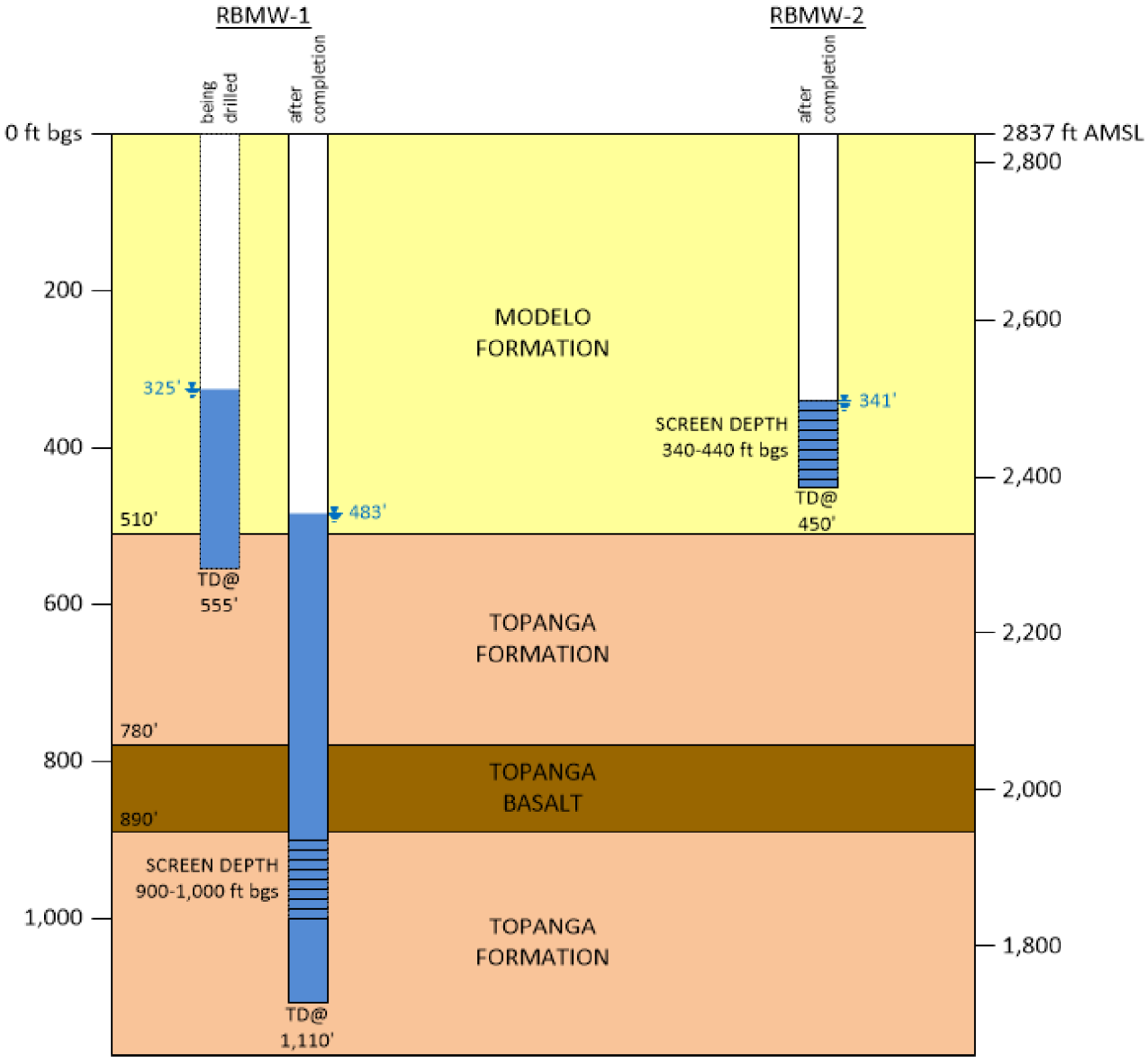

Figure 2: Hydrostatic Head/Water Level Measurements in RBMW-1 and RBMW-2 (modified after [2])

Three hydrostatic head measurements were made through RBMW-1 and RBMW-2 (Figure 2):

- With the well depth at 555 ft bgs (2,282 ft AMSL), the standing water level in the RBMW-1 OH was 325 ft bgs (2,512 ft AMSL). This may be considered as the potentiometric surface elevation of the shallowest water zone encountered at 382 ft bgs (2,455 ft AMSL).
- The standing water level in RBMW-2 after completion as a monitoring well was 341 ft bgs (2,496 ft AMSL). This level may be considered as the potentiometric surface elevation at 340 ft bgs (2,497 ft AMSL), since RBMW-2 was open to formation from this depth to 440 ft bgs (2,397 ft AMSL) at the time of measurement. Between the two RBMW-1 measurements, there is a 16 ft decrease in potentiometric surface elevation, which corresponds to 7 psi.
- The standing water level in RBMW-1 after completion as a monitoring well was 483 ft bgs (2,354 ft AMSL). This level may be considered to be the potentiometric surface elevation at 900 ft bgs (1,937 ft AMSL), since RBMW-1 was open to formation from this depth to 1,000 ft bgs (1,837 ft AMSL) at the time of measurement. The 142 ft decrease in potentiometric surface elevation corresponds to 61 psi.

These data indicate a pressure loss of 0.11–0.12 psi/ft, which is most likely associated with vertical flow as groundwater seeps into the surface.

The SS-25 wellhead elevation is 2,927 ft AMSL. Therefore, the equivalent depths for the potentiometric surfaces are 415–430 ft bgs for the shallow groundwater and 573 ft bgs for the deep groundwater. These values are the estimated depths to groundwater at the time of the RBMW-1 and RBMW-2 measurements in June 2018. Based on precipitation records (Section 7), the depths to groundwater at the time of the SS-25 incident in October 2015 are estimated to be similar; however, the depths to groundwater during earlier periods are estimated to be shallower (i.e., higher groundwater elevation).

5 Groundwater Chemistry

This study has analyzed the chemistry of the following samples:

- Three EPA samples from monitoring wells:
  - Samples RBMW-1 and RBMW-1-DUP, obtained from RBMW-1 well, which was open to formation between 900 ft bgs (1,937 ft AMSL) and 1,000 ft bgs (1,837 ft AMSL)
  - Sample RBMW-2, obtained from RBMW-2 well, which was open to formation between 340 ft bgs (2,497 ft AMSL) and 440 ft bgs (2,397 ft AMSL)

  These EPA samples were sampled using "the 'low flow' method consistent with EPA guidance" [2, p. 14] and are considered to be the most representative sample of the native groundwaters.
- Three grab samples obtained from RBMW-1 during drilling as follows:
  - At 382 ft bgs (2,455 ft AMSL) when water was first encountered
  - At 555 ft bgs (2,282 ft AMSL) when RCAR (dry drilling) technique had to be abandoned in favor of rotary drilling due to hole stability problems
  - At 325 ft bgs (2,512 ft AMSL) from the surface of water standing in the borehole upon completion of the operations to free stuck pipe at 555 ft bgs (2,282 ft AMSL), which was the total depth of the well at the time
- Seven surface seep samples obtained from surface seeps near SS-25 (four other surface seeps could not be sampled due to low flow)

The samples are described in Table A-1 and Table A-3, and the water chemistry data are tabulated in Table A-2 and Table A-4 in Appendix A.

5.1 Groundwater Type

Groundwater chemistry was evaluated using Piper plots. A Piper plot is constructed as follows (Figure 3):

- The cation and anion concentration of a given water sample is calculated in terms of milliequivalent mole percent.
- The cation concentration is plotted on the lower left triangular plot. A line is projected from this point parallel to the Mg axis to the diamond plot.
- The anion concentration is plotted on the lower right triangular plot. A line is projected from this point parallel to the SO_4 axis to the diamond plot.
- On the diamond plot, the water sample concentration is marked at the intersection of the two projection lines.

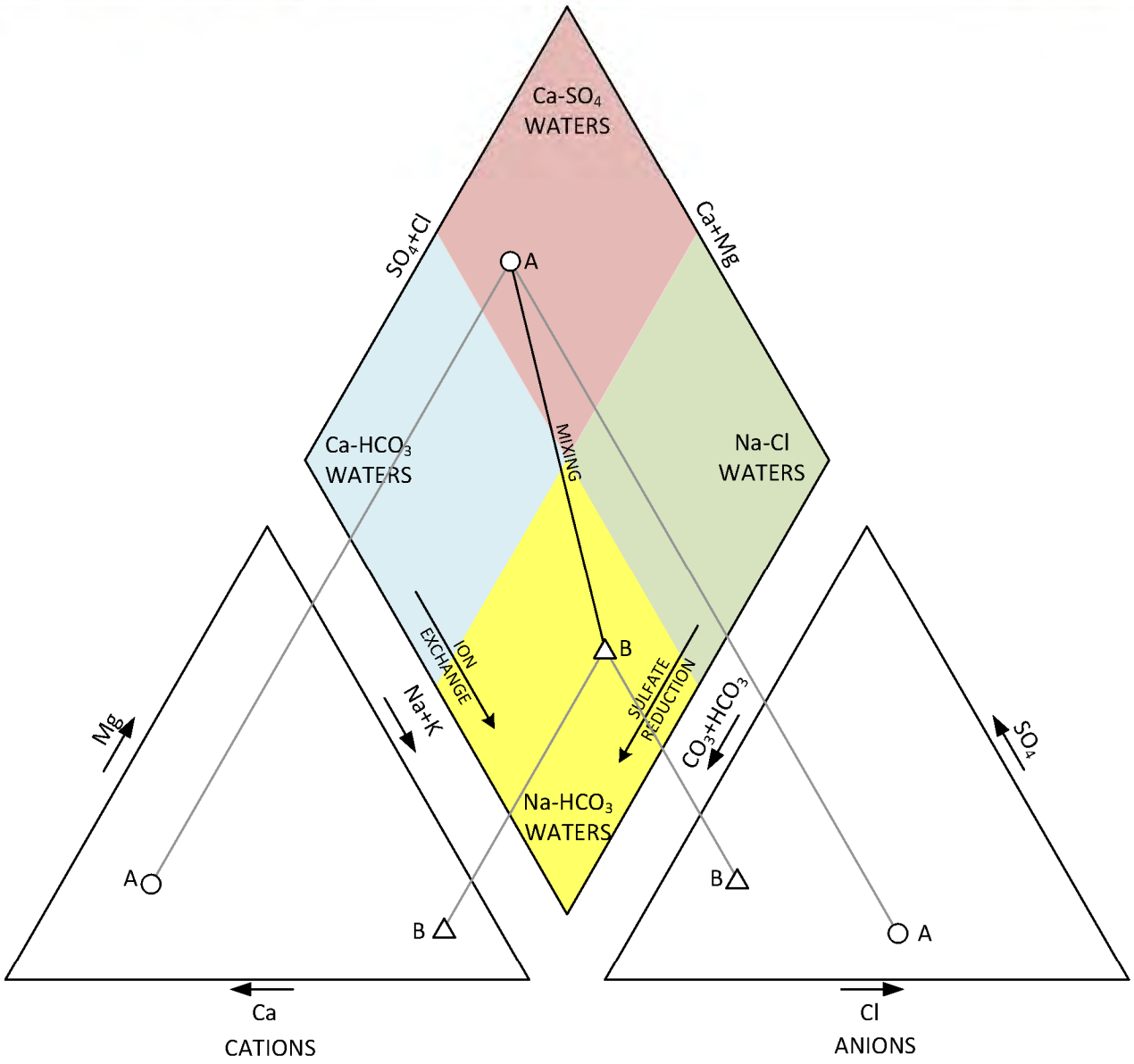

Figure 3: Piper Plot Construction and Uses

The Piper plot allows for rapid classification of the water samples as follows [1]:

- Ca-SO_4 waters, which are typical of gypsum groundwaters and mine discharge plot on the top of the diamond plot (red region)
- Ca-HCO_3 waters, which are typical of shallow, fresh groundwaters, plot on the left of the diamond plot (blue region)
- Na-Cl waters, which are typical of marine and deep ancient groundwaters, plot on the right of the diamond plot (green region).
- Na-HCO_3 waters, which are typical of deeper groundwaters influenced by ion exchange, plot on the bottom of the diamond plot (yellow region).

The Piper plot also identifies the ongoing groundwater processes [8]:

- Mixing of two groundwater regimes are indicated by a line connecting the two samples on the diamond plot.
- Ion exchange, by which groundwater exchanges Ca^{2+} and Mg^{2+} ions in return for Na^{+} ion, will plot parallel to the Na+K axis on the diamond plot. Clays in subsurface formations have high ion-exchange capacities due to their "large surface area of particles per unit volume" [9]. Also, clays "exhibit a selective preference of one ion over another" [9]. In general, clays prefer divalent ions (e.g., Ca^{2+}, Mg^{2+}) over monovalent ions (e.g., Na^{+}, K^{+}) [9]. Therefore, as groundwater flows through formations containing clay, the divalent ions are adsorbed on to the clay surfaces and replaced by monovalent ions.
- Sulfate reduction, by which SO_4^{2-} ions are consumed through the following general reaction [10]:

$$SO_4^{2-} + 9H^{+} + 8e^{-} \rightarrow HS^{-} + 4H_2O$$

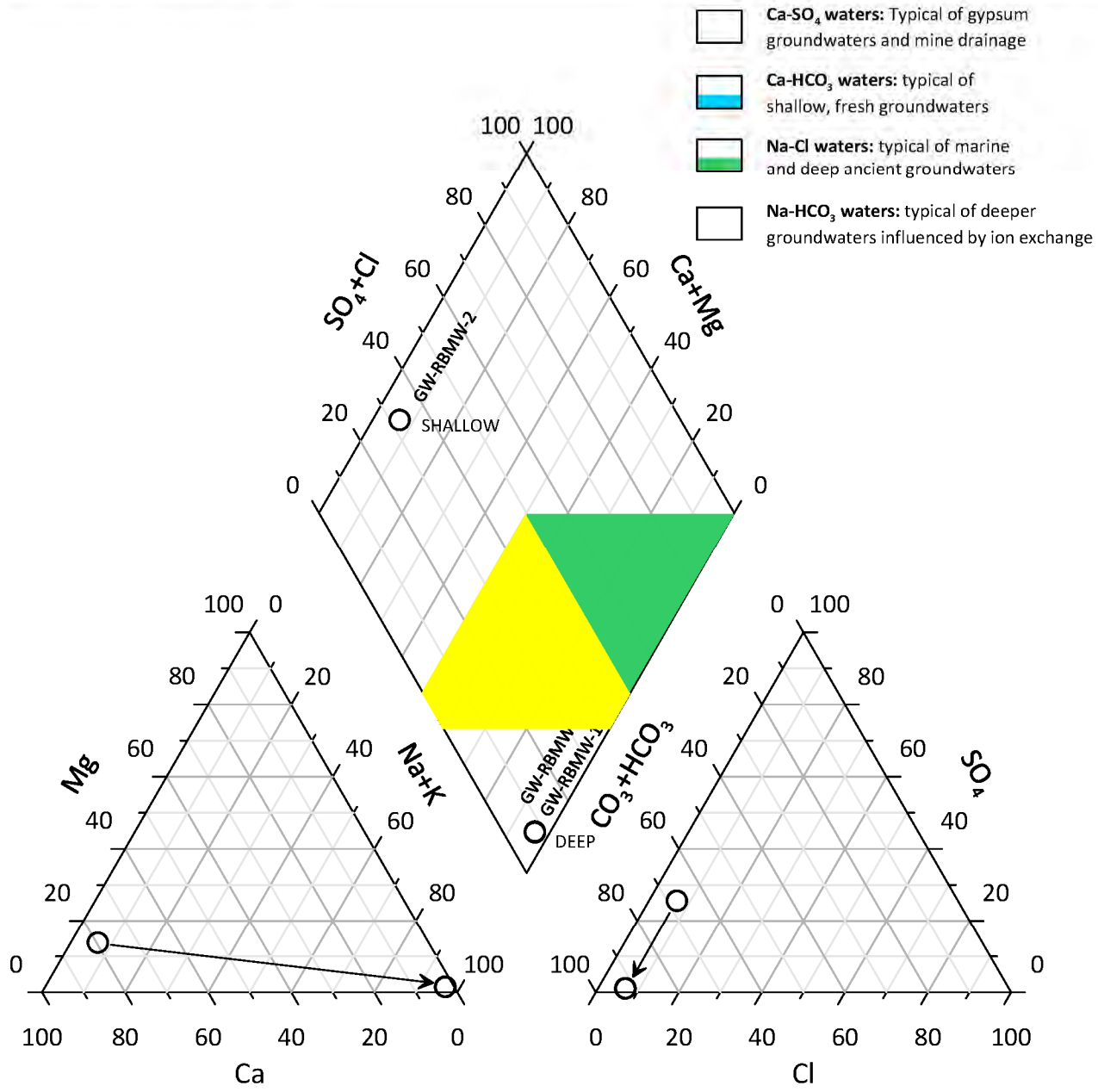

Figure 4: Piper Plot for EPA Water Samples

Figure 4 shows the ionic chemistry of the EPA samples from RBMW-1 and RBMW-2. (The two samples from RBMW-1 did not have any significant differences.) The shallow sample (obtained between 340 ft bgs and 440 ft bgs in RBMW-2) was of the Ca-HCO_3 type, which is typical of shallow, fresh groundwater, whereas the deeper samples (obtained between 900 ft bgs and 1,000 ft bgs in RBMW-1) were of the Na-HCO_3 type, which is typical of deeper groundwaters influenced by ion exchange.

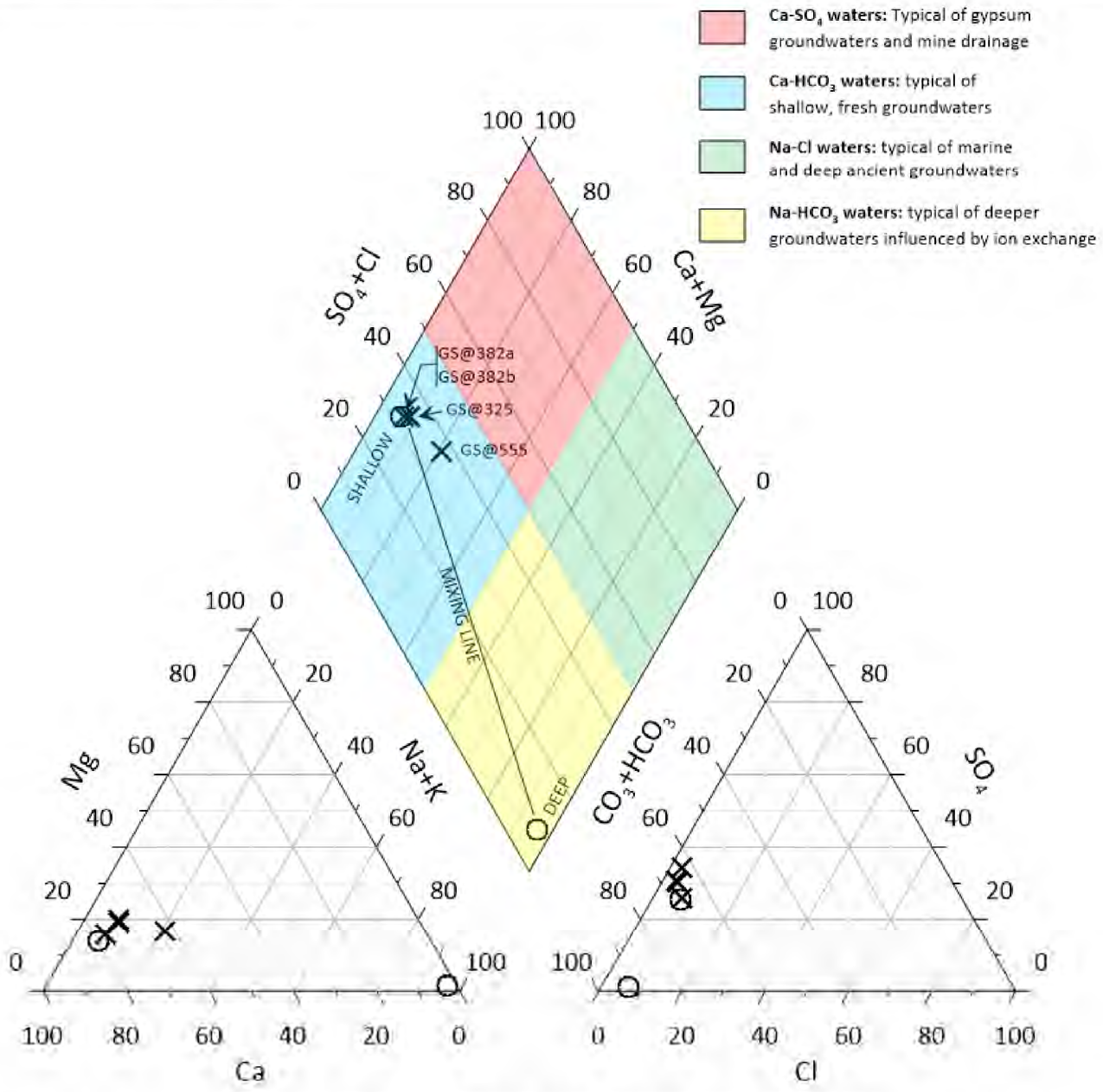

Figure 5: Piper Plot Comparing Grab Samples with EPA Samples

Figure 5 compares the three grab sample results with the EPA sample results. The grab samples from 382 ft bgs and 325 ft bgs are almost identical to the shallow groundwater sample GB-RBMW-2. The 555 ft bgs grab sample appears to be a shallow groundwater that has undergone some ion exchange.

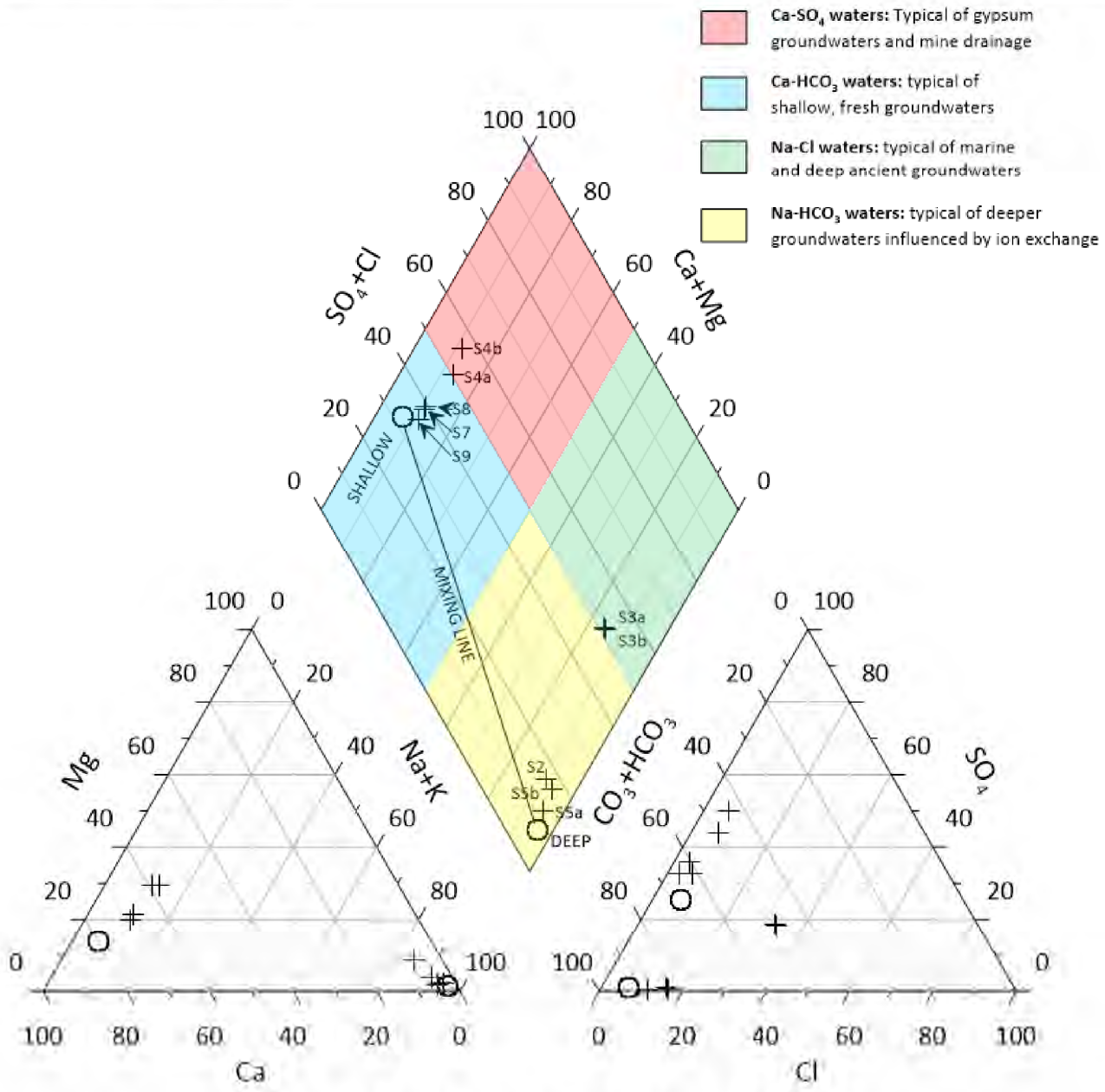

Figure 6: Piper Plot Comparing Seep Samples with EPA Samples

The surface seep samples are compared to the EPA samples in Figure 6. Seeps 7, 8, and 9 are consistent with shallow groundwater chemistry, and seeps 2 and 5 are similar to the deep groundwater chemistry. Seep 4 is close to the shallow groundwater chemistry; in fact, seep 4 appears to be shallow groundwater that has not yet undergone sulfate reduction. Similarly, seep 3 appears to be deep groundwater that has not yet undergone sulfate reduction.

Appendix B plots the surface seep chemistry results on a regional geologic map. The following are plausible geographic explanations for the difference in seep chemistries:

- Seeps obtained from quaternary landslide debris are consistent with shallow groundwater chemistry; seeps obtained from other surface formations (Modelo or Topanga) are consistent with deep groundwater chemistry.
- Seeps acquired to the south are consistent with shallow groundwater chemistry; seeps acquired to the north are consistent with deep groundwater chemistry. This suggests that the subsurface flow of groundwater may be from south to north.

These data are consistent with the change in groundwater chemistry as the water infiltrates the subsurface. As water moves across layers, the calcium ions are preferentially exchanged for sodium ions. This is a common occurrence in groundwater. As ion exchange occurs, the groundwater is expected to become more basic (pH increases) [11], which is consistent with the water chemistry data in Appendix A.

5.2 Groundwater Source

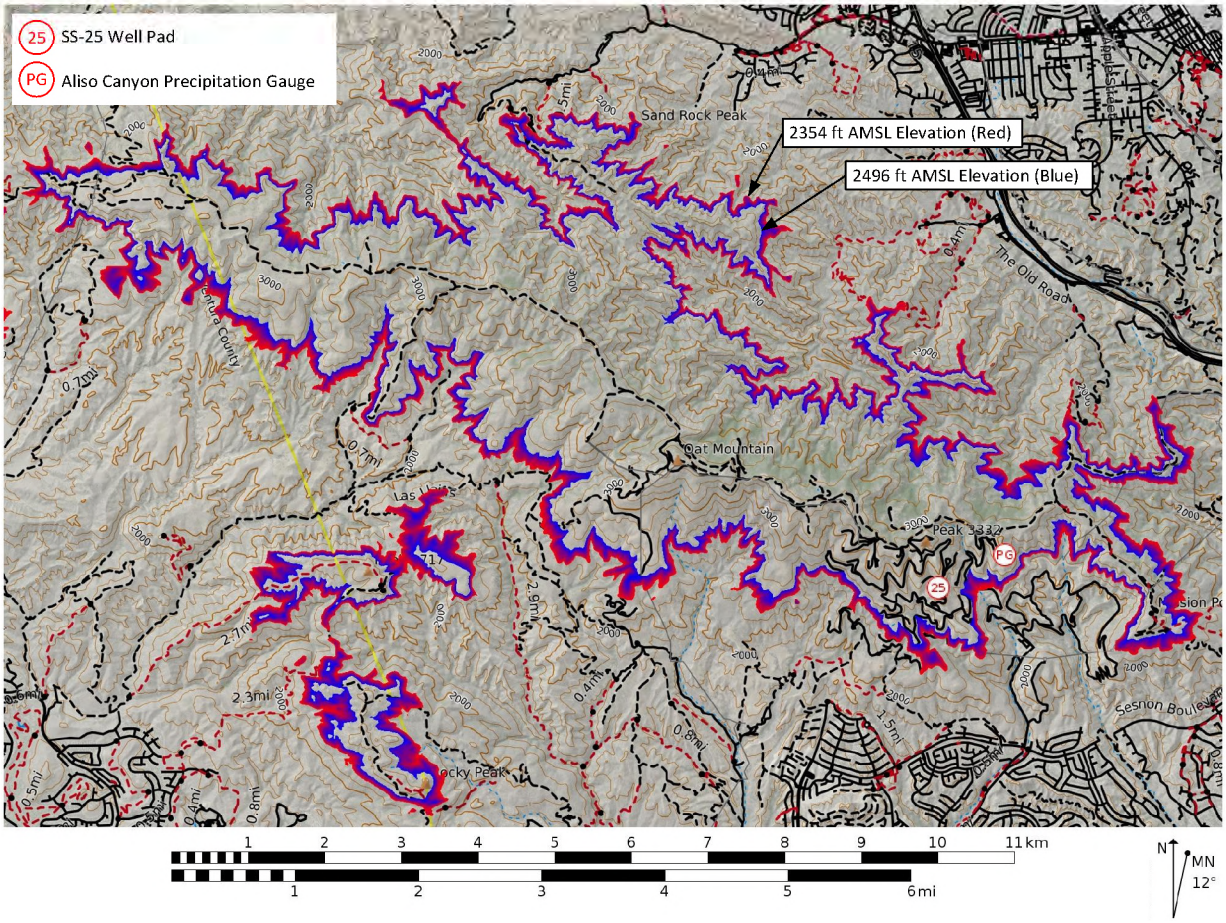

Figure 7: Regional Elevation Contour Map [12]

As described in Section 2, the potentiometric surface elevations are 2,496 ft AMSL (for shallow regime) and 2,354 ft AMSL (for deep regime). Therefore, the source of groundwater must lie above these elevations. Figure 7 shows the elevation map of the Aliso Canyon field. The 2,354 ft AMSL and

2,496 ft AMSL levels are marked[ii]. The source of groundwater must lie within these contours, but there are no surface bodies of water (lakes, rivers, etc.) within these contours. Therefore, by process of elimination, the source of groundwater must be the precipitation that falls inside these contours.

[ii] In Figure 7, the red-blue shaded (filled) region is the elevations between 2,354 ft AMSL and 2,496 ft AMSL. The red edge of the shaded area is the lower (2,354 ft AMSL) elevation; the blue edge of the shaded area is the higher (2,496 ft AMSL) contour.

6 Well Log Analysis

This study analyzed several geophysical logs, which were run in both RBMW-1 and SS-25 wells, for the presence of water. The types of logs that could be run in SS-25 were limited due to the presence of the 11 3/4-in. surface casing. In addition, it was anticipated that the formations around the SS-25 wellbore would likely have been disturbed because of the uncontrolled flow of gas and kill fluids during the SS-25 incident. Therefore, logs run in RBMW-1 were used to understand the subsurface hydrology, and SS-25 logs were re-interpreted based on these learnings.

6.1 RBMW-1 Well Logs

Several OH logs were run in RBMW-1, which was drilled approximately 600 ft south of SS-25 location. Logs were drilled both with the well TD at 555 ft bgs (when hole stability problems were encountered and addressed) and at 1,110 ft bgs (final depth). Table 1 summarizes the logs that were run at each depth.

Table 1: Geophysical Well Logs Run in RBMW-1 to Investigate Subsurface Geology and Groundwater

Logs Run at 555 ft TD	Logs Run at 1,110 ft TD
• Fluid temperature and differential temperature (Advisian) • Fluid electrical conductivity (EC) and differential EC (Advisian) • Formation conductivity (Advisian) • Natural gamma ray (Advisian) • Nuclear magnetic resonance (NRM) (Advisian)	• Fluid temperature and differential temperature (Advisian) • Fluid EC and differential EC (Advisian) • Formation conductivity (Advisian) • Natural gamma ray (Advisian) • NRM (Advisian) • Array Induction Imager Tool (AIT)-Platform Express (PEX) (Schlumberger) • Dielectric scanner (Schlumberger) • Spectral gamma ray (Schlumberger) • Formation micro imager (FMI) (Schlumberger) • Modular sonic imaging platform (Schlumberger) • Combinable magnetic resonance and Litho Scanner (Schlumberger)

Figure 8 is the composite display of geophysical logs run in and analyzed for the RBMW-1 well.

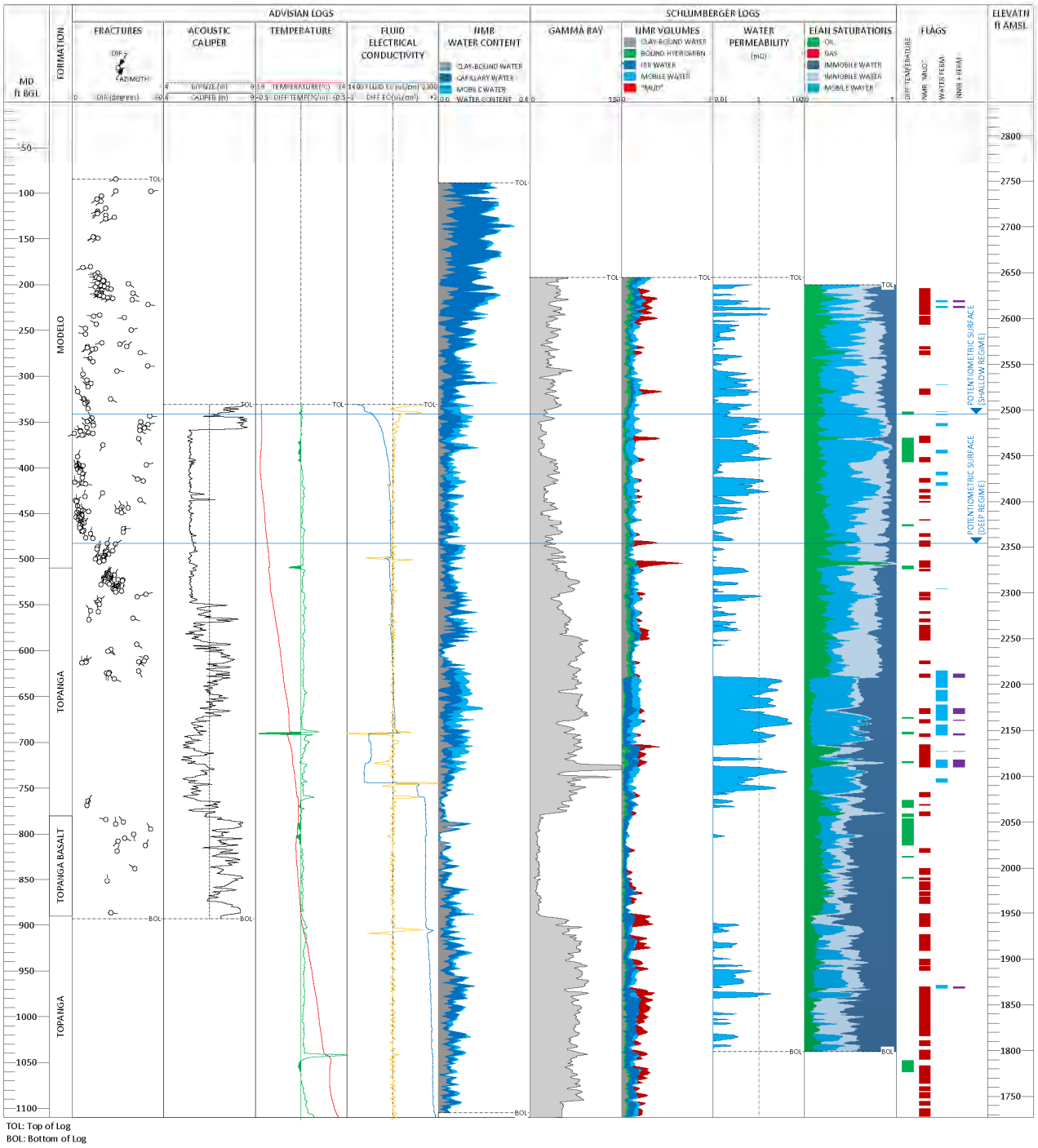

Figure 8: Composite Geophysical Logs for RBMW-1

The following observations may be made from the composite log:

- The fractures track indicates that there is extensive fracturing in the Modelo formation and in the portion of the Topanga formation down to about 650 ft bgs. There is some fracturing in the Topanga basalt. The log stops just below the Topanga basalt, so no observations are made regarding the lower Topanga formation under the basalt.

- The caliper log shows a smooth bore to about 550 ft (except near 350 ft). This is consistent with hole problems at 555 ft and the depths below being drilled with complete loss of returns.
- The temperature track, especially the differential temperature curve, is a possible indicator of water flow. In general, temperature increases with depth, so the differential temperature is typically slightly positive. Possible water flow zones are identified when differential temperature is negative. This process identifies two thicker and 11 thinner water flow zones.
- The fluid EC track does not provide much information related to water flow.
- The Advisian NMR track shows a thick layer with mobile water between 600–750 ft bgs.
- The gamma ray track is presented for correlation purposes.
- The Schlumberger NMR track provides two observations:
  - There is a thick layer of mobile water between 600–750 ft bgs, consistent with the Advisian NMR measurements.
  - The Schlumberger NMR track also suggests the presence of fractures. After the borehole was drilled it was filled with and stood full of fluid (i.e., 'mud') while the logs were being run. During this time, the fluid likely invaded permeable or fractured zones. These permeable or fractured zones are marked as 'mud' in the NMR track.
- The Schlumberger permeability track estimates permeability from correlations. These correlations are not very accurate, but suggest the presence of a thick layer of water between 600–750 ft bgs consistent with the NMR logs.
- The Schlumberger ELAN saturations track show presence of mobile water throughout the well.
- The flags track marks possible water locations as follows:
  - Differential temperature flag (green) is marked when the differential temperature is negative.
  - NMR mud flag (red) is marked when the Schlumberger NMR track indicates the presence of fluid invasion (i.e., 'mud') into permeable zones or fractures.
  - Water permeability flag (blue) is marked when Schlumberger water porosity is 1 mD or greater.
  - NMR and water flag (purple) is marked when both NMR mud and water permeability flags are marked.

The RBMW-1 composite log suggests that water is present in distinct permeable or fractured layers. However, it is difficult to correlate the location of these layers with data from logs that are run in cased holes.

6.2 SS-25 Logs

Since SS-25 had surface casing installed to 990 ft bgs, it was not possible to run OH logs (e.g., NMR, acoustic imaging, etc.), and we had to rely on interpreted cased hole log data to identify potential water zones.

Figure 9 shows a composite of geophysical logs run in the SS-25. The wellbore schematic is also shown with the locations of corrosion and casing holes marked.

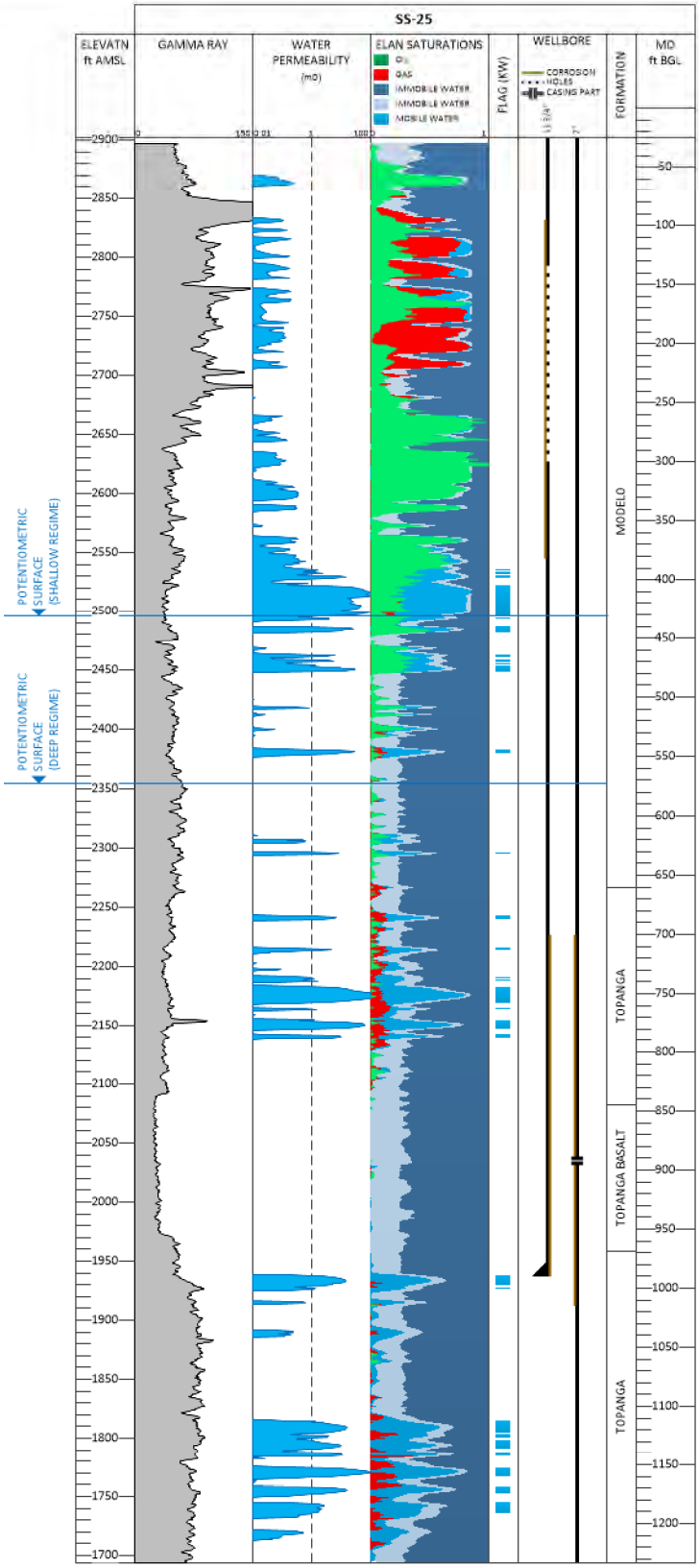

Figure 9: Composite Geophysical Logs for SS-25

The following observations may be made from the SS-25 composite log:

- The ELAN saturations track indicates the presence of gas in three distinct zones:
  - Between 80–230 ft bgs, opposite holes discovered in the 11 3/4 in. surface casing
  - Between 650–800 ft bgs
  - Between 1,120–1,220 ft bgs
- The water permeability track (for permeability greater than 1 mD) and mobile water in ELAN saturation tracks are correlated and likely mark the water zones. There are four groups of water zones:
  - Between 390–480 ft bgs, but most prominently between 400–430 ft bgs
  - Between 740–790 ft bgs. This zone also shows residual gas saturation.
  - Between 990–1,000 ft bgs. This zone is at the 11 3/4 in. casing shoe.
  - Between 1,110–1,190 ft bgs. This zone also shows residual water saturation.

Similar to RBMW-1, this composite log is consistent with water flowing in distinct highly permeable or fractured layers. A key observation is that the 11 3/4 in. casing shoe at 990 ft was placed in a water-bearing zone at the time the well was originally drilled in 1953.

7 Precipitation Analysis

As previously described, the only feasible source for the groundwater is precipitation that falls on the Aliso Canyon field above the 2,354 ft AMSL elevation. Therefore, historical precipitation records were analyzed for the region to see if they could provide insight into the behavior of the groundwater.

The following describes the precipitation characteristics for Los Angeles County [13, p. 7]:

> Precipitation (rainfall) in the Los Angeles area occurs primarily in the form of winter orographic rainfall associated with extra tropical cyclones of North Pacific origin. Major storms consist of one or more frontal systems and occasionally last four days or longer. Air masses and frontal systems associated with major storms commonly extend for 500 to 1,000 miles in length and produce rainfall simultaneously throughout the [Los Angeles] County. Major storms approach Southern California from the west or northwest with southerly winds which continue until frontal passage. The mountain ranges lie directly across the path of the inflow of warm, moist air, and orographic effects greatly intensify precipitation.

In addition, "nearly all precipitation occurs during the months of December through March" [13, p. 7]. Therefore, Los Angeles authorities have adopted a 'rain year' concept to analyze annual precipitation. A rain year starts on October 01 and continues until September 30 of the next year. For example, '2014–2015 rain year' starts on October 01, 2014, and ends on September 30, 2015. The rain year concept has also been adopted for this report. The SS-25 incident occurred at the beginning of the 2015–2016 rain year.

Precipitation data are available from two sources:

- An ALERT (Automatic Local Evaluation in Real Time) rain gauge (ALERT ID 302, Auto Raingage Reference ID 446), operated by Los Angeles County Public Works, located within the Aliso Canyon facility. This gauge is located near Porter tanks 1 and 2, approximately 3,135 ft east-northeast of SS-25, at 2,950 ft AMSL elevation[iii]. Daily precipitation data are usually available starting in 1995, but they are not complete.
- An annual total precipitation for the San Fernando Valley (SFV) as calculated by Los Angeles County authorities. Data are available online starting with the 1996–1997 rain year[iv]. Data quality is high. However, SFV is at 900 ft AMSL elevation. Since precipitation is dominated by orographic effects, it is expected to be higher at higher elevations than in the SFV. The normal annual SFV precipitation is 17.60 in.

[iii] Although Los Angeles County Public Works lists the elevation for this gauge as 2,367 ft, the correct elevation has been verified as 2,950 ft AMSL.

[iv] Data for previous rain years may be available by mail but were not analyzed in this report.

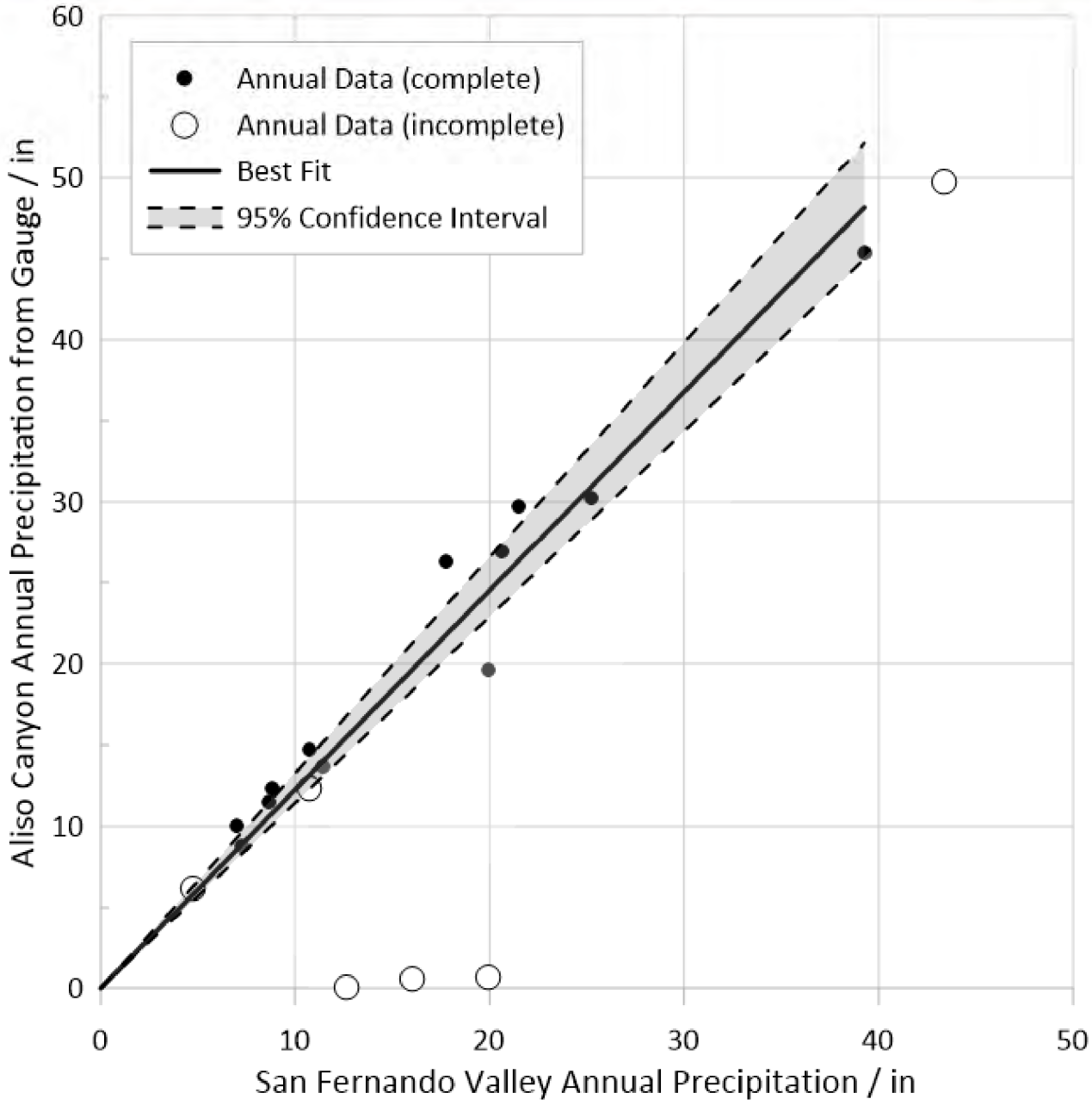

Figure 10: Correlation of Aliso Canyon's Precipitation with San Fernando Valley's Precipitation

Figure 10 correlates the Aliso Canyon's precipitation gauge measurements with SFV's total precipitation. Neglecting the years for which Aliso Canyon gauge data are incomplete, the correlation determines that Aliso Canyon's precipitation is 1.226 ± 0.037 times the SFV precipitation (R=0.99). Based on this correlation, the normal annual Aliso Canyon precipitation is estimated at 21.58 in.

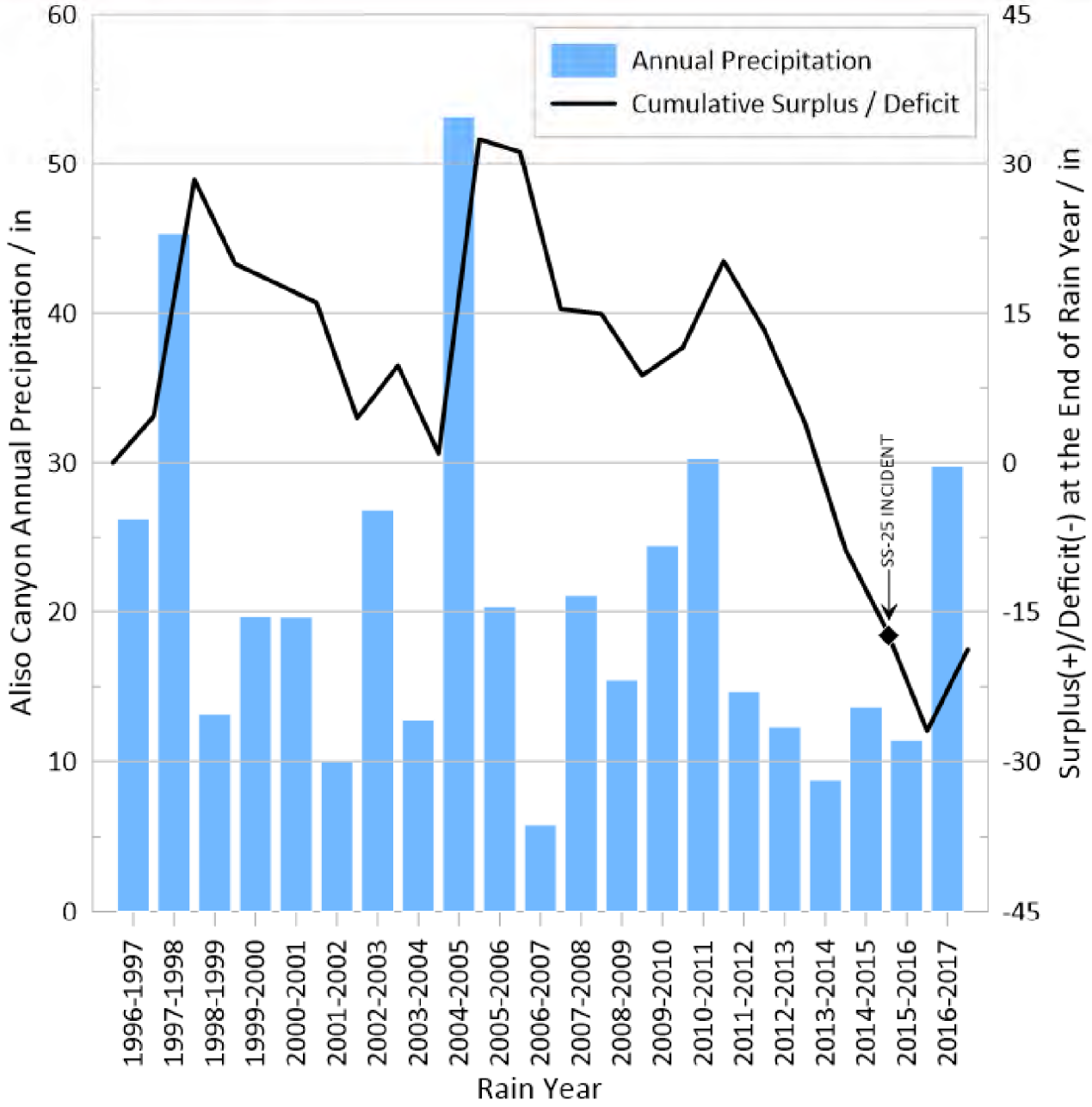

Figure 11: Aliso Canyon Annual Precipitation (1996–2017)

Figure 11 shows the Aliso Canyon's precipitation for rain years starting with 1996–1997. Data are taken from the Aliso Canyon's rain gauge for those years with complete records and estimated from SFV's precipitation for the remaining years. In addition, a cumulative precipitation surplus[v] (positive) or deficit (negative) is also shown.

[v] Cumulative surplus at the end of a rain year is calculated as follows:

- Take the cumulative surplus at the end of the previous rain year,
- Add total precipitation during the current rain year, and
- Subtract the normal annual precipitation of 21.58 in.

Cumulative surplus is set to zero at the end of the 1995–1996 rain year.

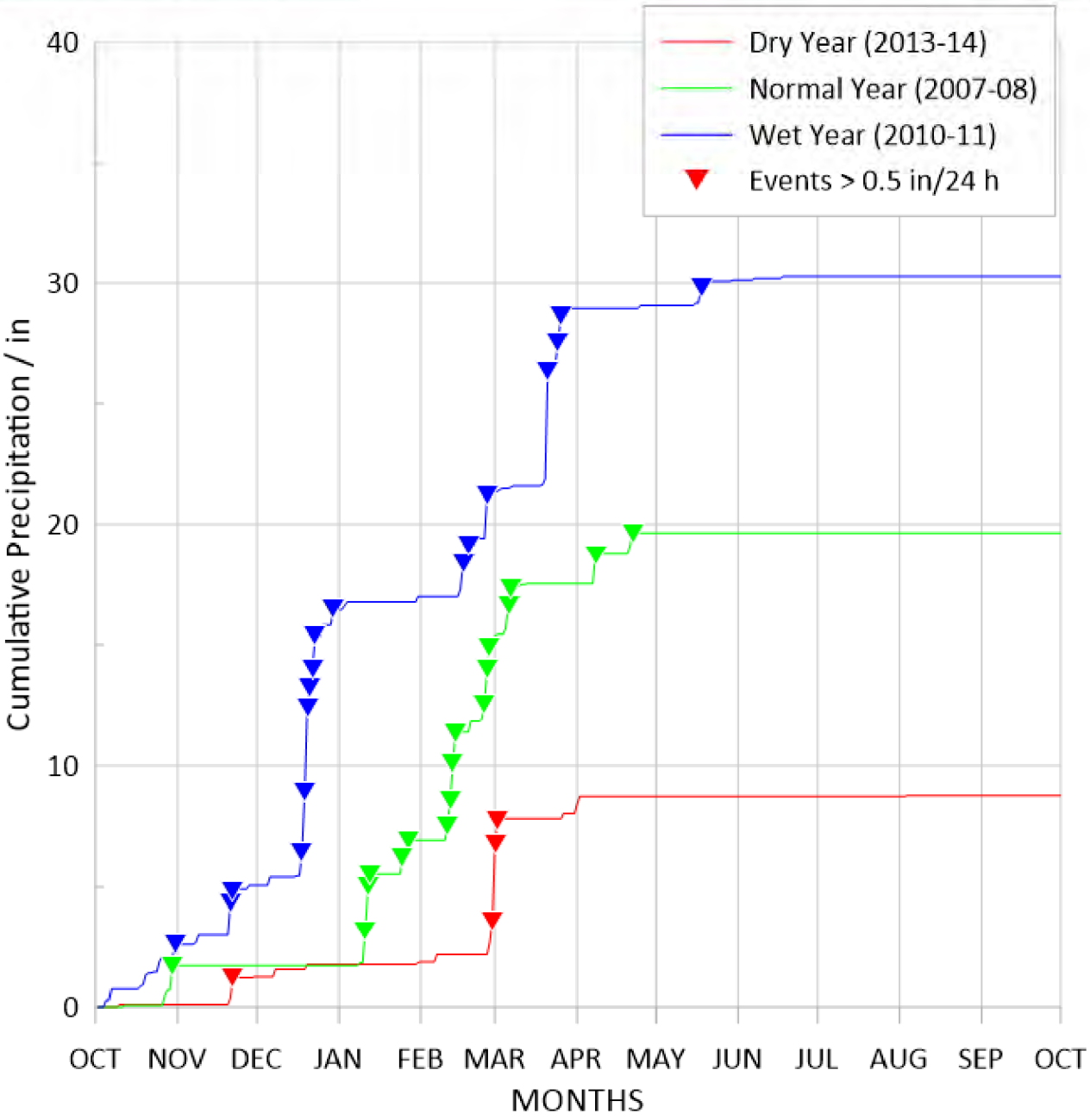

Figure 12: Annual Distribution of Rainfall in Aliso Canyon for Typical Dry, Normal, and Wet Years

Figure 12 shows daily distribution of annual precipitation for three typical years:

- The 2013–2014 rain year was drier than normal.
- The 2007–2008 rain year was close to normal.
- The 2010–2011 rain year was wetter than normal.

Note that the sudden increases in cumulative precipitation (marked by arrows) show the storms producing rain in the Santa Susana Mountains. Most of these storms occurred during the months of

December through March, consistent with the precipitation characteristics described earlier in this section.

Since precipitation is the source of groundwater, groundwater level should be related to precipitation level and groundwater level will vary within a given rain year. The groundwater level will rise during the rainy period from December to March, reaching its highest level at the end of the rainy period in March. The groundwater will then fall during the dry period from March to November, reaching its lowest level at the beginning of the subsequent rainy period. In addition, groundwater level will also vary from year-to-year: it will rise after wetter-than-normal rain years, it will remain steady after normal rain years, and it will fall after drier-than-normal rain years.

With this observation, the precipitation data can be used to estimate the relative groundwater level between 1997 and 2018 (Figure 13). This figure shows that the estimated groundwater level at the time of the SS-25 incident was the lowest it had been since at least 1997, and that the groundwater level in June 2018, when RBMW-1 and RBMW-2 were sampled, was similar to the level at the time of the SS-25 incident.

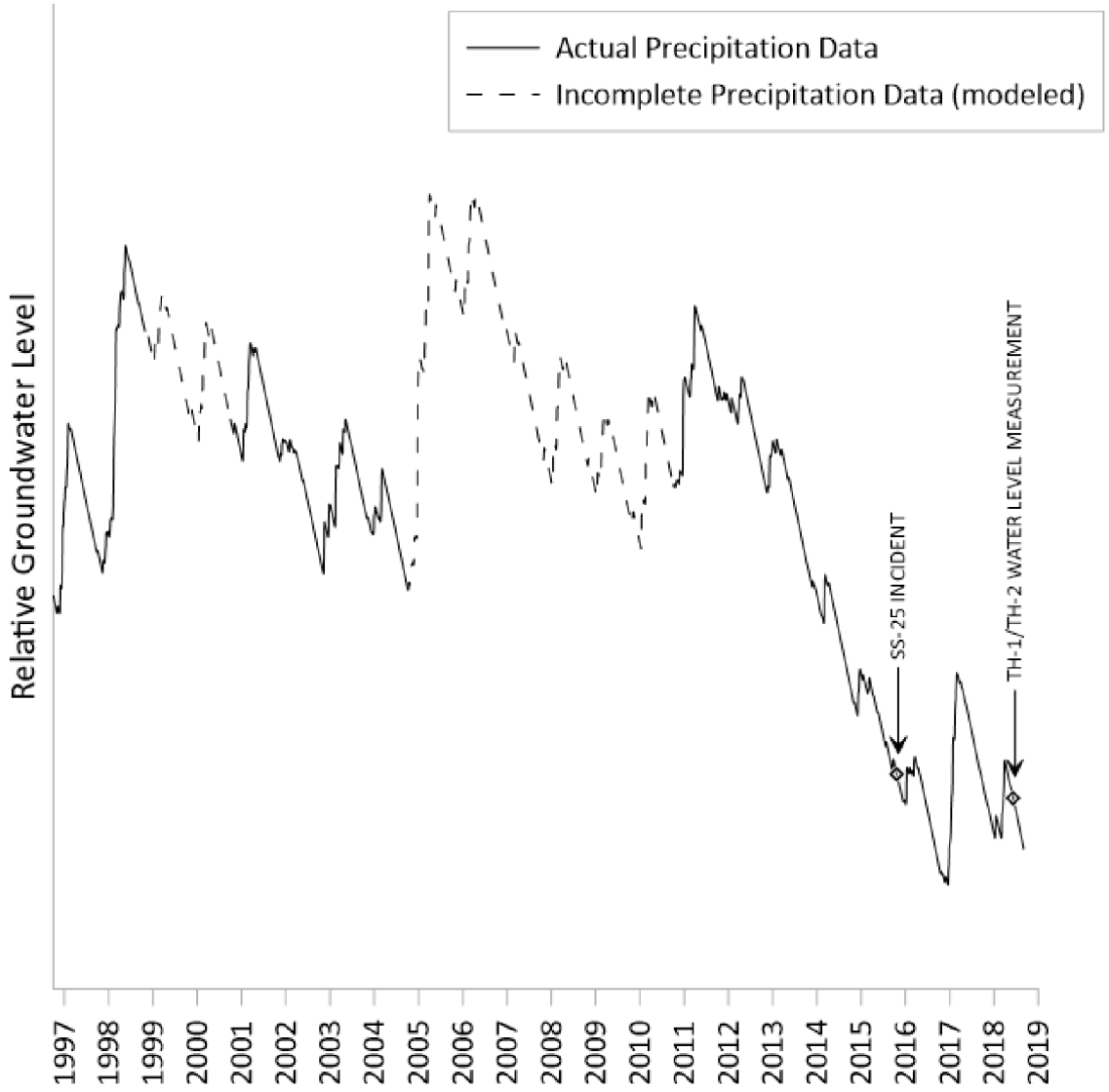

Figure 13: Conceptual Groundwater Level in Aliso Canyon (1996–2018)

8 Conceptual Groundwater Model

Figure 14 depicts the conceptual groundwater model that was developed based on data presented in this report.

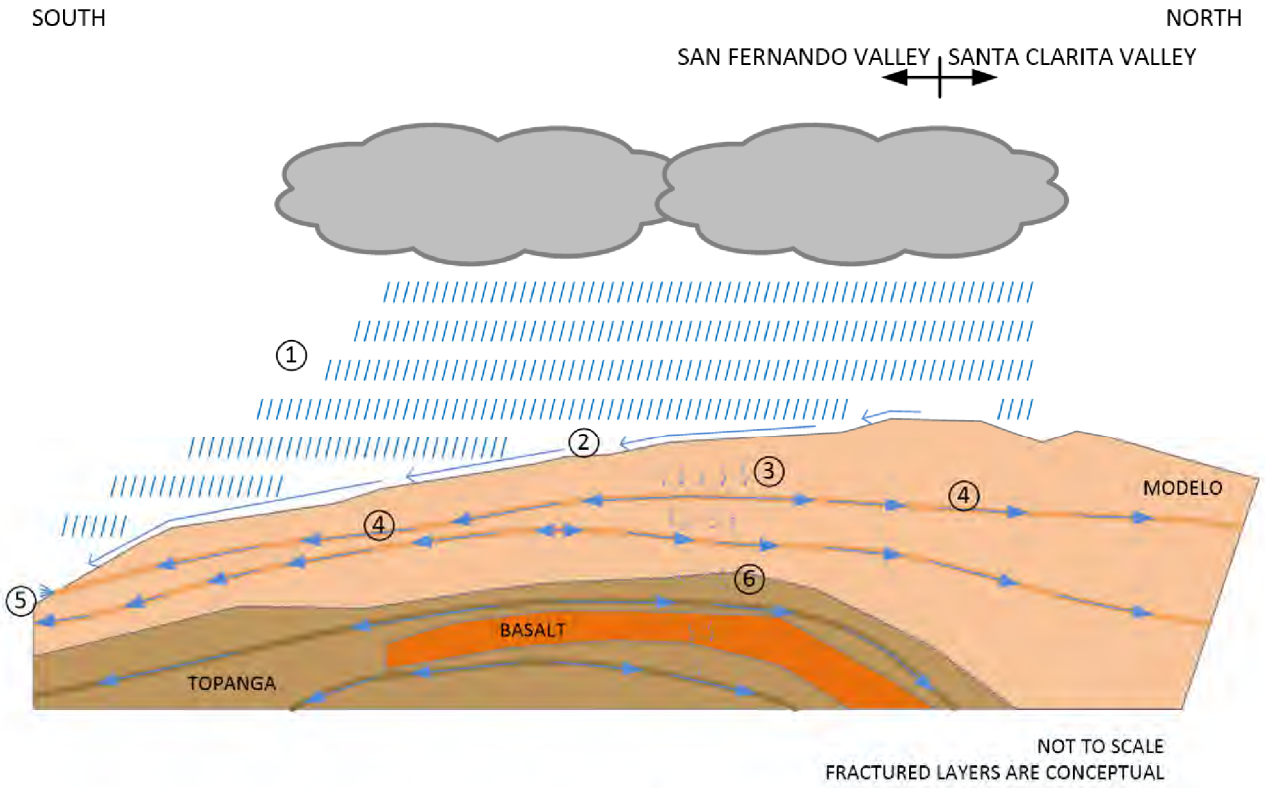

Figure 14: Conceptual Hydrologic Model

Precipitation falls on the Santa Susana Mountains around the Aliso Canyon field ①. Most of the precipitation flows on the surface as runoff ②. Remaining precipitation infiltrates into the ground and seeps vertically down ③. When water encounters permeable (most likely fractured) layers, some of it will enter the layer and move laterally within the permeable layer ④ to surface seeps ⑤ or to aquifers underlying the adjacent valleys to the south and north. Depending on the orientation of the layer, the movement may be to the south towards the SFV or north towards the Santa Clarita Valley (SCV); since shallower formations (above the older Santa Susana thrust fault) on the northern portion of the Aliso Canyon field dip to the north, a significant portion of the flow may be to the north towards the SCV. Remaining water continues to seep downward, losing pressure and undergoing ion exchange in the process ⑥.

As precipitation varies from month-to-month and year-to-year, the groundwater level will also vary. It will rise during the rainy season (December–March) and after wetter-than-normal years, and will fall during the dry season (April–November) and after drier-than-normal years.

9 SS-25 Implications

In SS-25, corrosion was observed visually on the outer surface of 7 in. production casing between 700 ft and 1,015 ft MD. In addition, corrosion was inferred from logs on the inner surface of the 11 3/4 in. surface casing at corresponding depths, between 700 ft MD and the casing shoe at 990 ft MD. Corrosion was further inferred from logs on the outer surface of the 11 3/4 in. surface casing between 95 ft and 395 ft. Finally, holes were observed in the 11 3/4 in. surface casing between 134 ft and 300 ft MD.

Corrosion requires the presence of water. Therefore, discovery of corrosion implies that water was present at the indicated depths at some point or throughout the life of the well. The groundwater investigated during the present study was the likely source of such water.

The 11 3/4 in. × 7 in. annulus corrosion was located between 700 ft and 1,015 ft MD (1,912–2,227 ft AMSL). These depths are below the June 2018 potentiometric surface elevation of 2,354 ft AMSL for the deeper groundwater regime. As discussed in Section 7, the June 2018 potentiometric surface elevation was likely among the lowest elevations since at least October 1996, and possibly during the well lifetime. Therefore, it was likely that the groundwater infiltrated into the annulus provided that there was a path.

ELAN analysis of the SS-25 logs (Figure 15, right side) indicates that the 11 3/4 in. surface casing shoe at 990 ft MD was placed in a high-permeability, likely fractured, 9 ft thick, water-bearing zone at the time of well construction in 1953[vi]. This situation provides the likely path of the groundwater to infiltrate into the 11 3/4 in. × 7 in. casing annulus.

The surface casing corrosion between 95 ft and 395 ft MD corresponds to 2,532–2,832 ft AMSL elevations. These elevations are above the June 2018 potentiometric surface elevation of 2,496 ft AMSL for the shallower groundwater regime. However, as discussed in Section 7, the June 2018 potentiometric surface elevation is likely among the lowest elevations since at least October 1996, and possibly during the well lifetime; the potentiometric surface elevation was almost certainly higher at some point during (if not most of) the well lifetime. Therefore, it is possible that the groundwater was the source of the water resulting in corrosion outside the 11 3/4 in. surface casing.

ELAN analysis of SS-25 logs (Figure 15) also provided insight into the path taken by the gas (and accompanying kill fluids during kill attempts) that escaped SS-25 during the October 2015–February 2016 incident. The interpretation is that the ELAN gas saturations were residuals from gas escaping into the zones at those depths.

[vi] The placement of the shoe into the water-bearing zone in 1953 was likely inadvertent.

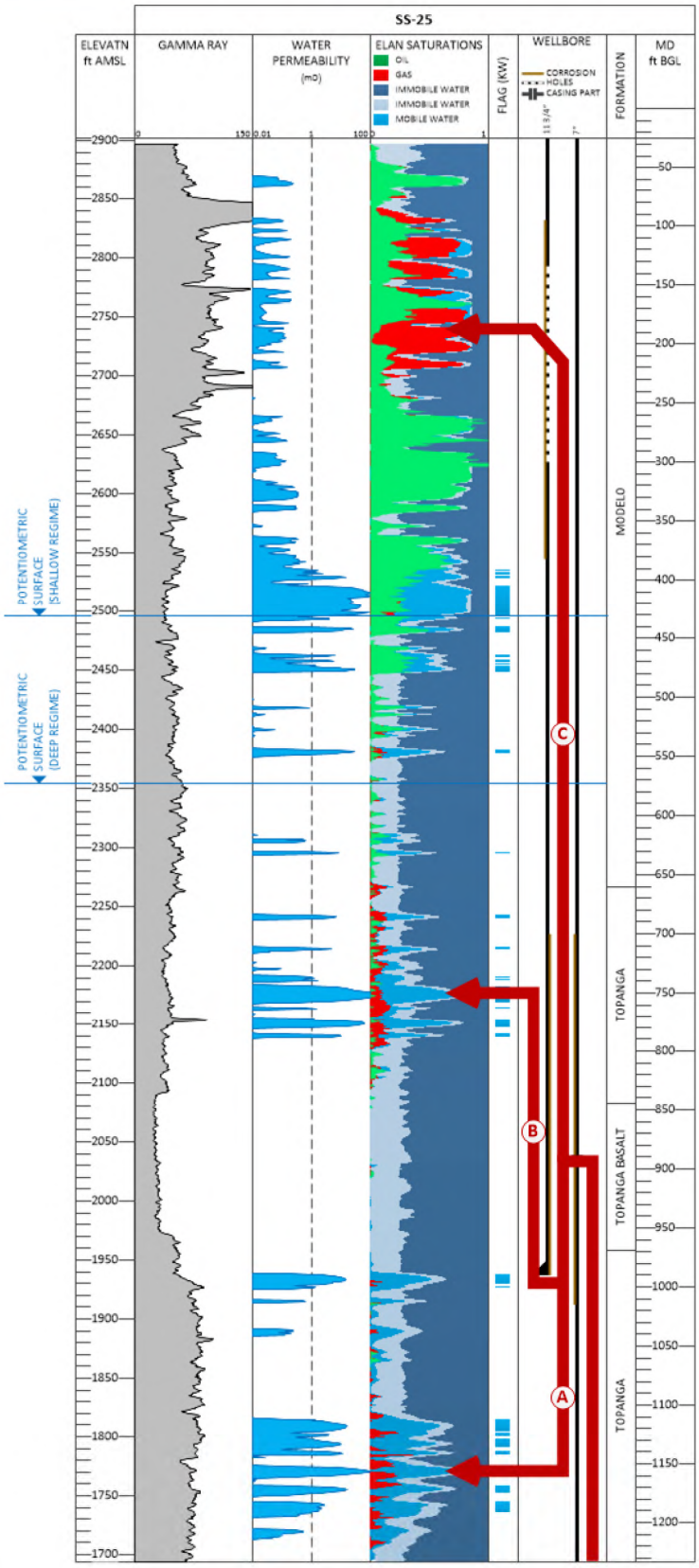

Figure 15: Possible Leak Paths for Escaping Gas

Figure 15 shows that there were three paths for the gas after it escaped from the 7 in. production casing at the parting located at 892 ft MD:

- The first path (marked "A" in Figure 15) was down the 11 3/4 in. × 7 in. annulus to the surface casing shoe, down outside the 7 in. production casing, and into the (lower) Topanga formation between 1,113 ft and 1,222 ft MD (1,705–1,814 ft AMSL).
- The second path (marked "B" in Figure 15) was down the 11 3/4 in. × 7 in. annulus to the surface casing shoe, around the surface casing shoe, up outside the surface casing, and into the (upper) Topanga formation between 656 ft and 798 ft MD (2,129–2,271 ft AMSL).
- The third path (marked "C" in Figure 15) was up the 11 3/4 in. × 7 in. annulus to holes between 134 ft and 300 ft MD and into the Modelo formation between 84 ft and 230 ft MD (corresponding to 2,697–2,843 ft AMSL).

10 References

[1] E. P. Poeter, "Lecture Notes, Colorado School of Mines, GEGN 467 - Ground Water Engineering, Water Chemistry 2 - Sampling and Presentation," [Online]. Available: http://inside.mines.edu/~epoeter/_GW/18WaterChem2/WaterChem2pdf.pdf.

[2] Geosyntec Consultants, "Subsurface Assessment Report, Investigative Order R4-2016-0035, Aliso Canyon Gas Storage Facility, Los Angeles County, California," Los Angeles, CA, 2018.

[3] State Water Rights Board Referee, "Report of Referee, Volume I: Text and Plates," Superior Court of California in and for the County of Los Angeles, 1962.

[4] State Water Rights Board Referee, "Report of Referee, Volume II: Appendices," Superior Court of the State of California in and for the County of Los Angeles, 1962.

[5] California Department of Toxic Substances Control, "Santa Susana Field Lab," [Online]. Available: www.dtsc.ca.gov/SiteCleanup/Santa_Susana_Field_Lab/index.cfm OR www.dtsc-ssfl.com.

[6] County of Los Angeles Department of Public Works, "Hydrologic Reports," [Online]. Available: http://dpw.lacounty.gov/wrd/report/.

[7] F. C. Hodges and E. R. Murray-Aaron, "Newhall-Portero, Aliso Canyon, Del Valle, and Oak Canyon Oil Fields," *California Oil Fields, Summary of Operations, Twenty-Ninth Annual Report of the State Oil and Gas Supervisor,* pp. 5-29, 1943.

[8] A. M. Piper, "A Graphic Procedure in the Geochemical Interpretation of Water Analyses," U.S. Geological Survey , Washington, D.C., 1953.

[9] W. Back and B. B. Hanshaw, "Chemical Geohydrology," U.S. Geological Survey, Washington, D.C., 1965.

[10] Z. Miao, M. L. Brusseau, K. C. Carroll, C. Carreón-Diazconti and B. Johnson, "Sulfate reduction in groundwater: characterization and applications for remediation," *Environmental Geochemistry and Health,* vol. 34, no. 4, pp. 539-550, 2012.

[11] "Geology 304 - Study Guide and Lecture Notes, Groundwater Chemical Evolution," January 2013. [Online]. Available: https://web.viu.ca/earle/geol304/304g.pdf.

[12] "CalTopo," [Online]. Available: https://caltopo.com/map.html.

[13] County of Los Angeles Department of Public Works, "Hydrologic Report 2014-2015".

[14] J. M. Carter, D. G. Driscoll, J. E. Williamson and V. A. Lindquist, "Atlas of Water Resources in the Black Hills Area, South Dakota," U.S. Geological Survey, 2002.

Appendix A Water Chemistry Data

Table A-1: List of EPA and Grab Samples

Sample Type	Sample ID	Sampling Well	Sampling Depth
EPA Sample	GW-RBMW-1	RBMW-1	900–1,000 ft bgs
EPA Sample	GW-RBMW-1-DUP	RBMW-1	900–1,000 ft bgs
EPA Sample	GW-RBMW-2	RBMW-2	340–440 ft bgs
Grab Sample	W-TH1-382	RBMW-1	382 ft bgs
Grab Sample	W-TH1-382-DUP	RBMW-1	382 ft bgs
Grab Sample	W-TH1-555	RBMW-1	555 ft bgs
Grab Sample	W-TH1-325	RBMW-1	325 ft bgs
See Table A-2 for water chemistry data.			

Table A-2: Water Chemistry Data for Grab Samples and EPA Samples [2]

Parameter	Units	Water Quality Objectives[1]	MCLs[2]	Sample ID and Date						
				W-TH1-382	W-TH1-382-DUP	W-TH1-555	TH1-W-325	GW-RBMW-1 Topanga (deep)	GW-RBMW-1-DUP Topanga (deep)	GW-RBMW-2 Modelo (shallow)
				3/20/2018	3/20/2018	3/28/2018	4/5/2018	6/8/2018	6/8/2018	6/8/2018
Total Dissolved Solids (SM 2540C)										
Total Dissolved Solids	mg/L	800	500*	865	875	970	650	1,090	1,090	1,010
Metals (EPA Method 200.7/200.8/245.1)										
Antimony	mg/L	NE	0.006	0.002	0.002	0.00185 J	0.000367 J	0.00168	0.00174	0.000207 J
Arsenic	mg/L	NE	0.010	0.225 J	0.244 J	0.0309	ND<0.00438	ND<0.00438	ND<0.00438	ND<0.00438
Barium	mg/L	NE	1	0.184 J	0.129 J	0.407	0.0812	0.175	0.179	0.0537
Beryllium	mg/L	NE	0.004	ND<0.000290	ND<0.000290	ND<0.000290	0.000457	0.00058 J	ND<0.00029	ND<0.00029
Cadmium	mg/L	NE	0.005	0.00938	0.00962	0.0146	0.00165 J	0.000288 J	0.000336 J	0.000967 J
Chromium (total)	mg/L	NE	0.050	ND<0.0541	ND<0.0541	0.0156	0.00668 J	0.00915 J	0.00747 J	ND<0.00271
Cobalt	mg/L	NE	NE	ND<0.0589	ND<0.0589	ND<0.0589	ND<0.00295	ND<0.00295	ND<0.00295	ND<0.00295
Copper	mg/L	NE	1.3**	0.00557	0.0113	0.0312	0.0273	0.0150	0.0147	0.00476
Lead	mg/L	NE	0.015**	0.000329 J	0.000591 J	0.00602 J	0.00129	0.019	0.0194	ND<0.00009
Mercury	mg/L	NE	0.002	ND<0.0000453	ND<0.0000453	ND<0.0000453	ND<0.0000453	0.000057 J	0.0000527 J	ND<0.0000453
Molybdenum	mg/L	NE	NE	52.9	53.6	43.6	0.0927	0.0211	0.0151	0.125
Nickel	mg/L	NE	0.1	0.109	0.108	0.108	0.0180	0.00686	0.00643	0.0521
Selenium	mg/L	NE	0.05	0.0048	0.00431	0.0122 B	0.00950 B	0.000879 J	0.000955 J	0.00379
Silver	mg/L	NE	0.1*	ND<0.000111	ND<0.000111	ND<0.000111	ND<0.000111	0.00707	0.00732	0.0222
Thallium	mg/L	NE	0.002	0.000248 J	0.000240 J	0.00298 J	ND<0.000101	ND<0.000101	ND<0.000101	ND<0.000101
Vanadium	mg/L	NE	NE	ND<0.0488	ND<0.0488	ND<0.0244	0.0151	0.00471 J	0.00434 J	0.00445 J
Zinc	mg/L	NE	5.0*	ND<0.0704	0.119 J	0.106	ND<0.00352	1.30	1.32	0.0895
Benzene, Toluene, Ethylbenzene, and Total Xylenes (EPA 8021 B)										
Benzene	µg/L	NE	1	ND<0.25	ND<0.25	ND<0.25	ND<0.25	0.46 J	0.52	ND<0.25
Toluene	µg/L	NE	150	ND<0.19	ND<0.19	ND<0.19	ND<0.19	150	170	0.24 J
Ethylbenzene	µg/L	NE	300	ND<0.25	ND<0.25	ND<0.25	ND<0.25	ND<0.25	ND<0.25	ND<0.25
Xylenes (total)	µg/L	NE	1750	ND<0.21	ND<0.21	ND<0.21	ND<0.21	ND<0.21	0.72	0.33 J
p/m-Xylene	µg/L	NE	NE	ND<0.49	ND<0.49	ND<0.49	ND<0.49	ND<0.49	ND<0.49	ND<0.49
o-Xylene	µg/L	NE	NE	ND<0.21	ND<0.21	ND<0.21	ND<0.21	ND<0.21	0.72	0.33 J
Total Petroleum Hydrocarbons as Crude Oil (EPA 8015B (M))										
TPH as Crude Oil	µg/L	NE	NE	ND<190	ND<190	ND<190	ND<190	420	1100	480
Polycyclic Aromatic Hydrocarbons (EPA 8270 [SIM])										
Acenaphthene	µg/L	NE	NE	ND<0.059	ND<0.059	ND<0.058	ND<0.060	ND<0.062	ND<0.074	ND<0.073
Acenaphthylene	µg/L	NE	NE	ND<0.072	ND<0.072	ND<0.071	ND<0.074	ND<0.076	ND<0.074	ND<0.073
Anthracene	µg/L	NE	NE	ND<0.066	ND<0.066	ND<0.065	ND<0.068	ND<0.069	ND<0.060	ND<0.059
Benzo (a) Anthracene	µg/L	NE	NE	ND<0.075	ND<0.075	ND<0.075	ND<0.077	ND<0.079	ND<0.073	ND<0.071
Benzo (a) Pyrene	µg/L	NE	0.2	ND<0.099	ND<0.099	ND<0.098	ND<0.100	ND<0.100	ND<0.067	ND<0.066
Benzo (b) Fluoranthene	µg/L	NE	NE	ND<0.083	ND<0.083	ND<0.082	ND<0.085	ND<0.087	ND<0.068	ND<0.066
Benzo (g,h,i) Perylene	µg/L	NE	NE	ND<0.092	ND<0.092	ND<0.092	ND<0.095	ND<0.097	ND<0.074	ND<0.073
Benzo (k) Fluoranthene	µg/L	NE	NE	ND<0.078	ND<0.078	ND<0.077	ND<0.080	ND<0.082	ND<0.071	ND<0.070
Dibenzothiophene	µg/L	NE	NE	ND<0.11	ND<0.11	ND<0.11	ND<0.11	ND<0.067	ND<0.077	ND<0.076
Chrysene	µg/L	NE	NE	ND<0.064	ND<0.064	ND<0.064	ND<0.066	ND<0.079	ND<0.066	ND<0.065
Dibenz (a,h) Anthracene	µg/L	NE	NE	ND<0.075	ND<0.075	ND<0.074	ND<0.077	ND<0.120	ND<0.080	ND<0.079
Fluoranthene	µg/L	NE	NE	ND<0.072	ND<0.072	ND<0.071	ND<0.074	ND<0.076	ND<0.085	ND<0.084
Fluorene	µg/L	NE	NE	ND<0.071	ND<0.071	ND<0.070	ND<0.073	ND<0.074	ND<0.100	ND<0.100
Indeno (1,2,3-c,d) Pyrene	µg/L	NE	NE	ND<0.080	ND<0.080	ND<0.079	ND<0.082	ND<0.084	ND<0.082	ND<0.081
1-Methylnaphthalene	µg/L	NE	NE	ND<0.072	ND<0.072	ND<0.072	ND<0.074	ND<0.076	ND<0.110	ND<0.110
2-Methylnaphthalene	µg/L	NE	NE	ND<0.073	ND<0.073	ND<0.072	ND<0.075	ND<0.076	ND<0.075	ND<0.073
Naphthalene	µg/L	NE	NE	ND<0.071	ND<0.071	ND<0.071	ND<0.073	1.0	0.80	0.57
Phenanthrene	µg/L	NE	NE	ND<0.065	ND<0.065	ND<0.065	ND<0.067	ND<0.069	ND<0.070	ND<0.068
Pyrene	µg/L	NE	NE	ND<0.069	ND<0.069	ND<0.069	ND<0.071	ND<0.073	ND<0.071	ND<0.070
Radionuclides (EPA Method 900/903/903.1/Ra-05)										
Gross Alpha Particle Activity	pCi/L	NE	15	153 ± 8.68	-	569 ± 17.5	11.8 ± 2.32	7.65 ± 1.56	10.2 ± 2.60	9.88 ± 2.89
Uranium	pCi/L	NE	20	139 ± 7.31	-	166 ± 7.59	7.28 ± 1.78	0.746 ± 0.911	0.373 ± 0.808	7.33 ± 1.99
Radium-226	pCi/L	NE	5[3]	1.50 ± 0.382	-	0.928 ± 0.271	0.289 ± 0.169	0.101 ± 0.085	0.043 ± 0.063	0.187 ± 0.109
Radium-228	pCi/L	NE	5[3]	0.000 ± 0.506	-	0.000 ± 0.615	0.000 ± 0.569	0.043 ± 0.666	0.017 ± 0.738	0.125 ± 0.748
Methane (RSK - 175M)										
Methane	µg/L	NE	NE	2.34	2.04	0.431 J	77.6	7220	4910	16.9
Mercaptans (LACSD 258)										
Mercaptans	mg/L	NE	NE	0.067 J	ND<0.062	0.088 J	ND<0.062	ND<0.062	ND<0.062	ND<0.062
Major and Minor Cations (EPA Method 200.7)										
Sodium	mg/L	NE	NE	26.3	28.1	99.7	10.7	475	469	15.3
Potassium	mg/L	NE	NE	4.51 J	3.89 J	5.30	0.978	5.05	5.20	1.26
Magnesium	mg/L	NE	NE	36.0 B	35.4 B	43.2 B	13.3 B	3.97	3.98	18
Calcium	mg/L	NE	NE	215	224	266	106	9.24	9.47	171
Major and Minor Anions (EPA Method 300.0)										
Nitrate (as N)	mg/L	10	10	ND<0.053	ND<0.053	ND<0.053	0.18	ND<0.045	ND<0.045	ND<0.045
Chloride	mg/L	150	250*	17	15	15	28	44	44	27
Sulfate	mg/L	300	250*	190	190	230	140	10	10	140
Alkalinity	mg/L	NE	NE	431	422	440 BU	378	881	866	385
Bromide	mg/L	NE	NE	ND<0.058	ND<0.058	0.063 J	0.14	0.11	0.12	0.12
Trace Elements (EPA Method 200.7/200.8)										
Lithium	mg/L	NE	NE	ND<0.0803	ND<0.0803	ND <0.00402	ND <0.00402	0.0521	0.0542	ND<0.0402
Strontium	mg/L	NE	NE	1.18	1.22	2.08	0.498	0.403	0.415	0.748
Boron	mg/L	8	NE	0.173	0.178	0.476 J	0.0899	1.67	1.8	0.0887
Iron	mg/L	NE	0.3*	14.4	13.9	38.5	3.11	4.46	3.83	0.0266
Manganese	mg/L	NE	0.05*	0.443	0.457	0.619	0.0743	0.0623	0.0587	0.0569
pH										
pH by Field Method	pH units	6.5 - 8.5	NE	8.19	-	8.34	7.15	8.32	8.32	6.75

Notes:

"-" = Not analyzed

1: Basin Plan Objective - Designated by the LARWQCB for San Fernando Basin, west of Highway 405.

2: Maximum Contaminant Levels (MCLs), Title 22 of California Code of Regulations, February 2013; a conservative screening level that may not be applicable to seep water, surface water, or oil field groundwater.

3: Screening level value of 5 combines radium-226 & -228.

***: Values are not actually MCLs, but secondary MCLs. Secondary MCLs address esthetics such as taste and odor and are only enforceable for community water systems.

****: Values referred to as MCLs for lead and copper are not actually MCLs; instead, they are called "Action Levels" under the lead and copper rule.

J: Analyte was detected at a concentration below the reporting limit and above the laboratory method detection limit. Reported value is estimated.

B: B Analyte was present in the associated method blank

NE: Not established

mg/L: Milligrams per liter

µg/L: Micrograms per liter

pCi/L: Picocuries per liter

ND<X: Not detected above the listed laboratory Method Detection Limit

Table A-3: List of Seep Samples

Sample Type	Sample ID	Sampling Elevation	Geologic Formation	
N/A	Seep-1	2,000 ft AMSL	Ttus/Ttls	Topanga (upper/lower interface)
Seep Sample	Seep-2-20170801	2,210 ft AMSL	Tm/Tml	Modelo (Monterey Shale) (upper/lower interface)
Seep Sample	Seep-3-20170801	2,040 ft AMSL	Tm/Tml	Modelo (Monterey Shale) (upper/lower interface)
Seep Sample	Seep-3-DUP-20170801	2,040 ft AMSL	Tm/Tml	Modelo (Monterey Shale) (upper/lower interface)
Seep Sample	Seep-4-20170801	1,740 ft AMSL	Qls/Tm	Quaternary landslide on Modelo (Monterey Shale) (upper)
Seep Sample	Seep-4 (Regional Board)	1,740 ft AMSL	Qls/Tm	Quaternary landslide on Modelo (Monterey Shale) (upper)
Seep Sample	Seep-5-20170801	2,140 ft AMSL	Ttls	Topanga (lower)
Seep Sample	Seep-5 (Regional Board)	2,140 ft AMSL	Ttls	Topanga (lower)
N/A	Seep-6	2,120 ft AMSL	Ttus	Topanga (lower)
Seep Sample	Seep-7-20170801	2,180 ft AMSL	Qls/Tml	Quaternary landslide on Modelo (Monterey Shale) (lower)
Seep Sample	Seep-8-20170801	2,180 ft AMSL	Qls/Tml	Quaternary landslide on Modelo (Monterey Shale) (lower)
Seep Sample	Seep-9-20170801	2,210 ft AMSL	Qls/Tml	Quaternary landslide on Modelo (Monterey Shale) (lower)
N/A	Seep-10	2,350 ft AMSL	Qls/Tml	Quaternary landslide on Modelo (Monterey Shale) (lower)
N/A	Seep-11	2,220 ft AMSL	Tm	Quaternary landslide on Modelo (Monterey Shale) (upper)
See Table A-4 for water chemistry data. Seeps 1, 6, 10 and 11 could not be sampled due to insufficient flow.				

Table A-4: Water Chemistry Data for Seep Samples [2]

Parameter	Units	Sample ID and Date										
		Seep-2-20170801	Seep-3-20170801	Seep-3-DUP-20170801	Seep-4-20170801	Seep-4 (Regional Board)	Seep-5-20170801	Seep-5 (Regional Board)	Seep-7-20170801	Seep-8-20170801	Seep-9-20170801	Seep-Blank-20170801
		8/1/2017	8/1/2017	8/1/2017	8/1/2017	8/1/2017	8/1/2017	8/1/2017	8/1/2017	8/1/2017	8/1/2017	8/1/2017
Total Dissolved Solids (SM 2540C)												
Total Dissolved Solids	mg/L	1,540	2,300	2,300	1,300	1,321	1,260	1,358	765	865	945	ND<1
Metals (EPA Method 200.7/200.8/245.1)												
Antimony	mg/L	ND<0.001	0.000188 J	0.000198 J	0.000253 J	ND<0.001	0.000167 J	0.0004 J	ND<0.001	ND<0.001	0.000156 J	ND<0.001
Arsenic	mg/L	0.0122	0.00655 J	0.0122 J	0.00585 J	ND<0.001	0.00573 J	0.0006	ND<0.0150	0.00941 J	ND<0.0150	ND<0.0150
Barium	mg/L	0.169	0.104	0.107	0.0215	0.0187	0.161	0.1365	0.0362	0.0397	0.0558	ND<0.0100
Beryllium	mg/L	ND<0.001	ND<0.001	ND<0.001	ND<0.001	ND<0.001	ND<0.001	ND<0.001	ND<0.001	ND<0.001	ND<0.001	ND<0.001
Cadmium	mg/L	ND<0.001	ND<0.001	ND<0.001	ND<0.001	ND<0.0004	0.000819 J	0.0004	0.000138 J	0.000265 J	ND<0.001	ND<0.001
Chromium (total)	mg/L	ND<0.010	ND<0.010	ND<0.010	ND<0.010	0.0091 J	0.00368 J	0.0018	ND<0.010	ND<0.010	ND<0.010	ND<0.010
Cobalt	mg/L	ND<0.010	ND<0.010	ND<0.010	ND<0.010	0.0002 J	ND<0.010	0.0007	ND<0.010	ND<0.010	ND<0.010	ND<0.010
Copper	mg/L	0.000416 J	0.00520	0.00208	0.00109	ND<0.01	0.00633	0.001	0.000976 J	0.00112	0.00103	ND<0.001
Lead	mg/L	0.000159 J	0.000239 J	0.000237 J	0.000199 J	ND<0.00	0.00268	0.0002	ND<0.001	ND<0.001	ND<0.001	ND<0.001
Mercury	mg/L	ND<0.0002	ND<0.0002	ND<0.0002	ND<0.0002	ND<0.0000	ND<0.0002	0.00001	ND<0.0002	ND<0.0002	ND<0.0002	ND<0.0002
Molybdenum	mg/L	0.0200	0.0133	0.0139	0.00476 J	0.00120	ND<0.010	0.0029	0.0505	0.0623	0.0546	ND<0.010
Nickel	mg/L	0.00133	0.00487	0.00348	0.00411	0.00060	0.00745	0.0026	0.00722	0.0132	0.00762	ND<0.001
Selenium	mg/L	0.000832 J	0.00115	0.00136	ND<0.001	0.0004 J	0.000850 J	0.0016	0.00600	0.000972 J	0.00358	ND<0.001
Silver	mg/L	ND<0.001	ND<0.001	ND<0.001	ND<0.001	ND<0.001	ND<0.001	ND<0.001	ND<0.001	ND<0.001	ND<0.001	ND<0.001
Thallium	mg/L	ND<0.001	ND<0.001	ND<0.001	0.000130 J	ND<0.001	0.000106 J	ND<0.001	ND<0.001	ND<0.001	ND<0.001	ND<0.001
Vanadium	mg/L	ND<0.010	0.00309 J	0.00338 J	ND<0.010	0.0005	0.0113	0.0063	0.00674 J	0.00361 J	ND<0.010	ND<0.010
Zinc	mg/L	0.0405	ND<0.010	0.00987 J	ND<0.010	ND<0.001	0.0348	0.00619	ND<0.010	ND<0.010	ND<0.010	ND<0.010
Benzene, Toluene, Ethylbenzene, and Total Xylenes (EPA 8021 B)												
Benzene	µg/L	ND<0.5	ND<0.5	ND<0.5	ND<0.5	ND<1.0	ND<0.5	ND<1.0	ND<0.5	ND<0.5	ND<0.5	ND<0.5
Toluene	µg/L	ND<0.5	ND<0.5	ND<0.5	ND<0.5	ND<1.0	ND<0.5	ND<1.0	ND<0.5	ND<0.5	ND<0.5	ND<0.5
Ethylbenzene	µg/L	ND<0.5	ND<0.5	ND<0.5	ND<0.5	ND<1.0	ND<0.5	ND<1.0	ND<0.5	ND<0.5	ND<0.5	ND<0.5
Xylenes (total)	µg/L	ND<0.5	ND<0.5	ND<0.5	ND<0.5	ND<1.0	ND<0.5	ND<1.0	ND<0.5	ND<0.5	ND<0.5	ND<0.5
p/m-Xylene	µg/L	ND<1	ND<1	ND<1	ND<1	ND<1	ND<1	ND<1	ND<1	ND<1	ND<1	ND<1
o-Xylene	µg/L	ND<0.5	ND<0.5	ND<0.5	ND<0.5	ND<1.0	ND<0.5	ND<1.0	ND<0.5	ND<0.5	ND<0.5	ND<0.5
Total Petroleum Hydrocarbons as Crude Oil (EPA 8015B (M))												
TPH as Crude Oil	µg/L	ND<250	ND<240	ND<240	ND<240	ND<0.3	ND<240	250	-	-	ND<230	-
Polycyclic Aromatic Hydrocarbons (EPA 8270 [SIM])												
Acenaphthene	µg/L	ND<0.19	ND<0.19	ND<0.19	ND<0.19	ND<0.01	ND<0.19	ND<0.01	-	-	ND<0.19	-
Acenaphthylene	µg/L	ND<0.19	ND<0.19	ND<0.19	ND<0.19	ND<0.01	ND<0.19	ND<0.01	-	-	ND<0.19	-
Anthracene	µg/L	ND<0.19	ND<0.19	ND<0.19	ND<0.19	ND<0.01	ND<0.19	ND<0.01	-	-	ND<0.19	-
Benzo (a) Anthracene	µg/L	ND<0.19	ND<0.19	ND<0.19	ND<0.19	ND<0.01	ND<0.19	ND<0.01	-	-	ND<0.19	-
Benzo (a) Pyrene	µg/L	ND<0.19	ND<0.19	ND<0.19	ND<0.19	ND<0.01	ND<0.19	ND<0.01	-	-	ND<0.19	-
Benzo (b) Fluoranthene	µg/L	ND<0.19	ND<0.19	ND<0.19	ND<0.19	ND<0.01	ND<0.19	ND<0.01	-	-	ND<0.19	-
Benzo (g,h,i) Perylene	µg/L	ND<0.19	ND<0.19	ND<0.19	ND<0.19	ND<0.01	ND<0.19	ND<0.01	-	-	ND<0.19	-
Benzo (k) Fluoranthene	µg/L	ND<0.19	ND<0.19	ND<0.19	ND<0.19	ND<0.01	ND<0.19	ND<0.01	-	-	ND<0.19	-
Dibenzothiophene	µg/L	ND<0.19	ND<0.19	ND<0.19	ND<0.19	ND<0.01	ND<0.19	ND<0.01	-	-	ND<0.19	-
Chrysene	µg/L	ND<0.19	ND<0.19	ND<0.19	ND<0.19	ND<0.01	ND<0.19	ND<0.01	-	-	ND<0.19	-
Dibenz (a,h) Anthracene	µg/L	ND<0.19	ND<0.19	ND<0.19	ND<0.19	ND<0.01	ND<0.19	ND<0.01	-	-	ND<0.19	-
Fluoranthene	µg/L	ND<0.19	ND<0.19	ND<0.19	ND<0.19	ND<0.01	ND<0.19	ND<0.01	-	-	ND<0.19	-
Fluorene	µg/L	ND<0.19	ND<0.19	ND<0.19	ND<0.19	ND<0.01	ND<0.19	ND<0.01	-	-	ND<0.19	-
Indeno (1,2,3-c,d) Pyrene	µg/L	ND<0.19	ND<0.19	ND<0.19	ND<0.19	ND<0.01	ND<0.19	ND<0.01	-	-	ND<0.19	-
1-Methylnaphthalene	µg/L	ND<0.19	ND<0.19	ND<0.19	ND<0.19	ND<0.01	ND<0.19	ND<0.01	-	-	ND<0.19	-
2-Methylnaphthalene	µg/L	ND<0.19	ND<0.19	ND<0.19	ND<0.19	ND<0.01	ND<0.19	ND<0.01	-	-	ND<0.19	-
Naphthalene	µg/L	ND<0.19	ND<0.19	ND<0.19	ND<0.19	0.0031	ND<0.19	0.0035	-	-	ND<0.19	-
Phenanthrene	µg/L	ND<0.19	ND<0.19	ND<0.19	ND<0.19	ND<0.01	ND<0.19	ND<0.01	-	-	ND<0.19	-
Pyrene	µg/L	ND<0.19	ND<0.19	ND<0.19	ND<0.19	ND<0.01	ND<0.19	ND<0.01	-	-	ND<0.19	-
Radionuclides (EPA Method 900/908/903.1/Ra-05)												
Gross Alpha Particle Activity	pCi/L	0.000 ± 0.601	1.76 ± 1.25	1.64 ± 1.33	1.15 ± 0.569	-	1.29 ± 0.643	-	6.25 ± 2.27	-	5.18 ± 1.33	-
Uranium	pCi/L	0.000 ± 0.516	0.322 ± 0.698	0.000 ± 0.557	0.107 ± 0.631	-	0.215 ± 0.666	-	3.76 ± 1.38	-	4.40 ± 1.47	-
Radium-226	pCi/L	0.161 ± 0.125	0.201 ± 0.137	0.182 ± 0.131	0.263 ± 0.154	-	0.263 ± 0.153	-	0.241 ± 0.147	-	0.161 ± 0.124	-
Radium-228	pCi/L	0.319 ± 0.654	0.000 ± 0.631	0.000 ± 0.603	0.000 ± 0.510	-	0.000 ± 0.483	-	0.034 ± 0.637	-	0.000 ± 0.571	-
Methane (RSK - 175M)												
Methane	µg/L	141	0.378 J	0.407 J	1140	901	1.32	ND<5.0	0.0800 J	0.0840 J	0.100 J	0.127 J
Mercaptans (LACSD 25S)												
Mercaptans	mg/L	ND<0.1	ND<0.1	ND<0.1	ND<0.1	-	ND<0.1	-	ND<0.1	ND<0.1	ND<0.1	ND<0.1
Major and Minor Cations (EPA Method 200.7)												
Sodium	mg/L	637	848	848	62.2	52.9	568	482	35.5	37.0	41.0	ND<0.5
Potassium	mg/L	6.69	7.93	8.31	2.75	2.4	4.36	2.60	2.19	2.16	1.60	ND<0.5
Magnesium	mg/L	14.2	44.7	46.5	76.7	73.4	6.53	4.7	34.8	39.6	44.1	0.0441 J
Calcium	mg/L	30.3	57.7	59.2	246	242.6	14.9	20.0	201	204	227	ND<0.1
Major and Minor Anions (EPA Method 300.0)												
Nitrate (as N)	mg/L	0.10	0.92	0.93	ND<0.1	ND<0.03	0.61	ND<0.03	0.65	0.11	ND<0.1	-
Chloride	mg/L	150	450	460	47	47	94	87	26	18	17	-
Sulfate	mg/L	15	340	340	420	505	2.0	3.7	190	230	250	-
Alkalinity	mg/L	1,140	930	945	496	464	1,010	638	372	406	511	-
Bromide	mg/L	1.2	4.1	4.0	0.13	0.253	0.086 J	0.58	0.14	ND<0.1	0.071 J	-
Trace Elements (EPA Method 200.7/200.8)												
Lithium	mg/L	0.0322 J	0.0389 J	0.0404 J	0.0175 J	0.0424	0.0672	0.0575	ND<0.05	ND<0.05	ND<0.05	ND<0.05
Strontium	mg/L	0.810	2.74	2.82	2.92	2.91	0.624	0.631	1.33	1.45	1.67	ND<0.03
Boron	mg/L	3.96	5.89	5.97	0.497	0.4682	2.92	3.40	0.402	0.408	0.377	ND<0.05
Iron	mg/L	0.310	0.655	0.659	0.0275 J	1.1973 J	4.93	0.75	0.0413 J	0.0174 J	0.372	ND<0.1
Manganese	mg/L	0.0536	0.0289	0.0223	0.0283	0.0276	0.0880	0.0713	0.000592 J	0.0395	0.0733	ND<0.001
pH												
pH by Field Method	pH units	8.40	8.36	6.76	NC	6.5	8.3	8.2	7.51	7.61	7.28	-

Notes:

"-" = Not analyzed

J: Analyte was detected at a concentration below the reporting limit and above the laboratory method detection limit. Reported value is estimated

B: B Analyte was present in the associated method blank

mg/L: Milligrams per liter

µg/L: Micrograms per liter

pCi/L: Picocuries per liter

ND<X: Not detected above the listed laboratory Method Detection Limit

Appendix B Water Seeps on Geologic Map

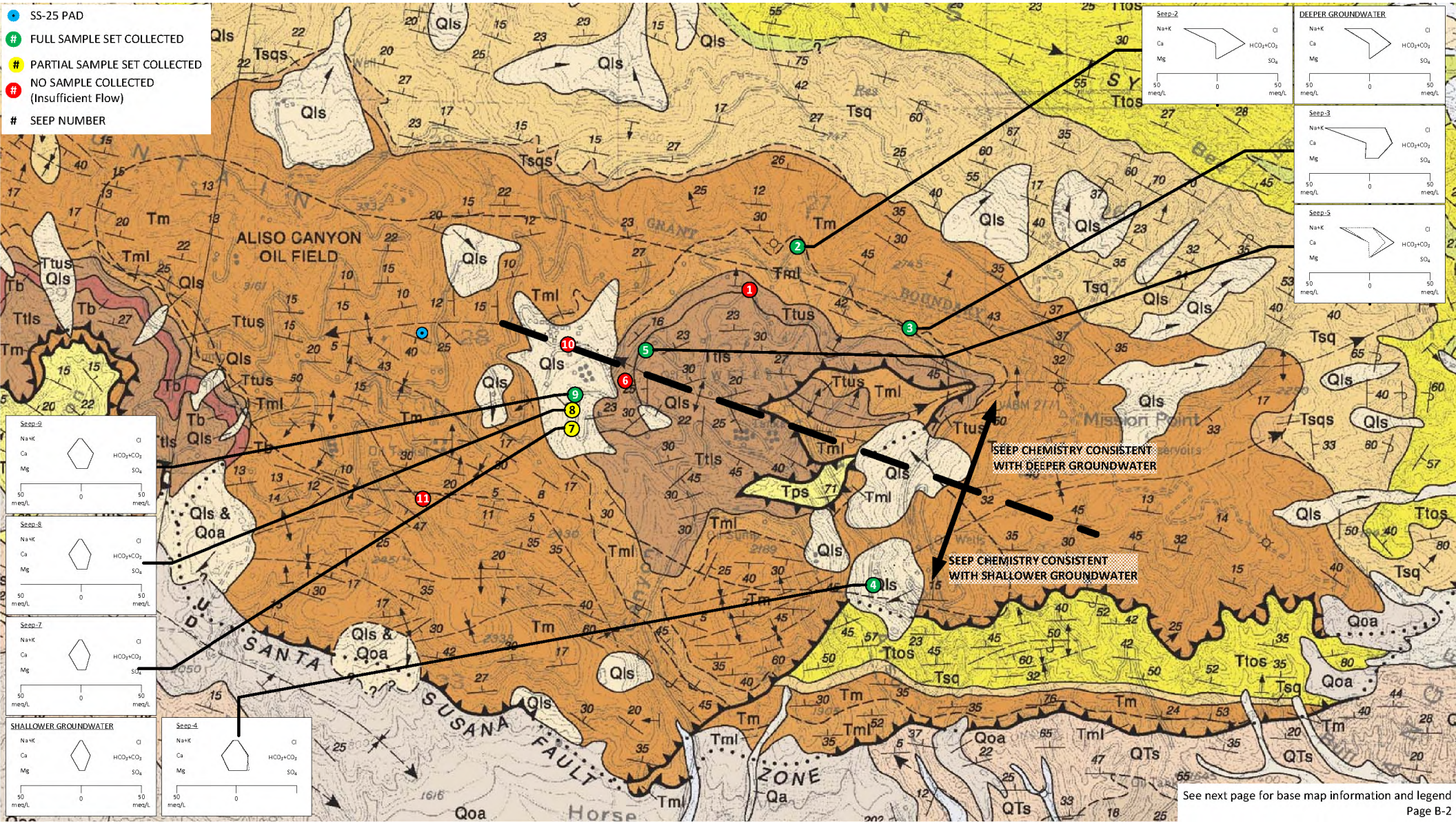

See next page for base map information and legend
Page B-2

af
Qa
Qg

SURFICIAL SEDIMENTS

Unconsolidated alluvial deposits; generally undissected

af *artificial cut and fill*

Qg *gravel and sand of major stream channels*

Qa *alluvial gravel, sand and clay of valley and floodplain areas*

Qls

LANDSLIDE DEBRIS

Qos
Qoa

OLDER SURFICIAL SEDIMENTS

Dissected, weakly consolidated alluvial deposits

Qos *older sandy alluvium, including slope wash, derived from Chatsworth Formation (**Kcs**)*

Qoa *older alluvium composed largely of angular pebble-size fragments of Miocene shale and some of sandstone (**Tm, Tsq, and Ttos**) in light gray to tan silty matrix in part indurated by calcareous caliche; crudely bedded to massive; about 200 ft (60m) thick; blends northward upslope in Browns Canyon drainage area into old debris-flow landslides (**Qls**); slightly deformed and much dissected where elevated; but at Horse Flats top surface of deposition preserved; late Pleistocene age; mapped as slope wash, older alluvium, and Saugus Formation (upper member) by Barrows 1975; Evans and Miller 1978; and Saul 1979; probably in places equivalent to Pacoima Formation of Oakeshott 1958; Barrows et al. 1975; and Dibblee 1991*

— UNCONFORMITY —

QTs
Ts | Tsr

SAUGUS FORMATION

Mostly terrestrial, weakly consolidated; Pleistocene and Pliocene age

QTs *light gray to brown pebble-cobble conglomerate, sandstone and lesser amounts of grayish to reddish brown, soft siltstone/claystone; conglomerate composed of granitic, gneissic, metavolcanic, quartzitic, gabbroic and anorthositic detritus in sandy matrix; deposited by westward-flowing streams; Pleistocene age; south of Santa Susana fault mapped as middle member of Saugus Formation by Barrows et al. 1975, Evans and Miller 1978, and Saul 1979 [in adjacent San Fernando quadrangle (Dibblee 1991) **QTs** west of Elsmere Canyon should be shown as **Ts**]*

Ts *(in Newhall area) similar to **QTs**, but correlative in age with units **Tsr** and **Tps** in part; probably Pliocene age*

Tsr *Sunshine Ranch Member (of Hazzard 1940, in Treiman 1987; Barrows et al. 1974; Evans and Miller 1978; and Saul 1979; type area extends eastward from lower Aliso Canyon to Van Norman Reservoir, Hazzard 1940); terrestrial deposits similar to **QTs**, but south of Santa Susana fault composed largely of more indurated greenish gray claystone, siltstone and fine grained sandstone, and contains in lower part brackish marine layers of oyster shells; in exposures northwestward from San Fernando Pass, consists mostly of interbedded conglomerate and fine grained sediments that locally contain few thin layers of peat, unit intertongues westward into **Tps**; mostly Pliocene age*

Tps
Tp | Tpg

PICO FORMATION

Marine clastic; mostly Pliocene age

Tps *south of Santa Susana fault: Pico sandstone (included in Saugus Formation by Kew 1924; Pico Formatioin by Butler 1977, Lant 1977, Yeats 1979; Pico and Saugus Formatioins by Evans and Miller 1978) mostly light gray to nearly white, soft friable sandstone, locally pebbly, contains abundant whole and fragmented bivalve shells west of Browns Canyon; deposited under marine to lagoonal conditions; grades upward into terrestrial Saugus Formation; unconformable on Miocene formations*

Tpg *conglomerate in lower Limekiln Canyon: gray massive conglomerate of cobbles of granitic and metavolcanic rocks in sandstone matrix; nonmarine (?), unconformable on Monterey Shale (**Tml**), overlain by Saugus Formation*

Tp *and **Tps** north of Santa Susana fault: Pico Formation of Kew 1924, Winterer and Durham 1958, 1962; **Tps** mostly light gray semi-friable sandstone, locally pebbly; upper beds contain bivalve shell fragments; intertongues into Saugus Formations (**Ts**); **Tp** mostly gray micaceous siltstone-claystone, bedded to massive, includes few thin sandstone layers*

Ttos
Ttoc

TOWSLEY FORMATIOIN

Marine clastic; early Pliocene age (Repettian Stage) and possibly latest Miocene ("Delmontian Stage")

Ttos *light gray to tan coherent to semi-friable sandstone, medium grained to locally gritty and pebbly, bedded; includes minor micaceous siltstone; grades laterally northward into Saugus Formation (**Ts**) in San Fernando Pass area*

Ttoc *gray micaceous silty claystone and siltstone; minor sandstone*

Holocene
Pleistocene
Pliocene
QUATERNARY
CENOZOIC

Tsq
Tsqs

SISQUOC SHALE

(Included in Modelo Formation by Kew 1924; Winterer and Durham 1958, 1962; Saul 1979; same lithologic unit as Sisquoc Formation in northern Ventura basin) marine clastic; late Miocene age (Mohnian to "Delmontian" Stage)

Tsq *dark gray to brownish gray clay shale, bleaches to light gray; crumbly with spheroidal to sub-platy fracture, gypsiferous in fractures, some layers contain large tan dolomitic concretions; includes some thin interbedded semi-siliceous layers; about 1000 ft (300 m) thick*

Tsqs *light gray coherent to semi-friable sandstone*

Tm
Tml

MONTEREY SHALE

(Modelo Formation of Kew 1924; Winterer and Durham 1958, 1962; Barrovs et al. 1974; Evans and Miller 1978; Saul 1979; same lithologic unit as Monterey Shale of northern Ventura basin); marine biogenic; nearly 2000 ft. (610m) thick north of Santa Susana fault, very thin south of it; middle and late Miocene age

Tm *upper part: thin bedded siliceous shale, dark gray brown but weathers cream-white, hard, platy, brittle, porcelaneous, locally cherty, closely fractured, some layers fissile, about 1500 ft (485m) thick; middle and late Miocene age (mostly Mohnian Stage); south of Santa Susana fault: soft, white weathering thin-bedded, fissile diatomaceous semi-siliceous shale*

Tml *lower part: thin-bedded, fissile semi-siliceous shale to soft shaly claystone, dark brown, weathers cream white; includes some calcareous shale, and thin tan-weathering hard dolomite strata that are increasingly abundant upward, unit as thick as 500 ft (150m); middle Miocene age (Luisian-Relizian Stage)*

Tlsc

DETRITAL SEDIMENTS OF LINDERO CANYON

(Included in Topanga Formation of Weber 1984; unconformable on Chatsworth Formation; best exposed in Lindero Canyon, Thousaad Oaks quadrangle) marine transgressive clastic; Miocene age [Luisian (?) Stage]

Tlsc *crudely bedded brown to gray conglomerate composed of cobbles of metavolcanic, granitic and quartzitic rocks, and of sandstone derived from Chatsworth Formation; sparsely fossiliferous; contains minor interbeds of light gray calcareous sandstone*

Ttus
Tb
Ttls

TOPANGA FORMATION

(Of Yeats 1979; Topanga Group of Saul 1979) marine transgressive clastic; middle Miocene age

Ttus *upper sandstone: light gray to white semi-friable, locally pebbly, massive to vaguely bedded; about 150 ft (45m) thick*

Tb *basalt flow (or diabase sill?); black, massive fine grained weakly coherent where weathered, present north of Santa Susana fault only; probably correlative with Conejo Volcanics to west*

Ttls *lower sandstone: light gray to tan, semi-friable to somewhat hard, massive to vaguely bedded; as thick as 600 ft (180m), base unexposed; present north of Santa Susana fault only*

— UNCONFORMITY —

Tll
Tllg

LLAJAS FORMATION

Marine clastic; middle Eocene age

Tll *gray micaceous claystone-siltstone and some interbeds of light gray to tan soft sansdstone*

Tllg *basal cobble conglomerate as thick as 50 ft (17m) with cobbles of granitic, metavolcanic and quartzitic rocks*

Tsu
Tsi

SANTA SUSANA FORMATION

Mostly marine clastic; Paleocene age

Tsu *dark gray micaceous claystone, crumbly with ellipsoidal fracture; includes few thin sandstone layers*

Tsi *Simi Conglomerate Member: gray to brown cobble conglomerate with smooth rounded cobbles up to 1 ft (1/3m) in diameter of pinkish-gray quartzite, metavolcanic and granitic rocks in gray sandstone matrix; possibly in part nonmarine, deposited as fan delta*

Kcsh
Kcs

CHATSWORTH FORMATION

(Of Colburn et al. 1981; "Chico" Formation of Kew 1924; Evans and Miller 1978) marine clastic; late Cretaceous age (Maestrichtian and Campanian Stages)

Kcsh *gray micaceous shale and siltstone; includes some sandstone strata; included in Martinez Formation (Paleocene) by Evans and Miller 1978*

Kcs *light gray to light brown, hard, thick bedded sandstone; locally gritty; includes few thin layers of micaceous siltstone; base not exposed*

Miocene
Eocene
Paleocene
Upper
TERTIARY
CRETACEOUS
MESOZOIC

GEOLOGIC MAP OF THE OAT MOUNTAIN AND NORTH 1/2 CANOGA PARK QUADRANGLES

LOS ANGELES COUNTY, CALIFORNIA

BY THOMAS W. DIBBLEE, JR., 1992

EDITED BY HELMUT E. EHRENSPECK, 1992

EDITED BY JOHN A. MINCH, 2008

Topographic base maps from available USGS 7.5-minute quadrangle

OAT MOUNTAIN, CA 1952	CANOGA PARK, CA 1952
PHOTOREVISED 1969	PHOTOREVISED 1967
DMA 2252 I SE – Series V895	DMA 2252 II NE – Series V895

GEOLOGIC SYMBOLS

not all symbols shown on each map

FORMATION CONTACT *dashed where inferred or indefinite dotted where concealed*

MEMBER CONTACT *between units of a formation* **Prominent bed**

CONTACT BETWEEN SURFICIAL SEDIMENTS *located only approximately in places*

FAULT: *Dashed where indefinite or inferred, dotted where concealed, queried where existence is doubtful. Parallel arrows indicate inferred relative lateral movement. Relative vertical movement is shown by U/D (U=upthrown side, D=downthrown side). Short arrow indicates dip of fault plane. Sawteeth are on upper plate of low angle thrust fault.*

U 25 ? D

FOLDS: *overturned* — **ANTICLINE** — **SYNCLINE**

arrow on axial trace of fold indicates direction of plunge; dotted where concealed by surficial sediments

Strike and dip of sedimentary rocks: 18 inclined; 20 inclined (approximate); 80 overturned; horizontal; vertical

Strike and dip of metamorphic or igneous rock foliation or flow banding or compositional layers: 75 inclined; inclined (approximate); vertical; 80 overturned

OTHER SYMBOLS: Direction of landslide movement; outline of water bodies shown on map; water well; oil well; springs

Appendix C RBMW-1 NMR Log

Schlumberger

NMR Processed Result

COMPANY: Southern California Gas Company
WELL: TH-1
FIELD: Aliso Canyon
COUNTY: Los Angeles
STATE: California
COUNTRY: USA

API No:

Location — Field: Lat: 34.3135336 Long: -118.5634409

Other Services: ConPr_R06_L002Up_CMRT_NEXT

Permanent Datum: MSL Elev: 0 ft
Log Measured From: DF 2837.98 ft above Perm. Datum
Drilling Measured from: DF

Elevations:
K.B. 0 ft
D.F. 2837.98 ft
G.L. 2836.48 ft

Date	21-Apr-2018	
Run No.	FOUR	
Depth Driller	1112 ft	
Depth Logger (Schl)	1113 ft	
Btm. Log Interval	1103 ft	
Top Log Interval	200 ft	
Casing-Driller	11.75 in @ 80 ft	
Casing-Logger	82.5 ft	
Bit Size	8.5 in	
Type Fluid in Hole	ABOND, Fluid	
Dens. | Visc.	8.5 lbm/gal | 48 s	
pH | Fluid loss	8.2 | 8.2 in3	
Source of Sample	Active Tank	
Rm @ Meas.Temp.	3.86 ohm.m @ 68.4 degF	
Rmf @ Meas.Temp.	3.25 ohm.m @ 68.2 degF	
Rmc @ Meas.Temp.	4.44 ohm.m @ degF	
Source: Rmf | Rmc	Calculated | Pressed	
Rm @ BHT	3.39881 @ 78.6 degF	
Circulation Stopped	12:30:00	
Logger on Bottom	12:10:00	
Max Rec.Temp.	78.6 deg F	
Equipment | Location	3705 | Bakersfield	
Recorded by:	Brett Tucker / Arona Ndiaye	
Witnessed by:		

FOLD HERE

The well name, location and borehole reference data were furnished by the customer

ANY INTERPRETATION, RESEARCH, ANALYSIS, DATA, RESULTS, ESTIMATES, OR RECOMMENDATION FURNISHED WITH THE SERVICES OR OTHERWISE COMMUNICATED BY SCHLUMBERGER TO CUSTOMER AT ANY TIME IN CONNECTION WITH THE SERVICES ARE OPINIONS BASED ON INFERENCES FROM MEASUREMENTS, EMPIRICAL RELATIONSHIPS AND/OR ASSUMPTIONS, WHICH INFERENCES, EMPIRICAL RELATIONSHIPS AND/OR ASSUMPTIONS ARE NOT INFALLIBLE, AND WITH RESPECT TO WHICH PROFESSIONALS IN THE INDUSTRY MAY DIFFER. ACCORDINGLY, SCHLUMBERGER CANNOT AND DOES NOT WARRANT THE ACCURACY, CORRECTNESS OR COMPLETENESS OF ANY SUCH INTERPRETATION, RESEARCH, ANALYSIS, DATA, RESULTS, ESTIMATES OR RECOMMENDATION. CUSTOMER ACKNOWLEDGES THAT IT IS ACCEPTING THE SERVICES "AS IS", THAT SCHLUMBERGER MAKES NO REPRESENTATION OR WARRANTY, EXPRESS OR IMPLIED, OF ANY KIND OR DESCRIPTION IN RESPECT THERETO, SPECIFICALLY CUSTOMER ACKNOWLEDGES THAT SCHLUMBERGER DOES NOT WARRANT THAT ANY INTERPRETATION, RESEARCH, ANALYSIS, DATA, RESULTS, ESTIMATES, OR RECOMMENDATION IS FIT FOR A PARTICULAR PURPOSE, INCLUDING BUT NOT LIMITED TO COMPLIANCE WITH ANY GOVERNMENT REQUEST OR REGULATORY REQUIREMENT. CUSTOMER FURTHER ACKNOWLEDGES THAT SUCH SERVICES ARE DELIVERED WITH THE EXPLICIT UNDERSTANDING AND AGREEMENT THAT ANY ACTION TAKEN BASED ON THE SERVICES RECEIVED SHALL BE AT ITS OWN RISK AND RESPONSIBILITY AND NO CLAIM SHALL BE MADE AGAINST SCHLUMBERGER AS A CONSEQUENCE THEREOF.

Ser. Order #: | OP Vers.: | Process Date: 1/16/2019 | Center: Houston | Baseline: Techlog | Log Analyst: Tianmin JIANG

Remarks:

Remarks:

CMR-NG is a new generation CMR tool which can measure continuous 2D T1-T2 downhole log. The 1D T1 or T2 log can be generated from the measured T1-T2 log.

The standard 1D CMR interpretation is based on 1D T2 distribution with T2 cutoffs to get fluid bin porosities, BFV/FFV and permeability.

In the 2D interpretation, the common T1-T2 peak are extracted from T1-T2 log. These extracted T1-T2 peak will be identified to be from different formation fluids based on the T1/T2 ratio and T2. The calculated volume of each T1-T2 peak will be the fluid porosity of the corresponding formation fluid. The 2D interpretation can give detailed formation fluid porosities and saturation.

Legend

Track1: T2 bin porosities with bit size and caliper
Track2: Depth track with tool tension and gamma ray, tool standoff DSOZ and RSOZ, mudcake thickness H_MC from ADT
Track3: Measure resistivity
Track4: NMR permeability based on SDR and Timur-Coates equations
Track5: NMR BFV/FFV with density-neutron porosities
Track6: Spectrolith/ELAN track
Track7: Mud-Corrected CMR-NG T2 distribution with T2LM and T2 Cutoff
Track8: Formation Tops
Track9: CMR processing zonation
Track10: CMR-NG T1 distribution with T1LM
Track11: CMR-NG T2 distribution with T2LM
Track12: NMR Cluster volumes from 2D NMR
Track13: Fluid porosities from 2D NMR
Track14: Total Oil porosity from ADT and NMR
Track15: Total Water porosity from ADT and NMR
Track16: Water saturation from ADT and NMR

Zone 1

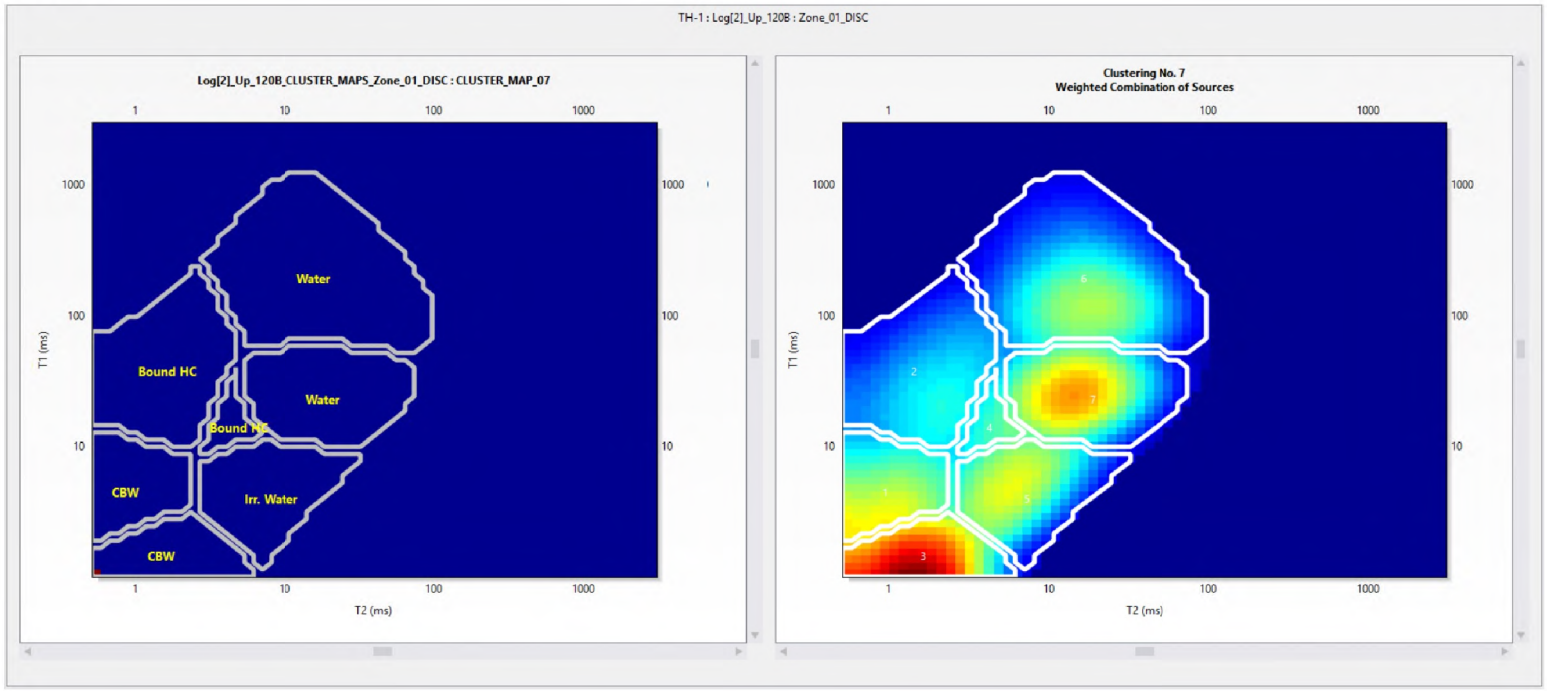
TH-1 : Log[2]_Up_120B : Zone_01_DISC
Log[2]_Up_120B_CLUSTER_MAPS_Zone_01_DISC : CLUSTER_MAP_07
Water
Bound HC
Water
Bound HC
CBW
Irr. Water
CBW
T1 (ms)
T2 (ms)
Clustering No. 7
Weighted Combination of Sources
T1 (ms)
T2 (ms)

Zone 2

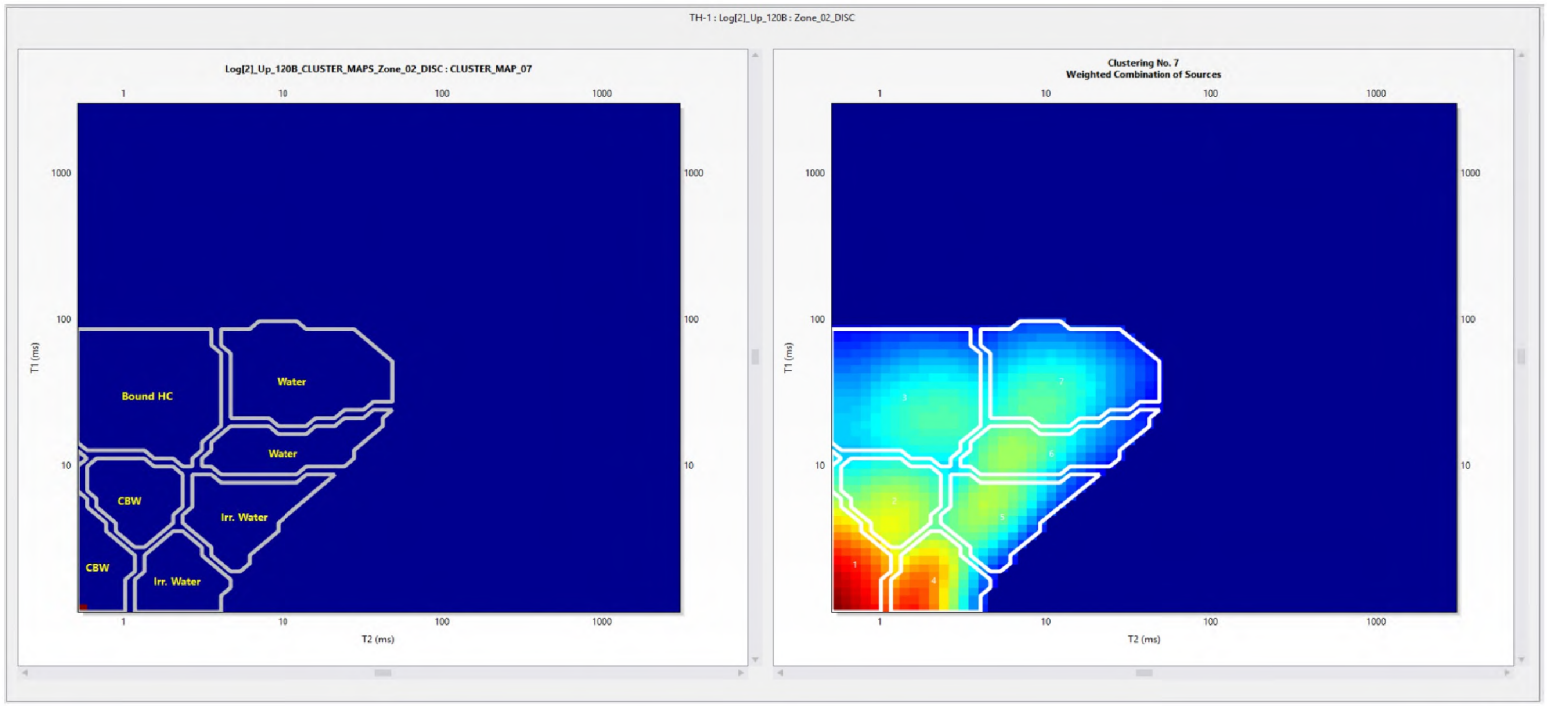
TH-1 : Log[2]_Up_120B : Zone_02_DISC
Log[2]_Up_120B_CLUSTER_MAPS_Zone_02_DISC : CLUSTER_MAP_07
Bound HC
Water
Water
CBW
Irr. Water
CBW
Irr. Water
T1 (ms)
T2 (ms)
Clustering No. 7
Weighted Combination of Sources
T1 (ms)
T2 (ms)

Zone 3

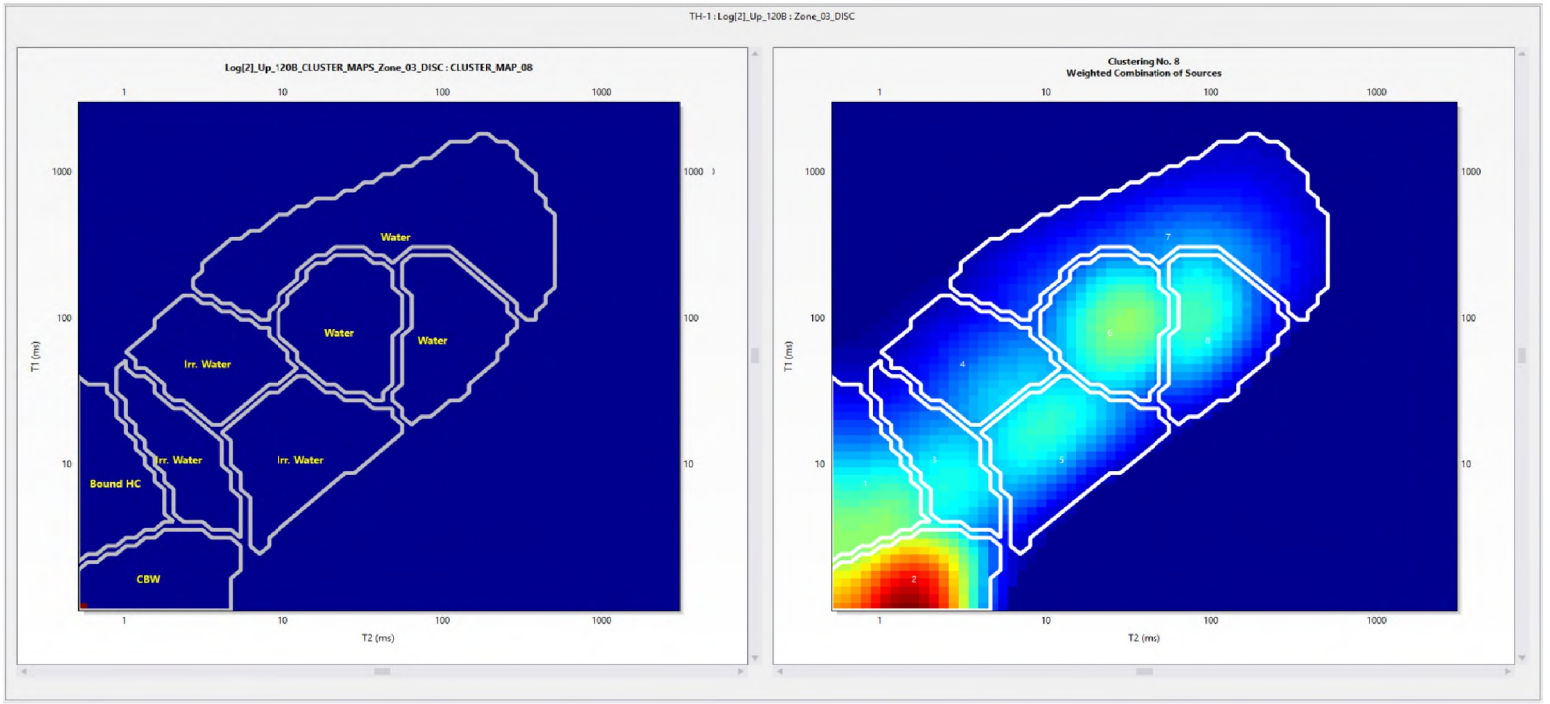
TH-1 : Log[2]_Up_120B : Zone_03_DISC
Log[2]_Up_120B_CLUSTER_MAPS_Zone_03_DISC : CLUSTER_MAP_08
Water
Water
Water
Irr. Water
Irr. Water
Irr. Water
Bound HC
CBW
T1 (ms)
T2 (ms)
Clustering No. 8
Weighted Combination of Sources

Zone 4

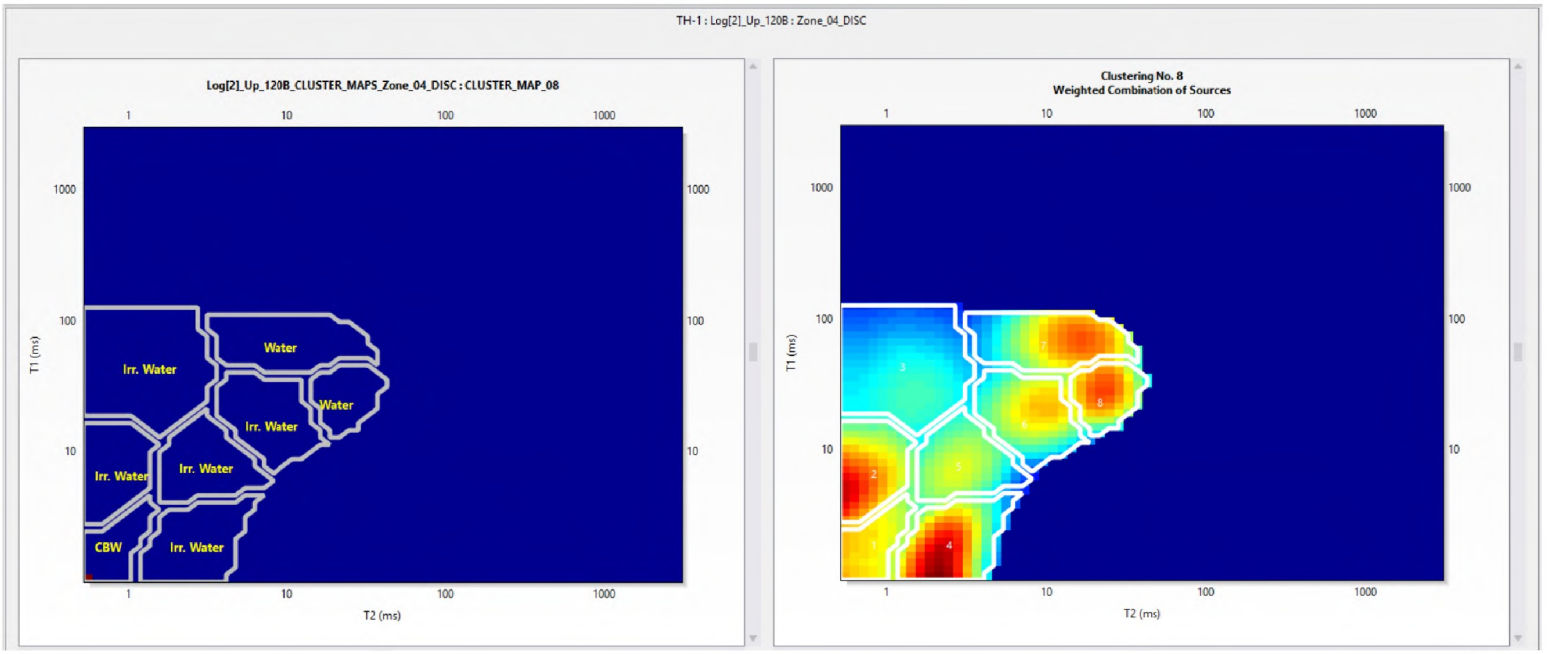
TH-1 : Log[2]_Up_120B : Zone_04_DISC
Log[2]_Up_120B_CLUSTER_MAPS_Zone_04_DISC : CLUSTER_MAP_08
Water
Water
Irr. Water
Irr. Water
Irr. Water
Irr. Water
Irr. Water
CBW
T1 (ms)
T2 (ms)
Clustering No. 8
Weighted Combination of Sources

Zone 5

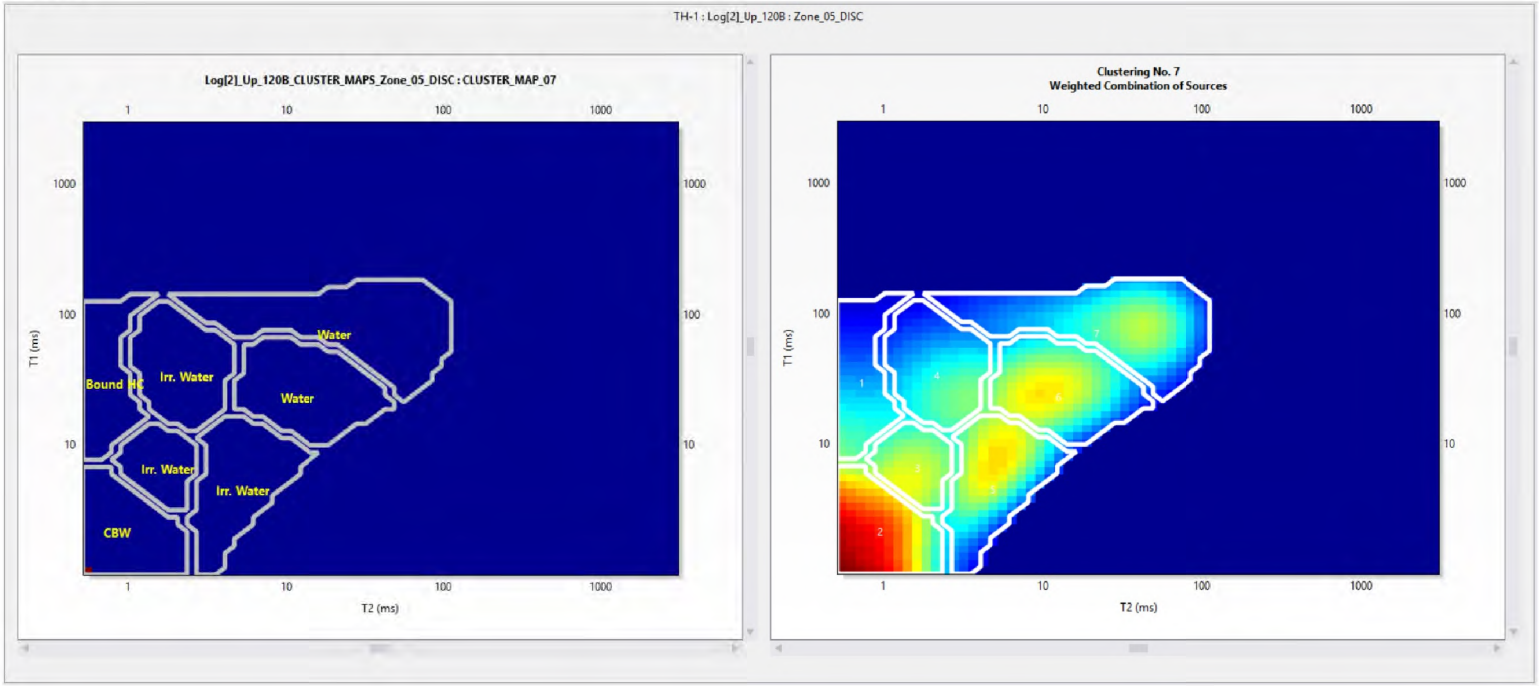

Standard Answers

Parameters		Permeability	Timur	SDR
T2 Cutoff:	19 (ms)	Computed:	yes	yes
		Multiplier:	1	4
		Porosity Exponent:	4	4
		Phi Ratio/T2LM Exp:	2	2
		Bound Fluid Min:	0.02 (ft3/ft3)	

Bin Porosities (ms)

0.5 1 3 10 33 100 300 1000 3000

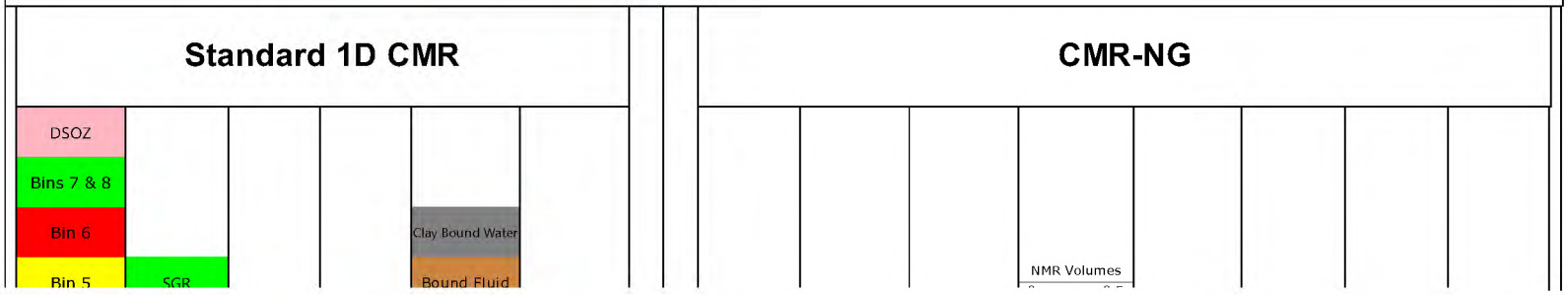

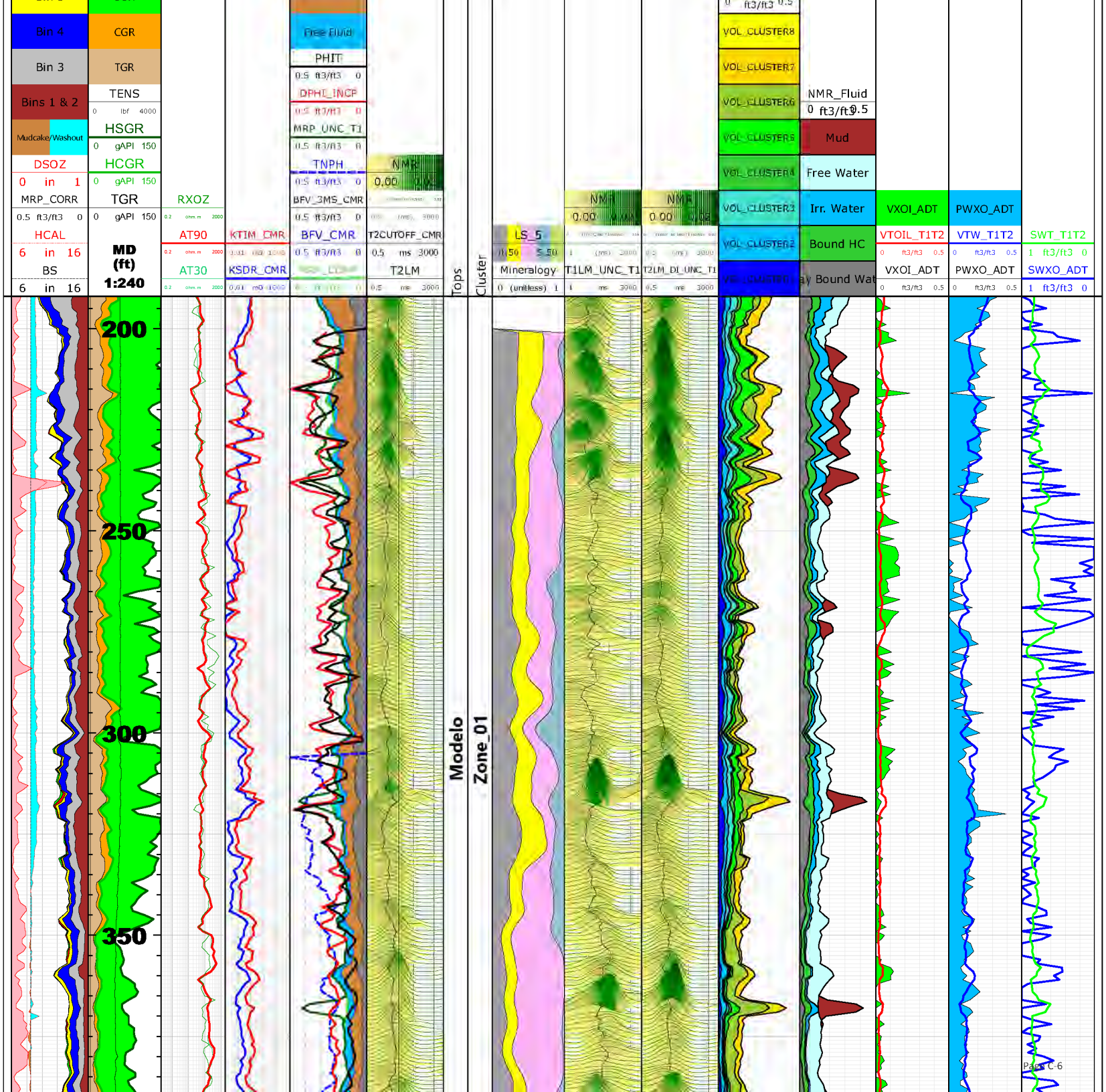
Bin 4
CGR
Bin 3
TGR
Bins 1 & 2
TENS
0 lbf 4000
Mudcake/Washout
HSGR
0 gAPI 150
DSOZ
HCGR
0 in 1
0 gAPI 150
MRP_CORR
TGR
0.5 ft3/ft3 0
0 gAPI 150
HCAL
MD (ft)
6 in 16
1:240
BS
6 in 16
RXOZ
AT90
AT30
KTIM_CMR
KSDR_CMR
Free Fluid
PHIT
0.5 ft3/ft3 0
DPHI_INCP
MRP_UNC_T1
TNPH
BFV_3MS_CMR
BFV_CMR
NMR
0.00
T2CUTOFF_CMR
0.5 ms 3000
T2LM
Tops
Modelo
Zone_01
Cluster
LS_5
Mineralogy
0 (unitless) 1
T1LM_UNC_T1
T2LM_DI_UNC_T1
VOL_CLUSTER8
VOL_CLUSTER7
VOL_CLUSTER6
VOL_CLUSTER5
VOL_CLUSTER4
VOL_CLUSTER3
VOL_CLUSTER2
NMR_Fluid
0 ft3/ft3 0.5
Mud
Free Water
Irr. Water
Bound HC
Bound Wat
VXOI_ADT
PWXO_ADT
VTOIL_T1T2
VTW_T1T2
SWT_T1T2
VXOI_ADT
PWXO_ADT
SWXO_ADT
200
250
300
350

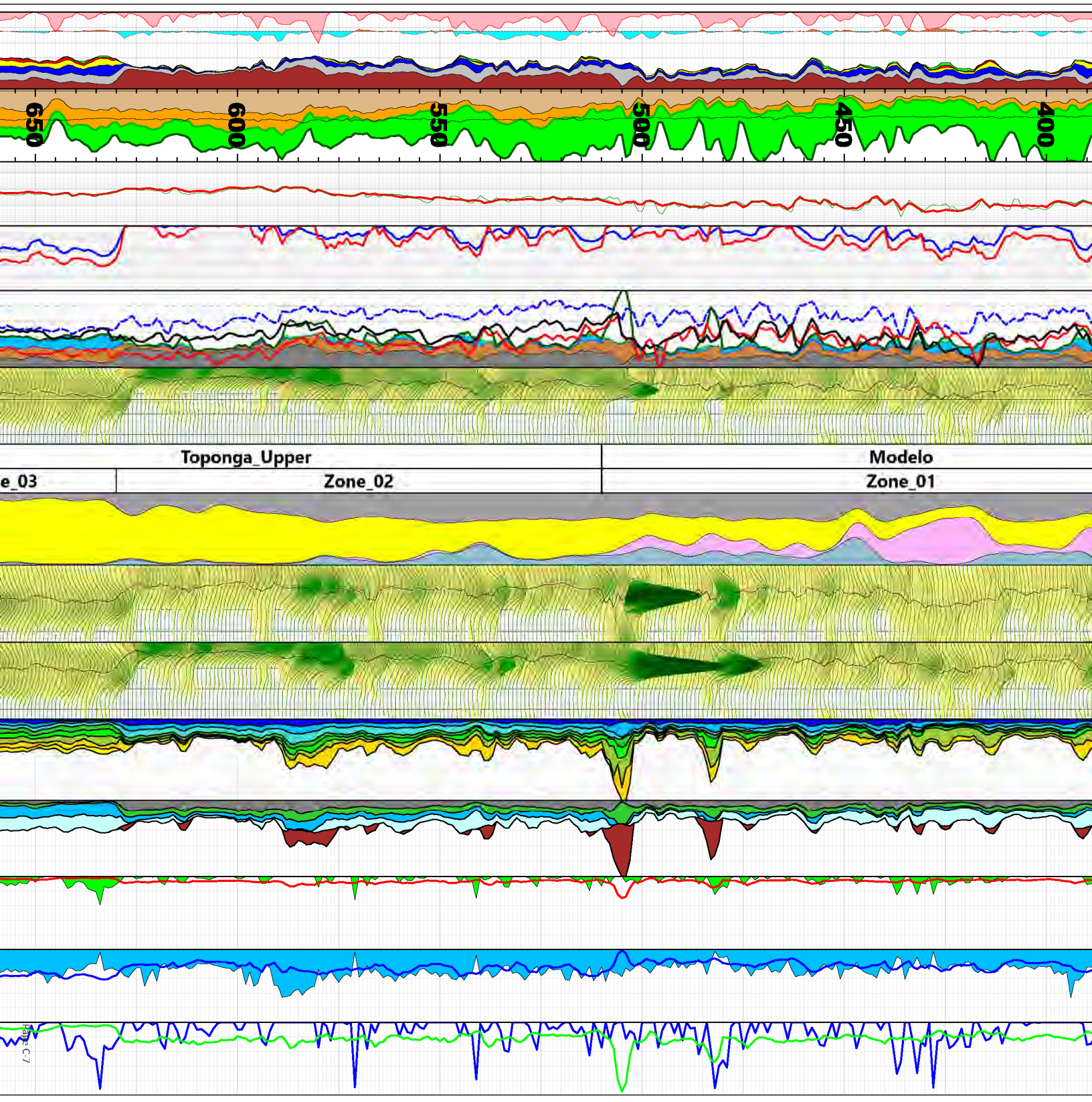
650
600
550
500
450
400
Toponga_Upper
Modelo
e_03
Zone_02
Zone_01

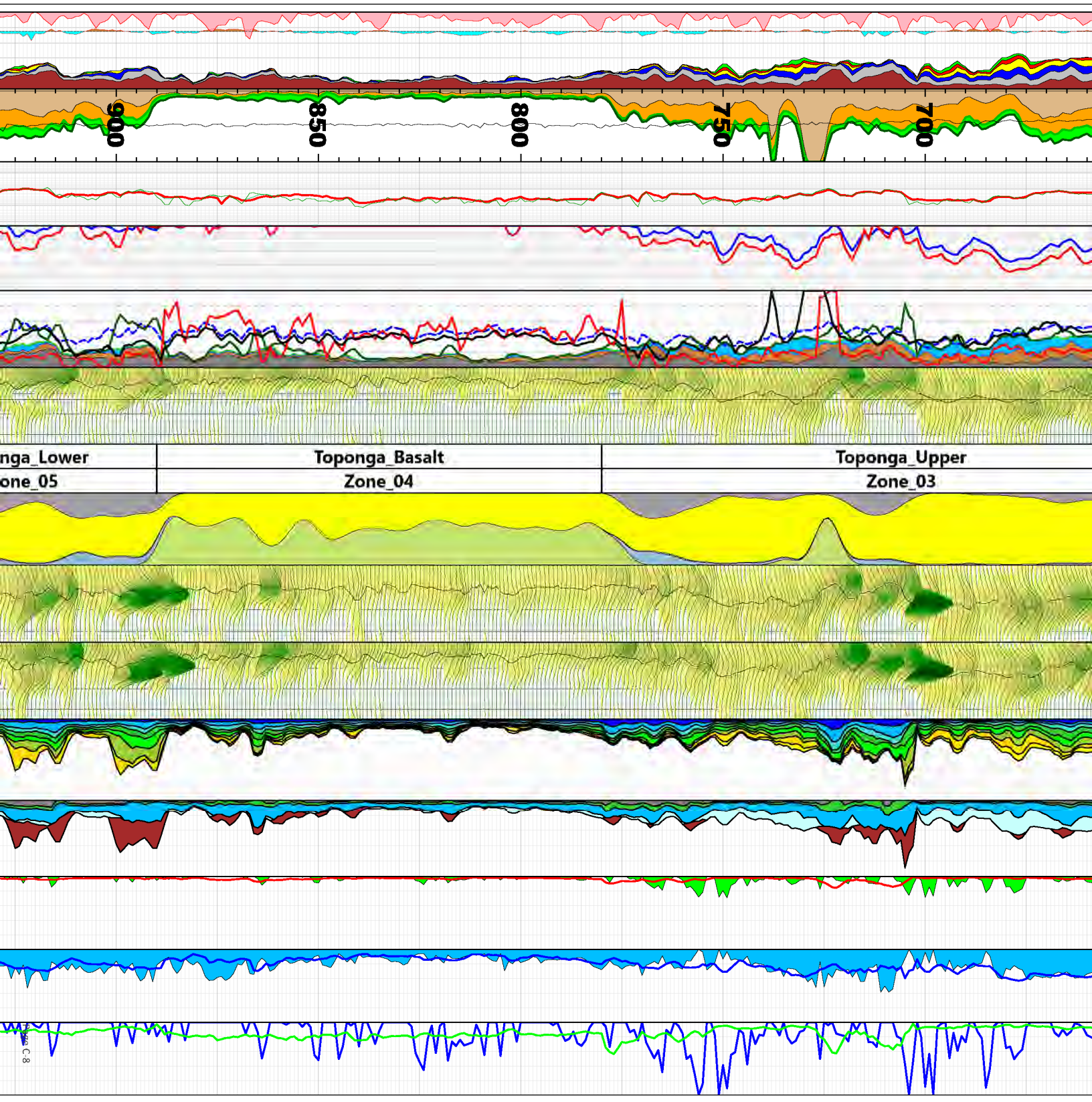
900
850
800
750
700
nga_Lower
one_05
Toponga_Basalt
Zone_04
Toponga_Upper
Zone_03

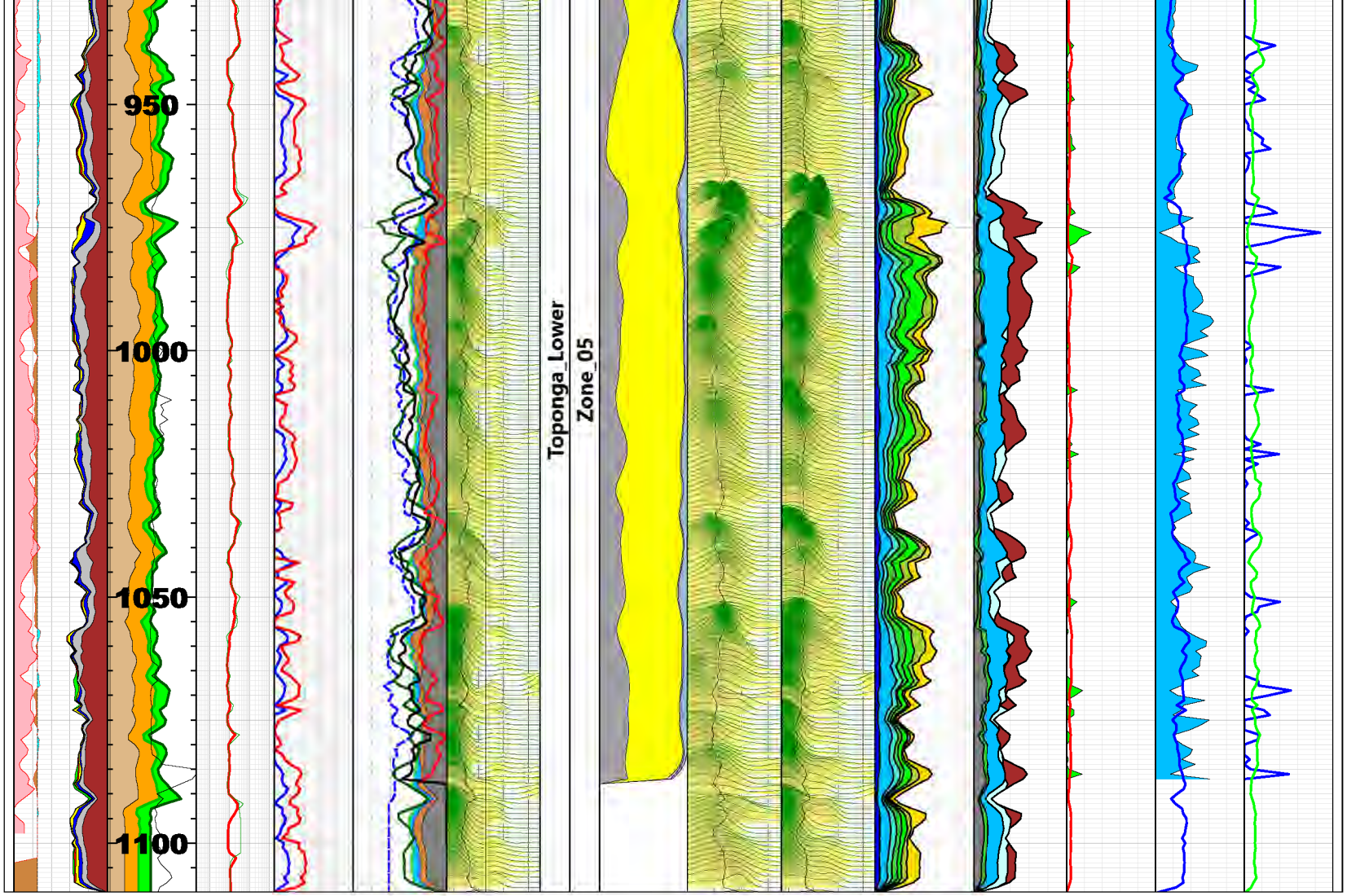
950
1000
1050
1100
Toponga_Lower
Zone_05

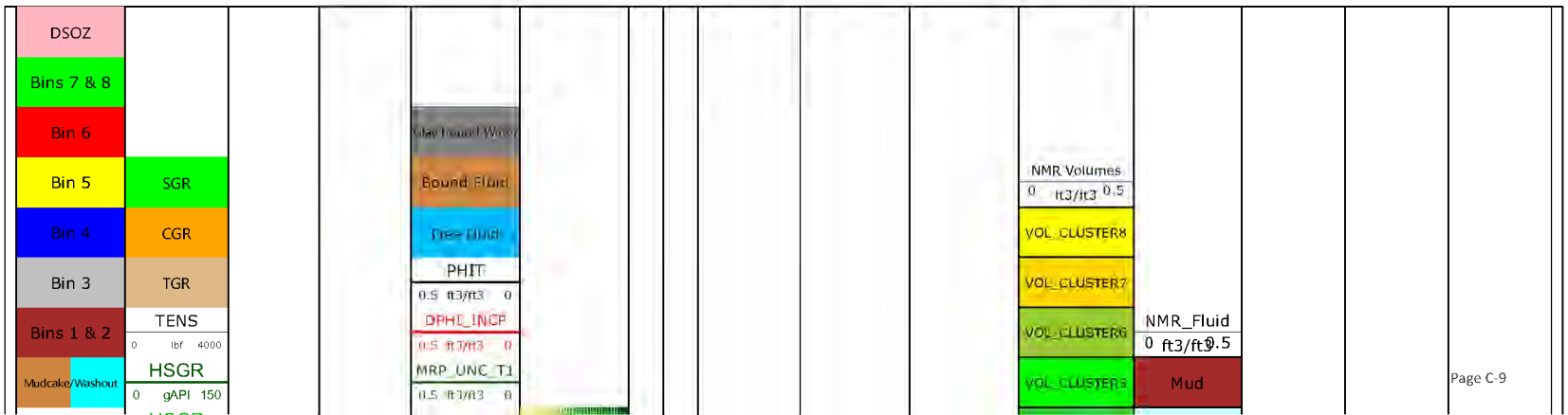
DSOZ
Bins 7 & 8
Bin 6
Bin 5
Bin 4
Bin 3
Bins 1 & 2
Mudcake/Washout
SGR
CGR
TGR
TENS
0 lbf 4000
HSGR
0 gAPI 150
Bound Fluid
Free Fluid
PHIT
0.5 ft3/ft3 0
DPHI_INCP
0.5 ft3/ft3 0
MRP_UNC_T1
0.5 ft3/ft3 0
NMR Volumes
0 ft3/ft3 0.5
VOL_CLUSTER8
VOL_CLUSTER7
VOL_CLUSTER6
VOL_CLUSTER5
NMR_Fluid
0 ft3/ft3 0.5
Mud

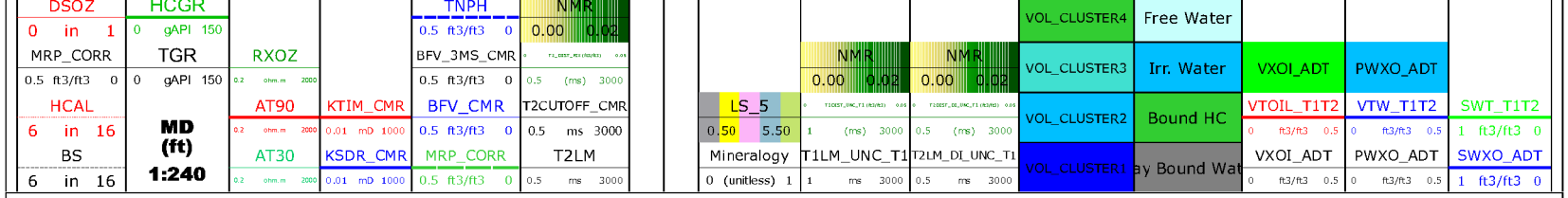

COMPANY: Southern California Gas Company

Schlumberger

WELL: TH-1
FIELD: Aliso Canyon
COUNTY: Los Angeles
STATE: California
COUNTRY: USA

API No.:

Date Processed: 1/16/2019

Appendix D RBMW-1 ELAN Log

Schlumberger

ELAN Analysis

COMPANY:	Southern California Gas Company
WELL:	TH-1
FIELD:	Aliso Canyon
COUNTY:	Los Angeles
STATE:	California
COUNTRY:	USA

API No:

Other Services:

Location — Field:
Lat: 34.3135336 Long: -118.5634409

Permanent Datum:	MSL	Elev: 0 ft	Elevations:
Log Measured From:	DF	2837.98 ft above Perm. Datum	K.B. 0 ft
Drilling Measured from:	DF		D.F. 2837.98 ft
			G.L. 2836.48 ft

Date	21-Apr-2018	
Run No.	FOUR	
Depth Driller	1112 ft	
Depth Logger (Schl)	1113 ft	
Btm. Log Interval	1103 ft	
Top Log Interval	200 ft	
Casing-Driller	11.75 in @ 80 ft	
Casing-Logger	82.5 ft	
Bit Size	8.5 in	
Type Fluid in Hole	ABOND, Fluid	
Dens. | Visc.	8.5 lbm/gal | 48 s	
pH | Fluid loss	8.2 | 8.2 in3	
Source of Sample	Active Tank	
Rm @ Meas.Temp.	3.86 ohm.m @ 68.4 degF	
Rmf @ Meas.Temp.	3.25 ohm.m @ 68.2 degF	
Rmc @ Meas.Temp.	4.44 ohm.m @ degF	
Source: Rmf | Rmc	Calculated | Pressed	
Rm @ BHT	3.39881 @ 78.6 degF	
Circulation Stopped	12:30:00	
Logger on Bottom	12:10:00	
Max Rec.Temp.	78.6 deg F	
Equipment | Location	3705 | Bakersfield	
Recorded by:	Brett Tucker / Arona Ndiaye	
Witnessed by:		

FOLD HERE

The well name, location and borehole reference data were furnished by the customer

ANY INTERPRETATION, RESEARCH, ANALYSIS, DATA, RESULTS, ESTIMATES, OR RECOMMENDATION FURNISHED WITH THE SERVICES OR OTHERWISE COMMUNICATED BY SCHLUMBERGER TO CUSTOMER AT ANY TIME IN CONNECTION WITH THE SERVICES ARE OPINIONS BASED ON INFERENCES FROM MEASUREMENTS, EMPIRICAL RELATIONSHIPS AND/OR ASSUMPTIONS, WHICH INFERENCES, EMPIRICAL RELATIONSHIPS AND/OR ASSUMPTIONS ARE NOT INFALLIBLE, AND WITH RESPECT TO WHICH PROFESSIONALS IN THE INDUSTRY MAY DIFFER. ACCORDINGLY, SCHLUMBERGER CANNOT AND DOES NOT WARRANT THE ACCURACY, CORRECTNESS OR COMPLETENESS OF ANY SUCH INTERPRETATION, RESEARCH, ANALYSIS, DATA, RESULTS, ESTIMATES OR RECOMMENDATION. CUSTOMER ACKNOWLEDGES THAT IT IS ACCEPTING THE SERVICES "AS IS", THAT SCHLUMBERGER MAKES NO REPRESENTATION OR WARRANTY, EXPRESS OR IMPLIED, OF ANY KIND OR DESCRIPTION IN RESPECT THERETO, SPECIFICALLY CUSTOMER ACKNOWLEDGES THAT SCHLUMBERGER DOES NOT WARRANT THAT ANY INTERPRETATION, RESEARCH, ANALYSIS, DATA, RESULTS, ESTIMATES, OR RECOMMENDATION IS FIT FOR A PARTICULAR PURPOSE, INCLUDING BUT NOT LIMITED TO COMPLIANCE WITH ANY GOVERNMENT REQUEST OR REGULATORY REQUIREMENT. CUSTOMER FURTHER ACKNOWLEDGES THAT SUCH SERVICES ARE DELIVERED WITH THE EXPLICIT UNDERSTANDING AND AGREEMENT THAT ANY ACTION TAKEN BASED ON THE SERVICES RECEIVED SHALL BE AT ITS OWN RISK AND RESPONSIBILITY AND NO CLAIM SHALL BE MADE AGAINST SCHLUMBERGER AS A CONSEQUENCE THEREOF.

Ser. Order # | OP Vers.: | Process Date: 2/5/2019 | Center: Bakersfield | Baseline: Techlog | Log Analyst: J. Little/ T. Jiang

Remarks:

Remarks:

The saturation equation used is Dual Water
Formation water salinity is 9.2 ppk.
Lithology is from LithoScanner spectroscopy data.

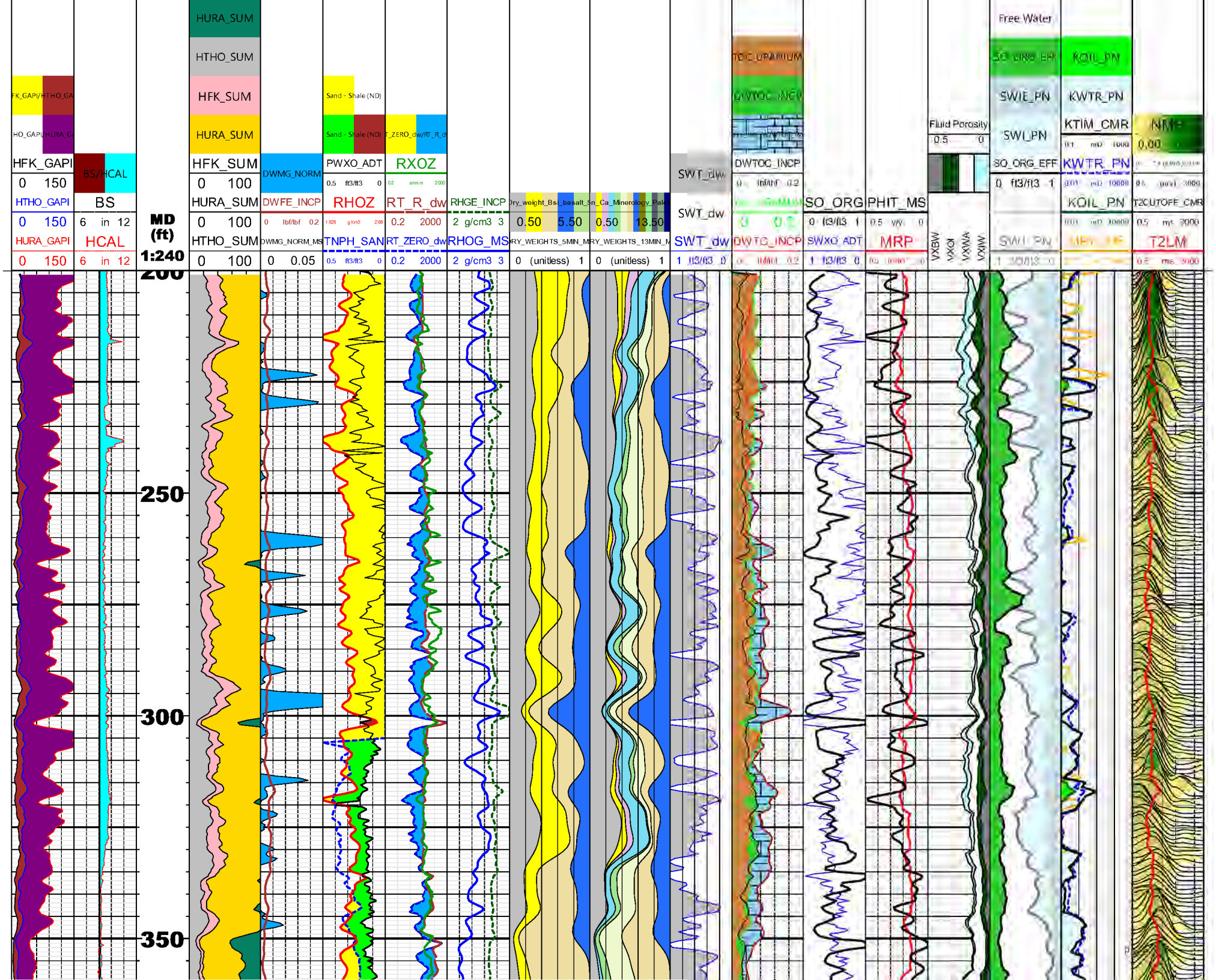
HFK_GAPI/HTHO_GA
HO_GAPI/HURA_GA
HFK_GAPI
0 150
HTHO_GAPI
0 150
HURA_GAPI
0 150
BS/HCAL
BS
6 in 12
HCAL
6 in 12
MD (ft)
1:240
200
250
300
350
HURA_SUM
HTHO_SUM
HFK_SUM
HFK_SUM
0 100
HURA_SUM
0 100
HTHO_SUM
0 100
DWMG_NORM
DWFE_INCP
0 lbf/lbf 0.2
DWMG_NORM_MS
0 0.05
Sand - Shale (ND)
Sand - Shale (ND)
PWXO_ADT
0.5 ft3/ft3 0
RHOZ
TNPH_SAN
0.5 ft3/ft3 0
RXOZ
T_ZERO_dw/RT_R_d
0.2 ohm.m 2000
RT_R_dw
0.2 2000
RT_ZERO_dw
0.2 2000
RHGE_INCP
2 g/cm3 3
RHOG_MS
2 g/cm3 3
Dry_weight_Bsl_basalt_Sn_Ca_Minerology_Pal
0.50 5.50
RY_WEIGHTS_5MIN_M
0 (unitless) 1
0.50 13.50
RY_WEIGHTS_13MIN_M
0 (unitless) 1
SWT_dw
SWT_dw
1 ft3/ft3 0
TOC_URANIUM
DWTOC_NCW
DWTOC_INCP
SO_ORG
0 ft3/ft3 1
SWXO_ADT
1 ft3/ft3 0
PHIT_MS
0.5 v/v 0
MRP
Fluid Porosity
0.5 0
VXBW
VXOI
VXWA
VXW
Free Water
SO_ORG_EFF
0 ft3/ft3 1
SWIE_PN
SWI_PN
KOIL_PN
KWTR_PN
KTIM_CMR
0.1 mD 1000
KWTR_PN
0.001 mD 10000
KOIL_PN
0.001 mD 10000
NMR
0.00
T2CUTOFF_CMR
0.5 ms 3000
T2LM
0.5 ms 3000

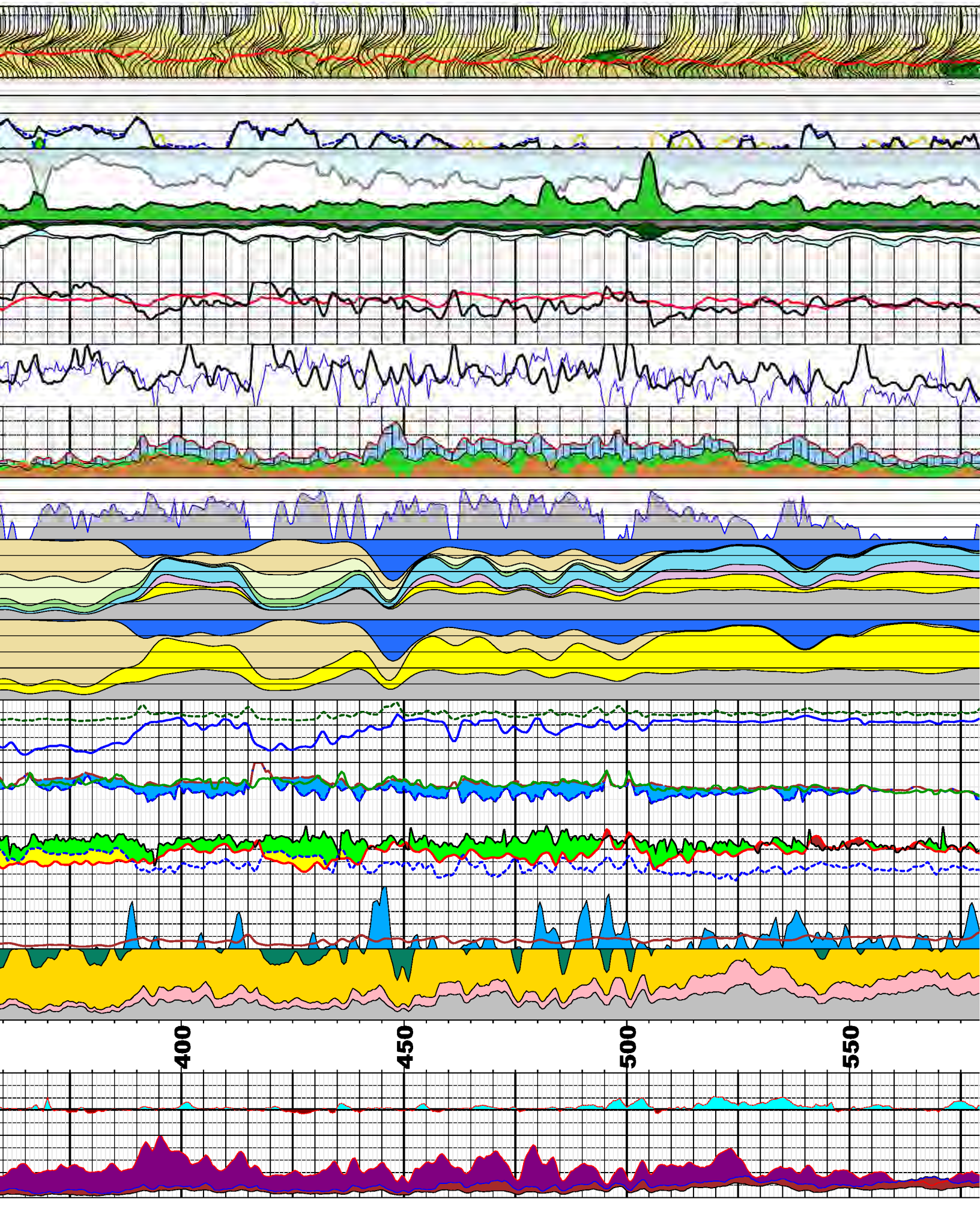
400
450
500
550

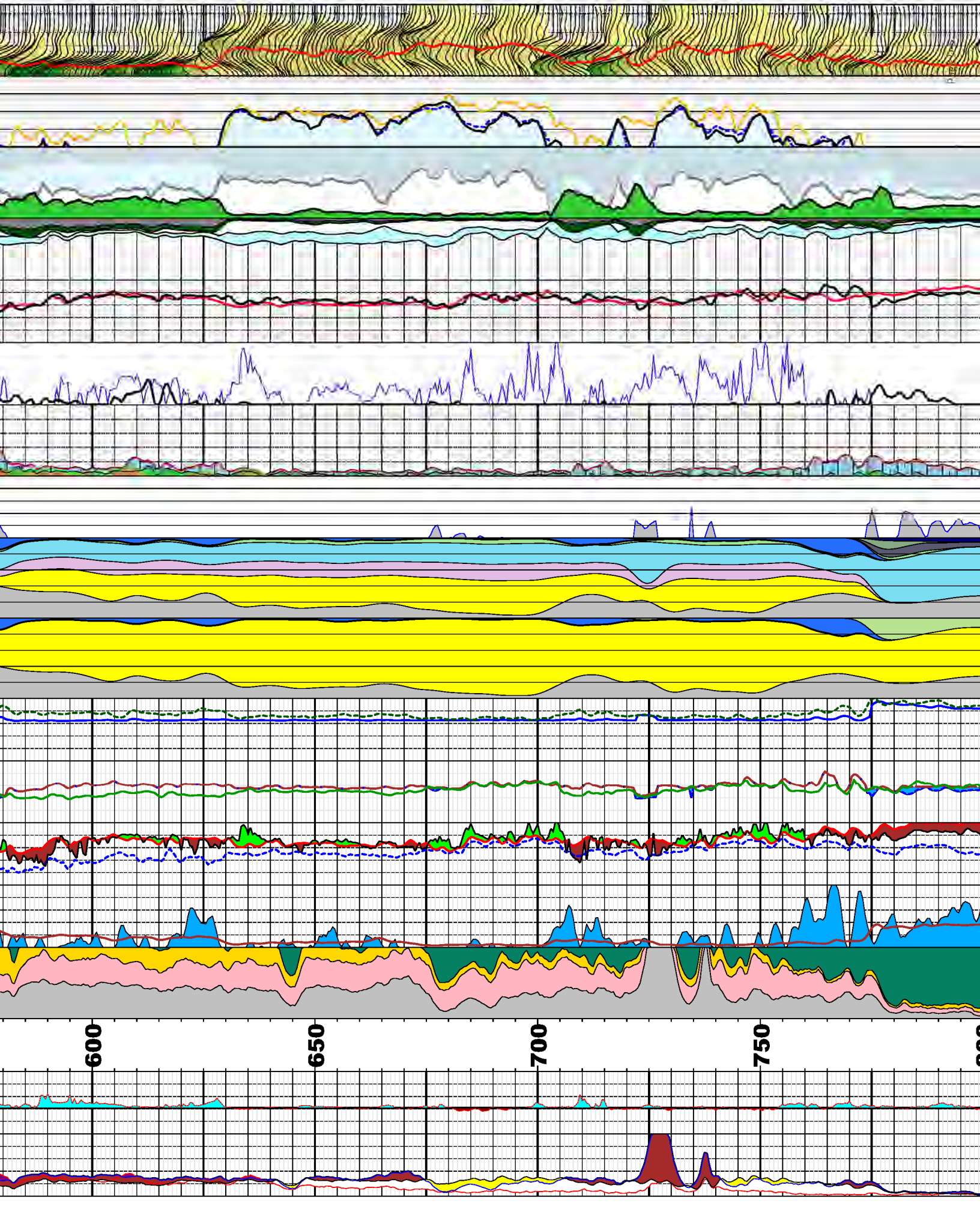
600
650
700
750

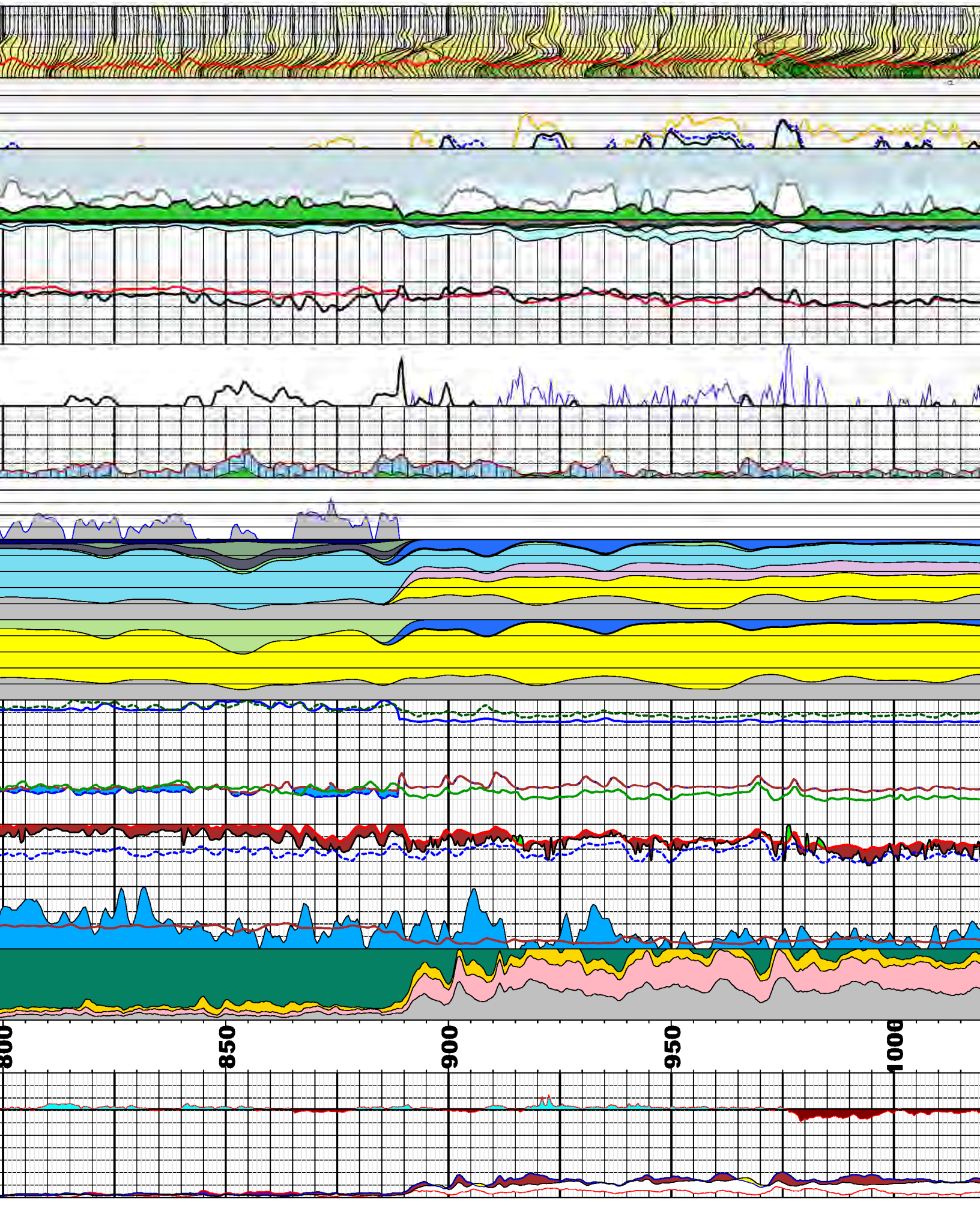
800
850
900
950
1000

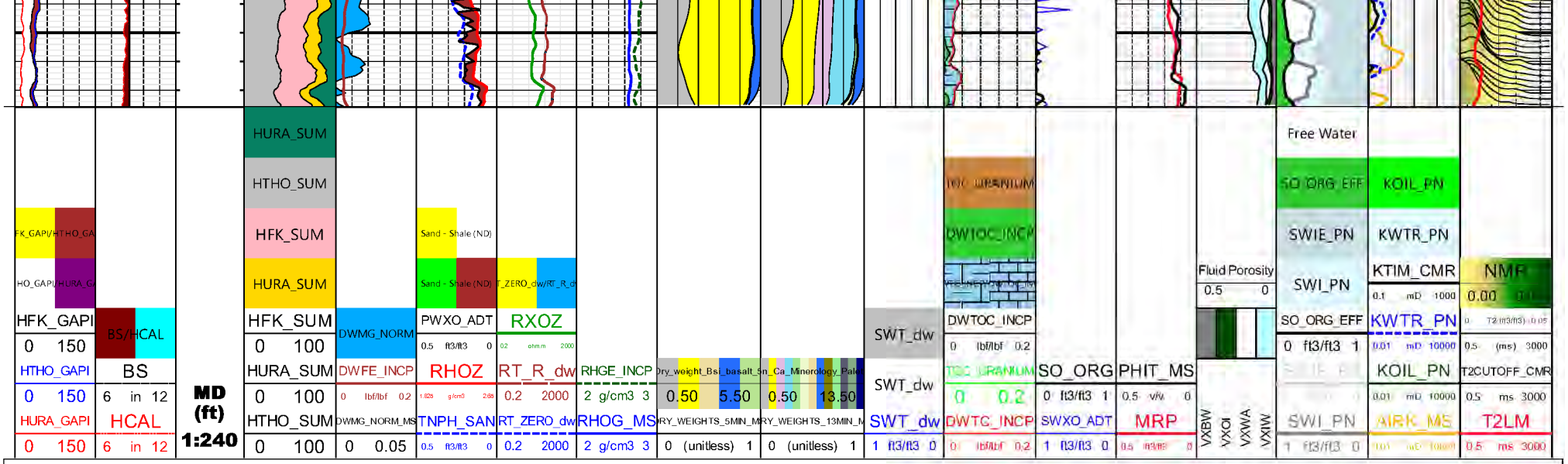

COMPANY: Southern California Gas Company

Schlumberger

WELL: TH-1
FIELD: Aliso Canyon
COUNTY: Los Angeles
STATE: California
COUNTRY: USA

API No.:

Date Processed: 2/5/2019

Appendix E SS-25 ELAN Log

Schlumberger

ELAN Analysis

COMPANY:	Southern California Gas Company
WELL:	Standard Sesnon 25
FIELD:	Aliso Canyon
COUNTY:	Los Angeles
STATE:	California
COUNTRY:	USA

COMPANY: Southern California Gas Company
WELL: Standard Sesnon 25
FIELD: Aliso Canyon
COUNTY: Los Angeles
STATE: California
COUNTRY: USA

API No: 04-037-00776

Other Services:

Location | Field:

Permanent Datum:	GL	Elev: 2927 ft	Elevations:
Log Measured From:	KB	6.35 ft above Perm. Datum	K.B. 2933.35 ft
Drilling Measured from:	KB		D.F. ft
			G.L. 2927 ft

Date	16-Nov-2017	
Run No.	One	
Depth Driller	990 ft	
Depth Logger (Schl)	990 ft	
Btm. Log Interval	930 ft	
Top Log Interval	11 ft	
Casing-Driller	11.75 in @ 939 ft	
Casing-Logger	938 ft	
Bit Size	16 in	
Type Fluid in Hole	Air	
Dens. | Visc.	0.1 lbm/gal | -999.25 s	
pH | Fluid loss	-999.25 | -999.25 in3	
Source of Sample	Active Tank	
Rm @ Meas.Temp.	500 ohm.m @ 68 degF	
Rmf @ Meas.Temp.	-999.25 ohm.m @ 68 degF	
Rmc @ Meas.Temp.	-999.25 ohm.m @ degF	
Source: Rmf | Rmc	| Pressed	
Rm @ BHT	170.887 @ -999.25 degF	
Circulation Stopped		
Logger on Bottom	14:23:00	
Max Rec.Temp.	-999.25 deg F	
Equipment | Location	3080 | Ventura	
Recorded by:	Lopez/Kartawidjaja	
Witnessed by:	Blade Energy Partners/T. McMahon	

FOLD HERE

The well name, location and borehole reference data were furnished by the customer

ANY INTERPRETATION, RESEARCH, ANALYSIS, DATA, RESULTS, ESTIMATES, OR RECOMMENDATION FURNISHED WITH THE SERVICES OR OTHERWISE COMMUNICATED BY SCHLUMBERGER TO CUSTOMER AT ANY TIME IN CONNECTION WITH THE SERVICES ARE OPINIONS BASED ON INFERENCES FROM MEASUREMENTS, EMPIRICAL RELATIONSHIPS AND/OR ASSUMPTIONS, WHICH INFERENCES, EMPIRICAL RELATIONSHIPS AND/OR ASSUMPTIONS ARE NOT INFALLIBLE, AND WITH RESPECT TO WHICH PROFESSIONALS IN THE INDUSTRY MAY DIFFER. ACCORDINGLY, SCHLUMBERGER CANNOT AND DOES NOT WARRANT THE ACCURACY, CORRECTNESS OR COMPLETENESS OF ANY SUCH INTERPRETATION, RESEARCH, ANALYSIS, DATA, RESULTS, ESTIMATES OR RECOMMENDATION. CUSTOMER ACKNOWLEDGES THAT IT IS ACCEPTING THE SERVICES "AS IS", THAT SCHLUMBERGER MAKES NO REPRESENTATION OR WARRANTY, EXPRESS OR IMPLIED, OF ANY KIND OR DESCRIPTION IN RESPECT THERETO, SPECIFICALLY CUSTOMER ACKNOWLEDGES THAT SCHLUMBERGER DOES NOT WARRANT THAT ANY INTERPRETATION, RESEARCH, ANALYSIS, DATA, RESULTS, ESTIMATES, OR RECOMMENDATION IS FIT FOR A PARTICULAR PURPOSE, INCLUDING BUT NOT LIMITED TO COMPLIANCE WITH ANY GOVERNMENT REQUEST OR REGULATORY REQUIREMENT. CUSTOMER FURTHER ACKNOWLEDGES THAT SUCH SERVICES ARE DELIVERED WITH THE EXPLICIT UNDERSTANDING AND AGREEMENT THAT ANY ACTION TAKEN BASED ON THE SERVICES RECEIVED SHALL BE AT ITS OWN RISK AND RESPONSIBILITY AND NO CLAIM SHALL BE MADE AGAINST SCHLUMBERGER AS A CONSEQUENCE THEREOF.

Ser. Order # DWBE-00028 | OP Vers.: | Process Date: 2/8/2019 | Center: Bakersfield | Baseline: Techlog | Log Analyst: J. Little/ T. Jiang

Remarks:

Remarks:

Lithology is from LithoScanner spectroscopy data.
Porosity and Saturation are from PNX.

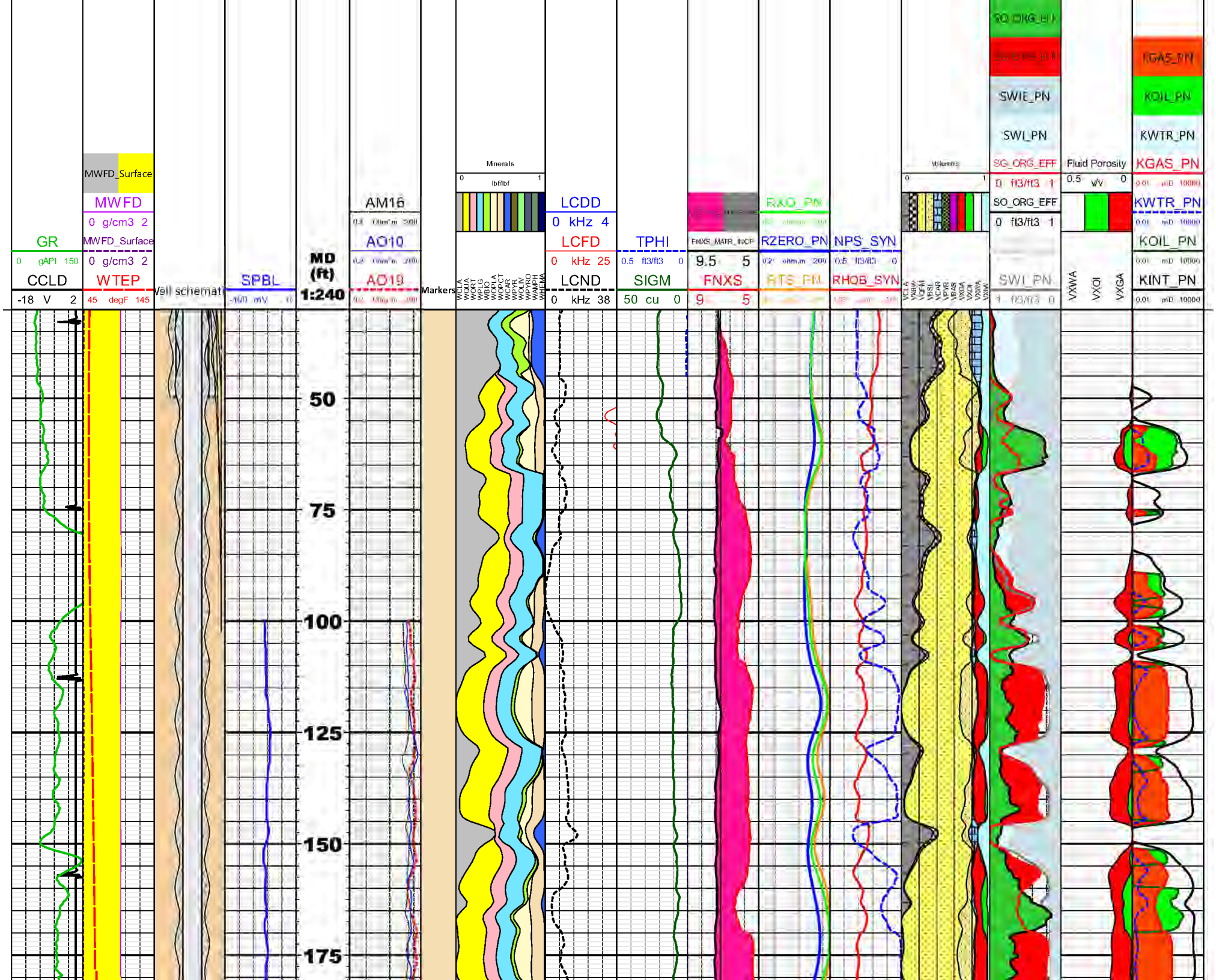
GR
0 gAPI 150
CCLD
-18 V 2
MWFD_Surface
MWFD
0 g/cm3 2
MWFD_Surface
0 g/cm3 2
WTEP
45 degF 145
Well schemati
SPBL
MD (ft)
1:240
AM16
AO10
AO19
Markers
Minerals
0 lbf/lbf 1
LCDD
0 kHz 4
LCFD
0 kHz 25
LCND
0 kHz 38
TPHI
0.5 ft3/ft3 0
SIGM
50 cu 0
FNXS_MATR_INCP
9.5 5
FNXS
9 5
RXO_PN
RZERO_PN
RTS_PN
NPS_SYN
RHOB_SYN
Volumes
0 1
SO_ORG_EFF
SWIE_PN
SWL_PN
SG_ORG_EFF
0 ft3/ft3 1
SO_ORG_EFF
0 ft3/ft3 1
SWI_PN
Fluid Porosity
0.5 v/v 0
VXWA
VXOI
VXGA
KGAS_PN
KOIL_PN
KWTR_PN
KGAS_PN
KWTR_PN
KOIL_PN
KINT_PN
50
75
100
125
150
175

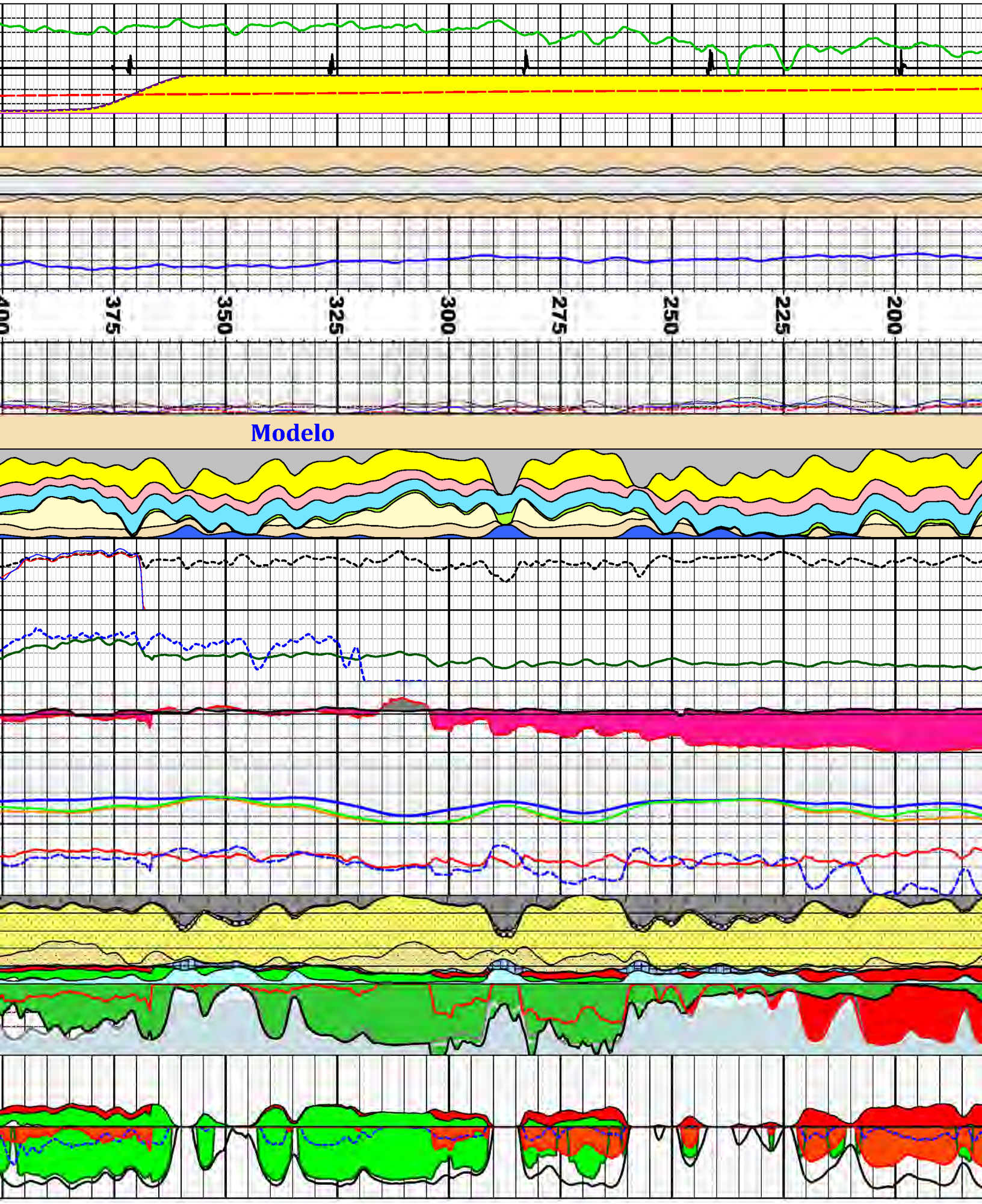
400
375
350
325
300
275
250
225
200
Modelo

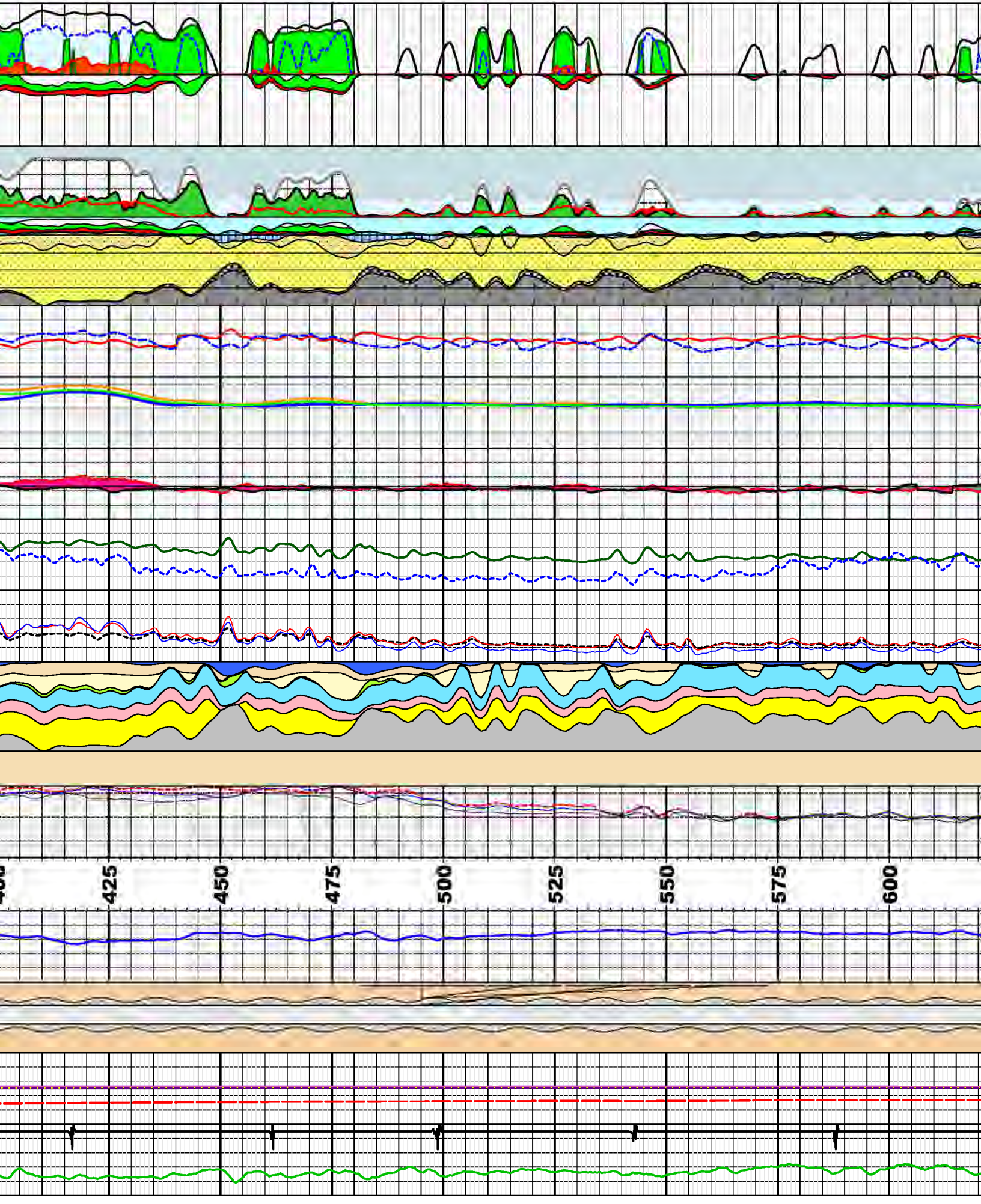
425
450
475
500
525
550
575
600

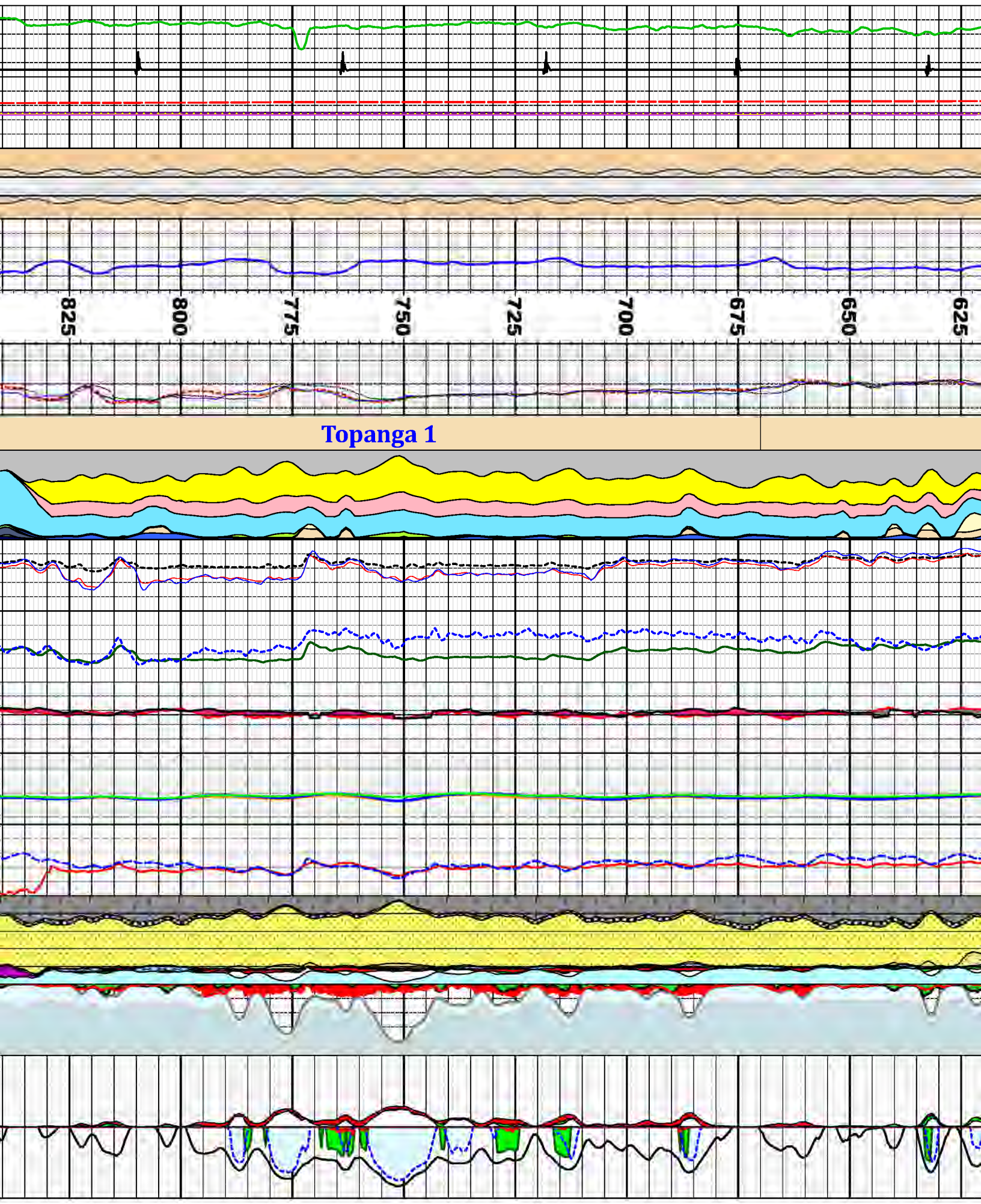
825
800
775
750
725
700
675
650
625
Topanga 1

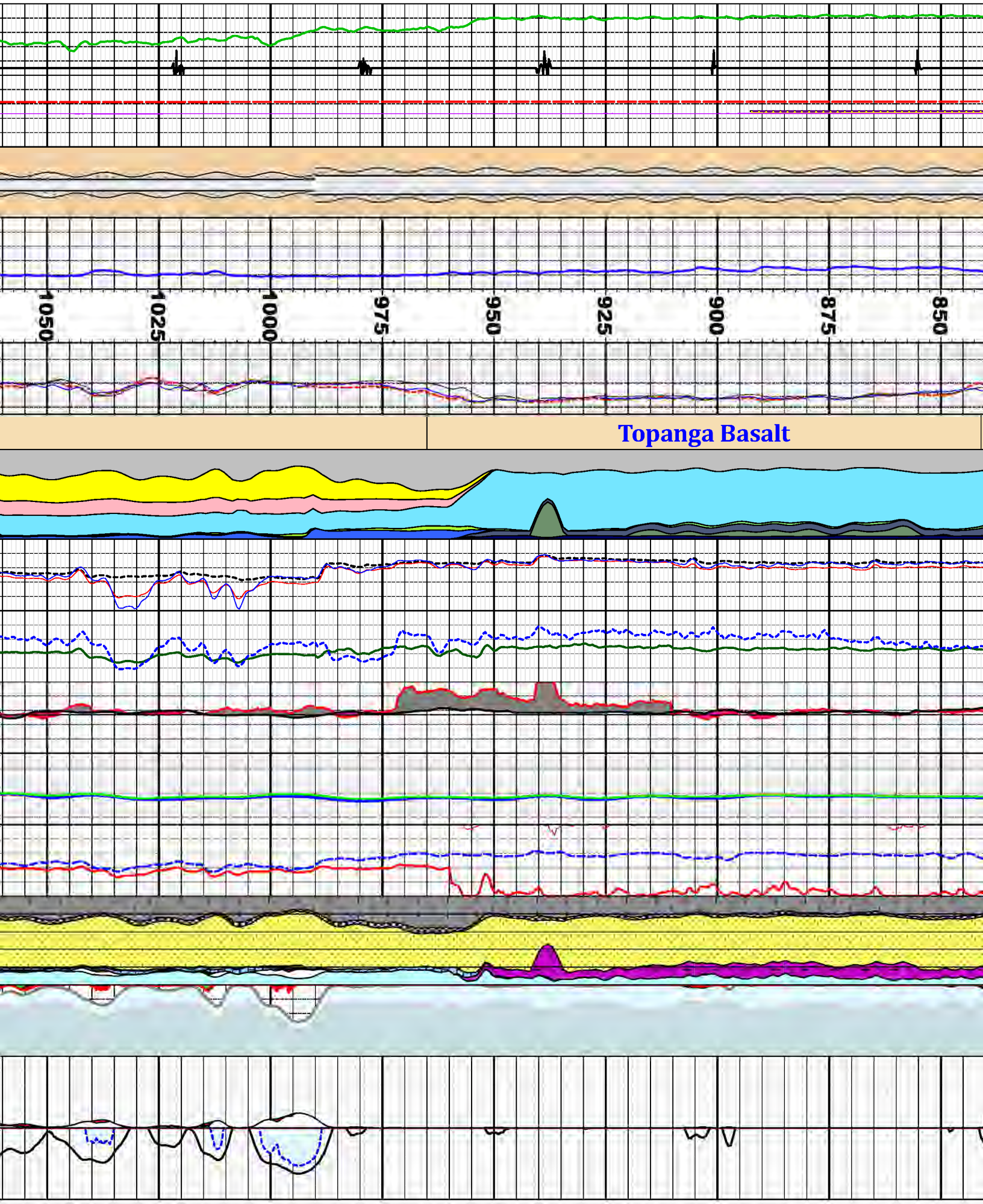
1050
1025
1000
975
950
925
900
875
850
Topanga Basalt

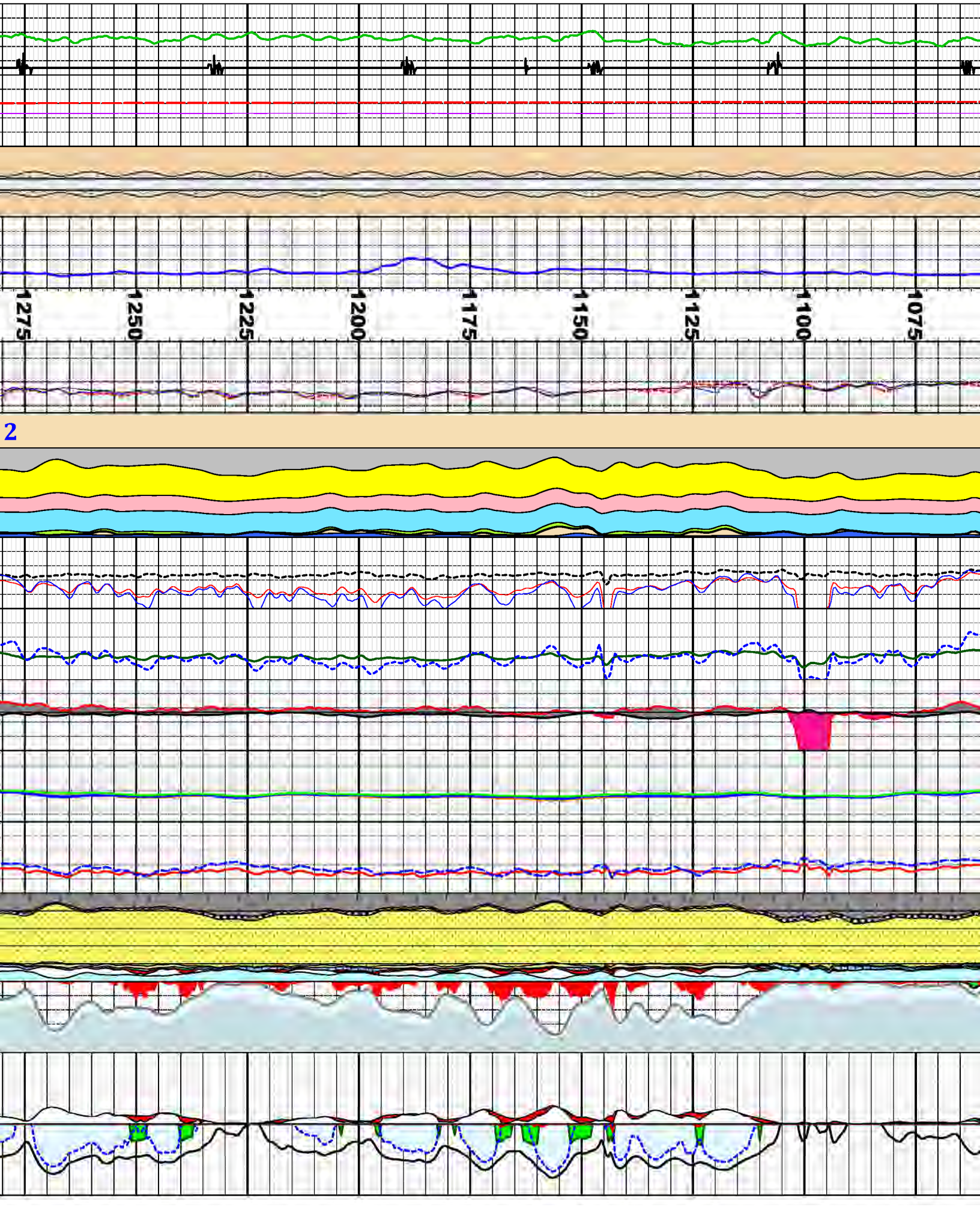
1275
1250
1225
1200
1175
1150
1125
1100
1075
2

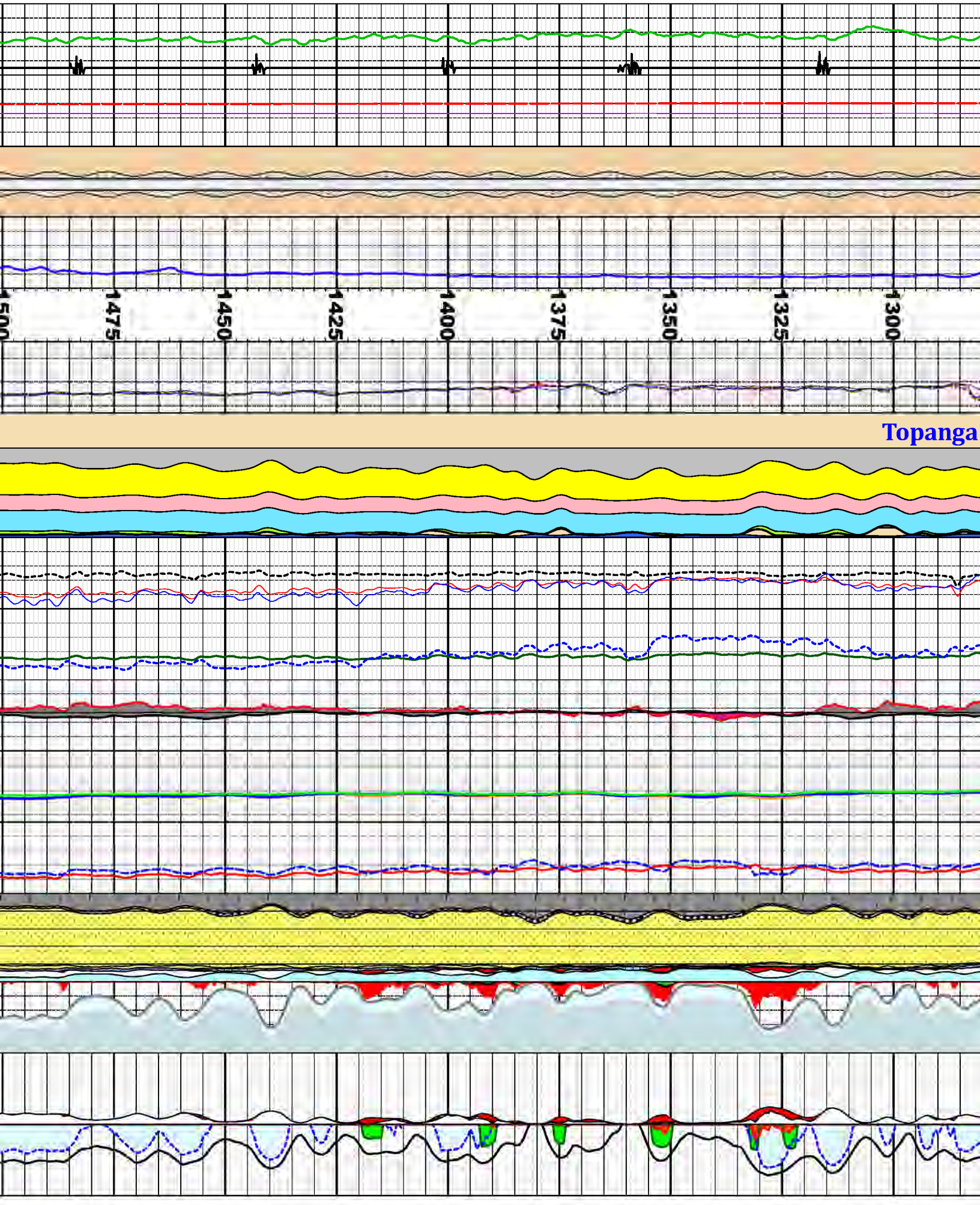
1500
1475
1450
1425
1400
1375
1350
1325
1300
Topanga

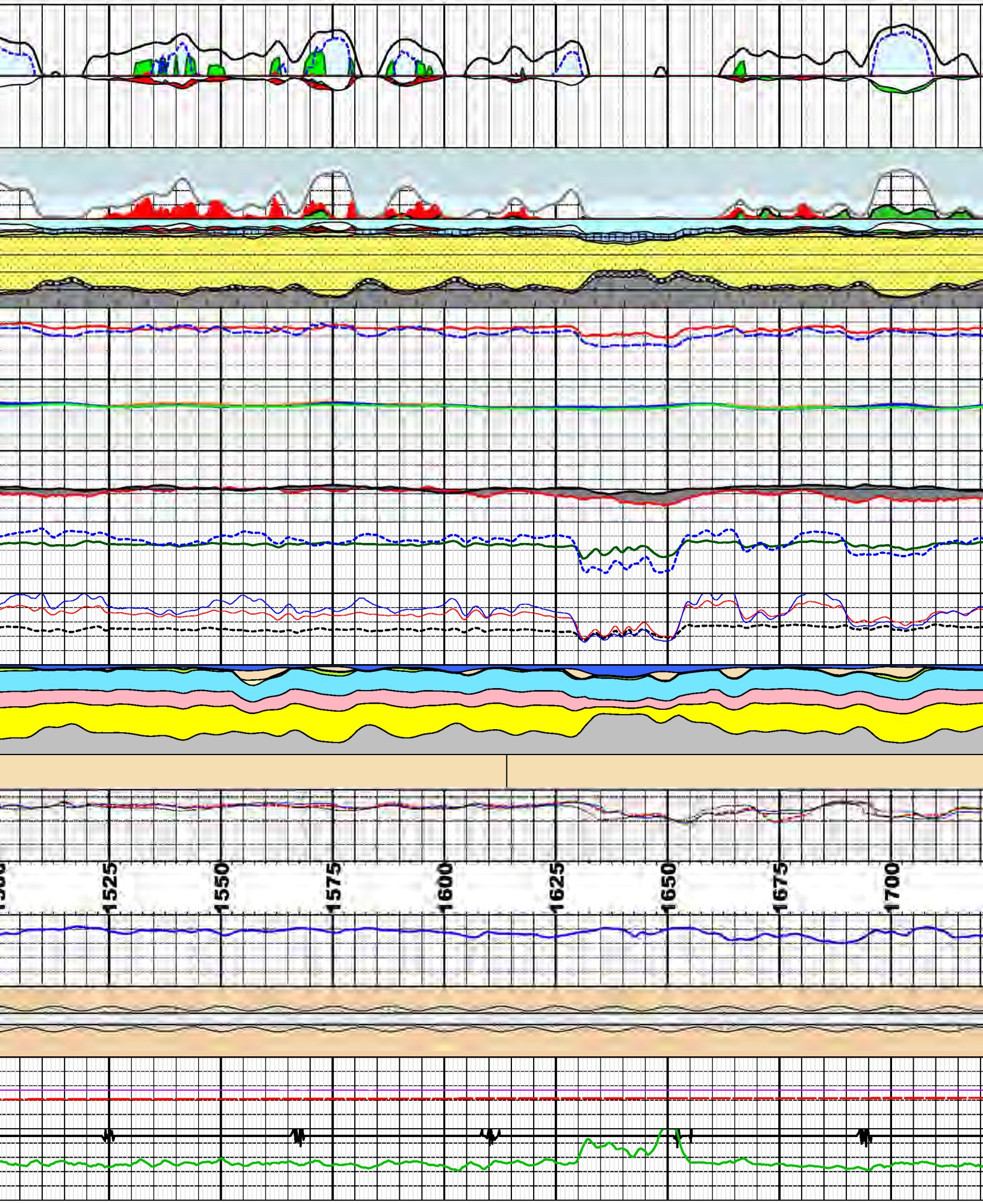
1525
1550
1575
1600
1625
1650
1675
1700

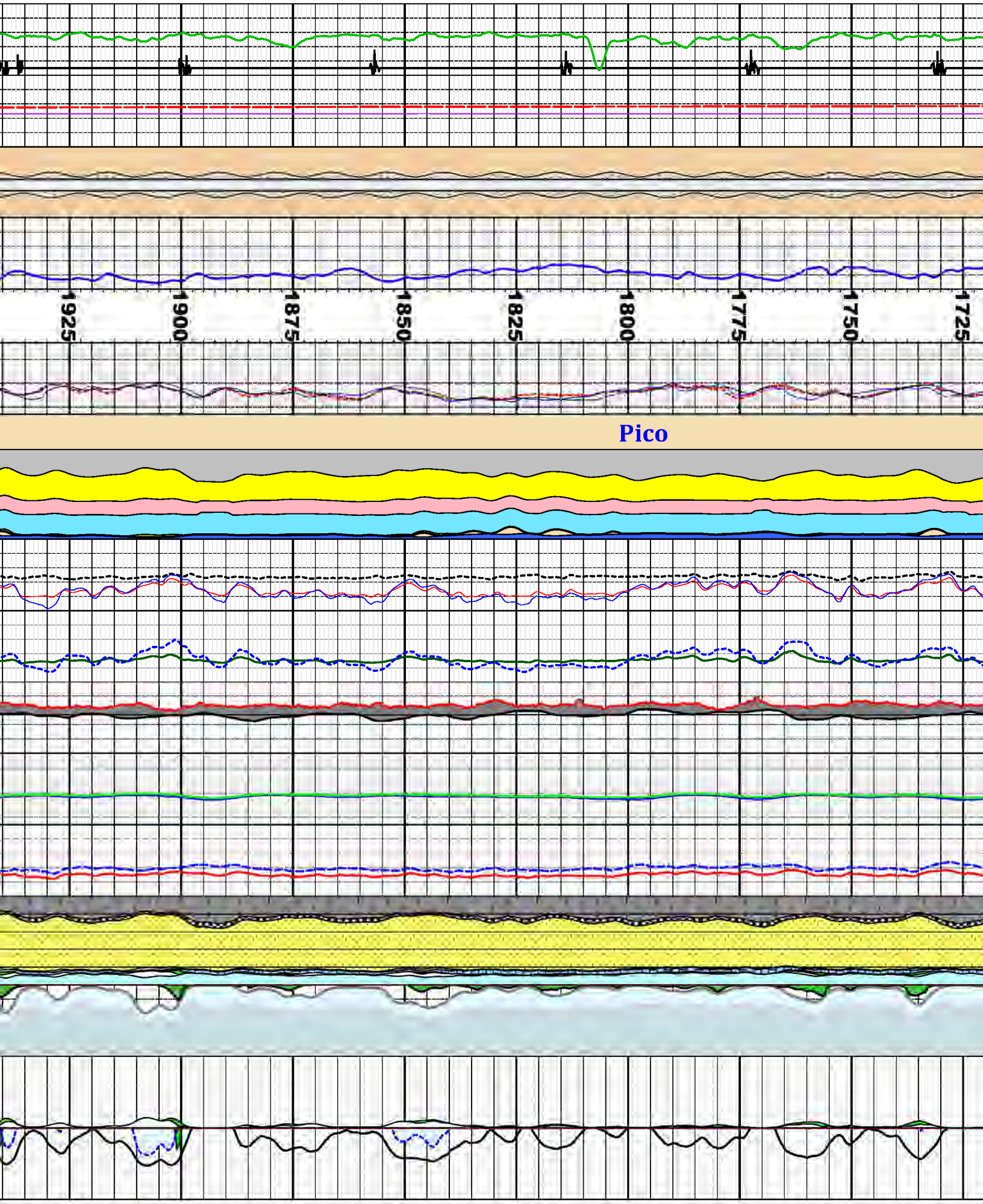
1925
1900
1875
1850
1825
1800
1775
1750
1725
Pico

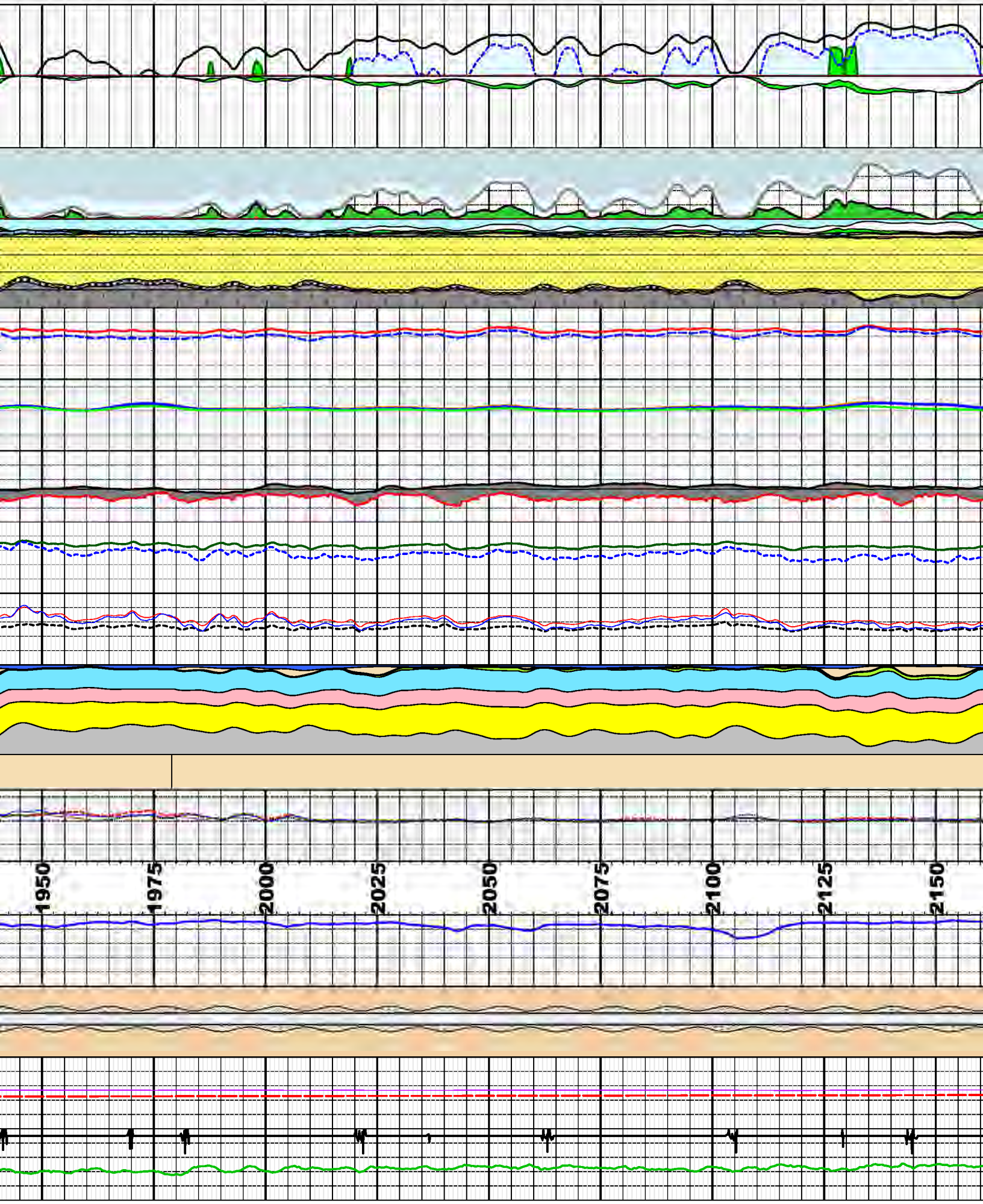
1950
1975
2000
2025
2050
2075
2100
2125
2150

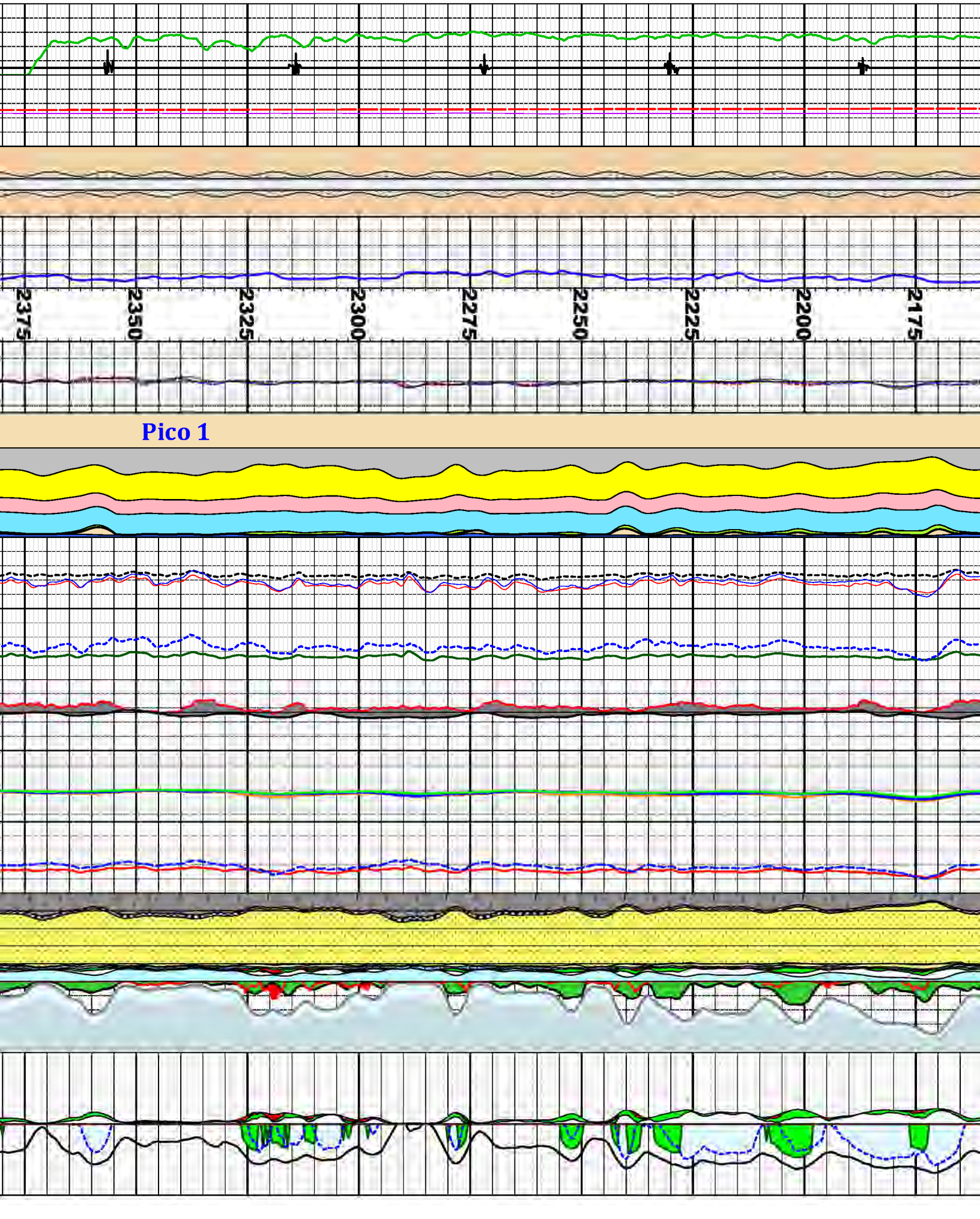
2375
2350
2325
2300
2275
2250
2225
2200
2175
Pico 1

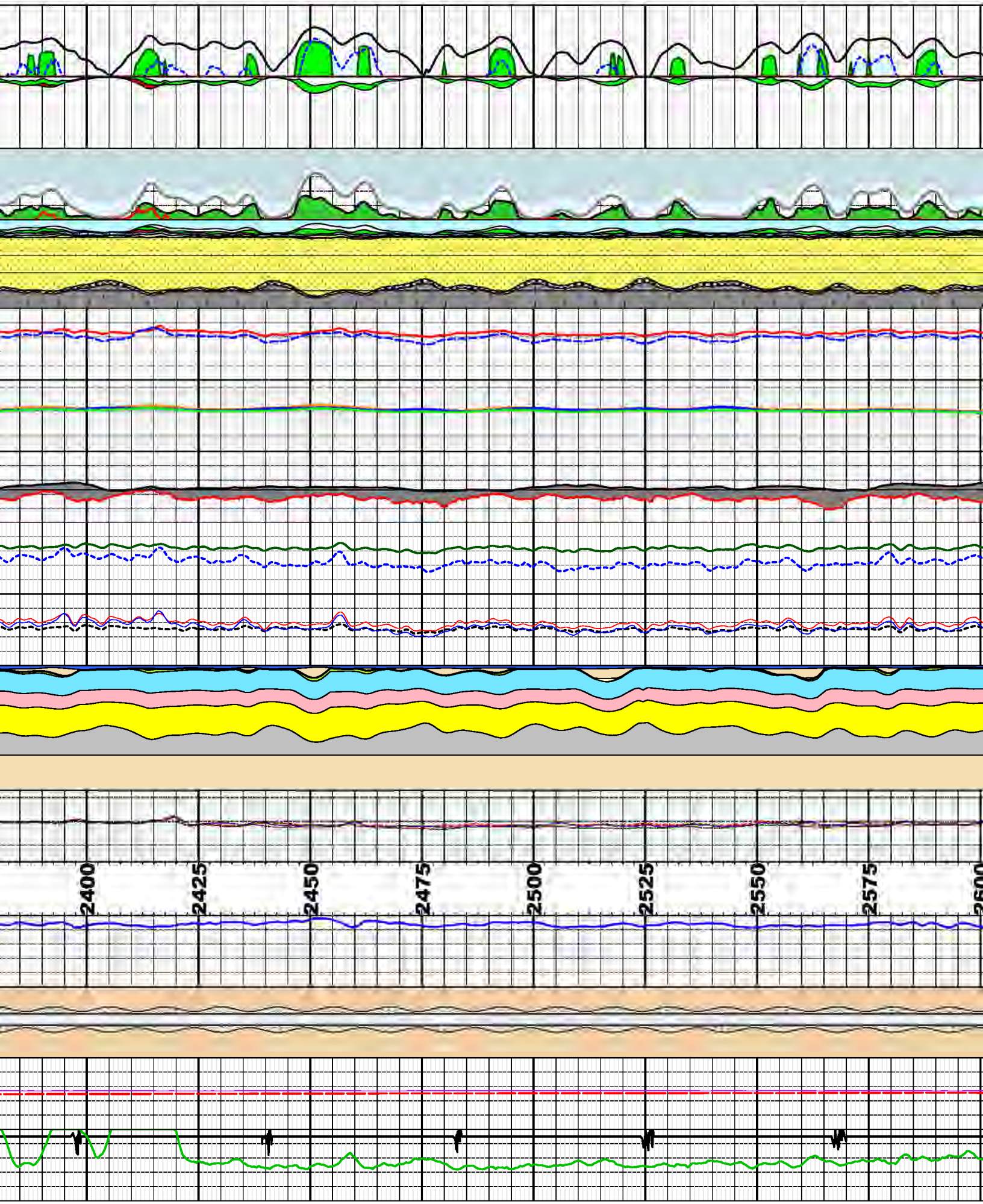
2400
2425
2450
2475
2500
2525
2550
2575

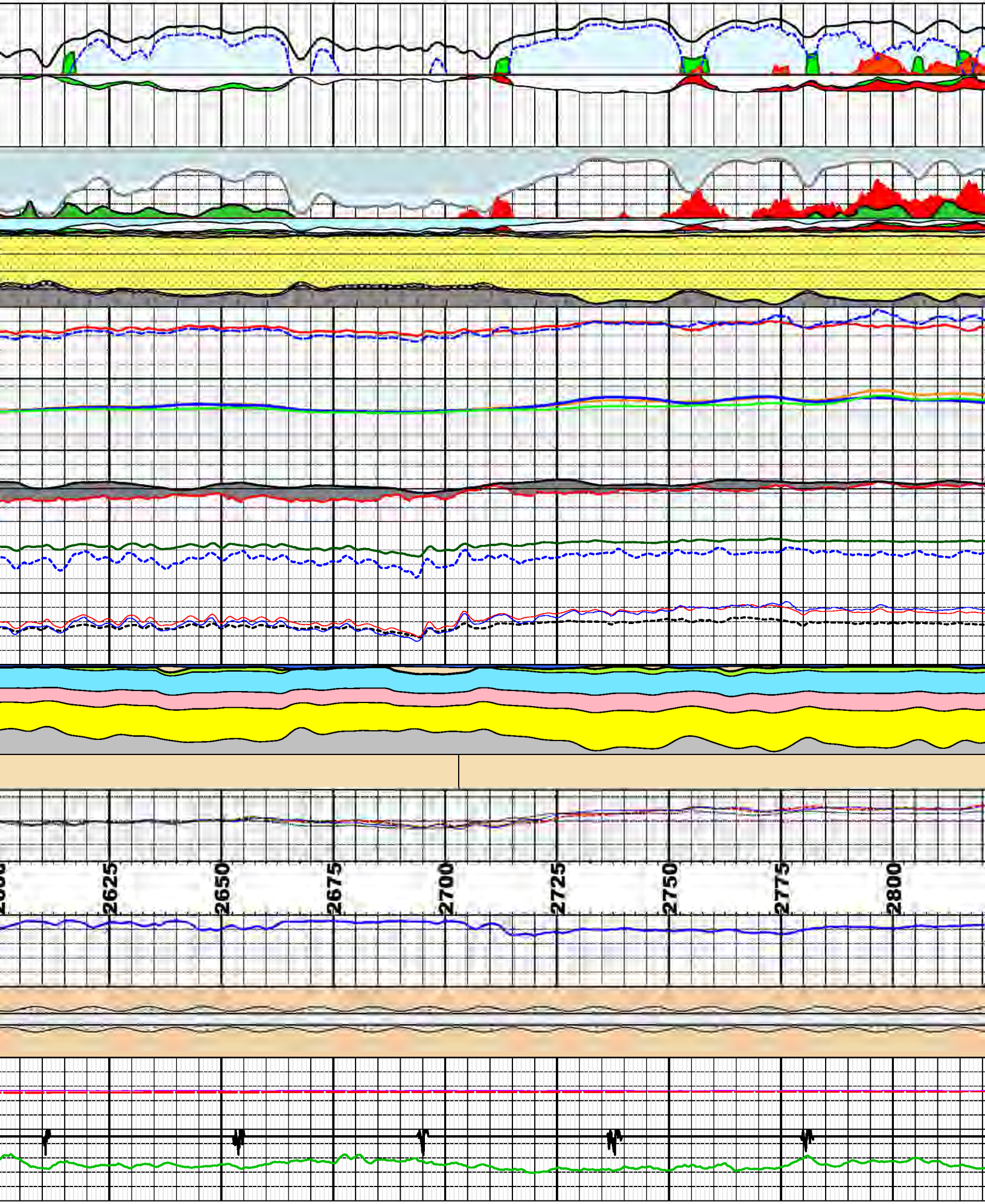
2625
2650
2675
2700
2725
2750
2775
2800

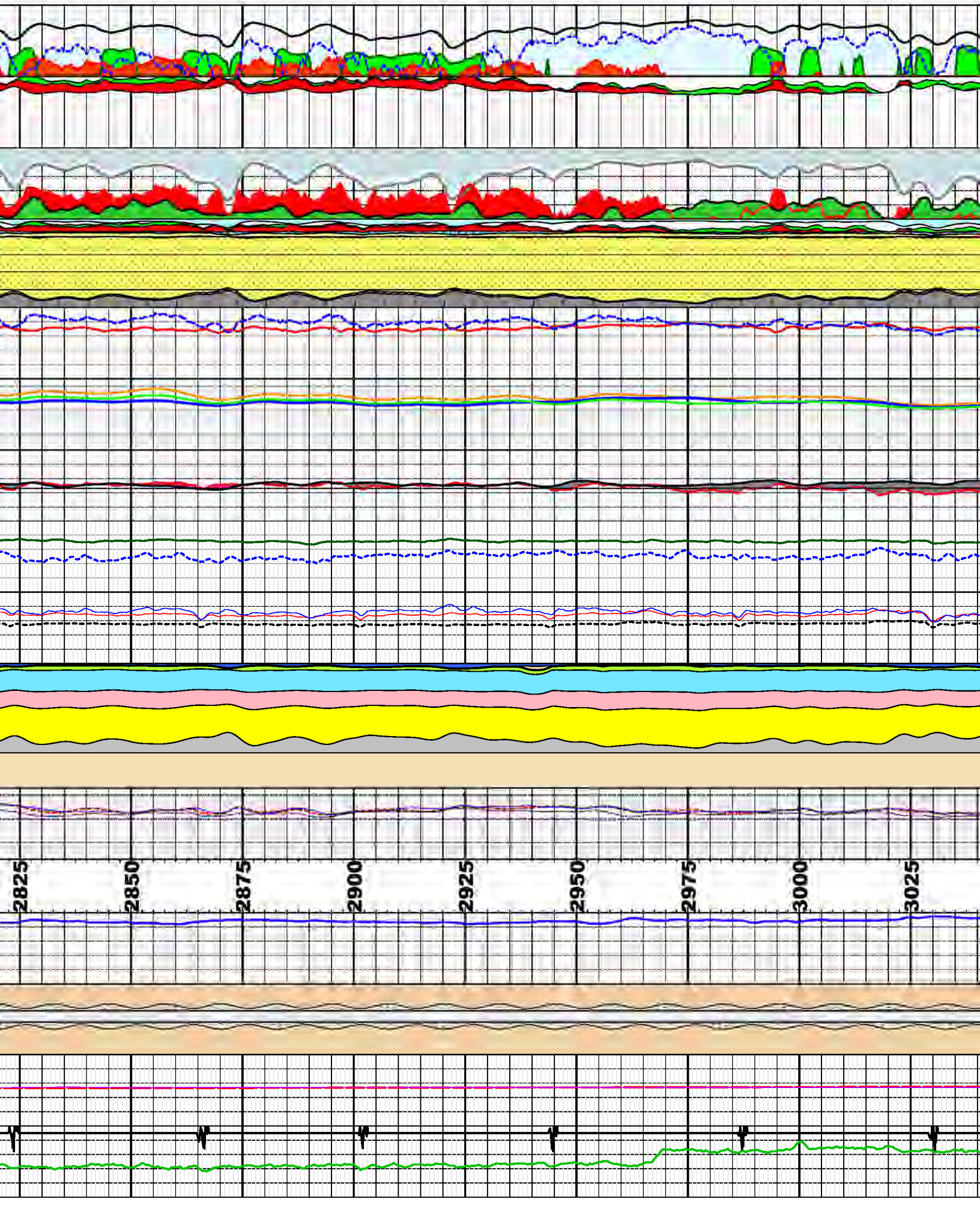
2825
2850
2875
2900
2925
2950
2975
3000
3025

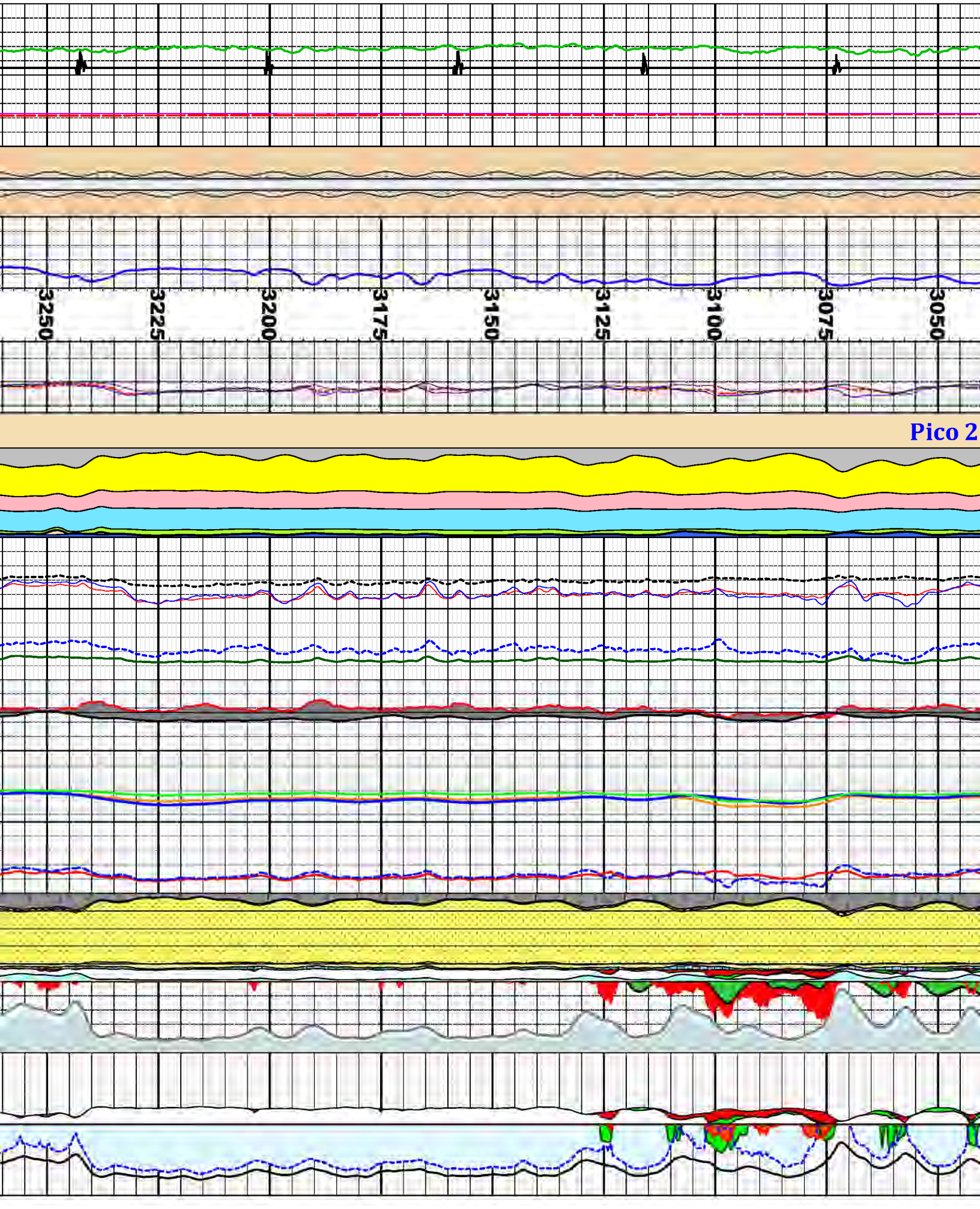
3250
3225
3200
3175
3150
3125
3100
3075
3050
Pico 2

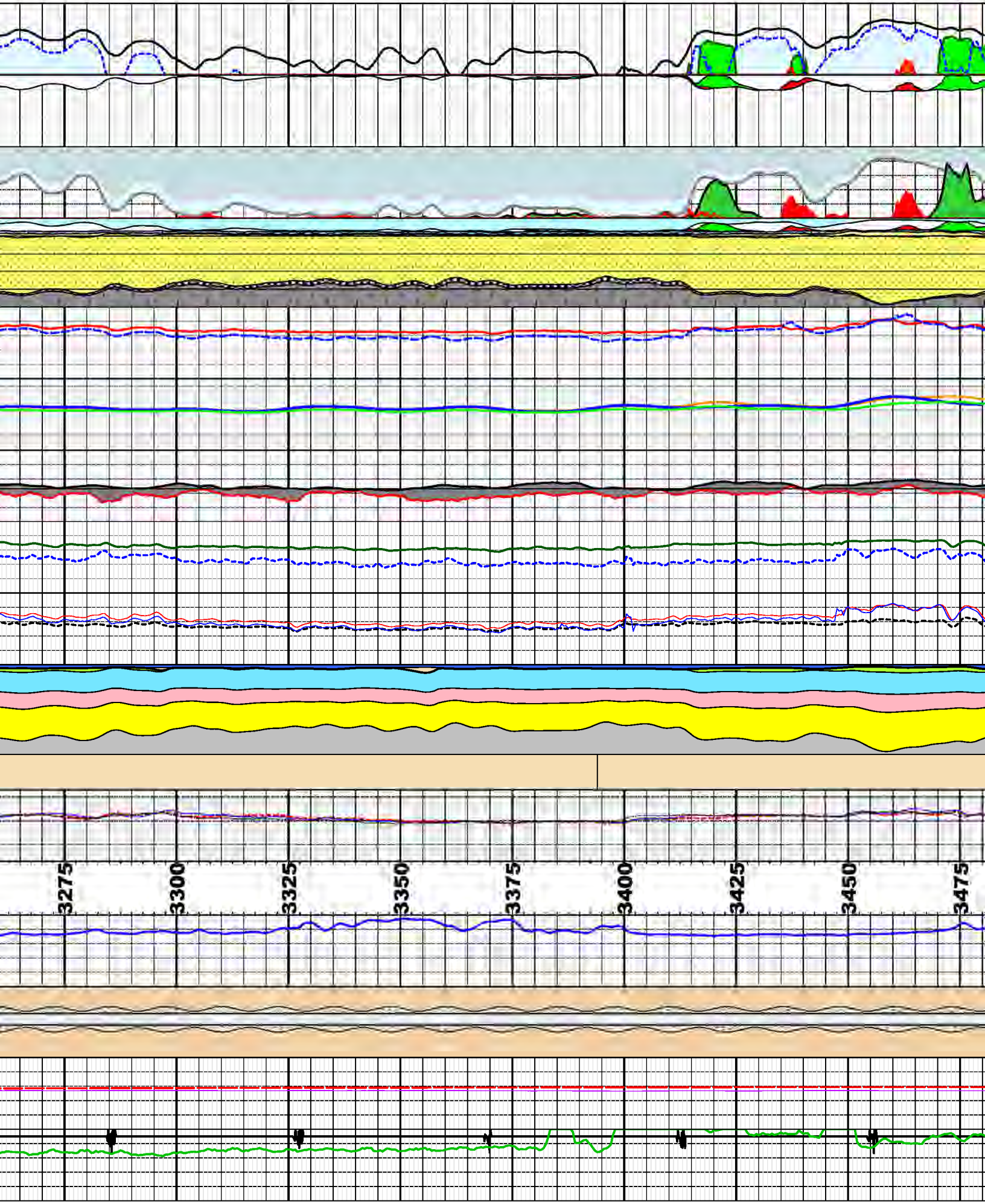
3275
3300
3325
3350
3375
3400
3425
3450
3475

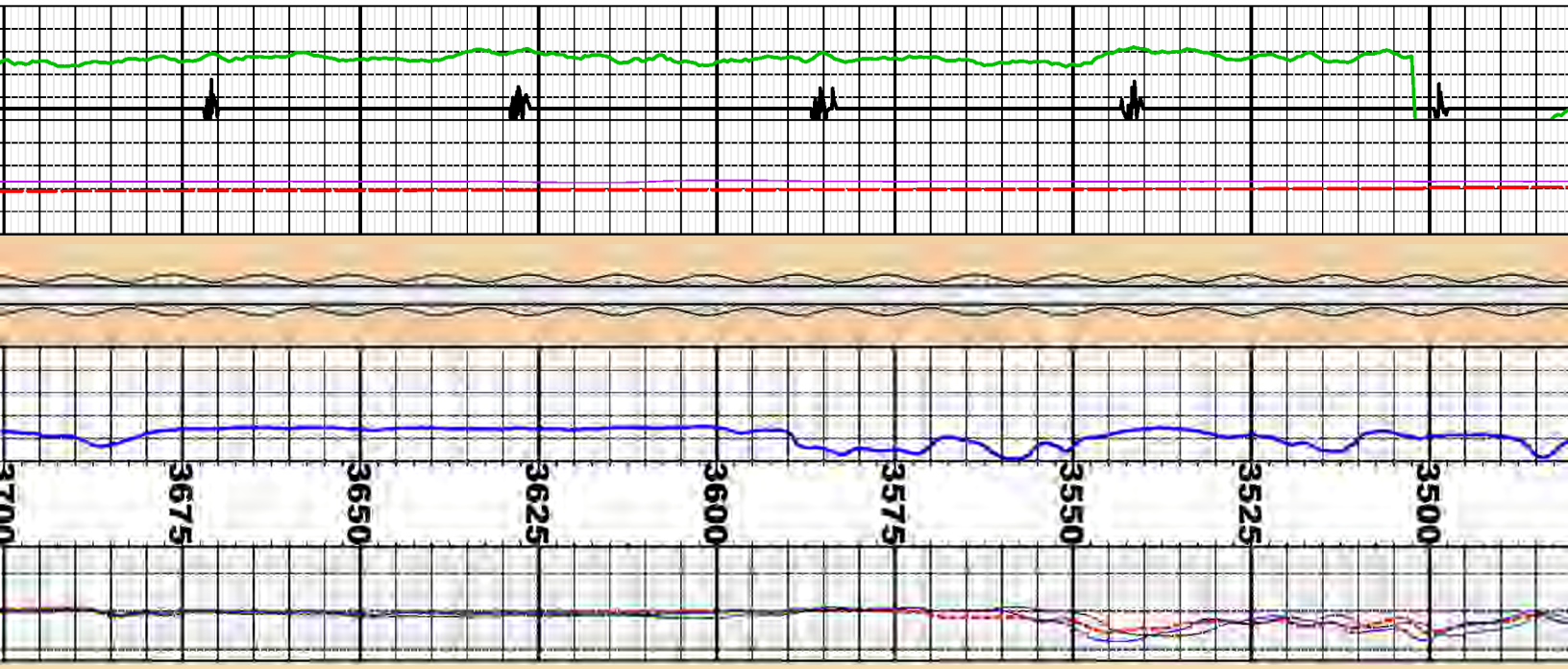

ico 3

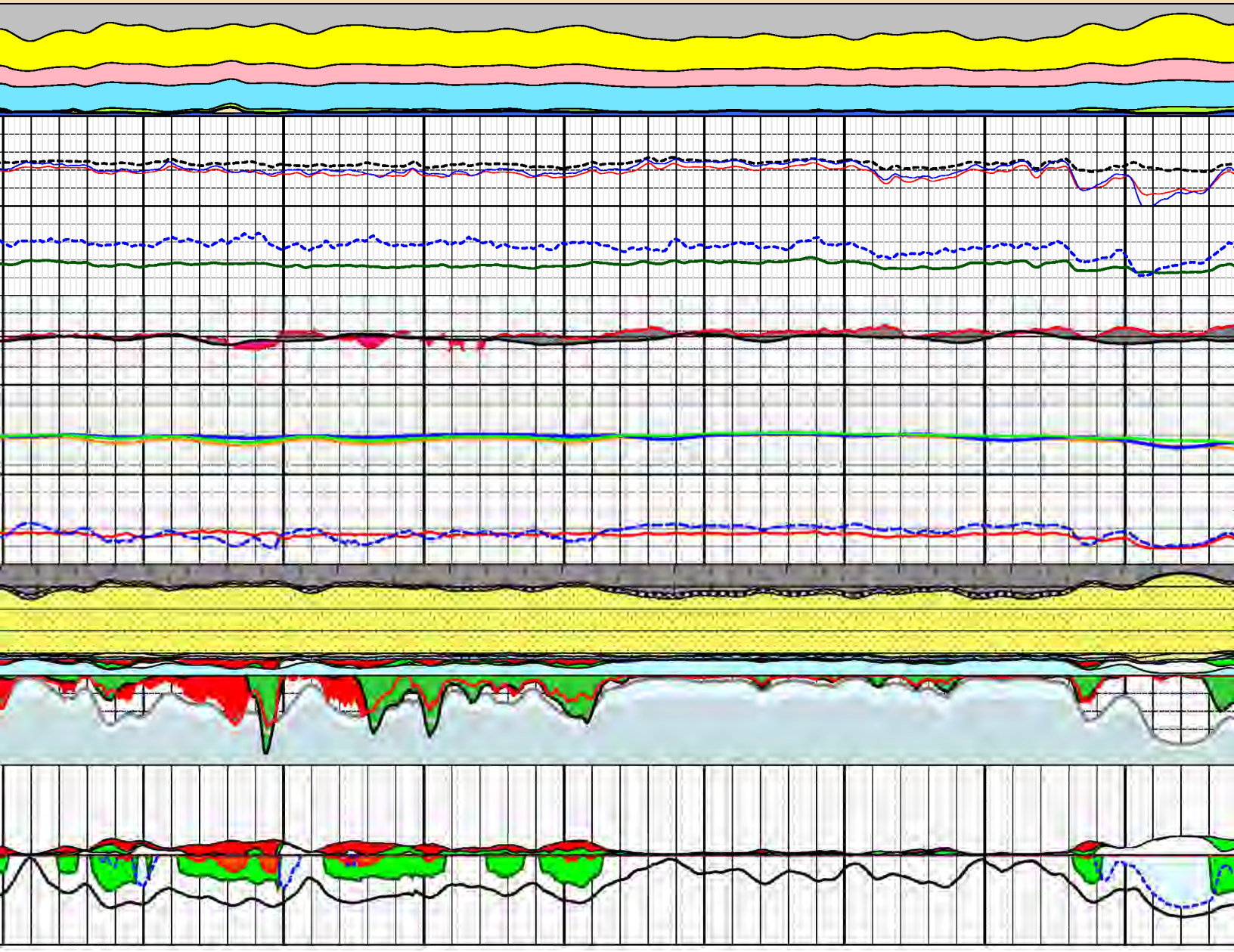

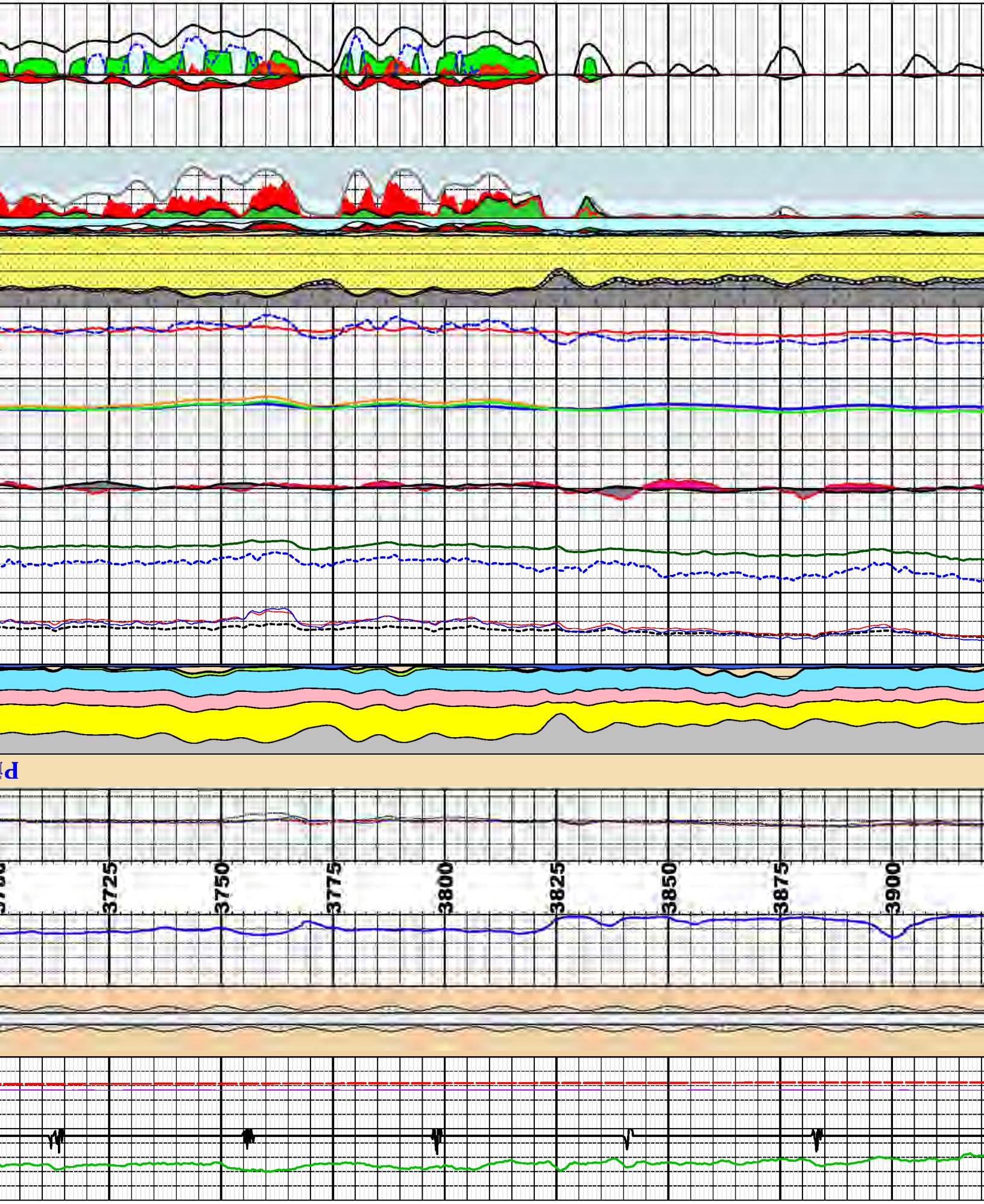
3725
3750
3775
3800
3825
3850
3875
3900

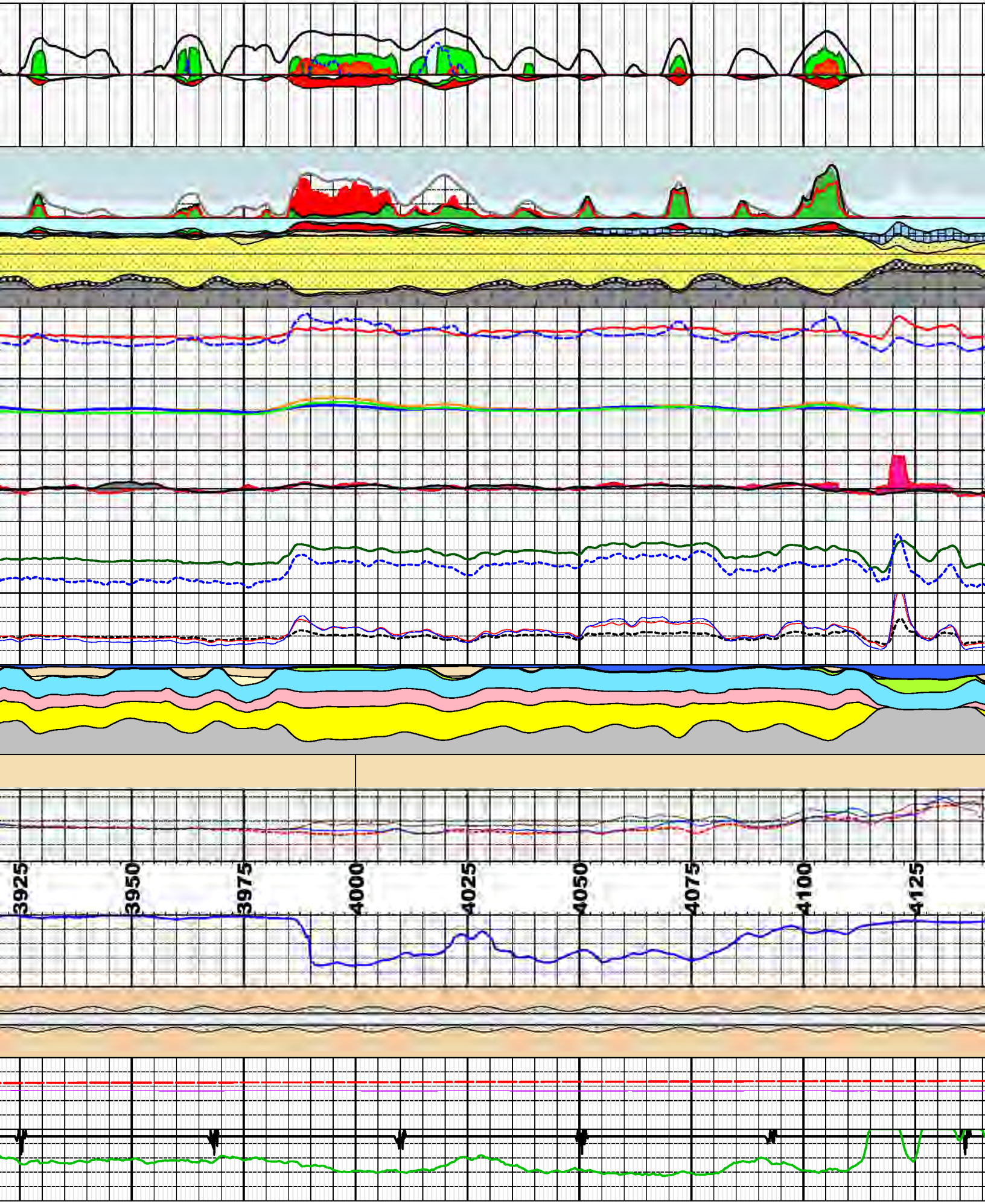
3925
3950
3975
4000
4025
4050
4075
4100
4125

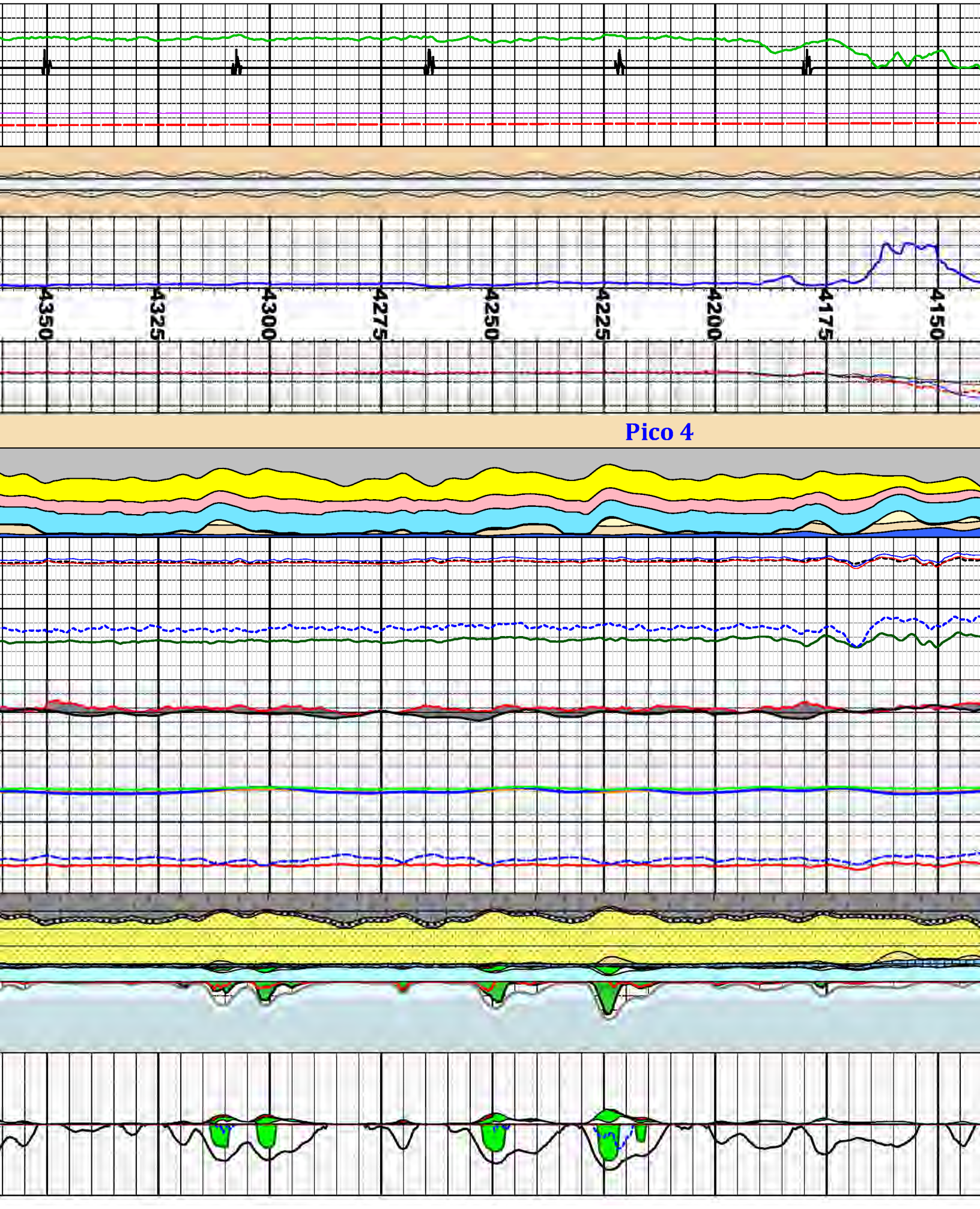
4350
4325
4300
4275
4250
4225
4200
4175
4150
Pico 4

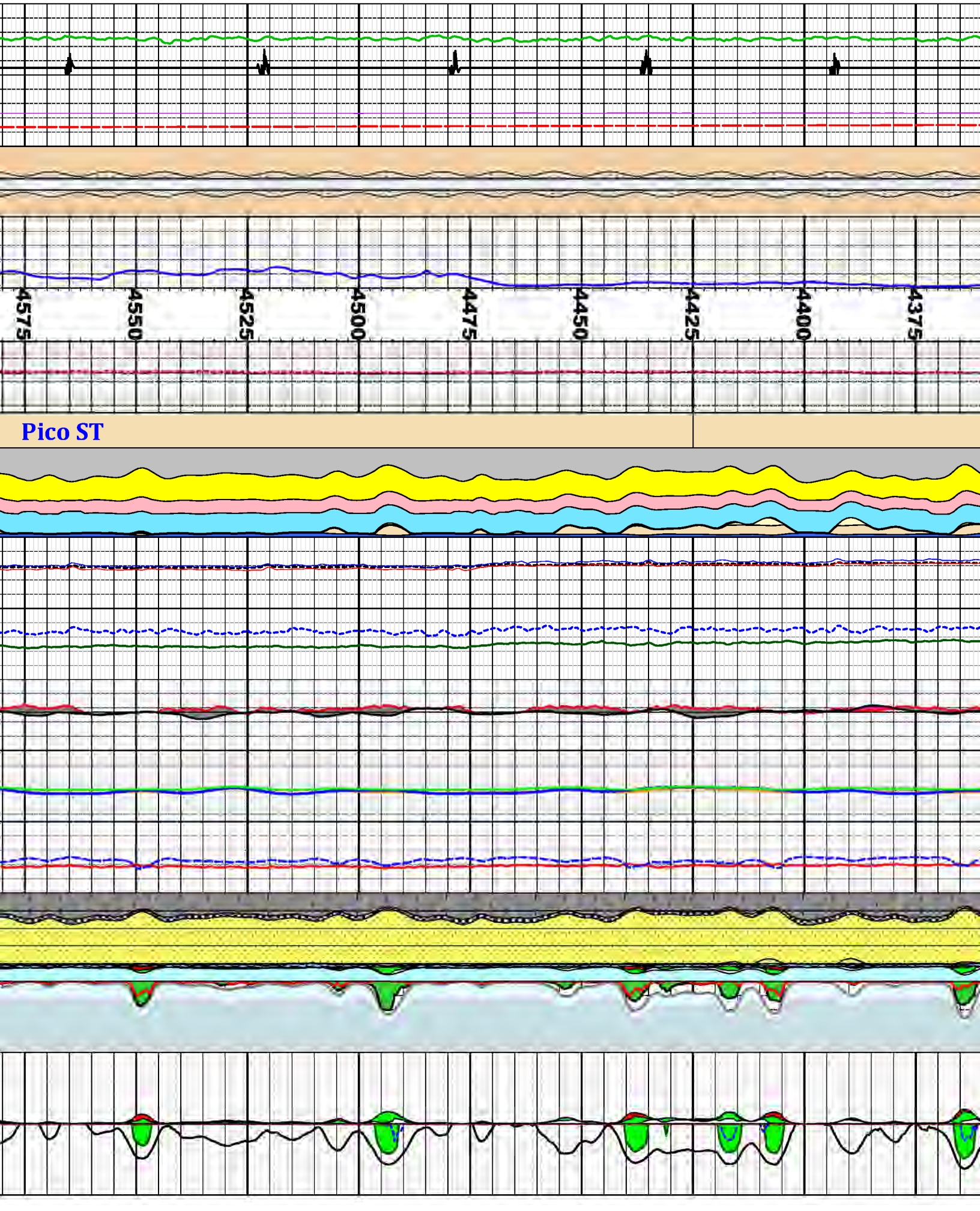
4575
4550
4525
4500
4475
4450
4425
4400
4375
Pico ST

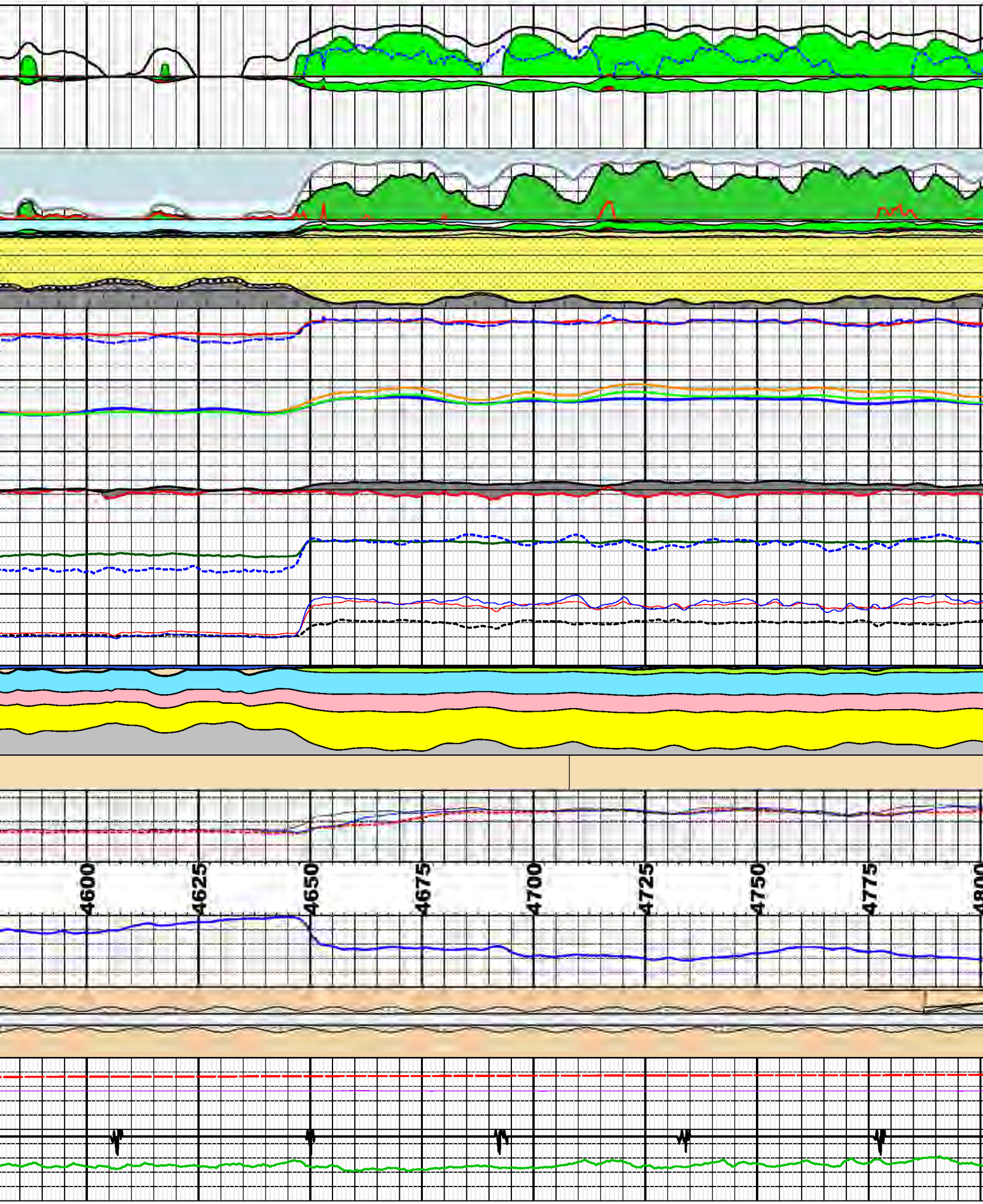
4600
4625
4650
4675
4700
4725
4750
4775

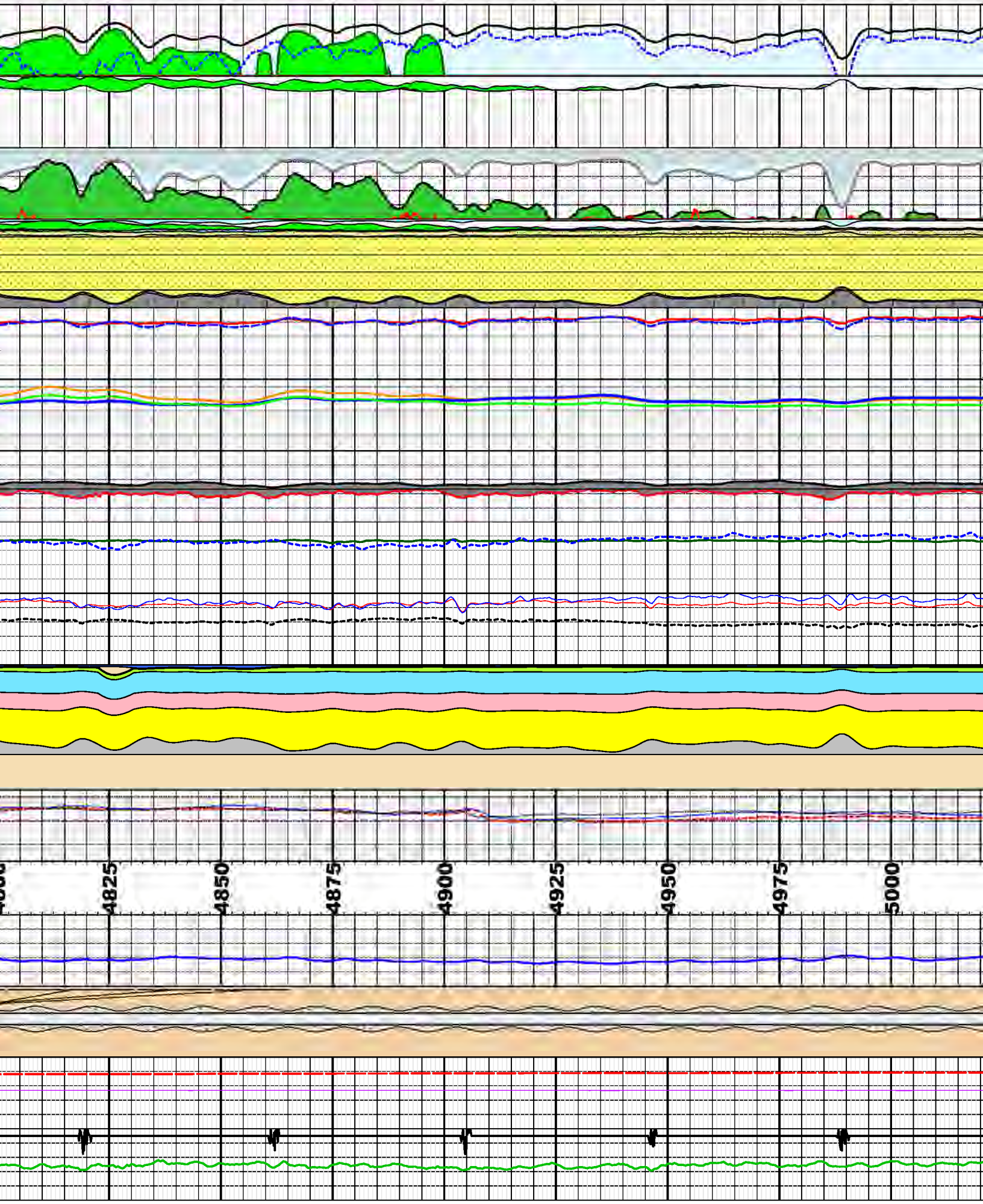
4825
4850
4875
4900
4925
4950
4975
5000

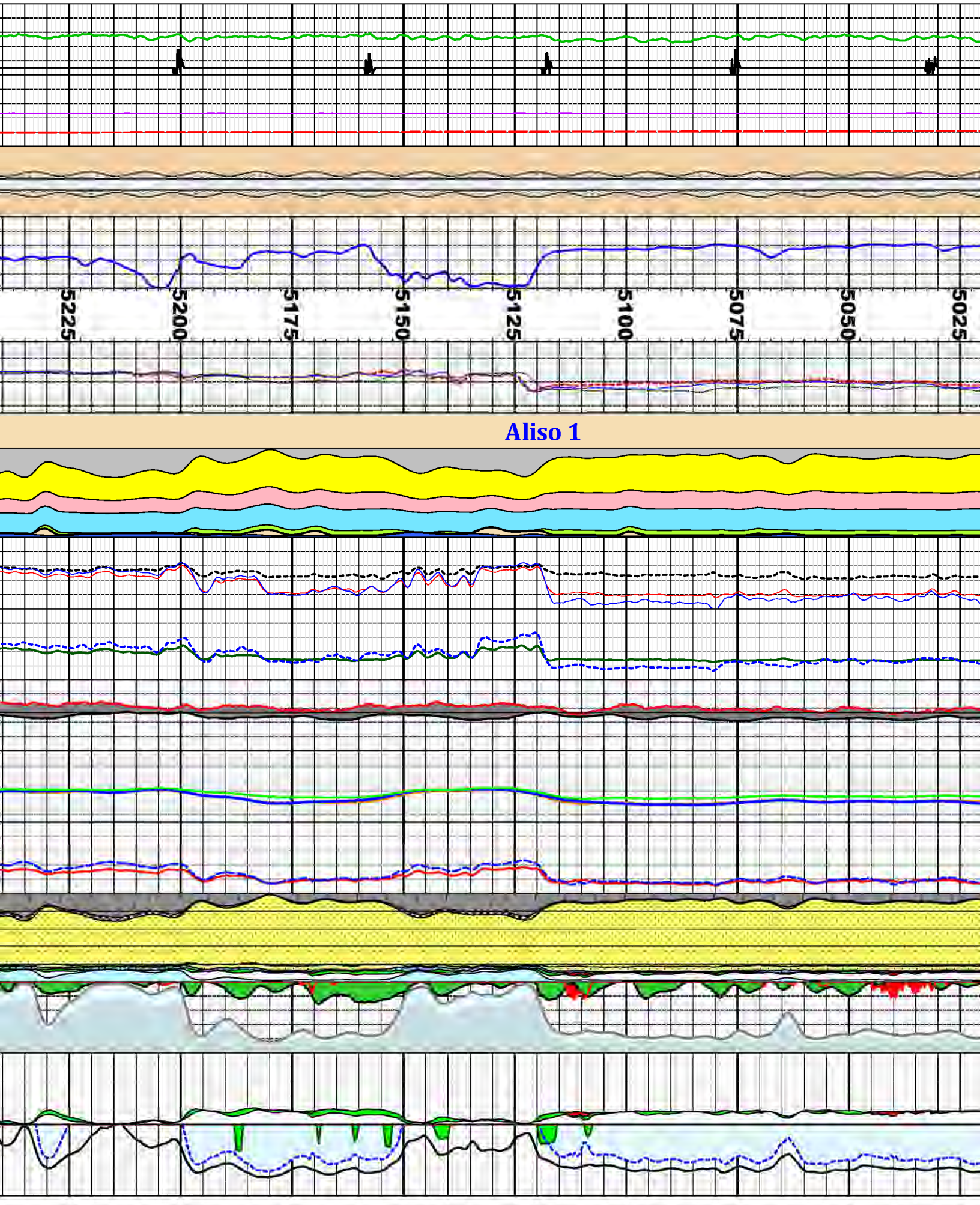
5225
5200
5175
5150
5125
5100
5075
5050
5025
Aliso 1

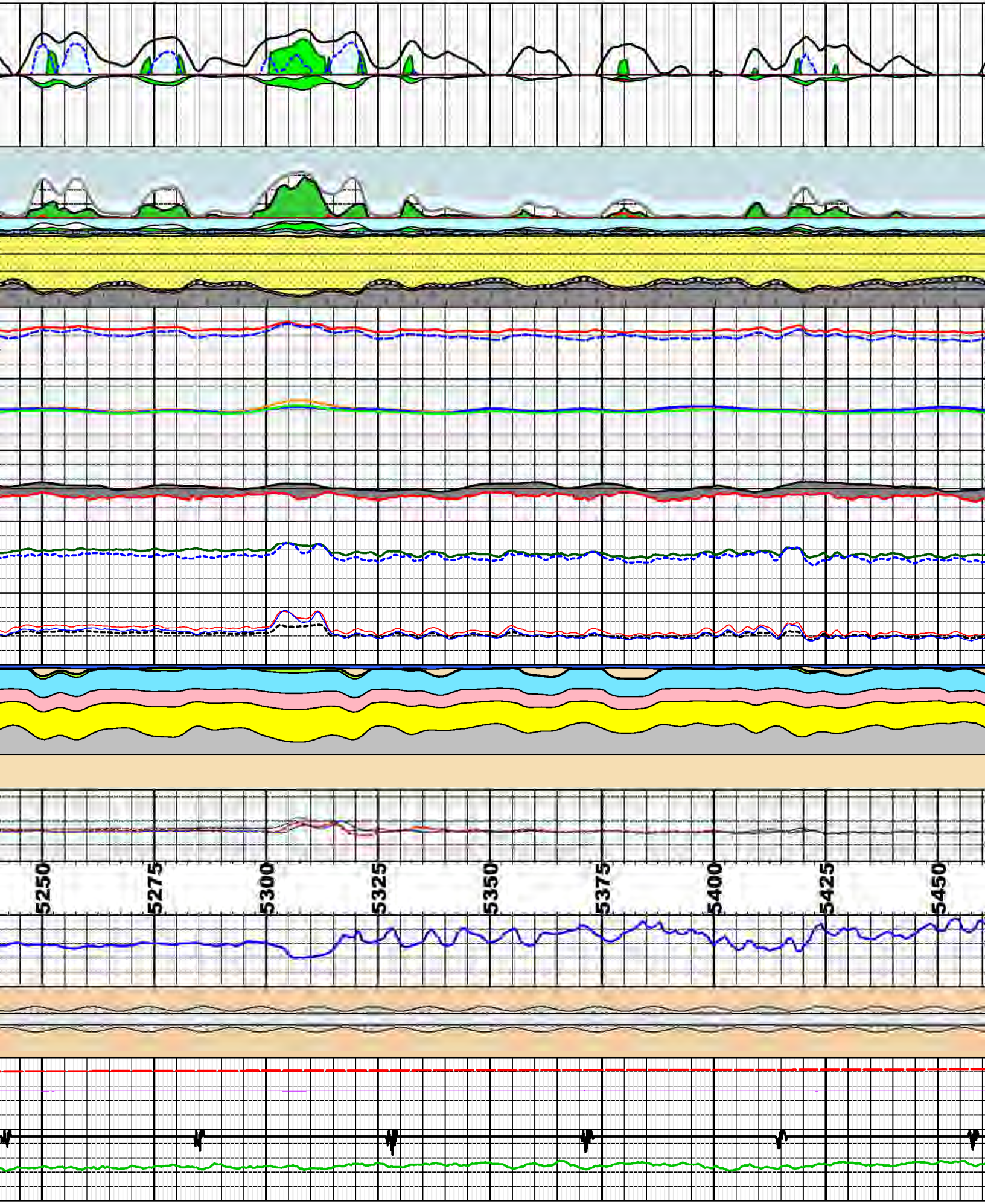
5250
5275
5300
5325
5350
5375
5400
5425
5450

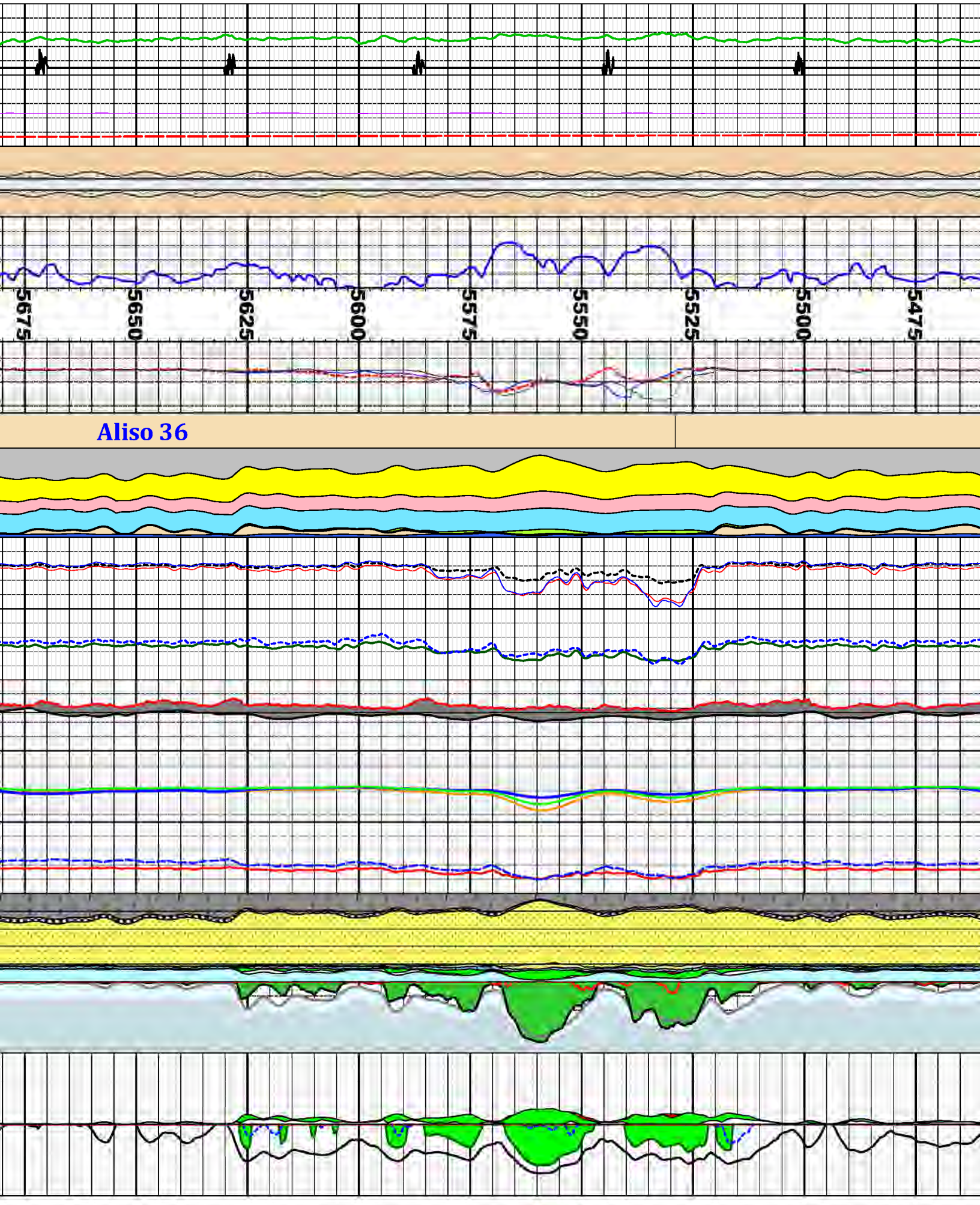
5675
5650
5625
5600
5575
5550
5525
5500
5475
Aliso 36

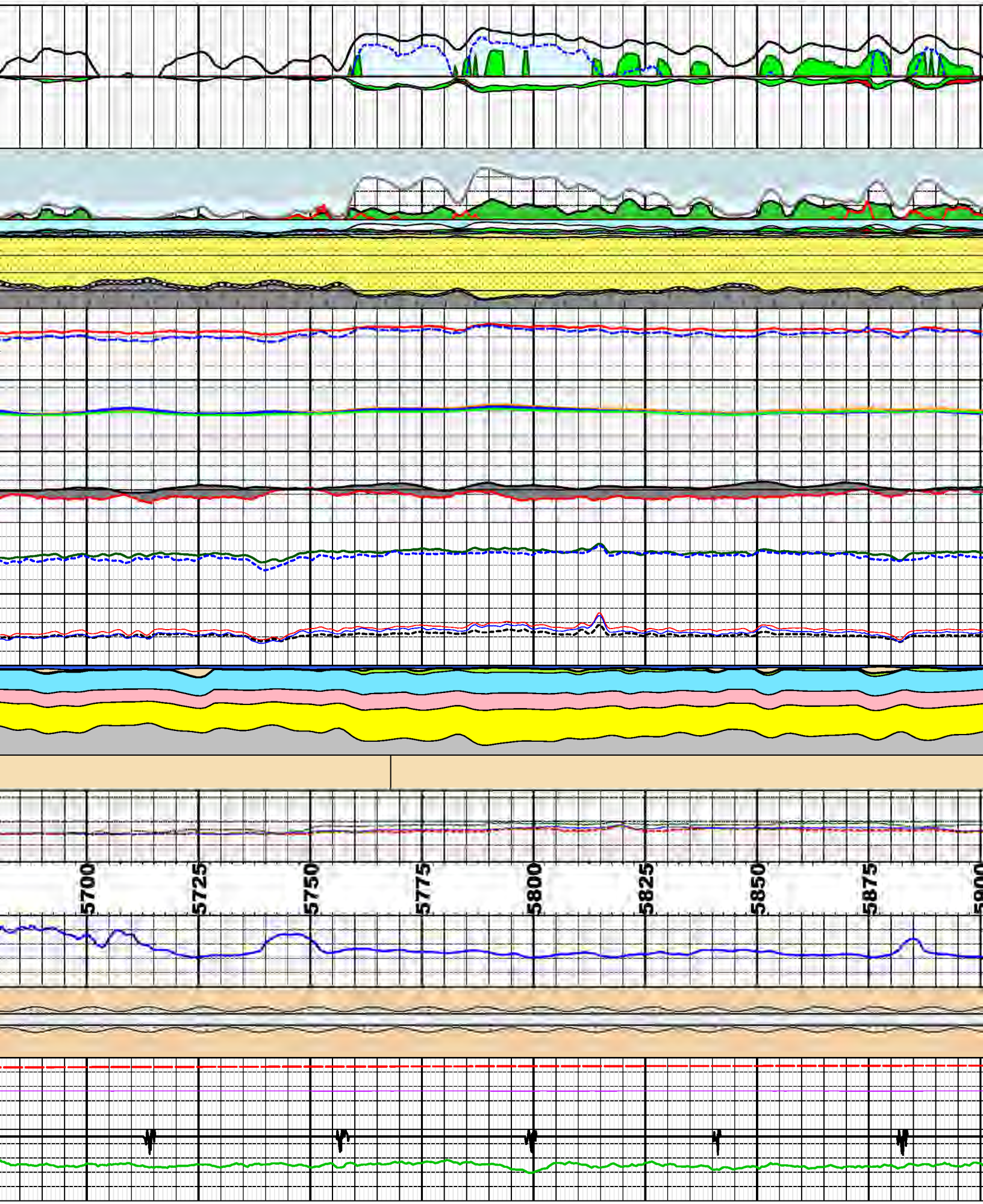
5700
5725
5750
5775
5800
5825
5850
5875

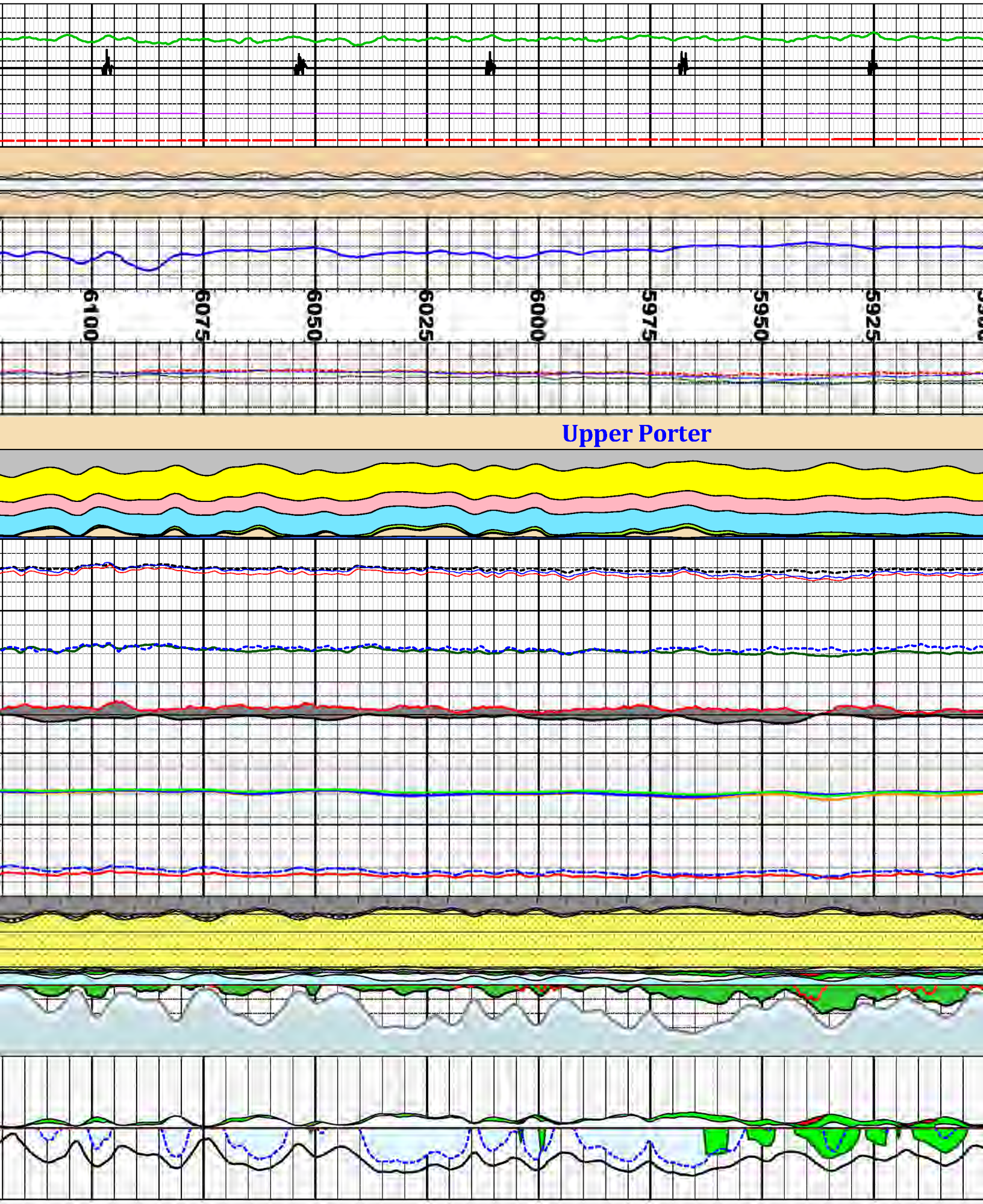
6100
6075
6050
6025
6000
5975
5950
5925
Upper Porter

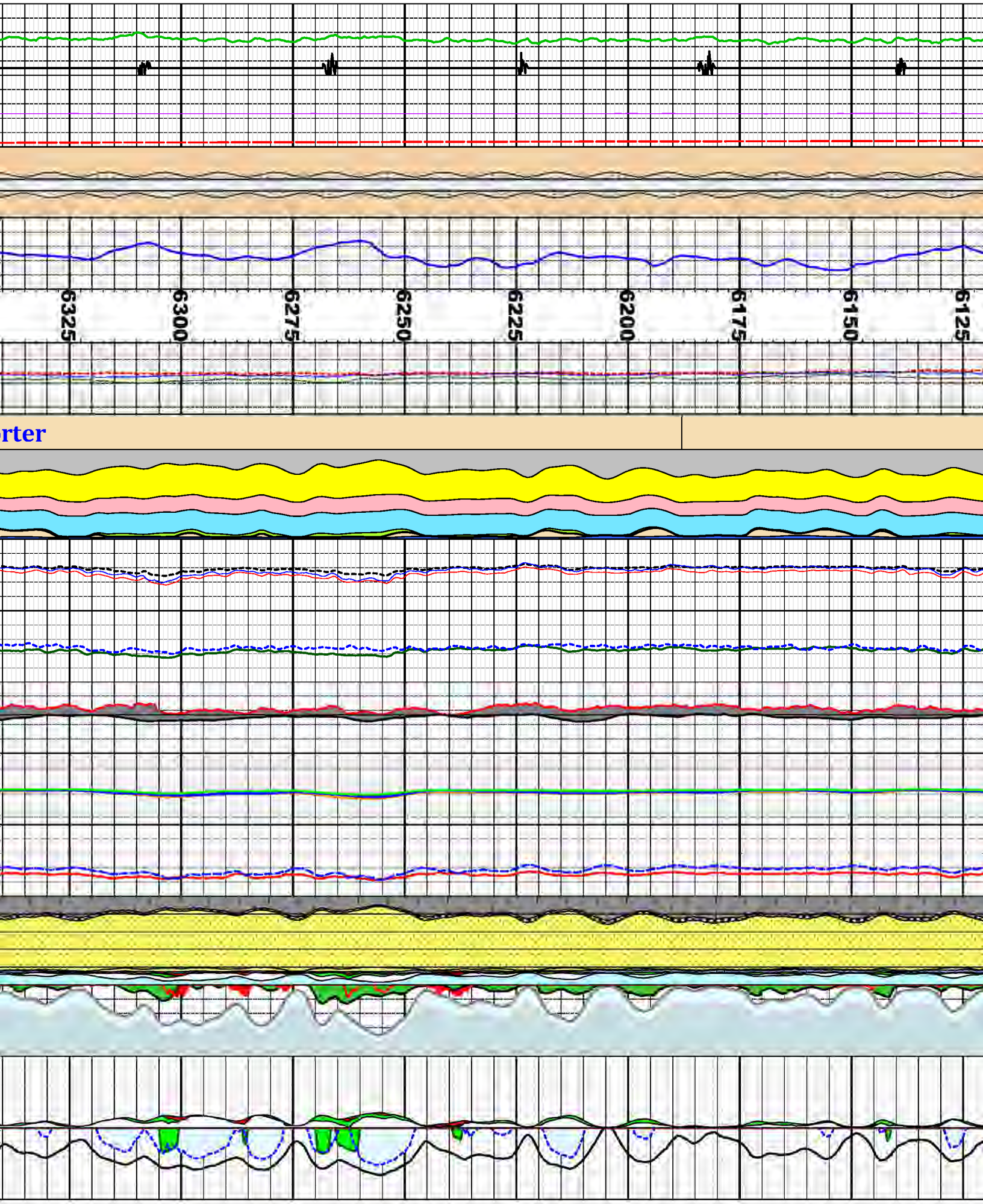
6325
6300
6275
6250
6225
6200
6175
6150
6125
rter

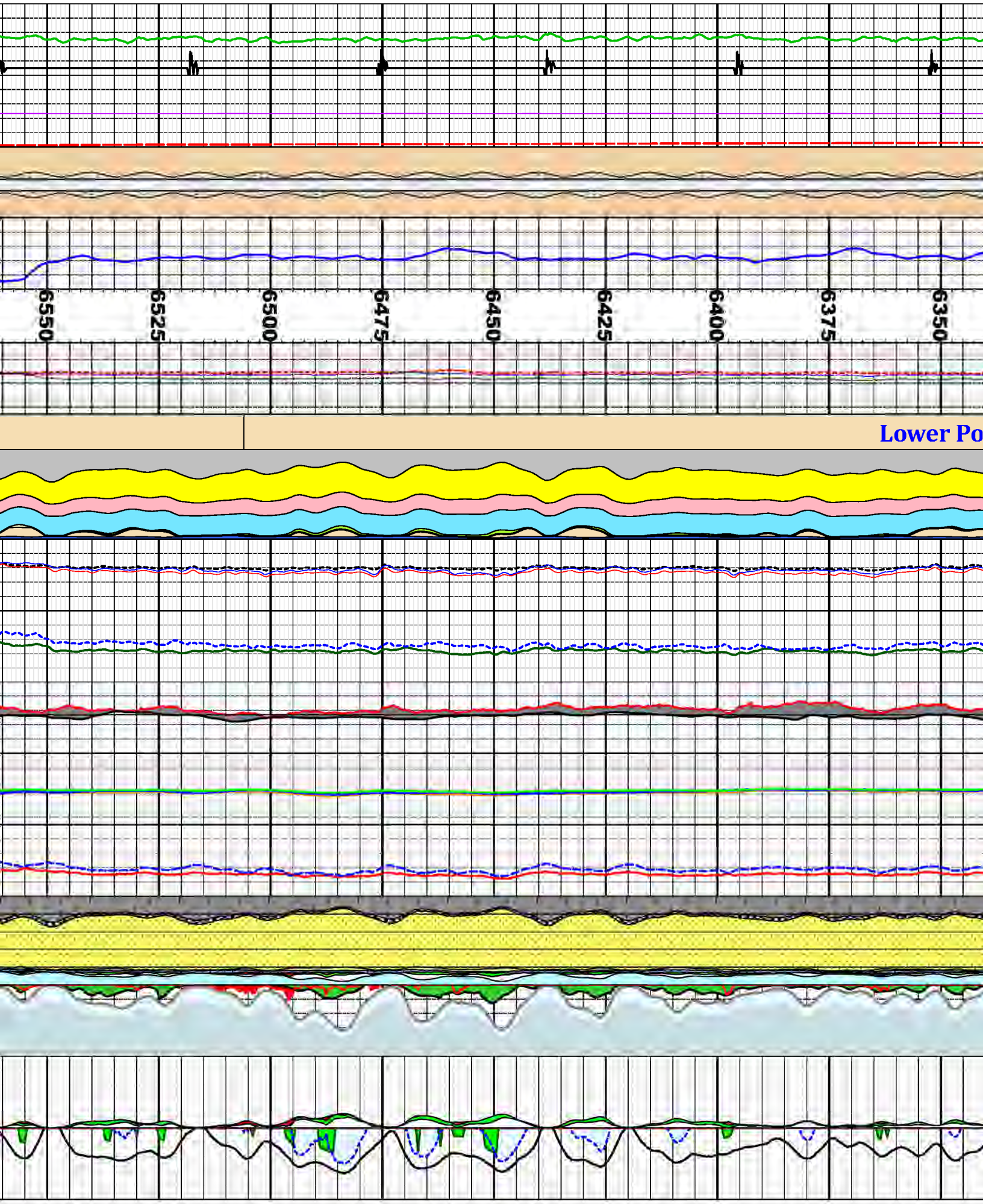
6550
6525
6500
6475
6450
6425
6400
6375
6350
Lower Po

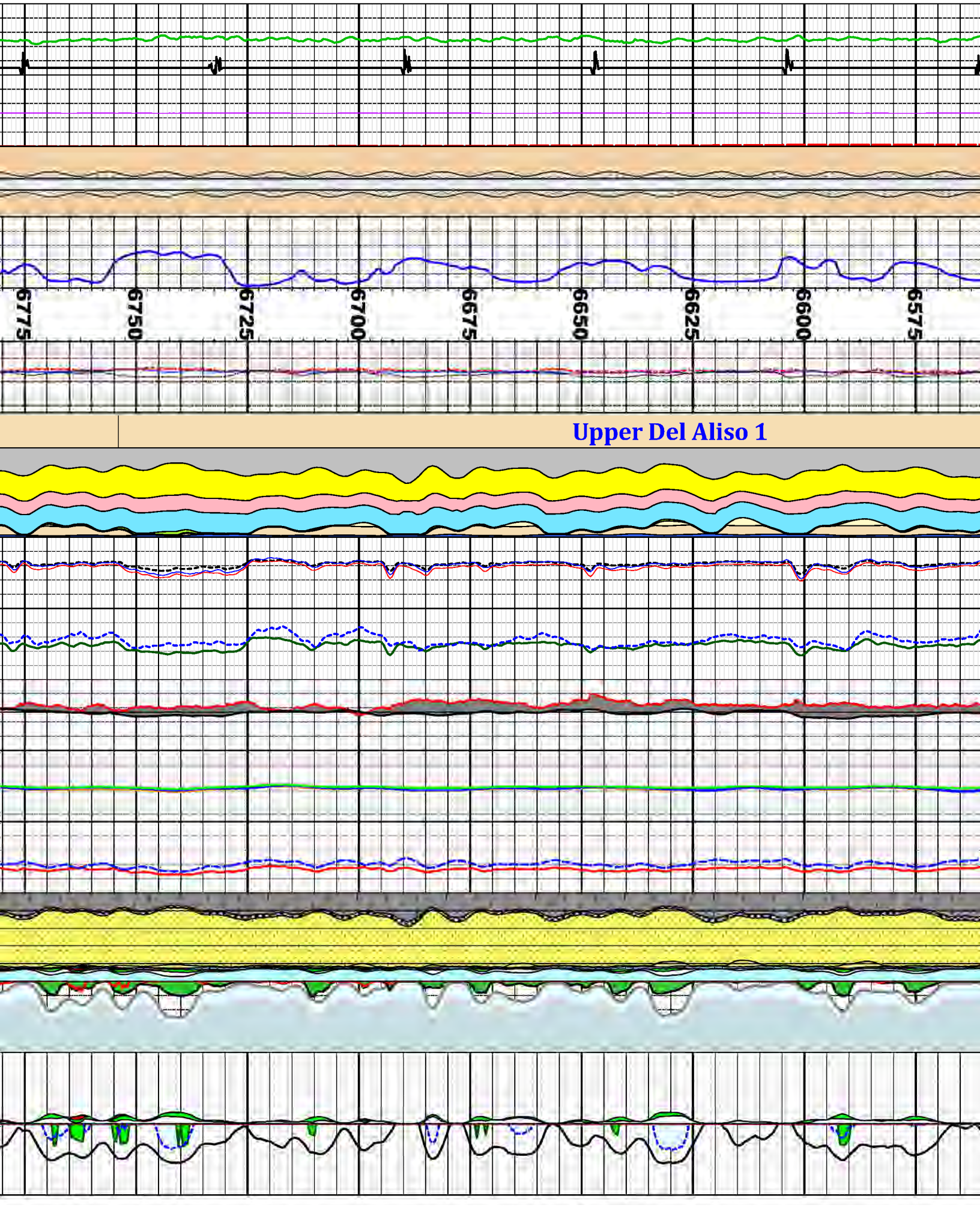
6775
6750
6725
6700
6675
6650
6625
6600
6575
Upper Del Aliso 1

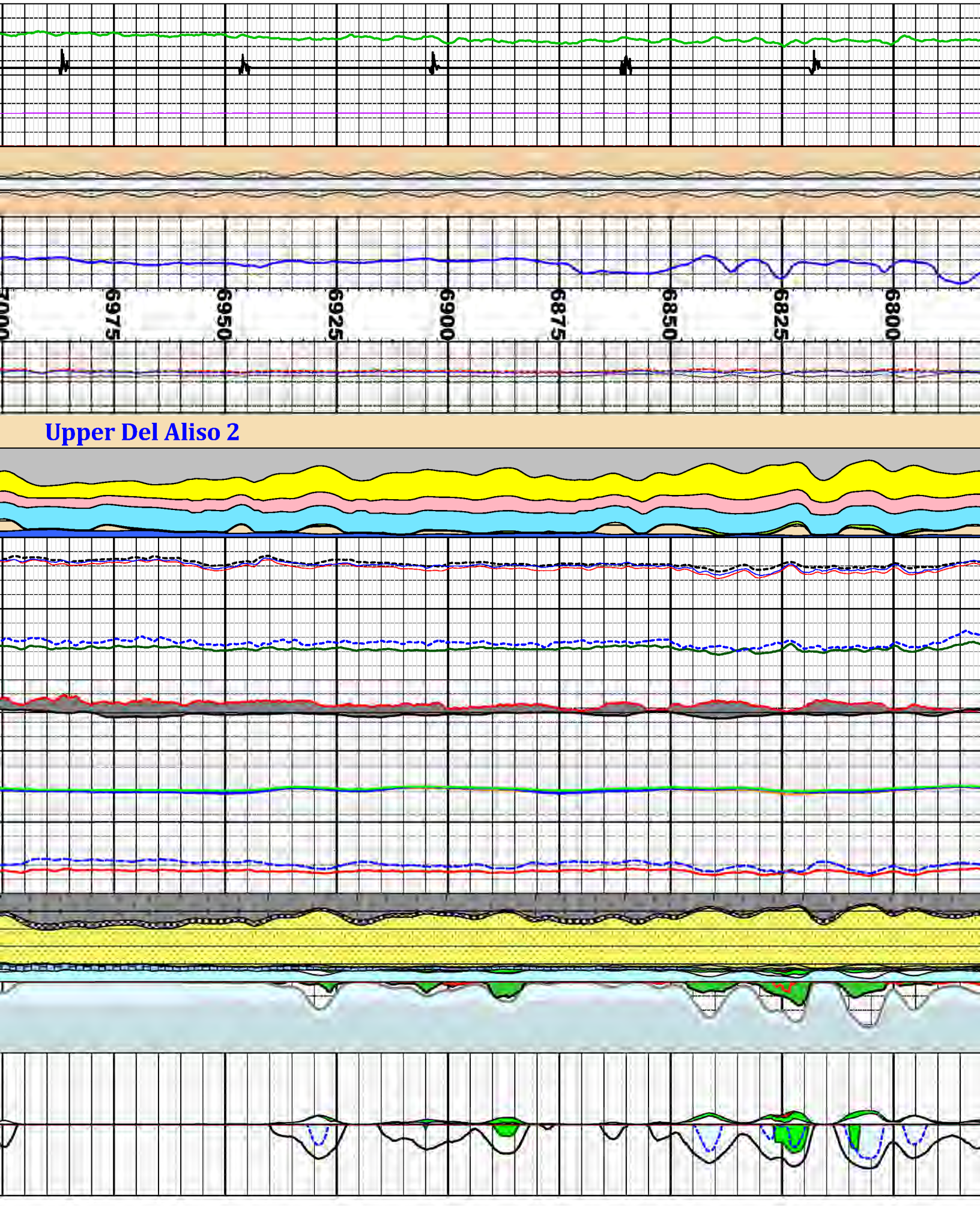
7000
6975
6950
6925
6900
6875
6850
6825
6800
Upper Del Aliso 2

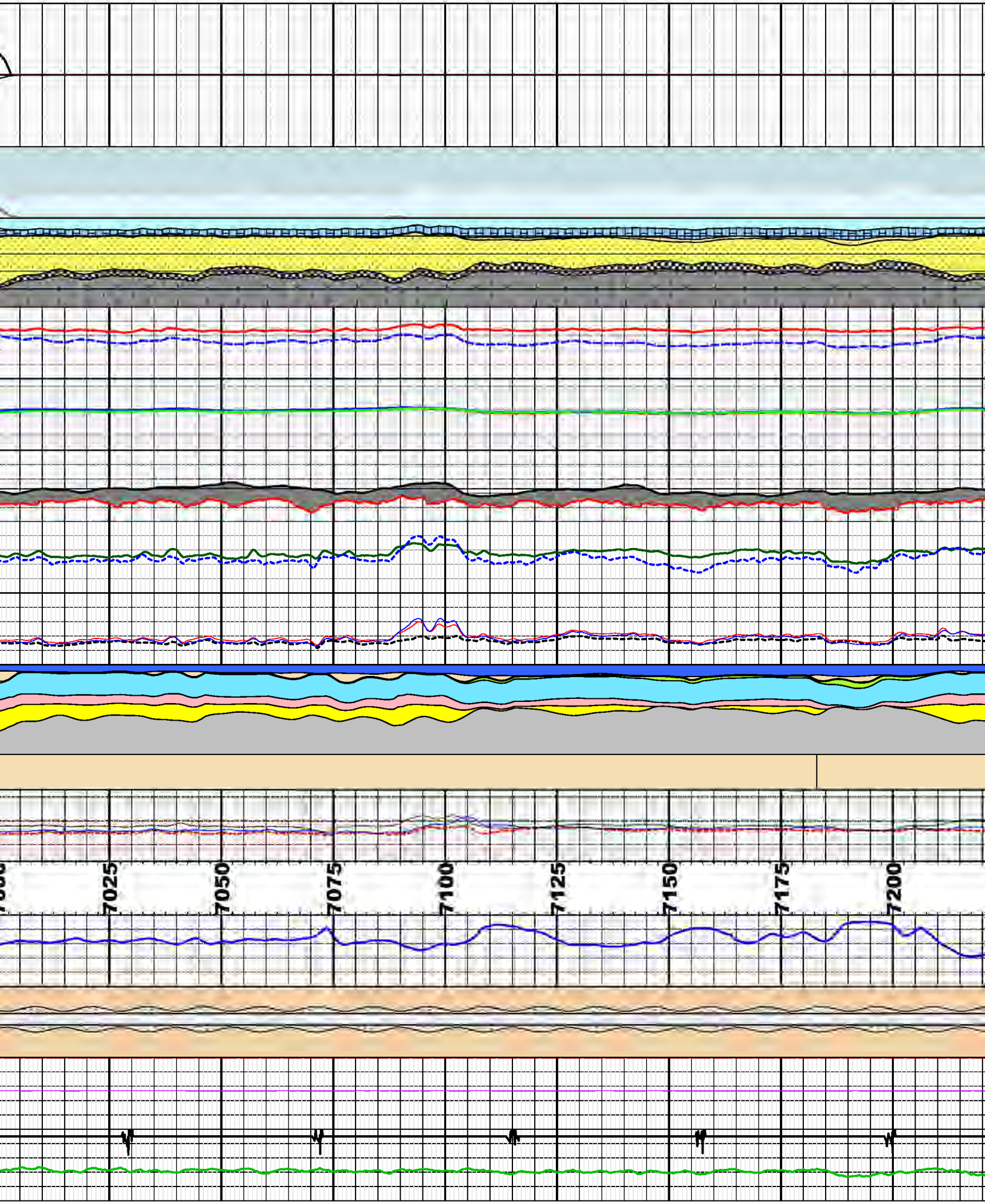
7025
7050
7075
7100
7125
7150
7175
7200

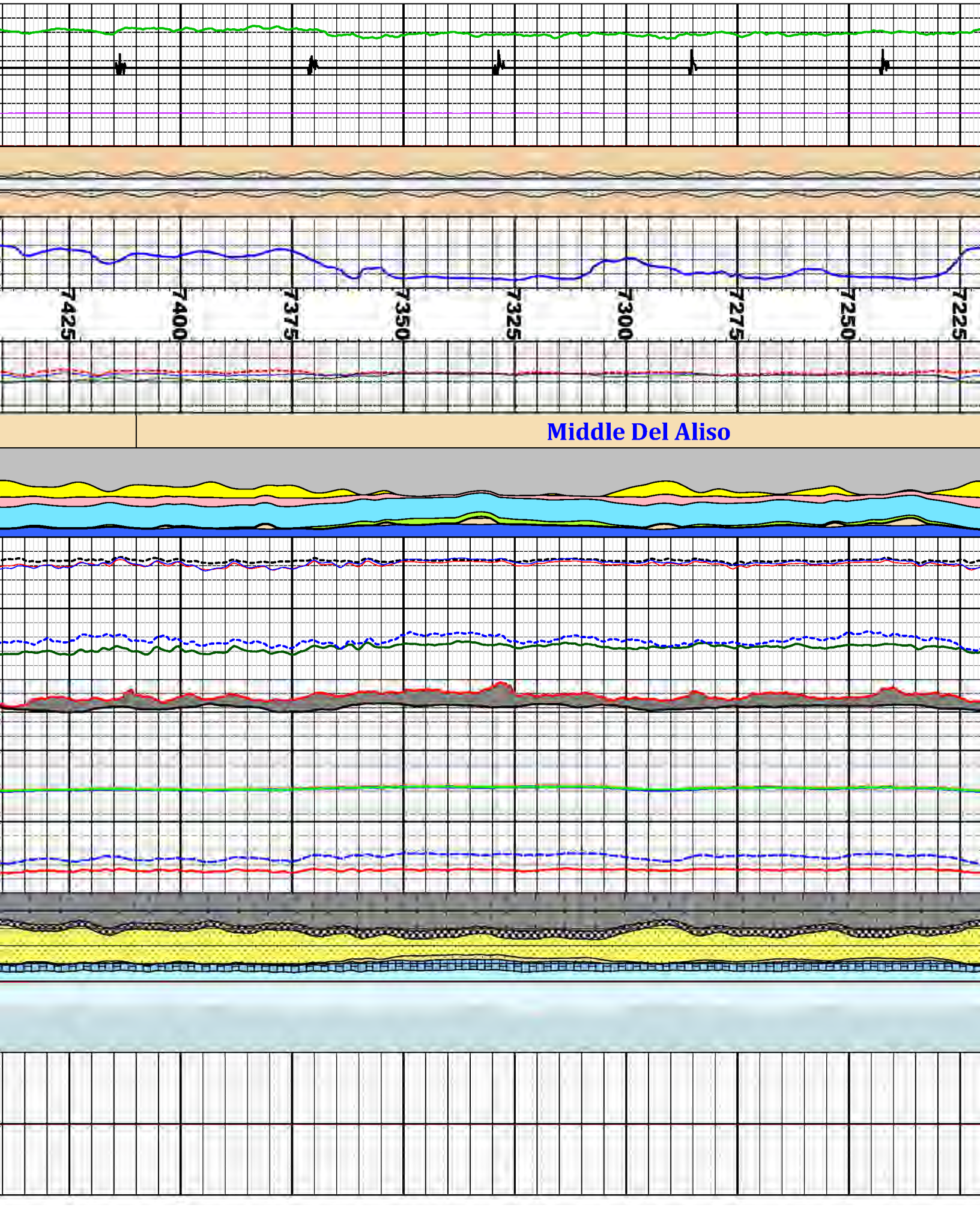
7425
7400
7375
7350
7325
7300
7275
7250
7225
Middle Del Aliso

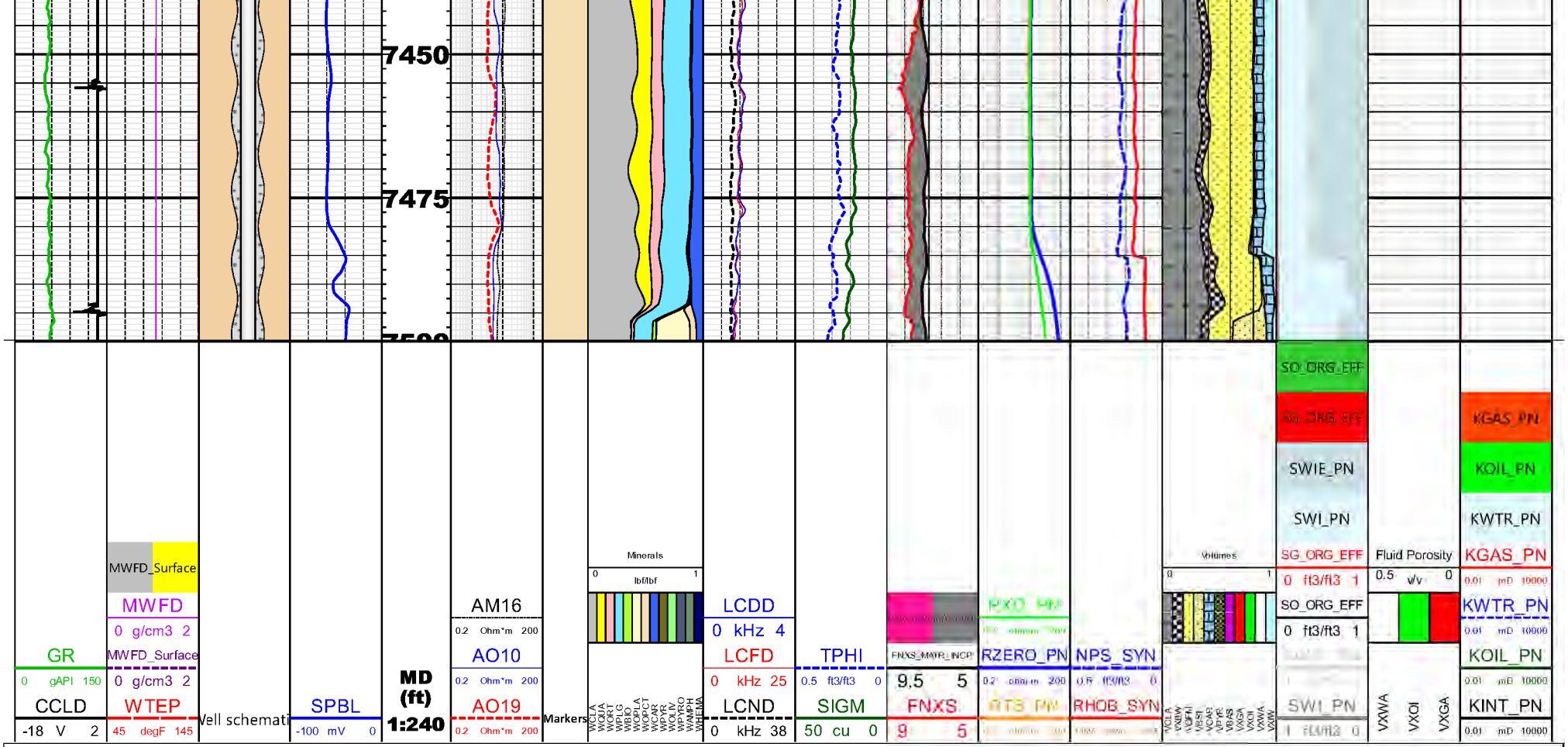

COMPANY: Southern California Gas Company

Schlumberger

WELL: Standard Sesnon 25
FIELD: Aliso Canyon
COUNTY: Los Angeles
STATE: California
COUNTRY: USA

API No.: 04-037-00776

Date Processed: 2/8/2019

SS-25 RCA Supplementary Report

SS-25 Geology Summary

Purpose:
Report to characterize the geology penetrated by the Aliso Canyon SS-25 wellbore in support of the Aliso Canyon Root Cause Analysis (RCA).

Date:
May 31, 2019

BLADE ENERGY PARTNERS

2600 Network Boulevard, Suite 550
Frisco, Texas 75034

+1 972-712-8407 (phone)
+1 972-712-8408 (fax)

16285 Park Ten Place, Suite 600
Houston, Texas 77084

1-800-319-2940 (toll free)
+1 281-206-2000 (phone)
+1 281-206-2005 (fax)

www.blade-energy.com

Blade Energy Partners Limited, and its affiliates ('Blade') provide our services subject to our General Terms and Conditions ('GTC') in effect at time of service, unless a GTC provision is expressly superseded in a separate agreement made with Blade. Blade's work product is based on information sources which we believe to be reliable, including information that was publicly available and that was provided by our client; but Blade does not guarantee the accuracy or completeness of the information provided. All statements are the opinions of Blade based on generally-accepted and reasonable practices in the industry. Our clients remain fully responsible for all clients' decisions, actions and omissions, whether based upon Blade's work product or not; and Blade's liability solely extends to the cost of its work product.

Abstract

The gas storage well Standard Sesnon 25 (SS-25) in the Aliso Canyon Gas Storage Field located in Los Angeles County, California started leaking gas in October 2015. A relief well was drilled, and SS-25 was brought under control. The leak stopped in February 2016.

In January 2016, as part of their investigation of the leak, the California Public Utilities Commission (CPUC) and the Division of Oil, Gas, and Geothermal Resources (DOGGR) selected and gave provisional authority to Blade Energy Partners (Blade) to perform an independent RCA. The Blade Team and parties under Blade's direction were responsible for directing the work of subcontractors who performed the extraction of SS-25's wellhead and tubing and casing and the preservation and protection of associated evidence. Blade RCA Reports, including this report, document and describe the key activities undertaken in support of the RCA effort.

This report summarizes the geologic data acquired and the geologic understanding developed during the RCA. The geologic information and understanding are characterized at regional, field and well levels. Existing literature, which focuses principally on the deeper productive, hydrocarbon-bearing formations, is used as a starting point. Data acquired during the project, including logs run in SS-25 and its neighboring wells, geophysical measurements acquired at the SS-25 well site and geologic field work, are used to supplement the existing data. Particular emphasis is placed on the shallow, unproductive formations above the older Santa Susana Thrust (OSST) fault, in particular on the Modelo, Topanga and Topanga Basalt formations.

This report also describes characterizing elements such as faults and fault traces, lost circulation zones and swelling clays. Surface gas vents, are described, and casing failures are analyzed on basis of geology. Finally, geologic influences and controls on the groundwater presence and movement are evaluated.

Table of Contents

1 Introduction 6

1.1 Abbreviations and Acronyms 6

2 Geologic Overview 7

3 Regional Setting 9

3.1 Transverse Range Province 9

3.2 Santa Susana Thrust 10

3.2.1 Santa Susana Fault Displacement and Slip Rate 12

4 Field Setting 13

4.1 Data 13

4.2 Subsurface Structure 14

5 Well Setting 17

5.1 Subsurface Stratigraphy 18

5.2 Shallow Stratigraphy – Lithology and Structure 32

5.2.1 Modelo 32

5.2.2 Topanga 32

5.2.3 Topanga Basalt 34

5.3 Shallow Geology 37

5.3.1 SS-25 Location Boreholes 37

5.3.2 Shallow Geophysical Investigation 38

5.3.3 RBMW-1 (TH-1) and SS-25 Log Comparison 40

5.3.4 SS-25 Other Characterizing Elements 43

5.4 Gas Vents 44

6 Casing Failure Wells: Evaluation by Fault Block and Formation 46

7 Groundwater Geology 49

7.1 Principal Findings 49

7.2 Influencing and Characterizing Geologic Elements 49

7.3 Boreholes Drilled for Groundwater Data Collection and Analysis 50

7.4 TH-1 – Geophysical Composite Log Analysis 51

7.4.1 Learning Implications for SS-25 57

7.5 Groundwater Composition Compared to Formation Mineralogy 57

7.6 Groundwater Geologic Conceptual Model 58

8 References 60

List of Figures

Figure 1: NASA Landsat Photograph of the Transverse Range Province 9
Figure 2: Southern California Geomorphic Provinces 10
Figure 3: Major Faults of the Ventura Basin–Transverse Range Province 11
Figure 4: South-North Cross-Section Through the Oat Mountain Quadrangle 11
Figure 5: West-East Cross-Section Across the Aliso Canyon Field 14
Figure 6: South-North Cross-Section Across the Aliso Field 15
Figure 7: Location Maps 18
Figure 8: SS-25 OH Logs 20
Figure 9: SS-25 and P-39A Relief Well Log Comparison 21
Figure 10: Modelo and Topanga Formations 24
Figure 11: Overthrust Pico Formation 25
Figure 12: Overthrust Pico Formation to Subthrust Aliso A-1 Zone 26
Figure 13: Aliso A-1 to Upper Del Aliso 1 Zone 27
Figure 14: Upper Del Aliso 2 to Sesnon 12 Zone 28
Figure 15: Correlation of SS-25, SS-25A, and SS-25B Wells 29
Figure 16: Comparison of SS-25B and SS25 Wells and the P39A Relief Well 30
Figure 17: Modelo Formation West of SS-25 32
Figure 18: Topanga Unconsolidated Sands East of SS-25 33
Figure 19: Structure Map Upper Topanga 33
Figure 20: Structure Map Lower Topanga 34
Figure 21: Contact of the Upper Topanga Sands and Topanga Basalt 35
Figure 22: Exposure (a) and Features (b, c) of the Topanga Basalt (Diabase) 36
Figure 23: Structure Map of the Topanga Basalt 36
Figure 24: Location of Shallow Boreholes 37
Figure 25: Core Photographs of Fractured Modelo in Borehole BH-1 38
Figure 26: ERT North-South Line 5B 39
Figure 27: Seismic Line 1 (Refraction) P-Wave Velocity 40
Figure 28: TH-1 OH Log Curves and Interpretation 41
Figure 29: SS-25 CH Log Curves and Interpretation 42
Figure 30: Location of Gas Vents Along Roadcuts East and West of SS-25 44
Figure 31: Gas Vents at the Base of the East and West Roadcuts 45
Figure 32: Location of Casing Failure Wells Evaluated Geologically 46
Figure 33: Aliso Canyon Field Fault Blocks 47
Figure 34: Casing Failure Wells by Fault Block, Formation, and Zone 48
Figure 35: Shear Fracturing and Overburden Unloading along Bedding Planes in B-1 Borehole Core 50
Figure 36: Composite Log Geophysical Log Track Information for RBMW-1 (TH-1) in Figure 37 53
Figure 37: Composite Geophysical Log for Borehole TH-1 (RBMW-1) 54
Figure 38: Detail of Fault and Dragging Zones from TH-1 FMI Log 55
Figure 39: TH-1 Geophysical Logs Compared to the Porter 39A Relief Well Mudlog 56
Figure 40: FMI - Strike Direction Rose Diagrams for the TH-1 Borehole 57
Figure 41: Groundwater and Grab Sample Composition versus Formation Mineralogy 58
Figure 42: Conceptual Groundwater Model 59

List of Tables

Table 1: Slip Rates for the Santa Susana Thrust Fault 12
Table 2: Sequence and Approximate Age of Major Tectonic Events..... 16
Table 3: SS-25 Summary of Formation Tops and Geologic Descriptions of Penetrated Formations 22
Table 4: SS-25A, SS-25B, and P39A Formation Tops..... 31

1 Introduction

This report, prepared as part of the RCA project, describes the geology of the formations penetrated by SS-25 and their structural history. The report examines the shallower geology from surface to approximately 1,100 ft because of the discovery of production casing failure at 892 ft, as well as significant corrosion observed in the 11 3/4 in. surface casing between 95 and 382 ft.

1.1 Abbreviations and Acronyms

Term	Definition
Blade	Blade Energy Partners, Ltd.
CH	Cased Hole (see also OH)
CPUC	California Public Utilities Commission
DOGGR	Division of Oil, Gas, and Geothermal Resources
DTS	Distributed Temperature Sensing
ERT	Electrical Resistivity Tomography
FMI	Formation MicroImager
FTIR	Fourier Transform Infrared Spectroscopy
GTC	General Terms and Conditions
MD	Measured Depth
NMR	Nuclear Magnetic Resonance
OH	Open Hole (see also CH)
OSST	Older Santa Susana Thrust (Fault) (see also YSST)
RCA	Root Cause Analysis
RBMW	Regional Board (Groundwater) Monitoring Well
SoCalGas	Southern California Gas
SP	Spontaneous Potential
SS	Standard Sesnon
TD	Total Depth
TH	Test Hole
Vsh	Shale Volume
XRD	X-Ray Diffraction
XRF	X-Ray Fluorescence
YSST	Younger Santa Susana Thrust (Fault) (see also OSST)

2 Geologic Overview

SS-25 is located in the Aliso Canyon Gas Storage Field in Los Angeles County, California. The well lies within the structurally complex and seismically active Transverse Range geomorphic province. The field underlies the southern flank of the Santa Susana Mountains in the southeastern portion of the Ventura Basin at the leading edge of the Santa Susanna thrust fault. The surface terrain is rugged, with vertical relief of over 2,000 ft between the surface elevation of SS-25 and the floor of the San Fernando Valley to the south. SS-25 is situated on a north-south trending ridge off the main east-west ridgeline of the Santa Susana Mountains.

This area underwent extensive compressional tectonic deformation from the late Miocene to the early Pleistocene due to movement of the Pacific Plate northward along the trace of the San Andres fault. Uplift of the Aliso anticline occurred from the late Miocene to the early Pliocene, with major faulting (Ward, Frew, and Roose faults) occurring in the late Pliocene to early Pleistocene. Two major thrusting events (Santa Susana thrusts), which occurred in the Pleistocene, thrusted older sediments over younger ones. These north-dipping thrusts are the dominant structural features in the area. Approximately 4,200 ft of thrusted rock from the north has been extensively broken and fractured near SS-25.

SS-25, which was drilled in 1953 and completed in 1954, is located in the field's central fault block. It penetrates 8,749 ft of predominantly unconsolidated marine sediments of sand, siltstones, clays, and porcellanite (chert) of the Modelo, Topanga, and Pico formations, which are of Miocene-Pliocene age. A volcanic intrusion, the Topanga Basalt, is a diabase of predominantly plagioclase-pyroxene composition, which intruded as a sill or sills into the middle portion of the Topanga sands. The primary casing failure at 892 ft was adjacent to the Topanga Basalt. SS-25 penetrates a major Miocene-Pliocene unconformity at 8,182 ft, which is above the (formerly) productive Sesnon sands.

The overthrust portion of the field has been unproductive. Productive formations in the field have been the Pico formation (Aliso, Porter, and Del Aliso sands) and the gas storage formation of the Modelo (Sesnon), which are all located below the Younger Santa Susana thrust fault (YSST). SS-25 originally produced from the Modelo (Sesnon zones) before being converted to a gas storage well.

Before the present RCA project, geologic studies of the Aliso Canyon Field focused on the deeper productive units below the YSST, with little information available about the upper overlying stratigraphy. In SS-25, the unproductive overlying stratigraphy constitutes approximately half of the total depth (4,200 ft). The primary tool utilized by geologists to evaluate the geology of a field, or an individual well that is placed in the field context, is the available open hole (OH) electric logs core, production, and well test data. At Aliso Canyon, historical practices were in large part to set the surface casing at 800–1,000 ft. This was most likely due to widespread loss of circulation issues across the field, as outlined in the drilling records in the weathered shallow formations. Therefore, OH logging coverage is absent in most wells from the surface down to 800–1,000 ft. However, SS-25 is one of the few wells that had OH coverage starting at 85 ft. In addition, even where OH log coverage is available, the extensive deformation in the overthrusted stratigraphic formations presents difficulties in well-to-well correlation.

The present study uses Lant's 1977 MS thesis [1] as a starting point, which identifies the Modelo, Topanga, and Topanga Basalt formations on cross-sections, as well as references from the available literature. Mudlogs from the P-39A relief well and the nearby, newly drilled SS-4A well are used for site-specific lithology information. This information is augmented with Litho Scanner high-definition spectroscopy service, nuclear magnetic resonance (NMR), and fullbore formation MicroImager (FMI) logs

from SS-25 as well as the nearby hydrologic test well, a Regional Board monitoring well #1 (RBMW-1, also known as TH-1).

The well-scale geologic evaluation focuses on the shallow geology of SS-25 because of the discovery of a production casing failure at 892 ft and identification of substantial corrosion in the 11 3/4 in. surface casing from 95 to 382 ft. The 7 in. casing failure occurred in the Lower Topanga adjacent to an andesitic diabase (named Topanga Basalt), and the near-surface corrosion occurred in the highly weathered and fractured Modelo formation.

A shallow geophysical investigation (Appendix A) identified a highly weathered zone, 200–300 ft thick, just below the surface. This shallow zone evidenced the presence of both high-resistivity frozen areas and low-resistivity areas, with these features being attributed to gas and kill fluids, respectively, escaping from the SS-25 wellbore during the incident.

3 Regional Setting

3.1 Transverse Range Province

SS-25 is located in the eastern Santa Susana Mountains, in the central portion of the Transverse Range geomorphic province, which has undergone substantial compressional deformation. Figure 1 is a NASA Landsat photo of the Transverse Range province highlighting the west-east orientation of the mountain ranges and the significant degree of faulting resulting from tectonic forces. Figure 1 also shows the location of the Aliso Canyon Field in the eastern portion of the Santa Susana mountain range.

One of California's 11 provinces, the Transverse Range province is characterized by a complex series of mountain ranges and valleys distinguished by an anomalous dominant west-east trend of the mountain ranges (as compared to the northwest-southeast trend of the adjacent expansive Coast and Peninsular Ranges). This distinguishing structural style of the Transverse Ranges is controlled by north-south compressional deformation, which is attributed to the convergence between the "big bend" of the San Andres fault, which separates the North American and Pacific plates, and motion of the Pacific plate (Figure 2) [2] [3] [4] [5]. Mountain ranges in this province, including the Santa Susana Mountains, have been rotated in a clockwise direction, and all are still undergoing continual stress and deformation.

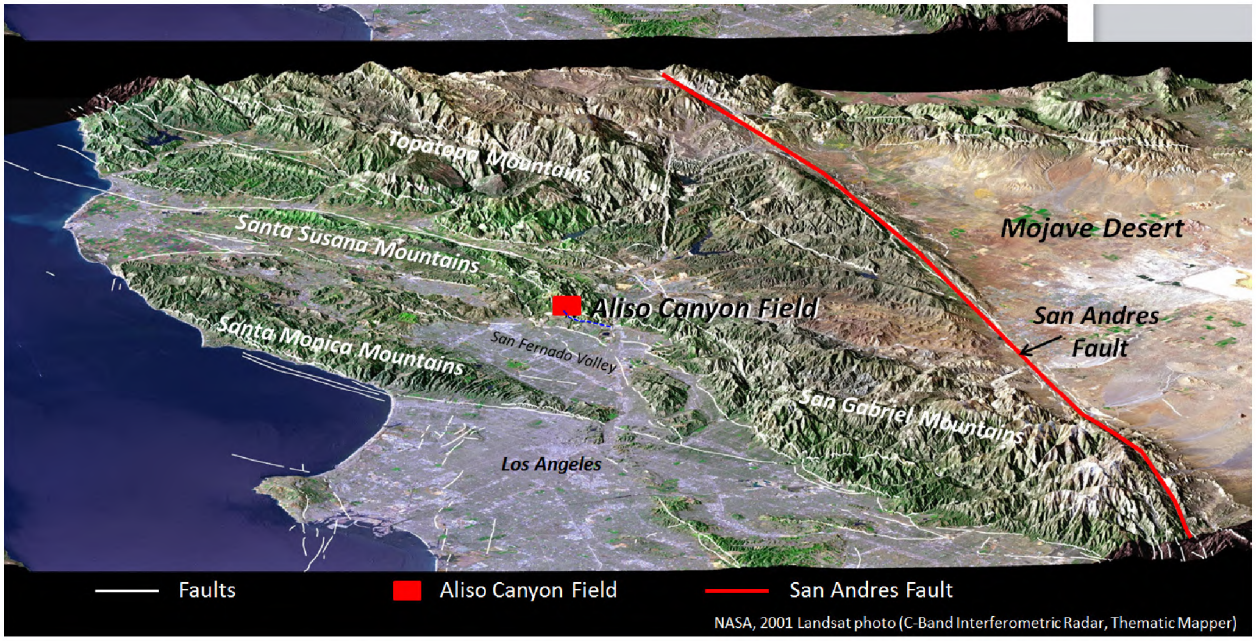

Figure 1: NASA Landsat Photograph of the Transverse Range Province

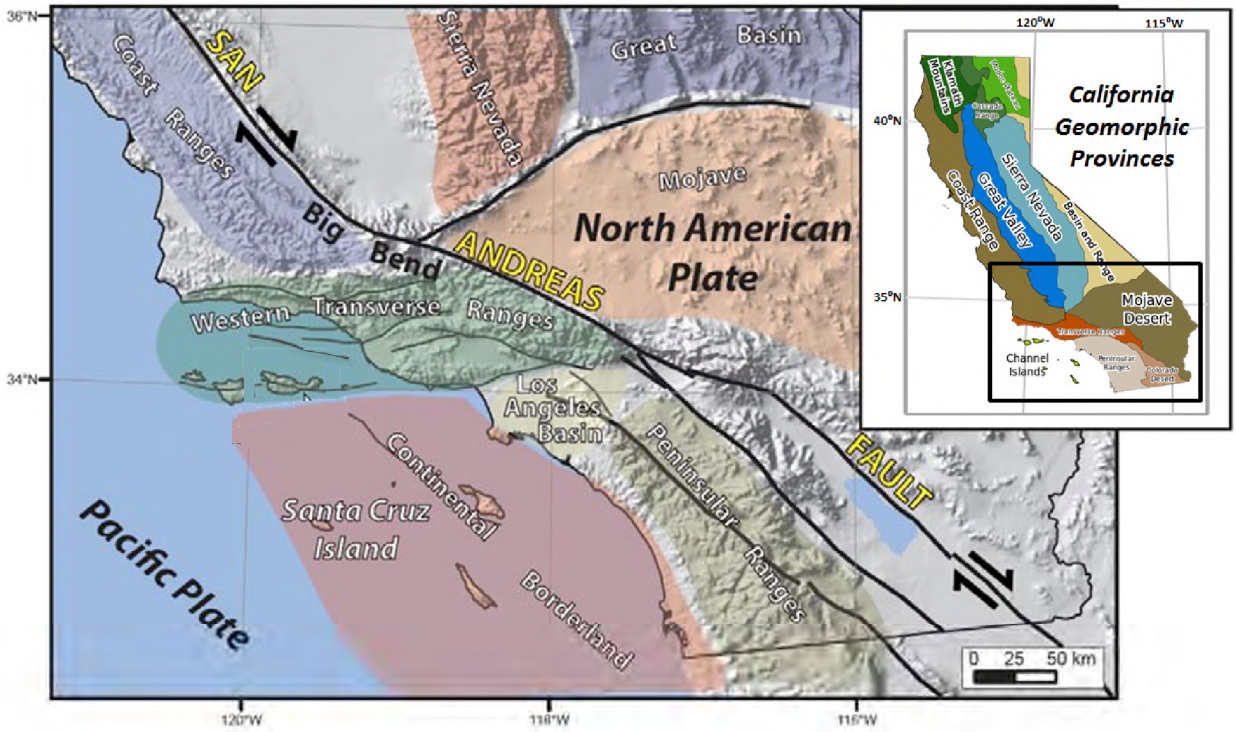

Figure 2: Southern California Geomorphic Provinces

3.2 Santa Susana Thrust

The Santa Susana thrust is the dominant geologic feature in the Aliso Canyon Field. The SS-25 wellbore surface location is approximately 5,150 ft north and 3,060 ft west of the surface trace of the Santa Susana thrust fault. The SS-25 wellbore penetrates the thrust fault twice, crossing the Older Santa Susana thrust fault (OSST) at approximately 1,635 ft and YSST at 4,200 ft.

Figure 3 shows the relative regional position of the Santa Susana thrust among the similar east-west trending major faults of the Ventura Basin of the Transverse Range province.

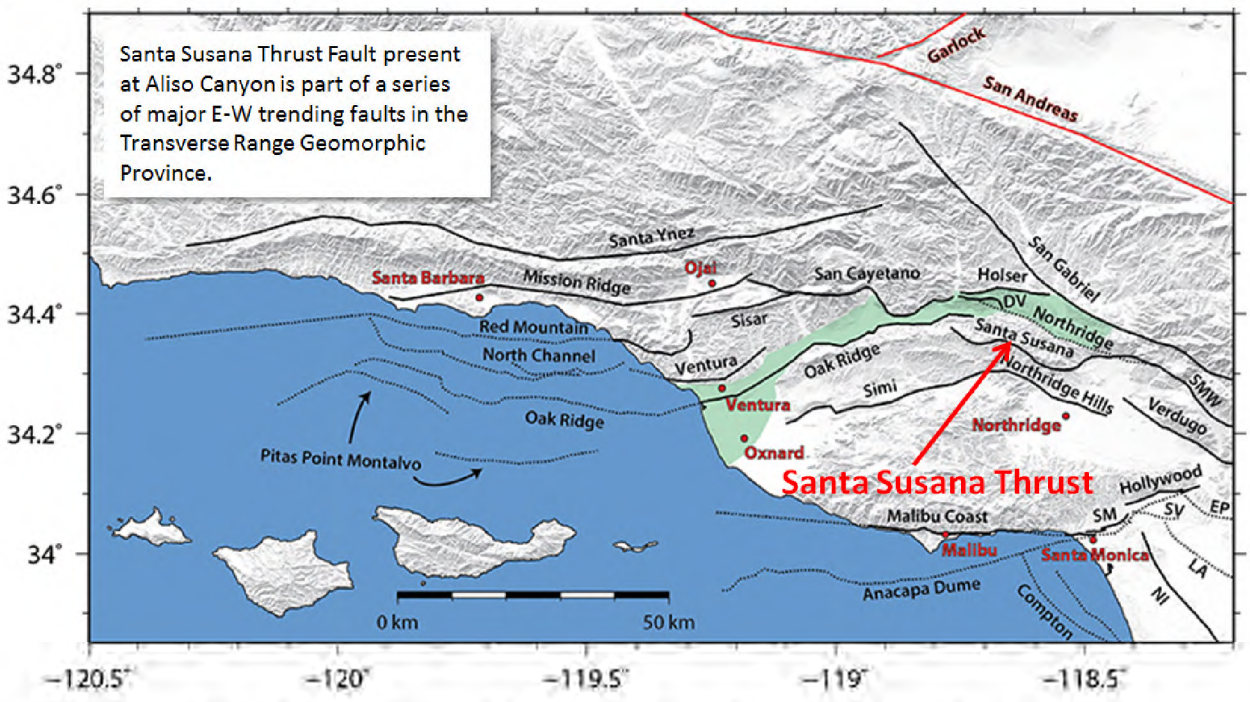

Figure 3: Major Faults of the Ventura Basin–Transverse Range Province

Figure 4, a north-south cross-section through the Oat Mountain quadrangle from Dibblee's geologic map [6], illustrates the significant compressional forces that shaped the geology of the area around the Aliso Canyon Field. Compressional forces caused buckling, folding, and uplifting, with the eventual overthrust of the older Modelo and Topanga from the north over the younger Pico sediments of the south along the Santa Susana thrust. The cross-section also depicts the older development of the Aliso anticline and deeper faults (Ward, Frew, Sub-Frew, and Roosa) in the Aliso Canyon Field. Because these deeper faults developed prior to the Santa Susana thrust, they were subsequently truncated by the Santa Susana thrust fault.

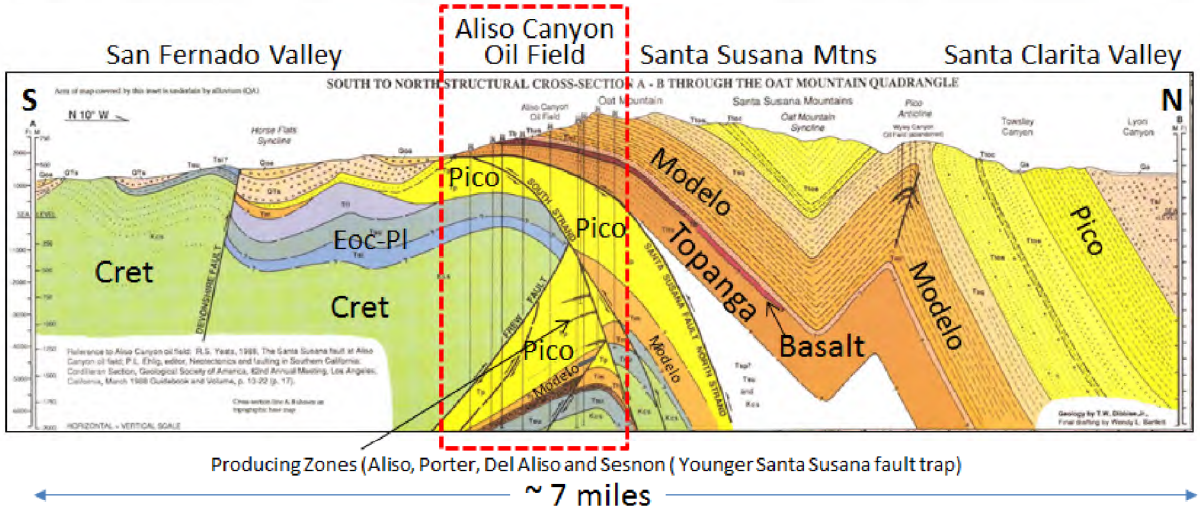

Figure 4: South-North Cross-Section Through the Oat Mountain Quadrangle

3.2.1 Santa Susana Fault Displacement and Slip Rate

Published slip rates for the Santa Susana range from 2.8 mm/year to 9.8 mm/year [7] [8] [9] [10] [11]. The most recent estimate is from the Southern California Earthquake Center, 2019, of 5–7 mm/year (Table 1).

Table 1: Slip Rates for the Santa Susana Thrust Fault

Source	Date	Slip Rate
Peterson and Wesnousky [7]	1994	2–8 mm/year
Yeats [8]	2001	7.0–9.8 mm/year
USGS Earthquake Hazards Program [9]	Current	>5 mm/year
Southern California Earthquake Center [10]	Current	5–7 mm/year
UCERF3 California Earthquake Rupture Forecast [11]	Current	2.1 mm–9.8 mm/year Best estimate: 6 mm/year

Horizontal displacement along the Santa Susana thrust fault has been estimated as ranging from 1.5–3 miles, with an estimated vertical displacement of 5,000 ft. Hazzard proposed a maximum north-south displacement of 8,000 ft for the Santa Susana thrust, with the northern block thrust southward for 18 miles along the southern side of the Santa Susana Mountains [12]. Ingram suggested vertical displacement of 5,000 ft with a horizontal displacement of 2–3 miles [13].

4 Field Setting

4.1 Data

Available data on the geologic interpretation of the Aliso Canyon Field is almost exclusively focused on the oil-productive formations that occur below the YSST. This leaves nearly half of the penetrated stratigraphy of the field largely without geologic interpretation. The exception is an MS thesis by Kevin Lant [1], which includes correlations of the overthrust Modelo, Topanga, and Topanga Basalt formations (shown on cross-sections only) and describes the major faults of the field. A thick section of the overthrust Pico remains undifferentiated. To evaluate SS-25 and surrounding wells, the present study subdivides the overthrust Pico stratigraphy into four sections based on petrofacies interpreted from coarsening upwards sequences on the resistivity logs and mudlog descriptions.

The following data sources were used in the present study:

- Southern California Gas (SoCalGas) and DOGGR well records
- SoCalGas historical studies, well records and second party reports
- Published literature
- On-site fieldwork
- Laboratory analysis of field and borehole samples collected during the RCA project
- Geophysical survey data work conducted for the RCA project
- Well logging data acquired during the RCA project

Lant's 1977 thesis on the Structure of Aliso Canyon [1] provided a valuable resource for fault picks and shallow formation tops. This thesis, in conjunction with a network of comprehensive, field-wide, well-tied structural cross-sections, structure picks, and maps of all the major faults, provided some of the data required but not found in the data sources listed in the preceding bulleted list.

The following are the limitations of the data used by the present study:

- Data collection in old fields with numerous previous operators through time is always problematic because of missing files and logs.
- Data provided by SoCalGas (reports, formations tops, maps, core data and well records) do not contain information on the formations above the YSST.
- Only a few short intervals of dipmeter data were located, but only in deeper sections.
- Formation tops (picks) provided by SoCalGas were all below the YSST and represent work by different interpreters; these were only modified in this study if required to provide consistent interpretation.
- Older well logs include primarily spontaneous potential (SP) and resistivity logs. Few density logs are available, and these cover only short sections of the deeper, productive units.
- The vast majority of OH logs covered only the drilled section below surface casing shoes, which generally started at approximately 800–1,000 ft. Therefore, OH electric log coverage in the shallow 0–1,100 ft section of interest for the present study was extremely limited.

4.2 Subsurface Structure

As illustrated in Figure 5 and Figure 6, the subsurface penetrated by SS-25 is characterized by two main tectonic thrusting events, which are the most significant geologic features at Aliso Canyon Field. The first event, the OSST at 1,635 ft, thrusted Middle Miocene age rock (Modelo and Topanga formations) over younger sections of Pliocene age rock (Pico formation). The second event, the YSST at 4,200 ft, thrusted thick sections of Pico over Pico. These thrusts resulted in an extremely thick Pico section of sands, claystones, and clay, represented in yellow in Figure 5 and Figure 6. The Pico Formation in SS-25 accounts for 75% of the penetrated section. At SS-25, the thrust plane of OSST cuts through interbedded sands and clays, and YSST cuts along a Pico claystone unit at 4,200 ft. YSST provides the structural trap for the subthrust Pliocene Pico reservoirs and gas storage reservoirs in the Miocene Modelo or Sesnon S1–S14 zones in SS-25. Structural dip of the OSST at SS-25 is 15° east. The YSST has a steep dip of 55° northeast. Formation dip angles above the YSST are to the northeast; whereas formation dip angles below the YSST are to the southwest. Pliocene and Miocene formations below the YSST are productive and comprise the Aliso, Porter, Del Aliso, and Sesnon zones.

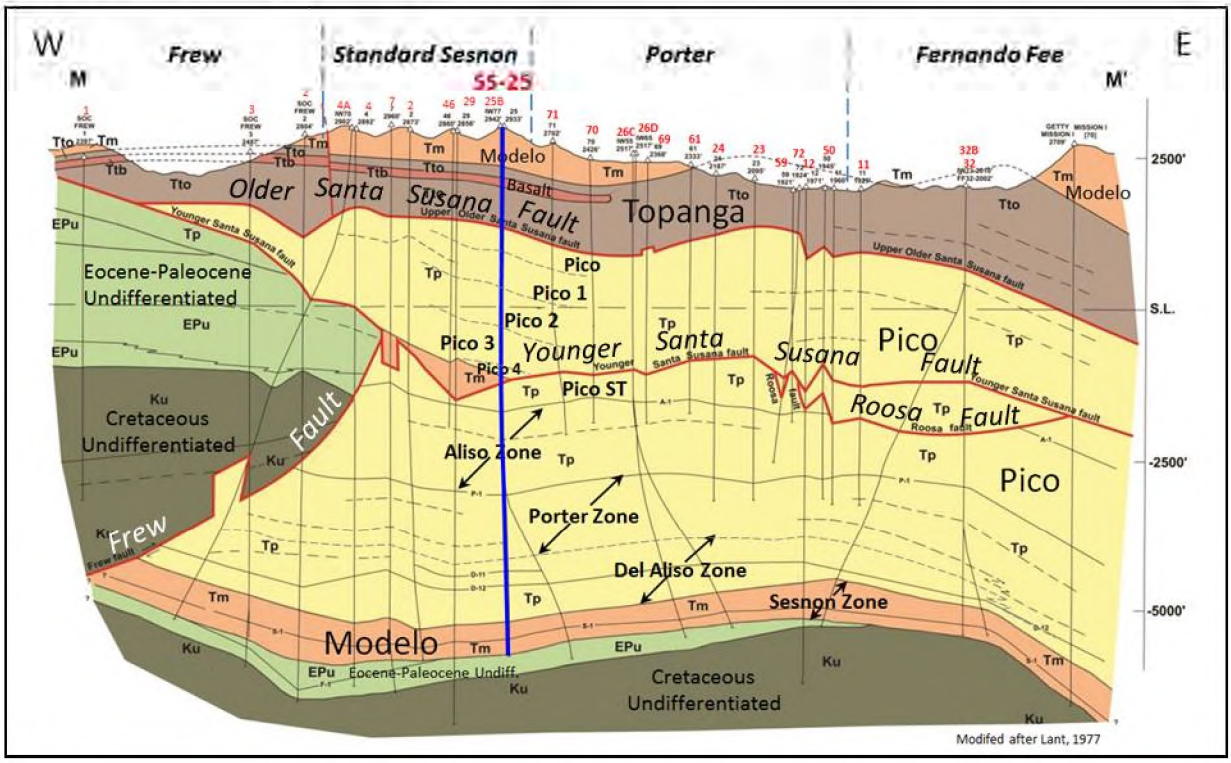

Figure 5: West-East Cross-Section Across the Aliso Canyon Field

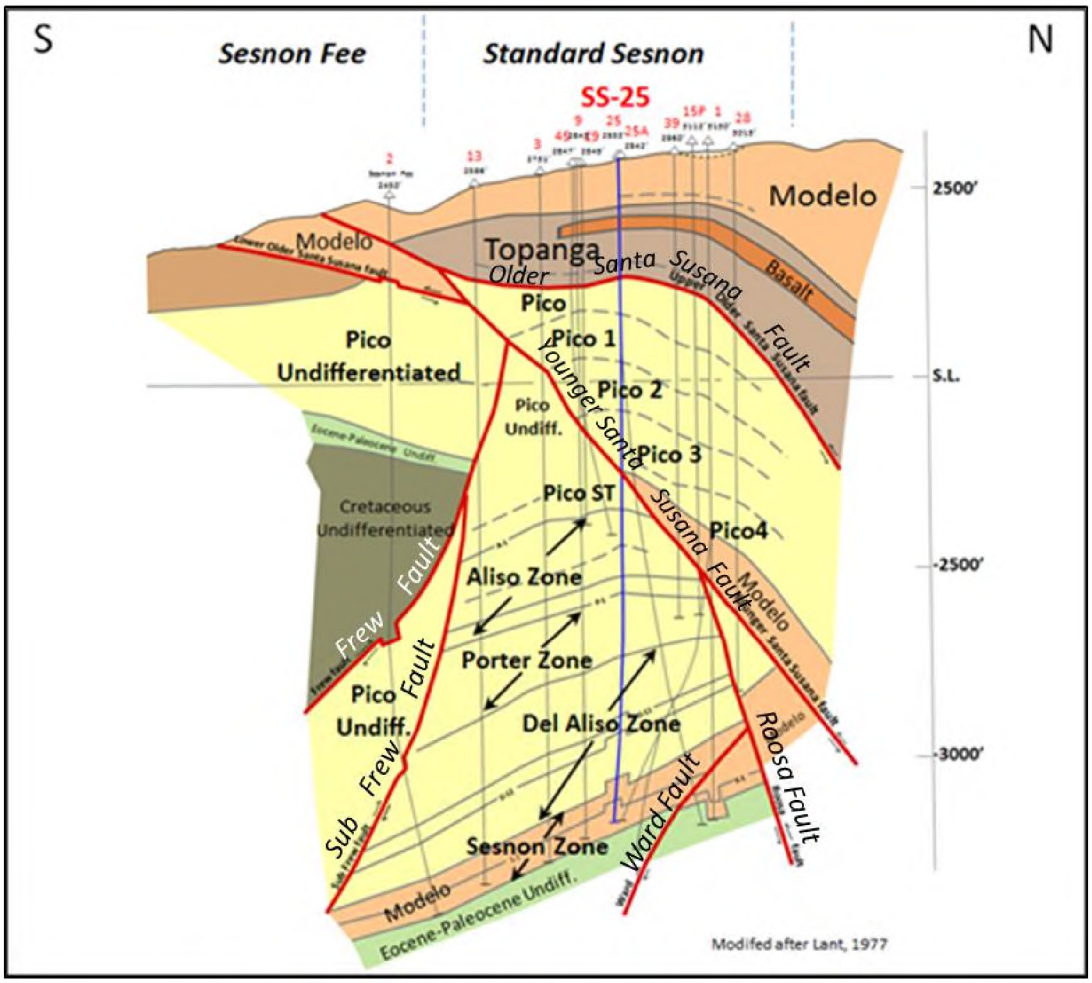

Figure 6: South-North Cross-Section Across the Aliso Field

All faults at Aliso Canyon are reverse faults, consistent with a compressional tectonic setting. The Aliso Canyon area had undergone a significant deformational history even prior to the thrusting of the Santa Susana fault. Compression during the late Miocene to late Pliocene was responsible for the development of the Ward, Frew, Sub-Frew, and Roosa faults. The Frew and Roosa faults were subsequently truncated when the thrusting events of the OSST and YSST occurred, creating a complex structural deformation history for the area (Table 2) [1] [14].

Table 2: Sequence and Approximate Age of Major Tectonic Events

Timing		Structural Event	Fault Type	Description
Youngest	Early Pleistocene	Younger Santa Susana thrusting event (YSST)	Reverse	Offset and folds to OSST
	Early Pleistocene	Older Santa Susana thrusting event (OSST)	Reverse	Formation of the Santa Susana Mountains
	Late Pliocene – Early Pleistocene	Roosa fault formation	Reverse	Development of the Roosa fault zone
	Late Pliocene – Early Pleistocene	Frew and sub-Frew fault formation	Reverse	Development of the Frew fault zone
	Late Pliocene	Ward fault formation	Reverse	L. Pliocene-Quaternary time crustal shortening
Oldest	Late Miocene – Early Pliocene	Aliso anticline formation	N/A	Uplift-formation of the Aliso anticline
Sources: [1] [14]				

Small-scale faults and shear fractures (microfaults) are present due to the significant compressional deformation history of the area in the overthrust section above OSST. These features are not large enough to detect on old log data sets. An FMI geophysical log run in the nearby RBMW-1 detected nine faults, an extensive amount of shear fractures (microfaults, both conductive and resistive) and a number of small-scale faults. Difficulties also occur in correlation between wells surrounding SS-25; this is most noticeable in the Pico section, with good correlations valid over only one or two adjacent wells.

5 Well Setting

The surface terrain (Figure 7) is rugged with vertical relief of more than 2,000 ft between the surface elevation of SS-25 and the floor of the San Fernando Valley to the south. SS-25 is situated on a north-south-trending ridge off the main east-west ridgeline of the Santa Susana Mountains. This north-south ridge is flanked by deep drainage areas carved into the Modelo formation. Extensively weathered, fractured, and contorted, Modelo siltstone, shale, and porcellanite are found at the surface location and in the roadcuts surrounding the SS-25 well site. On physical inspection, outcrops crumble to the touch.

The data used for studying the well setting include:

- 1950s-vintage electric logs (SP and resistivity) in SS-25 and other Aliso Canyon Field wells
- Modern logs and continuous mudlog from the Porter 39A (P-39A) relief well
- Geophysical survey of the SS-25 site (Appendix A), including cores acquired from several shallow boreholes drilled at the SS-25 site
- Data acquired from cased hole (CH) logs run in SS-25 acquired for the RCA project
- Data acquired from the nearby RBMW-1 (TH-1) hydrology test well, including FMI, NMR, and Litho Scanner logs
- Surface sampling and laboratory analysis of nearby outcrops of the Topanga Basalt (Appendix B), which were used to improve the Litho Scanner log interpretation model for SS-25 and RBMW-1 (TH-1) wells
- Professional papers describing the regional structure and lithology [2] [15] [16] [17]

The data listed were integrated through a geophysical software model built using the Petrel E&P platform. This geophysical software model was used to develop internal structural, stratigraphic, and lithologic understanding of SS-25 subsurface geology.

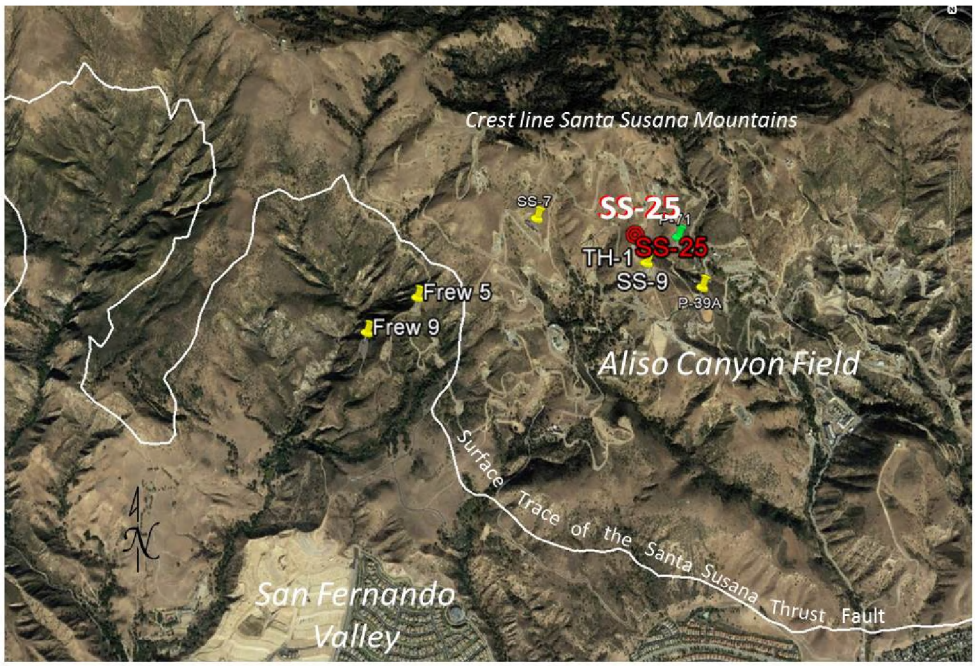

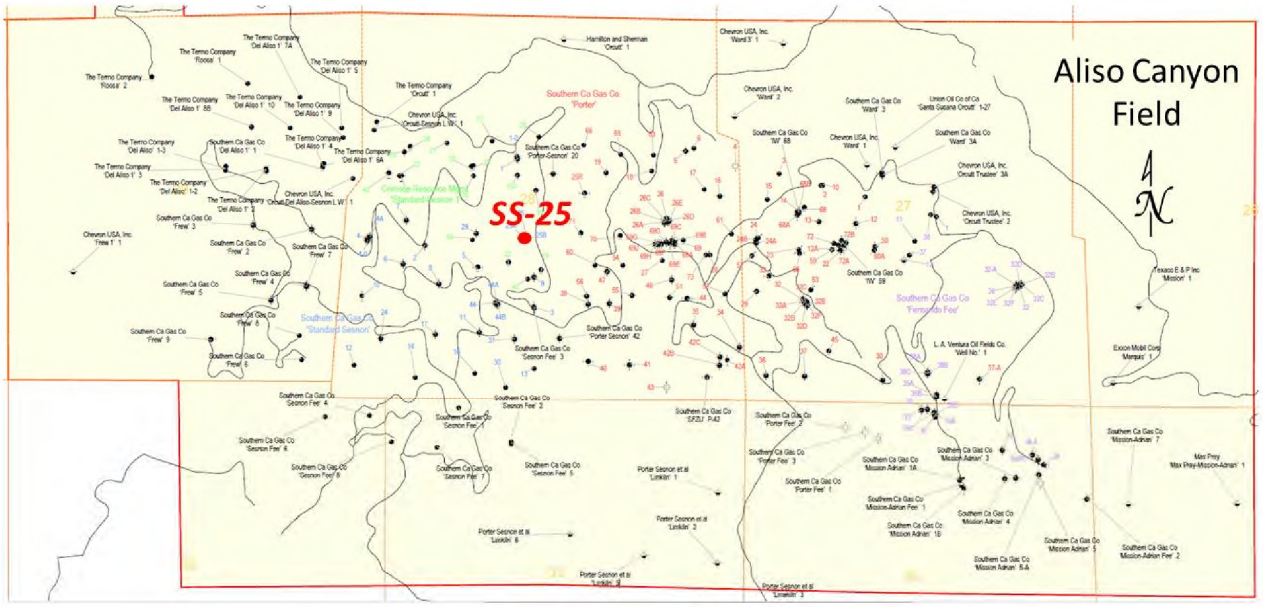

Figure 7: Location Maps

5.1 Subsurface Stratigraphy

Formations penetrated by the SS-25 wellbore consist of 1,635 ft of OSST overthrust Modelo and Topanga formations, 6,547 ft of the Pico formation, and 567 ft of YSST subthrust Modelo (Sesnon). Sediments are primarily unconsolidated sediments of the Pliocene Pico formation, composed of largely sands, claystone, and clay. The upper 4,200 ft of the stratigraphy was largely undifferentiated overthrust Pico sands with no hydrocarbon production. This interval was subdivided into five intervals (Pico and Pico 1 through Pico 4) based on log curve motifs and lithology information derived from the P-39A mudlogs.

The composite log in Figure 8 shows the stratigraphic section present in the SS-25 wellbore. Figure 8 also shows the OH electric logs, stratigraphy, faults, and shale volume (Vsh) lithology interpretation for SS-25. Figure 9 shows a well log comparison between SS-25 and P39A. In SS-25 and P-39A relief well log comparison, formation tops have been flattened on the tops so that a direct comparison between the stratigraphy and lithology of the two wells can be evaluated. The P-39A surface location is approximately 1,600 ft from the surface location of SS-25 (Figure 7). At approximately 3,500 ft measured depth (MD) (approximately top of Pico 3) in the P-39A relief well, the wellbore is directly adjacent to and tracks the SS-25 wellbore to total depth (TD). Note the excellent correlations between the two wells and in the fault locations. The P-39A mudlog is also shown and provides an excellent source for lithology prediction for the SS-25 wellbore.

Table 3 shows the formation and zone tops, thicknesses, dip angles, and general lithologic descriptions for SS-25. Figure 10 through Figure 14[i] contain a more detailed breakdown of 48 lithology-based subzones, including their associated thicknesses and descriptions; this breakdown was developed by contrasting SS-25 logs and Vsh curves with the logs and mudlog of the P-39A relief well[ii].

[i] Headers for Figure 11 through Figure 14 are the same as for Figure 10.

[ii] The displays of Figure 10 through Figure 14 were developed originally by Blade to aid in the various lithology scale requirements needed in the casing extraction and the analysis of the SS-25 well.

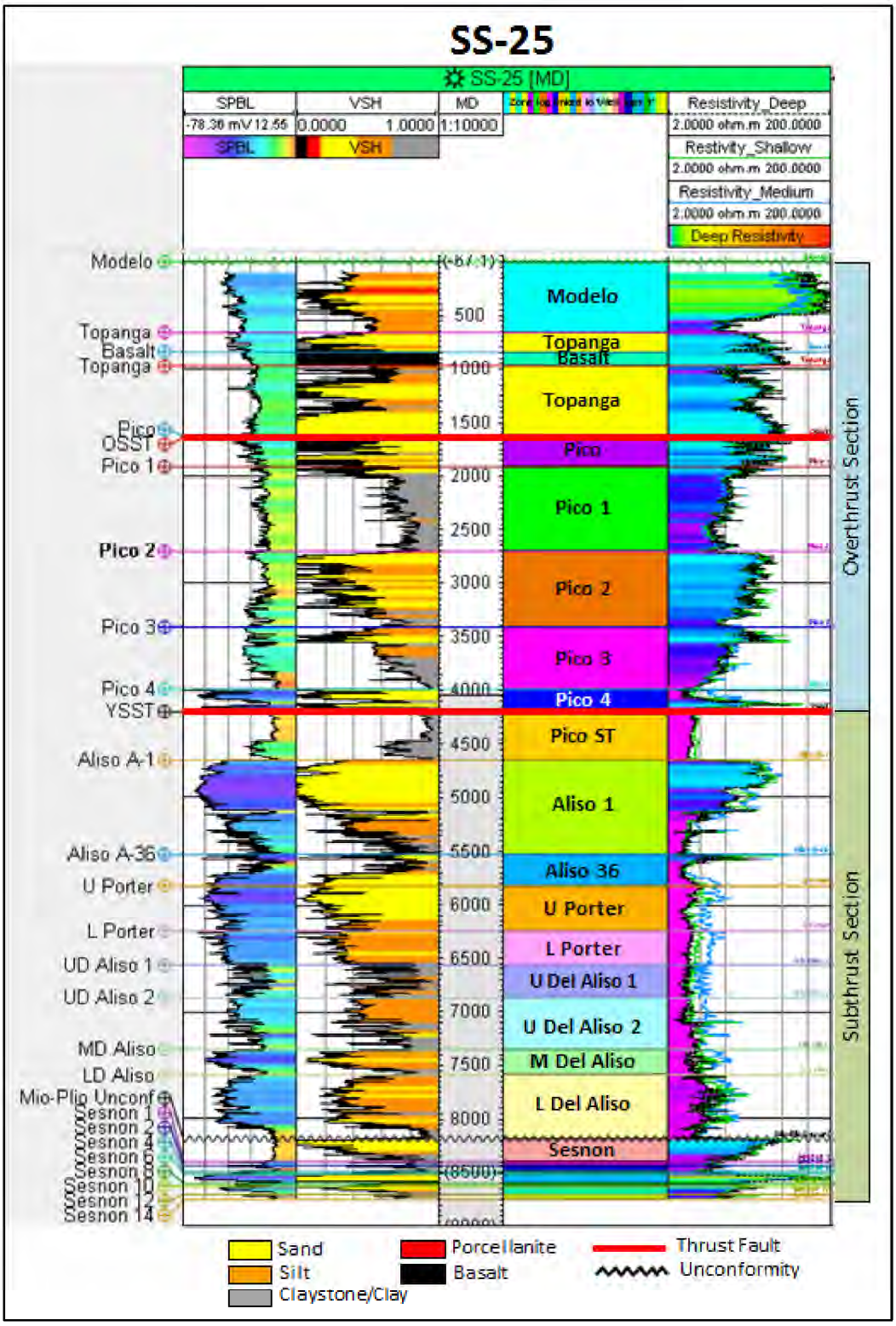

Figure 8: SS-25 OH Logs

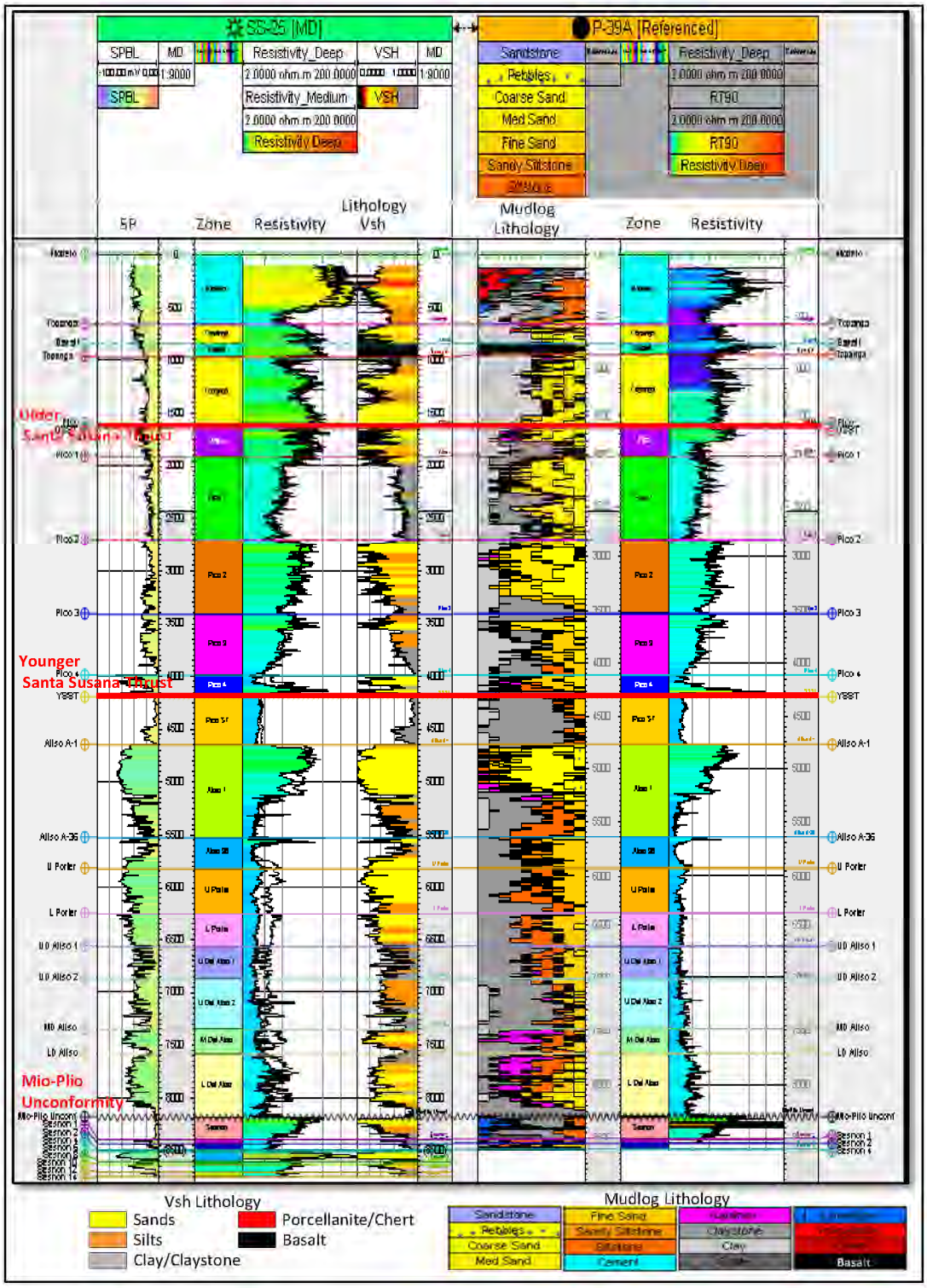

Figure 9: SS-25 and P-39A Relief Well Log Comparison

Table 3: SS-25 Summary of Formation Tops and Geologic Descriptions of Penetrated Formations

Age	Formation	Zone	Geological Description	Top (MD-ft)	Base (MD-ft)	Thickness (ft)	Bed/ Thrust Dip Angle
Middle Miocene	Modelo	Modelo	Interbedded porcellanite, siltstones, sands, organic shales, and soft clays, tar-bearing, lost circulation area, highly fractured	0	660	660	14°E
	Topanga	Topanga	Slightly consolidated f-vf grained sand, some pebbles, interbedded with soft greenish blue gray clay	660	845	185	14°E
		Topanga Basalt	Volcanic, basalt (plag-puroxene diabase)	845	969	124	15°E
		Topanga	Unconsolidated sand, C-f grained, bluish gray to gray white sticky clay	969	1,635	666	15°E
		Older Santa Susana Thrust Fault		1,635			15°NE
Upper Pliocene	Pico	Pico	Kaolinitic sand, c-m grained, soft, sticky claystone and clay	1,635	1,912	277	26°NE
		Pico 1	Unconsolidated sand, c-m grained, interbedded claystone	1,912	2,702	795	26°NE
		Pico 2	Massive unconsolidated sand, claystone	2,707	3,412	705	26°NE
		Pico 3	Unconsolidated sand, silts, sticky clay	3,412	3,992	580	26°NE
		Pico 4	Unconsolidated kaolinitic sand, silts	3,992	4,200	208	26°NE
		Young Santa Susana Thrust Fault		4,200			55°N
	Pico	Pico ST	Claystone, minor siltstone	4,200	4,650	450	18°S-SW
		Aliso 1	Massive unconsolidated sand, kaolinite	4,650	5,527	877	18°S-SW
		Aliso 36	Claystone, siltstone, unconsolidated, sand	5,527	5,820	293	18°S-SW
		Upper Porter	Claystone, siltstone, unconsolidated, sand	5,820	6,245	425	16°SW
		Lower Del Aliso	Sand, siltstone, claystone interbeds	6,245	6,566	321	18°S-SW
Lower Pliocene		Upper Del Aliso 1	Sand, siltstone, claystone interbeds	6,566	6,871	305	18°S-SW
		Upper Del Aliso 2	Claystone, minor siltstone, and sand	6,871	7,350	479	18°S-SW
		Middle Del	Kaolinite, claystone,	7,350	7,588	238	20°S-SW

Age	Formation	Zone	Geological Description	Top (MD-ft)	Base (MD-ft)	Thickness (ft)	Bed/ Thrust Dip Angle
		Aliso	siltstone, sand				
		Lower Del Aliso	Kaolinite, siltstone, sand	7,588	8,182	594	18°S-SW
		Miocene-Pliocene Unconformity		8,182			21°S-SW
Middle Miocene	Modelo	Senson Cap Rock	Cap Rock, hard, limestone, claystone and shale	8,182	8,395	213	15°S-SW
		S1	Sand and siltstone interbeds	8,395	8,434	39	15°S-SW
		S2	Sand and siltstone interbeds	8,434	8,492	58	15°S-SW
		S4	Sand	8,492	8,509	17	15°S-SW
		S6	Sand	8,509	8,600	91	15°S-SW
		S8	Siltstone, sand and claystone	8,600	8,628	28	15°S-SW
		S10	Siltstone, sand and claystone	8,628	8,702	74	15°S-SW
		S12	Siltstone, sand and claystone	8,702	8,748	46	15°S-SW
		S14	Not penetrated	8,748	TD	1	15°S-SW
		Total Well Depth (TD)		8,749			

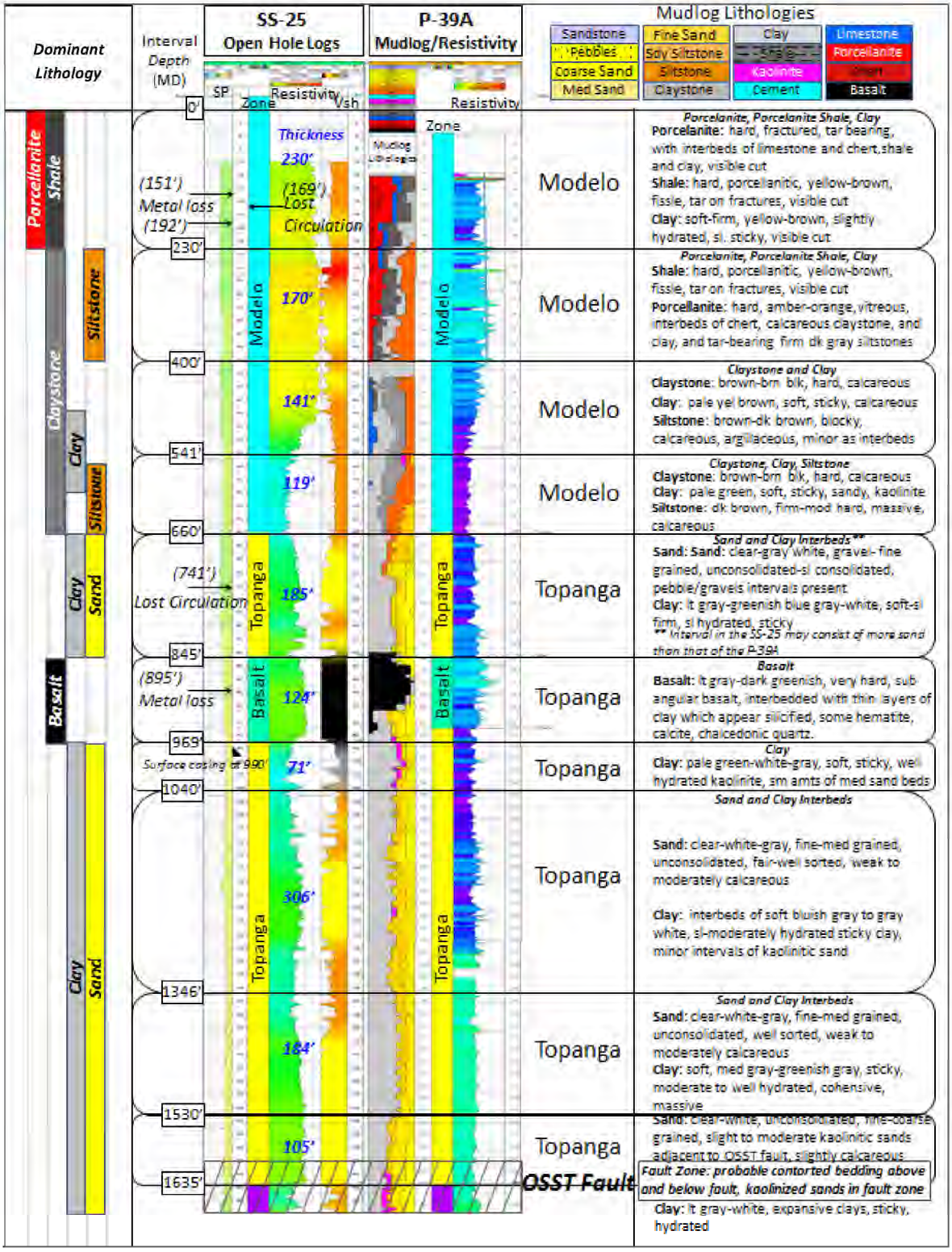

Figure 10: Modelo and Topanga Formations

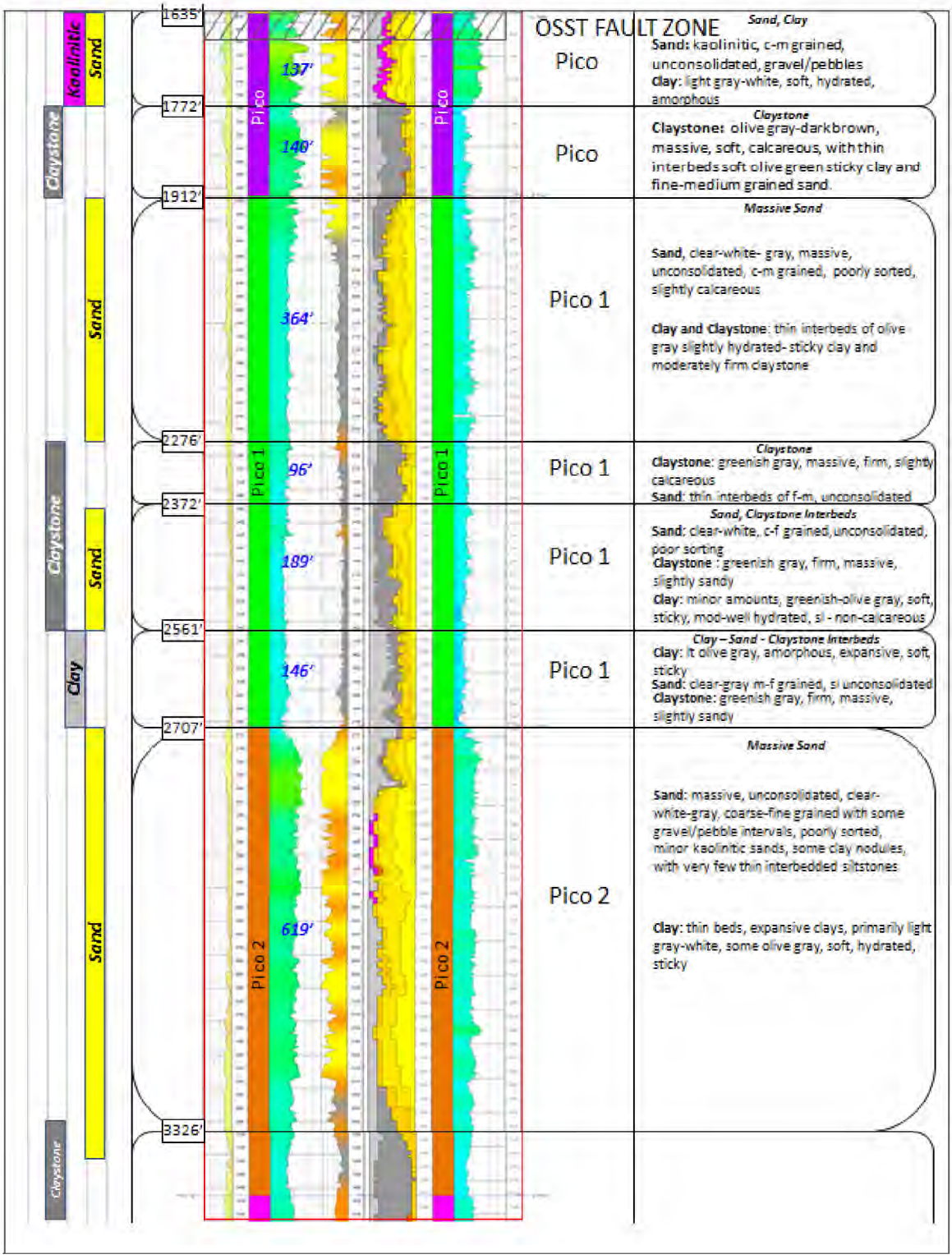

Figure 11: Overthrust Pico Formation

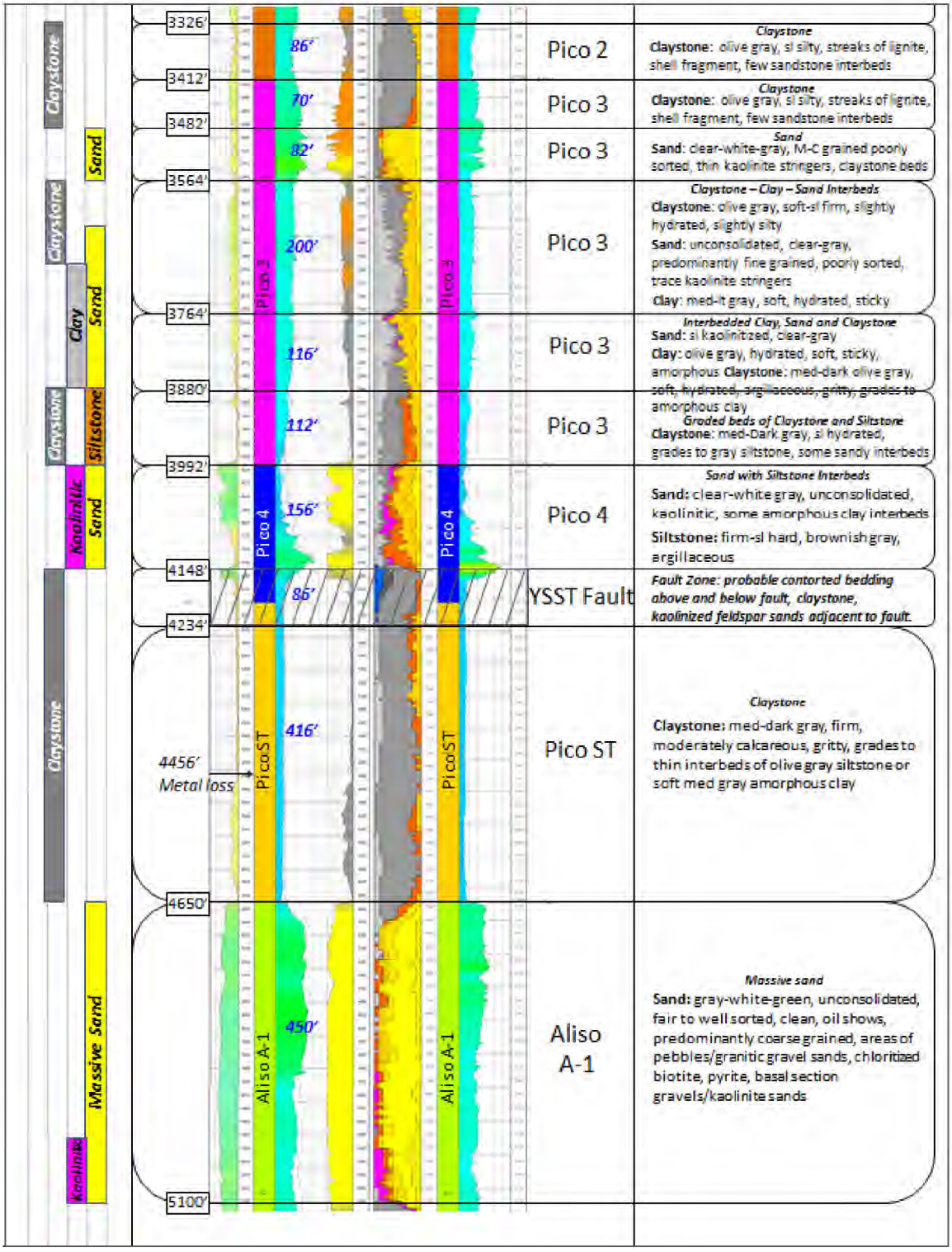

Figure 12: Overthrust Pico Formation to Subthrust Aliso A-1 Zone

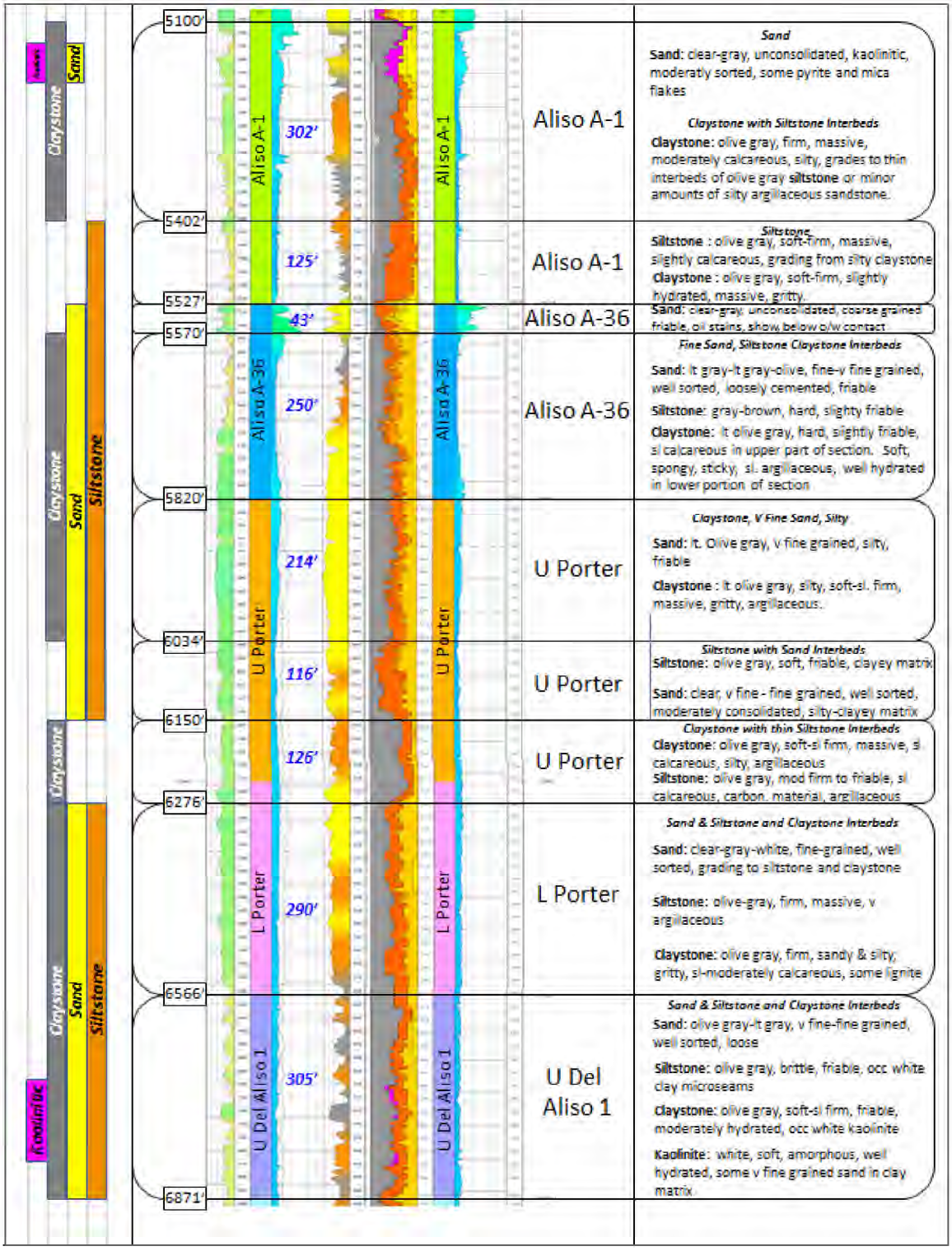

Figure 13: Aliso A-1 to Upper Del Aliso 1 Zone

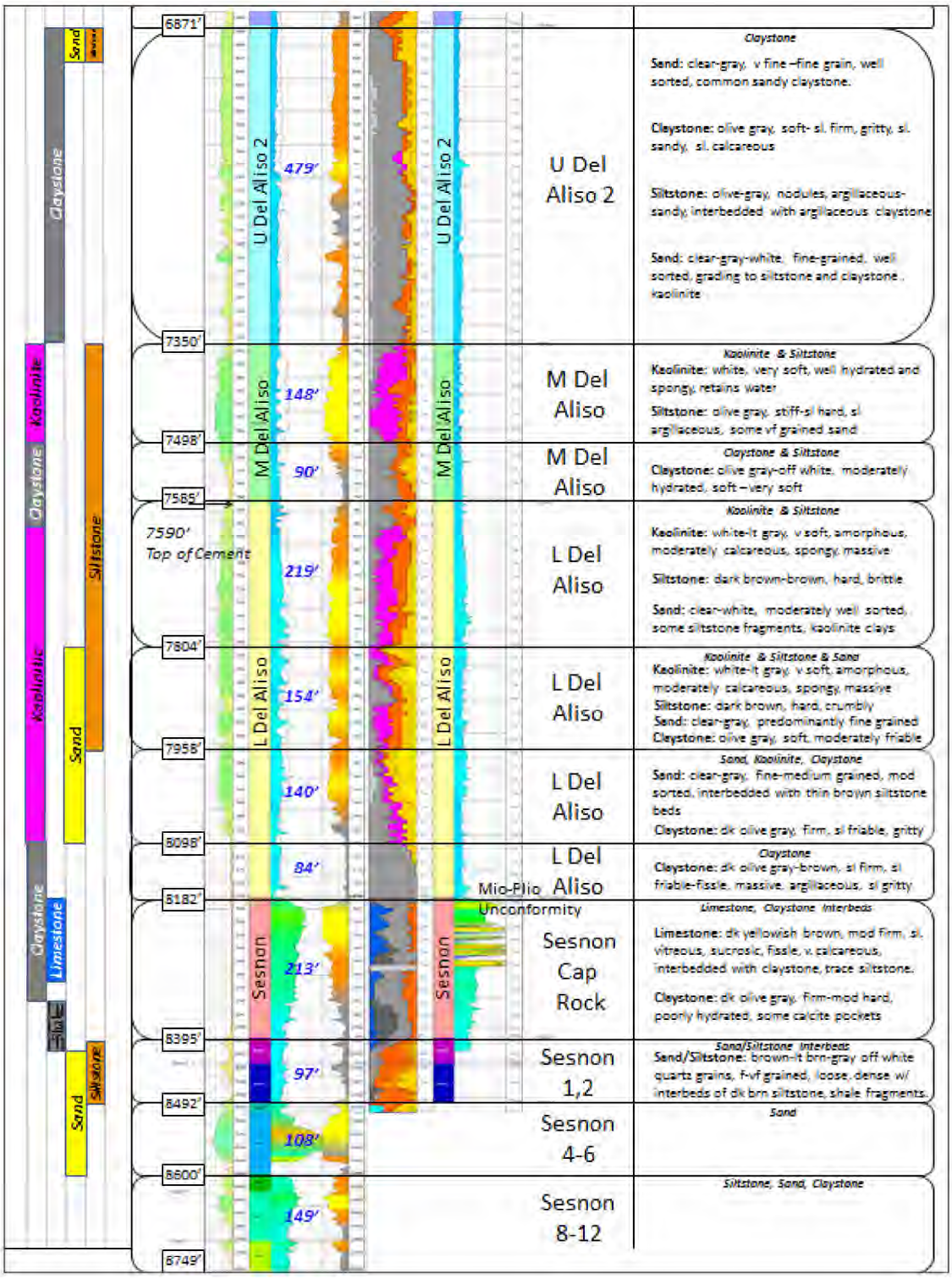

Figure 14: Upper Del Aliso 2 to Sesnon 12 Zone

Based on these formation breakdowns, a correlation was made between SS-25 and the other two pre-incident wells drilled from the SS-25 well site (SS-25A and SS-25B). This correlation is shown in the

structural west-east electric log cross-section in Figure 15. Figure 16 and Table 4 extend the correlation to the more distant P-39A relief well.

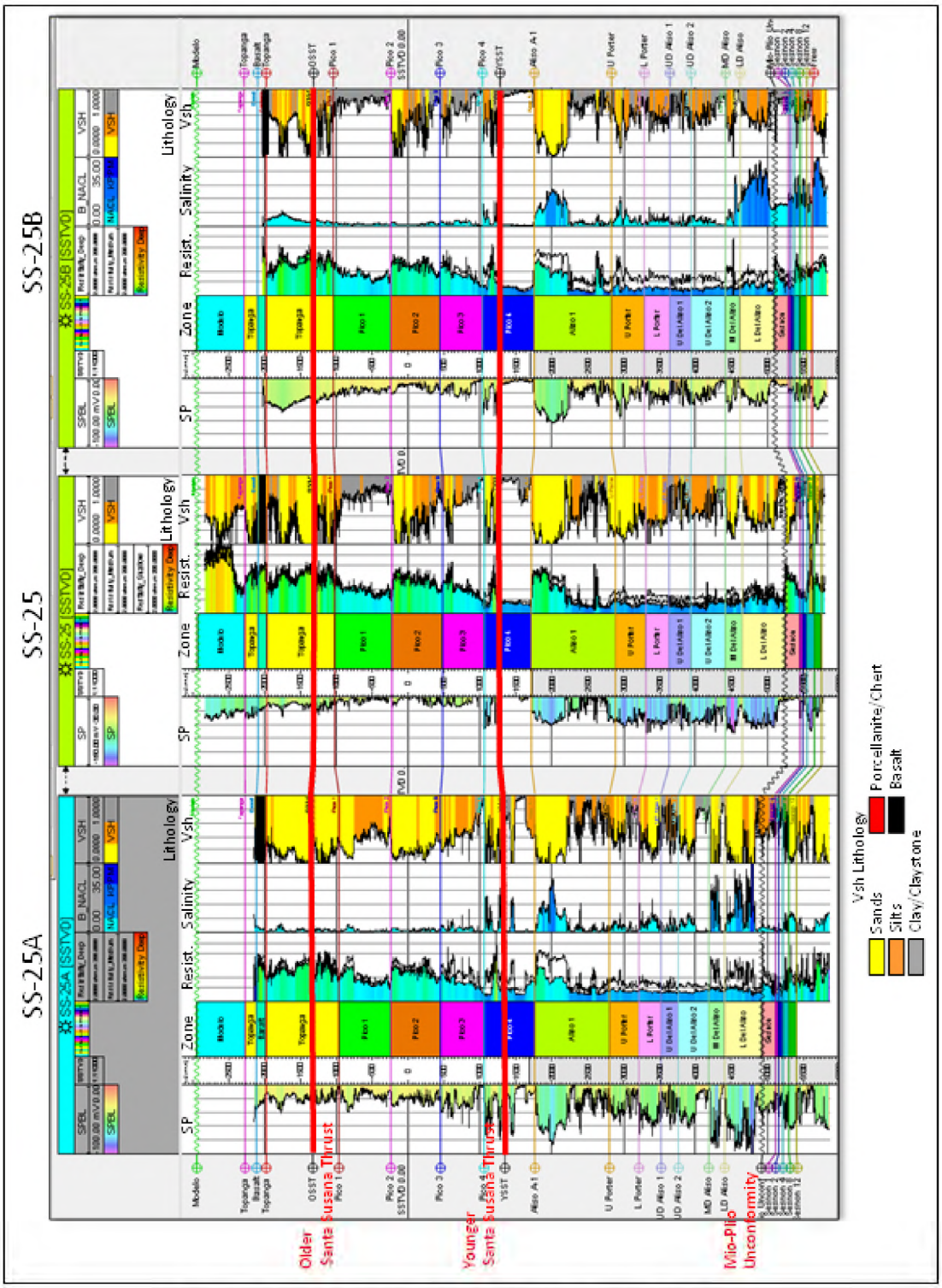

Figure 15: Correlation of SS-25, SS-25A, and SS-25B Wells

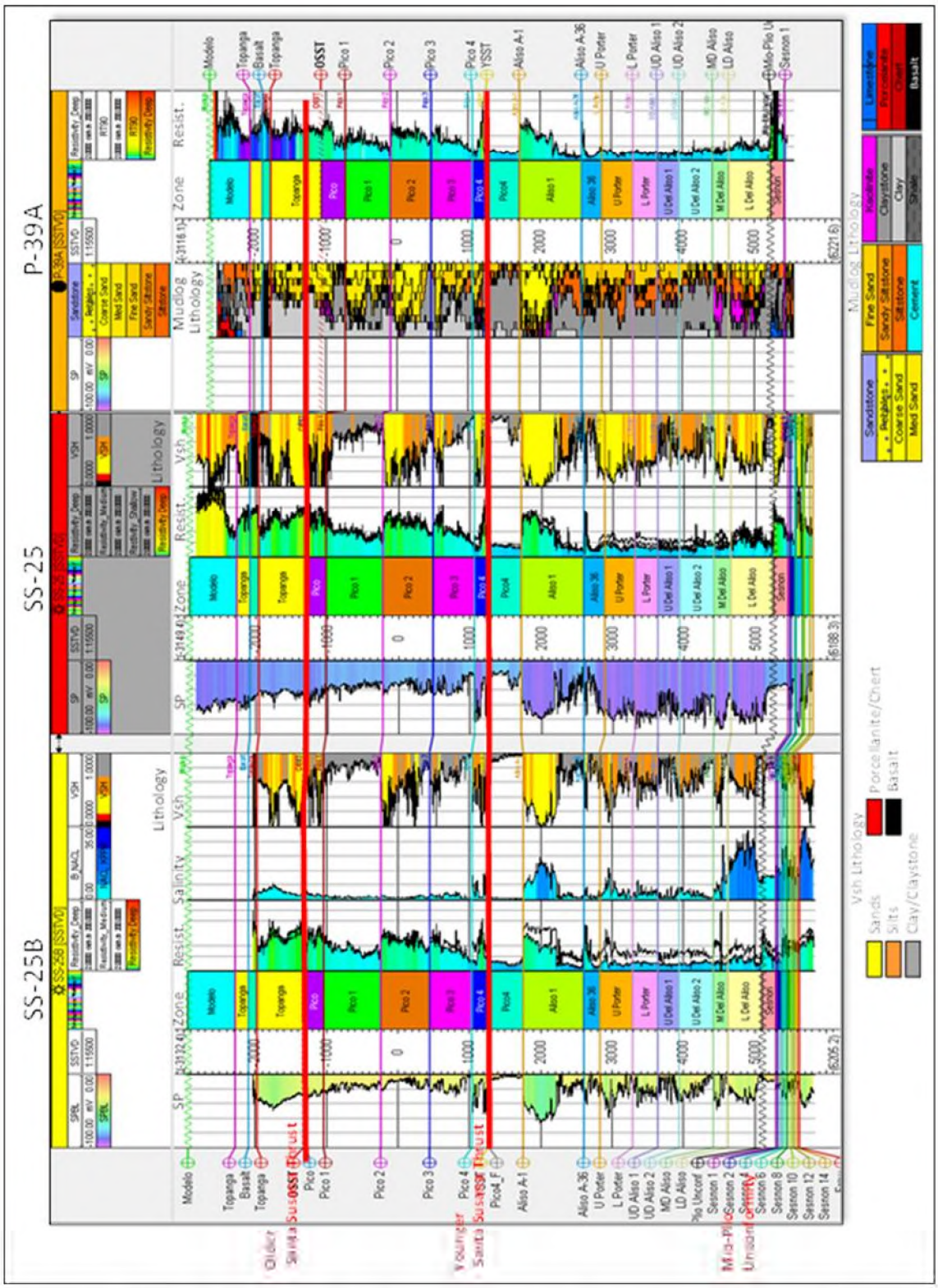

Figure 16: Comparison of SS-25B and SS25 Wells and the P39A Relief Well

Table 4: SS-25A, SS-25B, and P39A Formation Tops

Age	Formation	Zone	SS-25A		SS-25B		P-39A	
			Top (MD-ft)	Base (MD-ft)	Top (MD-ft)	Base (MD-ft)	Top (MD-ft)	Base (MD-ft)
Middle Miocene	Modelo	Modelo	0	660	0	658	0	560
	Topanga	Topanga	670	841	658	845	560	735
		Topanga Basalt	841	965	845	965	735	850
		Topanga	965	1,614	965	1,619	850	1,602
		Older Santa Susana Thrust Fault	1,614		1,619		1,602	
Upper Pliocene	Pico	Pico	1,614	1,979	1,619	1,900	1,602	2,011
		Pico 1	1,979	2,703	1,900	2,700	2,011	2,835
		Pico 2	2,703	3,394	2,700	3,385	2,835	3,522
		Pico 3	3,394	4,000	3,385	3,977	3,522	4,110
		Pico 4	4,000	4,425	3,977	4,208	4,110	4,306
		Young Santa Susana Thrust Fault	4,425		4,208		4,306	
	Pico	Pico ST	4,425	4,708	4,208	4,696	4,306	4,774
		Aliso 1	4,708	5,529	4,696	5,547	4,774	5,644
		Aliso 36	5,529	5,768	5,547	5,775	5,644	5,926
		Upper Porter	5,768	6,188	5,775	6,250	5,926	6,364
		Lower Del Aliso	6,188	6,506	6,250	6,633	6,364	6,702
Lower Pliocene		Upper Del Aliso 1	6,506	6,754	6,633	6,960	6,702	7,010
		Upper Del Aliso 2	6,754	7,183	4,960	7,512	7,010	7,479
		Middle Del Aliso	7,183	7,410	7,512	7,733	7,479	7,708
		Lower Del Aliso	7,410	7,945	7,733	8,250	7,708	8,293
		Miocene-Pliocene Unconformity	7945		8250		8293	
Middle Miocene	Modelo	Sesnon Cap Rock	7,945	8,134	8,250	8,448	8,293	8,513
		S1	8,134	8,180	8,448	8,483	8,513	8,556
		S2	8,180	8,240	8,483	8,534	8,556	8,607
		S4	8,240	8,272	8,534	8,583	8,607	TD
		S6	8,272	8,326	8,583	8,624		
		S8	8,326	8,384	8,624	8,678		
		S10	8,384	8,436	8,678	8,716		
		S12	8,436	8,484	8,716	8,758		
		S14	8,486	8,674	8,758	8,798		
Eocene	Frew	Frew	8,674	TD	8,798	TD		
Total Well Depth (TD)			8,905		9,030		8,623	

5.2 Shallow Stratigraphy – Lithology and Structure

5.2.1 Modelo

The Modelo formation is the eastern equivalent of the Monterey formation, which is the primary hydrocarbon source rock in California. The section penetrated by SS-25 is 660 ft thick. It is characterized by approximately 200–300 ft of an extensively weathered section of siltstones, cherts (porcellanite), and clays. The interval is tar-bearing, and tar has been observed in fractures in cores. The section is highly stratified and thin bedded. Outcrops on the road cuts just below the SS-25 well site are predominantly siltstone and are so extensively weathered that they are completely decomposed and crumble to the touch (Figure 17).

The top of the Modelo is at the surface and is severely eroded. There are few wells that have geophysical coverage over this shallow section; most are covered by surface casing. SS-25, with logs beginning at 85 ft, is a rare exception. There was no available data to attempt a construction of a structure map internal to the formation in the immediate area around SS-25. The Modelo is anticipated to have a similar strike and dip direction, as found in the underlying Upper Topanga: a strike direction of 18°NE and a dip of 14°NE.

Figure 17: Modelo Formation West of SS-25

5.2.2 Topanga

The Topanga section penetrated by SS-25 consists of three units: an upper 185-ft section of predominantly fine-grained marine sandstones interbedded with green-blue clays; a middle 124-ft section, which is an intrusive igneous diabase of plagioclase-pyroxene composition; and a lower 666-ft section of unconsolidated coarse-to-fine-grained marine sandstones and gray clays. The formation is not productive at Aliso Canyon. Sections of the weathered massive sands of the Topanga are exposed in the central portion of the field, as seen in a roadcut approximately 1/2 mile east of the SS-25 well site (Figure 18).

Figure 19 and Figure 20 show structure maps of the Upper and Lower Topanga in the central portion of the field surrounding SS-25. The structural strike of the Upper Topanga at SS-25 is 18°NE, with dip of 14° to the east. The Lower Topanga section was slightly different, striking in the same direction of 18°NE with a dip of 15°. The top of the Lower Topanga section below the intrusive basalt is also the base of the basalt.

Figure 18: Topanga Unconsolidated Sands East of SS-25

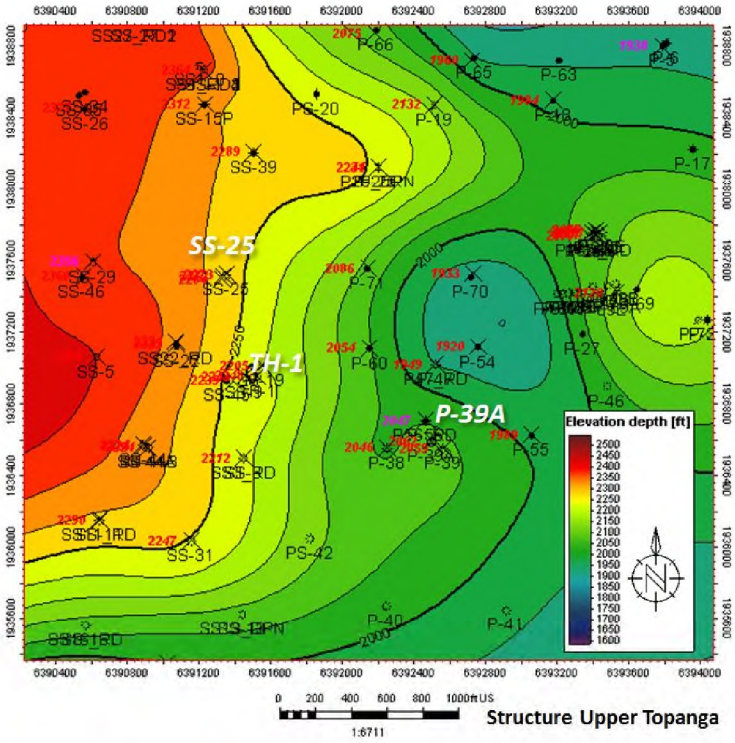

Figure 19: Structure Map Upper Topanga

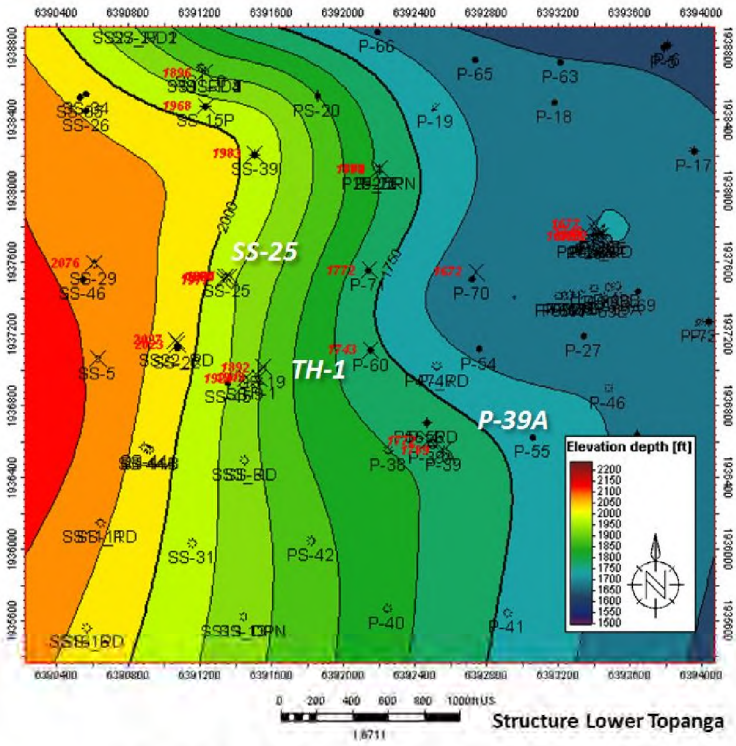

Figure 20: Structure Map Lower Topanga

5.2.3 Topanga Basalt

Laboratory analysis for the RCA project (Appendix B) indicates that the volcanic intrusives penetrated by SS-25 are most likely plagioclase-pyroxene diabases, historically called the Topanga Basalt. The intrusive unit is 124 ft thick in SS-25. It is present over a large section of the central Aliso Canyon Field but terminates abruptly to the south. Thrusted upwards by both OSST and YSST, the Topanga Basalt outcrops approximately 3,500 ft west of the SS-25 well site, near the F-5 and F-9 well sites, as identified by published geologic surface maps [6] [18] [19].

The Topanga Basalt in the outcrops is medium-dark gray in color. Crystals are visible, suggesting a slower subsurface cooling history, as expected in a sill. Fracturing is extensive and is a result of the thrusting. Some sections intertongue with Topanga sands. Spheroids and onion skin weathering are present. It is possible that there were several episodes of magma injection because layers of different crystal sizes are observed, and amygdules are found deeper in the section.

Figure 21 and Figure 22 show the Topanga Basalt outcrops. Figure 21 shows contact of the highly weathered Upper Topanga sands and the intrusive Topanga Basalt from a roadcut near the F-9 well site. Figure 22 shows (a) the road cut exposure of the Topanga Basalt (diabase); (b) basalt spheroids and onion skin weathering; and (c) basalt diabase coarse crystals.

The basalt outcrops were sampled for elemental and mineralogical geochemistry information to develop an igneous petrophysical model for use in evaluating SS-25 and TH-1 Litho Scanner logs. The failure of SS-25 production casing occurred in the basalt section at a depth of 892 ft. Eight samples of the least-weathered rock were collected as the best surface representation of the subsurface Topanga Basalt. Although coring was the intended sampling technique, surface conditions precluded use of the coring

equipment, and hand samples were obtained instead. Outcrop samples were from very competent rock that was very resistant to breakage by a 10-lb sledge hammer.

Thin section, Fourier transform infrared spectroscopy (FTIR), and X-ray diffraction (XRD) analyses were conducted on all eight samples. From thin section analysis, the Topanga Basalt is most likely not a basalt, but a hypabyssal diabase sill that is predominantly plagioclase and pyroxene, with lesser abundances of biotite, amphibole, and olivine. Chlorite is abundant in all hand samples and, along with iron oxides, has extensively replaced biotite, amphibole, and olivine. Secondary (diagenetic) minerals are abundant, but, other than chlorite, do not represent a major contribution to the geochemistry of the subsurface basalt. Most of the resistive shear fractures observed in the TH-1 borehole FMI results were present over the basalt interval.

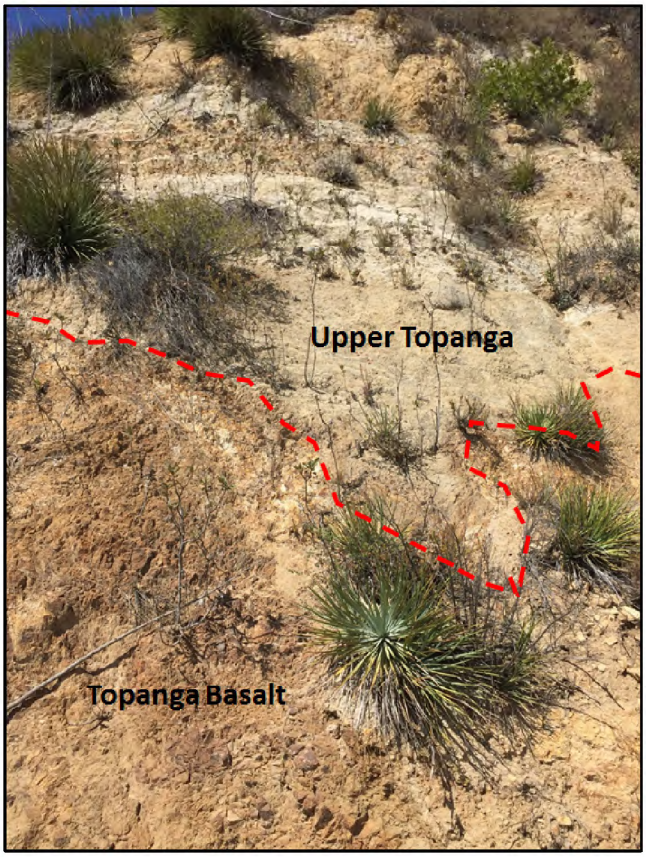

Figure 21: Contact of the Upper Topanga Sands and Topanga Basalt

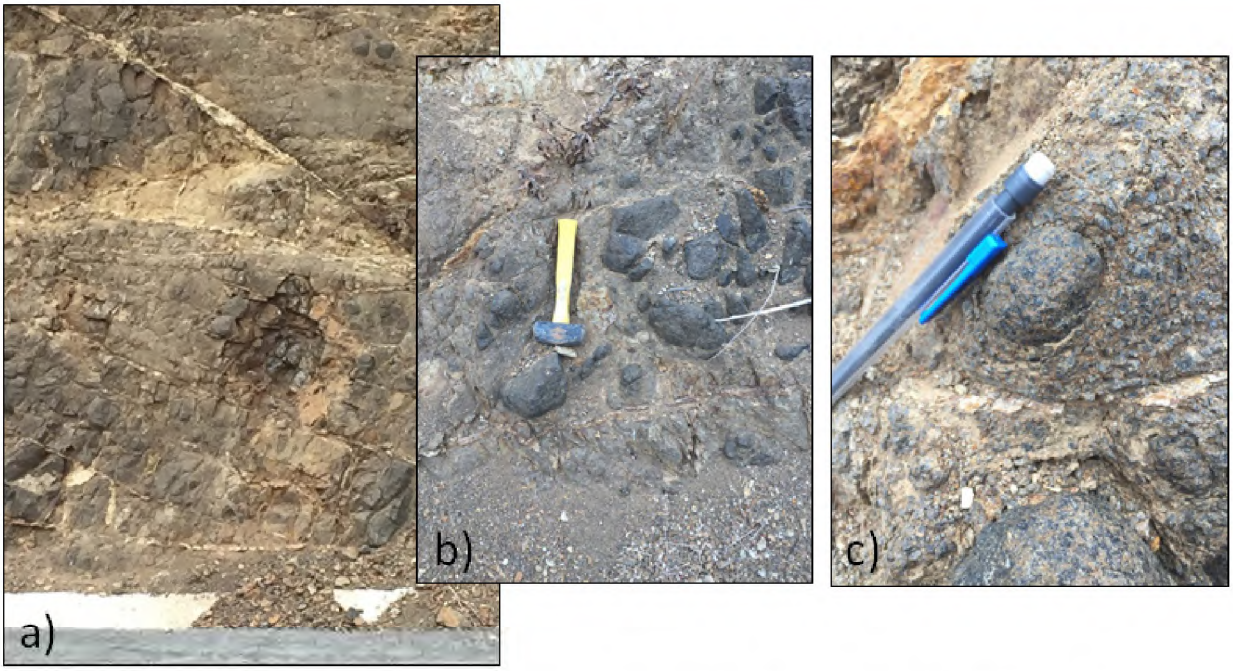

Figure 22: Exposure (a) and Features (b, c) of the Topanga Basalt (Diabase)

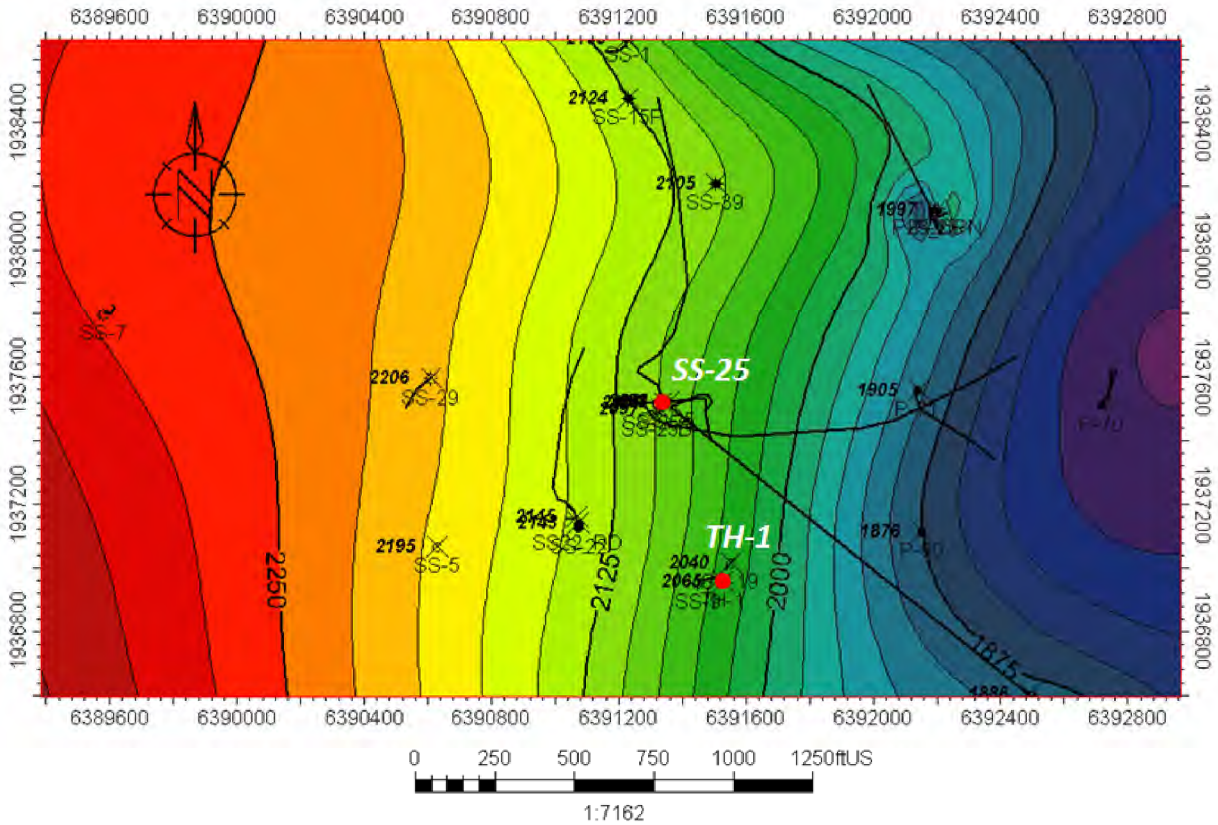

Figure 23: Structure Map of the Topanga Basalt

5.3 Shallow Geology

5.3.1 SS-25 Location Boreholes

Additional data gathering was conducted for a better understanding of the shallow geology of SS-25. Four shallow boreholes were drilled and cored by Advisian (Appendix A) on the SS-25 well site to evaluate the conditions of the shallow subsurface at the SS-25 well site. Televiewer data from the boreholes were collected and analyzed by Advisian. The boreholes reached depths ranging from 120–150 ft. Figure 24 shows the locations of the four boreholes on the SS-25 well site. Well site examination of the cores revealed highly weathered and extensively fractured siltstones, shales, chert, and clay of the Modelo formation. Of particular notice were the near-vertical fractures observed in some of the cores. Fracture types observed were of three types: (1) fractures filled with anhydrite, calcite, or tar; (2) open fractures; and (3) fractures stained with dead oil and iron on their surfaces.

Figure 24: Location of Shallow Boreholes

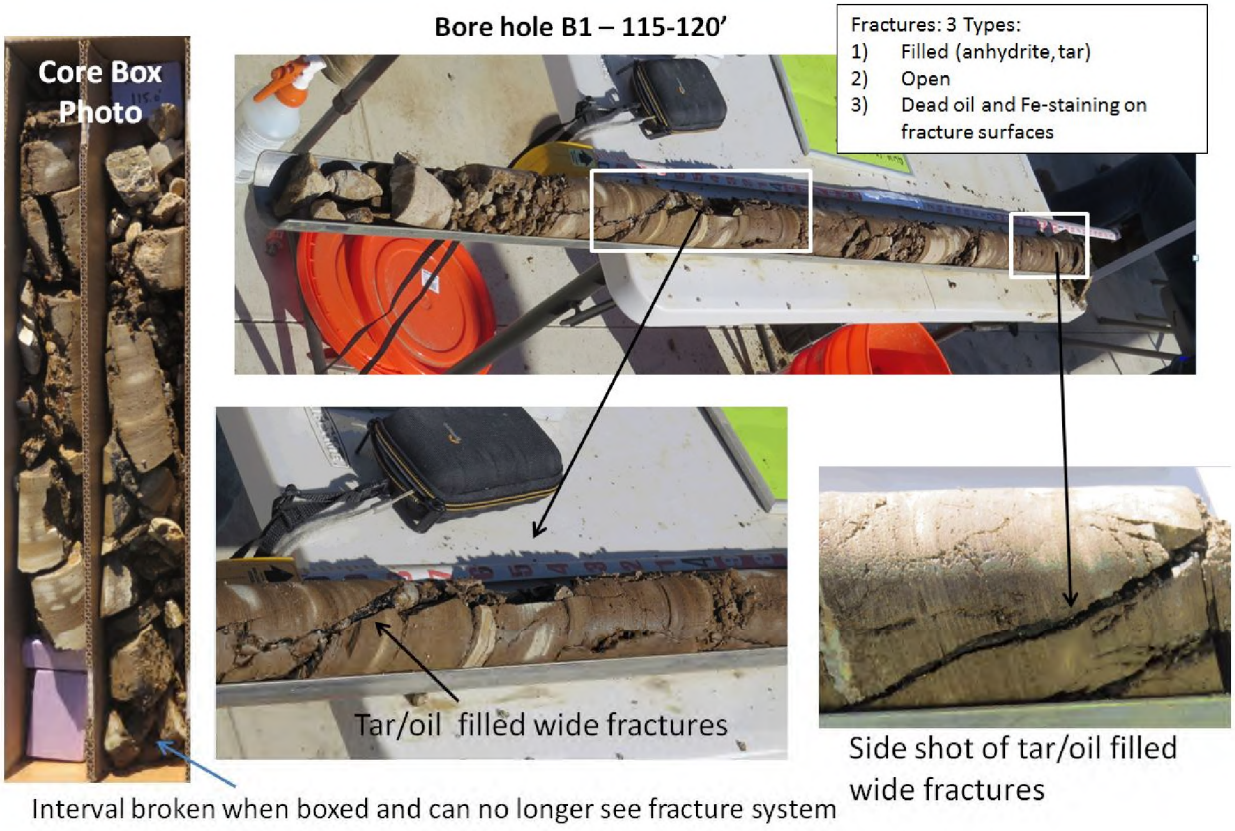

Figure 25: Core Photographs of Fractured Modelo in Borehole BH-1

Fractures were best observed while cores were still in the core tray because the highly weathered rock tended to crumble and break as the cores were being placed in core boxes, destroying the continuity of the lithology and fractures. Figure 25 shows core photographs taken between 115 and120 ft in the BH-1 borehole. A large near-vertical tar-filled fracture ran almost the entire length of the 5-ft core.

The optical televiewer logs from all four boreholes (but primarily BH-3 and BH-4) indicate that the shallow rock is highly weathered, with zones of spalling and open joints and fractures to depths of 100 ft. At depths below approximately 50 ft, thin bedding, less than 1-in. thick, becomes apparent.

5.3.2 Shallow Geophysical Investigation

A shallow geophysical investigation was conducted by Advisian (Appendix A) around the SS-25 well site. Despite the challenge presented by the rough terrain, data from 15 electrical resistivity tomography (ERT) lines and four shallow seismic lines were investigated.

ERT identified two zones of anomalously high (>500 ohm-m) resistivity. The zones are located north and south of the SS-25 wellhead and have been interpreted as associated with subsurface freezing. This interpretation is supported by temperature logs and distributed temperature sensing (DTS) results, as well as the anomalously high resistivities and the shape of the features appearing to be inconsistent with the lithology, stratigraphy, and structure of the Modelo formation. These high-resistivity features are depicted in pink in the lower right of Figure 26 (ERT line 5B).

Features with anomalously low resistivity (in dark blue in the lower right of Figure 26) are interpreted as possible kill fluid zones. Although core samples (fracture and matrix) from adjacent boreholes were tested

in the laboratory for the presence of $CaCl_2$ kill fluid, SEM, XRD, and X-ray fluorescence (XRF) analyses indicated only a very small amount of $CaCl_2$. The lack of $CaCl_2$ is not definitive, however, because the boreholes were not drilled directly into the low-resistivity features, and water circulation during coring may have flushed $CaCl_2$ from the core.

Geophysical logs run in the boreholes indicate that the rock is unsaturated to the borehole TD (120–150 ft), with no indication of perched aquifers at these depths.

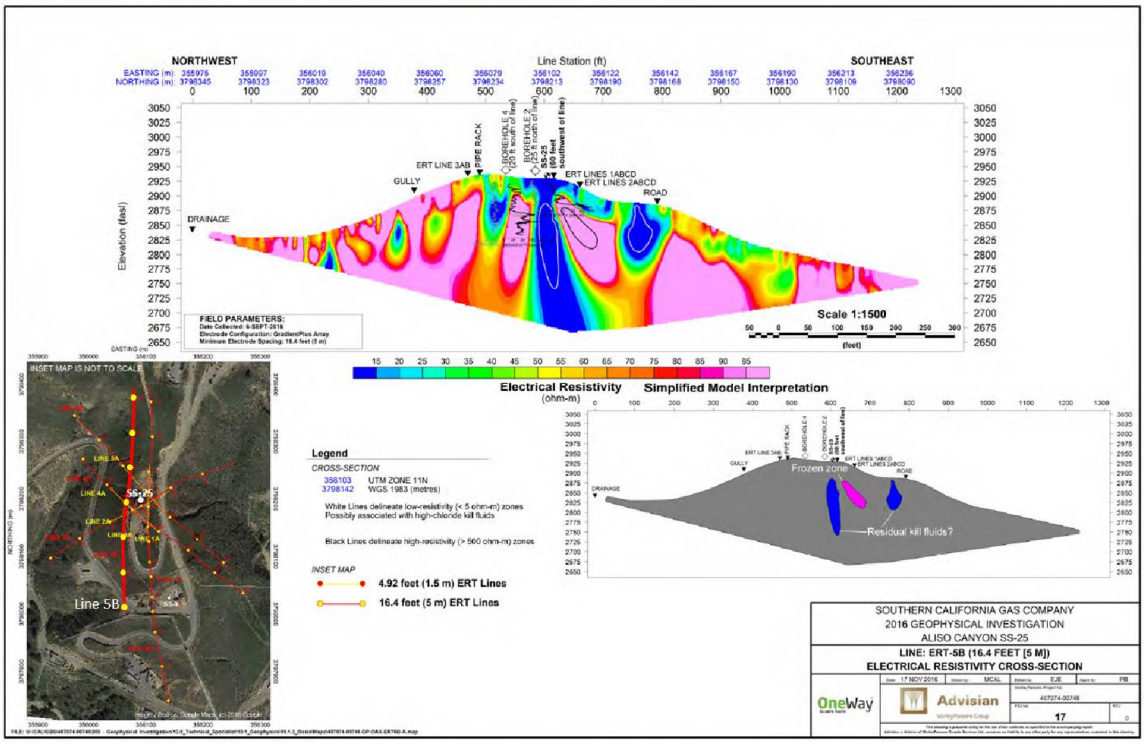

Figure 26: ERT North-South Line 5B

Seismic line 1 shows velocities indicative of highly weathered rock (less than 2,000 m/s) from surface to a depth of 200–300 ft. Below these depths, velocities increase relatively rapidly to more than 2,500 m/s, indicating a change to relatively competent rock. Seismic line 1 (Figure 27), a north-south line run over the SS-25 well site, shows an abrupt increase in P-wave velocity below the slower, weathered Modelo. The cross-section clearly shows the extent of the highly weathered upper 200-300 ft of the Modelo formation.

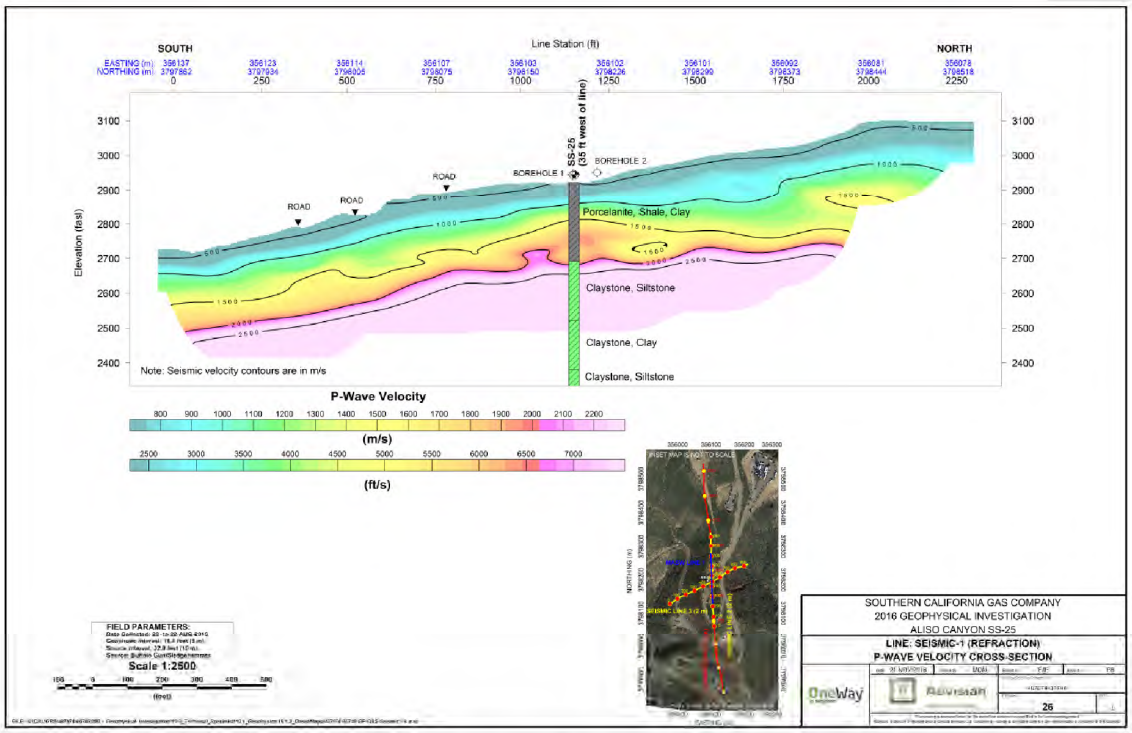

Figure 27: Seismic Line 1 (Refraction) P-Wave Velocity

5.3.3 RBMW-1 (TH-1) and SS-25 Log Comparison

Because of the presence of surface casing in SS-25, only CH logs, specifically the Litho Scanner service, could be run in that well, limiting the amount of data collected. However, a shallow test well (RBMW-1, also known as TH-1) was drilled about 600 ft south of the SS-25 well site to investigate the presence and contamination of potential groundwater. OH logs, including the Litho Scanner service, NMR, Dielectric Scanner multifrequency dielectric dispersion service, and FMI MicroImager, were run in the RBMW-1 (TH-1) well. Data from RBMW-1 (TH-1) OH logs (Figure 28) were compared with the SS-25 CH log data (Figure 29) and used to improve the SS-25 log data interpretation.

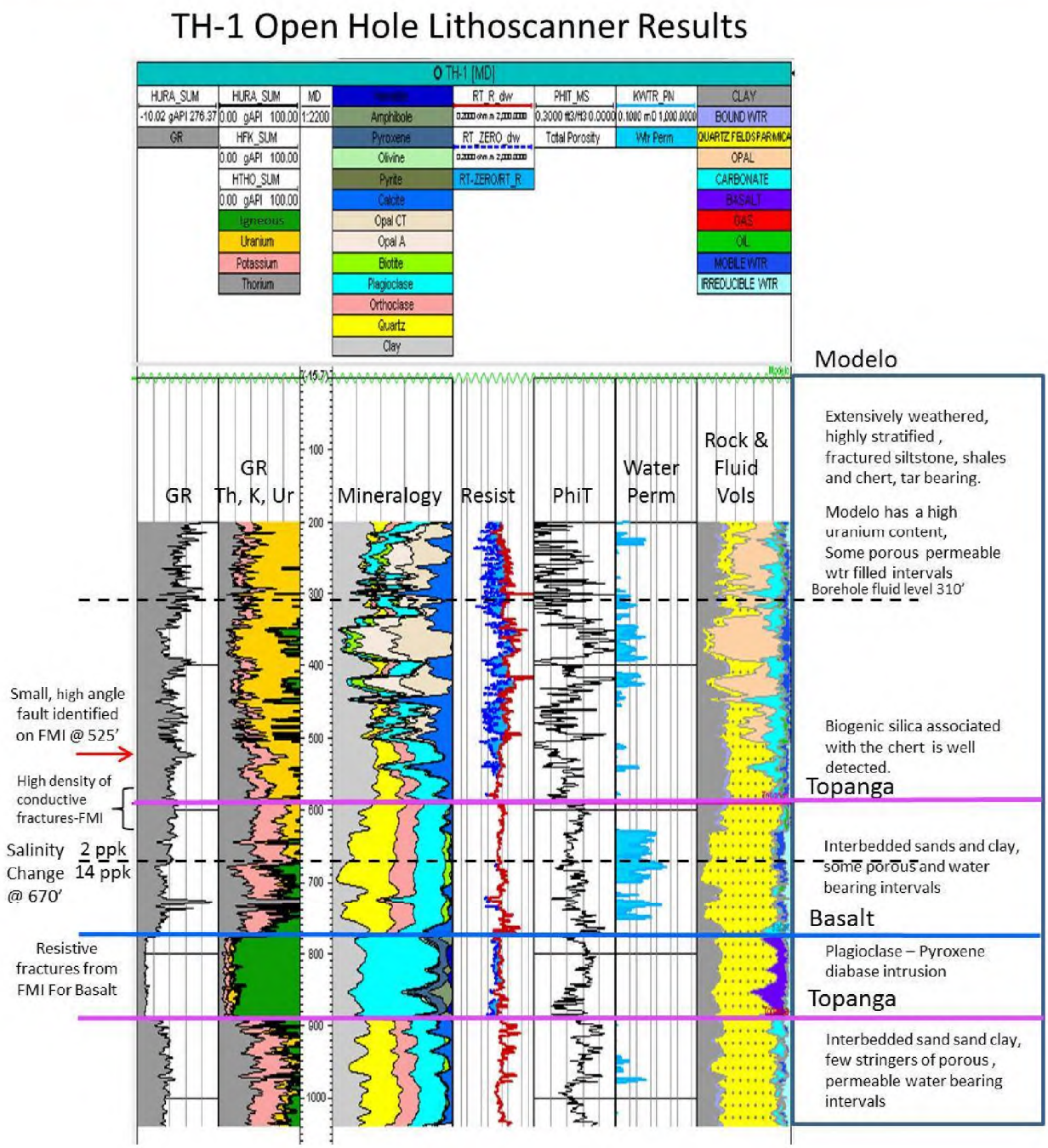

Figure 28: TH-1 OH Log Curves and Interpretation

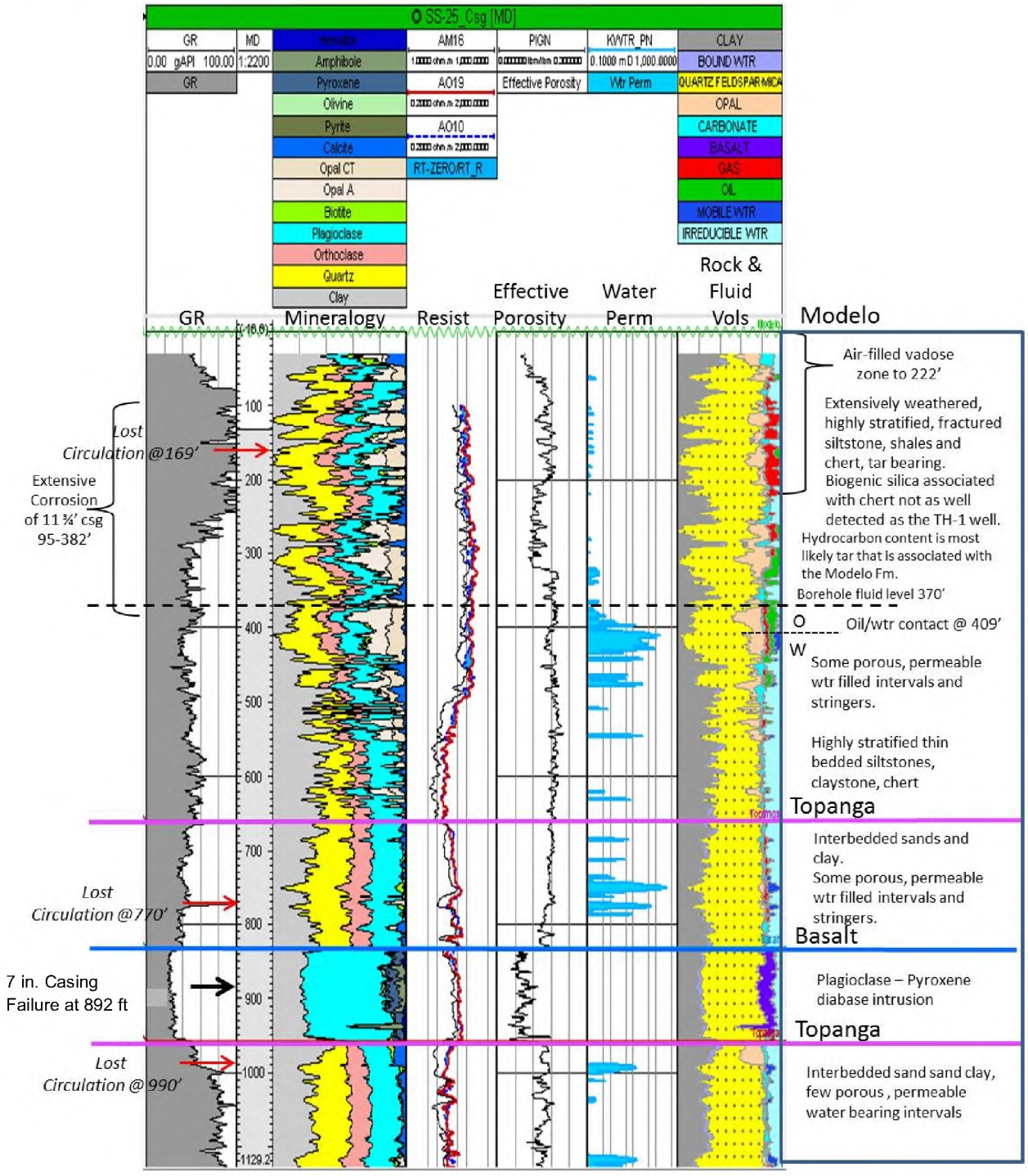

Figure 29: SS-25 CH Log Curves and Interpretation

First, mineralogy fractions compare well between the two wells, except that SS-25 CH data do not differentiate the biogenic silica from quartz in the Modelo formation.

RBMW-1 (TH-1) results (Figure 28) show elevated uranium content through the entire Modelo section. The Dielectric Scanner data show a large salinity change from 2,000 ppm in the Modelo to 14,000 ppm in the Topanga. Petrophysical modeling was conducted with the objective of differentiating 13 minerals, the

detrital nonmarine minerals from marine sedimentation and from the volcanic intrusives. This modeling was able to distinguish detrital quartz from biogenic silica and volcanic quartz. Water-permeable intervals are consistent with those observed in SS-25 in the lower Modelo and Upper Topanga intervals. FMI results from RBMW-1 (TH-1) indicate a small fault at 525 ft and also that the basalt fractures are resistive. Also observed is a high density of conductive fractures and microfractures in the interval from 580 ft to 635 ft in the Upper Topanga section.

SS-25 results (Figure 29) include the identification of a tar- or air-filled "vadose" zone to 222 ft, which is consistent with the Advisian borehole data that indicate unsaturated formations. The identification of Modelo hydrocarbons is consistent with the Modelo and tar in the shallow borehole core fractures. Both wells show the highly stratified nature of the Modelo, interbedded siltstones with cherts and clays. An oil-water contact was observed in SS-25, but this may be a tar mat. Some porous permeable intervals are present in the lower portion of the Modelo and Upper Topanga. The basalt section in both wells does not contain any water-permeable sections. The Lower Topanga has two water-permeable intervals.

5.3.4 SS-25 Other Characterizing Elements

Lost Circulation Potential

Lost circulation has been observed in a number of wells in the overthrust Modelo and Topanga formations. Lost circulation in SS-25 occurred at 169 ft in the Modelo and at 741 ft and 990 ft in the Topanga formations. Lost circulation in the RBMW-1 (TH-1) borehole was encountered at 555 ft and, despite significant efforts to contain it, continued throughout the remaining drilling to TD at 1,110 ft.

Hydrocarbon-Bearing Zones

Tar is present in the Middle Miocene Modelo, as observed in the shallow boreholes drilled, the mudlogs, and surface outcrops in Aliso Canyon.

The Upper Pliocene Aliso zone between 4,650 and 5,820 ft is an oil-producing zone and is actively being waterflooded. Formation tests in SS-25 resulted in hydrocarbon shows in the Aliso A-1 zones 4,661–4,781 ft; 4,725–4,860 ft; and 4,795–4,910 ft.

The Middle Miocene Sesnon zone from 8,395 ft to TD is a former oil-producing zone, which is currently being used as a gas storage reservoir.

Swelling Clays

Expansive clays appear to be present throughout the stratigraphic section penetrated by SS-25. Descriptions in the P-39A mudlog include "hydrated, sticky, fluffy" with respect to clay and claystone sections. XRD data for the Sesnon (Modelo) in the P-42A and FF32-A wells also identified an expansive clay with smectite, along with non-swelling clays with illite and kaolinite. XRD data were not located for other wells or formations.

Fault Zones

The area above and below the OSST and YSST thrust faults would be expected to be highly broken with contorted beds. Sands adjacent to both of these faults are kaolinitic, as observed from mudlogs, suggesting alteration of the feldspars due to introduction of fluids along the fault planes. The YSST is a sealed fault and is a trap for hydrocarbons below it; consequently, it is not expected to be a zone of lost circulation.

5.4 Gas Vents

A number of several small (inch-wide) gas vent holes were observed at the base of the roadcuts adjacent to the asphalt road on both the eastern and western sides of the SS-25 well site ridge, in the highly weathered, fractured Modelo formation. Gas emanating from these vents was reported by SoCalGas staff during the SS-25 incident.

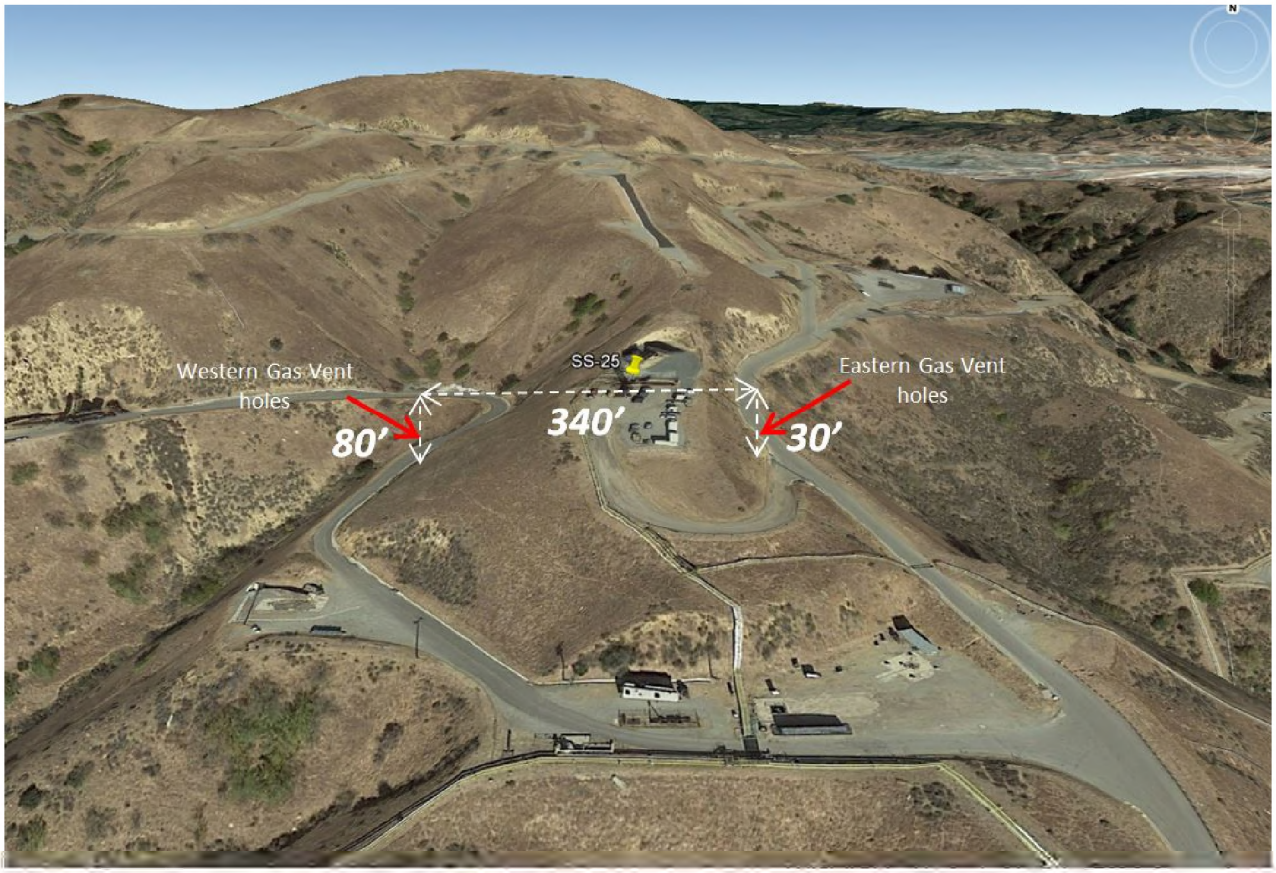

Figure 30: Location of Gas Vents Along Roadcuts East and West of SS-25

Figure 30 shows the locations of these roadside vents with respect to the SS-25 well site. The total distance as measured from Google Earth is approximately 340 ft across the ridge crossing the SS-25 well site. Figure 31 shows the gas vents at the base of the roadcuts east and west of the S-25 well site. The base of the eastern roadcut is approximately 30 ft lower than the surface elevation of SS-25, whereas the western road cut base is 80 ft lower.

These gas vent observations indicate that the gas escaped from SS-25 in an east-west direction across the ridge during the SS-25 incident. Gas may have entered the formation through the extensively corroded 11 3/4 in. surface casing (between 134 and 300 ft) and traveled through the highly weathered and fractured Modelo to exit adjacent to the asphalt roads near the roadcuts.

Inspection up and down the roads on either side of the ridge did not reveal any indication of animal burrowing, so these vents are most likely the direct result of gas escaping through the formation during the blowout.

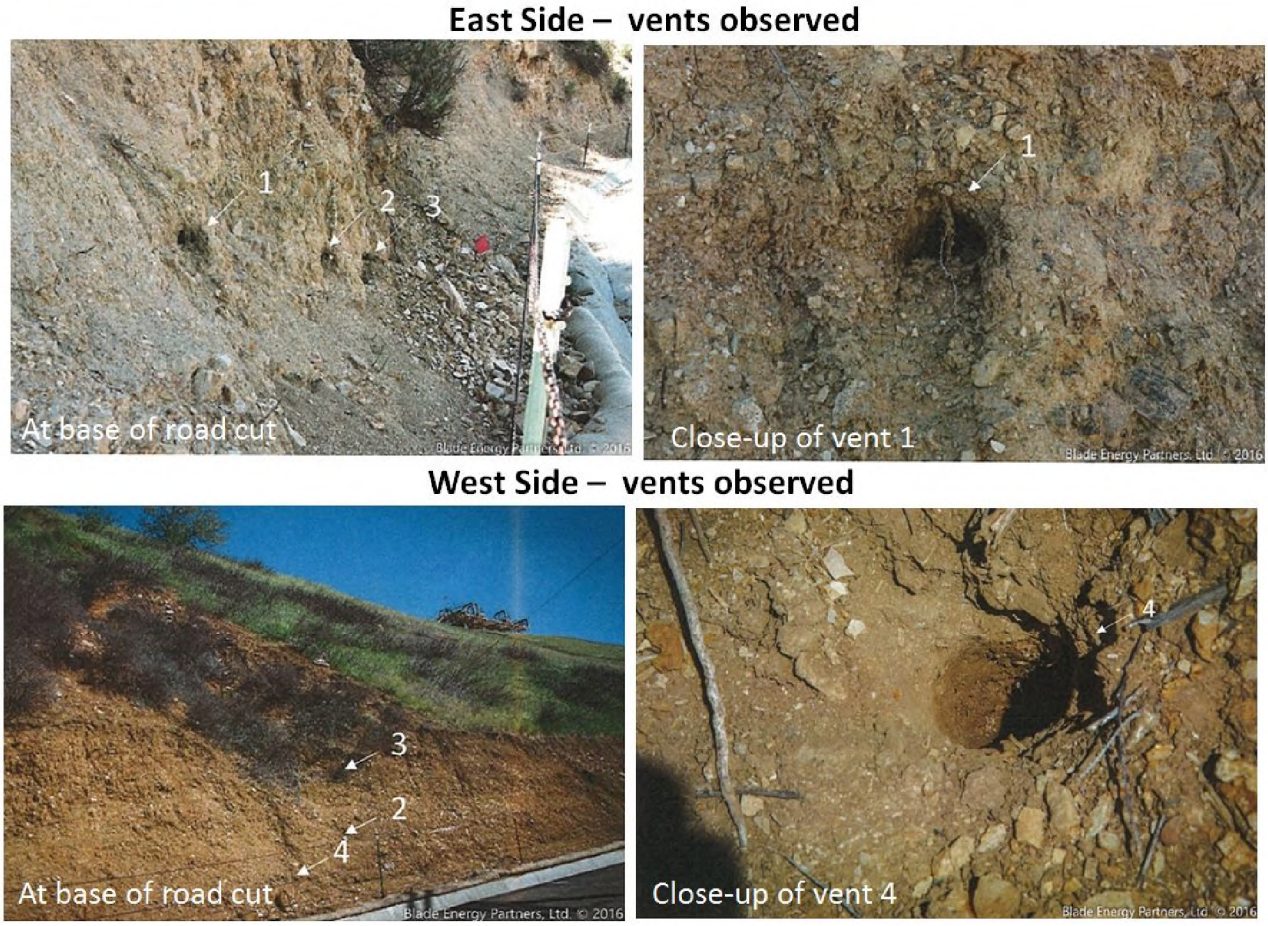

Figure 31: Gas Vents at the Base of the East and West Roadcuts

6 Casing Failure Wells: Evaluation by Fault Block and Formation

An engineering search of well histories of wells within a 3,000-ft radius of SS-25 identified 71 wells with casing problems between 1952 and 2016 (Figure 32). The types of casing problems identified are casing leak, casing collapse, parted casing, deformed casing, split casing, collar leak, severe deformation, and tight spot. These wells were evaluated geologically to determine whether casing failure is related to geological formation, fault block, or distance from a major fault.

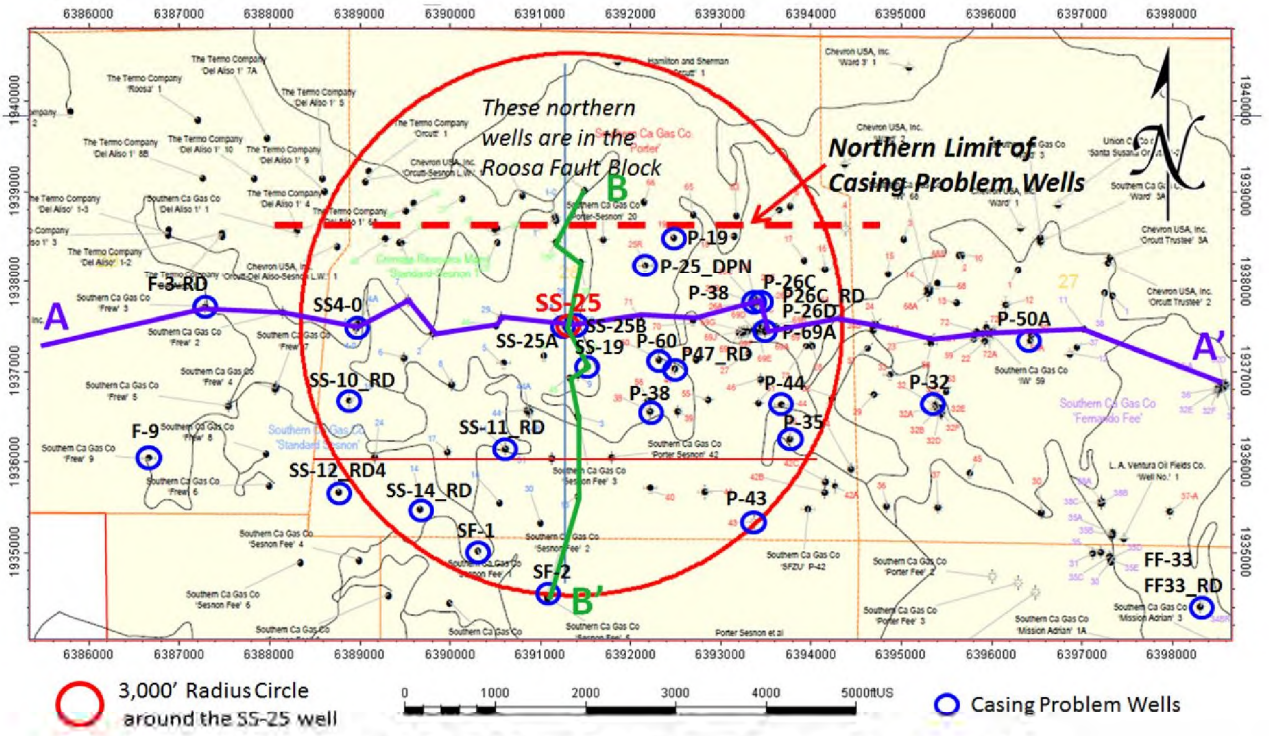

Figure 32: Location of Casing Failure Wells Evaluated Geologically

Seven Aliso Canyon Field fault blocks were identified, with four (1–4) characterized as major blocks. Wells were categorized by these fault blocks. Figure 33 presents two central cross-sections through Aliso Canyon Field, where (a) is a west-east cross-section and (b) is a north-south cross-section. Cross-section locations are included on the map in Figure 32. The fault blocks are identified in these cross-sections with generalized degrees of structural deformation noted in cross-hatches.

In Figure 33, the cross-hatched areas are where the more extensive damage is expected. The densest cross-hatching, indicating the most extensive damage, is seen fault block 1, which is expected due to the block's tectonic history of displacement and uplift and subsequent movement by the later YSST fault. Fault block 2 is expected to have the next most extensive deformation due to its displacement and uplift. Thrust planes are expected to exhibit shear zones of deformation above and below fault picks. Difficulties in log correlations above the two Santa Susana thrust zones suggest smaller scale faults and deformations, which have not been recognized before this study and are difficult to discern with only old electric logs. These smaller scale faults, as well as fractures, can be conduits for fluid and gas migration. As discussed earlier, fractures found in the shallow boreholes can be open or filled. Filled fractures indicate fluid movement through them at some time in the past; whereas open fractures are existing conduits for fluid

movement. Older faults (Frew, Sub-Frew, Ward, and Roosa) are expected to have some associated deformation, fractures, gouges, or breccia along their traces. Internal correlations from logs in these older fault blocks (3–7) are generally pretty good, suggesting that the overall interior of the fault blocks saw the least amount of deformation.

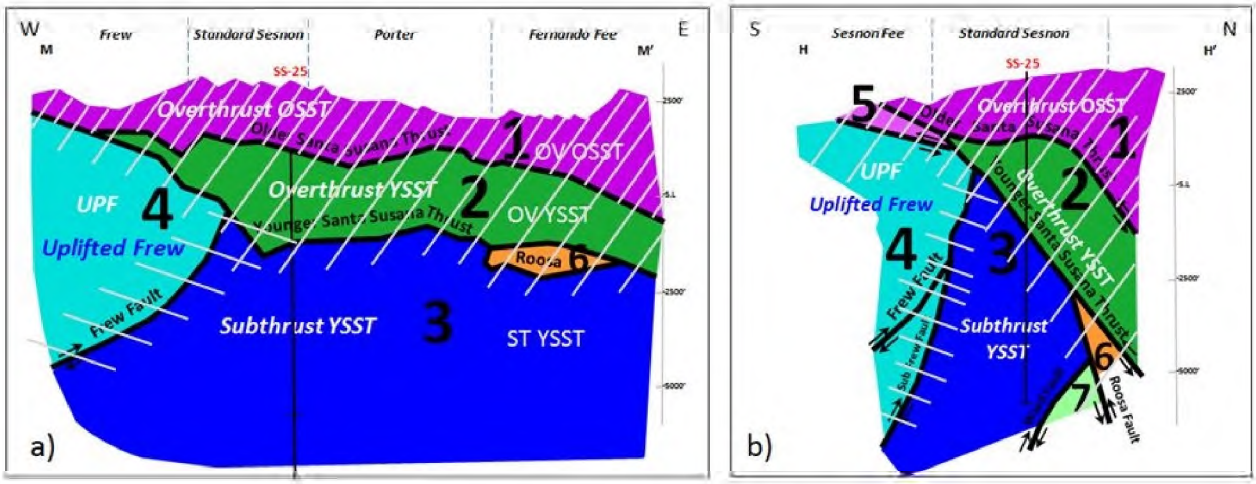

Figure 33: Aliso Canyon Field Fault Blocks

Figure 34 shows the evaluation of formation or zone by fault block. (A well may be identified more than once due to multiple casing problems). The results do not show a correlation for fault block, formation, or zone as the source of casing problems. In fact, the casing problems seem to be evenly distributed throughout the fault blocks, considering the size of and number of well penetrations in each fault block.

Most wells with casing problems (21 of the 71) are located in fault block 3, the subthrust section below YSST. However, this fault block is also the largest and has the most well penetrations. No casing problems are associated with the fault blocks 6 or 7.

Similarly, no correlation has been found between casing problems and stratigraphic formation or zone. Figure 34 shows that, after considering the thickness of each formation and multiple incidences of casing problems in some wells, the casing problems are again evenly distributed between different formations and zones. For example, the Pico overthrust has ten casing problems associated with seven wells. However, the Pico overthrust is also a field-wide, undifferentiated, thick section, so is expected to have a higher number of casing problem occurrences than the differentiated, thinner zones below YSST.

Two of the five wells with casing problems in the highly fractured Modelo formation are direct offsets to SS-25 (P-60 with casing leaks at 318 ft and 325–355 ft and SS-19 with a casing leak at 31 ft). These are all shallow Modelo depths where lost circulation while drilling is common.

Similarly, no correlation has been found between the casing problems and distance from major faults. However, it is possible that small-scale, undetected faults or fractures may be involved with casing problems; unfortunately, data to evaluate this possibility do not exist.

Aliso Canyon Casing Problem Wells by Faultblock

	OV OSST 1	OV YSST 2	ST YSST 3	FREW FB 4	L OSST 5
1	FF-34	P26C_RD	F-3_RD	F-3_RD	FF33_RD
2	P-19	P-50A	FF-33	F-9	FF-34
3	P-60	SS4-0	FF34A_RD	SF-1	FF-34A
4	SS-5	SS7_RD	MA-3	SF-2	
5	SS14_RD	SS-25A	P25_DPN	SS4-0	
6		SS-25B	P-26C	SS-4A	
7			P-26D	SS10_RD	
8			P-32	SS11_RD	
9			P-35	SS12_RD4	
10			P-38		
11			P-43		
12			P-44		
13			P47_RD		
14			P-69A		
15			SS4-0		
16			SS-4A		
17			SS12_RD4		
18			SS-19		
19			SS-25B		
20			SS-44		
21			W-3		
Total:	5	6	21	9	3

Well Casing Problems by Formation

Formation/Zone	Wells by Casing Problem Incident *										Totals	# Wells
Modelo	FF-34	FF-34	FF-34A	P-19	P-19	P-60	P-60	P-60	SS14_RD	SS14_RD	10	5
Topanga	FF33_RD	SS-5	SS14_RD								3	3
Pico	P-26C_RD	P-50A	P-50A	SS4-0	SS7_RD	SS7_RD	SS12_RD4	SS-25A	SS-25A	SS-25B	10	7
Pico ST	P-35	P-38	P-43	P-44	SF-1	SS11_RD	SS-19	SS-44	SS-44		9	8
Aliso A-1	P-32										1	1
Aliso A-36	P26C	P-69A									2	2
Lower Porter	P25_DPN	P25_DPN									2	1
UD Aliso 1	FF-33										1	1
UD Aliso 2	P25_DPN	P25_DPN	P-26C	SS4-0	SS-25B						5	4
MD Aliso	P25_DPN	P-69A									2	2
LD Aliso	P47_RD	P-69A	P-69A	SS-4A	W-3						5	4
Sesnon Cap Rock	F-3-RD	F-3-RD	FF34A_RD	MA-3	P25_DPN	P25_DPN	P25_DPN	P25_DPN	P47_RD	SS12_RD4	10	6
Sesnon 1	P-69A										1	1
Sesnon 6	P-26D										1	1
Sesnon 8	P-69A										1	1
Sesnon 14	P25_DPN										1	1
Eoc-Plio Undiff	F-3_RD	F-3_RD	F-9	SF-2	SS4-0	SS-4A					6	5
Cret 3	SS10_RD										1	1

** Some wells have multiple incidents of casing problems in the same formation* Total # of incidents: 71

No casing problems were found in the Basalt, U Porter, Sesnon 2, 4, 10, 12, 14, Cret 1, 2, 4 ,5

Figure 34: Casing Failure Wells by Fault Block, Formation, and Zone

7 Groundwater Geology

7.1 Principal Findings

Principal findings related to groundwater are:

- Groundwater that entered the TH-1 (RBMW-1) borehole while drilling is associated with faults.
- No apparent relationship of the presence of groundwater could be established between log porosity, permeability, mobile water, or lithology in the RBMW-1 (TH-1) borehole geophysical logs.
- Groundwater entered the TH-1 borehole at depths of 382 ft and 555 ft (sustained fluid level). Both of these depths are associated with faults that have dragging zones. Groundwater encountered at 555 ft was not controlled during the duration of drilling to TD, so lower fault zones could not be evaluated for groundwater potential.
- Two additional closely spaced faults at 980 ft and 1,000 ft, identified in the RBMW-1 (TH-1) have clear drag zones. Both are in the Lower Topanga below the basalt in a cluster of four faults. There may be groundwater associated with these faults.
- Nine faults were identified in the RBMW-1 (TH-1) borehole. This is a significant number of faults considering the shallow well depth (1,110 ft).
- The shallow section penetrated by the RBMW-1 (TH-1) is extremely shattered. The amount of microfaults (sheared fractures) observed was dense in the penetrated 1,110 ft TD. Microfaults are defined by Schlumberger borehole geologists as having less than 1 ft of throw. Determination of all of structural elements in the FMI run on the TH-1 was visually determined by trained borehole geoscientists at Schlumberger.
- The basalt appears to be a barrier in the RBMW-1 (TH-1). It has the most resistive (non-conductive) fractures.
- Shallow groundwater compositions were found to be different between the Modelo and Topanga samples. The groundwater appears to have a relationship with the changes in the formation minerology between the Modelo and Topanga. Modelo waters are calcium-rich, which is consistent with the predominant calcite-silica (opal and opal CT)-clay-quartz mineralogy found in the section. The Topanga groundwater is sodium-rich, which is consistent with the formation sodium feldspar (plagioclase)-orthoclase-quartz-clay mineralogy.

7.2 Influencing and Characterizing Geologic Elements

The nature and distribution of groundwater at Aliso Canyon Field is influenced or characterized by a variety of geologic processes or character:

- Severe structural deformation (thrusting, faulting, shear fracturing, joints, folding) resulting from regional compressional forces
- Significant overburden unloading of overlying stratigraphy. Thousands of feet of overburden section are absent. Bedding plane joints at Aliso Canyon have been calcite-filled in the upper 200 ft; below this depth, it is unknown. Open joints provide for fluid migration (Figure 35).

- Unconsolidated nature of the lithology: porous and permeable sediments
- Mechanical and chemical weathering processes
- Limited annual rainfall in the area
- Steep, deeply eroded terrain of the area, which redirects slope runoff

Figure 35: Shear Fracturing and Overburden Unloading along Bedding Planes in B-1 Borehole Core

7.3 Boreholes Drilled for Groundwater Data Collection and Analysis

Attention to evaluating the groundwater at Aliso Canyon was initiated when the Aliso Canyon RCA project identified corrosion on the outside of the 11 3/4 in. surface casing and the 7 in. production string. The RCA project commenced a study of the groundwater and associated geology to evaluate groundwater as a possible source of water for the corrosion.

Prior to the RCA project, not much information was available regarding the presence or geologic controls on groundwater at Aliso Canyon Field. As with many oil and gas fields, the overlying stratigraphy above hydrocarbon productive zones, especially unproductive shallow, near-surface formations, received little attention. In development drilling programs, after drilling a few wells, a set interval, generally in the hundreds of feet, is chosen to cover potential lost circulation zones encountered near surface. This is followed by determination of the depth of surface casing installation; hence, once a standard practice is determined, the shallow stratigraphic section generally is not considered again unless there are issues.

Two shallow boreholes, the RBMW-1 (TH-1) and RBMW-2, were drilled to approximately 1,100 ft and 450 ft TD, respectively, to investigate the shallow groundwater and the associated geology. These wells were drilled from the SS-9 well pad, located about 600 ft south of the SS-25 well site. This site was chosen as an area unaffected by the SS-25 incident and because of the limited access to the SS-25 well site. Both boreholes were later converted to groundwater monitoring wells. Both boreholes encountered groundwater.

For this evaluation, geophysical logs run on the RBMW-1 (TH-1), which had two encounters of groundwater in the borehole, were integrated into a composite log and evaluated to better understand the geologic controls on groundwater in the vicinity of SS-25. The primary geophysical log sets include Schlumberger Litho Scanner utilized to provide the mineralogy, rock and fluid volumes of the formations (Modelo and Topanga, including the Topanga Basalt), FMI to provide structural information on bedding, faulting, fractures, property information and the NMR data for mobile water and property information.

The RBMW-1 (TH-1) encountered groundwater at 382 ft, and later the water rose to a level of 325 ft. The second occurrence of groundwater was at 555 ft. At 555 ft there were hole stability issues, and after addressing the hole stability problems, drilling continued with complete loss of circulation; hence, additional groundwater-bearing zones could not be detected during the drilling to TD at 1,110 ft.

7.4 TH-1 – Geophysical Composite Log Analysis

A composite log was created from key log curves selected from the Litho Scanner, FMI and NMR log suites to integrate the mineralogy , rock, and fluid properties and fault, shear fracture (microfault) type and direction with the two groundwater occurrences identified during the drilling of the RBMW-1 (TH-1) borehole (Figure 37). Log curve track information is provided in Figure 36. The composite log was used to help determine the geologic controls on the presence of groundwater.

It should be noted that mobile water from the NMR for the entire well is low, predominantly less than 10% volume.

The two groundwater occurrences at 382 ft and 555 ft were studied to assess the geologic controls on their presence. The two groundwater occurrences were evaluated first for relationships:

1. The groundwater at 382 ft is located in the Modelo formation in a dominantly porcellanite (chert) section, with essentially no porosity, but has some water permeability and mobile water associated with the depth and adjacent footages. A fault was identified with dragging zones above and below the fault; the fault is low dip angle, approximately 15°. Shear fractures and conductive lithology fractures are associated with the dragging zones (Figure 37). Faulting is responsible for groundwater at this depth.
2. The groundwater at 555 ft is located in the lower Modelo in an interbedded siltstone and clay section. It has porosity but only two small thin low water permeability intervals with low mobile water. For an interval that continued to be a lost circulation zone throughout the remaining drilling of the well, the property information on the low side does not fit. A fault is present at 545 ft with thick (approximately 100 ft) upper and lower dragging zones. It is a near-vertical fault with a dip angle of 80°. A dense cluster of shear fractures are associated with the fault (Figure 37). Faulting is a more plausible explanation for the presence of groundwater at this depth. Figure 38 is a larger FMI display of the fault associated with the groundwater at 555 ft. The fault is circled in pink with black angled lines showing the increasing/decreasing bedding dip angle in the upper and lower dragging zones. Bed dips are found in the fifth track and are colored green. Undisturbed Modelo beds dip 14°; the dragging zone beds dip from 14–70°. This fault has the largest displacement of any of the nine faults found in the borehole.

Property and shear fracture information above the 555 ft interval was compared with sections without groundwater. However, some of these “dry” intervals had better water permeability and mobile water. Therefore, a relationship could not be established.

The two occurrences of groundwater encountered in the RBMW-1 (TH-1) were in fault zones with upper and lower dragging zones. It was determined that groundwater was associated with the faulting. It is quite common to have groundwater associated with faulting.

There are nine faults identified on the FMI fracture fault orientation track, circled in pink on Figure 37. Correspondence with three Houston Schlumberger borehole geologists on the method of FMI fault, microfault, and fracture determination was clarifying. Classifying the different structural and bedding, scour features on the FMI is done visually by the borehole geologists. Those classified as faults show more significant observable displacement in the image section and are associated with deformed bedding, fault breccia and fault gouge. Conversely, those classified as microfaults typically have negligible structural deformation and very minor displacement.

The remaining seven faults were reviewed for groundwater potential:

- There was no occurrence of groundwater while drilling in the two shallowest faults at 165 ft and 235 ft. These are very shallow depths; the weathering profile for this area is 200–300 ft.
- The fault at 735 ft observed bedding angles did not suggest any fault dragging zones, and there were few conductive shear fractures (microfractures) adjacent to the fault; it did not have the characteristics defined from the two groundwater intervals encountered. It appears it is a smaller fault with minor displacement.
- The fault at 980 ft bedding planes did not display an appreciable dragging zone, but was in a cluster of conductive shear fractures (microfaults). It does not meet the same criteria as found in the 382 ft and 55 ft groundwater occurrence faults.
- The remaining four faults occur in a cluster below the base of the basalt in the Lower Topanga. They are at depths of 980 ft, 1,000 ft, 1,040 ft, and 1,060 ft. The upper faults at 980 ft with a near-vertical dip angle of 80° and the lower dip angle fault at 1,000 ft have dragging zones above and below. A number of conductive shear zone (microfaults) are associated with the two faults. The faults at 980 ft and 1,000 ft appear like they are good candidates for groundwater presence. The other two faults may be smaller contributors.

Feldspar alteration to kaolinite was observed in the mud log below the basalt in the Porter 39A (P-39A) relief well. The kaolinitic section is 40 ft thick. Fresh water is required for the alteration; the thickness suggests that a significant amount of water has flowed through this section for some time. The basalt may be a vertical barrier. The faulted section below the basalt in the TH-1 (RBMW-1) may have similarities with the Porter 39A section (Figure 39).

Data collected by the FMI geophysical log are the first clear evidence seen to date in the shallow subsurface of the degree of deformation that compressional forces imposed on the formations in the OSST overthrusted section in Aliso Canyon.

In particular, the structural detection and directional information collected on faults, microfaults, conductive and resistive fracturing, and bed boundaries reveal the scale of just how finely shattered and sheared and faulted the Modelo and Topanga formations are. Surface outcrops reveal significant deformational features but hide the presence and frequency of smaller scaled structural information due to significant weathering processes/features, erosional surfaces, landslides, vegetation, and soil cover.

Smaller scale deformation (faults/fractures) down to the micro-level was expected in the subsurface overthrusted section of the Aliso Canyon Field area due to the long-term effects of compressional deformation, which displaced the Modelo and Topanga and sections of the Pico up to 3–18 miles from the north with vertical displacement estimated from 5,000 ft to 8,000 ft. However, there was no available

data to determine the degree and extent of that deformation. The RCA study collected and integrated subsurface log information and identified a groundwater relationship to the faults.

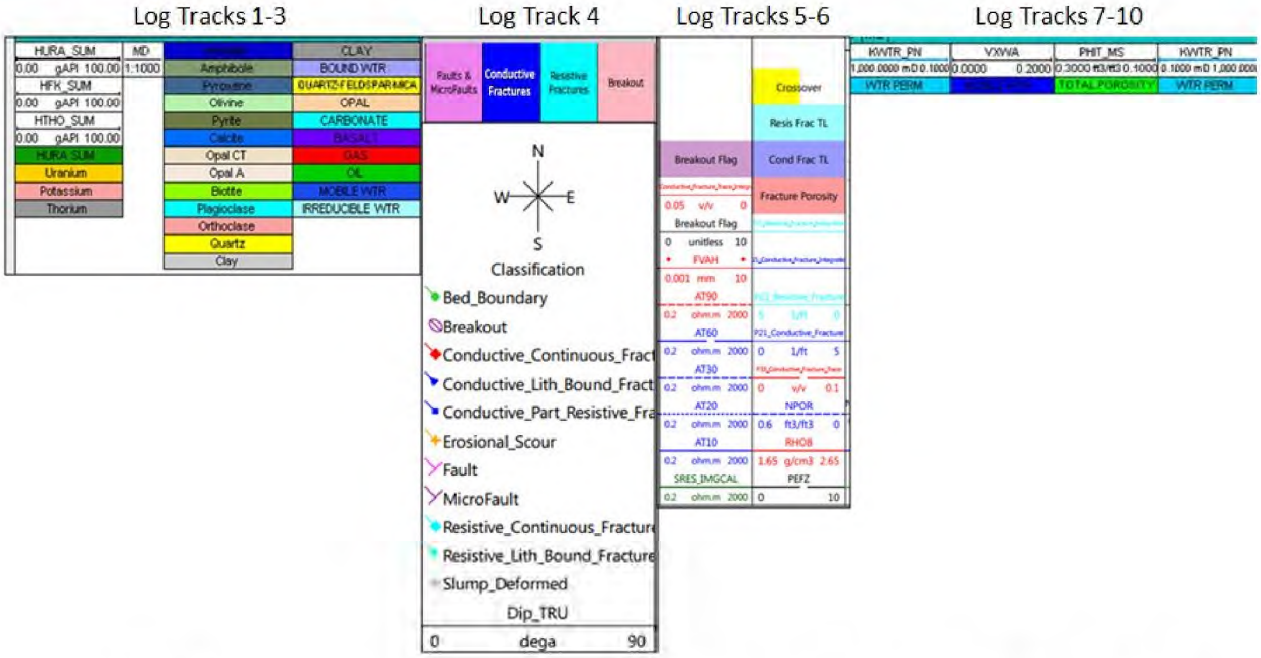

Figure 36: Composite Log Geophysical Log Track Information for RBMW-1 (TH-1) in Figure 37

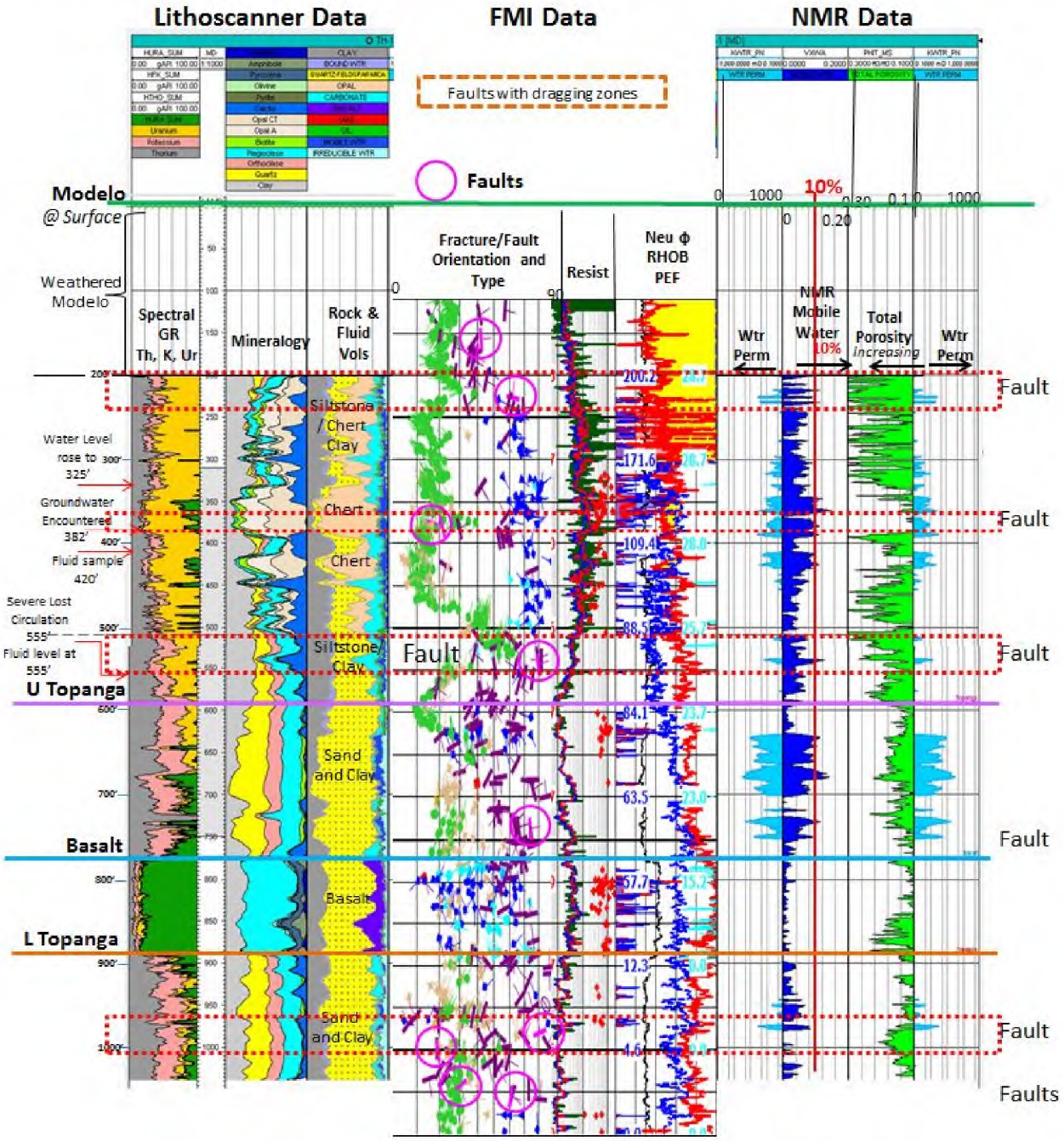

Figure 37: Composite Geophysical Log for Borehole TH-1 (RBMW-1)

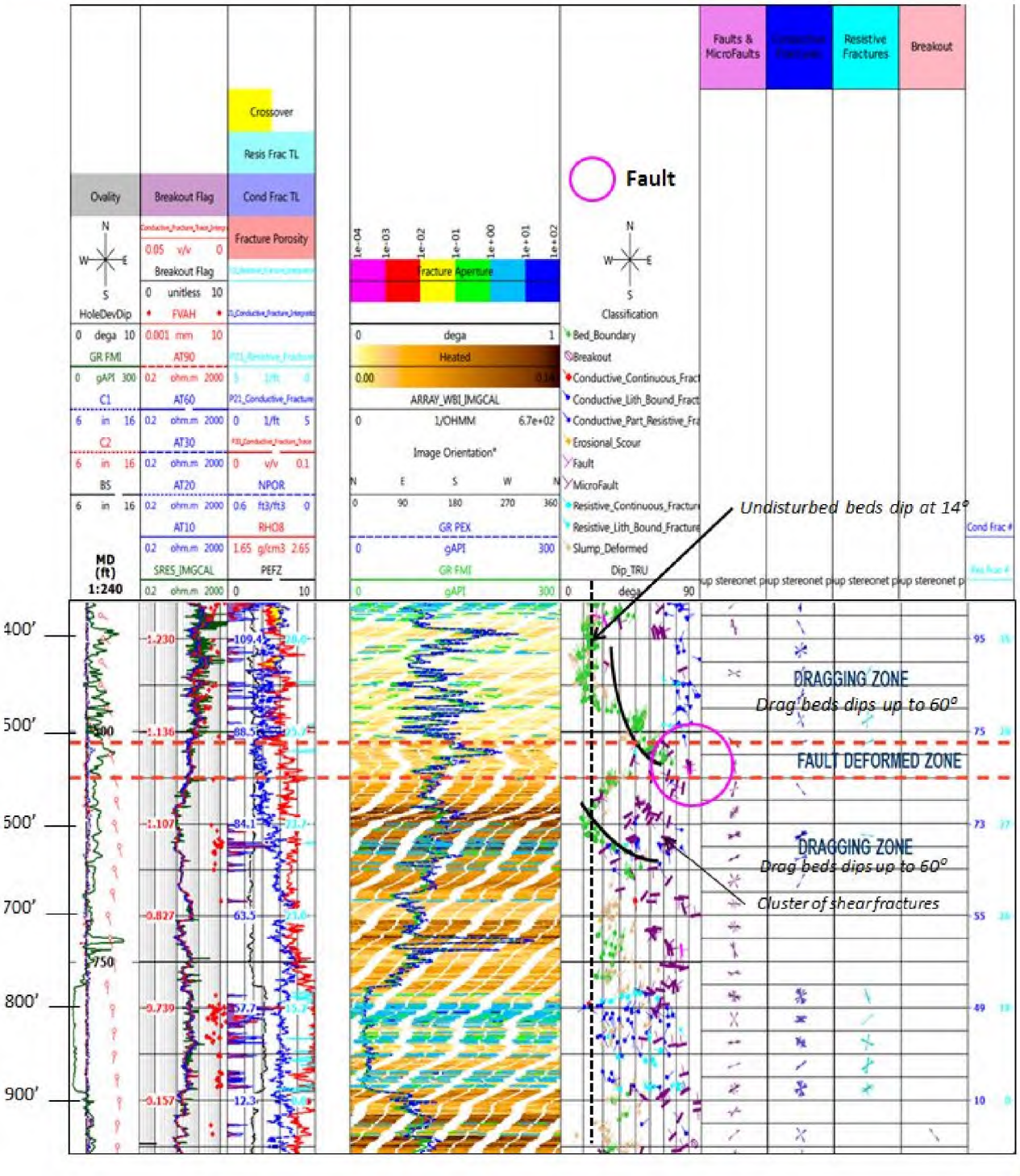

Figure 38: Detail of Fault and Dragging Zones from TH-1 FMI Log

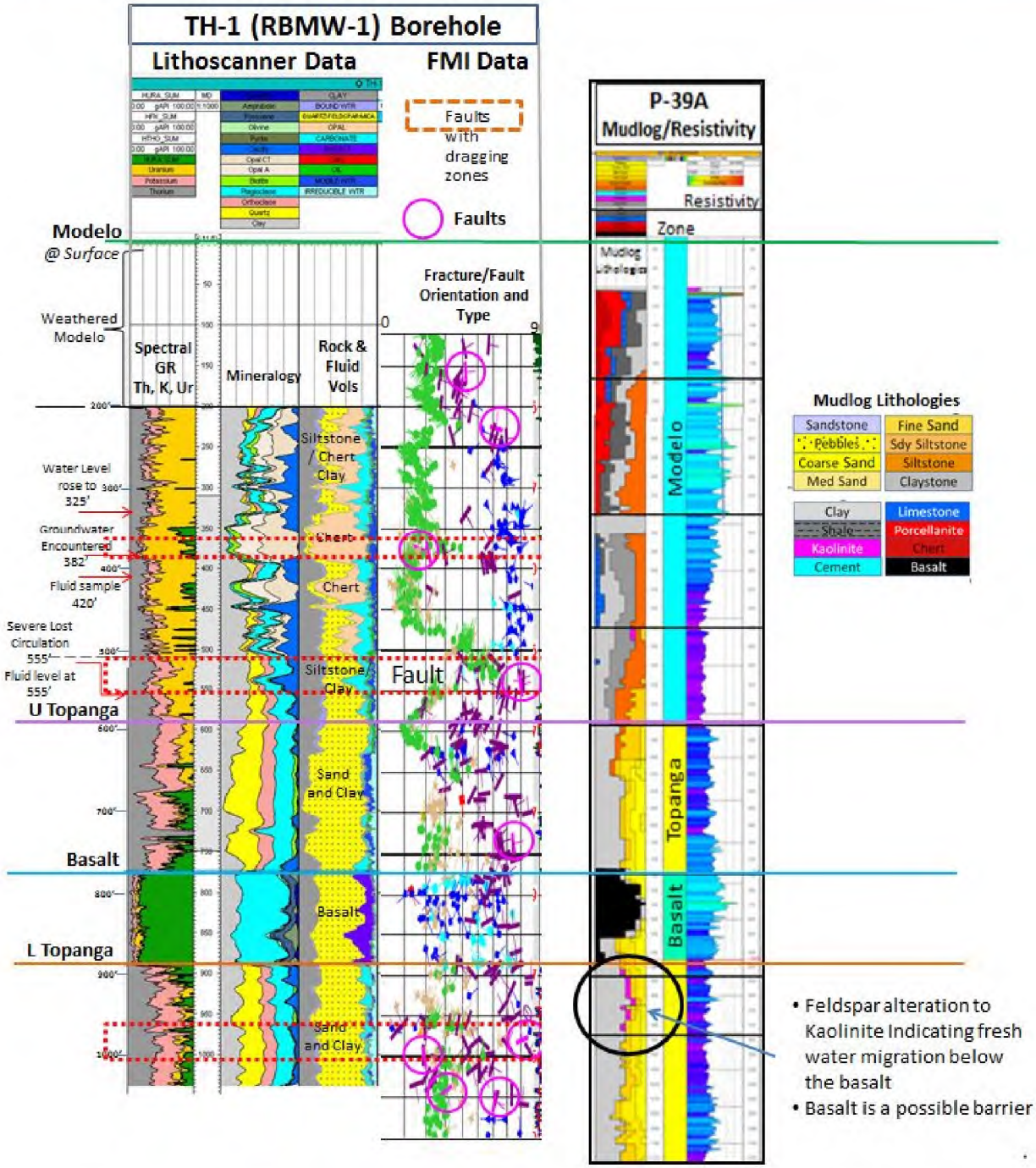

Figure 39: TH-1 Geophysical Logs Compared to the Porter 39A Relief Well Mudlog

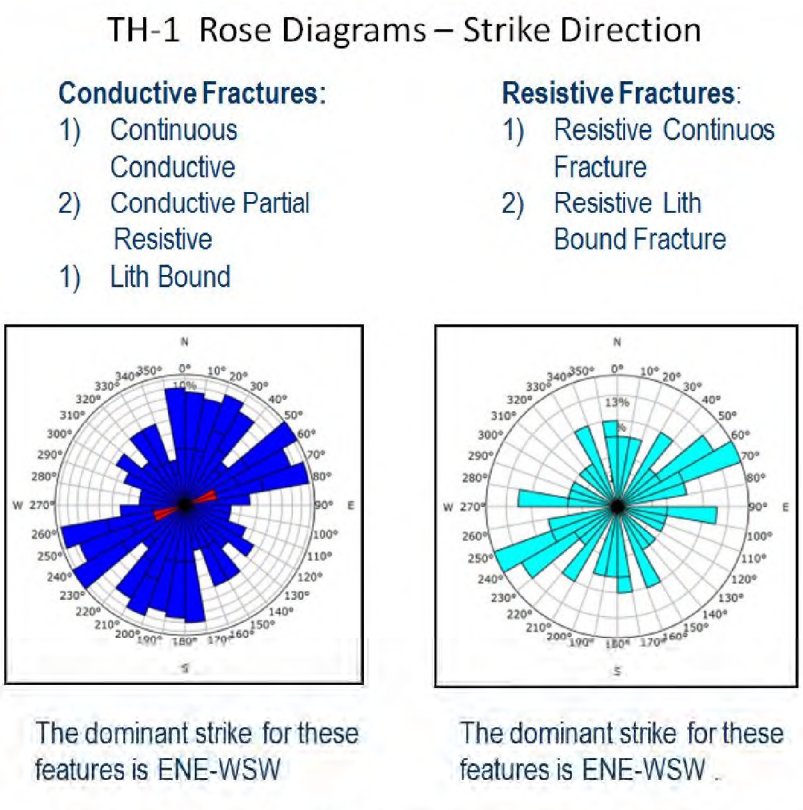

Figure 40: FMI - Strike Direction Rose Diagrams for the TH-1 Borehole

Rose diagrams show the strong ENE–WSW strike direction for the conductive and resistive fractures in the RBMW-1 (TH-1) borehole (Figure 40).

7.4.1 Learning Implications for SS-25

The groundwater encountered at lost circulation zones at 381 ft and 555 ft in RBMW-1 (TH-1) boreholes were found to be associated with faulting and conductive shear fractures, as shown from the evidence in the FMI fracture fault orientation and type analysis, and drilling records.

From drilling records, it was determined that lost circulation zones encountered while drilling SS-25 occurred in the Modelo at 169 ft, and in the Topanga at 770 ft just above the basalt and at 990 ft just below the basalt. Applying the learnings of RBMW-1 (TH-1), it is suspected that the lost circulation zones in SS-25 are also associated with faults and conductive shear fractures.

Corrosion caused the 7 in. casing rupture in SS-25 at 892 ft, between the two lost circulation zones at 770 ft and 990 ft. The 11 3/4 in. casing shoe was set at 990 ft at the deeper Topanga lost circulation zone. Corrosion of the 11 3/4 in. casing occurred 95–382 ft, so the lost circulation zone at 169 ft is located between the upper and lower limits of the corrosion.

7.5 Groundwater Composition Compared to Formation Mineralogy

Figure 41 compares the groundwater composition of samples taken from the RBMW-1 (TH-1) and RBMW-2 groundwater monitoring wells to the mineralogy of the formations from which they were sampled (i.e., Modelo and Topanga). The Upper Modelo groundwater is calcium-rich, while the Topanga groundwater is sodium-rich.

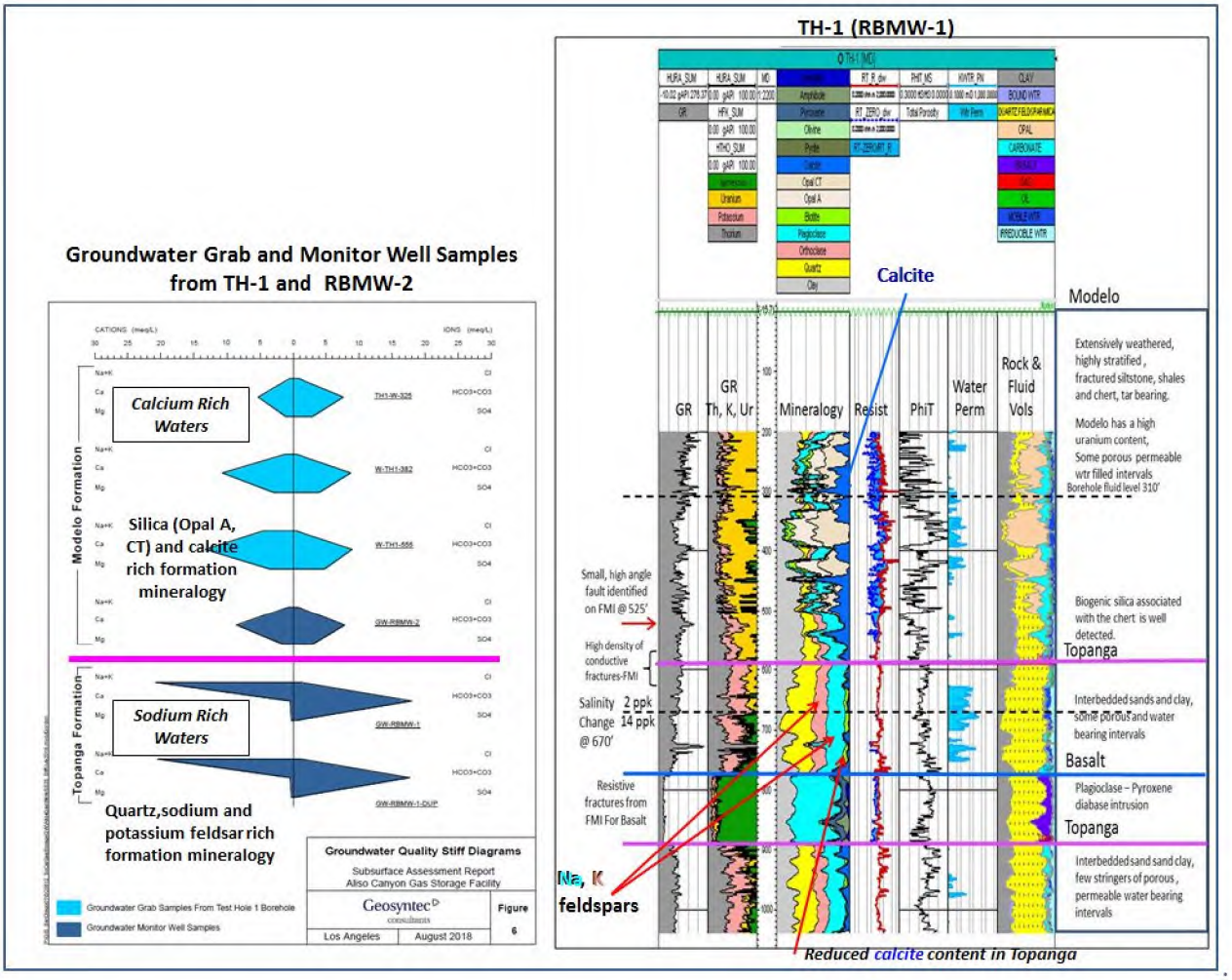

Figure 41: Groundwater and Grab Sample Composition versus Formation Mineralogy

When comparing the calcium-rich groundwater of the Modelo with the formation mineralogy, it is consistent with the calcite that is present almost throughout the entire Modelo section. The Modelo mineralogy is predominantly silica (Opal A, Opal CT), calcite-clay, which represents the lithology changes from the underlying Topanga.

The sodium-rich groundwater of the Topanga also is consistent with the formation's mineralogy. The Topanga mineralogy includes quartz, sodium, and potassium feldspar and clay.

7.6 Groundwater Geologic Conceptual Model

A west to east conceptual model (Figure 42) was constructed to represent the many possibilities of precipitation pathways to the subsurface in the extensively complex faulted and fractured Modelo and Topanga formations at Aliso Canyon. The rainwater pathways appear to be many from direction percolation into the Modelo, or outcrop charge, or along faults, or a combination of fault to fault to formation. It is impossible to predict the pathways. The upper portion of the figure is an east to west satellite image of the Aliso Canyon Field located on the southern slopes of the Santa Susana Mountains. Yellow dashed lines represent runoff from slopes into the white dashed drainage areas. Topography on

the surface, as well as the structural deformation and lithologic differences in the subsurface, contribute to the subsurface presence of groundwater complexity.

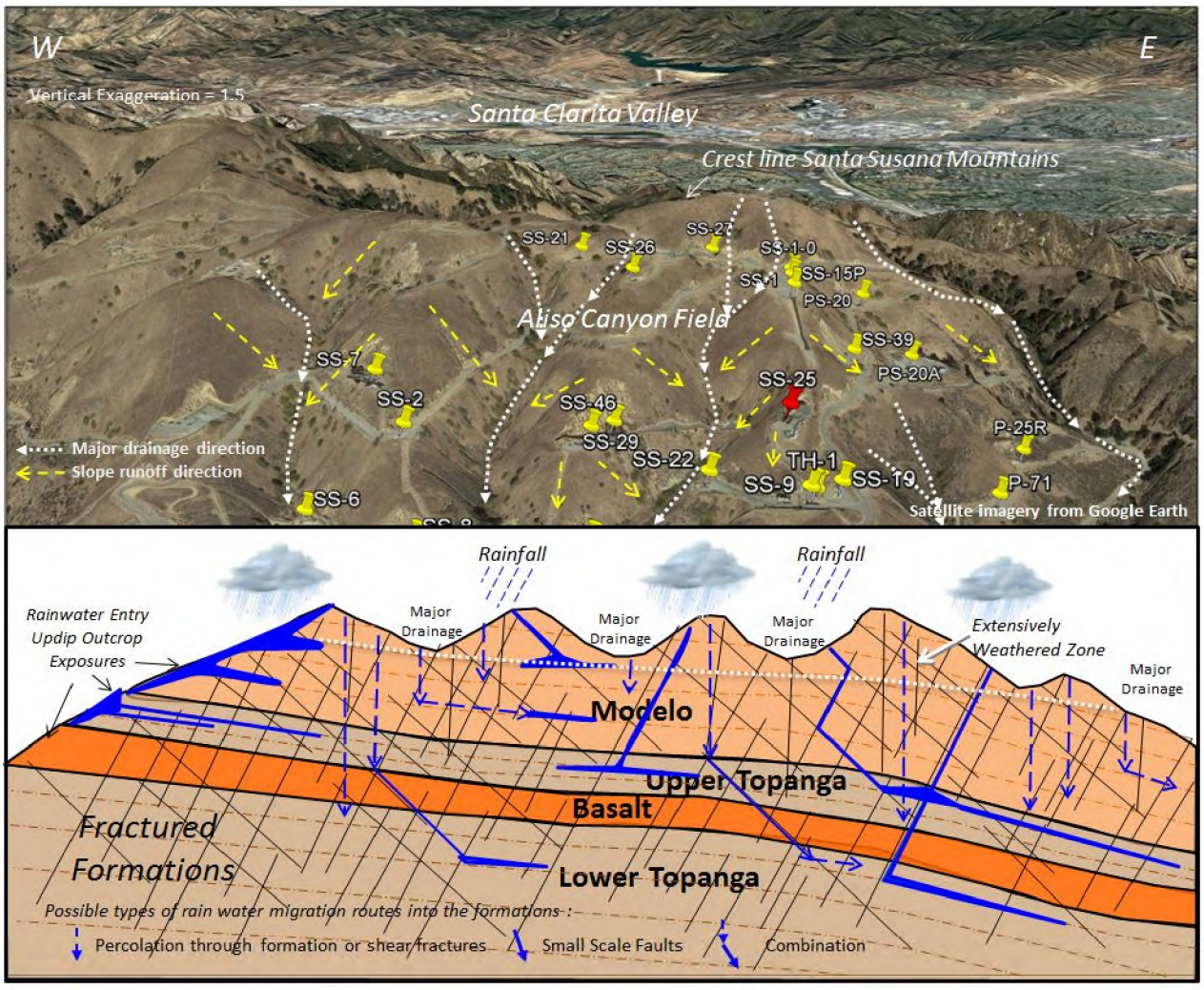

Figure 42: Conceptual Groundwater Model

8 References

[1] K. Lant, Structure of the Aliso Canyon Area, Eastern Ventura Basin, Athens, OH: Master's Thesis, Ohio University, 1977.

[2] C. Wentworth and R. Yerkes, Geologic Setting and Activity in the San Fernando Area, California (USGS Professional Paper 733), U.S. Geological Survey, 1971.

[3] J. Savage, W. H. Prescott, M. Lisowski and N. E. King, "Strain in Southern California-Measured uniaxial north-south regional contraction," *Science,* vol. 202, pp. 883-885, 1978.

[4] W. Thatcher, "Crustal deformation studies and earthquake prediction research," in *Earthquake Prediction, an international review*, Washington, D.C., American Geophysical Union, 1981, pp. 394-410.

[5] D. Morton and R. Yerkes, Recent Reverse Faulting in the Transverse Ranges, California-Introduction (USGS Professional Paper 1339), U.S. Geological Survey, 1987.

[6] T. Dibblee, Geologic Map of the Oat Mountain and Canoga Park (North 1/2) Quadrangles, Los Angeles County, California. 1:2400, Map DF-36, 1992.

[7] M. Petersen and S. Wesnousky, "Fault slip rates and earthquake histories for active faults in southern California," *Bulletin of the Seismological Society of America,* Vols. 84, No. 5, pp. 1608-1649, 1994.

[8] R. Yeats, "Neogene Tectonics of the east Ventura and San Fernando basins, California: an overview," *Pacific Section American Association of Petroleum Geologists, Guidebook 77,* pp. 9-36, 2001.

[9] U.S. Geologic Survey, "Quaternary Fault and Fold Database of the United States, Sierra Madre fault zone, Santa Susana section (Class A) No. 105a," 01 Jun 2000. [Online]. Available: https://earthquake.usgs.gov/cfusion/qfault/show_report_AB_archive.cfm?fault_id=105&section_id=a. [Accessed 21 Feb 2019].

[10] Southern California Earthquake Data Center, "Significant Earthquakes and Faults, Santa Susana Fault Zone," [Online]. Available: http://scedc.caltech.edu/significant/santasusana.html. [Accessed 21 Feb 2019].

[11] U.S. Geological Survey, "UCERF3: USGS Third Uniform California Earthquake Rupture Forecast," 2015. [Online]. Available: http://pubs.usgs.gov/of/2013/1165/data/ofr2013-1165_FaultSectionData.xlsx.

[12] J. Hazzard, "Some features of Santa Susana Thrust, vicinity of the Aliso Canyon Field, Los Angeles County, California (abstract)," *American Association of Petroleum Geologist Bulletin,* vol. 28, no. 12, pp. 1780-1781, 1944.

[13] W. Ingram, "Aliso Canyon Oil Field," *Summary of Operations - California Oil Fields,* vol. 45, no. 1, pp. 64-73, 1959.

[14] J. Evans and R. Miller, Geology of the southwestern part of the Oat Mountain Quadrangle, Los Angeles County, California, California Division of Mines and Geology, 1978.

[15] E. Winterer and D. Durham, Geology of Southeastern Ventura Basin, Los Angeles County California (USGS Professional Paper 334-H), U.S. Geological Survey, 1962, pp. 275-366.

[16] R. Saul, "Geology of the southeast slope of the Santa Susana Mountains and geologic effects of the San Fernando earthquake," in *San Fernando, earthquake of 9 February 1971: California*

Division of Mines and Geology Bulletin 196, 1975, pp. 53-70.

[17] R. Yeats, Late Cenezoic structure of the Santa Susana fault zone in Recent Reverse Faulting in the Transverse Ranges (USGS Professional Paper 1339), U.S. Geological Survey, 1987, pp. 1-5.

[18] R. Yerkes and R. Campbell, "Preliminary Geologic Map of the Oat Mountain 7.5' Quadrangle, Southern California," *USGS Open-File Report OF-93-525,* p. 1 plate, 1993.

[19] J. Evans and R. Miller, Geologic Map and Sections of the Southwestern Part of the Oat Mountain Quadrangle, Los Angeles County, California Map Sheet 33, California Division of Mines and Geology, 1978, p. 1 Plate.

Appendix A Shallow Subsurface Geophysical Investigation Report

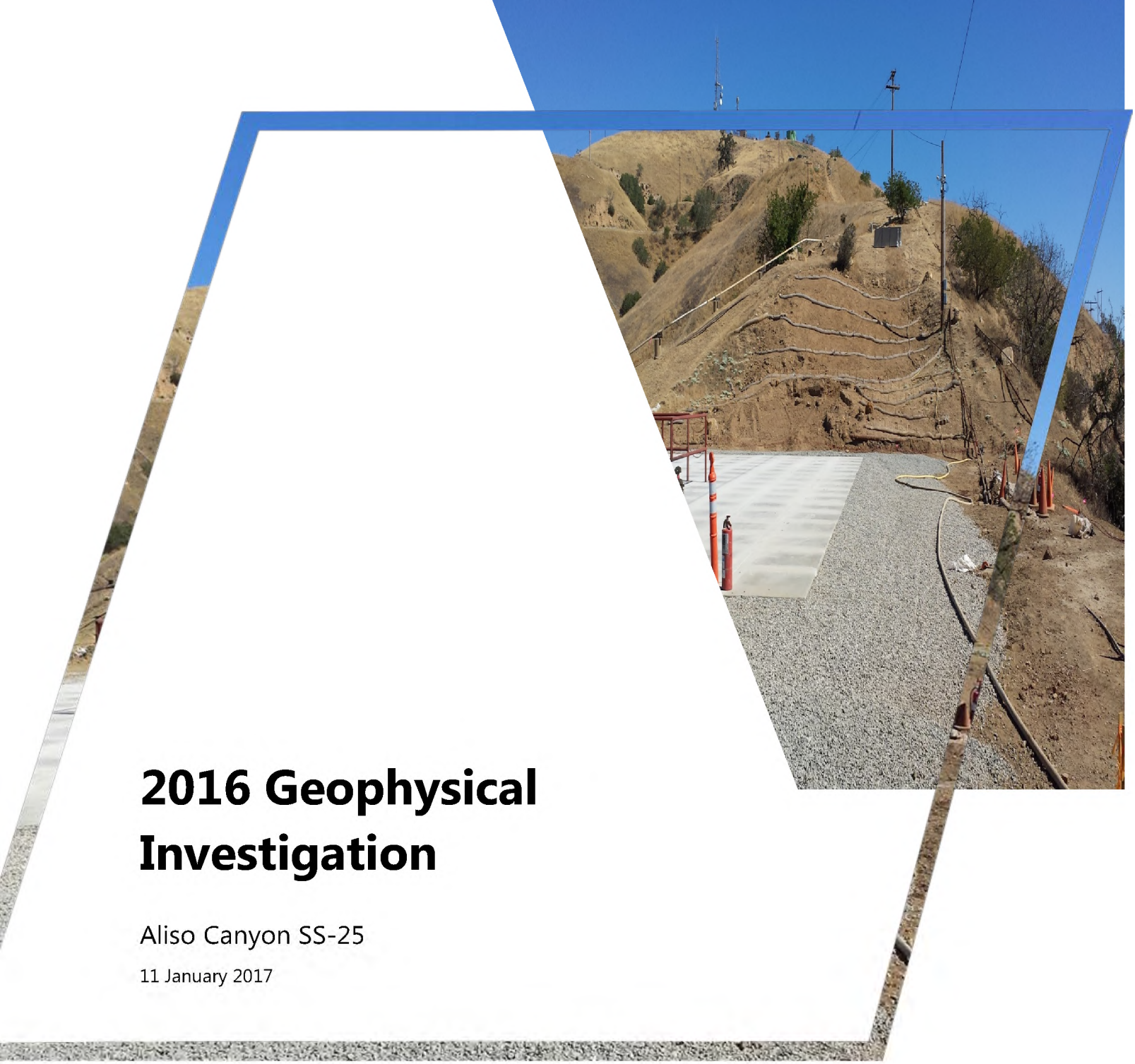

2016 Geophysical Investigation

Aliso Canyon SS-25

11 January 2017

151 Canada Olympic Rd SW
Calgary AB T3B 6B7
Canada

407074-00748-200-GP-REP-0001

Disclaimer

The information presented in this document was compiled and interpreted exclusively for the purposes stated in Section 1 of the document. WorleyParsons provided this report for Southern California Gas Company solely for the purpose noted above.

WorleyParsons has exercised reasonable skill, care, and diligence to assess the information acquired during the preparation of this report, but makes no guarantees or warranties as to the accuracy or completeness of this information. The information contained in this report is based upon, and limited by, the circumstances and conditions acknowledged herein, and upon information available at the time of its preparation. The information provided by others is believed to be accurate but cannot be guaranteed.

WorleyParsons does not accept any responsibility for the use of this report for any purpose other than that stated in Section 1 and does not accept responsibility to any third party for the use in whole or in part of the contents of this report. Any alternative use, including that by a third party, or any reliance on, or decisions based on this document, is the responsibility of the alternative user or third party.

Any questions concerning the information or its interpretation should be directed to Alastair McClymont or Paul Bauman.

Investigation: Aliso Canyon SS-25

Rev	Description	Author	Review	Advisian Approval	Date
0	Issued as Final	A. M. A. McClymont	P. Bauman/ R. Beck	A. M. A. McClymont	11-Jan-17

Table of Contents

Executive Summary vii

1 Introduction 1

1.1 Background 1

1.2 Geophysical Survey Objectives 1

2 Field Geophysical Investigation 2

2.1 Positional Control 4

2.2 Electrical Resistivity Tomography (ERT) Survey 4

2.3 Seismic Reflection and Refraction Survey 5

2.4 Multichannel Analysis of Surface Waves (MASW) Survey 6

2.5 Surface-Based Nuclear Magnetic Resonance (NMR) Survey 6

2.6 Ground-Penetrating Radar (GPR) Survey 7

2.7 Borehole Geophysical Logging Survey 7

3 Results and Interpretation 8

3.1 ERT Survey 8

3.1.1 4.92 Feet (1.5 M) ERT Lines (1A, 2A, 3A, 4A, and 5A) 9

3.1.2 16.4 Feet (5 M) ERT Lines (1B, 2B, 3B, 4B, 5B, and 6B) 9

3.1.3 32.8 feet (10 M) ERT Lines (1C and 2C) 12

3.1.4 22.5 M ERT Lines (1D and 2D) 13

3.2 Seismic Reflection and Refraction Survey 13

3.2.1 Seismic Line 1 14

3.2.2 Seismic Line 2 and Seismic Line 3 14

3.3 MASW Survey 15

3.4 Borehole Geophysical Logging Results 15
4 Conclusions 19
5 Closure 20
6 References 21

Tables within Text

Table A Individual line parameters for the ERT survey 2
Table B Individual line parameters for the seismic survey 3
Table C Geotechnical borehole locations 15
Table D Intervals logged by each geophysical tool (in feet) 16

Figures within Text

Figure A Zoomed In Sections of ERT Line 2b (Left) and ERT Line 4b (Right) Showing Low-Resistivity (Dark Blue) Zones under the SS-25 Well Pad 10
Figure B Zoomed in Sections of ERT Line 1B (left) and ERT Line 5B (right), Showing High-Resistivity (Pink) Zones under the SS-25 Well Pad 11
Figure C Polar Projection Plot of All Bedding Orientations 17
Figure D Polar Projection Plot of All Fracture and Joint Orientations 17

Figures

Figure 1 Site Location Map
Figure 2 ERT Basemap – 4.92 feet (1.5 m) and 16.4 feet (5 m) Minimum Electrode Spacing

Figure 3	ERT Basemap – 32.8 feet (10 m) and 73.8 feet (22.5 m) Minimum Electrode Spacing
Figure 4	Seismic Basemap
Figure 5	SS-25 Basemap with NMR and Geotechnical Borehole Locations
Figure 6A	3D View: 4.92 feet (1.5 m) ERT Lines – Color Scale 10 ohm-m to 100 ohm-m
Figure 6B	3D View: 4.92 feet (1.5 m) ERT Lines - Color Scale 100 ohm-m to 1000 ohm-m
Figure 7	Line: ERT-1A (4.92 feet [1.5 m]) – Electrical Resistivity Cross-Section
Figure 8	Line: ERT-2A (4.92 feet [1.5 m]) – Electrical Resistivity Cross-Section
Figure 9	Line: ERT-3A (4.92 feet [1.5 m]) – Electrical Resistivity Cross-Section
Figure 10	Line: ERT-4A (4.92 feet [1.5 m]) – Electrical Resistivity Cross-Section
Figure 11	Line: ERT-5A (4.92 feet [1.5 m]) – Electrical Resistivity Cross-Section
Figure 12A	3D View: 16.4 feet (5 m) ERT Lines – Color Scale 10 ohm-m to 100 ohm-m
Figure 12B	3D View: 16.4 feet (5 m) ERT Lines – Color Scale 100 ohm-m to 1000 ohm-m
Figure 13	Line: ERT-1B (16.4 feet [5 m]) – Electrical Resistivity Cross-Section
Figure 14	Line: ERT-2B (16.4 feet [5 m]) – Electrical Resistivity Cross-Section
Figure 15	Line: ERT-3B (16.4 feet [5 m]) – Electrical Resistivity Cross-Section
Figure 16	Line: ERT-4B (16.4 feet [5 m]) – Electrical Resistivity Cross-Section
Figure 17	Line: ERT-5B (16.4 feet [5 m]) – Electrical Resistivity Cross-Section
Figure 18	Line: ERT-6B (16.4 feet [5 m]) – Electrical Resistivity Cross-Section
Figure 19A	3D View: 32.8 feet (10 m) ERT Lines – Color Scale 10 ohm-m to 100 ohm-m
Figure 19B	3D View: 32.8 feet (10 m) ERT Lines – Color Scale 100 ohm-m to 1000 ohm-m
Figure 20	Line: ERT-1C (32.8 feet [10 m]) – Electrical Resistivity Cross-Section
Figure 21	Line: ERT-2C (32.8 feet [10 m]) – Electrical Resistivity Cross-Section
Figure 22A	3D View: 73.8 feet (22.5 m) ERT Lines – Color Scale 10 ohm-m to 100 ohm-m
Figure 22B	3D View: 73.8 feet (22.5 m) ERT Lines – Color Scale 100 ohm-m to 1000 ohm-m
Figure 23	Line: ERT-1D (73.8 feet [22.5 m]) – Electrical Resistivity Cross-Section

Figure 24 Line: ERT-2D (73.8 feet [22.5 m]) – Electrical Resistivity Cross-Section
Figure 25 Line: Seismic-1 (Reflection) – Seismic Reflection Cross-Section
Figure 26 Line: Seismic-1 (Refraction) – P-Wave Velocity Cross-Section
Figure 27 Line: Seismic-2 – Reflection and P-Map Velocity Cross-Section
Figure 28 Line: Seismic-3 – Reflection and P-Map Velocity Cross-Section
Figure 29 ERT Line 1B, Seismic Line 2, MASW-1 – ERT, Seismic Refraction, MASW

Photographs

Photo 1 SS-25
Photo 2 Collecting ERT Data
Photo 3 Setting up Seismic Line on Steep Slope
Photo 4 Augering Holes for Buffalo Gun on Steep Slopes
Photo 5 Buffalo Gun Shots
Photo 6 Sledgehammer Source Used When Collecting MASW Data
Photo 7 Working on Steep Slopes
Photo 8 Fire Suppression Team

Appendix List

Appendix 1: Geophysical Methodologies
Appendix 2: Surface-Based and Borehole NMR Survey Results
Appendix 3: Geophysical Borehole Logs
Appendix 4: ERT Conductivity Cross-Sections
Appendix 5: Existing Lithological and Geophysical Logs Provided by Blade Energy

Executive Summary

As part of a forensic investigation of the SS-25 gas storage well methane leak, WorleyParsons Canada Services Ltd., operating as Advisian, carried out surface and borehole geophysical investigations. Surface geophysical investigations included electrical resistivity tomography (ERT), seismic refraction, seismic reflection, multi-channel analysis of surface waves (MASW), ground penetrating radar (GPR), and nuclear magnetic resonance (NMR). Borehole logging services included natural gamma, induction conductivity, optical televiewer, NMR, temperature, and fluid conductivity. The objective of the geophysical surveys was to map structures and physical properties, beneath the SS-25 well pad.

Site conditions were very challenging for all surface geophysical investigation methods. Extreme relief is problematic for data acquisition and processing for all methods. Very soft ground conditions and a thick weathered zone were particularly problematic for seismic reflection data acquisition. Moderately conductive near-surface conditions eliminated any useful depth of investigation from a GPR survey. In addition, induced electrical fields into nearby pipelines overwhelmed the NMR signal, during the surface-based NMR investigation. Nevertheless, significant observations and conclusions from the surface geophysical data have been determined. The maximum depth of investigation of the surface geophysics program was approximately 1,000 feet (305 m), with higher resolution information being limited to the top 200 feet (61 m).

Extensively weathered bedrock is observed to outcrop at the surface and in road cuts surrounding the SS-25 knoll (at depths of ~130' from well surface elevation). Compressional wave (P-wave) seismic refraction velocities of less than 6562 feet per second (f/s; 2000 meters per second [m/s]) indicate that the rock is extensively and ubiquitously weathered to a depth of approximately 200 feet (61 m). Very low P-wave velocities of less than 3281 f/s (1000 m/s) are observed in the top 100 feet (30 m). Below a depth of approximately 200 feet (61 m), bedrock P-wave velocities quickly rise to 8202 f/s (2,500 m/s).

The borehole cuttings log from well P-39A, an offset well to SS-25 integrated with Geosyntec borehole core descriptions and core photos indicates more than 200 feet of extensively weathered and fractured siltstone and claystone with increasing amounts of underlying porcellanite and shale with depth, which supports this velocity layering and the observation of a thick, weathered zone, as determined by seismic refraction. In addition, the MASW section shows very low<656 f/s; (<200 m/s) to low (<1312 f/s; <400 m/s) shear wave (S-wave) velocities to the maximum depth of investigation of 100 feet (30 m). The optical televiewer imagery shows extensive weathering and fracturing, to the maximum depth of logging of almost 115 feet (35 m); weathering is so significant that no distinct bedding is observed until depths below 59 feet (18 m).

ERT identified two zones of anomalously high (>500 ohm-m) resistivity. These zones, one located north of SS-25, and a second zone located in proximity to well SS-9, are tentatively interpreted as being associated with subsurface freezing. The larger zone, north of SS-25, comes to within 50 feet of the surface and appears as a massive, steeply dipping, monolithic feature. Geophysical logs from within geotechnical borehole BH2 confirm that electrical resistivities start to increase dramatically above this interpreted frozen zone, at a depth below 40 feet. The interpretation of this feature being a frozen zone is supported by third party temperature logs and distributed temperature sensing (DTS)

results, the anomalously high resistivities, and the geometry of the features which appears to disregard lithologies and structure.

The ERT results also identified numerous zones of very high (>200 mS/m) conductivity (i.e. low resistivity, <5 ohm-m). These zones have been interpreted as accumulations of high salinity well kill fluid. The geophysical logs from geotechnical borehole BH3, which was located adjacent to one of these zones on ERT line 2B, indicated a notable decrease in resistivities between the depths of 60 and 100 feet, consistent with the location of the observed low-resistivity ERT anomaly. The natural gamma log over the same interval showed no significant variation over the same interval, indicating that the observed resistivity changes are associated with an increased salt concentration and not increasing clay content.

Televiewer results were limited to primarily two boreholes, BH3 and BH4, due to shallow obstructions in the other two boreholes. Specific results below are primarily from the BH3 and BH4 borehole data, which indicate extensive weathering, spalling, and fracturing. Distinct bedding is observed only below a depth of 59 feet (18 m). Fracturing is observed up to a depth of 114 feet (35 m). The general strike of the observed shale beds is north-northwest (329 degrees from true north), with a dip of 31 degrees to the west-southwest (239 degrees). The major observed fracture strike is south-southeast (158 degrees), with a 60 degree dip to the east-northeast (68 degrees). At least four fractures were observed to dip steeply, at angles greater than 70°.

Examination of the core descriptions and photos provided by Geosyntec from the full depth of the two obstructed boreholes shows extensively fractured sections with open, closed and filled fractures throughout. Notably, the core from BH1 has an extensive amount of subvertical fractures. Vertical to subvertical fractures may have acted as vertical pathways for kill fluids in the SS-25 knoll, and these are likely associated with vertically elongated low resistivity zones observed on some of the ERT lines.

Borehole NMR showed no evidence of perched water tables above the maximum depth of logging of about 35 m. However, borehole NMR did indicate significant water contents in the unsaturated zone, generally varying between 10% and 15%, between the ground surface to depths of over 100 feet. However, any fluids introduced during drilling and penetrating the borehole wall may be influencing this value. Indications of small percentages of "mobile" water are likely related to water trapped in dead-ended fractures.

No subsurface fault strands could be identified with confidence from the seismic reflection data or any other data sets. Nevertheless, televiewer data from within the four geotechnical boreholes confirm the presence of numerous fractures, and the seismic refraction data show that the rock mass surrounding the SS-25 well pad is extensively weathered to depths of at least 200 feet (61 m).

1 Introduction

WorleyParsons Canada Services Ltd., operating as Advisian, was retained by the Southern California Gas Company (SoCal) to undertake a geophysical site assessment as part of the Aliso Canyon Root-Cause Analysis. Blade Energy Partners (Blade), on behalf of SoCal, is undertaking a root-cause analysis of a methane leak at the site of gas storage well SS-25. The SS-25 well pad is located within SoCal's Aliso Canyon natural gas storage facility, near Los Angeles, California (the Site; Figure 1). The objective of the geophysical investigation was to provide information on subsurface structures and physical properties that would assist Blade with their investigation.

1.1 Background

At Aliso Canyon natural gas is stored thousands of feet below ground within depleted oil reservoirs. The gas is piped to and from the surface by way of a network of 115 gas storage wells over an area of approximately 2 square miles (SoCal 2016a). On October 23, 2015, a natural gas leak was discovered by SoCal employees in the vicinity of well SS-25. Following initial attempts to stem the leak, temporary control of well SS-25 was achieved on February 11, 2016 (SoCal 2016b).

The Aliso Canyon storage facility resides within the Santa Susana Mountains, within Los Angeles County. The Santa Susana Mountains are bounded to the south by the San Fernando Valley, across the roughly east-west trending Santa Susanna Fault. The geological units underlying the Site are comprised of Cretaceous sediments, overlain by Miocene marine sandstone, siltstone, and shale sediments, with some volcanic rocks (Langenheim et al. 2011). The region is subject to north-south shortening across east-west trending tectonic structures, including the Santa Susana Fault, which is a major north-dipping thrust fault. The Site is located within the seismically active area of southern California, and is close to the epicentre of the 1994 Northridge Earthquake.

1.2 Geophysical Survey Objectives

As part of Blade's root-cause analysis, Advisian was requested to undertake a geophysical survey over and around the SS-25 well pad (shown in Photo 1). The objectives of the geophysical survey were to map structures and physical properties beneath the well pad. These structures may include faults and any fault deformation, voids, lithological layer boundaries, and the location of groundwater aquifers. To meet these objectives, several geophysical investigation methods were tested and utilized at the Site, including electrical resistivity tomography (ERT), high-resolution seismic reflection and seismic refraction, multichannel analysis of surface waves (MASW), surface-based nuclear magnetic resonance (NMR), and ground-penetrating radar (GPR).

Following the completion of the initial geophysical survey, a subsequent borehole logging program was undertaken by Advisian within four boreholes, located on and near the SS-25 well pad, which extended to maximum depths of approximately 120 feet (37 meters [m]). The borehole logging program included downhole natural gamma, formation conductivity, optical televiewer, temperature, and borehole NMR logging tools.

2 Field Geophysical Investigation

The locations of all geophysical survey measurements are shown in Figure 2 (featuring higher resolution, shallow-looking ERT lines), Figure 3 (featuring lower resolution, deep-looking ERT lines), Figure 4 (featuring seismic reflection, refraction and MASW lines), and Figure 5 (showing location of geotechnical boreholes and surface-based NMR measurements). Line parameters for all of the ERT lines are shown in Table A. Line parameters for the seismic survey, including the MASW line, are shown in Table B.

Most of the ERT and seismic lines were centered at different orientations over the SS-25 well pad (Photo 1). Because of the extremely variable topography and obstructions at surface, including infrastructure around the SS-25 well pad (site conditions shown in Photos 1 to 8), care was taken to orient the lines in such a way as to avoid obstacles and minimize topographic gradients.

In addition to the ERT and seismic investigations, a surface-based NMR survey was undertaken at two locations on the SS-25 well pad and on the sloping ground to the west of the well pad (Figure 5). A GPR unit was tested at the Site but, due to unfavourable conditions at the Site, it was determined that a GPR survey would not provide useful information, and this technique was excluded from the program. Method descriptions for the individual geophysical techniques are provided in Appendix 1. All of the surface geophysical data collected as part of the field program were acquired between August 15 and September 6, 2016.

Some initial results of the surface geophysical program were used to locate four geotechnical boreholes. A geophysical logging program was completed within these boreholes that included natural gamma, formation conductivity, temperature, optical televiewer and NMR downhole tools. The borehole logging program was completed between September 19 and 23, 2016.

Table A Individual line parameters for the ERT survey

ERT Line	Minimum Electrode Spacing	Line Length	Approximate Depth of Investigation
ERT Line 1A	4.92 feet (1.5 m)	394 feet (120 m)	65 feet (20 m)
ERT Line 2A	4.92 feet (1.5 m)	394 feet (120 m)	65 feet (20 m)
ERT Line 3A	4.92 feet (1.5 m)	394 feet (120 m)	65 feet (20 m)
ERT Line 4A	4.92 feet (1.5 m)	394 feet (120 m)	65 feet (20 m)
ERT Line 5A	4.92 feet (1.5 m)	394 feet (120 m)	65 feet (20 m)
ERT Line 1B	16.4 feet (5 m)	1,312 feet (400 m)	197 feet (60 m)

ERT Line	Minimum Electrode Spacing	Line Length	Approximate Depth of Investigation
ERT Line 2B	16.4 feet (5 m)	1,312 feet (400 m)	197 feet (60 m)
ERT Line 3B	16.4 feet (5 m)	1,312 feet (400 m)	197 feet (60 m)
ERT Line 4B	16.4 feet (5 m)	1,312 feet (400 m)	197 feet (60 m)
ERT Line 5B	16.4 feet (5 m)	1,312 feet (400 m)	197 feet (60 m)
ERT Line 6B	16.4 feet (5 m)	1,312 feet (400 m)	197 feet (60 m)
ERT Line 1C	32.8 feet (10 m)	2,625 feet (800 m)	394 feet (120 m)
ERT Line 2C	32.8 feet (10 m)	2,625 feet (800 m)	394 feet (120 m)
ERT Line 1D	73.82 feet (22.5 m)	5,906 feet (1800 m)	984 feet (300 m)
ERT Line 2D	73.82 feet (22.5 m)	5,906 feet (1800 m)	984 feet (300 m)

Table B Individual line parameters for the seismic survey

Seismic Line	Geophone Interval	Shot Interval	Seismic Source
Seismic Line 1	16.4 feet (5 m)	32.8 feet (10 m)	Buffalo Gun/Weight Drop
Seismic Line 2	6.56 feet (2 m)	13.12 feet (4 m)	Buffalo Gun/Weight Drop
Seismic Line 3	6.56 feet (2 m)	13.12 feet (4 m)	Buffalo Gun/Weight Drop
MASW Line 1	6.56 feet (2 m)	13.12 feet (4 m)	Sledgehammer

2.1 Positional Control

All geophysical data sets were georeferenced by measuring positions using high-precision handheld Trimble GeoXH 6000 series global positioning system (GPS) receivers. GPS positions were subsequently differentially corrected (post-processed) using data from a publicly available GPS base station, located approximately 6 miles from the Site in Santa Clarita (SKYB; NOAA 2016). Except for a few outliers, the processed coordinates had accuracies of less than 4 inches (10 centimeters [cm]) in both horizontal and vertical directions. For the purposes of this report, all line positions (eastings and northings) are projected to the North American Datum 1983, Universal Transverse Mercator (UTM) Zone 11 North. Distances are given in terms of feet, and elevations are plotted as feet above sea level (fasl), relative to the EGM96 (Global) Geoid.

2.2 Electrical Resistivity Tomography (ERT) Survey

A total of 15 ERT lines were acquired at the Site (locations shown in Figures 2 and 3). Survey parameters for each ERT line are listed in Table A. The ERT profiles were designed to provide information on the structure and physical properties of geological layers, and the location of any water or solutes in the subsurface. The ERT technique measures the electrical resistivity of subsurface geological materials by injecting electrical current into the ground. In general, fine-grained materials like clays and silts have lower resistivities than coarse grained materials, like sands and gravels. However, the bulk electrical resistivity of a material also depends on the composition of any pore fluids, whereby increases in salinity will lower bulk resistivities. A complete method description is available in Appendix 1.

The ERT data were acquired using a 12-channel ABEM LS Terrameter system. Different electrode intervals were utilized to image targets at different depths. In general, shorter electrode intervals provide higher resolution of targets, but a shallower depth of investigation than do longer electrode intervals. Minimum electrode intervals of either 4.92 feet (1.5 m) 16.4 feet (5 m), 32.8 feet (10 m), and 73.82 feet (22.5 m) were used providing maximum idealised depths of investigation of approximately 65 feet (20 m), 197 feet (60 m), 394 feet (120 m), and 984 feet (300 m) below ground surface, respectively. In general, signal to noise levels of the recorded data decreased with increasing electrode intervals, as it became more difficult to transmit current over longer distances. This was especially apparent for the data acquired with a minimum electrode interval of 73.82 feet (22.5 m), for which the measured reception voltages were noted to have high standard deviations. To provide good lateral and vertical resolution of structures, apparent resistivity data were recorded using a modified gradient array configuration. The data were processed by Advisian using RES2DINV tomographic inversion software. The results are displayed as electrical resistivity cross-sections, and a colormap is used to indicate relative changes in resistivity (in ohm-m), where warm colors (reds and pinks) indicate high resistivities and cool colors (light and dark blues) indicate low resistivities.

2.3 Seismic Reflection and Refraction Survey

Three 2D seismic reflection profiles were acquired across the SS-25 well pad (Figure 4) to image geological horizons within a depth range of approximately 98 feet (30 m) to 980 feet (300 m), and examine them for evidence of fault deformation. High-resolution seismic reflection profiles are designed to image strata at depths shallower than can be imaged by conventional exploration seismic surveys. A complete method description is available in Appendix 1.

Two different sets of survey parameters were used for the seismic reflection and refraction survey to attempt to resolve features at different depths. A single approximately 2,345 foot (715 m) long seismic profile (Seismic Line 1) was acquired from south to north and centered on the SS-25 well pad. This profile used a geophone interval of 16.4 feet (5 m), and a source interval of 32.8 feet (10 m). In order to image shallower depths at higher spatial resolution, a second seismic line (Seismic Line 2) was acquired along the central portion of Seismic Line 1, using a geophone interval of 6.56 feet (2 m) and a source interval of 13.12 feet (4 m). A third seismic line (Seismic Line 3) was also centered over the well pad, but was acquired approximately perpendicular to the other seismic lines in a southwest-northeast orientation using the same geophone and source intervals as Seismic Line 2 (Figure 4).

Where vehicle access was possible, a truck-mounted accelerated weight drop, with a beam weight of 40 kilograms (88 pounds) was used as a seismic source. At most locations, where vehicle access was not possible, a portable near-surface seismic source (Buffalo Source) that fires blank shotgun shells into the soil was used to generate seismic energy. At the Buffalo Source shot locations, a gas-powered hand auger was used to drill holes to depths of up to 4 feet (Photo 4), which were then filled with water to enhance seismic coupling with the ground.

The seismic data were acquired using six networked 24-channel Geometrics seismographs (enabling data to be recorded on a 144-channel seismic array), and single 40 Hz geophones (in land casings with spikes). The recorded data were analysed in real time to assess noise conditions. Because of wind and traffic noise at the Site, attempts were made to limit acquisition of the seismic data to relatively quiet periods in the morning and late afternoon. A minimum of seven stacks were recorded at each shot point; but at some locations, up to nine stacks were required to produce acceptable signal to noise ratios. Shot gathers were recorded in SEG-2 format using a sampling interval of 0.125 milliseconds (ms), and a total time window of 1.25 seconds.

Seismic reflection processing was performed by Absolute Imaging Inc. in Calgary, Alberta. Processed data sets were delivered to Advisian as filtered and unfiltered structure stacks, and filtered and unfiltered migrated (post-stack Kirchhoff migration) sections. Filtering included time-variant spectral whitening (5-10-400-500 Hz), Coherent Noise attenuation, and an Ormsby bandpass filter (20/25-55/65 Hz). A processing datum of 1,000 m above sea level (3,281 fasl) was used for all lines. Tomography-based refraction statics corrections were performed using a replacement velocity of 3937 f/s (1,200 m/s). The data were migrated using a Post Stack Kirchoff Migration algorithm, but the migrated results were deemed inferior to the unmigrated structure stacks and are not included in this report. An approximate elevation scale is shown on the right-hand axis of each of the displayed seismic reflection cross-sections; the scale is based on a time-to-depth conversion using the replacement velocity of 3937 f/s (1,200 m/s).

The seismic data were also processed with seismic refraction analysis to produce compressional-wave (P-wave) velocity tomograms. Seismic refraction processing was performed by Advisian using commercially available software. First break picks were made in Rayfract inversion software; and P-wave velocity models were produced using Rayfract's iterative least-squares tomography algorithm, based on finite elements. The P-wave velocity models are displayed using colormaps, for which warm colors (reds and pinks) represent fast velocities, and cool colors (blues and greens) represent low velocities.

2.4 Multichannel Analysis of Surface Waves (MASW) Survey

A single MASW line, with a north-south orientation, was acquired across the SS-25 well pad for the purpose of determining shallow (depths less than 98 feet [30 m]) shear-wave (S-wave) velocity structure beneath the pad (location shown in Figure 4). S-wave velocity models are produced from MASW data by analysing the frequency dispersion characteristics of surface waves recorded on seismic shot gathers (otherwise considered a source of noise to seismic reflection surveys). A complete method description of the MASW techniques is provided in Appendix 1.

The MASW seismic data were collected using a similar setup as used for the seismic reflection and refraction lines. The data were acquired using geophone and source intervals of 6.56 feet (2 m) and 13.12 feet (4 m), respectively. An active spread of 72 channels was used, and source seismic energy was generated by striking a sledgehammer against a plate on the ground (Photo 6). In order to record the low-frequency surface waves used for the MASW processing, spiked geophones with peak frequency responses of 4.5 Hz were used. MASW processing was performed by Advisian using commercially available SurfSeis software. The S-wave velocity model was generated by analyzing the frequency dispersion characteristics of the recorded surface waves on each shot record, and utilizing an inversion routine that solves for the best-fitting 1-D S-wave velocity with depth profile. The 1-D profiles are stitched together to produce a 2-D model of S-wave velocity. The P-wave and S-wave velocity models are displayed using colormaps, for which warm colors (reds and pinks) represent fast velocities and cool colors (blues and greens) represent low velocities.

2.5 Surface-Based Nuclear Magnetic Resonance (NMR) Survey

A limited surface-based nuclear magnetic resonance (NMR) survey was undertaken at two sites on and adjacent to the SS-25 well pad (Figure 5). The purpose of the surface-based NMR survey was to determine changes in water content within the ground underlying the SS-25 well pad. The survey was completed on August 18 and 19 by a specialist from VistaClara Inc. based in Mukilteo, Washington, and with the assistance of the Advisian field crew.

All surface-NMR measurements made at the Site were highly impacted by electromagnetic noise. Despite significant efforts to reduce noise at the Site, by switching off Site powerlines and deploying an extensive optimized network of noise cancellation coils, accurate measures of water content using this method could not be obtained. A complete description of the surface-based NMR survey and results is contained in Appendix 2.

2.6 Ground-Penetrating Radar (GPR) Survey

A GPR system was tested at the Site for the purpose of imaging shallow strata and subsurface deformation structures, like voids or faults. The GPR method is a high-resolution technique that uses high-frequency electromagnetic pulses to image shallow geological structures in a cross-sectional format. An UltraGPR unit was tested with a nominal source frequency of 30 megahertz (MHz). Initial tests indicated poor signal penetration through the relatively electrically conductive soils, as well as interference reflections from above-ground infrastructure, including powerlines. Based on these conditions, a GPR survey was not conducted.

2.7 Borehole Geophysical Logging Survey

At four open boreholes, a variety of downhole instruments were used to collect subsurface data. Natural gamma, induction conductivity, temperature, and optical televiewer logs were collected from the surface to a maximum achievable depth. Borehole 1 (BH1) sloughed or collapsed, and logging was limited to the upper 30.3 feet (9.24 m). Borehole 2 (BH2) also sloughed or collapsed, resulting in logging being limited to the upper 49.1 feet (14.97 m). Borehole 3 (BH3) remained open allowing logging to 114.1 feet (34.78m). Similarly, Borehole 4 (BH4) remained open to a depth of 97.2 feet (29.63 m). At all four locations, temperature logs were collected despite the boreholes being dry. However, temperature logs in the air filled boreholes are not presented. Natural gamma, induction conductivity, and temperature logs were collected at 1 inch (2.5 cm) increments at each location. Optical televiewer data were collected at 0.08 inch (2.1 mm) vertical increments and 720 pixels per turn.

Geophysical logs are presented in Appendix 3 with representative interpreted structure. For clarity, not all bedding planes are included. Lithology data is from core descriptions from a Geosyntec report which was focused on geotechnical index properties and strength testing of the site subsurface conditions.

3 Results and Interpretation

On many figures, a simplified lithology log is displayed for SS-25, which was largely derived from an offset well mudlog and provided by Blade (Clayton 2016a; see Appendix 5). The simplified lithology log also features the original downhole electrical resistivity logs measured within SS-25 by Schlumberger in 1953 (also provided in Appendix 5). Lab core descriptions from the four shallow geotechnical boreholes drilled on and around the SS-25 well pad show that, between surface and depths of approximately 100 feet, the geology is porcellanite of the Modelo formation, grading upward into a more siltstone dominated Modelo member (Clayton 2016b; see Appendix 5). Furthermore, geologic core descriptions from the four shallow geotechnical boreholes indicate that shallow rock is extensively fractured, with some fractures having subvertical orientations (Geosyntec, 2016, Clayton 2016b). The fractures were observed to be of four basic types; open, closed, filled with gypsum/ anhydrite, or with tar or iron oxide film on fracture surfaces (Clayton 2016b; see Appendix 5). Some of the natural gamma and formation resistivity geophysical borehole logs acquired by Advisian in 2016 within the shallow geotechnical boreholes are also shown. On the ERT resistivity cross-section figures, simplified model interpretations have been included to highlight pertinent features interpreted from the geophysical data.

3.1 ERT Survey

The processed ERT cross-sections are displayed in terms of electrical resistivity. For all of the resistivity cross-sections, a colormap is used to indicate relative changes in resistivity (in ohm-m), where warm colors (reds and pinks) indicate high resistivities and cool colors (light and dark blues) indicate low resistivities. In order to accentuate subtle changes in lithology, most of the resistivity cross-sections are displayed using a linear scale of resistivities ranging between 10 ohm-m and 100 ohm-m. On these figures, areas of extremely high resistivities of greater than 500 ohm-m are delineated using black contour lines; areas of extremely low resistivities of less than 5 ohm-m are delineated using white contour lines. Complementary cross-sections of the ERT data, displayed in terms of electrical conductivity (the inverse of electrical resistivity), are provided in Appendix 4.

The following subsections describe the results of the ERT surveys by group, from the shallowest looking, highest resolution ERT profiles, collected with a minimum electrode spacing of 4.92 feet (1.5 m), to the deepest looking, lowest resolution ERT profiles, acquired with a minimum electrode spacing of 73.82 feet (22.5 m). Furthermore, because of the severe topography and the inherent limitations of modelling resistivity changes between electrode locations, the accuracy of the models generally decrease with increasing minimum electrode spacing, especially in parts of the models under sharp changes in topography (e.g. beneath valleys and hills). Consequently, certain anomalies apparent in the models produced using minimum electrode intervals of 32.8 feet (10 m) or 73.82 feet (22.5 m) may be processing artefacts, and are not associated with real features.

3.1.1 4.92 Feet (1.5 M) ERT Lines (1A, 2A, 3A, 4A, and 5A)

The 'A' series of five ERT lines were all acquired with a minimum electrode spacing of 4.92 feet (1.5 m). The processed cross-sections have a depth of investigation of approximately 65 feet (20 m) below ground surface. Figure 6 displays a 3D rendering of ERT lines 1A, 2A, 3A, 4A, and 5A, and shows that, in general, regions of relatively high resistivity and low resistivity correlate between cross-sections. Individual cross-sections, with interpretations, for ERT lines 1A, 2A, 3A, 4A, and 5A are shown in Figures 7, 8, 9, 10, and 11, respectively.

Given the range of resistivities displayed (10 ohm-m to 100 ohm-m), the cross-sections are relatively heterogeneous and it is difficult to distinguish geological layering. However, on the cross-sections for ERT1A and ERT2A, a relatively high resistivity layer can be delineated (pink zones on Figures 7 and 8). The relatively high resistivities within this layer may be associated with higher air-filled pore spaces. The top of this layer on ERT line 1A (Figure 7) coincides with an increase in resistivity and a decrease in gamma counts on the borehole logs from BH1 and BH2. The corresponding lithology logs over this interval indicate that this layer may be associated with increased gravel content. On all of the cross-sections, zones of unusually low resistivities of less than 5 ohm-m are delineated. These low resistivities are much less than would be expected for typical lithologies, including clay, and would indicate relatively saline conditions. Based on communications with Blade, these low resistivity zones are interpreted to be associated with high-chloride kill fluids that were used in large quantities at the SS-25 well pad to stem the gas leak (Krishnamurthy 2016, pers. comm.) In addition, core log descriptions and photos from the shallow geotechnical boreholes note/show the presence of subvertical open fractures. The BH1 borehole in particular has extensive subvertical fractures (Geosyntec 2016). Similarly, on the cross-sections from lines ERT3A and ERT4A, these zones are elongated vertically and extend from surface to depths greater than 80 feet (the maximum depth of investigation for these profiles). The vertical fractures may have acted as conduits for the infiltrating kill fluids.

3.1.2 16.4 Feet (5 M) ERT Lines (1B, 2B, 3B, 4B, 5B, and 6B)

The 'B' series of six ERT lines were all acquired with a minimum electrode spacing of 16.4 feet (5 m). The processed cross-sections have a depth of investigation of approximately 200 feet (60 m) below ground surface, allowing deeper targets to be imaged, but at lower resolution. Figures 12a and 12b display 3D renderings of ERT lines 1B, 2B, 3B, 4B, and 5B plotted using two different resistivity scales (ERT line 6B does not cross the SS-25 well pad and is not shown). As for the 'A' series lines shown in Figure 6, Figure 12a shows the lines using a linear resistivity scale that extends from 10 ohm-m to 100 ohm-m. In order to highlight the location of high resistivity zones that are present at depth on the north side of SS-25 (orange and red zones in Figure 12b), the display is shown using a modified linear resistivity scale that extends from 100 ohm-m to 1,000 ohm-m.

Individual cross-sections, with interpretations for ERT lines 1B, 2B, 3B, 4B, 5B, and 6B are shown in Figures 13, 14, 15, 16, 17, and 18, respectively. They are plotted using a linear range of resistivities from 10 ohm-m to 100 ohm. As for the shallow looking 'A' series lines, regions of unusually low resistivities (less than 5 ohm-m) are delineated on the parts of the 'B' series lines that cross the SS-25 well pad. Given that these low resistivity zones are localized to areas under the well pad, they are likely

associated with the high-chloride kill fluids used at the SS-25 well pad. On many of the cross-sections, and as was observed for the 'A' series lines, these zones are elongated vertically and, in places, extend to depths greater than 200 feet (the maximum depth of investigation of the 'B' series lines). For example, on line ERT 2B and ERT3B low resistivity zones extend from near the surface location of SS-25 to depths of over 200 feet (Figures 14 and 15). Although none of the geotechnical boreholes were located directly on any of the ERT lines, borehole BH3 was located close to ERT lines 2B and 4B on the southwest side of SS-25. Between depths of 60 and 100 feet below ground surface, an interval of low resistivities logged within borehole BH3 approximately coincides with two of the low resistivity zones delineated at the same location on ERT lines 2B and 4B (see zoomed in sections of these lines in Figure A, below). It is also notable that the corresponding natural gamma log across this same interval indicates no significant change in lithology across this interval. Consequently, it is likely that the low resistivities within this interval are associated with an increased salt concentration, rather than an increase in clay content.

Figure A Zoomed In Sections of ERT Line 2b (Left) and ERT Line 4b (Right) Showing Low-Resistivity (Dark Blue) Zones under the SS-25 Well Pad

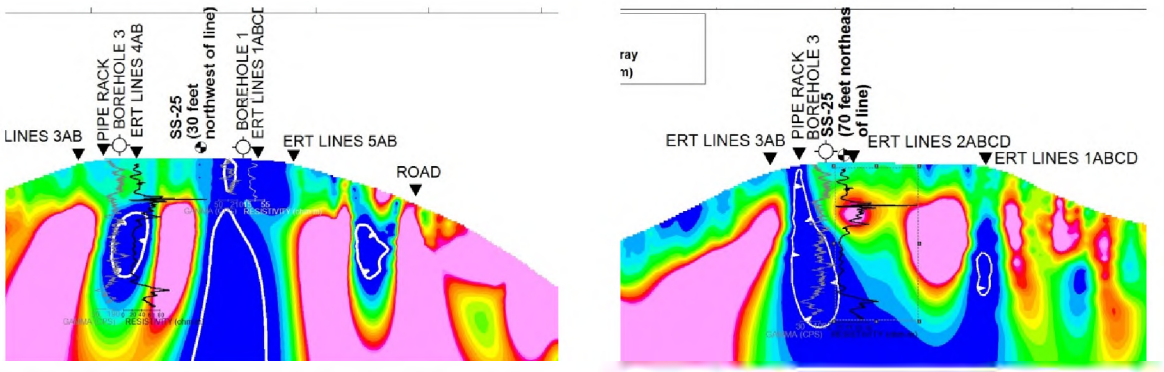

Note that zones with resistivities lower than 5 ohm-m, delineated by white lines on the left side of both ERT sections, approximately coincide with an interval of low resistivities logged at depths between 60 feet and 100 feet within borehole BH3 (black lines are the resistivity log). The corresponding gamma log (grey lines) indicates no significant change in lithology across this interval. Refer to Figures 14 and 16 for complete versions of these figures.

In addition to the very low resistivity zones of less than 5 ohm-m, there exist numerous other vertically elongated lower resistivity zones (blue colours). Such vertical banding is apparent on ERT lines 2B, 4B, and 5B (Figures 14, 16, and 17). It is possible that the low resistivity bands are where kill fluids have preferentially infiltrated through subvertical fractures, rather than through the less fractured higher resistivity bands. In addition to providing flowpaths for the kill fluids, the zones with open fractures may also provide preferential pathways for gas to migrate across the site. Line ERT 6B extended to the south of the SS-25 well pad and crosses the SS-9 well pad. It is notable that similar banding is also observed beneath the location of the SS-9 well pad. Although kill fluids are not known to have been used near the SS-9 well pad, it is possible that some fluid may have migrated to this area (Figure 18).

In addition to the low resistivity regions, localized zones of unusually high resistivity (greater than 500 ohm-m) are observed on parts of ERT lines 1B, 3B, and 5B that cross the north side of the SS-25 well pad (Figures 13, 15 and 17). The tops of these zones are at about 100 feet (31 m) below ground on ERT lines 1B and 3B, but may be as shallow as 50 feet (15 m) below ground on ERT line 5B. As shown in the zoomed sections of ERT lines 1B and 5B shown in Figure B (below), the resistivity log for borehole BH2 (which was located close to these lines) shows a rapid increase to over 200 ohm-m at a depth of approximately 40 feet (12.2 m), consistent with the trend of increasing resistivity to over 100 ohm-m, observed on the ERT sections for lines 1B and 5B at approximately the same location (Figure 13). Given the vertically elongated shape of these zones on ERT lines 1B and 3B, and the absence of such high resistivities elsewhere, these features are unlikely to be associated with typical geological units expected for this Site. Borehole televiewer data, from within the four geotechnical boreholes, confirms that the bedding beneath the Site dips moderately (mean dip of 31°; see Section 3.4) and not at steep angles as the ERT data would appear to indicate.

Figure B Zoomed in Sections of ERT Line 1B (left) and ERT Line 5B (right), Showing High-Resistivity (Pink) Zones under the SS-25 Well Pad

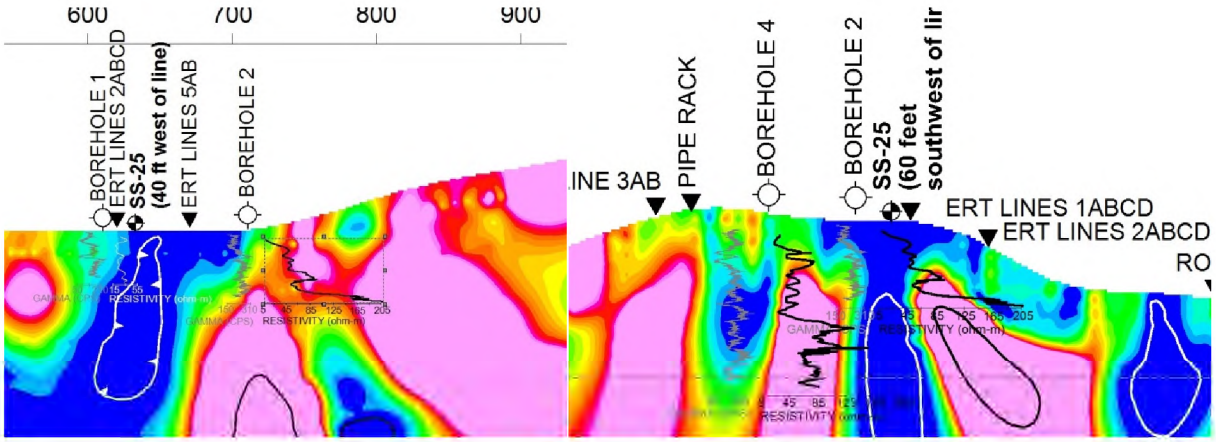

Note that high-resistivity zones (greater than 500 ohm-m), delineated by black lines on both ERT sections lie beneath shallow borehole BH2. The resistivity log from BH2 exhibits a rapid increase in resistivity near the base of the borehole, at an approximate depth of 40 feet, which is coincident with increasing resistivities with depth toward the high resistivity zones. Refer to Figures 13 and 17 for complete versions of these figures.

A borehole temperature log from within SS-25 indicated the presence of a frozen zone (i.e. temperatures less than 0° Celsius; 32° Fahrenheit) extending over depths greater than 100 feet (30 m) below ground surface (Krishnamurthy 2016, pers. comm.) The presence of a high-resistivity zone extending to depths as shallow as 50 feet (15.2 m)to the southeast of SS-25 on ERT line 5B, and the increase in resistivities observed at a depth of 40 (12.2 m) feet on the resistivity log for BH2, indicate that the frozen zone may extend to depths as shallow as 40 feet (12.2 m; Figures 13 and 17) Given the location of the resistive anomalies below the break in topographic slope on the north side of the SS-25 well pad (as visible on Figure 13), it is possible that the resistive anomalies are controlled by a relatively steep-dipping fault zone. The presence of a steeply dipping fault zone at this location is

also consistent with subvertical fractures observed within cores recovered from borehole BH2. Two small zones of high resistivity are also delineated on ERT Line 6B, near the SS-9 well pad (Figure 18). Although there is no other evidence to confirm the cause of the high resistivity zones at this location, it is possible that leaking gas has migrated from SS-25 to this location along another fracture zone or fault zone and given rise to other frozen zones near the SS-9 well pad.

3.1.3 32.8 feet (10 M) ERT Lines (1C and 2C)

The 'C' series of two ERT lines were all acquired with a minimum electrode spacing of 32.8 feet (10 m). The processed cross-sections have a depth of investigation of approximately 400 feet (120 m) below ground surface. Figures 19a and 19b display a 3D renderings of ERT lines 1C and 2C. Figure 19a show the lines plotted using a linear resistivity scale ranging between 10 ohm-m and 100 ohm-m. As for Figure 12b, to highlight the relatively high-resistivity features, in Figure 19b the cross-sections are displayed using a linear resistivity scale extending between 100 ohm-m and 1,000 ohm-m.

Individual cross-sections, with interpretations for ERT lines 1C and 2C, are shown in Figures 20 and 21, respectively. They are plotted using a linear range of resistivities from 10 ohm-m to 100 ohm. No distinct geological layers can be discerned on either cross-section. The cross-section for ERT line 1C reveals low resistivity (less than 5 ohm-m) zones beneath the SS-25 well pad, possibly associated with high-chloride kill fluids (Figure 20). Another distinct low resistivity zone occurs in the vicinity of the SS-9 well pad, at a line distance of 600 feet (Figure 20). This feature is likely associated with the low resistivity zone observed on ERT line 6b (Figure 18) and may indicate that high-chloride kill fluids have migrated from beneath SS-25 toward SS-9 along a fracture zone or fault zone. A third smaller low resistivity zone is observed at a line distance of 2200 feet, north of and uphill from the SS-25 well pad. The cause of this feature is undetermined but may also be associated with high-chloride kill fluids that have migrated from around SS-25. Three small high-resistivity zones (greater than 500 ohm-m) are delineated, including one that occurs near the north side of the SS-25 well pad and overlaps with the high-resistivity feature delineated on ERT Line 1B. The other two high-resistivity zones may also indicate frozen zones resulting from migrating gas, but further evidence is required to confirm this.

On the cross-section for ERT Line 2C, which extends from southwest to northeast across the Site (Figure 21), a series of vertically elongated bands of intermittent high and low resistivities are apparent under the SS-25 well pad. Given the relatively shallow dip of bedding, these features are unlikely to be associated with lithological changes. As was interpreted from ERT lines 2B, 4B, and 5B, the vertically elongated low resistivity zones may be associated with high-chloride kill fluids that have preferentially infiltrated along near-vertical fracture zones or fault zones. Likewise, the high resistivity bands, under the SS-25 well pad and elsewhere, may be indicative of frozen zones caused by gas that has migrated along fracture zones or fault zones. However, we also cannot rule out the possibility that these features are processing artefacts caused by the steep topography along this part of the line and/or interference from metal infrastructure, including pipelines that extend in a north-south direction across the SS-25 well pad. Such features become more pronounced for the data collected with relatively large electrode spacings. Consequently, we have only highlighted the larger high-resistivity zones under the SS-25 well pad on the simplified model interpretation shown in Figure 21.

3.1.4 22.5 M ERT Lines (1D and 2D)

The 'D' series of two ERT lines were all acquired with a minimum electrode spacing of 73.82 feet (22.5 m); the processed cross-sections have a depth of investigation of approximately 1,000 feet (300 m) below ground surface. Figure 22 displays a 3D rendering of ERT lines 1D and 2D. The cross-sections shown in Figure 22 are displayed using a linear resistivity scale extending between 10 ohm-m and 100 ohm-m so as to highlight lithological changes. Unlike the shallower looking ERT lines, two general layers with contrasting resistivities can be distinguished on both sections, which can be interpreted as either changes in lithology or changes in water content.

Individual cross-sections, with interpretations, for ERT lines 1D and 2D are shown in Figures 23 and 24, respectively. They are plotted using a linear range of resistivities from 10 ohm-m to 100 ohm. On both cross-sections, a relatively high-resistivity layer (pink; greater than 100 ohm-m) is interpreted to extend to depths of approximately 300 feet (91 m) to 500 feet (152 m) below ground surface, and overlay a relatively low resistivity layer (blue; less than 10 ohm-m). Based on the interpreted lithology log for SS-25 (which is based on an offset well mudlog), the shallow, higher resistivity layer is interpreted to correspond to the interval dominated by shale, porcellanite, claystone and siltstone of the Modelo formation. In contrast, the deeper low-resistivity layer is interpreted to be associated with the underlying interval dominated by clay, basalt and sand of the upper Topanga formation. It is possible that the upper Topanga formation is water saturated (i.e. an aquifer), which may also explain the decreased resistivities over this interval. The two contrasting resistivity layers are also consistent with the original downhole electrical resistivity logs from SS-25, which show the Modelo formation to be generally more resistive than the Topanga (Appendix 5).

Small localized zones of unusually low-resistivity (less than 5 ohm-m) and unusually high-resistivity (greater than 500 ohm-m) have been delineated in Figures 23 and 24, but these discrete features may result from modelling artefacts introduced because of noisy data and/or sharp changes in topography.

3.2 Seismic Reflection and Refraction Survey

The seismic reflection sections are plotted using a variable area display, for which blue and red colors indicate relatively strong negative and positive reflection amplitudes, respectively. A simplified elevation scale has been added to the right hand axis of the seismic reflection cross-sections and is based on the replacement velocity of 3937 f/s (1,200 m/s) used during processing. The replacement velocity is used during processing to produce static, vertical shifts in seismic data in order to bring specific points into alignment with some common elevation feature. In reality, the velocities are variable with depth such that the true elevation of reflections may differ slightly from that shown.

The seismic refraction sections are displayed as a color-shaded grid, showing variations in P-wave velocities. The cross-sections are shown using a linear scale that ranges between 1,640 f/s (500 m/s) and 8,200 f/s (2,500 m/s).

3.2.1 Seismic Line 1

Seismic line 1 was acquired using geophone and source intervals of 16.4 feet (5 m) and 32.8 feet (10 m), respectively. It was centered over and extends from south to north along the eastern side of the SS-25 well pad, and follows the same line path as used for ERT Lines 1A, 1B, 1C and 1D. The processed seismic reflection section for Seismic Line 1 is shown in Figure 25. In general, there are few coherent reflections which can be attributed to geological layers. This is largely because the seismic energy is rapidly attenuated within the highly weathered bedrock, and because the contrast in elastic properties between layers is likely to be very weak within the weathered zone. Nevertheless, a series of relatively high-amplitude, discontinuous reflections are visible across most of the cross-section at elevations of between 2,500 fasl and 2,700 fasl (760 m above sea level [masl] and 825 masl; 'R1' in Figure 25). These elevations approximately correspond to a change in lithology identified in SS-25, from shale and porcelanite to claystone and siltstone.

On the corresponding P-wave velocity model for Seismic Line 1 (Figure 26), velocities indicative of highly weathered rock (less than 6,561 f/s [2,000 m/s]) are present from surface to depths of approximately 200 to 300 feet (61 to 91 m). Below these depths, velocities increase relatively rapidly to over 8,200 f/s (2,500 m/s), indicating a change to relatively competent rock with fewer fractures and/or reduced pore space. These depths are also broadly consistent with the change in lithology from shale and porcelanite to claystone and siltstone shown in the predicted lithology log for SS-25 (which is based on the adjacent well mud log).

3.2.2 Seismic Line 2 and Seismic Line 3

Seismic Line 2 and Seismic Line 3 were acquired using geophone intervals of 16.4 feet (5 m) and source intervals of 32.8 feet (10 m). Seismic Line 2 is centered over the SS-25 well pad, extends from south to north along a portion of Seismic Line 1, and follows the same line path as used for ERT Lines 1A, 1B, 1C and 1D. Seismic Line 3 was also centered over the SS-25 well pad but oriented at an oblique angle to Seismic line 3, with an orientation from southwest to northeast.

Similar to Seismic Line 1, the reflection sections for both Seismic Line 2 and Seismic Line 3 (top panels in Figure 27 and Figure 28) show few coherent reflection horizons, but a series of relatively high-amplitude, discontinuous reflections are visible on each cross-section at elevations of between 2,500 fasl to 2,700 fasl (approximately 760 masl to 825 masl; 'R1' in Figures 27 and 28). These elevations approximately correspond to a change in lithology identified in SS-25, from shale and porcelanite to claystone and siltstone.

Although the depths of investigation for the refraction data collected on Seismic Line 2 and Seismic Line 3 are less than those for Seismic Line 1, velocities in excess of 8,200 f/s (approximately 2,500 m/s) are detected at elevations generally lower than 2700 fasl (approximately 825 masl). This is consistent with the findings from Seismic Line 1, where the 8,200 f/s (2,500 m/s) contour is interpreted to correspond to a change from weathered rock to competent rock, and approximately coincides with a change in lithology from shale and porcelanite to claystone and siltstone as shown in the geological log from SS-25 (Figure 26).

3.3 MASW Survey

A single MASW line was acquired across the SS-25 well pad along the same line path used for Seismic Line 1, Seismic Line 2, ERT 1A, ERT 1B, ERT 1C, and ERT 1D. The resulting S-wave velocity cross-section for MASW Line 1 is plotted as a color-shaded grid in the lower panel of Figure 29. The grid is plotted using a linear S-wave velocity scale that ranges between 656 f/s and 1,312 f/s (200 m/s and 400 m/s). So as to facilitate comparison with the ERT and seismic refraction data acquired along the same line path, in Figure 29 the resistivity cross-section from ERT Line 1B (upper panel) and the P-wave velocity section from Seismic Line 2 (middle panel) are also plotted. Unlike the ERT and seismic refraction lines, the depth of investigation of the MASW profile is only about 100 feet (about 30 m).

The average S-wave velocity of the soil beneath the SS-25 well pad is approximately 984 f/s (300 m/s). As per the US National Earthquake Hazard Reduction Program classification system (www.nehrp.gov), a V_s^{30} measurement (the average S-wave velocity down to a depth of 30 m [approximately 100 feet]) of 984 f/s (300 m/s) places the site into the category of Site Class 'D' (stiff soil). Over shallow depths of the S-wave velocity model, at least four layers can be interpreted. These layers may be indicative of bedding. In places, the S-wave velocities are as low as 492 f/s (150 m/s; within the dark blue regions shown in the lower panel of Figure 29), which may be interpreted as very weak soil, possibly containing open voids. It should be noted that S-wave velocities are typically classified as rock when they exceed 2500 f/s (approximately 760 m/s).

3.4 Borehole Geophysical Logging Results

Detailed borehole geophysical logs for boreholes BH1, BH2, BH3, and BH4 are provided in Appendix 3. Table C lists the boreholes by location, and Table D lists the intervals logged by each geophysical tool within each of the four geotechnical boreholes. The geotechnical lithology descriptions indicate that the logged intervals vary between siltstone, sandstone, shale and porcellanite, consistent with the predicted mud log for SS-25. The depth intervals of the logs for each tool vary due to various factors, including the length of the tool and whether spurious data points had to be removed. Due to the collapse of parts of boreholes BH1 and BH2, only boreholes BH3 and BH4 were logged to depths greater than 50 feet (15 m).

Table C Geotechnical borehole locations

Name	Coordinates (WGS84; UTM Zone 11N)	Geographic Coordinates	Location Description
BH1	356100 E; 3798196 N	34.31504640° N; 118.56396462° W	30 feet east of SS-25
BH2	356103 E; 3798220 N	34.31525984° N; 118.56394159°W	80 feet northeast of SS-25
BH3	356072 E; 3798179 N	34.31489403° N; 118.56427170° W	90 feet southwest of SS-25
BH4	356086 E; 3798220 N	34.31526271° N; 118.56412372° W	80 feet northwest of SS-25

Table D Intervals logged by each geophysical tool (in feet)

Name	Optical Televiewer	Natural Gamma	Formation Conductivity	Fluid Conductivity	Temperature	NMR
BH1	2.8 to 30.3	2.0 to 33.2	5.1 to 36.5	none	2.0 to 39.0	2.0 to 34.5
BH2	3.1 to 46.1	0.7 to 43.5	3.7 to 46.8	none	1.8 to 49.0	0.9 to 44.3
BH3	3.8 to 114.2	0.9 to 127.2	4.1 to 130.5	105.8 to 132.8	1.9 to 132.7	0.9 to 123.9
BH4	2.2 to 97.0	2 to 91.5	7.2 to 94.8	none	1.9 to 97.2	1.3 to 92.7

The optical televiewer logs from all four boreholes (data is primarily from boreholes BH3 and BH4) indicate that shallow rock is highly weathered with zones of spalling, and open joints and fractures to depths of up to 100 feet (30 m). At depths below about 50 feet (15 m), thin bedding (less than 1 inch (2.5 cm) thick) becomes more apparent. Geometric analysis of the beds (n=185) shows that the mean dip of the beds is 31°, with a mean dip direction of 239 (i.e. to the west-southwest; Figure C and provided in Appendix 3). Where they can be picked (n=19), fracture and joint orientations and apertures have been measured. The orientations of the fractures and joints appear to have a bimodal distribution with a main cluster (n=14) with mean dips of approximately 63° and a mean dip direction of 068 (to the east-northeast; Figure D). A second minor cluster has too few points (n=5) to determine an accurate dip and dip direction, but they appear to dip moderately to the west-southwest, similar to the bedding orientations. Four fractures/joints were observed to dip at subvertical angles of greater than 70°. Additional subvertical fractures were observed within cores extracted from boreholes BH1 and BH2 at depths greater than were logged by the televiewer (Geosyntec 2016). These latter subvertical fractures were not imaged by the televiewer because the deepest section of the boreholes collapsed before the logging program could begin. The geometric distribution of bedding and fractures from the logged portions of the boreholes is shown in the structure and rose diagram plots below, and are provided in Appendix 3.

Although open fractures were observed, in-situ fracture apertures could not be measured accurately from the televiewer images. This is because the friable weathered rock along the borehole wall appears to have collapsed into the borehole in places, artificially enlarging the apertures.

Figure C Polar Projection Plot of All Bedding Orientations

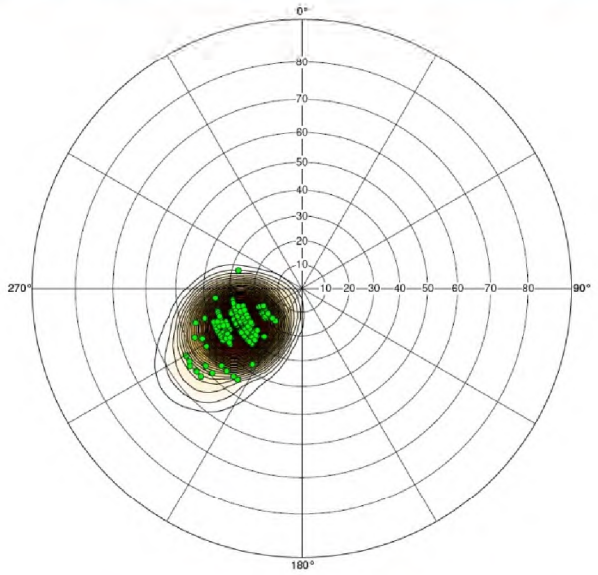

Figure D Polar Projection Plot of All Fracture and Joint Orientations

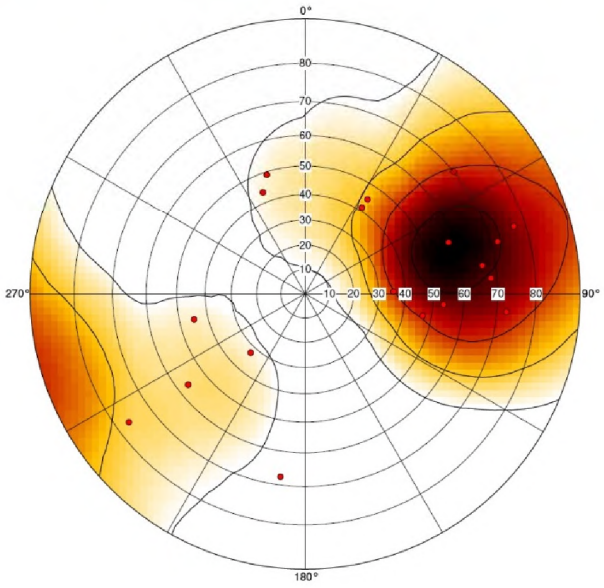

Natural gamma and formation conductivity logs show minor variations associated with lithological changes, including between 48 feet and 54 feet in borehole BH3, where natural gamma counts and

formation conductivities decrease slightly, indicating a decreased clay content. Because the boreholes were all predominantly dry, the temperature logs only reflect small variations in air temperature of between 70°F to 75°F (21°C and 24°C). Fluid conductivity was only measured near the base of borehole BH3, where water was present within the borehole.

The NMR logs reveal that water content within the unsaturated shale and porcellanite is generally less than 15% (0.15). In places water contents are as high as 25% (0.25) and these likely reflect minor changes in lithology and/or degree of fracturing. The fraction of this water that is "mobile" (blue boxes plotted on the borehole logs in Appendix 3) is likely associated with water trapped within fractures. The fractions of water that are "clay bound" or "capillary" (green and maroon boxes plotted on the borehole logs in Appendix 3) are likely associated with water that is held in tension within the unsaturated zone. For example, on the log for borehole BH3, between depths of 83 feet and 89 feet, a slight increase in water content within darker coloured bands of shale is associated with an increase in clay content (as shown by the increased gamma counts).

Over some intervals, the borehole NMR tool could not sample the formation to obtain an accurate result. This occurs between depths of 16 feet and 23 feet on the log for borehole BH3, where a zone of unusually low water content coincides with the collapse of the borehole wall shown on the televiewer image. In addition, the relatively high water contents measured near the base of borehole BH3 may be associated with residual drilling water sitting at the bottom of the borehole, rather than ambient conditions.

4 Conclusions

The 2016 geophysical investigation at Aliso Canyon has led to the following conclusions:

a) Zones of unusually low electrical resistivities (less than 5 ohm-m) were mapped under the SS-25 well pad. These zones extend from the ground surface to depths of up to 500 feet (150 m). These zones are interpreted to be associated with chloride-rich kill fluids used to stem the original gas leak. Zones of unusually high electrical resistivities (greater than 500 ohm-m) were imaged in places on the north side of the SS-25 well pad. These zones extend from depths as shallow as 50 feet (15 m) and extend to depths of greater than 200 feet (61 m). These high resistivities approximately correlate with a zone with temperatures below freezing (less than 32°F; 0°C), identified from temperature logs and distributed temperature sensing data acquired within the SS-25 well. An additional two small zones of high electrical resistivities were also imaged at similar depths close to the SS-9 well pad.

b) The bedrock is extensively weathered to significant depth. Beneath the SS-25 well pad, a layer with P-wave velocities less than 2,000 m/s (6,562 f/s) extends to a depth of approximately 200 feet (61 m). Based on correlation with SS-25 mud log data, this layer coincides with an interval of siltstone, shale and porcelanite within the Modelo formation. Shallow S-wave velocities of between 200 m/s (656 f/s) and 400 m/s (1,312 f/s), observed at depths of up to 100 feet (30 m) also indicate highly weathered rock.

c) Geophysical logs from four geotechnical boreholes drilled on and around the SS-25 well pad indicate that unsaturated conditions persist to depths of at least 150 feet (46 m; i.e. there is no indication of perched aquifers within this zone). The formation water content is generally less than 15% within the unsaturated zone, with some short intervals in excess of 20% that are associated with variations in clay content and/or degree of fracturing of the rock.

d) No subsurface fault strands could be identified with any confidence from the surface geophysical data, but fractures were observed from televiewer data images that may be linked to fault deformation.

e) Borehole televiewer logs indicate that the shallow rock is highly weathered, with spalling, and open joints and fractures observed to depths up to 100 feet (30 m). Thin (less than 1 inch thick [2.5 cm]) shale beds have a mean dip of 31° and dip direction of 239 ° (west-southwest). The orientations of the fractures and joints exhibit a main cluster with a dip of 63°, and a mean dip direction of 068 ° (east-northeast). Four of these fractures were observed to dip steeply at angles greater than 70°. A second minor cluster of fractures and joints appears to parallel the orientation of the bedding. Televiewer logs were not obtainable at depths greater than 30 feet and 46 feet, respectively, in the BH1 and BH2 boreholes, fracture orientation and dip of fractures, subvertical fractures were not captured in the reported results.

f) Zones of unusually low electrical resistivities (less than 5 ohm-m) were mapped under the SS-25 well pad. These zones extend from the ground surface to depths of up to 500 feet (150 m). These zones are interpreted to be associated with chloride-rich kill fluids used to stem the original gas leak.

5 Closure

We trust that this report satisfies your current requirements and provides suitable documentation for your records. If you have any questions or require further details, please contact the undersigned at any time.

Report Prepared by

Alastair McClymont, Ph.D., P.Geo. (AB)
Senior Geophysicist

Senior Review by

REGISTERED GEOLOGIST
RALPH M. BECK
No. 6330
Exp. 10/31/18
GEOLOGIST
STATE OF CALIFORNIA

Paul D. Bauman, M.Sc., P.Eng (AB)., P.Geoph. (AB)
Principal Geophysicist, Technical Director

Ralph M. Beck, PG
Director, Decommissioning & Restoration

6 References

Clayton, Carol – Blade Energy, 2016a. Powerpoint file SS-25_P-39A mudlog description by major lith zone_PLOT Copy.pptx, emailed to Alastair McClymont on 10 October, 2016.

Clayton, Carol – Blade Energy, 2016b. Word document file 'SS-25 Lithology Interpretation from P-39A Mudlogs.docx', sent by FTP site to Alastair McClymont on 9 November, 2016.

Geosyntec, 2016. Targeted Geotechnical Evaluation – SS-25 well site, Aliso Canyon gas storage facility, Los Angeles County, California. Draft technical report provided by Geosyntec Consultants to Southern California Gas Company. 21 October, 2016.

Krishnamurthy, Ravi – Blade Energy, 2016. Telephone communication, August 19, 2016

Langenheim, V.E., Wright, T.L., Okaya, D.A., Yeats, R.S., Fuis, G.S., Thygesen, K., Thybo, H. 2011. Structure of the San Fernando Valley region, California - Implications for seismic hazard and tectonic history. Geosphere; vol. 7, no. 2; p. 528-572; doi: 10.1130/GES00597.1.

NOAA (National Oceanic and Atmospheric Administration), 2016. National Oceanic and Atmospheric Administration National Geodetic Survey, CORS GPS base station data archive: http://www.ngs.noaa.gov/CORS/standard1.shtml.

SoCal (Southern California Gas Company), 2016a. Aliso Canyon Storage Facility website: https://www.socalgas.com/stay-safe/pipeline-and-storage-safety/aliso-canyon-storage-facility).

SoCal (Southern California Gas Company), 2016b. SoCal press release, February 11, 2016: https://www.alisoupdates.com/1443738468372/SoCalGas-Temporarily-Controls-Flow-of-Gas-021116-2.pdf.

Figures

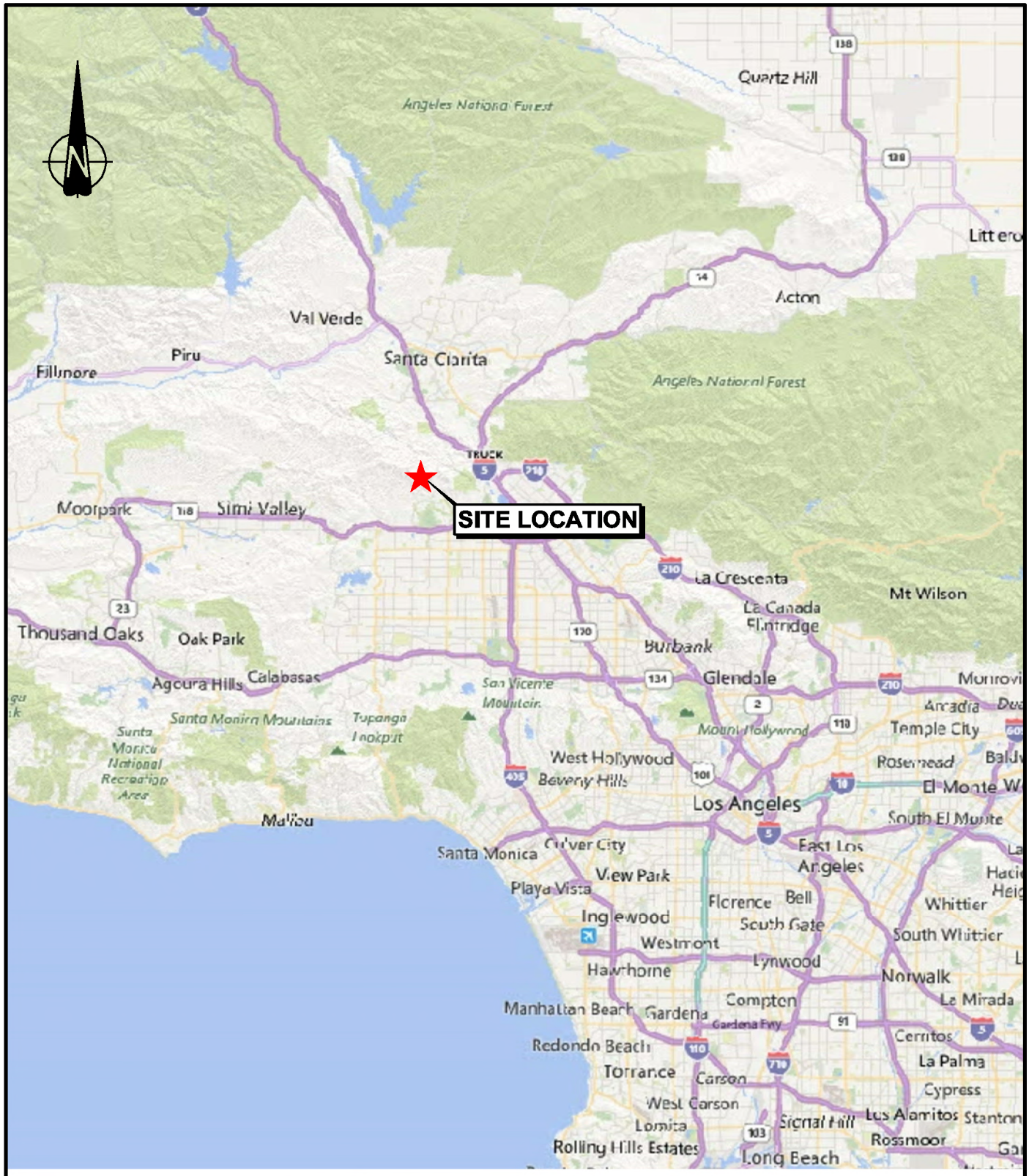

IMAGE PROVIDED BY BING MAPS © 2016 DIGITAL GLOBE, © 2016 GEOEYE, ©2016 MICROSOFT CORPORATION

m 0 5 10 15 20 25 km

1:500000

SOUTHERN CALIFORNIA GAS COMPANY
2016 GEOPHYSICAL INVESTIGATION
ALISO CANYON SS-25

SITE LOCATION MAP

Date: 05-OCT-16	Drawn by: B.M.F.	Edited by: -	App'd by: PB

OneWay to zero harm

Advisian WorleyParsons Group

WorleyParsons Project No. 407074-00748-200

FIG No. 1 | REV A

"This drawing is prepared for the use of our customer as specified in the accompanying report. WorleyParsons Canada Services Ltd. assumes no liability to any other party for any representations contained in this drawing."

USER NAME: blairfrk
ISSUING OFFICE: sCAD
PLOT DATE & TIME: 5/10/2016 9:23:40 AM
SAVE DATE & TIME: 5/10/2016 9:22:29 AM

FILE LOCATION: U:\CAL\GBS\407074-00748\200 - GEOPHYSICAL INVESTIGATION\11.0_FIGURES_&_MAPS\11.4_CAD_FILES\00748-200-00-EN-DWG-SITELOCMAP.DWG

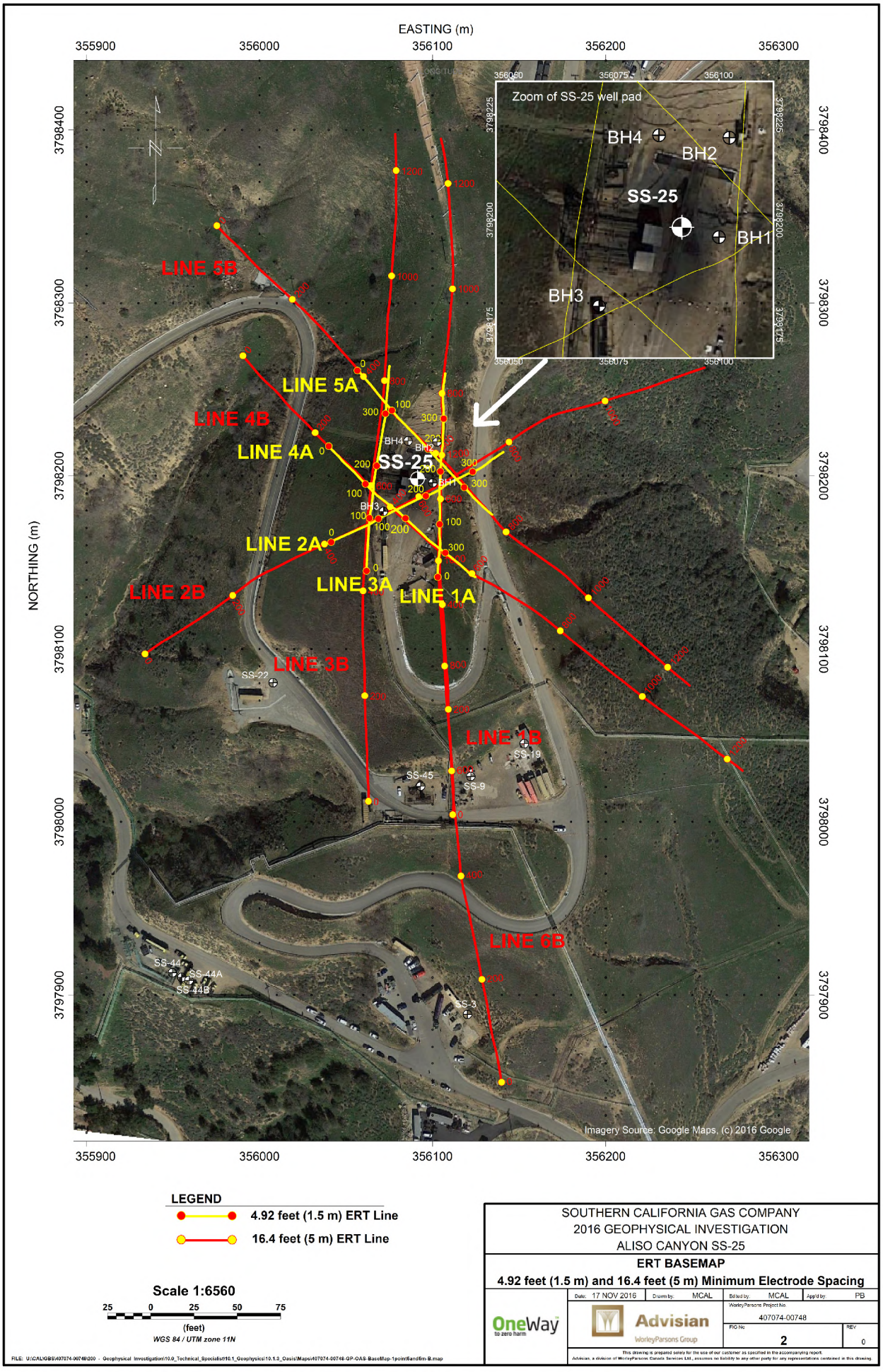

LEGEND

- 4.92 feet (1.5 m) ERT Line
- 16.4 feet (5 m) ERT Line

Scale 1:6560

25 0 25 50 75

(feet)

WGS 84 / UTM zone 11N

FILE: U:\CAL\GIS\407074-00748\200 - Geophysical Investigation\10.0_Technical_Specialist\10.1_Geophysics\10.1.3_Oasis\Maps\407074-00748-GP-OAS-BaseMap-1point5and6m-B.mxd

SOUTHERN CALIFORNIA GAS COMPANY
2016 GEOPHYSICAL INVESTIGATION
ALISO CANYON SS-25

ERT BASEMAP

4.92 feet (1.5 m) and 16.4 feet (5 m) Minimum Electrode Spacing

Date: 17 NOV 2016	Drawn by: MCAL	Edited by: MCAL	Appd by: PB
		Worley Parsons Project No. 407074-00748	
		FIG No. 2	REV 0

OneWay to zero harm

Advisian WorleyParsons Group

This drawing is prepared solely for the use of our customer as specified in the accompanying report. Advisian, a division of WorleyParsons Canada Services Ltd., assumes no liability to any other party for any representations contained in this drawing.

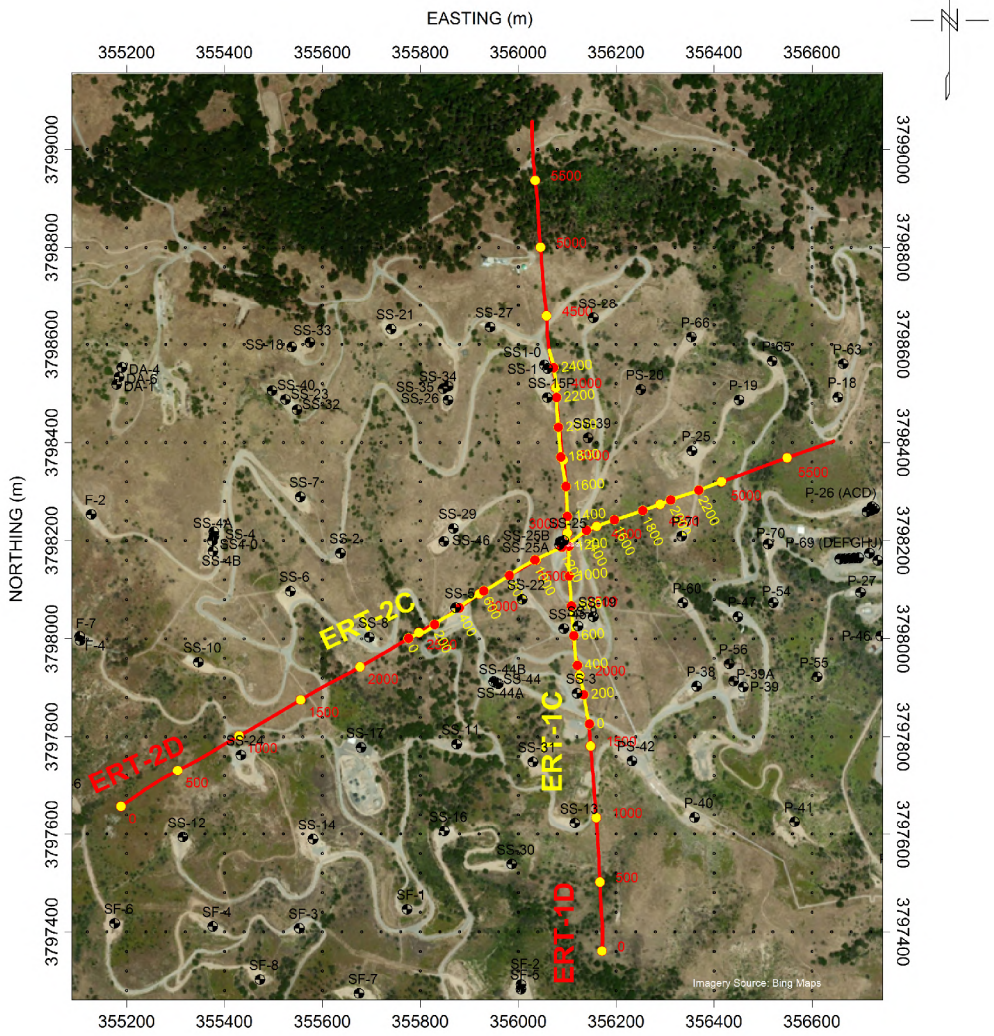

LEGEND

- 32.8 feet (10 m) ERT Line
- 73.8 feet (22.5 m) ERT Line

Scale 1:32808

100 0 100 200 300 400

(feet)

WGS 84 / UTM zone 11N

SOUTHERN CALIFORNIA GAS COMPANY
2016 GEOPHYSICAL INVESTIGATION
ALISO CANYON SS-25

ERT BASEMAP

32.8 feet (10 m) and 73.8 feet (22.5 m) Minimum Electrode Spacing

Date: 17 NOV 2016	Drawn by: MCAL	Edited by: EJE	Approved by: PB
Oneway	Advisian	Project No. 407074-00748	
		Fig No. 3	Rev 0

This drawing is prepared solely for the use of our customer as specified in the accompanying report. Advisian, a division of WorleyParsons Consulting Services, LLC, assumes no liability to any other party for any representations or opinions in this drawing.

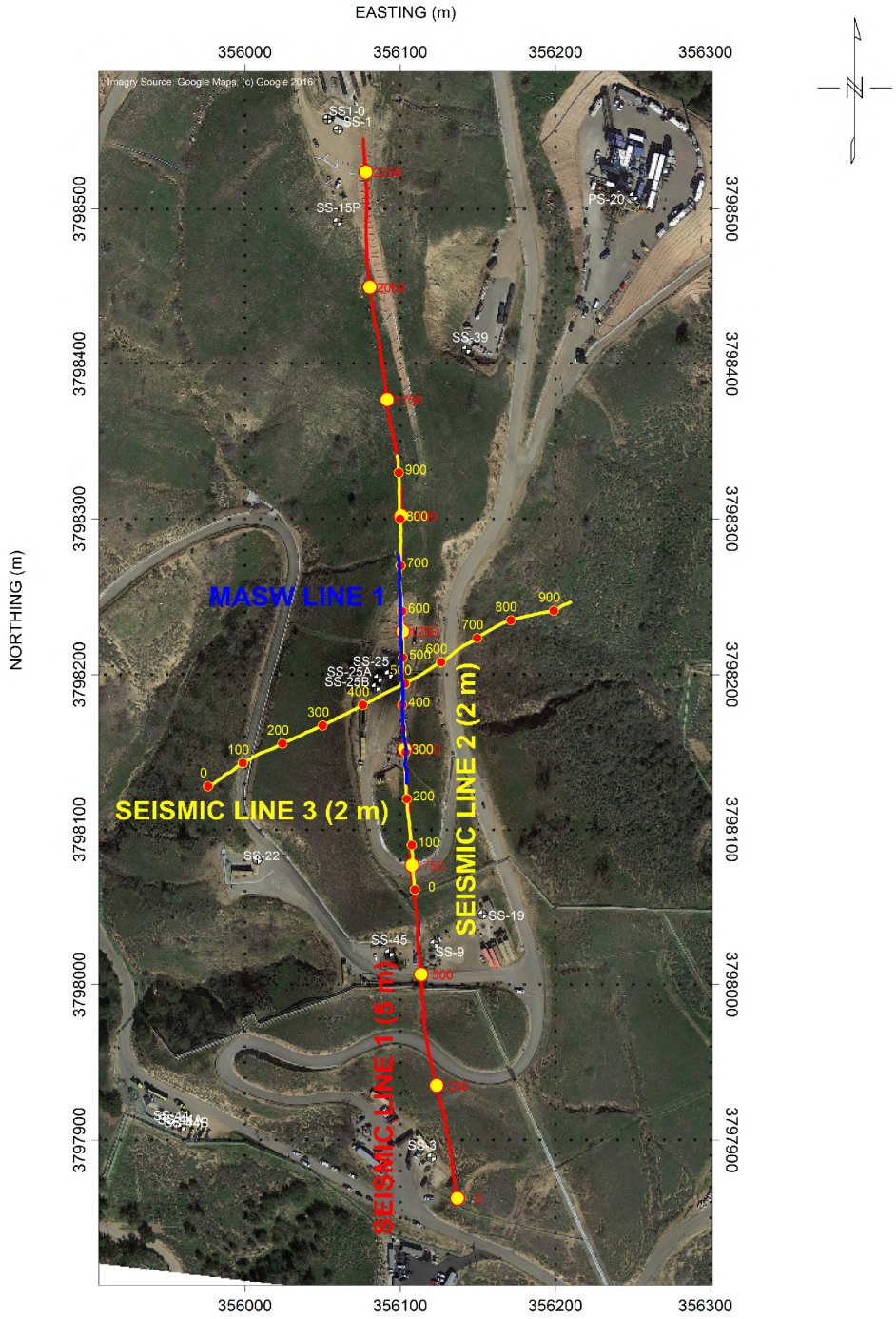

LEGEND

- 6.56 feet (2 m) Seismic Line
- 16.4 feet (5 m) Seismic Line
- MASW Seismic Line

Scale 1:9842

50 0 50 100

(feet)

WGS 84 / UTM zone 11N

FILE: U:\CAL\GIS\407074-00748\200 - Geophysical Investigation\10.0_Technical_Specialist\10.1_Geophysics\10.13_Oasis\Maps\407074-00748-GP-OAS-BaseMap-Seismic-A.mxd

SOUTHERN CALIFORNIA GAS COMPANY
2016 GEOPHYSICAL INVESTIGATION
ALISO CANYON SS-25

SEISMIC BASEMAP

Date: 17-NOV-2016	Drawn by: EJE	Edited by: EJE	Appd by: PB
		Worley Parsons Project No. 407074-00748	
		FIG No. 4	REV 0

OneWay to zero harm

Advisian WorleyParsons Group

This drawing is prepared solely for the use of our customer as specified in the accompanying report. Advisian, a division of WorleyParsons Canada Services Ltd., assumes no liability to any other party for any representations contained in this drawing.

SOUTHERN CALIFORNIA GAS COMPANY
2016 GEOPHYSICAL INVESTIGATION
ALISO CANYONE SS-25

SS-25 BASEMAP WITH NMR AND GEOTECHNICAL BOREHOLE LOCATIONS

Scale 1:2297

10 0 10 20

(feet)

WGS 84 / UTM zone 11N

Date: 17 NOV 2016	Drawn by: EJE	Edited by: EJE	Appd by: PB
		WorleyParsons Project No. 407074-00748	
		FIG No. 5	REV 0

OneWay to zero harm

Advisian WorleyParsons Group

This drawing is prepared solely for the use of our customer as specified in the accompanying report. Advisian, a division of WorleyParsons Canada Services Ltd., assumes no liability to any other party for any representations contained in this drawing.

FILE: U:\CAL\GIS\407074-00748\200 - Geophysical Investigation\10.0_Technical_Specialist\10.1_Geophysics\10.1.3_Oasis\Maps\407074-00748-GP-OAS-NMR-Basemap-A.map

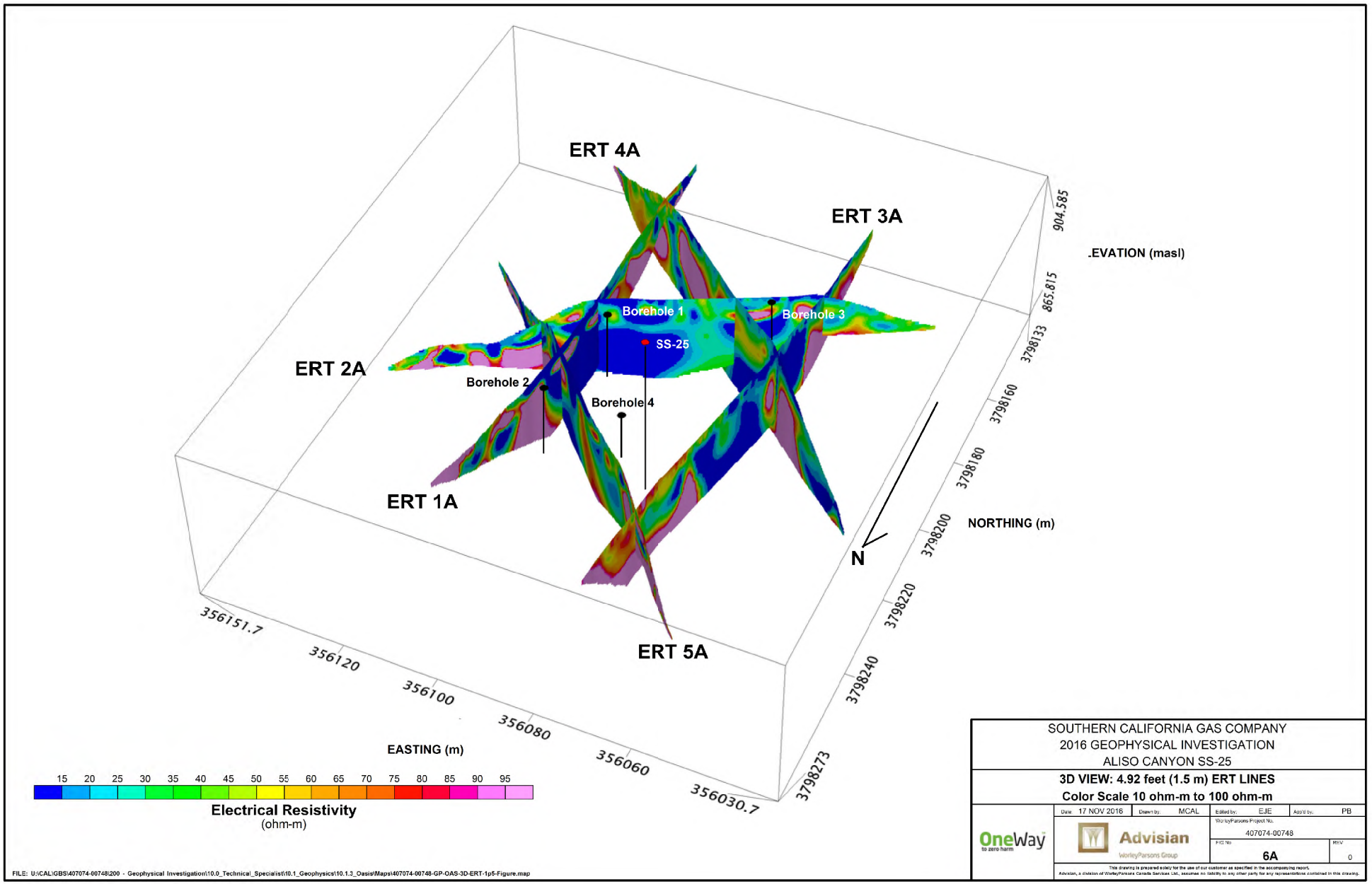

SOUTHERN CALIFORNIA GAS COMPANY
2016 GEOPHYSICAL INVESTIGATION
ALISO CANYON SS-25

3D VIEW: 4.92 feet (1.5 m) ERT LINES
Color Scale 10 ohm-m to 100 ohm-m

Date: 17 NOV 2016	Drawn by: MCAL	Edited by: EJE	Appd by: PB

OneWay to zero harm

Advisian WorleyParsons Group

WorleyParsons Project No.: 407074-00748

FIG No: 6A

REV: 0

This drawing is prepared solely for the use of our customer as specified in the accompanying report. Advisian, a division of WorleyParsons Canada Services Ltd., assumes no liability to any other party for any representations contained in this drawing.

FILE: U:\CAL\GBS\407074-00748\200 - Geophysical Investigation\10.0_Technical_Specialist\10.1_Geophysics\10.1.3_Oasis\Maps\407074-00748-GP-OAS-3D-ERT-1p5-Figure.map

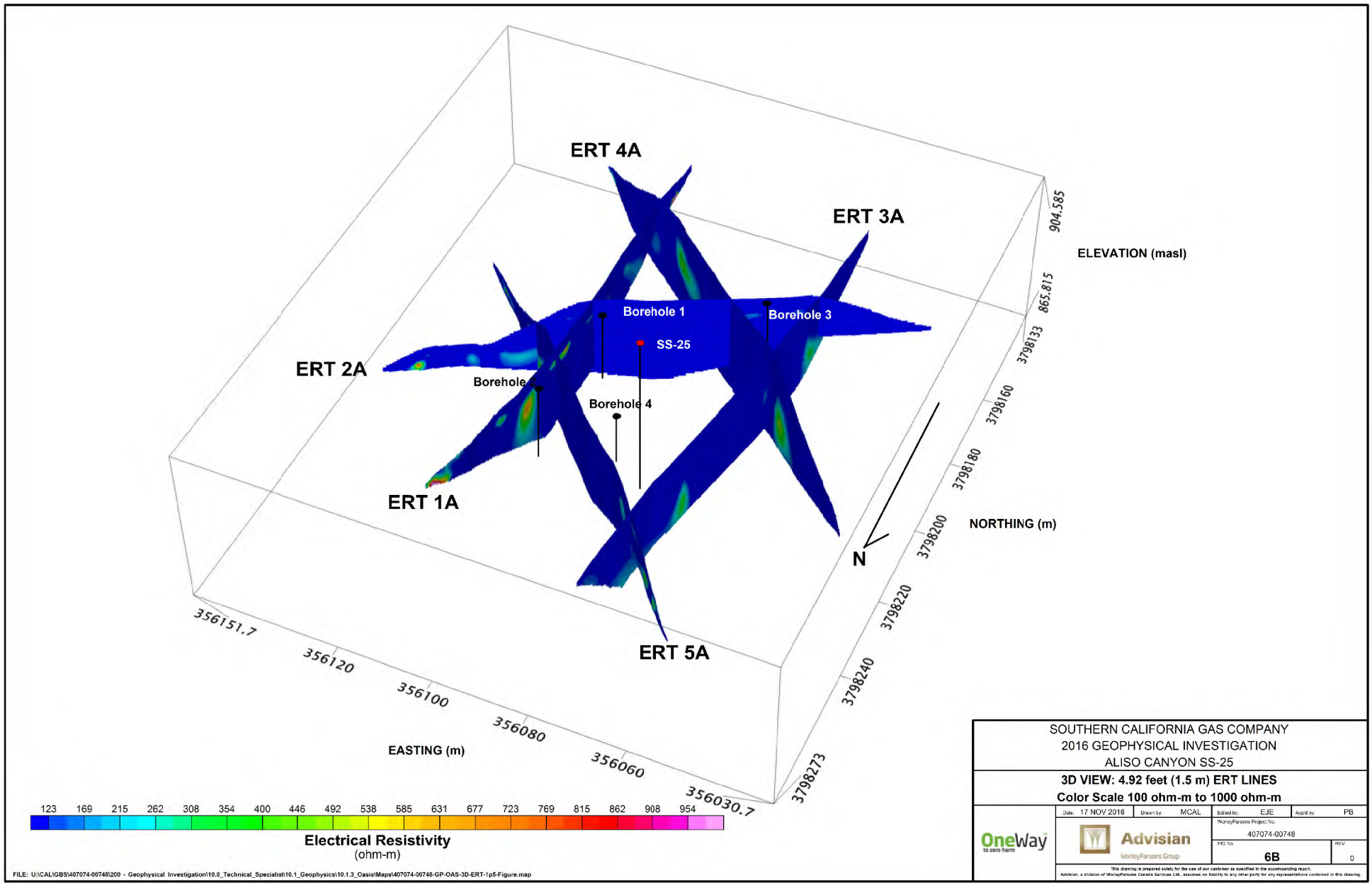

SOUTHERN CALIFORNIA GAS COMPANY
2016 GEOPHYSICAL INVESTIGATION
ALISO CANYON SS-25

3D VIEW: 4.92 feet (1.5 m) ERT LINES
Color Scale 100 ohm-m to 1000 ohm-m

Date: 17 NOV 2016	Drawn by: MCAL	Edited by: EJE	App'd by: PB
		WorleyParsons Project No. 407074-00748	
		FIG No. 6B	REV 0

OneWay to zero harm

Advisian WorleyParsons Group

This drawing is prepared solely for the use of our customer as specified in the accompanying report. Advisian, a division of WorleyParsons Canada Services Ltd., assumes no liability to any other party for any representations contained in this drawing.

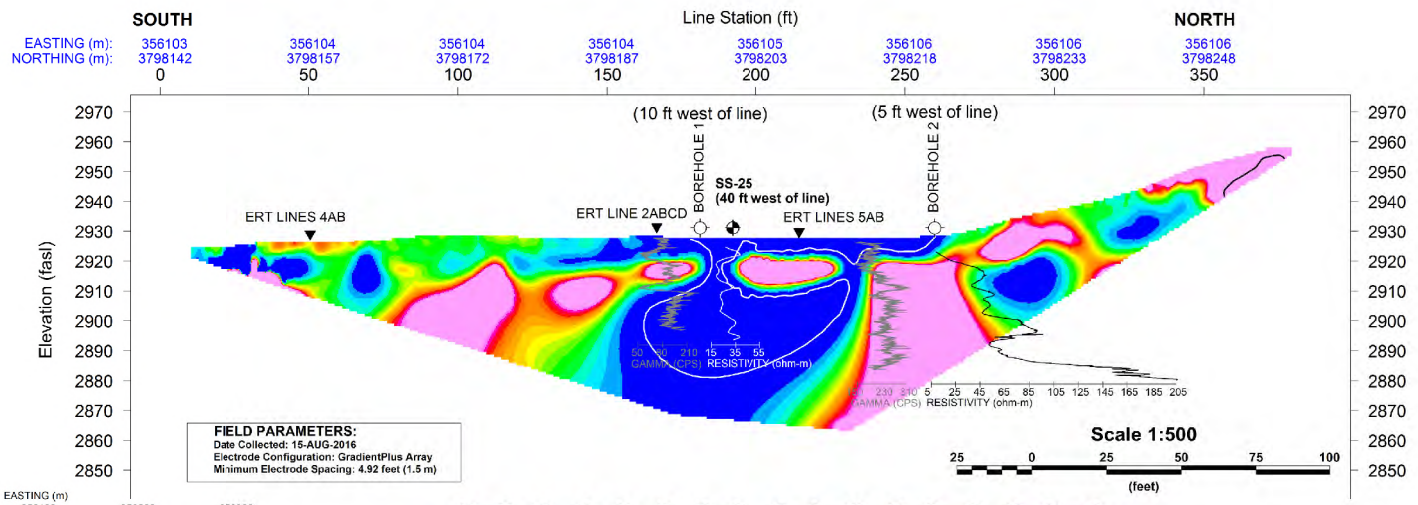

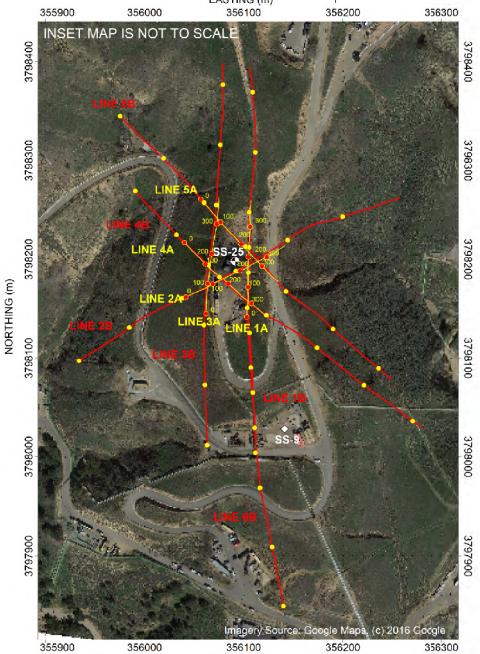

15 20 25 30 35 40 45 50 55 60 65 70 75 80 85 90 95

Electrical Resistivity
(ohm-m)

Legend

CROSS-SECTION

356103 UTM ZONE 11N
3798142 WGS 1983 (metres)

White Lines delineate low-resistivity (< 5 ohm-m) zones
Possibly associated with high-chloride kill fluids

Geotechnical Boreholes

Resistivity Log (ohm-m)

Gamma Log (cps)

INSET MAP

4.92 feet (1.5 m) ERT Lines

16.4 feet (5 m) ERT Lines

Simplified Model Interpretation

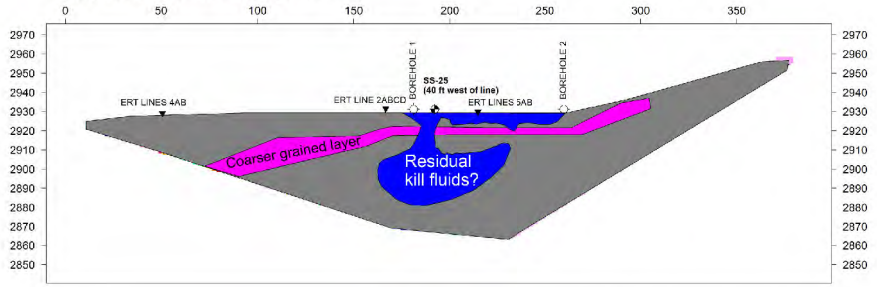

SOUTHERN CALIFORNIA GAS COMPANY
2016 GEOPHYSICAL INVESTIGATION
ALISO CANYON SS-25

LINE: ERT-1A (4.92 FEET [1.5 M])
ELECTRICAL RESISTIVITY CROSS-SECTION

Date: 17 NOV 2016	Drawn by: MCAL	Edited by: EJE	Appr'd by: PB
		WorleyParsons Project No: 407074-00748	
		FIG No: 7	REV: 0

OneWay to zero harm

Advisian WorleyParsons Group

This drawing is prepared solely for the use of our customer as specified in the accompanying report. Advisian, a division of WorleyParsons Canada Services Ltd., assumes no liability to any other party for any representations contained in this drawing.

FILE: U:\CAL\GBS\407074-00748\200 - Geophysical Investigation\10.0_Technical_Specialist\10.1_Geophysics\10.1.3_Oasis\Maps\407074-00748-GP-OAS-ERT1-A.map

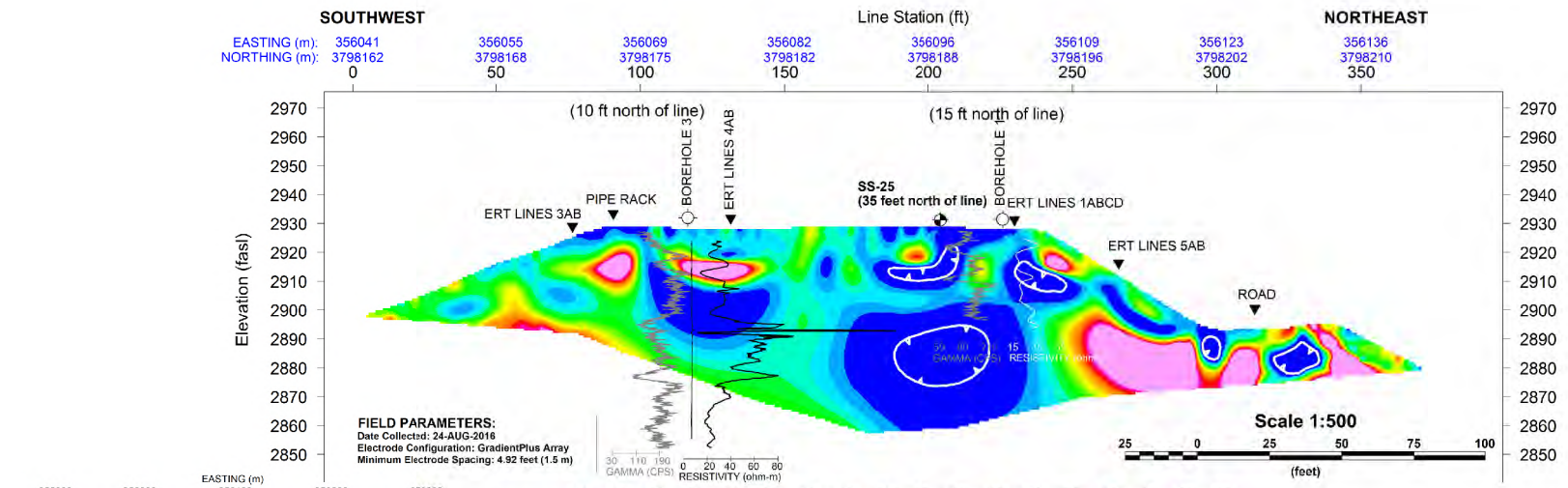

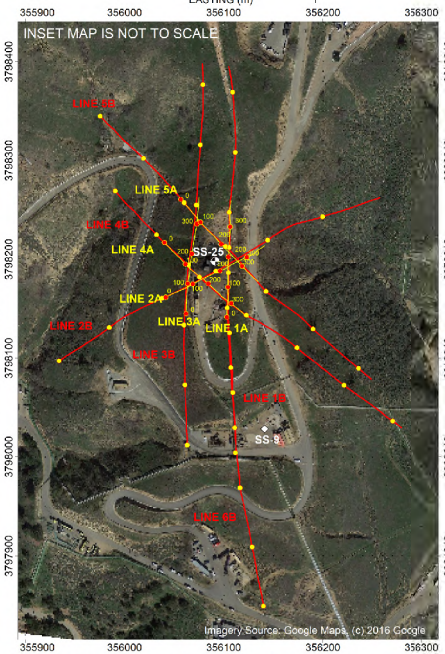

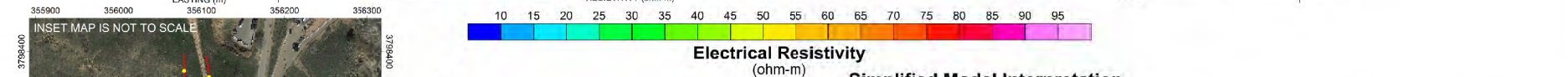

Legend

CROSS-SECTION

356103 UTM ZONE 11N
3798142 WGS 1983 (metres)

White Lines delineate low-resistivity (< 5 ohm-m) zones
Possibly associated with high-chloride kill fluids

Geotechnical Boreholes

Resistivity Log (ohm-m)

Gamma Log (cps)

INSET MAP

4.92 feet (1.5 m) ERT Lines

16.4 feet (5 m) ERT Lines

Simplified Model Interpretation

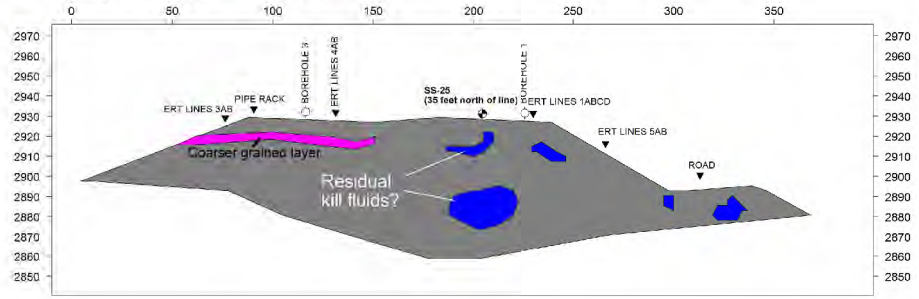

SOUTHERN CALIFORNIA GAS COMPANY
2016 GEOPHYSICAL INVESTIGATION
ALISO CANYON SS-25

LINE: ERT-2A (4.92 FEET [1.5 M])
ELECTRICAL RESISTIVITY CROSS-SECTION

Date:	Drawn by:	Edited by:	Appd by:
17 NOV 2016	MCAL	EJE	PB

WorleyParsons Project No: 407074-00748
FIG No: 8
REV: 0

OneWay
Advisian
WorleyParsons Group

This drawing is prepared solely for the use of our customer as specified in the accompanying report. Advisian, a division of WorleyParsons Canada Services Ltd., assumes no liability to any other party for any representations contained in this drawing.

FILE: U:\CAL\GBS\407074-00748\200 - Geophysical Investigation\10.0_Technical_Specialist\10.1_Geophysics\10.1.3_Oasis\407074-00748-GP-OAS-ERT3-A.map

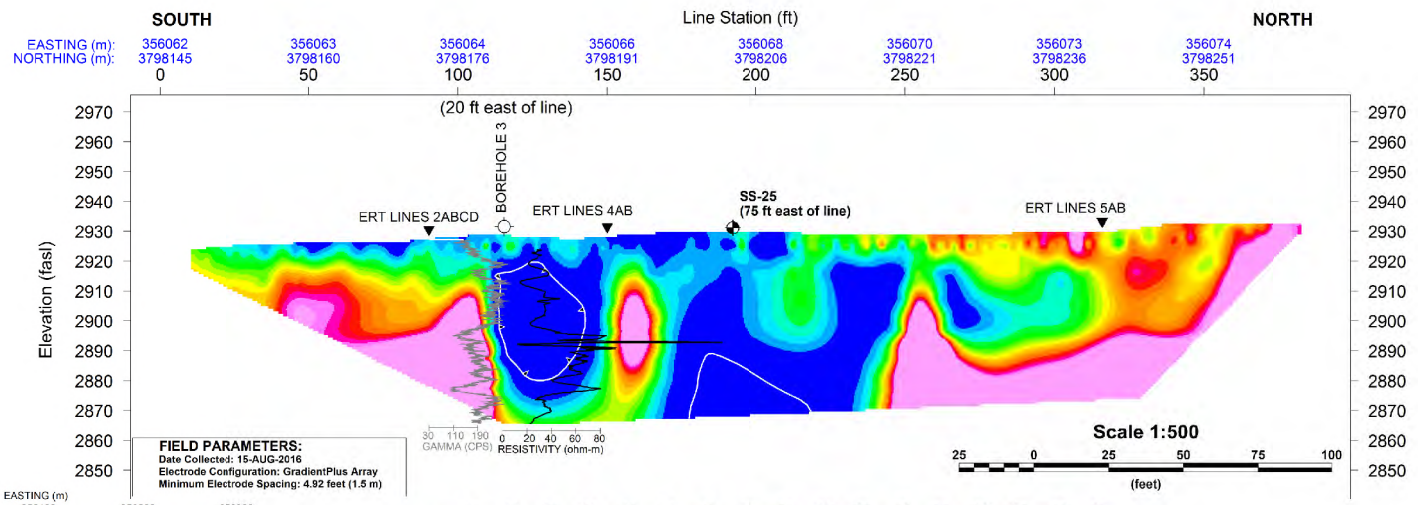

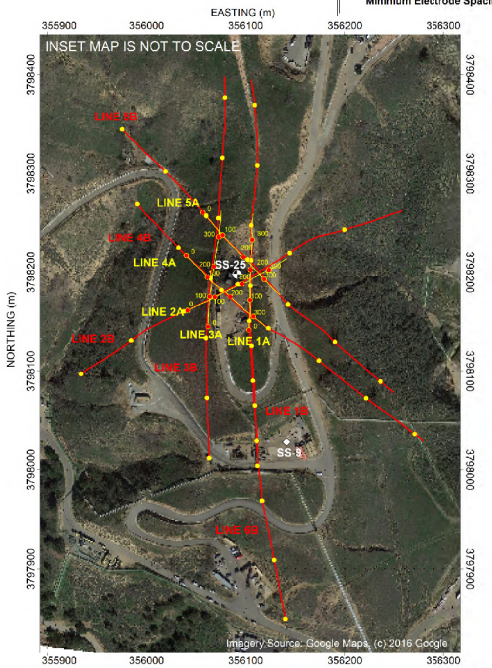

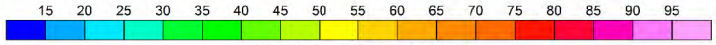

Legend

CROSS-SECTION

356103 UTM ZONE 11N
3798142 WGS 1983 (metres)

White Lines delineate low-resistivity (< 5 ohm-m) zones
Possibly associated with high-chloride kill fluids

Geotechnical Boreholes

Resistivity Log (ohm-m)

Gamma Log (cps)

INSET MAP

4.92 feet (1.5 m) ERT Lines

16.4 feet (5 m) ERT Lines

Simplified Model Interpretation

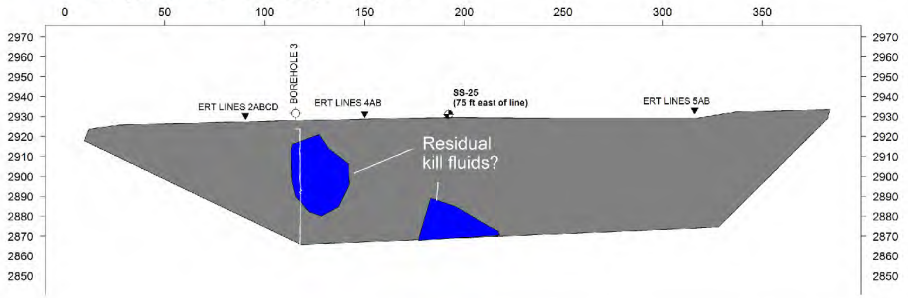

SOUTHERN CALIFORNIA GAS COMPANY
2016 GEOPHYSICAL INVESTIGATION
ALISO CANYON SS-25

LINE: ERT-3A (4.92 FEET [1.5 M])
ELECTRICAL RESISTIVITY CROSS-SECTION

Date: 17 NOV 2016	Drawn by: MCAL	Edited by: EJE	Appr'd by: PB
		WorleyParsons Project No: 407074-00748	
		FIG No: 9	REV: 0

OneWay to zero harm

Advisian WorleyParsons Group

This drawing is prepared solely for the use of our customer as specified in the accompanying report. Advisian, a division of WorleyParsons Canada Services Ltd., assumes no liability to any other party for any representations contained in this drawing.

FILE: U:\CAL\GBS\407074-00748\200 - Geophysical Investigation\10.0_Technical_Specialist\10.1_Geophysics\10.1.3_Oasis\407074-00748-GP-OAS-ERT2-A.map

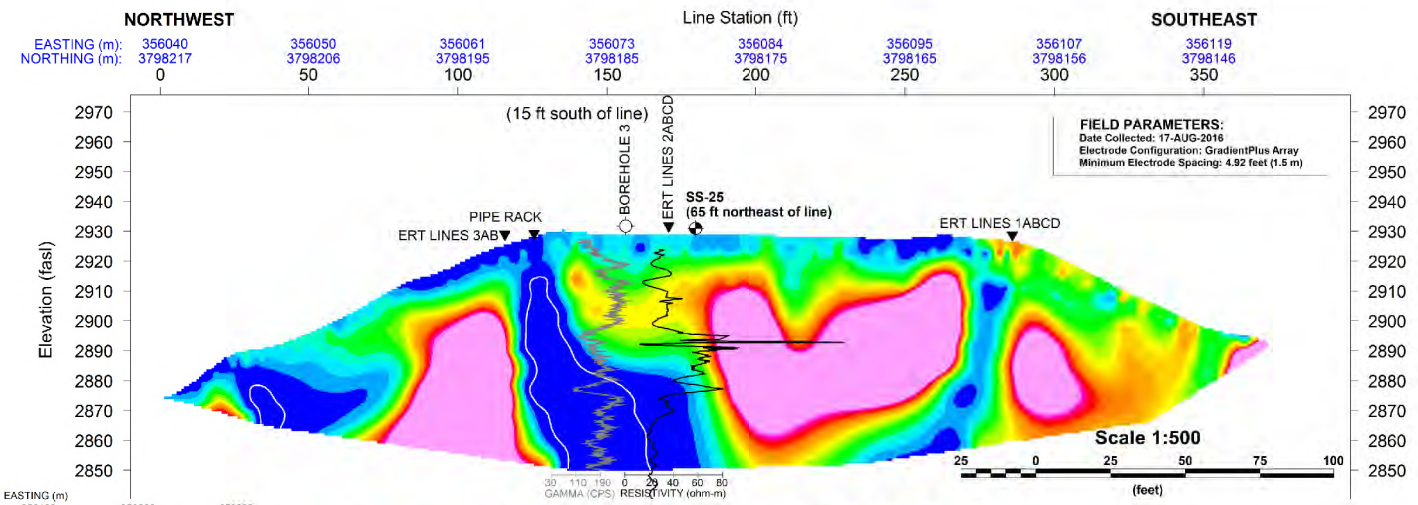

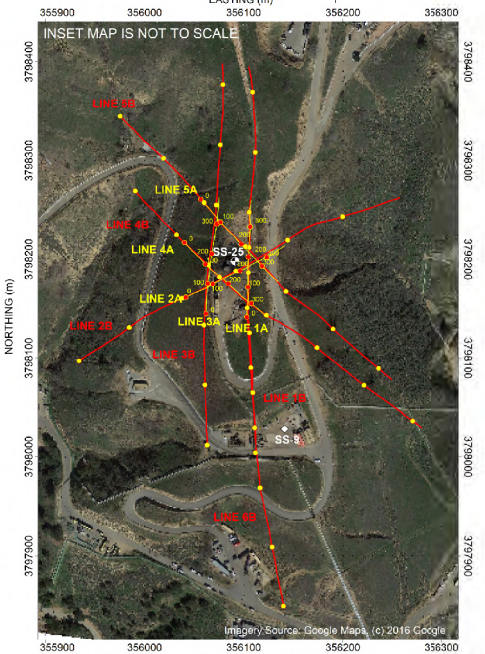

10 15 20 25 30 35 40 45 50 55 60 65 70 75 80 85 90 95

Electrical Resistivity
(ohm-m)

Legend

CROSS-SECTION

356103 UTM ZONE 11N
3798142 WGS 1983 (metres)

White Lines delineate low-resistivity (< 5 ohm-m) zones
Possibly associated with high-chloride kill fluids

Geotechnical Boreholes

Resistivity Log (ohm-m)

Gamma Log (cps)

INSET MAP

4.92 feet (1.5 m) ERT Lines

16.4 feet (5 m) ERT Lines

Simplified Model Interpretation

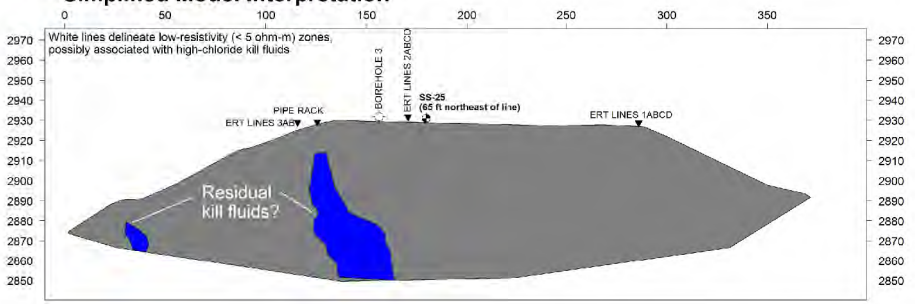

SOUTHERN CALIFORNIA GAS COMPANY
2016 GEOPHYSICAL INVESTIGATION
ALISO CANYON SS-25

LINE: ERT-4A (4.92 FEET [1.5 M])
ELECTRICAL RESISTIVITY CROSS-SECTION

Date: 17 NOV 2016	Drawn by: MCAL	Edited by: EJE	Appd by: PB

OneWay

Advisian
WorleyParsons Group

WorleyParsons Project No: 407074-00748
FIG No: 10
REV: 0

This drawing is prepared solely for the use of our customer as specified in the accompanying report. Advisian, a division of WorleyParsons Canada Services Ltd., assumes no liability to any other party for any representations contained in this drawing.

FILE: U:\CAL\GBS\407074-00748\200 - Geophysical Investigation\10.0_Technical_Specialist\10.1_Geophysics\10.1.3_Oasis\407074-00748-GP-OAS-ERT4-A.map

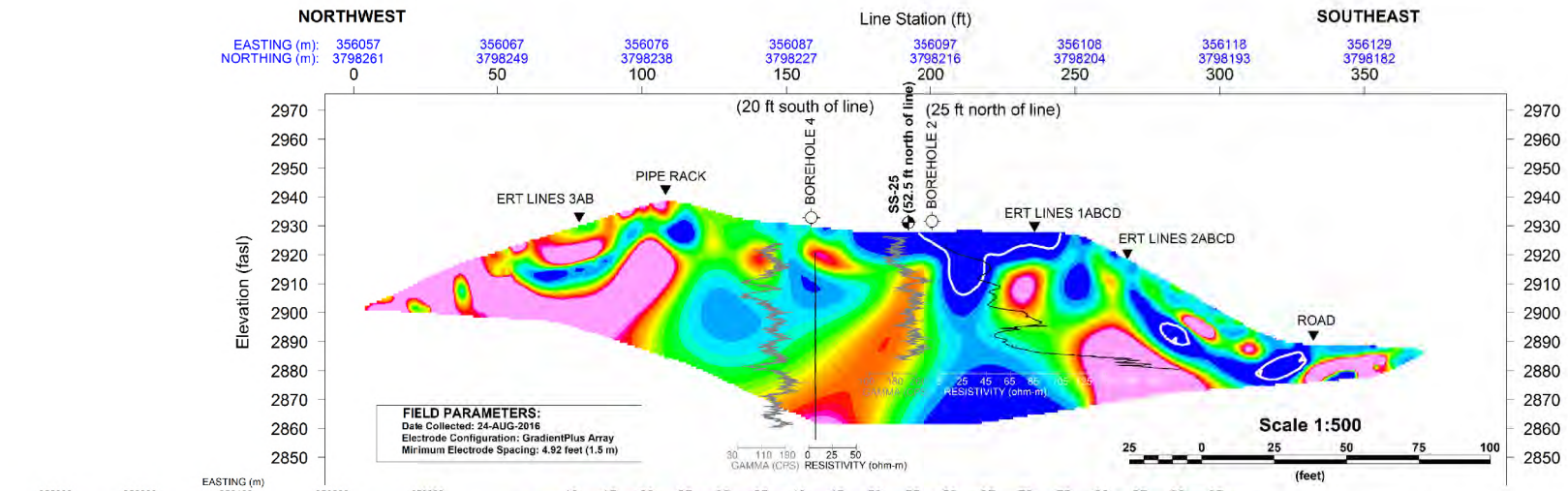

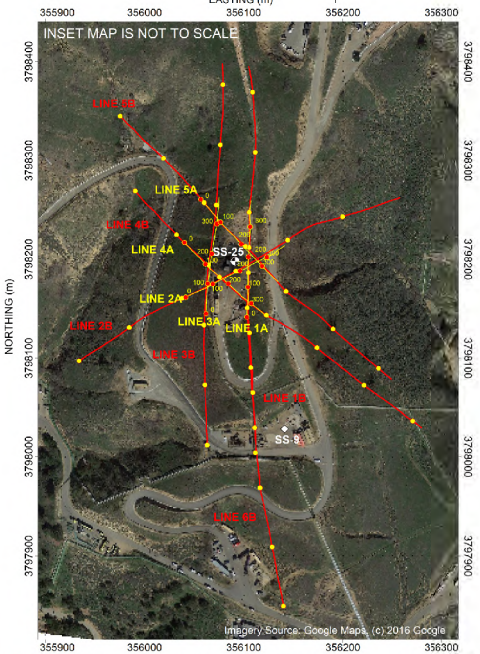

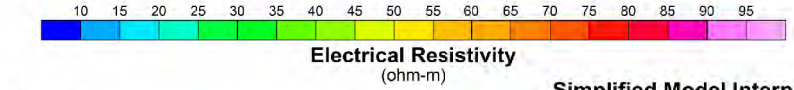

Legend

CROSS-SECTION

356103 UTM ZONE 11N
3798142 WGS 1983 (metres)

White Lines delineate low-resistivity (< 5 ohm-m) zones
Possibly associated with high-chloride kill fluids

Geotechnical Boreholes

Resistivity Log (ohm-m)

Gamma Log (cps)

INSET MAP

4.92 feet (1.5 m) ERT Lines

16.4 feet (5 m) ERT Lines

Simplified Model Interpretation

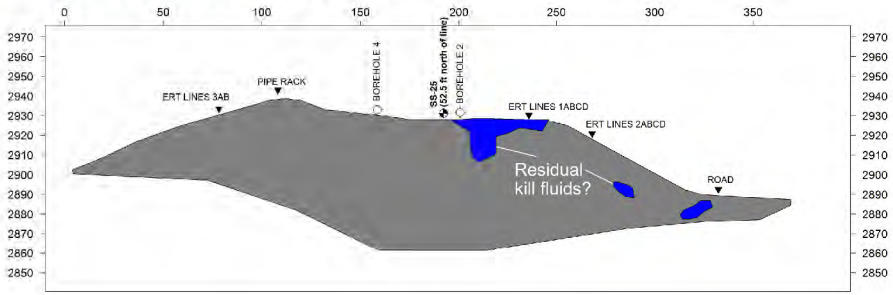

SOUTHERN CALIFORNIA GAS COMPANY
2016 GEOPHYSICAL INVESTIGATION
ALISO CANYON SS-25

LINE: ERT-5A (4.92 FEET [1.5 M])
ELECTRICAL RESISTIVITY CROSS-SECTION

Date: 17 NOV 2016	Drawn by: MCAL	Edited by: EJE	Appd by: PB
		WorleyParsons Project No: 407074-00748	
		FIG No: 11	REV: 0

OneWay
Advisian WorleyParsons Group

This drawing is prepared solely for the use of our customer as specified in the accompanying report. Advisian, a division of WorleyParsons Canada Services Ltd., assumes no liability to any other party for any representations contained in this drawing.

FILE: U:\CAL\GBS\407074-00748\200 - Geophysical Investigation\10.0_Technical_Specialist\10.1_Geophysics\10.1.3_Oasis\Maps\407074-00748-GP-OAS-ERT5A.map

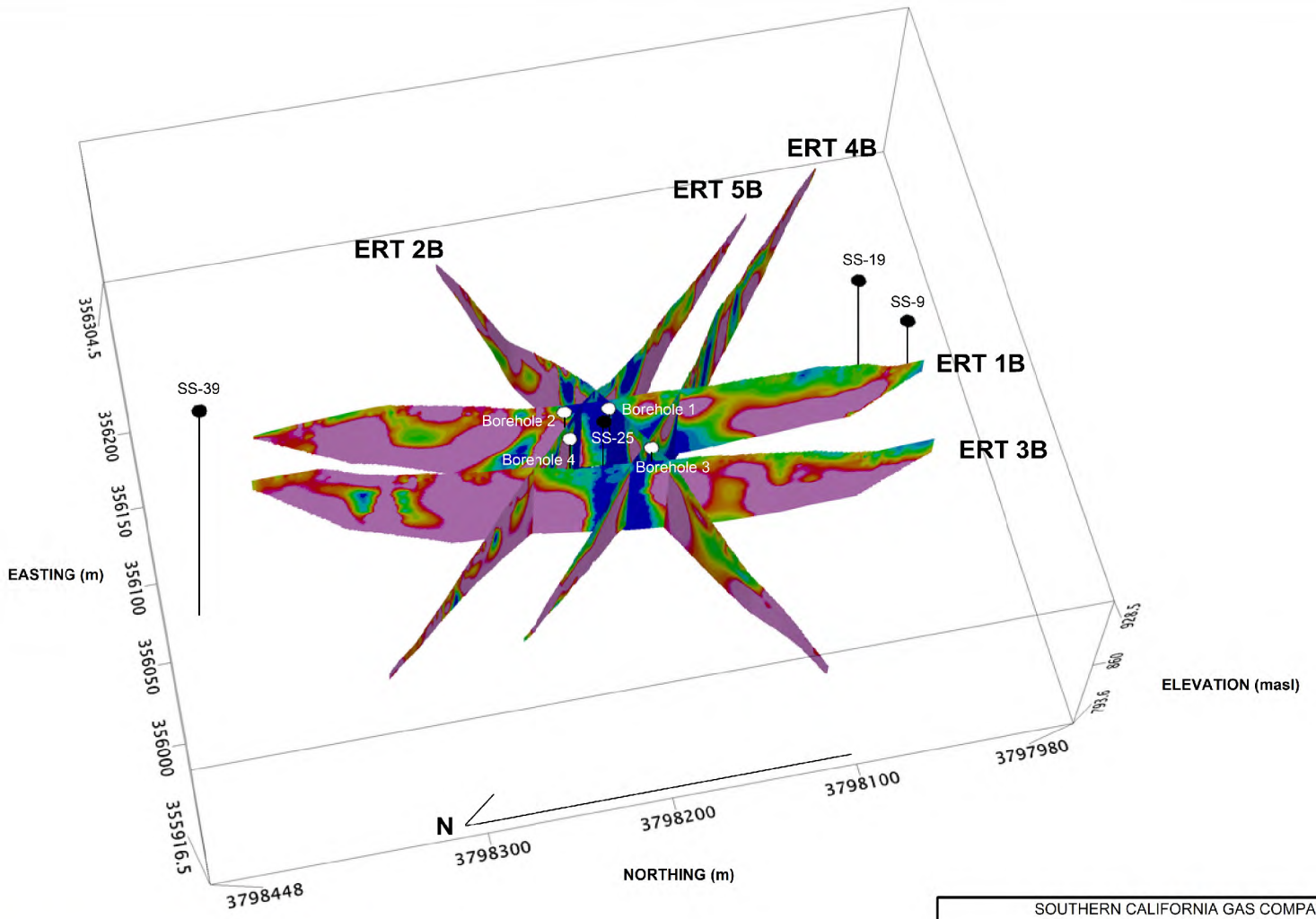

FILE: U:\CAL\GBS\407074-00749\200 - Geophysical Investigation\10.0_Technical_Specialist\10.1_Geophysics\10.1.3_Oasis\Maps\407074-00748-GP-OAS-3D-ERT-6m-Figure.map

SOUTHERN CALIFORNIA GAS COMPANY
2016 GEOPHYSICAL INVESTIGATION
ALISO CANYON SS-25

3D VIEW: 16.4 feet (5 m) ERT LINES
Color Scale 10 ohm-m to 100 ohm-m

Date: 17 NOV 2016	Drawn by: MCAL	Edited by: EJE	Appd by: PB

OneWay to zero harm

Advisian WorleyParsons Group

WorleyParsons Project No. 407074-00748

FIG No. 12A

REV 0

This drawing is prepared solely for the use of our customer as specified in the accompanying report. Advisian, a division of WorleyParsons Canada Services Ltd., assumes no liability to any other party for any representations contained in this drawing.

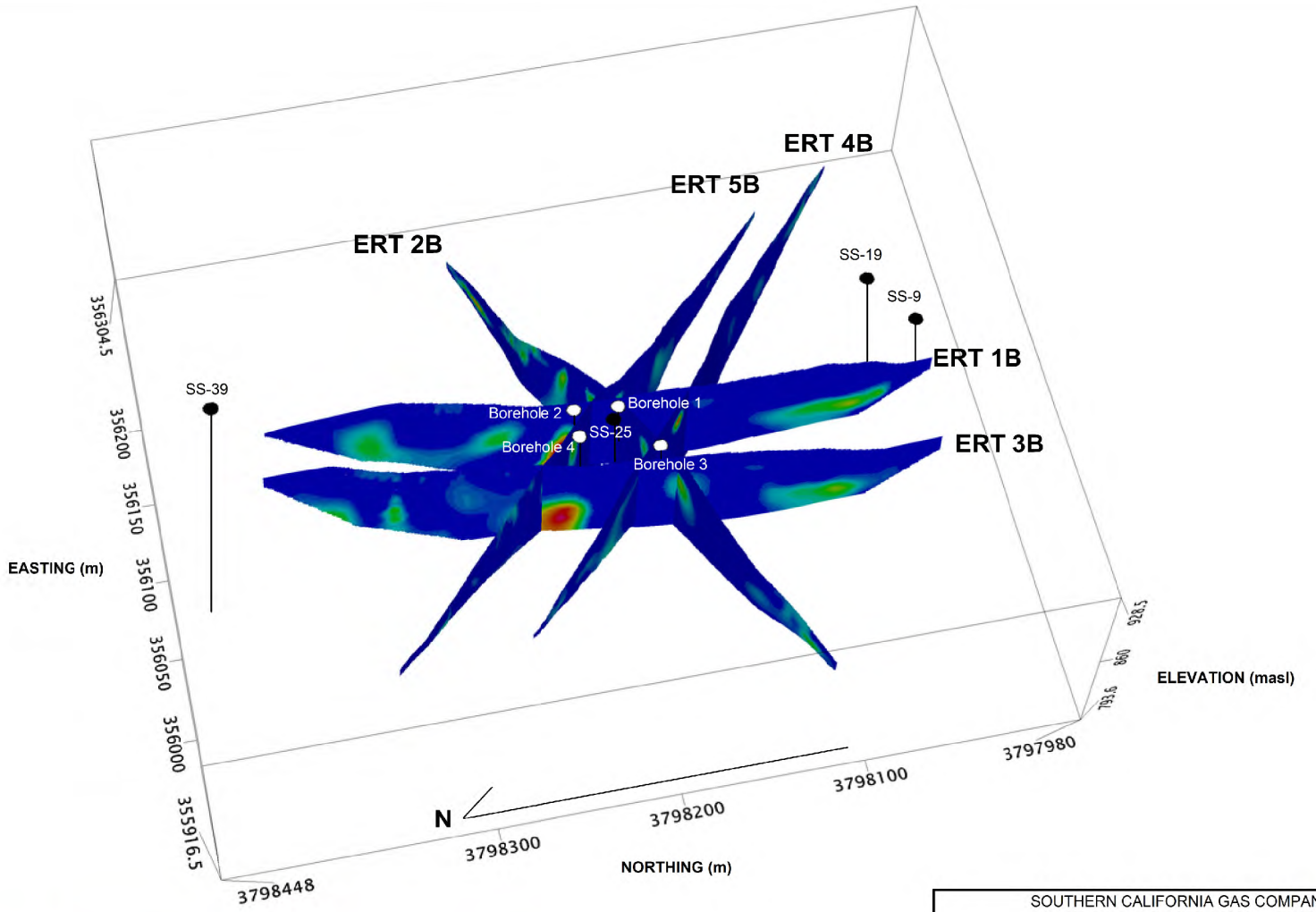

FILE: U:\CAL\GBS\407074-00748\200 - Geophysical Investigation\10.0_Technical_Specialist\10.1_Geophysics\10.1.3_Oasis\Maps\407074-00748-GP-OAS-3D-ERT-5m-Figure.map

SOUTHERN CALIFORNIA GAS COMPANY
2016 GEOPHYSICAL INVESTIGATION
ALISO CANYON SS-25

3D VIEW: 16.4 feet (5 m) ERT LINES
Color Scale 100 ohm-m to 1000 ohm-m

Date: 17 NOV 2016	Drawn by: MCAL	Edited by: EJE	Appd by: PB

OneWay to zero harm

Advisian WorleyParsons Group

WorleyParsons Project No.: 407074-00748

FIG No.: 12B

REV: 0

This drawing is prepared solely for the use of our customer as specified in the accompanying report. Advisian, a division of WorleyParsons Canada Services Ltd., assumes no liability to any other party for any representations contained in this drawing.

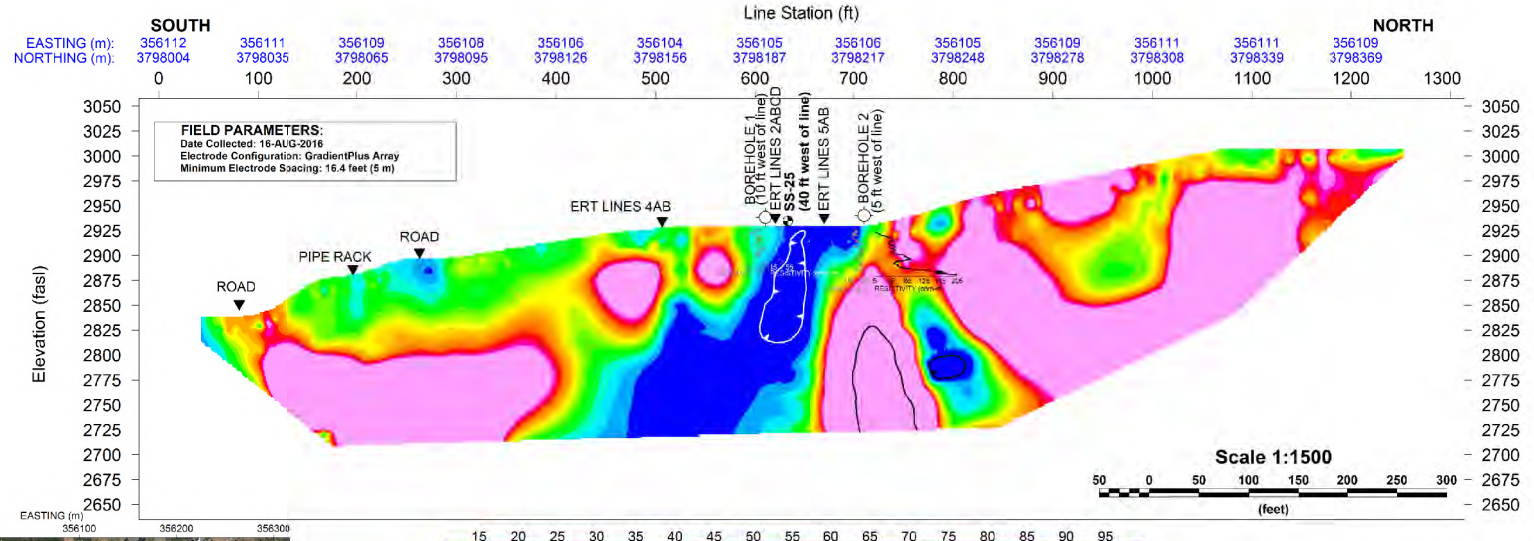

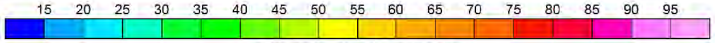

Electrical Resistivity
(ohm-m)

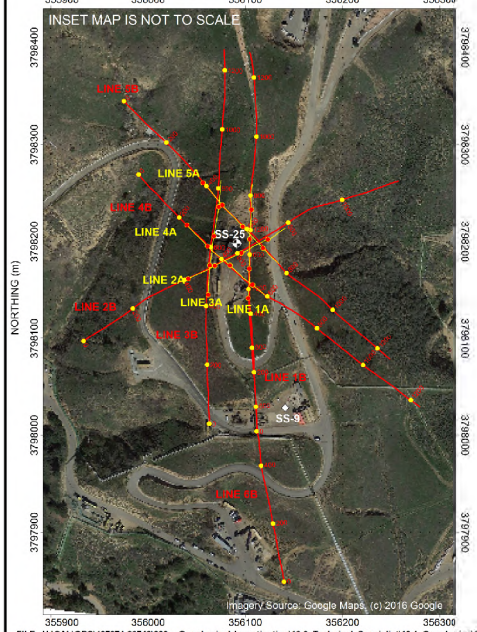

Legend

CROSS-SECTION

356103 UTM ZONE 11N
3798142 WGS 1983 (metres)

White Lines delineate low-resistivity (< 5 ohm-m) zones
Possibly associated with high-chloride kill fluids

Black Lines delineate high-resistivity (> 500 ohm-m) zones

INSET MAP

4.92 feet (1.5 m) ERT Lines

16.4 feet (5 m) ERT Lines

Simplified Model Interpretation

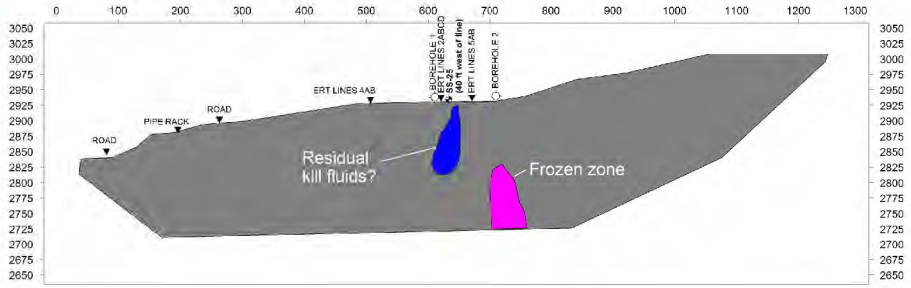

SOUTHERN CALIFORNIA GAS COMPANY
2016 GEOPHYSICAL INVESTIGATION
ALISO CANYON SS-25

LINE: ERT-1B (16.4 FEET [5 M])
ELECTRICAL RESISTIVITY CROSS-SECTION

Date: 17 NOV 2016	Drawn by: MCAL	Edited by: EJE	Appd by: PB
		WorleyParsons Project No.: 407074-00748	
		FIG No.: 13	REV: 0

OneWay
Advisian WorleyParsons Group

This drawing is prepared solely for the use of our customer as specified in the accompanying report.
Advisian, a division of WorleyParsons Canada Services Ltd., assumes no liability to any other party for any representations contained in this drawing.

FILE: U:\CAL\GBS\407074-00748\200 - Geophysical Investigation\10.0_Technical_Specialist\10.1_Geophysics\10.1.3_Oasis\Maps\407074-00748-GP-OAS-ERT1B-A.map

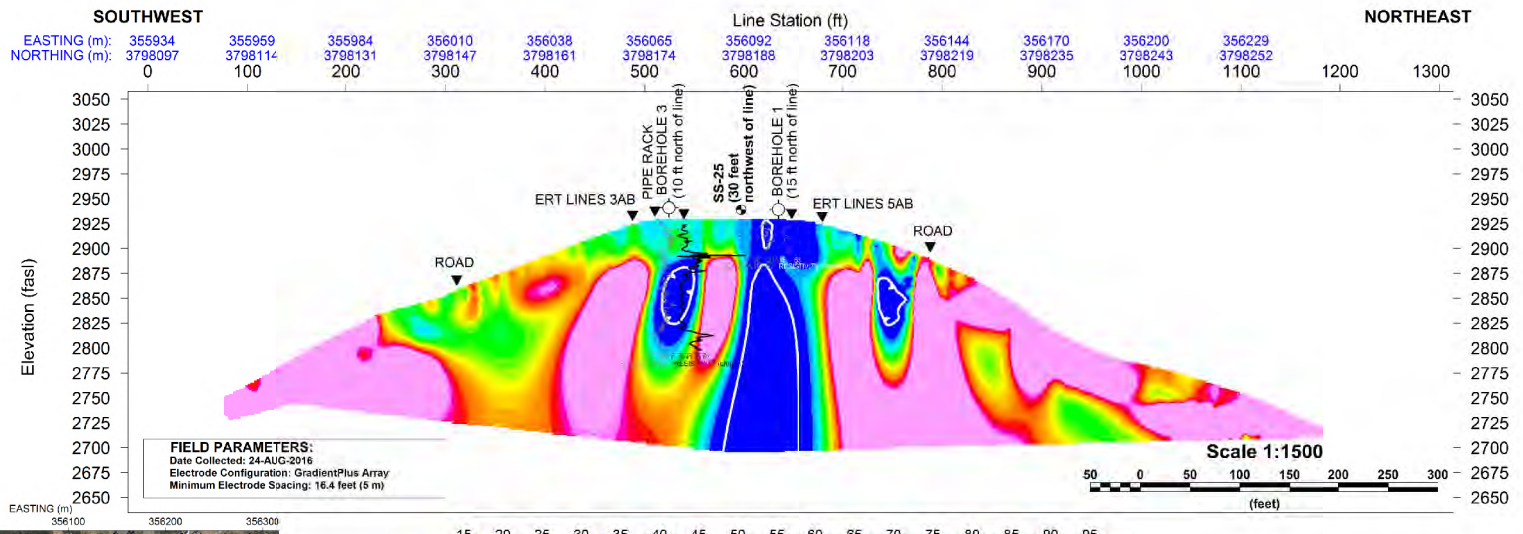

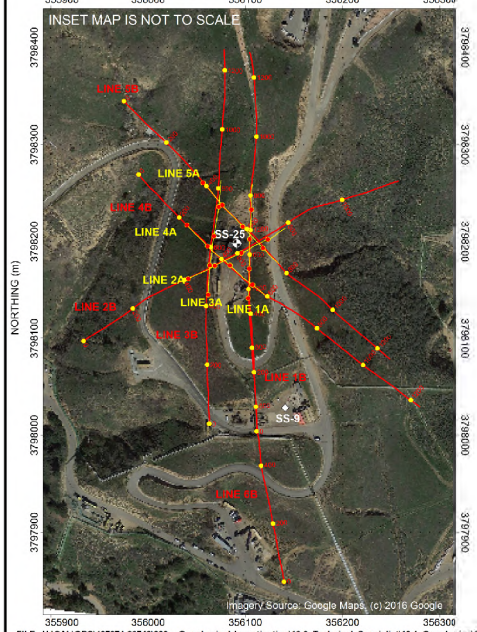

15 20 25 30 35 40 45 50 55 60 65 70 75 80 85 90 95

Electrical Resistivity
(ohm-m)

Legend

CROSS-SECTION

356103 UTM ZONE 11N
3798142 WGS 1983 (metres)

White Lines delineate low-resistivity (< 5 ohm-m) zones
Possibly associated with high-chloride kill fluids

INSET MAP

4.92 feet (1.5 m) ERT Lines

16.4 feet (5 m) ERT Lines

Simplified Model Interpretation

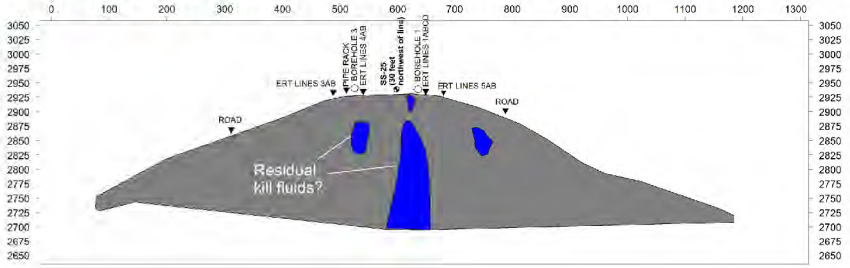

FILE: U:\CAL\GBS\407074-00748\200 - Geophysical Investigation\10.0_Technical_Specialist\10.1_Geophysics\10.1.3_Oasis\Maps\407074-00748-GP-OAS-ERT4B-A.map

SOUTHERN CALIFORNIA GAS COMPANY
2016 GEOPHYSICAL INVESTIGATION
ALISO CANYON SS-25

LINE: ERT-2B (16.4 FEET [5 M])
ELECTRICAL RESISTIVITY CROSS-SECTION

Date: 17 NOV 2016	Drawn by: MCAL	Edited by: EJE	Appd by: PB

OneWay
Advisian
WorleyParsons Group

WorleyParsons Project No.: 407074-00748
FIG No.: 14
REV: 0

This drawing is prepared solely for the use of our customer as specified in the accompanying report.
Advisian, a division of WorleyParsons Canada Services Ltd., assumes no liability to any other party for any representations contained in this drawing.

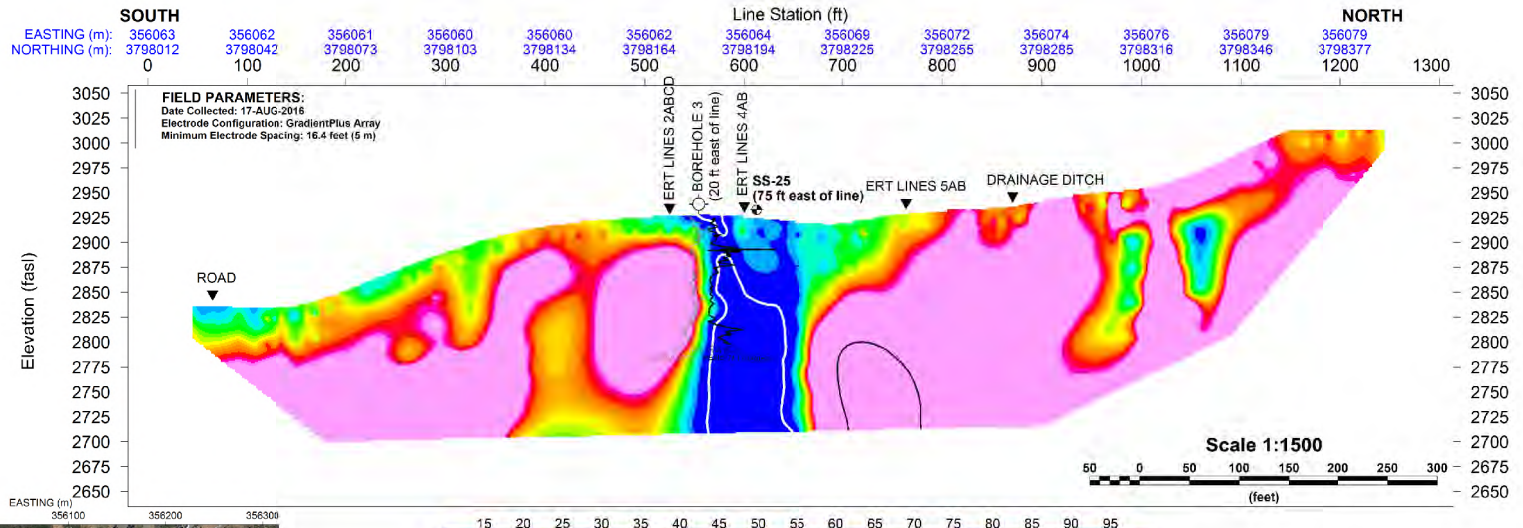

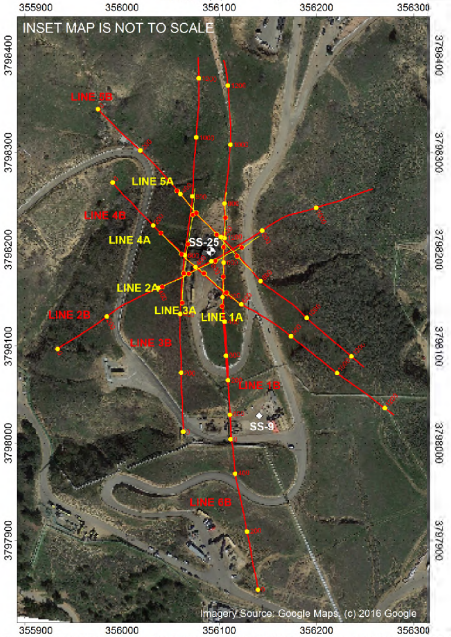

15 20 25 30 35 40 45 50 55 60 65 70 75 80 85 90 95

Electrical Resistivity
(ohm-m)

Legend

CROSS-SECTION

356103 UTM ZONE 11N
3798142 WGS 1983 (metres)

White Lines delineate low-resistivity (< 5 ohm-m) zones
Possibly associated with high-chloride kill fluids

Black Lines delineate high-resistivity (> 500 ohm-m) zones

INSET MAP

4.92 feet (1.5 m) ERT Lines

16.4 feet (5 m) ERT Lines

Simplified Model Interpretation

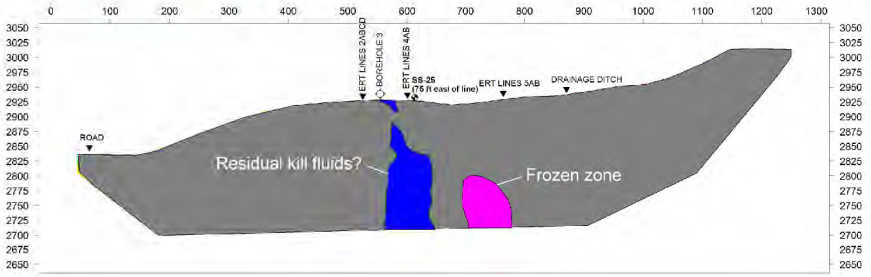

SOUTHERN CALIFORNIA GAS COMPANY
2016 GEOPHYSICAL INVESTIGATION
ALISO CANYON SS-25

LINE: ERT-3B (16.4 FEET [5 M])
ELECTRICAL RESISTIVITY CROSS-SECTION

Date:	Drawn by:	Edited by:	Appd by:
17 NOV 2016	MCAL	EJE	PB

WorleyParsons Project No.: 407074-00748
FIG No.: 15
REV: 0

OneWay
Advisian
WorleyParsons Group

This drawing is prepared solely for the use of our customer as specified in the accompanying report.
Advisian, a division of WorleyParsons Canada Services Ltd., assumes no liability to any other party for any representations contained in this drawing.

FILE: U:\CAL\GBS\407074-00748\200 - Geophysical Investigation\10.0_Technical_Specialist\10.1_Geophysics\10.1.3_Oasis\407074-00748-GP-OAS-ERT2B-A.mxd

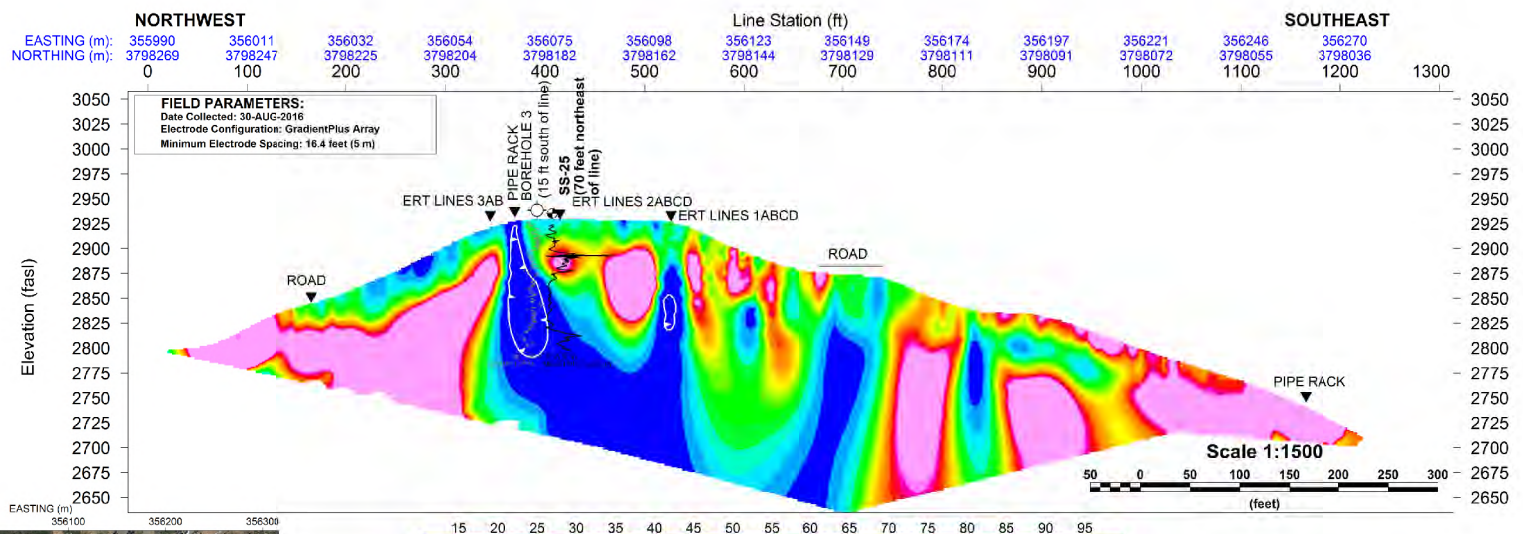

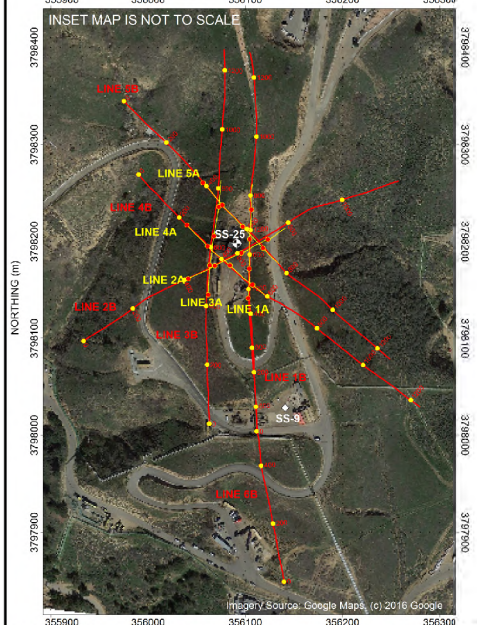

Legend

CROSS-SECTION

356103 UTM ZONE 11N
3798142 WGS 1983 (metres)

White Lines delineate low-resistivity (< 5 ohm-m) zones
Possibly associated with high-chloride kill fluids

Black Lines delineate high-resistivity (> 500 ohm-m) zones

INSET MAP

4.92 feet (1.5 m) ERT Lines

16.4 feet (5 m) ERT Lines

Simplified Model Interpretation

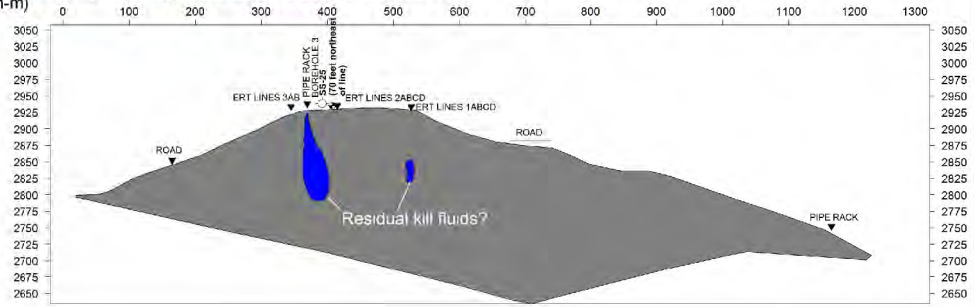

SOUTHERN CALIFORNIA GAS COMPANY
2016 GEOPHYSICAL INVESTIGATION
ALISO CANYON SS-25

LINE: ERT-4B (16.4 FEET [5 M])
ELECTRICAL RESISTIVITY CROSS-SECTION

Date: 17 NOV 2016	Drawn by: MCAL	Edited by: EJE	Appd by: PB

OneWay
Advisian
WorleyParsons Group

WorleyParsons Project No.: 407074-00748
RIG No.: 16
REV: 0

This drawing is prepared solely for the use of our customer as specified in the accompanying report.
Advisian, a division of WorleyParsons Canada Services Ltd., assumes no liability to any other party for any representations contained in this drawing.

FILE: U:\CAL\GBS\407074-00748\200 - Geophysical Investigation\10.0_Technical_Specialist\10.1_Geophysics\10.1.3_Oasis\Maps\407074-00748-GP-OAS-ERT3B-A.map

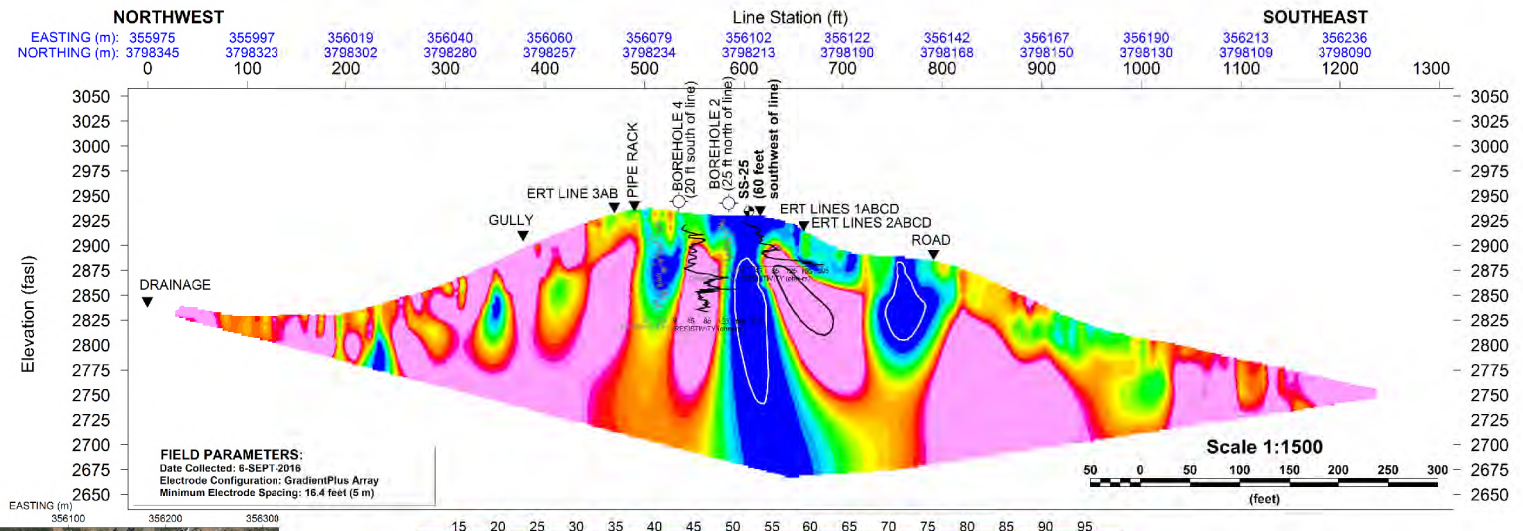

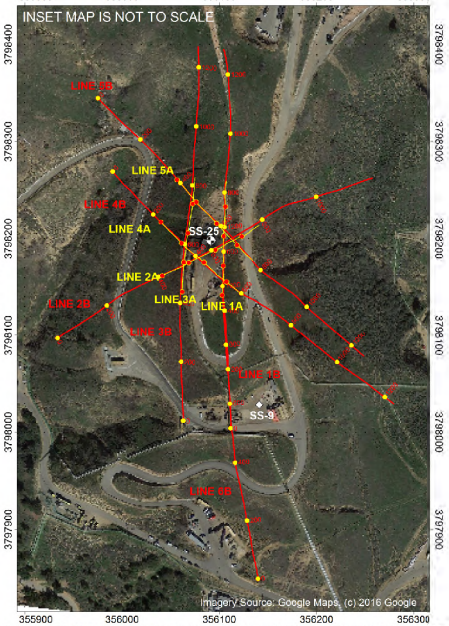

Simplified Model Interpretation

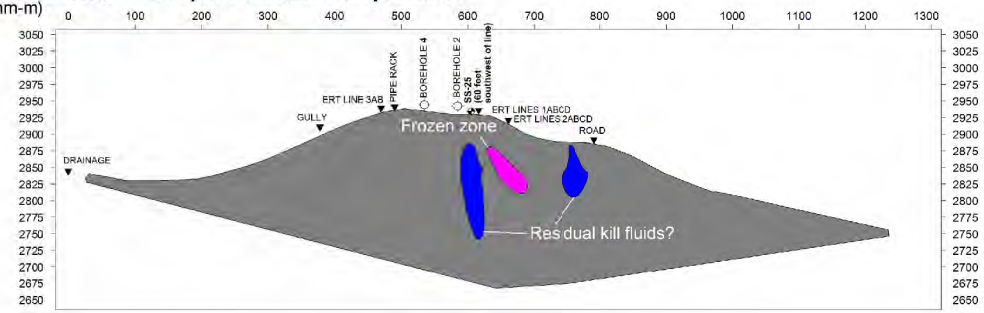

Legend

CROSS-SECTION

356103 UTM ZONE 11N
3798142 WGS 1983 (metres)

White Lines delineate low-resistivity (< 5 ohm-m) zones
Possibly associated with high-chloride kill fluids

Black Lines delineate high-resistivity (> 500 ohm-m) zones

INSET MAP

4.92 feet (1.5 m) ERT Lines

16.4 feet (5 m) ERT Lines

SOUTHERN CALIFORNIA GAS COMPANY
2016 GEOPHYSICAL INVESTIGATION
ALISO CANYON SS-25

LINE: ERT-5B (16.4 FEET [5 M])
ELECTRICAL RESISTIVITY CROSS-SECTION

Date: 17 NOV 2016	Drawn by: MCAL	Edited by: EJE	Appd by: PB
		WorleyParsons Project No. 407074-00748	
		FIG No. 17	REV 0

OneWay
Advisian WorleyParsons Group

This drawing is prepared solely for the use of our customer as specified in the accompanying report. Advisian, a division of WorleyParsons Canada Services Ltd., assumes no liability to any other party for any representations contained in this drawing.

FILE: U:\CAL\GBS\407074-00748\200 - Geophysical Investigation\10.0_Technical_Specialist\10.1_Geophysics\10.1.3_Oasis\Maps\407074-00748-GP-OAS-ERT6B-A.map

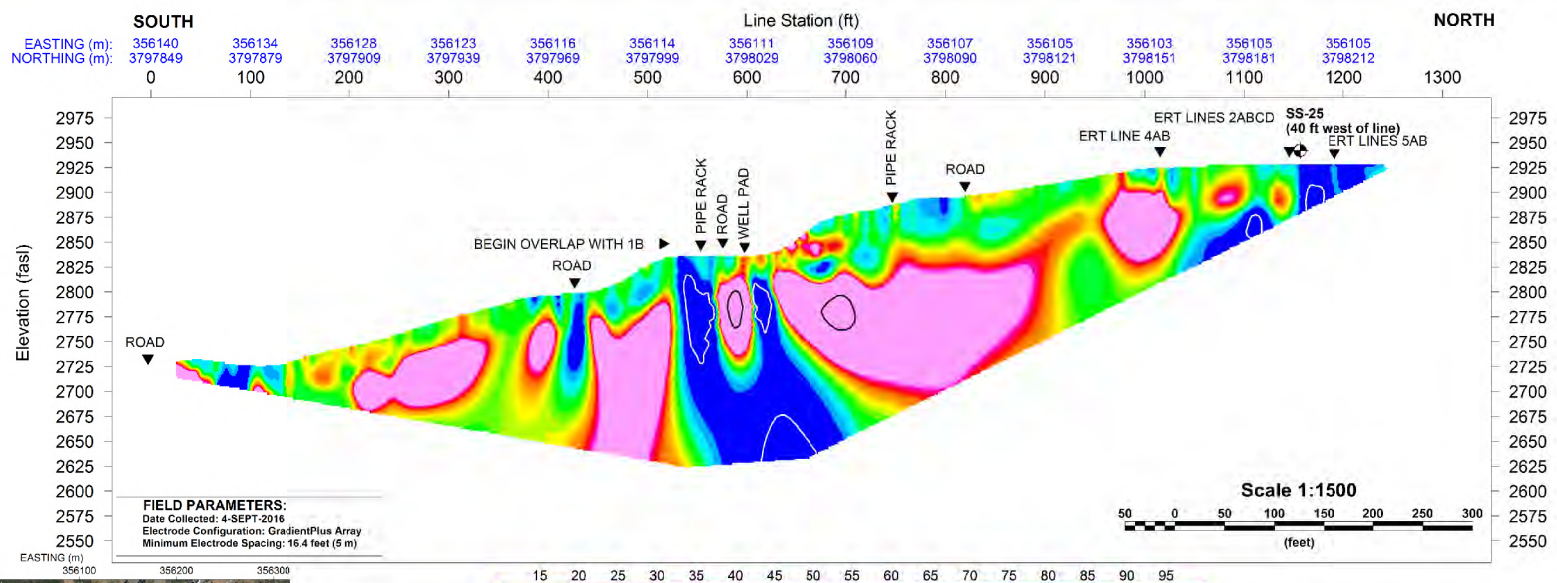

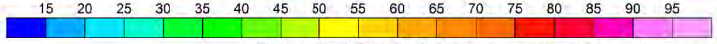

Electrical Resistivity (ohm-m)

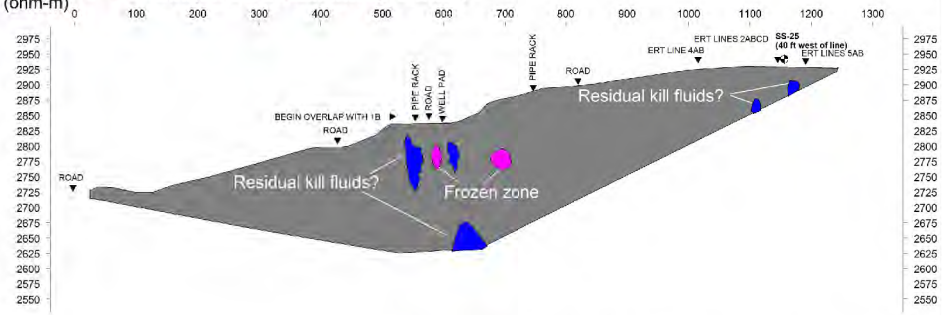

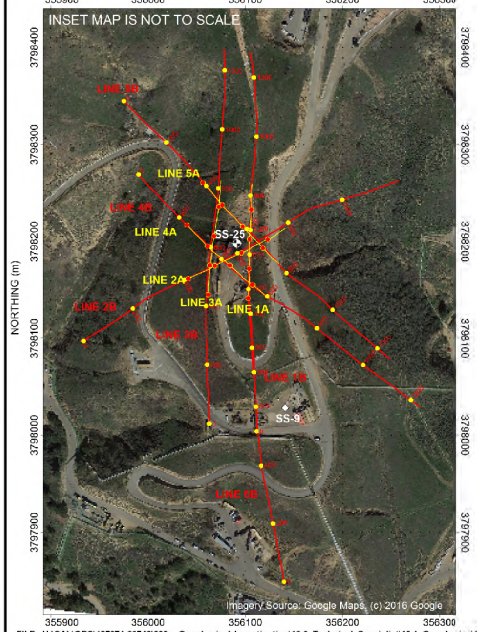

Legend

CROSS-SECTION

356103 UTM ZONE 11N
3798142 WGS 1983 (metres)

White Lines delineate low-resistivity (< 5 ohm-m) zones
Possibly associated with high-chloride kill fluids

Black Lines delineate high-resistivity (> 500 ohm-m) zones

INSET MAP

4.92 feet (1.5 m) ERT Lines

16.4 feet (5 m) ERT Lines

SOUTHERN CALIFORNIA GAS COMPANY
2016 GEOPHYSICAL INVESTIGATION
ALISO CANYON SS-25

LINE: ERT-6B (16.4 FEET [5 M])
ELECTRICAL RESISTIVITY CROSS-SECTION

Date: 17 NOV 2016	Drawn by: MCAL	Edited by: EJE	Appd by: PB

OneWay
Advisian WorleyParsons Group

WorleyParsons Project No. 407074-00748
FIG No. 18
REV 0

This drawing is prepared solely for the use of our customer as specified in the accompanying report. Advisian, a division of WorleyParsons Canada Services Ltd., assumes no liability to any other party for any representations contained in this drawing.

FILE: U:\CAL\GBS\407074-00748\200 - Geophysical Investigation\10.0_Technical_Specialist\10.1_Geophysics\10.1.3_Oasis\Maps\407074-00748-GP-OAS-ERT5B-A.map

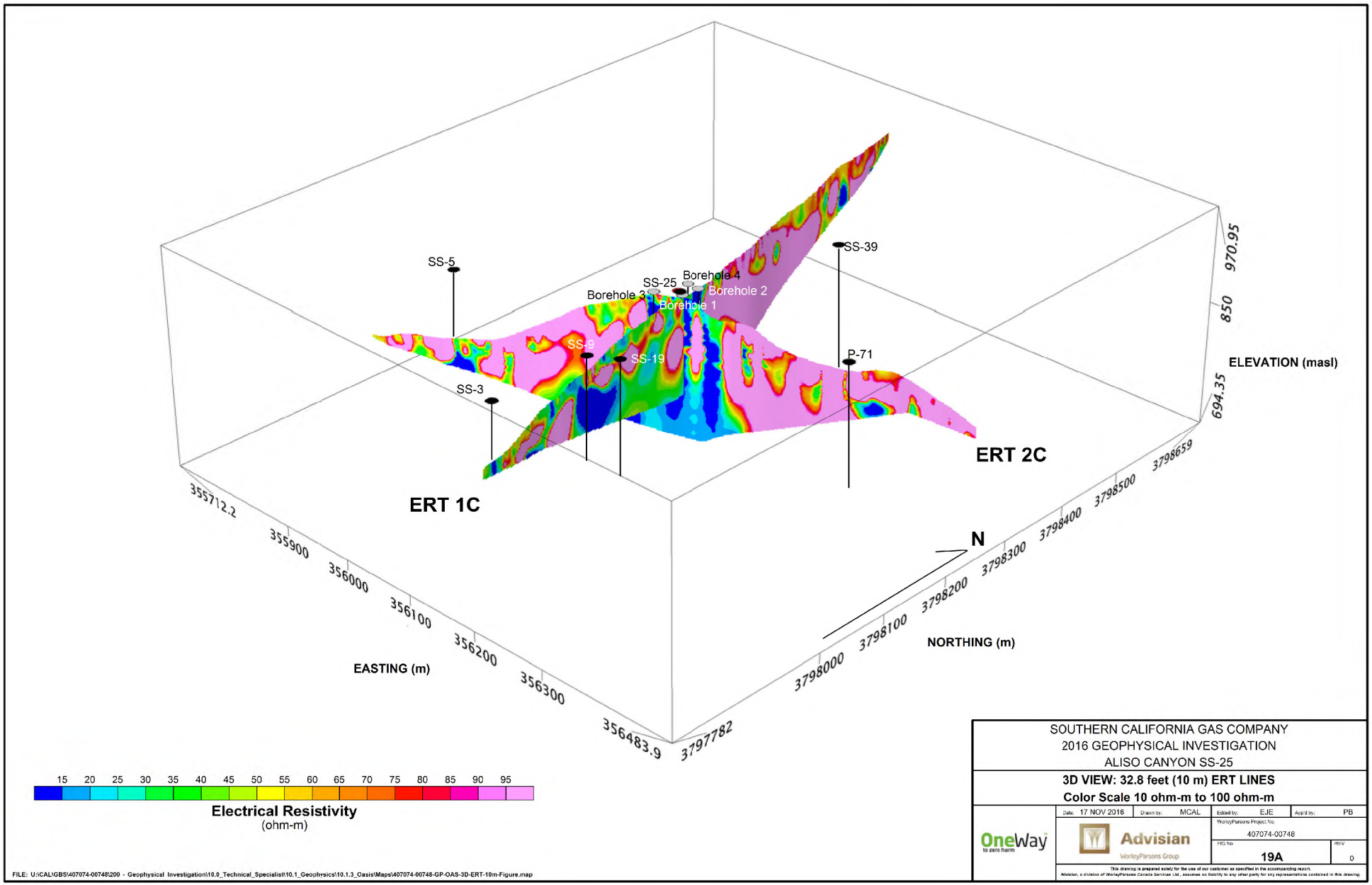

SOUTHERN CALIFORNIA GAS COMPANY
2016 GEOPHYSICAL INVESTIGATION
ALISO CANYON SS-25

3D VIEW: 32.8 feet (10 m) ERT LINES
Color Scale 10 ohm-m to 100 ohm-m

Date: 17 NOV 2016	Drawn by: MCAL	Edited by: EJE	Appd by: PB

OneWay to zero harm

Advisian WorleyParsons Group

WorleyParsons Project No. 407074-00748

FIG No. 19A

REV 0

This drawing is prepared solely for the use of our customer as specified in the accompanying report.
Advisian, a division of WorleyParsons Canada Services Ltd., assumes no liability to any other party for any representations contained in this drawing.

FILE: U:\CAL\GBS\407074-00748\200 - Geophysical Investigation\10.0_Technical_Specialist\10.1_Geophysics\10.1.3_Oasis\Maps\407074-00748-GP-OAS-3D-ERT-10m-Figure.map

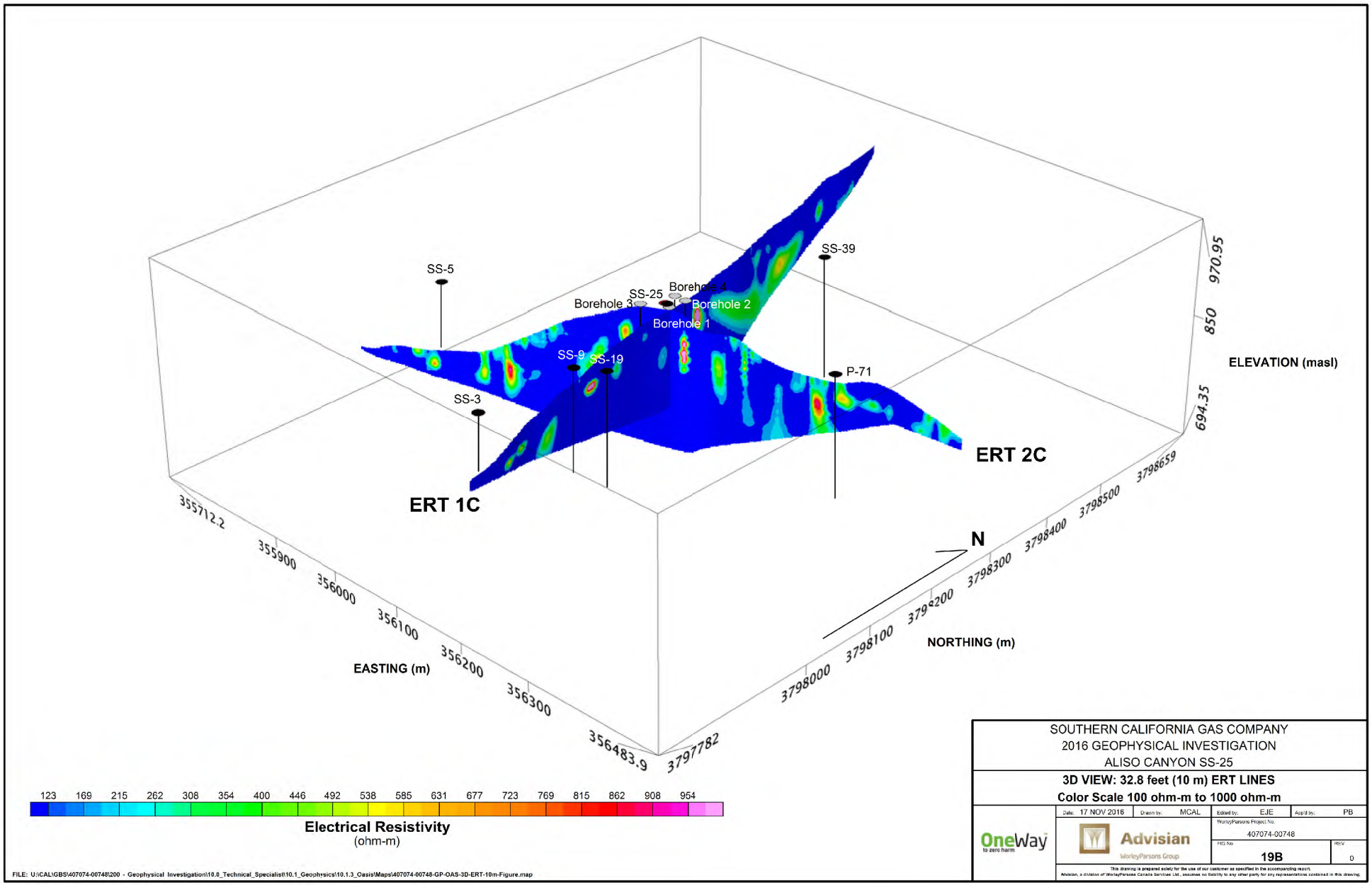

FILE: U:\CAL\GBS\407074-00748\200 - Geophysical Investigation\10.0_Technical_Specialist\10.1_Geophysics\10.1.3_Oasis\Maps\407074-00748-GP-OAS-3D-ERT-10m-Figure.map

SOUTHERN CALIFORNIA GAS COMPANY
2016 GEOPHYSICAL INVESTIGATION
ALISO CANYON SS-25

3D VIEW: 32.8 feet (10 m) ERT LINES
Color Scale 100 ohm-m to 1000 ohm-m

Date: 17 NOV 2016	Drawn by: MCAL	Edited by: EJE	Appd by: PB

OneWay to zero harm

Advisian WorleyParsons Group

WorleyParsons Project No. 407074-00748

FIG No. 19B REV 0

This drawing is prepared solely for the use of our customer as specified in the accompanying report.
Advisian, a division of WorleyParsons Canada Services Ltd., assumes no liability to any other party for any representations contained in this drawing.

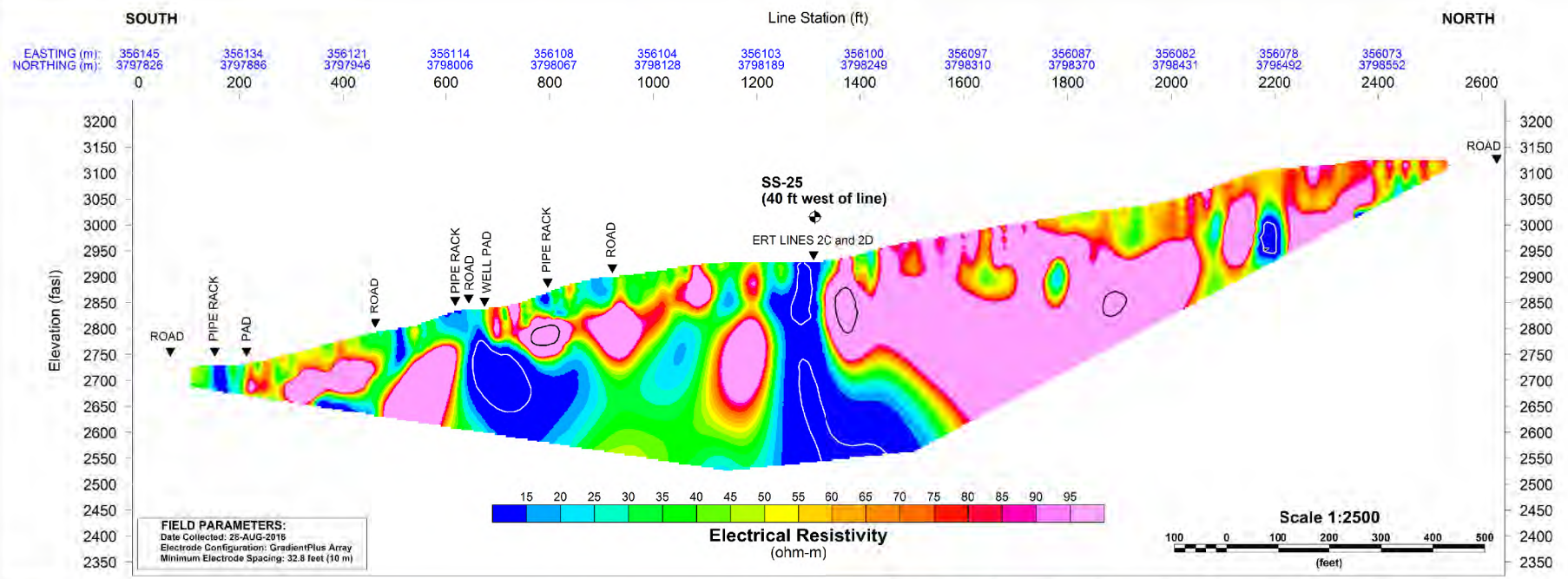

Legend

CROSS-SECTION

356103 UTM ZONE 11N
3798142 WGS 1983 (metres)

White Lines delineate low-resistivity (< 5 ohm-m) zones
Possibly associated with high-chloride kill fluids

Black Lines delineate high-resistivity (> 500 ohm-m) zones

INSET MAP

32.8 feet (10 m) ERT Lines

73.8 feet (22.5 m) ERT Lines

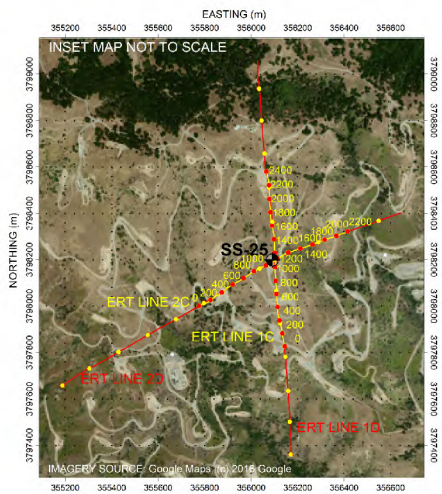

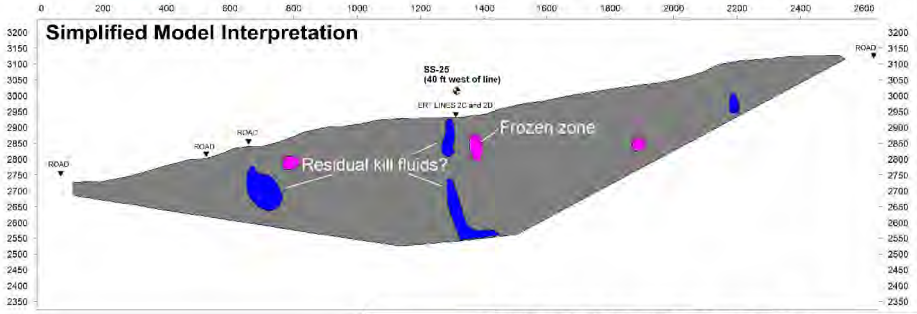

SOUTHERN CALIFORNIA GAS COMPANY
2016 GEOPHYSICAL INVESTIGATION
ALISO CANYON SS-25

LINE: ERT-1C (32.8 feet [10 m])
ELECTRICAL RESISTIVITY CROSS-SECTION

Date: 17 NOV 2016	Drawn by: MCAL	Edited by: EJE	Appd by: PB

OneWay
Advisian
WorleyParsons Project No.: 407074-00748
FIG No.: 20
REV: 0

This drawing is prepared solely for the use of our customer as specified in the accompanying report. Advisian, a division of WorleyParsons Canada Services Ltd., assumes no liability to any other party for any representations contained in this drawing.

FILE: U:\CAL\GBS\407074-00748\200 - Geophysical Investigation\10.0_Technical_Specialist\10.1_Geophysics\10.1.3_Oasis\Maps\407074-00748-GP-OAS-ERT1C-A.map

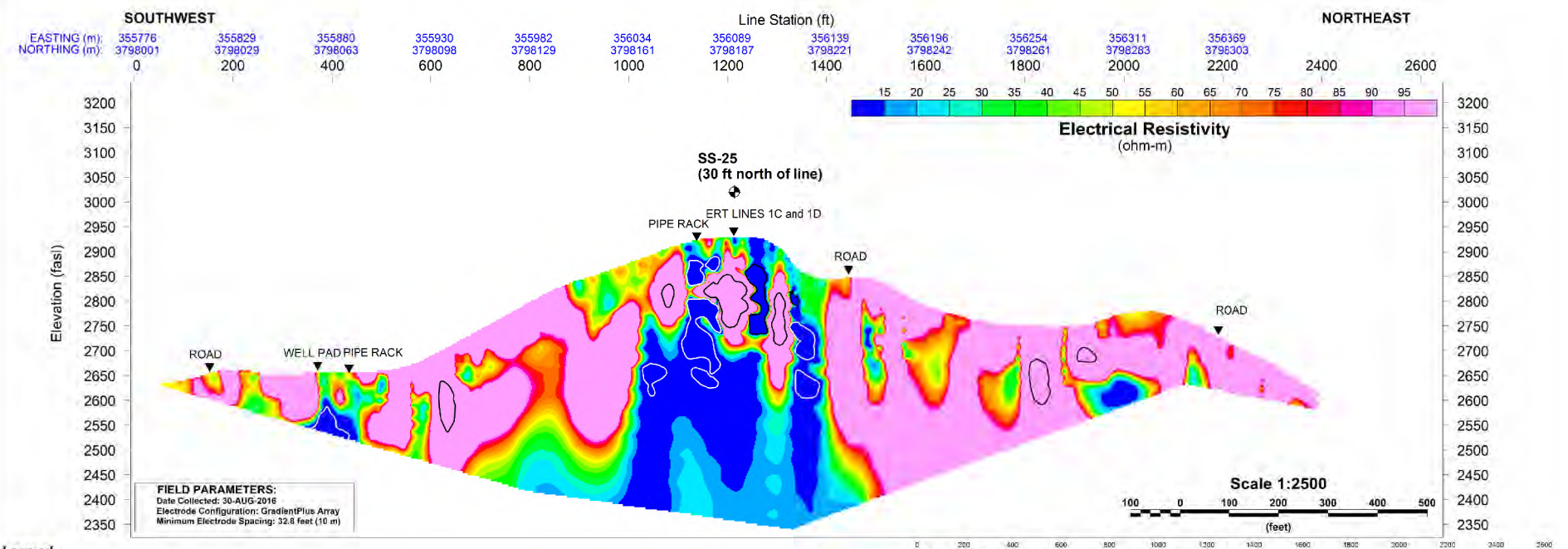

Legend

CROSS-SECTION

356103 UTM ZONE 11N
3798142 WGS 1983 (metres)

White Lines delineate low-resistivity (< 5 ohm-m) zones
Possibly associated with high-chloride kill fluids

Black Lines delineate high-resistivity (> 500 ohm-m) zones

INSET MAP

32.8 feet (10 m) ERT Lines

73.8 feet (22.5 m) ERT Lines

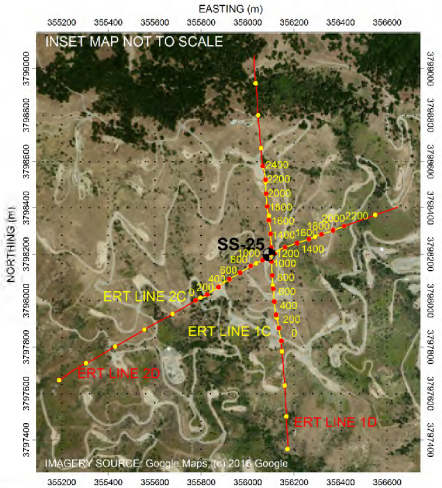

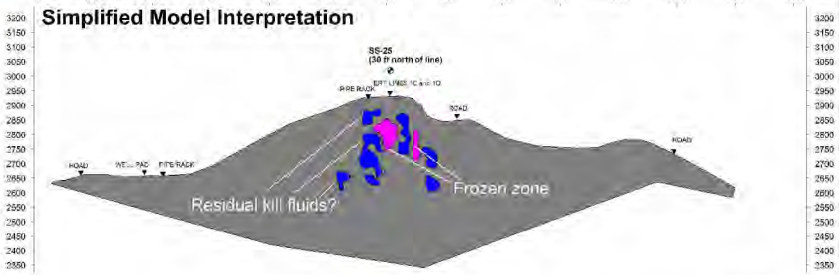

SOUTHERN CALIFORNIA GAS COMPANY
2016 GEOPHYSICAL INVESTIGATION
ALISO CANYON SS-25

LINE: ERT-2C (32.8 FEET [10 M])
ELECTRICAL RESISTIVITY CROSS-SECTION

Date: 17 NOV 2016	Drawn by: MCAL	Edited by: EJE	Appd by: PB

OneWay
Advision
WorleyParsons Project No.: 407074-00748
FIG No.: 21
REV: 0

This drawing is prepared solely for the use of our customer as specified in the accompanying report. Advision, a division of WorleyParsons Canada Services Ltd., assumes no liability to any other party for any representations contained in this drawing.

FILE: D:\CAL\GBS\407074-00748\200 - Geophysical Investigation\10.0_Technical_Specialist\10.1_Geophysics\10.1.3_Oasis\407074-00748-GP-OAS-ERT2C-A.map

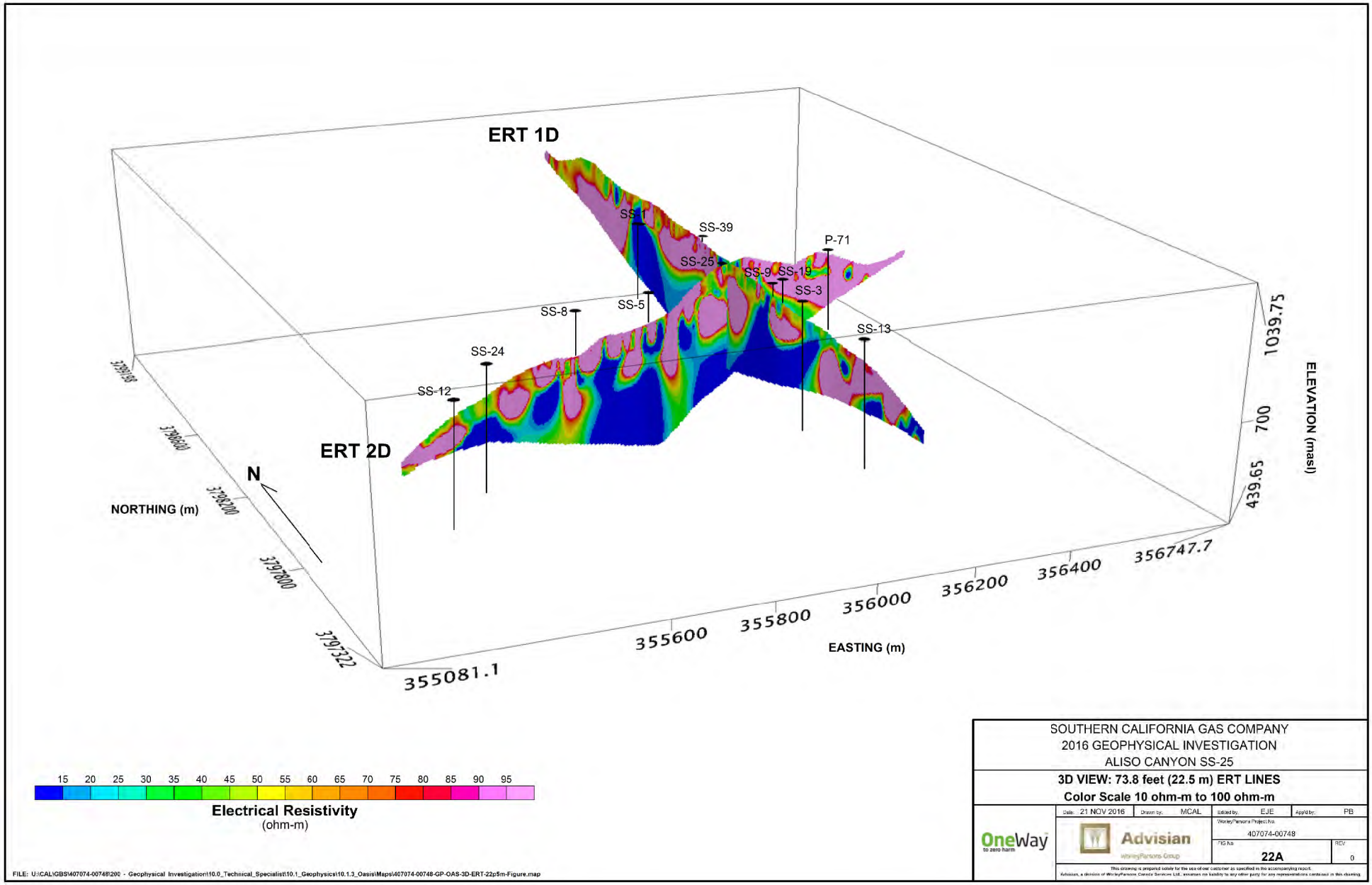

SOUTHERN CALIFORNIA GAS COMPANY
2016 GEOPHYSICAL INVESTIGATION
ALISO CANYON SS-25

3D VIEW: 73.8 feet (22.5 m) ERT LINES
Color Scale 10 ohm-m to 100 ohm-m

Date: 21 NOV 2016	Drawn by: MCAL	Edited by: EJE	Appvd by: PB

OneWay to zero harm

Advisian WorleyParsons Group

WorleyParsons Project No.
407074-00749

FIG No.
22A

REV
0

This drawing is prepared solely for the use of our customer as specified in the accompanying report. Advisian, a division of WorleyParsons Canada Services Ltd., assumes no liability to any other party for any representations contained in this drawing.

FILE: U:\CAL\GBS\407074-00748\200 - Geophysical Investigation\10.0_Technical_Specialist\10.1_Geophysics\10.1.3_Oasis\Maps\407074-00748-GP-OAS-3D-ERT-22p5m-Figure.map

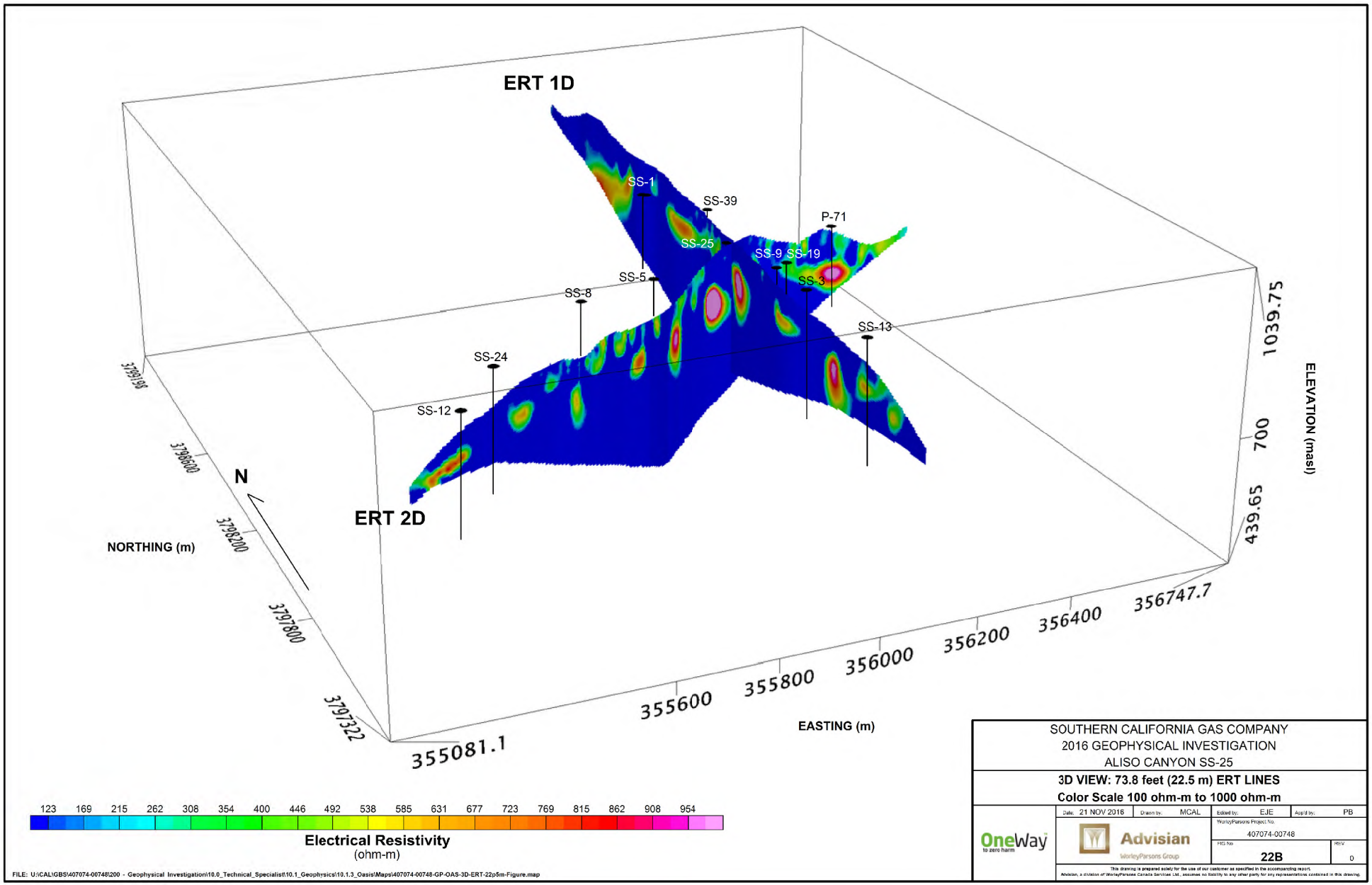
ERT 1D
ERT 2D
SS-1
SS-39
P-71
SS-25
SS-9
SS-19
SS-5
SS-3
SS-8
SS-13
SS-24
SS-12
N
NORTHING (m)
3799198
3798600
3798200
3797800
3797322
EASTING (m)
355081.1
355600
355800
356000
356200
356400
356747.7
ELEVATION (masl)
1039.75
700
439.65
123 169 215 262 308 354 400 446 492 538 585 631 677 723 769 815 862 908 954
Electrical Resistivity
(ohm-m)
FILE: U:\CAL\GBS\407074-00748\200 - Geophysical Investigation\10.0_Technical_Specialist\10.1_Geophysics\10.1.3_Oasis\Maps\407074-00748-GP-OAS-3D-ERT-22p5m-Figure.map
SOUTHERN CALIFORNIA GAS COMPANY
2016 GEOPHYSICAL INVESTIGATION
ALISO CANYON SS-25
3D VIEW: 73.8 feet (22.5 m) ERT LINES
Color Scale 100 ohm-m to 1000 ohm-m
Date: 21 NOV 2016
Drawn by: MCAL
Edited by: EJE
Appd by: PB
WorleyParsons Project No.
407074-00748
FIG No
22B
REV
0
OneWay
to zero harm
Advisian
WorleyParsons Group
This drawing is prepared solely for the use of our customer as specified in the accompanying report.
Advisian, a division of WorleyParsons Canada Services Ltd., assumes no liability to any other party for any representations contained in this drawing.

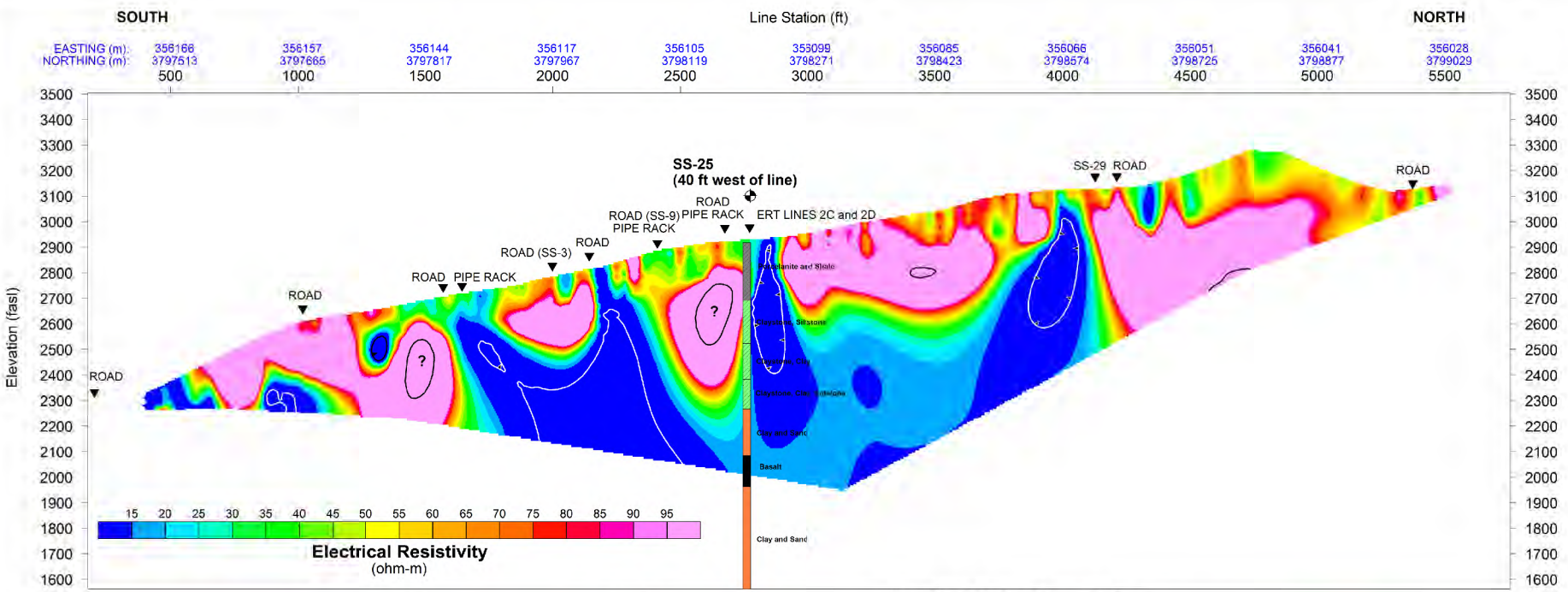

Legend

CROSS-SECTION

356103 UTM ZONE 11N
3798142 WGS 1983 (metres)

White Lines delineate low-resistivity (< 5 ohm-m) zones
Possibly associated with high-chloride kill fluids

Black Lines delineate high-resistivity (> 500 ohm-m) zones

INSET MAP

32.8 feet (10 m) ERT Lines

73.8 feet (22.5 m) ERT Lines

FIELD PARAMETERS:
Date Collected: 25-AUG-2016
Electrode Configuration: GradientPlus Array
Minimum Electrode Spacing: 73.8 feet (22.5 m)

Scale 1:5000

250 0 250 500 750 1000
(feet)

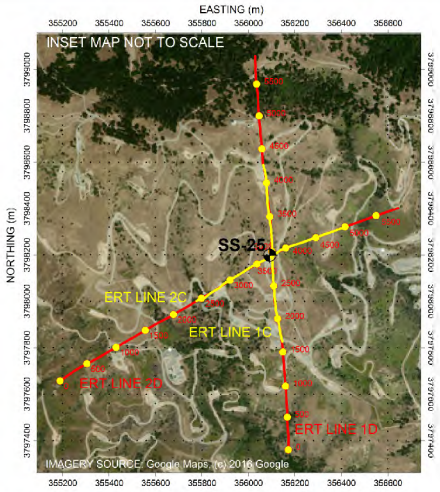

Simplified Model Interpretation

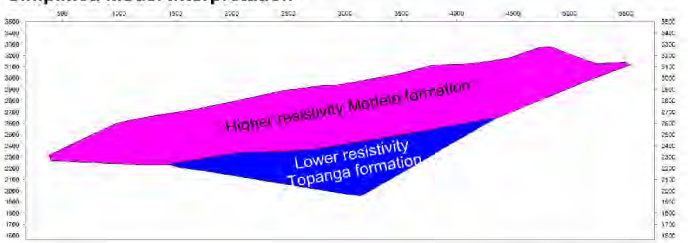

SOUTHERN CALIFORNIA GAS COMPANY
2016 GEOPHYSICAL INVESTIGATION
ALISO CANYON SS-25

LINE: ERT-1D (73.8 feet [22.5 m])
ELECTRICAL RESISTIVITY CROSS-SECTION

Date: 21 NOV 2016	Drawn by: MCAL	Edited by: EJE	Appd by: PB

OneWay
Advisian
Worley/Parsons Project No: 407074-00748
FIG No: 23
REV: 0

This drawing is prepared solely for the use of our customer as specified in the accompanying report. Advisian, a division of Worley/Parsons Canada Services Ltd., assumes no liability to any other party for any representations contained in this drawing.

FILE: U:\CAL\GBS\407074-00748\200 - Geophysical Investigation\10.0_Technical_Specialist\10.1_Geophysics\10.1.3_Oasis\Maps\407074-00748-GP-OAS-ERT1D-A.map

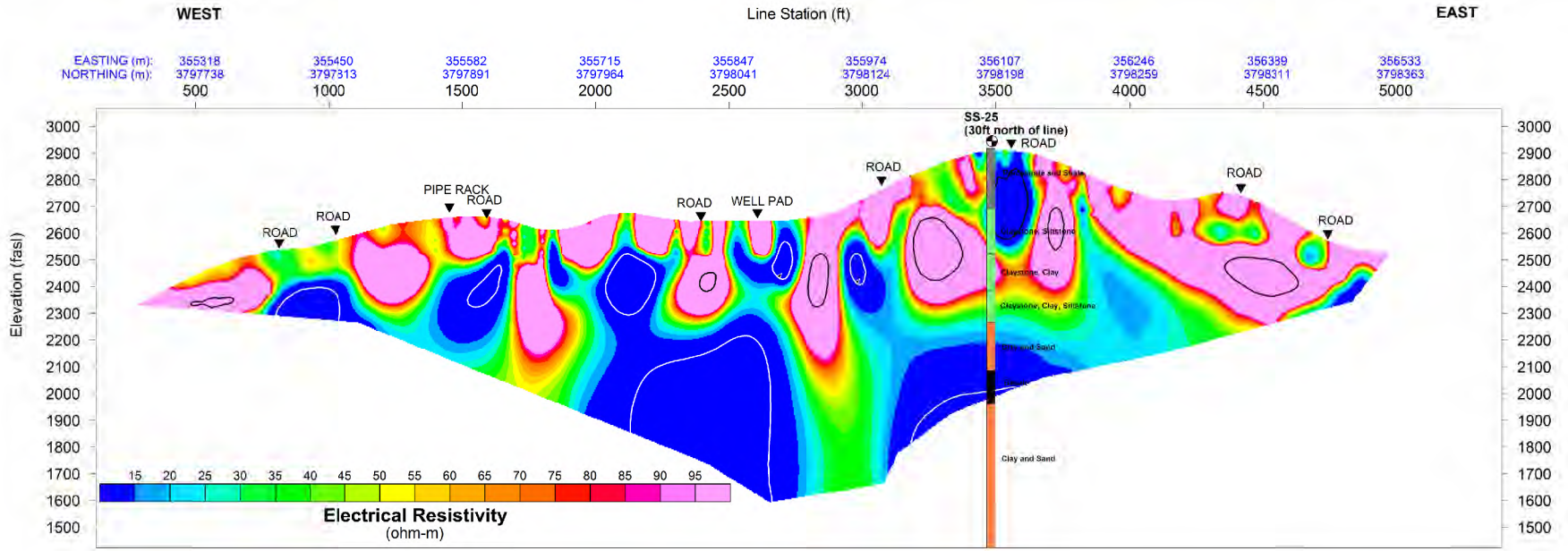

Legend

CROSS-SECTION

356103 UTM ZONE 11N
3798142 WGS 1983 (metres)

White Lines delineate low-resistivity (< 5 ohm-m) zones
Possibly associated with high-chloride kill fluids

Black Lines delineate high-resistivity (> 500 ohm-m) zones

INSET MAP

32.8 feet (10 m) ERT Lines

73.8 feet (22.5 m) ERT Lines

FIELD PARAMETERS:
Date Collected: 27-AUG-2016
Electrode Configuration: GradientPlus Array
Minimum Electrode Spacing: 73.8 feet (22.5 m)

Scale 1:5000

250 0 250 500 750 1000
(feet)

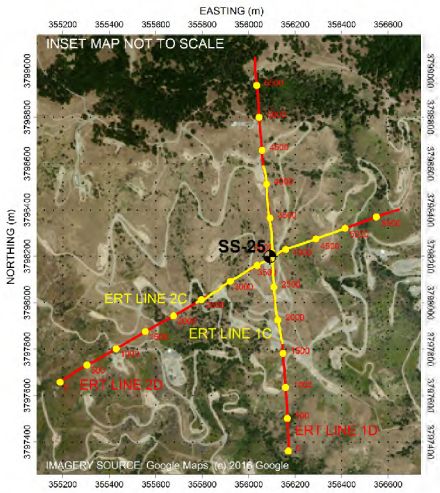

Simplified Model Interpretation

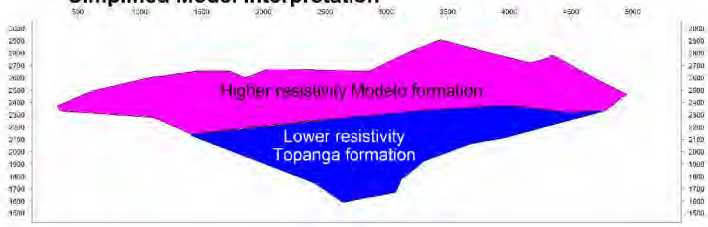

SOUTHERN CALIFORNIA GAS COMPANY
2016 GEOPHYSICAL INVESTIGATION
ALISO CANYON SS-25

LINE: ERT-2D (73.8 FEET [22.5 M])
ELECTRICAL RESISTIVITY CROSS-SECTION

Date: 21 NOV 2016	Drawn by: MCAL	Edited by: EJE	Appd by: PB
OneWay	Advisian	WorleyParsons Project No: 407074-00748	
		FIG No: 24	REV: 0

This drawing is prepared solely for the use of our customer as specified in the accompanying report.
Advisian, a division of WorleyParsons Canada Services Ltd., assumes no liability to any other party for any representations contained in this drawing.

FILE: U:\CAL\GBS\407074-00748\200 - Geophysical Investigation\10.0_Technical_Specialist\10.1_Geophysics\10.1.3_Oasis\Maps\407074-00748-GP-OAS-ERT2D-A.map

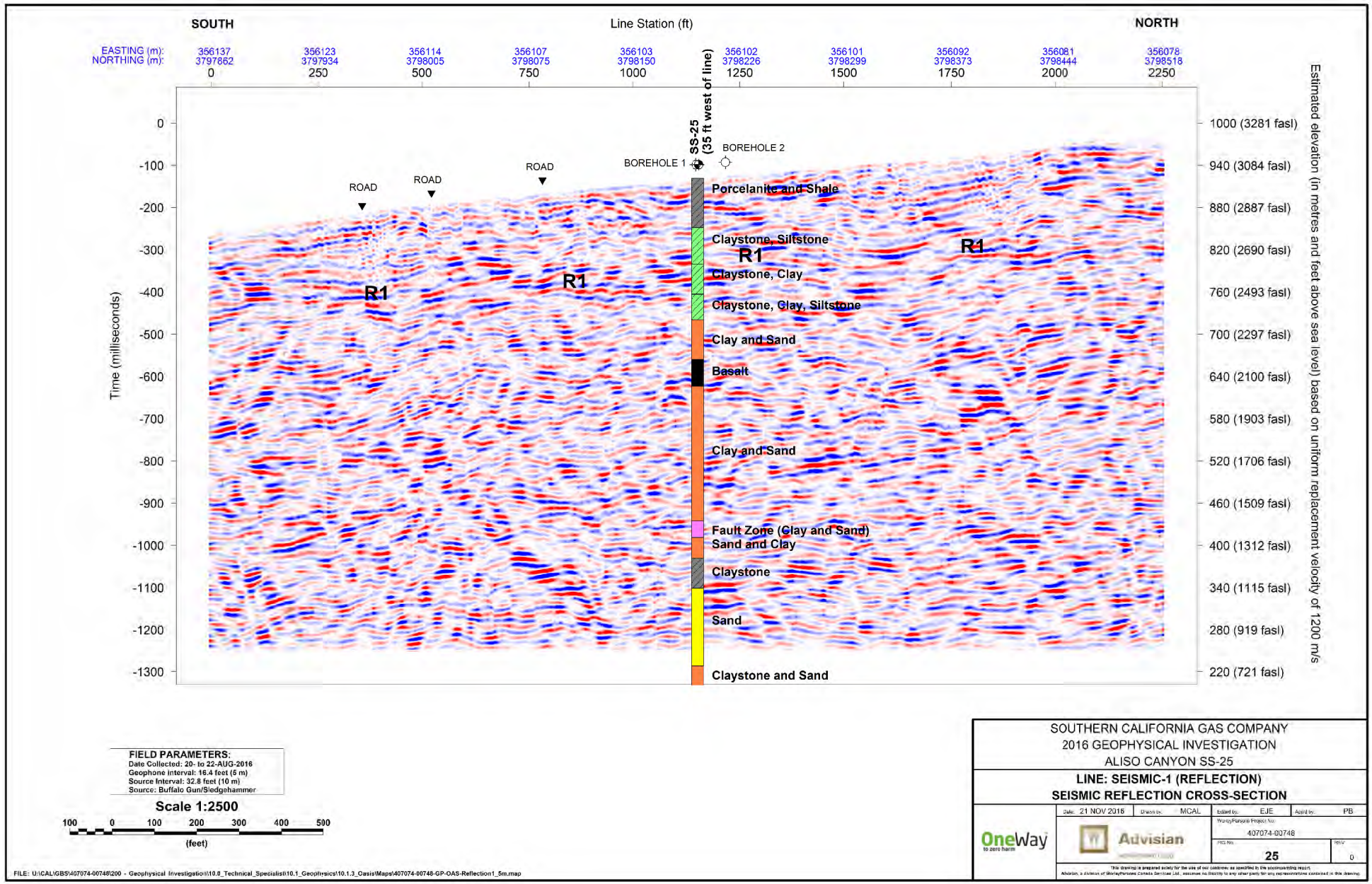

FIELD PARAMETERS:
Date Collected: 20- to 22-AUG-2016
Geophone Interval: 16.4 feet (5 m)
Source Interval: 32.8 feet (10 m)
Source: Buffalo Gun/Sledgehammer

Scale 1:2500

100 0 100 200 300 400 500
(feet)

SOUTHERN CALIFORNIA GAS COMPANY
2016 GEOPHYSICAL INVESTIGATION
ALISO CANYON SS-25

LINE: SEISMIC-1 (REFLECTION)
SEISMIC REFLECTION CROSS-SECTION

Date: 21 NOV 2016	Drawn by: MCAL	Edited by: EJE	Appd by: PB

OneWay to zero harm
Advisian
WorleyParsons Project No: 407074-00748
FIG No. 25
REV 0

This drawing is prepared solely for the use of our customer as specified in the accompanying report. Advisian, a division of WorleyParsons Canada Services Ltd., assumes no liability to any other party for any representations contained in this drawing.

FILE: U:\CAL\GBS\407074-00748\200 - Geophysical Investigation\10.0_Technical_Specialist\10.1_Geophysics\10.1.3_Oasis\Maps\407074-00748-GP-OAS-Reflection1_5m.map

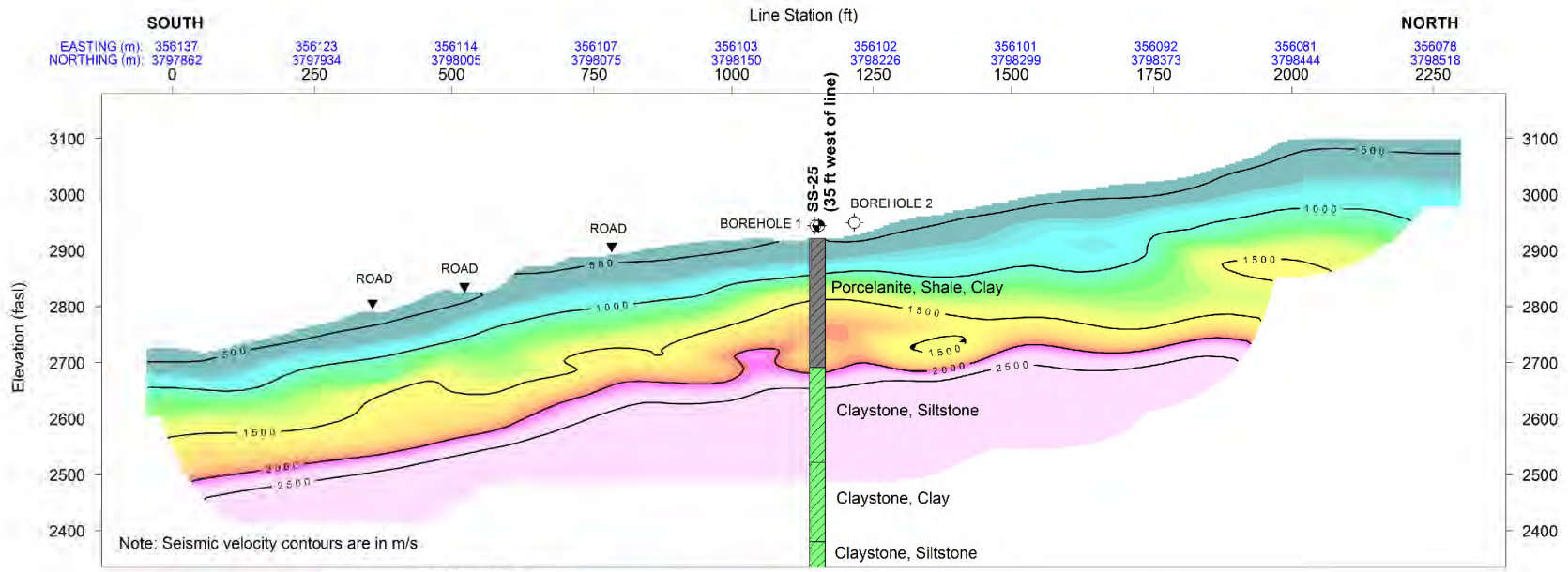

P-Wave Velocity

800 900 1000 1100 1200 1300 1400 1500 1600 1700 1800 1900 2000 2100 2200

(m/s)

2500 3000 3500 4000 4500 5000 5500 6000 6500 7000

(ft/s)

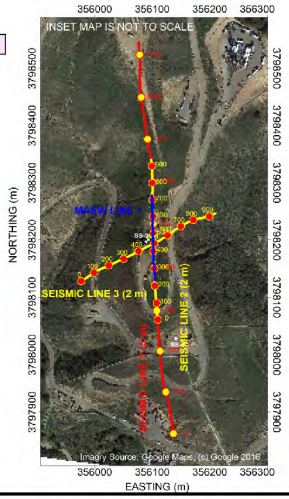

FIELD PARAMETERS:
Date Collected: 20- to 22-AUG-2016
Geophone interval: 16.4 feet (5 m)
Source Interval: 32.8 feet (10 m)
Source: Buffalo Gun/Sledgehammer

Scale 1:2500

100 0 100 200 300 400 500

(feet)

SOUTHERN CALIFORNIA GAS COMPANY
2016 GEOPHYSICAL INVESTIGATION
ALISO CANYON SS-25

LINE: SEISMIC-1 (REFRACTION)
P-WAVE VELOCITY CROSS-SECTION

Date: 21 NOV 2016	Drawn by: MCAL	Edited by: EJE	Appd by: PB

OneWay to zero harm

Advisian

WorleyParsons Project No.: 407074-00748

FIG No.: 26 REV: 0

This drawing is prepared solely for the use of our customer as specified in the accompanying report. Advisian, a division of WorleyParsons Canada Services Ltd., assumes no liability to any other party for any representations contained in this drawing.

FILE: U:\CAL\GBS\407074-00748\200 - Geophysical Investigation\10.0_Technical_Specialist\10.1_Geophysics\10.1.3_Oasis\Maps\407074-00748-GP-OAS-Seismic1-A.map

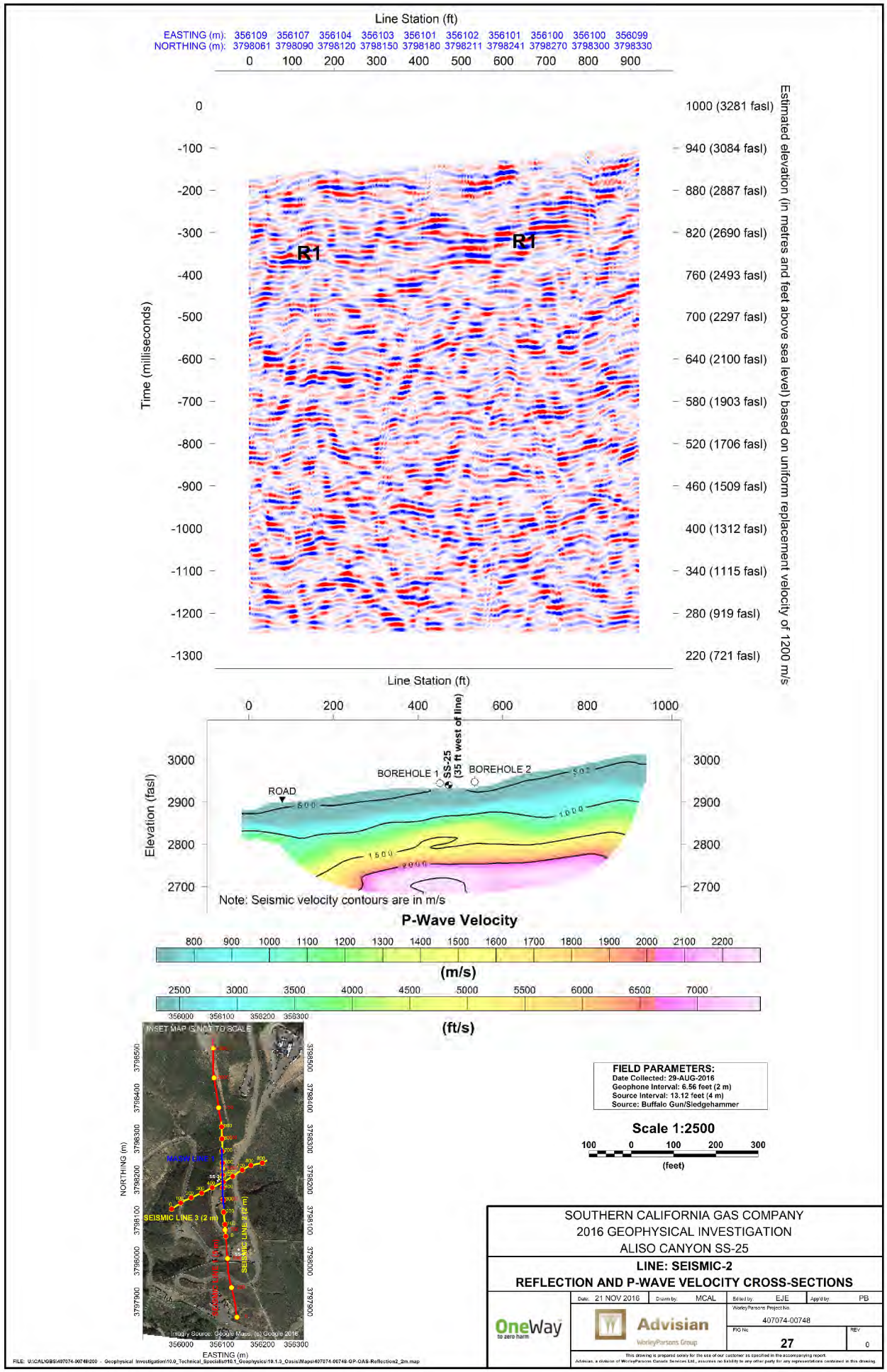
Line Station (ft)
EASTING (m): 356109 356107 356104 356103 356101 356102 356101 356100 356100 356099
NORTHING (m): 3798061 3798090 3798120 3798150 3798180 3798211 3798241 3798270 3798300 3798330
0 100 200 300 400 500 600 700 800 900
Time (milliseconds)
0 -100 -200 -300 -400 -500 -600 -700 -800 -900 -1000 -1100 -1200 -1300
1000 (3281 fasl) 940 (3084 fasl) 880 (2887 fasl) 820 (2690 fasl) 760 (2493 fasl) 700 (2297 fasl) 640 (2100 fasl) 580 (1903 fasl) 520 (1706 fasl) 460 (1509 fasl) 400 (1312 fasl) 340 (1115 fasl) 280 (919 fasl) 220 (721 fasl)
Estimated elevation (in metres and feet above sea level) based on uniform replacement velocity of 1200 m/s
R1
R1
Line Station (ft)
0 200 400 600 800 1000
Elevation (fasl)
3000 2900 2800 2700
SS-25 (35 ft west of line)
BOREHOLE 1
BOREHOLE 2
ROAD
500
1000
1500
2000
Note: Seismic velocity contours are in m/s
P-Wave Velocity
800 900 1000 1100 1200 1300 1400 1500 1600 1700 1800 1900 2000 2100 2200
(m/s)
2500 3000 3500 4000 4500 5000 5500 6000 6500 7000
(ft/s)
INSET MAP IS NOT TO SCALE
MAIN LINE
SEISMIC LINE 3 (2 m)
SEISMIC LINE 4 (2 m)
SEISMIC LINE 5 (2 m)
SEISMIC LINE 6 (2 m)
NORTHING (m)
EASTING (m)
Imagery Source: Google Maps, (c) Google 2016
FIELD PARAMETERS:
Date Collected: 29-AUG-2016
Geophone Interval: 6.56 feet (2 m)
Source Interval: 13.12 feet (4 m)
Source: Buffalo Gun/Sledgehammer
Scale 1:2500
100 0 100 200 300
(feet)
SOUTHERN CALIFORNIA GAS COMPANY
2016 GEOPHYSICAL INVESTIGATION
ALISO CANYON SS-25
LINE: SEISMIC-2
REFLECTION AND P-WAVE VELOCITY CROSS-SECTIONS
Date: 21 NOV 2016
Drawn by: MCAL
Edited by: EJE
Appd by: PB
Worley Parsons Project No.
407074-00748
FIG No.
27
REV
0
OneWay to zero harm
Advisian WorleyParsons Group
This drawing is prepared solely for the use of our customer as specified in the accompanying report.
Advisian, a division of WorleyParsons Canada Services Ltd., assumes no liability to any other party for any representations contained in this drawing.
FILE: U:\CALGBS\407074-00748\200 - Geophysical Investigation\10.0_Technical_Specialist\10.1_Geophysics\10.1.3_Oasis\Maps\407074-00748-GP-OAS-Reflection2_2m.map

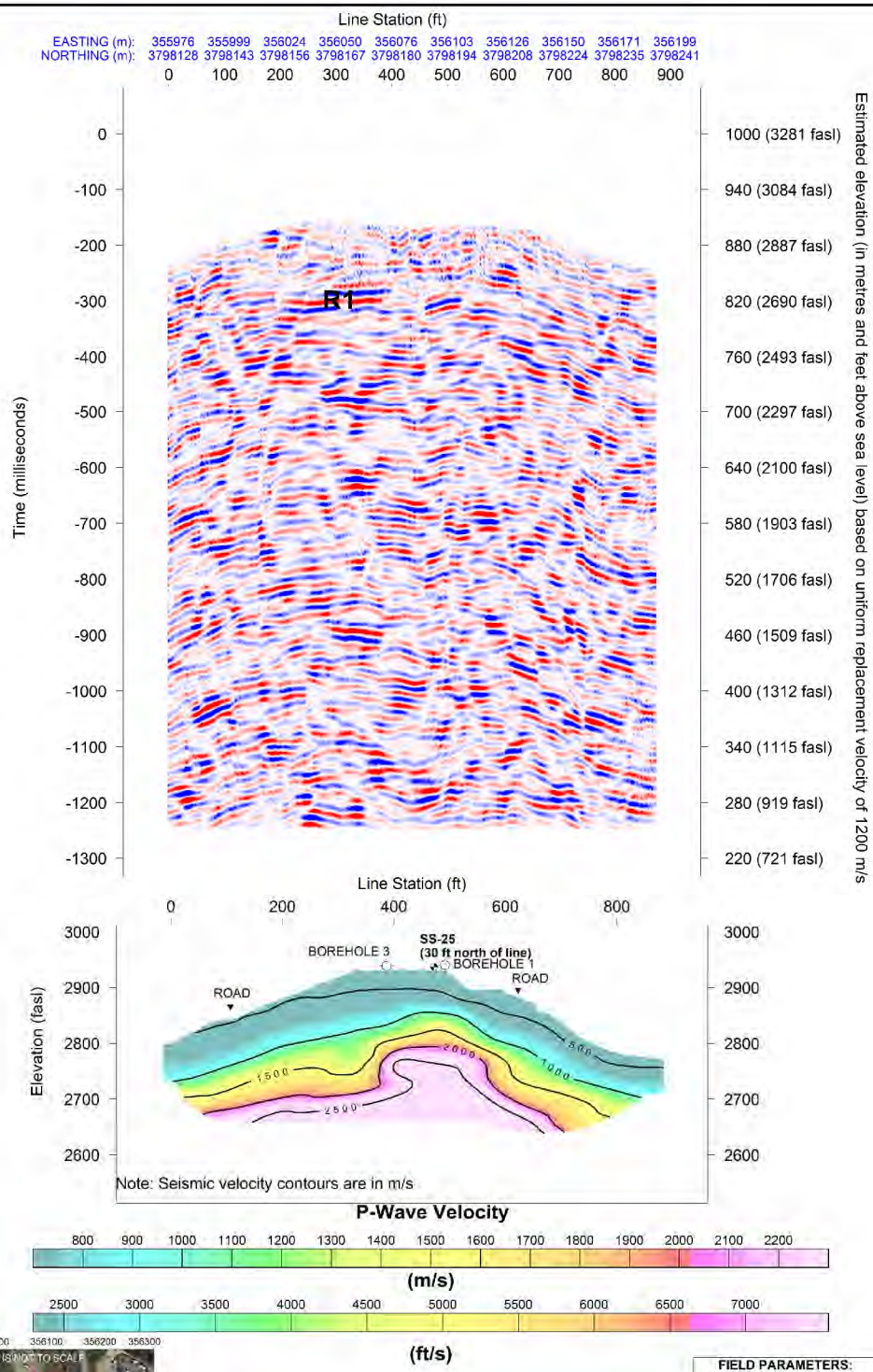

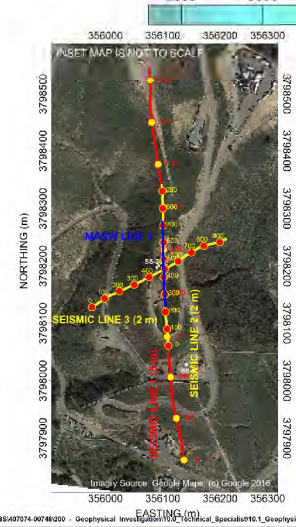

FIELD PARAMETERS:
Date Collected: 01-SEPT-2016
Geophone Spacing: 6.56 feet (2 m)
Shot Spacing: 13.12 feet (4 m)
Source: Buffalo Gun/Sledgehammer

Scale 1:2500

100 0 100 200 300
(feet)

SOUTHERN CALIFORNIA GAS COMPANY
2016 GEOPHYSICAL INVESTIGATION
ALISO CANYON SS-25

LINE: SEISMIC-3
REFLECTION AND P-WAVE VELOCITY CROSS-SECTIONS

Date: 21 NOV 2016	Drawn by: MCAL	Edited by: EJE	Appd by: PB
		WorleyParsons Project No. 407074-00748	
		FIG No. 28	REV 0

OneWay to zero harm
Advisian WorleyParsons Group

This drawing is prepared solely for the use of our customer as specified in the accompanying report.
Advisian, a division of WorleyParsons Canada Services Ltd., assumes no liability to any other party for any representations contained in this drawing.

FILE: U:\CAL\GBS\407074-00748\200 - Geophysical Investigation\10.0_Technical_Specialist\10.1_Geophysics\10.1.3_Oasis\407074-00748-GP-OAS-Reflection3_2m.map

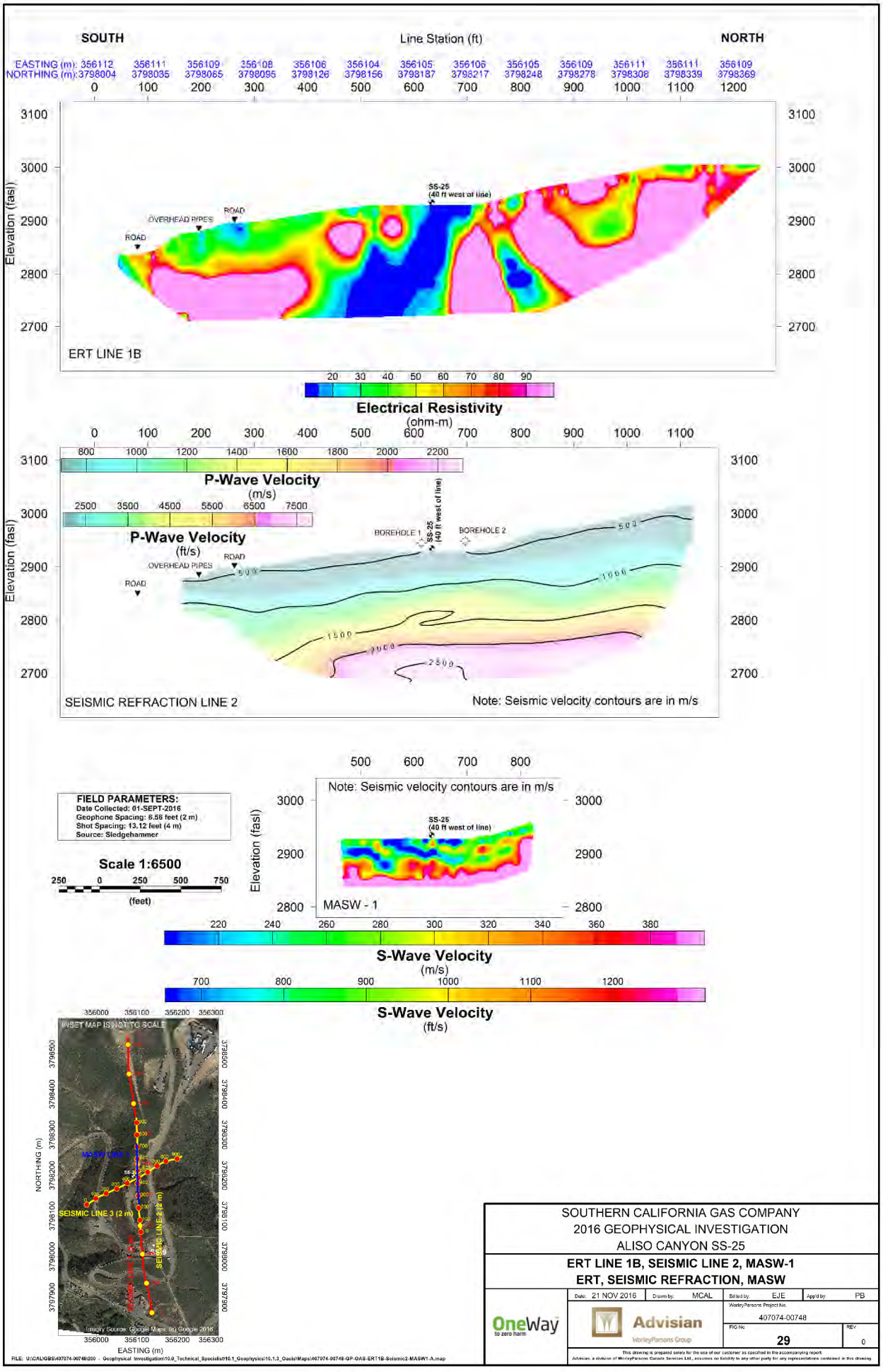

SOUTHERN CALIFORNIA GAS COMPANY
2016 GEOPHYSICAL INVESTIGATION
ALISO CANYON SS-25

ERT LINE 1B, SEISMIC LINE 2, MASW-1
ERT, SEISMIC REFRACTION, MASW

Date: 21 NOV 2016	Drawn by: MCAL	Edited by: EJE	Appd by: PB
		Worley Parsons Project No. 407074-00748	
		FIG No. 29	REV 0

OneWay to zero harm

Advisian WorleyParsons Group

This drawing is prepared solely for the use of our customer as specified in the accompanying report. Advisian, a division of WorleyParsons Canada Services Ltd., assumes no liability to any other party for any representations contained in this drawing.

FILE: U:\CALGBS\407074-00748\200 - Geophysical Investigation\10.0_Technical_Specialist\10.1_Geophysics\10.1.3_Oasis\Maps\407074-00748-GP-OAS-ERT1B-Seismic2-MASW1-A.map

Photographs

Advisian
WorleyParsons Group

PHOTO 1: SS-25

PHOTO 2: Collecting ERT Data

PHOTO 3: Setting up seismic line on steep slope

PHOTO 4: Augering holes for buffalo gun shots on steep slopes

PHOTO 5: Buffalo gun shots

PHOTO 6: Sledgehammer source used when collecting MASW data

PHOTO 7: Working on steep slopes

PHOTO 8: Fire suppression team

Appendices

Appendix 1: Geophysical Methodologies

APPENDIX 1 GEOPHYSICAL METHODOLOGIES

1 Surface-Based Geophysical Methods

1.1 Electrical Resistivity Tomography (ERT)

ERT is a technique for mapping the distribution of subsurface electrical resistivity (or its inverse, conductivity) in a cross-sectional format. Resistivity data are collected through a linear array of electrodes coupled to a direct current (DC) resistivity transmitter and receiver, and an electronic switching box. The spacing between electrodes controls the horizontal and vertical resolution of the data (smaller spacing results in higher resolutions). Similarly, the length of the array controls the depth of investigation (longer arrays yield greater investigation depths). Data collection is carried out in a sequential and automated fashion that takes advantage of all possible combinations of current injection and potential measurement electrodes. The data are downloaded to a computer for processing and analysis, which includes the application of a two-dimensional (2-D) finite difference or finite element inversion routine. The final product is a 2-D cross-section plotting resistivity (in ohm-m), or conductivity (in millisiemens per meter [mS/m]), versus depth.

The electrical resistivity or electrical conductivity of a formation is dependent on the mineral content of the grains and the concentration of salts in any pore water. Fine-grained materials like clays and silts typically have relatively low resistivities, whereas dry granular material like sands and gravels will exhibit relatively high resistivities. Similarly, fresh water has a relatively high resistivity and saline water has a relatively low resistivity.

1.2 Seismic Reflection

The seismic reflection technique measures the travel times and amplitudes of seismic waves reflecting off subsurface horizons. For each horizon, the reflections from different shot points are stacked together to produce a cross-section of the reflectivity of the earth. The method is used extensively in oil exploration where reflections from sedimentary layers down to depths of 15,000 feet (4572 m) show the strata and structure needed to identify potential exploration wells.

Shallow, high-resolution seismic reflection surveys are conducted in a similar manner to conventional reflection surveys, except that the geophones and shot points are spaced at smaller intervals, and higher frequency seismic signals are generated and recorded. Parameters that determine the quality of a seismic reflection include the thickness of the strata and the velocity and density contrasts between layers. The ability to detect individual stratum is dependent on the frequency content of the downward propagating energy. A rule of thumb is that seismic reflection methods can resolve an individual bed that has a thickness greater than one-quarter the wavelength of the seismic pulse. Therefore, higher frequency

waves are capable of resolving smaller beds than lower frequency waves. The main limitation of a high frequency seismic energy source is that the depth of penetration is less than for lower frequencies.

1.3 Seismic Refraction

The seismic refraction method uses the propagation of compressional waves in the subsurface to determine the velocity structure of the ground. Seismic energy is produced by a source (e.g. sledge hammer, weight drop, or dynamite), and spreads downwards and laterally through the earth. An array of receivers (geophones) measures the arrival of that energy at points on a line. Increasing vertical velocity gradients with depth will cause seismic energy to refract back to the surface. Decreasing vertical velocity gradients are rare but, where present, will bend rays away from the surface and create shadow zones that cannot be imaged. The travel path that the energy takes from each shot to each receiver can be represented by a curved ray path. Typically, seismic energy that has propagated through bedrock material will arrive with faster apparent velocities along the seismic array than seismic energy that has travelled through overburden.

The picked travel times of the first-arriving energy can be used as input to seismic inversion software (e.g. Rayfract), which solves for the velocity model of the subsurface that best fits the observed travel times. The accuracy of each travel-time pick is determined by the frequency of the first-arriving energy and the signal-to-noise (S/N) ratio. Factors that can reduce the frequency and/or S/N ratios include soft or spongy soils, wind noise, traffic noise, and the distance between the shot and the receiver (signal strength will reduce proportionally with increasing length of the ray path). The maximum depth of investigation of a velocity model is determined by the deepest refracted ray path. As a general rule, the longer the horizontal offset between a shot and a receiver, the greater the depth of penetration.

1.4 Multi-Channel Analysis of Surface Waves (MASW)

When seismic waves are generated from an active seismic source (i.e. a weight drop or sledge hammer), both surface and body waves (including compressional and shear waves) are generated, propagating in all directions. In conventional seismic methods, it is the measurement of the body wave arrival (reflection/ refraction) that is of interest, whereas the surface wave arrival is generally considered to be a source of noise. A Rayleigh wave is a particular type of surface wave that travels along or near the ground surface and is characterized by relatively low velocities, low frequencies, and high amplitudes. Surface wave velocity is dispersive, or frequency-dependent (i.e. the sampling depth of a particular frequency component of a surface wave is directly proportional to its wavelength). Therefore, information on the shallow subsurface can be derived from measurements of low frequency components of Rayleigh waves.

The process for acquiring multichannel shot records is similar to that of acquiring seismic reflection shot records, utilizing an active seismic source and a linear receiver array, and collecting data in a roll along common-midpoint (CMP) acquisition mode. Dispersion curves are extracted from each shot record using a wavefield-transformation method. From these dispersion curves, the fundamental mode of the surface

wave is extracted, removing all other reflected or scattered waves and ambient noise (Kansas Geological Survey 2006, internet site). The extracted dispersion curves are then inverted to obtain one-dimensional (1-D) shear wave velocity (Vs) profiles (i.e. a single 1-D profile for each shot record). Multiple profiles are then combined, resulting in a 2-D cross-section of Vs versus depth. As Vs is also described as 'stiffness', sharp contrasts in Vs may indicate voids, fractures, subsidence-prone areas, or bedrock surface.

Advantages to surface-wave imaging are the ease with which the high-amplitude waves are generated (i.e. utilizing a truck-mounted weight drop or sledgehammer), and the relative insensitivity to ambient, mechanical, or electrical noise.

1.5 Surface-Based Nuclear Magnetic Resonance (NMR)

The surface NMR sounding method operates under similar principles to the borehole NMR technique, except that the surface NMR system uses the Earth's magnetic field instead of the much stronger local magnetic field generated inside the borehole probe. In a surface NMR survey, the NMR response of groundwater is probed using large wire loops (up to 656 feet [200 m] on a side) which are laid out on the surface. Short current pulses are generated through the wire loops to energize the hydrogen nuclei in the groundwater at their resonant frequency. After the transmission pulse, the surface loops switch to receive mode and record the NMR signal generated by the energized water molecules. From the recorded NMR signals, a vertical profile of water content distribution beneath the loop can be calculated. Like the borehole NMR method, the decay behaviour of the measured NMR signal also provides information about the pore spaces in which the water is contained.

Surface NMR surveys have an advantage over borehole NMR logging surveys in that no drilling is required. However, surface NMR surveys have a limited depth of investigation that is dictated by the size of the surface loop used (in general, the greater the loop size, the deeper the depth of investigation). In addition, they are sensitive to cultural electromagnetic noise (radio signals, nearby powerlines, etc.) that can severely affect data quality.

1.6 Ground-Penetrating Radar (GPR)

GPR is a shallow, non-invasive, subsurface investigation technique capable of mapping interfaces in a cross-sectional format. GPR measures the propagation time of high frequency electromagnetic pulses that are reflected from interfaces between materials of different electrical properties. Typically, radar reflections occur with abrupt changes in moisture content, grain size, porosity, or soil texture, or off of massive buried objects such as pipelines or underground storage tanks. GPR is analogous to the reflection seismic technique that uses the travel time of acoustic pulses to identify interfaces. GPR is best suited to investigations in coarse-grained materials (i.e. sand size or larger).

GPR investigations for geological applications can be performed at frequencies ranging from 12.5 MHz to 500 MHz. Higher frequencies provide data of higher vertical resolution, while lower frequencies improve the depth of investigation. For example, 500 MHz would provide a resolution of approximately 0.32 feet

(10 cm) and a depth of investigation of approximately 3.278 feet (1 m) in a sandy soil. Conversely, 12.5 MHz antennas may provide a depth of investigation of 131 feet (40 m) or greater with a resolution of 9.84 feet (3 m) in a sandy soil.

2 Borehole Geophysical Logging Methods

The Mount Sopris logging instrument is a small geophysical borehole logging system used to collect various downhole geophysical logs, including, but not limited to, density, spectral gamma, natural gamma ray, formation induction conductivity, and temperature. All the logs acquired for this program, with the exception of the nuclear magnetic resonance (NMR) logs, were acquired using the Mount Sopris logging system. The tools are typically lowered down wells or boreholes with measurements being taken at regular, pre-determined intervals (usually every 1 inch (2.5 cm) or 2 inches (5 cm). A Vista Clara Inc. Dart borehole NMR system was also used to log the locations.

2.1 Optical Borehole Televiewer

The ALT 40mm (1.57 inch) Optical Borehole Televiewer or OBI40 is an advanced slimhole logging tool designed for the optimum optical imaging of the surface wall of open and cased wells, either in air or clear water. Designed to complement the ALT Acoustic Televiewers (ABI40 - FAC40) in dry well situations, it operates with the ALTLogger, MGXII and Matrix logging systems. It can be run on any standard wireline (mono, 4 or 7 conductor, coax). The optical televiewer is fully downhole digital. It includes a high precision deviation sensor (APS544) allowing accurate orientation of the image and borehole. This tool can provide detailed, oriented, structural and geological information.

2.2 Nuclear Magnetic Resonance (NMR)

Similar to the medical magnetic resonance imaging technique, the borehole NMR technique responds to changes in water content. Permanent magnets within the borehole NMR tool project a strong magnetic field several inches beyond the borehole that polarizes water molecules within the formation. By emitting a series of radio frequency pulses and recording the returning signal, the NMR tool is able to measure the response of water in the formation surrounding the borehole. The characteristics of the measured NMR signal reflect the quantity of water (volumetric water content) as well as a qualitative measure of hydraulic conductivity at a given depth. The total amplitude of the signal directly indicates the total amount of water, whereas the decay behaviour of the signal over time conveys more detailed information about the pore spaces in which the water is contained (i.e. whether that water is bound in tight pore spaces or whether the water is relatively mobile in large pore spaces).

A Dart borehole NMR system, manufactured by Vista Clara Inc., was used for this program. Measurements are made in step mode, whereby the probe is held at a specific depth for a specified length of time until an adequate signal can be recorded. In order to record high quality signals, measurement intervals of up

to five minutes were required at each depth station. Typically, measurements are made at intervals of 10 inches (0.25 m) or 20 inches (0.5 m).

2.3 Natural Gamma Ray

The natural gamma ray probe counts naturally emitted gamma rays of all energy levels using a scintillation counter. Borehole gamma logging is one of the primary instruments used for correlating stratigraphy between boreholes. A borehole gamma tool measures the natural or background gamma radiation emitted from surrounding geologic materials. Typically, fine-grained materials such as clays and shales contain significant amounts of naturally-occurring radioactive minerals, while coarse-grained deposits such as sands, sandstones or limestone often contain very little of such material. Thus, a gamma tool will typically measure high radiation counts in clays and low counts in sands.

The detector is a thallium-activated sodium iodide crystal that is 0.874 inches (2.22 cm) in diameter and 3 inches (7.62 cm) in length. The probe records counts of radiation emitted from material in a sphere with an approximate radius of 8 inches (0.2 m). Data are recorded as raw counts per second (cps). The influence of earth materials decreases with the square root of distance from the detector.

2.4 Formation Induction Conductivity

The formation conductivity measurements are recorded using an electrical induction tool to measure the electrical conductivity of the surrounding geologic material. A transmitter coil, located at one end of the probe, is energised with an alternating electrical current, which creates a primary magnetic field. This primary magnetic field induces an electrical current to flow within the surrounding formation, which in turn creates a secondary magnetic field. The receiver coil, located at the opposite end of the probe, measures the strength of both the primary and secondary magnetic fields. Under "low conductivity" conditions (typical of geologic material) the ratio of the secondary to primary fields is directly proportional to the conductivity of the formation. Typically, fine-grained materials such as clays and shales are conductive, while coarse-grained deposits such as sands, sandstones, or limestone will have lower conductivities.

Formation or annular material within a radius of 4 inches (0.10 m) from the probe contributes very little to the measured conductivity, thus making borehole effects negligible. The peak conductivity response is 11 inches (0.28 m) from the tool. The operating frequency is 39.2 kHz. Data is received as apparent conductivity in mS/m.

2.5 Temperature and Fluid Conductivity

The Mount Sopris fluid temperature/fluid resistivity probe typically provides information concerning the borehole fluid character and flow. The temperature sensor has a temperature range of -4 to +176 degrees Fahrenheit (–20 to +80 degrees Celsius), with a resolution of 0.18 degrees Fahrenheit (0.1 degrees

Celsius). The fluid temperature tool can provide information on the movement of water through a borehole. If there is no flow in or adjacent to a borehole, the temperature will increase as a function of the geothermal gradient. The movement of water through a borehole will provide variations in the temperature gradient. When combined with information about the lithology from other logs the fluid temperature tool can be used to identify lithologic units that are producing water. Combined with information about the fluid resistivity the quality of the water can be quickly assessed.

Appendix 2: Surface-Based and Borehole NMR Survey Results

Surface NMR Measurements at SoCal Gas

August, 2016

NMR theory

Hydrologic Properties from NMR

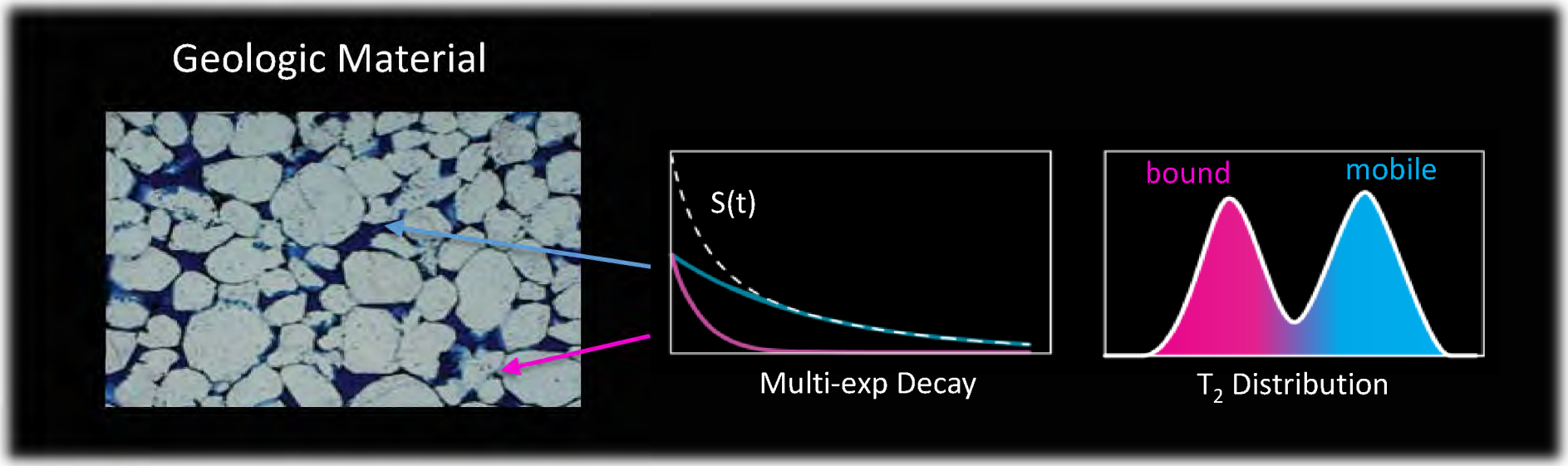

NMR Provides

- Water Content
- Porosity (Lithology Independent)
- Pore Size V/S
- Pore Size V/S Distribution
- Bound versus Mobile WC

Surface-based GMR

Use Earth's field as background field
and large surface coil for NMR excitation and detection

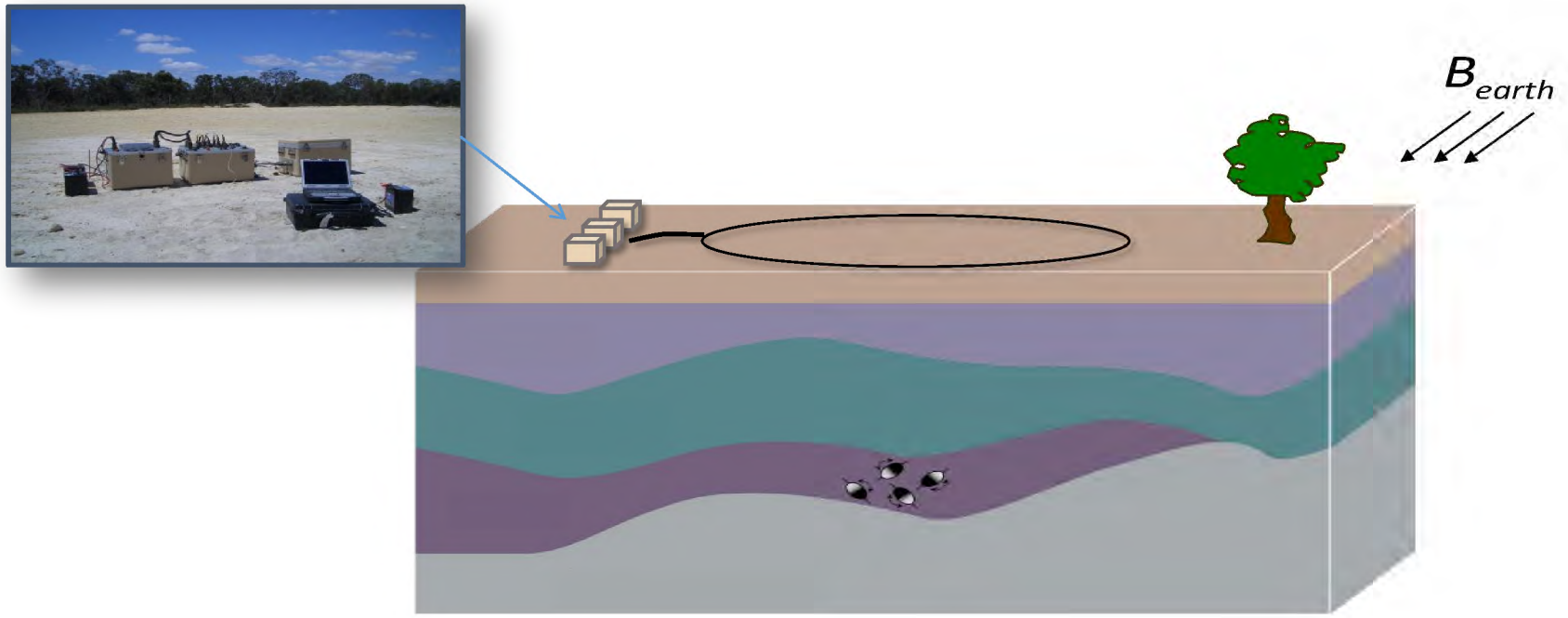

Surface-based GMR Field Procedures

- Measurement loop typically 20-150 m diameter
- Data collection takes 1 – 4 hours per loop location

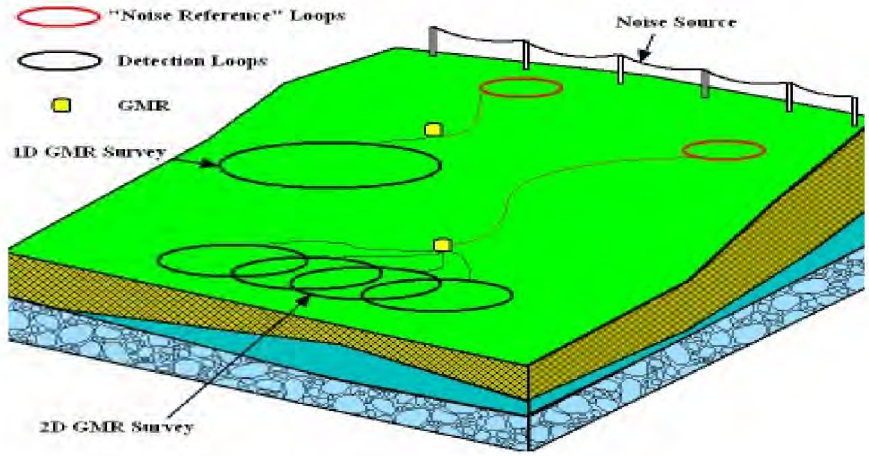

- Multi-channel architecture used for
  - Noise Reference and Cancellation
  - Multi-coil 2D imaging
- Maximum depth of investigation 100-150m

Surface-based GMR Measurement

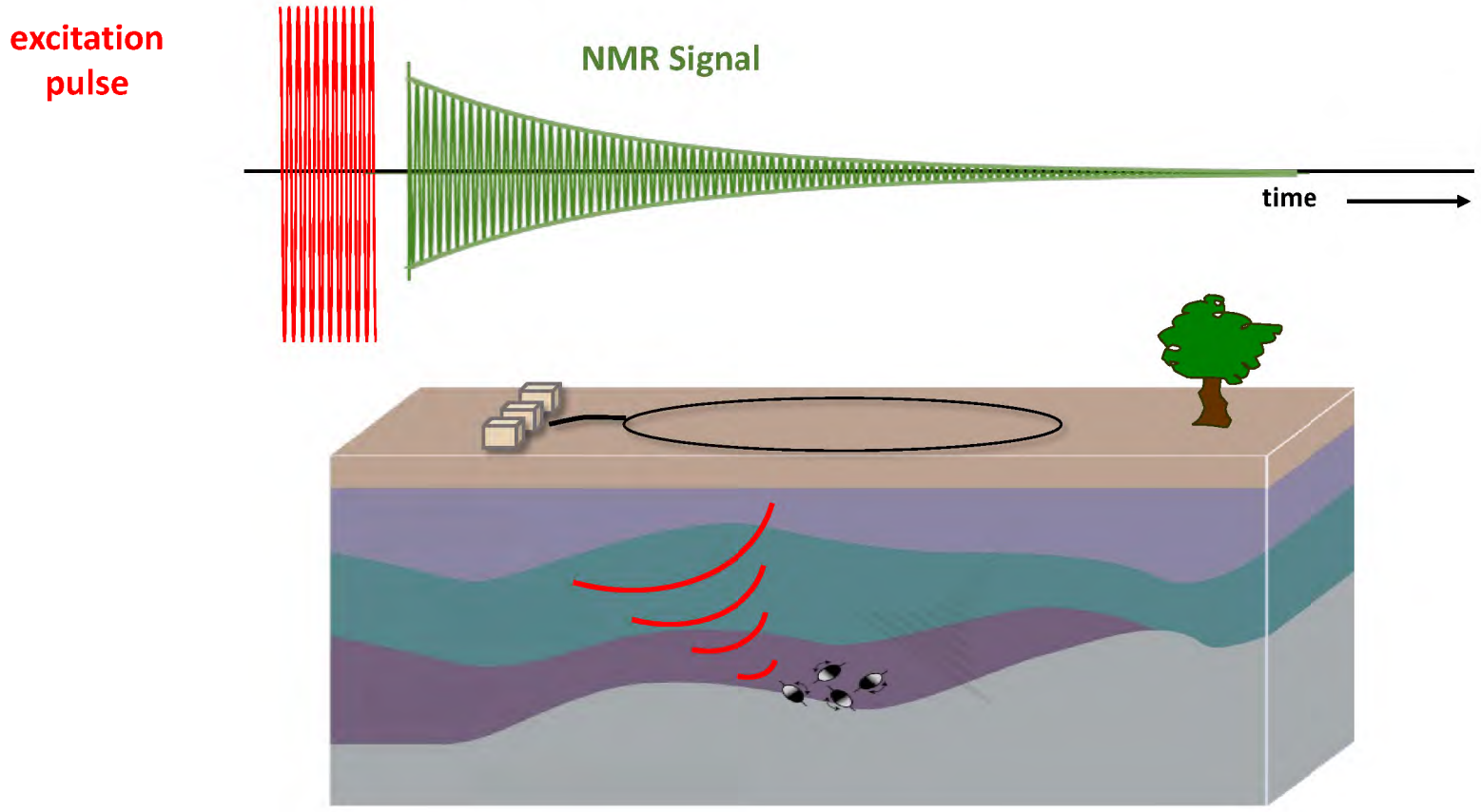

Summary

A surface-NMR survey was conducted with the aim of imaging the distribution of groundwater at the well pad. The survey was carried out by Advisian and Vista Clara using the multi-channel GMR instrument. The surface-NMR method enables direct detection of groundwater and provides information about water content and water mobility. The NMR signals, however, are extremely small in amplitude (nanovolts) and so the presence of electromagnetic noise (e.g. from powerlines) can limit signal detection.

All surface-NMR measurements performed at this site were highly impacted by electromagnetic noise, despite significant efforts to reduce noise during the survey by switching off site power and deploying an extensive optimized network of noise cancellation coils. It is likely one of the most significant and problematic noise sources was the metal pipeline running directly through the survey site. The pipeline acted as an antenna channeling electromagnetic noise from far away sources and radiate the noise incoherently near the NMR measurement coils.

Three survey configurations were implemented over the course of two days in an attempt to reduce the impact of noise. On the first day, data were acquired directly over the well pad using both open square and figure 8 loop configurations. Data from the first day of surveys was not usable due to the high level of noise. Data from the second day was also strongly impacted by noise, but noise levels were reduced enough to draw qualitative speculations regarding groundwater at the site.

Upon applying filtering and noise cancellation to the data from the second day, the noise level was reduced to a voltage at which water contents in the range of ~5% would be observable. No NMR signals, however, were observed at this level. This result is consistent with there being less than 5% mobile water content within the investigation zone of the coil (the area of the coil to ~40m depth). It should be noted, however, there is a chance that the very aggressive noise filtering applied to the data may have removed some NMR signals which were present. It should also be noted that some liquid water at the site may not have been detected because it was immobile resulting in short T2 signals which would not have been detected.

Laboratory NMR measurements on a sample of Modello sandstone taken from the site indicate that most water in the Modello is “bound” with T2 decay times less than 25ms. Such short signals would not have been detected in these surveys given the use of relatively long pulses (30ms) required for deep imaging and given the additional clipping of early time signals resulting from strong noise filtering. The NMR signals observed in the Modello, however, would be easily detectable with logging NMR measurement.

Day 1 – Measurement 1

Measurements were first attempted with the detection loop directly over the pad.

- Detection loop: 40m square loop centered over pad
- Noise loop 1: Large loop deployed to North
- Noise loop 2: Large loop deployed to West
- Noise loop 3: Large loop deployed to South

- Total stacks acquired: 49

Result: Averaged and filtered noise levels >400nV normalized; no meaningful conclusion on groundwater can be drawn.

Day 1 – Measurement 2

The loop shape was changed to a figure 8, which provides enhanced noise rejection at the expense of imaging depth. Unfortunately very large noise spikes started in the afternoon immediately after deploying the figure 8 coil.

- Detection loop: ~20m Figure 8 loop centered over pad
- Noise loop 1: Large loop deployed to North
- Noise loop 2: Large loop deployed to West
- Noise loop 3: Large loop deployed to South

- Total stacks acquired: 25

Result: Averaged and filtered noise levels >400nV normalized; no meaningful conclusion on groundwater can be drawn.

Day 2 – Measurement 1

The loop was moved to the western flank in order to increase the distance from the metal pipeline. The center of the coil was located approximately 25m down slope from the top of the pad.

- Detection loop: ~40m circle deployed to west of pad along slope
- Noise loop 1: Large loop deployed to South
- Noise loop 2: Large loop deployed to North
- Noise loop 3: Small loop on road to West

- Total stacks acquired: 89

Result: Averaged and filtered noise levels >150-200nV normalized. Only qualitative conclusions can be drawn. These data are elaborated upon in the following pages

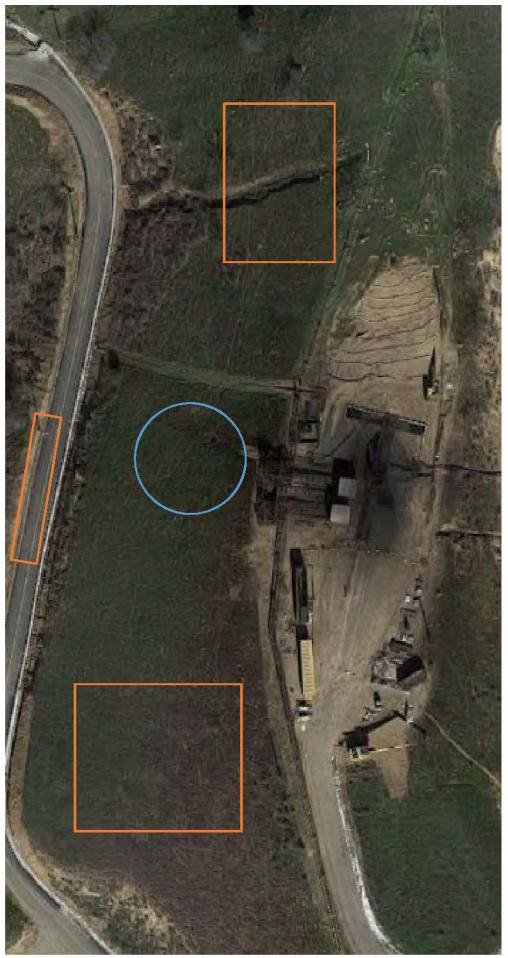

Example Raw Data

Good NMR Data
Other Site

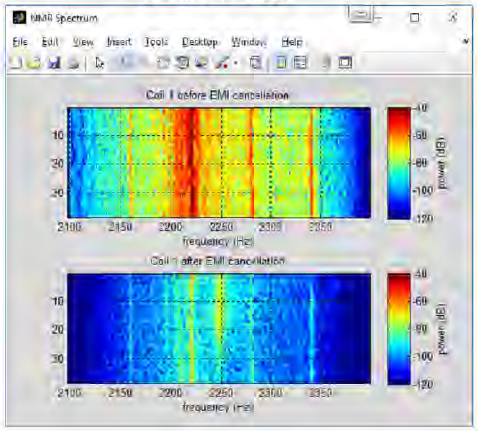

SoCal Data
This Site

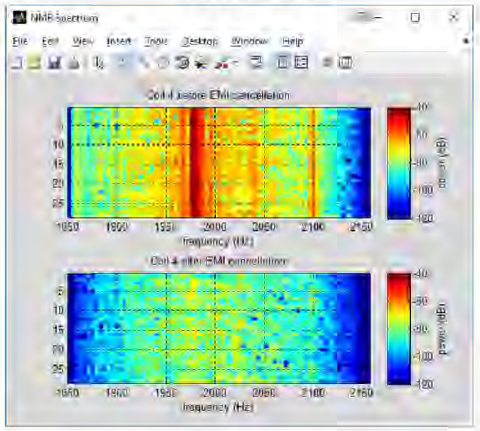

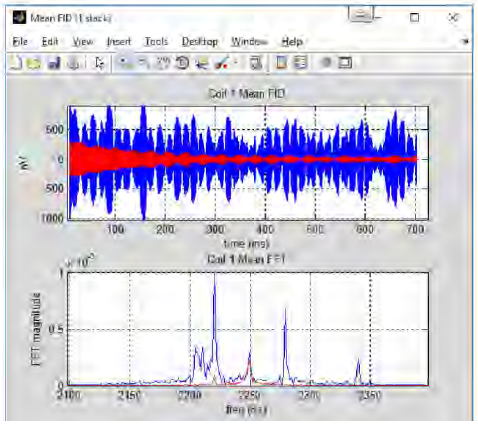

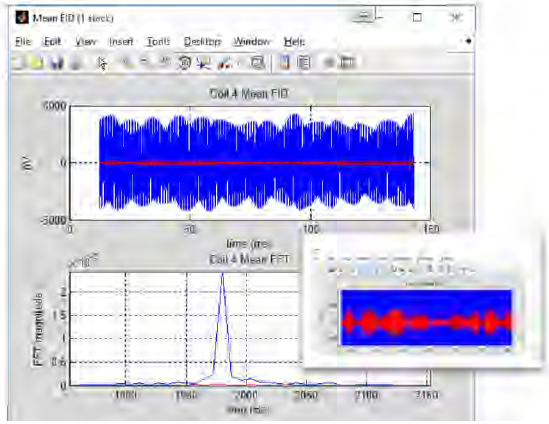

For comparison, we show good NMR data from another site (left) along side the SoCal data (right). The top figure shows the frequency spectra from multiple measurements before application of noise cancellation (above) and after noise cancellation (below). Powerline harmonics are observed as lines of noises at a fixed frequency. Spike noise sources appear as wideband distortions across the spectra. In the lower figure, the time domain signals are shown before noise cancellation (blue) and after noise cancellation red.

In the good data example, the noise is very effectively cancelled; powerline harmonics are removed leaving a background noise level of less than -110dB. The NMR signal is observed in the top figure as a diffuse yellow line in the center of the spectrum. In the lower figure, the NMR signal is observed as a clear signal decaying with time ~300nV.

In the SoCal data, noise cancellation significantly reduces noise but levels remain around -90dB. In the lower panel, the record levels are reduced only to ~500nV. No clear NMR decays are observed, but the noise level is too high to assess if small NMR signals may be present.

Inversion of the SoCal data

Although no NMR signals are observed, we are still able to invert the recorded data. In this case, the algorithm will fit the noise in the data falsely as NMR signals from water. This allows us to quantify the variance in water content estimates associated with the noise levels and thus provides a basis for estimating an upper bound on the water content.

Here we observe water contents in the ranging up to 5% by volume. We do not interpret this as detected NMR signals but rather as an indication there is less than 5% mobile water content within the sensitive volume of the coil.

The depth of investigation for this coil configuration is approximately 45 meters if we assume a resistive subsurface (>50 ohm-m). If the subsurface is significantly more conductive, the depth of investigation for the coil would be significantly reduced.

We note that the very aggressive filtering that had to be applied to this data may have also resulted in cancellation of some NMR signals. Thus, we cannot have full certainty in the assessment that mobile water content is less than 5%.

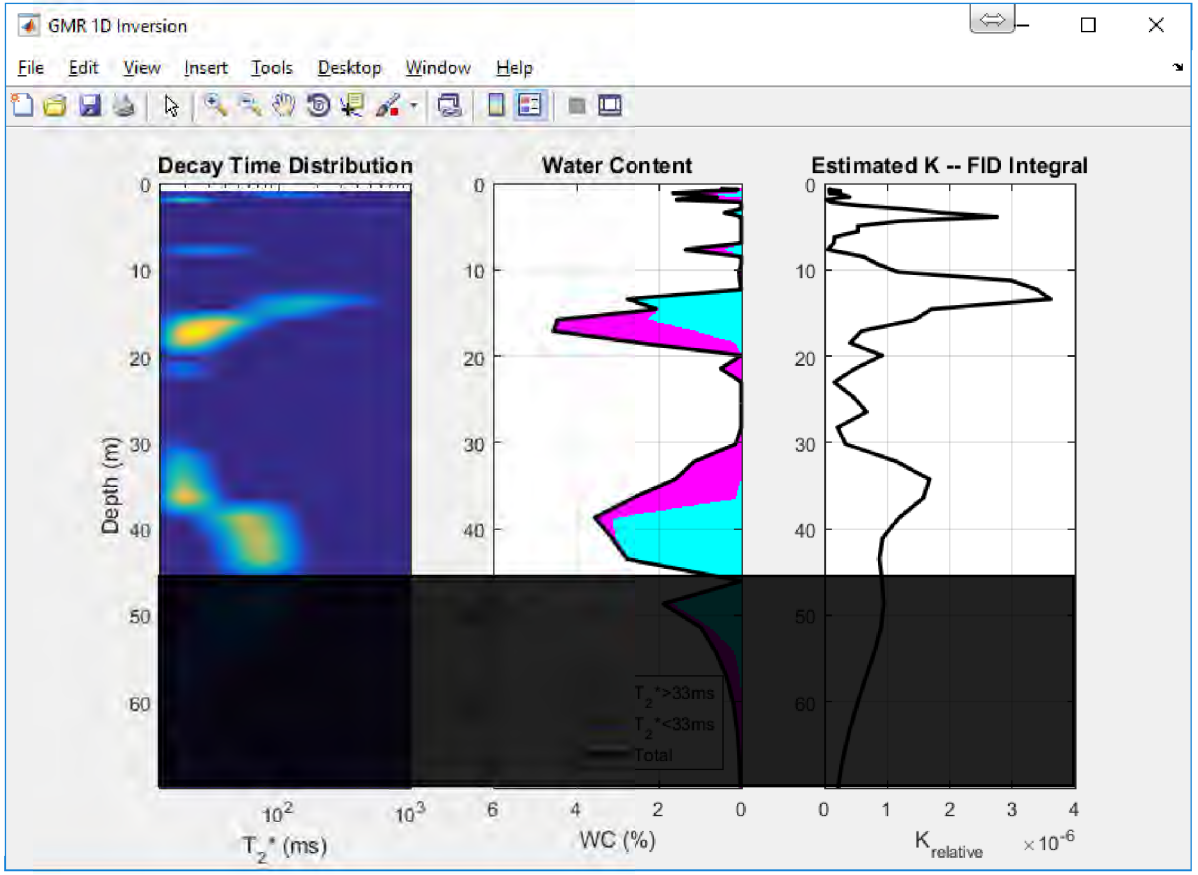

Possible bound water not detected

It is also possible that water contents may significantly exceed 5% but may be too short to have been detected. The requirement for relatively long acquisition pulses (30ms) and aggressive data filtering reduces detection of very short NMR signals. The effective "dead time" for the field data was ~25ms. This means signals decaying on a time scale shorter than 25ms (i.e. T2<25ms) would not be clearly detected.

In order to assess the NMR response of the Modello Sandstone at the site, a sample was taken back to the Vista Clara laboratory, was saturated with water, and was measured in an NMR rock core analyzer. The result at left shows the NMR response of water in the Modello Sandstone. We find that most of the NMR signals in the Modello are associated with bound water with T2<25ms. In fact, only about 20% of the water has T2 values longer than 25ms. As such, it is expected that much of the water in the Modello may not have been detected given the effective dead time associated with the required acquisition and processing procedures at this site.

We note that logging NMR measurements are much more similar to laboratory NMR measurements and are able to measure water signals with T2 down to ~1ms.

Laboratory NMR measurement on Modello Sandstone taken from site and saturated with water

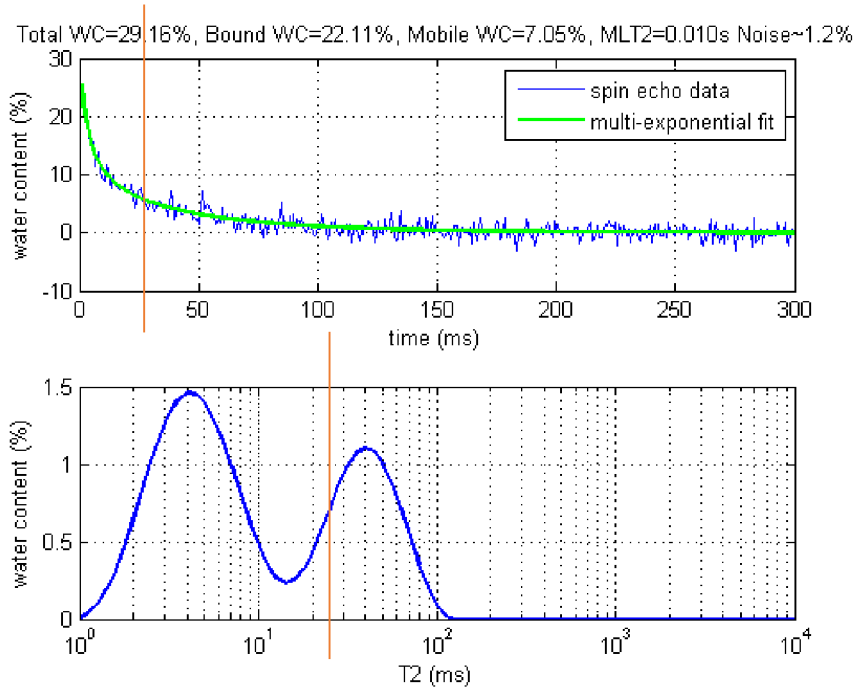

Dart NMR Logging Data
Aliso Canyon

Data Acquired by Advisian

Data Analyzed by Vista Clara

September, 2016

NMR Logging Method Overview

The NMR logging method uses the physics of nuclear magnetic resonance to directly measure fluid hydrogen in groundwater. The downhole NMR sonde contains magnets that polarize the fluid hydrogen, creating a net nuclear magnetization with a magnitude proportional to the number of fluid hydrogen present. Radio-frequency coils within the probe transmit EM pulses to excite this hydrogen magnetization and to measure its time-varying behavior. The recorded NMR signal decays over time and provides useful information about the hydrogeologic properties of the investigated material.

The initial amplitude of the NMR signal directly reflects the quantity of hydrogen in the formation or the volumetric water content (porosity if saturated). The decay time of the signal T_2 indicates whether the water is in "bound" small pores (with high surface-area-to-volume ratio) or is mobile in large pores spaces. In heterogeneous materials, the T_2 distribution provides an indication of the relative pore-size distribution with shorter T_2 components being associated with smaller pores and longer T_2 components being associated with larger pores. In the case of a suspension, the T_2 decay time may be interpreted to reflect the surface-area-to-volume ratio of the suspension. Given the sensitivity to water content and pore size, the NMR data may also be used to estimate permeability or hydraulic conductivity.

The configuration of the Vista Clara Dart NMR logging tool allows data to be acquired in a dual-frequency mode. Data acquired using a lower RF frequency is sensitive to water at a radial distance of ~3 inches from the tool (diameter ~6 inches). Data acquired using a higher RF frequency is sensitive to water at a lesser radial distance of ~2.5 inches (diameter ~5 inches). In most cases, the formation is sufficiently homogeneous radially that data at these different radial distances are identical. As such, these two datasets are typically combined by averaging to generate a combined dual-frequency log.

Because an NMR signal is only detected from fluids, no signal is observed from frozen water. An increase in ice content would be apparent as a decrease in water content.

“Mobile” and “Bound” Water

The T_2 distribution can be subdivided to estimate the fraction of water that is more bound and more mobile. The total integral of the T_2 distribution is the total water content so the area under a subdivided range of the distribution represents the total amount of water having T_2 within that range.

Using standard cutoff times derived from oil reservoir sandstones, water with T_2 longer than 33ms is estimated as “mobile” water; water with T_2 less than 33ms is estimated as “bound” water. Because these standard cutoff times are based on reservoir sandstones, in other rock/sediment types, the cutoffs and definitions of “bound” and “mobile” should not be considered in a definite sense but rather a way to distinguish “more bound” water from “more mobile” water.

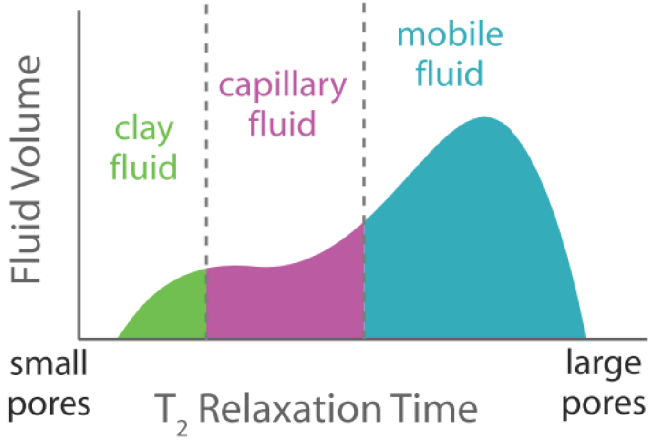

Data Processing

Data were processed with the following parameters (selectable as options in Vista Clara's NMR processing software):

- Spike noise removal was implement to remove periodic noise spikes.
- Dual-frequency data were combined in final processing. Uncombined individual frequency data were visualized in preprocessing to assess variability between the frequency shells.
- A regularization value of 10 was used in all cases.
- Da ta were acquired at the native 0.25 m vertical resolution and were processed at 1m resolution which incorporated averaging over 4 neighboring depth levels.
- Data were calibrated for 100% water content using tests with the probe immersed in a water tank and were implement before and after the data acquisition campaign.

Example Log

An example NMR log is shown below. In all panels, depth below the well head is on the y-axis. The panel at left shows the T_2 distribution at every depth level. Water signals are shown in warm colors, with the position of the signal along the horizontal axis indicating the T_2 decay time of the signal on a logarithmic scale [e.g. $\log_{10}(-2)$ s = 10^{-2} s = 10ms]. Water constricted in smaller geometries (small pores) will plot towards the left of the distribution (short T_2) and water in large spaces (large pores or fractures) will plot to the right of the distribution (long T_2). The second panel shows the total water content, mobile fraction and capillary fraction at every depth level.

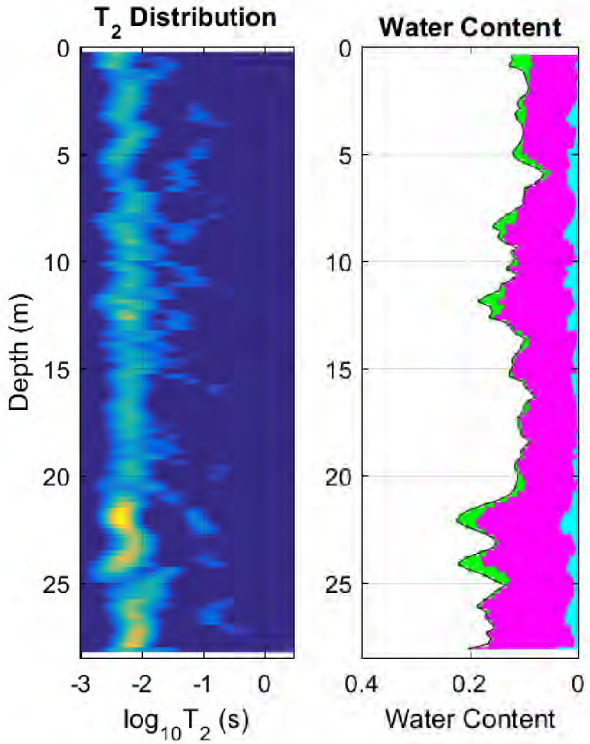

Data Quality Characteristics

In general, the quality from the Aliso Canyon data is very high. These measurements were not affected by external noise sources and so have excellent signal to noise. In general water content is between 10-20% throughout most of the logs, and is primarily estimated as bound data. This character is consistent with the logged intervals being partially saturated, with mobile water content drained, and primarily capillary water retained. It is possible the capillary water is native or may have been introduced during drilling. The lower section of BH3, the deepest zone logged appears to enter the saturated zone, marked by a significant increase in mobile water content. There are not any obvious zones where water content decreases, as might be anticipated in a frozen interval.

Laboratory NMR measurement on Modello Sandstone taken from site and saturated with water

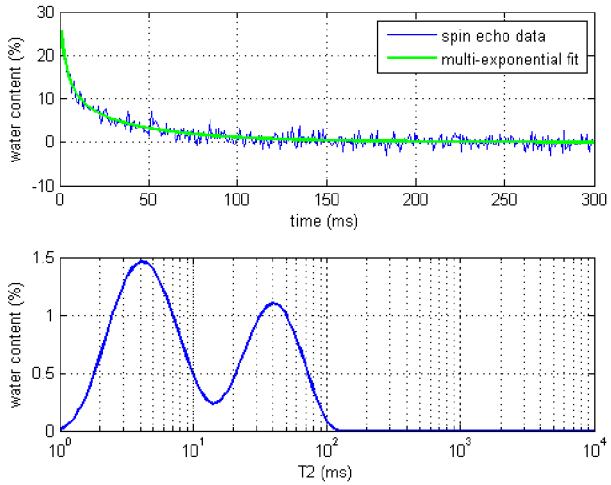

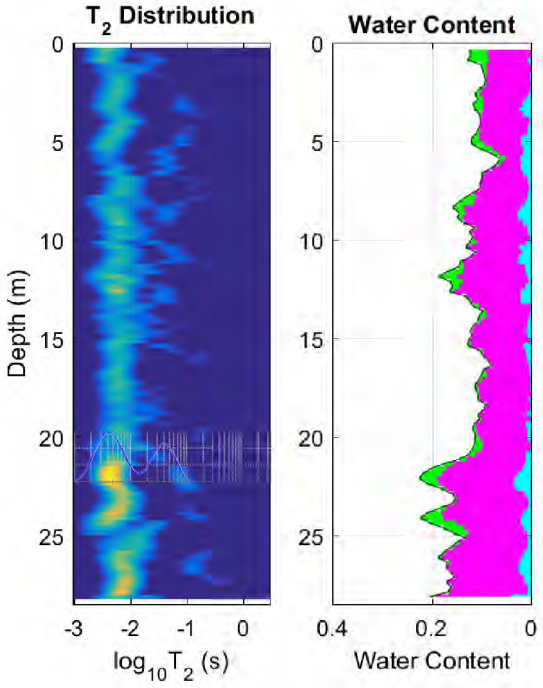

Appendix 3: Geophysical Borehole Logs

Advisian
WorleyParsons Group

Project Name:
Aliso Canyon SS-25 Geophysical Surveys

Borehole:
BH1

Project #: 407074-00748	Drilling Company: Cascade Drilling	Casing Diameter: ..	Location: SS-25
Client: SoCal Gas	Drilling Method: HSA (8" Auger), Rig: CME85	Casing Depth: ..	Latitude: 34.31504640
Logs: Various, see notes	Depth driller: 150 feet	Coring Diameter: 3.75 inches	Longitude: -118.56396462
Date: 2016-09-23	Depth logger: 30.3 feet (9.24 mbgs)	Coring Depths: 42 to 150 feet	Elevation: 2915.22 ft
Location (LLD): SS-25	Stick Up: n/a	Drilling Diameter: 7.5 inches to 42 feet	Notes: Optical Televiewer OBI40 (064905), Natural Gamma 2PGA (2425), Inductive Conductivity 2PIA (6051), Temperature 2PFA (), Magnetic Declination: 12.239 E
Logged by: R. Shinduke	Fluid Type: n/a	Console Type, Serial #: 2510, 0630	
Depths Relative to: Ground Level	Fluid Level: n/a	Probe(s) Model, Serial #: various	

This drawing is prepared solely for the use of our customer as specified in the accompanying report. WorleyParsons Canada Services Ltd. assumes no liability to any other party for any representations contained in this drawing."

Lithology Legend

- Poorly-graded gravels, gravel-sand mixtures, little or no fines
- Silty sands, sand-silt mixtures
- Inorganic silts and very fine sands, rock flour, silty or clayey fine sands or clayey silts with slight plasticity
- No recovery
- Modelo Formation

Structural Legend

- Closed Joint

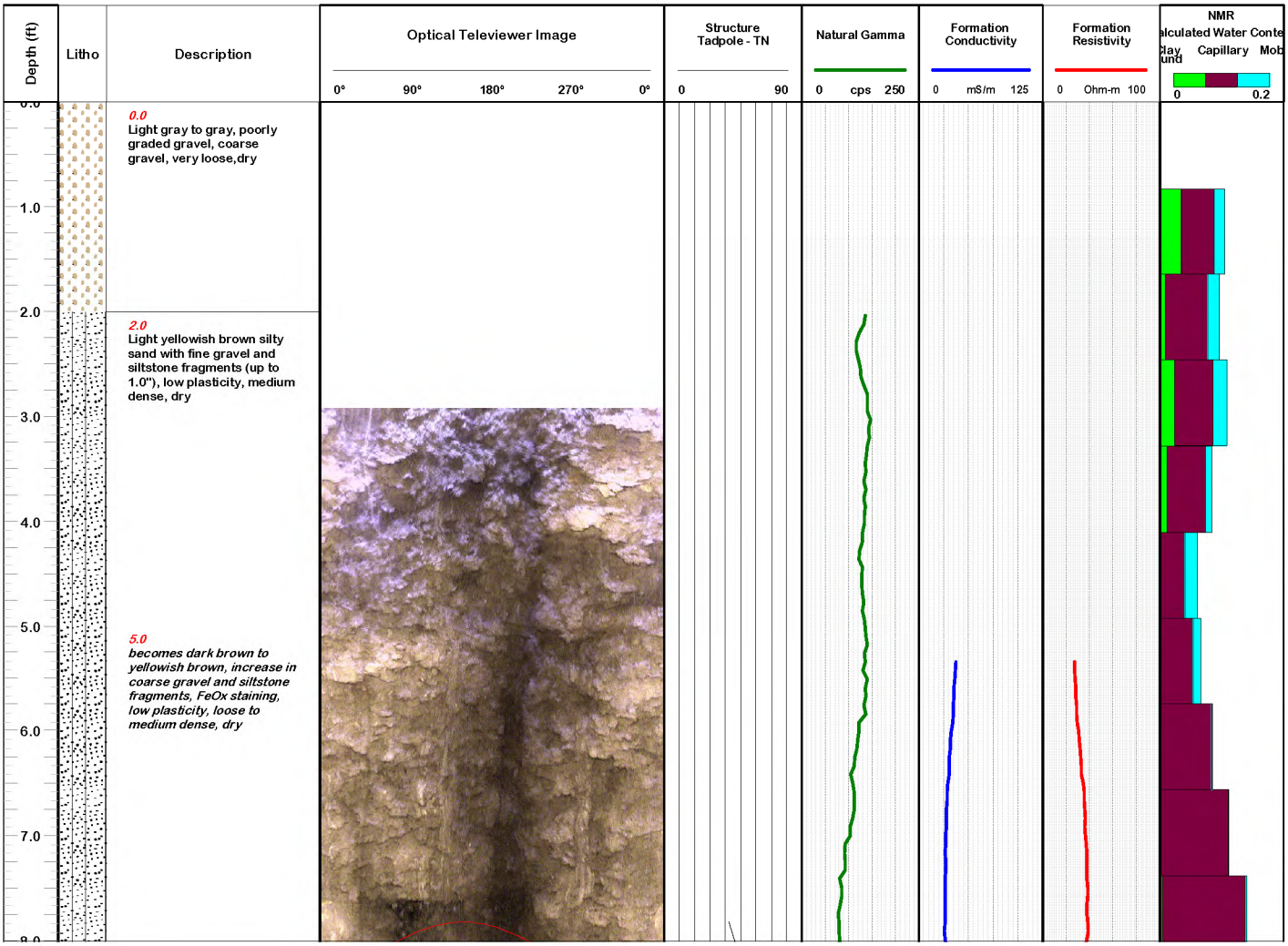

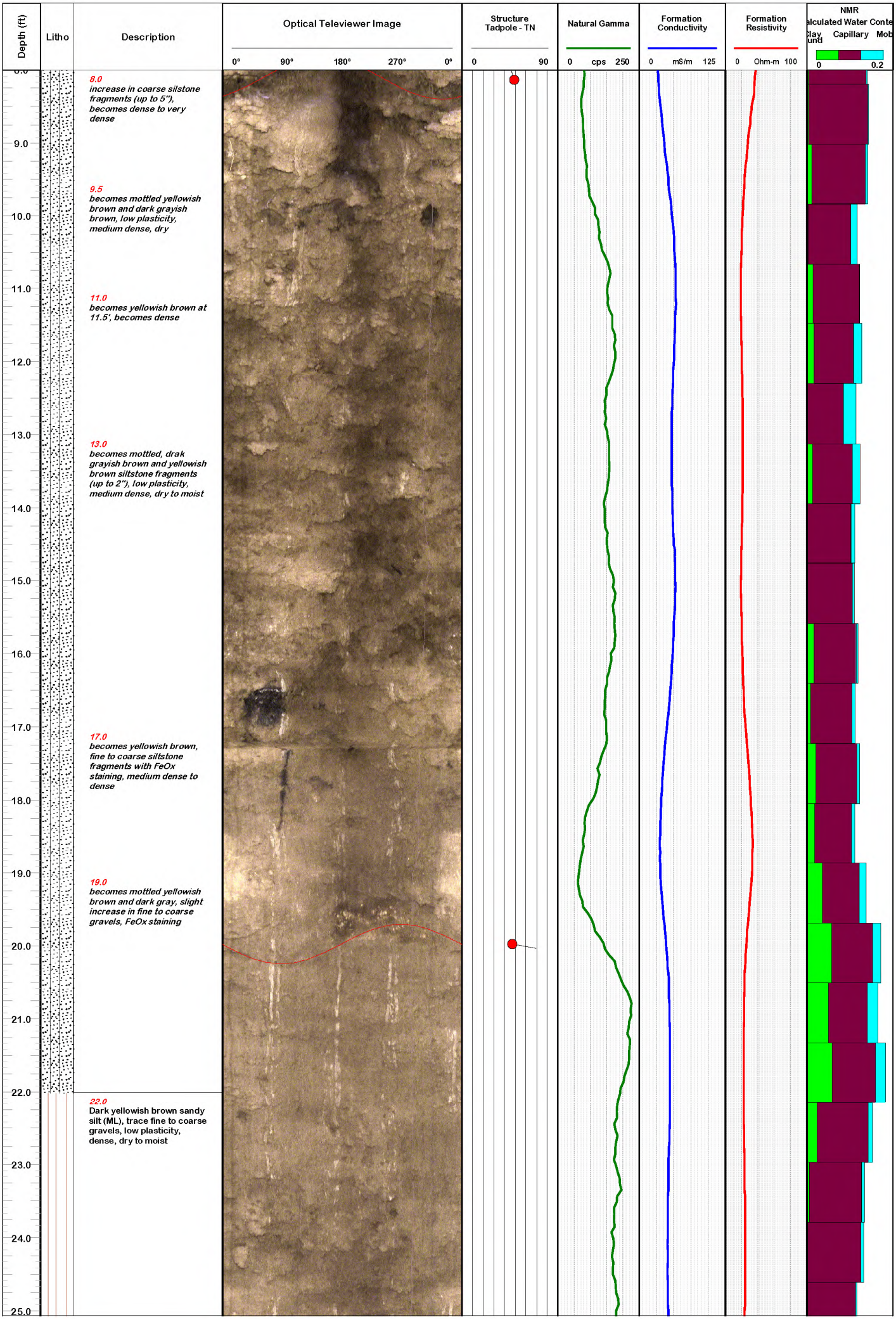
Depth (ft)
Litho
Description
Optical Televiewer Image
0° 90° 180° 270° 0°
Structure
Tadpole - TN
0 90
Natural Gamma
0 cps 250
Formation
Conductivity
0 mS/m 125
Formation
Resistivity
0 Ohm-m 100
NMR
Capillary
Mob
0 0.2
8.0
increase in coarse silstone fragments (up to 5"), becomes dense to very dense
9.5
becomes mottled yellowish brown and dark grayish brown, low plasticity, medium dense, dry
11.0
becomes yellowish brown at 11.5', becomes dense
13.0
becomes mottled, drak grayish brown and yellowish brown siltstone fragments (up to 2"), low plasticity, medium dense, dry to moist
17.0
becomes yellowish brown, fine to coarse siltstone fragments with FeOx staining, medium dense to dense
19.0
becomes mottled yellowish brown and dark gray, slight increase in fine to coarse gravels, FeOx staining
22.0
Dark yellowish brown sandy silt (ML), trace fine to coarse gravels, low plasticity, dense, dry to moist
9.0
10.0
11.0
12.0
13.0
14.0
15.0
16.0
17.0
18.0
19.0
20.0
21.0
22.0
23.0
24.0
25.0

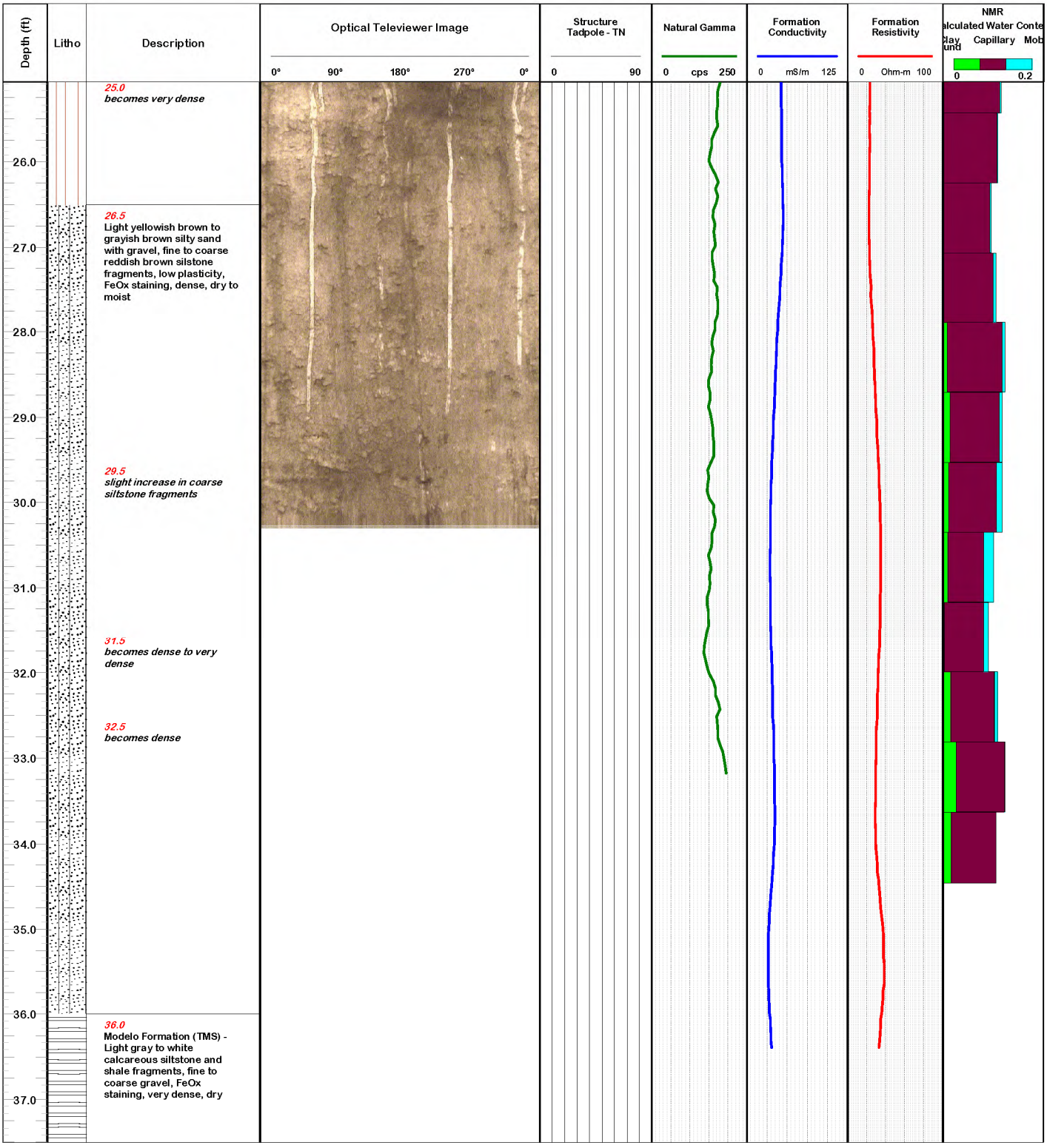
Depth (ft)
Litho
Description
Optical Televiewer Image
0°
90°
180°
270°
0°
Structure
Tadpole - TN
0
90
Natural Gamma
0
cps
250
Formation
Conductivity
0
mS/m
125
Formation
Resistivity
0
Ohm-m
100
NMR
Capillary
Mob
0
0.2
25.0
becomes very dense
26.5
Light yellowish brown to grayish brown silty sand with gravel, fine to coarse reddish brown silstone fragments, low plasticity, FeOx staining, dense, dry to moist
29.5
slight increase in coarse siltstone fragments
31.5
becomes dense to very dense
32.5
becomes dense
36.0
Modelo Formation (TMS) - Light gray to white calcareous siltstone and shale fragments, fine to coarse gravel, FeOx staining, very dense, dry
26.0
27.0
28.0
29.0
30.0
31.0
32.0
33.0
34.0
35.0
36.0
37.0

Advisian
WorleyParsons Group

Project Name:
Aliso Canyon SS-25 Geophysical Surveys

Borehole:
BH2

Project #: 407074-00748	Drilling Company: Cascade Drilling	Casing Diameter:	Location: SS-25
Client: SoCal Gas	Drilling Method: HSA (8" Auger), Rig: CME85	Casing Depth:	Latitude: 34.31525984
Logs: Various, see notes	Depth driller: 120 feet	Coring Diameter: 3.75 inches	Longitude: -118.56394159
Date: 2016-09-23	Depth logger: 49.2 feet (14.99 mbgs)	Coring Depths: 45 to 120 feet	Elevation: 2914.91 ft
Location (LLD): SS-25	Stick Up: n/a	Drilling Diameter: 7.5 inches to 45 feet	Notes: Optical Televiewer OBI40 (064905), Natural Gamma 2PGA (2425), Inductive Conductivity 2PIA (6051), Temperature 2PFA () Magnetic Declination: 12.239 E
Logged by: R. Shinduke	Fluid Type: n/a	Console Type, Serial #: 2510, 0630	
Depths Relative to: Ground Level	Fluid Level: n/a	Probe(s) Model, Serial #: various	

This drawing is prepared solely for the use of our customer as specified in the accompanying report. WorleyParsons Canada Services Ltd. assumes no liability to any other party for any representations contained in this drawing."

Lithology Legend

- Poorly-graded gravels, gravel-sand mixtures, little or no fines
- Silty sands, sand-silt mixtures
- No recovery
- Modelo Formation

Structural Legend

- Bedding
- Closed Joint

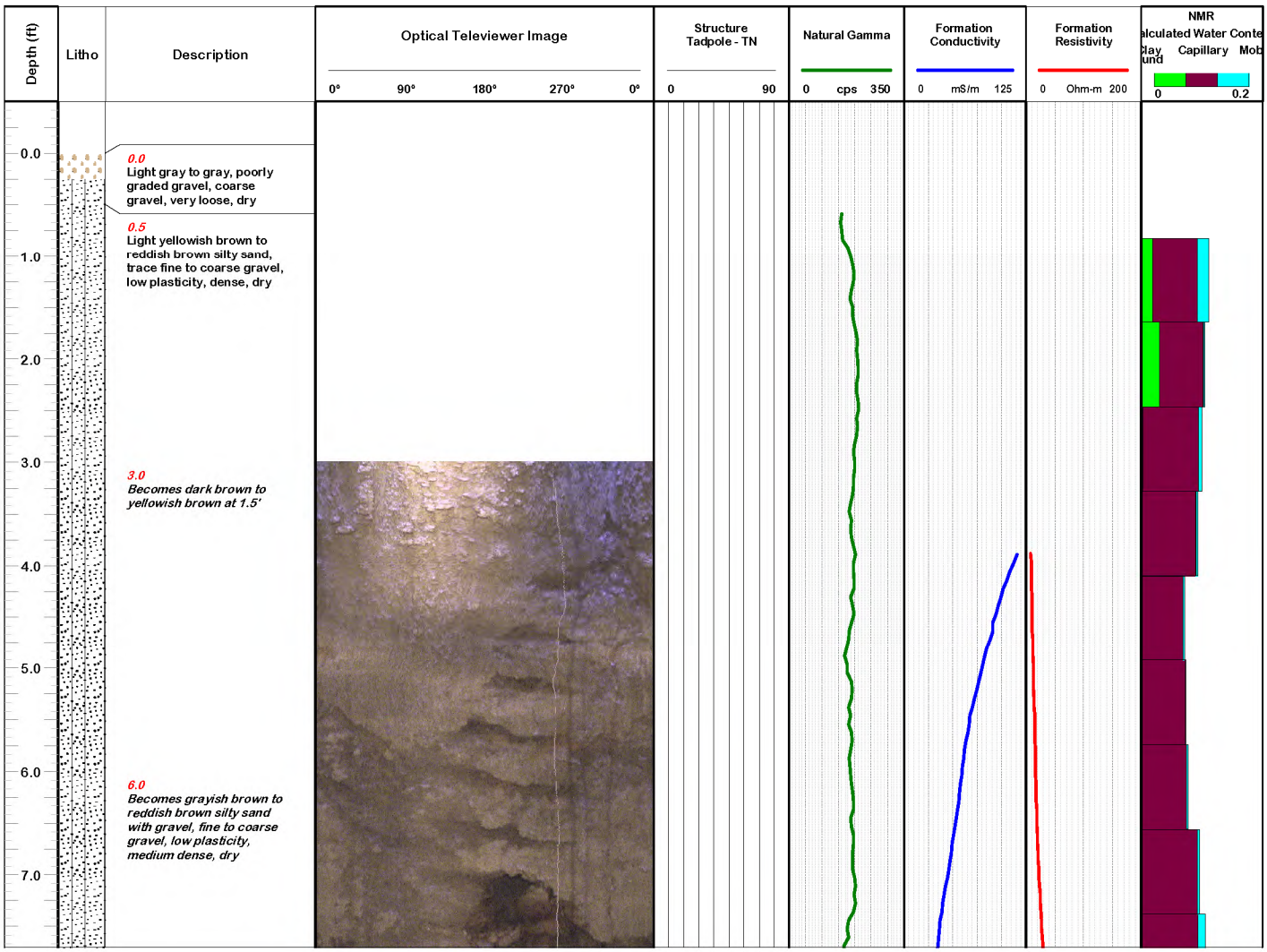

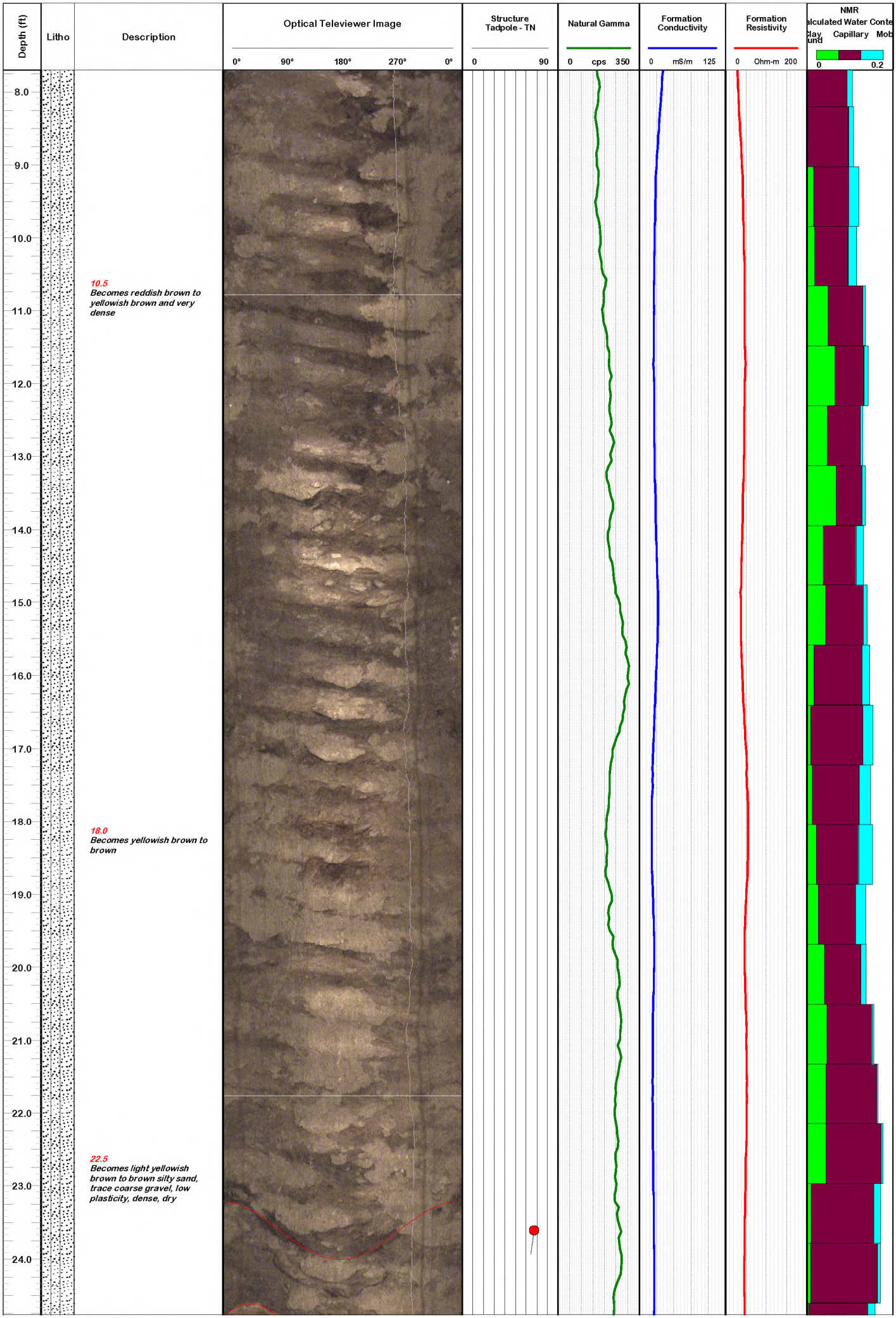
Depth (ft)
Litho
Description
Optical Televiewer Image
0°
90°
180°
270°
0°
Structure
Tadpole - TN
0
90
Natural Gamma
0
cps
350
Formation
Conductivity
0
mS/m
125
Formation
Resistivity
0
Ohm-m
200
NMR
Capillary
Mob
0
0.2
8.0
9.0
10.0
11.0
12.0
13.0
14.0
15.0
16.0
17.0
18.0
19.0
20.0
21.0
22.0
23.0
24.0
10.5
Becomes reddish brown to yellowish brown and very dense
18.0
Becomes yellowish brown to brown
22.5
Becomes light yellowish brown to brown silty sand, trace coarse gravel, low plasticity, dense, dry

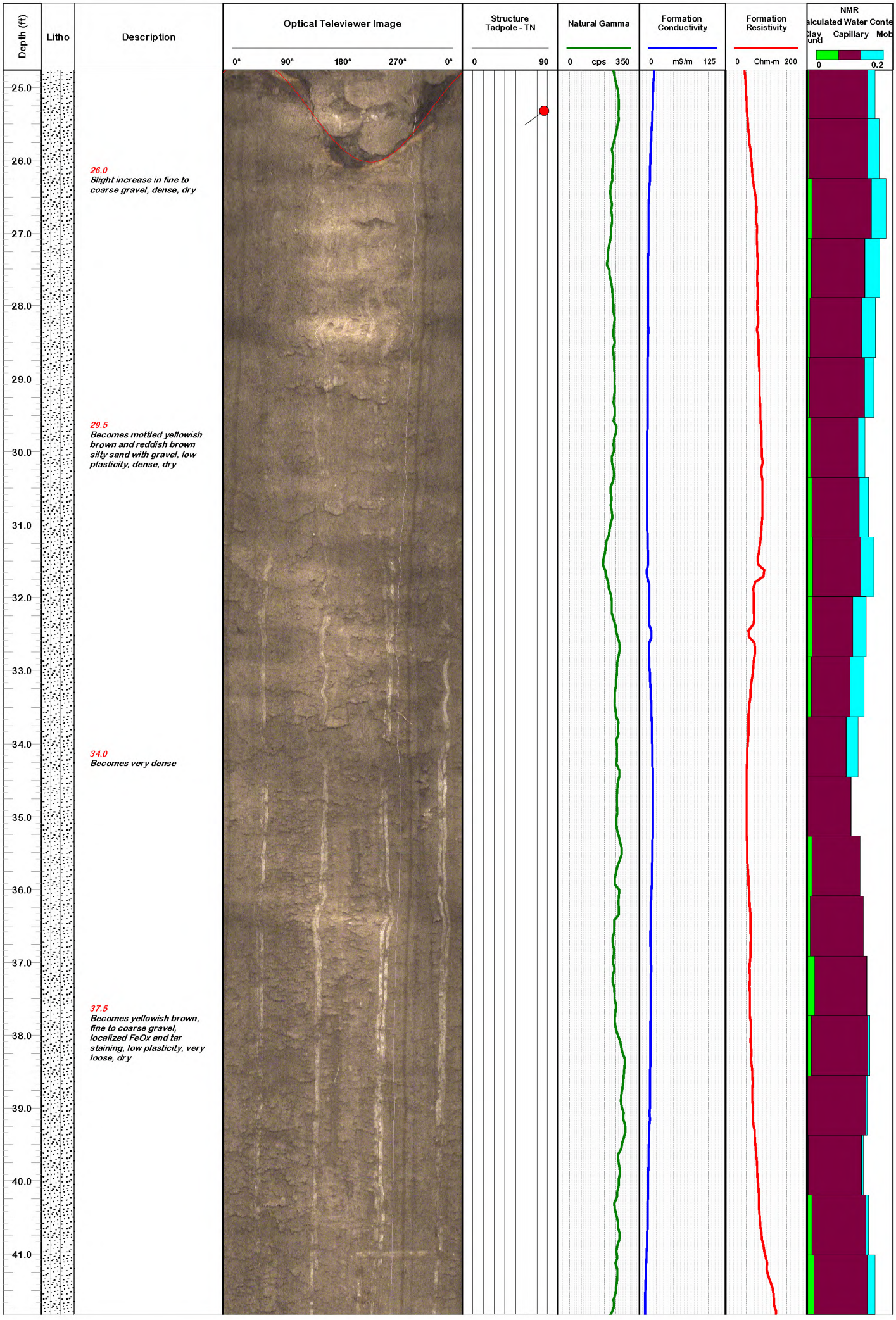
Depth (ft)
Litho
Description
Optical Televiewer Image
0° 90° 180° 270° 0°
Structure
Tadpole - TN
0 90
Natural Gamma
0 cps 350
Formation
Conductivity
0 mS/m 125
Formation
Resistivity
0 Ohm-m 200
NMR
Capillary
Mob
0 0.2
25.0
26.0
27.0
28.0
29.0
30.0
31.0
32.0
33.0
34.0
35.0
36.0
37.0
38.0
39.0
40.0
41.0
26.0
Slight increase in fine to coarse gravel, dense, dry
29.5
Becomes mottled yellowish brown and reddish brown silty sand with gravel, low plasticity, dense, dry
34.0
Becomes very dense
37.5
Becomes yellowish brown, fine to coarse gravel, localized FeOx and tar staining, low plasticity, very loose, dry

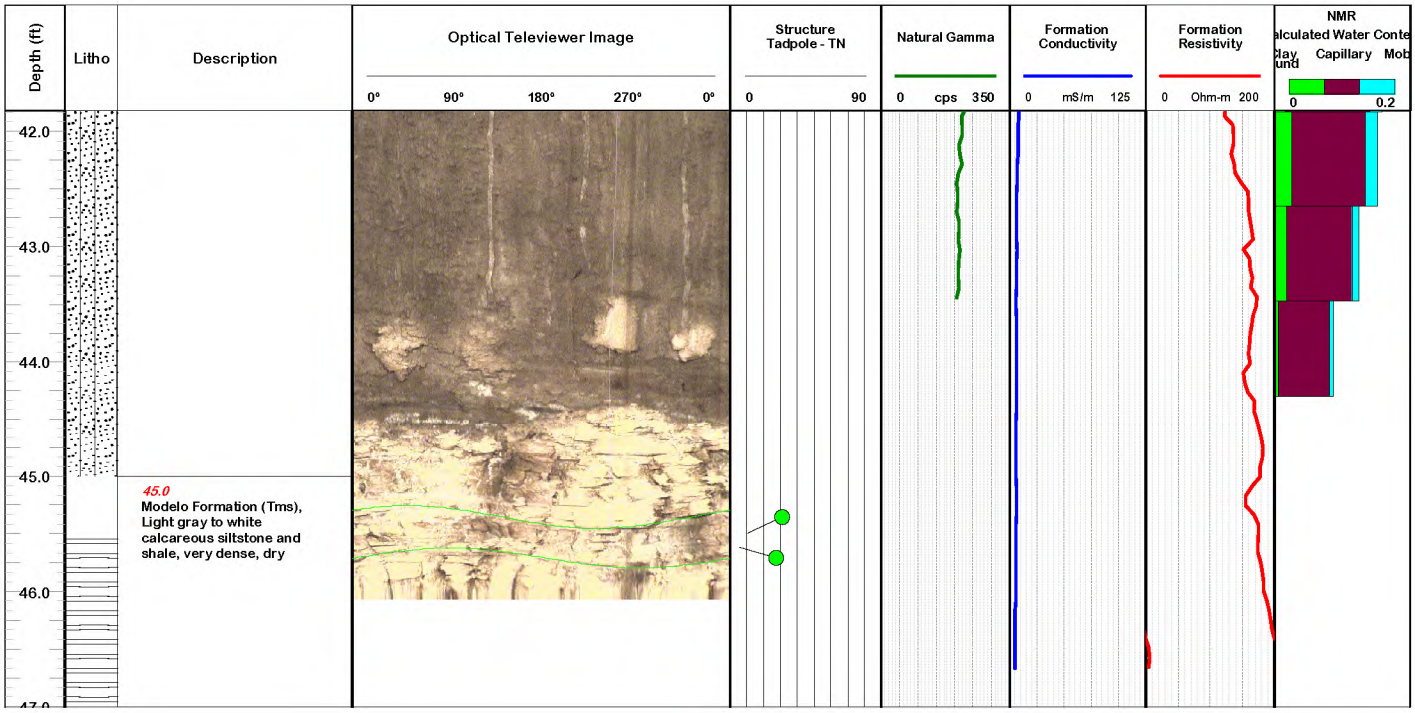
Depth (ft)
Litho
Description
Optical Televiewer Image
0°
90°
180°
270°
0°
Structure
Tadpole - TN
0
90
Natural Gamma
0
cps
350
Formation
Conductivity
0
mS/m
125
Formation
Resistivity
0
Ohm-m
200
NMR
Capillary
Mob
0
0.2
42.0
43.0
44.0
45.0
46.0
45.0
Modelo Formation (Tms), Light gray to white calcareous siltstone and shale, very dense, dry

Advisian
WorleyParsons Group

Project Name: Aliso Canyon SS-25 Geophysical Surveys			**Borehole: BH3**
Project #: 407074-00748	Drilling Company: Cascade Drilling	Casing Diameter: ..	Location: SS-25
Client: SoCal Gas	Drilling Method: HSA (8" Auger), Rig: CME85	Casing Depth: ..	Latitude: 34.31489403
Logs: Various, see notes	Depth driller: 135 feet	Coring Diameter: 3.75 inches	Longitude: -118.56427170
Date: 2016-09-23	Depth logger: 133 feet (40.55 mbgs)	Coring Depths: 135 feet	Elevation: 2913.93 ft
Location (LLD): SS-25	Stick Up: n/a	Drilling Diameter: 7.5 inches to 45 feet	Notes: Optical Televiewer OBI40 (064905), Natural Gamma 2PGA (2425), Inductive Conductivity 2PIA (6051), Temperature 2PFA () Magnetic Declination: 12.239 E
Logged by: R. Shinduke	Fluid Type: n/a	Console Type, Serial #: 2510, 0630	
Depths Relative to: Ground Level	Fluid Level: n/a	Probe(s) Model, Serial #: various	

This drawing is prepared solely for the use of our customer as specified in the accompanying report. WorleyParsons Canada Services Ltd. assumes no liability to any other party for any representations contained in this drawing."

Lithology Legend

- Well-graded sands
- Silty sands, sand-silt mixtures
- Inorganic silts and very fine sands, rock flour, silty or clayey fine sands or clayey silts with slight plasticity
- No recovery
- Modelo Formation

Structural Legend

- Bedding
- Closed Joint

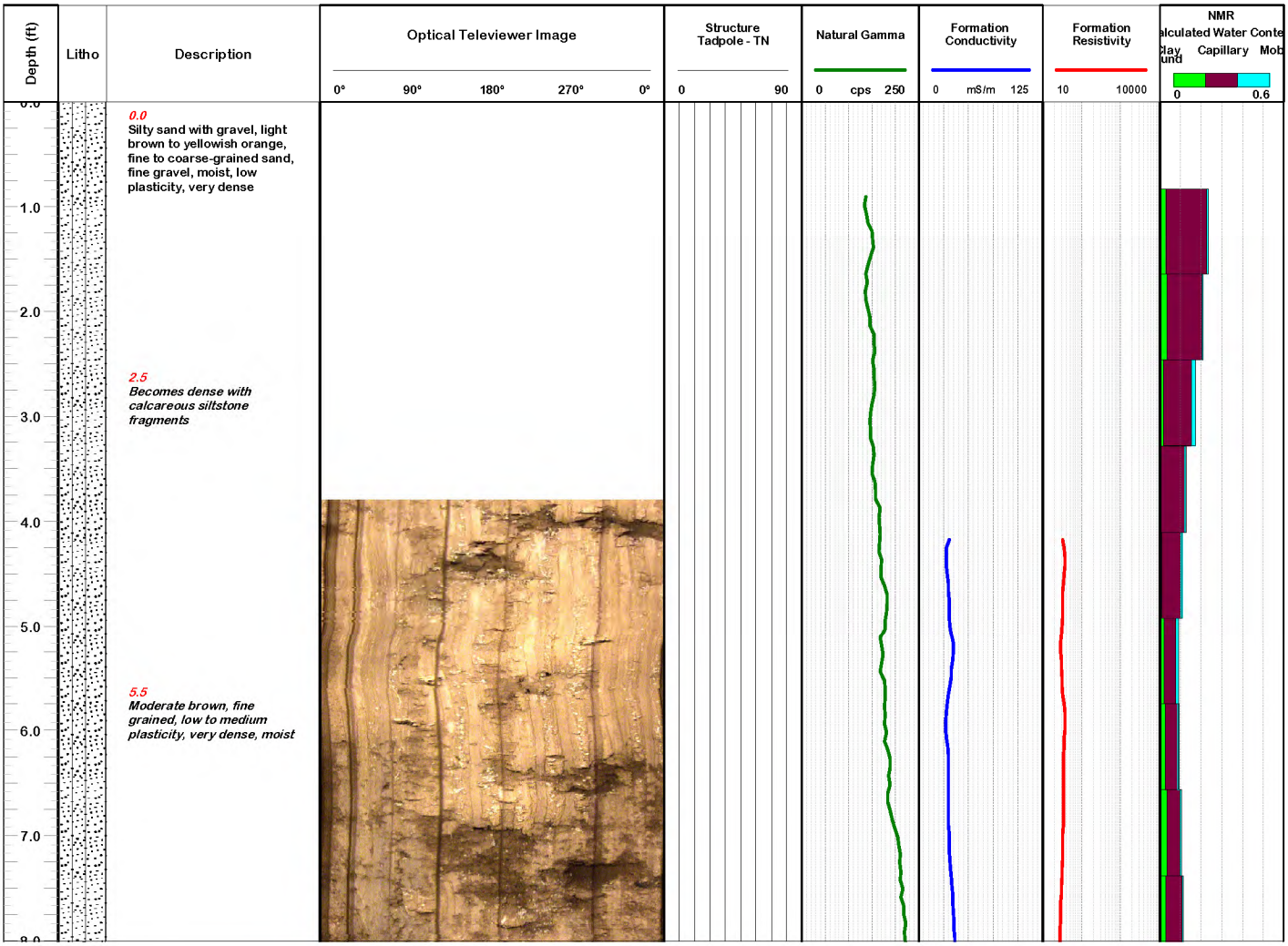

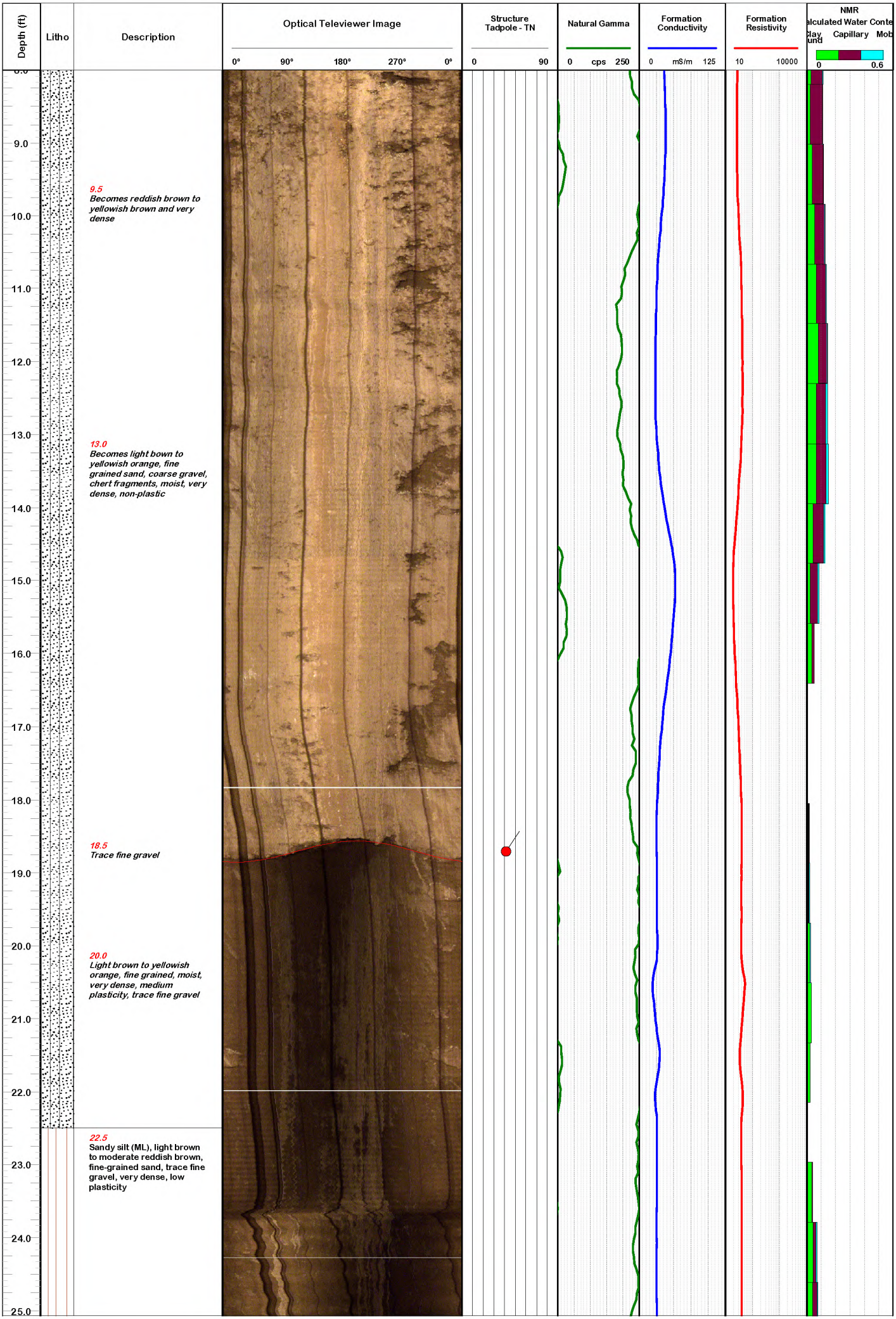
Depth (ft)
Litho
Description
Optical Televiewer Image
0°
90°
180°
270°
0°
Structure
Tadpole - TN
0
90
Natural Gamma
0
cps
250
Formation
Conductivity
0
mS/m
125
Formation
Resistivity
10
10000
NMR
Capillary
Mob
0
0.6
9.0
10.0
11.0
12.0
13.0
14.0
15.0
16.0
17.0
18.0
19.0
20.0
21.0
22.0
23.0
24.0
25.0
9.5
Becomes reddish brown to yellowish brown and very dense
13.0
Becomes light bown to yellowish orange, fine grained sand, coarse gravel, chert fragments, moist, very dense, non-plastic
18.5
Trace fine gravel
20.0
Light brown to yellowish orange, fine grained, moist, very dense, medium plasticity, trace fine gravel
22.5
Sandy silt (ML), light brown to moderate reddish brown, fine-grained sand, trace fine gravel, very dense, low plasticity

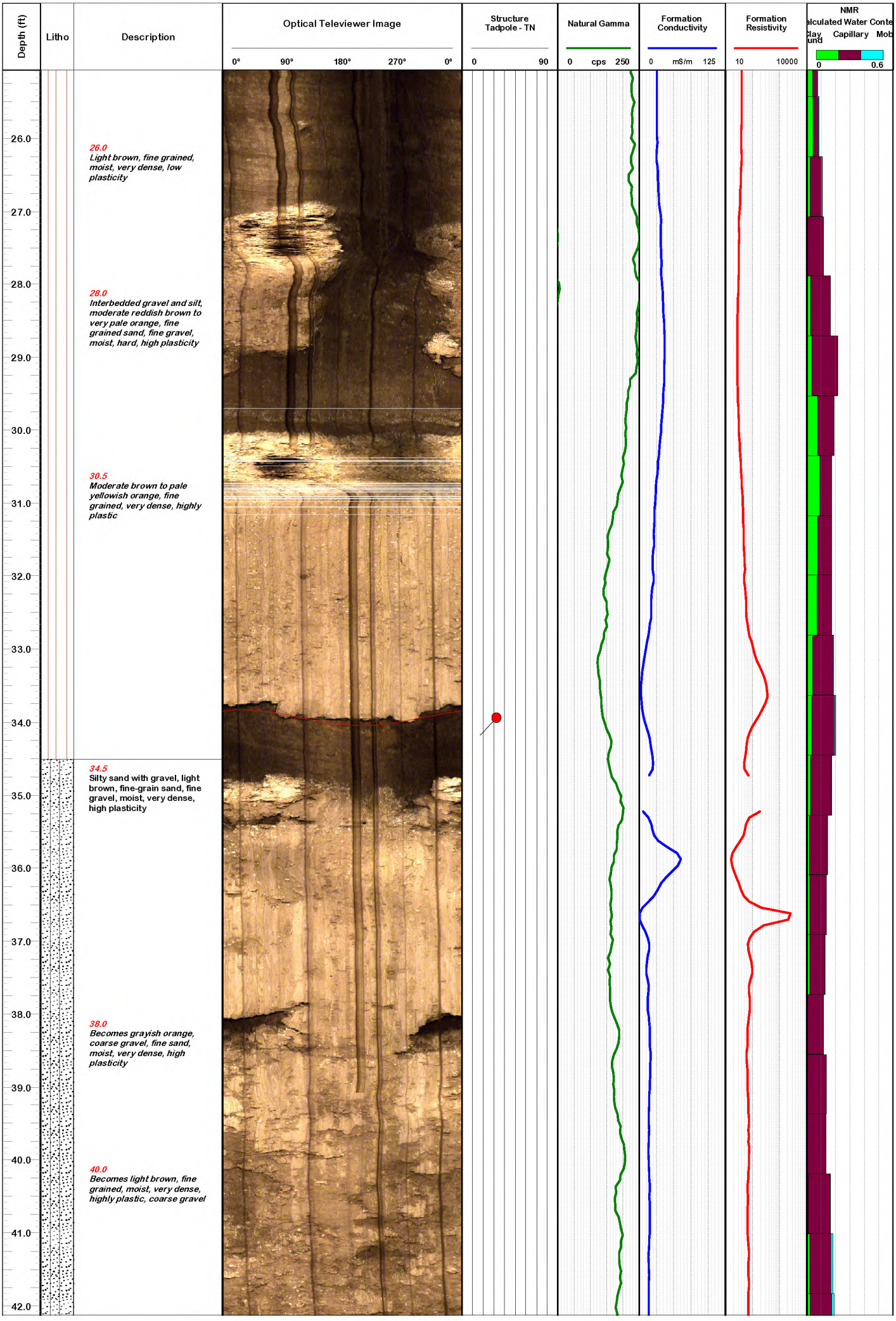
Depth (ft)
Litho
Description
Optical Televiewer Image
0° 90° 180° 270° 0°
Structure
Tadpole - TN
0 90
Natural Gamma
0 cps 250
Formation
Conductivity
0 mS/m 125
Formation
Resistivity
10 10000
NMR
Capillary Mob
0 0.6
26.0
Light brown, fine grained, moist, very dense, low plasticity
28.0
Interbedded gravel and silt, moderate reddish brown to very pale orange, fine grained sand, fine gravel, moist, hard, high plasticity
30.5
Moderate brown to pale yellowish orange, fine grained, very dense, highly plastic
34.5
Silty sand with gravel, light brown, fine-grain sand, fine gravel, moist, very dense, high plasticity
38.0
Becomes grayish orange, coarse gravel, fine sand, moist, very dense, high plasticity
40.0
Becomes light brown, fine grained, moist, very dense, highly plastic, coarse gravel
26.0
27.0
28.0
29.0
30.0
31.0
32.0
33.0
34.0
35.0
36.0
37.0
38.0
39.0
40.0
41.0
42.0

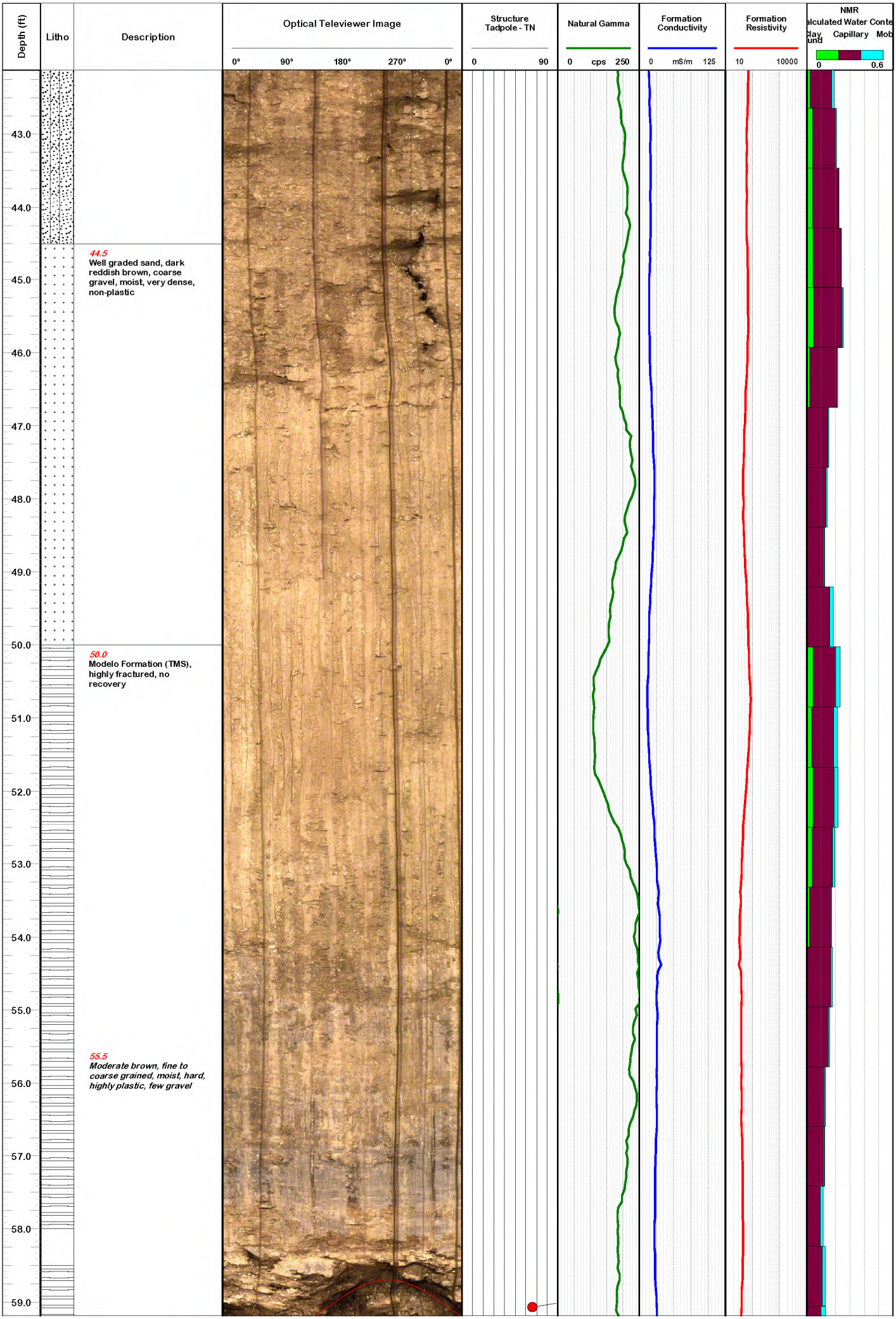
Depth (ft)
Litho
Description
Optical Televiewer Image
0°
90°
180°
270°
0°
Structure
Tadpole - TN
0
90
Natural Gamma
0
cps
250
Formation
Conductivity
0
mS/m
125
Formation
Resistivity
10
10000
NMR
Capillary
Mob
0
0.6
44.5
Well graded sand, dark reddish brown, coarse gravel, moist, very dense, non-plastic
50.0
Modelo Formation (TMS), highly fractured, no recovery
55.5
Moderate brown, fine to coarse grained, moist, hard, highly plastic, few gravel
43.0
44.0
45.0
46.0
47.0
48.0
49.0
50.0
51.0
52.0
53.0
54.0
55.0
56.0
57.0
58.0
59.0

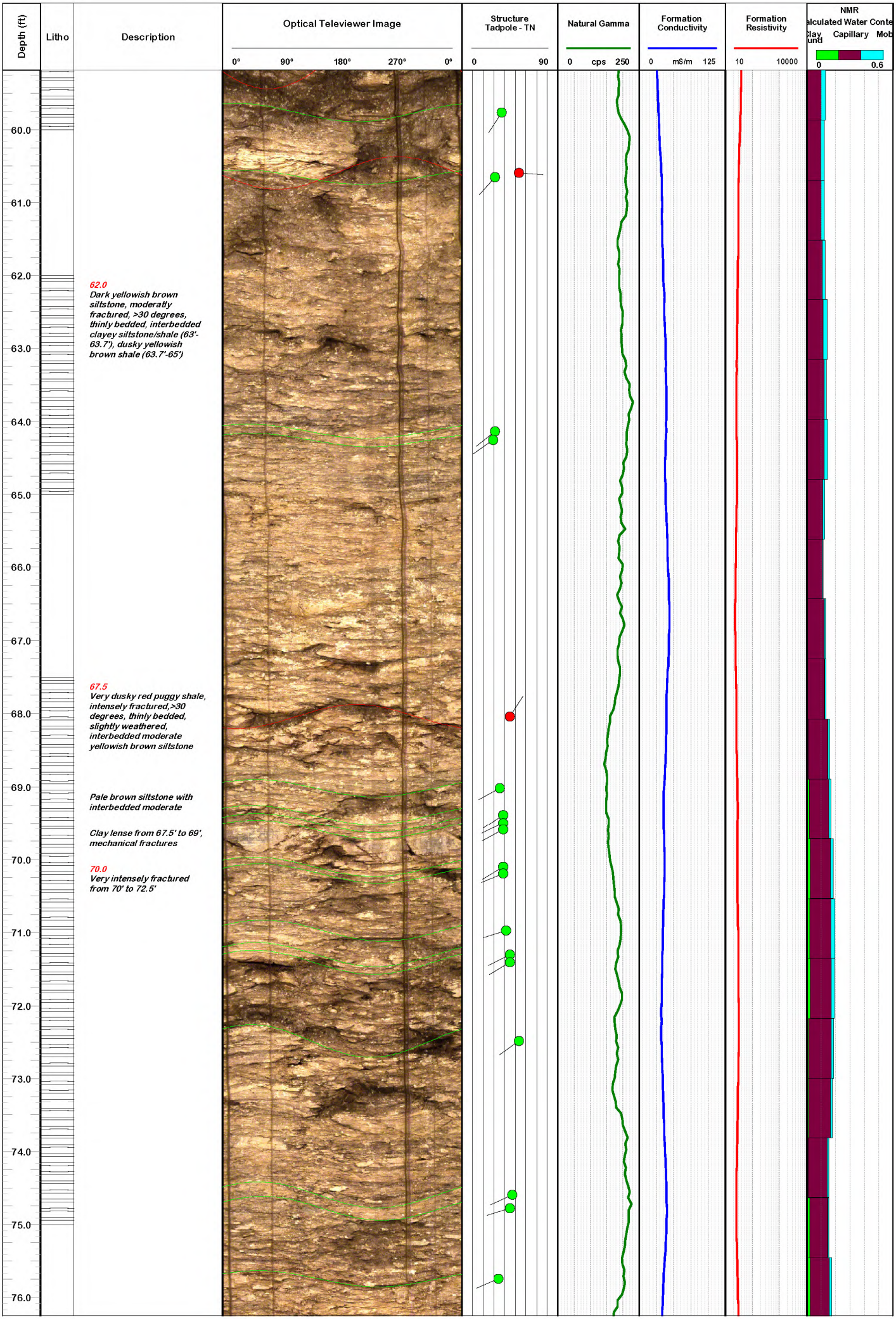
Depth (ft)
Litho
Description
Optical Televiewer Image
0°
90°
180°
270°
0°
Structure
Tadpole - TN
0
90
Natural Gamma
0
cps
250
Formation
Conductivity
0
mS/m
125
Formation
Resistivity
10
10000
NMR
Capillary
Mob
0
0.6
60.0
61.0
62.0
63.0
64.0
65.0
66.0
67.0
68.0
69.0
70.0
71.0
72.0
73.0
74.0
75.0
76.0
62.0
Dark yellowish brown siltstone, moderatly fractured, >30 degrees, thinly bedded, interbedded clayey siltstone/shale (63'-63.7'), dusky yellowish brown shale (63.7'-65')
67.5
Very dusky red puggy shale, intensely fractured,>30 degrees, thinly bedded, slightly weathered, interbedded moderate yellowish brown siltstone
Pale brown siltstone with interbedded moderate
Clay lense from 67.5' to 69', mechanical fractures
70.0
Very intensely fractured from 70' to 72.5'

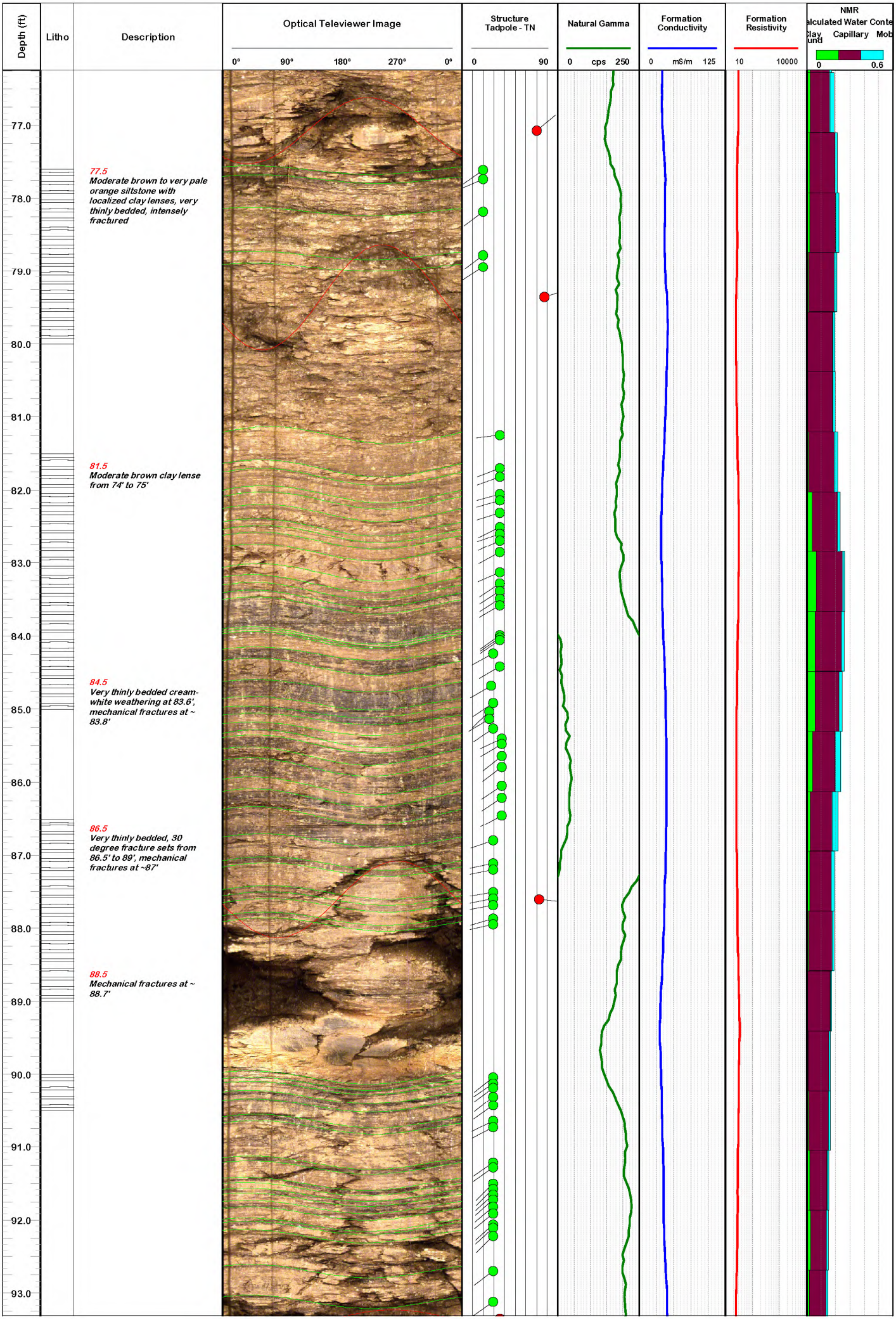
Depth (ft)
Litho
Description
Optical Televiewer Image
0°
90°
180°
270°
0°
Structure
Tadpole - TN
0
90
Natural Gamma
0
cps
250
Formation
Conductivity
0
mS/m
125
Formation
Resistivity
10
10000
NMR
Capillary
Mob
0
0.6
77.0
78.0
79.0
80.0
81.0
82.0
83.0
84.0
85.0
86.0
87.0
88.0
89.0
90.0
91.0
92.0
93.0
77.5
Moderate brown to very pale orange siltstone with localized clay lenses, very thinly bedded, intensely fractured
81.5
Moderate brown clay lense from 74' to 75'
84.5
Very thinly bedded cream-white weathering at 83.6', mechanical fractures at ~ 83.8'
86.5
Very thinly bedded, 30 degree fracture sets from 86.5' to 89', mechanical fractures at ~87'
88.5
Mechanical fractures at ~ 88.7'

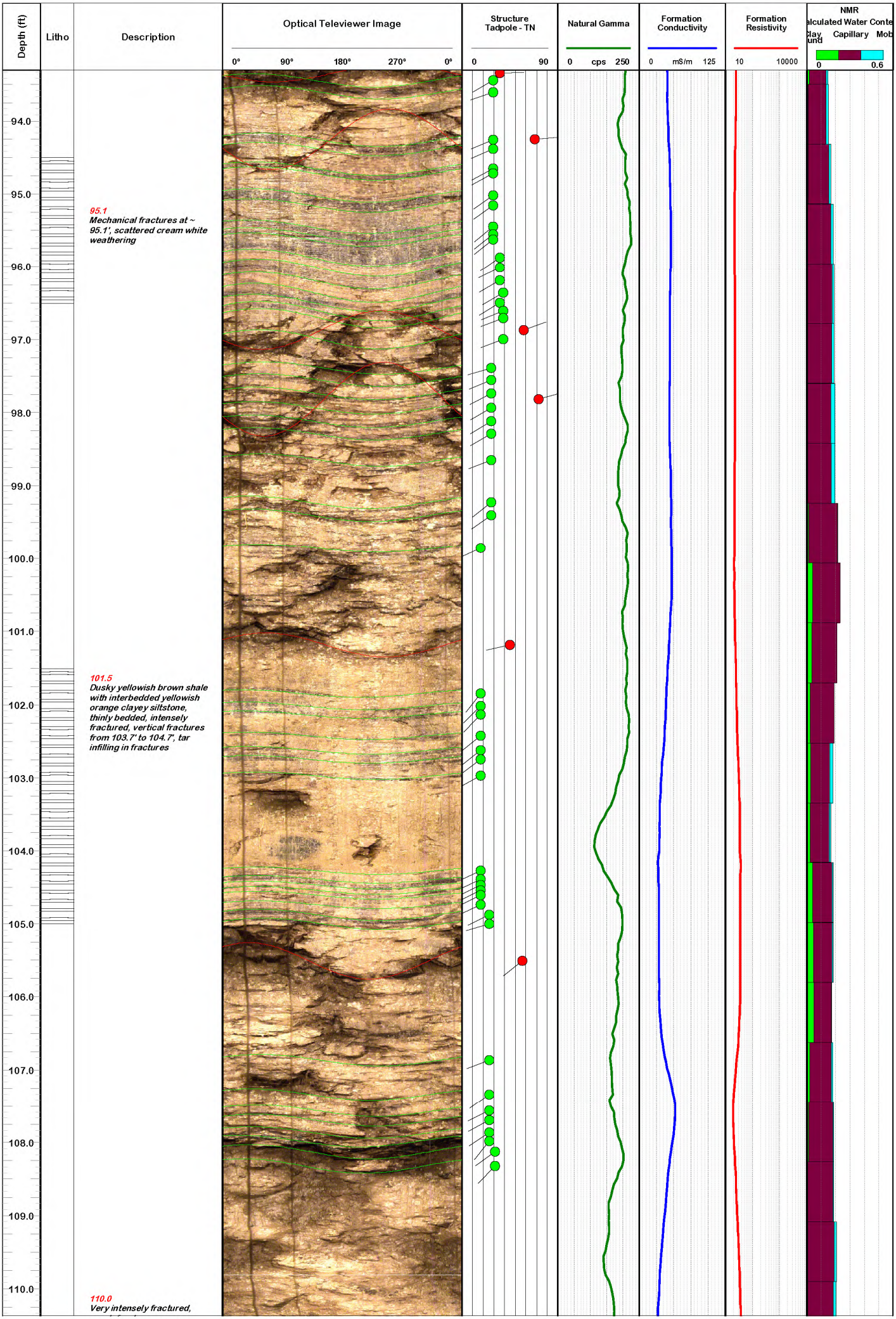
Depth (ft)
Litho
Description
Optical Televiewer Image
0°
90°
180°
270°
0°
Structure
Tadpole - TN
0
90
Natural Gamma
0
cps
250
Formation
Conductivity
0
mS/m
125
Formation
Resistivity
10
10000
NMR
Capillary
Mob
0
0.6
94.0
95.0
96.0
97.0
98.0
99.0
100.0
101.0
102.0
103.0
104.0
105.0
106.0
107.0
108.0
109.0
110.0
95.1
Mechanical fractures at ~ 95.1', scattered cream white weathering
101.5
Dusky yellowish brown shale with interbedded yellowish orange clayey siltstone, thinly bedded, intensely fractured, vertical fractures from 103.7' to 104.7', tar infilling in fractures
110.0
Very intensely fractured,

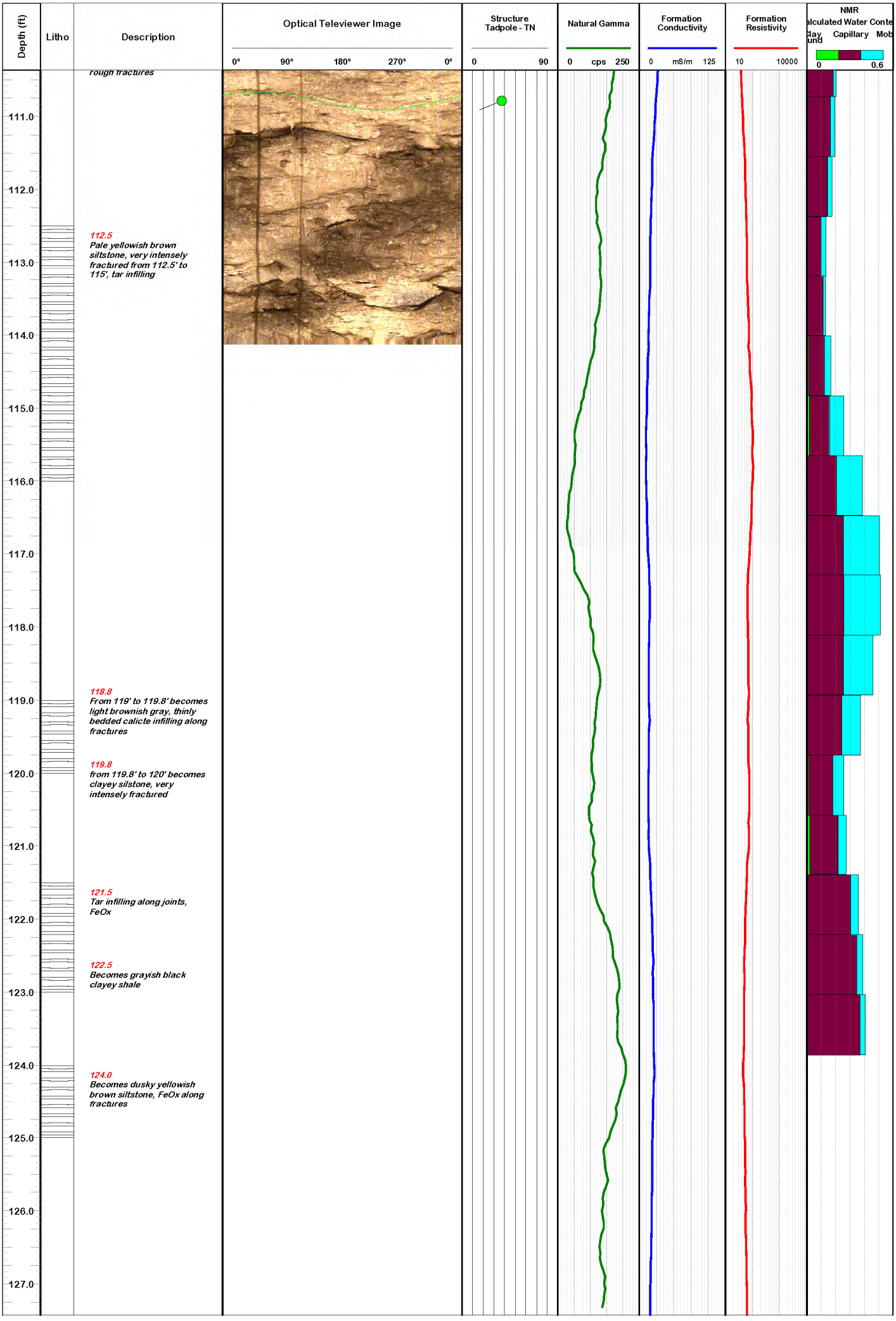
Depth (ft)
Litho
Description
Optical Televiewer Image
0° 90° 180° 270° 0°
Structure
Tadpole - TN
0 90
Natural Gamma
0 cps 250
Formation
Conductivity
0 mS/m 125
Formation
Resistivity
10 10000
NMR
Capillary Mob
0 0.6
rough fractures
112.5
Pale yellowish brown siltstone, very intensely fractured from 112.5' to 115', tar infilling
118.8
From 119' to 119.8' becomes light brownish gray, thinly bedded calicte infilling along fractures
119.8
from 119.8' to 120' becomes clayey silstone, very intensely fractured
121.5
Tar infilling along joints, FeOx
122.5
Becomes grayish black clayey shale
124.0
Becomes dusky yellowish brown siltstone, FeOx along fractures
111.0
112.0
113.0
114.0
115.0
116.0
117.0
118.0
119.0
120.0
121.0
122.0
123.0
124.0
125.0
126.0
127.0

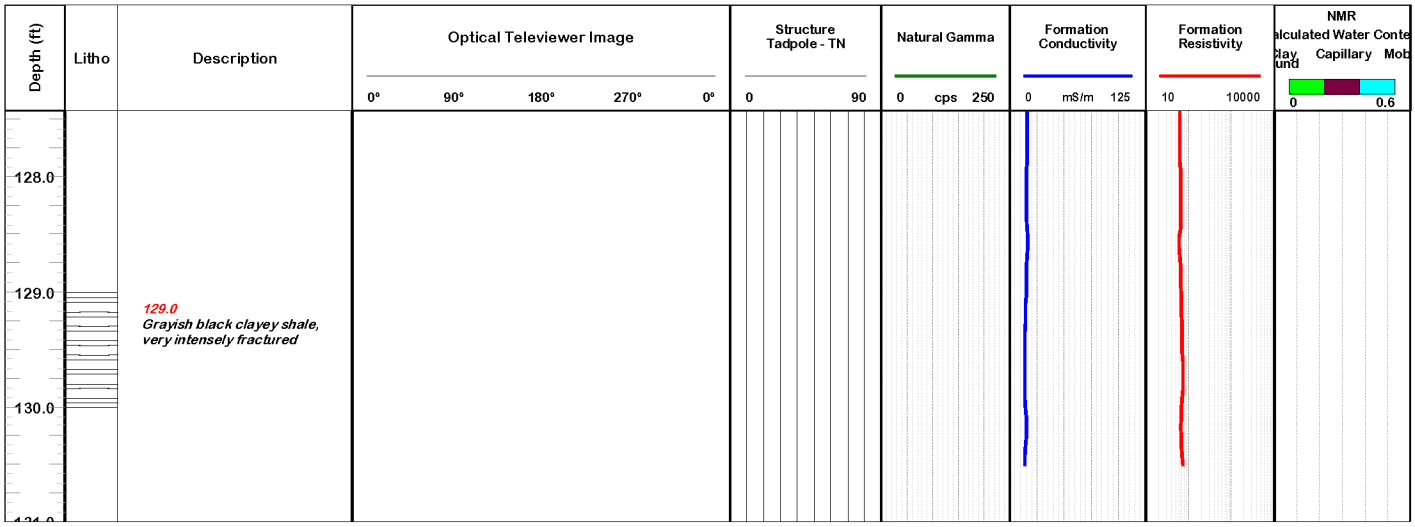
Depth (ft)
Litho
Description
Optical Televiewer Image
0°
90°
180°
270°
0°
Structure
Tadpole - TN
0
90
Natural Gamma
0
cps
250
Formation
Conductivity
0
mS/m
125
Formation
Resistivity
10
10000
NMR
Capillary
Mob
0
0.6
128.0
129.0
130.0
129.0
Grayish black clayey shale,
very intensely fractured

Advisian
WorleyParsons Group

Project Name: Aliso Canyon SS-25 Geophysical Surveys			**Borehole: BH4**
Project #: 407074-00748	Drilling Company: Cascade Drilling	Casing Diameter: ..	Location: SS-25
Client: SoCal Gas	Drilling Method: HSA (8" Auger), Rig: CME84	Casing Depth: ..	Latitude: 34.31526271
Logs: Optical Televiewer	Depth driller: 150 ft	Coring Diameter: 3.75 inches	Longitude: -118.56412372
Date: 2016-09-23	Depth logger: 29.64 mbgs (97.2')	Coring Depths: 102.5 feet	Elevation: 2914.74 ft
Location (LLD): SS-25	Stick Up: n/a	Drilling Diameter: 7.5 inches to 70 feet	Notes: Optical Televiewer OBI40 (064905), Natural Gamma 2PGA (2425), Inductive Conductivity 2PIA (6051), Temperature 2PFA () Magnetic Declination: 12.239 E
Logged by: R. Shinduke	Fluid Type: n/a	Console Type, Serial #: 2510/0630	
Depths Relative to: Ground Level	Fluid Level: n/a	Probe(s) Model, Serial #:	

This drawing is prepared solely for the use of our customer as specified in the accompanying report. WorleyParsons Canada Services Ltd. assumes no liability to any other party for any representations contained in this drawing."

Lithology Legend

- Silty sands, sand-silt mixtures
- No recovery
- Modelo Formation

Structural Legend

- Closed Joint
- Bedding

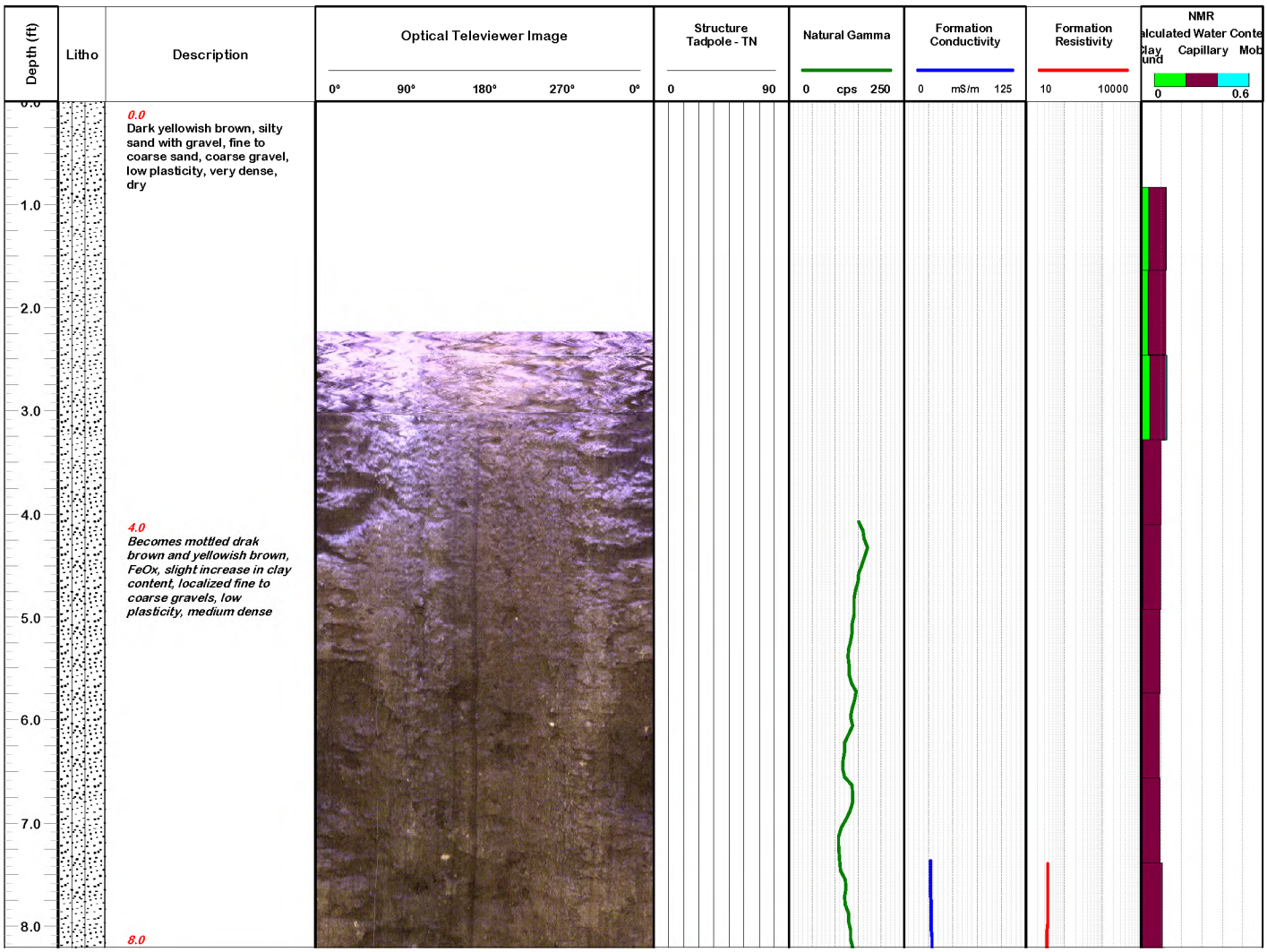

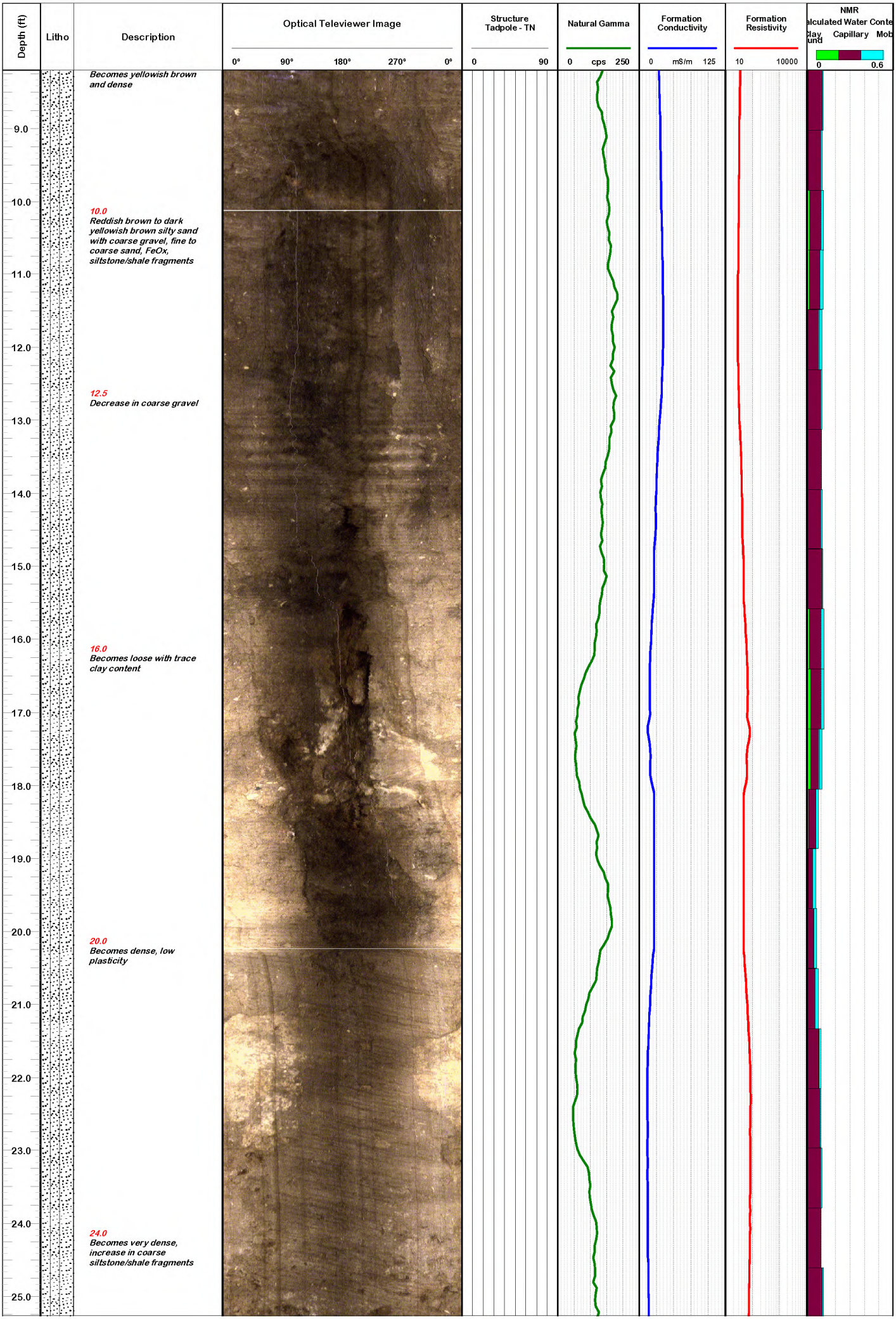
Depth (ft)
Litho
Description
Optical Televiewer Image
0°
90°
180°
270°
0°
Structure
Tadpole - TN
0
90
Natural Gamma
0
cps
250
Formation
Conductivity
0
mS/m
125
Formation
Resistivity
10
10000
NMR
Capillary
Mob
0
0.6
Becomes yellowish brown and dense
9.0
10.0
10.0
Reddish brown to dark yellowish brown silty sand with coarse gravel, fine to coarse sand, FeOx, siltstone/shale fragments
11.0
12.0
12.5
Decrease in coarse gravel
13.0
14.0
15.0
16.0
16.0
Becomes loose with trace clay content
17.0
18.0
19.0
20.0
20.0
Becomes dense, low plasticity
21.0
22.0
23.0
24.0
24.0
Becomes very dense, increase in coarse siltstone/shale fragments
25.0

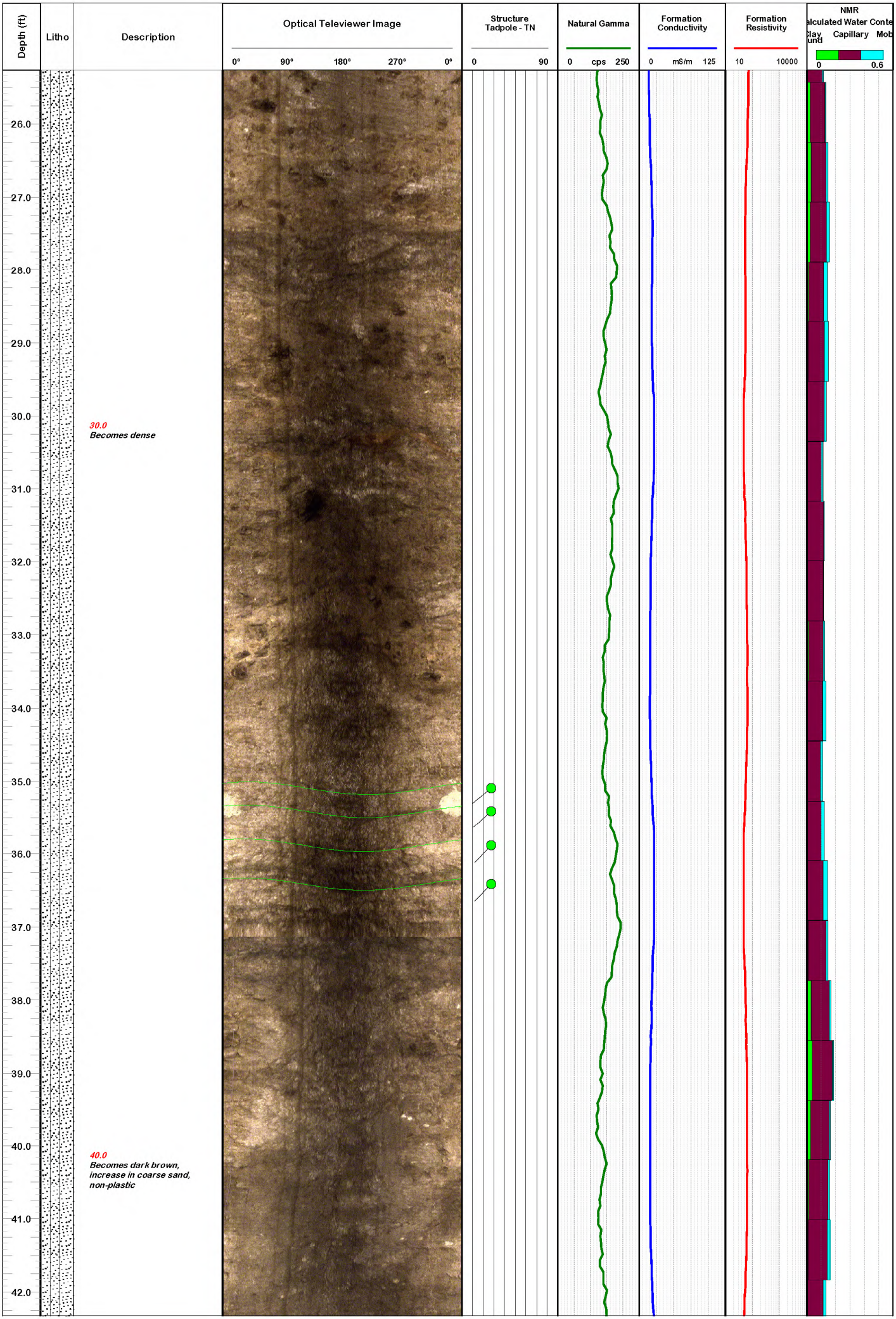
Depth (ft)
Litho
Description
Optical Televiewer Image
0°
90°
180°
270°
0°
Structure
Tadpole - TN
0
90
Natural Gamma
0
cps
250
Formation
Conductivity
0
mS/m
125
Formation
Resistivity
10
10000
NMR
Capillary
Mob
0
0.6
26.0
27.0
28.0
29.0
30.0
31.0
32.0
33.0
34.0
35.0
36.0
37.0
38.0
39.0
40.0
41.0
42.0
30.0
Becomes dense
40.0
Becomes dark brown,
increase in coarse sand,
non-plastic

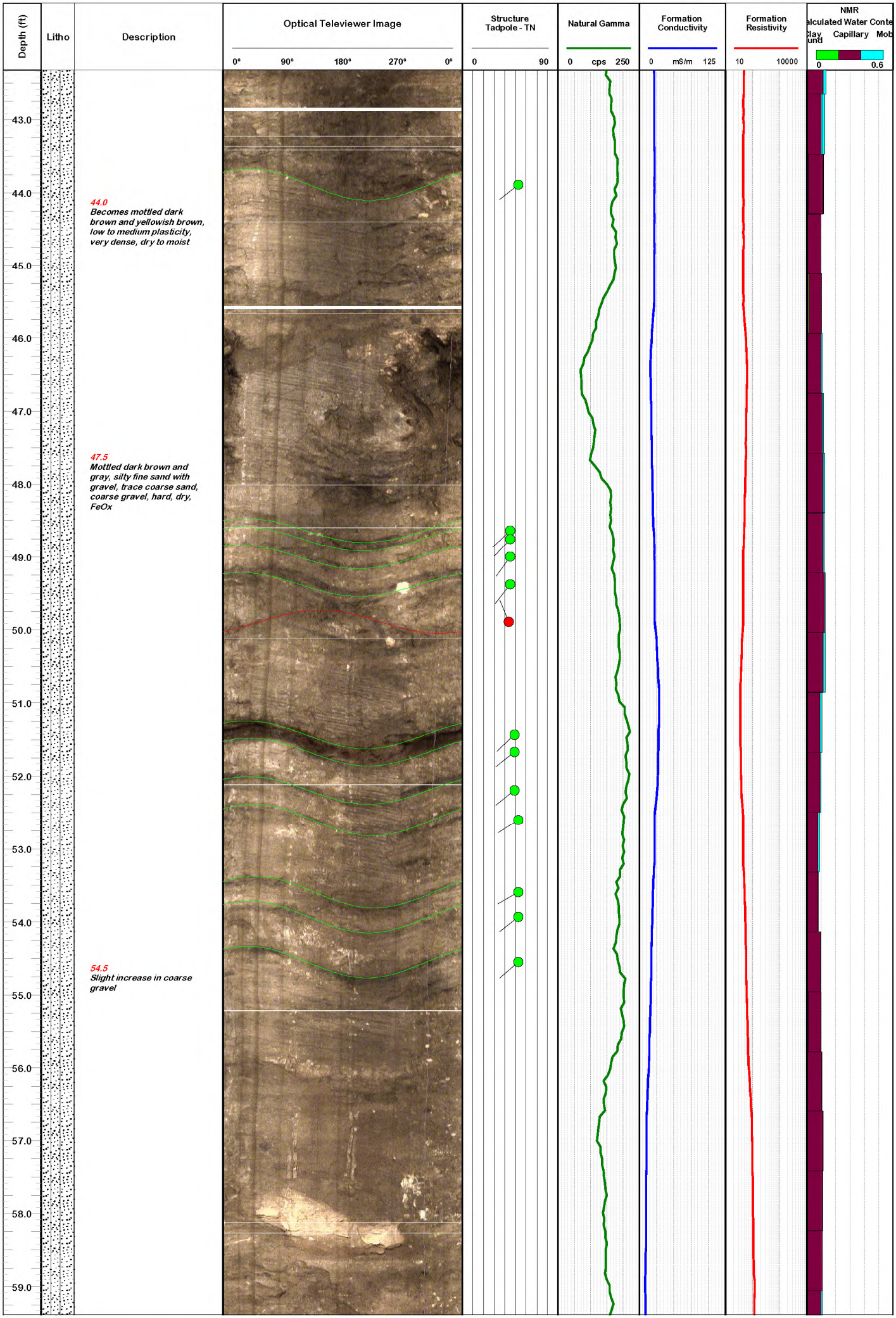
Depth (ft)
Litho
Description
Optical Televiewer Image
0° 90° 180° 270° 0°
Structure
Tadpole - TN
0 90
Natural Gamma
0 cps 250
Formation
Conductivity
0 mS/m 125
Formation
Resistivity
10 10000
NMR
Capillary
Mob
0 0.6
43.0
44.0
45.0
46.0
47.0
48.0
49.0
50.0
51.0
52.0
53.0
54.0
55.0
56.0
57.0
58.0
59.0
44.0
Becomes mottled dark brown and yellowish brown, low to medium plasticity, very dense, dry to moist
47.5
Mottled dark brown and gray, silty fine sand with gravel, trace coarse sand, coarse gravel, hard, dry, FeOx
54.5
Slight increase in coarse gravel

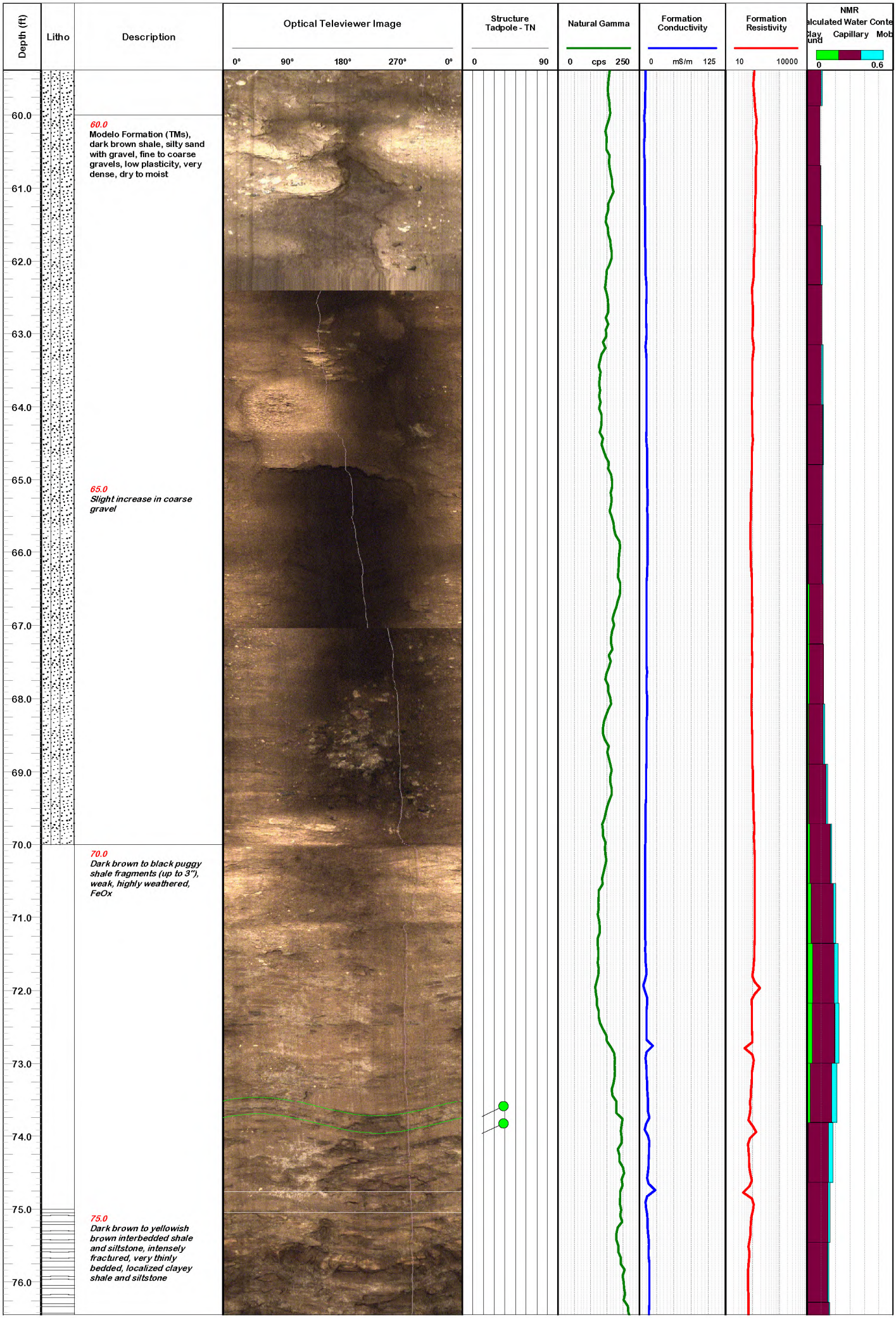
Depth (ft)
Litho
Description
Optical Televiewer Image
0°
90°
180°
270°
0°
Structure
Tadpole - TN
0
90
Natural Gamma
0
cps
250
Formation
Conductivity
0
mS/m
125
Formation
Resistivity
10
10000
NMR
Capillary
Mob
0
0.6
60.0
Modelo Formation (TMs), dark brown shale, silty sand with gravel, fine to coarse gravels, low plasticity, very dense, dry to moist
65.0
Slight increase in coarse gravel
70.0
Dark brown to black puggy shale fragments (up to 3"), weak, highly weathered, FeOx
75.0
Dark brown to yellowish brown interbedded shale and siltstone, intensely fractured, very thinly bedded, localized clayey shale and siltstone
60.0
61.0
62.0
63.0
64.0
65.0
66.0
67.0
68.0
69.0
70.0
71.0
72.0
73.0
74.0
75.0
76.0

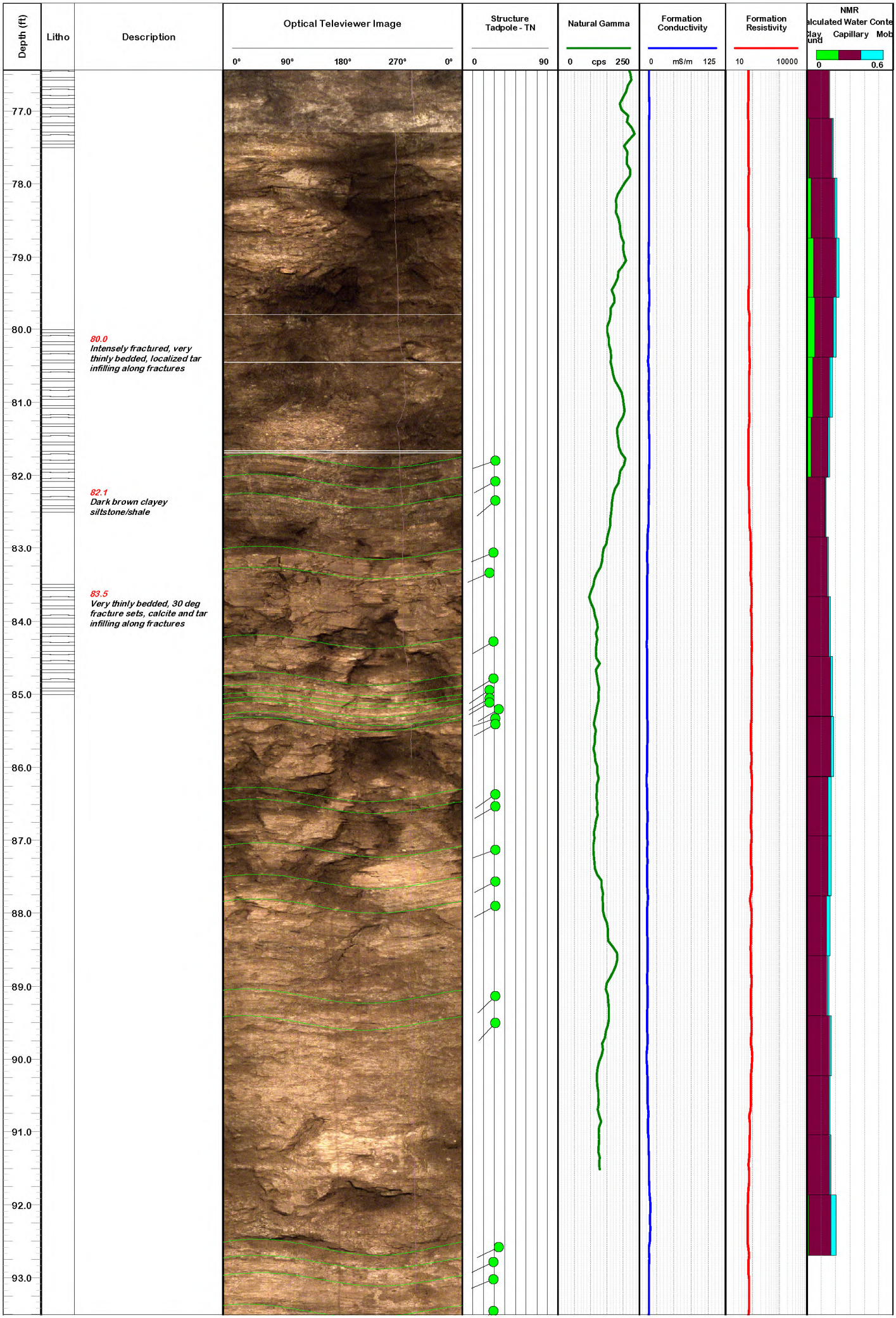
Depth (ft)
Litho
Description
Optical Televiewer Image
0°
90°
180°
270°
0°
Structure
Tadpole - TN
0
90
Natural Gamma
0
cps
250
Formation
Conductivity
0
mS/m
125
Formation
Resistivity
10
10000
NMR
Capillary
Mob
0
0.6
77.0
78.0
79.0
80.0
81.0
82.0
83.0
84.0
85.0
86.0
87.0
88.0
89.0
90.0
91.0
92.0
93.0
80.0
Intensely fractured, very thinly bedded, localized tar infilling along fractures
82.1
Dark brown clayey siltstone/shale
83.5
Very thinly bedded, 30 deg fracture sets, calcite and tar infilling along fractures

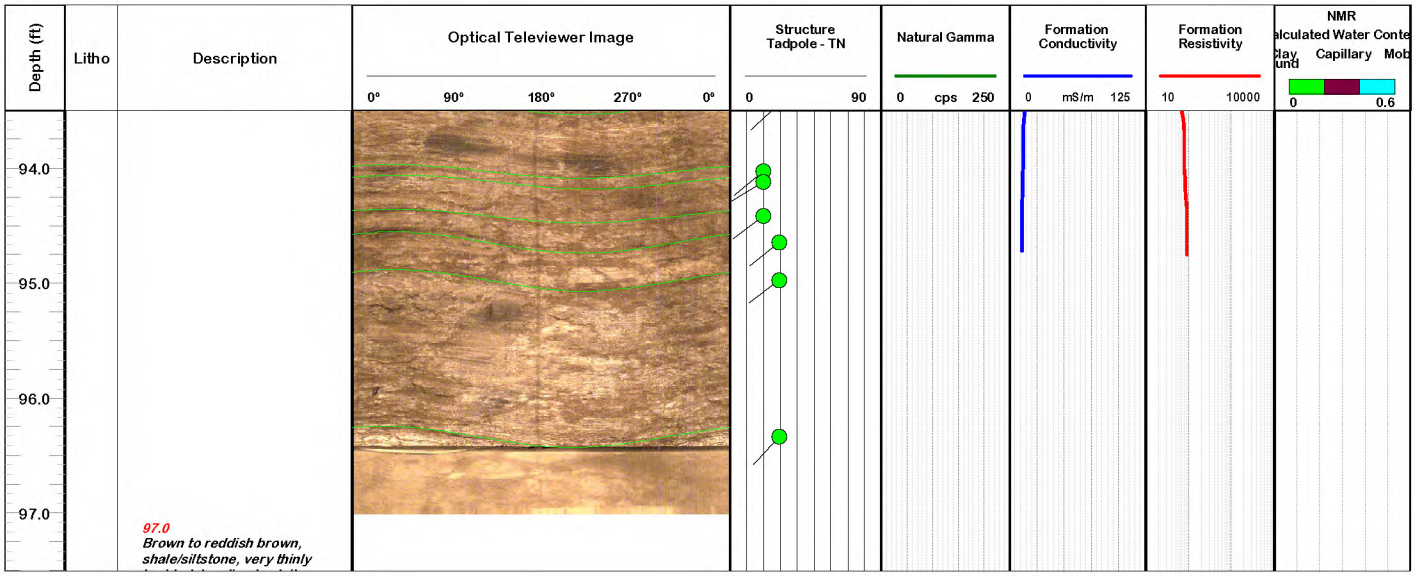
Depth (ft)
Litho
Description
Optical Televiewer Image
0°
90°
180°
270°
0°
Structure
Tadpole - TN
0
90
Natural Gamma
0
cps
250
Formation
Conductivity
0
mS/m
125
Formation
Resistivity
10
10000
NMR
Capillary
Mob
0
0.6
94.0
95.0
96.0
97.0
97.0
Brown to reddish brown,
shale/siltstone, very thinly

All Bedding Compilation: Dip

Limited Dataset:
Televiewer data are primarily from the BH-3 and BH-4 boreholes, which are partially representative of the four boreholes. Obstructions in the BH-1 and BH-2 boreholes did not permit complete logging of all of the boreholes, see chart.
Depths greater than 50' are extensively weathered and appear in sample retrieval as rubble (gravel). More competent rock with bedding planes are generally observed below 50'.

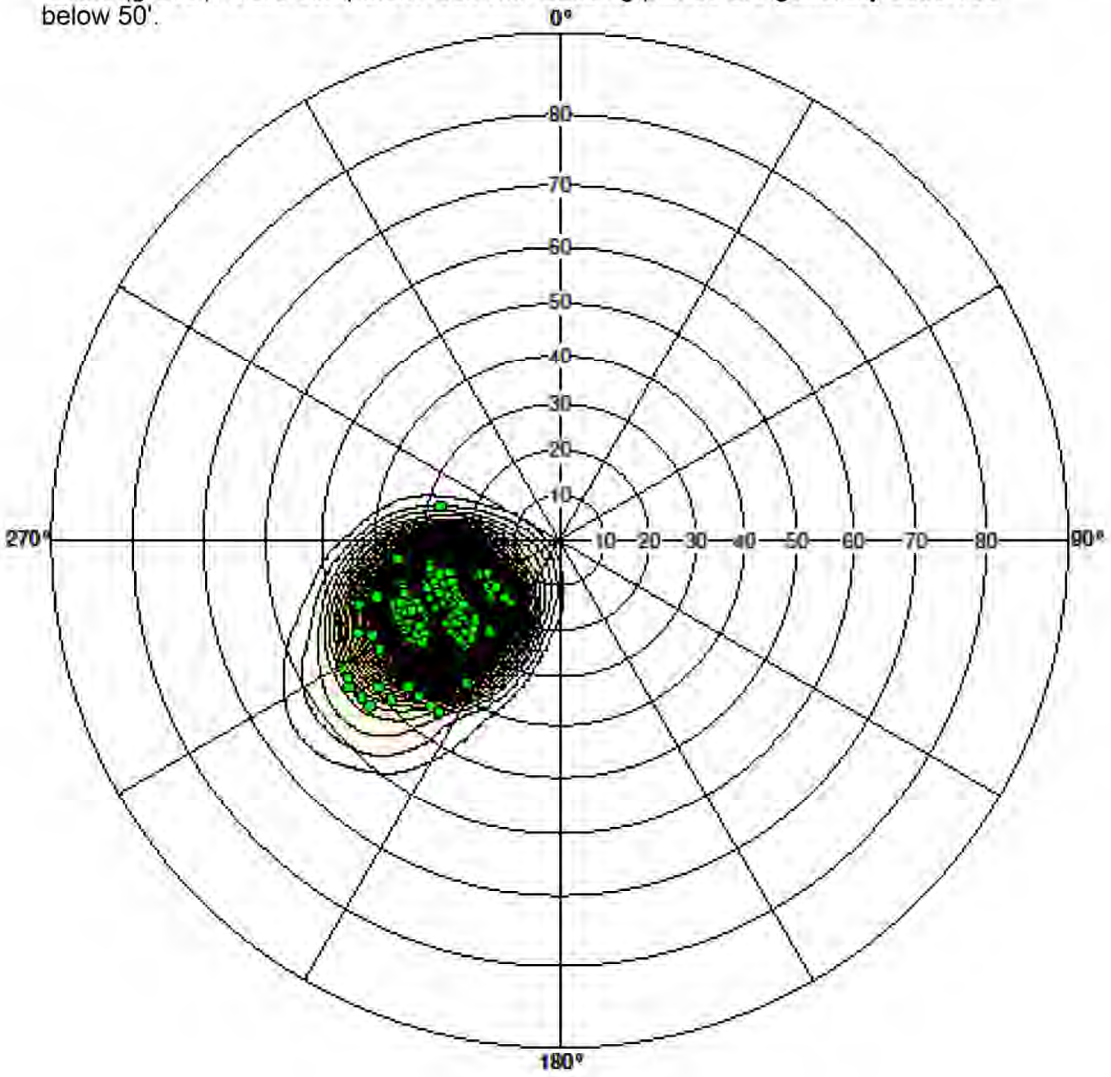

Plot: BH1 + BH2 + BH3 + BH4 (Bedding)

Attibute : Type

Symbol	Code - Description	Nb Points	Azi Mean	Dip Mean
◆	2 - Bedding / Banding / Foliation	185	238.91	30.98

Azimuths as a percent of total Log

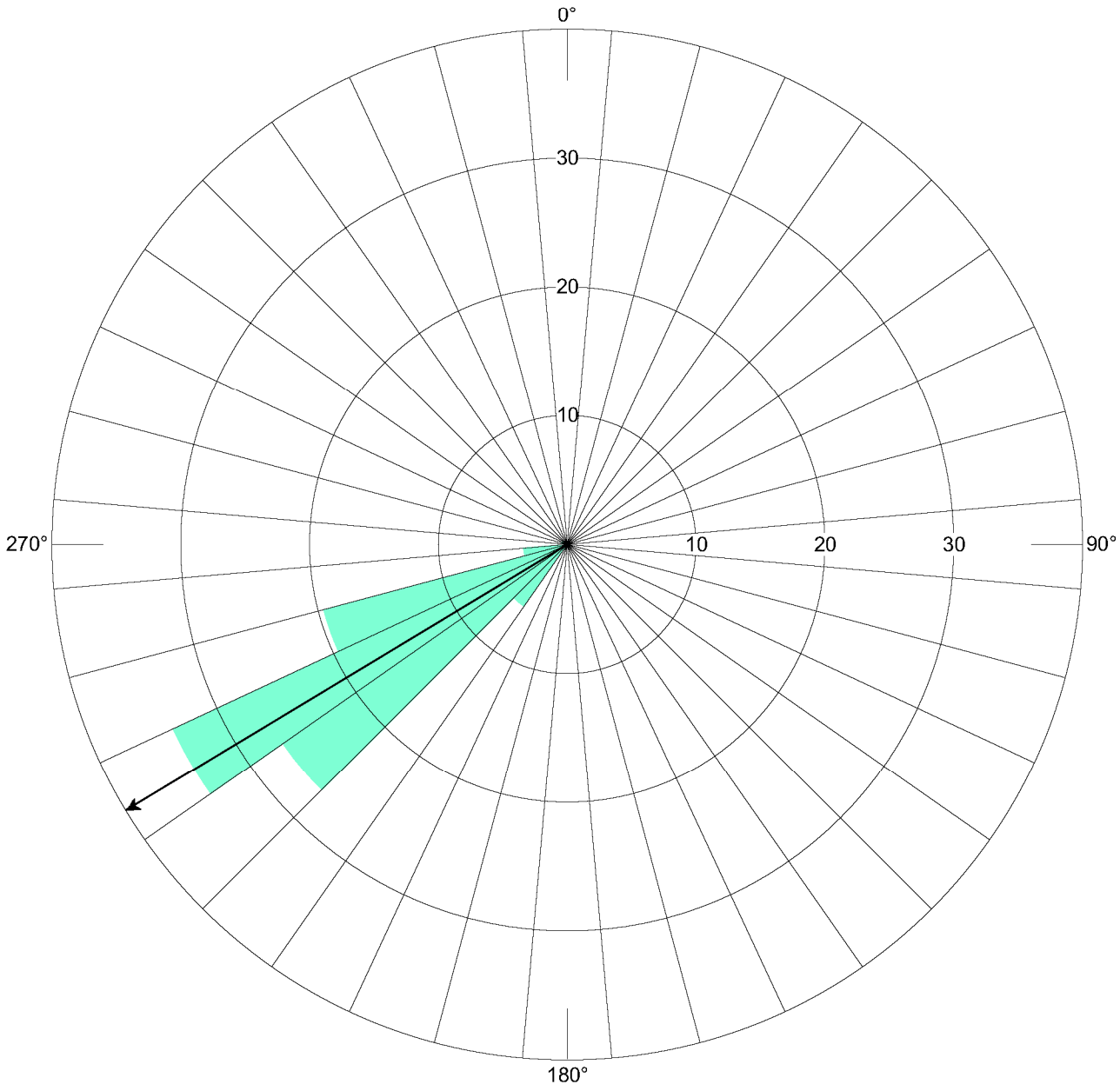

Plot: BH1 + BH2 + BH3 + BH4 (Bedding)

Name	Nb Points	Azi Mean	Dip Mean	Azi Min	Dip Min	Azi Max	Dip Max
All	185	238.91	30.98	212.97	17.74	285.97	53.67

BH 1-4 Joints / Fractures Compilation: Dip

Limited Dataset:

Televiewer data are primarily from the BH-3 and BH-4 boreholes, which are not wholly representative of the site due to sub vertical fractures found in the core description/photos.
Obstructions in the boreholes did not permit complete logging of all boreholes, see chart.
Extensively fractured intervals were described in Geosyntec core descriptions in all four boreholes.
A significant amount of subvertical fractures were observed in the core of BH-1, which was only logged to 30'.
Depths greater than 50' are extensively weathered and appear in sample retrieval as rubble (gravel).
Hence, BH-1 and BH-2 fractured zones are not represented in the plot below.

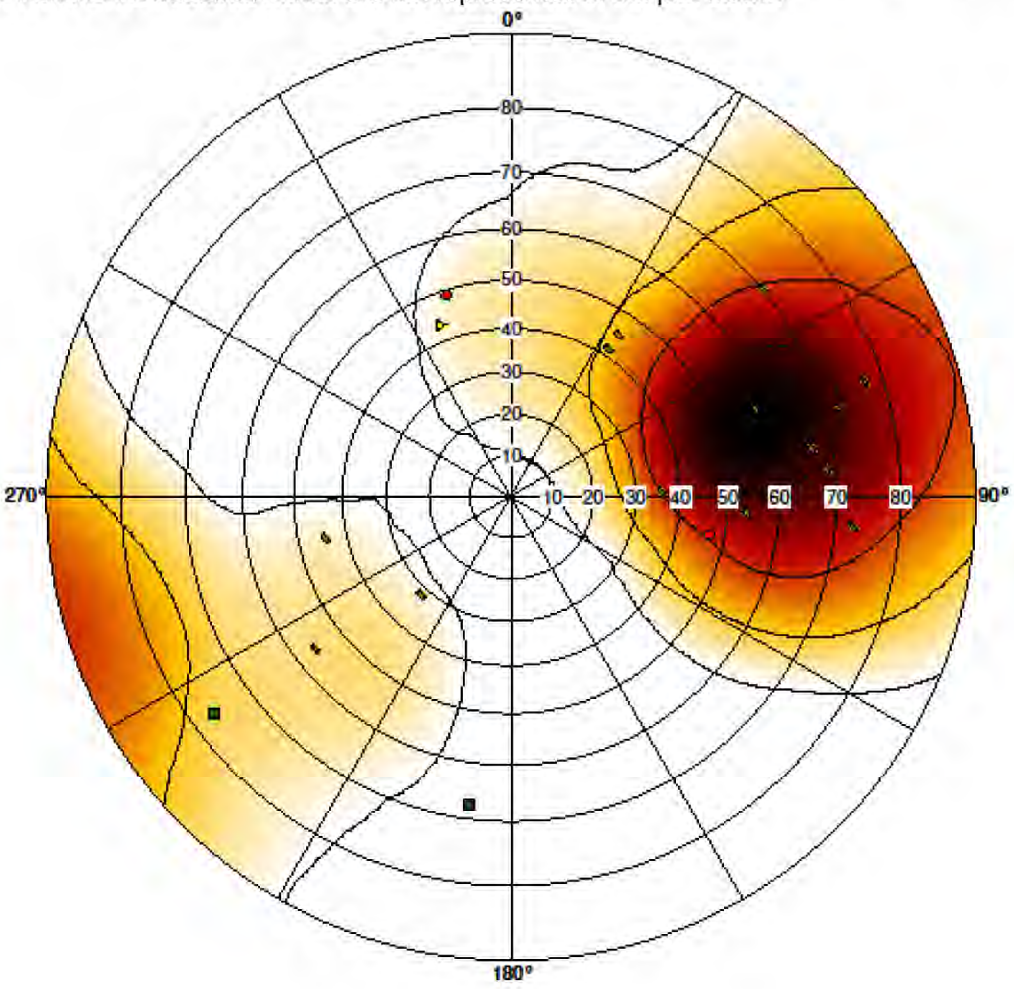

Wulff Plot (Dip) - UH - CAL_BH1-4
Plot: Structure - Tadpole - BH1-4
Depth: from 8.14 to 110.79 [ft]

Attribute : CAL_BH1-4

Symbol	Code - Description	Nb Points	Azi Mean	Dip Mean
●	#3 - BH1 - Joint / Fracture	2	40.00	29.69
■	#8 - BH2 - Joint / Fracture	2	211.42	70.84
◆	#10 - BH3 - Joint / Fracture	14	72.09	64.00
▷	#12 - BH4 - Joint / Fracture	1	337.64	43.83

All Structures Compilation: Dip

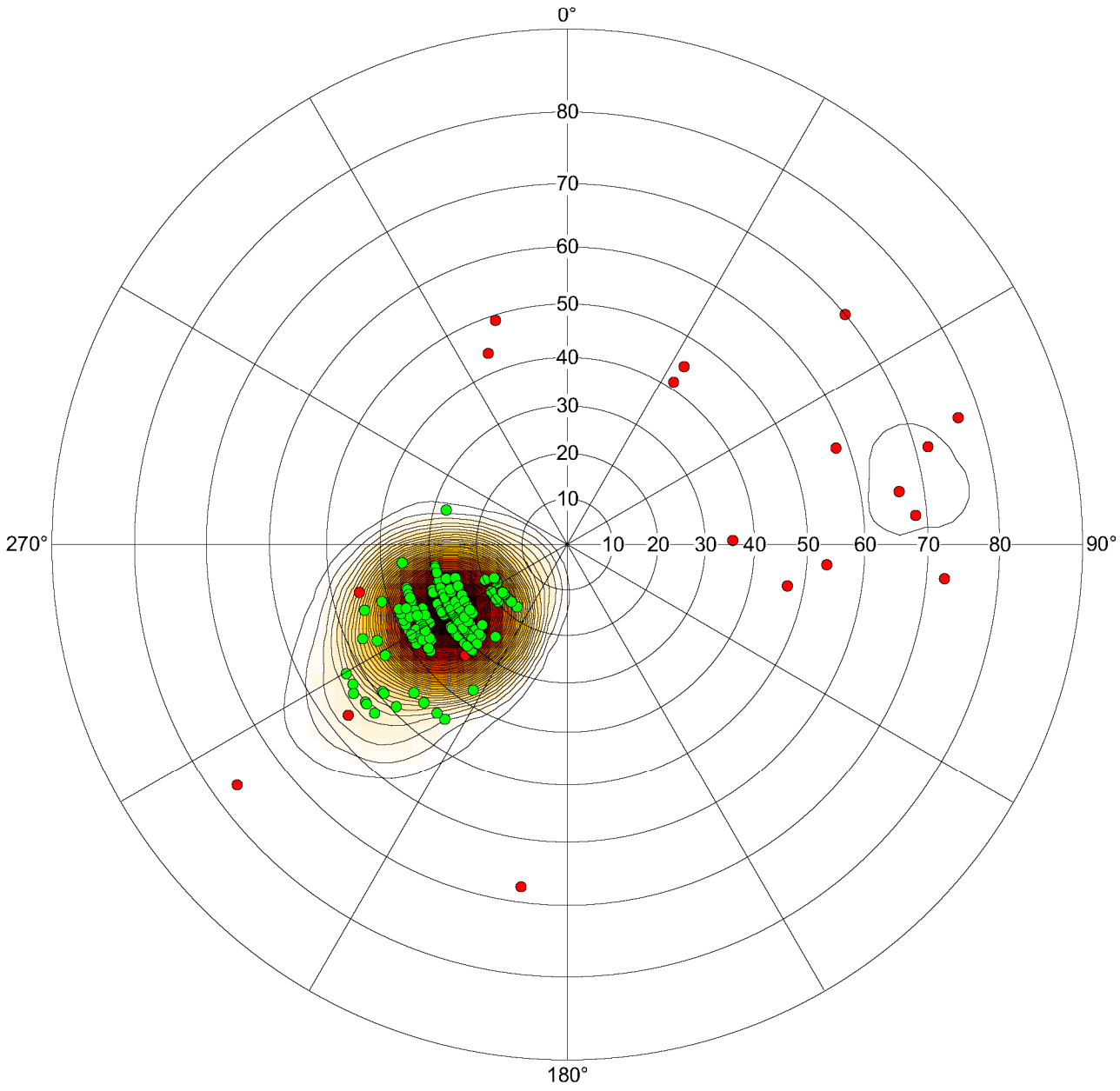

Plot: BH1 + BH2 + BH3 + BH4 (All Structures)

Attibute : Type

Symbol	Code - Description	Nb Points	Azi Mean	Dip Mean
	1 - Joint / Fracture	19	68.42	63.22
	2 - Bedding / Banding / Foliation	185	238.91	30.98

Appendix 4: ERT Conductivity Cross-Sections

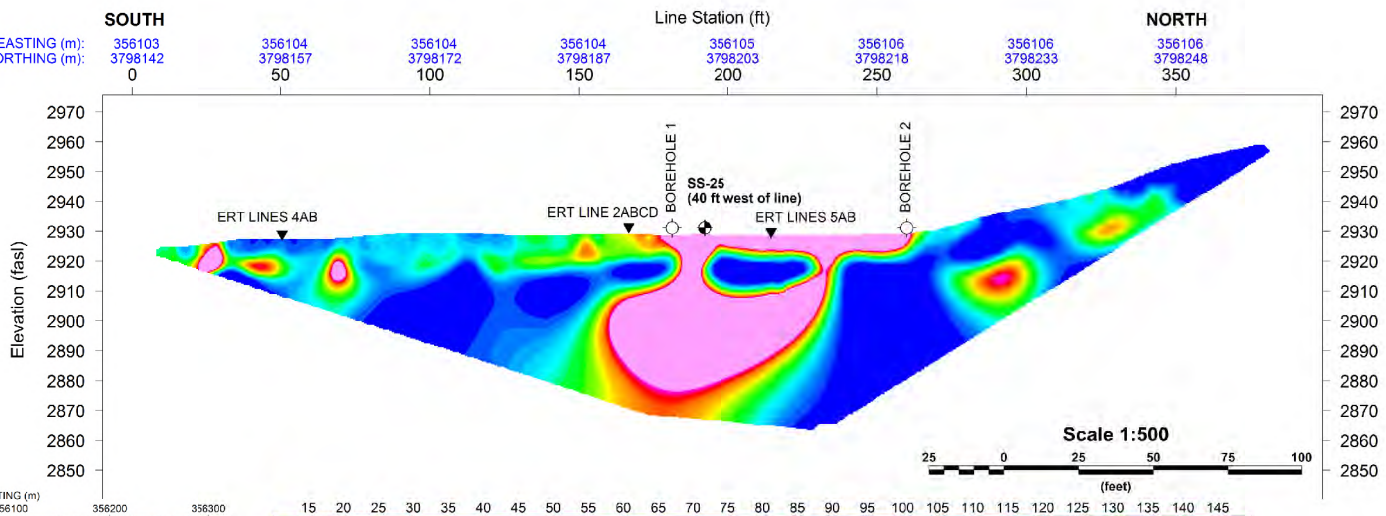

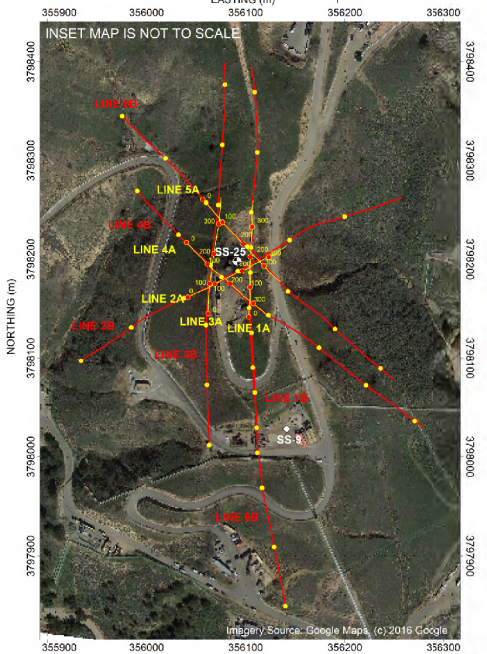

Legend

CROSS-SECTION

356103 UTM ZONE 11N
3798142 WGS 1983 (metres)

INSET MAP

4.92 feet (1.5 m) ERT Lines

16.4 feet (5 m) ERT Lines

FIELD PARAMETERS:
Date Collected: 15-AUG-2016
Electrode Configuration: GradientPlus Array
Minimum Electrode Spacing: 4.92 feet (1.5 m)

SOUTHERN CALIFORNIA GAS COMPANY
2016 GEOPHYSICAL INVESTIGATION
ALISO CANYON SS-25

LINE: ERT-1A (4.92 feet [1.5 M])
CONDUCTIVITY CROSS-SECTION

Date: 16 AUG 2016	Drawn by: MCAL	Edited by: EJE	Appd by: PB
		WorleyParsons Project No: 407074-00748	
		P/G No: APP4-1	REV: 0

OneWay
Advisian WorleyParsons Group

This drawing is prepared solely for the use of our customer as specified in the accompanying report.
Advisian, a division of WorleyParsons Canada Services Ltd., assumes no liability to any other party for any representations contained in this drawing.

FILE: U:\CAL\GBS\407074-00748\200 - Geophysical Investigation\10.0_Technical_Specialist\10.1_Geophysics\10.1.3_Oasis\Maps\407074-00748-GP-OAS-ERT1-A.map

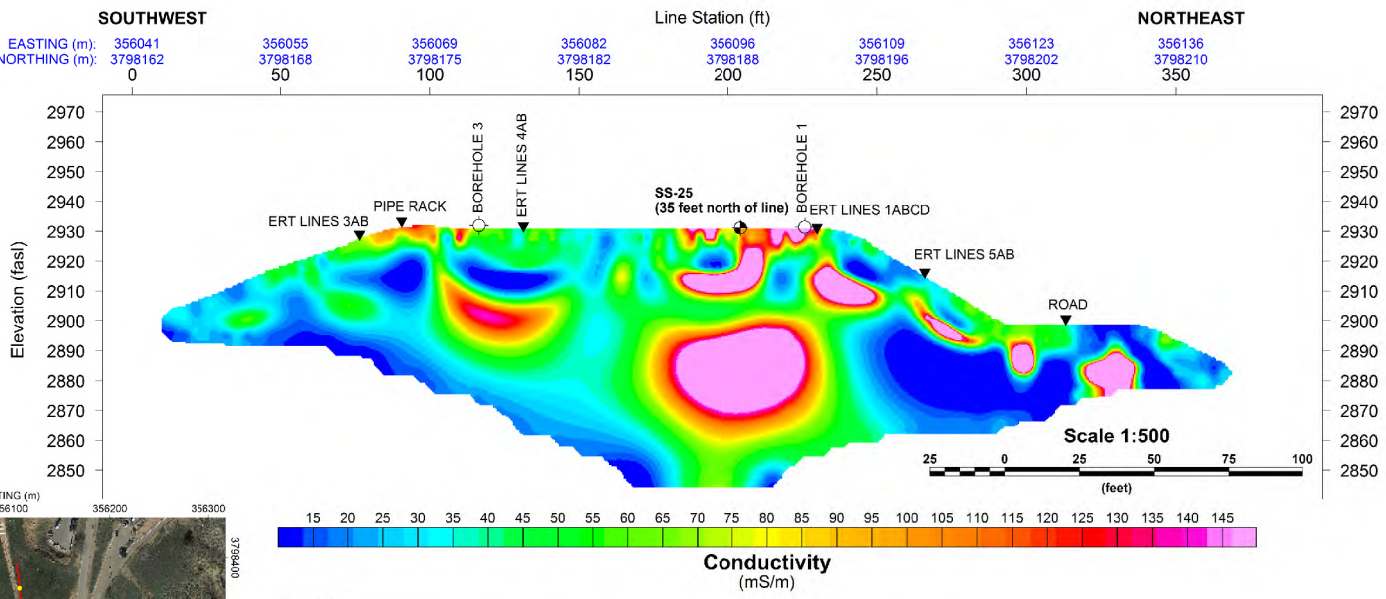

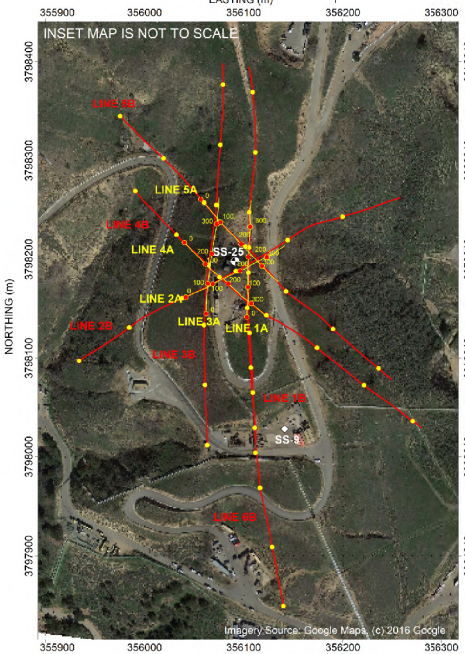

Legend

CROSS-SECTION

356103 UTM ZONE 11N
3798142 WGS 1983 (metres)

INSET MAP

4.92 feet (1.5 m) ERT Lines

16.4 feet (5 m) ERT Lines

FIELD PARAMETERS:
Date Collected: 24-AUG-2016
Electrode Configuration: GradientPlus Array
Minimum Electrode Spacing: 4.92 feet (1.5 m)

SOUTHERN CALIFORNIA GAS COMPANY
2016 GEOPHYSICAL INVESTIGATION
ALISO CANYON SS-25

LINE: ERT-2A (4.92 FEET [1.5 M])
CONDUCTIVITY CROSS-SECTION

OneWay to zero harm

Advisian WorleyParsons Group

Date	Drawn by	Edited by	Appr'd by
16 AUGUST 2016	MCAL	EJE	PB

WorleyParsons Project No: 407074-00748

FIG No: APP4-2

REV: 0

This drawing is prepared solely for the use of our customer as specified in the accompanying report. Advisian, a division of WorleyParsons Canada Services Ltd., assumes no liability to any other party for any representations contained in this drawing.

FILE: U:\CAL\GBS\407074-00748\200 - Geophysical Investigation\10.0_Technical_Specialist\10.1_Geophysics\10.1.3_Oasis\407074-00748-GP-OAS-ERT3-A.map

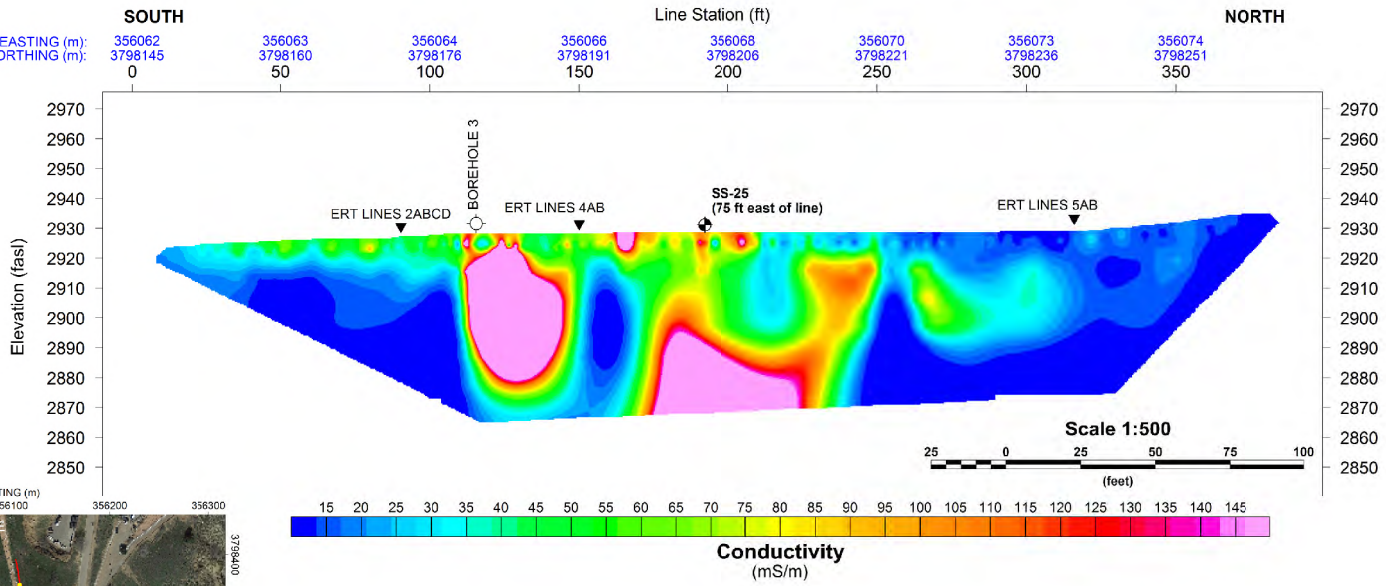

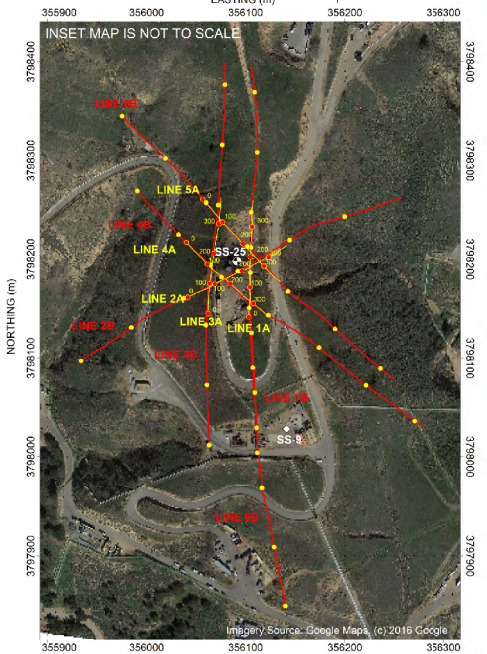

Legend

CROSS-SECTION

356103 UTM ZONE 11N
3798142 WGS 1983 (metres)

INSET MAP

4.92 feet (1.5 m) ERT Lines

16.4 feet (5 m) ERT Lines

FIELD PARAMETERS:
Date Collected: 15-AUG-2016
Electrode Configuration: GradientPlus Array
Minimum Electrode Spacing: 4.92 feet (1.5 m)

SOUTHERN CALIFORNIA GAS COMPANY
2016 GEOPHYSICAL INVESTIGATION
ALISO CANYON SS-25

LINE: ERT-3A (4.92 FEET [1.5 M])
CONDUCTIVITY CROSS-SECTION

Date: 16 AUG 2016	Drawn by: MCAL	Edited by: EJE	Appr'd by: PB
		WorleyParsons Project No: 407074-00748	
		FIG No: APP4-3	REV: 0

OneWay to zero harm

Advisian WorleyParsons Group

This drawing is prepared solely for the use of our customer as specified in the accompanying report. Advisian, a division of WorleyParsons Canada Services Ltd., assumes no liability to any other party for any representations contained in this drawing.

FILE: U:\CAL\GBS\407074-00748\200 - Geophysical Investigation\10.0_Technical_Specialist\10.1_Geophysics\10.1.3_Oasis\407074-00748-GP-OAS-ERT2-A.map

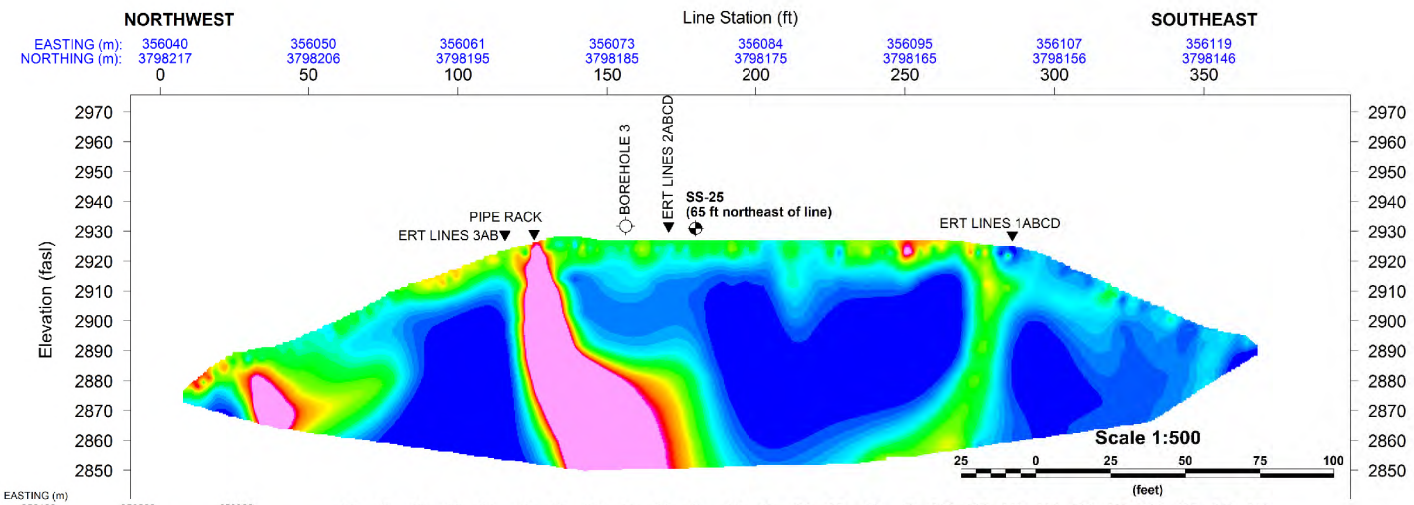

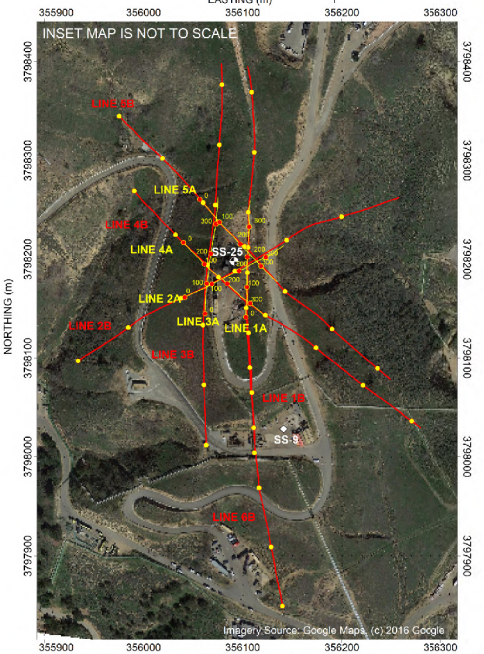

15 20 25 30 35 40 45 50 55 60 65 70 75 80 85 90 95 100 105 110 115 120 125 130 135 140 145

Conductivity
(mS/m)

Legend

CROSS-SECTION

356103 UTM ZONE 11N
3798142 WGS 1983 (metres)

INSET MAP

4.92 feet (1.5 m) ERT Lines

16.4 feet (5 m) ERT Lines

FIELD PARAMETERS:
Date Collected: 17-AUG-2016
Electrode Configuration: GradientPlus Array
Minimum Electrode Spacing: 4.92 feet (1.5 m)

SOUTHERN CALIFORNIA GAS COMPANY
2016 GEOPHYSICAL INVESTIGATION
ALISO CANYON SS-25

LINE: ERT-4A (16.4 FEET [1.5 M])
CONDUCTIVITY CROSS-SECTION

Date: 16 AUG 2016	Drawn by: MCAL	Edited by: EJE	Appd by: PB
		WorleyParsons Project No: 407074-00748	
		FIG No: APP4-4	REV: 0

OneWay to zero harm

Advisian WorleyParsons Group

This drawing is prepared solely for the use of our customer as specified in the accompanying report. Advisian, a division of WorleyParsons Canada Services Ltd., assumes no liability to any other party for any representations contained in this drawing.

FILE: U:\CAL\GBS\407074-00748\200 - Geophysical Investigation\10.0_Technical_Specialist\10.1_Geophysics\10.1.3_Oasis\407074-00748-GP-OAS-ERT4-A.map

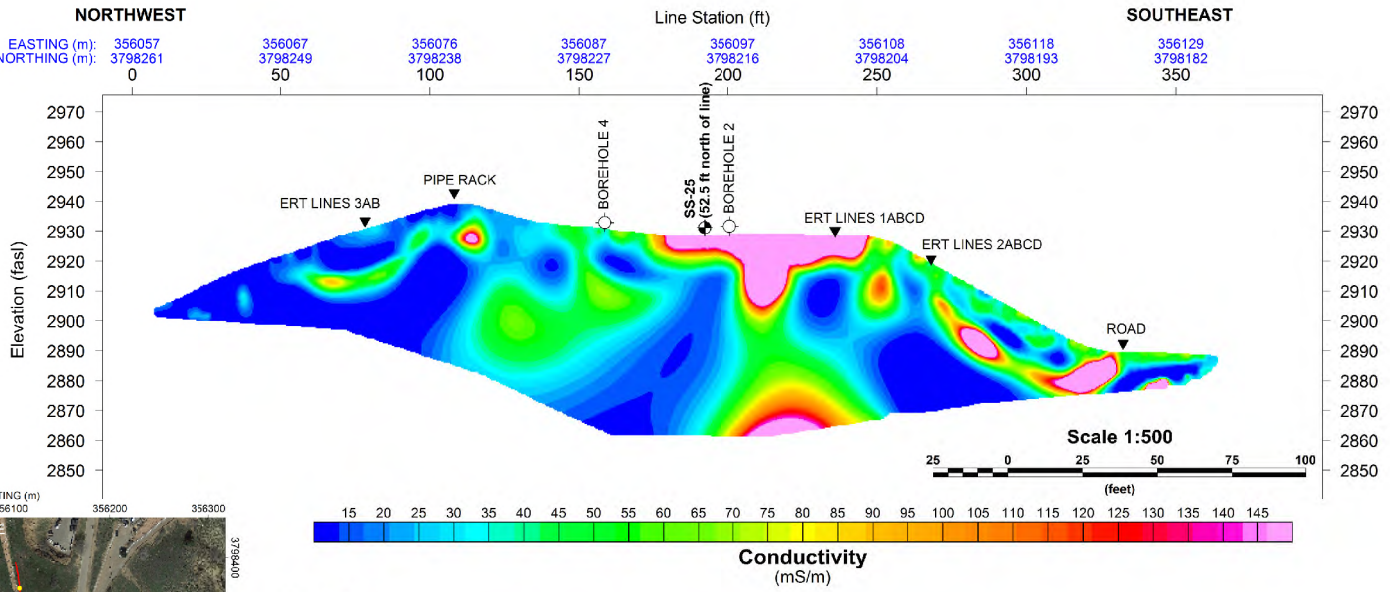

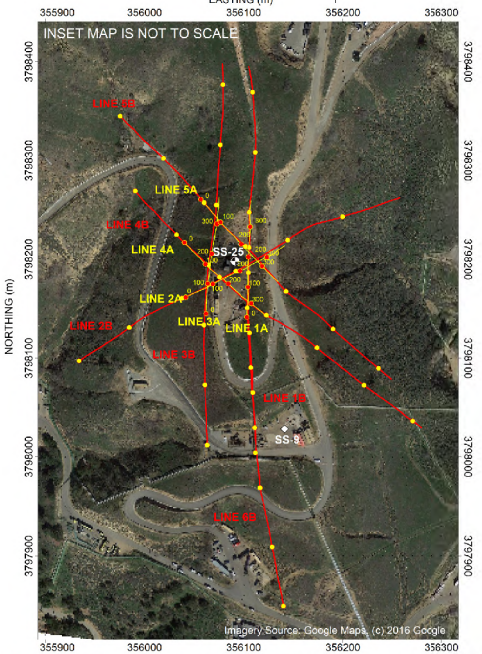

Legend

CROSS-SECTION

356103 UTM ZONE 11N
3798142 WGS 1983 (metres)

INSET MAP

4.92 feet (1.5 m) ERT Lines

16.4 feet (5 m) ERT Lines

FIELD PARAMETERS:
Date Collected: 24-AUG-2016
Electrode Configuration: GradientPlus Array
Minimum Electrode Spacing: 4.92 feet (1.5 m)

SOUTHERN CALIFORNIA GAS COMPANY
2016 GEOPHYSICAL INVESTIGATION
ALISO CANYON SS-25

LINE: ERT-5A (4.92 FEET [1.5 M])
CONDUCTIVITY CROSS-SECTION

Date: 25 AUG 2016	Drawn by: MCAL	Edited by: EJE	Appd by: PB
		WorleyParsons Project No: 407074-00748	
		FIG No: APP4-5	REV: 0

OneWay to zero harm
Advisian WorleyParsons Group

This drawing is prepared solely for the use of our customer as specified in the accompanying report. Advisian, a division of WorleyParsons Canada Services Ltd., assumes no liability to any other party for any representations contained in this drawing.

FILE: U:\CAL\GBS\407074-00748\200 - Geophysical Investigation\10.0_Technical_Specialist\10.1_Geophysics\10.1.3_Oasis\Maps\407074-00748-GP-OAS-ERT5A.map

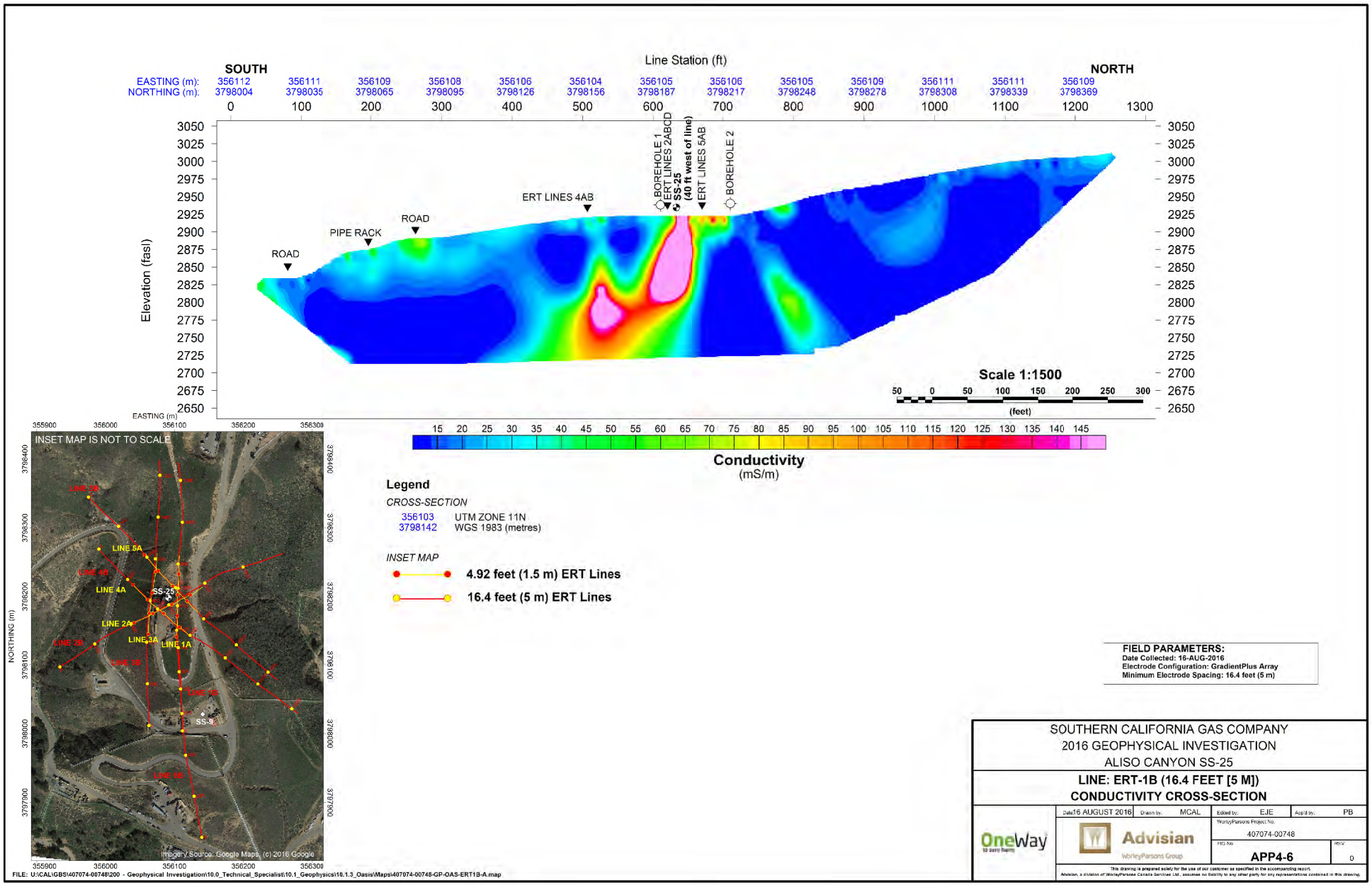
SOUTH
NORTH
Line Station (ft)
EASTING (m): 356112 356111 356109 356108 356106 356104 356105 356106 356105 356109 356111 356111 356109
NORTHING (m): 3798004 3798035 3798065 3798095 3798126 3798156 3798187 3798217 3798248 3798278 3798308 3798339 3798369
0 100 200 300 400 500 600 700 800 900 1000 1100 1200 1300
Elevation (fasl)
3050 3025 3000 2975 2950 2925 2900 2875 2850 2825 2800 2775 2750 2725 2700 2675 2650
ROAD
PIPE RACK
ROAD
ERT LINES 4AB
BOREHOLE 1
ERT LINES 2ABCD
SS-25
(40 ft west of line)
ERT LINES 5AB
BOREHOLE 2
Scale 1:1500
50 0 50 100 150 200 250 300
(feet)
EASTING (m)
355900 356000 356100 356200 356300
15 20 25 30 35 40 45 50 55 60 65 70 75 80 85 90 95 100 105 110 115 120 125 130 135 140 145
Conductivity
(mS/m)
INSET MAP IS NOT TO SCALE
LINE 3B
LINE 5A
LINE 4B
LINE 4A
SS-25
LINE 2A
LINE 2B
LINE 3A
LINE 1A
LINE 3B
LINE 1B
SS-9
LINE 5B
NORTHING (m)
3798400 3798300 3798200 3798100 3798000 3797900
Imagery Source: Google Maps, (c) 2016 Google
Legend
CROSS-SECTION
356103 UTM ZONE 11N
3798142 WGS 1983 (metres)
INSET MAP
4.92 feet (1.5 m) ERT Lines
16.4 feet (5 m) ERT Lines
FIELD PARAMETERS:
Date Collected: 16-AUG-2016
Electrode Configuration: GradientPlus Array
Minimum Electrode Spacing: 16.4 feet (5 m)
FILE: U:\CAL\GBS\407074-00748\200 - Geophysical Investigation\10.0_Technical_Specialist\10.1_Geophysics\10.1.3_Oasis\Maps\407074-00748-GP-OAS-ERT1B-A.map
SOUTHERN CALIFORNIA GAS COMPANY
2016 GEOPHYSICAL INVESTIGATION
ALISO CANYON SS-25
LINE: ERT-1B (16.4 FEET [5 M])
CONDUCTIVITY CROSS-SECTION
Date 16 AUGUST 2016
Drawn by: MCAL
Edited by: EJE
Appd by: PB
OneWay
Advisian
WorleyParsons Group
WorleyParsons Project No.
407074-00748
FIG No.
APP4-6
REV
0
This drawing is prepared solely for the use of our customer as specified in the accompanying report.
Advisian, a division of WorleyParsons Canada Services Ltd., assumes no liability to any other party for any representations contained in this drawing.

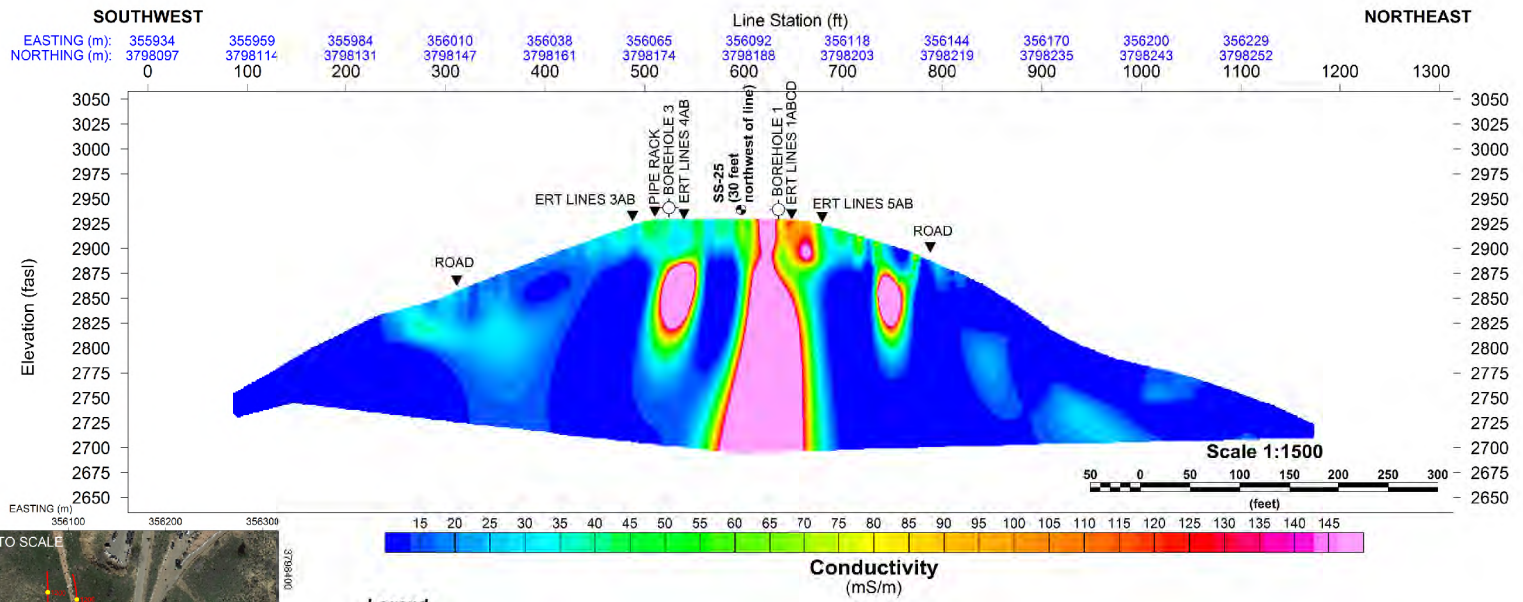

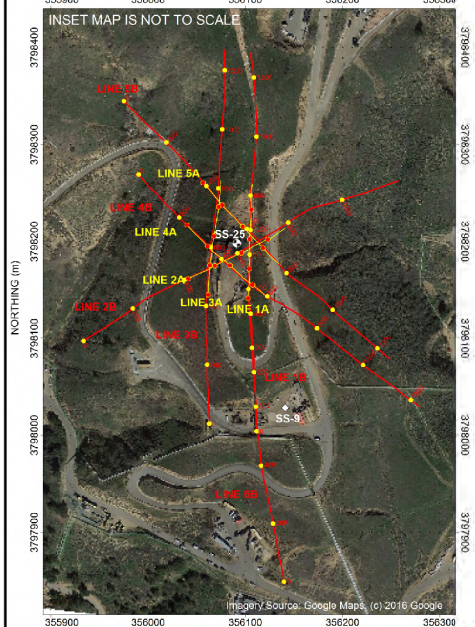

Legend

CROSS-SECTION

356103 UTM ZONE 11N
3798142 WGS 1983 (metres)

INSET MAP

4.92 feet (1.5 m) ERT Lines

16.4 feet (5 m) ERT Lines

FIELD PARAMETERS:
Date Collected: 24-AUG-2016
Electrode Configuration: GradientPlus Array
Minimum Electrode Spacing: 16.4 feet (5 m)

SOUTHERN CALIFORNIA GAS COMPANY
2016 GEOPHYSICAL INVESTIGATION
ALISO CANYON SS-25

LINE: ERT-2B (16.4 FEET [5 M])
CONDUCTIVITY CROSS-SECTION

Date: 25 AUGUST 2016	Drawn by: MCAL	Edited by: EJE	App'd by: PB
OneWay	Advisian WorleyParsons Group	WorleyParsons Project No. 407074-00748	
		FIG No. APP4-7	REV 0

This drawing is prepared solely for the use of our customer as specified in the accompanying report. Advisian, a division of WorleyParsons Canada Services Ltd., assumes no liability to any other party for any representations contained in this drawing.

FILE: U:\CAL\GBS\407074-00748\200 - Geophysical Investigation\10.0_Technical_Specialist\10.1_Geophysics\10.1.3_Oasis\Maps\407074-00748-GP-OAS-ERT4B-A.map

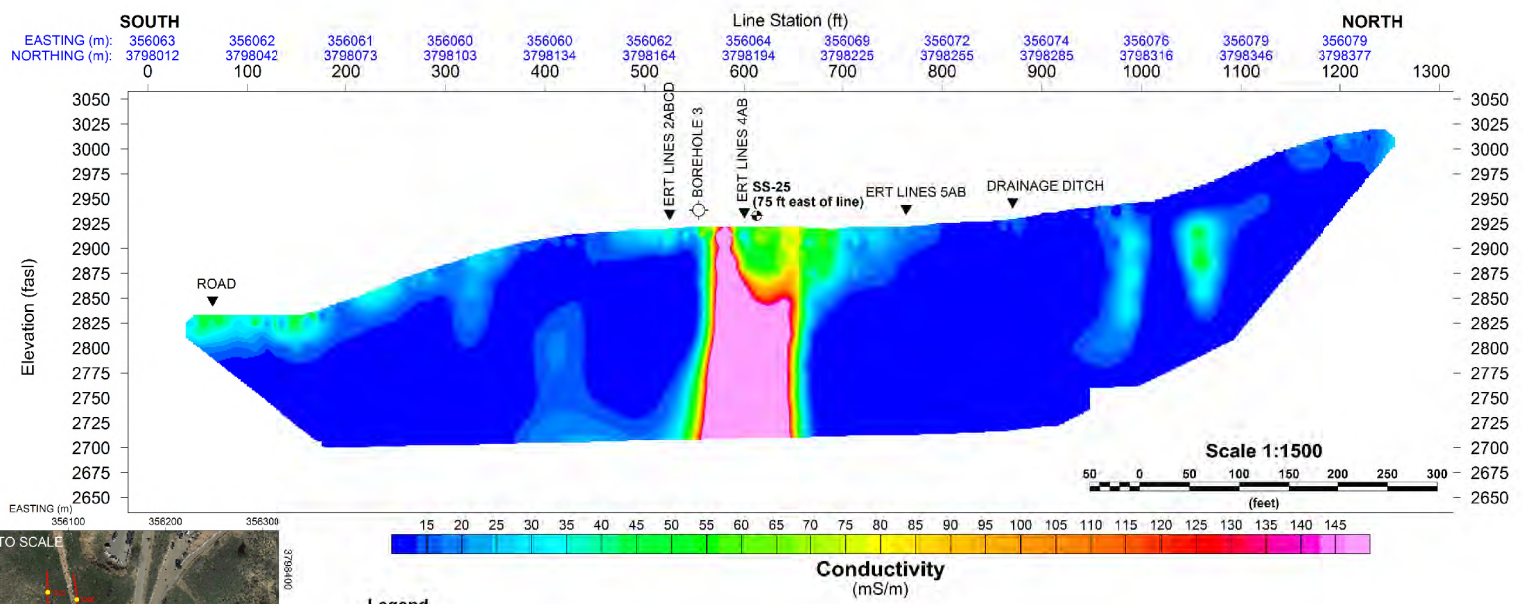

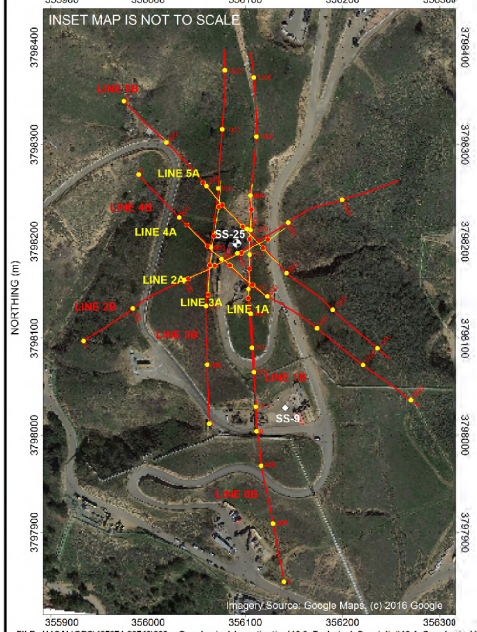

Legend

CROSS-SECTION

356103 UTM ZONE 11N
3798142 WGS 1983 (metres)

INSET MAP

4.92 feet (1.5 m) ERT Lines

16.4 feet (5 m) ERT Lines

FIELD PARAMETERS:
Date Collected: 17-AUG-2016
Electrode Configuration: GradientPlus Array
Minimum Electrode Spacing: 16.4 feet (5 m)

SOUTHERN CALIFORNIA GAS COMPANY
2016 GEOPHYSICAL INVESTIGATION
ALISO CANYON SS-25

LINE: ERT-3B (16.4 FEET [5 M])
CONDUCTIVITY CROSS-SECTION

Date: 16 AUG 2016	Drawn by: MCAL	Edited by: EJE	Appd by: PB

OneWay
Advision
WorleyParsons Group

WorleyParsons Project No. 407074-00748

FIG No. APP4-8 REV 0

This drawing is prepared solely for the use of our customer as specified in the accompanying report.
Advision, a division of WorleyParsons Canada Services Ltd., assumes no liability to any other party for any representations contained in this drawing.

FILE: U:\CAL\GBS\407074-00748\200 - Geophysical Investigation\10.0_Technical_Specialist\10.1_Geophysics\10.1.3_Oasis\407074-00748-GP-OAS-ERT2B-A.map

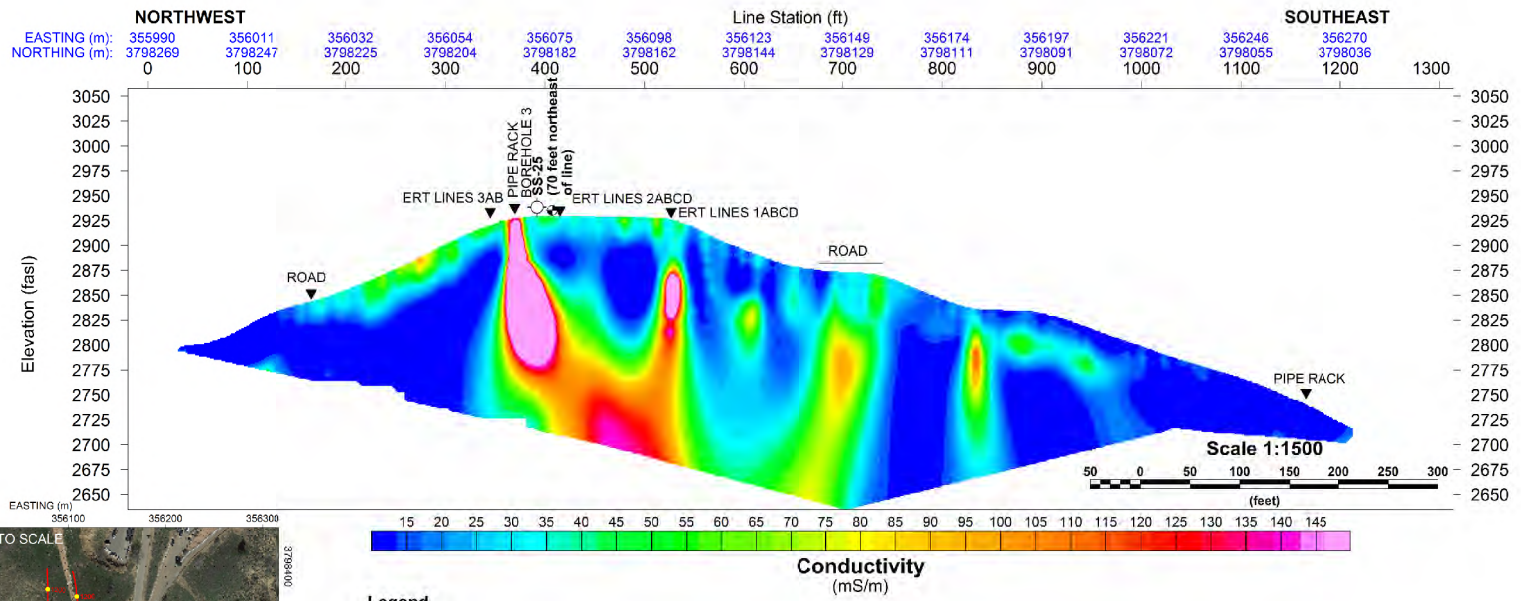

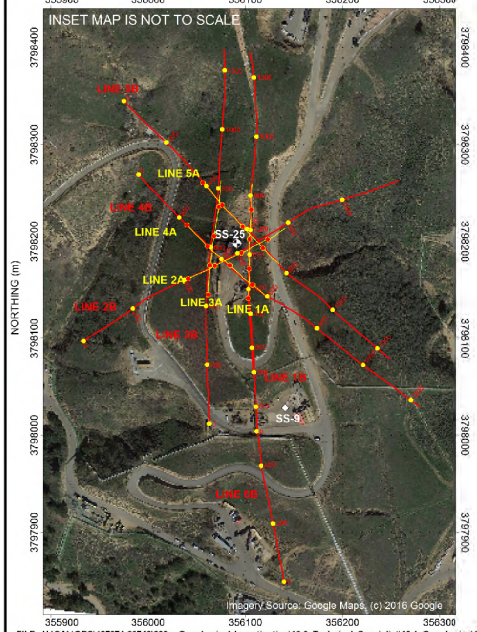

Legend

CROSS-SECTION

356103 UTM ZONE 11N
3798142 WGS 1983 (metres)

INSET MAP

4.92 feet (1.5 m) ERT Lines

16.4 feet (5 m) ERT Lines

FIELD PARAMETERS:
Date Collected: 30-AUG-2016
Electrode Configuration: GradientPlus Array
Minimum Electrode Spacing: 16.4 feet (5 m)

SOUTHERN CALIFORNIA GAS COMPANY
2016 GEOPHYSICAL INVESTIGATION
ALISO CANYON SS-25

LINE: ERT-4B (16.4 FEET [5 M])
CONDUCTIVITY CROSS-SECTION

Date: 1 SEPT 2016	Drawn by: MCAL	Edited by: EJE	Appd by: PB

OneWay
Advisian
WorleyParsons Group

WorleyParsons Project No. 407074-00748
RIG No. APP4-9
REV. 0

This drawing is prepared solely for the use of our customer as specified in the accompanying report. Advisian, a division of WorleyParsons Canada Services Ltd., assumes no liability to any other party for any representations contained in this drawing.

FILE: U:\CAL\GBS\407074-00748\200 - Geophysical Investigation\10.0_Technical_Specialist\10.1_Geophysics\10.1.3_Oasis\Maps\407074-00748-GP-OAS-ERT3B-A.map

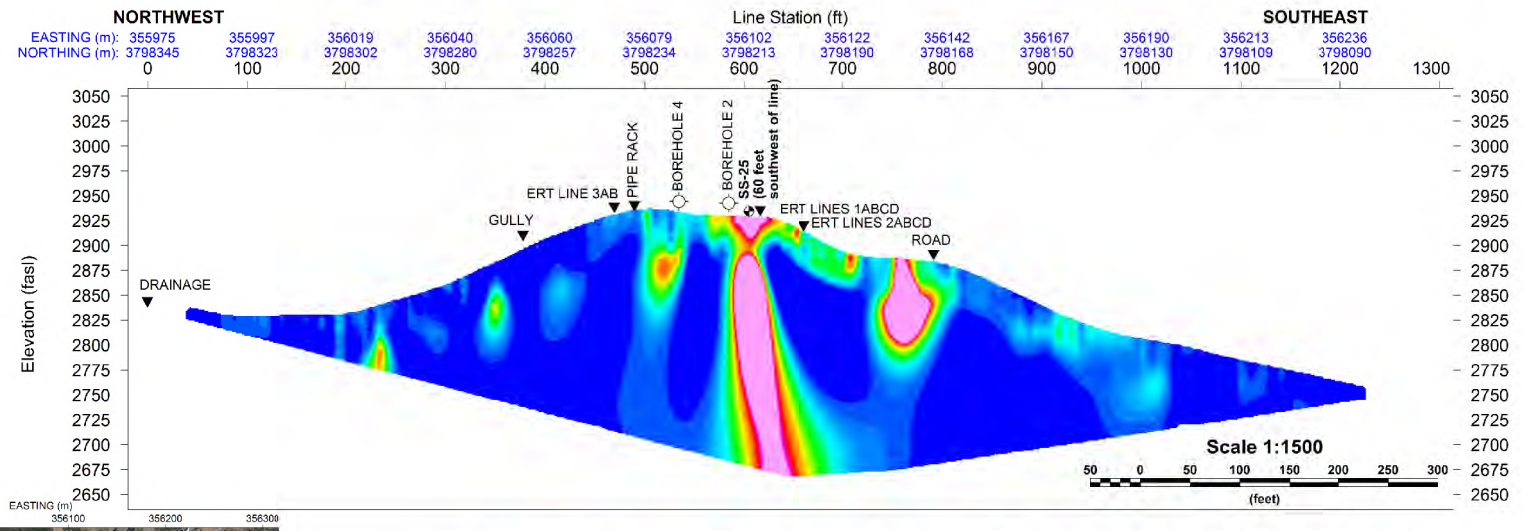

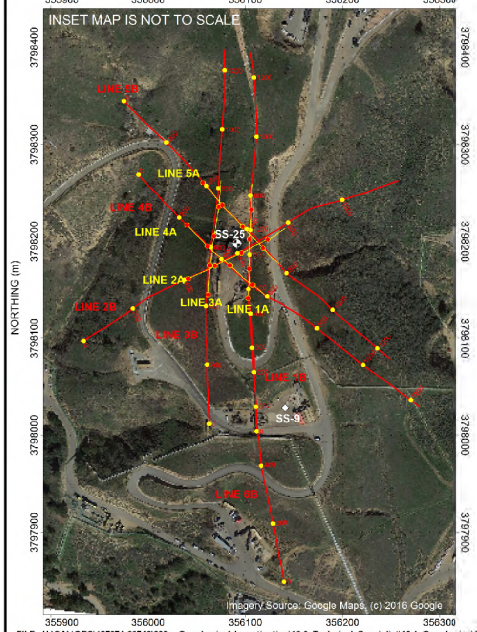

Legend

CROSS-SECTION

356103 UTM ZONE 11N
3798142 WGS 1983 (metres)

INSET MAP

4.92 feet (1.5 m) ERT Lines

16.4 feet (5 m) ERT Lines

FIELD PARAMETERS:
Date Collected: 6-SEPT-2016
Electrode Configuration: GradientPlus Array
Minimum Electrode Spacing: 16.4 feet (5 m)

SOUTHERN CALIFORNIA GAS COMPANY
2016 GEOPHYSICAL INVESTIGATION
ALISO CANYON SS-25

LINE: ERT-5B (16.4 FEET [5 M])
CONDUCTIVITY CROSS-SECTION

Date: 7 SEPT 2016	Drawn by: MCAL	Edited by: EJE	Appd by: PB

OneWay
Advision WorleyParsons Group

WorleyParsons Project No. 407074-00748

FIG No. APP4-10 REV 0

This drawing is prepared solely for the use of our customer as specified in the accompanying report. Advision, a division of WorleyParsons Canada Services Ltd., assumes no liability to any other party for any representations contained in this drawing.

FILE: U:\CAL\GBS\407074-00748\200 - Geophysical Investigation\10.0_Technical_Specialist\10.1_Geophysics\10.1.3_Oasis\Maps\407074-00748-GP-OAS-ERT6B-A.map

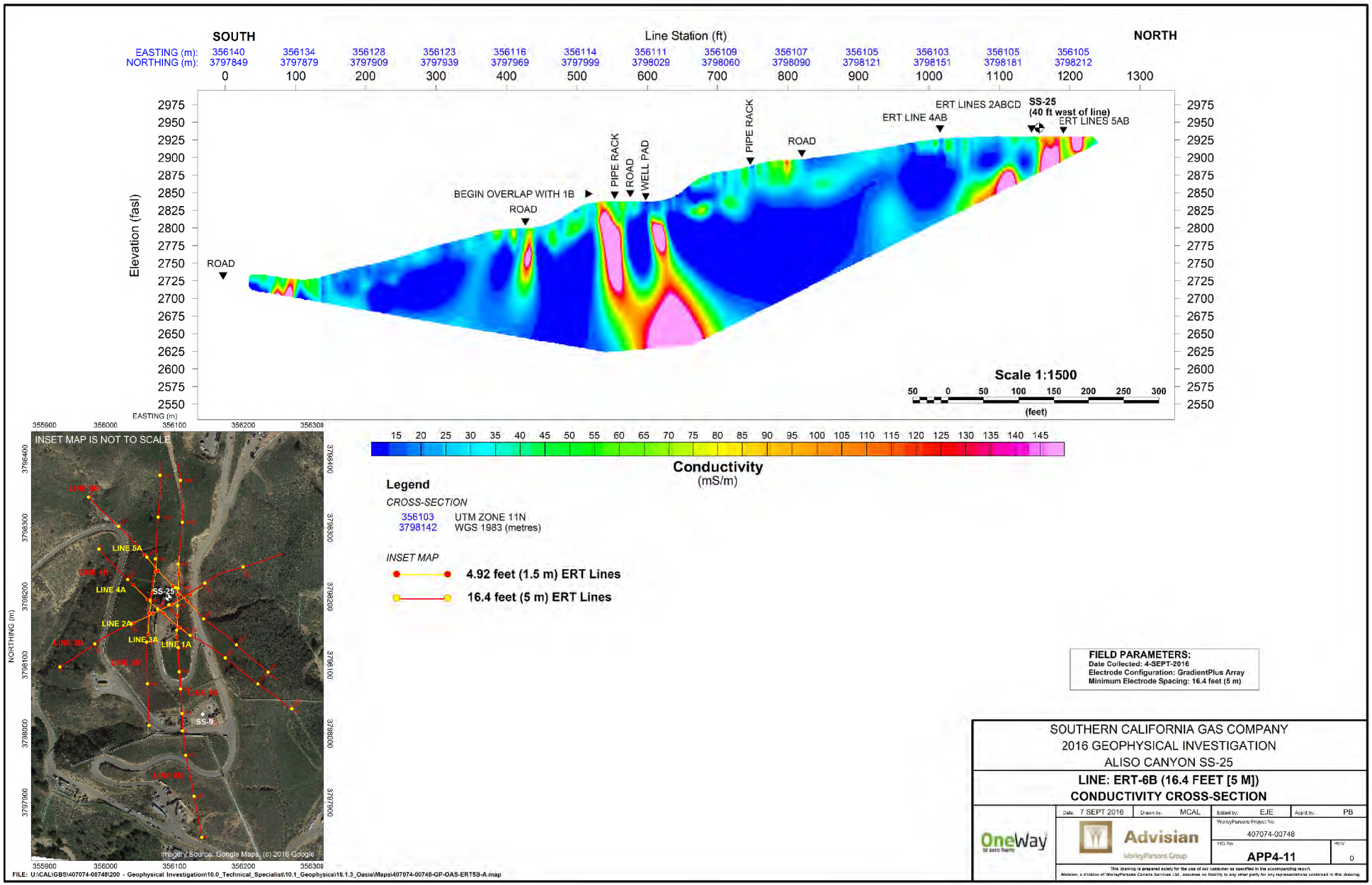

FIELD PARAMETERS:
Date Collected: 4-SEPT-2016
Electrode Configuration: GradientPlus Array
Minimum Electrode Spacing: 16.4 feet (5 m)

SOUTHERN CALIFORNIA GAS COMPANY
2016 GEOPHYSICAL INVESTIGATION
ALISO CANYON SS-25

LINE: ERT-6B (16.4 FEET [5 M])
CONDUCTIVITY CROSS-SECTION

Date:	Drawn by:	Edited by:	Appd by:
7 SEPT 2016	MCAL	EJE	PB

WorleyParsons Project No.: 407074-00748
FIG No.: APP4-11
REV: 0

OneWay
Advisian
WorleyParsons Group

This drawing is prepared solely for the use of our customer as specified in the accompanying report. Advisian, a division of WorleyParsons Canada Services Ltd., assumes no liability to any other party for any representations contained in this drawing.

FILE: U:\CAL\GBS\407074-00748\200 - Geophysical Investigation\10.0_Technical_Specialist\10.1_Geophysics\10.1.3_Oasis\Maps\407074-00748-GP-OAS-ERT5B-A.map

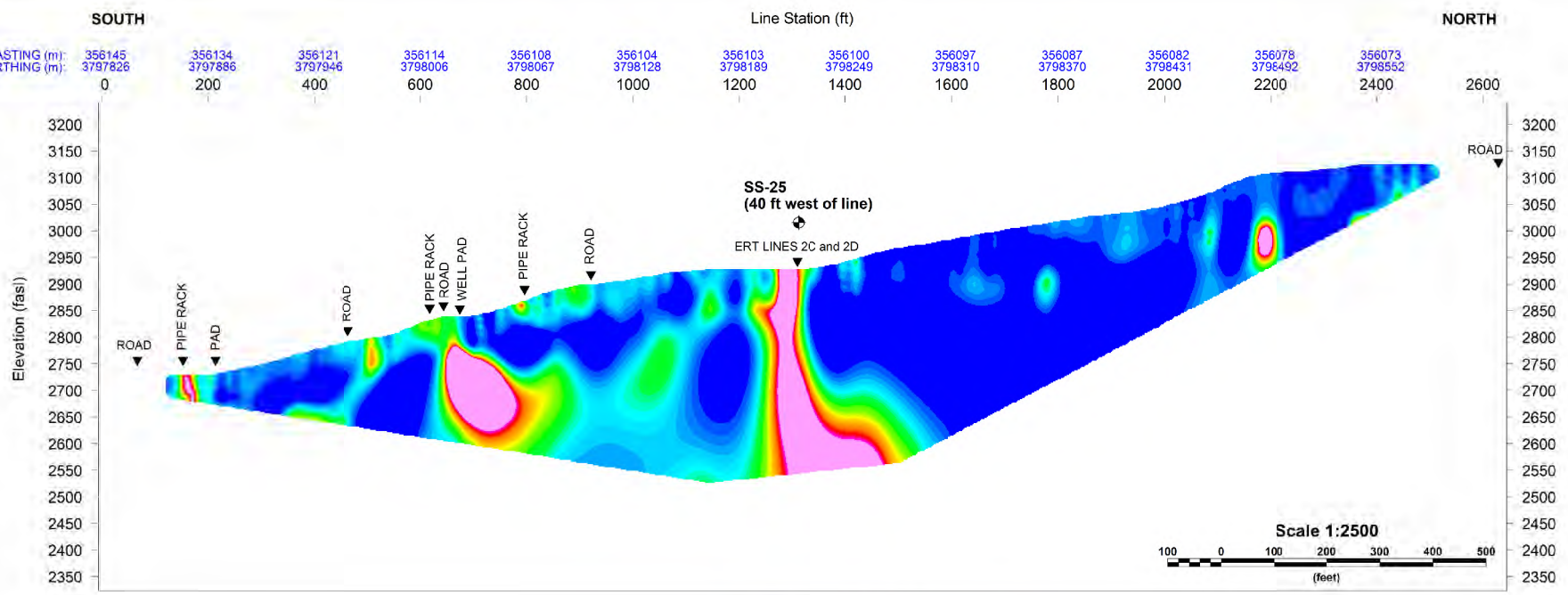

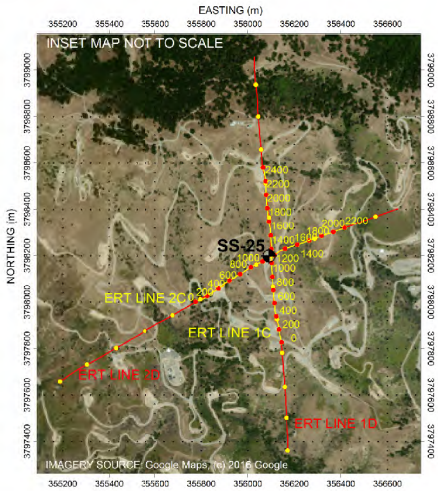

Legend

CROSS-SECTION

356103 UTM ZONE 11N
3798142 WGS 1983 (metres)

INSET MAP

32.8 feet (10 m) ERT Lines

73.8 feet (22.5 m) ERT Lines

FIELD PARAMETERS:
Date Collected: 28-AUG-2016
Electrode Configuration: GradientPlus Array
Minimum Electrode Spacing: 32.8 feet (10 m)

SOUTHERN CALIFORNIA GAS COMPANY
2016 GEOPHYSICAL INVESTIGATION
ALISO CANYON SS-25

LINE: ERT-1C (32.8 feet [10 m])
CONDUCTIVITY CROSS-SECTION

Date: 29-AUG-2016	Drawn by: MCAL	Edited by: EJE	Appd by: PB
OneWay to zero harm	Advisian	Worley Parsons Project No. 407074-00748	
		FIG No. APP4-12	REV 0

This drawing is prepared solely for the use of our customer as specified in the accompanying report. Advisian, a division of WorleyParsons Canada Services Ltd., assumes no liability to any other party for any representations contained in this drawing.

FILE: U:\CAL\GBS\407074-00748\200 - Geophysical Investigation\10.0_Technical_Specialist\10.1_Geophysics\10.1.3_Oasis\Maps\407074-00748-GP-OAS-ERT1C-A.map

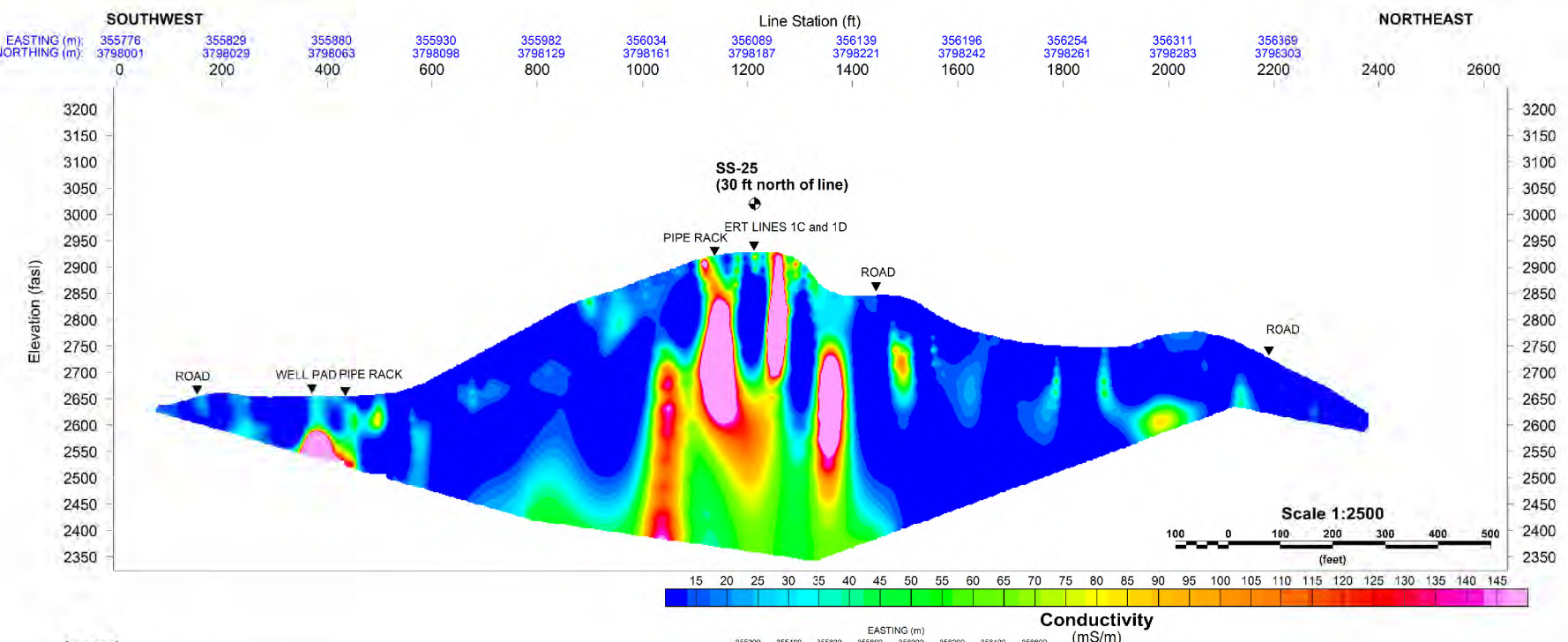

Legend

CROSS-SECTION

356103 UTM ZONE 11N
3798142 WGS 1983 (metres)

INSET MAP

32.8 feet (10 m) ERT Lines

73.8 feet (22.5 m) ERT Lines

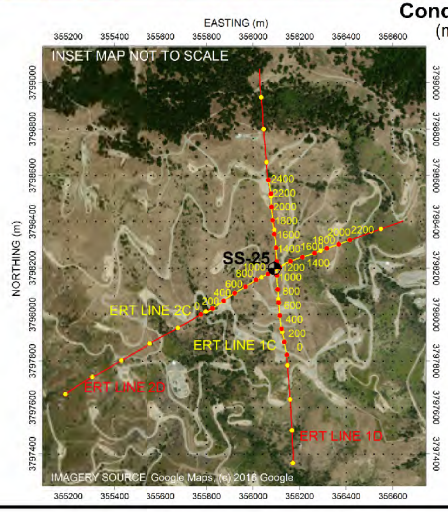

FIELD PARAMETERS:
Date Collected: 30-AUG-2016
Electrode Configuration: GradientPlus Array
Minimum Electrode Spacing: 32.8 feet (10 m)

SOUTHERN CALIFORNIA GAS COMPANY
2016 GEOPHYSICAL INVESTIGATION
ALISO CANYON SS-25

LINE: ERT-2C (32.8 FEET [10 M])
CONDUCTIVITY CROSS-SECTION

Date: 31-AUG-2016	Drawn by: MCAL	Edited by: EJE	Appd by: PB

WorleyParsons Project No.: 407074-00748

FIG No.: APP4-13 REV: 0

OneWay to zero harm

Advisian

This drawing is prepared solely for the use of our customer as specified in the accompanying report. Advisian, a division of WorleyParsons Canada Services Ltd., assumes no liability to any other party for any representations contained in this drawing.

FILE: D:\CAL\GBS\407074-00748\200 - Geophysical Investigation\10.0_Technical_Specialist\10.1_Geophysics\10.1.3_Oasis\407074-00748-GP-OAS-ERT2C-A.map

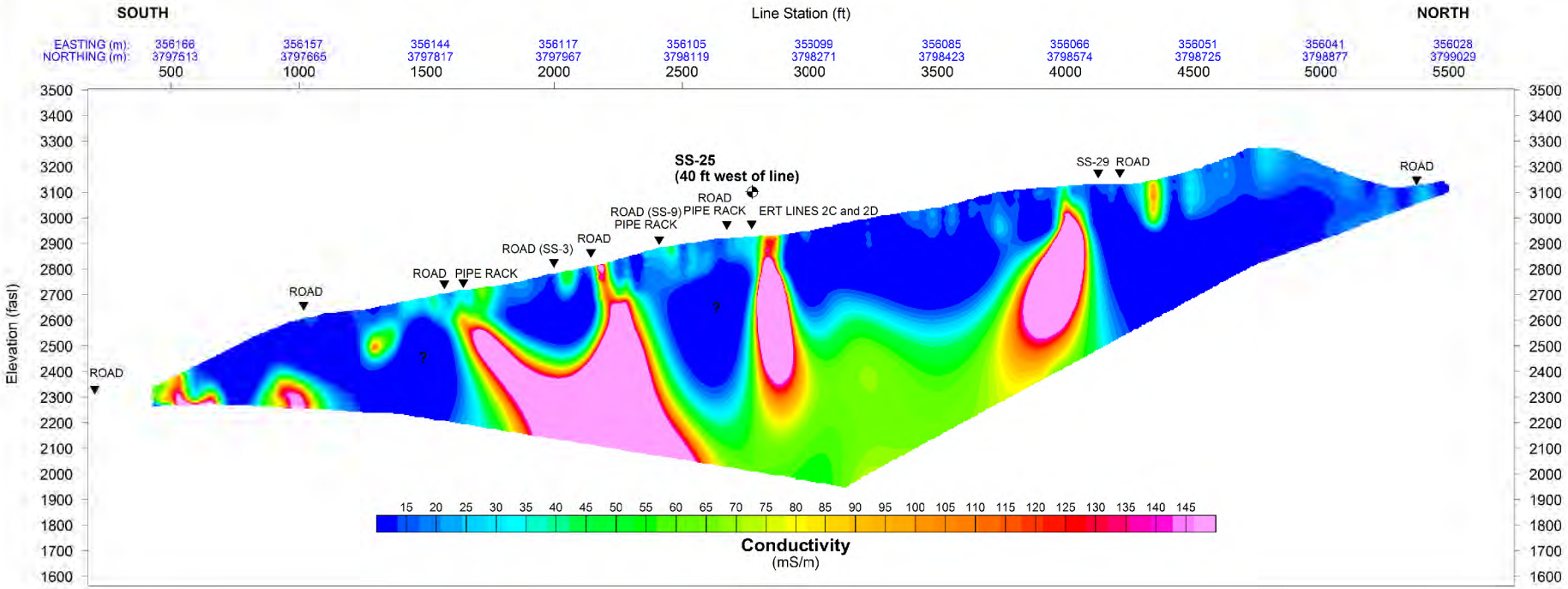

Legend

CROSS-SECTION

356103 UTM ZONE 11N
3798142 WGS 1983 (metres)

INSET MAP

32.8 feet (10 m) ERT Lines

73.8 feet (22.5 m) ERT Lines

FIELD PARAMETERS:
Date Collected: 25-AUG-2016
Electrode Configuration: GradientPlus Array
Minimum Electrode Spacing: 73.8 feet (22.5 m)

Scale 1:5000

250 0 250 500 750 1000
(feet)

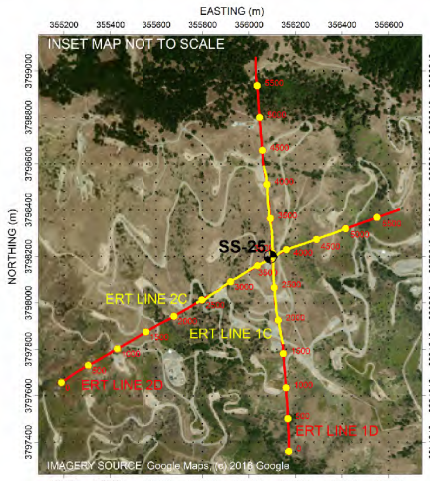

FILE: U:\CAL\GBS\407074-00748\200 - Geophysical Investigation\10.0_Technical_Specialist\10.1_Geophysics\10.1.3_Oasis\Maps\407074-00748-GP-OAS-ERT1D-A.map

SOUTHERN CALIFORNIA GAS COMPANY
2016 GEOPHYSICAL INVESTIGATION
ALISO CANYON SS-25

LINE: ERT-1D (73.8 feet [22.5 m])
CONDUCTIVITY CROSS-SECTION

OneWay to zero harm

Advisian

Date: 29 AUGUST 2016 | Drawn by: MCAL | Edited by: EJE | Appd by: PB
WorleyParsons Project No: 407074-00748
F.G No: APP4-14
Rev: 0

This drawing is prepared solely for the use of our customer as specified in the accompanying report. Advisian, a division of WorleyParsons Canada Services Ltd., assumes no liability to any other party for any representations contained in this drawing.

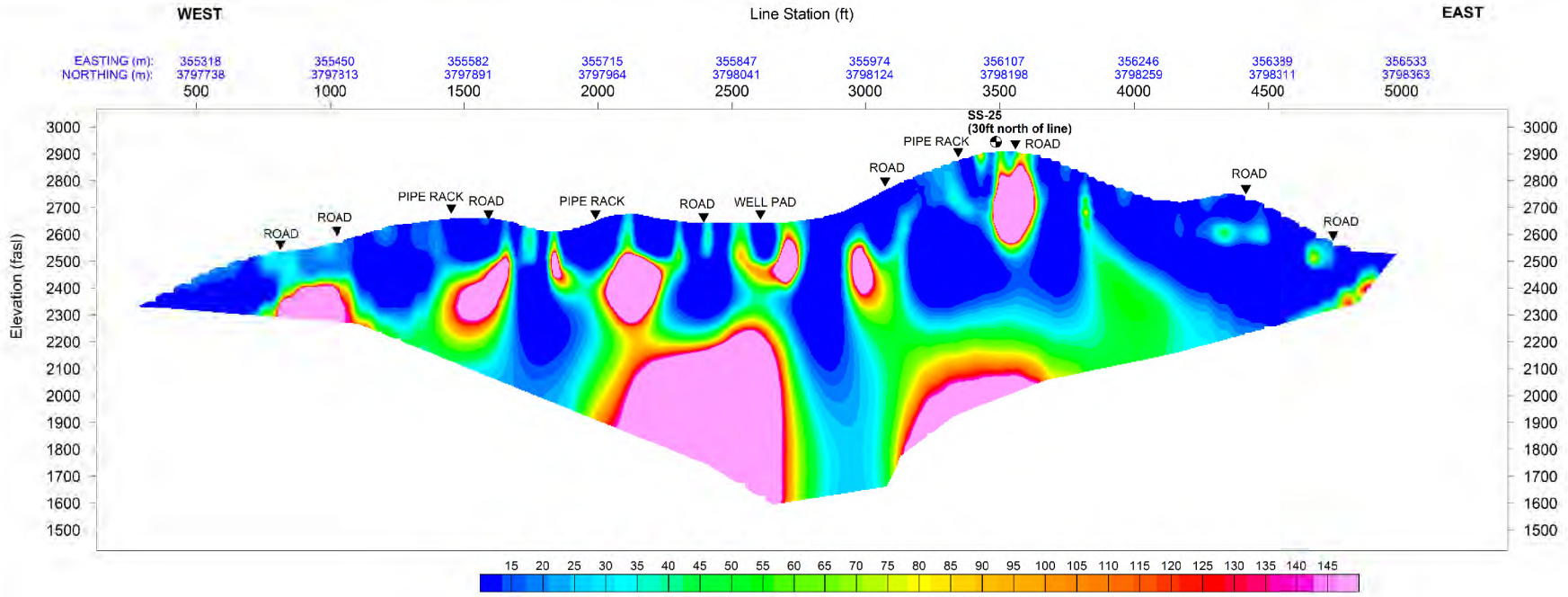

Legend

CROSS-SECTION

356103 UTM ZONE 11N
3798142 WGS 1983 (metres)

INSET MAP

32.8 feet (10 m) ERT Lines

73.8 feet (22.5 m) ERT Lines

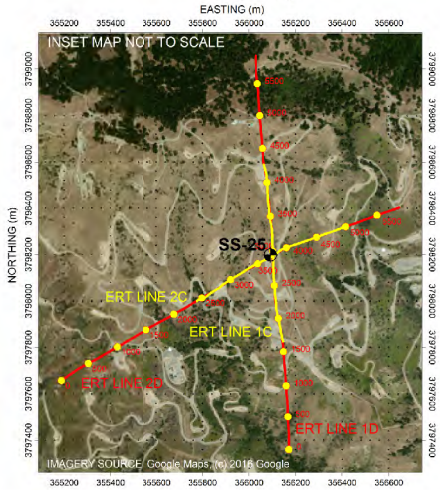

FIELD PARAMETERS:
Date Collected: 27-AUG-2016
Electrode Configuration: GradientPlus Array
Minimum Electrode Spacing: 73.8 feet (22.5 m)

Scale 1:5000

250 0 250 500 750 1000
(feet)

FILE: U:\CAL\GBS\407074-00748\200 - Geophysical Investigation\10.0_Technical_Specialist\10.1_Geophysics\10.1.3_Oasis\Maps\407074-00748-GP-OAS-ERT2D-A.map

SOUTHERN CALIFORNIA GAS COMPANY
2016 GEOPHYSICAL INVESTIGATION
ALISO CANYON SS-25

LINE: ERT-2D (73.8 FEET [22.5 M])
CONDUCTIVITY CROSS-SECTION

Date:	Drawn by:	Edited by:	Appd by:
16 AUG 2016	MCAL	EJE	PB

WorleyParsons Project No.: 407074-00748
FIG No.: APP4-15
REV: 0

OneWay to zero harm

Advisian

This drawing is prepared solely for the use of our customer as specified in the accompanying report. Advisian, a division of WorleyParsons Canada Services Ltd., assumes no liability to any other party for any representations contained in this drawing.

Appendix 5: Existing Lithological and Geophysical Logs Provided by Blade Energy

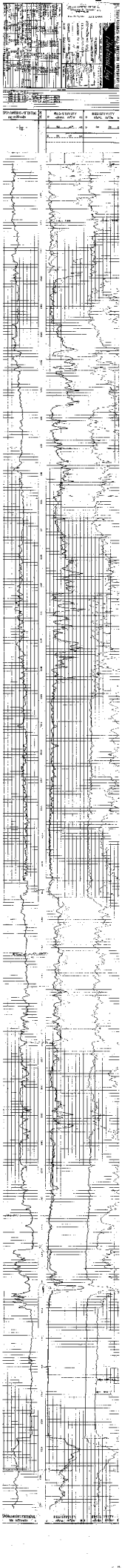

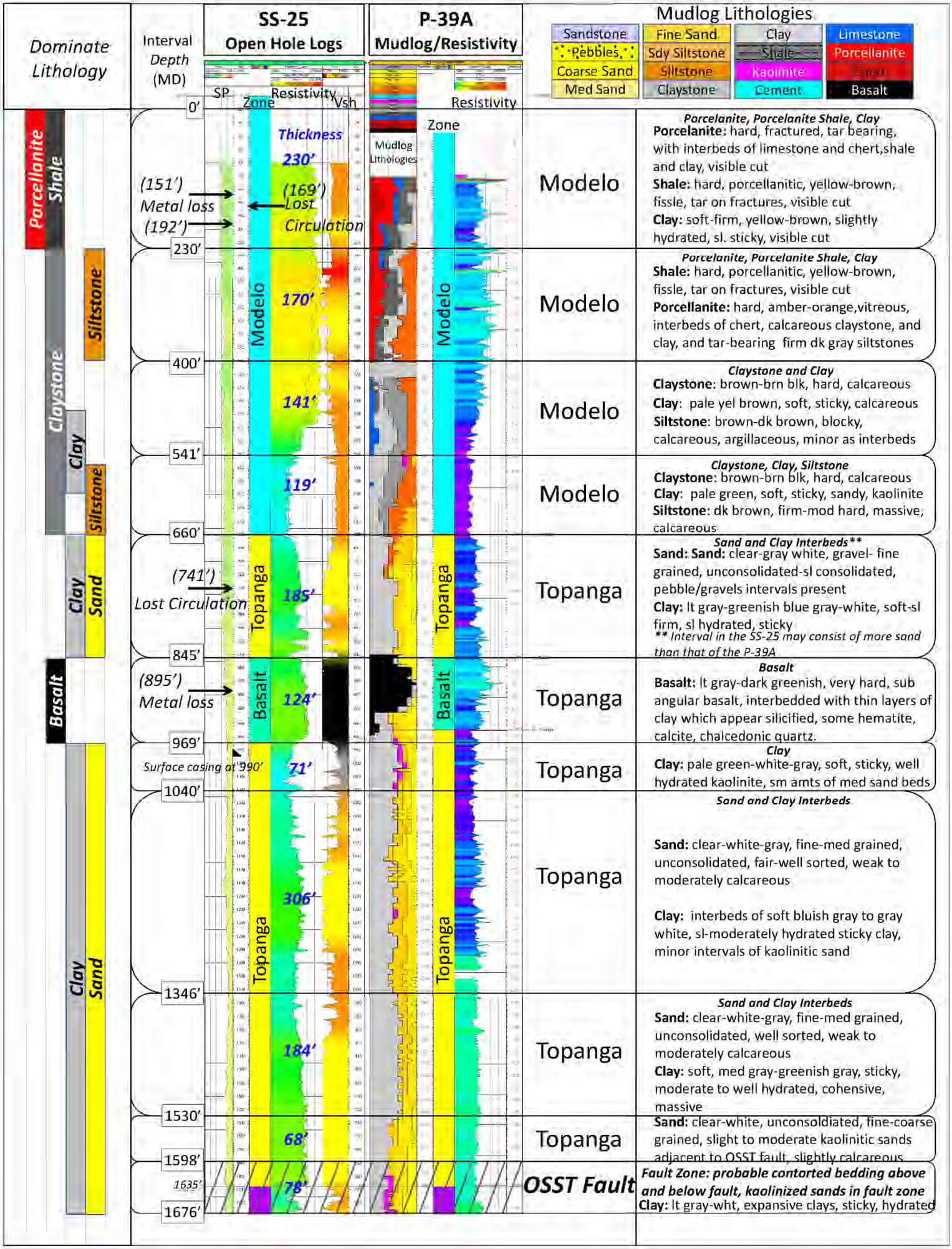
Dominate Lithology
Interval Depth (MD)
SS-25 Open Hole Logs
P-39A Mudlog/Resistivity
SP
Zone
Resistivity
Vsh
Mudlog Lithologies
Sandstone
Pebbles
Coarse Sand
Med Sand
Fine Sand
Sdy Siltstone
Siltstone
Claystone
Clay
Shale
Kaolinite
Cement
Limestone
Porcellanite
Chert
Basalt
Porcellanite Shale
Siltstone
Claystone
Clay
Siltstone
Clay Sand
Basalt
Clay Sand
0'
230'
400'
541'
660'
845'
969'
1040'
1346'
1530'
1598'
1635'
1676'
Thickness
230'
(151') Metal loss
(192')
(169') Lost Circulation
170'
141'
119'
(741') Lost Circulation
185'
(895') Metal loss
124'
Surface casing at 990'
71'
306'
184'
68'
78'
Modelo
Topanga
Basalt
OSST Fault
Porcelanite, Porcelanite Shale, Clay
Porcelanite: hard, fractured, tar bearing, with interbeds of limestone and chert,shale and clay, visible cut
Shale: hard, porcellanitic, yellow-brown, fissle, tar on fractures, visible cut
Clay: soft-firm, yellow-brown, slightly hydrated, sl. sticky, visible cut
Porcelanite, Porcelanite Shale, Clay
Shale: hard, porcellanitic, yellow-brown, fissle, tar on fractures, visible cut
Porcellanite: hard, amber-orange,vitreous, interbeds of chert, calcareous claystone, and clay, and tar-bearing firm dk gray siltstones
Claystone and Clay
Claystone: brown-brn blk, hard, calcareous
Clay: pale yel brown, soft, sticky, calcareous
Siltstone: brown-dk brown, blocky, calcareous, argillaceous, minor as interbeds
Claystone, Clay, Siltstone
Claystone: brown-brn blk, hard, calcareous
Clay: pale green, soft, sticky, sandy, kaolinite
Siltstone: dk brown, firm-mod hard, massive, calcareous
Sand and Clay Interbeds**
Sand: Sand: clear-gray white, gravel- fine grained, unconsolidated-sl consolidated, pebble/gravels intervals present
Clay: lt gray-greenish blue gray-white, soft-sl firm, sl hydrated, sticky
** Interval in the SS-25 may consist of more sand than that of the P-39A
Basalt
Basalt: lt gray-dark greenish, very hard, sub angular basalt, interbedded with thin layers of clay which appear silicified, some hematite, calcite, chalcedonic quartz.
Clay
Clay: pale green-white-gray, soft, sticky, well hydrated kaolinite, sm amts of med sand beds
Sand and Clay Interbeds
Sand: clear-white-gray, fine-med grained, unconsolidated, fair-well sorted, weak to moderately calcareous
Clay: interbeds of soft bluish gray to gray white, sl-moderately hydrated sticky clay, minor intervals of kaolinitic sand
Sand and Clay Interbeds
Sand: clear-white-gray, fine-med grained, unconsolidated, well sorted, weak to moderately calcareous
Clay: soft, med gray-greenish gray, sticky, moderate to well hydrated, cohensive, massive
Sand: clear-white, unconsoldiated, fine-coarse grained, slight to moderate kaolinitic sands adjacent to OSST fault, slightly calcareous
Fault Zone: probable contorted bedding above and below fault, kaolinized sands in fault zone
Clay: lt gray-wht, expansive clays, sticky, hydrated

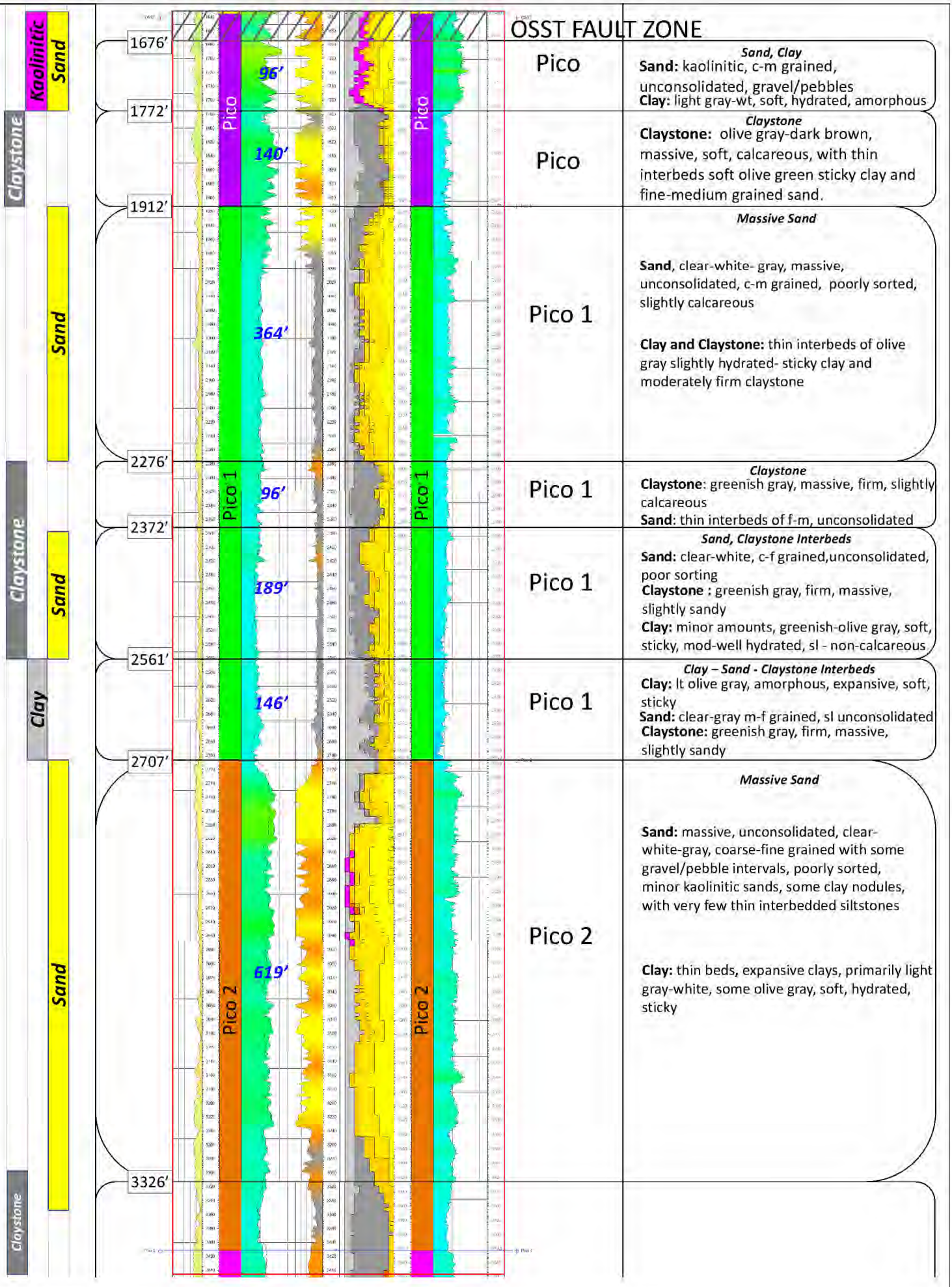
OSST FAULT ZONE
Kaolinitic Sand
Claystone
Sand
Claystone
Sand
Clay
Sand
Claystone
1676′
1772′
1912′
2276′
2372′
2561′
2707′
3326′
96′
140′
364′
96′
189′
146′
619′
Pico
Pico 1
Pico 2
Pico
Pico 1
Pico 2
Pico
Pico 1
Pico 1
Pico 1
Pico 2
Sand, Clay
Sand: kaolinitic, c-m grained, unconsolidated, gravel/pebbles
Clay: light gray-wt, soft, hydrated, amorphous
Claystone
Claystone: olive gray-dark brown, massive, soft, calcareous, with thin interbeds soft olive green sticky clay and fine-medium grained sand.
Massive Sand
Sand, clear-white- gray, massive, unconsolidated, c-m grained, poorly sorted, slightly calcareous
Clay and Claystone: thin interbeds of olive gray slightly hydrated- sticky clay and moderately firm claystone
Claystone
Claystone: greenish gray, massive, firm, slightly calcareous
Sand: thin interbeds of f-m, unconsolidated
Sand, Claystone Interbeds
Sand: clear-white, c-f grained,unconsolidated, poor sorting
Claystone : greenish gray, firm, massive, slightly sandy
Clay: minor amounts, greenish-olive gray, soft, sticky, mod-well hydrated, sl - non-calcareous
Clay – Sand - Claystone Interbeds
Clay: lt olive gray, amorphous, expansive, soft, sticky
Sand: clear-gray m-f grained, sl unconsolidated
Claystone: greenish gray, firm, massive, slightly sandy
Massive Sand
Sand: massive, unconsolidated, clear-white-gray, coarse-fine grained with some gravel/pebble intervals, poorly sorted, minor kaolinitic sands, some clay nodules, with very few thin interbedded siltstones
Clay: thin beds, expansive clays, primarily light gray-white, some olive gray, soft, hydrated, sticky

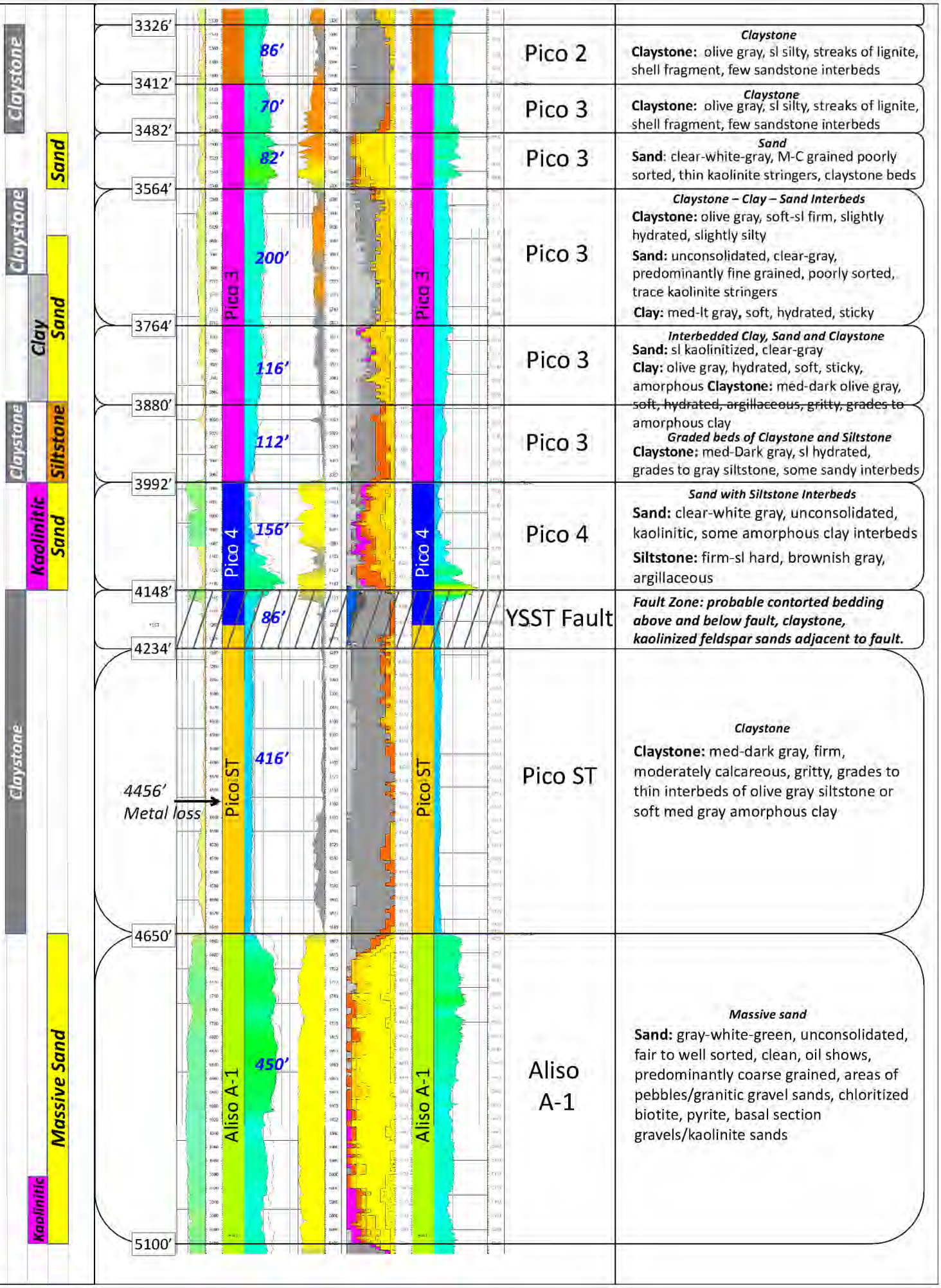
Claystone
Sand
Claystone
Clay
Sand
Claystone
Siltstone
Kaolinitic
Sand
Claystone
Massive Sand
Kaolinitic
3326′
3412′
3482′
3564′
3764′
3880′
3992′
4148′
4234′
4650′
5100′
86′
70′
82′
200′
116′
112′
156′
86′
416′
450′
Pico 3
Pico 3
Pico 4
Pico 4
Pico ST
Pico ST
Aliso A-1
Aliso A-1
4456′
Metal loss
Pico 2
Pico 3
Pico 3
Pico 3
Pico 4
YSST Fault
Pico ST
Aliso A-1
Claystone
Claystone: olive gray, sl silty, streaks of lignite, shell fragment, few sandstone interbeds
Claystone
Claystone: olive gray, sl silty, streaks of lignite, shell fragment, few sandstone interbeds
Sand
Sand: clear-white-gray, M-C grained poorly sorted, thin kaolinite stringers, claystone beds
Claystone – Clay – Sand Interbeds
Claystone: olive gray, soft-sl firm, slightly hydrated, slightly silty
Sand: unconsolidated, clear-gray, predominantly fine grained, poorly sorted, trace kaolinite stringers
Clay: med-lt gray, soft, hydrated, sticky
Interbedded Clay, Sand and Claystone
Sand: sl kaolinitized, clear-gray
Clay: olive gray, hydrated, soft, sticky, amorphous Claystone: med-dark olive gray, soft, hydrated, argillaceous, gritty, grades to amorphous clay
Graded beds of Claystone and Siltstone
Claystone: med-Dark gray, sl hydrated, grades to gray siltstone, some sandy interbeds
Sand with Siltstone Interbeds
Sand: clear-white gray, unconsolidated, kaolinitic, some amorphous clay interbeds
Siltstone: firm-sl hard, brownish gray, argillaceous
Fault Zone: probable contorted bedding above and below fault, claystone, kaolinized feldspar sands adjacent to fault.
Claystone
Claystone: med-dark gray, firm, moderately calcareous, gritty, grades to thin interbeds of olive gray siltstone or soft med gray amorphous clay
Massive sand
Sand: gray-white-green, unconsolidated, fair to well sorted, clean, oil shows, predominantly coarse grained, areas of pebbles/granitic gravel sands, chloritized biotite, pyrite, basal section gravels/kaolinite sands

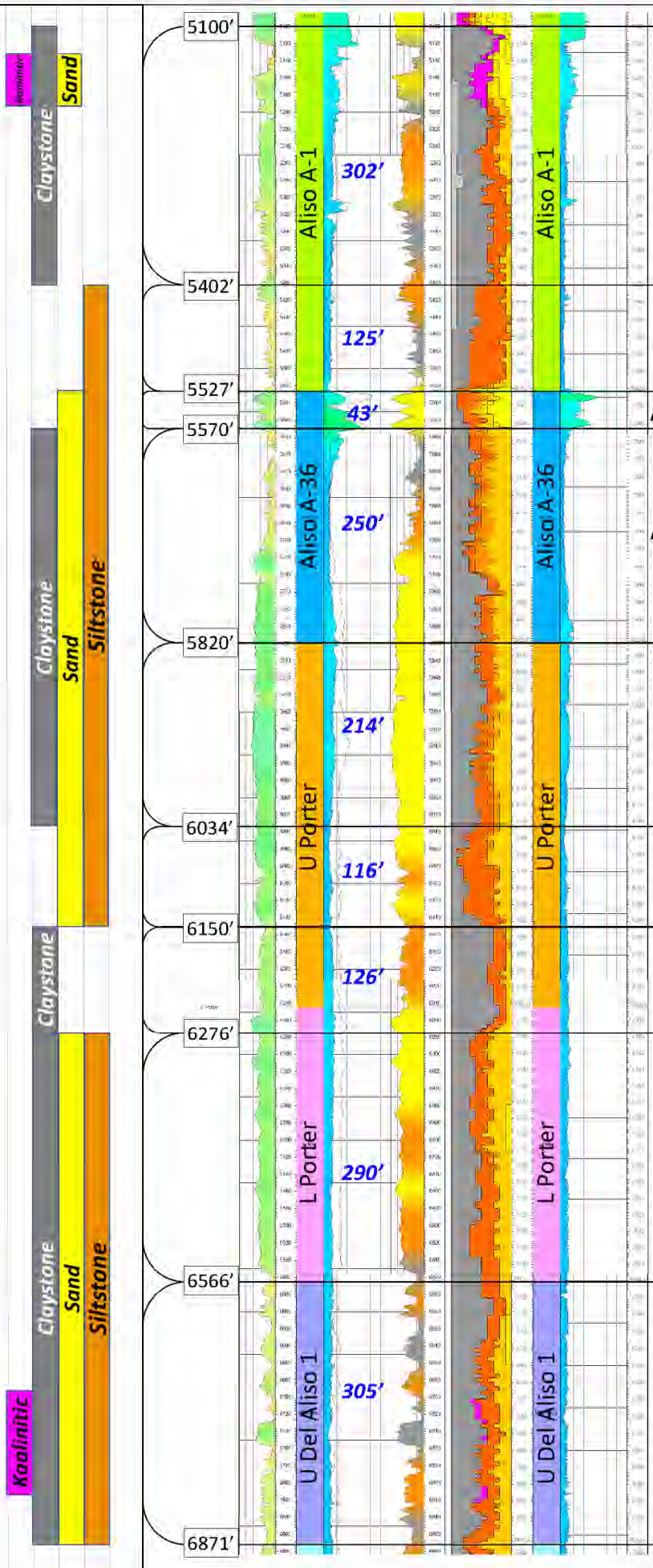

Aliso A-1

Sand

Sand: clear-gray, unconsolidated, kaolinitic, moderatly sorted, some pyrite and mica flakes

Claystone with Siltstone Interbeds

Claystone: olive gray, firm, massive, moderately calcareous, silty, grades to thin interbeds of olive gray **siltstone** or minor amounts of silty argillaceous sandstone.

Aliso A-1

Siltstone

Siltstone : olive gray, soft-firm, massive, slightly calcareous, grading from silty claystone

Claystone : olive gray, soft-firm, slightly hydrated, massive, gritty.

Aliso A-36

Sand: clear-gray, unconsolidated, coarse grained friable, oil stains, show, below o/w contact

Aliso A-36

Fine Sand, Siltstone Claystone Interbeds

Sand: lt gray-lt gray-olive, fine-v fine grained, well sorted, loosely cemented, friable

Siltstone: gray-brown, hard, slighty friable

Claystone: lt olive gray, hard, slightly friable, sl calcareous in upper part of section. Soft, spongy, sticky, sl. argillaceous, well hydrated in lower portion of section

U Porter

Claystone, V Fine Sand, Silty

Sand: lt. Olive gray, v fine grained, silty, friable

Claystone : lt olive gray, silty, soft-sl. firm, massive, gritty, argillaceous.

U Porter

Siltstone with Sand Interbeds

Siltstone: olive gray, soft, friable, clayey matrix

Sand: clear, v fine - fine grained, well sorted, moderately consolidated, silty-clayey matrix

U Porter

Claystone with thin Siltstone Interbeds

Claystone: olive gray, soft-sl firm, massive, sl calcareous, silty, argillaceous

Siltstone: olive gray, mod firm to friable, sl calcareous, carbon. material, argillaceous

L Porter

Sand & Siltstone and Claystone Interbeds

Sand: clear-gray-white, fine-grained, well sorted, grading to siltstone and claystone

Siltstone: olive-gray, firm, massive, v argillaceous

Claystone: olive gray, firm, sandy & silty, gritty, sl-moderately calcareous, some lignite

U Del Aliso 1

Sand & Siltstone and Claystone Interbeds

Sand: olive gray-lt gray, v fine-fine grained, well sorted, loose

Siltstone: olive gray, brittle, friable, occ white clay microseams

Claystone: olive gray, soft-sl firm, friable, moderately hydrated, occ white kaolinite

Kaolinite: white, soft, amorphous, well hydrated, some v fine grained sand in clay matrix

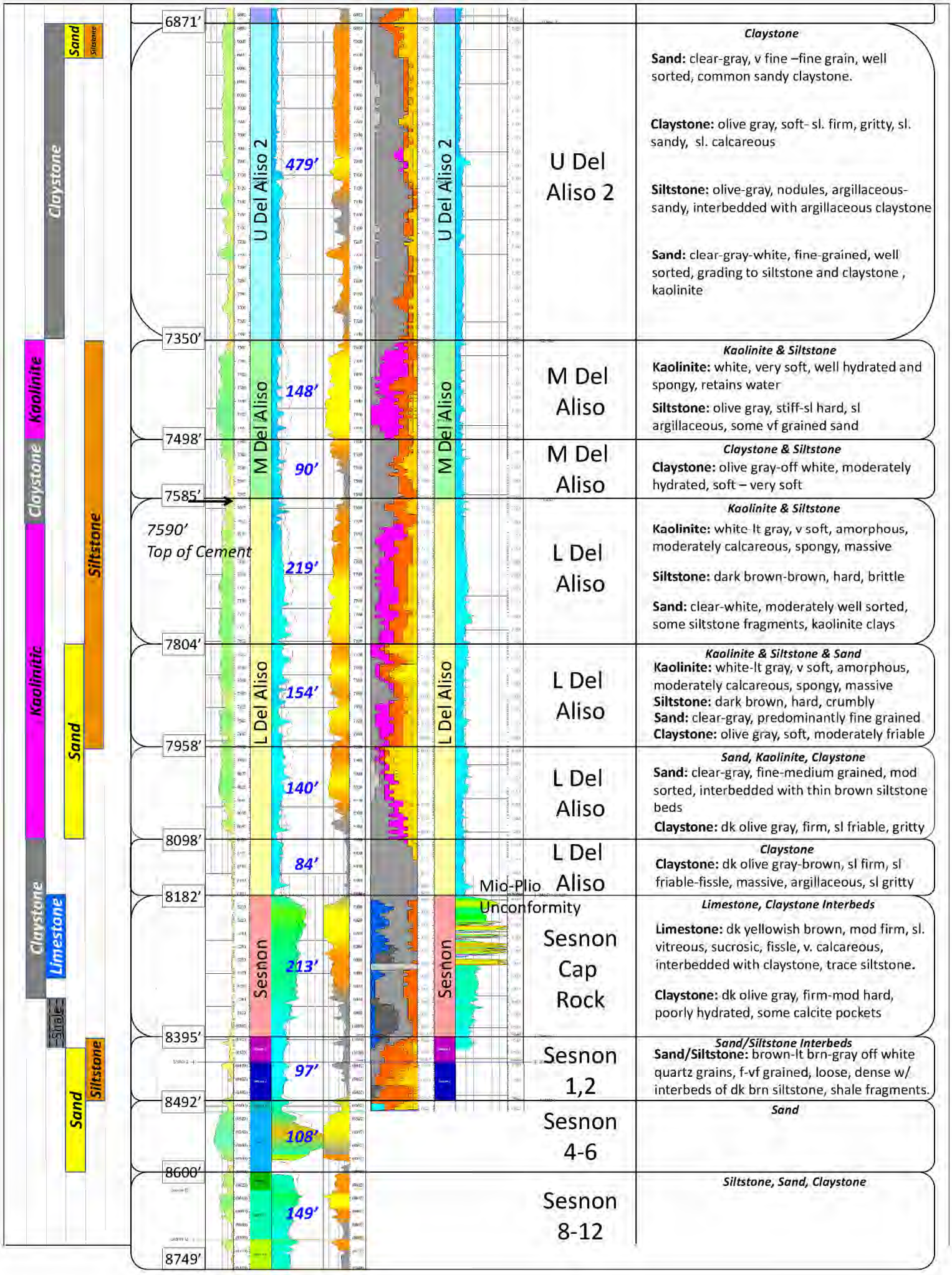
Sand
Siltstone
Claystone
Kaolinite
Claystone
Siltstone
Kaolinitic
Sand
Claystone
Limestone
Shale
Sand
Siltstone
6871'
7350'
7498'
7585'
7590'
Top of Cement
7804'
7958'
8098'
8182'
8395'
8492'
8600'
8749'
U Del Aliso 2
479'
M Del Aliso
148'
90'
L Del Aliso
219'
154'
140'
84'
Seshon
213'
97'
108'
149'
Mio-Plio
Unconformity
U Del
Aliso 2
M Del
Aliso
M Del
Aliso
L Del
Aliso
L Del
Aliso
L Del
Aliso
L Del
Aliso
Sesnon
Cap
Rock
Sesnon
1,2
Sesnon
4-6
Sesnon
8-12
Claystone
Sand: clear-gray, v fine –fine grain, well sorted, common sandy claystone.
Claystone: olive gray, soft- sl. firm, gritty, sl. sandy, sl. calcareous
Siltstone: olive-gray, nodules, argillaceous-sandy, interbedded with argillaceous claystone
Sand: clear-gray-white, fine-grained, well sorted, grading to siltstone and claystone , kaolinite
Kaolinite & Siltstone
Kaolinite: white, very soft, well hydrated and spongy, retains water
Siltstone: olive gray, stiff-sl hard, sl argillaceous, some vf grained sand
Claystone & Siltstone
Claystone: olive gray-off white, moderately hydrated, soft – very soft
Kaolinite & Siltstone
Kaolinite: white-lt gray, v soft, amorphous, moderately calcareous, spongy, massive
Siltstone: dark brown-brown, hard, brittle
Sand: clear-white, moderately well sorted, some siltstone fragments, kaolinite clays
Kaolinite & Siltstone & Sand
Kaolinite: white-lt gray, v soft, amorphous, moderately calcareous, spongy, massive
Siltstone: dark brown, hard, crumbly
Sand: clear-gray, predominantly fine grained
Claystone: olive gray, soft, moderately friable
Sand, Kaolinite, Claystone
Sand: clear-gray, fine-medium grained, mod sorted, interbedded with thin brown siltstone beds
Claystone: dk olive gray, firm, sl friable, gritty
Claystone
Claystone: dk olive gray-brown, sl firm, sl friable-fissle, massive, argillaceous, sl gritty
Limestone, Claystone Interbeds
Limestone: dk yellowish brown, mod firm, sl. vitreous, sucrosic, fissle, v. calcareous, interbedded with claystone, trace siltstone.
Claystone: dk olive gray, firm-mod hard, poorly hydrated, some calcite pockets
Sand/Siltstone Interbeds
Sand/Siltstone: brown-lt brn-gray off white quartz grains, f-vf grained, loose, dense w/ interbeds of dk brn siltstone, shale fragments.
Sand
Siltstone, Sand, Claystone

Appendix B Petrological Analysis of Igneous Outcrop Samples

Schlumberger

PETROLOGY

Detailed Thin Section Analysis for Igneous Outcrop Samples

Prepared for:
Client: Southern California Gas
Well: TH1-1
Field: Aliso Canyon
Location: Los Angeles County, California
API/UWI: N/A
Final: Yes

Prepared by:
Schlumberger Reservoir Laboratories
6350 West Sam Houston Parkway North
Houston, TX 77041
(713) 482-0700

September 2018

Project No.: 2018USHO-P194

Schlumberger for Third Party Data: Confidential

Disclaimer

The following disclaimer applies to this report and any interpretation provided by any of the Laboratories that comprise the Schlumberger Reservoir Laboratories:

Any interpretation, research, analysis, or recommendation furnished with the services or otherwise communicated by Schlumberger Reservoir Laboratories to Customer at any time in connection with the services are opinions based on inferences from measurements and empirical relationships and assumptions, which inferences and assumptions are not infallible, and with respect to which professionals in the industry may differ. Accordingly, Schlumberger Reservoir Laboratories cannot and does not warrant the accuracy, correctness or completeness of any such interpretation or description.

Customer acknowledges that It is accepting the services “as is”, that Schlumberger Reservoir Laboratories makes no representation or warranty, express or implied, of any kind or description in respect thereto, and that such services are delivered with the explicit understanding and agreement that any action customer may take based on the services received shall be at its own risk and responsibility and customer shall have no claim against Schlumberger Reservoir Laboratories as a consequence thereof.

Customer confirms that Schlumberger Reservoir Laboratories has made no promise or statement regarding the services that is inconsistent with these terms, or that has created or amounted to a warranty that the services would conform to any such promise or statement, and Schlumberger Reservoir Laboratories disclaims any and all warranties regarding the same.

Schlumberger for Third Party Data: Confidential

Executive Summary

Hand samples of the Topanga Basalt were collected from its outcrop area in the Aliso Canyon, Los Angeles County, California, in an effort to determine a good approximation of the elemental and mineralogical geochemistry of the same formation in the subsurface of the Aliso Canyon gas field. The outcrop area is near at least two exposed thrust faults and the outcrop is highly fractured and exhibited extensive areas of regolith, particularly near its contact with the overlying Topanga Upper Sandstone. The outcrop also exhibits extensive 'onion-skin' weathering that results in the formation of spheroids that vary in size from a few inches to 18" in diameter. The spheroids were easily disaggregated, but contained crystals discernable without magnification. The size of the crystals in the spheroids is indicative not of an extrusive basalt, but of a hypabyssal intrusive diabase. The presence of stringers of the overlying Topanga Upper Sandstone and the underlying Topanga Lower Sandstone in the 'basalt' is also indicative of an intrusive body. The rock is therefore labeled diabase rather than basalt and most likely represents a sill instead of a lava flow. Its formal name, Topanga Basalt, remains unchanged. The original intent of the sampling program was to obtain at least 16 1.5" x 20" core samples of the Topanga Basalt from its outcrop, but due to local regulations, coring was delayed and parred down to only eight locations. Once all local regulations were fulfilled, it was discovered that the extensive fracturing and weathering of the outcrop precluded the ability to obtain a quality core. Hand samples that represented the eight coring locations were chosen instead. Of the eight hand samples, six were chosen to represent the least weathered 'basalt' sample from that location; two samples from spheroids were chosen to represent moderate weathering, and one sample was chosen from regolith to represent the highest degree of weathering. The six least weathered samples are most likely the best surface representation of the subsurface Topanga Basalt. Thin section, Fourier Transform Infrared Spectroscopy (FTIR), and XRF analyses were conducted on all eight samples and the results of the detailed thin section analysis are reported here. FTIR results are also shown on the thin section description pages, but it should be noted and emphasized that FTIR was designed for and is calilbrated for sedimentary rocks, not igneous rocks. The results of the FTIR analysis are an approximation of the mineralogy of the basalt, but are not necessarily the true mineralogy of the system. The thin section analysis is a better approximation of the mineralogy of the Topanga Basalt, but it is not known if the fractured and weathered outcrop is a true representation of the subsurface basalt. Samples SGC-6HS and SGC-8HS1 were the least weathered outcrop samples and therefore the closest approximation of the subsurface rock, assuming that the fracturing and extensive weathering of the outcrop is due to uplift during thrusting and subsequent subaerial exposure of the outcrop. From the thin section analysis, the Topanga Basalt is most likely not a basalt, but a hypabyssal diabase sill that is predominantly plagioclase and pyroxene, with lesser abundances of biotite, amphibole, and olivine. Chlorite is abundant in all hand samples and, along with iron oxides, has extensively replaced biotite, amphibole, and olivine. Secondary (diagenetic) minerals are abundant, but other than chlorite, do not represent a major contribution to the geochemistry of the subsurface basalt.

Schlumberger for Third Party Data: Confidential

Analytical Procedures

Detailed Thin Section Analysis

Sample Preparation: Samples were impregnated with a low-viscosity, fluorescent blue-dye or red-dye epoxy resin under vacuum to highlight porosity. The impregnated samples were surfaced, mounted to standard (27 x 46 millimeter) thin section slides, and ground to a thickness of approximately 30 microns. The thin sections were then stained with a mixture of potassium ferricyanide and Alizarin Red "S" to aid in the identification of carbonate minerals. Thin sections are occasionally stained with sodium cobaltinitrate to aid in the identification of potassium feldspar.

Sample Imaging: Using a Nikon polarizing microscope, the prepared thin sections were examined and digitally imaged under transmitted plane-polarized, transmitted cross-polarized, and/or reflected UV light. The microscope is equipped with a Spot Insight digital camera, reflected light source, and various UV filters. All thin section images were taken in plane-polarized light, unless otherwise noted.

Thin Section Deliverables

The PDF document contains the Petrology Testing Matrix and one page for each sample analyzed petrographically. Zip file(s) for thin section images accompany the PDF. These files contain high-resolution, un-annotated versions (JPEGs) of the images included in the PDF's sample pages. Within the detailed thin section zip file(s), the filenames of lower magnification images end with "TS-01" and the filenames of higher magnification images end with "TS-02." If there are any additional images included, these images will end with TS-03, TS-04, etc.

Schlumberger for Third Party Data: Confidential

Table P1. Petrology Testing Matrix

Formation	Sample ID	Core Depth	HRA Class	Matrix/Interstitial Components (EDX)	Lithotype	FTIR	TS Scan	Det. TS	Det. SEM	XRD
Topanga Basalt	SGC-1 HSA	Outcrop	N/A	N/A	Diabase	X		X		
	SGC-2 HS	Outcrop	N/A	N/A	Diabase	X		X		
	SGC-4HS	Outcrop	N/A	N/A	Diabase	X		X		
	SGC-5 HS	Outcrop	N/A	N/A	Diabase	X		X		
	SGC-6 HS	Outcrop	N/A	N/A	Diabase	X		X		
	SGC-8 HS1	Outcrop	N/A	N/A	Diabase	X		X		
	SGC-8 HS2	Outcrop	N/A	N/A	Diabase	X		X		
	SGC-9W	Outcrop	N/A	N/A	Weathered diabase	X		X		
					TOTAL	**8**	**0**	**8**	**0**	**0**

Schlumberger for Third Party Data: Confidential

Client:	Southern California Gas	Project No.:	2018USHO-P194	Sample ID:	SGC-1 HSA	HRA
Well:	TH1-1	Formation:	Topanga Basalt	Core Depth:	Outcrop	N/A

THIN SECTION ANALYSIS

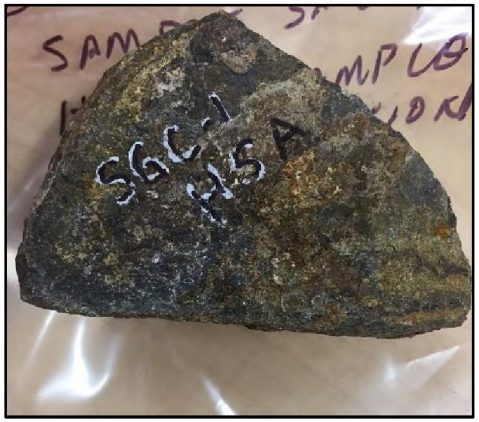

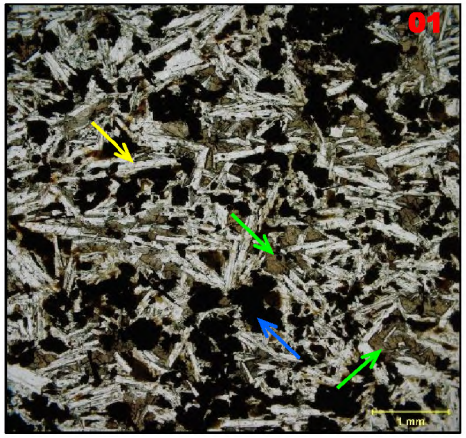

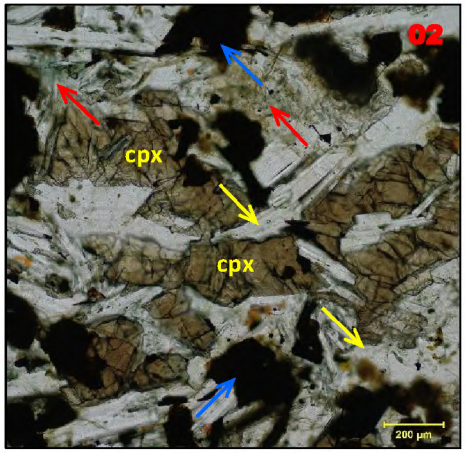

Diabase

Composition

predominantly plagioclase laths (yellow arrows, Images 01 and 02) with pyroxene (green arrows, Image 01; cpx, Image 02); amphiboles, biotite, and minor olivine are extensively altered and recognizable by crystal morphology only; additional minerals include chlorite (red arrows, Image 02), magnetite, hematite, amorphous iron oxides, rutile/anatase, and ilmenite

Texture

randomly oriented, twinned plagioclase laths that are 200 microns to 1 mm in length; pyroxene (cpx, Image 02) forms ophitic to subophitic texture that encloses plagioclase (yellow arrows, Images 01 and 02); this texture is typical of hypabyssal diabase

Clay Minerals

chlorite (red arrows, Image 02) is the predominant clay mineral observable at thin section scale; chlorite forms fibrous and platy masses that coat and replace grains and occurs as radiating crystals that also replace grains; chlorite color in thin section varies from bright green to greenish yellow; chlorite often exhibits anomalously high interference colors; very fine crystals of clays with high interference colors almost entirely replace certain minerals (blue arrows, Images 01 and 02)

Detrital Grains

Not applicable

Fossils

Not applicable

Organic Material

None observed

Diagenetic Minerals

chlorite is the predominant weathering product in this sample; other secondary minerals include iron oxides (hematite, limonite, goethite, and amorphous form), epidote, ilmenite, rutile/anatase, calcite, dolomite, ferroan dolomite, rhodochrosite, and magnesite; dark masses in images are partially opaque minerals and partially transparent reddish brown minerals that appear opaque in the images; in reflected light, the opaque minerals are magnetite, hematite, and rare pyrite; the transparent part of these minerals are extensively weathered crystals of amphibole, biotite, and/or olivine that have been replaced by very fine clays with high interference colors.

Additional Comments: hand sample selected was the least weathered sample from SGC-1 location

FTIR (Mineralogy in Relative Wt %)

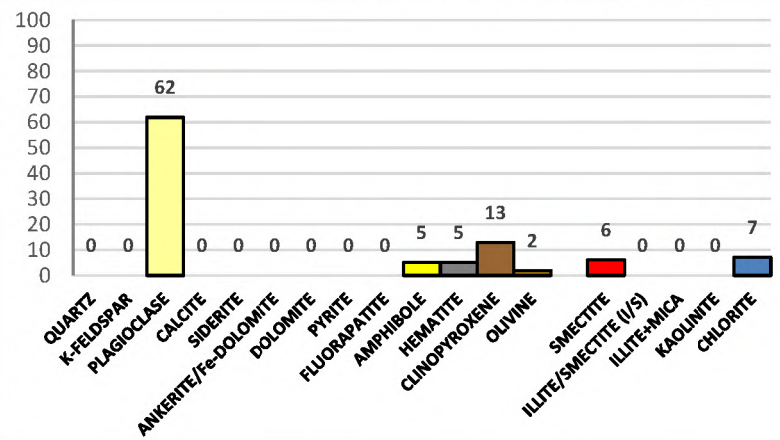

Total Expandable Clays (wt.%)	0

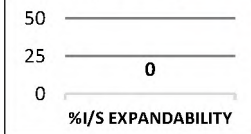

TRA	As-Received Grain Density (g/cc)	Effective Dry Grain Density (g/cc)	Gas Filled Porosity (% of BV)	Hydrocarbon-Filled Porosity (% of BV)	Effective Porosity (% of BV)	Effective Water Saturation (% of PV)	Effective Gas Saturation (% of PV)	Effective Oil Saturation (% of PV)	Bound Hydrocarbon (% of BV)	Clay-Bound Water (% of BV)	Structural Water (% of BV)	Pressure-Decay Permeability (nD)
	N/A	N/A	N/A	N/A	N/A	N/A	N/A	N/A	N/A	N/A	N/A	N/A
TOC/RE	As-Received Bulk Density (g/cc)	LECO TOC (wt%)		S1 (mg/g)	S2 (mg/g)	S3 (mg/g)	Tmax (°C)	HI	OI	S1*100 /TOC	PI	Calc Ro (%Ro)
	N/A	N/A		N/A	N/A	N/A	N/A	N/A	N/A	N/A	N/A	N/A

Schlumberger for Third Party Data: Confidential

Client:	Southern California Gas	Project No.:	2018USHO-P194	Sample ID:	SGC-2 HS	HRA
Well:	TH1-1	Formation:	Topanga Basalt	Core Depth:	Outcrop	N/A

THIN SECTION ANALYSIS

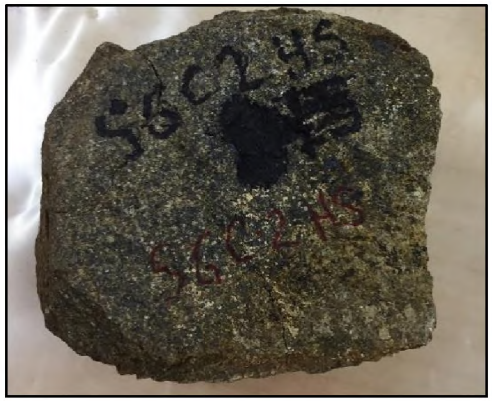

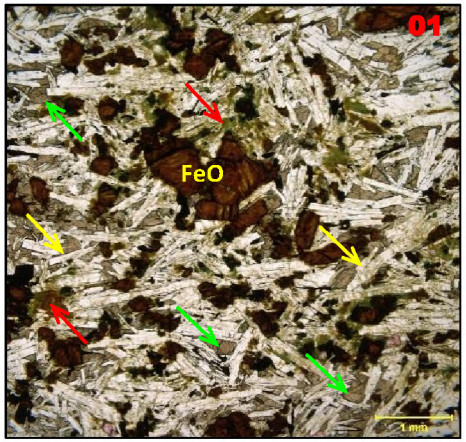

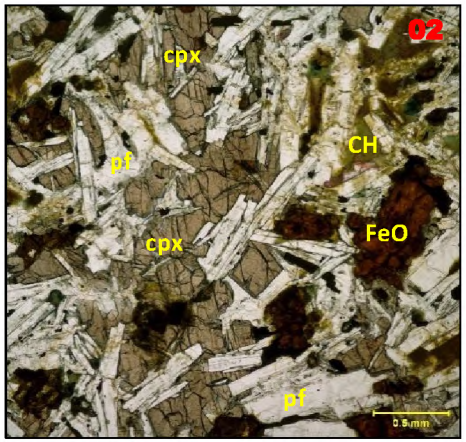

Diabase

Composition

predominantly plagioclase laths (yellow arrows, Image 01; pf, Image 02) with pyroxene (green arrows, Image 01; cpx, Image 02); amphiboles, biotite, and minor olivine are extensively altered and recognizable by crystal morphology only; additional minerals include chlorite (red arrow, Image 01; CH, Image 02), magnetite, hematite, amorphous iron oxides (FeO, Images 01 and 02), rutile/anatase, and ilmenite

Texture

randomly oriented, twinned plagioclase laths (yellow arrow, Image 01; pf, Image 02) are up to 1.5 mm in length; pyroxene (cpx, Image 02) forms ophitic to subophitic texture that encloses plagioclase; this texture is typical of hypabyssal diabase

Clay Minerals

chlorite (red arrows, Image 01; CH, Image 02) is the predominant clay mineral observable at thin section scale; chlorite forms fibrous and platy masses that coat and replace grains and occurs as radiating crystals that also replace grains; chlorite color in thin section varies from bright green to greenish yellow; chlorite often exhibits anomalously high interference colors

Detrital Grains

Not applicable

Fossils

Not applicable

Organic Material

None observed

Diagenetic Minerals

chlorite is the predominant weathering product in this sample; other secondary minerals include iron oxides (hematite, limonite, goethite, and amorphous form), epidote, ilmenite, rutile/anatase, calcite, dolomite, ferroan dolomite, rhodochrosite, and magnesite; the reddish brown minerals labeled FeO in Images 01 and 02 are mostly amorphous iron oxides, but show some platy, aligned zones with high interference colors that are indicative of chlorite, as well as patchy, mildly pleochroic zones that are indicative of biotite and/or amphibole; these minerals are therefore most likely originally biotite and amphibole that have been replaced by chlorite and subsequent amorphous iron oxides

Additional Comments: hand sample selected was the least weathered sample from SGC-2 location

FTIR (Mineralogy in Relative Wt %)

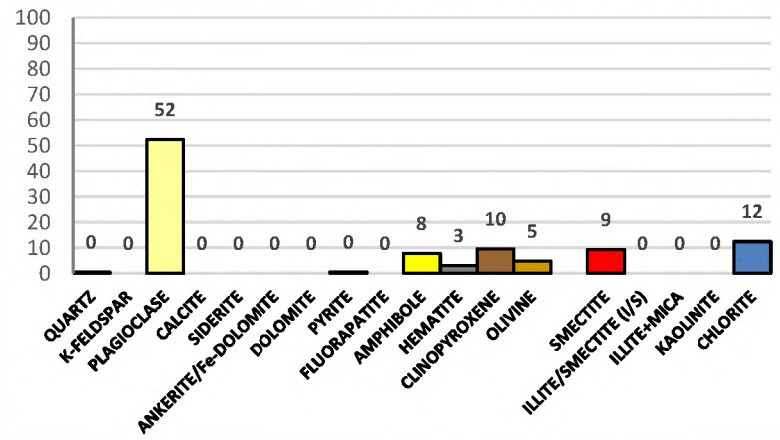

Total Expandable Clays (wt.%)	0

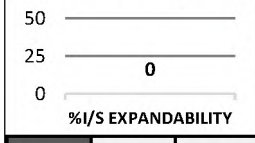

TRA	As-Received Grain Density (g/cc)	Effective Dry Grain Density (g/cc)	Gas Filled Porosity (% of BV)	Hydrocarbon-Filled Porosity (% of BV)	Effective Porosity (% of BV)	Effective Water Saturation (% of PV)	Effective Gas Saturation (% of PV)	Effective Oil Saturation (% of PV)	Bound Hydrocarbon (% of BV)	Clay-Bound Water (% of BV)	Structural Water (% of BV)	Pressure-Decay Permeability (nD)
	N/A	N/A	N/A	N/A	N/A	N/A	N/A	N/A	N/A	N/A	N/A	N/A
TOC/RE	As-Received Bulk Density (g/cc)	LECO TOC (wt%)		S1 (mg/g)	S2 (mg/g)	S3 (mg/g)	Tmax (°C)	HI	OI	S1*100 /TOC	PI	Calc Ro (%Ro)
	N/A	N/A		N/A	N/A	N/A	N/A	N/A	N/A	N/A	N/A	N/A

Schlumberger for Third Party Data: Confidential

Client:	Southern California Gas	Project No.:	2018USHO-P194	Sample ID:	SGC-4HS	HRA
Well:	TH1-1	Formation:	Topanga Basalt	Core Depth:	Outcrop	N/A

THIN SECTION ANALYSIS

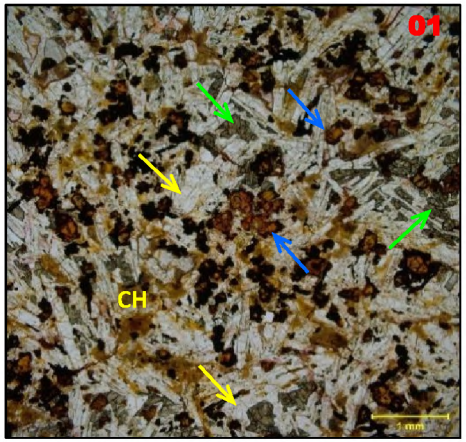

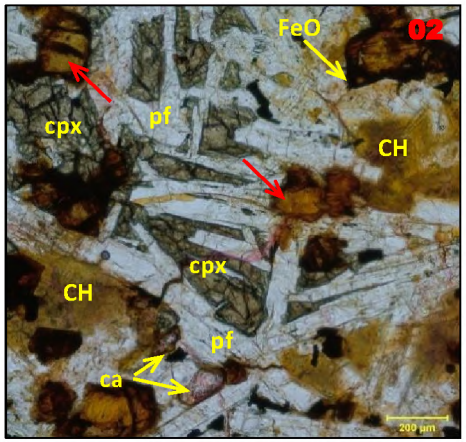

Diabase

Composition

predominantly plagioclase laths (yellow arrows, Image 01; pf, Image 02) with pyroxene (green arrows, Image 01; cpx, Image 02); amphiboles, biotite, and minor olivine are extensively altered and recognizable by crystal morphology only; additional minerals include chlorite (CH, Images 01 and 02), magnetite, hematite, and other iron oxides (blue arrows, Image 01; FeO, Image 02), rutile/anatase, and ilmenite

Texture

randomly oriented, twinned plagioclase laths (yellow arrows, Image 01; pf, Image 02) are up to 1.5 mm in length; pyroxene (cpx, Image 02) forms ophitic to subophitic texture that encloses plagioclase; this texture is typical of hypabyssal diabase

Clay Minerals

chlorite (CH, Images 01 and 02) is the predominant clay mineral observable at thin section scale; chlorite forms fibrous and platy masses that coat and replace grains and occurs as radiating crystals that also replace grains; chlorite color in thin section varies from bright green to greenish yellow; chlorite often exhibits anomalously high interference colors

Detrital Grains

Not applicable

Fossils

Not applicable

Organic Material

None observed

Diagenetic Minerals

chlorite is the predominant weathering product in this sample; other secondary minerals include iron oxides (hematite, limonite, goethite, and amorphous form), epidote, ilmenite, rutile/anatase, calcite (ca, Image 02), dolomite, ferroan dolomite, rhodochrosite, and magnesite; the reddish brown minerals labeled FeO form rims around crystals that have been replaced by very fine platy minerals that are aligned and exhibit the high interference colors that are indicative of chlorite (red arrows, Image 02), as well as patchy, mildly pleochroic zones that are indicative of biotite and/or amphibole; these crystals were most likely originally biotite and amphibole

Additional Comments: hand sample SGC-4HS is representative of the center portion of a spheroid of diabase that formed as a result of 'onion-skin' weathering

FTIR (Mineralogy in Relative Wt %)

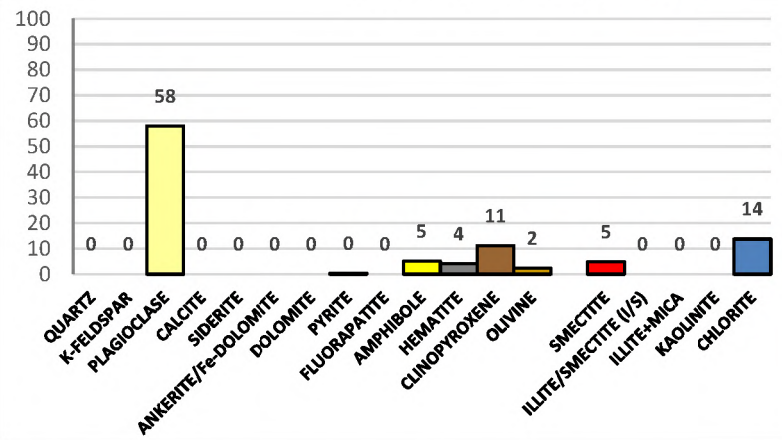

Total Expandable Clays (wt.%)	0

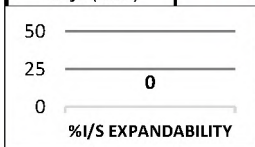

TRA	As-Received Grain Density (g/cc)	Effective Dry Grain Density (g/cc)	Gas Filled Porosity (% of BV)	Hydrocarbon-Filled Porosity (% of BV)	Effective Porosity (% of BV)	Effective Water Saturation (% of PV)	Effective Gas Saturation (% of PV)	Effective Oil Saturation (% of PV)	Bound Hydrocarbon (% of BV)	Clay-Bound Water (% of BV)	Structural Water (% of BV)	Pressure-Decay Permeability (nD)
	N/A	N/A	N/A	N/A	N/A	N/A	N/A	N/A	N/A	N/A	N/A	N/A
TOC/RE	As-Received Bulk Density (g/cc)	LECO TOC (wt%)		S1 (mg/g)	S2 (mg/g)	S3 (mg/g)	Tmax (°C)	HI	OI	S1*100 /TOC	PI	Calc Ro (%Ro)
	N/A	N/A		N/A	N/A	N/A	N/A	N/A	N/A	N/A	N/A	N/A

Schlumberger for Third Party Data: Confidential

Client:	Southern California Gas	Project No.:	2018USHO-P194	Sample ID:	SGC-5 HS	HRA
Well:	TH1-1	Formation:	Topanga Basalt	Core Depth:	Outcrop	N/A

THIN SECTION ANALYSIS

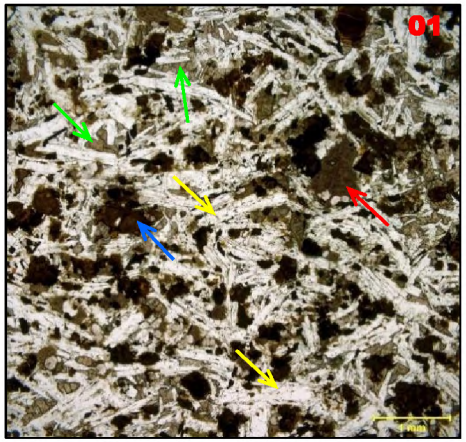

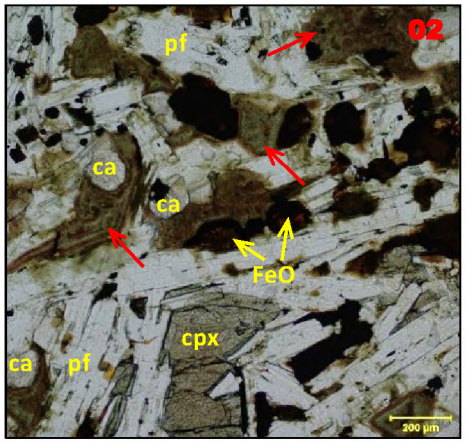

Diabase

Composition

predominantly plagioclase laths (yellow arrows, Image 01; pf, Image 02) with pyroxene (green arrows, Image 01; cpx, Image 02); amphiboles, biotite, and minor olivine are extensively altered and recognizable by crystal morphology only; additional minerals include chlorite (red arrow, Image 01), magnetite, hematite, and iron oxides (blue arrow, Image 01; FeO, Image 02), rutile/anatase, and ilmenite

Texture

randomly oriented, twinned plagioclase laths (yellow arrows, Image 01; pf, Image 02) are up to 1.5 mm in length; pyroxene (cpx, Image 02) forms ophitic to subophitic texture that encloses plagioclase; this texture is typical of hypabyssal diabase

Clay Minerals

chlorite is the predominant clay mineral observable at thin section scale; chlorite forms fibrous and platy masses that coat and replace grains and occurs as radiating crystals (red arrows, Images 01 and 02) that also replace grains; chlorite color in thin section varies from bright green to greenish yellow; chlorite often exhibits anomalously high interference colors

Detrital Grains

Not applicable

Fossils

Not applicable

Organic Material

None observed

Diagenetic Minerals

chlorite is the predominant weathering product in this sample; other secondary minerals include iron oxides (hematite, limonite, goethite, and amorphous form), epidote, ilmenite, rutile/anatase, calcite (ca, Image 02), dolomite, ferroan dolomite, rhodochrosite, and magnesite; the reddish brown minerals labeled FeO are mostly amorphous oxides that have replaced zones of very fine platy minerals that are aligned and exhibit the high interference colors that are indicative of chlorite (red arrows, Image 02), as well as patchy, mildly pleochroic zones that are indicative of biotite and/or amphibole; these crystals were most likely originally biotite and/or amphibole; hematite or a similar iron oxide rims areas now filled with radial chlorite

Additional Comments: hand sample selected was the least weathered sample from SGC-5 location

FTIR (Mineralogy in Relative Wt %)

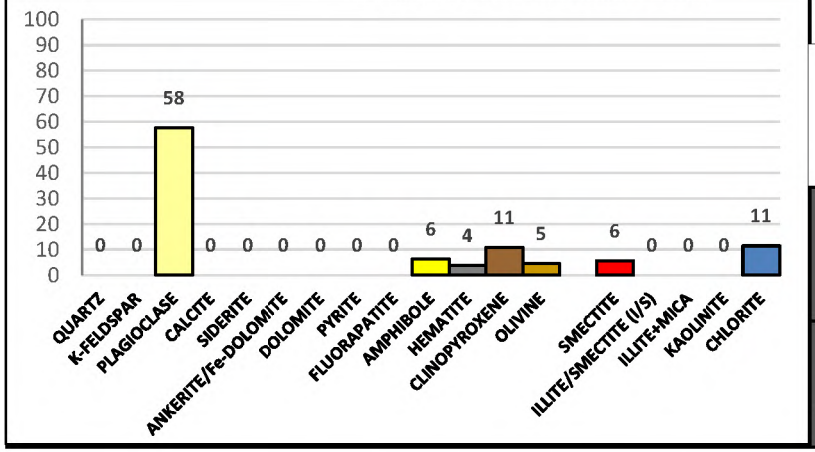

Total Expandable Clays (wt.%)	0

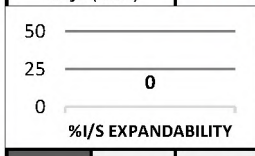

TRA	As-Received Grain Density (g/cc)	Effective Dry Grain Density (g/cc)	Gas Filled Porosity (% of BV)	Hydrocarbon-Filled Porosity (% of BV)	Effective Porosity (% of BV)	Effective Water Saturation (% of PV)	Effective Gas Saturation (% of PV)	Effective Oil Saturation (% of PV)	Bound Hydrocarbon (% of BV)	Clay-Bound Water (% of BV)	Structural Water (% of BV)	Pressure-Decay Permeability (nD)
	N/A	N/A	N/A	N/A	N/A	N/A	N/A	N/A	N/A	N/A	N/A	N/A
TOC/RE	As-Received Bulk Density (g/cc)	LECO TOC (wt%)		S1 (mg/g)	S2 (mg/g)	S3 (mg/g)	Tmax (°C)	HI	OI	S1*100 /TOC	PI	Calc Ro (%Ro)
	N/A	N/A		N/A	N/A	N/A	N/A	N/A	N/A	N/A	N/A	N/A

Schlumberger for Third Party Data: Confidential

Client:	Southern California Gas	Project No.:	2018USHO-P194	Sample ID:	SGC-6 HS	HRA
Well:	TH1-1	Formation:	Topanga Basalt	Core Depth:	Outcrop	N/A

THIN SECTION ANALYSIS

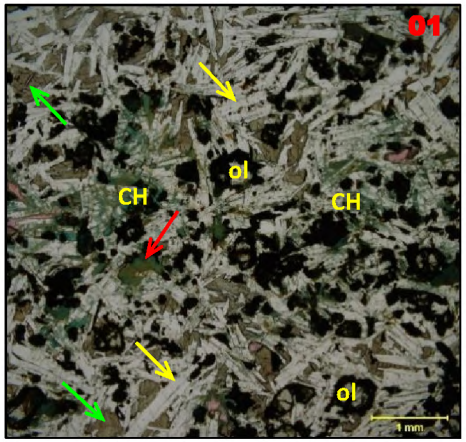

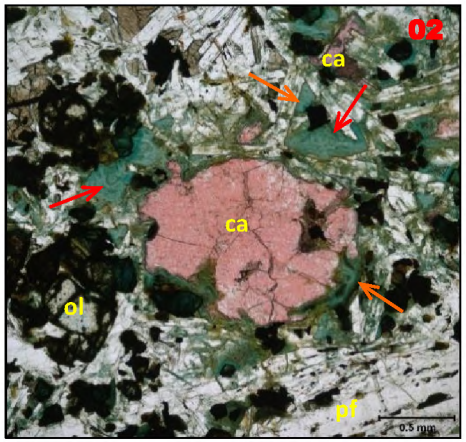

Diabase

Composition

predominantly plagioclase laths (yellow arrows, Image 01; pf, Image 02) with pyroxene (green arrows, Image 01); minor olivine (ol, Images 01 and 02) is weathered, but some crystals are recognizable by crystal morphology and high interference colors; additional minerals include chlorite (CH, Image 01; red arrows, Image 01), magnetite, hematite (orange arrows, Image 02), and other iron oxides (opaque minerals, Images 01 and 02), rutile/anatase, and ilmenite

Texture

randomly oriented, twinned plagioclase laths (yellow arrows, Image 01; pf, Image 02) are up to 1 mm in length; pyroxene forms ophitic to subophitic texture that encloses plagioclase; this texture is typical of hypabyssal diabase

Clay Minerals

chlorite is the predominant clay mineral observable at thin section scale; chlorite forms fibrous and platy masses that coat and replace grains and occurs as radiating, zoned crystals (red arrows, Images 01 and 02) that also replace grains; chlorite color in thin section varies from bright green to greenish yellow; chlorite often exhibits anomalously high interference colors

Detrital Grains

Not applicable

Fossils

Not applicable

Organic Material

None observed

Diagenetic Minerals

chlorite is the predominant weathering product in this sample; other secondary minerals include iron oxides (hematite, limonite, goethite, and amorphous form), epidote, ilmenite, rutile/anatase, calcite (pink crystals, Image 01; ca, Image 02), dolomite, ferroan dolomite, rhodochrosite, and magnesite; opaque rims of iron oxide minerals are common; reddish brown hematite (orange arrows, Images 01 and 02) rims radiated chlorite

Additional Comments: hand sample selected was the least weathered sample from SGC-6 location; this sample appeared in hand specimen to be one of the least weathered of all of the hand samples collected

FTIR (Mineralogy in Relative Wt %)

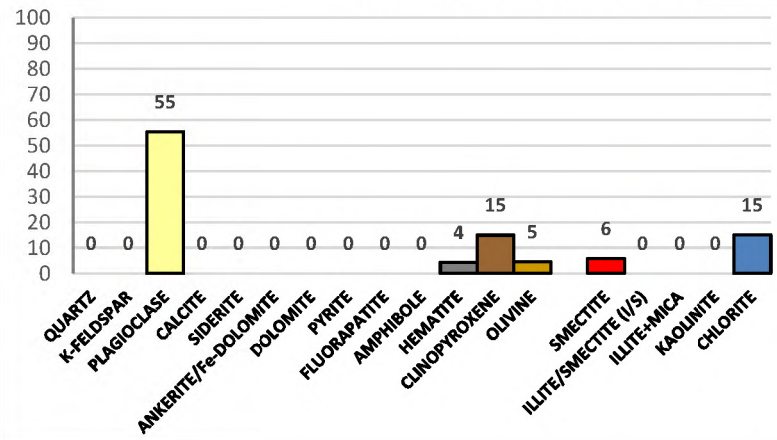

Total Expandable Clays (wt.%)	0

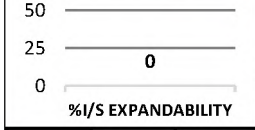

TRA	As-Received Grain Density (g/cc)	Effective Dry Grain Density (g/cc)	Gas Filled Porosity (% of BV)	Hydrocarbon-Filled Porosity (% of BV)	Effective Porosity (% of BV)	Effective Water Saturation (% of PV)	Effective Gas Saturation (% of PV)	Effective Oil Saturation (% of PV)	Bound Hydrocarbon (% of BV)	Clay-Bound Water (% of BV)	Structural Water (% of BV)	Pressure-Decay Permeability (nD)
	N/A	N/A	N/A	N/A	N/A	N/A	N/A	N/A	N/A	N/A	N/A	N/A
TOC/RE	As-Received Bulk Density (g/cc)	LECO TOC (wt%)		S1 (mg/g)	S2 (mg/g)	S3 (mg/g)	Tmax (°C)	HI	OI	S1*100 /TOC	PI	Calc Ro (%Ro)
	N/A	N/A		N/A	N/A	N/A	N/A	N/A	N/A	N/A	N/A	N/A

Schlumberger for Third Party Data: Confidential

Client:	Southern California Gas	Project No.:	2018USHO-P194	Sample ID:	SGC-8 HS1	HRA
Well:	TH1-1	Formation:	Topanga Basalt	Core Depth:	Outcrop	N/A

THIN SECTION ANALYSIS

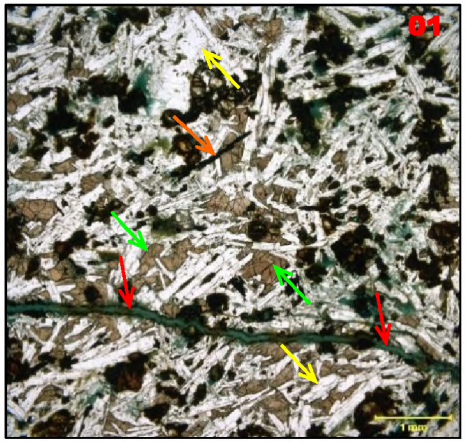

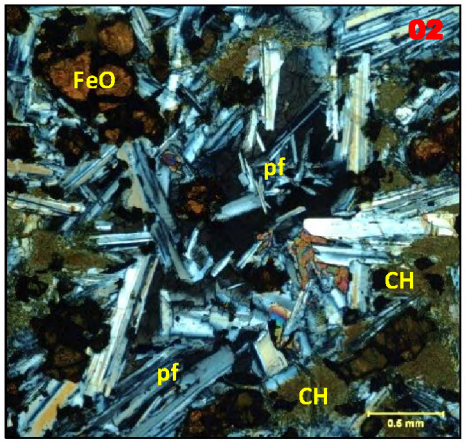

Diabase

Composition

predominantly plagioclase laths (yellow arrows, Image 01; pf, Image 02) with pyroxene (green arrows, Image 01); biotite, amphibole, and minor olivine are extensively weathered and recognizable by crystal morphology only; additional minerals include chlorite (green patches, Image 01; CH, Image 02), magnetite (orange arrow, Image 01), hematite, and other iron oxides, rutile/anatase, and ilmenite

Texture

randomly oriented plagioclase laths exhibit twinning (pf, Image 02) under cross Nicols are up to 1.25 mm in length; pyroxene forms ophitic to subophitic texture that encloses plagioclase; this texture is typical of hypabyssal diabase

Clay Minerals

chlorite is the predominant clay mineral observable at thin section scale; chlorite forms fibrous and platy masses that coat and replace grains and occurs as radiating, zoned crystals that also replace grains and fill a fracture (red arrows, Image 01); chlorite color in thin section varies from bright green to greenish yellow; chlorite often exhibits anomalously high interference colors

Detrital Grains

Not applicable

Fossils

Not applicable

Organic Material

None observed

Diagenetic Minerals

chlorite is the predominant weathering product in this sample; other secondary minerals include iron oxides (hematite, limonite, goethite, and amorphous form), epidote, ilmenite, rutile/anatase, calcite, dolomite, ferroan dolomite, rhodochrosite, and magnesite; opaque rims of iron oxide minerals are common; amorphous iron oxide (FeO, Image 02) has patches of very fine clays that exhibit high interference colors, as well as areas that are mildly pleochroic; these minerals were most likely initially biotite and/or amphiboles that were replaced by chlorite and iron oxides

Additional Comments: hand sample selected was the least weathered sample from SGC-8 location; this sample appeared in hand specimen to be one of the least weathered of all of the hand samples collected; Image 02 taken in crossed Nicols; thin section is slightly > 30 um thick

FTIR (Mineralogy in Relative Wt %)

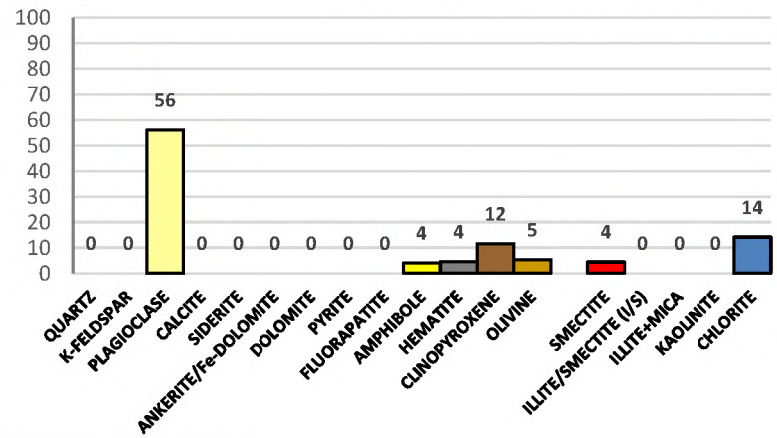

Total Expandable Clays (wt.%)	0

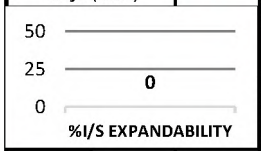

TRA	As-Received Grain Density (g/cc)	Effective Dry Grain Density (g/cc)	Gas Filled Porosity (% of BV)	Hydrocarbon-Filled Porosity (% of BV)	Effective Porosity (% of BV)	Effective Water Saturation (% of PV)	Effective Gas Saturation (% of PV)	Effective Oil Saturation (% of PV)	Bound Hydrocarbon (% of BV)	Clay-Bound Water (% of BV)	Structural Water (% of BV)	Pressure-Decay Permeability (nD)
	N/A	N/A	N/A	N/A	N/A	N/A	N/A	N/A	N/A	N/A	N/A	N/A
TOC/RE	As-Received Bulk Density (g/cc)	LECO TOC (wt%)		S1 (mg/g)	S2 (mg/g)	S3 (mg/g)	Tmax (°C)	HI	OI	S1*100 /TOC	PI	Calc Ro (%Ro)
	N/A	N/A		N/A	N/A	N/A	N/A	N/A	N/A	N/A	N/A	N/A

Schlumberger for Third Party Data: Confidential

Client:	Southern California Gas	Project No.:	2018USHO-P194	Sample ID:	SGC-8 HS2	HRA
Well:	TH1-1	Formation:	Topanga Basalt	Core Depth:	Outcrop	N/A

THIN SECTION ANALYSIS

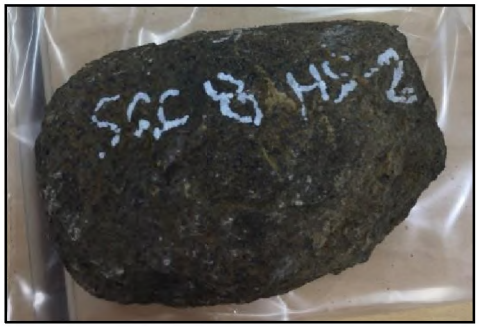

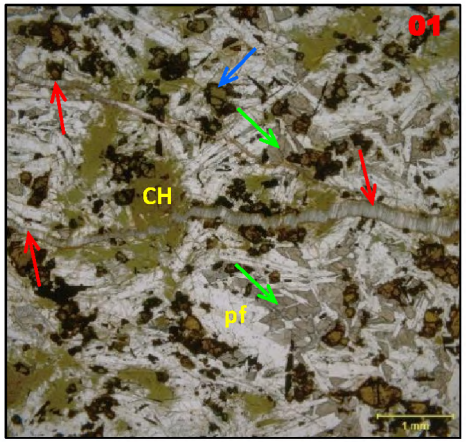

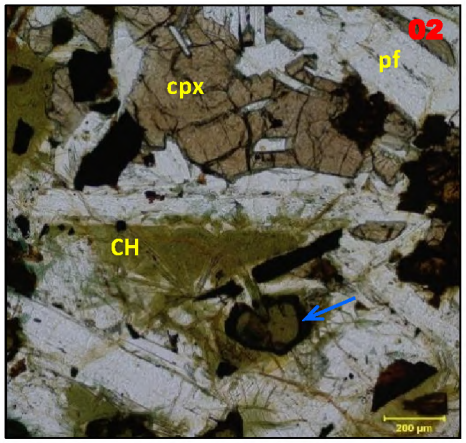

Diabase

Composition

predominantly plagioclase laths (pf, Images 01 and 02) with pyroxene (green arrows, Image 01; cpx, Image 02); biotite, amphibole, and minor olivine are extensively weathered and recognizable by crystal morphology only; additional minerals include chlorite (CH, Image 02), magnetite, hematite, and other iron oxides, rutile/anatase, and ilmenite

Texture

randomly oriented plagioclase laths exhibit twinning (pf, Image 02) under cross Nicols are up to 1.25 mm in length; pyroxene forms ophitic to subophitic texture that encloses plagioclase; this texture is typical of hypabyssal diabase

Clay Minerals

chlorite is the predominant clay mineral observable at thin section scale; chlorite forms fibrous and platy masses that coat and replace grains and occurs as radiating, zoned crystals that also replace grains; chlorite color in thin section varies from bright green to greenish yellow; chlorite often exhibits anomalously high interference colors

Detrital Grains

Not applicable

Fossils

Not applicable

Organic Material

None observed

Diagenetic Minerals

chlorite is the predominant weathering product in this sample; other secondary minerals include iron oxides (hematite, limonite, goethite, and amorphous form), epidote, ilmenite, rutile/anatase, calcite, dolomite, ferroan dolomite, rhodochrosite, and magnesite; opaque rims of iron oxide minerals (blue arrows, Images 01 and 02) are common and generally enclose chlorite in this sample; a set of fractures (red arrows, Image 01) is filled with very fine crystals that exhibit anomalously high interference colors; the fill mineral is most likely calcite, but the very small size of the crystals make identification difficult in thin section

Additional Comments: hand sample SGC-8 HS2 was taken from a spheroid of weathered diabase adjacent to hand sample SGC-8 HS1 and was chosen as a comparison between those areas that exhibited 'onion-skin' weathering and those that did not

FTIR (Mineralogy in Relative Wt %)

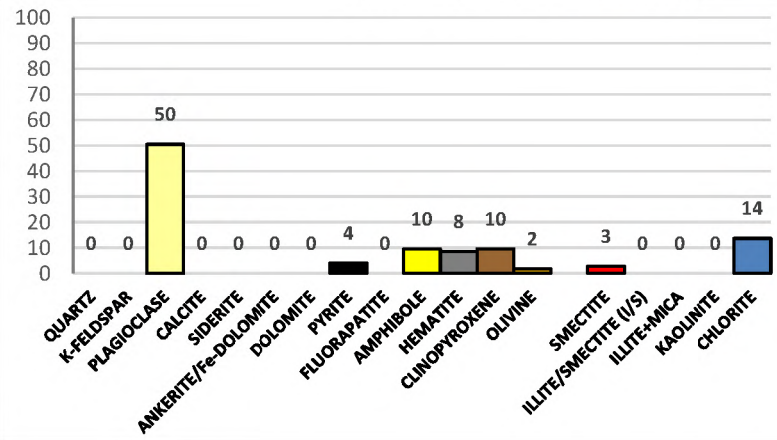

Total Expandable Clays (wt.%)	0

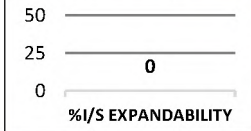

TRA	As-Received Grain Density (g/cc)	Effective Dry Grain Density (g/cc)	Gas Filled Porosity (% of BV)	Hydrocarbon-Filled Porosity (% of BV)	Effective Porosity (% of BV)	Effective Water Saturation (% of PV)	Effective Gas Saturation (% of PV)	Effective Oil Saturation (% of PV)	Bound Hydrocarbon (% of BV)	Clay-Bound Water (% of BV)	Structural Water (% of BV)	Pressure-Decay Permeability (nD)
	N/A	N/A	N/A	N/A	N/A	N/A	N/A	N/A	N/A	N/A	N/A	N/A
TOC/RE	As-Received Bulk Density (g/cc)	LECO TOC (wt%)		S1 (mg/g)	S2 (mg/g)	S3 (mg/g)	Tmax (°C)	HI	OI	S1*100 /TOC	PI	Calc Ro (%Ro)
	N/A	N/A		N/A	N/A	N/A	N/A	N/A	N/A	N/A	N/A	N/A

Schlumberger for Third Party Data: Confidential

Client:	Southern California Gas	Project No.:	2018USHO-P194	Sample ID:	SGC-9W	HRA
Well:	TH1-1	Formation:	Topanga Basalt	Core Depth:	Outcrop	N/A

THIN SECTION ANALYSIS

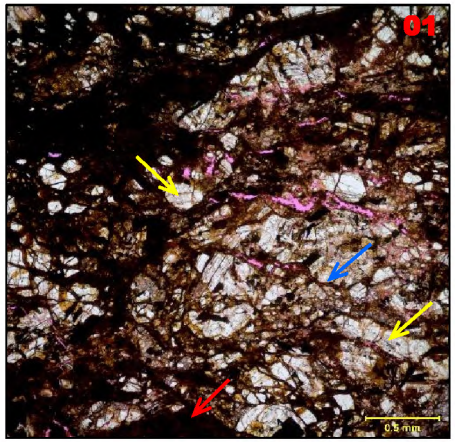

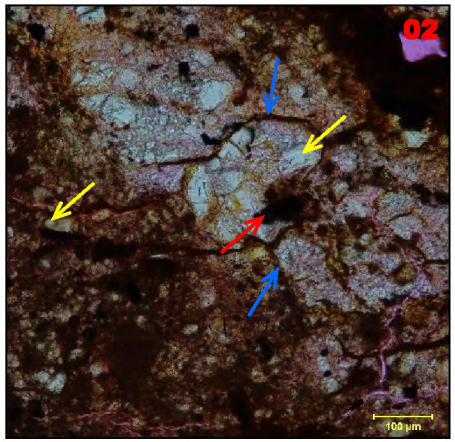

Weathered diabase

Composition

twinned plagioclase laths (yellow arrows, Images 01 and 02) are broken and weathered; pyroxene is also broken and weathered and less abundant than in other samples

sample is comprised of crushed mineral fragments bimodal in size; larger fragments are up to 100 microns in length and are contained in patches rimmed by hematite (blue arrows, Images 01 and 02) and surrounded by a finer grained 'matrix' that appears to be predominantly clays, iron oxides, and very small fragments of plagioclase and pyroxene

Clay Minerals

chlorite is the only discernable clay in thin section

Detrital Grains

Not applicable

Fossils

Not applicable

Organic Material

None observed

Diagenetic Minerals

chlorite is the predominant weathering product in this sample; other secondary minerals include iron oxides (hematite, limonite, and goethite); opaque iron oxide minerals (red arrows, Images 01 and 02) are common; the fuchsia epoxy combines with limonite and hematite to give this sample a pinkish coloring in thin section

Additional Comments: Sample SGC-9Wwas specially chosen to represent the most weathered end member from the diabase outcrop area

FTIR (Mineralogy in Relative Wt %)

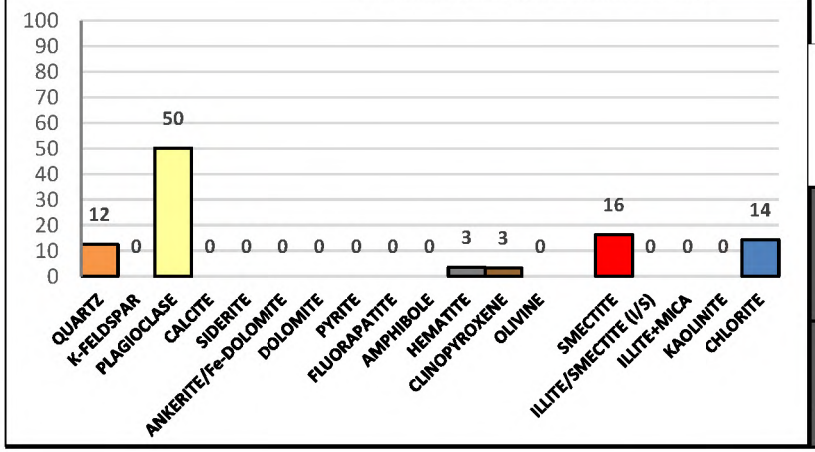

Total Expandable Clays (wt.%)	0

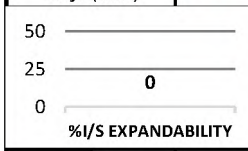

TRA	As-Received Grain Density (g/cc)	Effective Dry Grain Density (g/cc)	Gas Filled Porosity (% of BV)	Hydrocarbon-Filled Porosity (% of BV)	Effective Porosity (% of BV)	Effective Water Saturation (% of PV)	Effective Gas Saturation (% of PV)	Effective Oil Saturation (% of PV)	Bound Hydrocarbon (% of BV)	Clay-Bound Water (% of BV)	Structural Water (% of BV)	Pressure-Decay Permeability (nD)
	N/A	N/A	N/A	N/A	N/A	N/A	N/A	N/A	N/A	N/A	N/A	N/A
TOC/RE	As-Received Bulk Density (g/cc)	LECO TOC (wt%)		S1 (mg/g)	S2 (mg/g)	S3 (mg/g)	Tmax (°C)	HI	OI	S1*100 /TOC	PI	Calc Ro (%Ro)
	N/A	N/A		N/A	N/A	N/A	N/A	N/A	N/A	N/A	N/A	N/A

Schlumberger for Third Party Data: Confidential

Schlumberger

Routine Core Analysis Report

Prepared for: Southern California Gas

Well: TH-1 1

Schlumberger Confidential

Prepared by:
Schlumberger Reservoir Laboratories
6350 W. Sam Houston Parkway N, Suite 200
Houston, Texas 77041, USA
(713) 482-0700

Date: Sep 28 2018

Project No: 2018USHO-P194

Disclaimer

The following disclaimer applies to this report and any interpretation provided by any of the Laboratories that comprise the Schlumberger Reservoir Laboratories:

Any interpretation, research, analysis, or recommendation furnished with the services or otherwise communicated by Schlumberger Reservoir Laboratories to Customer at any time in connection with the services are opinions based on inferences from measurements and empirical relationships and assumptions, which inferences and assumptions are not infallible, and with respect to which professionals in the industry may differ. Accordingly, Schlumberger Reservoir Laboratories cannot and does not warrant the accuracy, correctness or completeness of any such interpretation or description.

Customer acknowledges that It is accepting the services "as is", that Schlumberger Reservoir Laboratories makes no representation or warranty, express or implied, of any kind or description in respect thereto, and that such services are delivered with the explicit understanding and agreement that any action customer may take based on the services received shall be at its own risk and responsibility and customer shall have no claim against Schlumberger Reservoir Laboratories as a consequence thereof.

Customer confirms that Schlumberger Reservoir Laboratories has made no promise or statement regarding the services that is inconsistent with these terms, or that has created or amounted to a warranty that the services would conform to any such promise or statement, and Schlumberger Reservoir Laboratories disclaims any and all warranties regarding the same.

Schlumberger Confidential

Quality Assurance Process

Schlumberger is committed to providing unsurpassed services in reservoir sampling and analyses while maintaining high standards of safety and quality. Our objective is to deliver the most accurate and reliable sampling processes and fluid and rock property measurements available in the industry. This objective requires persistent innovation and ongoing development of state-of-the-art technologies and equipment.

A rigorous quality assurance program, continuous employee training and enforcement of strict safety standards maintain our compliance with quality, health, safety, and environment (QHSE) requirements. Proactive integration of QHSE objectives and management goals at every level supports the communication and implementation of QHSE policies and standards. Schlumberger requires that qualified engineering technologists perform all laboratory measurements according to specified analytical procedures designed for obtaining accurate and reliable data.

The lab-generated data undergo the following five levels of quality checks to establish the integrity of the reported results.

a) Establish quality of measurement during data generation.
b) Lab supervisor and manager confirm the overall quality of the generated data.
c) Project manager reviews and processes generated data and generates reports.
d) Technical advisors confirm consistency of reported data.
e) Project manager finalizes reports.

Hence, the completion of each project requires that a qualified and experienced team of engineers perform a variety of independent reviews of all technical data to confirm the consistency and accuracy of the report as per pre-established quality checklists designed for each operation and based on the level of complexity. All property measurements and calculation procedures are maintained in company archives for a period of one year. This information is available for review by clients upon request.

The file and laboratory records information is listed below to provide access reference to all records related to this project. For any questions, please do not hesitate to contact the undersigned project manager.

File No.: 2018USHO-P194

Laboratory Procedures

Micah Alexander
Routine Core Analysis Supervisor

Reviewed by

X	Fabrice Pairoys	Data Assurance Team Lead
X	Gloria Besil	Data Quality Engineer

Project Management

Dustin Mortensen
Project Engineer

Schlumberger Confidential

Table of Contents

Disclaimer i
Quality Assurance ii
Summary 1
Table 1. Density Data 2

Schlumberger Confidential

Summary

Eight samples were selected for bulk density and grain density as shown below.

Experimental Program

Bulk density was calculated for all samples using the mass and bulk volume measured by immersion of the rocks in water. The average mass of the samples was 18.74 grams with a minimum and maximum mass of 5.84 grams and 30.15 grams respectively.

Grain volume was measured at ambient conditions using a CoreTest PHI-220 system. This measurement is based on helium expansion and Boyle's law.

System Quality Assurance & Control QA/QC

A set of rock sample standards for the PHI-220 system are tested daily to ensure the good calibration of the system. In addition, every fifth client sample is re-run to check repeatability.

a) For grain density, a rock standard of known density (such as Berea for sandstone rocks, Indiana limestone for carbonate rocks...) is measured on the PHI-220 apparatus after every fifth client's sample;

b) For pore volume, several metallic cylinders with inner holes of different diameters, covering a wide range of porosities, are tested on PHI-220 system. This step is performed every morning before the test to ensure a good data quality of pore volume measurements made on the client's samples;

Reference

1. Recommended Practices for Core Analysis, American Petroleum Institute, Recommended Practice 40, 2nd edition, Feb.1998, pages 6-35 and 6-55.

Schlumberger Confidential

Table 1. Density Data

Sample ID	Depth	Sample Mass (g)	Bulk Density (g/cm^3)	Post BD Sample Mass (g)	Grain Density (g/cm^3)
SGC-1 HSA	N/A	14.10	2.72	13.74	2.81
SGC-2 HS	N/A	25.86	2.56	24.39	2.80
SGC-4HS	N/A	25.83	2.80	25.65	2.81
SGC-5 HS	N/A	9.541	2.66	9.085	2.85
SGC-6 HS	N/A	17.15	2.74	16.86	2.81
SGC-8 HS1	N/A	30.15	2.76	29.80	2.81
SGC-8 HS2	N/A	21.45	2.76	21.13	2.81
SGC-9W	N/A	5.835	2.28	5.557	2.60

Schlumberger Confidential

SS-25 RCA Supplementary Report

SS-25 7 in. Casing Load Analysis

Purpose:
Evaluate and analyze the 7 in. casing loads to determine the load conditions that could cause the production casing failure observed in the well.

Date:
May 31, 2019

BLADE ENERGY PARTNERS

2600 Network Boulevard, Suite 550
Frisco, Texas 75034

+1 972-712-8407 (phone)
+1 972-712-8408 (fax)

16285 Park Ten Place, Suite 600
Houston, Texas 77084

1-800-319-2940 (toll free)
+1 281-206-2000 (phone)
+1 281-206-2005 (fax)

www.blade-energy.com

Blade Energy Partners Limited, and its affiliates ('Blade') provide our services subject to our General Terms and Conditions ('GTC') in effect at time of service, unless a GTC provision is expressly superseded in a separate agreement made with Blade. Blade's work product is based on information sources which we believe to be reliable, including information that was publicly available and that was provided by our client; but Blade does not guarantee the accuracy or completeness of the information provided. All statements are the opinions of Blade based on generally-accepted and reasonable practices in the industry. Our clients remain fully responsible for all clients' decisions, actions and omissions, whether based upon Blade's work product or not; and Blade's liability solely extends to the cost of its work product.

Abstract

The gas storage well Standard Sesnon 25 (SS-25) in the Aliso Canyon Gas Storage Field located in Los Angeles County, California started leaking gas in October 2015. A relief well was drilled, and SS-25 was brought under control. The leak stopped in February 2016.

In January 2016, as part of their investigation of the leak, the California Public Utilities Commission (CPUC) and the Division of Oil, Gas, and Geothermal Resources (DOGGR) selected and gave provisional authority to Blade Energy Partners (Blade) to perform an independent Root Cause Analysis (RCA). The Blade Team and parties under Blade's direction were responsible for directing the work of subcontractors who performed the extraction of the SS-25's wellhead, tubing, casings, and the preservation and protection of associated evidence. Blade's RCA Reports, including this report, document and describe the key activities undertaken in support of the RCA effort.

Numerous observations, including log data and downhole video, confirmed the 7 in. casing failure and leak at approximately 895 ft MD. The parted casing was extracted from the well in November 2017. Significant external corrosion was observed with accompanying wall loss at the location of the failure. A longitudinal rupture (indicative of a burst failure) was observed when the parted casing was recovered.

A detailed analysis of the 7 in. production casing was conducted to estimate the loads and the stresses caused by the loads applied to the casing leading up to the leak event. Load conditions were determined based on data collected during the RCA. The evaluation of the reduced casing burst strength caused by a reduction in casing wall thickness identified the remaining wall thickness (as a percent of nominal thickness) at which the casing would rupture when exposed to the well injection pressure.

Two methods of casing design were used in the analysis: Working Stress Design (WSD) and Reliability-Based Design (RBD). WSD is the conventional method of casing design used in the oil and gas industry. This method assumes maximum loads and minimum strength to calculate a Safety Factor (SF). SF of one or greater is the design criterion to determine if the design is acceptable. However, WSD has limitations when attempting to predict failure. For example, SF less than one does not indicate the casing will fail. Because of the limitations of WSD, RBD was used to estimate the probability of failure of the production casing for a range of remaining wall thickness. The RBD analysis showed that when the casing Remaining Body Wall (RBW) was below 30%, rupture of the casing could have been expected based on the load conditions.

Table of Contents

1 Introduction 7
1.1 Abbreviations and Acronyms 8
2 Data and Assumptions 9
2.1 Initial Condition Temperature Profile 9
2.2 Injection Conditions 9
2.3 Casing Pre-Tension 10
2.4 Wellbore Schematic 11
2.5 Wellbore Tubulars and Configuration 12
2.6 Directional Profile 13
3 Casing Load Analysis Methodology 14
3.1 Working Stress Design 14
3.2 Reliability-Based Design 14
4 Results and Discussion 17
4.1 Thermal Analysis 17
4.2 Load Analysis of the 7 in. Casing with Top of Cement Sensitivity Analysis 19
4.3 Effect of Wall Loss, Top of Cement at 7,000 ft MD 27
4.4 Effect of Wall Loss with Top of Cement at 990 ft MD 38
5 Conclusions 40
6 References 41
Appendix A **Detailed Results with Wall Loss, Top of Cement at 7,000 ft MD A-1**
Appendix B **Detailed Results with Effect of Wall Loss, Top of Cement at 990 ft MD B-1**

List of Figures

Figure 1: SS-25 Initial Condition Temperature Profile 9
Figure 2: SS-25 Well Schematic 11
Figure 3: SS-25 Tubular Specifications 12
Figure 4: SS-25 Well Configuration 12
Figure 5: SS-25 Directional Profile 13
Figure 6: SS-25 Trajectory-Dogleg Severity 13
Figure 7: Level-4 Reliability-Based Design Analysis 15
Figure 8: Consideration of Corrosion Wall Loss in Wall Thickness Distribution 16
Figure 9: SS-25 Withdrawal Temperature Profile 17
Figure 10: Steady State Injection Temperature Profiles for Different Inlet Temperatures 18
Figure 11: SS-25 Worst Case Cool Down Temperature Profile 19
Figure 12: Design Envelope–7 in. Casing Section from 0 ft to 895 ft MD with Top of Cement at 7,000 ft ... 22

Figure 13: Design Envelope–7 in. Casing Section from 896 ft to 2,398 ft MD with Top of Cement at 7,000 ft 22
Figure 14: Design Envelope–7 in. Casing Section from 0 ft to 895 ft MD with Top of Cement at 990 ft 25
Figure 15: Design Envelope–7 in. Casing Section from 896 ft to 2,398 ft MD with Top of Cement at 990 ft 25
Figure 16: Probability of Exceedance and Failure vs. Remaining Body Wall, Load Case "Steady State Gas Injection at 2,700 psi and 70°F Surface Temperature", Top of Cement at 7000 ft MD 37
Figure 17: Probability of Exceedance and Failure vs. Remaining Body Wall, Load Case "Injection at 2,700 psi with the Worst Case Cool Down" Temperature Profile, Top of Cement at 7000 ft MD 37
Figure 18: Probability of Exceedance and Probability of Failure for Load Case "Steady State Gas Injection at 2,700 psi and 70°F Surface Temperature", Top of Cement at 990 ft MD 38
Figure 19: Probability of Exceedance and Probability of Failure for Load Case "Injection at 2,700 psi with the Worst Case Cool Down Temperature Profile", Top of Cement at 990 ft MD 39
Figure 20: Probability of Exceedance vs. Remaining Body Wall for Triaxial Failure Mode A-3
Figure 21: Probability of Failure vs. Remaining Body Wall for Burst Failure Mode A-3
Figure 22: Probability of Exceedance vs. Remaining Body Wall for Triaxial Failure Mode A-5
Figure 23: Probability of Failure vs. Remaining Body Wall for Burst Failure Mode A-6
Figure 24: Probability of Exceedance vs. Remaining Body Wall for Triaxial Failure Mode A-8
Figure 25: Probability of Failure vs. Remaining Body Wall for Burst Failure Mode A-8
Figure 26: Probability of Exceedance vs. Remaining Body Wall for Triaxial Failure Mode A-11
Figure 27: Probability of Failure vs. Remaining Body Wall for Burst Failure Mode A-12
Figure 28: Probability of Exceedance vs. Remaining Body Wall for Triaxial Failure Mode B-13
Figure 29: Probability of Failure vs. Remaining Body Wall for Burst Failure Mode B-13
Figure 30: Probability of Exceedance vs. Remaining Body Wall for Triaxial Failure Mode B-15
Figure 31: Probability of Failure vs. Remaining Body Wall for Burst Failure Mode B-16
Figure 32: Probability of Exceedance vs. Remaining Body Wall for Triaxial Failure Mode B-17
Figure 33: Probability of Failure vs. Remaining Body Wall for Burst Failure Mode B-17
Figure 34: Probability of Failure vs. Remaining Body Wall for Triaxial Failure Mode B-20
Figure 35: Probability of Failure vs. Remaining Body Wall for Burst Failure Mode B-20

List of Tables

Table 1: Minimum Safety Factors 14
Table 2: Load Assumption for the 7 in. Casing 20
Table 3: Minimum Safety Factors for the 7 in. Casing with Top of Cement at 7,000 ft 21
Table 4: Internal and External Pressure, Axial Force, and Temperature at Depth of Interest (895 ft) 23
Table 5: Stresses at Depth of Interest (895 ft) 23
Table 6: Minimum Safety Factors for the 7 in. Casing with Top of Cement at 990 ft 24
Table 7: Internal and External Pressure, Axial Force, and Temperature at the Depth of Interest (895 ft) 26
Table 8: Stresses at Depth of Interest (895 ft) 26
Table 9: Minimum Safety Factors for the 7 in. Casing with 80% Remaining Body Wall 27
Table 10: Minimum Safety Factors for the 7 in. Casing with 70% Remaining Body Wall 28
Table 11: Minimum Safety Factors for the 7 in. Casing with 65% Remaining Body Wall 28
Table 12: Reliability-Based Design and Probability of Failure for the 7 in. Casing with 65% Remaining Body Wall 29
Table 13: Minimum Safety Factors for the 7 in. Casing with 60% Remaining Body Wall 30

Table 14: Reliability-Based Design and Probability of Failure for the 7 in. Casing with 60% Remaining Body Wall....30
Table 15: Minimum Safety Factors for the 7 in. Casing with 50% Remaining Body Wall....31
Table 16: Reliability-Based Design and Probability of Failure for the 7 in. Casing with 50% Remaining Body Wall....31
Table 17: Minimum Safety Factors for the 7 in. Casing with 40% Remaining Body Wall....32
Table 18: Reliability-Based Design and Probability of Failure for the 7 in. Casing with 40% Remaining Body Wall....32
Table 19: Minimum Safety Factors for the 7 in. Casing with 30% Remaining Body Wall....33
Table 20: Reliability—Based Design and Probability of Failure for the 7 in. Casing with 30% Remaining Body Wall....34
Table 21: Minimum Safety Factors for the 7 in. Casing with 20% Remaining Body Wall....35
Table 22: Reliability-Based Design and Probability of Failure for the 7 in. Casing with 20% Remaining Body Wall....35
Table 23: Probability of Exceedance vs. Remaining Body Wall for the 7 in. Casing for Triaxial Failure Mode A-1
Table 24: Probability of Failure vs. Remaining Body Wall for the 7 in. Casing for Burst Failure Mode.... A-2
Table 25: Probability of Exceedance vs. Remaining Body Wall for the 7 in. Casing for Triaxial Failure Mode A-4
Table 26: Probability of Failure vs. Remaining Body Wall for the 7 in. Casing for Burst Failure Mode.... A-5
Table 27: Probability of Exceedance vs. Remaining Body Wall for the 7 in. Casing for Triaxial Failure Mode A-7
Table 28: Probability of Failure vs. Remaining Body Wall for the 7 in. Casing for Burst Failure Mode.... A-7
Table 29: Probability of Exceedance vs. Remaining Body Wall for the 7 in. Casing for Triaxial Failure Mode A-9
Table 30: Probability of Failure vs. Remaining Body Wall for the 7 in. Casing for Burst Failure Mode.... A-10
Table 31: Minimum Safety Factors for the 7 in. Casing with 80% Remaining Body Wall....B-1
Table 32: Minimum Safety Factors for the 7 in. Casing with 70% Remaining Body Wall....B-2
Table 33: RBD Probability of Failure for the 7 in. Casing with 70% Remaining Body Wall....B-2
Table 34: Minimum Safety Factors for the 7 in. Casing with 65% Remaining Body Wall....B-3
Table 35: RBD Probability of Failure for the 7 in. Casing with 65% Remaining Body Wall....B-3
Table 36: Minimum Safety Factors for the 7 in. Casing with 60% Remaining Body Wall....B-4
Table 37: RBD Probability of Failure for the 7 in. Casing with 60% Remaining Body Wall....B-4
Table 38: Minimum Safety Factors for the 7 in. Casing with 50% Remaining Body Wall....B-5
Table 39: RBD Probability of Failure for the 7 in. Casing with 50% Remaining Body Wall....B-6
Table 40: Minimum Safety Factors for the 7 in. Casing with 40% Remaining Body Wall....B-6
Table 41: RBD Probability of Failure for the 7 in. Casing with 40% Remaining Body Wall....B-7
Table 42: Minimum Safety Factors for the 7 in. Casing with 30% Remaining Body Wall....B-8
Table 43: RBD Probability of Failure for the 7 in. Casing with 30% Remaining Body Wall....B-8
Table 44: Minimum Safety Factors for the 7 in. Casing with 20% Remaining Body Wall....B-9
Table 45: RBD Probability of Failure for the 7 in. Casing with 20% Remaining Body Wall....B-10
Table 46: Probability of Exceedance vs. Remaining Body Wall for the 7 in. Casing for Triaxial Failure Mode B-11
Table 47: Probability of Failure vs. Remaining Body Wall for the 7 in. Casing for Burst Failure Mode....B-12
Table 48: Probability of Exceedance vs. Remaining Body Wall for the 7 in. Casing for Triaxial Failure Mode B-14
Table 49: Probability of Failure vs. Remaining Body Wall for the 7 in. Casing for Burst Failure Mode....B-15

Table 50: Probability of Exceedance vs. Remaining Body Wall for the 7 in. Casing for Triaxial Failure Mode B-16
Table 51: Probability of Failure vs. Remaining Body Wall for the 7 in. Casing for Burst Failure Mode..... B-17
Table 52: Probability of Exceedance vs. Remaining Body Wall for the 7 in. Casing for Triaxial Failure Mode B-18
Table 53: Probability of Failure vs. Remaining Body Wall for the 7 in. Casing for Burst Failure Mode..... B-19

1 Introduction

The objective of the casing load analysis was to examine conditions under which casing failure could have occurred in the upper part of well SS-25. Specifically, the goal was to examine if the casing had been subjected to overload conditions that caused the leak incident on October 23, 2015. The reduction in wall thickness caused by metal loss from corrosion was a key parameter of the analysis.

The stresses on the 7 in. casing depend upon:

- The load conditions.
- The temperature change from the initial to the final load condition.
- The effective point of fixity of the casing.
- The RBW of the 7 in. casing.

A set of load cases was proposed to represent expected casing loads during the life of the well, particularly during the period immediately preceding the October 23, 2015 incident. Initial conditions (including applied overpull) were assumed to have created the casing stress state when the casing was run and cemented. Changes to the stress state caused by changes in pressure and temperature were calculated for each subsequent load case. For the injection load cases, an injection pressure of 2,700 psi was assumed based on reported conditions on and immediately before October 23, 2015. Because temperature of the casing decreased during injection, cool down temperature profiles were calculated for typical injection conditions. In addition, a cool down temperature profile recorded on November 8, 2015 [1] was considered because this represented measured temperature cool down of the casing and was the lowest temperature the casing likely experienced throughout its life.

The Top of Cement (TOC) was assumed to be the point of fixity for the 7 in. casing, and the TOC was confirmed by log data. The change in temperature of the uncemented casing above the TOC affected the axial force and stress state. Therefore, a TOC of 7,000 ft measured depth (MD) was assumed as the base case. However, over the long history of well usage, formation sloughing and cave-in at the 11 3/4 in. casing shoe (990 ft MD) may have led to bridging in the annulus. Bridging could have caused the 7 in. casing to behave as if it had been fixed at or just below the 11 3/4 in. shoe. This possibility was examined as a sensitivity case.

Finally, the RBW was a key sensitivity parameter reflecting wall reduction from corrosion. RBW was expressed as a percent of nominal wall with no wall loss as the base case.

For completeness, WSD checks were performed and the Safety Factors (SF) were reported. However, violation of WSD criteria does not imply failure—it merely implies inadequacy of design. Failure can only occur when the ultimate limit state of the tubular in the mode of interest is exceeded. Therefore, failure of casing was examined using the tension-burst limit state from API Technical Report 5C3 [2]. To account for uncertainties in the material properties and geometric parameters of the casing, a reliability-based approach was used to calculate the Probability of Failure (POF) of the casing for any given load case. The commercial software tool StrinGnosis[i] V 3.1was used in performing the probabilistic analyses. API Technical Report 5C3 [2] describes the basis of the statistical distributions for various strength-defining parameters, including wall thickness. A POF greater than 10^{-1} (greater than 90%) is interpreted as failure

[i] StrinGnosis is a tubular mechanics and wellbore heat transfer program developed and marketed by Blade Technology Corporation, LLC.

of the casing. Therefore, for any given load case, if the POF of the casing is lower than 10^{-1}, it is not considered a failure, even if the corresponding WSD factor of safety is less than the minimum required.

1.1 Abbreviations and Acronyms

Term	Definition
CPUC	California Public Utilities Commission
DLS	Dogleg Severity
DOGGR	Division of Oil, Gas, and Geothermal Resources, subsurface regulatory agency of the California state government
HPT	High-Precision Temperature
ID	Internal Diameter
klbf	Thousand Pounds Force
MD	Measured Depth
OCTG	Oil Country Tubular Goods
OD	Outside Diameter
POE	Probability of Exceedance
POF	Probability of Failure
RBD	Reliability-Based Design
RBW	Remaining Body Wall
RCA	Root Cause Analysis
SoCalGas	Southern California Gas Company, operator of Aliso Canyon Gas Storage Field
SF	Safety Factor
SS	Steady State
SS	Standard Sesnon
TOC	Top of Cement
TVD	True Vertical Depth
VME	Von Mises Equivalent
WSD	Working Stress Design

2 Data and Assumptions

The following sections discuss the well data used and key assumptions made when performing the analysis.

2.1 Initial Condition Temperature Profile

Figure 1 shows the initial condition temperature profile used in the analysis. It shows the long-term effects of gas injection near the bottom [3]. The temperature profile near the surface is affected by the hilly terrain–the well sits on a ridge with steep slopes on three sides of the site. The geothermal gradient is based on the Versa-Line's High-Precision Temperature (HPT) log run in April 2016. The cooling at the top (0–500 ft region) reflects the effect of cooling caused by the topography and structure of the well site. The cooling at the bottom is a consequence of injecting gas over a long period.

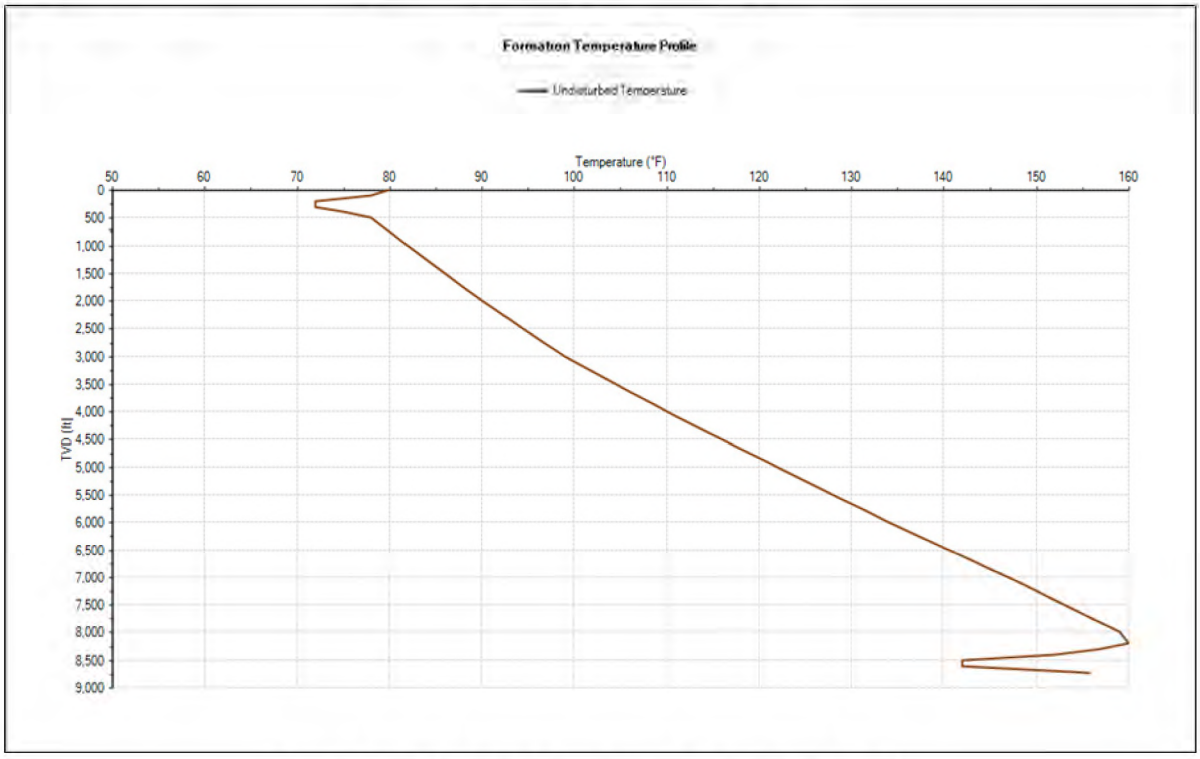

Figure 1: SS-25 Initial Condition Temperature Profile

2.2 Injection Conditions

The 7 in. casing was exposed to surface pressure variations during injection and withdrawal. The highest surface pressures occurred during injection. Based on the source material, the maximum injection pressure observed during the 2015 injection period was 2,700 psi [4]. This was the assumed pressure for the analysis in this report. The gas specific gravity was assumed to be 0.56.

2.3 Casing Pre-Tension

The 7 in. casing was installed with an imposed pre-tension caused by overpull. Based on data from the well work done in 1973 to convert well SS-25 from an oil well to a gas storage well, a pre-tension load was applied to match the tension of 196,000 lbf at the surface when the casing was landed [5]. This pre-tension was included in all of the analyses reported in this report.

2.4 Wellbore Schematic

Figure 2 shows the configuration of the well after it had been converted to gas storage in 1972 with the 7 in. casing TOC at 7,000 ft MD—the base case.

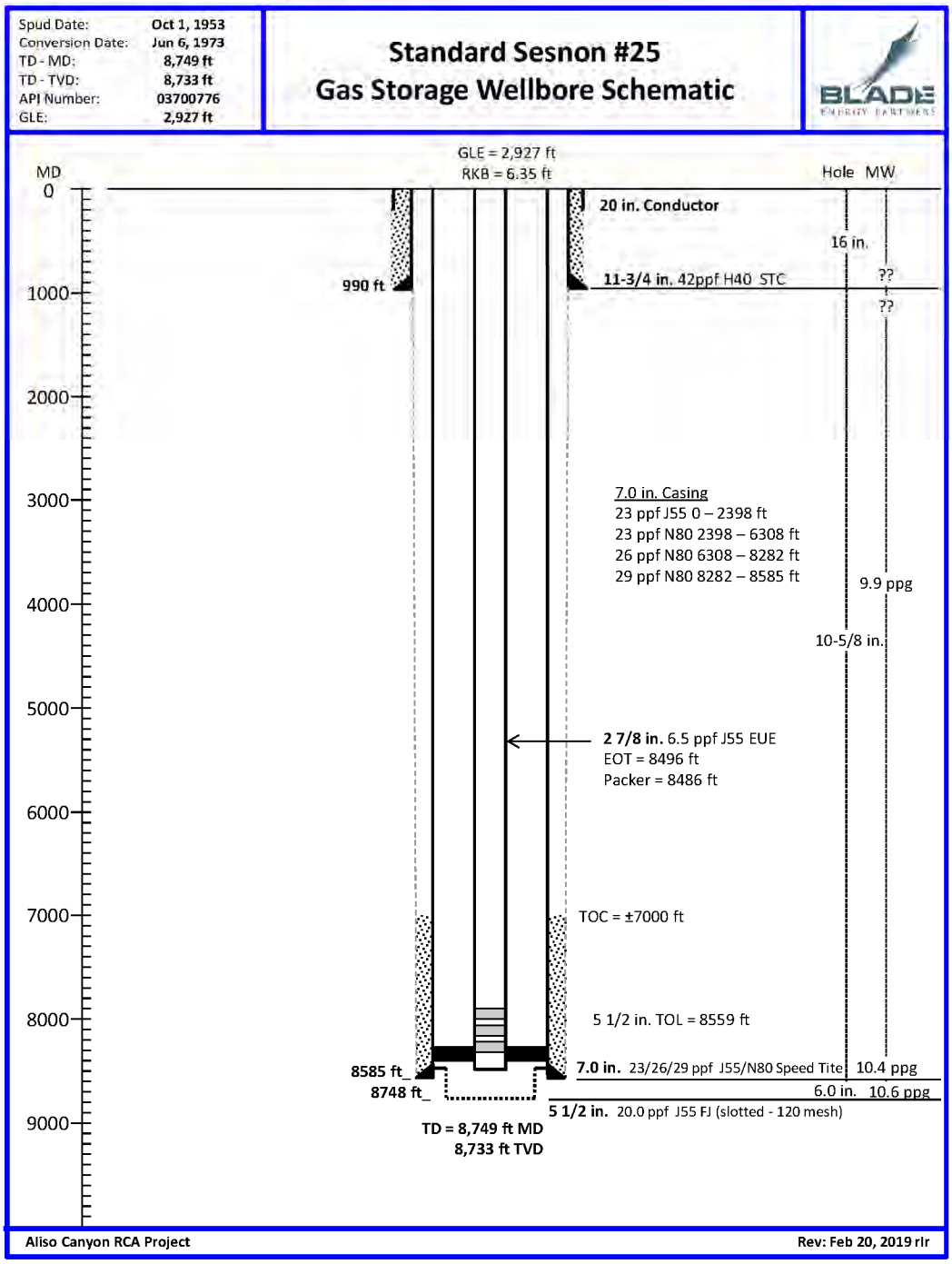

Figure 2: SS-25 Well Schematic

2.5 Wellbore Tubulars and Configuration

Figure 3 shows specifications and ratings of the tubulars used in the well; the tubular performance properties are the nominal API ratings without any wall loss.

String	Section	Name	Type	OD (in)	Weight (ppf)	Wall Thk (in)	OD / Wall Thk	Grade	Burst (psi)	Collapse (psi)	PBYS (klbf)	Tubular Type
1	1	Surface	Casing	11 3/4	42.00	0.333	35.29	H40	1,984	1,038	477.76	API
2	1	Production	Casing	7	23.00	0.317	22.08	J55	4,359	3,269	366.05	API
2	2	Production	Casing	7	23.00	0.317	22.08	N80	6,340	3,832	532.44	API
2	3	Production	Casing	7	26.00	0.362	19.34	N80	7,240	5,411	603.93	API
2	4	Production	Casing	7	29.00	0.408	17.16	N80	8,160	7,026	675.95	API
3	1	Production	Liner	5 1/2	20.00	0.361	15.24	J55	6,318	6,616	320.55	API
4	1	Production	Tubing	2 7/8	6.50	0.217	13.25	J55	7,265	7,676	99.66	API

Figure 3: SS-25 Tubular Specifications

Figure 4 shows the well and casing configuration details.

String	Sect	Name	Type	OD (in)	Weight (ppf)	ID (in)	Wall Thk (in)	Grade	Connection	Top MD (ft)	Bottom MD (ft)	TOC MD (ft)	Hole Size (in)	Fluid	Fluid Dens (ppg)	Tubular Type
1	1	Surface	Casing	11 3/4	42.00	11.084	0.333	H40	(none)	0.00	990.00	0.00	16.000	Fresh Water	8.33	API
2	1	Production	Casing	7	23.00	6.366	0.317	J55	Speed Tite	0.00	2,398.00	2,398.00	10.625	WBM 10.4 ppg	10.40	API
2	2	Production	Casing	7	23.00	6.366	0.317	N80	Speed Tite	2,398.00	6,308.00	6,308.00	10.625	WBM 10.4 ppg	10.40	API
2	3	Production	Casing	7	26.00	6.276	0.362	N80	Speed Tite	6,308.00	8,282.00	7,000.00	10.625	WBM 10.4 ppg	10.40	API
2	4	Production	Casing	7	29.00	6.184	0.408	N80	Speed-Tite	8,282.00	8,585.00	8,282.00	10.625	WBM 10.4 ppg	10.40	API
3	1	Production	Liner	5 1/2	20.00	4.778	0.361	J55	(none)	8,559.00	8,749.00	8,559.00	10.625	WBM 10.4 ppg	10.40	API
4	1	Production	Tubing	2 7/8	6.50	2.441	0.217	J55	(none)	0.00	8,496.00			Fresh Water	8.33	API

Figure 4: SS-25 Well Configuration

The focus of the analysis was on the 7 in. production casing—the pressure-containing tubular that failed.

2.6 Directional Profile

SS-25 was drilled as a vertical well. However, the well was sidetracked at approximately 4,000 ft. Figure 5 shows the directional profile, and Figure 6 [6] shows Dogleg Severity (DLS) (deg/100 ft).

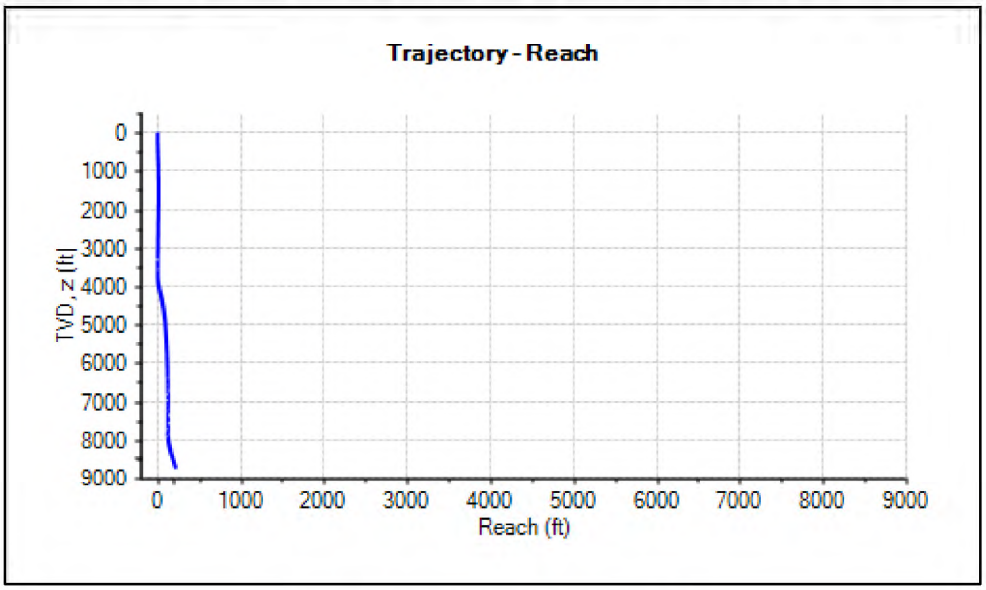

Figure 5: SS-25 Directional Profile

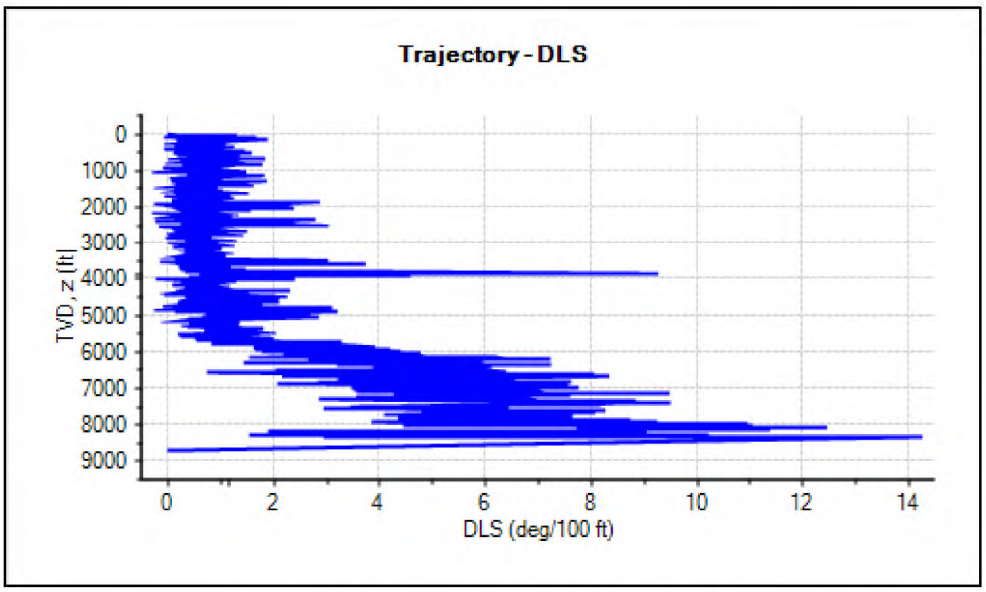

Figure 6: SS-25 Trajectory-Dogleg Severity

3 Casing Load Analysis Methodology

3.1 Working Stress Design

WSD is the traditional approach to the design of well tubulars. In general, strength is based on minimum performance properties, and load is based on reasonable and conservative assumptions. The SF is calculated as the ratio of the strength to the load and is compared to a recommended design factor (minimum acceptable SF). Table 1 lists the design factors considered in the study; these are representative of standard industry practice.

Table 1: Minimum Safety Factors

Failure Mode	Casing Minimum SF
Triaxial	1.25
Burst	1.1
Collapse	1.1
Compression	1.4
Tension	1.4

The yield strength of casing material decreases with increasing temperature. A 3% decrease in yield strength per 100°F increase in temperature above 70°F was assumed, which is a reasonable assumption for low-carbon steels and is consistent with standard industry practices.

For completeness, WSD was used to check each load case considered in this analysis. If the recommended minimum SF were not met in any load case, the design was inadequate. Because our interest was failure (and not design), we used limit state strength and probabilistic methods, as discussed in this report. The non-satisfaction of WSD criteria was therefore assumed a trigger to progress to Reliability-Based Design (RBD) approaches.

3.2 Reliability-Based Design

Consideration of uncertainty is imperative in all design approaches. In traditional WSD, the uncertainty in load and strength is addressed using elastic strength estimates based on minimum properties, conservative load assumptions, and a prescribed minimum SF. The goal is to ensure that material is used only within its elastic limit. This design method has been used widely and successfully by the oil and gas industry for decades.

WSD relies on the demonstration of design adequacy through satisfaction of prescribed design factors, such that only an allowable fraction of minimum strength is used in design. One limitation of the approach is the lack of insight into the implications of not satisfying these prescribed SF.

RBD methods have been in use for decades in the design of load-bearing structures. In RBD, it is explicitly recognized that strength and load are stochastic (i.e., of random distribution) in nature because they depend upon parameters that exhibit uncertainty and variability. For example, for tubulars, strength is based on parameters such as diameter, wall thickness, yield strength, and ultimate tensile strength. It is well recognized that because of the manufacturing and measurement processes involved, there is uncertainty in these parameters. For this reason, manufacturing specifications set allowable limits and ranges on many of these parameters. Likewise, load parameters also have uncertainty and variability

associated with them. For example, in well design, parameters that define loads, such as pore pressure, fracture pressure, and temperature are uncertain and cause variability in the magnitude of the load. Further, a given load considered in design may not occur at all and yet introduces uncertainty associated with the probability of occurrence of the load itself.

In RBD, strength and load are treated as random variables with known or measurable statistical distributions (probability density functions). Load effect distribution is more difficult to characterize because the required data are not always readily available, and RBD often requires the application of extreme value statistics. For this reason, the extreme event may be absent from available load data sets. In the most general applications of probabilistic design, both the load and the tubular ratings are treated as random variables. These probability distributions are developed based on rigorous statistical analysis of field load histories and actual test results on tubular performance. Reliability methods are then used to combine these distributions and quantify the *probability* that the load will exceed the strength under specified conditions. This is the POF, and its magnitude quantitatively conveys the risk of failure. In design, the maximum POF calculated should be less than a *target probability of failure*.

In practice, it is often difficult and cumbersome to obtain load data and rigorously quantify load side distributions. Moreover, designers often seek to understand whether a given tubular can withstand a given load at a *prescribed* magnitude. This is best answered by using a subset of RBD, known as *Level-4 RBD*. In Level-4 RBD, the load is deterministic at a prescribed (usually extreme) magnitude, and the strength is probabilistic, with distributions constructed from the statistical data on strength parameters (Figure 7). The failure probability, that is, the probability that the deterministic load exceeds the stochastic strength, is given by the yellow-shaded area under the strength probability density function to the left of the load distribution, which is a vertical line (it is deterministic). This is the POF if the load under consideration occurs at the assumed magnitude for the given tubular.

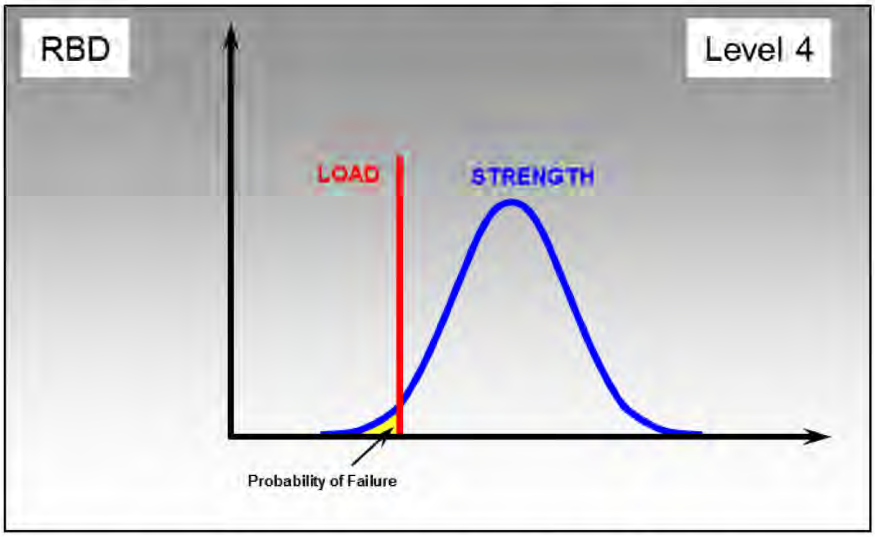

Figure 7: Level-4 Reliability-Based Design Analysis

Level-4 RBD was the approach used in this work to determine if the casing had been likely to fail for a given load condition. Tension-burst was the failure mode of interest in this work. The Klever-Stewart tension-burst limit state, as described in API Technical Report 5C3, was used as the limit state strength. Strength uncertainty was characterized by using statistical data on strength-defining parameters. The POF was calculated based on the Klever-Steward tension-burst limit state. Also, the Probability of Exceedance (POE) was calculated as the probability that the von Mises Equivalent (VME) stress exceeded the yield

strength of the casing. Although this does not necessarily imply failure, it is an important indicator of impending failure and is sometimes of interest in design situations where yielding is not acceptable. The POE is also indicative of the probability of connection failure because connection performance is usually referenced to the pipe body yield envelope.

In view of the fact that a key focus was to examine the effect of wall loss caused by corrosion, the wall thickness distribution was constructed as follows:

- The base case (no corrosion wall loss) condition used the statistics of the ensemble wall thickness distribution from the API Technical Report 5C3, which was based on data obtained by API from various manufacturers. The wall thickness distribution incorporated the API wall tolerance by definition[ii] and was considered as representative of Oil Country Tubular Goods (OCTG).
- Wall loss from corrosion was a sensitivity parameter and was expressed as percent wall loss (relative to the nominal wall thickness). This parameter must be considered in the wall thickness distribution. Because we started from the base case distribution, which did not include corrosion wall loss, the distribution was shifted to the left by the percent of wall loss. The shifted distribution was equivalent to the mean of the distribution being multiplied by the percent RBW.
- The standard deviation of the distribution remained the same; it accounted for wall loss occurring at the location of the minimum wall and was therefore the most conservative basis for consideration of corrosion wall loss.

This approach is illustrated in Figure 8.

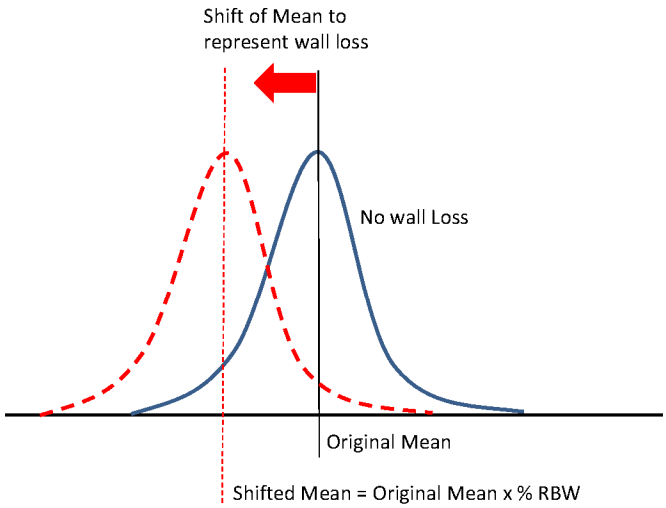

Figure 8: Consideration of Corrosion Wall Loss in Wall Thickness Distribution

In design, the target probabilities of failure are typically very low (of the order of 10^{-6} for tension-burst). However, in this work, our interest was failure. Therefore, we needed a criterion for failure (and not adequacy of design). In this work, the criterion for failure was that the POF was greater than 10^{-1} or 90%. Therefore, a calculated POF greater than 90% indicated imminent failure.

[ii] API allows for a 12.5% manufacturing wall tolerance. That is, the minimum wall thickness at any location can be at most 12.5% lower than the nominal wall thickness.

4 Results and Discussion

Analysis was performed using the commercial wellbore thermal analysis and tubular design program, StrinGnosis. Both WSD and RBD approaches were used in the analysis. The RBD approach was invoked only if the WSD SF did not meet minimum requirements. Ultimately, the RBD results were the basis for identifying casing failure.

4.1 Thermal Analysis

This section presents thermal analysis results.

SS-25 was used for injection (storage) and production (withdrawal) during its life. Because of the nature of the completion in this well, it was assumed that there was gas flow in the annulus between the tubing and the 7 in. casing.

4.1.1 Withdrawal

StrinGnosis was used to estimate a temperature profile for use when examining loads that occurred (or could have occurred) during the withdrawal phase. The case considered withdrawal of gas (assumed to be methane, specific gravity 0.56) at a rate of 20 MMscf/D for a long-term Steady State (SS) condition.

Figure 9 shows the resulting temperature profile (for the 7 in. casing).

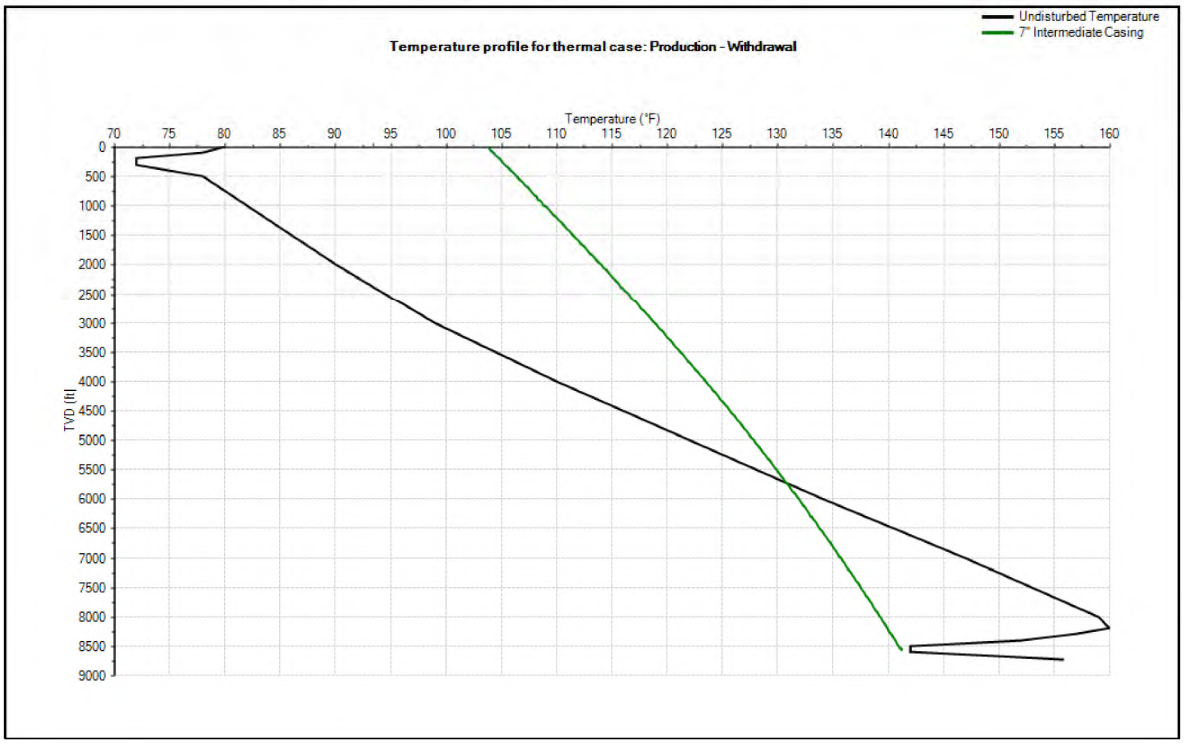

Figure 9: SS-25 Withdrawal Temperature Profile

4.1.2 Injection (Cool Down) Temperature Profile

Injection was of interest in this work because it presented conditions of highest internal pressure (burst load) and maximum cool down (thermally induced tension). Thermal analysis for a range of injection conditions (inlet temperature ranging from 30°F to 70°F) was performed using StrinGnosis. Figure 10 shows the resulting temperature profile of the 7 in. casing for the various cases. As expected, a lower injection inlet temperature resulted in lower overall casing temperature. These cases provided the temperature profiles of interest in the load analysis.

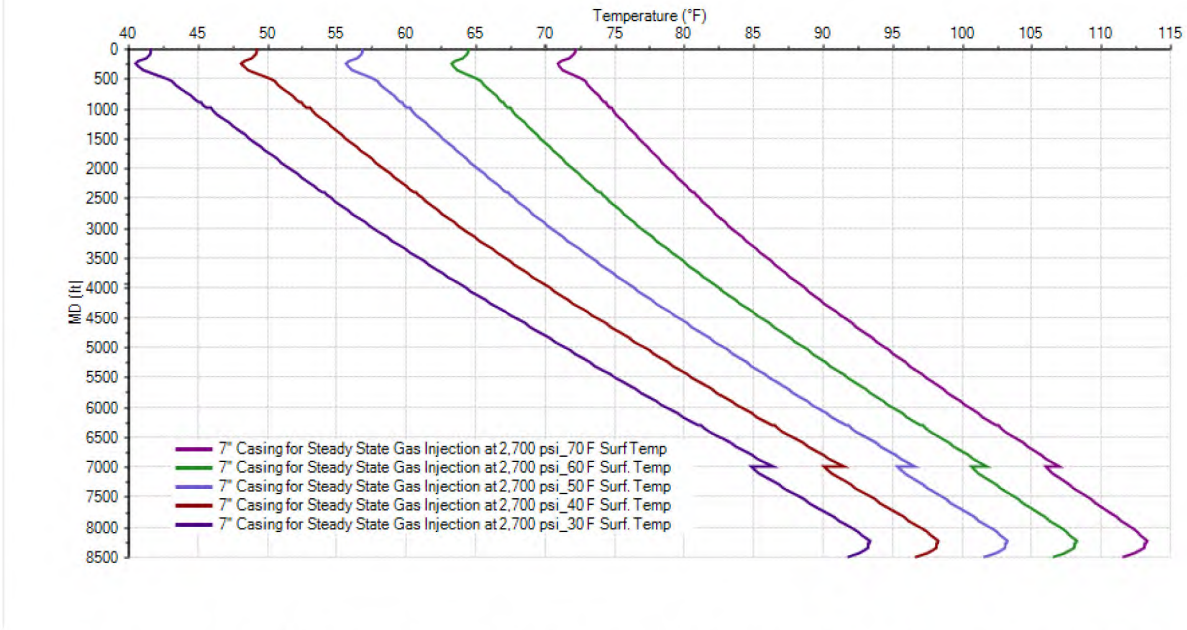

Figure 10: Steady State Injection Temperature Profiles for Different Inlet Temperatures

Several temperature profile measurements were also obtained from the well after the October 2015 incident. These measurements showed that the casing temperature was lower than the simulation results in Figure 10. This is likely because of the cooling effects caused by the topography and structure of the well site (which is not included in the model) or other possible causes for cool down such as cooling due to the expansion of the leaking gas. The Completion Profiler temperature profile run on November 8, 2015 and provided by SoCalGas [7] showed a cool down temperature profile (Figure 11). The profile showed that the wellbore temperature was lower than 20°F at shallow depths. This temperature profile was used in this analysis to represent the *worst case cool down* temperature profile.

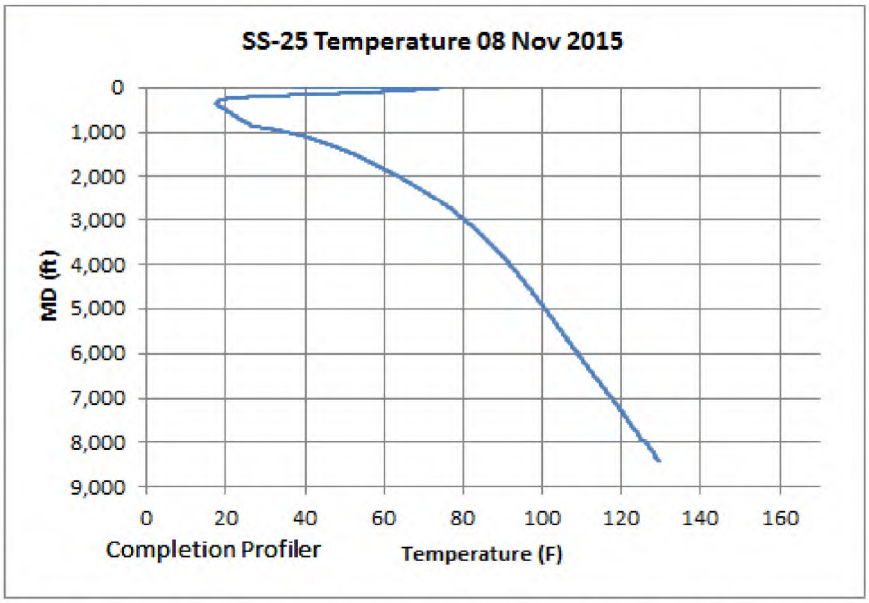

Figure 11: SS-25 Worst Case Cool Down Temperature Profile

4.2 Load Analysis of the 7 in. Casing with Top of Cement Sensitivity Analysis

The originally reported TOC from when the 7 in. casing was cemented in 1953 was at 7,000 ft MD and was the base case TOC assumption. However, considering the long service life of the well, it was highly likely that the formation in the openhole section above the TOC had caved in or collapsed around the casing, particularly at shallower depths. As a result, the casing may have behaved as if it were fixed at such locations. A shallower point of fixity could have led to higher stresses for a given thermal load. For this reason, the shallowest feasible point of fixity at the surface casing shoe (990 ft MD) was considered as a sensitivity.

Table 2 describes the load cases of interest. Several load cases were considered in the analysis to represent different operational conditions. Note the inclusion of the pre-tension in the initial condition (load case 1). Load cases 2–6 considered different simulated operational load conditions, and load cases 7 and 8 considered the *worst case cool down* temperature profile. The difference between load case 7 and 8 was the internal pressure. Load case 7 considered the maximum injection pressure, and load case 8 considered zero injection pressure (to investigate the effect of cool down only).

The internal pressure assumptions were based on the assumed internal fluid density and the surface pressure for the specific load case. The external pressure assumptions were a water gradient on the outside of the casing, which is typical for a casing design check. The external pressure for the initial condition assumed hydrostatic pressure of the drilling fluid and cement at the time the cement was placed in the annulus. The temperature profile was the assumed temperature for the specific load case determined from thermal modeling.

Table 2: Load Assumption for the 7 in. Casing

	Load Case	Internal Pressure	External Pressure	Temperature
1	Initial Condition with 41 klbf Overpull for Total of 196 klbf tension at surface	10.40 ppg fluid density hydrostatic pressure	0 psi pressure at hanger 10.40 ppg fluid density above TOC 15.80 ppg cement density below TOC	Undisturbed temperature
2	SS Gas Injection at 2,700 psi 70°F Surface Temperature	Pressure profile from simulation with 2,700 psi surface pressure and 30 MMscf/D gas injection rate	8.34 ppg fluid density hydrostatic pressure	Temperature profile for steady state gas injection with surface temperature of 70°F
3	SS Gas Injection at 2,700 psi 60°F Surface Temperature	Pressure profile from simulation with 2,700 psi surface pressure and 30 MMscf/D gas injection rate	8.34 ppg fluid density hydrostatic pressure	Temperature profile for steady state gas injection with surface temperature of 60°F
4	Withdrawal Operations	Pressure profile from simulation with 2,700 psi withdrawal operations	8.34 ppg fluid density hydrostatic pressure	Temperature profile for gas withdrawal of 20 MMscf/D from thermal simulation
5	Hot Shut-In	2,700 psi surface test pressure on top of a gas gradient	0 psi pressure at hanger 8.34 ppg fluid density above TOC 8.34 ppg fluid density below TOC	Withdrawal 20 MMscf/D
6	Cold Shut-In	2,700 psi surface test pressure on top of a gas gradient	0 psi pressure at hanger 8.34 ppg fluid density above TOC 8.34 ppg fluid density below TOC	Undisturbed temperature
7	Injection at 2,700 psi with the Worst Case Cool Down Temperature Profile	Pressure profile from a simulation with 2,700 psi surface pressure and 30 MMscf/D gas injection rate	8.34 ppf fluid density hydrostatic pressure	Cool down Completion Profiler temperature profile run on November 8, 2015 [7]
8	Worst Case Cool Down without Injection Pressure	Atmospheric pressure at surface on top of a gas gradient	8.34 ppf fluid density hydrostatic pressure	Cool down Completion Profiler temperature profile run on November 8, 2015 [7]

4.2.1 Base Case with No Wall Loss, Top of Cement at 7,000 ft MD

First, we considered the base case (no corrosion wall loss) with the TOC at the reported depth of 7,000 ft MD. Table 3 shows the SFs for the 7 in. casing loads, and Figure 12 and Figure 13 show design envelopes[iii] for the two critical sections of the 7 in. casing. The SFs for the loads considered were within the design SF requirements (Table 1), except for the tension SF for SS injection at 70°F and 60°F and injection with the worst case cool down temperature profile. The tension SFs for loads 2, 3, and 7 are below the minimum SF for tension. However, the focus of this study is on burst failure and not tension failure. The tension stress is included in the triaxial SF and is therefore considered. The SFs in red throughout this document are less than the minimum SFs in Table 1. The main conclusion was that without wall loss, mechanical failure due to tension was highly unlikely. Also note that the minimum tension SFs occurred near the surface and not at 895 ft, the depth of interest.

Table 3: Minimum Safety Factors for the 7 in. Casing with Top of Cement at 7,000 ft

		Burst		Collapse		Tension		Compression		Triaxial	
	Load Case	Pipe SF	MD (ft)	Pipe SF	MD (ft)	Pipe SF	MD (ft)	Pipe SF	MD (ft)	Pipe SF	MD (ft)
1	Initial Condition	-	-	>3	8,282	1.73	185	2.81	8,563	1.72	185
2	SS Gas Injection at 2,700 psi 70°F	1.61	0	>3	8,585	1.35	185	-	-	1.39	133
3	SS Gas Injection at 2,700 psi 60°F	1.61	0	>3	8,585	1.31	185	-	-	1.36	185
4	Withdrawal Operations	2.06	0	>3	8,282	1.76	185	2.74	8,563	1.81	104
5	Hot Shut-In	1.60	0	>3	8,585	1.64	185	2.99	8,563	1.55	52
6	Cold Shut-In	1.61	0	>3	8,585	1.50	185	2.98	8,563	1.48	52
7	Injection at 2,700 psi with the Worst Case Cool Down	1.61	0	>3	8,585	1.30	185	>3	8,563	1.35	185
8	Worst Case Cool Down without Injection	>3	0	1.7	6,308	1.59	185	2.64	8,563	1.57	185

[iii] The design envelopes represent the VME ellipses that indicate the combined stress limits of the casing. The rectangular box with the truncated lower right-hand corner represents the SF for the casing including burst, collapse, tension, and compression.

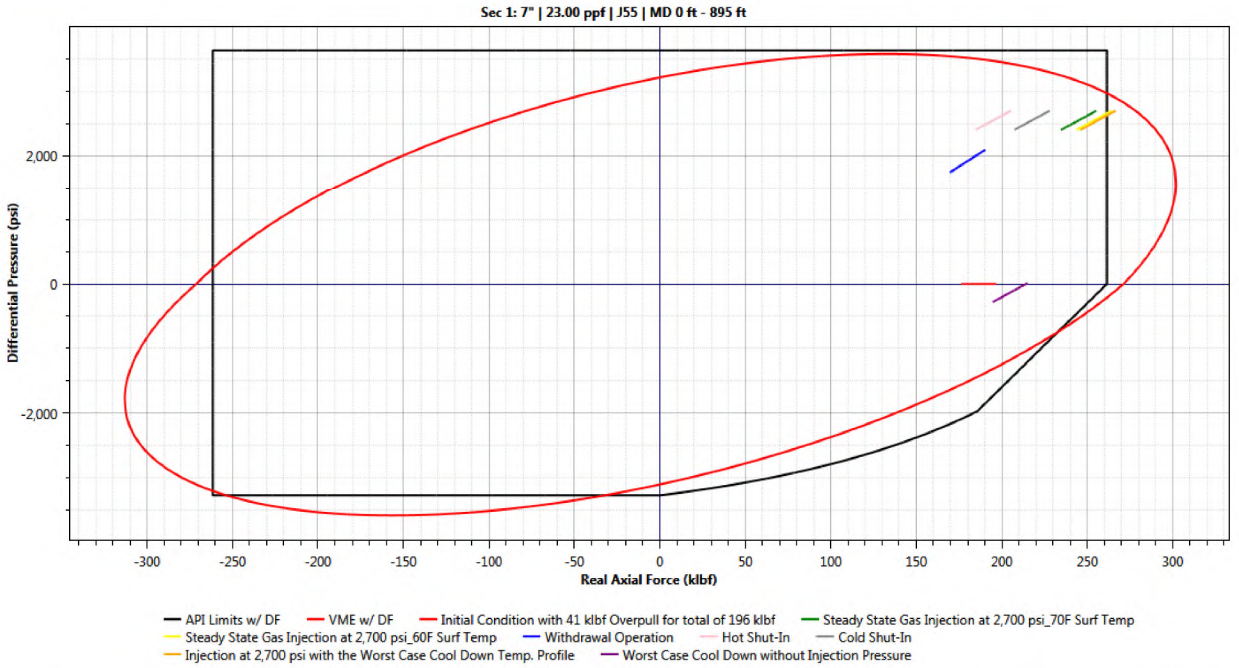

Figure 12: Design Envelope–7 in. Casing Section from 0 ft to 895 ft MD with Top of Cement at 7,000 ft

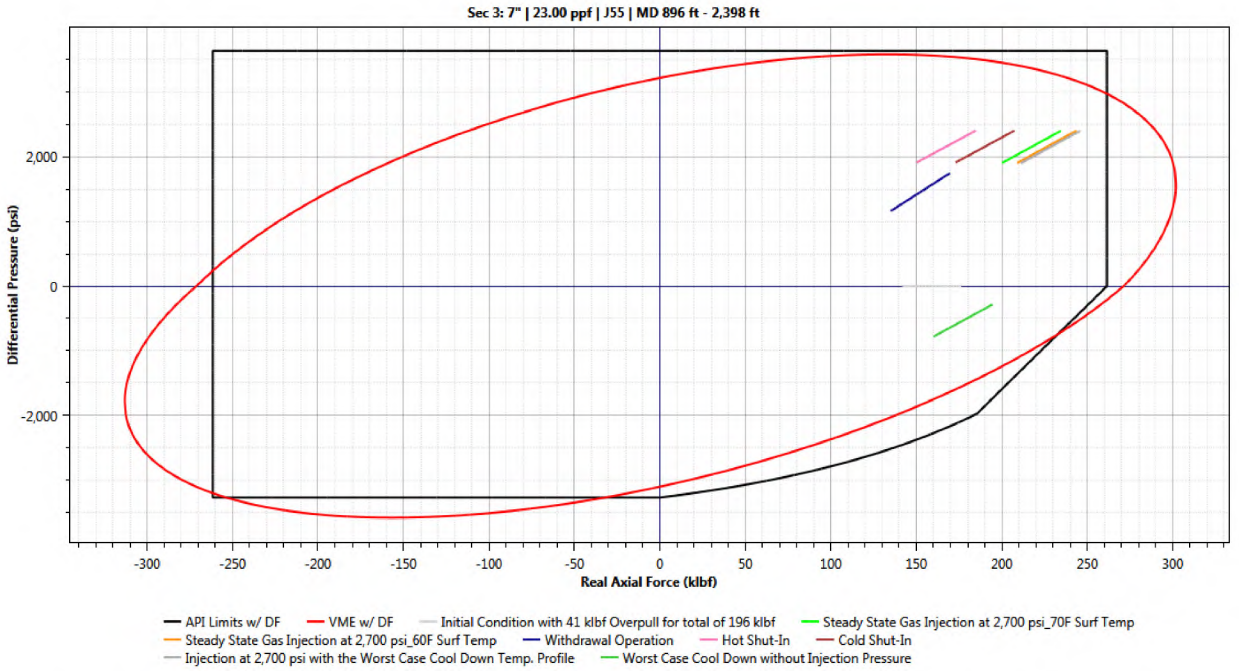

Figure 13: Design Envelope–7 in. Casing Section from 896 ft to 2,398 ft MD with Top of Cement at 7,000 ft

Table 4 and Table 5 show in more detail the load and the stresses at the depth of interest (895 ft) for all load cases. Tangential stress at the inside diameter (ID) of the casing is reported since it is higher than the stress at the outside diameter (OD). The true vertical depth (TVD) is approximately the same as MD in the upper part of the well.

Table 4: Internal and External Pressure, Axial Force, and Temperature at Depth of Interest (895 ft)

	Load Case	MD (ft)	TVD (ft)	Real Axial Force (lbf)	Internal Pressure (psi)	External Pressure (psi)	Temperature (°F)
1	Initial Condition	895	894.89	176,189	483	483	81.2
2	SS Gas Injection at 2,700 psi 70°F	895	894.89	234,645	2,791	388	74.4
3	SS Gas Injection at 2,700 psi 60°F	895	894.89	243,552	2,791	388	67.0
4	Withdrawal Operations	895	894.89	169,645	2,136	388	108.9
5	Hot Shut-In	895	894.89	184,752	2,793	387	109.4
6	Cold Shut-In	895	894.89	207,421	2,793	387	81.2
7	Injection at 2,700 psi with the Worst Case Cool Down	895	894.89	245,909	2,791	388	29.0
8	Worst Case Cool Down without Injection	895	894.89	194,544	106	388	29.0

Table 5: Stresses at Depth of Interest (895 ft)

Load Case	MD (ft)	TVD (ft)	Mean Axial Stress (psi)	Bending Stress OD (psi)	Tangential Stress ID (psi)	Radial Stress ID (psi)	Radial Stress OD (psi)	Max. VME Stress (psi)
Initial Condition	895	894.89	26,473	659	–483	–483	–483	27,615
SS Gas Injection at 2,700 psi 70°F	895	894.89	35,256	659	28,783	–2,791	–388	35,640
SS Gas Injection at 2,700 psi 60°F	895	894.89	36,594	659	28,785	–2,791	–388	36,514
Withdrawal Operations	895	894.89	25,489	659	20,825	–2,136	–388	25,995
Hot Shut-In	895	894.89	27,759	659	28,816	–2,793	–387	31,383
Cold Shut-In	895	894.89	31,165	659	28,816	–2,793	–387	33,181
Injection at 2,700 psi with the Worst Case Cool Down	895	894.89	36,948	659	28,778	–2,791	–388	36,747
Worst Case Cool Down without Injection	895	894.89	29,231	659	–3,818	–106	–388	31,968

4.2.2 Base Case with No Wall Loss, Top of Cement at 990 ft (Previous Shoe)

Next, we considered the possibility of formation collapsing around the 7 in. casing making it *fixed* at 990 ft. Table 6 shows SFs for this case, and Figure 14 and Figure 15 show the design envelope for the two critical sections of the 7 in. casing. The SF were within the minimum design SF requirements, except for the tension SF for the injection case with the worst case cool down temperature. SFs shown in red throughout this document are less than the minimum SF as shown in Table 1. The tension SF of 1.12 and triaxial SF of 1.21 became a concern because the condition of the casing after more than 60 years of service was unknown. The tension SFs for loads 2, 3, and 8 are slightly below the minimum SF for tension. However, the focus of this study was burst failure and not tension failure. The tension stress is included in the triaxial SF and was therefore considered. The results show that if the 7 in. casing had been fixed at a shallower depth resulting from collapse of formation, the axial loads and stresses would have been higher. However, the burst and VME SF still met minimum requirements. This suggested that without wall loss, a tension-burst failure was highly unlikely, even if the point of fixity had moved and was shallower because of the formation cave-in. Note that the minimum safety factors were located near the surface at not at 895 ft.

Table 6: Minimum Safety Factors for the 7 in. Casing with Top of Cement at 990 ft

		Burst		Collapse		Tension		Compression		Triaxial	
	Load Case	Pipe SF	MD (ft)	Pipe SF	MD (ft)	Pipe SF	MD (ft)	Pipe SF	MD (ft)	Pipe SF	MD (ft)
1	Initial Condition	-	-	2.12	6,308	1.73	185	2.21	8,563	1.73	185
2	SS Gas Injection at 2,700 psi 70°F	1.61	0	>3	8,585	1.38	185	>3	8,513	1.41	104
3	SS Gas Injection at 2,700 psi 60°F	1.61	0	>3	8,585	1.33	185	>3	8,513	1.37	185
4	Withdrawal Operations	2.06	0	>3	8,282	1.75	185	2.47	8,563	1.80	104
5	Hot Shut-In	1.60	0	>3	8,585	1.67	185	2.67	8,563	1.56	52
6	Cold Shut-In	1.61	0	>3	8,585	1.41	185	2.66	8,563	1.43	104
7	Injection at 2,700 psi with the Worst Case Cool Down	1.61	0	>3	8,585	1.12	185	2.90	8,563	1.21	185
8	Worst Case Cool Down without Injection	>3	0	1.79	6,308	1.34	185	2.39	8,563	1.32	185

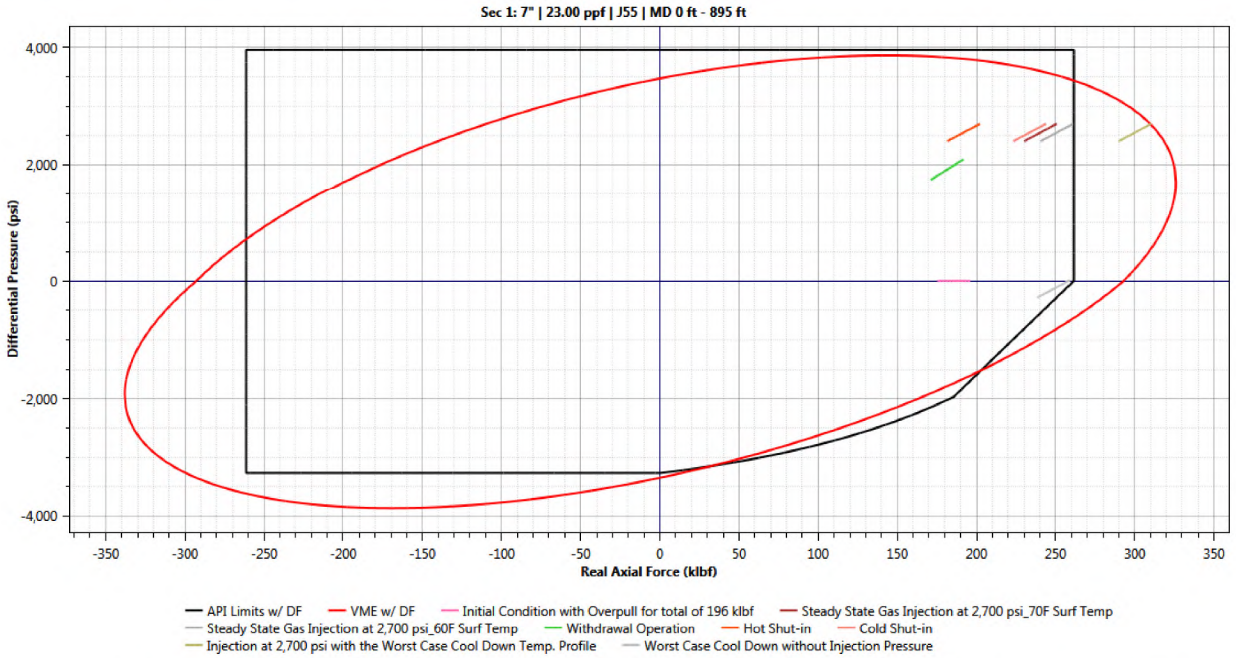

Figure 14: Design Envelope–7 in. Casing Section from 0 ft to 895 ft MD with Top of Cement at 990 ft

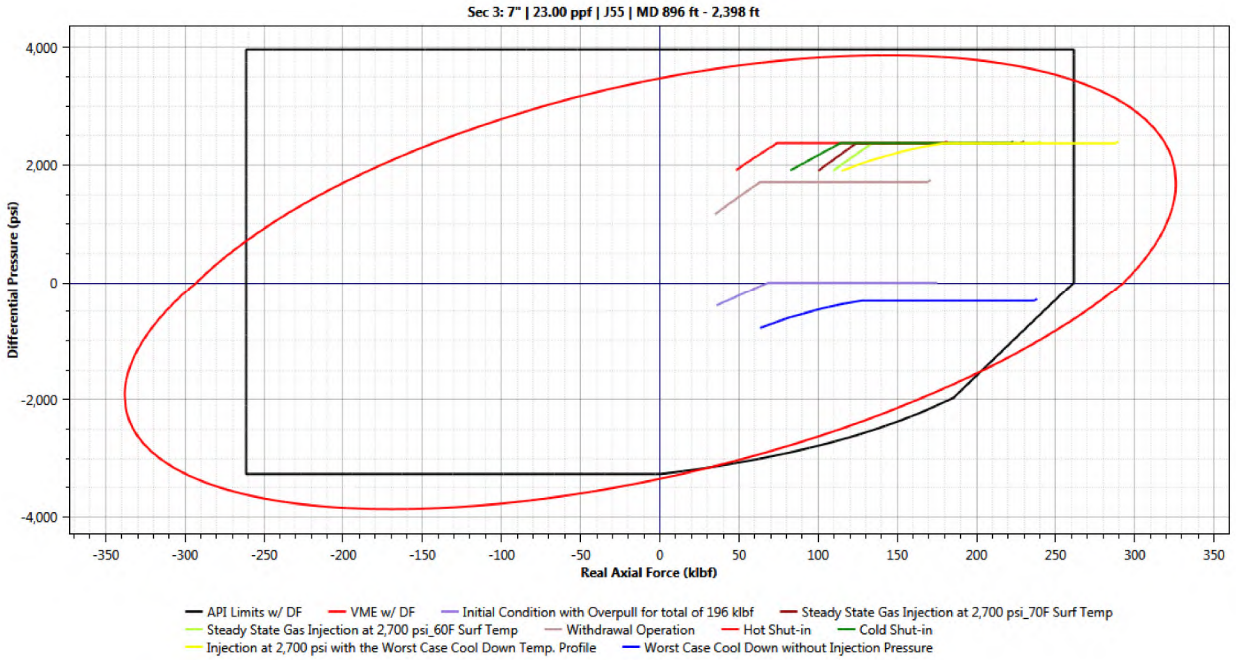

Figure 15: Design Envelope–7 in. Casing Section from 896 ft to 2,398 ft MD with Top of Cement at 990 ft

Table 7 and Table 8 show in more detail the load and the stresses at the depth of interest (895 ft) for all load cases with TOC at 990 ft.

Table 7: Internal and External Pressure, Axial Force, and Temperature at the Depth of Interest (895 ft)

	Load Case	MD (ft)	TVD (ft)	Real Axial Force (lbf)	Internal Pressure (psi)	External Pressure (psi)	Temperature (°F)
1	Initial Condition	895	894.89	175,356	483	483	81.2
2	SS Gas Injection at 2,700 psi 70°F	895	894.89	230,093	2,791	388	74.3
3	SS Gas Injection at 2,700 psi 60°F	895	894.89	240,459	2,791	388	67.0
4	Withdrawal Operations	895	894.89	171,200	2,136	388	108.9
5	Hot Shut-In	895	894.89	181,577	2,793	387	110.2
6	Cold Shut-In	895	894.89	223,356	2,793	387	81.2
7	Injection at 2,700 psi with the Worst Case Cool Down	895	894.89	289,763	2,791	388	29.0
8	Worst Case Cool Down without Injection	895	894.89	238,498	106	388	29.0

Table 8: Stresses at Depth of Interest (895 ft)

Load Case	MD (ft)	TVD (ft)	Mean Axial Stress (psi)	Bending Stress OD (psi)	Tangential Stress ID (psi)	Radial Stress ID (psi)	Radial Stress OD (psi)	Max. VME Stress (psi)
Initial Condition	895	894.89	26,348	659	–483	–483	–483	27,490
SS Gas Injection at 2,700 psi 70°F	895	894.89	34,572	659	28,783	–2,791	–388	35,206
SS Gas Injection at 2,700 psi 60°F	895	894.89	36,129	659	28,785	–2,791	–388	36,207
Withdrawal Operations	895	894.89	25,723	659	20,825	–2,136	–388	26,146
Hot Shut-In	895	894.89	27,282	659	28,816	–2,793	–387	31,152
Cold Shut-In	895	894.89	33,560	659	28,816	–2,793	–387	34,591
Injection at 2,700 psi with the Worst Case Cool Down	895	894.89	43,537	659	28,778	–2,791	–388	41,441
Worst Case Cool Down without Injection	895	894.89	35,835	659	–3,818	–106	–388	38,550

4.3 Effect of Wall Loss, Top of Cement at 7,000 ft MD

As noted earlier in this report, corrosion wall loss was observed in the extracted casing from the SS-25 well. We examined the effect of wall loss. A range of wall loss was considered. WSD was the initial basis for investigation. If the WSD SFs were lower than the design factors, the case was examined using Level-4 RBD and a POF and POE were computed. A POF in excess of 90% was assumed to indicate near-certainty of failure.

Wall loss was considered in the burst, collapse, and triaxial calculations and SF in this analysis. RBW was not considered in the tension SF, because corrosion is normally localized and does not occur around the entire circumference of the casing.

We first considered the TOC at the original installed depth of 7,000 ft MD. Recall that with this TOC, the stresses were, in general, lower than for a shallower TOC for all the load cases evaluated. Therefore, it was representative of the lower threshold of RBW, at which burst failure may be expected.

4.3.1 80% and 70% Remaining Body Wall

Table 9 and Table 10 show the results for 80% RBW and 70% RBW, respectively. As expected, the SFs decreased as RBW reduced. The SFs for burst and triaxial met the design requirements with the reduced wall. Note that the minimum SFs for some loads occurred at 895 ft for the 70% RBW case including injection, withdrawal, and shut-in.

Table 9: Minimum Safety Factors for the 7 in. Casing with 80% Remaining Body Wall

		Burst		Collapse		Tension		Compression		Triaxial	
	Load Case	Pipe SF	MD (ft)	Pipe SF	MD (ft)	Pipe SF	MD (ft)	Pipe SF	MD (ft)	Pipe SF	MD (ft)
1	Initial Condition	-	-	6.5	8,282	1.73	185	2.81	8,563	1.72	185
2	SS Gas Injection at 2,700 psi 70°F	1.61	0	>3	8,585	1.35	185	-	-	1.39	133
3	SS Gas Injection at 2,700 psi 60°F	1.61	0	>3	8,585	1.31	185	-	-	1.36	185
4	Withdrawal Operations	2.06	0	>3	8,282	1.76	185	2.74	8,563	1.81	104
5	Hot Shut-In	1.60	0	>3	8,585	1.64	185	2.99	8,563	1.52	895
6	Cold Shut-In	1.61	0	>3	8,585	1.50	185	2.98	8,563	1.48	895
7	Injection at 2,700 psi with the Worst Case Cool Down	1.61	0	>3	8,585	1.30	185	>3	8,563	1.35	185
8	Worst Case Cool Down without Injection	>3	0	1.74	6,308	1.59	185	2.64	8,563	1.57	185

Table 10: Minimum Safety Factors for the 7 in. Casing with 70% Remaining Body Wall

	Load Case	Burst		Collapse		Tension		Compression		Triaxial	
		Pipe SF	MD (ft)	Pipe SF	MD (ft)	Pipe SF	MD (ft)	Pipe SF	MD (ft)	Pipe SF	MD (ft)
1	Initial Condition	-	-	>3	8,282	1.73	185	2.81	8,563	1.72	185
2	SS Gas Injection at 2,700 psi 70°F	1.45	895	>3	8,585	1.35	185	-	-	1.31	895
3	SS Gas Injection at 2,700 psi 60°F	1.45	895	>3	8,585	1.31	185	-	-	1.30	895
4	Withdrawal Operations	1.97	895	>3	8,282	1.76	185	2.74	8,563	1.78	895
5	Hot Shut-In	1.43	895	>3	8,585	1.64	185	2.99	8,563	1.37	895
6	Cold Shut-In	1.44	895	>3	8,585	1.50	185	2.98	8,563	1.35	895
7	Injection at 2,700 psi with the Worst Case Cool Down	1.45	895	>3	8,585	1.30	185	3.27	8,563	1.29	895
8	Worst Case Cool Down without Injection	>3	0	1.74	6,308	1.59	185	2.64	8,563	1.57	185

4.3.2 65% Remaining Body Wall

Table 11 shows SFs for the 7 in. casing loads with 65% RBW. Importantly, for 65% RBW, for the first time, we saw that the triaxial SF was below the minimum required value of 1.25. The triaxial SF, which is the ratio of the yield strength to the VME stress, is indicative of impending yielding in a combined loading mode and is therefore more representative of casing response to tension-burst loading, which was of interest in this study. Clearly, any further reduction in RBW would have resulted in the triaxial SF falling below the minimum requirement. However, *violation of minimum SF requirements does not imply failure*. We needed to examine the violating load cases using Level-4 RBD to make reasonable conclusions about failure.

Table 11: Minimum Safety Factors for the 7 in. Casing with 65% Remaining Body Wall

	Load Case	Burst		Collapse		Tension		Compression		Triaxial	
		Pipe SF	MD (ft)	Pipe SF	MD (ft)	Pipe SF	MD (ft)	Pipe SF	MD (ft)	Pipe SF	MD (ft)
1	Initial Condition	-	-	>3	8,282	1.73	185	2.81	8,563	1.72	185
2	SS Gas Injection at 2,700 psi 70°F	1.35	895	>3	8,585	1.35	185	-	-	1.25	895
3	SS Gas Injection at 2,700 psi 60°F	1.35	895	>3	8,585	1.31	185	-	-	1.24	895
4	Withdrawal Operations	1.83	895	>3	8,282	1.76	185	2.74	8,563	1.70	895
5	Hot Shut-In	1.33	895	>3	8,585	1.64	185	2.99	8,563	1.29	895

	Load Case	Burst		Collapse		Tension		Compression		Triaxial	
		Pipe SF	MD (ft)	Pipe SF	MD (ft)	Pipe SF	MD (ft)	Pipe SF	MD (ft)	Pipe SF	MD (ft)
6	Cold Shut-In	1.34	895	>3	8,585	1.50	185	2.98	8,563	1.28	895
7	Injection at 2,700 psi with the Worst Case Cool Down	1.35	895	>3	8,585	1.30	185	>3	8,563	1.23	895
8	Worst Case Cool Down without Injection	>3	0	1.74	6,308	1.59	185	2.64	8,563	1.57	185

Table 12 shows RBD results and the POE[iv] for this case. Note that this table shows only POE (probability that the VME stress exceeds yield strength) results. This is because the API burst SFs (based on the historical API burst equation, a traditional basis for WSD) were still above the minimum requirement (1.1) according to WSD. As expected, because the triaxial SFs were slightly below 1.25, the POE was very low.

Table 12: Reliability-Based Design and Probability of Failure for the 7 in. Casing with 65% Remaining Body Wall

Load Case	MD (ft)	Internal Pressure (psi)	External Pressure (psi)	Real Axial Force (lbf)	Fail Mode	Min. SF	POF or POE (10^{x})	Failure Rate (1 in -)
SS Gas Injection at 2,700 psi 70°F	895	2,791	388	234,645	Triaxial	1.25	–7.3	20,396,576
SS Gas Injection at 2,700 psi 60°F	895	2,791	388	243,552	Triaxial	1.24	–7.1	11,674,154
Injection at 2,700 psi with the Worst Case Cool Down	895	2,791	388	245,909	Triaxial	1.23	–7.0	9,938,665

4.3.3 60% Remaining Body Wall

Table 13 shows SFs for the 7 in. casing loads with 60% RBW. The triaxial SFs for several loads (including operational loads) were below minimum WSD requirements. Table 14 shows RBD results, which indicated increasing POE. However, even at 60% RBW, the POF was exceedingly low, indicating that ductile rupture was still highly unlikely with RBW at 60% of nominal wall thickness (equivalent to 40% wall loss).

[iv] POE is shown in the table when the VME SF is less than the minimum design factor of 1.25. POF is shown when the uniaxial load SF is less than the minimum SF. The Fail Mode column in the table determines if the value shown in the POF or POE column is the POF or POE.

Table 13: Minimum Safety Factors for the 7 in. Casing with 60% Remaining Body Wall

	Load Case	Burst		Collapse		Tension		Compression		Triaxial	
		Pipe SF	MD (ft)	Pipe SF	MD (ft)	Pipe SF	MD (ft)	Pipe SF	MD (ft)	Pipe SF	MD (ft)
1	Initial Condition	-	-	>3	8,282	1.73	185	2.81	8,563	1.72	185
2	SS Gas Injection at 2,700 psi 70°F	1.24	895	>3	8,585	1.35	185	-	-	1.18	895
3	SS Gas Injection at 2,700 psi 60°F	1.24	895	>3	8,585	1.31	185	-	-	1.17	895
4	Withdrawal Operations	1.69	895	>3	8,282	1.76	185	2.74	8,563	1.60	895
5	Hot Shut-In	1.23	895	>3	8,585	1.64	185	2.99	8,563	1.20	895
6	Cold Shut-In	1.24	895	>3	8,585	1.50	185	2.98	8,563	1.20	895
7	Injection at 2,700 psi with the Worst Case Cool Down	1.24	895	>3	8,585	1.30	185	>3	8,563	1.17	895
8	Worst Case Cool Down without Injection	>3	0	1.74	6,308	1.59	185	2.64	8,563	1.57	185

Table 14: Reliability-Based Design and Probability of Failure for the 7 in. Casing with 60% Remaining Body Wall

Load Case	MD (ft)	Internal Pressure (psi)	External Pressure (psi)	Real Axial Force (lbf)	Fail Mode	Min. SF	POF or POE (10^x)	Failure Rate (1 in -)
SS Gas Injection at 2,700 psi 70°F	895	2,791	388	234,645	Triaxial	1.18	–6.4	2,432,666
SS Gas Injection at 2,700 psi 60°F	895	2,791	388	243,552	Triaxial	1.17	–6.2	1,571,136
Hot Shut-In	895	2,793	387	184,752	Triaxial	1.20	–7.1	12,730,222
Cold Shut-In	895	2,793	387	207,421	Triaxial	1.20	–6.9	7,998,053
Injection at 2,700 psi with the Worst Case Cool Down	895	2,791	388	245,909	Triaxial	1.17	–6.1	1,382,023

4.3.4 50% Remaining Body Wall

Table 15 shows SFs for the 7 in. casing loads with 50% RBW. At 50% RBW, the uniaxial API burst SFs also fell below the minimum required SF. The RBD results for triaxial and burst (Table 16) show the POF results were still quite low, implying that ductile rupture was unlikely.

Table 15: Minimum Safety Factors for the 7 in. Casing with 50% Remaining Body Wall

	Load Case	Burst		Collapse		Tension		Compression		Triaxial	
		Pipe SF	MD (ft)	Pipe SF	MD (ft)	Pipe SF	MD (ft)	Pipe SF	MD (ft)	Pipe SF	MD (ft)
1	Initial Condition	-	-	6.5	8,282	1.73	185	2.81	8,563	1.72	185
2	SS Gas Injection at 2,700 psi 70°F	1.04	895	>3	8,585	1.35	185	-	-	1.01	895
3	SS Gas Injection at 2,700 psi 60°F	1.04	895	>3	8,585	1.31	185	-	-	1.01	895
4	Withdrawal Operations	1.41	895	>3	8,282	1.76	185	2.74	8,563	1.38	895
5	Hot Shut-In	1.02	895	>3	8,585	1.64	185	2.99	8,563	1.01	895
6	Cold Shut-In	1.03	895	>3	8,585	1.50	185	2.98	8,563	1.02	895
7	Injection at 2,700 psi with the Worst Case Cool Down	1.04	895	>3	8,585	1.30	185	>3	8,563	1.01	895
8	Worst Case Cool Down without Injection	>3	0	1.74	6,308	1.59	185	2.64	8,563	1.57	185

Table 16: Reliability-Based Design and Probability of Failure for the 7 in. Casing with 50% Remaining Body Wall

Load Case	MD (ft)	Internal Pressure (psi)	External Pressure (psi)	Real Axial Force (lbf)	Fail Mode	Min. SF	POF or POE (10^x)	Failure Rate (1 in -)
SS Gas Injection at 2,700 psi 70°F	895	2,791	388	234,645	Burst	1.04	< 1E–9	> 1 E9
SS Gas Injection at 2,700 psi 70°F	895	2,791	388	234,645	Triaxial	1.01	–4.1	11,470
SS Gas Injection at 2,700 psi 60°F	895	2,791	388	243,552	Burst	1.04	< 1E–9	> 1 E9
SS Gas Injection at 2,700 psi 60°F	895	2,791	388	243,552	Triaxial	1.01	–3.9	9,424
Hot Shut-In	895	2,793	387	184,752	Burst	1.02	< 1E–9	> 1 E9
Hot Shut-In	895	2,793	387	184,752	Triaxial	1.01	–4.3	17,942
Cold Shut-In	895	2,793	387	207,421	Burst	1.03	< 1E–9	> 1 E9
Cold Shut-In	895	2,793	387	207,421	Triaxial	1.02	–4.3	18,488
Injection at 2,700 psi with the Worst Case Cool Down	895	2,791	388	245,909	Burst	1.04	< 1E–9	> 1 E9

Load Case	MD (ft)	Internal Pressure (psi)	External Pressure (psi)	Real Axial Force (lbf)	Fail Mode	Min. SF	POF or POE (10^x)	Failure Rate (1 in -)
Injection at 2,700 psi with the Worst Case Cool Down	895	2,791	388	245,909	Triaxial	1.01	–3.9	8,859

4.3.5 40% Remaining Body Wall

Table 17 shows the SFs for the casing loads with 40% RBW. Some of the SFs were less than one. This does not imply failure. The RBD results in Table 18 show the probability of failure in burst was low (1 in greater than 1 billion), which indicated rupture was not likely; however, the probability of exceeding yield strength was high (1 in 19).

Table 17: Minimum Safety Factors for the 7 in. Casing with 40% Remaining Body Wall

	Load Case	Burst		Collapse		Tension		Compression		Triaxial	
		Pipe SF	MD (ft)	Pipe SF	MD (ft)	Pipe SF	MD (ft)	Pipe SF	MD (ft)	Pipe SF	MD (ft)
1	Initial Condition	-	-	6.5	8,282	1.73	185	2.81	8,563	1.72	185
2	SS Gas Injection at 2,700 psi 70°F	0.83	895	>3	8,585	1.35	185	-	-	0.82	895
3	SS Gas Injection at 2,700 psi 60°F	0.83	895	>3	8,585	1.31	185	-	-	0.82	895
4	Withdrawal Operations	1.13	895	>3	8,282	1.76	185	2.74	8,563	1.12	895
5	Hot Shut-In	0.82	895	>3	8,585	1.64	185	2.99	8,563	0.81	895
6	Cold Shut-In	0.83	895	>3	8,585	1.50	185	2.98	8,563	0.82	895
7	Injection at 2,700 psi with the Worst Case Cool Down	0.83	895	>3	8,585	1.30	185	3.27	8,563	0.82	895
8	Worst Case Cool Down without Injection	>3	0	1.7	6,308	1.59	185	2.64	8,563	1.55	896

Table 18: Reliability-Based Design and Probability of Failure for the 7 in. Casing with 40% Remaining Body Wall

Load Case	MD (ft)	Internal Pressure (psi)	External Pressure (psi)	Real Axial Force (lbf)	Fail Mode	Min. SF	POF or POE (10^x)	Failure Rate (1 in -)
SS Gas Injection at 2,700 psi 70°F	895	2,791	388	234,645	Burst	0.83	< 1E–9	> 1 E9

Load Case	MD (ft)	Internal Pressure (psi)	External Pressure (psi)	Real Axial Force (lbf)	Fail Mode	Min. SF	POF or POE (10^x)	Failure Rate (1 in -)
SS Gas Injection at 2,700 psi 70°F	895	2,791	388	234,645	Triaxial	0.82	–1.4	24
SS Gas Injection at 2,700 psi 60°F	895	2,791	388	243,552	Burst	0.83	< 1E–9	> 1 E9
SS Gas Injection at 2,700 psi 60°F	895	2,791	388	243,552	Triaxial	0.82	–1.4	24
Withdrawal Operations	895	2,136	388	169,645	Triaxial	1.12	–6.0	994,458
Hot Shut-In	895	2,793	387	184,752	Burst	0.82	< 1E–9	> 1 E9
Hot Shut-In	895	2,793	387	184,752	Triaxial	0.81	–1.3	19
Cold Shut-In	895	2,793	387	207,421	Burst	0.83	< 1E–9	> 1 E9
Cold Shut-In	895	2,793	387	207,421	Triaxial	0.82	–1.4	24
Injection at 2,700 psi with the Worst Case Cool Down	895	2,791	388	245,909	Burst	0.83	< 1E–9	> 1 E9
Injection at 2,700 psi with the Worst Case Cool Down	895	2,791	388	245,909	Triaxial	0.82	–1.4	24

4.3.6 30% Remaining Body Wall

Table 19 and Table 20 show the results of the 30% RBW analysis. The SFs were significantly less than 1 and the burst POFs for most loads are around 10^{-2} (1 failure in a hundred). This indicated a wall thickness less than 30% would have resulted in a failure rate of 10^{-1} (1 failure in 10) predicting certainty for a ductile rupture.

Table 19: Minimum Safety Factors for the 7 in. Casing with 30% Remaining Body Wall

	Load Case	Burst		Collapse		Tension		Compression		Triaxial	
		Pipe SF	MD (ft)	Pipe SF	MD (ft)	Pipe SF	MD (ft)	Pipe SF	MD (ft)	Pipe SF	MD (ft)
1	Initial Condition	-	-	6.5	8,282	1.73	185	2.81	8,563	1.72	185
2	SS Gas Injection at 2,700 psi 70°F	0.62	895	>3	8,585	1.35	185	-	-	0.61	895
3	SS Gas Injection at 2,700 psi 60°F	0.62	895	>3	8,585	1.31	185	-	-	0.61	895
4	Withdrawal Operations	0.85	895	>3	8,282	1.76	185	2.74	8,563	0.83	895
5	Hot Shut-In	0.61	895	>3	8,585	1.64	185	2.99	8,563	0.60	895
6	Cold Shut-In	0.62	895	>3	8,585	1.50	185	2.98	8,563	0.61	895

	Load Case	Burst		Collapse		Tension		Compression		Triaxial	
		Pipe SF	MD (ft)	Pipe SF	MD (ft)	Pipe SF	MD (ft)	Pipe SF	MD (ft)	Pipe SF	MD (ft)
7	Injection at 2,700 psi with the Worst Case Cool Down	0.62	895	>3	8,585	1.30	185	>3	8,563	0.62	895
8	Worst Case Cool Down without Injection	>3	0	1.74	6,308	1.59	185	2.64	8,563	1.47	896

Table 20: Reliability—Based Design and Probability of Failure for the 7 in. Casing with 30% Remaining Body Wall

Load Case	MD (ft)	Internal Pressure (psi)	External Pressure (psi)	Real Axial Force (lbf)	Fail Mode	Min. SF	POF or POE (10^{x})	Failure Rate (1 in -)
SS Gas Injection at 2,700 psi 70°F	895	2,791	388	234,645	Burst	0.62	–2.1	121
SS Gas Injection at 2,700 psi 70°F	895	2,791	388	234,645	Triaxial	0.61	0	1
SS Gas Injection at 2,700 psi 60°F	895	2,791	388	243,552	Burst	0.62	–2.1	125
SS Gas Injection at 2,700 psi 60°F	895	2,791	388	243,552	Triaxial	0.61	0	1
Withdrawal Operations	895	2,136	388	169,645	Burst	0.85	< 1E–9	> 1 E9
Withdrawal Operations	895	2,136	388	169,645	Triaxial	0.83	–1.6	45
Hot Shut-In	895	2,793	387	184,752	Burst	0.61	–1.9	86
Hot Shut-In	895	2,793	387	184,752	Triaxial	0.60	0	1
Cold Shut-In	895	2,793	387	207,421	Burst	0.62	–2.0	100
Cold Shut-In	895	2,793	387	207,421	Triaxial	0.61	0	1
Injection at 2,700 psi with the Worst Case Cool Down	895	2,791	388	245,909	Burst	0.62	–2.1	128
Injection at 2,700 psi with the Worst Case Cool Down	895	2,791	388	245,909	Triaxial	0.62	0	1

4.3.7 20% Remaining Body Wall

Table 21 and Table 22 show the SFs and RBD results for 20% RBW. As expected, rupture was predicted with the RBD results showing a POF of 1 in 1 for most loads.

Table 21: Minimum Safety Factors for the 7 in. Casing with 20% Remaining Body Wall

	Load Case	Burst		Collapse		Tension		Compression		Triaxial	
		Pipe SF	MD (ft)	Pipe SF	MD (ft)	Pipe SF	MD (ft)	Pipe SF	MD (ft)	Pipe SF	MD (ft)
1	Initial Condition	-	-	6.5	8,282	1.73	185	2.81	8,563	1.72	185
2	SS Gas Injection at 2,700 psi 70°F	0.41	895	>3	8,585	1.35	185	-	-	0.40	895
3	SS Gas Injection at 2,700 psi 60°F	0.41	895	>3	8,585	1.31	185	-	-	0.40	895
4	Withdrawal Operations	0.56	895	>3	8,282	1.76	185	2.74	8,563	0.54	895
5	Hot Shut-In	0.41	895	>3	8,585	1.64	185	2.99	8,563	0.39	895
6	Cold Shut-In	0.41	895	>3	8,585	1.50	185	2.98	8,563	0.39	895
7	Injection at 2,700 psi with the Worst Case Cool Down	0.41	895	>3	8,585	1.30	185	3.27	8,563	0.40	895
8	Worst Case Cool Down without Injection	>3	0	1.7	896	1.59	185	2.64	8,563	1.31	896

Table 22: Reliability-Based Design and Probability of Failure for the 7 in. Casing with 20% Remaining Body Wall

Load Case	MD (ft)	Internal Pressure (psi)	External Pressure (psi)	Real Axial Force (lbf)	Fail Mode	Min. SF	POF or POE (10^x)	Failure Rate (1 in -)
SS Gas Injection at 2,700 psi 70°F	895	2,791	388	234,645	Burst	0.41	0	1
SS Gas Injection at 2,700 psi 70°F	895	2,791	388	234,645	Triaxial	0.40	0	1
SS Gas Injection at 2,700 psi 60°F	895	2,791	388	243,552	Burst	0.41	0	1
SS Gas Injection at 2,700 psi 60°F	895	2,791	388	243,552	Triaxial	0.40	0	1
Withdrawal Operations	895	2,136	388	169,645	Burst	0.56	–0.6	4
Withdrawal Operations	895	2,136	388	169,645	Triaxial	0.54	0	1

Load Case	MD (ft)	Internal Pressure (psi)	External Pressure (psi)	Real Axial Force (lbf)	Fail Mode	Min. SF	POF or POE (10^x)	Failure Rate (1 in -)
Hot Shut-In	895	2,793	387	184,752	Burst	0.41	0	1
Hot Shut-In	895	2,793	387	184,752	Triaxial	0.39	0	1
Cold Shut-In	895	2,793	387	207,421	Burst	0.41	0	1
Cold Shut-In	895	2,793	387	207,421	Triaxial	0.39	0	1
Injection at 2,700 psi with the Worst Case Cool Down	895	2,791	388	245,909	Burst	0.41	0	1
Injection at 2,700 psi with the Worst Case Cool Down	895	2,791	388	245,909	Triaxial	0.40	0	1

4.3.8 Summary of Remaining Body Wall Results with Wall Loss, Top of Cement at 7,000 ft MD

The results presented in Section 4.3.4 show that five load cases dictated the RBD results. These cases were:

- SS Gas Injection at 2,700 psi and 70°F Surface Temperature
- SS Injection at 2,700 psi and 60°F Surface Temperature
- Hot Shut-in
- Cold Shut-in
- Injection at 2,700 psi with the Worst Case Cool Down Temperature Profile

Of these, the first load (SS Gas Injection at 2,700 psi and 70°F Surface Temperature) was a reasonable operational load case whereas the last case (Injection at 2,700 psi with the Worst Case Cool Down temperature profile) was the most severe load based on the measured cool down temperature in the well. The effects of RBW on the POE and POF for these two load cases are depicted in Figure 16 and Figure 17, respectively. A review of the burst POF showed the threshold for greater than 90% POF or failure occurring between 30% RBW and 20% RBW. Ductile rupture was therefore predicted for RBW lower than 30%. The Hot Shut-in load was not a load of interest because the well was exposed to injection conditions when the leak event happened.

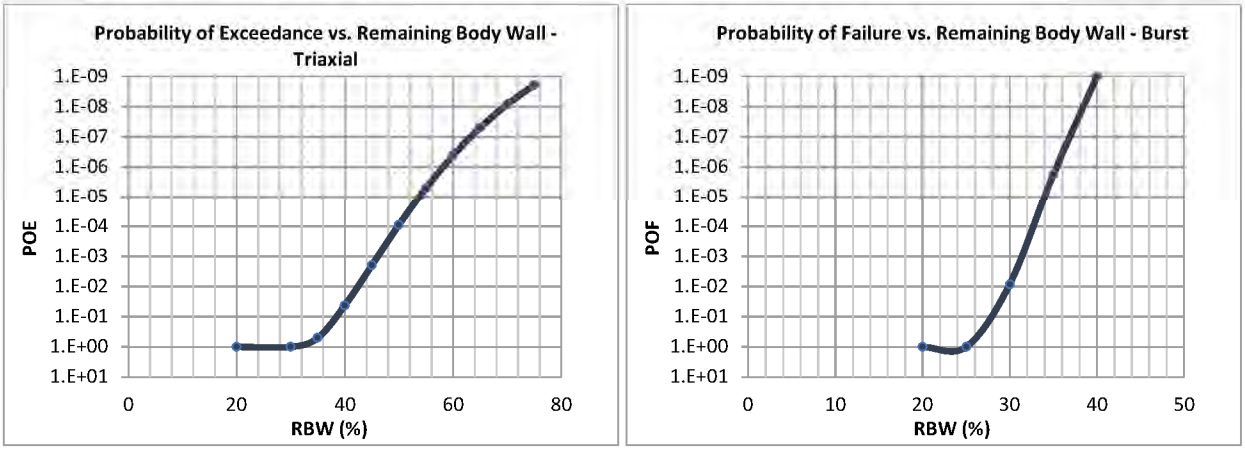

Figure 16: Probability of Exceedance and Failure vs. Remaining Body Wall, Load Case "Steady State Gas Injection at 2,700 psi and 70°F Surface Temperature", Top of Cement at 7000 ft MD

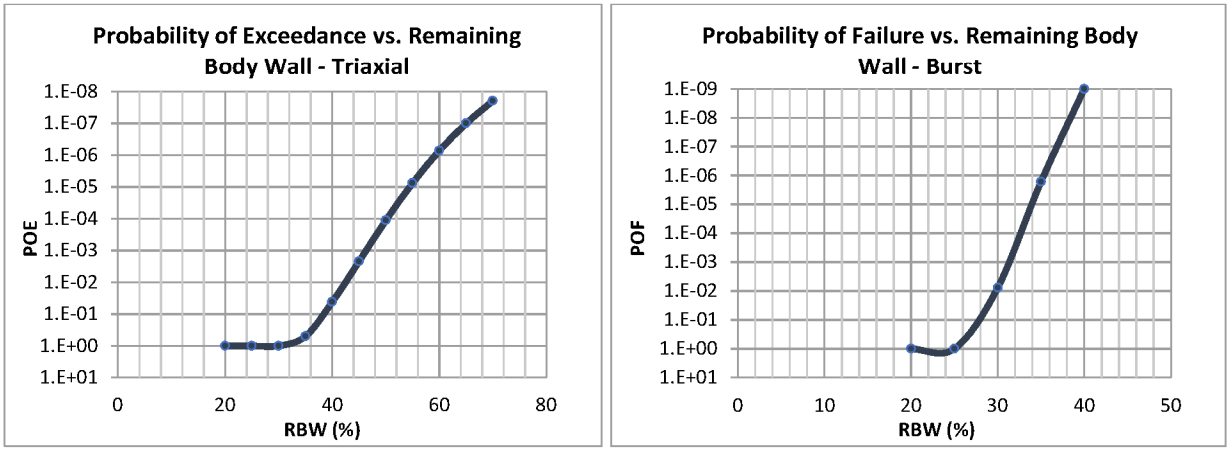

Figure 17: Probability of Exceedance and Failure vs. Remaining Body Wall, Load Case "Injection at 2,700 psi with the Worst Case Cool Down" Temperature Profile, Top of Cement at 7000 ft MD

Detailed results, including tabulated values of the POE and POF for these load cases, can be found in Appendix A.

4.4 Effect of Wall Loss with Top of Cement at 990 ft MD

As a sensitivity case, we looked at the possibility that because of the formation cave-in, the point of fixity of the 7 in. casing had shifted to 990 ft MD at the shoe of the surface casing. With a shallower point of fixity, the stresses for a given wall loss would have been higher (compared to TOC at 7,000 ft MD); therefore, higher POF (or POE) could have been expected. This sensitivity therefore established an upper bound for the wall loss required for ductile rupture.

Just as in the previous case, RBW ranging from 80% to 20% of nominal wall was investigated. Key results are discussed in this section. Detailed results, including tabulated SFs and probabilities of exceedance and failure, are provided in Appendix B.

The impact of a shallower TOC was best illustrated by looking at two load cases: "Steady State Gas Injection at 2,700 psi and 70°F Surface Temperature" and "Injection at 2,700 psi with the Worst Case Cool Down Temperature Profile". Figure 18 and Figure 19, respectively, show the POE and POF as a function of RBW for these two load cases. Results were not substantially different from the case with TOC at 7,000 ft MD, and ductile rupture was predicted for RBW less than 30%. In other words, regardless of the TOC, when the RBW was less than 30%, ductile rupture of the casing was considered imminent.

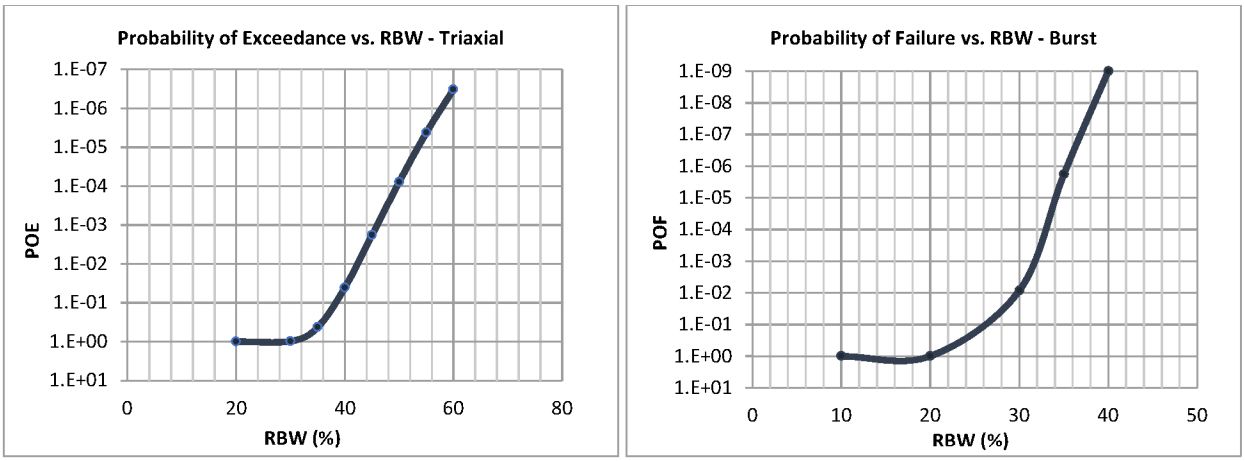

Figure 18: Probability of Exceedance and Probability of Failure for Load Case "Steady State Gas Injection at 2,700 psi and 70°F Surface Temperature", Top of Cement at 990 ft MD

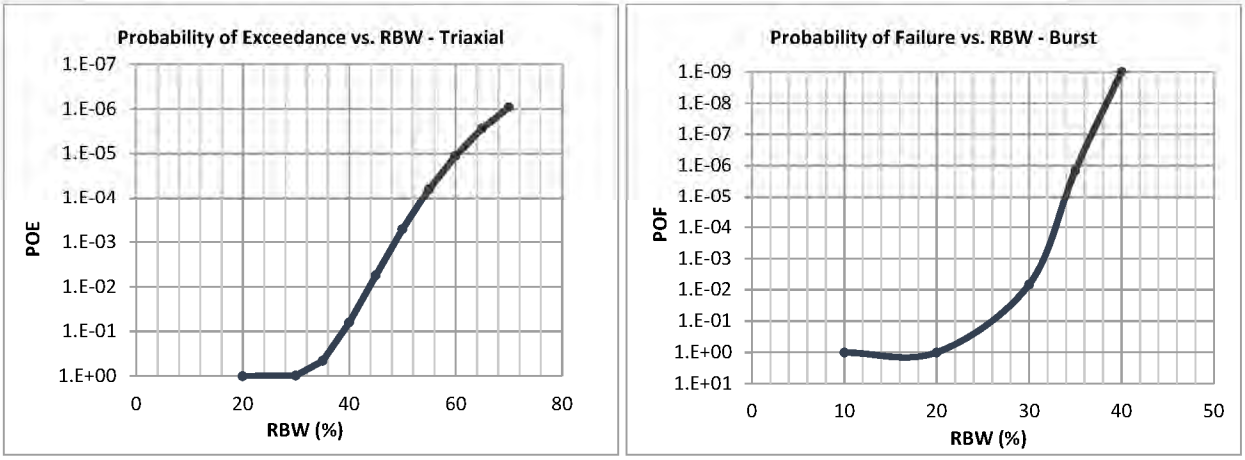

Figure 19: Probability of Exceedance and Probability of Failure for Load Case "Injection at 2,700 psi with the Worst Case Cool Down Temperature Profile", Top of Cement at 990 ft MD

5 Conclusions

The following is a summary of the study results:

- The results showed that for RBW less than 30% of nominal wall, ductile rupture of the casing would have been expected in a tension-burst failure mode for all injection cases. This was the case regardless of the extent of cool down during injection; therefore, wall loss was established as the key driver of failure. Thermally induced tension from cool down during injection increased the axial stress in which the highest stresses occur when the point of fixity was at the 11 3/4 in. casing shoe (990 ft).
- The results for predicting casing rupture were similar for a case where the casing was fixed at 7,000 ft, the original TOC, or if the casing was fixed at 990 ft. The point of fixity of the casing affected the axial stress when the casing was cooled or heated compared to the initial condition.

6 References

[1] SoCalGas, "Temperature Log, Nov 8, 2016, AC_BLD_0018125-AC_BLD_0018136 (SS-25 Completion Profiler Pages.pdf)".

[2] API, "Calculating Performance Properties of Pipe Used as Casing or Tubing, API Technical Report 5C3, Seventh Edition, June 2018".

[3] SoCalGas, "SS-25 Temperature Profile (SS-25 Geothermal Gradients Rev 2.xlsx)".

[4] SoCalGas, *SS25 Well Pressures, AC_CPUC_0000100 (SS-25 Well Documentation (from SoCalGas)_N.pdf, page 78).*

[5] SoCalGas, "Division of Oil and Gas History of Oil and Gas Well AC_BLD_0000089-AC_BLD_0000091 (SS-25 Well Documentation (from SoCalGas)_N.pdf, pages 67-69)".

[6] SoCalGas, "SS-25 Directional Survey (SS-25 Direct Svy Data Plots – WSW, Rev 9Apr16.xlsx)".

[7] SoCalGas, "Completion Profiler Temperature Data Nov 8, 2018 (Socalgas_SS25_11-8-15_PLT_Protechniques AC_BLD_0035419.xlsx)".

Appendix A Detailed Results with Wall Loss, Top of Cement at 7,000 ft MD

This appendix presents detailed results from the investigation of the effect of wall loss with the TOC at 7,000 ft MD for the four load cases of interest where factors of safety fell below minimum requirements with RBW lower than 65% of nominal wall.

A.1 Steady State Gas Injection at 2,700 psi and 70°F Surface Temperature

Table 23 and Table 24, respectively, show RBD results for the triaxial and burst failure modes.

As discussed in Section 4.3.2, when the RBW approaches 65%, the triaxial SFs and the POE start to become an issue. When the RBW is 65%, the probability of yielding the casing is extremely low for the gas injection at 2,700 psi and 70°F load case.

Table 24 shows that the burst failure mode becomes an issue when the RBW is less than 30% with a failure rate greater than 1 in 121.

Table 23: Probability of Exceedance vs. Remaining Body Wall for the 7 in. Casing for Triaxial Failure Mode

RBW (%)	Load Case	MD (ft)	Internal Pressure (psi)	External Pressure (psi)	Real Axial Force (lbf)	Fail Mode	Min. SF	POF or POE (10^{x})	Failure Rate (1 in -)
75	SS Gas Injection at 2,700 psi 70°F	895	2,791	388	234,645	Triaxial	1.36	–8.7	524,252,882
70	SS Gas Injection at 2,700 psi 70°F	895	2,791	388	234,645	Triaxial	1.31	–8.1	120,660,060
65	SS Gas Injection at 2,700 psi 70°F	895	2,791	388	234,645	Triaxial	1.25	–7.3	20,396,576
60	SS Gas Injection at 2,700 psi 70°F	895	2,791	388	234,645	Triaxial	1.18	–6.4	2,432,666
55	SS Gas Injection at 2,700 psi 70°F	895	2,791	388	234,645	Triaxial	1.10	–5.3	199,726
50	SS Gas Injection at 2,700 psi 70°F	895	2,791	388	234,645	Triaxial	1.01	–4.1	11,470
45	SS Gas Injection at 2,700 psi 70°F	895	2,791	388	234,645	Triaxial	0.92	–2.7	513

RBW (%)	Load Case	MD (ft)	Internal Pressure (psi)	External Pressure (psi)	Real Axial Force (lbf)	Fail Mode	Min. SF	POF or POE (10^x)	Failure Rate (1 in -)
40	SS Gas Injection at 2,700 psi 70°F	895	2,791	388	234,645	Triaxial	0.82	–1.4	24
35	SS Gas Injection at 2,700 psi 70°F	895	2,791	388	234,645	Triaxial	0.72	–0.4	2
30	SS Gas Injection at 2,700 psi 70°F	895	2,791	388	234,645	Triaxial	0.41	0	1
20	SS Gas Injection at 2,700 psi 70°F	895	2,791	388	234,645	Triaxial	0.40	0	1

Table 24: Probability of Failure vs. Remaining Body Wall for the 7 in. Casing for Burst Failure Mode

RBW (%)	Load Case	MD (ft)	Internal Pressure (psi)	External Pressure (psi)	Real Axial Force (lbf)	Fail Mode	Min. SF	POF or POE (10^x)	Failure Rate (1 in -)
55	SS Gas Injection at 2,700 psi 70°F	895	2,791	388	234,645	Burst	1.14	< 1E–9	> 1 E9
50	SS Gas Injection at 2,700 psi 70°F	895	2,791	388	234,645	Burst	1.04	< 1E–9	> 1 E9
45	SS Gas Injection at 2,700 psi 70°F	895	2,791	388	234,645	Burst	0.93	< 1E–9	> 1 E9
40	SS Gas Injection at 2,700 psi 70°F	895	2,791	388	234,645	Burst	0.83	< 1E–9	> 1 E9
35	SS Gas Injection at 2,700 psi 70°F	895	2,791	388	234,645	Burst	0.72	–5.7	560,752
30	SS Gas Injection at 2,700 psi 70°F	895	2,791	388	234,645	Burst	0.62	–2.1	121
25	SS Gas Injection at 2,700 psi 70°F	895	2,791	388	234,645	Burst	0.52	–0.1	1
20	SS Gas Injection at 2,700 psi 70°F	895	2,791	388	234,645	Burst	0.41	0	1

Figure 20 and Figure 21 show POE and POF versus RBW results from Table 23 and Table 24 for two failure modes.

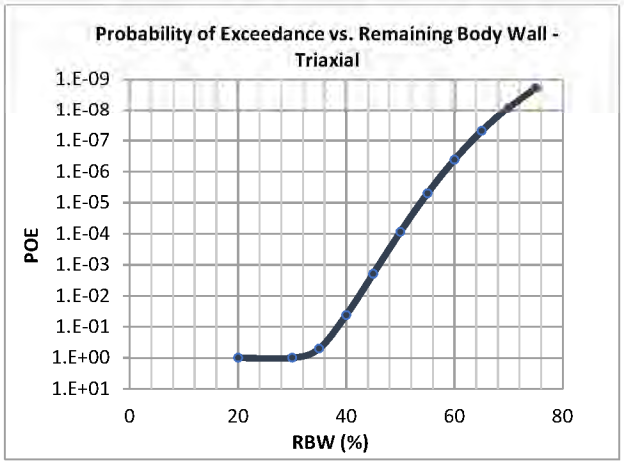

Figure 20: Probability of Exceedance vs. Remaining Body Wall for Triaxial Failure Mode

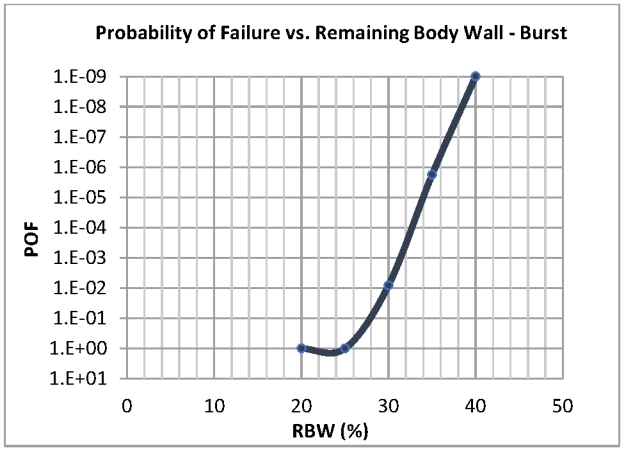

Figure 21: Probability of Failure vs. Remaining Body Wall for Burst Failure Mode

A.2 Steady State Gas Injection at 2,700 psi and 60°F Surface Temperature

Table 25 and Table 26, respectively, show RBD results for triaxial and burst failure modes.

As discussed in Section 4.3.2, when the RBW approaches 65%, the triaxial SFs and the POEs start to become an issue. When the RBW is 65%, the probability of yielding the casing is extremely low for the gas Injection at 2,700 psi and 60°F load case.

Table 26 shows that the burst failure mode becomes an issue when the RBW is less than 30% with a failure rate greater than 1 in 125.

Table 25: Probability of Exceedance vs. Remaining Body Wall for the 7 in. Casing for Triaxial Failure Mode

RBW (%)	Load Case	MD (ft)	Internal Pressure (psi)	External Pressure (psi)	Real Axial Force (lbf)	Fail Mode	Min. SF	POF or POE (10^{x})	Failure Rate (1 in -)
70	SS Gas Injection at 2,700 psi 60°F	895	2,791	388	243,552	Triaxial	1.30	–7.8	61,562,109
65	SS Gas Injection at 2,700 psi 60°F	895	2,791	388	243,552	Triaxial	1.24	–7.1	11,674,154
60	SS Gas Injection at 2,700 psi 60°F	895	2,791	388	243,552	Triaxial	1.17	–6.2	1,571,136
55	SS Gas Injection at 2,700 psi 60°F	895	2,791	388	243,552	Triaxial	1.10	–5.2	145,824
50	SS Gas Injection at 2,700 psi 60°F	895	2,791	388	243,552	Triaxial	1.01	–3.9	9,424
45	SS Gas Injection at 2,700 psi 60°F	895	2,791	388	243,552	Triaxial	0.92	–2.7	468
40	SS Gas Injection at 2,700 psi 60°F	895	2,791	388	243,552	Triaxial	0.82	–1.4	24
35	SS Gas Injection at 2,700 psi 60°F	895	2,791	388	243,552	Triaxial	0.72	–0.4	2
30	SS Gas Injection at 2,700 psi 60°F	895	2,791	388	243,552	Triaxial	0.61	0	1
25	SS Gas Injection at 2,700 psi 60°F	895	2,791	388	243,552	Triaxial	0.51	0	1
20	SS Gas Injection at 2,700 psi 60°F	895	2,791	388	243,552	Triaxial	0.40	0	1

Table 26: Probability of Failure vs. Remaining Body Wall for the 7 in. Casing for Burst Failure Mode

RBW (%)	Load Case	MD (ft)	Internal Pressure (psi)	External Pressure (psi)	Real Axial Force (lbf)	Fail Mode	Min. SF	POF or POE (10^x)	Failure Rate (1 in -)
55	SS Gas Injection at 2,700 psi 60°F	895	2,791	388	243,552	Burst	1.14	< 1E–9	> 1 E9
50	SS Gas Injection at 2,700 psi 60°F	895	2,791	388	243,552	Burst	1.04	< 1E–9	> 1 E9
45	SS Gas Injection at 2,700 psi 60°F	895	2,791	388	243,552	Burst	0.93	< 1E–9	> 1 E9
40	SS Gas Injection at 2,700 psi 60°F	895	2,791	388	243,552	Burst	0.83	< 1E–9	> 1 E9
35	SS Gas Injection at 2,700 psi 60°F	895	2,791	388	243,552	Burst	0.73	–5.8	590,709
30	SS Gas Injection at 2,700 psi 60°F	895	2,791	388	243,552	Burst	0.62	–2.1	125
25	SS Gas Injection at 2,700 psi 60°F	895	2,791	388	243,552	Burst	0.52	–0.1	1
20	SS Gas Injection at 2,700 psi 60°F	895	2,791	388	243,552	Burst	0.41	0	1

Figure 22 and Figure 23 show POE and POF versus RBW graphically.

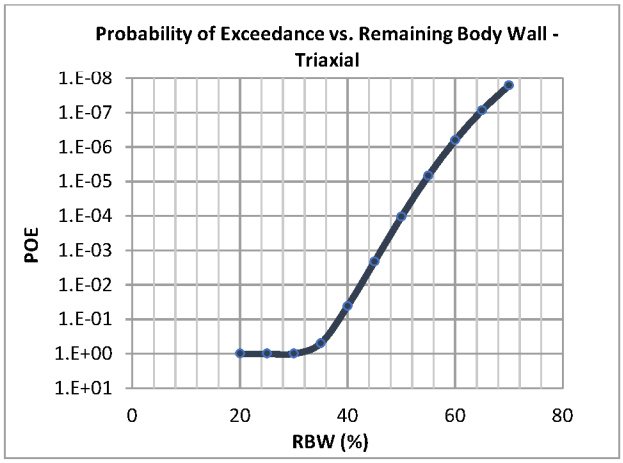

Figure 22: Probability of Exceedance vs. Remaining Body Wall for Triaxial Failure Mode

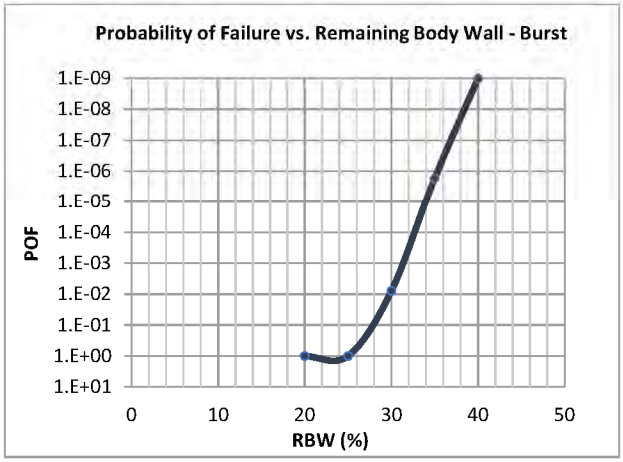

Figure 23: Probability of Failure vs. Remaining Body Wall for Burst Failure Mode

A.3 Cold Shut-In

Table 27 and Table 28, respectively, show RBD results for the triaxial and burst failure modes.

As discussed in Section 4.3.2, when the RBW approaches 65%, the triaxial SF and the POE start to become an issue. When the RBW is 60%, the probability of yielding the casing is very low for the Cold Shut-In load case.

Table 28 shows that the burst failure mode becomes an issue when the RBW is less than 30% with a failure rate greater than 1 in 100.

Table 27: Probability of Exceedance vs. Remaining Body Wall for the 7 in. Casing for Triaxial Failure Mode

RBW (%)	Load Case	MD (ft)	Internal Pressure (psi)	External Pressure (psi)	Real Axial Force (lbf)	Fail Mode	Min. SF	POF or POE (10^x)	Failure Rate (1 in -)
65	Cold Shut-in	895	2,793	387	207,421	Triaxial	1.28	–7.9	97,424,484
60	Cold Shut-in	895	2,793	387	207,421	Triaxial	1.20	–6.9	7,998,053
55	Cold Shut-in	895	2,793	387	207,421	Triaxial	1.11	–5.7	454,099
50	Cold Shut-in	895	2,793	387	207,421	Triaxial	1.02	–4.3	18,488
45	Cold Shut-in	895	2,793	387	207,421	Triaxial	0.92	–2.8	619
40	Cold Shut-in	895	2,793	387	207,421	Triaxial	0.82	–1.4	24
35	Cold Shut-in	895	2,793	387	207,421	Triaxial	0.71	–0.3	2
30	Cold Shut-in	895	2,793	387	207,421	Triaxial	0.61	0	1
25	Cold Shut-in	895	2,793	387	207,421	Triaxial	0.50	0	1
20	Cold Shut-in	895	2,793	387	207,421	Triaxial	0.39	0	1

Table 28: Probability of Failure vs. Remaining Body Wall for the 7 in. Casing for Burst Failure Mode

RBW (%)	Load Case	MD (ft)	Internal Pressure (psi)	External Pressure (psi)	Real Axial Force (lbf)	Fail Mode	Min. SF	POF or POE (10^x)	Failure Rate (1 in -)
55	Cold Shut-in	895	2,793	387	207,421	Burst	1.14	< 1E–9	> 1 E9
50	Cold Shut-in	895	2,793	387	207,421	Burst	1.03	< 1E–9	> 1 E9
45	Cold Shut-in	895	2,793	387	207,421	Burst	0.93	< 1E–9	> 1 E9
40	Cold Shut-in	895	2,793	387	207,421	Burst	0.83	< 1E–9	> 1 E9
35	Cold Shut-in	895	2,793	387	207,421	Burst	0.72	–5.6	426,563
30	Cold Shut-in	895	2,793	387	207,421	Burst	0.62	–2.0	100
25	Cold Shut-in	895	2,793	387	207,421	Burst	0.52	–0.1	1
20	Cold Shut-in	895	2,793	387	207,421	Burst	0.41	0	1

Figure 24 and Figure 25 show the results graphically.

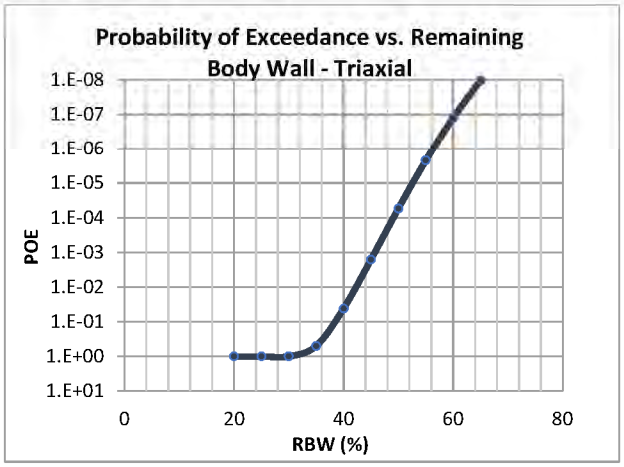

Figure 24: Probability of Exceedance vs. Remaining Body Wall for Triaxial Failure Mode

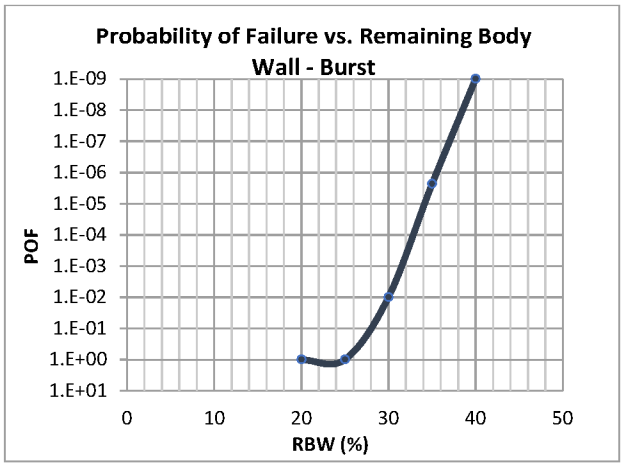

Figure 25: Probability of Failure vs. Remaining Body Wall for Burst Failure Mode

A.4 Injection at 2,700 psi with the Worst Case Cool Down Temperature Profile

Table 29 and Table 30 show RBD results for the triaxial and burst failure modes, respectively. The RBD results are similar to the steady state gas injection at 2,700 psi and 70°F Surface Temperature load case. That is, when the RBW approaches 65%, the triaxial failure mode is highly reliable, and when the RBD is below 30%, the burst mode POF becomes not acceptable.

Table 30 shows that the burst failure mode becomes an issue when the RBW is less than 30% with a failure rate greater than 1 in 128.

Table 29: Probability of Exceedance vs. Remaining Body Wall for the 7 in. Casing for Triaxial Failure Mode

RBW (%)	Load Case	MD (ft)	Internal Pressure (psi)	External Pressure (psi)	Real Axial Force (lbf)	Fail Mode	Min. SF	POF or POE (10^{x})	Failure Rate (1 in -)
70	Injection at 2,700 psi with the Worst Case Cool Down	895	2,791	388	245,909	Triaxial	1.29	–7.7	50,819,542
65	Injection at 2,700 psi with the Worst Case Cool Down	895	2,791	388	245,909	Triaxial	1.23	–7.0	9,938,665
60	Injection at 2,700 psi with the Worst Case Cool Down	895	2,791	388	245,909	Triaxial	1.17	–6.1	1,382,023
55	Injection at 2,700 psi with the Worst Case Cool Down	895	2,791	388	245,909	Triaxial	1.09	–5.1	132,651
50	Injection at 2,700 psi with the Worst Case Cool Down	895	2,791	388	245,909	Triaxial	1.01	–3.9	8,859
45	Injection at 2,700 psi with the Worst Case Cool Down	895	2,791	388	245,909	Triaxial	0.92	–2.6	453
40	Injection at 2,700 psi with the Worst Case Cool Down	895	2,791	388	245,909	Triaxial	0.82	–1.4	24

RBW (%)	Load Case	MD (ft)	Internal Pressure (psi)	External Pressure (psi)	Real Axial Force (lbf)	Fail Mode	Min. SF	POF or POE (10^{x})	Failure Rate (1 in -)
35	Injection at 2,700 psi with the Worst Case Cool Down	895	2,791	388	245,909	Triaxial	0.72	–0.4	2
30	Injection at 2,700 psi with the Worst Case Cool Down	895	2,791	388	245,909	Triaxial	0.62	0	1
25	Injection at 2,700 psi with the Worst Case Cool Down	895	2,791	388	245,909	Triaxial	0.51	0	1
20	Injection at 2,700 psi with the Worst Case Cool Down	895	2,791	388	245,909	Triaxial	0.40	0	1

Table 30: Probability of Failure vs. Remaining Body Wall for the 7 in. Casing for Burst Failure Mode

RBW (%)	Load Case	MD (ft)	Internal Pressure (psi)	External Pressure (psi)	Real Axial Force (lbf)	Fail Mode	Min. SF	POF or POE (10^{x})	Failure Rate (1 in -)
55	Injection at 2,700 psi with the Worst Case Cool Down	895	2,791	388	245,909	Burst	1.14	< 1E–9	> 1 bil
50	Injection at 2,700 psi with the Worst Case Cool Down	895	2,791	388	245,909	Burst	1.04	< 1E–9	> 1 bil
45	Injection at 2,700 psi with the Worst Case Cool Down	895	2,791	388	245,909	Burst	0.93	< 1E–9	> 1 bil
40	Injection at 2,700 psi with the Worst Case Cool Down	895	2,791	388	245,909	Burst	0.83	< 1E–9	> 1 bil
35	Injection at 2,700 psi with the Worst Case Cool Down	895	2,791	388	245,909	Burst	0.73	–5.7	606,617

RBW (%)	Load Case	MD (ft)	Internal Pressure (psi)	External Pressure (psi)	Real Axial Force (lbf)	Fail Mode	Min. SF	POF or POE (10^x)	Failure Rate (1 in -)
30	Injection at 2,700 psi with the Worst Case Cool Down	895	2,791	388	245,909	Burst	0.62	–2.1	128
25	Injection at 2,700 psi with the Worst Case Cool Down	895	2,791	388	245,909	Burst	0.52	–0.1	1
20	Injection at 2,700 psi with the Worst Case Cool Down	895	2,791	388	245,909	Burst	0.41	0	1

Figure 26 and Figure 27, respectively, show the POE and POF results graphically for this case.

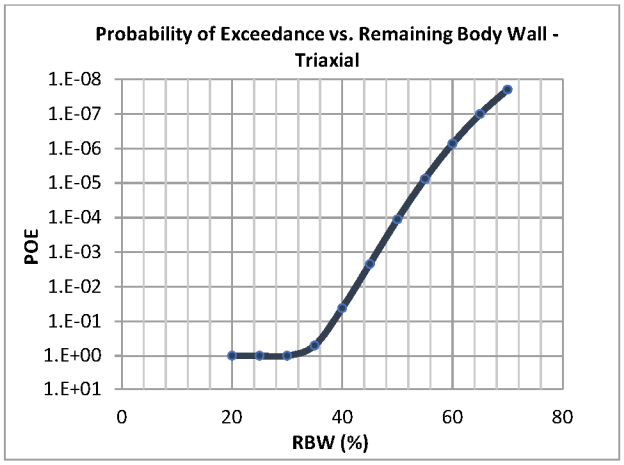

Figure 26: Probability of Exceedance vs. Remaining Body Wall for Triaxial Failure Mode

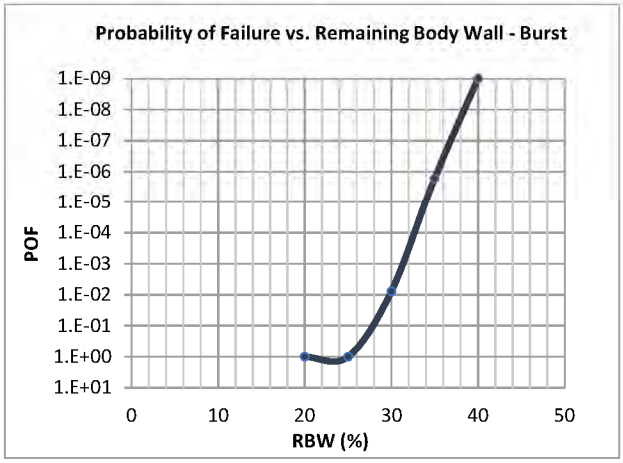

Figure 27: Probability of Failure vs. Remaining Body Wall for Burst Failure Mode

Appendix B Detailed Results with Effect of Wall Loss, Top of Cement at 990 ft MD

This appendix shows the detailed results for the effect of wall low (RBW ranging from 80% of nominal wall to 20% of nominal wall) for the case where the TOC is at 990 ft.

B.1 80% Remaining Body Wall

Table 31 shows SFs for the 7 in. casing loads with 80% RBW. These SFs are similar to the base case with the API tolerance wall thickness except for the triaxial SF of 1.21 at 185 ft. The tension SFs for loads 2, 3, and 8 are slightly below the minimum SF for tension. However, the focus of this study was burst failure and not tension failure. The tension stress is included in the triaxial SF and was therefore considered. The reliability of the injection at 2,700 psi with worst case cool down load will be assessed in Section B.2 where the 70% RBW case is analyzed.

Table 31: Minimum Safety Factors for the 7 in. Casing with 80% Remaining Body Wall

		Burst		Collapse		Tension		Compression		Triaxial	
	Load Case	Pipe SF	MD (ft)	Pipe SF	MD (ft)	Pipe SF	MD (ft)	Pipe SF	MD (ft)	Pipe SF	MD (ft)
1	Initial Condition	-	-	2.12	6,308	1.73	185	2.21	8,563	1.73	185
2	SS Gas Injection at 2,700 psi 70°F	1.61	0	>3	8,585	1.38	185	>3	8,513	1.41	104
3	SS Gas Injection at 2,700 psi 60°F	1.61	0	>3	8,585	1.33	185	>3	8,513	1.37	185
4	Withdrawal Operations	2.06	0	>3	8,282	1.75	185	2.47	8,563	1.80	104
5	Hot Shut-In	1.60	0	>3	8,585	1.67	185	2.67	8,563	1.52	895
6	Cold Shut-In	1.61	0	>3	8,585	1.41	185	2.66	8,563	1.43	104
7	Injection at 2,700 psi with the Worst Case Cool Down	1.61	0	>3	8,585	1.12	185	2.90	8,563	1.21	185
8	Worst Case Cool Down without Injection	>3	0	1.79	6,308	1.34	185	2.39	8,563	1.32	185

B.2 70% Remaining Body Wall

Table 32 shows SFs for the 7 in. casing loads with 70% RBW. As discussed in Section 4.2.2, the minimum SFs are similar to the base case. As expected, the burst and triaxial SFs are reduced because of the reduced wall thickness. The triaxial SF for gas injection at 2,700 psi with the Worst Case Cool Down temperature profile load case is 1.20 and below minimum WSD requirements of 1.25.

Table 32: Minimum Safety Factors for the 7 in. Casing with 70% Remaining Body Wall

	Load Case	Burst		Collapse		Tension		Compression		Triaxial	
		Pipe SF	MD (ft)	Pipe SF	MD (ft)	Pipe SF	MD (ft)	Pipe SF	MD (ft)	Pipe SF	MD (ft)
1	Initial Condition	-	-	2.12	6,308	1.73	185	2.21	8,563	1.73	185
2	SS Gas Injection at 2,700 psi 70°F	1.45	895	>3	8,585	1.38	185	>3	8,513	1.32	895
3	SS Gas Injection at 2,700 psi 60°F	1.45	895	>3	8,585	1.33	185	>3	8,513	1.30	895
4	Withdrawal Operations	1.97	895	>3	8,282	1.75	185	2.47	8,563	1.77	895
5	Hot Shut-In	1.43	895	>3	8,585	1.67	185	2.67	8,563	1.37	895
6	Cold Shut-In	1.44	895	>3	8,585	1.41	185	2.66	8,563	1.33	895
7	Injection at 2,700 psi with the Worst Case Cool Down	1.45	895	>3	8,585	1.12	185	2.90	8,563	1.20	895
8	Worst Case Cool Down without Injection	>3	0	1.79	6,308	1.34	185	2.39	8,563	1.32	185

Table 33 shows RBD results and the POE or POF for this case. The RBD triaxial failure mode is an indication of the probability of yielding the casing under the assumed load conditions. Yielding the casing does not predict casing failure or rupture. When the RBW is 70%, the probability of yielding the casing is less than 1 in one million for the Injection at 2,700 psi with Worst Case Cool Down temperature profile load case indicating very high reliability.

Table 33: RBD Probability of Failure for the 7 in. Casing with 70% Remaining Body Wall

Load Case	MD (ft)	Internal Pressure (psi)	External Pressure (psi)	Real Axial Force (lbf)	Fail Mode	Min. SF	POF or POE (10^x)	Failure Rate (1 in -)
Injection at 2,700 psi with the Worst Case Cool Down	895	2,791	388	289,763	Triaxial	1.20	–6.0	1,099,610

B.3 65% Remaining Body Wall

Table 34 shows SFs for the 7 in. casing loads with 65% RBW. The farther reduction in wall thickness is reflected in the burst and triaxial SFs. The triaxial SFs for some loads are below minimum WSD requirements.

Table 34: Minimum Safety Factors for the 7 in. Casing with 65% Remaining Body Wall

		Burst		Collapse		Tension		Compression		Triaxial	
	Load Case	Pipe SF	MD (ft)	Pipe SF	MD (ft)	Pipe SF	MD (ft)	Pipe SF	MD (ft)	Pipe SF	MD (ft)
1	Initial Condition	-	-	2.12	6,308	1.73	185	2.21	8,563	1.73	185
2	SS Gas Injection at 2,700 psi 70°F	1.35	895	>3	8,585	1.38	185	>3	8,513	1.25	895
3	SS Gas Injection at 2,700 psi 60°F	1.35	895	>3	8,585	1.33	185	>3	8,513	1.24	895
4	Withdrawal Operations	1.83	895	>3	8,282	1.75	185	2.47	8,563	1.69	895
5	Hot Shut-In	1.33	895	>3	8,585	1.67	185	2.67	8,563	1.29	895
6	Cold Shut-In	1.34	895	>3	8,585	1.41	185	2.66	8,563	1.26	895
7	Injection at 2,700 psi with the Worst Case Cool Down	1.35	895	>3	8,585	1.12	185	2.90	8,563	1.16	895
8	Worst Case Cool Down without Injection	>3	0	1.79	6,308	1.34	185	2.39	8,563	1.32	185

Because some of the loads have triaxial SFs less than 1.25 when the wall is reduced to 65% of nominal, RBD was used to evaluate the POE. Table 35 shows RBD results and the POE[v] for this case. The RBD triaxial failure mode is an indication of the probability of yielding the casing under the assumed load conditions. Yielding the casing does not predict casing failure or rupture. The POE is very low at 1 in 362,000 for an RBW of 65%.

Table 35: RBD Probability of Failure for the 7 in. Casing with 65% Remaining Body Wall

Load Case	MD (ft)	Internal Pressure (psi)	External Pressure (psi)	Real Axial Force (lbf)	Fail Mode	Min. SF	POF or POE (10^{x})	Failure Rate (1 in -)
SS Gas Injection at 2,700 psi 60°F	895	2,791	388	240,459	Triaxial	1.24	–7.1	14,487,550

[v] POE is shown in the table when the VME SF is less than the minimum design factor of 1.25. POF is shown when the uniaxial load SF is less than the minimum SF. The Fail Mode column in the table determines if the value shown in the POF or POE column is the POF or POE.

Load Case	MD (ft)	Internal Pressure (psi)	External Pressure (psi)	Real Axial Force (lbf)	Fail Mode	Min. SF	POF or POE (10^{x})	Failure Rate (1 in -)
Injection at 2,700 psi with the Worst Case Cool Down	895	2,791	388	289,763	Triaxial	1.16	–5.5	362,200

B.4 60% Remaining Body Wall

Table 36 shows SFs for the 7 in. casing loads with 60% RBW. As expected, because the RBW is reduced, the burst load SF decreases, and the POF or POE increases (Table 37). Similar to the previous discussion, the POE and POF are still very low.

Table 36: Minimum Safety Factors for the 7 in. Casing with 60% Remaining Body Wall

	Load Case	Burst		Collapse		Tension		Compression		Triaxial	
		Pipe SF	MD (ft)	Pipe SF	MD (ft)	Pipe SF	MD (ft)	Pipe SF	MD (ft)	Pipe SF	MD (ft)
1	Initial Condition	-	-	2.12	6,308	1.73	185	2.21	8,563	1.73	185
2	SS Gas Injection at 2,700 psi 70°F	1.24	895	>3	8,585	1.38	185	>3	8,513	1.18	895
3	SS Gas Injection at 2,700 psi 60°F	1.24	895	>3	8,585	1.33	185	>3	8,513	1.17	895
4	Withdrawal Operations	1.69	895	>3	8,282	1.75	185	2.47	8,563	1.60	895
5	Hot Shut-In	1.23	895	>3	8,585	1.67	185	2.67	8,563	1.20	895
6	Cold Shut-In	1.24	895	>3	8,585	1.41	185	2.66	8,563	1.19	895
7	Injection at 2,700 psi with the Worst Case Cool Down	1.24	895	>3	8,585	1.12	185	2.90	8,563	1.11	895
8	Worst Case Cool Down without Injection	>3	0	1.79	6,308	1.34	185	2.39	8,563	1.32	185

Table 37: RBD Probability of Failure for the 7 in. Casing with 60% Remaining Body Wall

Load Case	MD (ft)	Internal Pressure (psi)	External Pressure (psi)	Real Axial Force (lbf)	Fail Mode	Min. SF	POF or POE (10^{x})	Failure Rate (1 in -)
SS Gas Injection at 2,700 psi 70°F	895	2,791	388	230,093	Triaxial	1.18	–6.4	3,093,185

Load Case	MD (ft)	Internal Pressure (psi)	External Pressure (psi)	Real Axial Force (lbf)	Fail Mode	Min. SF	POF or POE (10^x)	Failure Rate (1 in -)
SS Gas Injection at 2,700 psi 60°F	895	2,791	388	240,459	Triaxial	1.17	–6.2	1,868,874
Hot Shut-In	895	2,793	387	181,577	Triaxial	1.20	–7.1	13,854,575
Cold Shut-In	895	2,793	387	223,356	Triaxial	1.19	–6.5	3,858,248
Injection at 2,700 psi with the Worst Case Cool Down	895	2,791	388	289,763	Triaxial	1.11	–4.9	89,143

B.5 50% Remaining Body Wall

Table 38 shows SFs for the 7 in. casing loads with 50% RBW. As expected, because the RBW is reduced, the burst load SF decreases, and the POF or POE increases (Table 39). Again, the POE and POF are very low, indicating no failure.

Table 38: Minimum Safety Factors for the 7 in. Casing with 50% Remaining Body Wall

		Burst		Collapse		Tension		Compression		Triaxial	
	Load Case	Pipe SF	MD (ft)	Pipe SF	MD (ft)	Pipe SF	MD (ft)	Pipe SF	MD (ft)	Pipe SF	MD (ft)
1	Initial Condition	-	-	2.12	6,308	1.73	185	2.21	8,563	1.73	185
2	SS Gas Injection at 2,700 psi 70°F	1.04	895	>3	8,585	1.38	185	>3	8,513	1.02	895
3	SS Gas Injection at 2,700 psi 60°F	1.04	895	>3	8,585	1.33	185	>3	8,513	1.01	895
4	Withdrawal Operations	1.41	895	>3	8,282	1.75	185	2.47	8,563	1.38	895
5	Hot Shut-In	1.02	895	>3	8,585	1.67	185	2.67	8,563	1.01	895
6	Cold Shut-In	1.03	895	>3	8,585	1.41	185	2.66	8,563	1.02	895
7	Injection at 2,700 psi with the Worst Case Cool Down	1.04	895	>3	8,585	1.12	185	2.90	8,563	0.98	895
8	Worst Case Cool Down without Injection	>3	0	1.79	6,308	1.34	185	2.39	8,563	1.32	185

Table 39: RBD Probability of Failure for the 7 in. Casing with 50% Remaining Body Wall

Load Case	MD (ft)	Internal Pressure (psi)	External Pressure (psi)	Real Axial Force (lbf)	Fail Mode	Min. SF	POF or POE (10^x)	Failure Rate (1 in -)
SS Gas Injection at 2,700 psi 70°F	895	2,791	388	230,093	Burst	1.04	< 1E–9	> 1 bil
SS Gas Injection at 2,700 psi 70°F	895	2,791	388	230,093	Triaxial	1.02	–4.1	12,874
SS Gas Injection at 2,700 psi 60°F	895	2,791	388	240,459	Burst	1.04	< 1E–9	> 1 bil
SS Gas Injection at 2,700 psi 60°F	895	2,791	388	240,459	Triaxial	1.01	–4.0	10,285
Hot Shut-In	895	2,793	387	181,577	Burst	1.02	< 1E–9	> 1 bil
Hot Shut-In	895	2,793	387	181,577	Triaxial	1.01	–4.3	18,250
Cold Shut-In	895	2,793	387	223,356	Burst	1.03	< 1E–9	> 1 bil
Cold Shut-In	895	2,793	387	223,356	Triaxial	1.02	–4.1	13,494
Injection at 2,700 psi with the Worst Case Cool Down	895	2,791	388	289,763	Burst	1.04	< 1E–9	> 1 bil
Injection at 2,700 psi with the Worst Case Cool Down	895	2,791	388	289,763	Triaxial	0.98	–3.3	1,955

B.6 40% Remaining Body Wall

Table 40 shows SFs for the 7 in. casing loads with 40% RBW.

Table 40: Minimum Safety Factors for the 7 in. Casing with 40% Remaining Body Wall

		Burst		Collapse		Tension		Compression		Triaxial	
	Load Case	Pipe SF	MD (ft)	Pipe SF	MD (ft)	Pipe SF	MD (ft)	Pipe SF	MD (ft)	Pipe SF	MD (ft)
1	Initial Condition	-	-	2.12	6,308	1.73	185	2.21	8,563	1.73	185
2	SS Gas Injection at 2,700 psi 70°F	0.83	895	>3	8,585	1.38	185	>3	8,513	0.82	895
3	SS Gas Injection at 2,700 psi 60°F	0.83	895	>3	8,585	1.33	185	>3	8,513	0.82	895
4	Withdrawal Operations	1.13	895	>3	8,282	1.75	185	2.47	8,563	1.12	895
5	Hot Shut-In	0.82	895	>3	8,585	1.67	185	2.67	8,563	0.81	895
6	Cold Shut-In	0.83	895	>3	8,585	1.41	185	2.66	8,563	0.82	895

	Load Case	Burst		Collapse		Tension		Compression		Triaxial	
		Pipe SF	MD (ft)	Pipe SF	MD (ft)	Pipe SF	MD (ft)	Pipe SF	MD (ft)	Pipe SF	MD (ft)
7	Injection at 2,700 psi with the Worst Case Cool Down	0.83	895	>3	8,585	1.12	185	2.90	8,563	0.82	895
8	Worst Case Cool Down without Injection	>3	0	1.79	6,308	1.34	185	2.39	8,563	1.31	896

Table 41 shows the POF or POE results for this case. The highest triaxial POE is 1 in 19. However, the burst POF is very low at < 1E–9.

Table 41: RBD Probability of Failure for the 7 in. Casing with 40% Remaining Body Wall

Load Case	MD (ft)	Internal Pressure (psi)	External Pressure (psi)	Real Axial Force (lbf)	Fail Mode	Min. SF	POF or POE (10^x)	Failure Rate (1 in -)
SS Gas Injection at 2,700 psi 70°F	895	2,791	388	230,093	Burst	0.83	< 1E–9	> 1 E9
SS Gas Injection at 2,700 psi 70°F	895	2,791	388	230,093	Triaxial	0.82	–1.4	25
SS Gas Injection at 2,700 psi 60°F	895	2,791	388	240,459	Burst	0.83	< 1E–9	> 1 E9
SS Gas Injection at 2,700 psi 60°F	895	2,791	388	240,459	Triaxial	0.82	–1.4	24
Withdrawal Operations	895	2,136	388	171,200	Triaxial	1.12	–6.0	977,494
Hot Shut-In	895	2,793	387	181,577	Burst	0.82	< 1E–9	> 1 E9
Hot Shut-In	895	2,793	387	181,577	Triaxial	0.81	–1.3	19
Cold Shut-In	895	2,793	387	223,356	Burst	0.83	< 1E–9	> 1 E9
Cold Shut-In	895	2,793	387	223,356	Triaxial	0.82	–1.4	23
Injection at 2,700 psi with the Worst Case Cool Down	895	2,791	388	289,763	Burst	0.83	< 1E–9	> 1 E9
Injection at 2,700 psi with the Worst Case Cool Down	895	2,791	388	289,763	Triaxial	0.82	–1.2	16

B.7 30% Remaining Body Wall

Table 42 shows SFs for the 7 in. casing loads with 30% RBW.

Table 42: Minimum Safety Factors for the 7 in. Casing with 30% Remaining Body Wall

	Load Case	Burst		Collapse		Tension		Compression		Triaxial	
		Pipe SF	MD (ft)	Pipe SF	MD (ft)	Pipe SF	MD (ft)	Pipe SF	MD (ft)	Pipe SF	MD (ft)
1	Initial Condition	-	-	2.12	6,308	1.73	185	2.21	8,563	1.73	185
2	SS Gas Injection at 2,700 psi 70°F	0.62	895	>3	8,585	1.38	185	3.45	8,513	0.61	895
3	SS Gas Injection at 2,700 psi 60°F	0.62	895	>3	8,585	1.33	185	3.62	8,513	0.61	895
4	Withdrawal Operations	0.85	895	>3	8,282	1.75	185	2.47	8,563	0.83	895
5	Hot Shut-In	0.61	895	>3	8,585	1.67	185	2.67	8,563	0.60	895
6	Cold Shut-In	0.62	895	>3	8,585	1.41	185	2.66	8,563	0.61	895
7	Injection at 2,700 psi with the Worst Case Cool Down	0.62	895	>3	8,585	1.12	185	2.90	8,563	0.62	895
8	Worst Case Cool Down without Injection	>3	0	1.79	6,308	1.34	185	2.39	8,563	1.25	896

Table 43 shows RBD results and the POFs and POEs for this case. The triaxial POE shows yield is likely and the burst POF is approximately 10^{-2} or 1 in a hundred for several loads. This indicates that the burst POF will increase to 10^{-1} or 1 in 10 when the RBW is less than 30%.

Table 43: RBD Probability of Failure for the 7 in. Casing with 30% Remaining Body Wall

Load Case	MD (ft)	Internal Pressure (psi)	External Pressure (psi)	Real Axial Force (lbf)	Fail Mode	Min. SF	POF or POE (10^x)	Failure Rate (1 in -)
SS Gas Injection at 2,700 psi 70°F	895	2,791	388	230,093	Burst	0.62	–2.1	118
SS Gas Injection at 2,700 psi 70°F	895	2,791	388	230,093	Triaxial	0.61	0	1
SS Gas Injection at 2,700 psi 60°F	895	2,791	388	240,459	Burst	0.62	–2.1	124
SS Gas Injection at 2,700 psi 60°F	895	2,791	388	240,459	Triaxial	0.61	0	1
Withdrawal Operations	895	2,136	388	171,200	Burst	0.85	< 1E–9	> 1 E9

Load Case	MD (ft)	Internal Pressure (psi)	External Pressure (psi)	Real Axial Force (lbf)	Fail Mode	Min. SF	POF or POE (10^x)	Failure Rate (1 in -)
Withdrawal Operations	895	2,136	388	171,200	Triaxial	0.83	−1.7	45
Hot Shut-In	895	2,793	387	181,577	Burst	0.61	−1.9	84
Hot Shut-In	895	2,793	387	181,577	Triaxial	0.60	0	1
Cold Shut-In	895	2,793	387	223,356	Burst	0.62	−2.0	109
Cold Shut-In	895	2,793	387	223,356	Triaxial	0.61	0	1
Injection at 2,700 psi with the Worst Case Cool Down	895	2,791	388	289,763	Burst	0.62	−2.2	147
Injection at 2,700 psi with the Worst Case Cool Down	895	2,791	388	289,763	Triaxial	0.62	0	1

B.8 20% Remaining Body Wall

Table 44 shows SFs for the 7 in. casing loads with 20% RBW.

Table 44: Minimum Safety Factors for the 7 in. Casing with 20% Remaining Body Wall

		Burst		Collapse		Tension		Compression		Triaxial	
	Load Case	Pipe SF	MD (ft)	Pipe SF	MD (ft)	Pipe SF	MD (ft)	Pipe SF	MD (ft)	Pipe SF	MD (ft)
1	Initial Condition	-	-	2.12	6,308	1.73	185	2.21	8,563	1.73	185
2	SS Gas Injection at 2,700 psi 70°F	0.41	895	>3	8,585	1.38	185	>3	8,513	0.40	895
3	SS Gas Injection at 2,700 psi 60°F	0.41	895	>3	8,585	1.33	185	>3	8,513	0.40	895
4	Withdrawal Operations	0.56	895	>3	8,282	1.75	185	2.47	8,563	0.54	895
5	Hot Shut-In	0.41	895	>3	8,585	1.67	185	2.67	8,563	0.39	895
6	Cold Shut-In	0.41	895	>3	8,585	1.41	185	2.66	8,563	0.40	895
7	Injection at 2,700 psi with the Worst Case Cool Down	0.41	895	>3	8,585	1.12	185	2.9	8,563	0.40	895
8	Worst Case Cool Down without Injection	>3	0	1.48	896	1.34	185	2.39	8,563	1.14	896

Table 45 shows RBD results and the POFs and POEs for this case indicating failure for all cases except Worst Case Cool Down without Injection.

Table 45: RBD Probability of Failure for the 7 in. Casing with 20% Remaining Body Wall

Load Case	MD (ft)	Internal Pressure (psi)	External Pressure (psi)	Real Axial Force (lbf)	Fail Mode	Min. SF	POF or POE (10^x)	Failure Rate (1 in -)
SS Gas Injection at 2,700 psi 70°F	895	2,791	388	230,093	Burst	0.41	0	1
SS Gas Injection at 2,700 psi 70°F	895	2,791	388	230,093	Triaxial	0.40	0	1
SS Gas Injection at 2,700 psi 60°F	895	2,791	388	240,459	Burst	0.41	0	1
SS Gas Injection at 2,700 psi 60°F	895	2,791	388	240,459	Triaxial	0.40	0	1
Withdrawal Operations	895	2,136	388	171,200	Burst	0.56	–0.6	4
Withdrawal Operations	895	2,136	388	171,200	Triaxial	0.54	0	1
Hot Shut-In	895	2,793	387	181,577	Burst	0.41	0	1
Hot Shut-In	895	2,793	387	181,577	Triaxial	0.39	0	1
Cold Shut-In	895	2,793	387	223,356	Burst	0.41	0	1
Cold Shut-In	895	2,793	387	223,356	Triaxial	0.40	0	1
Injection at 2,700 psi with the Worst Case Cool Down	895	2,791	388	289,763	Burst	0.41	0	1
Injection at 2,700 psi with the Worst Case Cool Down	895	2,791	388	289,763	Triaxial	0.40	0	1
Worst Case Cool Down without Injection	896	106	389	238,475	Triaxial	1.14	–4.9	75,095

B.9 7 in. Casing Reliability-Based Design—Summary of the Results with TOC at 990 ft

RBD results are summarized for critical loads "Steady State Gas Injection at 2,700 psi and 70°F Surface Temperature", "Steady State Injection at 2,700 psi and 60°F Surface Temperature", "Cold Shut-in," and "Injection at 2,700 psi with the Worst Case Cool Down Temperature Profile." The results for triaxial and burst failure modes are tabulated and presented in graphs showing POF versus RBW.

B.9.1 Steady State Gas Injection at 2,700 psi and 70°F Surface Temperature

Table 46 and Table 47, respectively, show RBD results for the triaxial and burst failure modes.

When the RBW is below 45%, the triaxial SFs and POEs start to become an issue. When the RBW is 40%, the probability of yielding the casing is 1 in 25 for the gas injection at 2,700 psi and 70°F load case. Table 47 shows that the burst failure mode becomes an issue when the RBW is less than 30% with a failure rate of 1 in 118.

Table 46: Probability of Exceedance vs. Remaining Body Wall for the 7 in. Casing for Triaxial Failure Mode

RBW (%)	Load Case	MD (ft)	Internal Pressure (psi)	External Pressure (psi)	Real Axial Force (lbf)	Fail Mode	Min. SF	POF or POE (10^x)	Failure Rate (1 in -)
65	SS Gas Injection at 2,700 psi 70°F	895	2,791	388	230,093	Triaxial	1.25	-	-
60	SS Gas Injection at 2,700 psi 70°F	895	2,791	388	230,093	Triaxial	1.18	–6.5	3,093,185
55	SS Gas Injection at 2,700 psi 70°F	895	2,791	388	230,093	Triaxial	1.10	–5.4	238,337
50	SS Gas Injection at 2,700 psi 70°F	895	2,791	388	230,093	Triaxial	1.02	–4.1	12,874
45	SS Gas Injection at 2,700 psi 70°F	895	2,791	388	230,093	Triaxial	0.92	–2.7	546
40	SS Gas Injection at 2,700 psi 70°F	895	2,791	388	230,093	Triaxial	0.82	–1.4	25
35	SS Gas Injection at 2,700 psi 70°F	895	2,791	388	230,093	Triaxial	0.72	–0.4	2
30	SS Gas Injection at 2,700 psi 70°F	895	2,791	388	230,093	Triaxial	0.61	0	1
25	SS Gas Injection at 2,700 psi 70°F	895	2,791	388	230,093	Triaxial	0.50	0	1
20	SS Gas Injection at 2,700 psi 70°F	895	2,791	388	230,093	Triaxial	0.40	0	1

Table 47: Probability of Failure vs. Remaining Body Wall for the 7 in. Casing for Burst Failure Mode

RBW (%)	Load Case	MD (ft)	Internal Pressure (psi)	External Pressure (psi)	Real Axial Force (lbf)	Fail Mode	Min. SF	POF or POE (10^x)	Failure Rate (1 in -)
55	SS Gas Injection at 2,700 psi 70°F	895	2,791	388	230,093	Burst	1.14	-	-
55	SS Gas Injection at 2,700 psi 70°F	895	2,791	388	230,093	Burst	1.14	< 1E–9	> 1 E9
50	SS Gas Injection at 2,700 psi 70°F	895	2,791	388	230,093	Burst	1.04	< 1E–9	> 1 E9
45	SS Gas Injection at 2,700 psi 70°F	895	2,791	388	230,093	Burst	0.93	< 1E–9	> 1 E9
40	SS Gas Injection at 2,700 psi 70°F	895	2,791	388	230,093	Burst	0.83	< 1E–9	> 1 E9
35	SS Gas Injection at 2,700 psi 70°F	895	2,791	388	230,093	Burst	0.72	–5.7	544,576
30	SS Gas Injection at 2,700 psi 70°F	895	2,791	388	230,093	Burst	0.62	–2.1	118
25	SS Gas Injection at 2,700 psi 70°F	895	2,791	388	230,093	Burst	0.52	0	1
20	SS Gas Injection at 2,700 psi 70°F	895	2,791	388	230,093	Burst	0.41	0	1

Figure 28 and Figure 29, respectively, show POE and POF versus RBW results from Table 46 and Table 47 for two failure modes.

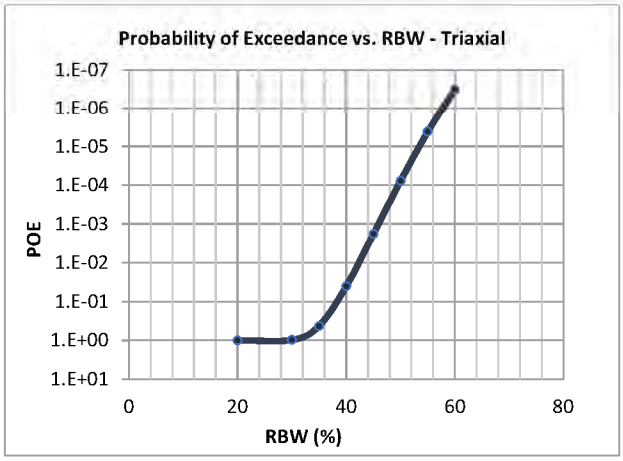

Figure 28: Probability of Exceedance vs. Remaining Body Wall for Triaxial Failure Mode

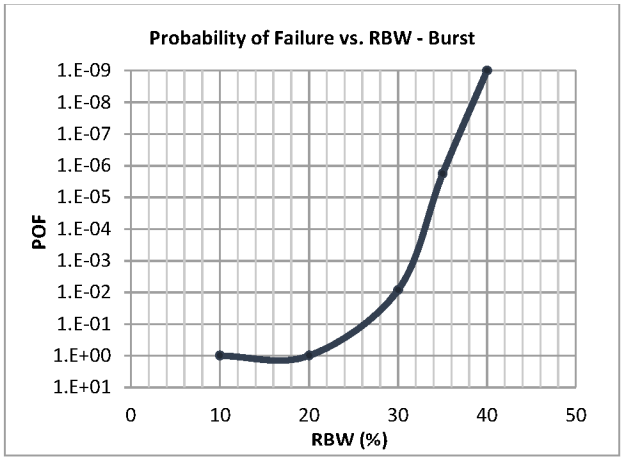

Figure 29: Probability of Failure vs. Remaining Body Wall for Burst Failure Mode

B.9.2 Steady State Gas Injection at 2,700 psi and 60°F Surface Temperature

Table 48 and Table 49, respectively, show RBD results for the triaxial and burst failure modes.

When the RBW is below 45%, the triaxial SFs and the POEs start to become an issue. When the RBW is 40%, the probability of yielding the casing is 1 in 24 for the gas injection at 2,700 psi and 60°F load case. Table 49 shows that the burst failure mode becomes an issue when the RBW is less than 30% with a failure rate of 1 in 124.

Table 48: Probability of Exceedance vs. Remaining Body Wall for the 7 in. Casing for Triaxial Failure Mode

RBW (%)	Load Case	MD (ft)	Internal Pressure (psi)	External Pressure (psi)	Real Axial Force (lbf)	Fail Mode	Min. SF	POF or POE (10^{x})	Failure Rate (1 in -)
65	SS Gas Injection at 2,700 psi 60°F	895	2,791	388	240,459	Triaxial	1.24	–7.2	14,487,550
60	SS Gas Injection at 2,700 psi 60°F	895	2,791	388	240,459	Triaxial	1.17	–6.3	1,868,874
55	SS Gas Injection at 2,700 psi 60°F	895	2,791	388	240,459	Triaxial	1.10	–5.2	166,073
50	SS Gas Injection at 2,700 psi 60°F	895	2,791	388	240,459	Triaxial	1.01	–4.0	10,285
45	SS Gas Injection at 2,700 psi 60°F	895	2,791	388	240,459	Triaxial	0.92	–2.7	491
40	SS Gas Injection at 2,700 psi 60°F	895	2,791	388	240,459	Triaxial	0.82	–1.4	24
35	SS Gas Injection at 2,700 psi 60°F	895	2,791	388	240,459	Triaxial	0.72	–0.4	2
30	SS Gas Injection at 2,700 psi 60°F	895	2,791	388	240,459	Triaxial	0.61	0	1
25	SS Gas Injection at 2,700 psi 60°F	895	2,791	388	240,459	Triaxial	0.51	0	1
20	SS Gas Injection at 2,700 psi 60°F	895	2,791	388	240,459	Triaxial	0.40	0	1

Table 49: Probability of Failure vs. Remaining Body Wall for the 7 in. Casing for Burst Failure Mode

RBW (%)	Load Case	MD (ft)	Internal Pressure (psi)	External Pressure (psi)	Real Axial Force (lbf)	Fail Mode	Min. SF	POF or POE (10^x)	Failure Rate (1 in -)
55	SS Gas Injection at 2,700 psi 60°F	895	2,791	388	240,459	Burst	1.14	-	-
50	SS Gas Injection at 2,700 psi 60°F	895	2,791	388	240,459	Burst	1.04	< 1E–9	> 1 E9
45	SS Gas Injection at 2,700 psi 60°F	895	2,791	388	240,459	Burst	0.93	< 1E–9	> 1 E9
40	SS Gas Injection at 2,700 psi 60°F	895	2,791	388	240,459	Burst	0.83	< 1E–9	> 1 E9
35	SS Gas Injection at 2,700 psi 60°F	895	2,791	388	240,459	Burst	0.73	–5.8	580,526
30	SS Gas Injection at 2,700 psi 60°F	895	2,791	388	240,459	Burst	0.62	–2.1	124
25	SS Gas Injection at 2,700 psi 60°F	895	2,791	388	240,459	Burst	0.52	–0.1	1
20	SS Gas Injection at 2,700 psi 60°F	895	2,791	388	240,459	Burst	0.41	0	1

Figure 30 and Figure 31, respectively, show POE and POF versus RBW results from Table 48 and Table 49 for two failure modes.

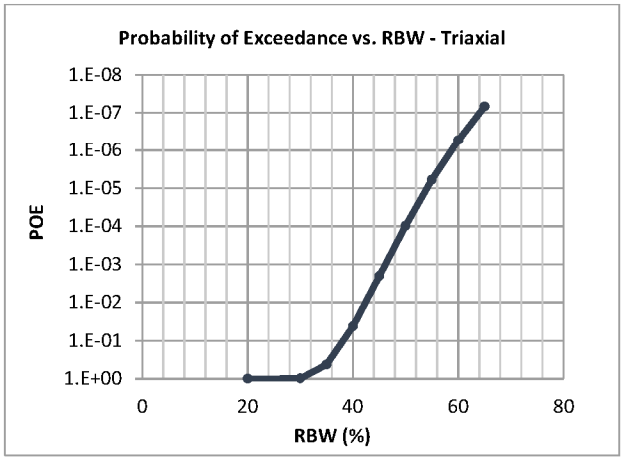

Figure 30: Probability of Exceedance vs. Remaining Body Wall for Triaxial Failure Mode

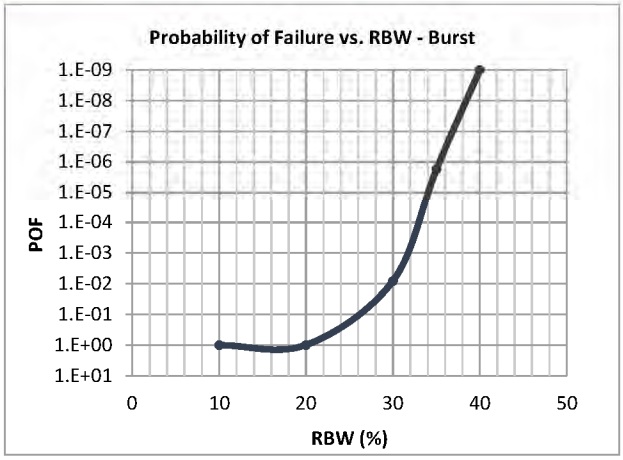

Figure 31: Probability of Failure vs. Remaining Body Wall for Burst Failure Mode

B.9.3 Cold Shut-In

Table 50 and Table 51, respectively, show RBD results for the triaxial and burst failure modes. When the RBW approaches 45%, the triaxial SFs and POEs start to become an issue. When the RBW is 40%, the probability of yielding the casing is 1 in 23 for the Cold Shut-In load case.

Table 51 shows that the burst failure mode becomes an issue when the RBW is less than 30% with a failure rate of 1 in 109, with the POF of 1 in 1 with 25% RBW.

Table 50: Probability of Exceedance vs. Remaining Body Wall for the 7 in. Casing for Triaxial Failure Mode

RBW (%)	Load Case	MD (ft)	Internal Pressure (psi)	External Pressure (psi)	Real Axial Force (lbf)	Fail Mode	Min. SF	POF or POE (10^x)	Failure Rate (1 in -)
65	Cold Shut-in	895	2,793	387	223,356	Triaxial	1.26	-	-
60	Cold Shut-in	895	2,793	387	223,356	Triaxial	1.19	–6.6	3,858,248
55	Cold Shut-in	895	2,793	387	223,356	Triaxial	1.10	–5.4	271,389
50	Cold Shut-in	895	2,793	387	223,356	Triaxial	1.02	–4.1	13,494
45	Cold Shut-in	895	2,793	387	223,356	Triaxial	0.92	–2.7	536
40	Cold Shut-in	895	2,793	387	223,356	Triaxial	0.82	–1.4	23
35	Cold Shut-in	895	2,793	387	223,356	Triaxial	0.72	–0.4	2
30	Cold Shut-in	895	2,793	387	223,356	Triaxial	0.61	0	1
20	Cold Shut-in	895	2,793	387	223,356	Triaxial	0.40	0	1

Table 51: Probability of Failure vs. Remaining Body Wall for the 7 in. Casing for Burst Failure Mode

RBW (%)	Load Case	MD (ft)	Internal Pressure (psi)	External Pressure (psi)	Real Axial Force (lbf)	Fail Mode	Min. SF	POF or POE (10^x)	Failure Rate (1 in -)
55	Cold Shut-in	895	2,793	387	223,356	Burst	1.14	-	-
50	Cold Shut-in	895	2,793	387	223,356	Burst	1.03	< 1E–9	> 1 E9
40	Cold Shut-in	895	2,793	387	223,356	Burst	0.83	< 1E–9	> 1 E9
35	Cold Shut-in	895	2,793	387	223,356	Burst	0.72	–5.7	483,073
30	Cold Shut-in	895	2,793	387	223,356	Burst	0.62	–2.0	109
25	Cold Shut-in	895	2,793	387	223,356	Burst	0.52	–0.1	1
20	Cold Shut-in	895	2,793	387	223,356	Burst	0.41	0	1

Figure 32 and Figure 33, respectively, show POE and POF versus RBW results from Table 50 and Table 51 for two failure modes.

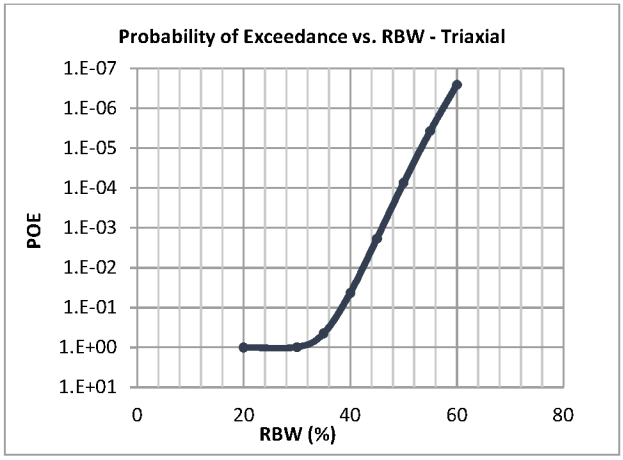

Figure 32: Probability of Exceedance vs. Remaining Body Wall for Triaxial Failure Mode

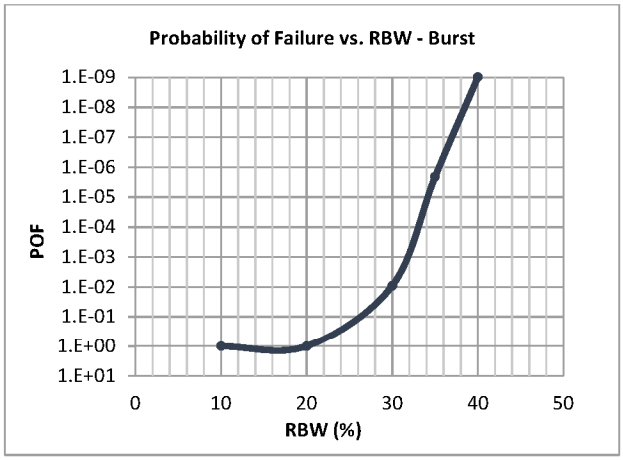

Figure 33: Probability of Failure vs. Remaining Body Wall for Burst Failure Mode

B.9.4 Injection at 2,700 psi with the Worst Case Cool Down Temperature Profile

Table 52 and Table 53, respectively, show RBD results for the triaxial and burst failure modes. The RBD results are similar to the SS Gas Injection at 2,700 psi and 70°F Surface Temperature load case. That is, when the RBW approaches 40%, the triaxial failure mode becomes an issue, and when the RBD is below 30%, the burst mode POF is not acceptable. When the RBW is 40%, the probability of yielding the casing is 1 in 24 for the gas injection at 2,700 psi and 1 in 16 for the Worst Case Cool Down temperature profile load case.

Table 53 shows that the burst failure mode becomes an issue when the RBW is less than 30% with a failure rate of 1 in 147.

Table 52: Probability of Exceedance vs. Remaining Body Wall for the 7 in. Casing for Triaxial Failure Mode

RBW (%)	Load Case	MD (ft)	Internal Pressure (psi)	External Pressure (psi)	Real Axial Force (lbf)	Fail Mode	Min. SF	POF or POE (10^x)	Failure Rate (1 in -)
70	Injection at 2,700 psi with the Worst Case Cool Down	895	2,791	388	289,763	Triaxial	1.20	–6.0	1,099,610
65	Injection at 2,700 psi with the Worst Case Cool Down	895	2,791	388	289,763	Triaxial	1.16	–5.6	362,200
60	Injection at 2,700 psi with the Worst Case Cool Down	895	2,791	388	289,763	Triaxial	1.11	–4.9	89,143
55	Injection at 2,700 psi with the Worst Case Cool Down	895	2,791	388	289,763	Triaxial	1.05	–4.2	15,719
50	Injection at 2,700 psi with the Worst Case Cool Down	895	2,791	388	289,763	Triaxial	0.98	–3.3	1,955
45	Injection at 2,700 psi with the Worst Case Cool Down	895	2,791	388	289,763	Triaxial	0.91	–2.3	182
40	Injection at 2,700 psi with the Worst Case Cool Down	895	2,791	388	289,763	Triaxial	0.82	–1.2	16

RBW (%)	Load Case	MD (ft)	Internal Pressure (psi)	External Pressure (psi)	Real Axial Force (lbf)	Fail Mode	Min. SF	POF or POE (10^x)	Failure Rate (1 in -)
35	Injection at 2,700 psi with the Worst Case Cool Down	895	2,791	388	289,763	Triaxial	0.72	–0.3	2
30	Injection at 2,700 psi with the Worst Case Cool Down	895	2,791	388	289,763	Triaxial	0.62	0	1
20	Injection at 2,700 psi with the Worst Case Cool Down	895	2,791	388	289,763	Triaxial	0.40	0	1

Table 53: Probability of Failure vs. Remaining Body Wall for the 7 in. Casing for Burst Failure Mode

RBW (%)	Load Case	MD (ft)	Internal Pressure (psi)	External Pressure (psi)	Real Axial Force (lbf)	Fail Mode	Min. SF	POF or POE (10^x)	Failure Rate (1 in -)
55	Injection at 2,700 psi with the Worst Case Cool Down	895	2,791	388	289,763	Burst	1.14	-	-
50	Injection at 2,700 psi with the Worst Case Cool Down	895	2,791	388	289,763	Burst	1.04	< 1E–9	> 1 E9
40	Injection at 2,700 psi with the Worst Case Cool Down	895	2,791	388	289,763	Burst	0.83	< 1E–9	> 1 E9
35	Injection at 2,700 psi with the Worst Case Cool Down	895	2,791	388	289,763	Burst	0.73	–5.9	702,898
30	Injection at 2,700 psi with the Worst Case Cool Down	895	2,791	388	289,763	Burst	0.62	–2.2	147
25	Injection at 2,700 psi with the Worst Case Cool Down	895	2,791	388	289,763	Burst	0.52	–0.1	1

RBW (%)	Load Case	MD (ft)	Internal Pressure (psi)	External Pressure (psi)	Real Axial Force (lbf)	Fail Mode	Min. SF	POF or POE (10^x)	Failure Rate (1 in -)
20	Injection at 2,700 psi with the Worst Case Cool Down	895	2,791	388	289,763	Burst	0.41	0	1

Figure 34 and Figure 35, respectively, show POE and POF versus RBW results from Table 52 and Table 53 for the two failure modes.

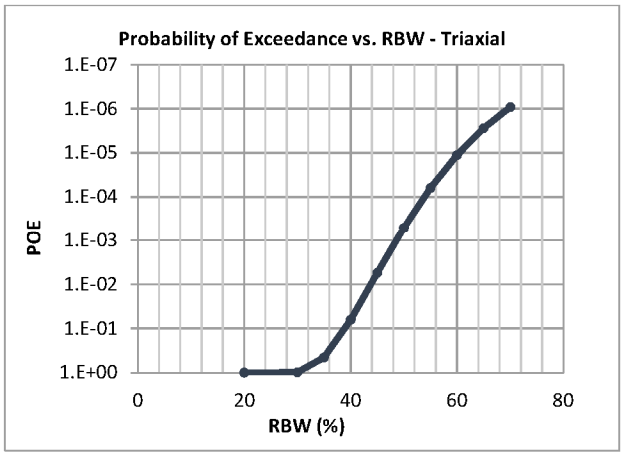

Figure 34: Probability of Failure vs. Remaining Body Wall for Triaxial Failure Mode

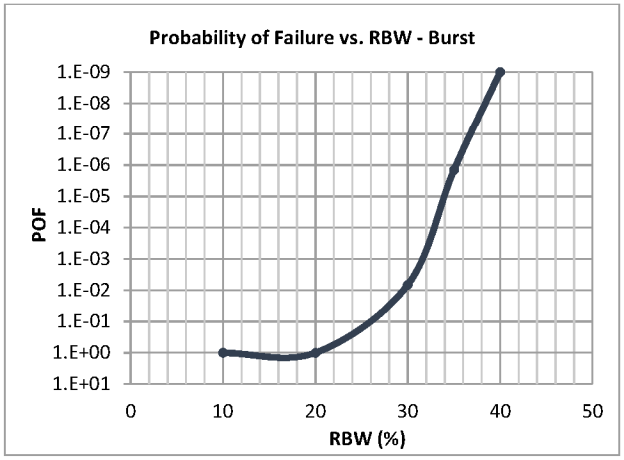

Figure 35: Probability of Failure vs. Remaining Body Wall for Burst Failure Mode

SS-25 RCA Supplementary Report

SS-25 Tubulars NDE Analysis

Purpose:
Summarize the results of the nondestructive examination (NDE) of the 2 7/8 in. tubing and 7 in. casing extracted from SS-25

Date:
May 31, 2019

BLADE ENERGY PARTNERS

2600 Network Boulevard, Suite 550
Frisco, Texas 75034

+1 972-712-8407 (phone)
+1 972-712-8408 (fax)

16285 Park Ten Place, Suite 600
Houston, Texas 77084

1-800-319-2940 (toll free)
+1 281-206-2000 (phone)
+1 281-206-2005 (fax)

www.blade-energy.com

Blade Energy Partners Limited, and its affiliates ('Blade') provide our services subject to our General Terms and Conditions ('GTC') in effect at time of service, unless a GTC provision is expressly superseded in a separate agreement made with Blade. Blade's work product is based on information sources which we believe to be reliable, including information that was publicly available and that was provided by our client; but Blade does not guarantee the accuracy or completeness of the information provided. All statements are the opinions of Blade based on generally-accepted and reasonable practices in the industry. Our clients remain fully responsible for all clients' decisions, actions and omissions, whether based upon Blade's work product or not; and Blade's liability solely extends to the cost of its work product.

Abstract

The gas storage well Standard Sesnon 25 (SS-25) in the Aliso Canyon Gas Storage Field (Aliso Canyon) located in Los Angeles County, California started leaking gas in October 2015. A relief well was drilled, and SS-25 was brought under control. The leak stopped in February 2016.

In January 2016, as part of their investigation of the leak, the California Public Utilities Commission (CPUC) and the Division of Oil, Gas, and Geothermal Resources (DOGGR) selected and gave provisional authority to Blade Energy Partners (Blade) to perform an independent Root Cause Analysis (RCA). The Blade Team and parties under Blade's direction were responsible for directing the work of subcontractors who performed the extraction of the SS-25's wellhead and tubing and casing and the preservation and protection of associated evidence. Blade RCA Reports, including this one, document and describe the key activities undertaken in support of the RCA effort.

The 2 7/8 in. tubing and 7 in. casing joints extracted from SS-25 in late 2017 were transported from Alison Canyon to Blade's RCA Storage Facility in Houston, Texas. The tubing and casing subsequently underwent a full-length pipe body nondestructive examination (NDE) to look for surface breaking cracks, or cracks within the wall of the pipe using a combination of electromagnetic, magnetic particle, and ultrasonic inspection techniques. From March through June 2018, 241 joints of tubing and 19 joints of casing were inspected at NOV Tuboscope's inspection facility in Houston. No cracks or significant flaws that were relevant to the RCA were found during the various inspections of either the tubing or the casing.

Table of Contents

1 Introduction 4
1.1 Abbreviations and Acronyms 4
2 NDE Process Overview 5
3 Tubing NDE Discussion 6
4 Casing NDE Discussion 7
5 Conclusions 8
6 References 8
Appendix A Tubing NDE Reconciliation A-1
Appendix B Casing NDE Reconciliation B-1
Appendix C NDE Photos C-1

List of Figures

Figure 1: Tubulars Storage at Blade's Houston Warehouse C-1
Figure 2: Loading Tubing Bolsters at Blade's Warehouse C-1
Figure 3: Offloading Tubing at Tuboscope C-2
Figure 4: Tubing Cleaning at Tuboscope C-2
Figure 5: Tubing after EMI Inspection C-3
Figure 6: Tubing FLUT Inspection C-3
Figure 7: Loading Out Casing Bolsters at Blade Warehouse C-4
Figure 8: Casing Bolsters Loaded C-4
Figure 9: Casing FLUT Inspection C-5

List of Tables

Table 1: Calibration Standard Reference Notch Configuration 5
Table 2: Tubing NDE Disposition A-1
Table 3: Casing Mechanical Testing Ring Sectioning Summary B-1
Table 4: Casing NDE Disposition B-2

1 Introduction

Phase 4 of the RCA work scope (NDE and Laboratory Metallurgical Examination) included the nondestructive examination of the tubing and casing extracted from SS-25. The objective was to conduct a full-length pipe body inspection for flaws that may be relevant to the RCA using a combination of electromagnetic, magnetic particle, and ultrasonic inspection techniques. Of specific interest were surface breaking cracks, or cracks within the wall of the pipe. The tubulars were transported from Aliso Canyon to Houston, Texas to be inspected because the inspection technology required was not available in California at the time.

The purpose of this report is to describe the Electromagnetic Inspection (EMI) and Full-Length Ultrasonic Testing (FLUT) of the 2 7/8 in. tubing and 7 in. casing that was done at NOV Tuboscope's Sheldon Road facility in Houston. The NDE was done in accordance with API 5CT, Annex A, A.2 [1] *"SR1 Supplementary non-destructive examination for Grades H40, J55, K55 and N80 Type 1"*, and Tuboscope's internal proprietary inspection and handling procedures.

Between March 3 and April 10, 2018, 241 joints of 2 7/8 in. 6.5 ppf J55 EUE tubing were inspected at Tuboscope. No cracks were found during the various inspections. The tubing was returned to the Blade RCA storage facility (warehouse) in Houston on April 18, 2018 for storage.

Between May 1 and June 5, 2018, 19 joints of 7 in. 23 ppf J55 casing were inspected at Tuboscope. No cracks were found during the various inspections. The casing was returned to the Blade warehouse on June 8, 2018 for storage.

1.1 Abbreviations and Acronyms

Term	Definition
Blade	Blade Energy Partners
COC	Chain of Custody
CPUC	California Public Utilities Commission
DOGGR-IT	Division of Oil, Gas, and Geothermal Resources Investigation Team
EDM	Electrical Discharge Machined
EMI	Electromagnetic Inspection
FLUT	Full Length Ultrasonic Inspection
ID	Inside Diameter
JSN	Joint Sequence Number
MPI	Magnetic Particle Inspection
NDE	Nondestructive Examination
OD	Outside Diameter
ppf	Pound Per Foot
RCA	Root Cause Analysis
SEA	Special End Area
SoCalGas	Southern California Gas Company
SR1	Supplementary Requirements #1

Term	Definition
VCI	Volatile Corrosion Inhibitor

2 NDE Process Overview

Blade shipped the tubing and casing joints in bolsters from the Blade warehouse to the Tuboscope's Sheldon Road inspection facility. Bolstering was the primary method used for preventing handling damage during transport and storage. Each joint was identified by a unique Joint Sequence Number (JSN). Tuboscope used these same JSNs for traceability and reporting the results of the inspection. Each joint also had a Chain of Custody (COC) form. The original COC forms, which originated in California, traveled with the joints as they were moved from the warehouse to the Tuboscope facility. Blade released custody of the tubulars to Tuboscope for the NDE work, and Tuboscope transferred custody back to Blade when the NDE work was completed and the tubulars were returned to the warehouse for storage.

The tubulars were stored at the Tuboscope facility for the duration of the NDE work. The movement and handling of the tubing at the Tuboscope facility was done using their internal corrosion resistant alloy procedures to ensure that the tubulars were not damaged during the inspection processes. The pipe movement within the facility and inspection work was tracked and documented using Tuboscope's internal inventory management system.

Blade provided Tuboscope with a separate joint of tubing and casing for use as calibration reference joints to confirm that the inspection systems performed as expected and that the proper sensitivity was obtained to detect flaws present in the material being inspected. Tuboscope cut the API SR1 Electromagnetic Discharge Machined (EDM) notches on the Inside Diameter (ID) and Outside Diameter (OD) listed in Table 1 onto the reference joints, which were in turn used to calibrate the FLUT and EMI inspection equipment and to ensure inspection repeatability.

Table 1: Calibration Standard Reference Notch Configuration

Notch Type	Angle (deg)	Surface	Width (in.)	Length (in.)
Longitudinal	0	ID and OD	0.020	1.000
Transverse	90	ID and OD	0.020	1.000
Left Hand Oblique	11	ID and OD	0.020	1.000
Right Hand Oblique	11	ID and OD	0.020	1.000
Left Hand Oblique	22	ID and OD	0.020	1.000
Right Hand Oblique	22	ID and OD	0.020	1.000
Left Hand Oblique	45	ID and OD	0.020	1.000
Right Hand Oblique	45	ID and OD	0.020	1.000

A key part of the calibration was ensuring that the combination of linear and rotational speed of the joint produced 100% coverage of the joint body based on the effective beam width of the ultrasonic testing transducers and the length of the EMI detection sensors. The API SR1 requirements are designed to detect flaws that exceed 12 1/2% of the nominal wall thickness of the pipe.

After calibration, the reference joints were run through EMI and FLUT units at the start of the inspection and then again at the end after all of the joints were inspected. Additionally, Tuboscope's procedures called for periodic standardization checks made by running the calibration reference joint through the

EMI and FLUT units after every 50 joints or after 4 hours shutdown time. If the EDM reference notches were not detected by the inspection equipment during these standardization checks, then all of the joints that had been inspected since the previous standardization check had to be reinspected.

Blade witnessed all the pipe movement and inspection work and documented the "as-found" and "as-left" condition of the tubulars at the beginning and end of each inspection shift. The California Public Utilities Commission (CPUC) witnessed the first days of the tubing inspection, and representatives of interested parties witnessed all of the casing and tubing inspections.

The overall NDE process is described below.

1. Blade loaded the bolstered joints onto trucks at the Blade warehouse.
2. Blade completed the COC forms releasing custody of the tubulars.
3. Blade escorted the trucks transporting the tubulars to the Tuboscope facility. Tuboscope completed the COC forms, accepting custody of the tubing.
4. Tuboscope unbolstered the joints and conducted a receiving inspection check for any transportation-related damage, which was witnessed by Blade.
5. Tuboscope cleaned the ID and OD of each joint to remove the Tectyl 846 corrosion inhibitor coating.
6. Tuboscope sent each joint through an automated full-length and full-body EMI and FLUT inspection. The automated inspection units cannot inspect the last 18–24 in. at each end of a joint. These areas therefore underwent a manual Special End Area (SEA) inspection.
7. Flaw indications detected during the inspections were proved-up and characterized manually with a handheld shear wave ultrasonic unit or by using magnetic particle inspection (MPI) methods. Any flaws that were proved-up and found to be relevant to the RCA would be later sectioned and analyzed at a laboratory in accordance with the SS-25 Metallurgical Protocol [2].
8. After inspection, Tuboscope rebolstered the joints. The reapplication of corrosion inhibitor to the OD and ID was not required because the joints were to be stored at Blade's climate-controlled warehouse.
9. Tuboscope signed the COC forms releasing custody of the tubulars. The tubulars were transported back to Blade's warehouse.
10. Blade completed the COC forms accepting custody of the tubing and conducted a receiving inspection to check for any transportation-related damage.

Appendix C includes photographs of several of the steps in the NDE process.

3 Tubing NDE Discussion

In August 2017, 244 joints of 2 7/8 in. 6.5 ppf J55 tubing were extracted from SS-25. All of the joints were transferred from Aliso Canyon to the Blade warehouse in Houston on October 24, 2017. Four additional 2 7/8 in. 6.5 ppf J55 tubing joints that did not come from SS-25 were also sent to be used as test joints. Blade prepared a 2 7/8 in. Tubing NDE Protocol [3], which went through several revisions after reviews and comments from CPUC and the Division of Oil, Gas, and Geothermal Resources Investigation Team (DOGGR-IT).

Blade sent the four test joints to Tuboscope in January 2018. Blade witnessed Tuboscope use them to successfully confirm that the planned cleaning and inspection techniques would work with the extracted

tubing. Tuboscope cut the EDM notches on one of the joints, and this joint was subsequently used as the calibration reference standard.

On March 5, 2018, Blade sent 241 joints of tubing to Tuboscope for inspection. During the receiving inspection, Tuboscope found 43 joints that were obviously too bent to be inspected by the automated inspection equipment. These joints were rebolstered without being cleaned or inspected. The tubing joints tested are listed in Appendix A.

Tuboscope cleaned the remaining 198 joints to remove the Tectyl 846 coating between March 12 and March 16. Tuboscope transferred the joints to their EMI unit where the joints went through an EMI and SEA inspection, as well as manual prove-up, between March 26 and March 28, 2018. Tuboscope then transferred the joints to their FLUT unit. Excessive surface roughness in 47 joints precluded them from FLUT inspection. The remaining 151 joints underwent a FLUT inspection and manual prove-up between March 29 and April 10, 2018.

Although both the EMI and FLUT inspections resulted in flaw indications, none of the flaws were confirmed as crack indications during the prove-up inspection. The indications turned out to be laps or gouges as a result of the manufacturing process, which were not relevant to the RCA. No cracks were found. As a consequence, Blade determined that inspecting the 43 bent joints that had been set aside during the receiving inspection was not required. Tuboscope rebolstered the joints, and they were sent back to the Blade warehouse for storage on April 18, 2018.

4 Casing NDE Discussion

In November 2017, 23 joints of 7 in. 23 ppf J55 casing were extracted from SS-25. All of the joints were transferred from Aliso Canyon to the Blade warehouse in Houston on December 5, 2017. Blade purchased an additional joint of 7 in. 23 ppf J55 casing in Houston to be used as a calibration reference joint. Blade prepared a 7 in. Casing NDE Protocol [4], which went through several revisions after reviews and comments from CPUC and DOGGR-IT.

Experience during the NDE of the 2 7/8 in. tubing showed that the rough surface condition of the tubing resulted in erroneous flaw indications during the FLUT inspection and caused an excessive and unnecessary amount of manual prove-ups. The surface condition of the 7 in. casing is at least as rough as the tubing. Therefore, Blade and Tuboscope decided to first do a full-length fluorescent Magnetic Particle Inspection (MPI) for each joint to better characterize the surface condition and facilitate a more meaningful prove-up inspection. This also obviated the need for a manual SEA inspection.

On May 1, 2018, Blade sent 19 joints of casing from SS-25 and one new joint to be used as a calibration joint to Tuboscope for inspection. The calibration notches were cut in this calibration joint. The casing joints tested are listed in Appendix B. Tuboscope did a receiving inspection and cleaned the ID and OD of each joint to remove the Tectyl 846 coating on May 7. Tuboscope transferred the joints to their EMI unit where they went through a full length MPI and an EMI inspection between May 11 and May 15. Tuboscope then transferred the joints to their FLUT unit, and the joints were inspected on May 16. Blade and Tuboscope reviewed the inspection results on May 18 and agreed on the criteria that were to be used to determine which flaw indications required further manual prove-up. The prove-up inspections were carried out between June 2 and June 5.

Although the MPI, EMI, and FLUT inspections found signs of flaws, none were confirmed as crack indications during the prove-up inspections. Again, the indications showed laps or gouges as a result of the manufacturing process, and therefore were irrelevant to the RCA. No cracks were detected.

Tuboscope rebolstered the joints, and they were sent back to the Blade warehouse for storage on June 8, 2018.

5 Conclusions

The objective of the NDE work was to conduct a full-length pipe body inspection of the tubing and casing extracted from SS-25 to look for flaws that may be relevant to the RCA. Of specific interest were surface breaking cracks, or cracks within the wall of the pipe. The inspections were done in accordance with the API SR1 NDE requirements and Tuboscope's internal proprietary procedures. Blade witnessed all of the inspection operations.

Tuboscope inspected 198 of the 244 joints of tubing extracted from SS-25. Flaws were detected, but no cracks. Of the 46 joints not inspected at Tuboscope, 43 were too bent to be inspected with the automated equipment, and 2 joints were examined separately by Blade at the warehouse.

Tuboscope inspected 19 of the 25 joints of casing extracted from SS-25. Although there were flaw indications, no cracks were detected. The other 6 joints were examined separately by Blade at the warehouse.

The NDE work did not locate any flaws in the tubing or casing that were relevant to the RCA. Tuboscope considers the details of their inspection results to be proprietary data. However, the inspection records are stored for 10 years and are available for review at their Sheldon Road inspection facility.

6 References

[1] American Petoleum Institutue, "API Specification 5CT - Specification for Casing and Tubing".

[2] Blade, "SS-25 Metallurgical Protocol ver 001 February 15th 2018.pdf".

[3] Blade, "SS-25 Tubing NDE Protocol (AC-RCA SS25 Phase 4 Tubing NDE Protocol Rev 001 2018-03-05.pdf)".

[4] Blade, "SS-25 Casing NDE Protocol (AC-RCA SS25 Phase 4 Casing NDE Protocol Rev 000, 2018-04-21.pdf)".

[5] Blade, "Phase 3 Tubulars Handling Protocol (AC-RCA Phase 3 Tubulars Handling Protocol Rev 004, 31-July-2017.pdf)".

Appendix A Tubing NDE Reconciliation

Between March 3 and April 10, 2018, 241 joints of 2 7/8 in. 6.5 ppf J55 EUE tubing were extracted from SS-25. The joints were visually inspected, cleaned of the Tectyl 846 corrosion inhibitor coating the ID and OD, and then bolstered in accordance with Blade's Tubulars Handling Protocol [5]. Two joints (T028 and T029) located near where the 7 in. casing had parted, were visually inspected, wrapped in VCI film without cleaning, and then crated. During the visual inspection at PS-20, 31 joints were found to be bent. One of these joints (T116) had a severe enough bend that it would not it would not fit in a bolster, and it was cleaned, inspected, coated, and crated. All of the joints were transferred from Aliso Canyon to the Blade warehouse in Houston on October 24, 2017.

On March 5, 2018, 241 joints of tubing were sent to Tuboscope for inspection. Joints T028, T029, and T116 were not sent to Tuboscope and were examined separately by Blade at the warehouse. During the receiving inspection at Tuboscope, 43 joints were set aside because they were too bent to be inspected. Therefore, 198 of the 244 joints were inspected at Tuboscope. Table 2 shows the final tubing NDE disposition.

Table 2: Tubing NDE Disposition

# Joints	JSN	Inspected at Tuboscope?	Comments
1	T001	No	Too bent; culled at Tuboscope
2	T002	No	Too bent; culled at Tuboscope
3	T003	Yes	
4	T004	Yes	
5	T005	No	Too bent; culled at Tuboscope
6	T006	Yes	
7	T007	Yes	
8	T008	No	Too bent; culled at Tuboscope
9	T009	No	Too bent; culled at Tuboscope
10	T010	No	Too bent; culled at Tuboscope
11	T011	Yes	
12	T012	No	Too bent; culled at Tuboscope
13	T013	No	Too bent; culled at Tuboscope
14	T014	Yes	
15	T015	Yes	
16	T016	Yes	
17	T017	Yes	
18	T018	No	Too bent; culled at Tuboscope
19	T019	Yes	
20	T020	Yes	
21	T021	No	Too bent; culled at Tuboscope
22	T022	No	Too bent; culled at Tuboscope

# Joints	JSN	Inspected at Tuboscope?	Comments
23	T023	No	Too bent; culled at Tuboscope
24	T024	No	Too bent; culled at Tuboscope
25	T025	Yes	
26	T026	Yes	
27	T027	Yes	
	T028	No	Not sent; examined at Blade warehouse
	T029	No	Not sent; examined at Blade warehouse
28	T030	No	Too bent; culled at Tuboscope
29	T031	Yes	
30	T032	Yes	
31	T033	No	Too bent; culled at Tuboscope
32	T034	No	Too bent; culled at Tuboscope
33	T035	Yes	
34	T036	No	Too bent; culled at Tuboscope
35	T037	Yes	
36	T038	Yes	
37	T039	Yes	
38	T040	No	Too bent; culled at Tuboscope
39	T041	Yes	
40	T042	No	Too bent; culled at Tuboscope
41	T043	Yes	
42	T044	No	Too bent; culled at Tuboscope
43	T045	Yes	
44	T046	No	Too bent; culled at Tuboscope
45	T047	Yes	
46	T048	No	Too bent; culled at Tuboscope
47	T049	Yes	
48	T050	No	Too bent; culled at Tuboscope
49	T051	No	Too bent; culled at Tuboscope
50	T052	Yes	
51	T053	No	Too bent; culled at Tuboscope
52	T054	Yes	
53	T055	Yes	
54	T056	No	Too bent; culled at Tuboscope
55	T057	No	Too bent; culled at Tuboscope
56	T058	Yes	
57	T059	Yes	

# Joints	JSN	Inspected at Tuboscope?	Comments
58	T060	Yes	
59	T061	Yes	
60	T062	No	Too bent; culled at Tuboscope
61	T063	Yes	
62	T064	Yes	
63	T065	Yes	
64	T066	Yes	
65	T067	Yes	
66	T068	Yes	
67	T069	Yes	
68	T070	Yes	
69	T071	Yes	
70	T072	No	Too bent; culled at Tuboscope
71	T073	Yes	
72	T074	No	Too bent; culled at Tuboscope
73	T075	Yes	
74	T076	Yes	
75	T077	Yes	
76	T078	Yes	
77	T079	Yes	
78	T080	No	Too bent; culled at Tuboscope
79	T081	Yes	
80	T082	Yes	
81	T083	Yes	
82	T084	Yes	
83	T085	Yes	
84	T086	No	Too bent; culled at Tuboscope
85	T087	Yes	
86	T088	Yes	
87	T089	Yes	
88	T090	Yes	
89	T091	Yes	
90	T092	Yes	
91	T093	Yes	
92	T094	Yes	
93	T095	Yes	
94	T096	No	Too bent; culled at Tuboscope

# Joints	JSN	Inspected at Tuboscope?	Comments
95	T097	Yes	
96	T098	Yes	
97	T099	Yes	
98	T100	Yes	
99	T101	Yes	
100	T102	Yes	
101	T103	Yes	
102	T104	No	Too bent; culled at Tuboscope
103	T105	Yes	
104	T106	Yes	
105	T107	Yes	
106	T108	Yes	
107	T109	Yes	
108	T110	Yes	
109	T111	Yes	
110	T112	No	Too bent; culled at Tuboscope
111	T113	Yes	
112	T114	Yes	
113	T115	Yes	
	T116	No	Not sent; examined at Blade warehouse
114	T117	Yes	
115	T118	Yes	
116	T119	Yes	
117	T120	Yes	
118	T121	Yes	
119	T122	Yes	
120	T123	Yes	
121	T124	Yes	
122	T125	Yes	
123	T126	Yes	
124	T127	Yes	
125	T128	Yes	
126	T129	Yes	
127	T130	Yes	
128	T131	Yes	
129	T132	Yes	
130	T133	Yes	

# Joints	JSN	Inspected at Tuboscope?	Comments
131	T134	Yes	
132	T135	Yes	
133	T136	Yes	
134	T137	Yes	
135	T138	Yes	
136	T139	Yes	
137	T140	No	Too bent; culled at Tuboscope
138	T141	No	Too bent; culled at Tuboscope
139	T142	Yes	
140	T143	Yes	
141	T144	Yes	
142	T145	Yes	
143	T146	Yes	
144	T147	No	Too bent; culled at Tuboscope
145	T148	Yes	
146	T149	Yes	
147	T150	No	Too bent; culled at Tuboscope
148	T151	Yes	
149	T152	No	Too bent; culled at Tuboscope
150	T153	Yes	
151	T154	Yes	
152	T155	Yes	
153	T156	Yes	
154	T157	Yes	
155	T158	No	Too bent; culled at Tuboscope
156	T159	Yes	
157	T160	No	Too bent; culled at Tuboscope
158	T161	Yes	
159	T162	No	Too bent; culled at Tuboscope
160	T163	Yes	
161	T164	Yes	
162	T165	Yes	
163	T166	Yes	
164	T167	Yes	
165	T168	Yes	
166	T169	Yes	
167	T170	Yes	

# Joints	JSN	Inspected at Tuboscope?	Comments
168	T171	Yes	
169	T172	Yes	
170	T173	Yes	
171	T174	Yes	
172	T175	Yes	
173	T176	Yes	
174	T177	Yes	
175	T178	Yes	
176	T179	Yes	
177	T180	Yes	
178	T181	Yes	
179	T182	Yes	
180	T183	Yes	
181	T184	Yes	
182	T185	Yes	
183	T186	Yes	
184	T187	Yes	
185	T188	Yes	
186	T189	Yes	
187	T190	Yes	
188	T191	Yes	
189	T192	Yes	
190	T193	Yes	
191	T194	Yes	
192	T195	Yes	
193	T196	Yes	
194	T197	Yes	
195	T198	Yes	
196	T199	Yes	
197	T200	Yes	
198	T201	Yes	
199	T202	Yes	
200	T203	Yes	
201	T204	Yes	
202	T205	Yes	
203	T206	Yes	
204	T207	Yes	

# Joints	JSN	Inspected at Tuboscope?	Comments
205	T208	Yes	
206	T209	Yes	
207	T210	Yes	
208	T211	Yes	
209	T212	Yes	
210	T213	Yes	
211	T214	Yes	
212	T215	Yes	
213	T216	Yes	
214	T217	Yes	
215	T218	Yes	
216	T219	Yes	
217	T220	Yes	
218	T221	Yes	
219	T222	Yes	
220	T223	Yes	
221	T224	Yes	
222	T225	Yes	
223	T226	Yes	
224	T227	Yes	
225	T228	Yes	
226	T229	Yes	
227	T230	Yes	
228	T231	Yes	
229	T232	Yes	
230	T233	Yes	
231	T234	Yes	
232	T235	Yes	
233	T236	Yes	
234	T237	Yes	
235	T238	Yes	
236	T239	Yes	
237	T240	Yes	
238	T241	Yes	
239	T242	Yes	
240	T243	Yes	
241	T244	Yes	

Appendix B Casing NDE Reconciliation

In November 2017, 23 joints of 7 in. 23 ppf J55 casing were extracted from SS-25. After extraction, the casing was cleaned and inspected in accordance with Blade's Tubulars Handling Protocol [5]. Each joint was then cut to remove a short section containing the made-up Speedtite connection. Additional short sections, which required special handling, were cut from several of the joints based on the results of the inspection. In the end, 27 short sections were wrapped in VCI and then individually crated for shipping. Of the 23 long joints, 21 long joints were ID and OD coated with Tectyl 846 corrosion inhibitor and then bolstered, and 2 long joints were wrapped in VCI and then bolstered for shipping. All of the bolsters and crates were transferred from Aliso Canyon to the Blade warehouse in Houston on December 4, 2017.

After the casing arrived at the Houston warehouse, Blade cut 24 in. long rings from 19 of the long sections for later mechanical testing. This required a change in the JSNs to maintain traceability, as documented in Table 3

Table 3: Casing Mechanical Testing Ring Sectioning Summary

# Joints	Original Parent JSN	Child 1 JSN	Child 2 JSN	Child 3 JSN
1	C001A	Not applicable; no ring was cut		
2	C002A	C002A1	C002A2	
3	C003A	C003A1	C003A2	
4	C004A	C004A1	C004A2	
5	C005A	C005A1	C005A2	
6	C006A	C006A1	C006A2	
7	C007A	C007A1	C007A2	
8	C008A	C008A1	C008A2	
9	C009A	C009A1	C009A2	
10	C010A	C010A1	C010A2	
1	C011A	C011A1	C011A2	
12	C012A	C012A1	C012A2	
13	C013A	C013A1	C013A2	
14	C014A	C014A1	C014A2	
15	C015A	C015A1	C015A2	
16	C016A	C016A1	C016A2	
17	C017A	C017A1	C017A2	
18	C018A	C018A1	C018A2	C018A3
19	C019A	C019A1	C019A2	
20	C020A	C020A1	C020A2	
21	C021A	Not applicable; no ring was cut		
22	C022A	Not applicable; no ring was cut		
23	C023B2	Not applicable; no ring was cut		

Rings were not cut from C001A, C021A, C022A, or C023B. These joints were also not sent to Tuboscope for inspection; C001 was too short, and Blade conducted a more detailed examination and inspection of the other three joints at the Blade warehouse. The test ring from C018A had to be removed at a location approximately 2 ft away from the end of the section. Note that only "long" casing sections were inspected at Tuboscope. The short, crated connection sections were inspected separately by Blade at the warehouse.

Two additional joints of casing were extracted from SS-25 in August 2018, and these were transported to Blade's warehouse on September 21, 2018. Blade inspected these joints at the warehouse, and they were not sent to Tuboscope for inspection.

A total of 25 joints of casing were extracted from SS-25, and 19 joints were sent to Tuboscope for inspection. Table 4 shows the final casing NDE disposition.

Table 4: Casing NDE Disposition

# Joints	JSN	Inspected at Tuboscope?
1	C001A	No; examined at Blade warehouse
2	C002A1	Yes
3	C003A1	Yes
4	C004A1	Yes
5	C005A1	Yes
6	C006A1	Yes
7	C007A1	Yes
8	C008A1	Yes
9	C009A1	Yes
10	C010A1	Yes
1	C011A1	Yes
12	C012A1	Yes
13	C013A1	Yes
14	C014A1	Yes
15	C015A1	Yes
16	C016A1	Yes
17	C017A1	Yes
18	C018A1	Yes
19	C019A1	Yes
20	C020A1	Yes
21	C021A	No; examined at Blade warehouse
22	C022A	No; examined at Blade warehouse
23	C023B2	No; examined at Blade warehouse
24	C025	No; examined at Blade warehouse
25	C026	No; examined at Blade warehouse

Appendix C NDE Photos

Figure 1: Tubulars Storage at Blade's Houston Warehouse

Figure 2: Loading Tubing Bolsters at Blade's Warehouse

Figure 3: Offloading Tubing at Tuboscope

Figure 4: Tubing Cleaning at Tuboscope

Figure 5: Tubing after EMI Inspection

Figure 6: Tubing FLUT Inspection

Figure 7: Loading Out Casing Bolsters at Blade Warehouse

Figure 8: Casing Bolsters Loaded

Figure 9: Casing FLUT Inspection

SS-25 RCA Supplementary Report

SS-25 Annular Flow Safety System Review

Purpose:
Provide the background and summary of the annular flow safety system used in SS-25 and how it was intended to work. A summary of the SS-25 completions, use of annular flow safety systems in other wells, and gas storage well regulatory requirements are included.

Date:
May 31, 2019

BLADE ENERGY PARTNERS

2600 Network Boulevard, Suite 550
Frisco, Texas 75034

+1 972-712-8407 (phone)
+1 972-712-8408 (fax)

16285 Park Ten Place, Suite 600
Houston, Texas 77084

1-800-319-2940 (toll free)
+1 281-206-2000 (phone)
+1 281-206-2005 (fax)

www.blade-energy.com

Blade Energy Partners Limited, and its affiliates ('Blade') provide our services subject to our General Terms and Conditions ('GTC') in effect at time of service, unless a GTC provision is expressly superseded in a separate agreement made with Blade. Blade's work product is based on information sources which we believe to be reliable, including information that was publicly available and that was provided by our client; but Blade does not guarantee the accuracy or completeness of the information provided. All statements are the opinions of Blade based on generally-accepted and reasonable practices in the industry. Our clients remain fully responsible for all clients' decisions, actions and omissions, whether based upon Blade's work product or not; and Blade's liability solely extends to the cost of its work product.

Abstract

The gas storage well Standard Sesnon 25 (SS-25) in the Aliso Canyon Gas Storage Field located in Los Angeles County, California started leaking gas in October 2015. A relief well was drilled, and SS-25 was brought under control. The leak stopped in February 2016.

In January 2016, as part of their investigation of the leak, the California Public Utilities Commission (CPUC) and the Division of Oil, Gas, and Geothermal Resources (DOGGR) selected and gave provisional authority to Blade Energy Partners (Blade) to perform an independent Root Cause Analysis (RCA). The Blade Team and parties under Blade's direction were responsible for directing the work of subcontractors who performed the extraction of the SS-25's wellhead and tubing and casing and the preservation and protection of associated evidence. Blade RCA Reports, including this report, document and describe the key activities undertaken in support of the RCA effort.

Well Standard Sesnon 25 (SS-25) was completed with a Camco annular flow safety system in July 1976. The safety system was removed and replaced in February 1979. Another attempt was made to repair and test the system in January 1980, when it was concluded the system did not function as designed. The internal components were then removed rendering the annular flow safety system inoperable.

The annular flow safety system was a means to shut off gas flow in the tubing-casing annulus in the event of a leak in the casing or uncontrolled flow at surface. The safety system is run with the completion tubing and packer and placed deep in the well above the packer, near the reservoir. There are numerous documents in the Aliso Canyon well files indicating problems with this type of safety system. Use of this device was discontinued in the 1980s, according to SoCalGas, because it did not work as designed and was unreliable. An operational downhole safety device was not in place in SS-25 when the well leaked on October 23, 2015.

A downhole safety device was not a regulatory requirement at the time because SS-25 does not meet the conditions for a *critical* well as defined in the 2015 California Code of Regulations.

Table of Contents

1 Introduction....4
1.1 Safety System Nomenclature....4
1.2 Abbreviations and Acronyms....5
2 SS-25 Operational Background....6
2.1 SS-25 SSSV Correspondence and Well Records....6
2.2 SSSVs Installed in Other Aliso Canyon Wells....8
2.3 Discussion of the Camco SC-1 Annular Flow Safety System....9
2.4 Discussion of the Otis Annular Flow Safety System....10
3 Gas Storage Regulations Summary....14
4 SS-25 Completion History....15
5 Conclusions....16
6 References....17

List of Figures

Figure 1: Camco SC-1 Annular Flow Safety System Diagram....11
Figure 2: SS-25 Wellbore Schematic Showing the Completion Run in 1979....12
Figure 3: SS-25 Wellbore Schematic Showing Details of the Completion Run in 1979....13

List of Tables

Table 1: SS-25 Well Activity Reports....7
Table 2: SS-25 Completion Summary....15

1 Introduction

The purpose of this report is to document the review of the history and problems with annular flow safety systems in SS-25. The well leaked natural gas to the atmosphere from October 23, 2015 to February 11, 2016 due to the failure of the 7 in. production casing.

SS-25 is located in the Aliso Canyon Gas Storage Field in Los Angeles County, California, and was equipped with a Camco SC-1 (Surface Controlled – First Generation) annular flow safety system in 1976 after the well was converted to a gas storage well. The annular flow safety system is sometimes referred to as a subsurface safety valve (SSSV) in the well files, not to be confused with modern day surface-controlled subsurface safety valves. Research into this system indicates that it was designed for wells that injected or produced through the production tubing-casing annulus. The Camco annular flow safety system was run as part of the tubing-packer completion equipment and set approximately 35 ft above the packer. The system operated by applying tubing pressure to hold the SSSV open and allowing flow in the annulus. When the tubing pressure was bled off, the SSSV was designed to close and shut off the injection or withdrawal through the annulus.

Other wells in the Aliso Canyon field had annulus flow safety systems installed when wells were converted from oil and gas to gas storage wells. Two wells of interest for the annulus flow safety system discussion are Frew 3 and FF-34A, which were equipped with Otis annulus flow safety systems. The Otis system was a competitor to the Camco safety system. Casing leaks in these two wells resulted in underground flow. The well records show the internal components of the Frew 3 safety system were removed prior to the leak. We found no records showing that the internal components of the FF-34A safety system were installed. These wells were killed by pumping down the tubing.

A downhole safety device was not a regulatory requirement for SS-25 because the well did not meet the conditions for a *critical* well. A summary of regulatory requirements for gas storage wells is included in Section 3.

1.1 Safety System Nomenclature

The subject of this document is an annular flow safety system which is a downhole safety device to control and isolate gas flow in the tubing by production casing annulus in the event of an emergency. This system is referred to by different names and terms in the well file and documents.

The original name was a Camco SC-1 Annular Flow Safety System. The well records sometimes refer to this system as a SSSV without specifying whether the valve is an annular gas flow safety valve system or a tubing flow safety valve.

Other similar terminology includes SSV which normally refers to a surface safety valve (SSV) installed on a wellhead or tree at the surface. The SSV is installed between the well and flow line so gas flow to and from well is through the SSV. The valve is actuated, meaning it is held open by applying pressure to the actuator. A pilot device that senses a condition such as high or low pressure causes the SSV to close if the pressure is outside a specified range. When pressure to the actuator is removed, the valve closes and stops gas flow. SSVs are commonly used on gas storage wells.

The term SCSSV or SC-SSV usually refers to a surface controlled subsurface safety valve installed for tubing flow that is closed in the event that pressure to keep the valve open is removed. SCSSVs are commonly used for offshore wells or where landslides are possible to shut in the tubing in the event the surface tree or flow line is damaged.

1.2 Abbreviations and Acronyms

Term	Definition
BHC	Bottomhole Choke
BHP	Bottomhole Pressure
FF	Fernando Fee
IW	Injection Well
NOI	Notice of Intent
SC-1	Surface Controlled—First Generation
SCSSV	Surface Controlled Subsurface Safety Valve
SoCalGas	Southern California Gas Company
SS	Standard Sesnon
SSV	Surface Safety Valve
SSSV	Subsurface Safety Valve

2 SS-25 Operational Background

SS-25 spudded on October 1, 1953 and completed as an oil producer in April 1954. The well was subsequently converted to gas storage in June 1973.

The Notice of Intention (NOI) to Rework Well was filed by SoCalGas on June 17, 1976 to clean out SS-25 and install an annular flow safety system [1]. DOGGR well records show a workover starting June 25, 1976 and ending July 9, 1976 [2]. The Tubing Detail document dated July 3, 1976 shows that Item 10, an SC-1 Safety System was installed [3].

An attempt was made to repair and function test the system in December 1978 [4]. The Camco annular flow safety system was pulled and replaced in February 1979 [5]. Another attempt to repair and test the system was made on January 28, 1980. The daily report stated "Pulled valve and pack-off. System apparently bad." [6].

A leak occurred in SS-25 in October 2015 allowing gas to escape to the atmosphere. A relief well was drilled to kill the well, and the bottom of SS-25 was sealed with cement in February 2016, which stopped the leak.

2.1 SS-25 SSSV Correspondence and Well Records

A discussion of the SS-25 SSSV system follows. It is based on SoCalGas internal correspondence and well records related to problems with annular flow safety systems in SS-25 and other wells. The well was converted to gas storage in 1973, but the system was not installed until 1976. The system operation was apparently problematic over the next several years, and a recommendation was made to replace the nonfunctioning SS-25 SSSV in December 1978.The following segment was extracted from a SoCalGas interoffice correspondence dated December 26, 1978 [4].

> It is recommended that we re-work SS-9 and SS-25. Both wells have Camco 2-1/2 in. SSSV's that failed during withdrawal. . . . Both of these valves failed by coming unlatched and smashing into the packoff above. Fortunately the packoff held and the valve fell back across the crossover flow ports, where the valve was then partially blocking the flow of gas. The reduction in rate was noticed and the wells were shut-in at the surface.
>
> This is at least the sixth such failure at Aliso for this type valve. Since we use few bottom-hole chokes anymore, it is critical that the SSSV stay in place since it is also our choke in most wells. Therefore it is further recommended that we replace these systems with Otis 2-1/2 in. SSSV's which have no history of coming loose.

The recommendation was approved and a work program was prepared to repair the SS-25 SSSV. The following segment was extracted from a SoCalGas interoffice correspondence dated December 27, 1978 [7].

> Attached are copies of letters just received from . . . with information concerning subsurface safety system failures in wells SS 9, SS 25, and IW 55. . . . Please add SS 25 to your schedule at this time with a "B" priority. . . . The question of replacing the defective Camco systems with Otis systems is under review. . . . However, if Camco cannot determine the source of their problem and correct it before such time as a rig is ready to complete one of the above wells, then an Otis system should be run.

Miscellaneous Work Order 99574 dated January 3, 1979 [8] was approved to replace the inoperable subsurface safety system as the following extracted segment indicates.

> Standard Sesnon 25 – Aliso Canyon
>
> Replace inoperable subsurface safety system
>
> Reason for request Tests conducted from December 13, through December 20, 1978 Indicate a leak in the safety valve control system and/or production packer. Such leakage renders the safety system inoperable. Priority "B".

A well program was prepared to pull and repair the SS-25 Downhole Safety System dated February 2, 1979 in an interoffice correspondence [9].

DOGGR well records show that a workover starting February 16, 1979 and ending February 20, 1979 [5] was carried out to install a new Camco system. The Tubing Detail document dated February 21, 1979 shows that Item 11, Camco "SC-1" safety system, was installed at a depth of 8,455 ft [10].

A review of the well service records indicates that the Camco SSSV installed during the 1979 workover would not test. Attempts to replace the SSSV and get a test were unsuccessful, and it was pulled on January 28, 1980. A comment in the well service records states "System apparently bad."

Table 1 shows the Well Activity Reports for SS-25 [6] including the 1979 workover. The wording in the Report Comments column replicates what was reported in the well file and has not been edited.

Table 1: SS-25 Well Activity Reports

Date	Report Comments
February 20, 1979	Rig removed safety valve system from well. The control line was gone, exchanged systems with Camco.
November 5, 1979	Hanson attempted to set BHC. Could not get choke to go through packoff nipple. Left choke in packoff nipple.
November 6, 1979	Ran bottom hole pressure (BHP) survey. Hanson pulled BHC from well. Discovered that backup ring on packing was too large to go through nipple. Changed ring. Set BHC.
November 13, 1979	Gurevich ran BHP survey. Found that BHC had been set in the safety valve nipple. Pulled loose OK.
November 14, 1979	Hanson located BHC in safety valve nipple. Pulled choke. Re-dressed choke and attempted to run in but could not get past safety valve nipple. Moved off of well.
November 15, 1979	Hanson ran in to set BHC but could not get past safety valve nipple.
November 16, 1979	Hanson again attempted to set BHC. No luck.
November 19, 1979	Hanson set 1.0 BHC.
January 4, 1980	Archer-Reed set CA-2 plug in pack-off nipple. Tested tubing. Pressure held tight. Pulled plug.
January 7, 1980	Camco pulled 1.0 BHC. Ran in to set SSSV. Could not get valve to stay in nipple. Checked running tool, prong was damaged. Shut down till Monday.
[No Date]	Camco ran in with broach. Found tight spot at 1356'. Beat through. Cleared out tight spot at 3590' and 3608'. Continued broaching tight spot at 1345' for remainder of day.
January 8, 1980	Camco finished broaching tight spot at 1346'. Ran and set SSSV. Could not get setting tool to release from valve. Wire broke at counter sheave. Dropped cutter bar and retrieved wire from well. Will change wire and fish for tools tomorrow.

Date	Report Comments
January 9, 1980	Camco attempted to fish for tools. Rope swelled up with rain water and would not thru pulleys. Shut down for day.
January 10, 1980	Camco fished all tools out of well OK. Set pack-off. Tested SSSV. S/I tubing (T) 2,500 psi, casing (C) 2,600 psi. Bled tubing to 2,000 psi, held OK. Bled tubing to 1,020 psi, held OK. Bled casing to 2,000 psi, valve closed and held OK. Pressure casing to 2,500 psi. Pressure tubing to 2,460 psi, valve opened OK. Requested instrument department install recording gauge on tubing. Will put well on withdrawal when gauge installed.
January 14, 1980	Inst. Dept. installed pressure recorder on tubing. Will have well put on withdrawal.
January 22, 1980	Camco attempted to pull SSSV. Could not latch. Ran in with spear. Slips on spear broke. Ran in with shear (sic) [spear?] and latched onto valve. Unable to pull. Shut down for night.
January 23, 1980	Camco pulled SSSV. Fishing neck was flared out and cracked along side. It has come out of nipple and hit pack-off. Set another SSSV and pack-off. Tested valve. Test no good. Tubing pressure built up 50 psi in 30 seconds.
January 24, 1980	Camco pulled pack-off and SSSV. Ran another SSSV and pack-off. Tested valve. Bled tubing from 2,100 psi to 1,750 psi, pressure rose 50 psi in one minute. Will test again in morning.
January 25, 1980	Tested SSSV. Blew tubing pressure to atmosphere, pressure did not get below 350 psi. Not enough to close valve. Pulled pack-off and SSSV.
January 28, 1980	Camco ran SSSV and pack-off. Tested valve. Blew tubing down to 550 psi. Opened 2" stack, pressure would not go below 280 psi. Bled casing from 2,160 psi to 1,900 psi. Pressure rose 50 psi/minute. Valve did not close. Pulled valve and pack-off. System apparently bad.

2.2 SSSVs Installed in Other Aliso Canyon Wells

A review of other Aliso Canyon well records found wells where an Otis annular flow safety system and a Baker surface controlled subsurface safety valve (SCSSV) were installed.

- Well SS-1. A 2 7/8 in. Otis system was installed in October 1977 according to the NOI to rework the well [11] and the well history [12].
- Well SS-9. A 2 7/8 in. Camco system was installed in September 1977 [13] at 8,527 ft. The system was inoperative and was pulled and replaced with another Camco system in February 1979 [14] at 8,529 ft. The Camco system was pulled and a 4 1/2 in. Baker T5 SCSSV was run in November 1994 [15] at 477 ft when the well was converted to large diameter tubing flow.
- Well SS-5. A 2 3/8 in. Otis system was installed in December 1977 [16] at 8,274 ft replacing the Camco system.
- Well Frew 3. A 2 7/8 in. Otis system was installed in September 1977 [17].
- Well SS-44A. A 2 7/8 in. Otis system was installed in July 1978 [18] at 8,780 ft.
- Well FF-34A. A 3 1/2 in. Otis system was installed in December 1979 [19].

2.2.1 Wells with Casing Leaks, Underground Flow and Well Kill Operations

Two wells (Frew 3 in 1984 and FF-34A in 1990) had casing leaks and underground flow and were killed by pumping down the tubing. These wells were equipped with Otis annular flow safety systems. SoCalGas personnel were questioned regarding the effectiveness of the safety systems in these wells when the leaks occurred [20]. SoCalGas stated that the safety systems had been removed before the leak events in these two wells because the systems were not reliable. A review of the well records showed that the internal components of the Frew 3 safety system were removed prior to the leak. We found no records showing that the internal components of the FF-34A safety system were installed. Additional details of the completions and the well kill operations can be found in a separate Blade report [21].

2.3 Discussion of the Camco SC-1 Annular Flow Safety System

The following is a summary of how the safety system was intended to work. This summary is based on discussions with knowledgeable people familiar with the Camco equipment used during this timeframe and supplemented with data request responses and details documented in the SS-25 well files. Figure 1 shows a diagram of the Camco SC-1 Annular Flow Safety System.

The SC-1 annular flow safety system mandrel (length 15.50 ft) is run as part of the completion equipment with the production tubing. After the tubing is landed, the PC-4 Safety Valve is run on slickline and landed and locked in the WP-1 nipple profile below the ports in the SC-1 Safety System (Figure 1). The PC-4 is spring loaded and nitrogen charged in the normally closed position where a sleeve covers and isolates the SC-1 ports.

The GS Packoff is run on slickline and is landed and locked in the DS-1 nipple profile above the ports in the SC-1 Safety System. The GS Packoff blocks flow in the tubing. The side port in the GS Packoff directs tubing pressure through the external control line to the PC-4 Safety Valve. Tubing pressure applied to the PC-4 Safety Valve causes the PC-4 sleeve to shift and expose the SC-1 ports, which allows communication from the reservoir to the casing or vice versa. When the tubing pressure is bled off, the PC-4 Safety Valve isolates the SC-1 ports, which prevents flow up the annulus. The GS Pack-off prevents flow up the tubing.

The inability to keep the PC-4 Safety Valve latched in the WP-1 nipple to achieve a complete pack-off between the WP-1 ported nipple and the PC-4 Safety Valve made the system inoperable. The problems with latching the PC-4 Safety Valve in the nipple profile are described in the reports shown in Table 1.

It was not possible to locate engineering drawings, catalogues, or other material for this system. Apparently, no patent was filed for this design. The design appears to be limited in application and was a special design. The system was not deployed worldwide or outside of California based on the research.

Some of the abbreviations, including PC, WP, GS, and DCRT used in the component names, are undefined because of the lack of proper documentation available in the records.

Refer to Figure 2 and Figure 3 for wellbore diagrams showing the SS-25 completion with more details.

2.4 Discussion of the Otis Annular Flow Safety System

Based on the information from Aliso Canyon well files, the Otis annular flow safety system competed with the Camco system. No details on the functionality, operation, or reliability of the Otis system were found in the well files. As discussed in this report, because of the numerous problems with the Camco system, recommendations were made to replace it with the Otis system, which had no history of coming loose according to a SoCalGas Interoffice Correspondence dated December 26, 1978 [4].

Relevant technical information of the 1970s Otis annular flow safety systems was unavailable.

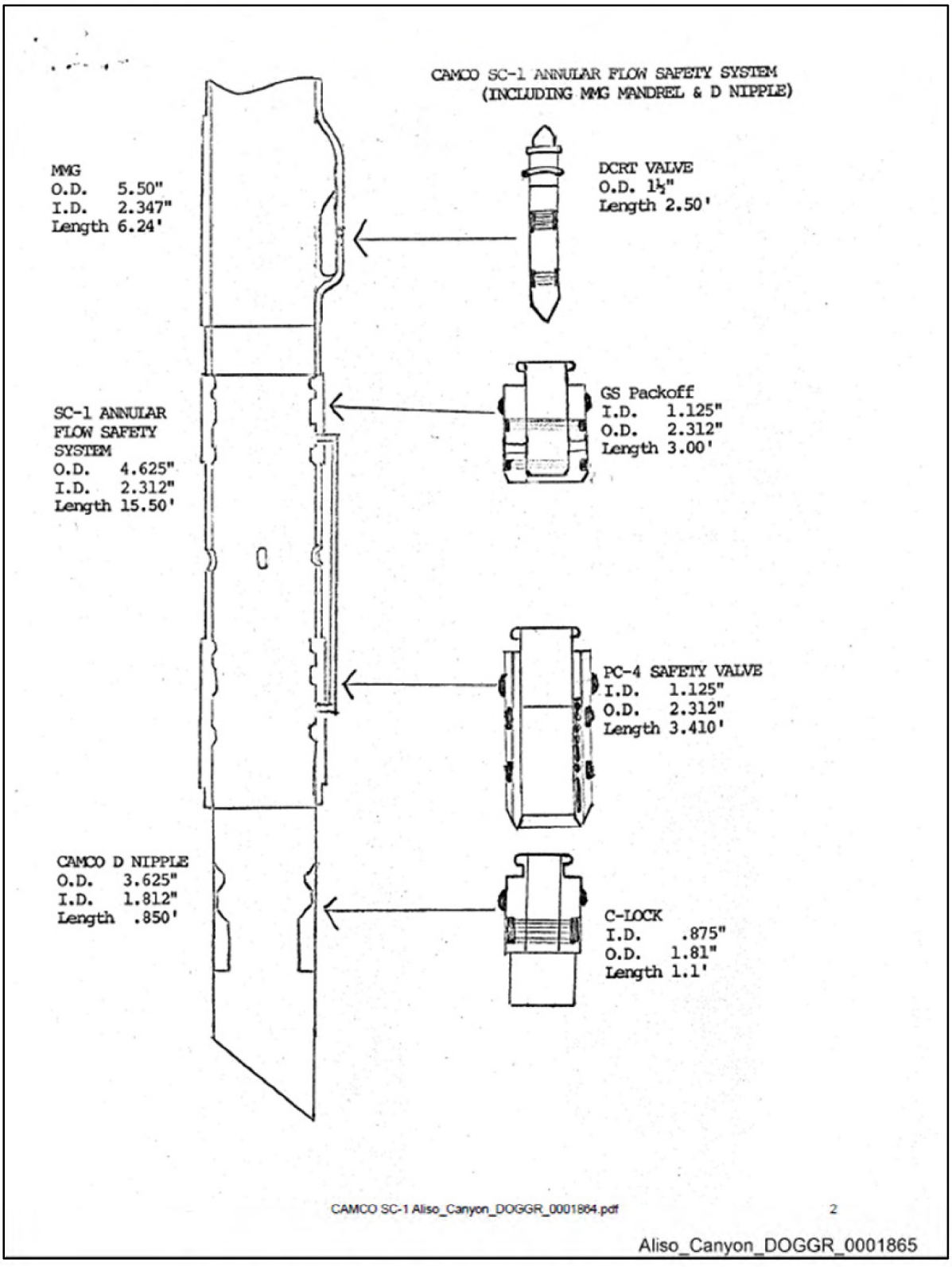

Figure 1: Camco SC-1 Annular Flow Safety System Diagram

Spud Date:	Oct 1, 1953
Conversion Date:	Jun 6, 1973
TD - MD:	8,749 ft
TD - TVD:	8,733 ft
API Number:	03700776
GLE:	2,927 ft

Standard Sesnon #25
Gas Storage Wellbore Schematic

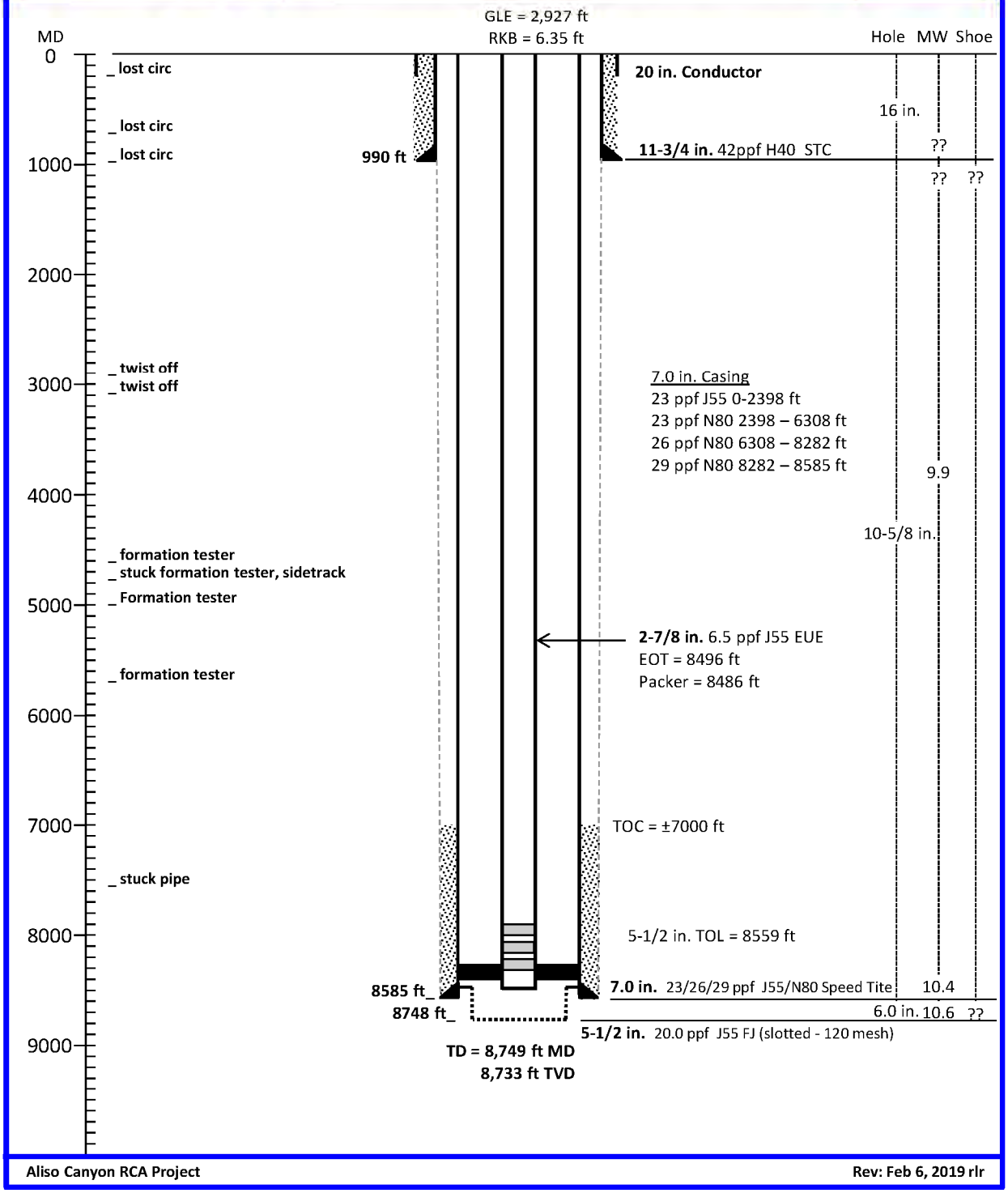

Aliso Canyon RCA Project — Rev: Feb 6, 2019 rlr

Figure 2: SS-25 Wellbore Schematic Showing the Completion Run in 1979

Spud Date:	Oct 1, 1953
Conversion Date:	June 6, 1973
TD - MD:	8,749 ft
TD - TVD:	8,733 ft
API Number:	03700776
GLE:	2,927 ft

Standard Sesnon #25
Gas Storage Completion Detail

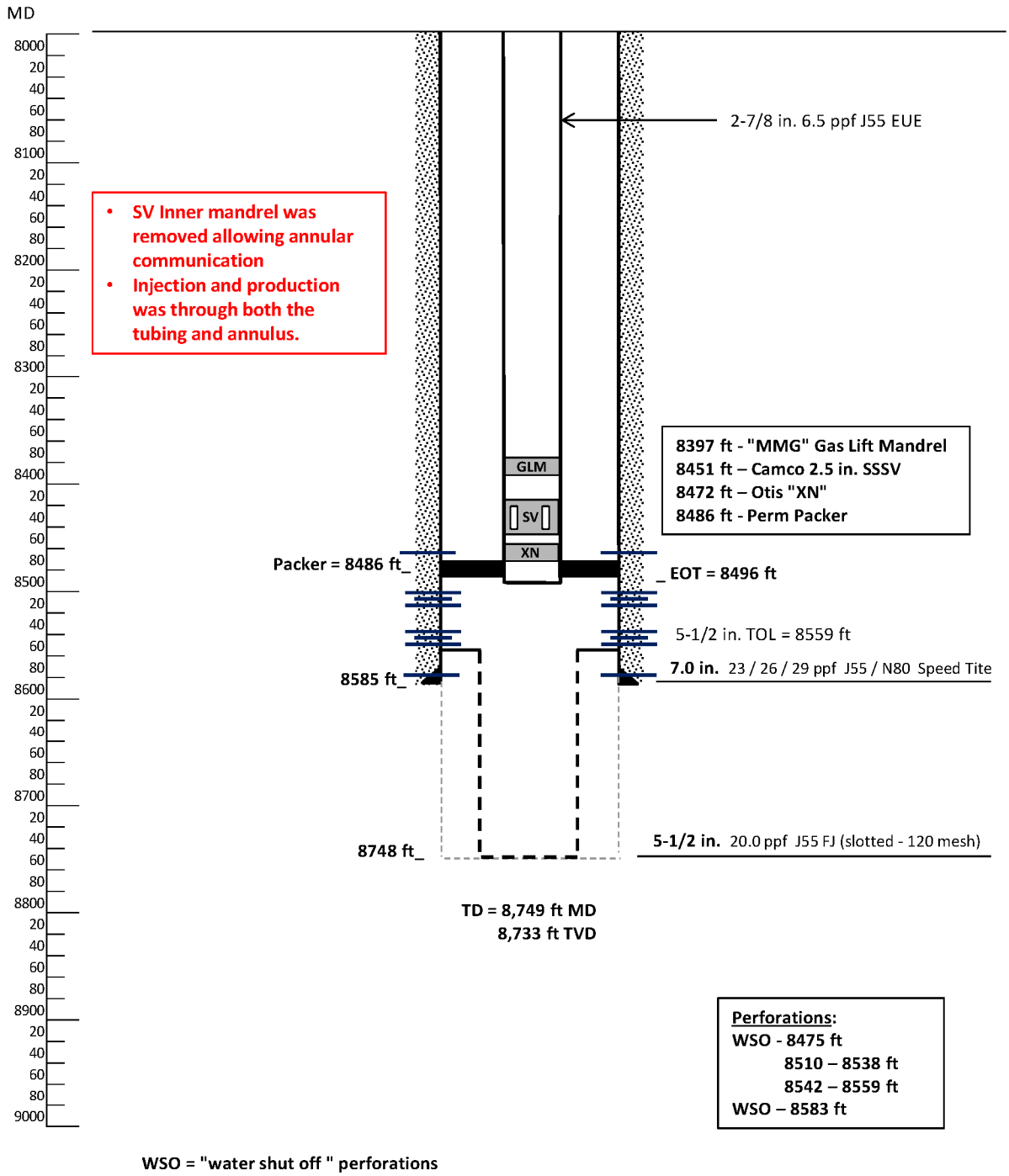

Aliso Canyon RCA Project — Rev: Feb 6, 2019 rlr

Figure 3: SS-25 Wellbore Schematic Showing Details of the Completion Run in 1979

3 Gas Storage Regulations Summary

The regulatory discussion is based on the 2015 California Statutes and Regulations which were in place when the SS-25 leak event happened.

A subsurface safety device for wells defined as *critical* is required by regulation. A *critical* well is a well located within a given distance from a public area, water, or wildlife preserve. SS-25 did not meet the conditions of a critical well; therefore, a subsurface safety device was not a requirement.

A summary of the California Statutes and Regulations document, Publication No. PRC10, 2015 version [22] relevant to SS-25, Gas Storage Projects, and Underground Injection Projects follows:

- 1724.9 Gas Storage Projects addresses the requirements for the approval of a gas storage project. It does not specifically mention well types, but it does list the data required by the Division prior to approval of a project including, (a) characteristics of the cap rock, (b) oil and gas reserves prior to injection, (c) list of proposed surface and subsurface safety devices, and (d) proposed waste water disposal method.
- 1724.10 Filing, Notification, Operating, and Testing Requirements for Underground Injection Projects do mention pipeline-quality gas injection wells and injection-withdrawal wells in a gas storage project.
  - 1724.10 (g) Exempts pipeline-quality gas injection wells from the requirement of equipping wells with tubing and packer set immediately above the approved zone of injection. There are provisions for exceptions where there is (1) no evidence of freshwater, (2) more than one string of casing cemented below the base of fresh water, and (3) other justification, as determined by the district deputy, based on documented evidence that fresh water and oil zones can be protected without the use of tubing and a packer.
  - 1724.10 (j) Requires a mechanical integrity test (MIT) for all injection wells. The MIT consists of two parts.
    - 1724.10 (j) (1) Prior to injecting, each injection well must pass a pressure test. Thereafter, the annulus of each well must be tested at least once every 5 years.
    - 1724.10 (j) (2) Injection wells shall demonstrate that there is no fluid migration behind the casing, tubing, or packer. Test frequency is given for water-disposal, waterflood, and steamflood wells. A test frequency for gas storage wells is not specified.
  - 1724.10 (k) Additional requirements or modifications of the above requirements may be necessary to fit specific circumstances and types of projects are given. One example cited includes a list of all injection-withdrawal wells in a gas storage project, showing casing-integrity test methods and dates, the types of safety valves used, submitted to the Division annually.
- 1724.3 Safety devices are required for wells that are defined as *critical*. Wells are deemed critical if they are located with a specified distance from public areas, bodies of water, airport runways, or wildlife preserves as stated in Article 2 §1720 of [22]. SS-25 does not meet the requirements for a critical well; therefore, a downhole safety device such as an annulus flow safety system was not a requirement.

4 SS-25 Completion History

Table 2 is a summary of the SS-25 completions from 1954 until the leak event in 2015. The Completion and Summary Comments are from the well file reports and are un-edited. The abbreviations, including KV, FH, DS, MMG, XN, and DCRT, are undefined because of the lack of complete documentation available to accurately define them. Figure 2 shows the completion run in 1979, and Figure 3 shows the details of the 1979 completion, which is also how the well was configured when it leaked in October 2015.

Table 2: SS-25 Completion Summary

No.	Date Run	Completion Summary and Comments	Completion Time Frame	Casing Exposed to Wellbore Fluids	Reference
1	February 16, 1954	2 7/8 in. tubing landed at 8,540' (no packer reported)	1 month	Yes	[23]
2	March 18, 1954	Guiberson KV-30 wall packer at 8525', five Guiberson gas lift valves and 2 7/8 in. tubing.	19 years 2 months	No	[23]
3	June 5, 1973	Converted to gas storage well. Baker FH packer at 8,453', Baker F nipple, Baker L sliding sleeve and 5 KBMG gas lift mandrels w/BK valve and 2 7/8 in. tubing.	3 years 1 month	Possible, depends if the sliding sleeve was open or closed.	[24]
4	July 8, 1976	Baker Retrieva-D packer at 8,480', Blast Joint, Camco no go nipple, Camco Blast Joint, D-S Nipple ½ in. Hyd. Control Line SC-1-Safety Annulus System, MMG Mandrel (empty) and 2 7/8 in. tubing.	2 years 7 months	Yes, assuming Safety system is annulus flow safety system.	[2], [25]
5	February 20, 1979	Baker packer at 8,486', Camco Blast Joint, Otis XN no go nipple [or Camco D no go nipple; conflicting records], Camco Blast Joint, Camco WP-1 nipple, Camco SC-1 Safety System, Camco DS-1 nipple, Camco MMG mandrel with DCRT valve and 2 7/8 in. tubing.	11 months	Yes, assuming Safety system is annulus flow safety system.	[10], [5]
6	January 28, 1980	Well service. Pulled SSSV valve and packoff. System apparently bad. (leaving the SSSV ports open between the tubing and annulus)	35 years 9 months	Yes, SSSV ports are open.	[6]
7	Leak Event October 23, 2015	SS-25 was killed 11 Feb 2016 and then plugged and abandoned in Sep 2018.	Not Applicable	Not Applicable	Not Applicable

5 Conclusions

Documents in the SS-25 well file indicate that the Camco system was not reliable and had caused operational problems in SS-25 and other wells. Well records show the SS-25 annular flow safety system internal components were removed in 1980 after a workover to repair the safety system. The records also show an Otis annular flow safety system was used in some Aliso Canyon wells, but information on the Otis system is limited. Numerous problems with the annular flow safety system are reported in the Aliso Canyon well files. SoCalGas eventually removed this type of downhole safety device from wells because of the operational problems and unreliable performance.

6 References

[1] SoCalGas, "Division of Oil and Gas Notice of Intent to Rework Well, AC_CPUC_0000024, (SS-25 Well Documentation (from SoCalGas)_N.pdf page 2)".

[2] SoCalGas, "Division of Oil and Gas History of Oil or Gas Well AC_CPUC_0000029 - AC_CPUC_0000030, SS-25 Well Documentation (from SoCalGas)_N.pdf, pages 7 - 8)".

[3] SoCalGas, "Tubing Detail, AC_CPUC_0000033, (SS-25 Well Documentation (from SoCalGas)_N.pdf, page 11)".

[4] SoCalGas, "Interoffice Correspondence, SS-9 and SS-25, December 26, 1978, AC_CPUC_0000073, (SS-25 Well Documentation (from SoCalGas)_N.pdf, page 51)".

[5] SoCalGas, "Division of Oil and Gas History of Oil or Gas Well AC_CPUC_0000031, (SS-25 Well Documentation (from SoCalGas)_N.pdf, page 9)".

[6] SoCalGas, "Well Activities Reports for SS 25, AC_CPUC_0000060 - AC_CPUC_0000061, (SS-25 Well Documentation (from SoCalGas)_N.pdf, page 38 - 39)".

[7] SoCalGas, "Interoffice Correspondence, Recommend SS 9, SS 25 and IW 55 for Repair Schedule, 27 December 1978, AC_CPUC_0000071 (SS-25 Well Documentation (from SoCalGas)_N.pdf, page 49)".

[8] SoCalGas, "Miscellaneous Work Order, 3 January 1979, AC_CPUC_0000070, (SS-25 Well Documentation (from SoCalGas)_N.pdf, page 48)".

[9] SoCalGas, *Interoffice Correspondence, Well Program for Standard Sesnon #25 - Aliso Canyon - Pull and Repair Down-Hole Safety System, February 2, 1979, AC_CPUC_0000074 - AC_CPUC_0000077 (SS-25 Well Documentation (from SoCalGas)_N.pdf pages 52 - 55).*

[10] SoCalGas, "Tubing Detail, AC_CPUC_0000032, (SS-25 Well Documentation (from SoCalGas)_N.pdf, page 10)".

[11] SoCalGas, "Division of Oil and Gas Notice of Intention to Rework Well, (SS-1 03700754_DATA_2-29-2008.pdf, pages 117 - 120)".

[12] SoCalGas, "Division of Oil and Gas History of Oil or Gas Well (SS-1 03700754_Data_2-29-2008.pdf pages 112 - 114)".

[13] SoCalGas, "Division of Oil and Gas History of Oil or Gas Well AC_BLD_0029456 - AC_BLD_0029458, (SS-9 Well File from SoCalGas.pdf pages 111 - 113)".

[14] SoCalGas, "Division of Oil and Gas History of Oil and Gas Well AC_BLD_0029451 - AC_BLD_0029452 (SS-9 Well File Data from SoCalGas.pdf, page 106 - 107)".

[15] SoCalGas, "Wellbore Schematic, AC_BLD_0029347, (SS-9 Well File Data from SoCalGas.pdf, page 2)".

[16] SoCalGas, "Tubing Detail, AC_BLD_0004019 (SS-5 Well File Data from SoCalGas.pdf, page 162)".

[17] SoCalGas, "Division of Oil and Gas History of Oil or Gas Well (Frew 3 History 03700666_DATA_03-20-2008.pdf, pages 39 - 40)".

[18] SoCalGas, "Division of Oil and Gas History of Oil or Gas Well (SS-44A 03721455_DATA_11-19-07.pdf, pages 89 - 93)".

[19] SoCalGas, "Division of Oil and Gas History of Oil or Gas Well (FF-34A History 03722044_DATA_10-03-2007.pdf, pages 29 - 36)".

[20] SoCalGas, Interviewee, *Data Clarification Meeting, Chatsworth, CA, 24 August 2018.* [Interview]. 24 August 2018.

[21] Blade, "Analysis of Aliso Canyon Gas Storage Wells with Casing Failures".

[22] State of California, *California Statutes and Regulations for Conservation of Oil, Gas, & Geothermal Resources,* 2015.

[23] SoCalGas, "Division of Oil and Gas History of Oil or Gas Well (SS-25 Well Documentation, AC_CPUC_0000034 - AC_CPUC_0000039 (from SoCalGas)_N.pdf, page 12 - 17)".

[24] SoCalGas, "Division of Oil and Gas History of Oil or Gas Well AC_CPUC_0000139 - AC_CPUC_0000141 (SS-25 Well Documentation (from SoCalGas)_N.pdf, pages 117 - 119)".

[25] SoCalGas, "Tubing Detail, AC_CPUC_0000120 (SS-25 Well Documentation (from SoCalGas)_N.pdf, page 98)".